

New Chemistry of Multiynes under Thermal and Metal-Catalyzed Conditions

BY

SASWATA GUPTA

B.Sc., Presidency College, Kolkata, 2013

M.Sc., Indian Institute of Technology Kharagpur, 2015

THESIS

Submitted as partial fulfillment of the requirements
for the degree of Doctor of Philosophy in Chemistry
in the Graduate College of the
University of Illinois at Chicago, 2021

Chicago, Illinois

Defense Committee: Daesung Lee, Advisor and Chair, Chemistry
Neal Mankad, Chemistry
Duncan Wardrop, Chemistry
Andy Nguyen, Chemistry
Peng Liu, University of Pittsburgh

This thesis is dedicated to my beloved parents

Mr. Nipendra Kumar Gupta and Mrs. Banasree Gupta

ACKNOWLEDGEMENTS

First and foremost, I would like to express my earnest gratitude to my advisor, Professor Daesung Lee, for his numerous insightful ideas, invaluable guidance, and endless encouragement to achieve several meaningful goals. He remained a true inspiration throughout my Ph.D. term. I appreciate his passion for teaching, and I admire the way he explains organic chemistry both during the course work as well as in our group meetings. He showed me how to work neatly and time-efficiently. I am honored to have the opportunity to work under his supervision.

I want to thank my committee members, Prof. Neal Mankad, Prof. Duncan Wardrop, Prof. Andy Nguyen of UIC, and Prof. Peng Liu of University of Pittsburgh for their time, helpful comments, and suggestions to make this thesis better. I would like to thank the excellent professors in our department, Prof. Daesung Lee, Prof. Vladimir Gevorgyan, Prof. Justin Mohr, Prof. Tom Driver, Prof. Leslie Aldrich for their brilliant teaching during my PhD coursework.

I would like to thank Prof. Yuanzhi Xia, Peipei Xie, Yongjia Lin of Wenzhou University and Prof. Peng Liu, Yu Zhang of University of Pittsburgh for contributing to the computational studies in several of my research projects. I would thank Professor Donald J. Wink of UIC for solving several X-ray structures in some of the chapters.

I also need to thank all the members of Lee's group whom I had an opportunity to work with: Dr. Matthew J. O'Connor, Dr. Venkata Sabbasani, Dr. Rajdip Karmakar, Dr. Hyunjin Lee, Dr. Fa-Jie Chen, Dr. Xinyu Guan, Dr. Sourav Ghorai, Dr. Anh Le, Siyuan Su, Hua Xu, and Erandi Liyanage Perera. I would like to give special thanks to Dr. Venkata Sabbasani and Siyuan Su for working in collaborative projects. It was a great pleasure working with them through the years together and I wish them the best in their future career. I also thank Prof. Mohr and his group members for sharing their ideas during our joint group meetings.

I am thankful to the Chemistry Department staffs, the late Ms. Rhonda Staudohar, Ms. Margaret

Shortall, Ms. Silvia Solis, Ms. Jennifer Kazin and Ms. Gloria Torres Mares for their official supports, Dr. Dan McElheny for training me NMR techniques, Dr. Randall Puchalski and Mr. Thomas Frueh for taking care of safety issues in lab, Brian Schwandt for making and fixing numerous glassware, and entire staff of Department of Chemistry for their support in the past years.

I would like to thank my roommates and friends in Chicago, especially, Navendu, Debanjan, Sumon, Sayantan, Proloy, Sujoy and Soumya with whom I have shared many memorable memories outside the lab. Lastly, I am sincerely grateful to my parents and relatives for their love, caring, blessings, and support throughout these years.

Thank you all.

SG

2021, Chicago

CONTRIBUTION OF AUTHORS

I would like to acknowledge several people who have contributed to the projects presented in this thesis.

Prof. Yuanzhi Xia and his group members Peipei Xia and Yongjia Lin of Wenzhou University contributed to the computational studies described in Chapters 2, 3 and 4. Prof. Peng Liu and Yu Zhang of University of Pittsburgh contributed to the computational studies described in Chapter 8. Prof. Donald J. Wink contributed to X-ray crystallographic studies in Chapters 4, 7 and 8. A part of the work including initial discovery described in Chapter 7 was done by Dr. Venkata R. Sabbasani. A portion of experimental works for projects described in Chapters 7 and 8 was done by Siyuan Su.

TABLE OF CONTENTS

<u>CHAPTER</u>	<u>PAGE</u>
PART I: THERMAL REACTIONS OF MULTIYNES: HEXADEHYDRO DIELS-ALDER (HDDA) REACTION	
1. Thermal Reactions of Multiynes	2
1.1. Thermal Dehydro Diels-Alder (DDA) Reactions	2
1.2. Hexadehydro Diels-Alder (HDDA) Reaction and Aryne Generation	7
1.2.1. Early examples of HDDA reaction	7
1.2.2. Hoya's approach and reaction mechanisms	9
1.2.3. Trapping methods of arynes.....	11
1.2.4. Multicomponent reactions with arynes	14
1.2.5. Metal-catalyzed reactions of HDDA-derived arynes	16
1.3. Strategy-Level Development of HDDA Reactions	17
1.3.1. Photochemical and domino HDDA reactions	17
1.3.2. Other variants of HDDA reactions.....	18
1.4. Other Thermal Processes of Multiynes	19
1.5. Summary	20
1.6. References.....	21
2. Intermolecular Alder-Ene Reaction of Arynes with Functionalized Alkenes	25
2.1. Introduction.....	26
2.1.1. Alder-ene reaction.....	26
2.1.2. Transition metal-catalyzed Alder-ene reaction	30
2.1.3. Allylic C–H bond functionalization	33
2.1.4. Aryne-ene reaction	34
2.2. Results and Discussions	38
2.2.1. Initial observation	38
2.2.2. Reaction profile of 1,1-disubstituted alkenes	39
2.2.3. Reaction profile of trisubstituted alkenes.....	40
2.2.4. Reaction profile of alkenyl alcohols	41
2.2.5. Reaction profile of 1,3-dienes.....	42
2.2.6. Stereoselectivity and regioselectivity.....	43
2.3. Conclusion	45
2.4. Experimental Details.....	46
2.4.1. General information	46
2.4.2. Preparation of substrates	47
2.4.3. General procedure for tandem HDDA-Alder-ene reaction	52
2.4.4. Characterization data.....	53
2.4.5. Computational details	69
2.5. Note.....	70
2.6. References.....	71

TABLE OF CONTENTS

<u>CHAPTER</u>	<u>PAGE</u>
3. Intermolecular Alder-Ene vs. Addition Reactions	74
3.1. Introduction.....	75
3.1.1. Addition reaction of arynes with polar functionalities	75
3.1.2. Reaction of arynes with carbonyl compounds	77
3.2. Results and Discussions	79
3.2.1. Reaction profile of alkenyl acids, amines, azides and aldehydes.....	79
3.2.2. Reaction profile of α,β -unsaturated aldehydes to form chromenes	80
3.2.3. Competition between Alder-ene reaction and chromene formation	82
3.2.4. Reaction profile of other electron-rich carbonyls	84
3.2.5. DFT calculations to support the selectivity.....	85
3.3. Conclusion	87
3.4. Experimental Details.....	88
3.4.1. General information	88
3.4.2. Experimental procedure	89
3.4.3. Characterization data.....	94
3.4.4. Computational details	106
3.5. Note.....	107
3.6. References.....	108
4. Alder-Ene Reaction to Form Benzocyclobutenes	111
4.1. Introduction.....	112
4.2. Results and Discussions	116
4.2.1. Initial design and optimization.....	116
4.2.2. Effect of substituents on the ene-donors	118
4.2.3. Reaction profile with different tethers	121
4.2.4. Competition experiments and DFT studies.....	121
4.2.5. Reactions of benzocyclobutene derivatives	123
4.3. Conclusion	125
4.4. Experimental Details.....	126
4.4.1. General information	126
4.4.2. Preparation of substrates	127
4.4.3. HDDA reaction to form benzocyclobutenes	135
4.4.4. Procedures for reactions of benzocyclobutene derivatives	136
4.4.5. Characterization data.....	140
4.4.6. Computational Details.....	159
4.5. Note.....	162
4.6. References.....	162
5. Diversity-Oriented Synthesis of Bioactive Natural Products of the <i>Selaginella</i> Family	166
5.1. Introduction.....	167
5.1.1. Alkynyl phenol natural products from the genus <i>Selaginella</i>	167
5.1.2. Biosynthesis and biological activity	169

TABLE OF CONTENTS

<u>CHAPTER</u>	<u>PAGE</u>
5.1.3. Previous syntheses	172
5.2. Diversity-Oriented Approach to Various Natural Products of the Selaginella Family	177
5.3. Results and Discussions	179
5.3.1. Total synthesis of selaginellin H	179
5.3.2. Synthetic progress to selaginpulvinin G	181
5.4. Conclusion	183
5.5. Experimental Details	184
5.5.1. General information	184
5.5.2. Experimental procedures and characterization data	184
5.6. References	196
PART II: METAL CATALYZED REACTIONS OF MULTIYNES: RUTHENIUM CARBENE COMPLEX	
6. Metal-Catalyzed Reactions of Multiynes	201
6.1. Platinum and Gold-Catalyzed Reaction	201
6.2. Ruthenium-Catalyzed Reaction: Enyne metathesis	203
6.2.1. Historical background and mechanisms	203
6.2.2. <i>Exo/endo</i> -mode selectivity	206
6.2.3. Tandem and domino metathesis	207
6.2.4. Enyne cross metathesis	208
6.2.5. Metallotropic [1,3]-shift	210
6.3. Metathesis and Metallotropy: Applications in Total Synthesis and Polymer Chemistry	211
6.4. Metal Complexes with Multiynes	213
6.5. Summary	215
6.6. References	216
7. Alkene-Chelated Ruthenium Alkylidenes: A Missing Link to New Catalysts	220
7.1. Introduction	221
7.1.1. Heteroatom-chelated ruthenium alkylidenes	221
7.1.2. Previous alkene and alkyne-chelated ruthenium alkylidenes	225
7.2. Results and Discussions	227
7.2.1. Enyne metathesis-based design to ruthenium alkylidenes	227
7.2.2. 1,5-Alkene chelates	229
7.2.2.1. Tandem RCM-CM approach with 1,n-diynes	229
7.2.2.2. RCM approach from ynamide-tethered 1,7-diynes	232
7.2.3. η^3 -Vinyl alkylidene chelates	234
7.2.3.1. RCM of 1,n-enynes	234
7.2.3.2. Heteroatom substituent effect	236
7.2.4. Catalytic activity studies	237
7.2.4.1. Structure-Activity relationships	237

TABLE OF CONTENTS

<u>CHAPTER</u>	<u>PAGE</u>
7.2.4.2. Benchmarking catalytic activity.....	239
7.3. Conclusion	242
7.4. Experimental Details.....	243
7.4.1. General information	243
7.4.2. General procedure for alkene-chelate formation.....	244
7.4.3. Characterization data of alkene-chelate	245
7.4.4. Catalytic activity studies	263
7.4.5. X-ray crystallographic data	285
7.5. Note.....	299
7.6. References.....	300
8. Ruthenabenzene: A Robust Precatalyst.....	305
8.1. Introduction.....	306
8.2. Results and Discussions	309
8.2.1. Initial design, structural requirements, and substituent effects	309
8.2.2. Tolerance of structural variations on the ruthenabenzene framework	312
8.2.3. Different mode of initiation and pathway selectivity	314
8.2.4. Mechanism of ruthenabenzene formation.....	316
8.2.5. Catalytic activity of ruthenabenzenes	318
8.3. Conclusion	322
8.5. Experimental Details.....	323
8.5.1. General information	323
8.5.2. Experimental procedures.....	324
8.5.3. Characterization data.....	343
8.5.4. Kinetic studies for RCM.....	358
8.5.5. Other reactivities of ruthenabenzenes	361
8.5.6. Recyclability and degradation experiments.....	363
8.5.7. Computational studies	367
8.5.8. X-ray crystallography data	378
8.5. Note.....	385
8.6. References.....	385
Appendices.....	393
Appendix I (Selected NMR spectra Chapter 2).....	393
Appendix II (Selected NMR spectra Chapter 3)	452
Appendix III (Selected NMR spectra Chapter 4)	489
Appendix IV (Selected NMR spectra Chapter 5).....	559
Appendix V (Selected NMR spectra Chapter 7)	578
Appendix VI (Selected NMR spectra Chapter 8).....	622
Appendix VII (Copyright permissions).....	693
VITA	697

LIST OF SCHEMES

<u>SCHEME</u>	<u>PAGE</u>
1.1. Different classes of dehydro Diels-Alder reactions	2
1.2. Selected examples of thermal dehydro Diels-Alder (DDA) reaction	4
1.3. Photochemical dehydro Diels-Alder (DDA) reaction.....	5
1.4. Transition metal-catalyzed dehydro Diels-Alder (DDA) reactions	6
1.5. Johnson's cycloaromatization of triynes.....	8
1.6. Ueda's tandem cyclization of tetraynes	9
1.7. Intra and intermolecular trapping of arynes generated through HDDA reactions	10
1.8. Concerted vs. stepwise mechanisms	11
1.9. Introduction of adjacent C–C and C–C/N/O bonds to arynes.....	12
1.10. Introduction of adjacent C–H and C–O/N/H/X bonds to arynes	13
1.11. Multicomponent reactions of HDDA arynes	14
1.12. Multicomponent reactions of HDDA-arynes involving nitriles and isonitriles	15
1.13. Silver-catalyzed dicarbene reactivity of arynes	16
1.14. Photochemical and domino HDDA reactions.....	13
1.15 Aza-HDDA and pentadehydro Diels-Alder reaction	17
1.16. Other thermal processes of multiynes.....	18
2.1. Alder-ene vs. Diels-Alder reaction	26
2.2. Thermal vs. Lewis Acid-catalyzed carbonyl-ene reaction.....	27
2.3. Alder-ene reaction with azodicarboxylate	28
2.4. Imino-ene reaction and application to the synthesis of papuamine	29
2.5. Imino-ene reaction and application to the synthesis of DEF ring of complestatin	30
2.6. Regio- and site-selectivity in the Ru-catalyzed Alder-ene reaction of diynes	31

LIST OF SCHEMES (continued)

<u>SCHEME</u>	<u>PAGE</u>
2.7. Alder-ene reaction catalyzed by Rh and Co.....	32
2.8. Metal-catalyzed Alder-ene reaction: Application in Total Synthesis	32
2.9. Transition metal-catalyzed allylic C–H functionalization	34
2.10. Examples of intermolecular aryne-ene reaction.....	35
2.11. Lauten’s intramolecular aryne-ene reaction and its application to crinine synthesis.....	36
2.12. Lee’s intramolecular aryne-ene reactions	37
2.13. Hoya’s aromatic ene reactions	37
2.14. Initial observation: Alder-ene reaction of arynes with methallyl alcohol	38
2.15. Reactivity of 1,1-di- and trisubstituted alkenes and isomers thereof	43
2.16. Regioselectivity in the Alder-ene reactions of arynes.....	44
3.1. Reaction of arynes with acids, amines, and azides	76
3.2. Regioselectivity of nucleophile addition to arynes	77
3.3. Reaction of arynes with carbonyl compounds	78
3.4. Reaction of arynes with α,β -unsaturated compounds.....	79
3.5. Mechanism of 2 <i>H</i> -chromene formation	82
3.6. DFT calculations for the reaction between an aryne and tiglic aldehyde and its deconjugated forms	86
4.1. Different protocols for the synthesis of benzocyclobutenes	113
4.2. Benzocyclobutene formation via radical and anion intermediates.....	114
4.3. Palladium-catalyzed and photoinduced cyclizations to form benzocyclobutenes	115
4.4. Aryne-mediated Alder-ene reaction driven by hydrogen bonding and steric pressure.....	116
4.5. Inter vs. intramolecular Alder-ene reaction	123

LIST OF SCHEMES (continued)

<u>SCHEME</u>	<u>PAGE</u>
4.6. The energy profiles of Alder-ene reactions and the origin of cis selectivity	124
4.7. Reactions of benzocyclobutene derivatives	125
5.1. Different classes of natural products from the genus <i>Selaginella</i>	168
5.2. Biosynthetic routes to Type C and D selaginellins	169
5.3. Biosynthetic routes to Type A and B selaginellins	170
5.4. PDE-4 inhibitory activities of selaginellins and selaginpuvilins	171
5.5. Yin's total synthesis of Selaginpulvillin A–F	173
5.6. Sherburn's four step synthesis of selaginpulvilin D	175
5.7. Baire's synthesis of selaginpulvilin D (TDDA approach)	176
5.8. Lee's synthesis of selaginpulvilin C (HDDA approach)	177
5.9. Diversity-oriented approach to various natural products of the <i>Selaginella</i> family	178
5.10. Synthesis of the triyne intermediate 5-27	180
5.11. Completion of synthesis of selaginellin H	181
5.12. Synthetic progress to selaginpulvilin G	182
6.1. Gold-catalyzed transformations of multiynes	201
6.2. Platinum-catalyzed bond-reorganization of multiynes	202
6.3. Earlier reports on enyne metathesis	204
6.4. Possible mechanism for enyne RCM	205
6.5. <i>Exo/endo</i> -mode selectivity in the enyne RCM of tartrate-tethered enynes	206
6.6. <i>Exo/endo</i> -mode selectivity in the RCM with silicon-tethered enynes	207
6.7. Group selectivity in tandem enyne metathesis	208
6.8. Regio- and stereoselectivity in enyne cross metathesis	209
6.9. Metathesis and metallotropic [1,3]-shift	211

LIST OF SCHEMES (continued)

<u>SCHEME</u>	<u>PAGE</u>
6.10. Metathesis and metallotropy – applications in total synthesis	212
6.11. Metathesis and metallotropy – applications in polymer chemistry	213
6.12. Metal complexes with multiynes	214
7.1. Heteroatom-chelated ruthenium alkylidene	222
7.2. Enyne metathesis approach to hydroxy- and ether-chelated ruthenium alkylidenes	224
7.3. Enyne metathesis approach to oxygen-chelated ruthenium alkylidenes	225
7.4. Alkene-chelated ruthenium alkylidenes: Snapper's and Grubbs'	226
7.5. Alkene and alkyne-chelated ruthenium alkylidenes	227
7.6. Alkene-chelated ruthenium alkylidenes generated through enyne RCM	228
7.7. Steric and electronic factors stabilizing alkene-chelates	229
7.8. Unusual mode of RCM of ynamide-tethered 1,7-diynes to generate alkene-chelates	233
8.1. Various synthetic routes to metallabenzenes	307
8.2. Various synthetic routes to metallabenzenes	308

LIST OF TABLES

<u>TABLE</u>	<u>PAGE</u>
2.1. Alder-ene reactions of functionalized 1,1-disubstituted alkenes with an aryne	39
2.2. Alder-ene reactions of functionalized trisubstituted alkenes with an aryne.....	40
2.3. Ene reactions of alkenyl alcohols with an aryne	41
2.4. Alder-ene vs. Diels-Alder reaction of 1,3-dienes reacting with an aryne	42
3.1. Alder-ene reactions of functionalized alkenes with an aryne	80
3.2. Reaction of α,β -unsaturated aldehydes with an aryne to generate 2 <i>H</i> -chromenes	81
3.3. The selectivity between Alder-ene and addition reactions of structurally elaborated aldehydes.....	83
3.4. Reactivity of alkenyl aldehydes and electron-rich carbonyl compounds with arynes	85
4.1. Effect of steric bulk and hydrogen bonding on the Alder-ene reaction of arynes.....	117
4.2. Effect of the substituents on the ene-donor.....	119
4.3. Reactivity of triynes of different tethers	122
7.1. Tandem CM-RCM of 1, <i>n</i> -diynes to generate 1,5-alkene-chelates.....	231
7.2. RCM 1, <i>n</i> -enynes to form η^3 -vinyl alkylidene chelates.....	235
7.3. Heteroatom substituent effect on the formation of η^3 -vinyl alkylidene complexes.....	237
7.4. Reactivity order of selected alkene-chelates for different metathesis process.....	241

LIST OF FIGURES

<u>FIGURES</u>	<u>PAGE</u>
7.1. Partial structure of 7-22a and 7-22b from X-ray	238
7.2. Catalytic activities of alkene-chelated ruthenium alkylidene complexes	240
8.1. A new approach to ruthenabenzenes.....	310
8.2. Selectivity in product distributions	311
8.3. Ruthenabenzene formation via ring-closing metathesis (RCM) → metallotropic [1,3]-shift (MTS) → RCM → aromatization sequence with ene-triynes.	313
8.4. Different modes of initiation and selectivity.....	315
8.5. Mechanisms of cycloaromatization to form ruthenabenzene.....	317
8.6. Reactivity of ruthenabenzene in various metathetic and non-metathetic reactions	319
8.7. Possible catalytic cycles.....	321

LIST OF ABBREVIATIONS

Ac	Acetyl
Ar	Aryl
BINOL	1,1'-Bi-2-naphthol
Boc	<i>t</i> -Butyloxycarbonyl
Bn	Benzyl
Bu (also <i>n</i> -Bu)	<i>n</i> -Butyl
<i>t</i> -Bu (also <i>t</i> -Bu)	<i>tert</i> -Butyl
CAN	Cerric ammonium nitrate
Cat.	Catalyst
Cp	Cyclopentadienyl
CM	Cross-Metathesis
δ	Chemical shifts in parts per million downfield from tetramethylsilane (NMR)
DBU	1,8-Diazabicyclo[5.4.0]undec-7-ene
DCC	<i>N,N'</i> -Dicyclohexylcarbodiimide
DCE	1,2-Dichloroethane
DCM	Dichloromethane
DDA	Dehydro Diels-Alder
DFT	Density functional theory
DHP	3,4-Dihydropyran
DIBAL-H	Diisobutylaluminum hydride
DMAP	4-Dimethylaminopyridine
DMP	Dess-Martin periodinane
DMF	Dimethylformamide
DMSO	Dimethyl sulfoxide

LIST OF ABBREVIATIONS (continued)

dr	Diastereomeric ratio
<i>E</i>	Entgegen (opposite, <i>trans</i>)
ee	Enantiomeric excess
equiv	equivalent
EI	Electron impact
ESI	Electrospray ionization
Et ₂ O	Diethyl ether
EtOAc	Ethyl acetate
EWG	Electron withdrawing group
FG	Functional group
G-I	Grubbs 1 st -Generation Catalyst
G-II	Grubbs 2 nd -Generation Catalyst
G-III	Grubbs 3 rd -Generation Catalyst
GH-I/ II	Grubbs-Hoveyda Catalyst, 1 st and 2 nd Generation
GSM	Growing string method
HDDA	Hexadehydro Diels-Alder
HMPA	Hexamethylphosphoramide
HOMO	Highest occupied molecular orbital
Hex (also <i>n</i> -Hex)	<i>n</i> -Hexyl
HRMS	High resolution mass spectrometry
Hz	Hertz
<i>i</i> -Pr	Isopropyl
INT	Intermediate
IR	Infra-red
<i>J</i>	Coupling constant (NMR)

LIST OF ABBREVIATIONS (continued)

Kcal	Kilocalorie
LAH	Lithium aluminum hydride
LG	Leaving group
LCMS	Liquid chromatography mass spectrometry
LRMS	Low resolution mass spectrometry
LUMO	Lowest unoccupied molecular orbital
MCR	Multicomponent reaction
MS	Molecular sieves
Ms	Methanesulfonyl (Mesyl)
mol	mole
Nu	Nucleophile
NBS	<i>N</i> -Bromosuccinimide
NHC	<i>N</i> -Heterocyclic carbene
NICS	Nucleus-independent chemical shift
NMR	Nuclear magnetic resonance
nOe	Nuclear Overhauser effect
<i>o</i> -DCB	<i>ortho</i> -Dichlorobenzene
PCC	Pyridiniumchlorochromate
PDE	Phosphodiesterase
Ph	Phenyl
PhH	Benzene
PhMe	Toluene
Ph(4-OMe)	4-Methoxyphenyl
ppm	Parts per million
PMB	<i>p</i> -Methoxybenzyl

LIST OF ABBREVIATIONS (continued)

Piv	Pivaloyl (<i>aka</i> trimethylacetyl)
Pr also (<i>n</i> -Pr)	<i>n</i> -Propyl
Pyr	pyridine; solvent, base, catalyst
RCM	Ring closing metathesis
RRM	Ring rearrangement metathesis
ROMP	Ring opening metathesis polymerization
SCF	Self consistent field
SMD	Solvation model based on density
rt	Room temperature
sol	solvent
TBAF	Tetra- <i>n</i> -butylammonium fluoride
TBS	<i>t</i> -Butyldimethylsilyl
TEA	Triethylamine
TES	Triethylsilyl
Tf	Trifluoromethanesulfonyl
TFA	Trifluoroacetic acid
THF	Tetrahydrofuran
THP	Tetrahydropyran
TIPS	Triisopropylsilyl
TLC	Thin layer chromatography
TMS	Trimethylsilyl
Ts	<i>p</i> -Toluenesulfonyl
TS	Transition State
Z	Zusammen (together, <i>cis</i>)

SUMMARY

This thesis consists of two main parts, Part I and Part II. The five chapters in Part I deal with the thermal reaction of multiynes focusing on the new reactivity of arynes generated *via* the hexadehydro Diels-Alder (HDDA) reactions. The last three chapters in Part II deal with metal-catalyzed reactions of multiynes focusing on the synthesis of novel ruthenium alkylidene complexes and investigating their catalytic activities.

Chapter 1 provides a brief overview of the thermal reactions of multiynes focusing on the history and development of dehydro Diels-Alder reactions. This chapter covers the discovery and development of HDDA reaction as a tool for aryne generation. This chapter also includes a systematic overview of the application of HDDA reaction for the synthesis of highly substituted aromatic compounds including several natural products.

In Chapter 2, an Alder-ene reaction of arynes generated *via* HDDA reaction with functionalized alkenes is described. This study led to the development of a formal allylic C–H functionalization reaction under mild reagent-free conditions. The reaction proceeded showed excellent functional group tolerance and high regioselectivity. New insight into the stereoselectivity of this reaction was obtained which was supported by DFT calculations.

In Chapter 3, the competition between Alder-ene reaction and addition reaction to arynes were investigated with functionalized alkenes having highly polar functional groups like amines, carboxylic acids and α,β -unsaturated aldehydes. Systematic investigation revealed the various factors affecting the selectivity between these two manifolds of reactions. The reaction of α,β -unsaturated aldehydes with arynes predominantly underwent an addition reaction to form 2*H*-chromene. The mechanism for this transformation was also established through DFT calculations.

Chapter 4 describes a novel intramolecular Alder-ene reaction to form benzocyclobutene. The high kinetic barrier to form a 4-membered ring was overcome by installing a maximum gearing effect through an internal hydrogen bonding. The reaction is *cis*-diastereoselective and the origin of this selectivity was

studied using DFT calculations.

In Chapter 5, a diversity-oriented approach for the synthesis of several bioactive natural products of the *Selaginella* family is reported. The strategy relies on HDDA mediated synthesis of the arene core followed by various standard synthetic manipulations that lead to a unique approach to access the different natural products of this family. This strategy accomplished the first synthesis of selaginellin H and made significant progress in the synthesis of selaginpulvin G.

In Chapter 6, a brief overview of the metal-catalyzed reactions of multiynes is described. It describes the origin and development of Pt- and Au-carbenoid mediated transformations of multiynes and Ru-alkylidene carbene catalyzed enyne metathesis of multiynes. This chapter also describes the application of these transformations in natural product synthesis, organometallics, and polymer chemistry.

Chapter 7 describes a unified approach for the synthesis of various alkene-chelated ruthenium alkylidene complexes. Both steric and electronic controls were used for the stabilization of these complexes. The structural properties of these complexes were studied through X-ray crystallography and the catalytic activities for these complexes were studied for various standard metathesis processes. Careful tuning leads to the development of catalysts with enhanced catalytic activities compared to standard metathesis catalysts.

Chapter 8 describes a novel approach for the synthesis of ruthenabenzenes relying on metathesis and metallotropic cascades of multiynes. This study develops these ruthenabenzene complexes as an aromatic equivalent of the Grubbs catalyst. These complexes show robust catalytic activities towards both metathetic and non-metathetic reactions and have high catalyst recoverability. DFT calculations reveal the mechanism for the formation of these complexes and also provides insight into how they show robust catalytic activities.

CHAPTER 1

Thermal Reactions of Multiynes

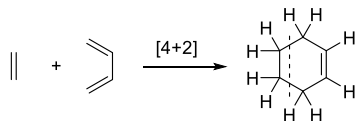
1. Thermal Reactions of Multiynes

Multiynes and other conjugated acyclic π -systems are important functionalities and finds immense applications in organic synthesis, polymer chemistry, and materials science. These multiynes can undergo myriads of thermal reactions particularly including cycloaddition and cyclization reactions that can create a wide variety of unsaturated and aromatic compounds. Furthermore, multiynes interact with various transition metal complexes of platinum, gold and ruthenium to promote metal carbenoid-mediated transformations. Multiynes can also form novel organometallic complexes that can be developed as new catalysts.

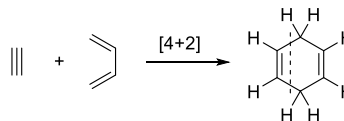
1.1. Thermal Dehydro Diels-Alder (DDA) Reactions

Diels-Alder (DA) reactions is one of the most well-known $[4 + 2]$ cycloaddition between a diene and a dienophile to form cyclohexene derivatives with a tetrahydrobenzene oxidation state.¹ A typical DA reaction is exothermic in nature as it involves the simultaneous formation of two σ -bonds at the cost of two π -bonds. Also, DA reaction is a thermally allowed concerted process according to the Woodward-Hoffmann rules although a stepwise mechanism a via diradical intermediate was proposed in some cases.² If one or both π -components of the diene are replaced by a triple bond the primary products will contain a cyclic allenic skeleton. In contrast to classical DA reactions, the initial products of these dehydro Diels-Alder

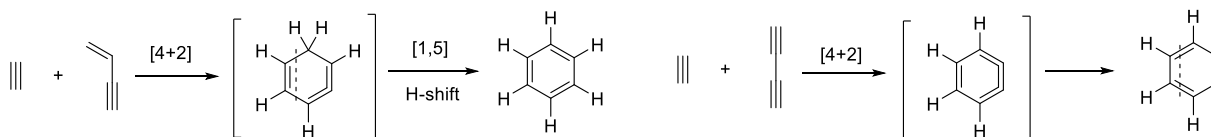
Diels-Alder Reaction



Didehydro Diels-Alder (DDA) Reaction



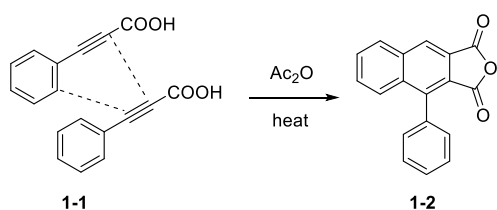
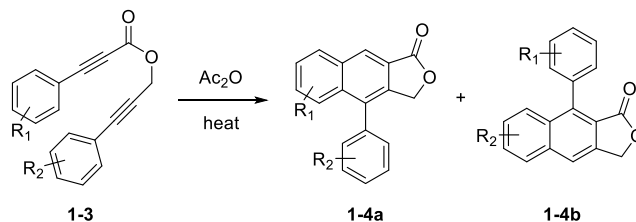
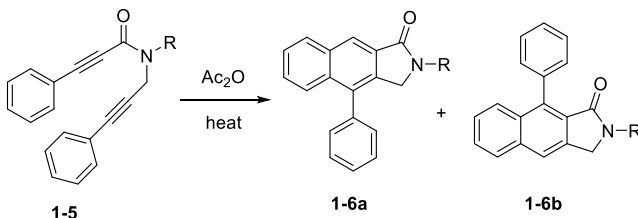
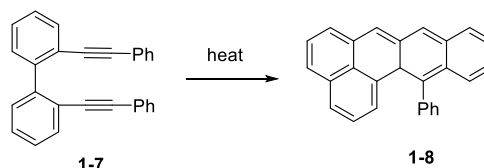
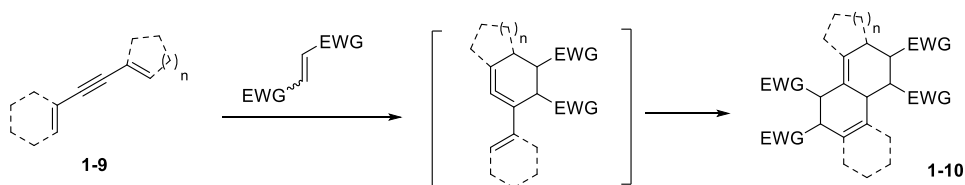
Hexadehydro Diels-Alder (HDDA) Reaction



Scheme 1.1. Different classes of dehydro Diels-Alder reactions

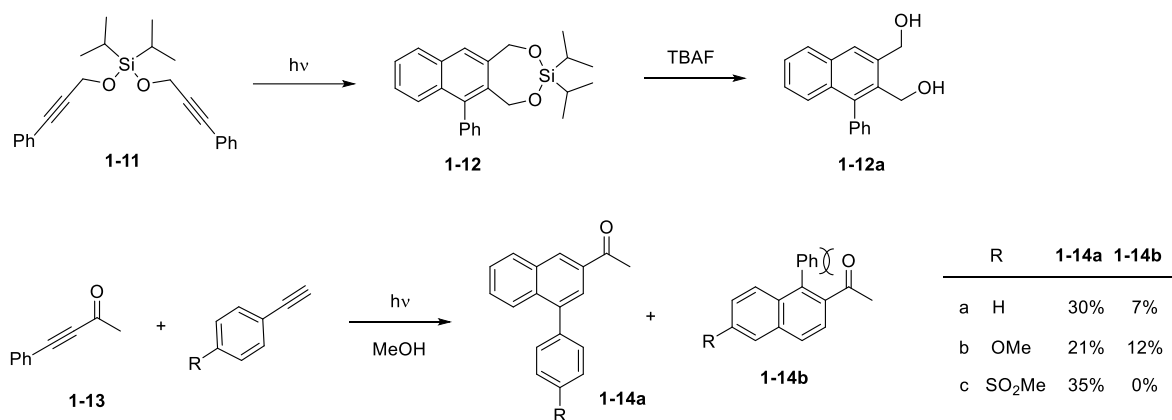
reactions, because of the considerable ring strain of the cyclic allene moiety, can behave as reactive intermediates to induce subsequent chemical transformations. These dehydrogenated versions of Diels-Alder reactions are collectively known as dehydro Diels-Alder (DDA) reactions.³ The DDA reactions could be further classified into DDA, TDDA, and HDDA reactions on the basis of the oxidation state of the products or the number of hydrogen atom deficiency in the products compared to the cyclohexene product obtained in a classical DA reaction (**Scheme 1.1**). The [4 + 2] cycloaddition reaction between an alkyne and butadiene would form 1,4-cyclohexadiene with an oxidation state of 1,4-dihydrobenzene, which thus is termed as the dehydro Diels-Alder (DDA) reaction. The reaction between an alkyne and a 1,3-enyne forms benzene as the end product via a [1,5] hydrogen shift of a cyclic allene intermediate, which is called as the tetrahydro Diels-Alder (TDDA) reaction. The reaction between an alkyne and a 1,3-diyne leading o-benzynes, which on the basis of number of hydrogen atom deficiency compared to the parent cyclohexene is termed as the hexadehydro Diels-Alder (HDDA) reaction.⁴

Interestingly, the first dehydro Diels-Alder reaction was reported 30 years before the Diels-Alder reaction was discovered. More than 120 years ago, Michael and Bucher reported the dimerization of 3-phenylpropionic acid **1-1** in the presence of acetic anhydride in a sealed tube to give dimeric anhydride **1-2** (**Scheme 1.2A**).⁵ The ester analogue of 3-phenylpropionic acid also form the dimeric diester. Substituted 3-arylpropionic acids can be used to introduce substituents at the naphthalene product formed. Also mixed anhydride prepared from different 3-arylpropionic acid chlorides and 3-arylpropionic acid can undergo DDA reaction to form mixed dimeric anhydride.⁶ The ratio of different regioisomeric dimers depends mostly on the nature of the substituents on the arylpropionic acids. The scope for this DDA reaction could be substantially improved if two different 3-arylpropionic acids are linked through different tethers like esters, ethers and amides. Klemm reported the cyclization of 3-arylpropionic acid propargyl esters **1-3** in acetic anhydride medium. In most cases, a mixture of different isomeric lactones **1-4a** and **1-4b** were obtained (**Scheme 1.2B**).⁷ The structural analogue of amides **1-5** can react in a similar manner to give mixture of isomeric lactams **1-6a** and **1-6b** (**Scheme 1.2C**).⁸

A. Dimerization of 3-phenylpropionic acid**B. DDA reaction of 3-arylpropionic acid propargyl ester****C. DDA reaction of 3-arylpropionic acid propargyl amide****D. DDA reaction from disubstituted diphenyl****E. DDA reaction with enyne as the diene component****Scheme 1.2. Selected examples of thermal dehydro Diels-Alder (DDA) reaction**

One or several C–C bond units can be a part of an aromatic system to provide a straightforward access to complex polycyclic molecules. For example, a smooth DDA reaction occurs from *o,o'*-disubstituted diphenyl **1-7** giving benzo[*b*]triphenyl **1-8** (**Scheme 1.2E**).⁹ Introducing enyne as the 1,3-diene component for a DDA reaction instead of arylacetylenes can bring about some fundamental differences; as opposed to arylacetylenes, the reaction of enynes do not disrupt aromaticity, thus the incipient cyclic allene intermediates are considerably stable to have longer lifetimes, which allow them to be engaged in the second DA reaction. Butz and coworkers reported the reaction of various dienynes **1-9** with electron-deficient alkenes (maleic anhydride, fumarates, *p*-benzoquinone). The initially formed cycloallenes undergo a second DA reaction providing compounds **1-10** as final products (**Scheme 1.2E**).¹⁰

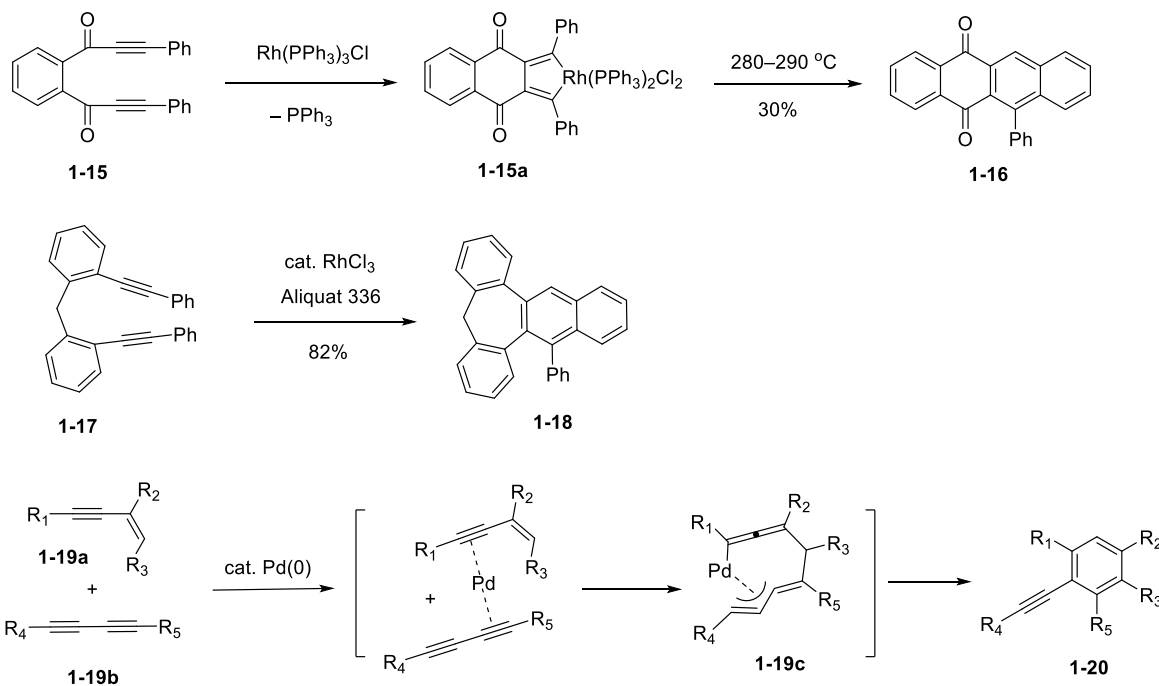
Photochemical and Metal-Catalyzed DDA Reactions: According to the Woodward-Hoffmann rules, the concerted Diels-Alder reaction is a thermally allowed but photochemically forbidden process because of the orbital symmetry. However, this rule is no longer applicable if the underlying reaction mechanism is a multistep process, and the first step is the formation of only one chemical bond which generally happens in DDA reactions. In 1948, Baddar observed that phenylpropionic anhydride can dimerize in presence of sunlight.¹¹ The photochemical dimerization of phenylacetylenes is known for a long time but it has limited preparative values because the yield of the products were very low and the reactions often were accompanied by azulene formation as a main pathway.



Scheme 1.3. Photochemical dehydro Diels-Alder (DDA) reaction

In 1995, Fleming reported the photochemical DDA cyclization of silyl bis(phenylpropargyl) ether **1-11** to naphthalene **1-12**, which was subsequently deprotected to generate diol **1-12a** (Scheme 1.3).¹² The scope of intermolecular photochemical DDA reactions is extended by employing ynone **1-13** and differently substituted arylacetylenes. In this reaction, the heteromolecular photochemical DDA reaction was predominately observed, and only traces of the homodimerization products were formed. Furthermore, the reaction is remarkably regioselective, and 4-substituted 2-acetylnaphthalenes **1-14a** was generated as a major product along with minor isomer **1-14b**. The selectivity could be explained by the unfavorable steric interaction in 1,2,6-substituted naphthalene **1-14b** (Scheme 1.3).¹³

The first example of a DDA reaction involving a transition metal complex was reported by Müller in the 1970s.¹⁴ Rhodium complex **1-15a**, obtained from diyne **1-15** upon treatment with the Wilkinson catalyst $\text{Rh}(\text{PPh}_3)_3\text{Cl}$, provided naphthacene **1-16** under harsh conditions and with low yields. The thermal cyclization of **1-15** to form **1-16** takes place under lower temperature than the metal-mediated reaction.



Scheme 1.4. Transition metal-catalyzed dehydro Diels-Alder (DDA) reactions

The first transition metal-catalyzed DDA reactions was reported nearly 20 years later. In the presence of RhCl_3 and a phase transfer catalyst (Aliquat 336 – methyltrioctylammonium chloride), diyne **1-17** underwent a smooth cyclization to generate compound **1-18**.¹⁵ Palladium can also catalyze certain DDA reactions; the reaction between enyne **1-19a** and diyne **1-19b** proceeds with high regioselectivity, giving benzenes **1-20** where R_1 is arranged in ortho position relative to the alkyne. Furthermore, only Z-configured enynes **1-19a** can participate in this reaction. The mechanism of this $\text{Pd}(0)$ -catalyzed DDA reaction of enynes with themselves or with diynes and triynes is still not fully elucidated, but the formation of metallacyclic species **1-19c** along the reaction pathway was suggested (Scheme 1.4).¹⁶

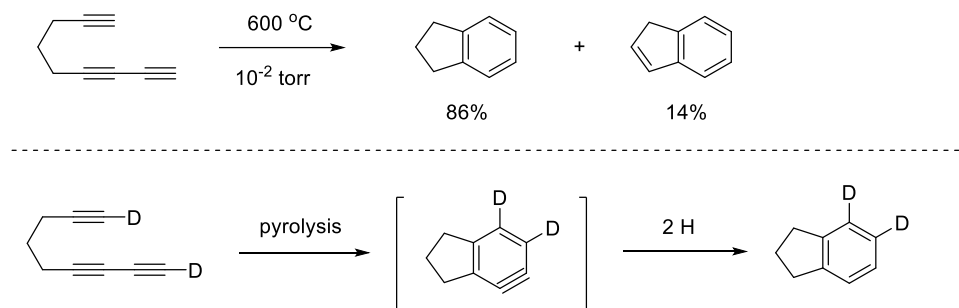
1.2. Hexadehydro Diels-Alder (HDDA) Reaction and Aryne Generation

The most oxidized version of DDA reactions is the hexadehydro Diels-Alder reaction, which involves a [4+2] cycloaddition between diynophiles and 1,3-diynes to form *o*-benzynes. Since the product from this reaction has six hydrogen atoms less than the product of Diels-Alder reaction, this reaction is named as hexadehydro Diels-Alder (HDDA) reaction.⁴ Benzyne or arynes are highly electrophilic transient intermediates which can form various carbon-carbon or carbon-heteroatom bonds, giving rise to various functionalized aromatic compounds.¹⁷ Traditionally, arynes are generated from aromatic precursors via metalation or base-mediated 1,2-elimination of aryl 1,2-dihalides or aryl halides, thermal decomposition of arenediazonium-2-carboxylate, and thermal, photochemical, or oxidative elimination of nitrogen from various precursors.¹⁸ Most of these reaction conditions are harsh involving the use of strong bases or high temperature. A milder method for aryne generation was reported by Kobayashi, which involves the 1,2-elimination of aryl silyl triflates by a source of fluoride such as CsF at room temperature.¹⁹ But this method has its own limitations, requiring super-stoichiometric quantity of the fluoride source and somewhat restricted capacity in the structural variations of aryl silyl triflates. On the other hand, the HDDA-based aryne formation does not require any external reagent and the precursor multiynes can be prepared through relatively simple operations. Therefore, diverse structural variations can be introduced onto the multiyne precursors to generate highly elaborated aromatic frameworks. In addition, no external reagents except heat are needed in HDDA reactions to form arynes so that the intrinsic properties of arynes can be explored. This is not true for other methods such as Kobayashi's method where the excess amount of somewhat basic CsF and its byproducts has a significant impact on the reaction profiles. In many occasions, completely different behaviors of the nucleophilic counterpart are manifested when arynes are generated by these two different methods.

1.2.1. Early examples of HDDA reaction

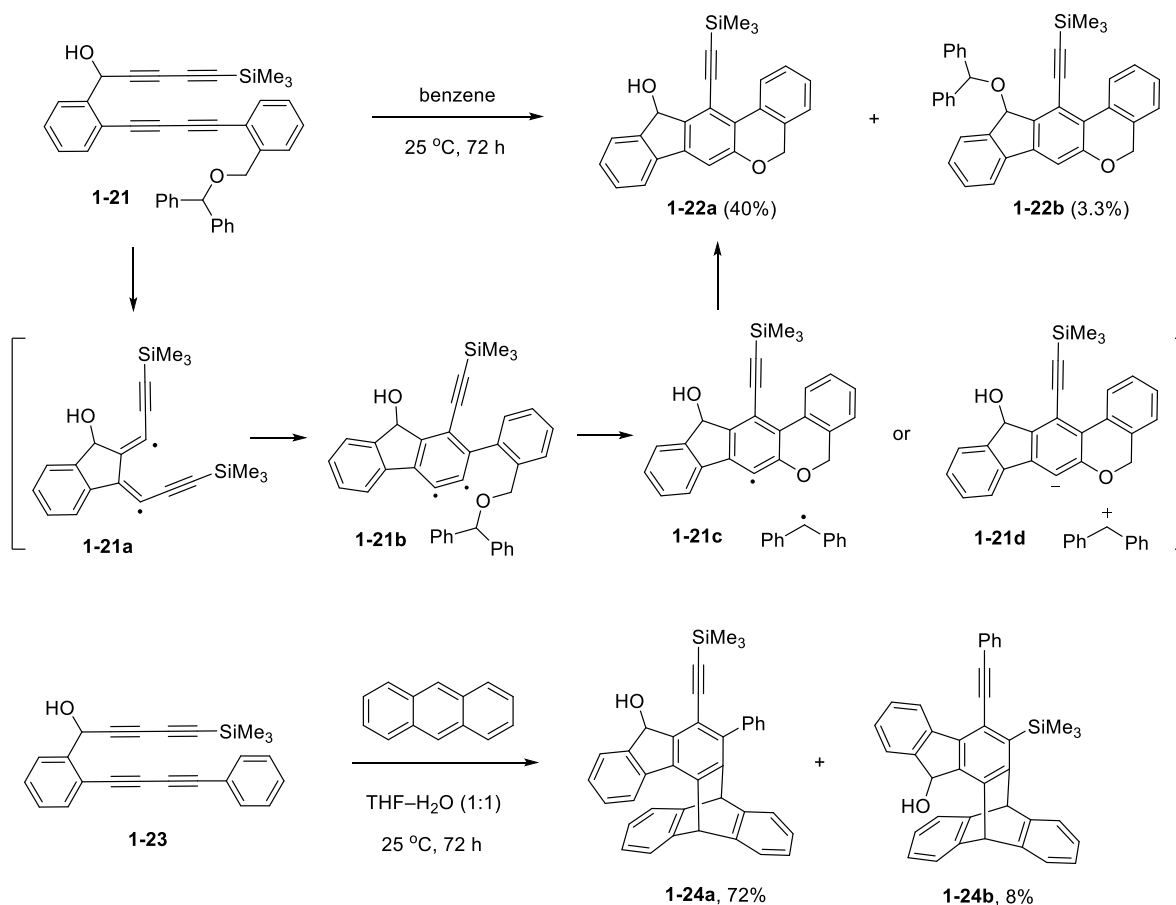
The trimerization of acetylene as observed by Berthelot in 1866 can be considered as the earliest example of the HDDA reaction involving an alkyne and a 1,3-diyne.²⁰ After almost 150 years later, Johnson

reported the cycloaromatization of 1,3,8-nonatriyne under flash vacuum thermolysis conditions to generate a mixture of indane and indene in 86% and 14% yield, respectively (**Scheme 1.5**).²¹ Deuterium labelling study showed no scrambling of deuterium labels, and it was suggested that cycloaromatization proceeds through a [4+2] cycloaddition manifold *via* an aryne intermediate.



Scheme 1.5. Johnson's cycloaromatization of triynes

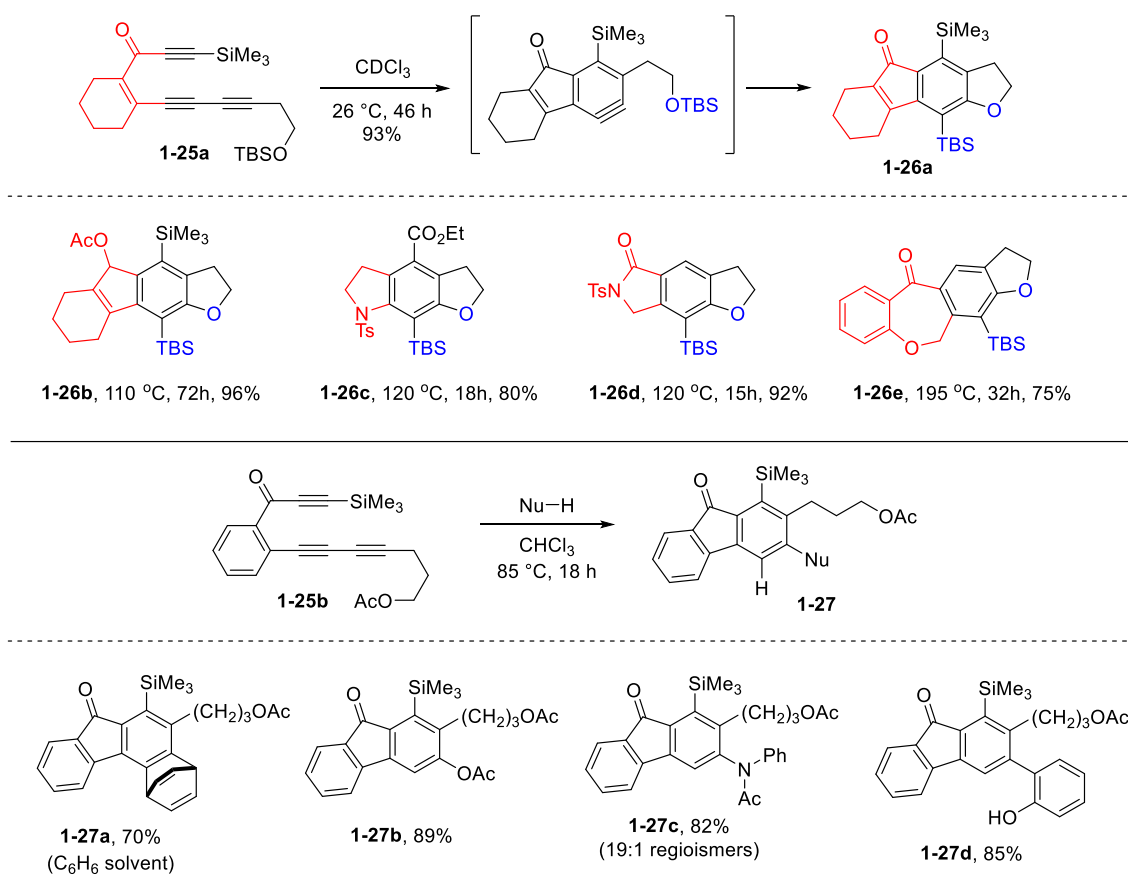
In the same year, the Ueda group independently reported a similar HDDA reaction where bis-1,3-diynes connected by a suitable tether could undergo tandem cyclizations to form fluorene-containing products.²² In stark contrast to the triynes, the reaction of tetraynes can undergo a similar reaction at room temperature. A stepwise radical mechanism was proposed wherein tetrayne **1-21** cyclized to form diradical **1-21a** as the first intermediate, which transforms into a 1,2-didehydrobenzene diradical **1-21b**. The intermediate **1-21b** can undergo intermolecular trapping of a tethered functionality to form radical-pair **1-21c** (or more likely ion-pair **1-21d**), recombination of which leads to product **1-22a** and **1-22b**. In the reaction of **1-23** that does not contain a trapping group, the putative intermediate could be trapped in an intermolecular fashion with anthracene to provide an isomeric mixture of compounds **1-24a** and **1-24b**, which are the consequence of the two different mode of initial ring closure of **1-23** (**Scheme 1.6**).



Scheme 1.6. Ueda's tandem cyclization of tetraynes

1.2.2. Hoye's approach and reaction mechanisms

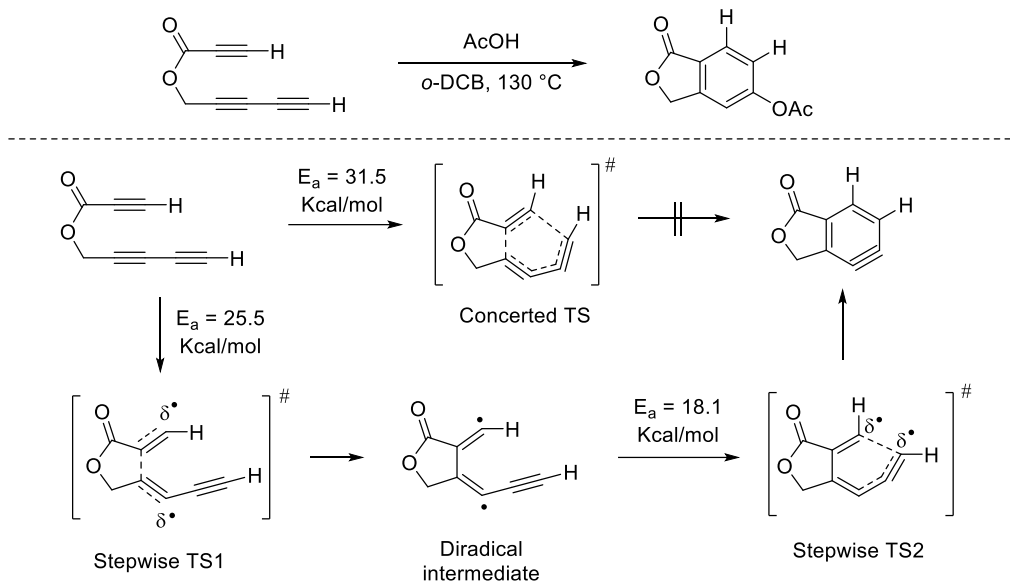
Following their serendipitous discovery of HDDA reaction while studying MnO_2 oxidation of suitably tethered multiynes, Hoye and co-workers undertook a systematic study on aryne generation (**Scheme 1.7**).⁴ As a representative example, the cyclohexenoyl tethered triyne **1-25a** underwent HDDA reaction at ambient temperature and the putative aryne intermediate was subsequently trapped by the pendant OTBS group via a retro-Brook type rearrangement to form **1-26a** in 93% yield. Similar reactions were examined with multiynes of different tether to form highly substituted arenes **1-26b–1-26-e** in good yield. The HDDA reactivity of the multiynes varies extensively with the nature of the tethers, which requires different reaction temperatures. A benzene tether instead of a cyclohexenyl tether significantly lower the



Scheme 1.7. Intra and intermolecular trapping of arynes generated through HDDA reactions

the reactivity of triene **1-25b**, which thus require 85 $^{\circ}\text{C}$ for reasonable reaction rate to provided products **1-27a–1-27d** after intermolecular trapping with benzene, acetic acid, phenyl acetanilide and phenol.

The mechanism for HDDA reaction was investigated by Hoyer and Houk by both experimental and computational methods.²³ Kinetic studies and DFT calculations indicate that a stepwise mechanism *via* forming diradical intermediates is energetically more favorable than a concerted [4 + 2] process (**Scheme 1.8**). The theoretical calculations of Houk and coworkers revealed that, based on the distortion/interaction analysis, a stepwise diradical mechanism is favorable for HDDA reactions and an extra alkynyl substituent accelerates the reaction by ~5 orders of magnitude by minimizing the distortion energy to achieve the diradical transition state.²³

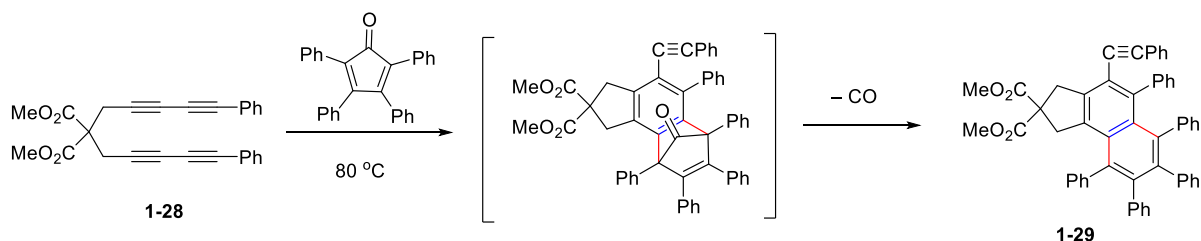


Scheme 1.8. Concerted vs. stepwise mechanisms

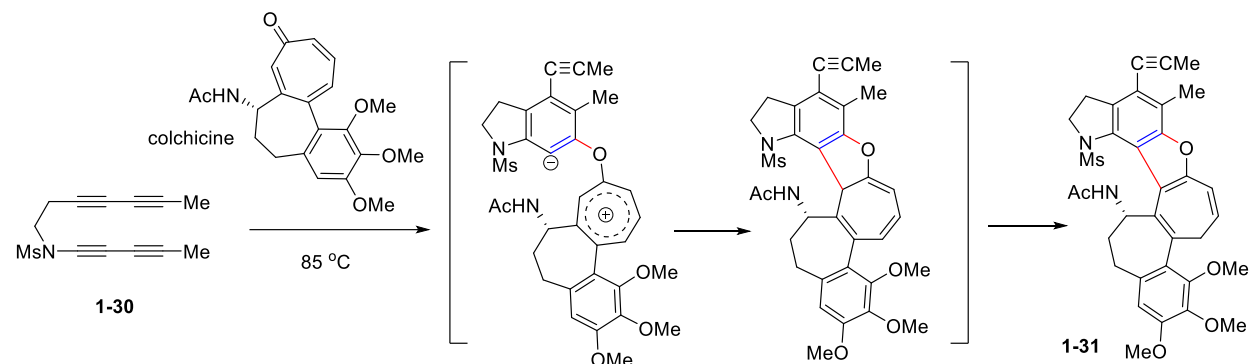
1.2.3. Trapping methods of arynes

Since HDDA reaction involves aryne generation under reagent-free thermal conditions, it allows the study of the intrinsic properties of the aryne intermediate. This allows discovery of a plethora of new reactions on arynes including the introduction of various new types of adjacent σ -bonds on the arynes. For instance, the most common way of introducing two adjacent C–C bonds onto an aryne scaffold involves a Diels-Alder reaction. For example, aryne generated from tetrayne **1-28** can be trapped with tetraphenylcyclopentadienone to form blue light-emitting aryl alkynyl naphthalene derivative **1-29**.²⁴ Introduction of adjacent C–C and C–O bonds can be exemplified by an unprecedented reactivity of the aryne generated from **1-30** with natural colchicine, in which the aryne intermediate engages with the colchicine molecule at the ketonic oxygen to generate the tropylium zwitterion **1-30a** which then collapses to the cycloheptatriene **1-30b**, which isomerizes to adduct **1-31** by a final [1,5]-H atom migration.²⁵ Introduction of adjacent C–C and C–N bonds can be exemplified by the reaction of aryne generated from **1-32** with simple imine to generate the acridine derivative **1-33** through an electrocyclic ring-opening, electrocyclization and rearomatization of the azetidine intermediate **1-32a** (Scheme 1.9).²⁶

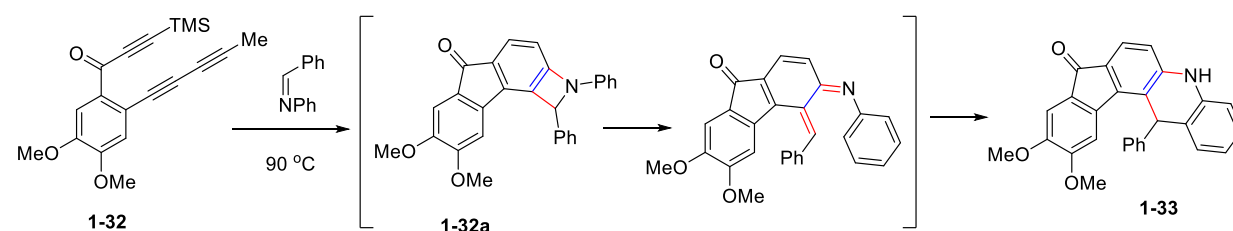
Introduction of C–C and C–C bonds



Introduction of C–C and C–O bonds



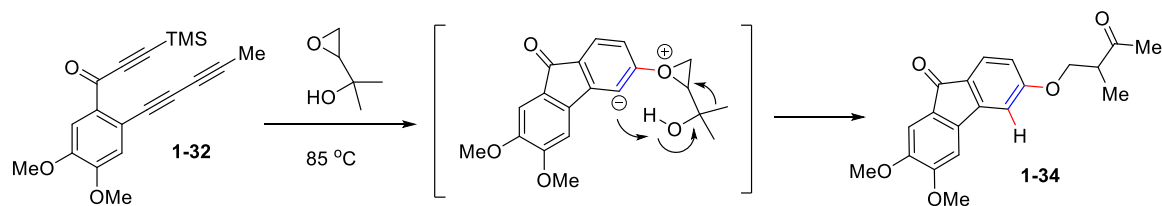
Introduction of C–C and C–N bonds



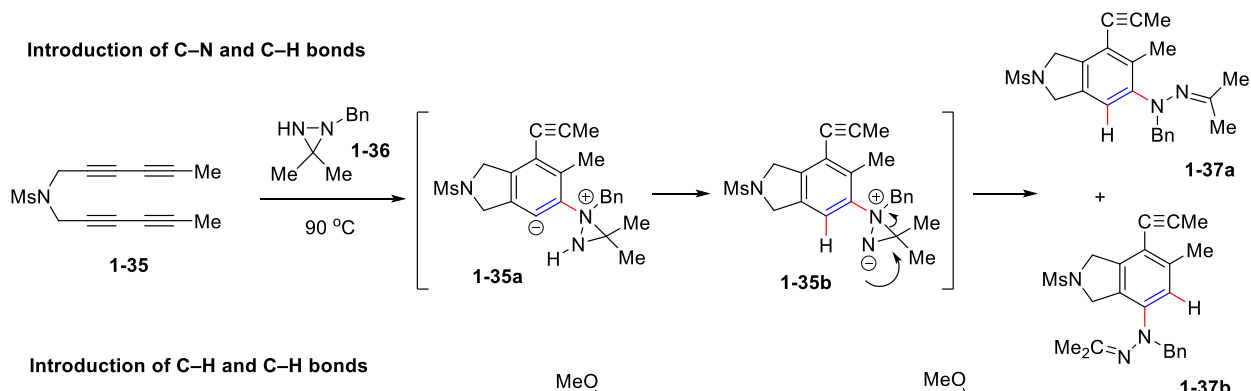
Scheme 1.9. Introduction of adjacent C–C and C–C/O/N bonds to arynes

An example of introducing adjacent C–O and C–H bonds is the reaction of aryne generated from **1-32** with a glycidol derivative to form the ketone **1-34** after a carbon skeleton rearrangement.²⁷ Introduction of adjacent C–N and C–H bonds can be demonstrated by an unusual reaction of HDDA-generated aryne from **1-35** with diaziridine **1-36** in which the adduct **1-35a** undergoes a proton transfer and ring-opening **1-35b** to form a regioisomeric mixture of hydrazones **1-37a** and **1-37b**.²⁸ Two adjacent C–H bonds can be introduced by using hydrogen donors such as cyclooctane or certain alcohols. For example, upon oxidizing tetraynol alcohol **1-38** with MnO_2 , aryne **1-38** was generated via HDDA reaction, which accepted H atoms from cyclooctane to form the fluorenone **1-38**.²⁹ This fluorenone is a precursor for the total synthesis of

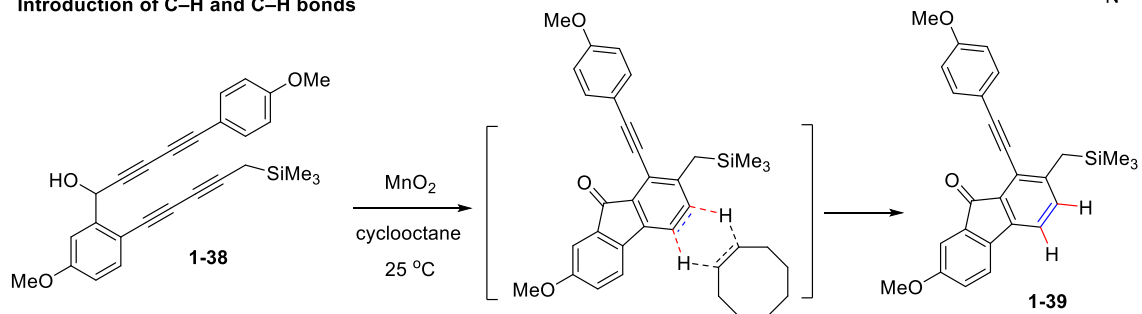
Introduction of C–O and C–H bonds



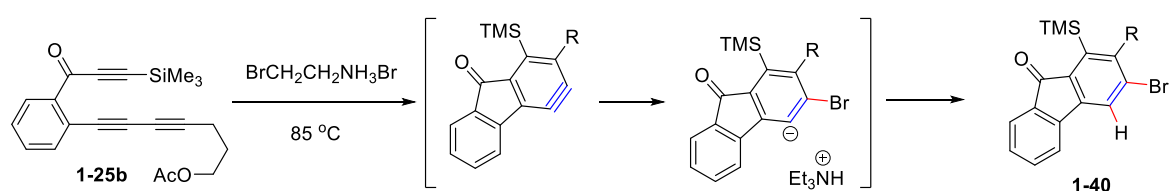
Introduction of C–N and C–H bonds



Introduction of C–H and C–H bonds



Introduction of C–X and C–H bonds

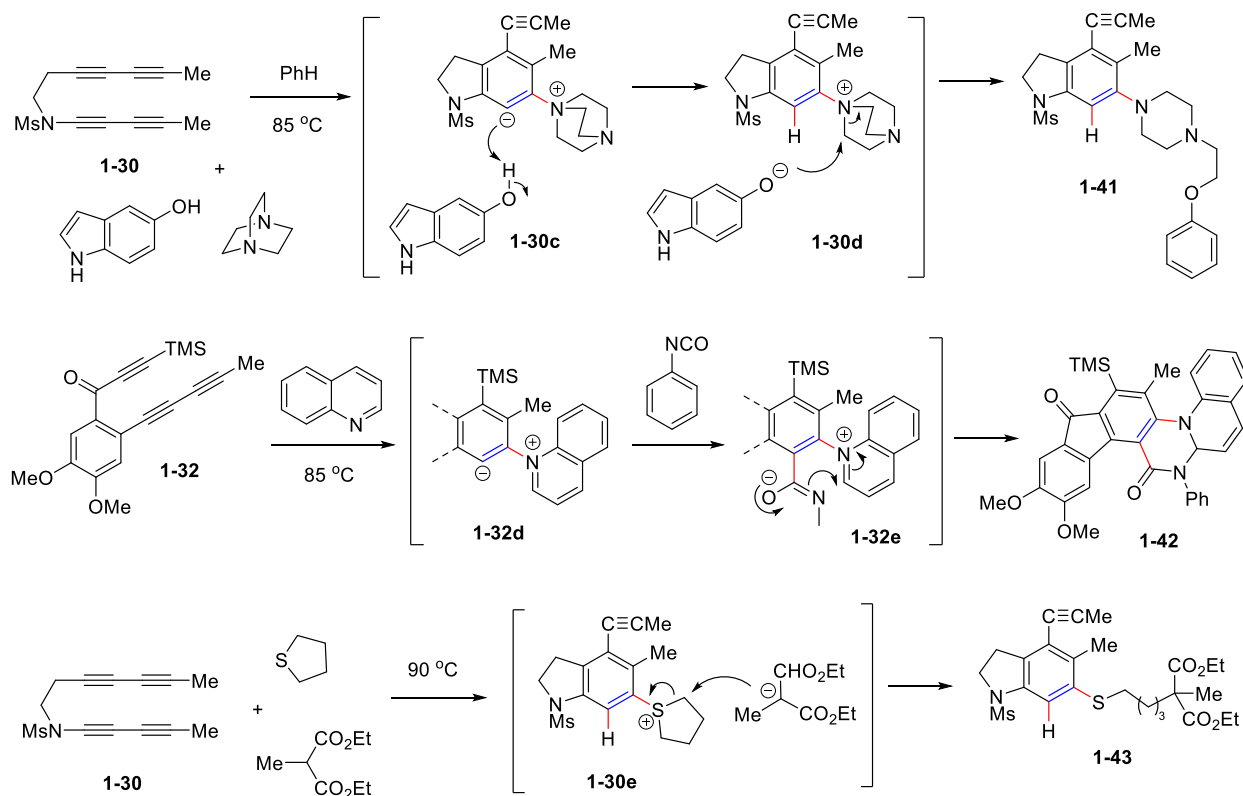


Scheme 1.10. Introduction of adjacent C–H and C–O/N/H/X bonds to arynes

selaginpulvin C. Introduction of C–H and C–halogen bonds on the arynes can be achieved in presence of halide source and sometimes in presence of transition metals. An example showing hydrobromination of arynes to form bromoarene **1-40** is demonstrated by arynes precursor **1-25b** in presence of a HBr salt of primary amine (Scheme 1.10).⁴

1.2.4. Multicomponent reactions with arynes

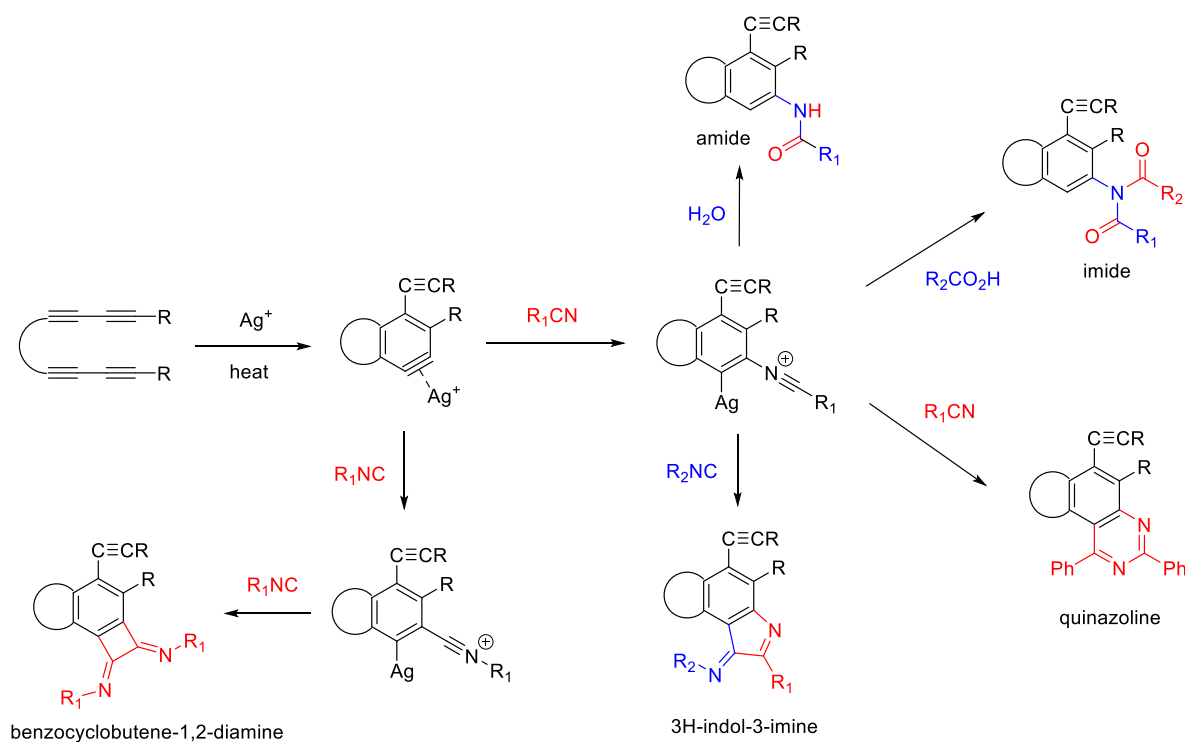
Due to their electrophilic nature, arynes can react with varieties of nucleophile. The initial intermediate formed from the interception of the nucleophile with arynes can generate another electrophilic species which can react with a second nucleophile, which thus constitute multicomponent coupling reactions. Arynes generated from Kobayashi precursor are known to undergo a wide variety of multicomponent reactions. The HDDA-derived arynes have been utilized in various multicomponent reactions by the groups of Hoyer, Lee and Hu. Hoyer and coworkers reported a three-component coupling reaction between arynes, cyclic tertiary amines, and aprotic nucleophiles (**Scheme 1.11**). The aryne formed from **1-30** reacts with DABCO to generate an ammonium intermediate **1-30c**. Abstraction of a proton by **1-30c** from a protic nucleophile to form intermediate **1-30d** followed by subsequent nucleophilic ring-opening generated three-component coupling product **1-41**.³⁰ The aryne generated from **1-32** can be



Scheme 1.11. Multicomponent reactions of HDDA arynes

intercepted with quinoline to form zwitterion intermediate **1-32d**. Trapping **1-32d** with phenyl isocyanate to form intermediate **1-32e** followed by subsequent ring closure generates product **1-42**.³¹ The reaction of an aryne generated from precursor **1-30** reacts with thiolane to form zwitterionic intermediates **1-30e** and **1-30f**, which reacts with weakly acidic protic nucleophile to form the product **1-43**.³²

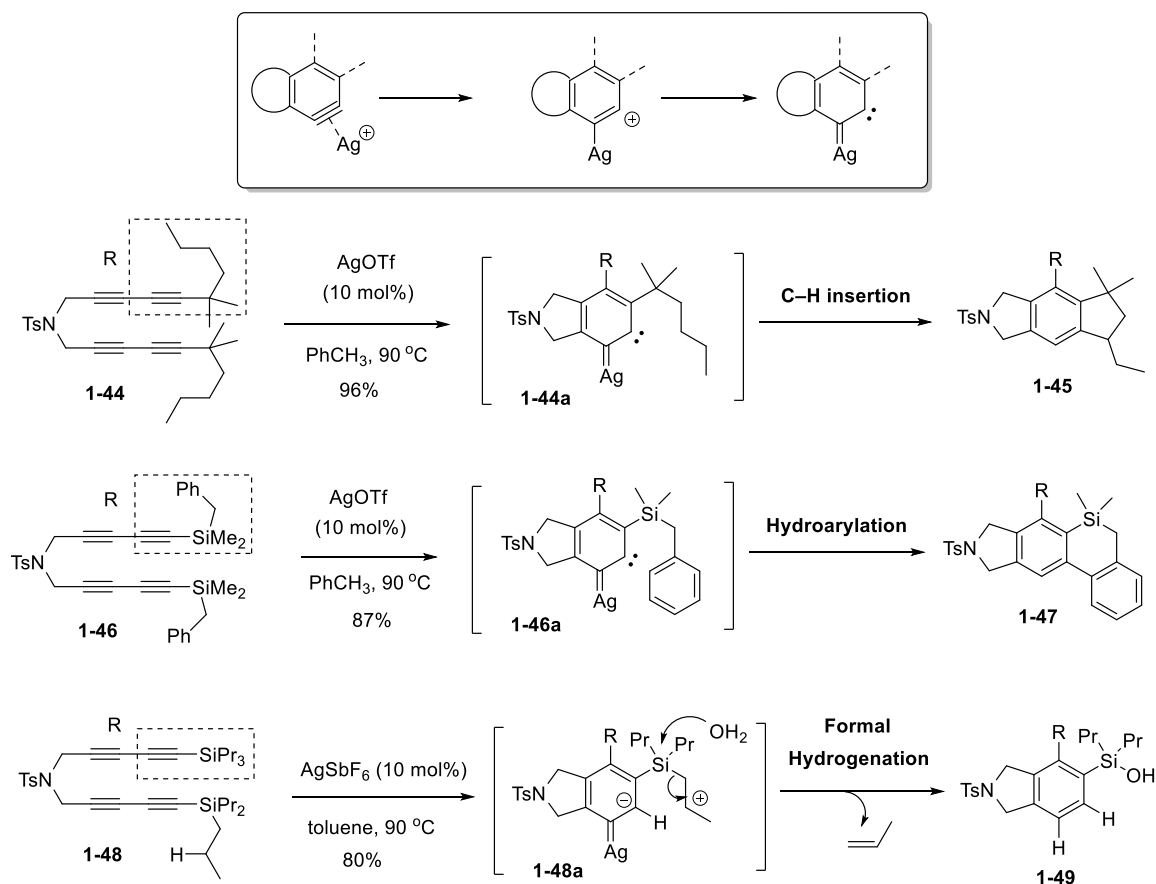
Multicomponent reactions of arynes with nitriles and isonitriles along with protic nucleophiles occurs in the presence of silver salts to form various aromatic and heterocyclic compounds. The silver cation interacts with arynes to increase their electrophilicity, thus making them react with weak nucleophiles such as nitrile to form a nitrilium ion intermediate. The nitrilium subsequently reacts with water or acetic acid to form amides or imides, respectively.³³ The nitrilium intermediate can also react with another nitrile or isonitrile molecule to generate quinazoline or 3*H*-indol-3-imine.³⁴ Isonitrile can also react with aryne to form a nitrilium intermediate, which can react with another isonitrile molecule to form benzocyclobutene-1,2-diamine (Scheme 1.12).³⁵



Scheme 1.12. Multicomponent reactions of HDDA-arynes involving nitriles and isonitriles

1.2.5. Metal-catalyzed reactions of HDDA-derived arynes

Various transition metal complexes of Ag, Cu, Fe or Ru can interact with arynes and thus affect their reactivity. Silver complexes can associate with arynes to form intermediates with enhanced electrophilicity allowing for them to react with a broad range of reacting counterparts, and thus reduces the possibility of side-reactions as well. The reactivity of arynes can be manifested as zwitterion or as a diradical, but in the presence of silver cation a new reactivity involving a formal dicarbene intermediate can be explored (**Scheme 1.13**). Tetrayne **1-44**, upon heating in the presence of catalytic AgOTf, forms a putative dicarbene intermediate **1-44a**, which undergoes C–H insertion to generate product **1-45**.³⁶ Similarly, the dicarbene intermediate **1-46a** generated from tetrayne **1-46** provided hydroarylation product **1-47**.³⁷ The mechanism of this net hydroarylation involves either C–H insertion of C(*sp*²)–H or electrophilic aromatic substitution.



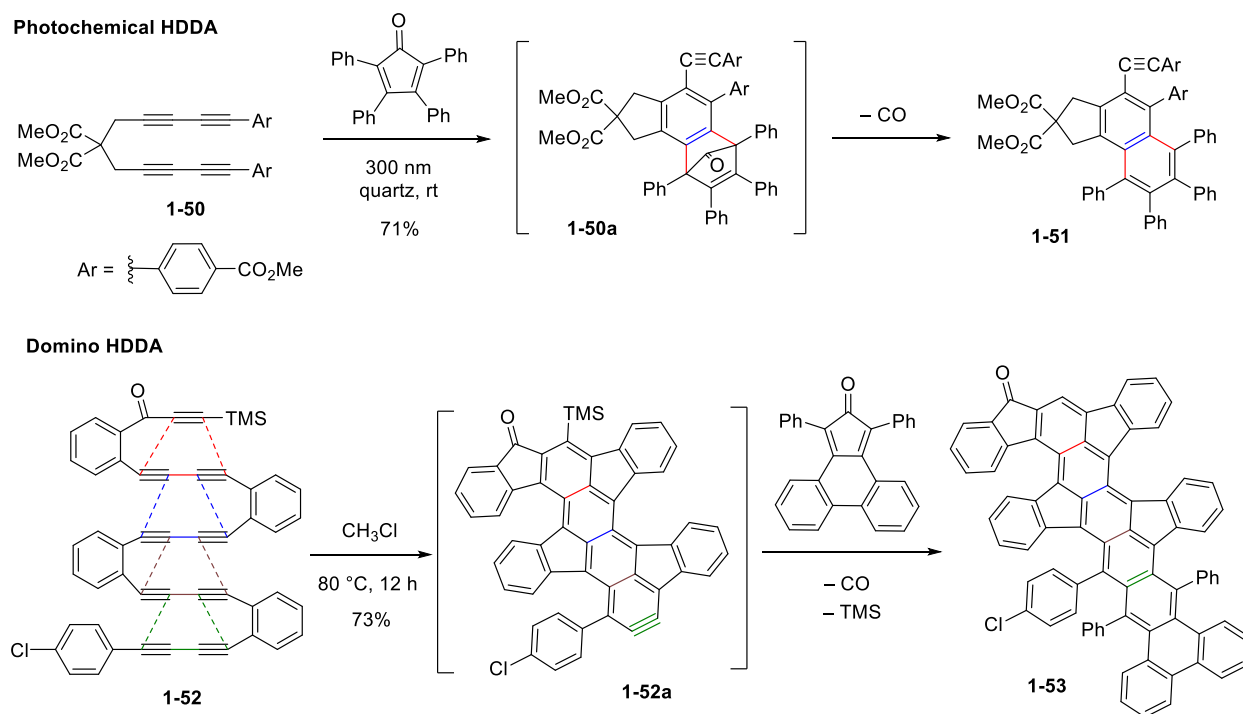
Scheme 1.13. Silver-catalyzed dicarbene reactivity of arynes

Tetrayne **1-48** containing a C–H bond at 2° and 3° β -carbon of a silyl group forms a silyl-stabilized carbocation at the β -carbon of the silyl group via a 1,5-hydride transfer in intermediate **1-48a**, which undergoes propene elimination by the participation of adventitious water to generate a formal aryne hydrogenation product **1-49**.³⁸

1.3. Strategy-Level Development of HDDA Reactions

1.3.1. Photochemical and domino HDDA reactions

Hoye and coworkers reported a photochemical HDDA reaction in 2017 (**Scheme 1.14**).³⁹ In this study, only tetraynes bearing two aromatic substituents at the terminal alkynes were employed. Tetrayne **1-50** tetraphenylcyclopentadienone upon irradiation with 300 nm quartz lamp form [4 + 2] adduct **1-50a**, which lead to final product **1-51** after CO extrusion. Although the photochemical HDDA reaction can be carried out at room temperature certain tetrayne with 4-methoxy phenyl substituent can be initiated at temperature as low as $-70\text{ }^{\circ}\text{C}$. When an unsymmetrically substituted tetrayne were subjected to same reaction under



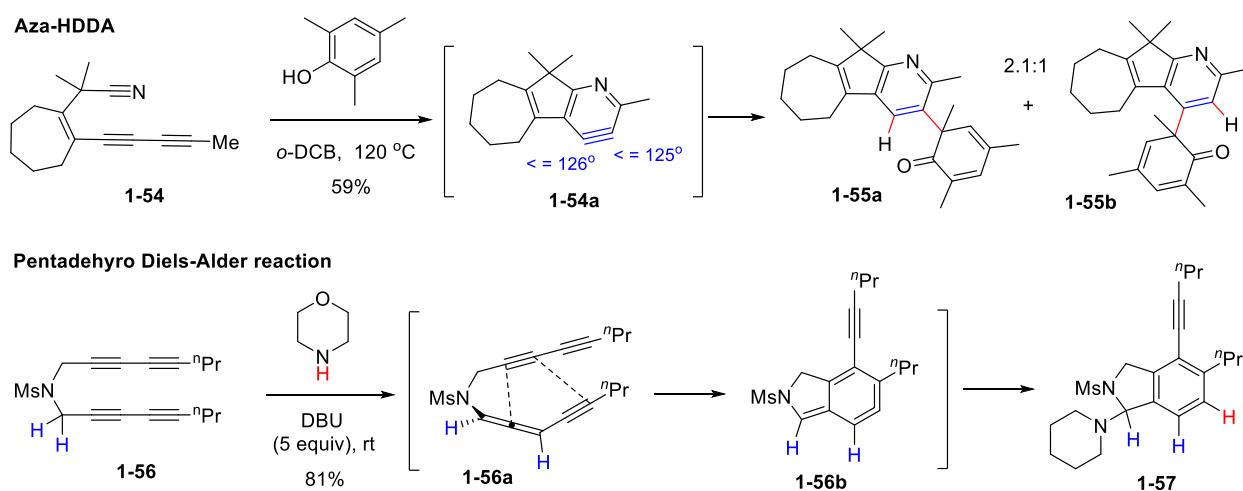
Scheme 1.14. Photochemical and domino HDDA reactions

photochemical and thermal initiation identical ratio of the products from isomeric benzyne were formed. This indicates that regardless of the mode of initiation the reaction proceeded through a common intermediate.

With an appropriate linear array of suitably tethered multiple diynes, a series of intramolecular cyclizations can successively occur to constitute a domino HDDA process. One of the most elaborated example of a domino HDDA process involves nonayne **1-52**, which undergoes four consecutive HDDA reactions to form tetracyne **1-52a**.⁴⁰ Trapping of the aryne via a Diels-Alder reaction with the cyclopentadienone followed by CO extrusion and desilylation generated product **1-53**.

1.3.2. Other variants of HDDA reactions

Replacement of the diynophile alkyne in triynes with a nitrile functionality will constitute an aza-HDDA reaction⁴¹ to form a pyridyne intermediate (**Scheme 1.15**). For example, upon heating enediynonitril **1-54** generates relatively undistorted 3,4-pyridyne pyridyne **1-54a**, which reacts with 2,4,6-trimethyl phenol to give a mixture of isomeric dienones **1-55a** and **1-55b** in a 2.1:1 ratio. Installation of the nitrile as a component of the diyne makes the resulting 2,3-pyridyne more distorted, which and shows higher selectivity to nucleophile trapping. Certain reactions are reported to give products that are HDDA-like

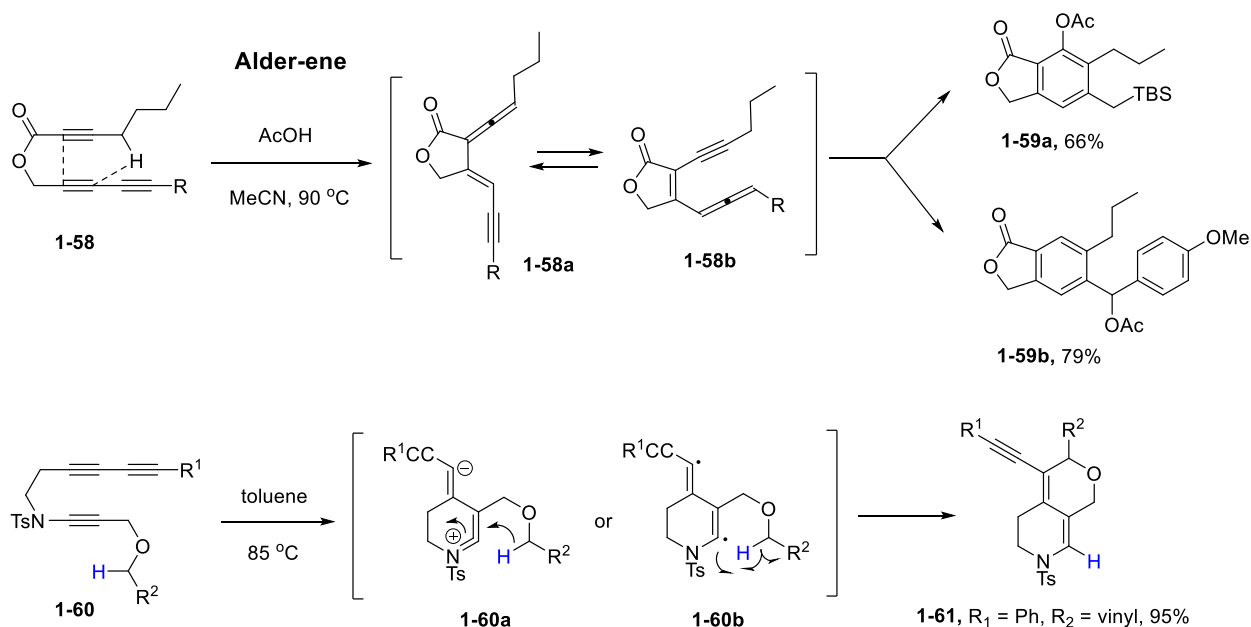


Scheme 1.15. Aza-HDDA and pentadehydro Diels-Alder reaction

but that do not proceed through an aryne intermediate. For example, tetrayne **1-56** generates product **1-57** upon treating with morpholine at ambient temperature. Mechanistic studies revealed that the reaction proceeds by an initial base-catalyzed isomerization to generate allenyne **1-56a**, which then cyclizes to the strained allene **1-56b**. This $\alpha,3$ -dehydrotoluene derivative is then captured by amine. This process was named as the pentadehydro Diels–Alder (PDDA) reaction, signifying that the cyclization occurs via an acyclic intermediate **1-56a**, whereon five of the component atoms are *sp*-hybridized.⁴²

1.4. Other Thermal Processes of Multiynes

Although multiynes mainly participate in HDDA reactions under thermal conditions other processes are also reported (**Scheme 1.16**). One such example involves the thermally induced Alder-ene reaction of ester-tethered 1,3,8-triynes to provide novel benzannulation products with concomitant incorporation of nucleophiles.⁴³ In this process, triyne **1-58** generates an allene-enyne intermediate **1-58a** via an Alder-ene initiation, which ultimately leads to the formation of discrete aromatic products after subsequent



Scheme 1.16. Other thermal processes of multiynes

transformations depending on the nature of the substituents. When **1-58a** contains a silyl substituent at the terminal position of the alkyne a nucleophile is incorporated on to the aromatic ring to generate **1-59a** whereas an aromatic substituent directs the nucleophile incorporation to the benzylic carbon atom connected to the aryl substituent to provide **1-59b**. The formation of **1-59b** is believed to be the consequence of involvement of a regioisomeric allene-ene intermediate **1-58b**. Lee and coworkers reported a facile thermal cyclization of ynamide-tethered 1,3,8-triynes **1-60** to form a 3,5,6,8-tetrahydro-1*H*-pyrano[3,4-*c*] skeleton **1-61**.⁴⁴ The mechanism of this unprecedented cyclization cannot be fully defined although the formation of either a strained keteniminium **1-60a** or a biradical intermediate **1-60b** followed by a 1,5-hydride or hydrogen shift is tentatively proposed as the elementary step in the reaction sequence. Although DFT calculation supports the biradical mechanism experimental results are not fully consistent with this diradical mechanism. Regardless of the actual mechanism, appropriate electronic activation at the hydrogen- or hydride-donating carbon leading to a stabilized radical or oxonium species is a key factor to a successful cyclization.

1.5. Summary

In summary, multiynes can undergo a wide variety of cycloaddition and cyclization processes under thermal conditions to form annulated products. The most prominent of them involves the DDA reactions out of which are TDDA and HDDA reactions to the for generate various arene products. HDDA reactions serves as a mild and efficient atom-economical process to generate arynes. HDDA-derived arynes have been utilized to introduce different types of adjacent σ -bonds to the aryne skeleton, which allow the synthesis of highly substituted aromatic and heteroaromatic compounds and found applications in the synthesis of certain natural products. Transition metals have also been used in the reactions of HDDA-derived arynes to promote new reactions including aryne-based multicomponent coupling of nitriles and isonitriles. Photochemical initiation of HDDA reaction was developed although it is restricted to a particular class of substrate. Domino HDDA reactions have been developed where appropriately tethered diynes undergoes successive intramolecular cyclizations to generate complex polyaromatic systems including

naphthynes and anthracynes. Other variants of HDDA reactions such as aza-HDDA can be achieved by replacing one of the terminal alkynes in triynes. In addition to the most common DDA type thermal process, multiynes can participate in other thermal cyclizations and benzannulations.

1.6. References

1. (a) Martin, J. G.; Hill, R. K. *Chem. Rev.* **1961**, *61*, 537–562. (b) Brieger, G.; Bennett, J. N. *Chem. Rev.* **1980**, *80*, 63. (c) Kagan, H. B.; Riant, O. *Chem. Rev.* **1992**, *92*, 1007. (d) Winkler, J. D. *Chem. Rev.* **1996**, *96*, 167–176. (e) Kumar, A. *Chem. Rev.* **2001**, *101*, 1. (f) Takao, K.-i.; Munakata, R.; Tadano, K.-i. *Chem. Rev.* **2005**, *105*, 4779.
2. Bobrowski, M.; Liwo, A.; Oldziej, S.; Jeziorek, D.; Ossowski, T. *J. Am. Chem. Soc.* **2000**, *122*, 8112.
3. Wessig, P.; Müller, G. *Chem. Rev.* **2008**, *108*, 2051.
4. (a) Hoye, T. R.; Baire, B.; Niu, D.; Willoughby, P. H.; Woods, B. P. *Nature*, **2012**, *490*, 208. Reviews: (b) Holden, C.; Greaney, M. F. *Angew. Chem., Int. Ed.* **2014**, *53*, 5746. (c) Diamond, O. J.; Marder, T. B. *Org. Chem. Front.* **2017**, *4*, 891. (d) Fluegel, L. L.; Hoye, T. R. *Chem. Rev.* **2021**, *121*, 2413.
5. (a) Michael, A.; Bucher, J. E. *Chem. Ber.* **1895**, *28*, 2511. (b) Michael, A.; Bucher, J. E. *Am. Chem. J.* **1898**, *20*, 89. (c) Bucher, J. E. *J. Am. Chem. Soc.* **1908**, *30*, 1244.
6. Baddar, F. G.; Moussa, G. E. M.; Omar, M. T. *J. Chem. Soc.* **1968**, 110.
7. (a) Klemm, L. H.; Gopinath, K. W.; Hsu Lee, D.; Kelly, F. W.; Trod, E.; McGuire, T. M. *Tetrahedron* **1966**, *22*, 1797. (b) Klemm, L. H.; Hsu Lee, D.; Gopinath, K. W.; Klopfenstein, C. E. *J. Org. Chem.* **1966**, *31*, 2376. (c) Klemm, L. H.; Klemm, R. A.; Santhanam, P. S.; White, D. V. *J. Org. Chem.* **1971**, *36*, 2169. (d) Klemm, L. H.; McGuire, T. M.; Gopinath, K. W. *J. Org. Chem.* **1976**, *41*, 2571.

8. Klemm, L. H.; McGuire, T. M. *J. Heterocycl. Chem.* **1972**, 9, 1215.
9. (a) Bossenbroek, B.; Shechter, H. *J. Am. Chem. Soc.* **1967**, 89, 7111. (b) Ipaktschi, J.; Staab, H. A. *Tetrahedron Lett.* **1967**, 3, 4403. (c) Müller, E.; Heiss, J.; Sauerbier, M.; Streichfuss, D.; Thomas, R. *Tetrahedron Lett.* **1968**, 9, 1195. (d) Bossenbroek, B.; Sander, D. C.; Curry, H. M.; Shechter, H. *J. Am. Chem. Soc.* **1969**, 91, 371. (e) Staab, H. A.; Ipaktschi, J. *Chem. Ber.* **1971**, 104, 1170.
10. (a) Butz, L. W.; Gaddis, A. M.; Butz, E. W. J.; Davis, R. E. *J. Org. Chem.* **1940**, 5, 379. (b) Butz, L. W.; Gaddis, A. M.; Butz, E. W. J.; Davis, R. E. *J. Am. Chem. Soc.* **1940**, 62, 995. (c) Butz, L. W.; Joshel, L. M. *J. Am. Chem. Soc.* **1941**, 63, 3344. (d) Joshel, L. M.; Butz, L. W.; Feldman, J. *J. Am. Chem. Soc.* **1941**, 63, 3348. (e) Butz, L. W.; Joshel, L. M. *J. Am. Chem. Soc.* **1942**, 64, 1311. (f) Nudenberg, W.; Butz, L. W. *J. Am. Chem. Soc.* **1943**, 65, 2059. (g) Butz, L. W.; Gaddis, A. M.; Butz, E. W. J. *J. Am. Chem. Soc.* **1947**, 69, 924.
11. Baddar, F. G.; ElAssal, L. S. *J. Chem. Soc.* **1948**, 1267.
12. Bradford, C. L.; Fleming, S. A.; Ward, S. C. *Tetrahedron Lett.* **1995**, 36, 4189.
13. Wessig, P.; Müller, G.; Pick, C.; Matthes, A. *Synthesis* **2007**, 464.
14. (a) Staab, H. A.; Draeger, B. *Chem. Ber.* **1972**, 105, 2320. (b) Wagner, F.; Meier, H. *Tetrahedron* **1974**, 30, 773.
15. Baidossi, W.; H. Schumann, H.; Blum, J. *Tetrahedron* **1996**, 52, 8349.
16. Gevorgyan, V.; Takeda, A.; Homma, M.; Sadayori, N.; Radhakrishnan, U.; Yamamoto, Y. *J. Am. Chem. Soc.* **1999**, 121, 6391.
17. Wenk, H. H.; Winkler, M.; Sander, W. *Angew. Chem., Int. Ed.* **2003**, 42, 502. (b) Pellissier, H.; Santelli, M. *Tetrahedron* **2003**, 59, 701. (c) Dyke, A. M.; Hester, A. J.; Lloyd-Jones, G. C. *Synthesis* **2006**, 4093. (d) Sanz, R. *Org. Prep. Proced. Int.* **2008**, 40, 215. (e) Chen, Y.; Larock, R. C. In *Modern Arylation Methods*; Akermann, L., Ed.; Wiley-VCH: Weinheim, Germany, **2009**; pp 401–

473. (f) Kitamura, T. *Aust. J. Chem.* **2010**, *63*, 987. (g) Tadross, P. M.; Stoltz, B. M. *Chem. Rev.* **2012**, *112*, 3550. (h) Bhunia, A.; Yetra, S. R.; Biju, A. T. *Chem. Soc. Rev.* **2012**, *41*, 3140. (i) Gampe, C. M.; Carreira, E. M. *Angew. Chem., Int. Ed.* **2012**, *51*, 3766. (j) Wu, C.; Shi, F. *Asian J. Org. Chem.* **2013**, *2*, 116. (k) Dubrovskiy, A. V.; Markina, N. A.; Larock, R. C. *Org. Biomol. Chem.* **2013**, *11*, 191.
18. (a) Matsumoto, T.; Hosoya, T.; Katsuki, M.; Suzuki, K. *Tetrahedron Lett.* **1991**, *32*, 6735. (b) Stiles, M.; Miller, R. G. *J. Am. Chem. Soc.* **1960**, *82*, 3802. (c) Wittig, G.; Hoffmann, R. W. *Org. Synth.* **1967**, *47*, 4. (d) Gilchrist, T. L.; Graveling, F. J.; Rees, C. W. *Chem. Commun.* **1968**, 821. (e) Campbell, C. D.; Rees, C. W. *J. Chem. Soc. C*, **1969**, 742.
19. Himeshima, Y.; Sonoda, T.; Kobayashi, H. *Chem. Lett.* **1983**, 1211.
20. (a) Berthelot, A. Jahresber. *Fortschritte Chem.* **1866**, 516. (b) Berthelot, A. *Ann. Chim. Phys.* **1866**, *9*, 445.
21. (a) Bradley, A. Z.; Johnson, R. P. *J. Am. Chem. Soc.* **1997**, *119*, 9917. (b) Kociolek, M. G.; Johnson, R. P. *Tetrahedron Lett.* **1999**, *40*, 4141. (c) Ajaz, A.; Bradley, A. Z.; Burrell, R. C.; Li, W. H. H.; Daoust, K. J.; Bovee, L. B.; DiRico, K. J.; Johnson, R. P. *J. Org. Chem.* **2011**, *76*, 9320.
22. (a) Miyawaki, K.; Suzuki, R.; Kawano, T.; Ueda, I. *Tetrahedron Lett.* **1997**, *38*, 3943. (b) Kimura, H.; Torikai, K.; Miyawaki, K.; Ueda, I. *Chem. Lett.* **2008**, *37*, 662.
23. (a) Marell, D. J.; Furan, L. R.; Woods, B. P.; Lei, X.; Bendelsmith, A. J.; Cramer, C. J.; Hoye, T. R.; Kuwata, K. T. *J. Org. Chem.* **2015**, *80*, 11744. (b) Liang, Y.; Hong, X.; Yu, P.; Houk, K. N. *Org. Lett.* **2014**, *16*, 5702. (c) Chen, M.; He, C. Q.; Houk, K. N. *J. Org. Chem.* **2019**, *84*, 1959.
24. Xu, F.; Hershey, K. W.; Holmes, R. J.; Hoye, T. R. *J. Am. Chem. Soc.* **2016**, *138*, 12739.
25. Ross, S. P.; Hoye, T. R. *Nat. Chem.* **2017**, *9*, 523.
26. Arora, S.; Sneddon, D. S.; Hoye, T. R. *Eur. J. Org. Chem.* **2020**, 2020, 2379.

27. Zhang, J.; Hoye, T. R. *Org. Lett.* **2019**, *21*, 2615.
28. Arora, S.; Palani, V.; Hoye, T. R. *Org. Lett.* **2018**, *20*, 8082.
29. Karmakar, R.; Lee, D. *Org. Lett.* **2016**, *18*, 6105.
30. Ross, S. P.; Hoye, T. R. *Org. Lett.* **2018**, *20*, 100.
31. Nobusue, S.; Yamane, H.; Miyoshi, H.; Tobe, Y. *Org. Lett.* **2014**, *16*, 1940.
32. Chen, J.; Palani, V.; Hoye, T. R. *J. Am. Chem. Soc.* **2016**, *138*, 4318.
33. Ghorai, S.; Lee, D. *Tetrahedron* **2017**, *73*, 4062.
34. (a) Ghorai, S.; Lin, Y.; Xia, Y.; Wink, D. J.; Lee, D. *Org. Lett.* **2020**, *22*, 626. (b) Ghorai, S.; Lin, Y.; Xia, Y.; Wink, D. J.; Lee, D. *Org. Lett.* **2020**, *22*, 642.
35. Ghorai, S.; Lee, D. *Org. Lett.* **2019**, *21*, 7390.
36. Yun, S. Y.; Wang, K. P.; Lee, N. K.; Mamidipalli, P.; Lee, D. *J. Am. Chem. Soc.* **2013**, *135*, 4668.
37. Lee, N. K.; Yun, S. Y.; Mamidipalli, P.; Salzman, R. M.; Lee, D.; Zhou, T.; Xia, Y. *J. Am. Chem. Soc.* **2014**, *136*, 4363.
38. Mamidipalli, P.; Yun, S. Y.; Wang, K. P.; Zhou, T.; Xia, Y.; Lee, D. *Chem. Sci.* **2014**, *5*, 2362.
39. Xu, F.; Xiao, X.; Hoye, T. R. *J. Am. Chem. Soc.* **2017**, *139*, 8400.
40. Xiao, X.; Hoye, T. R. *Nat. Chem.* **2018**, *10*, 838.
41. Thompson, S. K.; Hoye, T. R. *J. Am. Chem. Soc.* **2019**, *141*, 19575.
42. Wang, T.; Naredla, R. R.; Thompson, S. K.; Hoye, T. R. *Nature* **2016**, *532*, 484.
43. Karmakar, R.; Yun, S. Y.; Chen, J.; Xia, Y.; Lee, D. *Angew. Chem., Int. Ed.* **2015**, *54*, 6582.
44. Sabbasani, V. R.; Lee, D.; Xie, P.; Xia, Y.; Lee, D. *Chem. – Eur. J.* **2017**, *23*, 8161-8165.

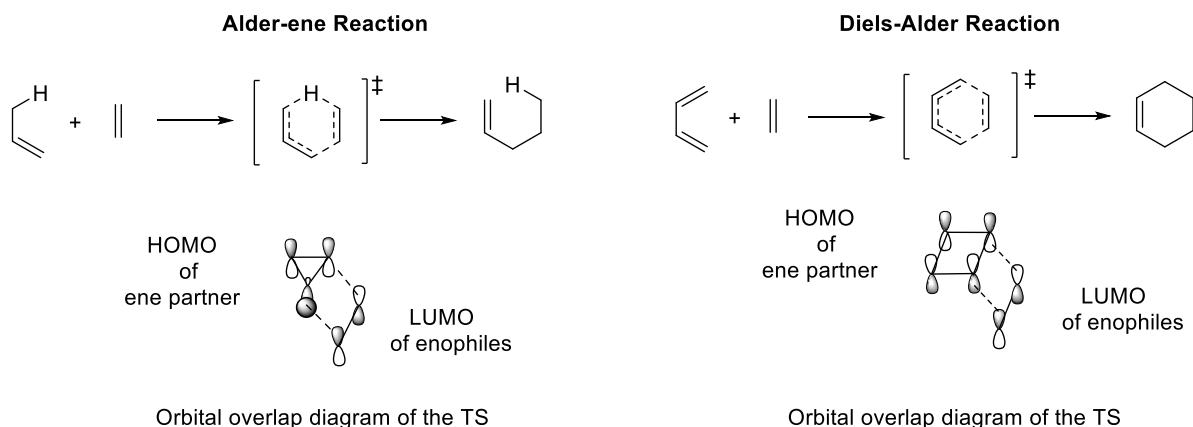
CHAPTER 2

Intermolecular Alder-Ene Reaction of Arynes with Functionalized Alkenes

2.1. Introduction

2.1.1. Alder-ene reaction

Ene reactions are a type of pericyclic reactions between a π -system (enophile) and an allylic or propargylic C–H bond-containing moiety (ene partner).¹ In this 6-electron process, a new C–C σ -bond is formed between those two moieties with a hydrogen atom and a π -bond migration.² Mechanistically, ene reaction proceed through a six-member transition state similar to Diels-Alder reaction between a conjugated diene and a dienophile (**Scheme 2.1**). In general, Alder-ene reactions occur through a suprafacial interaction between the HOMO of an ene-donor and the LUMO of an enophile.³ Although in rare occasions, a stepwise



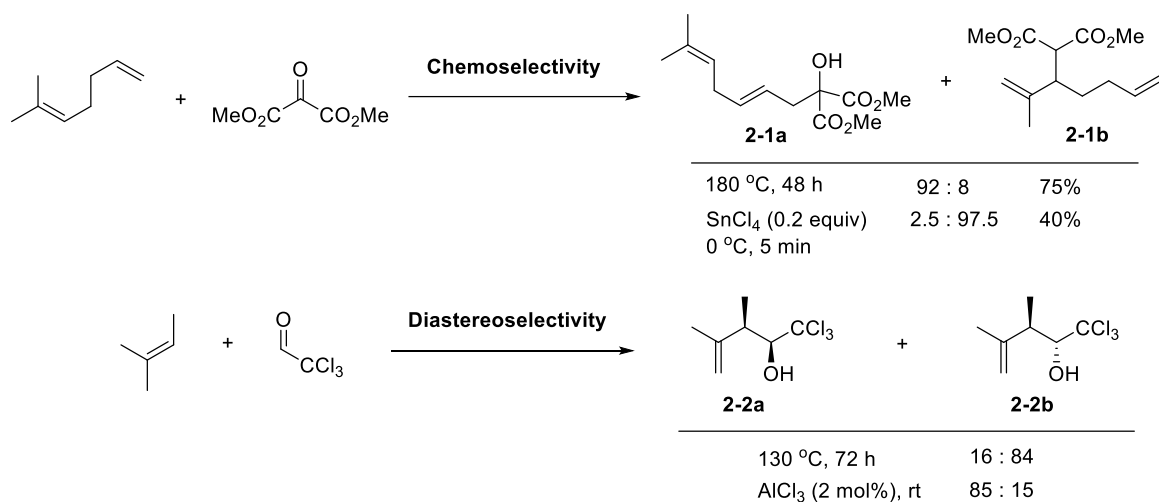
Scheme 2.1. Alder-ene vs. Diels-Alder reaction

a stepwise mechanism *via* biradical intermediate was also demonstrated.^{1c,4} A variety of ene-donors and enophiles have been successfully employed in this reaction. Alkene, alkyne, arene etc. are typical ene-donors and enophiles range from C–C multiple bonds, C=O, C=N, C=S, N=N, N=O, O=O, and so forth.³ After the discovery of the first ene reaction by Alder in 1943,^{1a,b} extensive developments were made over the last several decades. While the thermal Alder-ene reactions have been in use traditionally, various Lewis low temperature while the thermal processes requires relatively high temperature.⁵ Also, the Lewis acid-

*This chapter has been reprinted (adapted) with permission from Gupta, S.; Xie, P.; Xia, Y.; Lee, D. "Reactivity and Selectivity in the Intermolecular Alder–Ene Reactions of Arynes with Functionalized Alkenes" *Org. Lett.* **2017**, 19, 5162–5165. Copyright 2017, American Chemical Society.

acids have been found to catalyze this process.⁵ The Lewis acid-catalyzed processes can be performed at catalyzed Alder-ene reactions often occur in an asynchronous or stepwise manner and provide better and/or opposite chemo-, regio-, and stereoselectivity compared to that of thermal counterparts.⁶

The carbonyl-ene reaction is one of the most studied class of Alder-ene reactions. In 1984, Salmon demonstrated the difference in the chemoselectivity of a carbonyl-ene reaction with dienes and oxomalonates in thermal and SnCl₄-mediated conditions.^{6,7} When the reaction between 6-methyl-1,5-heptadiene and dimethyl oxomalonate was carried out in thermal conditions, the ene reaction of the less substituted alkene predominantly provide **2-1a** as the major product (**Scheme 2.2**). On the other hand, the reaction with SnCl₄ (0.2 equiv), more substituted alkene becomes more reactive toward the Lewis acid-coordinated carbonyl moiety, affording **2-1b** as the major product. While the thermal reaction is concerted and controlled mainly by steric factors, asynchronous nature of the Lewis-acid catalyzed reaction prefers the opposite selectivity through an electronic control. Gill and co-worker demonstrated the effect of Lewis-acid catalysis in the ene reactions between chloral or bromal with varieties of alkenes.⁸ The reaction of 2-methyl-2-butene with chloral under thermal conditions showed higher selectivity towards the formation of *anti*-diastereomer **2-2a** while AlCl₃-catalyzed reaction provided the *syn*-diastereomer **2-2b** more favorably.

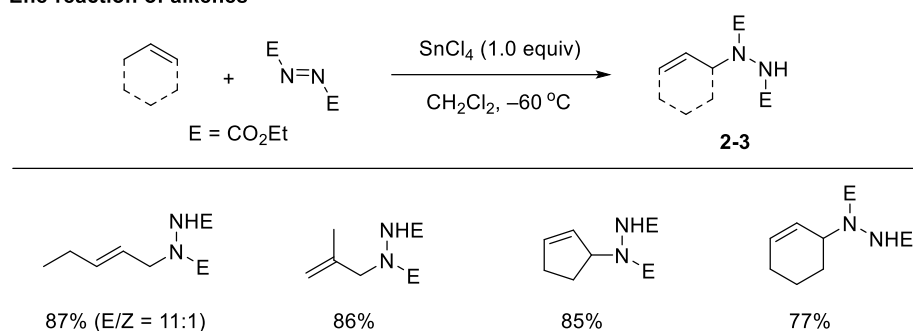


Scheme 2.2. Thermal vs. Lewis Acid-catalyzed carbonyl-ene reaction

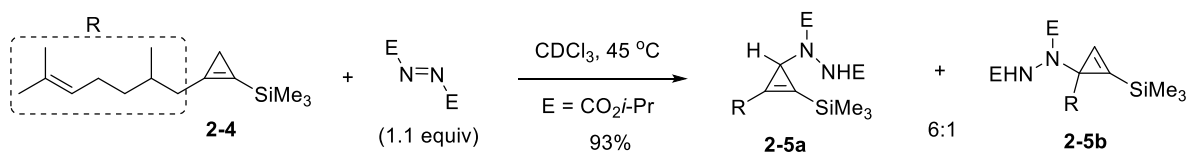
In 1993, Heathcock reported the first Lewis-acid mediated ene reaction of azodicarboxylate. Both cyclic and acyclic olefins undergo ene reaction with azodicarboxylate in presence of stoichiometric amount

of SnCl_4 provided products **2-3** (Scheme 2.3).⁹ In 2012, the Lee group demonstrated a novel $\text{C}(sp^3)\text{-H}$ animation of TMS-substituted cyclopropenes **2-4**, which proceeds via a tandem regioselective ene reaction between the cyclopropane and azodicarboxylate to generate a hydrazocarboxylate intermediate followed by a site-selective allylic transposition, generating *N*-substituted-cyclopropenes **2-5a** and **2-5b** in a 6:1 ratio.¹⁰ Lee and coworkers also reported a facile Alder-ene reaction of silylallenes **2-6** with diisopropyl azodicarboxylate in which the ene reaction occurs preferentially through the allenic $\text{C}(sp^2)\text{-H}$ in competition with allylic $\text{C}(sp^3)\text{-H}$ bonds to form product **2-7** at ambient temperature.¹¹

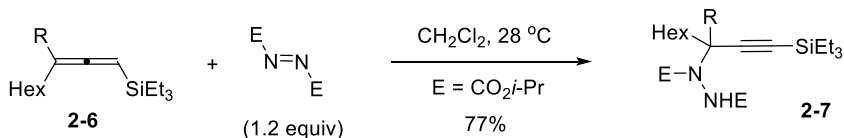
Ene-reaction of alkenes



Ene-reaction of silylcyclopropenes



Ene-reaction of silyl allenes

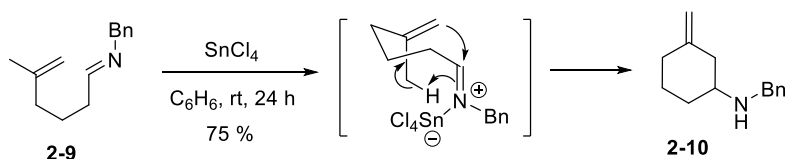


Scheme 2.3. Alder-ene reaction with azodicarboxylate

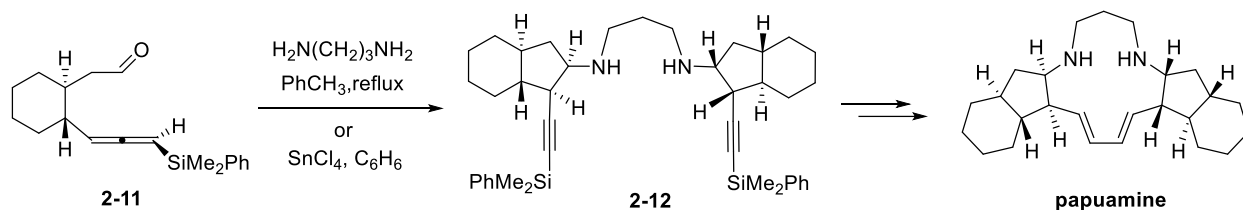
Similar to the carbonyl-ene reaction, the corresponding imino-ene reaction have been extensively studied over the last few decades and have been applied to the total synthesis of natural products.¹² While the carbonyl-ene reaction is an excellent tool for synthesis of a variety of homoallylic alcohol the imino-ene reaction is a synthetic tool to get access to various homoallylic amines. The ene reactions of imines are

usually catalyzed by Lewis acids. Demailly and Solladie reported a SnCl_4 -catalyzed intramolecular ene reaction of unactivated alkyl imines **2-8** to generate cyclohexyl amine derivative **2-9** (**Scheme 2.4**).¹³ An intramolecular double imino-ene reaction of silyllallene **2-11** provided mimeric product **2-12** either under thermal conditions or in presence of Lewis-acid catalyst, which was employed as the key intermediate in the synthesis of papuamine.¹⁴

Intramolecular Imino-ene reaction



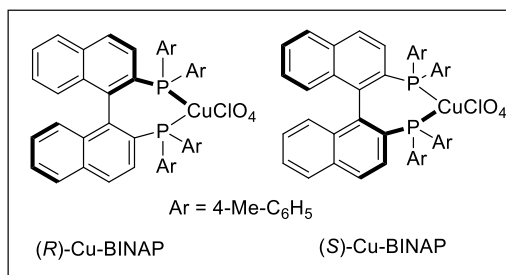
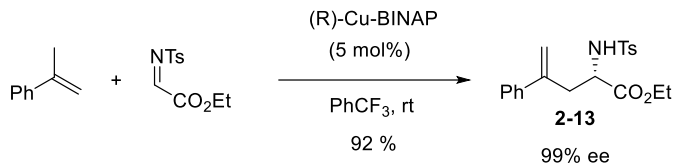
Application to total synthesis of papuamine



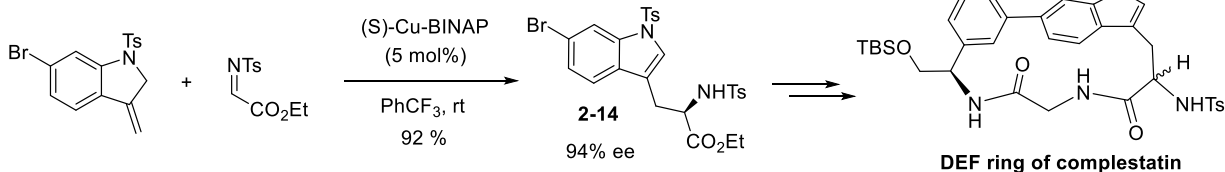
Scheme 2.4. Imino-ene reaction and application to the synthesis of papuamine

In 1988, the Lectka group reported an asymmetric imino-ene reaction (**Scheme 2.5**). In this study, α -amino ester derivatives **2-13** were generated with excellent enantoselectivity through the ene reaction of α -imino esters with olefins in presence of a chiral Cu-BINAP complex.¹⁵ The Rich group demonstrated the application of this reaction for the synthesis of 16- and 17-membered DEF ring systems of chloropeptin and complestatin from the ene reaction product **2-14**.¹⁶

Intermolecular Asymmetric Imino-ene reaction



Application to total synthesis of DEF rings of complestatin

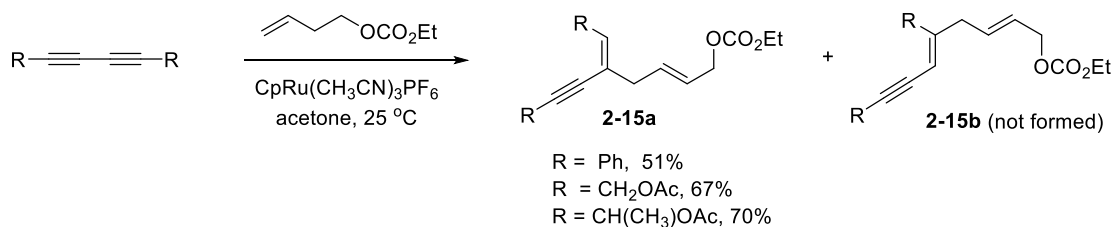


Scheme 2.5. Imino-ene reaction and application to the synthesis of DEF ring of complestatin

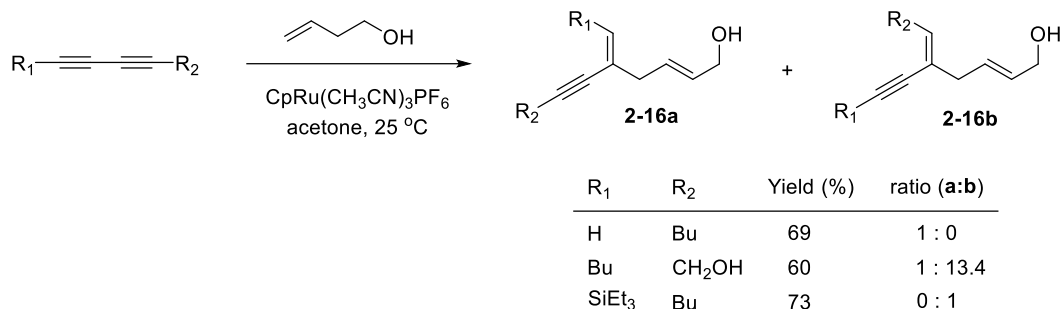
2.1.2. Transition metal-catalyzed Alder-ene reaction

Various transition metals including Ru, Pt, Co and Rh have been used as catalysts for Alder-ene reactions between alkenes and alkynes to form unsaturated molecular frameworks.¹⁷ One of the main challenges of the metal-catalyzed Alder-ene reactions of alkenes and alkynes is to control the regioselectivity in the product. In Ru-catalyzed Alder-ene reactions, regioselectivity is often unpredictable leading to mixtures of linear and branched isomers in varying ratios.¹⁸ The Trost group demonstrated that silylated alkynes generates *trans*-branched isomer exclusively on Alder-ene reaction with alkenes,¹⁹ while the Lee group demonstrated that borylated alkynes also shows excellent regioselectivity generating the unusual *cis*-branched isomer exclusively.²⁰ The Lee group also observed high level of regio- and site-selectivity in the Alder-ene reaction of 1,3-diyne and 1,3,5-triyne (**Scheme 6**). The regioselectivity profile of the Alder-ene reaction of symmetrical 1,3-diyne with 3-butenyl ethyl carbonate, symmetric diynes generated Alder-ene products **2-15a** as a single regioisomer and regioisomer **2-15b** was not observed. Two salient features of these reactions are the perfect regioselectivity for the branched isomer **2-15a** and the lack of reactivity of its alkyne moiety toward the second Alder-ene reaction. For unsymmetric diynes, the site

Regioselectivity with Symmetrical 1,3-Diynes



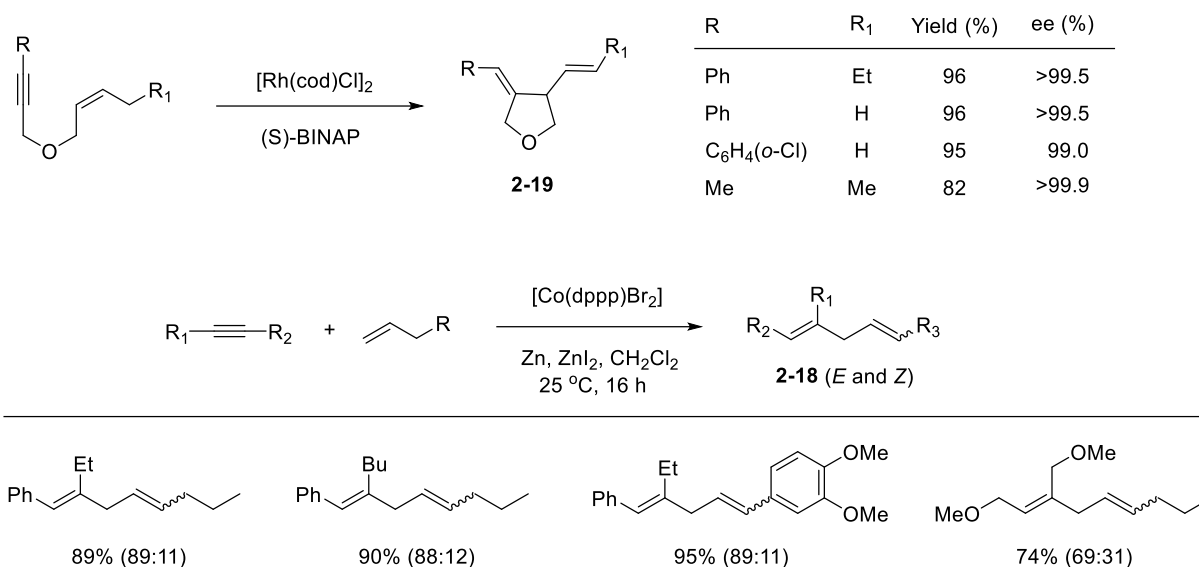
Site-Selectivity with Unsymmetrical 1,3-Diynes



Scheme 2.6. Regio- and site-selectivity in the Ru-catalyzed Alder-ene reaction of diynes

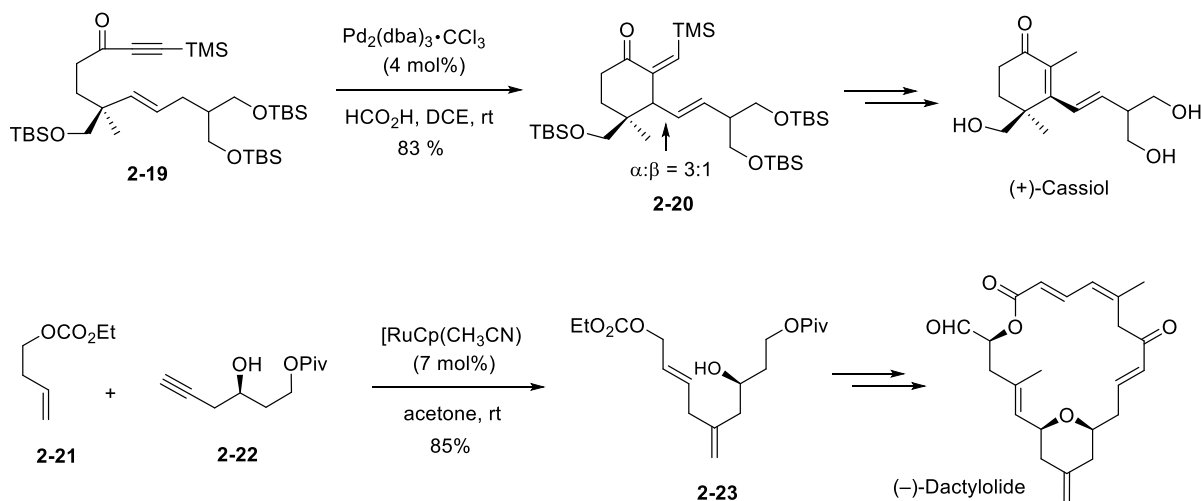
selectivity intricately depends on the interplay between steric factors and the electronic factor of the polar substituent at the propargylic sites. When R₁ = H and R₂ = Bu, the ene reaction occurs selectively from the terminal alkyne giving rise to branched alkene of the type **2-16a** exclusively. A polar substituent such as a hydroxyl group at the propargylic site directs the ene reaction to occur from the alkyne close to the hydroxyl group. When a silyl substitution is present on the alkyne, it directs the reaction to occur on the other alkyne, thus forming **2-16b** selectively.²¹

Other metals such as Rh, Co and Pd have also been used to catalyze Alder-ene reactions. Zhang and coworkers reported a highly enantioselective intramolecular Alder-ene reaction of 1,5-enyne catalyzed by a rhodium-BINAP complex to form chiral tetrahydrofurans **2-19** in excellent yield (**Scheme 2.7**).²² An inexpensive cobalt-diphosphine complex can also catalyze the intermolecular Alder-ene reaction of internal alkynes with terminal alkenes to form functionalized 1,4-dienes **2-18** in good yields with somewhat low *E/Z* selectivity at the newly formed disubstituted alkene.²³



Scheme 2.7. Alder-ene reaction catalyzed by Rh and Co

Transition metal-catalyzed Alder-ene reactions have been applied to the total synthesis of natural products. Trost and coworkers demonstrated a Pd-catalyzed intramolecular Alder-ene reaction of the enyne **2-19** to generate **2-20** as a 3:1 inconsequential diastereomeric mixtures. Double bond migration followed by desilylations lead to completion of the synthesis of (+)-cassiol (**Scheme 2.8**).²⁴



Scheme 2.8. Metal-catalyzed Alder-ene reaction: Application in Total Synthesis

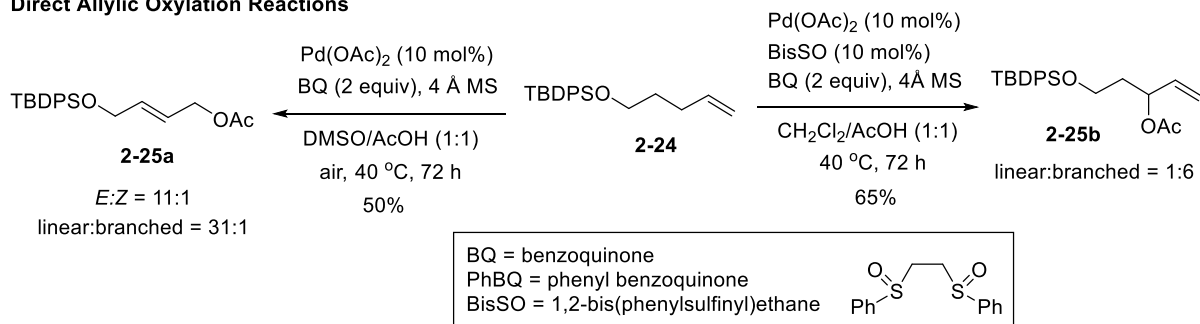
The Lee group demonstrated the prowess of Ru-catalyzed Alder-ene reaction in the total synthesis of (–)-dactylolide. A Ru-catalyzed ene reaction between alkene **2-21** and alkyne **2-22** generated 1,4-diene **2-23**, which was elaborated to the central 4-exomethylene tetrahydropyran, leading completion of (–)-dactylolide.²⁵

2.1.3. Allylic C–H bond functionalization

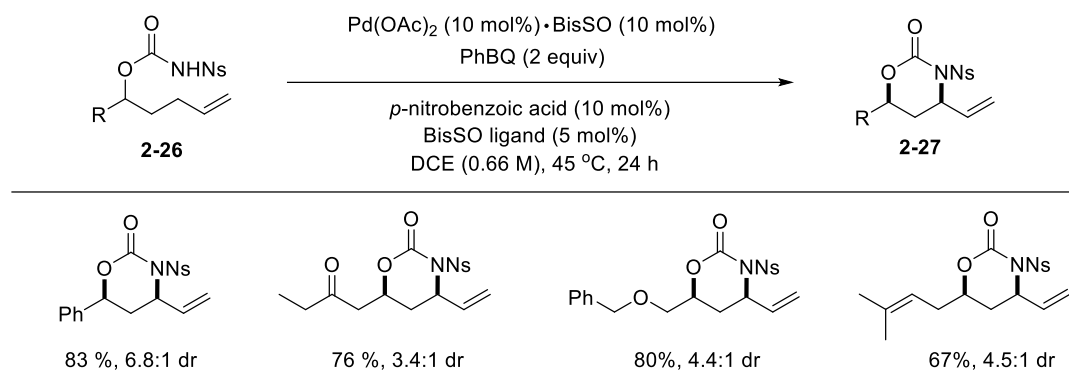
The functionalization of allylic C–H bonds is an important synthetic tool to incorporate C–O, C–N or C–C bonds at the allylic position. The direct Pd(II)-catalyzed allylation with various nucleophiles has emerged as a powerful method for allylic C–H functionalization.²⁶ A few representative examples for allylic hydroxylation, amination and alkylation are described. White and coworkers demonstrated that direct allylic oxidation could be achieved from terminal alkene **2-24** in a regioselective manner to give linear or branched acetates depending on the reaction conditions (**Scheme 2.9**).²⁷ The use of DMSO as a co-solvent led to the linear allylic acetate **2-25a**, whereas in the presence of 1,2-disulfoxide ligand formation of branched product **2-25b** becomes favorable.²⁷ A representative direct allylic amination is demonstrated by Rice and White, in which switching the *N*-protecting group from tosyl to a more electron-deficient nosyl group increases the reactivity. The reason for the higher reactivity of the nosyl amide is the consequence of the increased acidity, which provides a higher concentration of the deprotonated form as a better nucleophile. In Pd(0)-catalyzed oxidation of **2-26**, addition of a catalytic amount of *p*-nitrobenzoic acid provide good yield of 1,3-oxazinones **2-27** with high diastereoselectivities.²⁸ Young and White described a direct intermolecular allylic alkylation of resonance-stabilized nucleophiles such as α -nitrocarbonyl compounds, thus alkylated product **2-28** was obtained from 1-undecene and α -nitroacetophenone.²⁹

Alder-ene reactions can serve as an effective synthetic method to functionalize allylic C–H bonds with a concomitant 1,3-transposition of the involved alkenes. While the thermal Alder-ene reaction can still serve as a unique strategy to functionalize allylic C–H bond a majority of allylic C–H functionalization involves the use of transition metals, which provides broader reaction scope and better reactivity and selectivity control.

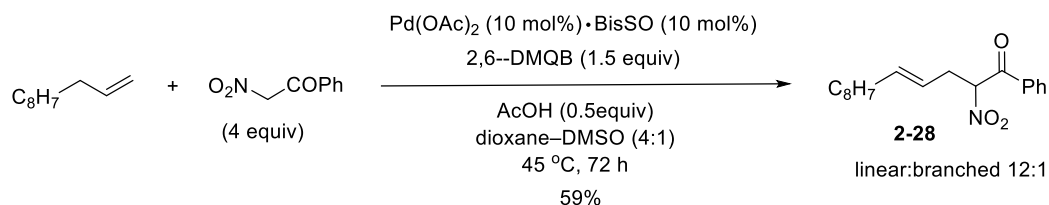
Direct Allylic Oxidation Reactions



Direct Allylic Amination Reactions



Direct Allylic Alkylation Reactions

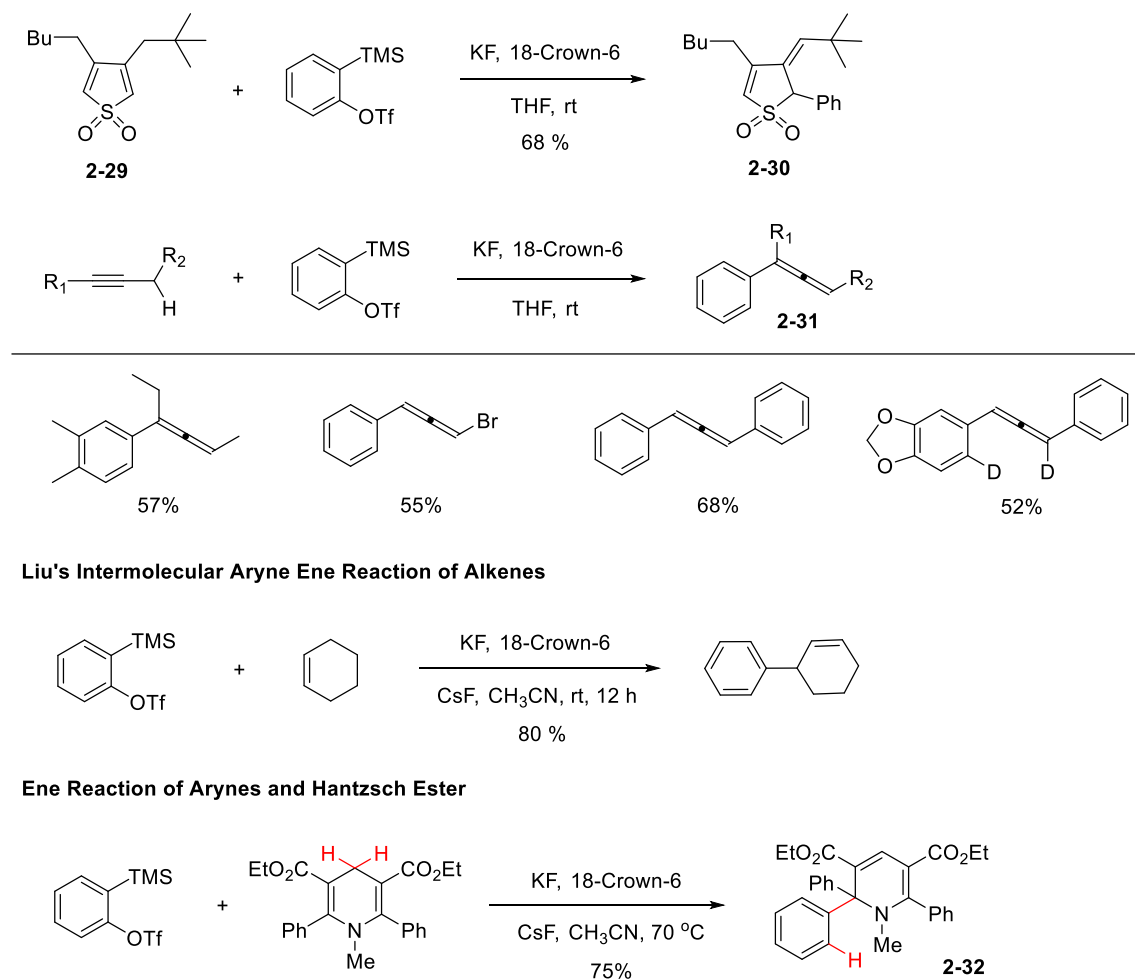


Scheme 2.9. Transition metal-catalyzed allylic C–H functionalization

2.1.4. Aryne-ene reaction

Arynes can serve as an excellent enophile for the Alder-ene reaction and is known to react with ene-donors both in inter and intramolecular fashions. In 1994, Nakayama observed the first intermolecular ene reaction of aryne. The benzyne generated from thermal decomposition of 2-carboxybenzenediazonium chloride was expected to undergo a Diels-Alder reaction with **2-29**, instead gave the ene reaction product **2-30** as the major product.³⁰ Since the discovery of Kobayashi's method, which served as a mild and efficient method for aryne generation, significant advancements have been made in discovering new reactivities of benzyne including Alder-ene reaction. In 2006, Chen and coworkers reported the

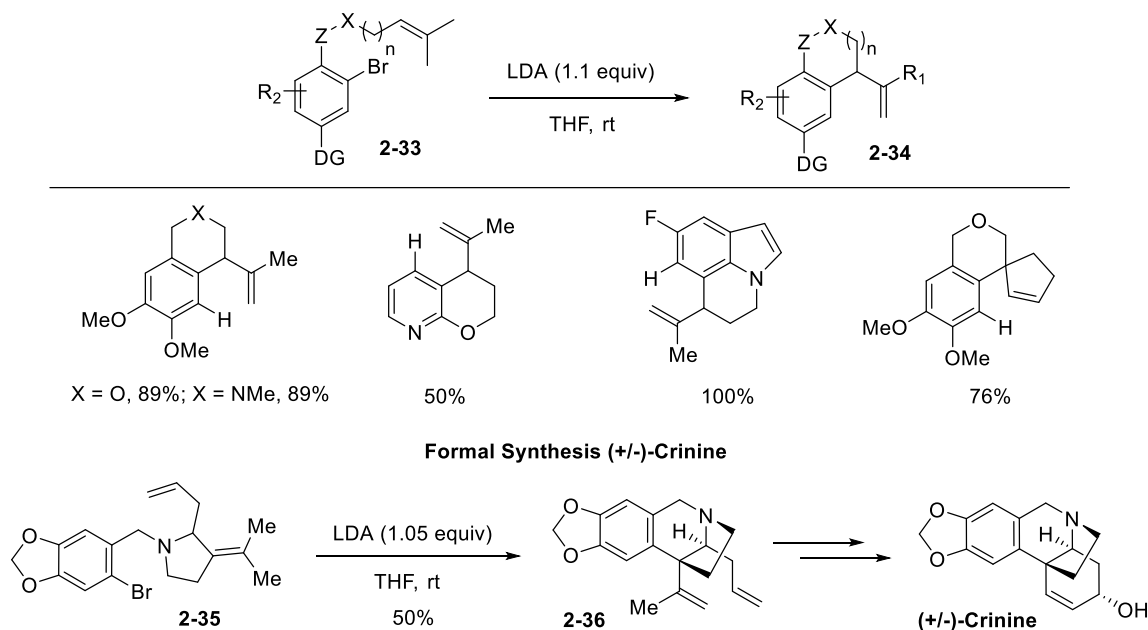
intermolecular ene reactions between aryne and alkynes to form allenes **2-31** in moderate yields.³¹ The Liu group demonstrated the intermolecular ene reaction of aryne with simple olefins. For example, benzyne generated from 1-trimethylsilyl-2-phenyl triflate reacts with cyclohexene to generate 2-phenylcyclohexene.³² Recently, Jones and coworkers reported an ene reaction of aryne with Hantzsch esters. For, example treating 1-trimethylsilyl-2-phenyl triflate with KF in the presence of the Hantzsch ester generated product **2-32** in 75% yield (**Scheme 2.10**).³³



Scheme 2.10. Examples of intermolecular aryne-ene reaction

In 2011, Lautens reported intramolecular ene reactions involving aryl bromides with a pendent ene-donor (**Scheme 2.11**).³⁴ When aryl bromide **2-33** was treated with LDA, the generated aryne underwent an intramolecular ene reaction with the tethered alkene to form wide variety of structurally complexdiversified

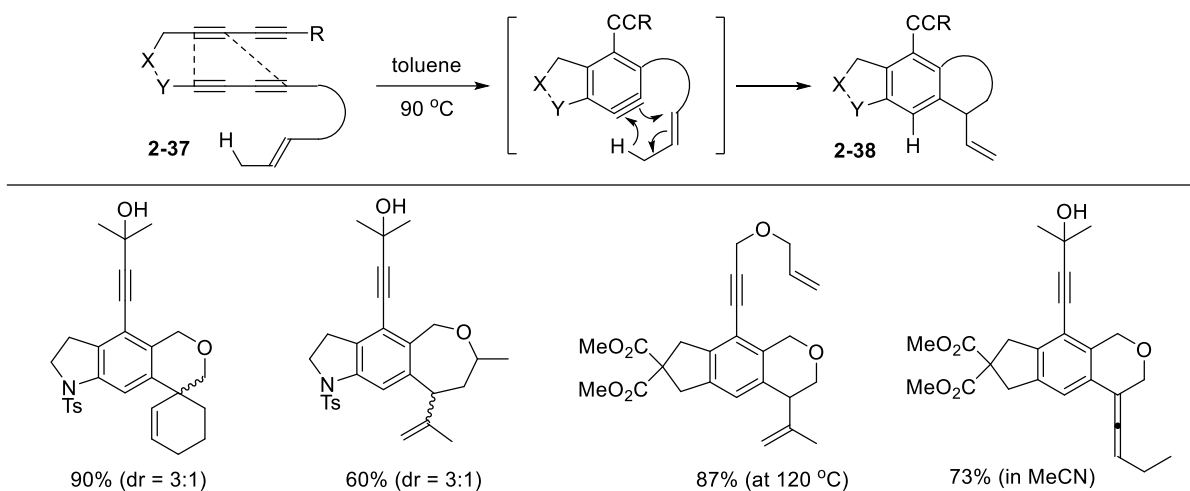
arenes **2-34** with high efficiency. This methodology was further applied for a formal synthesis of (\pm)-crinine starting from **2-35** via the formation of ene reaction product **2-36**.



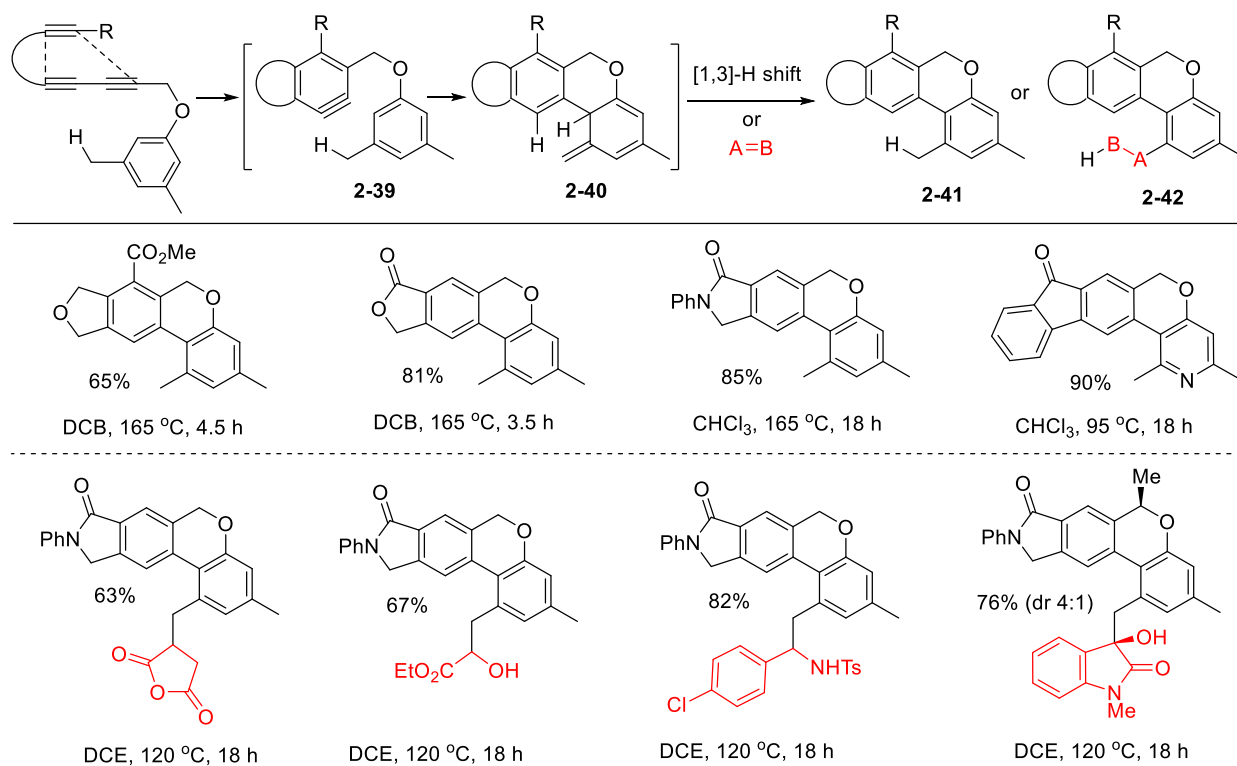
Scheme 2.11. Lauten's intramolecular aryne-ene reaction and its application to crinine synthesis

The Lee group demonstrated that arynes generated from tetraynes **2-37** via hexadehydro Diels-Alder (HDDA) reaction could undergo intramolecular Alder-ene reaction to generate various ene reaction products **2-38** (Scheme 2.12).³⁵ In these reactions, the reaction required temperature was found to be sensitive to the substrate structure such as presence of heteroatom, tether-length, and substituent patterns.

Hoye and coworkers reported an aromatic ene-reaction in which thermally generated aryne **2-39** can be engaged in an ene reaction to generate isotoluene **2-40** (Scheme 2.13).³⁶ This intermediate can undergo formal [1,3]-H shift to generate rearomatized product **2-41** or can be engaged in an intermolecular ene reaction with external enophiles to tricomponent generate product **2-41**.



Scheme 2.12. Lee's intramolecular aryne-ene reactions

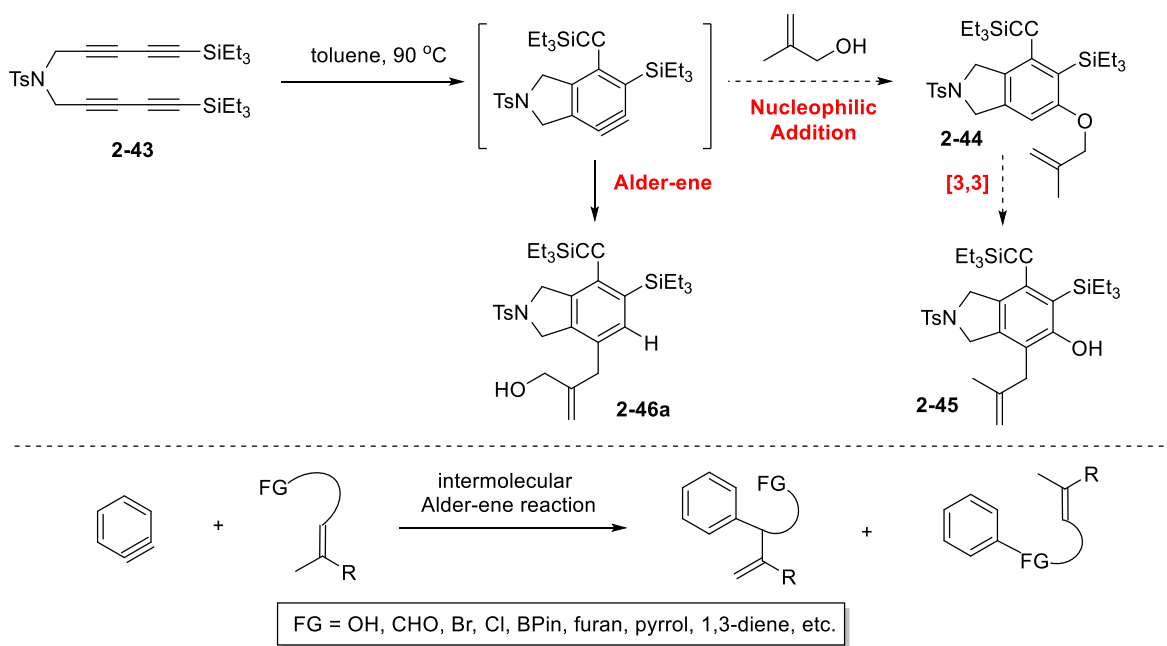


Scheme 2.13. Hoye's aromatic ene reactions

2.2. Results and Discussions

2.2.1. Initial observation

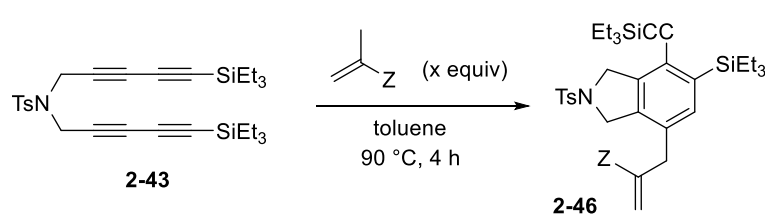
Arynes are electrophilic and reactive enough to react with various nucleophiles.³⁷ Alcohols are known to undergo addition to arynes to form aryl ethers. We envisioned that the tetrayne **2-43** under thermal condition would generate aryne through HDDA cycloaddition and might undergo addition with methallyl alcohol to generate aryl ether **2-44**, which may undergo a [3,3]-Claisen rearrangement to generate the phenolic compound **2-45** (Scheme 2.14). As opposed to the expectation, however, the reaction generated only compound **2-46** through an Alder-ene reaction. This result indicates that the ene reaction of the aryne with methallyl alcohol is more favorable than the ether formation. Even when this reaction was carried out in the presence of 5 equiv. of MeOH along with 5 equiv of methallyl alcohol, still the ene reaction product **2-46a** was obtained, indicating the significant preference of the ene reaction. This initial observation led to the investigation of intermolecular Alder-ene reaction of arynes with various ene-donors containing polar functional groups, which would provide insight into the reactivity and selectivity of intermolecular Alder-ene reactions of arynes and this will constitute a reagent-free allylic C–H bond functionalization.



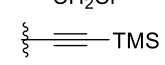
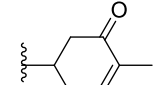
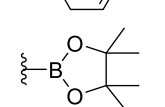
Scheme 2.14. Initial observation: Alder-ene reaction of arynes with methallyl alcohol

2.2.2. Reaction profile of 1,1-disubstituted alkenes

First, we examined the Alder-ene reactions by using a symmetrical tetrayne **2-43** and electronically deactivated ene-donor methyl methacrylate (**Table 2.1**). Reactions with varying amounts of the ene-donor showed that 5 equivalents of methyl methacrylate relative to the aryne precursor **2-43** provided the highest yield of the ene reaction product **2-46b** in 72% (entry 1), thus subsequent studies employed this stoichiometry unless otherwise noted. Under this optimized condition, the Alder-ene reactions of other 1,1-disubstituted alkenes bearing additional functional groups provided the corresponding Alder-ene products **2-46c-i** in good yields ranging from 55% to 81% (entries 2–8).



x	Yield (%)
1	10
2	43
3	55
4	61
5	72 ^a
10	65

entry	Z		yield (%) ^b
1	–CO ₂ Me	b	72 ^c
2	–CN	c	63
3	–Ph	d	55
4	–COC ₄ H ₉	e	81
5	–CH ₂ Cl	f	75
6		g	58
7		h	62
8		i	56

^aAll alkenes are used in 5 equiv relative to **2-43**. ^bIsolated yield.

^cWith a larger scale (1 mmol), **2-46** was obtained in 68% yield.

Table 2.1. Alder-ene reactions of functionalized 1,1-disubstituted alkenes with an aryne

2.2.3. Reaction profile of trisubstituted alkenes

Next, we examined the reactivity of trisubstituted alkenes containing a substituent including, an allylic bromide, a conjugated carboxylate, a ketal, dimethyl malonate moiety, a carbamate, an ester, an aldehyde, and a silyl ether (**Table 2.2**). The overall yields of the reaction involving these trisubstituted alkenes are slightly lower (ranging from 35 to 65%) than those of 1,1-disubstituted alkenes. It is worth noting that the geometrical isomers show stark difference in reactivity such that the *E*-isomer generates ene reaction product (entry 7) but the corresponding *Z*-isomer yields no ene reaction product (entry 8).

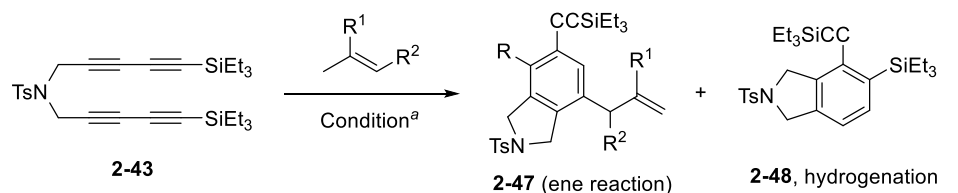
2-43 + $R^1-CH=CH-R^2$ (5 equiv) → **2-46**

entry	alkene	ene product	yield (%)
1		j	45
2		k	65
3		l	52
4		m	58
5		n	54
6		o	45
7		p	35
8		No ene reaction product	—

Table 2.2. Alder-ene reactions of functionalized trisubstituted alkenes with an aryl

2.2.4. Reaction profile of alkenyl alcohols

With the relative reactivity trend of differently substituted alkenes in hand, we next examined the reaction profiles of alkenyl alcohols (**Table 2.3**). In general, disubstituted alkenes containing a hydroxyl group provide only hydrogenation product **2-48** (entries 1–4).³⁸ Cyclooctadiene mono epoxide gave the ene reaction product (entry 4) but the TIPS ether of crotyl alcohol did not give either **2-47a** nor **2-48a** (entry 1)



entries	alkene		yield (%) ^b
1		a 0 (0) ^c	73 (0) ^c
2		b 0	47
3		c 0	61
4		d (d') 0 (52) ^d	54 (0) ^d
5		e 0	62
6		f 65	24
7		g 62	10
8		h 72	0
9		i 64	0
10		j 58	28

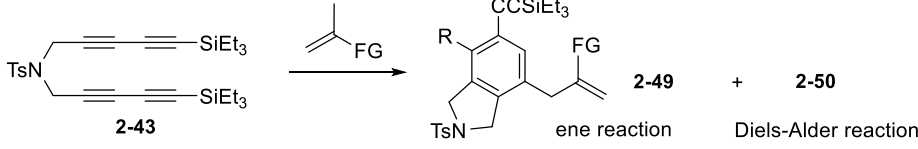
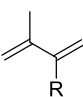
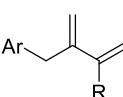
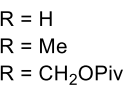
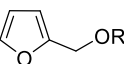
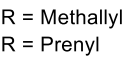
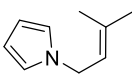
^aAlkene (5 equiv), toluene 90 °C, 4 h. ^bIsolated yield. ^cThe reaction led to polymerization of the aryne intermediate. ^dThe reaction provided Alder-ene product **2-47d'** in 52% yield.

Table 2.3. Ene reactions of alkenyl alcohols with an aryne

Trisubstituted alkenyl alcohols generated varying degree of the Alder-ene reaction and hydrogenation products depending on the disposition of allylic C–H bonds. Verbenol afforded only hydrogenation product because of the unreactive *trans*-geometry (entry 5) while prenyl alcohol and 6-methylhept-5-en-2-ol provided mainly Alder-ene products **2-47f** and **2-47g** along with **2-48** (entries 6 and 7). 1,1-Disubstituted alkenyl 1° and 2° alcohols provided exclusively Alder-ene products **2-47h** and **2-47i** (entries 8 and 9) except for an alkene containing an allylic 2° hydroxyl group, which also generated **2-48j** (entry 10). A notable observation from **Table 2.3** is the lack of aryl ethers albeit alcohols can undergo addition with arynes.

2.2.5. Reaction profile of 1,3-dienes

Recognizing the preferred Alder-ene reactivity of an aryne, we next examined the competition between an Alder-ene and a Diels-Alder reaction³⁸ by employing 1,3-dienes (**Table 2.4**). Acyclic dienes such as isoprene and 2,3-dimethyl butadiene provided only Alder-ene products **2-49a** and **2-49b** in 54% and 58%, respectively (entries 1 and 2) while the pivalate-substituted 2,3-dimethyl butadiene afforded a 1:1

			
entries	1,3-diene	yield (%)	
1		54	a
2		58	b
3		26	c
4		0	d
5		0	e
6		0	f

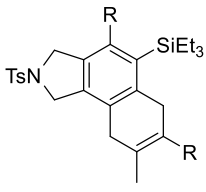
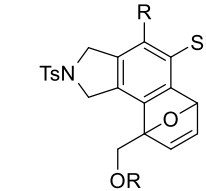
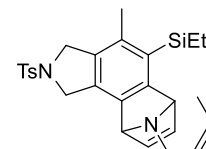
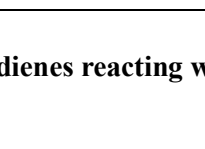
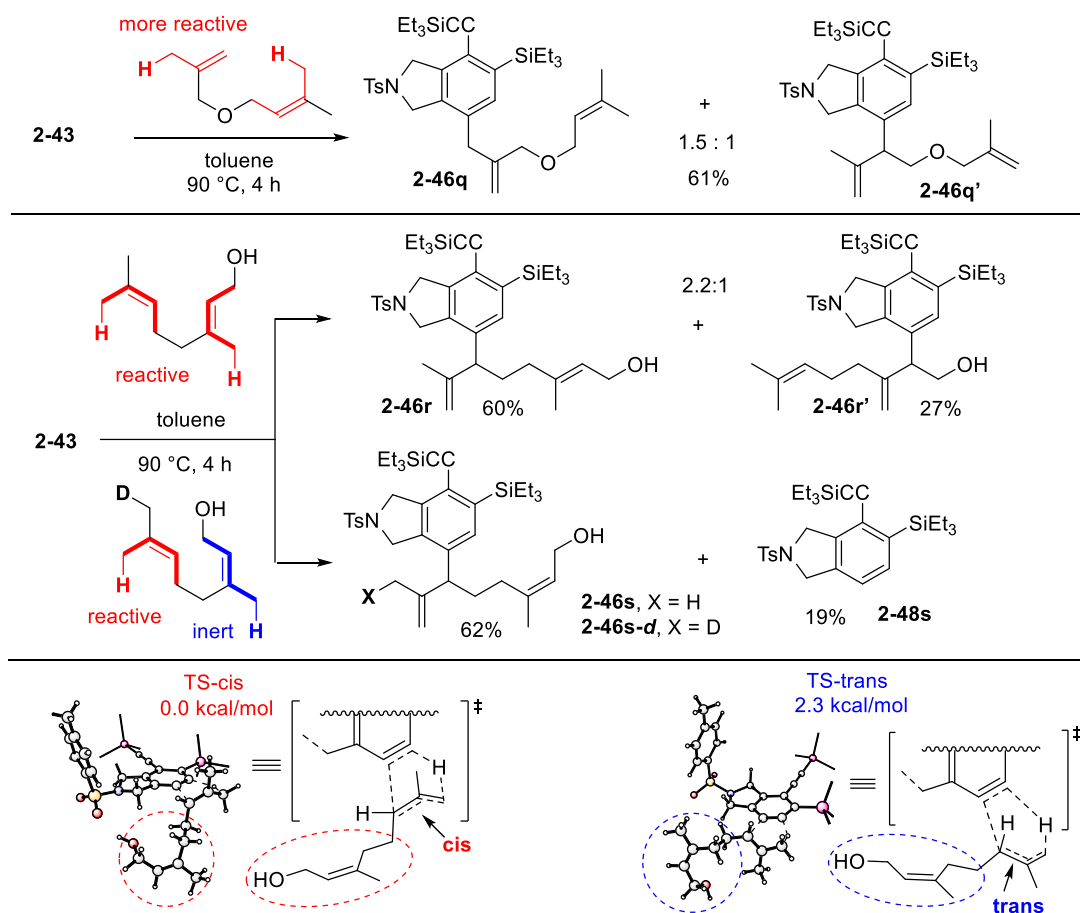
	0
	76
	72
	87

Table 2.4. Alder-ene vs. Diels-Alder reaction of 1,3-dienes reacting with an aryne

mixture of **2-49c** and Diels-Alder product **2-50c** in 52% overall yield (entry 3). From cyclic dienes such as furan and pyrrole regardless of the tethered alkene, only Diels-Alder reaction products **2-50d-f** were obtained in good yields (entries 4–6).

2.2.6. Stereoselectivity and regioselectivity

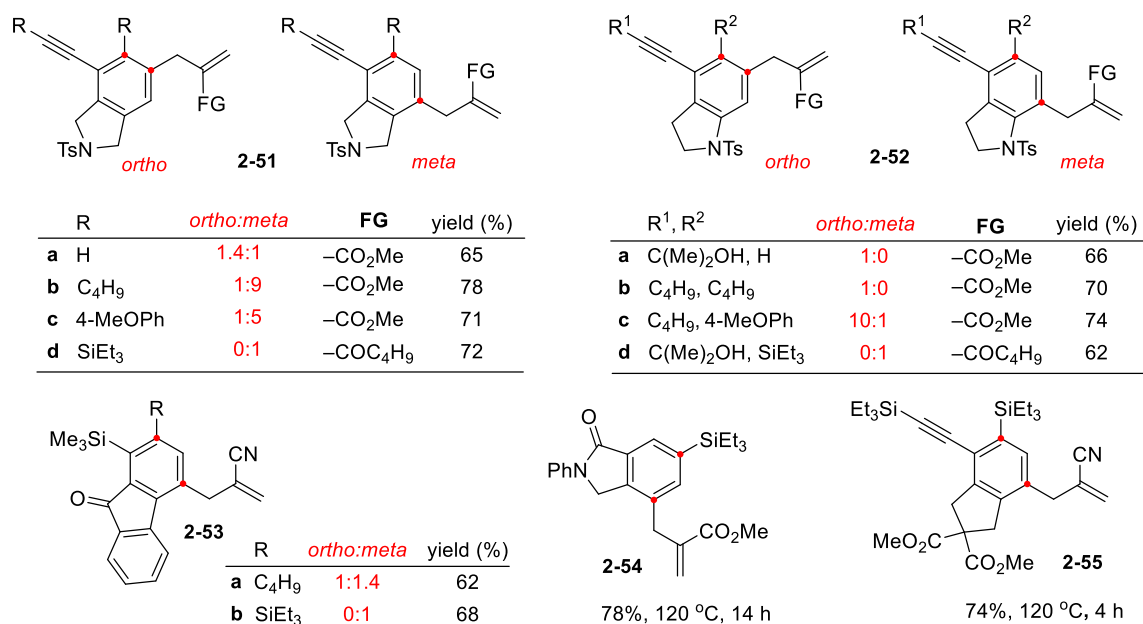
The reactivity difference between 1,1-disubstituted versus trisubstituted alkenes and the allylic C–H bonds of *cis*- and *trans*-disposed methyl groups are further examined (**Scheme 2.15**).³⁹ When methallylprenyl ether was heated with tetrayne **2-43**, a mixture of **2-46q** and **2-46q'** was obtained in 61% yield (1.5:1), which suggests that 1,1-disubstituted alkenes are slightly more reactive than trisubstituted alkenes. The reactivity of geometrical isomers of trisubstituted alkenes was examined with geraniol and nerol. The reaction with geraniol afforded a mixture of **2-46r** and **2-46r'** in 87% yield (2.2:1). On the other



Scheme 2.15. Reactivity of 1,1-di- and trisubstituted alkenes and isomers thereof

hand, nerol provided only single Alder-ene product **2-46s** (66%) along with a sizable amount of hydrogenation product **2-48s** (19%). The different product distribution indicates that the allylic C–H bonds on the methyl group *cis* to the substituent on the next carbon are reactive in the Alder-ene reaction, while the corresponding C–H bonds on the *trans* methyl group are inert. This is further confirmed by employing a deuterated nerol, which provided product **2-46s-d** where deuterium is completely retained in the methyl group. The transition state energies from DFT calculations⁴⁰ are consistent with this conclusion. The Alder-ene reaction with a *trans*-disposed methyl group leads to a transition state higher in energy by 3.4 kcal/mol than that of the *cis*-disposed methyl group. The *trans*-disposed methyl group becomes a pseudoequatorial substituent at the transition state, which develops an extra non-bonded interaction against the aryne moiety.

We also examined the regioselectivity (*ortho/meta*) of the Alder-ene reaction with other arynes (**Scheme 2.16**). The reaction of an *NTs*-tethered symmetrical tetrayne and methyl methacrylate afforded isoindolines **2-51a–d** in good yields where the ratio of *ortho:meta* changes from 1.4:1 (H) to only *meta* isomer **2-51d** (SiEt₃) depending on the steric bulk of the substituent. On the other hand, the reaction of an ynamide-tethered tetrayne afforded the *ortho*-isomer of indolines **2-52a–d** with Bu, H, and aryl substituent



Scheme 2.16. Regioselectivity in the Alder-ene reaction of arynes

on the aryne, but generated only the *meta*-isomer **2-52d** with SiEt₃ substituent. The aryne with a fluorenone skeleton showed substituent-dependent *ortho:meta* selectivity where a sterically less hindered butyl group afforded a 1.4:1 mixture of **2-53a-ortho** and **2-53a-meta** whereas a bulky SiEt₃ group confer an excellent control to generate only meta product **2-53b**. Similar selectivity was observed for *meta*-isomers of **2-54** and **2-55**. It is worth noting that the general regioselectivity in the Alder-ene products **2-51**, **2-53**, **2-54** and **2-55** is opposite to that of other nucleophile additions. Only indolines **2-52a–c** showed the same preference of a meta isomer in both Alder-ene reaction and other nucleophile addition reactions.

2.3. Conclusion

In summary, we have systematically investigated the reactivity and selectivity issues of the inter- and intramolecular Alder-ene reactions of arynes reacting with a variety of alkenes containing additional functional groups. In general, 1,1-disubstituted acyclic and cyclic alkenes are most favorable for Alder ene-reaction over other reactions such as hydrogenation by hydrogen transfer from an alcohol moiety or its direct addition to form aryl ethers. The reactivities of trisubstituted alkenes are slightly lower than 1,1-disubstituted alkenes and the disposition of the reacting allylic C–H bonds is crucial for their reactivity: the allylic C–H bonds of the carbon cis to the substituent on the next carbon are reactive but the corresponding C–H bonds on the trans position are inert. For acyclic 1,3-dienes containing allylic C–H bonds, an Alder-ene reaction is more favorable over a Diels-Alder reaction. On the other hand, alkene-tethered cyclic dienes such as furan and pyrrole participate in Diels-Alder reaction much more favorably over an Alder-ene process by the alkene moiety. High regioselectivity in Alder-ene reactions has been demonstrated by judiciously installing substituents with steric and electronic factors. Overall, the aryne-mediated Alder-ene reaction is an effective and green protocol for allylic C–H functionalization that has its own merit compared to other methods.

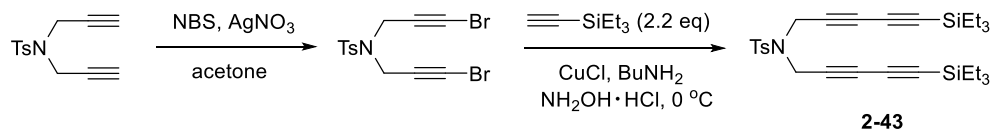
2.4. Experimental Details

2.4.1. General information

Reactions were carried out in oven-dried glassware unless otherwise noted. Compounds were purchased from Aldrich, Acros, or TCI America unless otherwise noted. Anhydrous acetonitrile and methanol from Sigma–Aldrich were used as purchased. Toluene and dichloromethane were distilled over calcium hydride (CaH_2) under nitrogen. Tetrahydrofuran was dried over sodiumbenzophenone ketyl. Acetic acid was used as purchased from Fischer Scientific. Column chromatography was performed using silica gel 60 Å (32–63 mesh) purchased from Silicycle Inc. Analytical thin layer chromatography (TLC) was performed on 0.25 mm E. Merck precoated silica gel 60 (particle size 0.040–0.063 mm). Yields refer to chromatographically and spectroscopically pure isolated compounds unless otherwise stated. ^1H NMR and ^{13}C NMR spectra were recorded on a Bruker AV-500 spectrometer. ^1H NMR chemical shifts (δ) are reported in parts per million (ppm) downfield of TMS and are referenced relative to the residual protected solvent peak (CDCl_3 (7.26 ppm)). ^{13}C chemical shifts (δ) are reported in parts per million downfield of TMS and are referenced to the carbon resonance of the solvent (CDCl_3 (77.2 ppm)). Multiplicities are indicated by s (singlet), d (doublet), t (triplet), q (quartet), quin (quintet), sext (sextet) or m (multiplet). ^1H NMR signals that fall within a ca. 0.3 ppm range are generally reported as a multiplet, with a range of chemical shift values corresponding to the peak or center of the peak. Coupling constants, J, are reported in Hz (Hertz). Electrospray ionization (ESI) and Electron impact (EI) mass spectra were recorded on a Waters Micromass Q-Tof Ultima and Micromass 70-VSE, respectively in the University of Illinois at Urbana–Champaign.

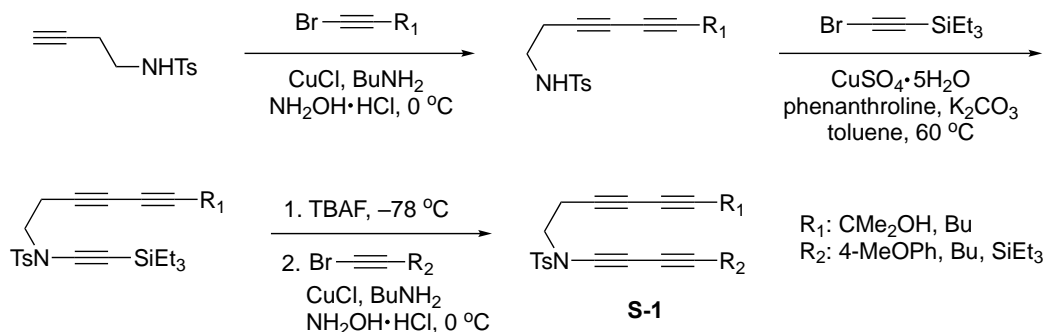
2.4.2. Preparation of substrates

Preparation of tetaryne **2-43**⁴¹



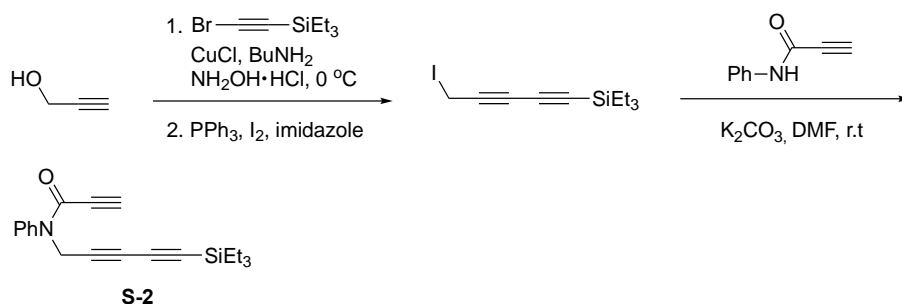
An acetone solution of diyne (**3** g, 12.1 mmol) was cooled down to $-78\text{ }^\circ\text{C}$ and degassed under vacuum and the flask was then filled with nitrogen using a balloon. To this flask was added NBS (5.4 g, 14.5 mmol) and AgNO_3 (205.9 mg, 1.21 mmol) and the reaction mixture warmed up to room temperature. After completion of the reaction (monitored by TLC), the reaction mixture was concentrated and purified by flash column chromatography (gradient elution, Hexanes–EtOAc, 20:1 to 5:1) to obtain the dibromide (**4.2** g, 85%) as a yellow solid.⁴² In a two-neck round bottom flask containing CuCl (80.5 mg, 0.81 mmol) was added 30% aqueous BuNH_2 solution under nitrogen flow. A pinch of $\text{NH}_2\text{OH} \cdot \text{HCl}$ was added until the blue color disappeared. Triethylsilyl acetylene (380 mg, 2.7 mmol) in CH_2Cl_2 was added at $0\text{ }^\circ\text{C}$ to the flask and the solution became yellow. A solution of alkynyl dibromide (**500** mg, 1.2 mmol) in CH_2Cl_2 was added dropwise at $0\text{ }^\circ\text{C}$. The reaction mixture was stirred for 5 min at room temperature. The nitrogen flow was removed, and the biphasic reaction mixture was transferred to a separatory funnel. Dichloromethane layer was separated and dried over anhydrous Na_2SO_4 . After filtration, the organic layer was concentrated and the crude material was purified by column chromatography (hexanes–EtOAc, 5:1) to obtain the tetrayne **2-43** (470 mg, 75%) as a yellow oil.

Preparation of tetaryne **S-1**⁴¹



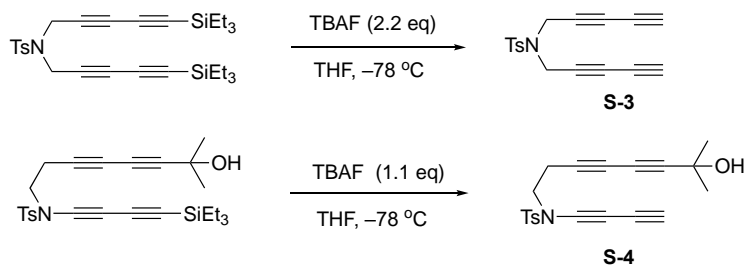
To a solution of a diyne tosylamide (1 g, 3.3 mmol) in toluene was added $\text{CuSO}_4\cdot 5\text{H}_2\text{O}$ (82.3 mg, 0.5 mmol), phenanthroline (118.8 mg, 1 mmol), K_2CO_3 (911 mg, 6.6 mmol) followed by triethylsilyl acetylene bromide (695 mg, 4.9 mmol) in toluene. The reaction mixture was heated at $65\text{ }^\circ\text{C}$ for 16 h. After completion, the reaction mixture was concentrated, filtered through a short pad of silica and washed with EtOAc (x3). The crude mixture was then purified by column chromatography (hexanes–EtOAc, 4:1) to obtain the ynamide (1.3 g, 85%) as a yellow oil.⁴³ To a solution of the ynamide (1.2 g, 2.7 mmol) in dry THF at $-78\text{ }^\circ\text{C}$ under nitrogen was added tetrabutylammonium fluoride (1 M soln in THF) (2.91 ml, 2.9 mmol) and the reaction was slowly warmed up. Upon completion, the reaction mixture was transferred to a separatory funnel, diluted with ethyl acetate, washed with water (x2) and then brine. The organic layer was separated, dried over anhydrous Na_2SO_4 , filtered, and concentrated under reduced pressure. The crude product was directly used for the next step. The triyne was subjected to coupling reaction with alkynyl bromide following typical procedure of Cadiot-Chodkiewicz coupling⁴⁴ to obtain unsymmetrical tetrayne **S-1** (200 mg, 65%) as a light-yellow oil.

Preparation of triyne amide S-2



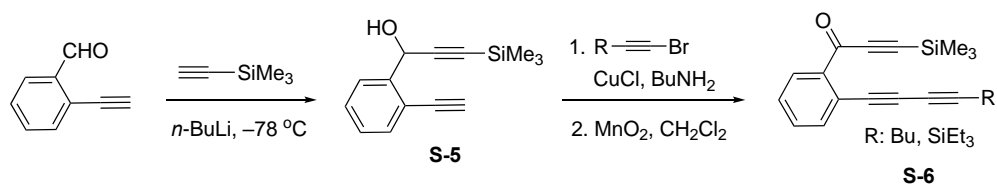
The diyne iodide was prepared by known literature procedure.⁴⁵ To a DMF solution of N-Phenyl propiolamide (150 mg, 1 mmol) was added K_2CO_3 (303 mg, 2.2 mmol) and the iodide (365.1 mg, 1.2 mmol) and stirred at rt for 16 h. The reaction mixture was concentrated, and the residue was purified by flash chromatography (hexanes–EtOAc, 5:1) to obtain the triyne amide **S-2** (202 mg, 63%) as a yellow oil.

Preparation of tetaryne S-3 and S-4



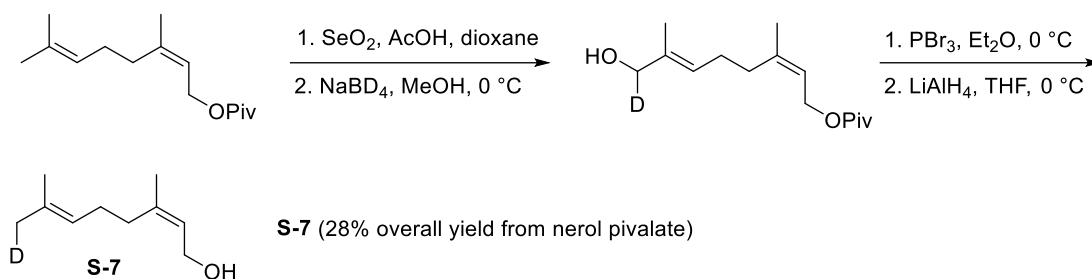
Tetraynes **S-3** and **S-4** was prepared by following the literature procedure for removal of trialkyl silyl group.

Preparation of triyne S-6



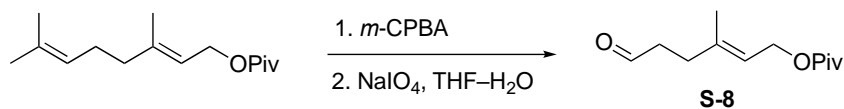
Triynes **S-6** were prepared from known compound **S-5**⁴⁶ via the coupling with bromoalkynes followed by oxidation with MnO_2 .

Preparation of deuterated nerol S-7



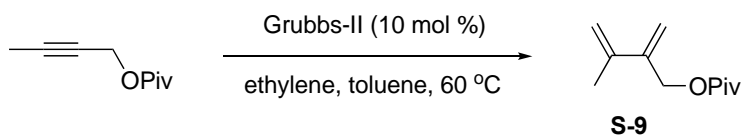
The nerol pivalate (1 g, 4.2 mmol) was dissolved in acetic acid–dioxane (5:1) mixture and SeO_2 (2.3 g, 21 mmol) was added. The mixture was stirred at room temperature for 3 h. After completion, the reaction mixture was filtered of through a short pad of celite, concentrated and purified by column chromatography (hexanes–EtOAc, 9:1). The obtained aldehyde was dissolved in MeOH under N_2 at 0°C and treated NaBD_4 (1.2 equiv) in portions and stirred for 30 min. The reaction mixture was quenched by addition of H_2O and the product was extracted with EtOAc. The organic layer was washed with brine (x2) to remove MeOH and dried over Na_2SO_4 , filtered and concentrated and was proceeded to the next step without further purification. The deuterated alcohol (150 mg, 0.6 mmol) was dissolved in Et_2O and PBr_3 (0.6 μL , 0.72 mmol) was added dropwise at 0°C . The reaction mixture was stirred for 2 h and then quenched by addition of H_2O . The product was extracted with Et_2O and the organic layer was washed with brine (x3), dried over Na_2SO_4 , filtered and concentrated. The crude material dissolved in anhydrous Et_2O was treated with LiAlH_4 (53 mg, 1.5 mmol) at 0°C . The reaction mixture was stirred for 30 min and quenched by adding 0.3 mL H_2O , 0.3 mL 1M NaOH followed by 0.6 mL H_2O to allow complete precipitation of Al salts. The supernatant was dried with anhydrous Na_2SO_4 and filtered through a short pad of silica. After concentration, the crude mixture was purified by column chromatography (hexanes–EtOAc, 5:1) to afford **S-7** (44 mg, 84% yield) as a colorless oil.

Preparation of S-8



Geranyl pivalate (500 mg, 2.1 mmol) was dissolved in CH_2Cl_2 at 30 °C and to it *m*-CPBA (398 mg, 2.3 mmol) was added. After 30 min, the reaction was quenched by addition of water and extracted with CH_2Cl_2 . The organic layer was dried over anhydrous Na_2SO_4 , filtered and concentrated under reduced pressure. The crude mixture was purified by column chromatography (hexanes–EtOAc, 20:1). The epoxide (200 mg, 0.8 mmol) was dissolved in THF– H_2O (1:1) and treated with NaIO_4 (202 mg, 0.96 mmol). After stirring for 6 h at room temperature, water was added to dissolve the white precipitate and the product was extracted with EtOAc. The organic layer was washed with brine (x2), dried over anhydrous Na_2SO_4 , filtered and concentrated. The crude aldehyde was further purified by column chromatography (hexanes–EtOAc, 5:1) to afford **S-8** (144 mg, 85%) as a yellow oil. The corresponding aldehyde from nerol was also prepared by the same procedure.

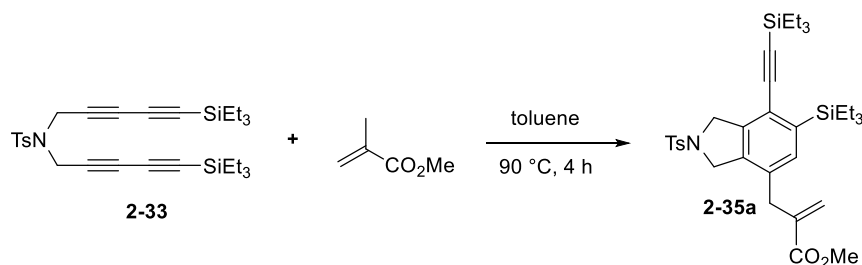
Preparation of diene S-9



To the pivalate (150 mg, 0.97 mmol) dissolved in toluene was added Grubbs-II catalyst (87 mg, 0.097mmol). The reaction mixture was then cooled to –78 °C and degassed under vacuum. After warming to 60 °C, ethylene gas (balloon) was bubbled into the reaction mixture for 15 min. The balloon was removed, and the reaction mixture was stirred for another 15 min. Toluene was removed under reduced pressure and the crude material was purified by flash chromatography (hexanes–EtOAc, 50:1) to afford pure 1,3-diene **S-9** (135 mg, 76%) as a colorless oil.

2.4.3. General procedure for tandem HDDA-Alder-ene reaction

Representative Procedure for the Tandem HDDAR–Intermolecular Alder-ene Reaction with 1.0 mmol Scale

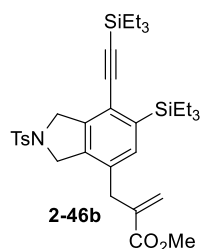


To a toluene solution (0.05 M) of tetrayne **1** (550 mg, 1.05 mmol) in a Schlenk tube was added methyl methacrylate (526 mg, 5.25 mmol). The reaction mixture was heated at 90 °C for 4 h, brought to room temperature, and concentrated under reduced pressure. The crude product was purified by column chromatography (hexanes–EtOAc, 4:1), providing product **2a** (445 mg, 68%) as a pale-yellow solid.

General Procedure for the Tandem HDDAR–Intermolecular Alder-ene Reactions

To a toluene solution (0.03–0.05 M) of tetrayne (0.05–0.06 mmol) in a Schlenk tube was added respective alkene (5 equiv). The reaction mixture was heated at 90 °C for 4 h, brought to room temperature, and concentrated under reduced pressure. The product was isolated by column chromatography (hexanes–EtOAc, 4:1).

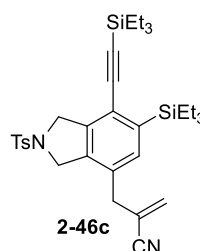
2.4.4. Characterization data



2-46b: This compound was isolated in (72% yield, 28mg) as a pale-yellow solid. ^1H

NMR (CDCl_3 , 500 MHz): δ 7.75 (d, J = 8.9 Hz, 2H), 7.31 (d, J = 7.5 Hz, 2H), 7.09 (s, 1H), 6.21 (s, 1H), 4.63 (s, 2H), 4.58 (s, 2H), 3.75 (s, 3H), 3.47 (s, 2H), 2.42 (s, 3H), 1.05 (t, J = 8.1 Hz, 9H), 0.88–0.91 (m, 15 H), 0.69 (q, J = 7.8 Hz, 6H); ^{13}C **NMR** (CDCl_3 ,

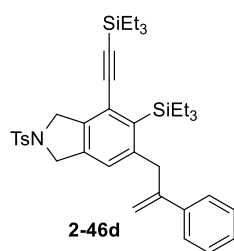
500 MHz): δ 166.9, 143.6, 140.5, 139.5, 138.1, 136.0, 135.7, 133.9, 132.1, 129.8, 126.4, 127.6, 121.9, 104.0, 100.0, 54.4, 53.4, 52.0, 35.4, 21.5, 7.4, 4.3, 3.1; **HRMS** (ESI) calcd for $\text{C}_{34}\text{H}_{50}\text{NO}_4\text{SSi}_2$ $[\text{M}+\text{H}]^+$ 624.2999, found 624.3004.



2-46c: This compound was isolated in (63% yield, 22 mg) as a pale-yellow oil. ^1H **NMR**

(CDCl_3 , 500 MHz): δ 7.75 (d, J = 8.2 Hz, 2H), 7.32 (d, J = 8.2 Hz, 2H), 7.13 (s, 1H), 5.92 (s, 1H), 5.61 (s, 1H), 4.64 (s, 2H), 4.59 (s, 2H), 3.42 (s, 3H), 1.05 (t, J = 8.2 Hz, 9H), 0.88–0.94 (m, 15 H), 0.69 (q, J = 7.8 Hz, 6H); ^{13}C **NMR** (CDCl_3 , 500 MHz): 143.8,

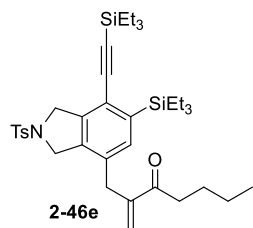
140.9, 140.4, 135.9, 135.5, 133.8, 131.4, 129.9, 128.9, 127.5, 123.1, 120.7, 117.9, 103.6, 100.7, 54.4, 53.2, 38.1, 24.8, 21.5, 7.4, 4.3, 3.1; **HRMS** (ESI) calcd for $\text{C}_{33}\text{H}_{47}\text{N}_2\text{O}_2\text{SSi}_2$ $[\text{M}+\text{H}]^+$ 591.2897, found 591.2896.



2-46d: This compound was isolated in (64% yield, 21 mg) as a colorless oil. ^1H **NMR**

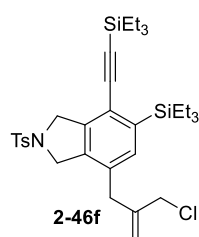
(CDCl_3 , 500 MHz): δ 7.74 (d, J = 8.6 Hz, 2H), 7.27–7.35 (m, 7H), 7.07 (s, 1H), 5.39 (s, 1H), 4.85 (s, 1H), 4.62 (s, 2H), 3.67 (s, 2H), 2.41 (s, 3H), 1.04 (t, J = 7.8 Hz, 9H), 0.83–0.87 (m, 15H), 0.68 (q, J = 7.9 Hz, 6H); ^{13}C **NMR** (CDCl_3 , 500 MHz): δ 145.3,

143.6, 140.5, 140.3, 139.2, 135.9, 135.8, 133.1, 129.8, 128.3, 127.6, 125.6, 121.5, 114.7, 104.1, 99.5, 54.4, 53.6, 39.2, 21.5, 7.45, 7.39, 4.3, 3.1; **HRMS** (ESI) calcd for $\text{C}_{38}\text{H}_{52}\text{NO}_2\text{SSi}_2$ $[\text{M}+\text{H}]^+$ 642.3257, found 642.3275.



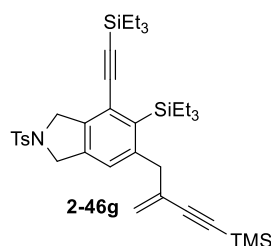
2-46e: This compound was isolated in (81% yield, 26mg) as a white solid. ^1H NMR (CDCl_3 , 500 MHz): δ 7.75 (d, J = 7.6 Hz, 2H), 7.31 (d, J = 7.6 Hz, 2H), 7.04 (s, 1H), 6.04 (s, 1H), 5.43 (s, 1H), 4.63 (s, 2H), 4.57 (s, 2H), 3.43 (s, 2H), 2.67 (t, J = 7.4 Hz, 2H), 1.52–1.58 (m, 2H), 1.30 (sext, J = 7.9 Hz, 2H), 1.05 (t, J = 8.3 Hz, 9H),

0.85–0.92 (m, 15H), 0.68 (q, J = 7.9 Hz, 6H); ^{13}C NMR (CDCl_3 , 500 MHz): δ 201.2, 146.4, 143.6, 140.4, 139.4, 136.0, 135.6, 133.9, 132.7, 129.8, 127.6, 121.7, 125.1, 104.0, 99.7, 54.5, 53.5, 37.5, 34.3, 26.6, 22.4, 21.5, 13.9, 7.4, 4.3, 3.1; **HRMS** (ESI) calcd for $\text{C}_{37}\text{H}_{56}\text{NO}_3\text{SSi}_2$ $[\text{M}+\text{H}]^+$ 650.3519, found 650.3539.



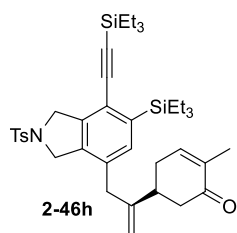
2-46f: This compound was isolated in (75% yield, 18 mg) as a colorless oil. ^1H NMR (CDCl_3 , 500 MHz): δ 7.75 (d, J = 8.1 Hz, 2H), 7.31 (d, J = 8.0 Hz, 2H), 7.13 (s, 1H), 5.18 (s, 1H), 4.81 (s, 1H), 4.63 (s, 2H), 4.60 (s, 2H), 3.89 (s, 2H), 3.38 (s, 2H), 2.40 (s, 3H), 1.05 (t, J = 8.0 Hz, 9H), 0.87–0.92 (m, 15H), 0.69 (q, J = 8.1 Hz, 6H); ^{13}C NMR

(CDCl_3 , 500 MHz): δ 143.6, 142.5, 140.6, 139.6, 136.1, 133.9, 133.8, 131.8, 129.8, 127.6, 122.1, 116.8, 103.9, 99.9, 54.4, 53.3, 47.4, 37.1, 21.5, 7.4, 4.3, 3.1; **HRMS** (ESI) calcd for $\text{C}_{33}\text{H}_{49}\text{NO}_2\text{SSi}_2\text{Cl}$ $[\text{M}+\text{H}]^+$ 614.2711, found 614.2742.

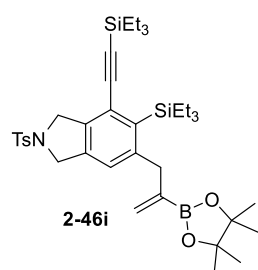


2-46g: This compound was isolated in (62% yield, 23mg) as a pale-yellow solid. ^1H NMR (CDCl_3 , 500 MHz): δ 7.75 (d, J = 7.8 Hz, 2H), 7.31 (d, J = 8.3 Hz, 2H), 7.14 (s, 1H), 5.43 (s, 1H), 5.08 (s, 1H), 4.60–4.65 (m, 4H), 3.32 (s, 2H), 2.40 (s, 3H), 1.05 (t, J = 7.9 Hz, 9H), 0.88–0.93 (m, 15H), 0.69 (q, J = 7.8 Hz, 6H); ^{13}C

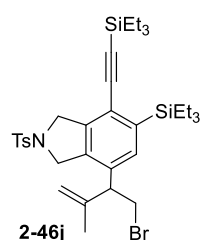
NMR (CDCl_3 , 500 MHz): δ 143.6, 140.3, 139.4, 136.0, 135.8, 134.0, 131.9, 129.8, 128.8, 127.6, 123.4, 121.9, 104.8, 104.1, 99.7, 94.9, 54.4, 53.4, 40.6, 27.3, 21.5, 7.49, 7.46, 4.3, 3.2, 0.2; **HRMS** (ESI) calcd for $\text{C}_{39}\text{H}_{56}\text{NO}_3\text{SSi}_2$ $[\text{M}+\text{H}]^+$ 674.3519, found 674.3517.



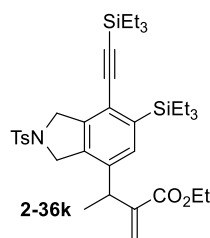
2-46h: This compound was isolated in (58% yield, 30mg) as a yellow solid. ^1H NMR (CDCl_3 , 500 MHz): 7.74 (d, $J = 8.2$ Hz, 2H), 7.31 (d, $J = 8.4$ Hz, 2H), 7.06 (s, 1H), 6.68–6.72 (m, 1H), 4.90 (s, 1H), 4.58–4.67 (m, 3H), 4.50–4.58 (m, 2H), 3.24 (s, 2H), 2.52–2.60 (m, 2H), 2.41 (s, 3H), 2.22–2.40 (m, 3H), 1.76 (m, 3H), 1.05 (t, $J = 7.7$ Hz, 9H), 0.86–0.92 (m, 15H), 0.68 (q, $J = 7.9$ Hz, 6H); ^{13}C NMR (CDCl_3 , 500 MHz): 199.1, 147.9, 144.0, 143.7, 140.6, 139.5, 136.0, 135.7, 135.6, 133.9, 132.6, 129.8, 127.5, 121.9, 112.2, 103.9, 99.9, 54.4, 53.4, 43.3, 40.5, 38.9, 31.6, 21.5, 15.6, 7.4, 4.3, 3.1; **HRMS** (ESI) calcd for $\text{C}_{37}\text{H}_{56}\text{NO}_2\text{SSi}_3$ $[\text{M}+\text{H}]^+$ 662.3340, found 662.3320.



2-46i: This compound was isolated in (56% yield, 18 mg) as a colorless oil. ^1H NMR (CDCl_3 , 500 MHz): δ 7.75 (d, $J = 8.3$ Hz, 2H), 7.30 (d, $J = 8.1$ Hz, 2H), 7.09 (s, 1H), 5.82 (s, 1H), 5.36 (s, 1H), 4.62 (s, 2H), 4.60 (s, 2H), 3.30 (s, 2H), 2.40 (s, 3H), 1.20 (s, 12H), 1.05 (t, $J = 7.7$ Hz, 9H), 0.86–0.92 (m, 15H), 0.68 (q, $J = 7.8$ Hz, 6H); ^{13}C NMR (CDCl_3 , 500 MHz): δ 143.5, 140.1, 138.9, 138.2, 136.0, 135.9, 134.3, 134.0, 130.4, 129.8, 127.6, 121.1, 104.3, 99.2, 83.7, 54.4, 53.6, 38.5, 24.7, 21.5, 7.5, 4.4, 3.2; **HRMS** (ESI) calcd for $\text{C}_{38}\text{H}_{59}\text{NO}_4\text{SSi}_3\text{B}$ $[\text{M}+\text{H}]^+$ 692.3796, found 692.3784.

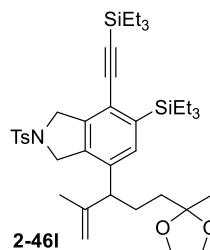


2-46j: This compound was isolated in (45% yield, 17mg) as a colorless oil. ^1H NMR (CDCl_3 , 500 MHz): δ 7.75 (d, $J = 7.2$ Hz, 2H), 7.30 (d, $J = 7.3$ Hz, 2H), 7.14 (s, 1H), 4.98 (s, 1H), 4.87 (s, 1H), 4.58–4.69 (m, 4H), 3.73 (dd, $J = 3.7, 6.2$ Hz, 1H), 3.59 (t, $J = 9.9$ Hz, 1H), 2.40 (s, 3H), 1.05 (t, $J = 7.8$ Hz, 9H), 0.87–0.93 (m, 15H); ^{13}C NMR (CDCl_3 , 500 MHz): δ 143.7, 143.3, 140.7, 139.4, 136.1, 134.0, 133.9, 132.5, 129.8, 127.6, 122.4, 113.5, 103.9, 100.1, 54.4, 53.4, 52.1, 33.3, 21.5, 7.4, 4.3, 3.2; **HRMS** (ESI) calcd for $\text{C}_{34}\text{H}_{51}\text{NO}_2\text{SSi}_2\text{Br}$ $[\text{M}+\text{H}]^+$ 672.2362, found 672.2365.



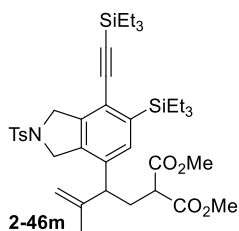
2-46k: This compound was isolated in (65% yield, 22mg) as a white solid. **¹H NMR** (CDCl₃, 500 MHz): δ 7.77 (d, *J* = 8.44, 2H), 7.31 (d, *J* = 8.8 Hz, 2H), 7.07 (s, 1H), 6.30 (s, 1H), 5.53 (s, 1H), 4.7 (s, 1H), 4.66 (s, 1H), 4.63 (s, 2H), 4.06 (dq, *J* = 8.0 Hz, 1.9 Hz, 2H), 3.83 (q, *J* = 7.4 Hz, 1H), 2.40 (s, 3H), 1.32 (d, 3H), 1.13 (t, *J* = 7.1 Hz, 3H),

1.04 (t, *J* = 7.4 Hz, 9H), 0.86–0.89 (m, 15H), 0.68 (q, *J* = 7.9 Hz, 6H); **¹³C NMR** (CDCl₃, 500 MHz): δ 166.4, 143.6, 143.5, 140.4, 139.4, 138.2, 135.2, 134.0, 132.3, 129.8, 127.6, 124.0, 121.6, 104.1, 99.5, 60.7, 54.4, 53.4, 37.6, 21.5, 19.4, 14.0, 7.45, 7.42, 4.34. 3.20; **HRMS** (ESI) calcd for C₃₆H₅₄NO₄SSi₂ [M+H]⁺ 652.3312, found 652.3299.



2-46l: This compound was isolated in (52% yield, 26mg) as a colorless oil. **¹H NMR** (CDCl₃, 500 MHz): δ 7.75 (d, *J* = 7.6 Hz, 2H), 7.29 (d, *J* = 7.8 Hz, 2H), 7.16 (s, 1H), 4.83 (s, 1H), 4.82 (s, 1H), 4.63 (s, 2H), 4.62 (s, 2H), 3.90–3.94 (m, 1H), 3.83–3.86 (m, 1H), 3.08 (t, *J* = 8.0 Hz, 1H), 2.39 (s, 3H), 1.85–1.93 (m, 1H), 1.73–1.82 (m, 1H), 1.48

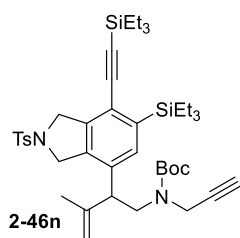
(s, 3H), 1.27 (s, 3H), 1.05 (t, *J* = 7.9 Hz, 9H), 0.89–0.91 (m, 15H), 0.68 (q, *J* = 7.9 Hz, 6H); **¹³C NMR** (CDCl₃, 500 MHz): δ 145.4, 143.5, 140.4, 139.0, 136.8, 136.0, 134.0, 132.8, 129.8, 127.6, 121.4, 112.0, 109.8, 104.1, 99.4, 64.6, 54.4, 53.4, 50.1, 37.1, 26.3, 23.8, 21.5, 20.3, 7.4, 4.3, 3.2; **HRMS** (ESI) calcd for C₃₉H₆₀NO₄SSi₂ [M+H]⁺ 694.3782, found 694.3779.



2-46m: This compound was isolated in (58%, 25mg) as a pale-yellow solid. **¹H NMR** (CDCl₃, 500 MHz): δ 7.76 (d, *J* = 8.4 Hz, 2H), 7.30 (d, *J* = 8.2 Hz, 2H), 7.13 (s, 1H), 4.91 (s, 1H), 4.86 (s, 1H), 4.61 (s, 1H), 3.73 (s, 4H), 3.69 (s, 1H), 3.25 (t, *J* = 7.2 Hz, 1H), 3.13 (t, *J* = 8.0 Hz, 1H), 2.38–2.45 (m, 1H), 2.21–2.28 (m, 1H), 1.48 (s, 1H),

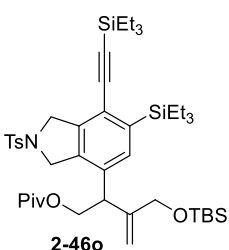
1.05 (t, 3H), 0.87–0.92 (s, 1H), 0.68 (q, 6H); **¹³C NMR** (CDCl₃, 500 MHz): δ 169.6, 169.5, 144.1, 143.6, 140.7, 139.4, 136.1, 135.3, 133.9, 129.8, 128.6, 127.6, 122.0, 112.8, 103.9, 99.9, 54.3, 53.2, 52.65, 52.61,

49.7, 47.6, 31.0, 21.5, 20.5, 7.5, 7.4, 4.3, 3.1; **HRMS** (ESI) calcd for $C_{39}H_{58}NO_6SSi_2$ $[M+H]^+$ 724.3523, found 724.3509.



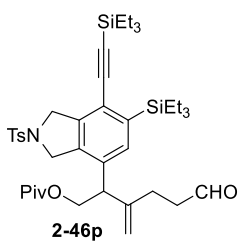
2-46n: This compound was isolated in (54% yield, 15mg) as yellow oil. **¹H NMR** (CDCl₃, 500 MHz): δ 7.74 (d, J = 7.8 Hz, 2H), 7.30 (d, J = 7.8 Hz, 2H), 7.18 (s, 1H), 4.89–4.97 (m, 1H), 4.87 (s, 1H), 4.51–4.72 (m, 4H), 3.85–3.99 (m, 1H), 3.36–3.56 (m, 2H), 2.40 (s, 3H), 2.14 (s, 1H), 1.53 (s, 3H), 1.43 (s, 9H), 1.05 (t, J = 7.8 Hz, 9H),

0.87–0.93 (m, 15H), 0.68 (q, J = 7.86, 6H); **¹³C NMR** (CDCl₃, 500 MHz): δ 154.8, 143.6, 140.6, 139.4, 136.4, 135.1, 134.7, 133.9, 133.3, 130.0, 129.8, 127.6, 112.9, 105.4, 103.9, 80.6, 79.1, 72.0, 54.3, 53.4, 48.0, 36.8, 36.1, 28.3, 21.5, 21.3, 7.4, 4.3, 3.1; **HRMS** (ESI) calcd for $C_{42}H_{63}N_2O_4SSi_2Br$ $[M+H]^+$ 747.4047, found 747.4033.



2-46o: This compound was isolated in (45% yield, 16 mg) as a yellow solid. **¹H NMR** (CDCl₃, 500 MHz): δ 7.76 (d, J = 8.3 Hz, 2H), 7.31 (d, J = 8.2 Hz, 2H), 7.17 (s, 1H), 5.24 (s, 1H), 4.92 (s, 1H), 4.61–4.67 (m, 4H), 4.32–4.38 (m, 2H), 3.89 (dd, J = 10.5, 14.0 Hz, 2H), 3.65 (t, J = 7.4 Hz, 1H), 2.4 (s, 3H), 1.05 (t, J = 8.0 Hz, 9H),

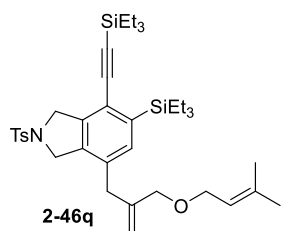
1.01 (s, 9H), 0.86–0.91 (m, 15H), 0.86 (s, 9H), 0.69 (q, J = 8.1 Hz, 6H); **¹³C NMR** (CDCl₃, 500 MHz): δ 178.1, 146.1, 143.6, 140.5, 139.4, 136.2, 134.0, 133.5, 133.2, 129.8, 127.6, 122.1, 111.8, 103.9, 99.9, 65.3, 64.7, 54.4, 53.4, 43.9, 29.7, 27, 25.8, 21.5, 18.3, 7.4, 4.3, 3.1, –5.4; **HRMS** (ESI) calcd for $C_{45}H_{74}NO_5SSi_3$ $[M+H]^+$ 824.4596, found 824.4621.



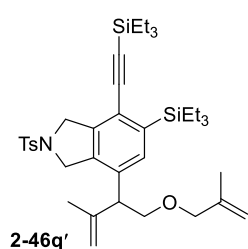
2-46p: This compound was isolated in (35% yield, 18mg) as a colorless oil. **¹H NMR** (CDCl₃, 500 MHz): δ 9.65 (t, J = 2.0 Hz, 1H), 7.77 (d, J = 8.1 Hz, 2H), 7.32 (d, J = 8.1 Hz, 2H), 7.15 (s, 1H), 4.97 (s, 1H), 4.95 (s, 1H), 4.61–4.70 (m, 4H), 4.28–4.39 (m, 2H), 3.55 (t, J = 7.4 Hz, 1H), 2.47 (t, J = 7.4 Hz, 2H), 2.41 (s, 3H),

2.09–2.24 (m, 2H), 1.05 (t, J = 7.8 Hz, 9H), 1.03 (s, 9H), 0.86–0.92 (m, 15H), 0.69 (q, J = 7.9 Hz, 6H); **¹³C**

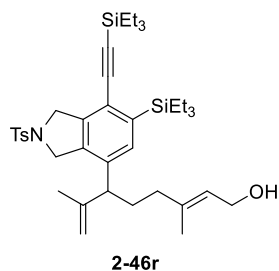
NMR (CDCl₃, 500 MHz): δ 200.9, 178.1, 144.9, 143.7, 140.7, 139.7, 136.14, 133.9, 133.2, 129.9, 128.3, 127.6, 122.4, 112.4, 103.8, 100.2, 64.3, 54.3, 53.4, 47.8, 41.7, 38.6, 27.0, 29.9, 21.5, 7.4, 4.3, 3.1; **HRMS** (ESI) calcd for C₃₈H₅₂NO₂SSi₂ [M+H]⁺ 736.3887, found 736.3888.



2-46q: This compound was isolated in (37% yield, 13mg) as a yellow oil. **¹H NMR** (CDCl₃, 500 MHz): δ 7.75 (d, *J* = 8.0 Hz, 2H), 7.30 (d, *J* = 8.3 Hz, 2H), 7.10 (s, 1H), 5.31 (t, *J* = 5.4 Hz, 1H), 5.06 (s, 1H), 4.14 (s, 1H), 4.63 (s, 2H), 4.59 (s, 2H), 3.89 (d, *J* = 7.0 Hz, 2H), 3.78 (s, 2H), 3.25 (s, 2H), 2.40 (s, 3H), 1.75 (s, 3H), 1.65 (s, 3H), 1.05 (t, *J* = 7.8 Hz, 9H), 0.86–0.92 (m, 15H), 0.68 (q, *J* = 8.1 Hz, 6H); **¹³C NMR** (CDCl₃, 500 MHz): δ 143.7, 143.6, 140.4, 139.01, 138.98, 136.1, 135.8, 134.0, 132.8, 129.8, 127.6, 121.6, 121.0, 113.8, 104.1, 99.5, 72.4, 66.7, 54.4, 53.4, 37.3, 25.8, 21.5, 18.0, 7.5, 4.3, 3.1; **HRMS** (ESI) calcd for C₃₈H₅₈NO₃SSi₂ [M+H]⁺ 664.3676, found 664.3701.

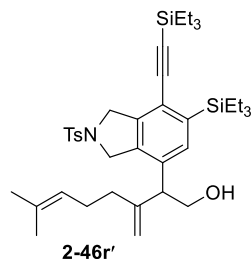


2-46q': This compound was isolated in (24% yield, 9mg) as a yellow oil. **¹H NMR** (CDCl₃, 500 MHz): δ 7.75 (d, *J* = 8.3 Hz, 2H), 7.29 (d, *J* = 8.3 Hz, 2H), 7.18 (s, 1H), 4.93 (s, 1H), 4.82 (d, *J* = 8.5 Hz, 2H), 4.57–4.69 (m, 4H), 3.79 (dd, *J* = 9.4, 13.0 Hz, 2H), 3.73 (dd, *J* = 3.2, 6.1, 1H), 3.59 (t, *J* = 9.1 Hz, 3H), 3.40 (t, *J* = 6.8 Hz, 1H), 2.40 (s, 3H), 1.58 (s, 3H), 1.11 (s, 3H), 1.05 (t, *J* = 7.9 Hz, 9H), 0.87–0.92 (m, 15H), 0.68 (q, *J* = 7.8 Hz, 6H); **¹³C NMR** (CDCl₃, 500 MHz): δ 143.5, 143.4, 141.9, 140.3, 139.0, 136.5, 135.0, 133.0, 130.0, 127.6, 112.6, 112.3, 104.2, 99.5, 75.2, 71.3, 54.5, 53.6, 49.8, 21.8, 21.5, 19.4, 7.4, 4.3, 3.2; **HRMS** (ESI) calcd for C₃₈H₅₈NO₃SSi₂ [M+H]⁺ 664.3676, found 664.3684.

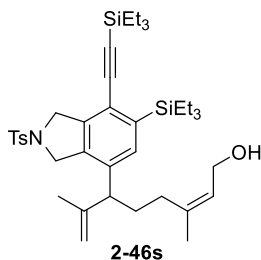


2-46r: This compound was isolated in (60% yield, 21 mg) as a colorless oil. **¹H NMR** (CDCl₃, 500 MHz): δ 7.75 (d, *J* = 8.1 Hz, 2H), 7.30 (d, *J* = 7.8 Hz, 2H), 7.16 (s, 1H), 5.32 (t, *J* = 6.9 Hz, 1H), 4.82 (s, 1H), 4.84 (s, 1H), 4.57–4.67 (m, 4H), 4.14 (d, *J* = 5.5 Hz, 2H), 3.06 (t, *J* = 6.6 Hz, 1H), 2.40 (s, 3H), 1.88–1.96 (m, 2H), 1.76–

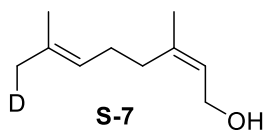
1.87 (m, 2H), 1.64 (s, 3H), 1.49 (s, 3H), 1.05 (t, $J = 7.8$ Hz, 1H), 0.88–0.91 (m, 15H), 0.68 (q, $J = 8.2$ Hz, 6H); ^{13}C NMR (CDCl_3 , 500 MHz): δ 145.4, 139.0, 132.8, 129.8, 127.6, 124.0, 111.9, 59.3, 54.4, 53.4, 49.5, 37.4, 30.1, 21.5, 20.5, 7.4, 4.3, 3.2; **HRMS** (ESI) calcd for $\text{C}_{39}\text{H}_{60}\text{NO}_3\text{SSi}_2$ $[\text{M}+\text{H}]^+$ 678.3832, found 678.3848.



2-46r': This compound was isolated in 27% yield (colorless oil) as a (2:3) inseparable mixture with geraniol. ^1H NMR (CDCl_3 , 500 MHz): δ 7.75 (d, $J = 8.4$ Hz, 2H), 7.30 (d, $J = 8.2$ Hz, 2H), 7.19 (s, 1H), 5.07 (s, 1H), 4.96 (t, $J = 8.0$ Hz, 1H) 4.93 (s, 1H), 4.55–4.70 (m, 4H), 3.91–3.97 (m, 1H), 3.73–3.79 (m, 1H), 3.38 (t, $J = 6.7$ Hz, 1H), 2.06–2.14 (m, 4H), 1.64 (s, 1H), 1.53 (s, 1H), 1.05 (t, $J = 7.8$ Hz, 9H), 0.86–0.92 (m, 15H), 0.68 (q, $J = 7.9$ Hz, 6H); ^{13}C NMR (CDCl_3 , 500 MHz): δ 153.6, 147.1, 143.6, 140.6, 139.5, 136.4, 134.1, 133.8, 133.2, 129.8, 127.6, 122.2, 111.6, 103.9, 99.9, 63.8, 54.4, 53.5, 51.2, 35.3, 29.7, 25.6, 21.5, 7.4, 4.3, 3.2; **HRMS** (ESI) calcd for $\text{C}_{39}\text{H}_{60}\text{NO}_3\text{SSi}_2$ $[\text{M}+\text{H}]^+$ 678.3832, found 678.3844.

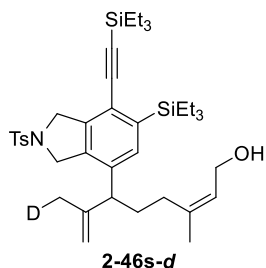


2-46s: This compound was isolated in (66%, 24mg, colorless oil) yield along with 19% hydrogenation product. ^1H NMR (CDCl_3 , 500 MHz): δ 7.75 (d, $J = 7.5$ Hz, 2H), 7.30 (d, $J = 8.5$ Hz, 2H), 7.15 (s, 1H), 5.39 (t, $J = 7.7$ Hz, 1H), 4.85 (s, 1H), 4.82 (s, 1H), 4.62 (s, 4H), 3.84–3.94 (m, 2H), 3.04 (t, $J = 6.5$ Hz, 1H), 2.40 (s, 3H), 1.97–2.03 (m, 1H), 1.84–1.89 (m, 2H), 1.73–1.79 (m, 1H), 1.71 (s, 3H), 1.50 (s, 3H), 1.05 (t, $J = 8.0$ Hz, 6H), 0.88–0.93 (m, 15 H), 0.69 (q, $J = 7.8$ Hz, 9H); ^{13}C NMR (CDCl_3 , 500 MHz): δ 145.4, 140.5, 139.2, 136.6, 136.0, 133.9, 132.6, 129.8, 127.6, 124.8, 121.5, 112.0, 104.0, 99.7, 58.9, 54.4, 53.4, 49.7, 30.6, 30.0, 23.3, 21.5, 20.4, 7.4, 4.3, 3.2; **HRMS** (ESI) calcd for $\text{C}_{39}\text{H}_{60}\text{NO}_3\text{SSi}_2$ $[\text{M}+\text{H}]^+$ 678.3832, found 678.3812.



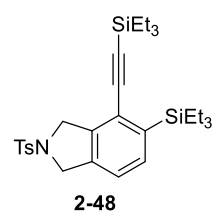
S-7: This compound was prepared in 28% overall yield from nerol pivalate (4 steps). ^1H NMR (CDCl_3 , 500 MHz): δ 5.44 (t, $J = 6.7$ Hz, 1H), 5.05–5.12 (m, 1H), 4.08 (d, $J = 7.03$ Hz, 2H), 2.03–2.13 (m, 4H), 1.75 (s, 3H), 1.67 (s, 2H), 1.60 (s, 3H); ^{13}C NMR

(CDCl₃, 500 MHz): δ 140.0, 132.4, 124.4, 123.8, 59.0, 32.0, 25.5, 25.3, 25.2, 23.4, 17.6; **HRMS** (EI) calcd for C₁₀H₁₇O²H [M]⁺ 155.1423, found 155.1420.



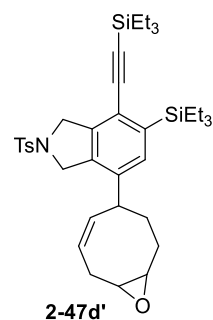
2-46s-d: This compound was isolated in (45% yield, 16 mg, colorless oil) along with hydrogenation product. **¹H NMR** (CDCl₃, 500 MHz): δ 7.75 (d, J = 6.5 Hz, 2H), 7.31 (d, J = 7.1 Hz, 2H), 7.15 (s, 1H), 5.39 (t, J = 7.0 Hz, 1H), 4.84 (s, 1H), 4.81 (s, 1H), 4.57–4.67 (m, 4H), 3.83–3.94 (m, 2H), 3.04 (t, J = 7.5 Hz, 1H), 2.40 (s, 3H), 1.97–2.06 (m, 1H), 1.83–1.90 (m, 2H), 1.73–1.79 (m, 1H), 1.71 (s, 3H),

1.48 (s, 2H), 1.05 (t, J = 7.3 Hz, 9H), 0.86–0.93 (m, 15H), 0.68 (q, J = 8.0 Hz, 6H); **¹³C NMR** (CDCl₃, 500 MHz): δ 145.3, 143.6, 140.5, 139.2, 139.1, 136.6, 136.0, 133.9, 132.6, 129.8, 127.6, 124.8, 121.5, 112.0, 104.0, 99.7, 58.9, 54.4, 53.4, 49.7, 30.6, 30.0, 23.3, 21.5, 20.3, 20.1, 20.0, 7.4, 4.3, 3.1. **HRMS** (ESI) calcd for C₃₉H₅₉NO₃SSi₂D [M+H]⁺ 679.3895, found 679.3882.



2-48: This compound was isolated in (73% yield, 22 mg) as a colorless oil from the reaction of crotyl alcohol on aryne. **¹H NMR** (CDCl₃, 500 MHz): δ 7.76 (d, J = 8.5 Hz, 2H), 7.31 (d, J = 7.6 Hz, 3H), 7.07 (d, J = 7.2 Hz, 1H), 4.64 (s, 4H), 2.40 (s, 3H), 1.06 (t, J = 8.0 Hz, 6H), 0.88–0.94 (m, 15H), 0.69 (q, J = 7.7 Hz, 9H); **¹³C NMR** (CDCl₃,

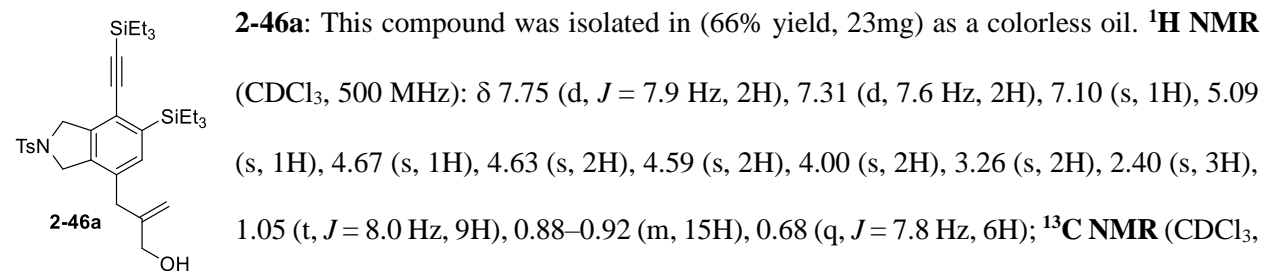
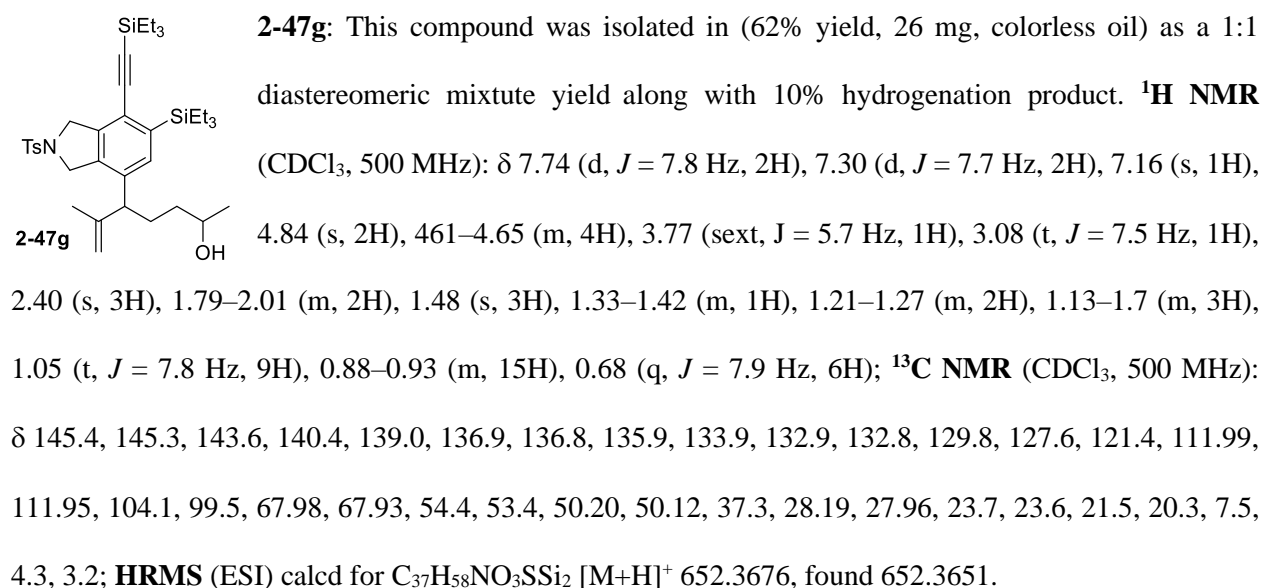
500 MHz): δ 143.6, 140.2, 138.9, 136.6, 134.6, 133.9, 129.8, 127.6, 123.8, 121.5, 103.9, 100.2, 54.4, 54.2, 21.5, 7.4, 4.3, 3.1; **HRMS** (ESI) calcd for C₂₉H₄₄NO₂SSi₂ [M+H]⁺ 526.2631, found 526.2614.



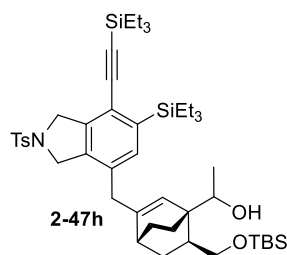
2-47d': This compound was isolated in (52% yield, 21 mg) as a yellow solid. **¹H NMR** (CDCl₃, 500 MHz): δ 7.76 (d, J = 8.4 Hz, 2H), 7.32 (d, J = 8.2 Hz, 2H), 7.22 (s, 1H), 5.57–5.63 (m, 1H), 5.26–5.32 (m, 1H), 4.56–4.67 (m, 4H), 3.63–3.70 (m, 1H), 3.24–3.28 (m, 1H), 3.00–3.04 (m, 1H), 2.90–2.98 (m, 1H), 2.51–2.59 (m, 1H), 2.41 (s, 3H), 2.19–2.26 (m, 1H), 1.79–1.93 (m, 2H), 1.57–1.64 (m, 1H), 1.05 (t, J = 7.8 Hz, 9H),

0.87–0.95 (m, 15H), 0.68 (q, J = 7.7 Hz, 6H); **¹³C NMR** (CDCl₃, 500 MHz): δ 144.2, 140.4, 139.9, 138.8,

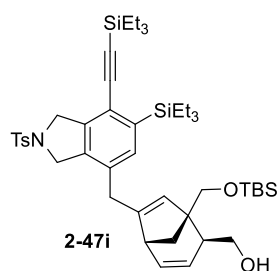
2-47f: This compound was isolated in (65% yield, 23mg, colorless oil) along with 24% of hydrogenation product. **¹H NMR** (CDCl₃, 500 MHz): δ 7.75 (d, *J* = 8.3 Hz, 2H), 7.31 (d, *J* = 8.1 Hz, 2H), 7.18 (s, 1H), 5.02 (s, 1H), 4.86 (s, 1H), 4.59–4.70 (m, 4H), 3.97 (dd, *J* = 11.5, 7.5 Hz, 1H), 3.80 (dd, *J* = 6.7, 10.9 Hz, 1H), 3.35 (t, *J* = 6.9 Hz, 1H), 2.41 (s, 3H), 1.57 (s, 3H), 1.05 (t, *J* = 7.6, 9H), 0.89–0.91 (m, 15H), 0.68 (q, *J* = 8.1 Hz, 6H); **¹³C NMR** (CDCl₃, 500 MHz): δ 143.6, 143.0, 140.7, 139.5, 136.4, 133.9, 132.7, 129.8, 127.6, 122.2, 113.3, 103.9, 100.0, 63.3, 54.4, 53.4, 52.3, 21.5, 21.4, 7.4, 4.3, 3.2; **HRMS** (ESI) calcd for C₃₄H₅₂NO₃SSi₂ [M+H]⁺ 610.3206, found 610.3188.



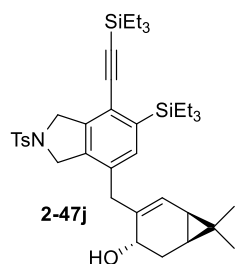
500 MHz): δ 146.0, 143.6, 140.5, 139.4, 136.1, 135.7, 135.7, 134.0, 132.6, 129.8, 127.6, 112.0, 104.0, 99.7, 65.5, 54.4, 53.4, 37.0, 21.5, 7.6, 4.3, 3.1; **HRMS** (ESI) calcd for $C_{33}H_{50}NO_3SSi_2$ $[M+H]^+$ 596.3050, found 596.3074.



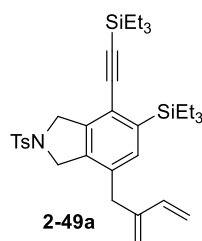
2-47h: This compound was isolated in (72% yield, 34 mg) as a white solid. **¹H NMR** (CDCl₃, 500 MHz): δ 7.75 (d, J = 8.1 Hz, 2H), 7.30 (d, J = 8.1 Hz, 2H), 7.07 (s, 1H), 5.65 (s, 1H), 4.63 (s, 2H), 4.58 (s, 2H), 4.17 (q, J = 6.4 Hz, 1H), 4.12–4.21 (m, 1H), 3.67 (dd, J = 9.6, 12.2 Hz, 2H), 3.24 (s, 2H), 2.40 (s, 3H), 2.18–2.22 (m, 1H), 2.06–2.15 (m, 1H), 1.97–2.06 (m, 1H), 1.58–1.65 (m, 1H), 1.46–1.54 (m, 1H), 1.30–1.42 (m, 2H), 1.19–1.26 (m, 1H), 1.10 (d, 3H), 1.05 (t, J = 7.8 Hz, 9H), 0.86–0.92 (m, 24 H), 0.68 (q, J = 7.6 Hz, 6H), 0.06 (s, 6H); **¹³C NMR** (CDCl₃, 500 MHz): δ 143.6, 141.8, 140.2, 139.0, 135.8, 135.4, 134.0, 133.4, 132.9, 129.8, 127.6, 121.3, 104.2, 99.4, 67.7, 66.8, 54.5, 53.4, 46.3, 42.7, 38.3, 34.9, 27.2, 25.9, 25.8, 24.8, 22.0, 21.5, 18.4, 7.4, 4.3, 3.1, –5.6; **HRMS** (ESI) calcd for $C_{47}H_{76}NO_4SSi_3$ $[M+H]^+$ 834.4803, found 834.4821.



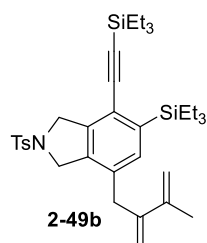
2-47i: This compound was isolated in (64% yield, 31 mg) as a yellow solid. **¹H NMR** (CDCl₃, 500 MHz): δ 7.74 (d, J = 8.0 Hz, 2H), 7.32 (d, J = 8.0 Hz, 2H), 7.07 (s, 1H), 5.72 (t, J = 7.1 Hz, 1H), 4.98 (dd, J = 3.0, 6.4 Hz, 1H), 4.94 (s, 1H), 4.62 (dd, J = 9.6, 14.5 Hz, 2H), 4.44 (dd, J = 13.4, 27.6 Hz, 2H), 3.62–3.76 (m, 5H), 3.28 (dd, J = 12.8, 15.6 Hz, 2H), 2.52 (t, J = 4.7 Hz, 1H), 2.42 (s, 3H), 2.03–2.07 (m, 1H), 1.59–1.66 (m, 2H), 1.46 (dd, J = 4.6, 5.2 Hz, 1H), 1.05 (t, J = 7.8 Hz, 9H), 0.89–0.92 (m, 15H), 0.88 (s, 9H), 0.69 (q, J = 7.6 Hz, 6H), 0.07 (s, 6H); **¹³C NMR** (CDCl₃, 500 MHz): δ 152.7, 143.7, 140.2, 139.2, 136.1, 135.3, 134.7, 133.9, 132.9, 129.8, 127.54, 127.48, 127.40, 121.6, 104.1, 99.6, 68.7, 64.5, 54.4, 53.1, 51.3, 44.2, 43.0, 39.8, 34.9, 25.7, 21.5, 18.2, 7.5, 4.3, 3.15, –5.5; **HRMS** (ESI) calcd for $C_{46}H_{72}NO_4SSi_3$ $[M+H]^+$ 818.4490, found 818.4473.



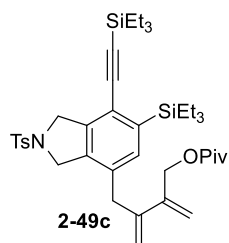
2-47j: This compound was isolated in (58% yield, 22 mg, yellow oil) along with 28% hydrogenation product. **¹H NMR** (CDCl₃, 500 MHz): δ 7.75 (d, *J* = 8.2 Hz, 2H), 7.31 (d, *J* = 7.5 Hz, 2H), 7.10 (s, 1H), 5.42–5.45 (m, 1H), 4.63 (s, 2H), 4.59 (s, 2H), 3.62 (t, *J* = 5.4, 1H), 3.29 (dd, *J* = 8.4, 15.6, 2H), 2.4 (s, 3H), 1.96–2.05 (m, 1H), 1.68–1.73 (1H, m), 1.07 (s, 3H), 1.05 (t, *J* = 7.9 Hz, 9H), 0.86–0.92 (m, 15H), 0.78 (s, 3H), 0.68 (q, 7.7 Hz, 6H) **¹³C NMR** (CDCl₃, 500 MHz): δ 143.6, 140.4, 139.3, 139.1, 136.1, 135.5, 134.0, 133.3, 129.8, 127.6, 125.2, 121.5, 104.1, 99.6, 65.5, 54.4, 53.5, 38.5, 28.8, 27.8, 23.0, 21.5, 17.4, 15.3, 7.4, 4.3, 3.1; **HRMS** (ESI) calcd for C₃₉H₅₈NO₃SSi₂ [M+H]⁺ 676.3676, found 676.3666.



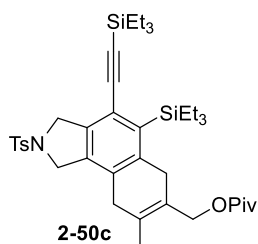
2-49a: This compound was isolated in (54% yield, 20 mg) as colorless oil. **¹H NMR** (CDCl₃, 500 MHz): δ 7.75 (d, *J* = 8.2 Hz, 2H), 7.31 (d, *J* = 8.2 Hz, 2H), 7.10 (s, 1H), 6.44 (dd, *J* = 10.2, 6.8 Hz, 1H), 5.18 (d, *J* = 17.5 Hz, 1H), 5.11 (s, 1H), 5.08 (d, *J* = 11.4 Hz, 1H), 4.64 (s, 2H), 4.62 (s, 1H), 4.56 (s, 2H), 3.38 (s, 2H), 2.41 (s, 3H), 1.05 (t, *J* = 7.8 Hz, 9H), 0.86–0.93 (m, 15H), 7.9 (q, *J* = 7.9 Hz, 6H), **¹³C NMR** (CDCl₃, 500 MHz): δ 143.6, 143.1, 140.3, 139.2, 138.4, 136.0, 135.8, 134.0, 133.0, 129.8, 127.6, 121.6, 118.0, 144.2, 104.1, 99.5, 54.4, 53.5, 35.3, 21.5, 7.4, 5.8, 3.1; **HRMS** (ESI) calcd for C₃₄H₅₀NO₂SSi₂ [M+H]⁺ 592.3101, found 592.3088.



2-49b: This compound was isolated in (58% yield, 22 mg) as a colorless oil. **¹H NMR** (CDCl₃, 500 MHz): δ 7.75 (d, *J* = 8.2 Hz, 2H), 7.31 (d, *J* = 8.3 Hz, 2H), 7.07 (s, 1H), 5.21 (s, 1H), 4.99 (s, 1H), 4.97 (s, 1H), 4.64 (s, 3H), 4.56 (s, 2H), 3.45 (s, 2H), 2.41 (s, 3H), 1.93 (s, 3H), 1.05 (t, *J* = 7.4 Hz, 6H), 0.86–0.92 (m, 15H), 0.68 (q, *J* = 8.2 Hz, 9H); **¹³C NMR** (CDCl₃, 500 MHz): δ 144.6, 143.6, 142.3, 140.3, 139.2, 135.9, 135.9, 135.6, 134.4, 134.2, 133.9, 133.8, 121.4, 114.7, 113.5, 104.2, 99.4, 54.4, 53.6, 37.3, 29.7, 21.5, 21.1, 7.4, 4.3, 3.2; **HRMS** (ESI) calcd for C₃₅H₅₂NO₂SSi₂ [M+H]⁺ 606.3257, found 606.3281.

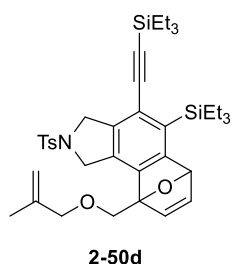


2-49c: This compound (26% yield, 11 mg) as pale-yellow solid. **¹H NMR** (CDCl₃, 500 MHz): δ 7.75 (d, *J* = 8.1 Hz, 2H), 7.31 (d, *J* = 8.2 Hz, 2H), 7.07 (s, 1H), 5.25 (s, 1H), 5.22 (s, 1H), 5.18 (s, 1H), 4.74 (s, 2H), 4.69 (s, 1H), 4.64 (s, 2H), 4.56 (s, 2H), 3.44 (s, 2H), 2.41 (s, 3H), 1.22 (s, 9H), 1.05 (t, *J* = 7.8 Hz, 9H), 0.87–0.90 (m, 15 H), 0.68 (q, *J* = 7.7 Hz, 6H); **¹³C NMR** (CDCl₃, 500 MHz): δ 180.1, 143.6, 141.9, 141.5, 140.4, 139.3, 135.9, 135.6, 133.9, 132.9, 129.8, 127.6, 121.7, 115.1, 115.0, 104.0, 99.7, 64.9, 54.4, 53.5, 41.9, 37.6, 27.2, 21.5, 7.4, 4.3, 3.1; **HRMS** (ESI) calcd for C₄₀H₆₀NO₄SSi₂ [M+H]⁺ 706.3782, found 706.3805.



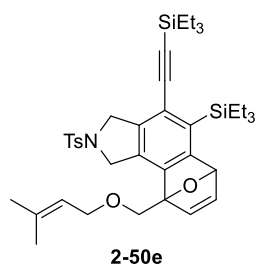
2-50c: This compound is isolated in (26% yield, 13mg) as a yellow solid. **¹H NMR** (CDCl₃, 500 MHz): δ 7.76 (d, *J* = 8.2 Hz, 2H), 7.31 (d, *J* = 7.9 Hz, 2H), 4.67 (s, 2H), 4.58–4.63 (m, 4H), 3.44 (s, 2H), 3.12 (t, *J* = 4.84 Hz, 2H), 2.41 (s, 3H), 1.84 (s, 3H), 1.20 (s, 9H), 1.01–1.09 (m, 15H), 0.91 (t, *J* = 7.7 Hz, 9H), 0.69

(q, *J* = 7.9 Hz, 6H); **¹³C NMR** (CDCl₃, 500 MHz): δ 178.6, 143.6, 141.0, 138.6, 137.4, 134.5, 133.9, 129.8, 128.7, 128.6, 127.6, 124.1, 122.6, 104.8, 101.5, 64.2, 55.2, 54.0, 38.9, 35.0, 34.1, 27.2, 21.5, 18.3, 7.9, 7.5, 5.8, 4.3; **HRMS** (ESI) calcd for C₄₀H₆₀NO₄SSi₂ [M+H]⁺ 706.3782, found 706.3781.

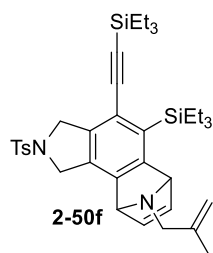


2-50d: This compound was isolated in (80% yield, 28 mg, pale-yellow solid) along with its regioisomer in a 10:1 ratio. **¹H NMR** (CDCl₃, 500 MHz): δ 7.73 (d, *J* = 7.9 Hz, 2H), 7.29 (d, *J* = 7.9 Hz, 2H), 6.99 (d, *J* = 5.9 Hz, 1H), 6.76 (d, *J* = 5.5 Hz, 1H), 5.83 (s, 1H), 5.02 (s, 1H), 4.96 (s, 1H), 4.44–4.74 (m, 4H), 4.07 (s, 2H), 2.40 (s, 3H),

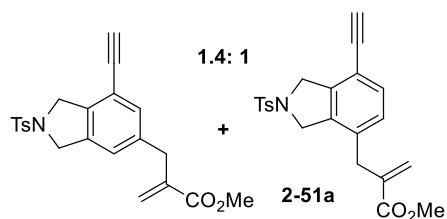
1.78 (s, 3H), 1.04 (t, *J* = 7.7 Hz, 9H), 0.87–0.92 (m, 15H), 0.68 (q, *J* = 8.1 Hz, 6H); **¹³C NMR** (CDCl₃, 500 MHz): δ 158.2, 144.6, 143.7, 142.2, 144.8, 141.4, 139.6, 133.7, 129.9, 129.3, 127.6, 119.7, 113.1, 104.7, 100.4, 91.3, 83.1, 75.9, 67.3, 54.2, 53.0, 21.5, 19.6, 7.6, 4.32, 4.29; **HRMS** (ESI) calcd for C₃₈H₅₄NO₄SSi₂ [M+H]⁺ 676.3312, found 676.3331.



2-50e: This compound was isolated in (72% yield, 26 mg, yellow solid) along with its regioisomer in a 10:1 ratio. **¹H NMR** (CDCl₃, 500 MHz): δ 7.73 (d, *J* = 8.4 Hz, 2H), 7.31 (d, *J* = 8.3 Hz, 2H), 6.99 (dd, *J* = 1.8, 4.0 Hz, 1H), 6.74 (d, *J* = 5.5 Hz, 1H), 5.81–5.83 (m, 1H), 5.4 (t, *J* = 7.3 Hz, 1H), 4.43–4.74 (m, 4H), 4.12–4.20 (m, 2H), 4.06–4.12 (m, 2H), 2.40 (s, 3H), 1.80 (s, 3H), 1.73 (s, 3H), 1.04 (t, *J* = 7.7 Hz, 9H), 0.87–0.92 (m, 15 H), 0.67 (q, *J* = 7.9 Hz, 6H); **¹³C NMR** (CDCl₃, 500 MHz): δ 158.2, 144.6, 143.6, 142.2, 141.7, 139.6, 137.7, 133.8, 129.9, 129.3, 127.6, 119.6, 104.7, 100.3, 91.3, 83.1, 68.3, 67.2, 54.2, 53.1, 25.9, 21.5, 18.1, 7.55, 7.46, 7.32, 7.30; **HRMS** (ESI) calcd for C₃₈H₅₄NO₄SSi₂ [M+H]⁺ 676.3312, found 676.3331.

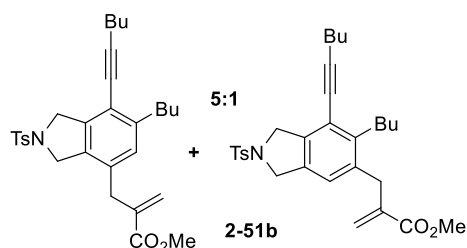


2-50f: This compound was isolated in (76% yield, 22 mg, colorless oil). **¹H NMR** (CDCl₃, 500 MHz): δ 7.75 (d, *J* = 8.1 Hz, 2H), 7.31 (d, *J* = 8.2 Hz, 2H), 6.68–6.94 (m, 2H), 4.41–4.83 (m, 8H), 2.41 (s, 3H), 1.72 (s, 3H), 1.04 (t, *J* = 7.4 Hz, 9H), 0.92–0.99 (m, 6H), 0.86–0.92 (m, 9H), 0.68 (q, *J* = 7.6 Hz, 6H); **¹³C NMR** (CDCl₃, 500 MHz): δ 143.7, 142.4, 141.5, 139.1, 133.8, 129.8, 127.6, 127.4, 112.6, 105.0, 99.9, 70.7, 70.4, 67.6, 55.9, 54.6, 52.8, 21.5, 21.2, 7.6, 7.5, 4.44, 4.35; **HRMS** (ESI) calcd for C₃₇H₅₃N₂O₂SSi₂ [M+H]⁺ 645.3366, found 645.3337.



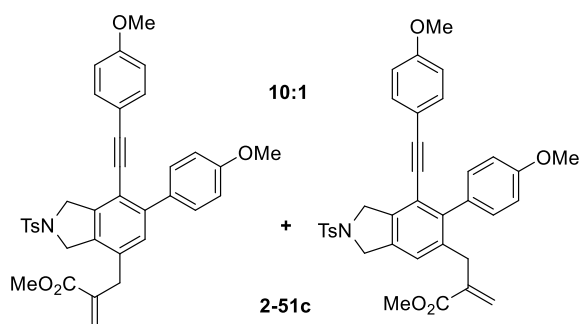
2-51a: These two mixtures of regioisomers were isolated in 1.4:1 total yield of 65% (22 mg, colorless oil). **¹H NMR** (CDCl₃, 500 MHz) *o*-isomer: δ 7.77 (d, *J* = 8.2 Hz, 2H), 7.32 (d, *J* = 8.4 Hz, 2H), 7.18 (s, 1H), 6.99 (s, 1H), 6.23 (s, 1H), 5.4 (s, 1H), 4.63 (s, 2H), 4.60 (s, 2H), 3.71 (s, H), 3.55 (s, 2H), 3.23 (s, 1H), 2.41 (s, 3H); *m*-isomer: δ 7.77 (d, *J* = 8.2 Hz, 2H), 7.32 (d, *J* = 8.4 Hz, 2H), 7.29 (d, *J* = 7.9 Hz, 2H), 7.01 (d, *J* = 7.8 Hz, 2H), 6.23 (s, 1H), 5.34 (s, 1H), 4.68 (s, 2H), 4.60 (s, 2H), 3.71 (s, 3H), 3.48 (s, 3H), 3.23 (s, 1H), 2.41 (s, 3H) **¹³C NMR** (CDCl₃, 500 MHz) (all discernable signal for both isomer): δ 166.9, 166.7, 143.7, 139.6, 139.2, 139.1, 137.7, 137.5, 136.7, 135.7,

134.1, 133.7, 131.7, 131.6, 129.9, 128.7, 127.6, 126.9, 126.7, 125.6, 117.1, 115.4, 81.6, 81.5, 54.03, 54.00, 53.6, 53.2, 52.1, 52.0, 37.7, 35.4, 21.5; **HRMS** (ESI) calcd for $C_{22}H_{22}NO_4S$ $[M+H]^+$ 608.2107, found 608.2083.



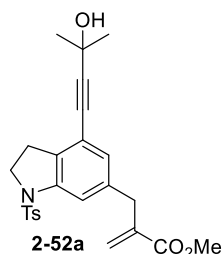
2-51b: These two mixtures of regioisomers were isolated in a total yield of (78%, 26mg) as a white solid. The characterization data for the major isomer is given. **1H NMR** ($CDCl_3$, 500 MHz):

δ 7.77 (d, J = 8.4 Hz, 2H), 7.31 (d, J = 8.2 Hz, 2H), 6.83 (s, 1H), 6.20 (s, 1H), 5.27 (s, 1H), 4.63 (s, 2H), 4.53 (s, 2H), 3.73 (s, 3H), 3.43 (s, 2H), 2.86 (t, J = 7.7 Hz, 2H), 2.45 (t, J = 6.8 Hz, 2H), 2.40 (s, 3H), 1.58–1.62 (m, 2H), 1.45–1.55 (m, 4H), 1.28–1.35 (m, 2H), 0.96 (t, J = 7.4 Hz, 3H), 0.90 (t, J = 7.2 Hz, 3H); **^{13}C NMR** ($CDCl_3$, 500 MHz): δ 166.9, 144.8, 143.6, 139.1, 138.1, 133.9, 132.5, 131.9, 129.8, 129.2, 127.6, 126.4, 123.0, 116.8, 98.4, 76.0, 54.4, 53.3, 52.2, 35.3, 33.9, 32.9, 30.9, 22.5, 22.0, 21.5, 19.3, 13.9, 13.6; **HRMS** (ESI) calcd for $C_{30}H_{38}NO_4S$ $[M+H]^+$ 508.2522, found 508.2522.

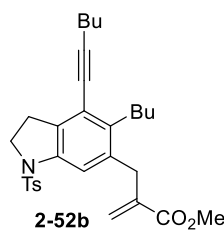


2-51c: These two mixtures of regioisomers were isolated in a total yield of (71%, 24mg) as a yellow solid. The characterization data for the major isomer is given. **1H NMR** ($CDCl_3$, 500 MHz):

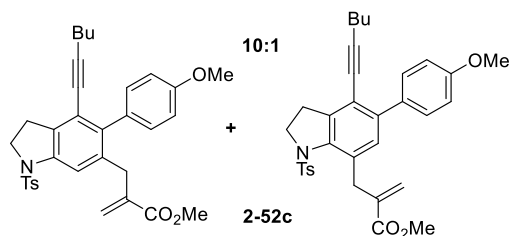
δ 7.81 (d, J = 8.1 Hz, 2H), 7.53 (d, J = 8.6 Hz, 2H), 7.33 (d, J = 8.2 Hz, 2H), 7.30 (d, J = 8.3 Hz, 2H), 7.08 (s, 1H), 6.95 (d, 2H, J = 8.2 Hz), 6.85 (d, J = 8.1 Hz, 2H), 6.24 (s, 1H), 5.39 (s, 1H), 4.80 (s, 2H), 4.65 (s, 2H), 3.85 (s, 3H), 3.82 (s, 3H), 3.74 (s, 3H), 3.52 (s, 2H), 2.41 (s, 3H); **^{13}C NMR** ($CDCl_3$, 500 MHz): δ 166.9, 159.9, 159.3, 143.7, 143.0, 139.6, 137.9, 133.8, 132.9, 132.8, 132.2, 130.8, 130.4, 129.9, 129.8, 127.6, 126.9, 126.7, 115.1, 115.1, 114.1, 113.9, 113.4, 96.6, 84.7, 55.4, 54.6, 53.4, 52.1, 35.4, 21.5; **HRMS** (ESI) calcd for $C_{36}H_{34}NO_6S$ $[M+H]^+$ 608.2107, found 608.2083.



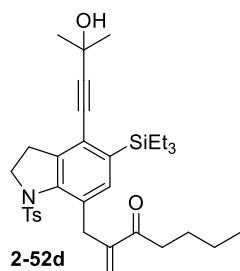
2-52a: This compound was isolated in (65% yield, 18mg) as a colorless oil. **¹H NMR** (CDCl₃, 500 MHz): δ 7.64 (d, *J* = 8.2 Hz, 2H), 7.46 (s, 1H), 7.22 (d, *J* = 8.4 Hz, 2H), 6.86 (s, 1H), 6.27 (s, 1H), 5.46 (s, 1H), 3.91 (t, *J* = 8.2 Hz, 2H), 3.76 (s, 3H), 3.59 (s, 2H), 2.92 (t, *J* = 8.5 Hz, 2H), 2.38 (s, 1H), 1.56 (s, 6H); **¹³C NMR** (CDCl₃, 500 MHz): δ 167.1, 144.2, 142.2, 139.8, 139.0, 133.6, 132.5, 127.4, 127.1, 126.6, 119.5, 115.7, 97.7, 79.3, 65.6, 51.9, 49.9, 38.0, 31.5, 27.3, 21.5; **HRMS** (ESI) calcd for C₂₅H₂₈NO₅S [M+H]⁺ 454.1688, found 454.1672.



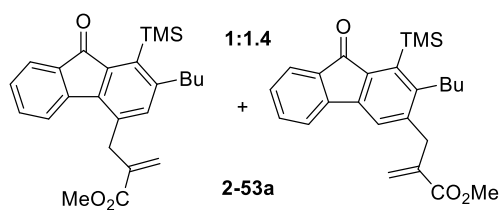
2-52b: This compound was isolated in (70% yield, 25mg) as a white solid. **¹H NMR** (CDCl₃, 500 MHz): δ 7.63 (d, *J* = 8.1 Hz, 2H), 7.3 (s, 1H), 7.20 (d, *J* = 8.2 Hz, 2H), 6.26 (s, 1H), 5.12 (s, 1H), 3.88 (t, *J* = 8.1 Hz, 2H), 3.81 (s, 3H), 3.62 (s, 2H), 2.91 (t, *J* = 8.7 Hz, 2H), 2.57–2.64 (m, 2H), 2.41 (t, *J* = 6.9 Hz, 2H), 2.37 (s, 3H), 1.51–1.56 (m, 2H), 1.40–1.48 (m, 4H), 1.33–1.39 (m, 2H), 0.85–0.95 (m, 6H); **¹³C NMR** (CDCl₃, 500 MHz): □□167.4, 144.0, 140.0, 139.5, 138.7, 135.7, 133.6, 133.1, 129.6, 127.5, 126.1, 121.2, 115.9, 97.7, 52.0, 49.9, 35.3, 32.7, 30.9, 30.6, 28.1, 23.1, 21.9, 21.5, 19.2, 13.9, 13.6; **HRMS** (ESI) calcd for C₃₀H₃₈NO₄S [M+H]⁺ 508.2522, found 508.2534.



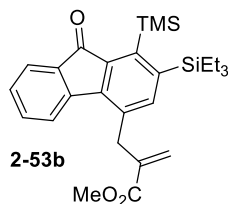
2-52c: This compound was isolated in (74% yield, 25 mg) as a yellow solid. **¹H NMR** (CDCl₃, 500 MHz): δ 7.68 (d, *J* = 8.2 Hz, 2H), 7.4 (s, 1H), 7.25 (d, *J* = 8.3 Hz, 2H), 7.06 (d, 2H, *J* = 8.2 Hz), 6.86 (d, *J* = 8.4 Hz, 2H), 6.23 (s, 1H), 5.13 (s, 1H), 3.93 (t, *J* = 8.1 Hz, 2H), 3.85 (s, 3H), 3.82 (s, 3H), 3.44 (s, 2H), 2.97 (t, *J* = 8.5 Hz, 2H), 2.4 (s, 3H), 2.14 (t, *J* = 7.2 Hz, 2H), 1.21–1.28 (m, 2H), 1.07–1.16 (m, 2H), 0.76 (t, *J* = 7.2 Hz, 3H); **¹³C NMR** (CDCl₃, 500 MHz): δ 167.4, 144.1, 140.0, 139.5, 138.7, 135.7, 133.1, 129.6, 127.4, 126.1, 11.2, 115.9, 97.7, 52.0, 49.9, 35.3, 32.7, 30.9, 30.6, 28.1, 23.1, 21.9, 21.5, 19.2, 13.9, 13.6; **HRMS** (ESI) calcd for C₃₃H₃₆NO₅S [M+H]⁺ 558.2314, found 558.2302.



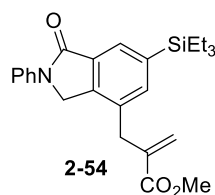
2-52d: This compound was isolated in (62% yield, 19mg) as a colorless oil. ^1H NMR (CDCl_3 , 500 MHz): δ 7.35 (d, J = 8.1 Hz, 2H), 7.14 (d, J = 7.9 Hz, 2H), 7.10 (s, 1H), 6.1 (s, 1H), 5.74 (s, 1H), 4.04 (s, 2H), 3.94 (t, J = 7.7 Hz, 2H), 2.62 (t, J = 7.7 Hz, 2H), 2.40 (m, 3H), 2.21 (t, J = 7.2 Hz, 2H), 1.52 (s, 6H), 1.24–1.30 (m, 0.84–0.92 (m, 20 H); ^{13}C NMR (CDCl_3 , 500 MHz): δ 201.5, 147.6, 144.2, 142.0, 141.2, 137.3, 136.3, 134.4, 132.7, 129.4, 127.7, 125.3, 122.4, 99.1, 80.9, 65.7, 52.2, 37.7, 34.4, 31.3, 29.1, 26.6, 22.4, 21.5, 13.9, 7.5, 3.2; **HRMS** (ESI) calcd for $\text{C}_{34}\text{H}_{48}\text{NO}_4\text{Si}$ $[\text{M}+\text{H}]^+$ 594.3073, found 594.3084.



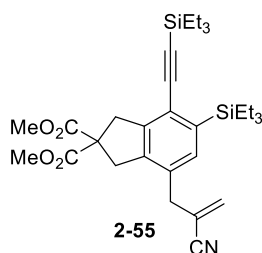
2-53a: This compound was isolated in (62% yield, 20mg) as a yellow solid. ^1H NMR (CDCl_3 , 500 MHz) major isomer: δ 7.59 (d, J = 8.2 Hz, 2H), 7.37–7.43 (m, 2H), 7.19–7.25 (m, 1H), 6.96 (s, 1H), 6.28 (s, 1H), 5.31 (s, 1H), 3.89 (s, 2H), 3.85 (s, 2H), 2.71–2.76 (m, 2H), 1.31–1.54 (m, 4H), 0.89–0.98 (m, 3H), 0.43 (s, 9H); minor isomer: δ 7.56 (d, J = 8.2 Hz, 2H), 7.37–7.43 (m, 2H), 7.33 (s, 1H), 7.20–7.25 (m, 1H), 6.31 (s, 1H), 5.35 (s, 1H), 3.81 (s, 3H), 3.70 (s, 2H), 2.71–2.76 (m, 2H), 1.31–1.54 (m, 4H), 0.89–0.98 (m, 3H), 0.44 (s, 9H); ^{13}C NMR (CDCl_3 , 500 MHz) (all discernable signal for both isomer): δ 195.3, 167.4, 167.3, 150.9, 149.0, 143.9, 143.2, 142.6, 142.3, 141.3, 139.2, 139.1, 137.9, 137.6, 134.5, 134.3, 134.2, 133.9, 133.8, 128.6, 128.1, 126.8, 126.7, 123.79, 123.75, 123.2, 122.7, 119.3, 52.2, 52.1, 36.4, 36.1, 35.9, 35.6, 35.2, 31.8, 22.8, 22.4, 14.1, 14.0, 2.9, 2.6; **HRMS** (ESI) calcd for $\text{C}_{25}\text{H}_{31}\text{O}_3\text{Si}$ $[\text{M}+\text{H}]^+$ 407.2042, found 407.2046.



2-53b: This compound was isolated in (68% yield, 24 mg) as a yellow solid. ^1H NMR (CDCl_3 , 500 MHz): δ 7.62 (d, J = 8.2 Hz, 2H), 7.37–7.44 (m, 2H), 7.35 (s, 1H), 7.24–7.28 (m, 1H), 6.29 (s, 1H), 5.31 (s, 1H), 3.92 (s, 2H), 3.85 (s, 2H), 2.04 (s, 3H), 0.84–0.97 (m, 15H), 0.42 (s, 9H); ^{13}C NMR (CDCl_3 , 500 MHz): δ 196.0, 167.4, 14.7, 146.1, 144.5, 143.8, 142.4, 141.8, 137.7, 134.5, 134.3, 134.1, 131.7, 129.1, 128.7, 126.9, 124.0, 123.8, 123.3, 121.9, 52.2, 35.3, 7.7, 5.5, 2.7; **HRMS** (ESI) calcd for $\text{C}_{27}\text{H}_{37}\text{O}_3\text{Si}_2$ $[\text{M}+\text{H}]^+$ 454.1688, found 454.1672.



2-54: This compound was isolated in (78% yield, 26mg) as a white solid. ^1H NMR (CDCl_3 , 500 MHz): δ 7.94 (s, 1H), 7.86 (d, J = 8.6 Hz, 2H), 7.49 (s, 1H), 7.40 (t, J = 7.4 Hz, 2H), 7.18 (t, J = 7.3 Hz, 1H), 6.3 (s, 1H), 5.46 (s, 1H), 4.81 (s, 2H), 3.76 (s, 3H), 3.74 (s, 2H), 0.96 (t, J = 6.8 Hz, 9H), 0.80–0.86 (m, 6H); ^{13}C NMR (CDCl_3 , 500 MHz): δ 168.0, 167.0, 139.9, 139.6, 138.9, 138.7, 138.5, 132.8, 132.1, 129.4, 129.2, 128.4, 126.4, 119.6, 52.1, 49.9, 34.5, 7.3, 3.3; **HRMS** (ESI) calcd for $\text{C}_{25}\text{H}_{32}\text{NO}_3\text{Si}$ $[\text{M}+\text{H}]^+$ 422.2151, found 422.2161.



2-55: This compound was isolated in (74% yield, 24mg) as a yellow oil. ^1H NMR (CDCl_3 , 500 MHz): δ 7.08 (s, 1H), 5.92 (s, 1H), 5.55 (s, 1H), 3.76 (s, 6H), 3.71 (s, 2H), 3.49–3.53 (m, 4H), 1.05 (t, J = 7.7 Hz, 9H), 0.90–0.96 (m, 15H), 0.69 (q, J = 7.7 Hz, 6H); ^{13}C NMR (CDCl_3 , 500 MHz): δ 172.0, 144.4, 139.6, 139.2, 135.1, 131.1, 130.1, 124.4, 121.2, 118.4, 105.0, 99.4, 60.0, 53.1, 38.2, 39.5, 38.2, 7.52, 7.46, 4.36, 3.17; **HRMS** (ESI) calcd for $\text{C}_{31}\text{H}_{46}\text{NO}_4\text{Si}_2$ $[\text{M}+\text{H}]^+$ 552.2965, found 552.2941.

2.4.5. Computational details

All DFT calculations were carried out with the Gaussian 09 suite of computational programs.^[1] The geometries of all stationary points were optimized using the B3LYP hybrid functional^[2] at the basis set level of 6-31+G(d). Frequencies were analytically computed at the same level of theory to obtain the free energies and to confirm whether the structures are minima (no imaginary frequency) or transition states (only one imaginary frequency). All transition state structures were confirmed to connect the proposed reactants and products by intrinsic reaction coordinate (IRC) calculations. All the energies given in the text are relative free energies in the gas phase, including dispersion corrections calculated by DFT-D3 (BJ) code developed by Grimme.^[3]

[1] Gaussian 09, Revision A.01, M. J. Frisch, G. W. Trucks, H. B. Schlegel, G. E. Scuseria, M. A. Robb, J. R. Cheeseman, G. Scalmani, V. Barone, B. Mennucci, G. A. Petersson, H. Nakatsuji, M. Caricato, X. Li,

H. P. Hratchian, A. F. Izmaylov, J. Bloino, G. Zheng, J. L. Sonnenberg, M. Hada, M. Ehara, K. Toyota, R. Fukuda, J. Hasegawa, M. Ishida, T. Nakajima, Y. Honda, O. Kitao, H. Nakai, T. Vreven, J. A. Montgomery, Jr., J. E. Peralta, F. Ogliaro, M. Bearpark, J. J. Heyd, E. Brothers, K. N. Kudin, V. N. Staroverov, R. Kobayashi, J. Normand, K. Raghavachari, A. Rendell, J. C. Burant, S. S. Iyengar, J. Tomasi, M. Cossi, N. Rega, J. M. Millam, M. Klene, J. E. Knox, J. B. Cross, V. Bakken, C. Adamo, J. Jaramillo, R. Gomperts, R. E. Stratmann, O. Yazyev, A. J. Austin, R. Cammi, C. Pomelli, J. W. Ochterski, R. L. Martin, K. Morokuma, V. G. Zakrzewski, G. A. Voth, P. Salvador, J. J. Dannenberg, S. Dapprich, A. D. Daniels, Ö. Farkas, J. B. Foresman, J. V. Ortiz, J. Cioslowski, D. J. Fox, Gaussian, Inc., Wallingford CT, **2009**.

[2] (a) Becke, A. D. *J. Chem. Phys.* **1993**, 98, 5648. (b) Becke, A. D. *J. Chem. Phys.* **1993**, 98, 1372. (c) Lee, C.; Yang, W.; Parr, R. G. *Phys. Rev. B* **1988**, 37, 785.

[3] (a) S. Grimme, J. Antony, S. Ehrlich, and S. Krieg, *J. Chem. Phys.* **2010**, 132, 154104. (b) S. Grimme, S. Ehrlich, and L. Goerigk, *J. Comp. Chem.* **2011**, 32, 1456.

2.5. Note

Computational study for this work has been carried out by Peipei Xie and Prof. Yuanzhi Xia from Wenzhou, University in China.

2.6. References

1. (a) Alder, K.; Pascher, F.; Schmidt, H. *Ber. Dtsch. Chem. Ges.* **1943**, 76, 27. (b) Nobel Lectures-Chemistry, 1942-1962. *Elsevier: Amsterdam* **1964**, p 253- 305. (c) Review: Hoffmann, H. M. R. *Angew. Chem., Int. Ed. Engl.* **1969**, 8, 556.
2. Woodward, R. B.; Hoffmann, R. *J. Am. Chem. Soc.* **1965**, 87, 2511.
3. (a) Paderes, G. D.; Jorgensen, W. L. *J. Org. Chem.* **1992**, 57, 1904. (b) Fernández, I.; Bickelhaupt, F. M. *J. Comput. Chem.* **2012**, 33, 509.
4. Bartlett, P. D. *Science* **1968**, 159, 833.
5. Snider, B. B. *Acc. Chem. Res.* **1980**, 13, 426 and the references therein.
6. Mikami, K.; Shimizu, M. *Chem. Rev.* **1992**, 92, 1021.
7. Salomon, M. F.; Pardo, S. N.; Salomon, R. G. *J. Am. Chem. Soc.* **1984**, 106, 3797.
8. Benner, J. P.; Gill, G. B.; Parrott, S. J.; Wallace, B.; Begley, M. J. *J. Chem. Soc., Perkin Trans. 1* **1984**, 315.
9. Brimble, M. A.; Heathcock, C. H. *J. Org. Chem.* **1993**, 58, 5261.
10. Sun, C.; Li, J.; Lee, D.; Huang, G.; Xia, Y. *Chem. Commun.* **2012**, 48, 10990.
11. Sabbasani, V. R.; Huang, G.; Xia, Y.; Lee, D. *Chem.-Eur. J.* **2015**, 21, 17210.
12. Borzilleri, R. M.; Weinreb, S. M. *Synthesis* **1995**, 347 and the references therein.
13. Demailly, G.; Solladie, G. *J. Org. Chem.* **1981**, 46, 3102.
14. Weinreb, S. M.; Parvez, M. *J. Am. Chem. Soc.* **1995**, 117, 10905.
15. Drury III, W. J.; Ferraris, D.; Cox, C.; Young, B.; Lectka, T. *J. Am. Chem. Soc.* **1998**, 120, 11006.
16. Elder, A. M.; Rich, D. H. *Org. Lett.* **1999**, 1, 1443.
17. (a) Trost, B. M.; Krische, M. J. *Synlett* **1998**, 1. (b) Pinkerton, A. B.; Toste, D. F.; Trost, B. M. *Chem. Rev.* **2001**, 101, 2067. (c) Cao, P.; Wang, B.; Zhang, X. *J. Am. Chem. Soc.* **2000**, 122, 6490. (d) Nevado, C.; Echavarren, A. M. *Chem. Soc. Rev.* **2004**, 33, 431.

18. (a) Trost, B. M.; Indolese, A. *J. Am. Chem. Soc.* **1993**, *115*, 4361. (b) Trost, B. M.; Indolese, A. F.; Müller, T. J. J.; Treptow, B. *J. Am. Chem. Soc.* **1995**, *117*, 615. (c) Trost, B. M.; Shen, H. C.; Pinkerton, A. B. *Chem.–Eur. J.* **2002**, *10*, 2341.
19. (a) Trost, B. M.; Machacek, M.; Schnaderbeck, M. J. *Org. Lett.* **2000**, *2*, 1761. (b) Trost, B. M.; Machacek, M. R. *Angew. Chem., Int. Ed.* **2002**, *41*, 4693. (c) Trost, B. M.; Machacek, M. R.; Ball, Z. T. *Org. Lett.* **2003**, *5*, 1895.
20. Hansen, E. C.; Lee, D. *J. Am. Chem. Soc.* **2005**, *127*, 3252.
21. Cho, E. J.; Lee, D. *J. Am. Chem. Soc.* **2017**, *129*, 6692.
22. Lei, A.; He, M.; Wu, S.; Zhang, X. *Angew. Chem., Int. Ed.* **2002**, *41*, 3457.
23. Gerhard, H.; Treutwein, J. *Angew. Chem., Int. Ed.* **2007**, *46*, 8500.
24. Trost, B. M.; Li, Y. *J. Am. Chem. Soc.* **1996**, *118*, 6625.
25. Yun, S. Y.; Hansen, E. C.; Volchkov, I.; Cho, E. J.; Lo, W. Y.; Lee, D. *Angew. Chem., Int. Ed.* **2010**, *49*, 4261.
26. Liron, F.; Oble, J.; Lorion, M. M.; Poli, G. *Eur. J. Org. Chem.* **2014**, *2014*, 5863–5883.
27. (a) Chen, M. S.; White, M. C. *J. Am. Chem. Soc.* **2004**, *126*, 1346. (b) Delcamp, J. H.; White, M. C. *J. Am. Chem. Soc.* **2006**, *128*, 15076. (c) Chen, M. S.; Prabakaran, N.; Labenz, N. A.; White, M. C. *J. Am. Chem. Soc.* **2005**, *127*, 6970.
28. Rice, G. T.; White, M. C. *J. Am. Chem. Soc.* **2009**, *131*, 11707.
29. (a) Young, A. J.; White, M. C. *J. Am. Chem. Soc.* **2008**, *130*, 14090. (b) Young, A. J.; White, M. C. *Angew. Chem., Int. Ed.* **2011**, *50*, 6824.
30. Nakayama, J.; Yoshimura, K. *Tetrahedron Lett.* **1994**, *35*, 2709.
31. Jayanth, T. T.; Jeganmohan, M.; Cheng, M.-J.; Chu, S.-Y.; Cheng, C.-H. *J. Am. Chem. Soc.* **2006**, *128*, 2232.
32. Chen, Z.; Liang, J.; Yin, J.; Yu, G. A.; Liu, S. H. *Tetrahedron Lett.* **2013**, *54*, 5785.

33. Trinchera, P.; Sun, W.; Smith, J. E.; Palomas, D.; Crespo-Otero, R.; Jones, C. R. *Org. Lett.* **2017**, *19*, 4644.
34. (a) Candito, D. A.; Panteleev, J.; Lautens, M. *J. Am. Chem. Soc.* **2011**, *133*, 14200. (b) Candito, D. A.; Dobrovolsky, D.; Lautens, M. *J. Am. Chem. Soc.* **2012**, *134*, 15572.
35. Karmakar, R.; Mamidipalli, P.; Yun, S. Y.; Lee, D. *Org. Lett.* **2013**, *15*, 1938.
36. Niu, D.; Hoye, T. R. *Nat. Chem.* **2014**, *6*, 34.
37. Karmakar, R.; Yun, S. Y.; Wang, K. P.; Lee, D. *Org. Lett.* **2014**, *16*, 6.
38. (a) Zhang M. X.; Shan, W.; Chen, Z.; Yin, J.; Yu, G. A.; Liu, S. H. *Tetrahedron Lett.* **2015**, *56*, 6833. (b) Pogula, V. D.; Wang, T.; Hoye, T. R. *Org. Lett.* **2015**, *17*, 856. (c) Nguyen, Q. L.; Baire, B.; Hoye, T. R. *Tetrahedron Lett.* **2015**, *56*, 3265. (d) Bhojgude, S. S.; Bhunia, A.; Biju, A. T. *Acc. Chem. Res.* **2016**, *49*, 1658.
39. Stereoselectivity of Alder-ene reactions: (a) Oppolzer, W.; Snieckus, V. *Angew. Chem., Int. Ed.* **1978**, *17*, 476. (b) Tshaen, D. M.; Turos, E.; Weinreb, S. M. *J. Org. Chem.* **1984**, *49*, 5058. (c) Thomas, B. E.; Houk, K. N. *J. Am. Chem. Soc.* **1993**, *115*, 790. (d) Griesbeck, A. G.; Bartoschek, A.; Neudörfl, J.; Miara, C. *Photochem. Photobiol.* **2006**, *82*, 1233.
40. All calculations were carried out with Gaussian 09 suite by B3LYP–D3/6-31+G* method in gas phase.
41. Hofmeister, H.; Annen, K.; Laurent, H.; Wiechert, H. *Angew. Chem., Int. Ed. Engl.* **1984**, *23*, 727–729.
42. Zhang, Y.; Hsung, R. P.; Tracey, M. R.; Kurtz, K. M. C.; Vera, E. L. *Org. Lett.* **2004**, *7*, 1151–1156.
43. a) Chodkiewicz, W. *Ann. Chim.* **1957**, *2*, 819; b) Cadiot, P.; Chodkiewicz, W. in *Chemistry of Acetylenes* (Ed.: H. G. Viehe), Marcel Dekker, New York, **1969**, pp. 597–647.
44. Karmakar, R.; Yun, S. Y.; Chen, J.; Xia, Y.; Lee, D. *Angew. Chem., Int. Ed.* **2015**, *54*, 6582–6586.
45. Hoye, T. R.; Baire, B.; Niu, D.; Willoughby, P. H.; Woods, B. P. *Nature* **2012**, *490*, 208–212.

CHAPTER 3

Intermolecular Alder-ene vs. Addition Reactions

3.1. Introduction*

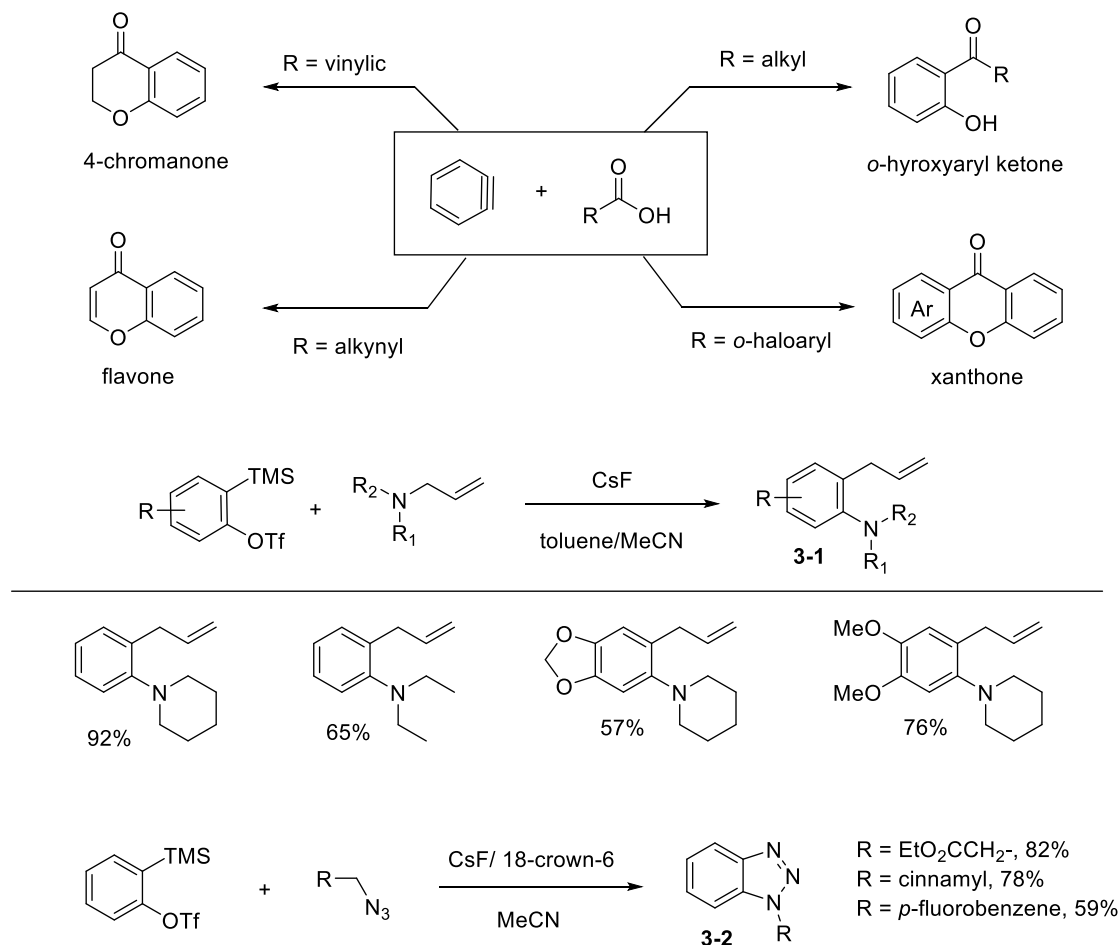
The Alder-ene reactions are an effective functionalization method for allylic C–H bonds with a concomitant 1,3-transposition of the involved alkenes.¹ Our study on intermolecular Alder-ene reaction of arynes with functionalized alkenes containing a polar functional group revealed a strong preference for an Alder-ene reaction over other processes such as addition reaction and hydrogen transfer.² For example, certain allylic alcohols reacted with arynes to form predominately Alder-ene product devoid of any addition products and acyclic 1,3-dienes also formed only Alder-ene product devoid of an Diels-Alder product. In order to expand the scope and utility of aryne-based transformations, it is desirable to obtain comprehensive information about the reactivity of arynes with structurally diverse alkenes containing a heteroatom functionality. Accordingly, we planned to explore the reactivity of arynes toward alkenes containing a polar functionality including carboxylic acid, amine, azide, and aldehyde. These polar functionalities are known to undergo addition reaction with arynes to form aryl esters and amines.³ Aldehyde are also known to form products via a [2+2] cycloaddition process.⁴ Exploring the reactivity of arynes with these functionalized alkenes would provide insight into the selectivity between Alder-ene reaction and addition reaction. The relationship between the selectivity trend and the structure of the alkene, the method of aryne generation, solvent, temperature is an important area to study.

3.1.1. Addition reaction of arynes with polar functionalities

Arynes are known to undergo addition reaction with acids, amines, and azides to form aryl esters, aryl amines, and triazoles (**Scheme 3.1**). Although the reaction of carboxylic acids with HDDA-derived arynes usually generates aryl esters through insertion into the O–H bond, arynes generated under the Kobayashi's protocol at elevated temperature undergo insertion to the C–O bond of the carboxylic acid to form *o*-hydroxyaryl ketone.⁵ With *o*-haloaryl carboxylic acid, a nucleophilic aromatic substitution led to

*This chapter has been reproduced from Gupta, S.; Xie, P.; Xia, Y.; Lee, D. "Reactivity of arynes toward functionalized alkenes: intermolecular Alder-ene vs. addition reactions" *Org. Chem. Front.* **2018**, 5, 2208–2213, with permission from The Royal Society of Chemistry.

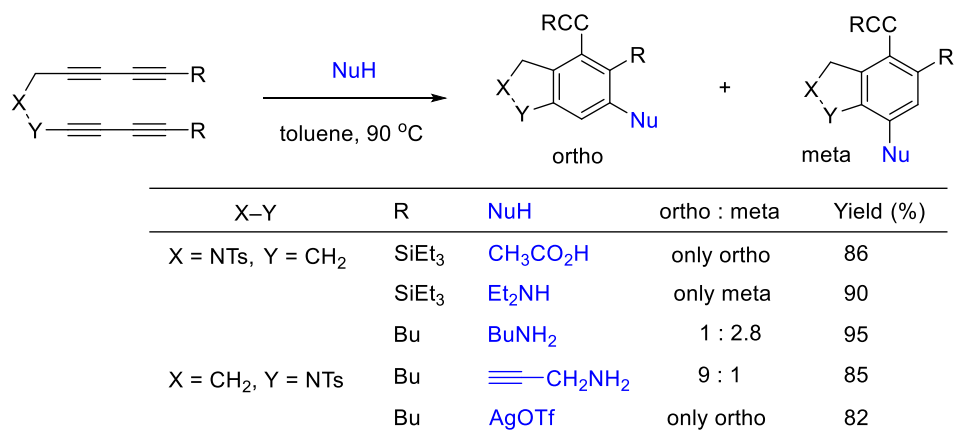
the formation of xanthenes. With acrylic and propiolic acids Michael addition of the phenolate ion led to the formation of 4-chromanone and flavones, respectively. Greaney and co-workers demonstrated the aza-Claisen rearrangement involving arynes and tertiary allyl amines, which leads to the formation of functionalized aryl amines **3-1**.⁶ Feringa and coworkers demonstrated a [3+2] cycloaddition of arynes generated from Kobayashi precursor with various azides to form substituted benzotriazoles **3-2**.⁷



Scheme 3.1. Reaction of arynes with acids, amines, and azides

Arynes generated through hexadehydro Diels-Alder (HDDA) reaction was trapped with different nitrogen and oxygen-based nucleophiles to probe into the regioselectivity of the reaction (**Scheme 3.2**). The regioselectivity was found to be profoundly influenced by not only the nature of the nucleophiles but also on the substituent on the aryne.⁸ This is the consequence of both the unfavorable steric interaction between

the incoming nucleophile and the nearby substituent and the inherent electronic bias induced by different substituents on the arynes. For silyl-substituted arynes, the addition of oxygen-based nucleophiles like carboxylic acids is predominately dictated by electronic effect of the silyl group which favors the *ortho*-addition. Addition of nitrogen nucleophiles is however controlled by their steric effect with 2° and 3° amines giving exclusive *meta*-addition product. Butyl substituent however lack strong electronic driving effect like the silyl group thus leading to lower regioselectivity. For the NTs-substituted arynes, regardless of nucleophile, the addition is exclusively controlled by electronic effect. The regioselectivity of the nucleophile addition can be explained by the structural distortion of the aryne core caused by the respective substituents, as demonstrated by the DFT calculations of Houk and co-workers for simpler systems.^{8b-d}

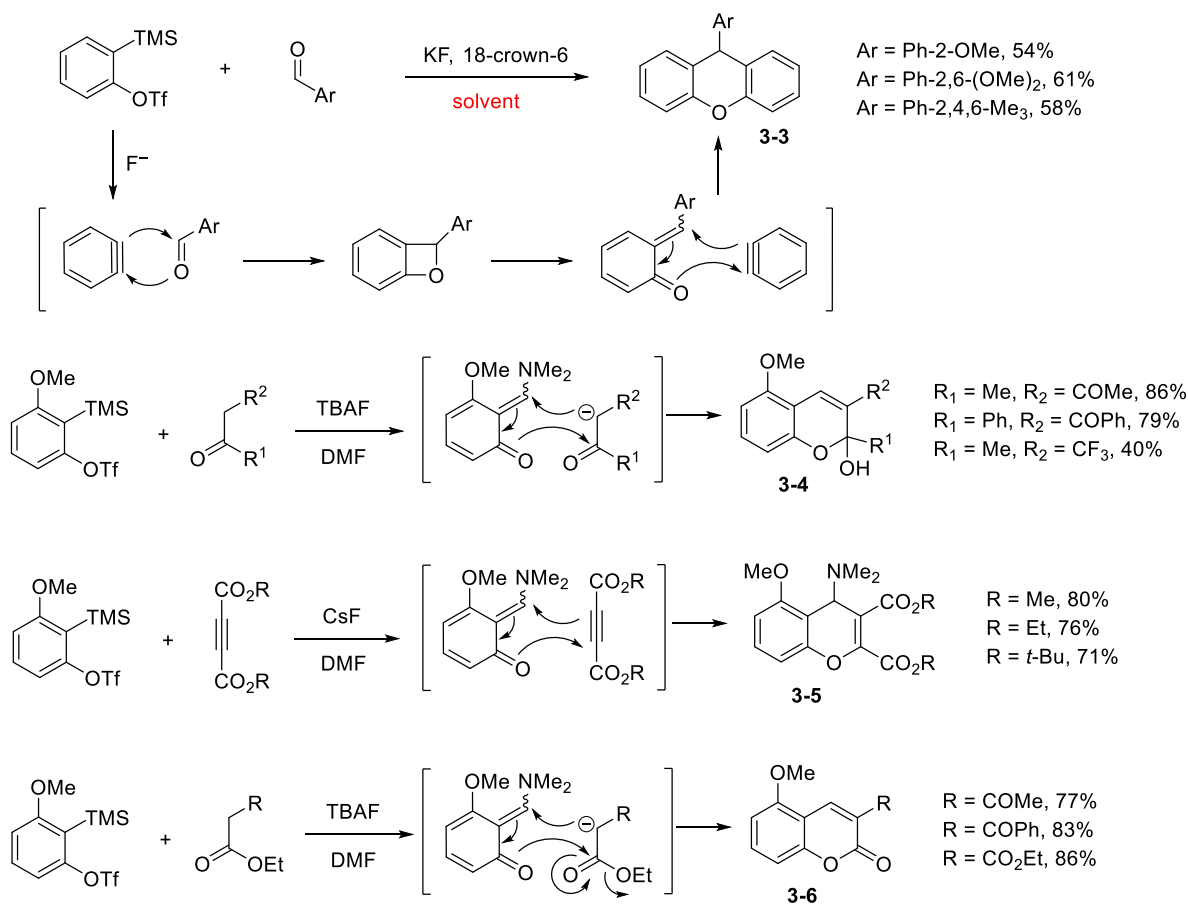


Scheme 3.2. Regioselectivity of nucleophile addition to arynes

3.1.2. Reaction of arynes with carbonyl compounds

Formation of adjacent C–O and C–C σ -bonds to an aryne is a powerful synthetic approach to form benzo-fused heterocycles containing oxygen atoms. The insertion of aryne into a C=O bond forms [2+2] cycloadduct, which undergoes cycloreversion to an *ortho*-quinone methide. This intermediate can undergo either intramolecular or intermolecular reactions with other components to form a variety of oxygen atom-containing heterocycles. Insertion of arynes to the C=O bond of aldehydes or formamides leads to the formation of various oxygen heterocycles including coumarin, chromene, xanthene and benzofuran derivatives. Yoshida and coworkers reported the synthesis of xanthene derivatives by reaction of arynes

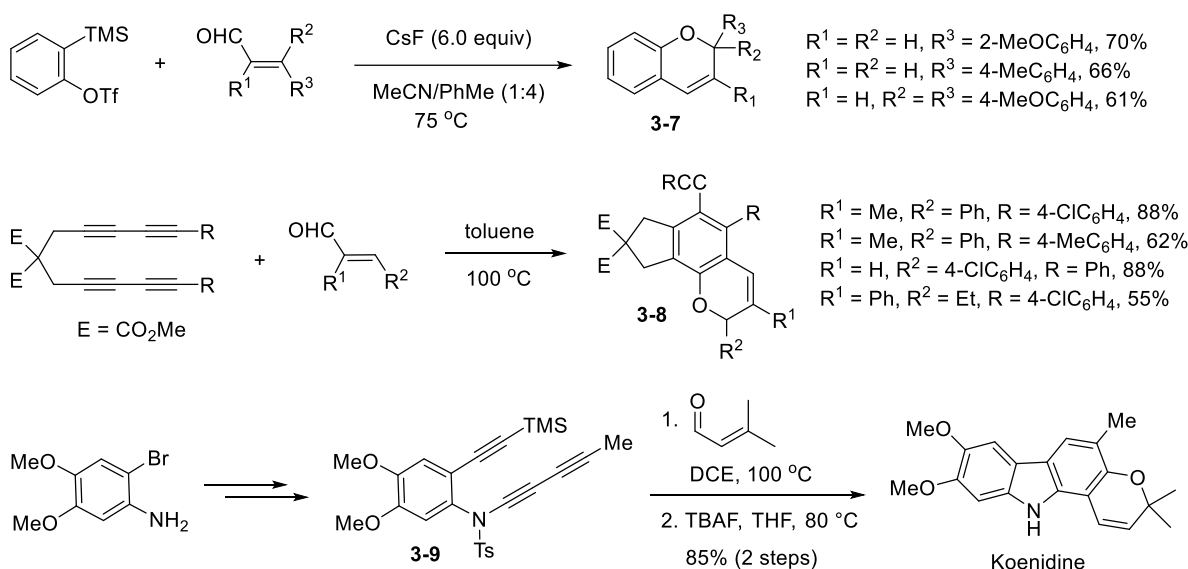
and aryl aldehyde to form 9-aryl-xanthenes **3-3** (Scheme 3.3).⁹ Domino reactions starting from the insertion of arynes into the C=O bond of formamides provide a new synthetic approach to the benzo-fused heterocycles containing an oxygen atom. Miyabe reported a three-component coupling reaction involving an aryne, formamide and a nucleophile having an active methylene group to form 2*H*-chromene derivatives **3-4**.¹⁰ Three-component couplings involving the hetero Diels-Alder reaction of the *ortho*-quinone methide and dienophiles lead to the formation of 4*H*-chromene derivatives **3-5**.¹¹



Scheme 3.3. Reaction of arynes with carbonyl compounds

Arynes are known to react with α,β -unsaturated aldehydes to form 2*H*-chromene (Scheme 3.4). Aryne intermediate undergoes [2+2] cycloaddition reaction with aldehyde followed by cycloreversion to an *ortho*-quinone methide intermediate, which then undergoes 6π -electrocyclization to form 2*H*-chromene. In 1972, Heaney and coworkers demonstrated the aryne generated from tetrachloroanthranilic acid reacts

with α,β -unsaturated aldehydes to form 2*H*-chromenes in 4–38% yield.¹² Later, Wu and co-workers utilized Kobayashi protocol to generate arynes, which react with different α,β -unsaturated aldehydes to form 2*H*-chromenes **3-7** in high yield.¹³ Hu and coworkers demonstrated the reactivity of arynes generated from tetraynes via HDDA reaction with various α,β -unsaturated aldehydes to form different 2*H*-chromenes **3-8** in excellent yields.¹⁴ Hoyer and coworkers demonstrated the utility of HDDA reaction of triyne **3-9** in the total synthesis of natural products mahanimbine and koenidine.¹⁵



Scheme 3.4. Reaction of arynes with α,β -unsaturated aldehydes

3.2. Results and Discussions

3.2.1. Reaction profile of alkenyl acids, amines, azides and aldehydes

Arynes generated from tetrayne **3-10** via a HDDA reaction react with alkenes having polar functional groups such as carboxylic acids, amines, azides, and aldehydes. It was found that the addition reaction of these alkenes outcompeted an Alder-ene reaction (**Table 3.1**). The reaction of *N*-methallyl piperidine afforded only addition product **3-12a** in 62% yield (entry 1), whereas *N*-methallyl morpholine afforded both Alder-ene product **3-11b** and addition product **3-12b** in 15% and 45% yield, respectively. This discrepancy is most likely because of the weaker nucleophilicity of morpholine (entry 2). The reaction of prenyl azide (3:1 mixture) generated [3 + 2] cycloadduct **3-12c** in 76% yield with a trace amount of its regioisomer

(entry 3). Methacrylic acid provided a mixture of both **3-11d** and **3-12d** in 33% and 40% yield (entry 4). While the reaction with methacrolein afforded exclusively Alder-ene product **3-11e**, the corresponding butyl-substituted aldehyde generated a 1:1 mixture of Alder-ene product **3-11f** and *2H*-chromene derivative **3-12f** in 46% yield (entry 5).

3-10, R¹ = Bu, SiEt₃

Entries	Alkene	Yield (%) ^b	Product	Yield (%) ^b
1		3-11a 0		3-12a 62
2		3-11b 15		3-12b 45
3		3-11c 0		3-12c 76 ^d
4		3-11d 33		3-12d 40
5		3-11e 55 ^e		3-12e 0
6		3-11f 23 ^f		3-12f 23

^aTetrayne **3-10** (20–50 mg), alkene (5 equiv.), toluene 90 °C, 4 h. ^bIsolated yield. ^c1-Azido-3-methylbut-2-ene and 3-azido-3-methylbut-1-ene exist in a 4 : 1 equilibrium ratio. ^d10 : 1 regioisomers. ^e5 : 1 regioisomers. ^f10 : 1 mixture.

Table 3.1. Alder-ene reactions of functionalized alkenes with an aryne

3.2.2. Reaction profile of α,β -unsaturated aldehydes to form chromenes

Having seen the change of product distribution between **3-12e** and **3-12f** by the slight structural change in the reacting aldehydes, the reactions with structurally diversified α,β -unsaturated aldehydes were also explored (**Table 3.2**). While mono- and disubstituted acrolein such as crotonaldehyde and tiglic aldehyde efficiently generated *2H*-chromenes **3-12g** and **3-12h** (entries 1 and 2), β,β -dimethylated acrolein

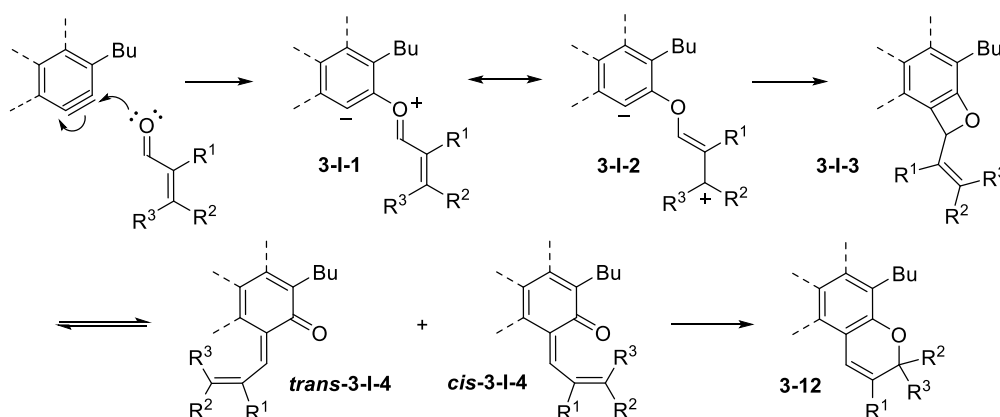
Entries	Alkenyl aldehyde	Product	Yield (%) ^b
1			71
2			65
3			86
4			84
5	n = 0		56
6	n = 1		62
7	n = 1		75
8	n = 3		65
9	n = 7		68

^aTetrayne **3-10** (20–50 mg), alkene (5 equiv.), toluene 90 °C. ^bIsolated yield.

Table 3.2. Reaction of α,β-unsaturated aldehydes with an aryne to generate 2H-chromenes

afforded product **3-12i** in 86% yield (entry 3). Also, the reaction of hexa-2,4-dienal afforded high yield of **3-12j** due to the development a bisallylic carbocationic character along the reaction (entry 4). Cycloalkenyl carboxaldehydes behave similarly to α,β-dimethyld acrolein, generating **3-12k** and **3-12l** in 56% and 62% yield, respectively (entries 5 and 6), while cycloalkylidenyl carboxaldehydes behave similarly to β,β-dimethyld acrolein, generating spirocyclic products **3-12m–3-12o** in good yields (entries 7–9).¹⁶

The proposed mechanism for the formation of *2H*-chromene is shown in **Scheme 3.5**. The overall sequence of events is initiated by the nucleophilic addition of the formyl group to form zwitterinonic intermediate **3-I-1** and its canonical form **3-I-2**, which cyclize to form oxacyclobutene **3-I-3**. Subsequent ring-opening to form **3-I-4** and/or **3-I-5** followed by 6π -electrocyclization generates *2H*-chromene **3-12**. The DFT (B3LYP/6-31+G*) calculated energy profiles prove the facile nature of this reaction pathway (see computational details section).¹⁷ From the reactions in **Table 3.2**, a general trend has emerged: no Alder-ene but only addition reaction occurs to generate *2H*-chromene derivatives (**3-12g–3-12o**) and the efficiency of the reaction decreases with the α -alkyl substituent but increases with the β -alkyl substituent. This trend can be rationalized by the stabilization of the developing β -carbocationic character by the β -alkyl substituent¹⁸ in the intermediate **3-I-2**. On the other hand, the α -alkyl substituent increases the steric hindrance when the aldehyde interacts with an aryne counterpart during the conversion of **3-I-2** to **3-I-3**.



Scheme 3.5. Mechanism of *2H*-chromene formation

3.2.3. Competition between Alder-ene reaction and chromene formation

With the reactivity trend of simple α,β -unsaturated aldehydes in hand, we next examined the reactions of structurally more elaborated α,β -unsaturated aldehydes (**Table 3.3**). Perillylaldehyde containing a 4-isopropenyl group provided both the Alder-ene product **3-11p** and aldehyde addition product **3-12p** in 24%

product (entry 3). Similarly, the citronellal-derived dialdehyde afforded product **3-12s** (46%) wherein the α,β -unsaturated aldehyde moiety solely participated in the reaction and the saturated aldehyde portion remained intact (entry 4). Finally, α,β -unsaturated dialdehyde containing an α - and a β -methyl substituents afforded chromene **3-12t** (72%) through the participation of only the β -methyl substituted α,β -unsaturated aldehyde moiety (entry 5).

3.2.4. Reaction profile of other electron-rich carbonyls

To diversify the pool of carbonyl groups that can react with arynes, other electron-rich carbonyl compounds were also examined (**Table 3.4**). As expected, the reactions of aldehydes with no possibility of the Alder-ene reaction such as acrolein and 4-dimethylaminocinnamaldehyde afforded *2H*-chromene derivatives **3-12u** and **3-12v** in good yields (entries 1 and 2). The reaction with β -diethylamino cinnamaldehyde afforded **3-12x**, which is the consequence of hydrolysis of the initially formed amino-substituted product during purification on silica gel (entry 3). A β -alkoxy-substituted enal afforded 5,6-spiroketal derivative **3-12y** in excellent yield (entry 4).¹⁹ Dimethylacrylamide and the corresponding thioamide²⁰ also generated chroman-4-one **3-12za** and thiochroman-4-one²¹ **3-12zb** in 56% and 51% yields, respectively (entries 5 and 6). The aryne generated from an ester-tethered triyne also reacts with β,β -dimethyl acrolein to afford **3-12aa** in excellent yield (entry 7). Interestingly, the benzyne generated from 1-trimethylsilyl-2-phenyl triflates with fluoride²² and from thermal decomposition of diazonium carboxylate in the presence of perillylaldehyde afforded only the Alder-ene product **3-11p'** in 75% and 42% yields without forming a *2H*-chromene derivative (entry 8). This is in sharp contrast to the reactivity of the arynes generated from tetrayne **3-10** via a hexadehydro Diels–Alder reaction, which preferentially engaged in the reaction with the same aldehyde to generate *2H*-chromene derivative **3-12p** as the major product and Alder-ene product **3-11p'** as the minor product (entry 1 in **Table 3.3**).

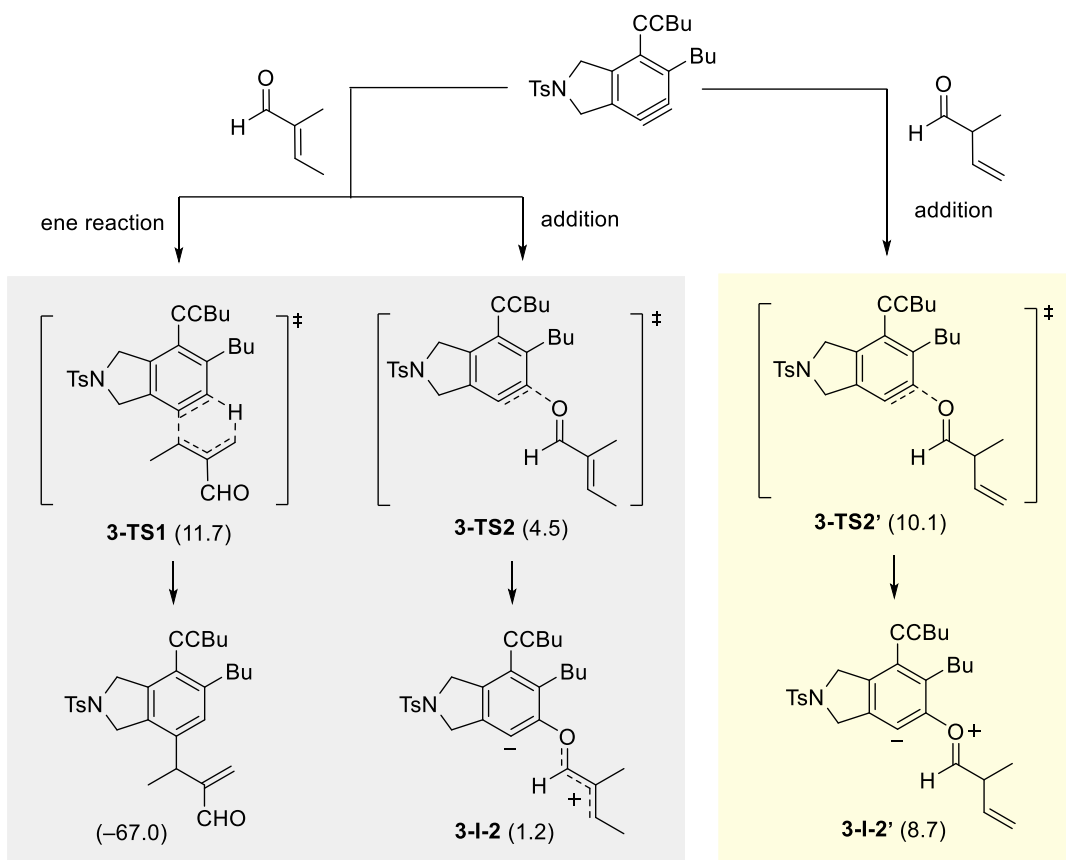
Entries	Aryne precursor	Alkene ^a	Product	Yield (%) ^b
1				72
2		R = 4-Me ₂ NPh		74
3				54
4				92
5				56
6		X = S		51
7				86
8				75

^aTetrayne **3-10** (20–50 mg), alkene (5 equiv.), toluene 90 → C. ^bIsolated yield. ^cBenzyne generated from the aprotic diazotization of anthranilic acid afforded **3-11p'** in 42% yield as a sole product.

Table 3.4. Reactivity of alkenyl aldehydes and electron-rich carbonyl compounds with arynes

3.2.5. DFT calculations to support the selectivity

To gain further insight into the reactivity and selectivity of different manifolds of reactions with arynes, we carried out DFT calculations (**Scheme 3.6**). As a representative reaction, we used the reaction between the aryne generated from symmetric tetrayne **3-10** and tiglic aldehyde. In the calculations, the transition state energies of competing Alder-ene and aldehyde addition reactions were compared wherein the Alder-ene reaction proceeds through a single transition state **3-TS1** (11.7 kcal mol⁻¹) to generate the



Scheme 3.6. DFT calculations for the reaction between an aryne and tiglic aldehyde and its deconjugated form

final ene reaction product ($-67.0 \text{ kcal mol}^{-1}$). On the other hand, the aldehyde addition reaction occurs via a multiple-step process, where the first transition state **3-TS2** ($4.5 \text{ kcal mol}^{-1}$) leads to an intermediate **3-I-2** ($1.2 \text{ kcal mol}^{-1}$). These calculated results clearly show that the interaction of the lone pair electrons of the aldehyde with the aryne is kinetically much more favorable to generate the relatively unstable zwitterionic intermediate compared to the abstraction of the allylic hydrogen to form the final Alder-ene product. For the reaction of β,γ -unsaturated aldehyde, the relative energy of transition state **3-TS2'** and intermediate **3-I-2'** indicate such addition is much less favorable, which corroborates the lack of the reactivity of saturated aldehydes towards the addition reaction to form oxacyclobutenes.

3.3. Conclusion

In summary, we have explored the reactions of arynes with functionalized alkenes focusing on the selectivity between Alder-ene and addition reaction manifolds. The reactions of 1,1-disubstituted alkenes containing a polar functional group such as methallyl amine, prenyl azide, and methacrylic acid predominantly provided addition products of the polar heteroatom functionalities over the Alder-ene reaction of the alkene moiety. The selectivity trend, however, intricately depends on the substituent patterns of the alkene moiety. The addition reaction of α,β -unsaturated aldehyde is generally much more favorable and efficient than the Alder-ene reaction. Except for 2-propenyl group-containing aldehydes such as methacrolein, all α,β -unsaturated aldehydes examined in this study preferentially participated in the addition reaction of the formyl group to generate 2*H*-chromene derivatives in high yields. DFT calculations show that the preferred mode of addition of α,β -unsaturated aldehyde is a kinetically favorable process compared to the corresponding Alder-ene reaction. Other electron-rich carbonyl compounds such as dimethyl acrylamide and acrylthioamide also participated in the addition reaction to generate chroman-4-one and thiochroman-4-one. It was observed that the structure of arynes and the method of their generation have a significant impact on the reactivity and selectivity between different manifolds of reactions. This implies that the species in the reaction medium including the reagents used for the formation of aryne intermediates and their byproducts are not innocent spectators, but they may alter the reactivity of arynes.

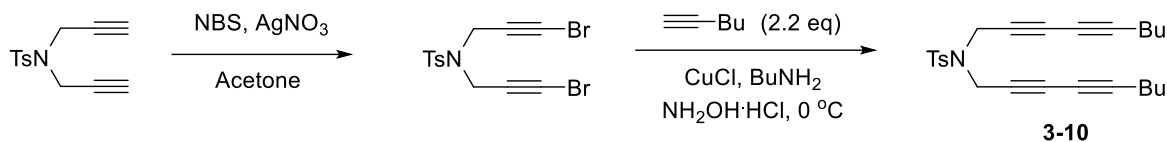
3.4. Experimental Details

3.4.1. General information

Reactions were carried out in oven-dried glassware unless otherwise noted. Compounds were purchased from Aldrich, Acros, Oakwood or TCI America unless otherwise noted. Anhydrous acetonitrile and methanol from Sigma-Aldrich were used as purchased. Toluene and dichloromethane were distilled over calcium hydride (CaH_2) under nitrogen. Tetrahydrofuran was dried over sodiumbenzophenone ketyl. Column chromatography was performed using silica gel 60 Å (32–63 mesh) purchased from Silicycle Inc. Analytical thin layer chromatography (TLC) was performed on 0.25 mm E. Merck precoated silica gel 60 (particle size 0.040–0.063 mm). Yields refer to chromatographically and spectroscopically pure isolated compounds unless otherwise stated. ^1H NMR and ^{13}C NMR spectra were recorded on a Bruker AV-500 spectrometer. ^1H NMR chemical shifts (δ) are reported in parts per million (ppm) downfield of TMS and are referenced relative to the residual proteated solvent peak (CDCl_3 (7.26 ppm)). ^{13}C chemical shifts (δ) are reported in parts per million downfield of TMS and are referenced to the carbon resonance of the solvent (CDCl_3 (77.2 ppm)). Multiplicities are indicated by s (singlet), d (doublet), t (triplet), q (quartet), quin (quintet), sext (sextet) or m (multiplet). ^1H NMR signals that fall within a ca. 0.3 ppm range are generally reported as a multiplet, with a range of chemical shift values corresponding to the peak or center of the peak. Coupling constants, J, are reported in Hz (Hertz). Electrospray ionization (ESI) and Electron impact (EI) mass spectra were recorded on a Waters Micromass Q-Tof Ultima and Micromass 70-VSE, respectively in the University of Illinois at Urbana-Champaign.

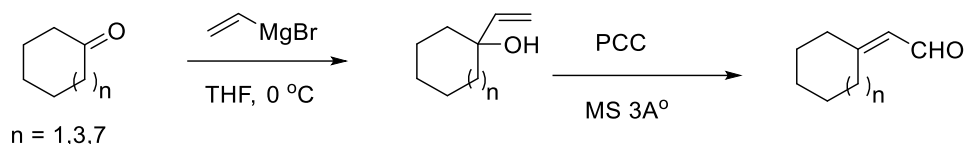
3.4.2. Experimental procedure

Preparation of tetrayne 3-10



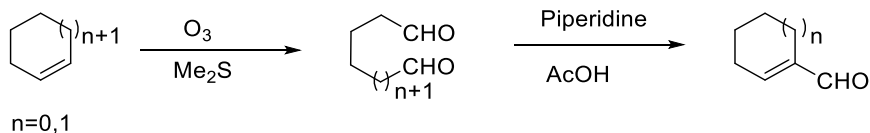
Tetrayne **3-10** was prepared by following the published procedure.²³

Preparation of cycloalkylidene Carboxaldehyde²⁴



To a THF solution of a cycloalkanone (2 mmol) was added 2.2 mL vinylmagnesium bromide (1 M in THF) at 0 °C. After completion, the reaction mixture was quenched by addition of sat. NH₄Cl solution and extracted with Et₂O (x2). The combined organic layer was washed with brine, dried over anhydrous Na₂SO₄, filtered, concentrated and purified by flash chromatography (SiO₂, hexanes–EtOAc, 10:1) to obtain alkynyl alcohol as colorless oil. The alcohol (1.4 mmol) was dissolved in CH₂Cl₂ as 3 Å MS (1.5 g) was added followed by pyridinium chlorochromate (2.1 mmol) in portions and stirred was 14 h. The reaction mixture was filtered over celite, concentrated, and purified by flash chromatography (SiO₂, hexanes–EtOAc, 10:1) to obtain the corresponding enal as white solid.

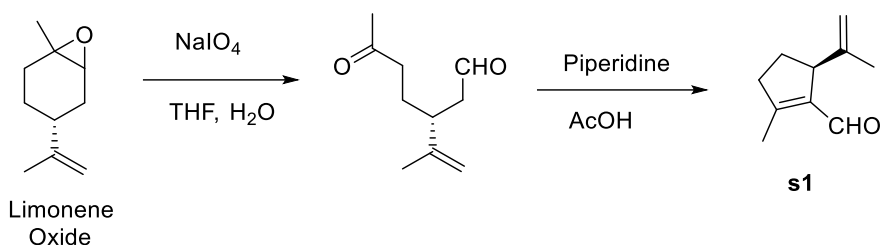
Preparation of cyclopalkenylcarboxaldehydes



Cycloalkene (2 mmol) was dissolved in MeOH (20 mL) and cooled to –78 °C and a stream of ozone gas was passed until the appearance of blue color. The excess ozone was removed by a stream of nitrogen and

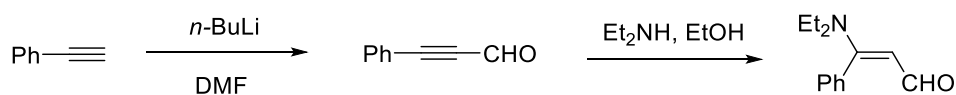
Me₂S (20 mmol) and the reaction mixture was slowly warmed to room temperature and stirred for 14 h. The reaction mixture was concentrated and dissolved in EtOAc and the organic layer was washed with brine (x4), dried over anhydrous Na₂SO₄, filtered, concentrated and purified by flash chromatography (SiO₂, hexanes–EtOAc, 5:1). The dialdehyde (1.5 mmol) was dissolved in dichloromethane followed by addition of Piperidine (2 mL) and AcOH (1.5 mL) and stirred for 15 min at ambient temperature. The reaction was quenched by adding water and organic layer washed with 1 M HCl, sat. NaHCO₃ and brine. The organic layer was dried over anhydrous Na₂SO₄, filtered, concentrated, and purified by flash chromatography (SiO₂, hexanes–EtOAc, 20:1) to obtain the desired cyclopalkenylcarboxaldehydes as colorless oil.

Preparation of limonene oxide derived aldehyde **s1**



The substrate **s1** was prepared from limonene oxide by following known literature procedure²⁵

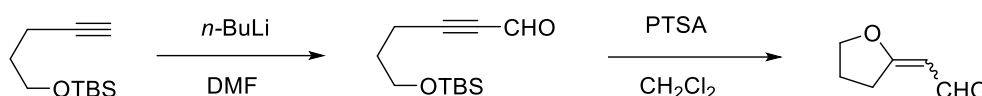
Preparation of β-diethylamino cinnamaldehyde



Phenylacetylene (5 mmol) was dissolved in dry THF and cooled to –40 °C and *n*-BuLi (2.5 M in Hexanes) was added dropwise while maintaining temperature between –40 °C to –35 °C and stirred for 45 min at same temperature. Then DMF (50 mmol) was added dropwise at –40 °C and stirred for 45 min and slowly warmed to room temperature and stirred for another 1 h. The reaction mixture was poured into 100 ml of 1 M HCl solution and the biphasic solution was transferred to a separatory funnel. The organic layer was washed with brine (x4), dried over anhydrous Na₂SO₄, filtered, concentrated, and purified by flash

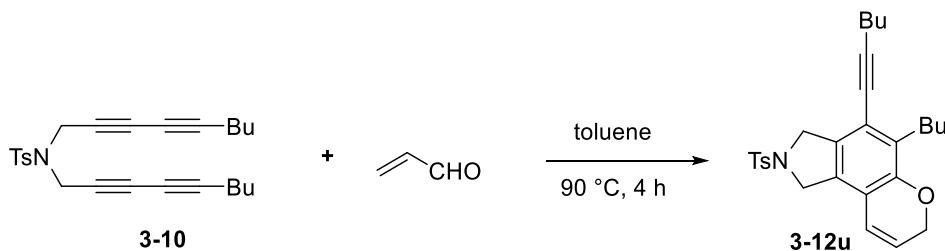
chromatography (SiO₂, hexanes–EtOAc, 10:1). The alkynyl aldehyde (1.2 mmol) was dissolved in EtOH and treated with Et₂NH (1.4 mmol) and stirred at room temperature for 16 h. EtOH was removed under reduced pressure and the residue was dissolved in EtOAc and washed with brine (x5). The organic layer was dried over anhydrous Na₂SO₄, filtered and concentrated to obtain β-diethylamino cinnamaldehyde as a red oil which was used without further purification.

Preparation of 2-(dihydrofuran-2(3H)-ylidene) acetaldehyde



The alkynyl aldehyde (1 mmol) prepared by the method described above was dissolved in dichloromethane, followed by addition of *p*-toluenesulfonic acid and stirred for 14 h. The deep purple solution was washed with brine (x2), dried over anhydrous Na₂SO₄, filtered, concentrated and purified by flash chromatography to obtain 2-(dihydrofuran-2(3H)-ylidene) acetaldehyde (SiO₂, hexanes–EtOAc, 2:1) as a colorless oil (76% yield,) with Z:E ratio (3:1).

Representative Procedure for the Tandem HDDAR–Intermolecular Alder-ene/Addition Reaction with 1.0 mmol Scale

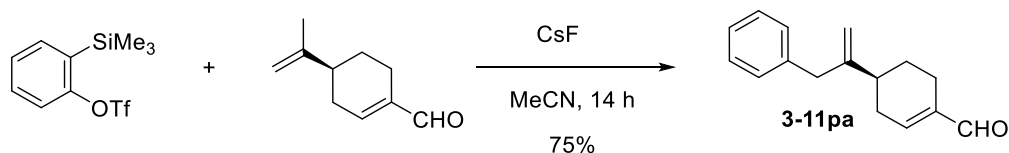


To a toluene solution (0.05 M) of tetrayne **3-10** (410 mg, 1 mmol) in a Shlenk tube was added acrolein (0.3 mL, 5 mmol). The reaction mixture was heated at 90 °C for 4 h, brought to room temperature, and concentrated under reduced pressure. The crude product was purified by column chromatography (SiO₂, hexanes–EtOAc, 4:1), providing product **3-12u** (324 mg, 72%) as white solid.

General Procedure for the Tandem HDDAR–Intermolecular Alder-ene/ Addition Reactions

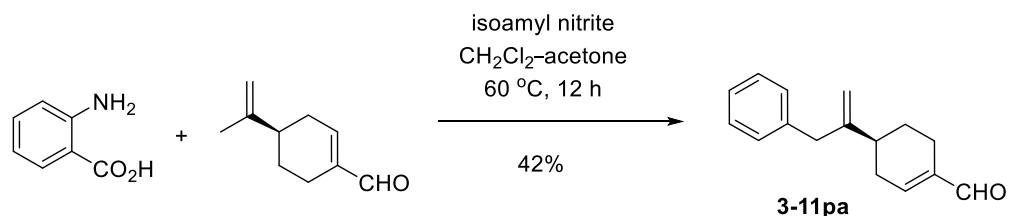
To a toluene solution (0.03–0.05 M) of tetrayne (0.05–0.06 mmol) in a Shlenk tube was added functionalized alkene (5 equiv). The reaction mixture was heated at 90 °C for 4 h, brought to room temperature, and concentrated under reduced pressure. The product was isolated by column chromatography (SiO₂, hexanes–EtOAc, 4:1; alder-ene product) or (SiO₂, hexanes–EtOAc, 10:1; addition product).

Reaction of Benzyne from Kobayashi Precursor and Perillaldehyde



2-Trimethylsilylphenyl trifluoromethanesulfonate (30 mg, 0.1 mmol) was dissolved in MeCN under N₂ and to it was added perillaldehyde (60 mg, 0.4 mmol) followed by CsF (62 mg, 0.4 mmol) and stirred for 14 h at ambient temperature. MeCN was removed under reduced pressure and 10 mL of EtOAc was added and organic layer was washed with brine (x2). The organic layer dried over anhydrous Na₂SO₄, filtered, concentrated, and purified by flash chromatography (SiO₂, hexanes–EtOAc: 20:1) to obtain **3-11p'** (75% yield, 30 mg) as a yellow solid.

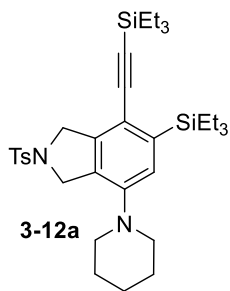
Reaction of Benzyne from Anthranilic acid and Perillaldehyde



A solution of perillaldehyde (602.4 mg, 4.0 mmol) and isoamyl nitrite (0.293 mL, 2.2 mmol) in CH₂Cl₂ was taken in a three-necked flask equipped with refluxing condenser and a dropping funnel and heated to

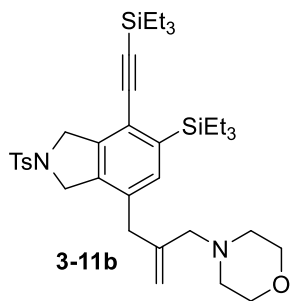
60 °C. Anthranilic acid (250 mg, 1.82 mmol) was dissolved in 8 mL acetone and added dropwisethrough the dropping funnel over 30 min. The mixture was refluxed for additional 12 h. After completion, the solvent was removed under reduced pressure and the residue was purified by column chromatography (SiO₂, hexanes–EtOAc: 20:1) to obtain **3-11pa** (42% yield, 173 mg) as a yellow solid.

3.4.3. Characterization data



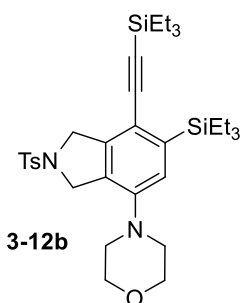
3-12a: This compound was isolated in (62% yield, 15 mg) as a colorless oil. ^1H NMR (CDCl_3 , 500 MHz): δ 7.75 (d, J = 8.0 Hz, 2H), 7.30 (d, J = 8.0 Hz, 2H), 6.81 (s, 1H), 4.57–4.60 (m, 4H), 2.88–2.92 (m, 4H), 2.40 (s, 3H), 1.64–1.70 (m, 4H), 1.60–1.54 (t, J = 7.8 Hz, 9H), 0.88–0.93 (m, 15H), 0.67 (q, J = 7.7 Hz, 6H); ^{13}C NMR (CDCl_3 , 500 MHz): δ 147.9, 143.5, 141.8, 140.6, 133.9, 129.8, 128.7, 127.6, 123.1,

116.0, 104.6, 98.0, 54.4, 53.8, 51.7, 26.3, 24.2, 21.5, 7.52, 7.48, 4.42, 3.25; **HRMS** (ESI) calcd for $\text{C}_{34}\text{H}_{53}\text{N}_2\text{O}_3\text{SSi}_2$ $[\text{M}+\text{H}]^+$ 609.3366, found 609.3348.



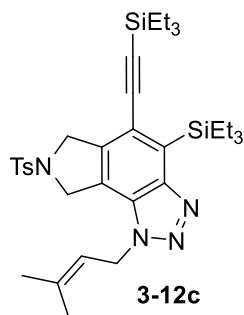
3-11b: This compound was isolated in (15% yield, 6 mg) as a yellow oil. ^1H NMR (CDCl_3 , 500 MHz): δ 7.75 (d, J = 8.1 Hz, 2H), 7.31 (d, J = 7.9 Hz, 2H), 7.14 (s, 1H), 4.98 (s, 1H), 4.81 (s, 1H), 4.63 (s, 2H), 4.61 (s, 2H), 3.63–3.68 (m, 4H), 3.25 (s, 2H), 2.40 (s, 3H), 2.26–2.32 (m, 4H), 1.05 (t, J = 7.9 Hz, 2H), 0.86–0.93 (m, 15H), 0.68 (q, J = 7.8 Hz, 2H); ^{13}C NMR (CDCl_3 , 500 MHz): δ 143.6,

140.3, 139.0, 136.2, 135.8, 134.0, 133.4, 122.8, 121.4, 115.1, 104.1, 99.5, 67.1, 63.5, 54.4, 53.5, 53.4, 38.3, 21.5, 7.5, 4.3, 3.1; **HRMS** (ESI) calcd for $\text{C}_{33}\text{H}_{51}\text{N}_2\text{O}_3\text{SSi}_2$ $[\text{M}+\text{H}]^+$ 611.3125, found 611.3135.



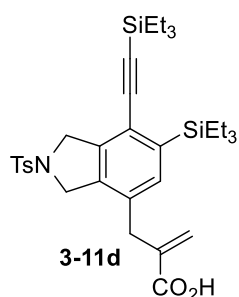
3-12b: This compound was isolated in (45% yield, 18 mg) as a yellow oil. ^1H NMR (CDCl_3 , 500 MHz): δ 7.77 (d, J = 7.9, 2H), 7.32 (d, J = 8.2 Hz, 2H), 6.83 (s, 1H), 4.59 (s, 4H), 3.78–3.84 (m, 4H), 2.91–2.97 (m, 4H), 2.41 (s, 3H), 1.04 (t, J = 7.8 Hz, 2H), 0.88–0.93 (m, 15H), 0.68 (q, J = 8.0 Hz, 2H); ^{13}C NMR (CDCl_3 , 500 MHz): δ 146.5, 143.7, 142.1, 141.0, 133.8, 129.8, 128.7, 127.6, 122.8, 117.2,

104.2, 98.7, 67.1, 54.2, 53.7, 50.7, 21.5, 7.50, 7.47, 4.4, 3.2; **HRMS** (ESI) calcd for $\text{C}_{33}\text{H}_{51}\text{N}_2\text{O}_3\text{SSi}_2$ $[\text{M}+\text{H}]^+$ 611.3125, found 611.3135.



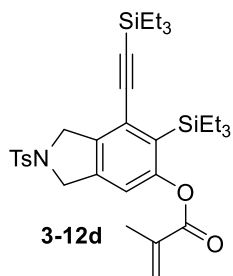
3-12c: This compound was isolated in (76% yield, 26 mg) as a colorless oil. ^1H NMR (CDCl_3 , 500 MHz): δ 7.76 (d, J = 8.2 Hz, 2H), 7.32 (d, J = 8.3 Hz, 2H), 5.33–5.26 (m, 1H), 5.18 (d, J = 6.2 Hz, 1H), 4.97 (s, 2H), 4.74 (s, 2H), 2.4 (s, 3H), 1.89 (s, 3H), 1.78 (s, 3H), 1.99 (q, J = 8.1 Hz, 6H), 1.08 (t, J = 7.2 Hz, 9H), 0.94 (t, J = 7.8 Hz, 9H), 0.72 (q, J = 7.5 Hz, 6H); ^{13}C NMR (CDCl_3 , 500 MHz): δ 152.1,

144.0, 139.7, 138.3, 134.2, 133.7, 129.9, 127.5, 127.0, 120.4, 118.9, 117.6, 115.7, 104.1, 99.9, 54.9, 53.4, 47.4, 25.7, 21.5, 18.4, 7.6, 7.5, 4.4, 4.3; **HRMS** (ESI) calcd for $\text{C}_{34}\text{H}_{51}\text{N}_4\text{O}_2\text{SSi}_2$ $[\text{M}+\text{H}]^+$ 635.3271, found 635.3257.



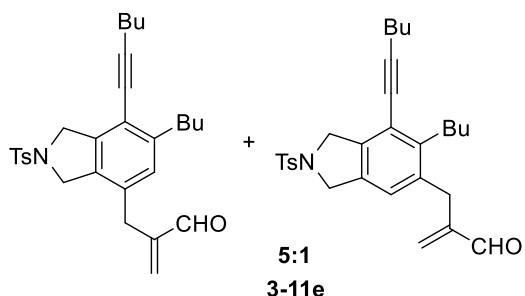
3-11d: This compound was isolated in (33% yield, 12 mg) as a yellow oil. ^1H NMR (CDCl_3 , 500 MHz): δ 7.75 (d, J = 8.2 Hz, 2H), 7.31 (d, J = 8.2 Hz, 2H), 7.11 (s, 1H), 6.34 (s, 1H), 4.64 (s, 2H), 4.59 (s, 2H), 3.44 (s, 2H), 2.39 (s, 3H), 1.05 (t, J = 8.0 Hz, 9H), 0.88 – 0.91 (m, 15H), 0.69 (q, J = 7.9 Hz, 6H); ^{13}C NMR (CDCl_3 , 500 MHz): δ 170.1, 143.6, 140.6, 139.6, 137.4, 136.0, 135.7, 133.9, 131.8, 129.8, 128.5,

127.6, 122.1, 103.9, 99.9, 54.4, 53.4, 35.0, 21.5, 7.4, 4.3, 3.1; **HRMS** (ESI) calcd for $\text{C}_{33}\text{H}_{48}\text{NO}_4\text{SSi}_2$ $[\text{M}+\text{H}]^+$ 610.2843, found 610.2842.



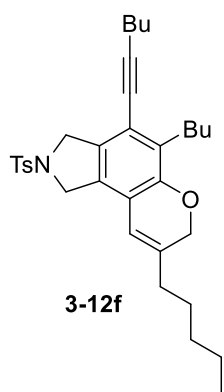
3-12d: This compound was isolated in (40% yield, 14 mg) as a yellow solid. ^1H NMR (CDCl_3 , 500 MHz): δ 7.75 (d, J = 8.3 Hz, 2H), 7.32 (d, J = 8.3 Hz, 2H), 6.72 (s, 1H), 6.27 (s, 1H), 5.75 (t, J = 1.3 Hz, 1H), 4.64 (s, 2H), 4.59 (s, 2H), 2.42 (s, 3H), 2.03 (s, 3H), 1.06 (t, J = 8.1 Hz, 9H), 0.86–0.94 (m, 15H), 0.70 (q, J = 8.4 Hz, 6H); ^{13}C NMR (CDCl_3 , 500 MHz): δ 166.5, 156.3, 143.8, 138.8, 138.0, 136.0,

133.6, 130.3, 129.9, 127.7, 125.4, 117.1, 103.6, 102.2, 54.3, 21.5, 18.4, 7.6, 7.4, 4.30, 4.25; **HRMS** (ESI) calcd for $\text{C}_{33}\text{H}_{48}\text{NO}_4\text{SSi}_2$ $[\text{M}+\text{H}]^+$ 610.2843, found 610.2841.



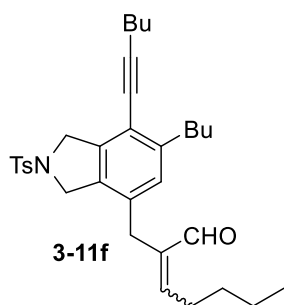
3-11e: This compound was isolated in (55% yield, 16 mg, colorless oil) as a 5:1 regioisomeric mixture. Characterization data for the major isomer is given. **¹H NMR** (CDCl₃, 500 MHz): δ 9.58 (s, 1H), 7.77 (d, *J* = 8.4 Hz, 2H), 7.31 (d, *J* = 8.1 Hz, 2H), 6.81 (s, 1H), 6.05 (s, 1H), 5.94 (s, 1H), 4.63 (s, 2H), 4.50 (s, 2H), 3.36 (s, 2H), 2.66 (t, *J* = 7.8 Hz, 2H), 2.41 (s, 3H), 1.62–1.56 (m, 2H), 1.54–1.46

(m, 4H), 1.36–1.28 (m, 2H), 0.96 (t, *J* = 7.8 Hz, 3H), 0.91 (t, *J* = 8.0 Hz, 3H); **¹³C NMR** (CDCl₃, 500 MHz): δ 193.6, 149.3, 147.7, 144.9, 143.6, 139.2, 135.0, 132.4, 131.3, 129.8, 129.3, 127.6, 116.9, 98.5, 75.9, 54.4, 53.2, 33.8, 32.9, 31.5, 30.8, 22.5, 21.9, 21.5, 19.3, 13.9, 13.6; **HRMS** (ESI) calcd for C₂₉H₃₆NO₃S [M+H]⁺ 478.2416, found 478.2401.



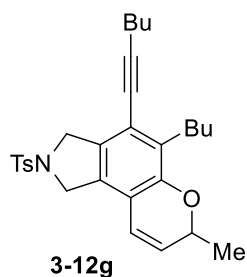
3-12f: This compound was isolated in (23% yield, 11 mg) as colorless oil. **¹H NMR** (CDCl₃, 500 MHz): δ 9.43 (s, 1H), 7.78 (d, *J* = 8.2 Hz, 2H), 7.33 (d, *J* = 7.8 Hz, 2H), 6.68 (t, *J* = 7.5 Hz, 1H), 6.61 (s, 1H), 4.62 (s, 4H), 3.39 (s, 2H), 2.60 (t, *J* = 7.5, 2H), 2.46–2.40 (m, 2H), 2.41 (s, 3H), 2.29 (q, *J* = 7.5 Hz, 2H), 1.60–1.54 (m, 2H), 1.51–1.40 (m, 6H), 1.34–1.24 (m, 6H), 0.95 (t, *J* = 7.2 Hz, 3H), 0.91–0.86 (m, 6H); **¹³C NMR** (CDCl₃, 500 MHz): δ 194.2, 157.1, 144.6, 143.6, 140.6, 138.9, 133.9, 132.3,

132.0, 129.8, 127.6, 127.3, 120.2, 116.3, 98.2, 76.0, 54.4, 53.5, 33.9, 32.9, 30.9, 30.5, 29.2, 26.7, 22.5, 21.9, 21.5, 19.3, 13.8; **HRMS** (ESI) calcd for C₃₃H₄₄NO₃S [M+H]⁺ 534.3042, found 534.3063.

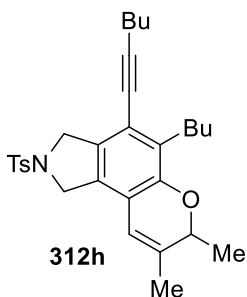


3-11f: This compound was isolated in (23% yield, 11 mg) as colorless oil. **¹H NMR** (CDCl₃, 500 MHz): δ 7.77 (d, *J* = 8.1 Hz, 2H), 7.31 (d, *J* = 7.8 Hz, 2H), 5.93 (s, 1H), 4.59 (s, 2H), 4.59 (s, 2H), 4.56 (s, 4H), 2.65 (t, *J* = 7.7 Hz, 2H), 2.44 (t, *J* = 7.5 Hz, 2H), 2.40 (s, 3H), 2.09 (t, *J* = 7.5 Hz, 2H), 1.61–1.55 (m, 2H), 1.53–1.41 (m, 6H), 1.37–1.28 (m, 6H), 0.96 (t, *J* = 7.2 Hz, 3H), 0.92–0.88 (m,

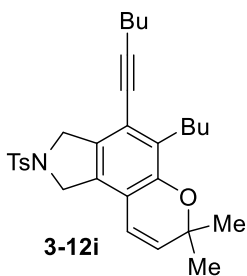
6H); **¹³C NMR** (CDCl₃, 500 MHz): δ 150.0, 143.5, 137.7, 134.0, 131.4, 131.1, 129.8, 128.4, 127.6, 117.6, 117.2, 115.1, 98.1, 76.6, 68.2, 54.2, 53.0, 33.4, 31.9, 31.5, 30.9, 27.5, 26.5, 22.8, 22.4, 21.9, 21.5, 19.3, 14.0, 13.6; **HRMS** (ESI) calcd for C₃₃H₄₄NO₃S [M+H]⁺ 534.3042, found 534.3037.



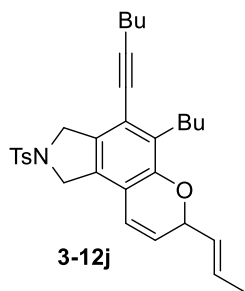
3-12g: This compound was isolated in (71% yield, 25 mg) as a white solid. $^1\text{H NMR}$ (CDCl_3 , 500 MHz): δ 7.77 (d, J = 8.2 Hz, 2H), 7.31 (d, J = 7.8 Hz, 2H), 6.17 (dd, J = 1.7, 8.3 Hz, 1H), 5.72 (dd, J = 3.6, 6.7 Hz, 1H), 4.924.86 (m, 1H), 4.60–4.49 (m, 4H), 2.67 (t, J = 7.5 Hz, 2H), 2.45 (t, J = 7.0 Hz, 2H), 2.41 (s, 3H), 1.61–1.56 (m, 2H), 1.51–1.41 (m, 4H), 1.37 (d, J = 5.9 Hz, 3H), 0.96 (t, J = 6.5 Hz, 3H), 0.91 (t, J = 7.2 Hz, 3H); $^{13}\text{C NMR}$ (CDCl_3 , 500 MHz): δ 150.4, 143.6, 134.0, 132.1, 130.7, 129.8, 129.0, 128.3, 127.6, 120.1, 118.7, 115.8, 98.5, 76.6, 71.1, 54.2, 52.9, 31.7, 30.9, 27.4, 22.7, 21.9, 21.5, 20.8, 19.3, 14.0, 13.6; **HRMS** (ESI) calcd for $\text{C}_{28}\text{H}_{34}\text{NO}_3\text{S}$ $[\text{M}+\text{H}]^+$ 464.2259, found 464.2251.



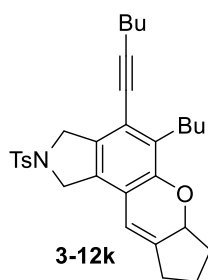
3-12h: This compound was isolated in (65% yield, 24 mg) as yellow solid. $^1\text{H NMR}$ (CDCl_3 , 500 MHz): δ 7.77 (d, J = 7.8 Hz, 2H), 7.31 (d, J = 8.1 Hz, 2H), 5.9 (s, 1H), 4.75 (q, J = 6.3 Hz, 1H), 4.59–4.51 (m, 4H), 2.67 (t, J = 7.5 Hz, 2H), 2.44 (t, J = 6.8 Hz, 2H), 2.40 (s, 3H), 1.82 (s, 3H), 1.61–1.54 (m, 2H), 1.52–1.43 (m, 4H), 1.38–1.32 (m, 2H), 1.28 (d, J = 6.8 Hz, 3H), 0.96 (t, J = 6.3 Hz, 3H), 0.91 (t, J = 7.3 Hz, 3H); $^{13}\text{C NMR}$ (CDCl_3 , 500 MHz): δ 148.2, 143.4, 137.3, 134.0, 131.9, 129.8, 128.1, 127.6, 117.6, 116.6, 115.2, 98.0, 76.6, 74.7, 54.2, 53.0, 31.8, 30.9, 27.5, 22.8, 21.9, 21.5, 19.5, 19.3, 18.4, 14.0, 13.6; **HRMS** (ESI) calcd for $\text{C}_{30}\text{H}_{38}\text{NO}_3\text{S}$ $[\text{M}+\text{H}]^+$ 492.2572, found 492.2562.



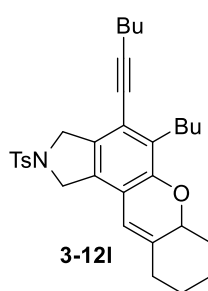
3-12i: This compound was isolated in (86% yield, 29 mg) as white solid. $^1\text{H NMR}$ (CDCl_3 , 500 MHz): δ 7.77 (d, J = 7.5 Hz, 2H), 7.31 (d, J = 7.7 Hz, 2H), 6.10 (d, J = 10.2 Hz, 1H), 5.63 (d, J = 11.8 Hz, 1H), 2.67 (t, J = 7.3 Hz, 2H), 2.45 (t, J = 7.0 Hz, 2H), 2.40 (s, 3H), 1.62–1.54 (m, 2H), 1.52–1.43 (m, 4H), 1.37 (s, 6H), 1.39–1.31 (m, 2H), 0.96 (t, J = 6.8 Hz, 3H), 0.92 (t, J = 7.5 Hz, 3H); $^{13}\text{C NMR}$ (CDCl_3 , 500 MHz): δ 149.9, 143.5, 133.9, 132.3, 131.9, 130.4, 129.8, 128.9, 127.6, 118.7, 118.6, 115.1, 98.3, 76.6, 75.9, 54.2, 52.9, 31.7, 30.9, 27.6, 27.3, 22.7, 21.9, 21.5, 19.3, 14.0, 13.6; **HRMS** (ESI) calcd for $\text{C}_{25}\text{H}_{38}\text{N}_3\text{O}_5\text{S}$ $[\text{M}+\text{H}]^+$ 534.3042, found 534.3037.



3-12j: This compound was isolated in (84% yield, 28 mg) as colorless oil. **¹H NMR** (CDCl₃, 500 MHz): δ 7.77 (d, *J* = 7.7 Hz, 2H), 7.32 (d, *J* = 8.2 Hz, 2H), 6.21 (d, *J* = 9.5 Hz, 1H), 5.96–5.69 (m, 2H), 5.62–5.54 (m, 1H), 5.17–5.12 (s, 1H), 4.59–4.57 (m, 4H), 2.67 (t, *J* = 7.2 Hz, 2H), 2.45 (t, *J* = 6.5 Hz, 2H), 2.41 (s, 3H), 1.68 (d, *J* = 5.6 Hz, 2H), 1.61–1.54 (m, 2H), 1.52–1.41 (m, 4H), 1.36–1.29 (m, 2H), 0.96 (t, *J* = 6.5 Hz, 3H), 0.90 (t, *J* = 7.2 Hz, 3H); **¹³C NMR** (CDCl₃, 500 MHz): δ 150.1, 143.6, 133.9, 132.1, 129.8, 129.2, 128.8, 127.6, 126.0, 120.2, 118.7, 115.8, 98.6, 76.6, 75.0, 54.2, 52.9, 31.7, 30.8, 27.5, 22.7, 21.9, 21.5, 19.3, 17.7, 14.0, 13.6; **HRMS** (ESI) calcd for C₃₁H₃₈NO₃S [M+H]⁺ 504.2572, found 504.2565.

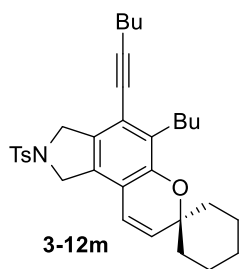


3-12k: This compound was isolated in (56% yield, 22 mg) as a colorless oil. **¹H NMR** (CDCl₃, 500 MHz): δ 7.76 (d, *J* = 7.6 Hz, 2H), 7.30 (d, *J* = 8.0 Hz, 2H), 6.02–5.99 (m, 1H), 4.75–4.69 (m, 1H), 4.65–4.46 (m, 4H), 2.69 (t, *J* = 7.5 Hz, 2H), 2.45 (t, *J* = 6.7 Hz, 2H), 2.40 (s, 3H), 2.34–2.29 (m, 1H), 1.94–1.84 (m, 2H), 1.73–1.64 (m, 1H), 1.61–1.55 (m, 2H), 1.51–1.43 (m, 4H), 1.38–1.31 (m, 2H), 0.96 (t, *J* = 6.6 Hz, 3H), 0.91 (t, *J* = 7.2 Hz, 3H); **¹³C NMR** (CDCl₃, 500 MHz): δ 150.9, 143.5, 143.2, 133.9, 131.9, 131.2, 129.8, 128.7, 127.6, 118.6, 117.6, 113.4, 98.1, 78.9, 76.7, 54.3, 53.2, 32.2, 31.9, 30.9, 28.4, 27.6, 22.6, 21.9, 21.7, 21.5, 19.4, 14.0, 13.6; **HRMS** (ESI) calcd for C₃₁H₃₈NO₃S [M+H]⁺ 504.2572, found 504.2578.

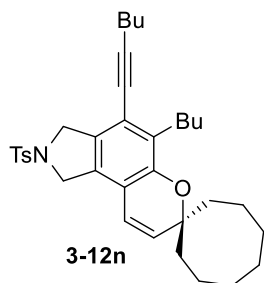


3-12l: This compound was isolated in (62% yield, 29 mg) as a colorless oil. **¹H NMR** (CDCl₃, 500 MHz): δ 7.76 (d, *J* = 8.2 Hz, 2H), 7.30 (d, *J* = 7.8 Hz, 2H), 5.80–5.77 (m, 1H), 4.87–4.81 (m, 1H), 4.56–4.49 (m, 4H), 2.65–2.60 (m, 2H), 2.44 (t, *J* = 7.2 Hz, 2H), 2.40 (s, 3H), 2.22–2.15 (m, 1H), 2.07–1.99 (m, 1H), 1.91–1.83 (m, 1H), 1.82–1.76 (m, 1H), 1.74–1.65 (m, 1H), 1.60–1.53 (m, 2H), 1.51–1.38 (m, 6H), 1.36–1.29 (m, 2H), 1.27–1.22 (m, 1H), 0.95 (t, *J* = 7.4 Hz, 3H), 0.90 (t, *J* = 7.2 Hz, 3H); **¹³C NMR** (CDCl₃, 500 MHz): δ 149.7, 143.5, 139.9, 134.0, 130.7, 130.4, 129.8, 128.1, 127.6, 117.5, 115.6, 112.8, 97.8, 77.2, 76.0, 54.2, 52.9,

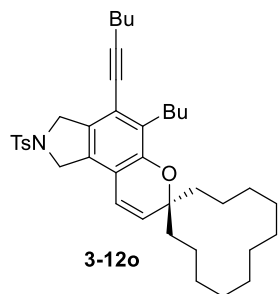
34.9, 33.1, 31.7, 30.9, 27.3, 26.7, 24.2, 24.2, 22.7, 21.9, 21.5, 19.3, 14.0, 13.6; **HRMS** (ESI) calcd for $C_{33}H_{42}NO_3S$ $[M+H]^+$ 532.2885, found 532.2885.



3-12m: This compound was isolated in (75% yield, 25 mg) as a white solid. **1H NMR** ($CDCl_3$, 500 MHz): δ 7.76 (d, J = 8.0 Hz, 2H), 7.31 (d, J = 7.8 Hz, 2H), 6.10 (d, J = 9.8 Hz, 2H), 5.62 (d, J = 9.9 Hz, 2H), 4.56 (s, 4H), 2.73 (t, J = 8.1 Hz, 2H), 2.45 (t, J = 7.1 Hz, 2H), 2.40 (s, 3H), 1.94–1.86 (m, 2H), 1.73–1.66 (m, 2H), 1.62–1.54 (m, 3H), 1.53–1.45 (m, 7H), 1.44–1.35 (m, 3H), 1.31–1.25 (m, 2H), 0.96 (t, J = 7.2 Hz, 3H), 0.93 (t, J = 7.6 Hz, 3H); **^{13}C NMR** ($CDCl_3$, 500 MHz): δ 150.1, 143.6, 134.0, 132.1, 130.8, 129.8, 129.2, 129.1, 128.7, 127.6, 125.9, 120.2, 118.7, 115.8, 98.6, 76.6, 75.0, 54.2, 52.9, 31.7, 30.8, 27.4, 22.7, 21.9, 21.5, 19.3, 17.7, 14.0, 13.6; **HRMS** (ESI) calcd for $C_{33}H_{42}NO_3S$ $[M+H]^+$ 532.2885, found 532.2885.

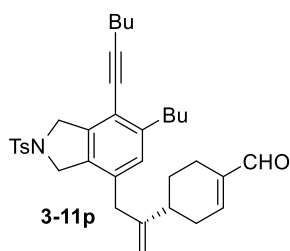


3-12n: This compound was isolated in (65% yield, 26 mg) as a white solid. **1H NMR** ($CDCl_3$, 500 MHz): δ 7.77 (d, J = 7.8 Hz, 2H), 7.31 (d, J = 8.6 Hz, 2H), 6.08 (d, J = 9.9 Hz, 1H), 5.73 (d, J = 9.8 Hz, 1H), 4.55 (s, 4H), 2.72–2.67 (m, 2H), 2.45 (t, J = 6.6 Hz, 2H), 2.40 (s, 3H), 2.09–1.98 (m, 2H), 1.75–1.62 (m, 6H), 1.60–1.53 (m, 4H), 1.53–1.43 (m, 8H), 1.40–1.32 (m, 2H), 0.96 (t, J = 7.2 Hz, 3H), 0.92 (t, J = 7.6 Hz, 3H); **^{13}C NMR** ($CDCl_3$, 500 MHz): δ 149.6, 143.5, 134.0, 132.3, 131.5, 130.2, 129.8, 128.9, 127.6, 118.5, 118.4, 115.6, 98.3, 80.3, 76.6, 54.2, 53.0, 34.2, 31.7, 30.9, 28.1, 27.5, 24.8, 22.9, 21.9, 21.5, 21.2, 19.3, 14.0, 13.6; **HRMS** (ESI) calcd for $C_{35}H_{46}NO_3S$ $[M+H]^+$ 560.3198, found 560.3198.

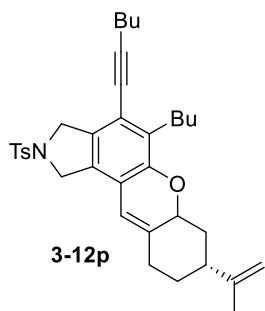


3-12o: This compound was isolated in (68% yield, 25 mg) as a white solid. **1H NMR** ($CDCl_3$, 500 MHz): δ 7.77 (d, J = 7.8 Hz, 2H), 7.31 (d, J = 8.2 Hz, 2H), 6.09 (d, J = 10.2 Hz, 1H), 5.69 (d, J = 10.9 Hz, 1H), 4.55 (s, 4H), 2.66 (t, J = 7.2 Hz, 2H), 2.45 (t, J = 6.4 Hz, 2H), 2.40 (s, 3H), 1.80–1.72 (m, 2H), 1.68–1.61 (m, 2H), 1.60–1.55 (m, 2H), 1.52–1.43 (m, 4H), 1.39–1.32 (m, 20H), 0.96 (t, J = 7.6

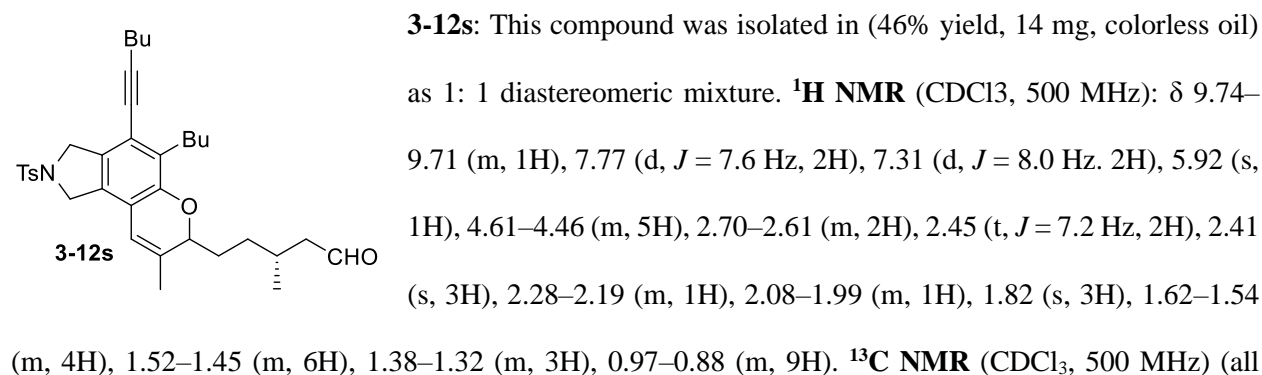
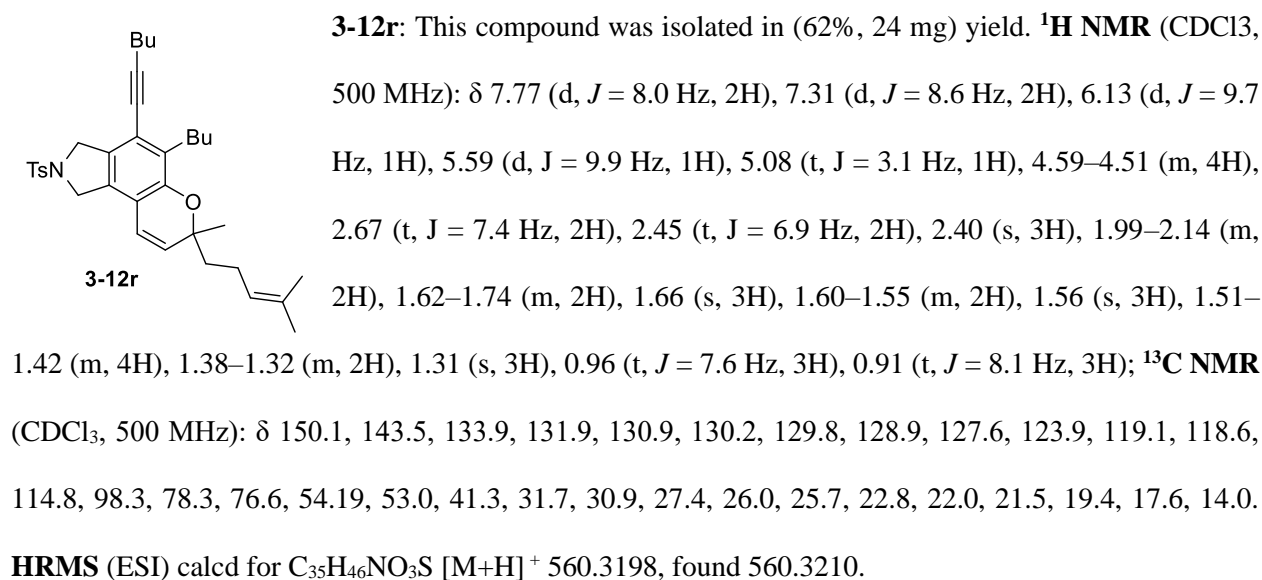
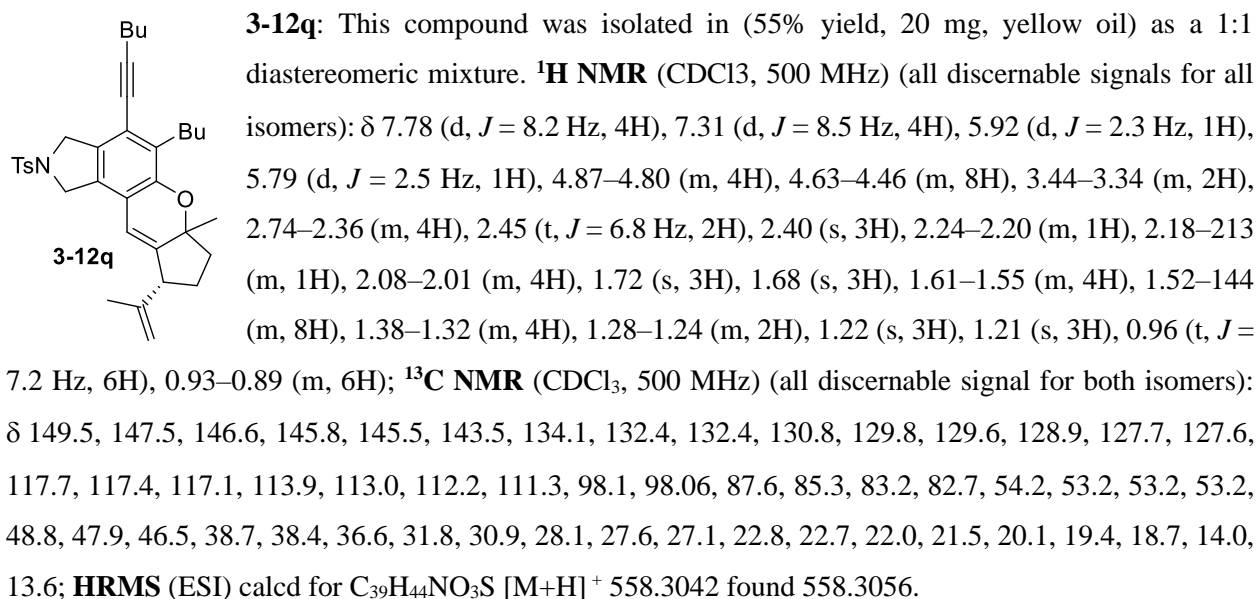
Hz, 3H), 0.92 (t, $J = 7.0$ Hz, 3H); ^{13}C NMR (CDCl_3 , 500 MHz): δ 149.8, 143.5, 134.0, 132.2, 131.1, 130.3, 129.8, 128.9, 127.6, 118.5, 115.9, 98.3, 80.5, 76.7, 54.2, 52.9, 32.6, 31.6, 30.9, 27.5, 26.3, 26.0, 22.8, 22.5, 22.1, 21.9, 21.5, 19.3, 18.9, 14.0, 13.6; **HRMS** (ESI) calcd for $\text{C}_{39}\text{H}_{54}\text{NO}_3\text{S}$ $[\text{M}+\text{H}]^+$ 616.3824, found 616.3835.



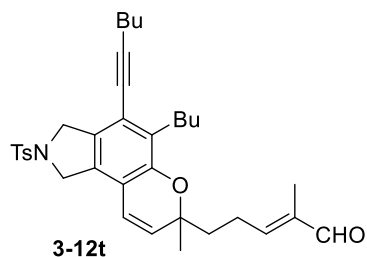
3-11p: This compound was isolated in (24% yield, 11 mg, colorless oil) as a 10:1 regioisomeric mixture. Characterization data for major isomer is given. ^1H NMR (CDCl_3 , 500 MHz): δ 9.43 (s, 1H), 7.76 (d, $J = 8.1$ Hz, 2H), 7.31 (d, $J = 7.7$, 2H), 6.82 (s, 1H), 6.79–6.76 (m, 1H), 4.85 (s, 1H), 4.63–4.60 (m, 2H), 4.59 (s, 1H), 4.56–4.47 (m, 2H), 3.22 (s, 2H), 2.67 (t, $J = 7.1$ Hz, 2H), 2.45 (t, $J = 6.4$ Hz, 2H), 2.26–2.14 (m, 2H), 2.14–2.02 (m, 2H), 1.91–1.84 (m, 1H), 1.62–1.55 (m, 4H), 1.54–1.44 (m, 4H), 1.34–1.28 (m, 2H), 0.96 (t, $J = 7.7$ Hz, 2H), 0.91 (t, $J = 7.3$ Hz, 2H); ^{13}C NMR (CDCl_3 , 500 MHz): δ 193.7, 150.0, 149.6, 143.6, 141.2, 139.1, 133.9, 132.8, 132.5, 129.8, 129.4, 127.5, 116.5, 111.1, 98.4, 76.0, 54.4, 53.3, 39.2, 38.7, 33.8, 32.9, 32.2, 30.9, 26.7, 22.5, 21.9, 21.6, 21.5, 19.3, 13.9, 13.6; **HRMS** (ESI) calcd for $\text{C}_{35}\text{H}_{44}\text{NO}_3\text{S}$ $[\text{M}+\text{H}]^+$ 558.3018, found 558.3029.



3-12p: This compound was isolated in (34% yield, 14 mg) as yellow oil. ^1H NMR (CDCl_3 , 500 MHz): δ 7.76 (d, $J = 8.1$ Hz, 2H), 7.30 (d, $J = 7.8$ Hz, 2H), 5.83 (s, 1H), 4.99–4.95 (m, 1H), 4.92 (s, 1H), 4.83 (s, 1H), 4.58–4.48 (m, 4H), 2.65 (t, $J = 7.5$ Hz, 2H), 2.61–2.56 (m, 1H), 2.44 (t, $J = 5.6$ Hz, 2H), 2.40 (s, 3H), 2.27–2.21 (m, 2H), 2.01–1.93 (m, 2H), 1.77 (s, 3H), 1.70–1.62 (m, 1H), 1.60–1.54 (m, 2H), 1.52–1.41 (m, 4H), 1.36–1.29 (m, 2H), 0.96 (t, $J = 7.5$ Hz, 2H), 0.91 (t, $J = 7.2$ Hz, 2H); ^{13}C NMR (CDCl_3 , 500 MHz): δ 150.0, 146.1, 143.5, 139.7, 133.9, 130.6, 129.8, 128.1, 127.6, 117.4, 116.3, 113.4, 111.1, 109.5, 97.9, 76.7, 73.4, 54.2, 52.9, 38.7, 35.7, 31.7, 30.9, 28.1, 27.8, 27.2, 22.6, 22.2, 21.9, 21.5, 19.3, 14.0, 13.6; **HRMS** (ESI) calcd for $\text{C}_{35}\text{H}_{44}\text{NO}_3\text{S}$ $[\text{M}+\text{H}]^+$ 558.3042, found 558.3040.



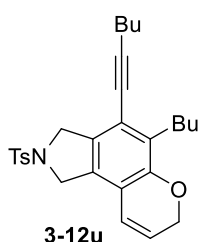
discernable signal for both isomers): δ 202.42, 148.2, 148.1, 143.5, 135.8, 135.0, 134.0, 131.6, 130.8, 129.8, 127.6, 117.7, 116.5, 115.92, 115.89, 98.2, 78.7, 78.6, 76.6, 54.2, 52.9, 51.1, 50.8, 32.7, 31.94, 31.92, 29.89, 29.78, 29.7, 28.0, 28.88, 27.57, 22.96, 21.5, 20.0, 19.7, 19.3, 13.9, 13.6; **HRMS** (ESI) calcd for $C_{35}H_{46}NO_4S$ $[M+H]^+$ 576.3148, found 576.3147.



3-12t: This compound was isolated in (72% yield, 26 mg) as a yellow oil.

1H NMR ($CDCl_3$, 500 MHz): δ 9.36 (s, 1H), 7.74 (d, J = 8.1 Hz, 2H), 7.32 (d, J = 7.9 Hz, 2H), 6.47 (t, J = 7.2 Hz, 1H), 6.19 (d, J = 9.9 Hz, 1H), 5.59 (d, J = 9.9 Hz, 1H), 4.56 (s, 4H), 2.67 (t, J = 7.0 Hz, 2H), 2.45 (t, J =

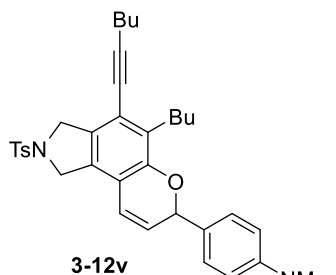
7.0 Hz, 2H), 2.41 (s, 3H), 1.92–1.77 (m, 2H), 1.69 (s, 3H), 1.62–1.54 (m, 3H), 1.53–1.41 (m, 4H), 1.39–1.32 (m, 1H), 1.35 (s, 3H), 0.95 (t, J = 7.4 Hz, 3H), 0.91 (t, J = 7.6 Hz, 3H); **^{13}C NMR** ($CDCl_3$, 500 MHz): δ 195.1, 153.8, 149.7, 139.5, 133.9, 131.9, 130.6, 129.9, 129.8, 129.2, 127.6, 119.9, 119.0, 114.5, 98.7, 78.1, 76.5, 54.1, 52.9, 39.7, 31.7, 30.8, 27.4, 26.2, 24.1, 22.8, 21.9, 21.5, 19.3, 14.0, 13.6, 9.1; **HRMS** (ESI) calcd for $C_{35}H_{44}NO_4S$ $[M+H]^+$ 574.2991, found 574.2998.



3-12u: This compound was isolated in (72% yield, 324 mg) as a white solid. **1H NMR**

($CDCl_3$, 500 MHz): δ 7.77 (d, J = 7.8 Hz, 2H), 7.31 (d, J = 8.2 Hz), 6.22 (d, J = 10.4, 1H), 5.85–5.80 (m, 1H), 4.74–4.70 (m, 2H), 4.57–4.53 (m, 4H), 2.65 (t, J = 7.6 Hz, 2H), 2.45 (t, J = 6.8 Hz, 2H), 2.41 (s, 3H), 1.61–1.54 (m, 2H), 1.53–1.40 (m, 4H), 1.37–1.30

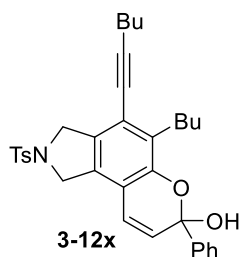
(m, 2H), 0.96 (t, J = 7.7 Hz, 3H), 0.90 (t, J = 8.0 Hz, 3H). **^{13}C NMR** ($CDCl_3$, 500 MHz): δ 151.2, 143.6, 133.9, 11.9, 131.1, 129.8, 129.2, 127.6, 123.4, 121.2, 118.7, 116.5, 98.6, 76.5, 65.2, 54.1, 52.9, 31.8, 30.8, 27.5, 22.8, 22.0, 21.5, 19.3, 13.9, 13.6; **HRMS** (ESI) calcd for $C_{28}H_{34}NO_3S$ $[M+H]^+$ 464.2259, found 464.2251.



3-12v: This compound was isolated in (74% yield, 28 mg) as a yellow solid.

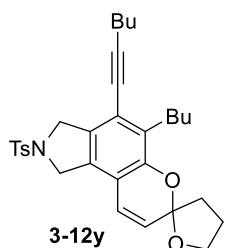
¹H NMR (CDCl₃, 500 MHz): δ 7.78 (d, *J* = 7.9 Hz, 2H), 7.32 (d, *J* = 8.1 Hz, 2H), 7.21 (d, *J* = 8.6 Hz, 2H), 6.65 (d, *J* = 8.4 Hz, 2H), 6.35 (d, *J* = 10.0 Hz, 1H), 5.87 (dd, *J* = 3.7, 5.8 Hz, 1H), 5.77–5.74 (m, 1H), 4.60 (s, 2H), 4.55 (s, 2H), 2.92 (s, 6H), 2.59 (t, *J* = 6.7 Hz, 2H), 2.44–2.38 (m, 5H), 1.58–

1.52 (m, 4H), 1.49–1.43 (m, 2H), 1.24–1.18 (m, 2H), 0.94 (t, *J* = 6.7 Hz, 3H), 0.8 (t, *J* = 7.0 Hz, 3H); **¹³C NMR** (CDCl₃, 500 MHz): δ 150.7, 150.1, 143.5, 134.0, 132.2, 130.6, 129.8, 128.4, 127.2, 126.4, 126.4, 124.6, 120.3, 118.7, 115.8, 112.2, 98.4, 76.4, 76.4, 54.2, 53.0, 40.4, 31.6, 30.8, 27.4, 22.6, 21.9, 21.5, 19.3, 14.0, 13.6. **HRMS** (ESI) calcd for C₃₆H₄₃N₂O₃S [M+H]⁺ 583.2994, found 583.2988.



3-12x: This compound was isolated in (54% yield, 18 mg) as white solid. **¹H NMR** (CDCl₃, 500 MHz): δ 7.78 (d, *J* = 7.8 Hz, 2H), 7.62 (d, *J* = 6.0 Hz, 2H), 7.44–7.37 (m, 3H), 7.32 (d, *J* = 6.64, 2H), 6.47 (d, *J* = 9.7 Hz, 2H), 5.94 (d, *J* = 10.3 Hz, 2H), 4.73–4.56 (m, 4H), 3.12 (s, 1H, –OH, D₂O exchangeable) 2.84–2.78 (m, 2H), 2.47

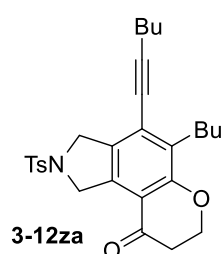
(t, *J* = 6.9 Hz, 2H), 2.41 (s, 3H), 1.64–1.57 (m, 2H), 1.54–1.46 (m, 4H), 1.37–1.31 (m, 2H), 0.97 (t, *J* = 6.5 Hz, 3H), 0.88 (t, *J* = 7.1 Hz, 3H); **¹³C NMR** (CDCl₃, 500 MHz): δ 145.7, 143.6, 142.7, 141.9, 140.8, 129.8, 128.7, 128.4, 127.6, 125.6, 124.4, 124.3, 121.4, 116.5, 111.7, 96.9, 96.4, 75.9, 54.8, 52.2, 33.1, 30.9, 30.0, 22.9, 22.0, 19.3, 13.9, 13.6. **HRMS** (ESI) calcd for C₃₄H₃₈NO₄S [M+H]⁺ 556.2522, found 556.2527.



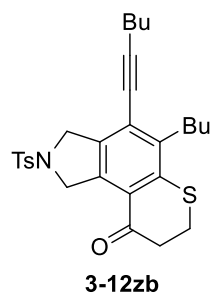
3-12y: This compound was isolated in (92% yield, 30 mg) as white solid. **¹H NMR** (CDCl₃, 500 MHz): δ 7.76 (d, *J* = 7.8 Hz, 2H), 7.30 (d, *J* = 8.1 Hz, 2H), 6.49 (d, *J* = 9.1 Hz, 1H), 5.79 (d, *J* = 9.5 Hz, 1H), 4.73–4.49 (m, 4H), 4.08–4.02 (m, 1H), 4.07–4.02 (m, 1H), 3.96–3.91 (m, 1H), 2.78–2.67 (m, 2H), 2.46 (t, *J* = 7.3 Hz, 2H), 2.40 (s,

3H), 2.48–2.38 (m, 1H), 2.37–2.32 (m, 1H), 2.13–2.05 (m, 1H), 2.04–1.96 (m, 1H), 1.61–1.57 (m, 2H), 1.53–1.43 (m, 4H), 1.39–1.34 (m, 2H), 0.96 (t, *J* = 7.3 Hz, 2H), 0.92 (t, *J* = 7.4 Hz, 2H); **¹³C NMR** (CDCl₃, 500 MHz): δ 148.8, 143.6, 133.8, 132.6, 130.9, 129.8, 129.3, 127.5, 123.5, 123.3, 118.9, 114.5, 104.9, 98.8,

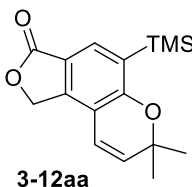
76.6, 68.4, 54.3, 53.1, 38.9, 31.8, 30.8, 27.6, 24.6, 22.9, 21.9, 21.5, 19.4, 14.0, 13.6. **HRMS** (ESI) calcd for $C_{31}H_{38}NO_4S$ $[M+H]^+$ 520.2522, found 520.2509.



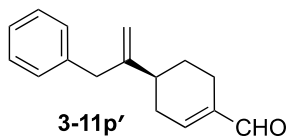
3-12za: This compound was isolated in (56% yield, 20 mg) as a yellow solid. **1H NMR** ($CDCl_3$, 500 MHz): δ 7.80 (d, J = 8.3 Hz, 2H), 7.30 (d, J = 7.8 Hz, 2H), 4.90–4.86 (m, 2H), 4.56–4.51 (m, 2H), 4.47 (t, J = 6.7 Hz, 2H), 2.75–2.69 (m, 4H), 2.49 (t, J = 6.7 Hz, 2H), 2.39 (s, 3H), 1.64–1.57 (m, 2H), 1.52–1.42 (m, 4H), 1.38–1.31 (m, 2H), 0.97 (t, J = 7.2 Hz, 2H), 0.92 (t, J = 7.6 Hz, 2H); **^{13}C NMR** ($CDCl_3$, 500 MHz): δ 192.1, 159.7, 143.4, 134.2, 134.1, 133.7, 131.7, 129.8, 127.6, 125.3, 115.7, 102.4, 76, 67.0, 55.9, 53.1, 37.8, 31.6, 30.6, 27.7, 22.8, 22.0, 21.5, 19.5, 13.9, 13.6; **HRMS** (ESI) calcd for $C_{28}H_{34}NO_4S$ $[M+H]^+$ 488.2209, found 488.2202.



3-12zb: This compound was isolated in (51% yield, 17 mg) as a yellow solid. **1H NMR** ($CDCl_3$, 500 MHz): δ 7.79 (d, J = 8.4 Hz, 2H), 7.29 (d, J = 8.2 Hz, 2H), 4.92 (s, 2H), 4.92 (s, 2H), 3.17–3.12 (m, 2H), 2.92–2.87 (m, 2H), 2.86–2.81 (m, 2H), 2.50 (t, J = 7.04 Hz, 2H), 2.39 (s, 3H), 1.64–1.57 (m, 2H), 1.52–1.46 (m, 4H), 1.44–1.36 (m, 2H), 0.99–0.92 (m, 6H); **^{13}C NMR** ($CDCl_3$, 500 MHz): δ 194.8, 143.5, 141.8, 141.1, 136.8, 136.4, 133.9, 129.8, 127.6, 125.2, 123.5, 102.6, 76.2, 56.9, 39.8, 32.1, 25.8, 23.0, 22.0, 21.5, 19.5, 13.8, 13.6; **HRMS** (ESI) calcd for $C_{28}H_{34}NO_4S$ $[M+H]^+$ 488.2209, found 488.2202; **HRMS** (ESI) calcd for $C_{28}H_{34}NO_3S_2$ $[M+H]^+$ 496.1980, found 496.1997.



3-12aa: This compound was isolated in (86% yield, 28 mg) as a white solid. **1H NMR** ($CDCl_3$, 500 MHz): δ 7.75 (s, 1H), 6.21 (d, J = 10.2 Hz, 1H), 5.72 (d, J = 9.7 Hz, 1H), 5.21 (s, 2H), 1.5 (s, 6H), 0.3 (s, 9H); **^{13}C NMR** ($CDCl_3$, 500 MHz): δ 171.2, 162.2, 144.9, 132.2, 131.6, 129.3, 117.5, 116.9, 113.4, 77.9, 69.3, 67.8, 28.3, -1.06; **HRMS** (ESI) calcd for $C_{16}H_{21}O_3Si$ $[M+H]^+$ 298.1260, found 298.1265.



3-11p': This compound was isolated in (75% yield, 38 mg) as a yellow solid.

¹H NMR (CDCl₃, 500 MHz): δ 9.41 (s, 1H), 7.31–7.27 (m, 2H), 6.79–6.76 (m, 1H), 4.90 (s, 1H), 4.81 (s, 1H), 3.42 (s, 2H), 2.51–2.37 (m, 2H), 2.28–

2.16 (m, 2H), 2.12–2.01 (m, 1H), 1.95–1.88 (m, 1H), 1.52–1.42 (m, 1H); **¹³C NMR** (CDCl₃, 500 MHz): δ 193.8, 151.9, 150.5, 141.2, 139.5, 129.0, 128.4, 126.2, 110.9, 42.0, 38.4, 32.4, 26.7, 21.6; **HRMS** (ESI) calcd for C₁₆H₁₈O [M+H]⁺ 226.1357, found 226.1359.

3.4.4. Computational details

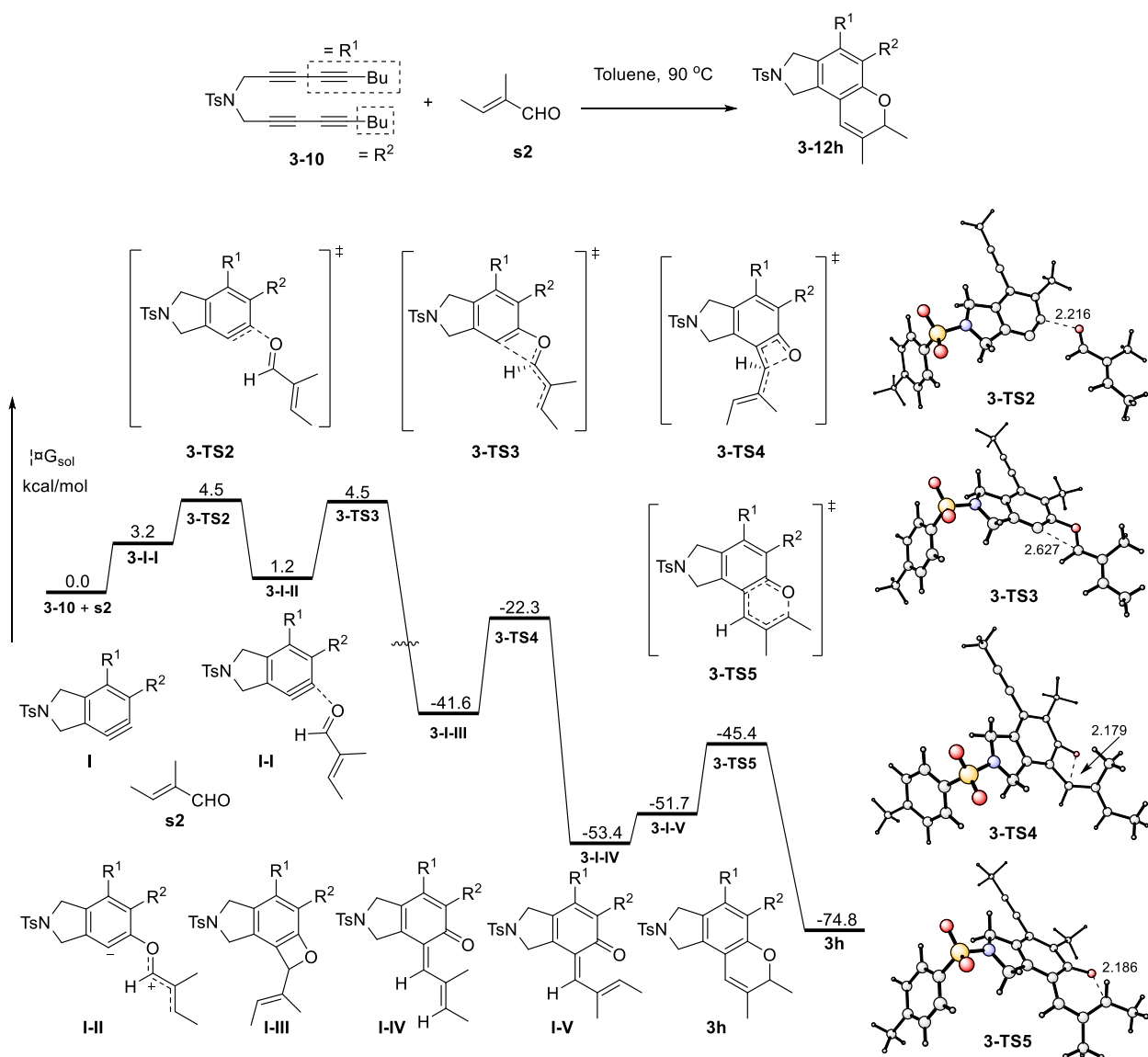
All DFT calculations were carried out with the Gaussian 09 suite of computational programs.^[1] The geometries of all stationary points were optimized using the B3LYP hybrid functional^[2] at the basis set level of 6-31+G(d). Frequencies were analytically computed at the same level of theory to obtain the free energies and to confirm whether the structures are minima (no imaginary frequency) or transition states (only one imaginary frequency). The solvent effect of toluene was evaluated by using the SMD polarizable continuum model by carrying out single point calculations at the M06/6-311+G(d,p) level.^[3] All transition state structures were confirmed to connect the proposed reactants and products by intrinsic reaction coordinate (IRC) calculations. All the energies given in the text are relative free energies corrected with solvation effects.

[1] Gaussian 09, Revision A.01, M. J. Frisch, G. W. Trucks, H. B. Schlegel, G. E. Scuseria, M. A. Robb, J. R. Cheeseman, G. Scalmani, V. Barone, B. Mennucci, G. A. Petersson, H. Nakatsuji, M. Caricato, X. Li, H. P. Hratchian, A. F. Izmaylov, J. Bloino, G. Zheng, J. L. Sonnenberg, M. Hada, M. Ehara, K. Toyota, R. Fukuda, J. Hasegawa, M. Ishida, T. Nakajima, Y. Honda, O. Kitao, H. Nakai, T. Vreven, J. A. Montgomery, Jr., J. E. Peralta, F. Ogliaro, M. Bearpark, J. J. Heyd, E. Brothers, K. N. Kudin, V. N. Staroverov, R. Kobayashi, J. Normand, K. Raghavachari, A. Rendell, J. C. Burant, S. S. Iyengar, J. Tomasi, M. Cossi, N. Rega, J. M. Millam, M. Klene, J. E. Knox, J. B. Cross, V. Bakken, C. Adamo, J. Jaramillo, R. Gomperts, R. E. Stratmann, O. Yazyev, A. J. Austin, R. Cammi, C. Pomelli, J. W. Ochterski, R. L. Martin, K. Morokuma, V. G. Zakrzewski, G. A. Voth, P. Salvador, J. J. Dannenberg, S. Dapprich, A. D. Daniels, Ö. Farkas, J. B. Foresman, J. V. Ortiz, J. Cioslowski, D. J. Fox, Gaussian, Inc., Wallingford CT, **2009**.

[2] (a) Becke, A. D. *J. Chem. Phys.* **1993**, 98, 5648. (b) Becke, A. D. *J. Chem. Phys.* **1993**, 98, 1372. (c) Lee, C.; Yang, W.; Parr, R. G. *Phys. Rev. B* **1988**, 37, 785.

[3] (a) Zhao, Y.; Truhlar, D. G. *Theor. Chem. Acc.* **2008**, 120, 215. (b) Zhao, Y.; Truhlar, D. G. *Acc. Chem. Res.* **2008**, 41, 157.

DFT-Calculated Reaction Mechanism



3.5. Note

Computational study for this work has been carried out by Peipei Xie and Prof. Yuanzhi Xia of Wenzhou University in China.

3.6. References

1. For general reviews on Alder-ene reactions: (a) Mikami, K.; Shimizu, M. *Chem. Rev.* **1992**, *92*, 1021. (b) Dias, L. C. *Curr. Org. Chem.* **2000**, *4*, 30. (c) Adams, W.; Krebs, O. *Chem. Rev.* **2003**, *103*, 4131. For a review on transition metal-catalyzed Alder-ene reactions: (d) Trost, B. M.; Frederiksen, M. U.; Rudd, M. T. *Angew. Chem., Int. Ed.* **2005**, *44*, 6630.
2. Gupta, S.; Xie, P.; Xia, Y.; Lee, D. *Org. Lett.* **2017**, *19*, 5162.
3. (a) Bhojgude, S. S.; Bhunia, A.; Biju, A. T. *Acc. Chem. Res.* **2016**, *49*, 1658. (b) Ross, S. P.; Baire, B.; Hoye, T. R. *Org. Lett.* **2017**, *19*, 5705. (c) Roy, T.; Biju, A. T. *Chem. Commun.* **2018**, *54*, 2580.
4. Miyabe, H. *Molecules* **2015**, *20*, 12558.
5. Dubrovski, A. V.; Larock, R. C. *Org. Lett.* **2010**, *12*, 3117.
6. Cant, A. A.; Bertrand, G. H. V.; Henderson, J. L.; Roberts, L.; Greaney, M. F. *Angew. Chem., Int. Ed.* **2009**, *48*, 5199.
7. Campbell-Verduyn, L.; Elsinga, P. H.; Mirfeizi, L.; Dierckx, R. A.; Feringa, B. L. *Org. Biomol. Chem.* **2008**, *6*, 3461.
8. (a) R. Karmakar, S. Y. Yun, K. P. Wang and D. Lee, *Org. Lett.*, 2014, *16*, 6. For theoretical studies on the regioselectivity of aryne reactions: (b) Cheong, P. H.-Y.; Paton, R. S.; Bronner, S. M.; Im, G.-Y. J.; Garg, N. K.; Houk, K. N. *J. Am. Chem. Soc.* **2010**, *132*, 1267. (c) Medina, J. M.; Mackey, J. L.; Garg, N. K.; Houk, K. N. *J. Am. Chem. Soc.* **2014**, *136*, 15798.
9. Yoshida, H.; Watanabe, M.; Fukushima, H.; Ohshita, J.; Kunai, A. *Org. Lett.* **2004**, *6*, 4049.
10. Yoshioka, E.; Kothani, S.; Miyabe, H. *Angew. Chem., Int. Ed.* **2011**, *50*, 6638.
11. Yoshioka, E.; Tamenaga, H.; Miyabe, H. *Tetrahedron Lett.* **2014**, *55*, 1402.
12. Heany, H.; Jablonski, J. M.; McCarty, C. T. *J. Chem. Soc., Perkin Trans. I* **1972**, 2903.

13. Zhang, T.; Huang, X.; Wu, L. *Eur. J. Org. Chem.* **2012**, 2012, 3507.
14. Meng, X.; Lv, S.; Cheng, D.; Hu, Q.; Ma, J.; Liu, B.; Hu, Y. *Chem. – Eur. J.* **2017**, 23, 6264.
15. Wang, T.; Hoye, T. R. *J. Am. Chem. Soc.* **2016**, 138, 13870.
16. Wang, T.; Oswood, C. J.; Hoye, T. R. *Synlett* **2017**, 28, 2933.
17. All calculations were carried out using Gaussian 09 suite of programs by (SMD)M06/6-311+G(d,p)//B3LYP/6-31+G* method in a toluene dispersed phase. All free energies values (in kcal mol⁻¹) discussed are relative to the energy sum of the corresponding aldehyde and benzyne intermediate.
18. Desimoni, G.; Tacconi, G. *Chem. Rev.* **1975**, 75, 651.
19. Reports on the synthesis of [5,6]-spiroketals: (a) Lindsey, C. C.; Wu, L. K.; Pettus, T. R. *Org. Lett.* **2006**, 8, 2365. (b) Marsini, M. A.; Huang, Y.; Lindsey, C. C.; Wu, K.-L.; Pettus, T. R. *Org. Lett.* **2008**, 10, 1477. (c) Zhou, G.; Zhu, J.; Xie, J.; Li, Y. *Org. Lett.* **2008**, 10, 721. (d) Brimble, M. A.; McLeod, M. C.; Wilson, Z. E.; Rathwell, D. C. K.; Yien, T.-Y. *Pure Appl. Chem.* **2012**, 84, 1379.
20. Palani, V.; Chen, J.; Hoye, T. R. *Org. Lett.* **2016**, 18, 6312.
21. (a) Fridén-Saxin, M.; Seifert, T.; Landergren, M. R.; Suuronen, T.; Lahtela-kakkonen, M.; Jarho, E. M.; Luthman, K. *J. Med. Chem.* **2012**, 55, 7104. (b) Conti, C.; Monaco, L. P.; Desideri, L. P. *Bioorg. Med. Chem.* **2011**, 19, 7357.
22. (a) Himeshima, Y.; Sonada, T.; Kobayashi, H. *Chem. Lett.* **1983**, 12, 1211. (b) Liu, S.; Li, Y.; Lan, Y. *Eur. J. Org. Chem.* **2017**, 2017, 6349.
23. Lee, N. M.; Yun, S. Y.; Mamidipalli, P.; Salzman, R. M.; Lee, D.; Zhou, T.; Xia, Y. *J. Am. Chem. Soc.* **2014**, 136, 4363.

24. Michno, D. M.; Dauben, W. G. *J. Org. Chem.* **1977**, *42*, 682.
25. Wolinsky, J.; Slabaugh, M. R.; Gibson, T. *J. Org. Chem.* **1964**, *29*, 3740.

CHAPTER 4

Alder-Ene Reaction to Form Benzocyclobutenes

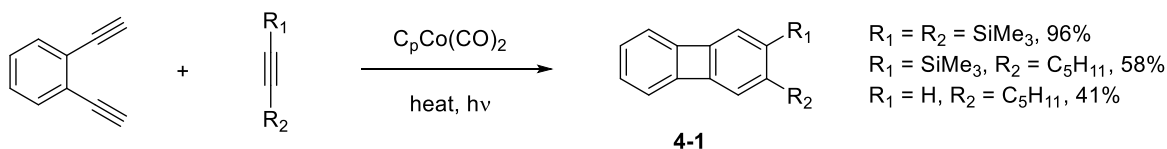
4.1. Introduction*

Benzocyclobutenes form a unique class of compounds that shows interesting reactivities through the opening of the four-membered ring. In particular, their property to undergo thermal electrocyclic ring-opening to give *ortho*-xylylenes and undergo a Diels-Alder reaction have been exploited over the past decades for the total synthesis of various polycyclic natural products.¹ The unique ring-opening reactivities have shown great applications in the synthesis of thermoset polymers² and various active pharmaceutical ingredients.³ Particularly, benzocyclobutenones demonstrated an unconventional mode of reactivity under transition-metal catalysis, which provides access a basis for the development of new synthetic routes to benzo-fused cyclic skeletons.⁴ The synthetic importance of this class of molecules has spurred a renewed demand to develop more convenient methods to synthesize benzocyclobutenones with a wide functional group tolerance starting from easily accessible materials.

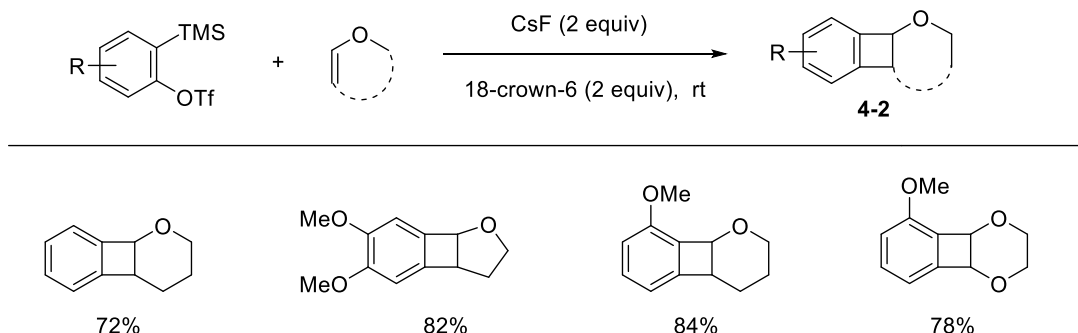
The earliest method for accessing a benzocyclobutene skeleton is a cobalt catalyzed [2+2+2]-cycloaddition reaction developed by Vollhardt and coworkers.⁵ In this reaction *o*-diethynylbenzene undergoes co-cyclization with alkynes in the presence of dicarbonyl(cyclopentadienyl)-cobalt catalyst to provide a versatile synthesis of the biphenylene nucleus **4-1** (**Scheme 4.1**). The [2+2] cycloaddition of arynes with electron-rich alkenes is one of the most common methods to synthesize benzocyclobutenes.⁶ Regioselectivity of this cycloaddition is dictated by the nature of substituents on the aryne. This method has been utilized as a platform to get access to stereo-defined 1,2-disubstituted benzocyclobutenes **4-2a** by employing arynes generated under the Kobayash's protocol and cyclic enol ethers including 2,3-dihydrofuran, 2,3-dihydro-3*H*-pyran, 1,4-dioxene.⁷

*This chapter has been reproduced from Gupta, S.; Lin, Y.; Xia, Y.; Wink, D. J.; Lee, D. "Alder-ene reactions driven by high steric strain and bond angle distortion to form benzocyclobutenes" *Chem. Sci.* **2019**, *10*, 2212–2217, with permission from The Royal Society of Chemistry.

Cobalt-catalyzed [2+2+2] cycloaddition



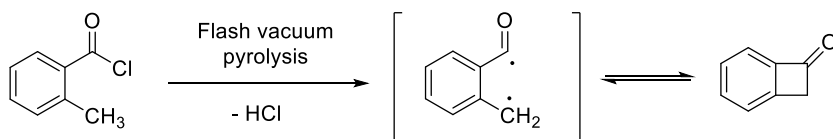
Cycloaddition of arynes and enol ethers



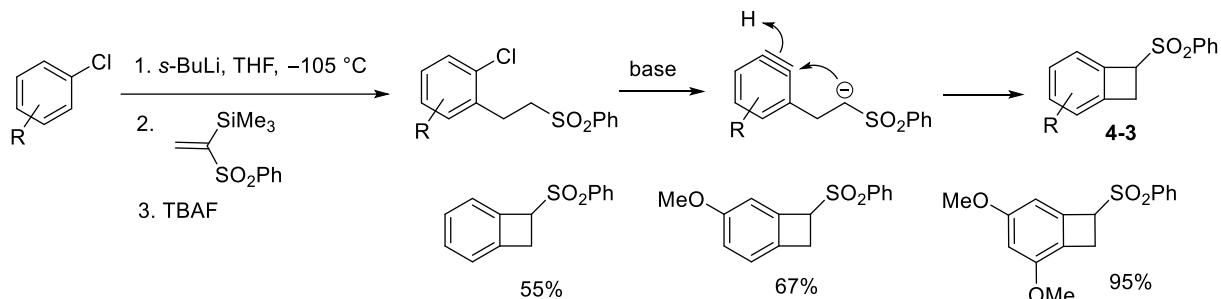
Scheme 4.1. Different protocols for the synthesis of benzocyclobutenes

Flash vacuum pyrolysis of aroyl chloride offers alternative access to benzocyclobutenones. This method requires rigorous heating conditions (around 630 °C), which diminish the practicality of the method (**Scheme 4.2**).⁸ Iwao reported a directed lithiation of chlorobenzene for the synthesis of benzocyclobutenes.⁹ Chlorobenzene and its MeO-, TBSO-, and Cl-substituted derivatives were lithiated at the *ortho*-position to the chloride with high regioselectivity by treatment with *sec*-BuLi in THF at –105 °C without forming benzyne. The lithiated species thus generated underwent smooth Michael addition on treatment with 1-(phenylsulfonyl)-1-(trimethylsilyl)ethene. After desilylation, the Michael adducts were treated with a strong base to generate 1-(phenylsulfonyl)benzocyclobutenes **4-3** via a benzyne intermediate. The four-membered ring can also be constructed by intramolecular nucleophilic addition of aryl lithium generated from (*o*-halophenyl)epoxides¹⁰ and (*o*-halophenyl)acetamides. Lithium-iodine exchange of *o*-iodo-*N*-methoxy-*N*-methyl phenylacetamides also provides a simple and efficient route to benzocyclobutenones.¹¹

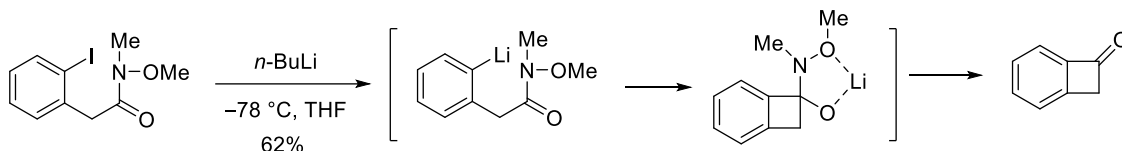
Flash Vacuum Pyrolysis



Directed Lithiation of Chlorobenzenes



Intramolecular nucleophilic addition of aryl lithium

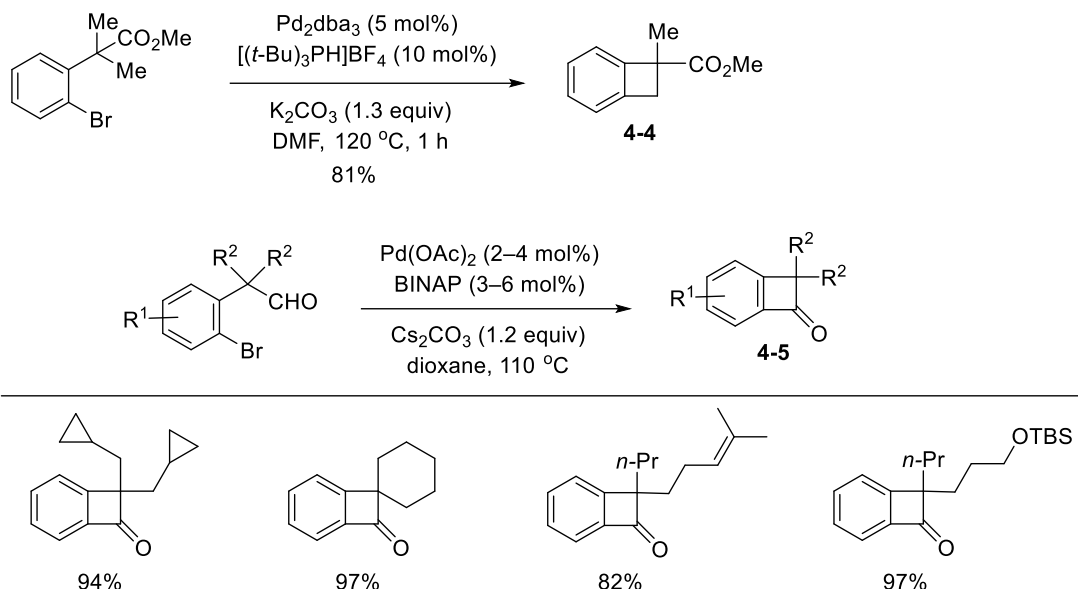


Scheme 4.2. Benzocyclobutene formation via radical and anion intermediates

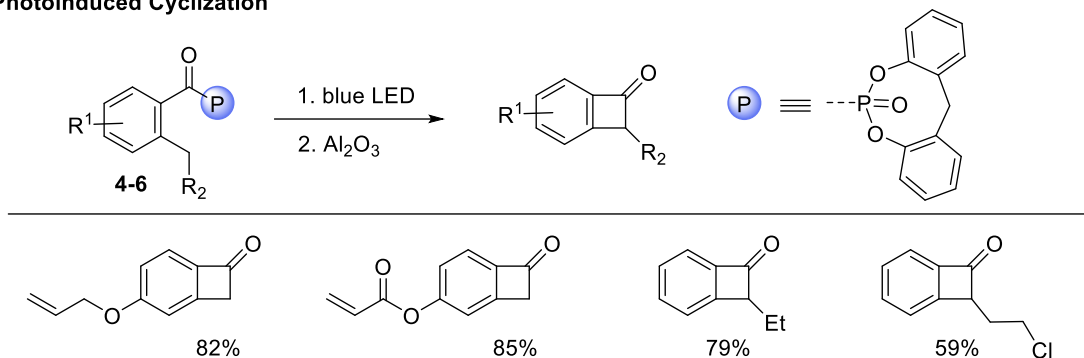
Palladium-catalyzed cyclization reaction is a powerful method for the synthesis of benzocyclobutenes. Baudoin and coworkers¹² demonstrated an efficient catalytic system for the synthesis of benzocyclobutenes by C–H activation of methyl groups (**Scheme 4.3**). The optimal conditions employed a combination of Pd(OAc)₂, P(*t*-Bu)₃, and K₂CO₃ in DMF. This method leads to the formation of various benzocyclobutenes **4-4** in 44–92% yield, including molecules that are hardly accessible by other methods. Martin and coworkers¹³ demonstrated an Pd-catalyzed intramolecular acylation for the synthesis of functionalized benzocyclobutenones **4-5** with diverse substituent pattern. The optimal condition for this method uses Pd(OAc)₂, Cs₂CO₃ and a bidentate diarylphosphine in dioxane at 110 °C.

Photo-induced cyclization *o*-alkylphenyl ketones is another atom-economical method to access benzocyclobutenols.¹⁴ Although this approach has a merit to avoid the use of an organolithium reagent it suffers from low yields. Murukami and coworkers¹⁵ has improved the efficiency of the photo-induced cyclization by using visible light with (*o*-alkylbenzoyl)-phosphonates **4-6** to form phosphonate-substituted

Palladium catalyzed cyclization



Photoinduced Cyclization



Scheme 4.3. Palladium-catalyzed and photoinduced cyclizations to form benzocyclobutenes

to form phosphonate-substituted benzocyclobutenols followed by subsequent elimination of phosphinate to generate benzocyclobutenones. The starting (*o*-alkylbenzoyl)phosphonates **4-6** can be readily prepared from aryl chlorides and phosphinic acid. In this reaction, the phosphonate plays a key role to facilitate construction of the four-membered ring. The mild reaction conditions allow for incorporation of a diverse array of functional groups that conventional methods hardly tolerate.

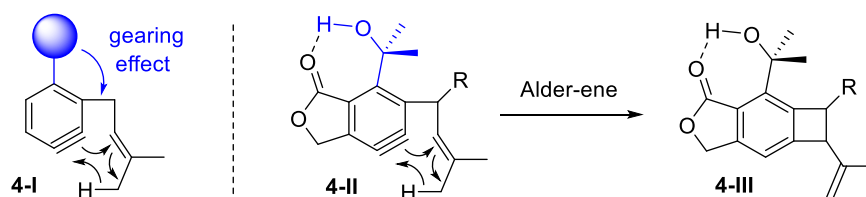
Although the Kobayashi's protocol for aryne formation and (*o*-alkylbenzoyl)phosphonate-based photochemical approach are mild and efficient they suffer from poor atom-economy. Intramolecular Alder-

ene reaction of aryne is a powerful method for formation of carbocyclic or heterocycles fused with arene skeletons. Intramolecular Alder-ene reaction has been conveniently used to access 5-, 6-, 7- or larger membered rings but accessing a strained 4-membered ring through Alder-ene reaction have never been reported. Thus, the development of an aryne-ene reaction to form 4-membered ring would broaden the chemistry of benzocyclobutenes.

4.2. Results and Discussions

4.2.1. Initial design and optimization

The paucity of four-membered ring formation via a thermal Alder-ene reaction is due to not only the ring-strain of the incipient ring but also the difficulty of overcoming the geometrical constraints for the required cyclic transition state. In the case of an aryne as an enophile, however, the relief of its high strain energy may provide a sufficient driving force for the reaction to proceed to form benzocyclobutenes.¹⁷ The calculated Gibbs free energy for the Alder-ene reaction suggests that the product formation has a sufficient thermodynamic driving force (ca. 50–63 kcal mol⁻¹). To overcome the expected kinetic barrier, installation of a structural element (**4-I**) is expected to be crucial, whereby the steric bulk of the substituent will gear the ene-donor alkene via angle distortion to attain an appropriate transition state (**Scheme 4.4**).¹⁶ In the actual substrate (**4-II**) the *ortho*-(dimethyl)methyl carbinol moiety is expected to serve as an effective gearing element through internal hydrogen bonding. In this hydrogen-bonded conformation, the steric pressure exerted by the *gem*-dimethyl group against the ene-donor moiety would promote its interaction with the aryne moiety more effectively, which would facilitate the formation of benzocyclobutene (**4-III**).



Scheme 4.4. Aryne-mediated Alder-ene reaction driven by hydrogen bonding and steric pressure

Having these concerns in mind, we designed propiolate-based triyne substrates **4-7a–h**, ynamide-based tetrayne **4-7i** and triyne **4-7j** (Table 4.1). These substrates contain a substituent that will impose a variable degree of steric interactions with the prenyl group at the transition state of the Alder-ene reaction. The prenyl group was chosen as the ene-donor based on its most favorable capacity for Alder-ene reactions.¹⁷ When triyne **4-7a** bearing a trimethylsilyl group (SiMe₃, TMS) was heated at 130 °C (toluene), complete conversion was reached after 30 h and the isolated product was identified as the Alder-ene product

Entry	R	Time (h)	Conversion ^b	Yield (%) ^c	
1	a	SiMe ₃	30	100	45 (10:1) ^d
2	b	SiEt ₃	30	75	48 ^e (7:1) ^d
3	c	SiMe ₂ ^t Bu	30	25	19 ^f
4	d	Si ⁱ Pr ₃	48	5<	— ^g
5	e	C(OH)Me ₂	14	100	67
6	f	C(OTBS)Me ₂	14	5<	— ^g
7	g	CMe ₃	40	95	49 (5:1) ^d
8	h	H	12	95	— ^h
9	i	CCBu	6	100	— ^h
10	j	C(OH)Me ₂	14	100	28 (5:1) ^{d,i}

4-7i

4-8i

4-7j

4-8j

^a20–25 mg scale of **4-7**. ^bDetermined by ¹H NMR of crude mixtures. ^cIsolated yield.

^dDiastereomeric ratios. ^e52% yield with 75% conversion at 150 °C, 40 h. ^fDetermined by ¹H NMR with an internal standard. ^gStarting material intact at 130 °C but decomposed at 170 °C.

^hNo product observed with decomposition of the starting materials. ⁱHeating at 90 °C

Table 4.1. Effect of steric bulk and hydrogen bonding on the Alder-ene reaction of arynes

4-8a in 45% yield (entry 1). Unexpectedly, the predominant diastereomer of **4-8a** (10:1 dr) was confirmed to have a *cis*-relationship between the silyloxy and the isopropenyl groups. Under the same conditions, triyne **4-7b** containing a triethylsilyl group (SiEt₃, TES) showed similar reactivity, affording product **4-8b** in 48% yield (entry 2). The reaction of **4-7c** containing a *tert*-butyldimethylsilyl group (SiMe₂^tBu, TBS) was much slower, resulting in 25% conversion after 30 h to produce **4-8c** in 19% yield (entry 3). Triyne **4-7d** containing a triisopropylsilyl group (SiⁱPr₃, TIPS) remained intact even after 48 h (entry 4), which seems to be the consequence of extreme steric bulk of the TIPS group that prohibits the formation of an aryne intermediate. Gratifyingly, triyne **4-7e** containing a (dimethyl)methyl carbinol moiety (CMe₂OH) afforded Alder-ene product **4-8e** as a single diastereomer (for nOe data showing the *cis*-relationship see Appendix III) in 65% yield with full conversion within 14 h (entry 5). The ¹H NMR of product **4-8e** shows a characteristic sharp singlet at 6.2 ppm suggesting a hydrogen-bonded hydroxyl group. To compare the role of hydrogen bonding, similar substrates without a free hydroxyl group such as **4-7f** and **4-7g** were tested. While the TBS ether **4-7f** showed little conversion (entry 7), *t*-butyl-containing substrate **4-7g** afforded **4-8g** (5:1 dr) in 45% yield at 75% conversion after 40 h (entry 6 and 7). Triyne **4-7h** containing an unsubstituted propiolate moiety did not provide an Alder-ene product although full conversion was achieved within 12 h (entry 8). As expected, this is the consequence of relatively facile formation of an aryne intermediate but the Alder-ene reaction did not occur due to the lack of the necessary gearing effect. By the same token, the failure of tetrayne **4-7i** in producing **4-8i** is the consequence of a small steric bulk of the 1-hexynyl substituent (entry 9). The important role of the hydrogen bonding was further demonstrated by triyne **4-7j** containing a CMe₂OH group, which provided **4-8j** in only 28% yield although full conversion was achieved (entry 10).

4.2.2. Effect of substituents on the ene-donors

Having identified the crucial elements for the 4-membered ring forming Alder-ene reaction of aryne species, we next examined the structural requirement of the ene-donor moiety (Table 4.2). Triyne **4-7k**, identical to **4-7e** but devoid of a silyloxy group, afforded **4-8k** in 72% yield (entry 1). In contrast, a free

Entry	R	Benzocyclobutene	Yield (%) ^{b,c}	
1			4-8k	72
2			4-8l	30
3			4-8m	— ^d
4			4-8n	— ^d
5			4-8o	67 ^e
6			4-8p	62
7			4-8q	56
8			4-8r	68
			4-8r' (R = SiEt ₃)	46 ^f
9			4-8s	42
10			4-8t	69
11			4-8u ^d	— ^d

^aConditions: toluene, 130 °C, 14 h. ^bIsolated yield. ^c*cis*-Diastereomer only. ^dDecomposition of polymerization of the aryne intermediates. ^e*E/Z*-mixture (2.5 : 1). ^fWith R = SiEt₃, **4-8r'** was obtained in 46% yield at 150 °C at 40 h. ^gIntermolecular Alder-ene reaction with β-pinene (5 equiv.) of **4-7u** provided **4-8u'** (see ref. 19).

Table 4.2. Effect of the substituents on the ene-donor

hydroxyl-containing substrate **4-7l** afforded product **4-8l** in significantly lower yield (30%) (entry 2). We surmise that an alternative hydrogen bonding by the secondary hydroxyl group may perturb the hydrogen bonding of the 3° hydroxyl group at the stage of the ene reaction. This hypothesis is supported by a new broad singlet at 5.6 ppm, which is significantly different from the characteristic signal in other products including **4-8e**. This clearly suggests the beneficial effect of the hydrogen bonding between 3° hydroxyl groups and the lactone carbonyl for the Alder-ene reaction. A structural limitation was recognized from the failure of triyne **4-7m** in generating Alder-ene product **4-8m** (entry 3). We assume that this failure is caused by the severe steric interaction between the aryne moiety and the incipient quaternary carbon center at the transition state of the ene reaction. Unexpectedly, triyne **4-7n** containing a trans-disubstituted ene-donor did not generate **4-8n** instead the starting material was decomposed (entry 4). Triyne **4-7o** containing a geraniol moiety afforded **4-8o** in 67% yield (*E/Z*, 2.5:1) (entry 5). On the other hand, triyne **4-7p** containing a nerol moiety afforded a single isomer **4-8p** in 62% yield, where only the methyl group reacted to become a methyldiene moiety (entry 6). This is consistent with the previous observations that only the distal allylic C–H bonds on the trans-position of ene-donor alkenes can participate in the intramolecular Alder-ene reaction.^{16c} Despite the possibility of forming an 8-membered ring, the exclusive formation of 4-membered ene product **4-8p** from a nerol-derived substrate **4-7p** suggests that a kinetic preference to form a 4-membered ring may override the thermodynamic preference to form an 8-membered ring. Triyne **4-7q** tethered with a 3-methylcyclohexen-1-ol moiety afforded cyclohexane-fused benzocyclobutene **4-8q** in 56% yield (entry 7). The reaction of triyne **4-7r** provided **4-8r** where the gem-dimethyl bridge should control the *cis*-ring junction stereochemistry, which was confirmed by nOe experiments and X-ray diffraction analysis (entry 8). As expected, **4-8r'** containing a triethylsilyl group was obtained in 46% yield at higher temperature with a longer reaction time (150 °C, 40 h) compared to **4-8r** which was obtained in 68% at 130 °C within 14 h. A cholesterol-derived triyne **4-7s** afforded **4-8s** in 42% yield (entry 9). The relatively low yield of **4-8s** is assumed to be the consequence of a conformationally restricted ene-donor methylene unit within the decaline system. On the other hand, triyne **4-7t** tethered with a cyclooctylidene moiety afforded benzocyclobutene **4-8t** in 69% yield, where the ene donor methylene conformation should

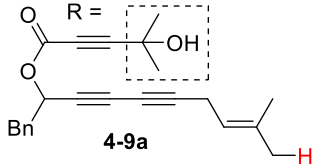
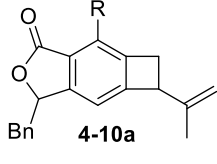
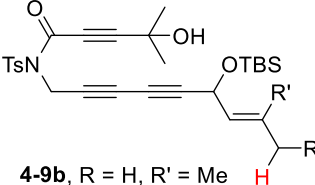
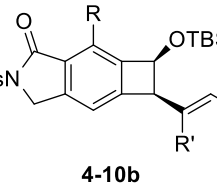
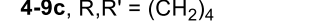
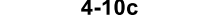
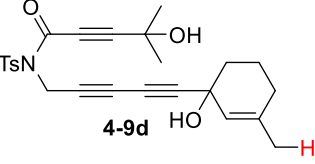
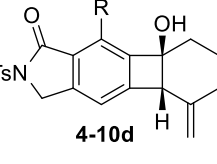
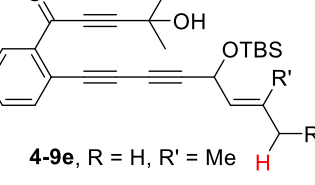
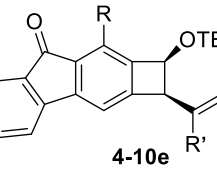


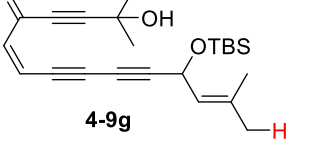
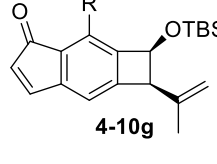
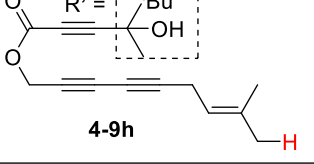
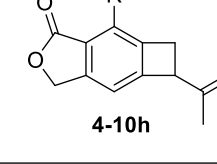
be more flexible to achieve an appropriate transition state for the ene reaction (entry 10). Under the same conditions, triyne **4-7u** bearing an alkyne ene-donor was consumed but the Alder-ene product **4-8u** was not obtained (entry 11). In the presence of β -pinene (5 equiv.) however, **4-7u** afforded product **4-8u'** in 76% yield via an intermolecular reaction. This suggests that the putative aryne intermediate was formed properly from **4-7r** but the Alder-ene reaction between the aryne and the tethered propyne moiety failed. This is presumably because of the difficulty in accessing the required transition state with the alkyne moiety of linear geometry.

4.2.3. Reaction profile with different tethers

Next, we investigated the effect of the tether of triynes on the efficiency of the Alder-ene reaction (Table 4.3). Triyne **4-9a** with a benzylic substituent afforded **4-10a** as a 1:1 mixture of diastereomers in 62% yield (entry 1). Imide-tethered triynes **4-9b** and **4-9c** containing a gem-dimethyl or a cyclohexylidene moiety provided **4-10b** and **4-10c** in 72 and 56% yield (entries 2 and 3). Triyne **4-9d** with a 3-methyl cyclohexen-1-ol moiety afforded **4-10d** in relatively low yield (42%). In the same vein, arene-tethered triynes **4-9e** and **4-9f** afforded **4-10e** and **4-10f** in 87 and 76% yield (entries 5 and 6). Triyne **4-9g** with an enone tether generate indenone **4-10g** in 56% yield (entry 7). A racemic chiral alcohol **4-9h** with sterically differentiated methyl and tert-butyl groups did not lead to the relative stereochemical induction, thus affording **4-10h** as a 1:1 diastereomer in 87% yield (entry 8).

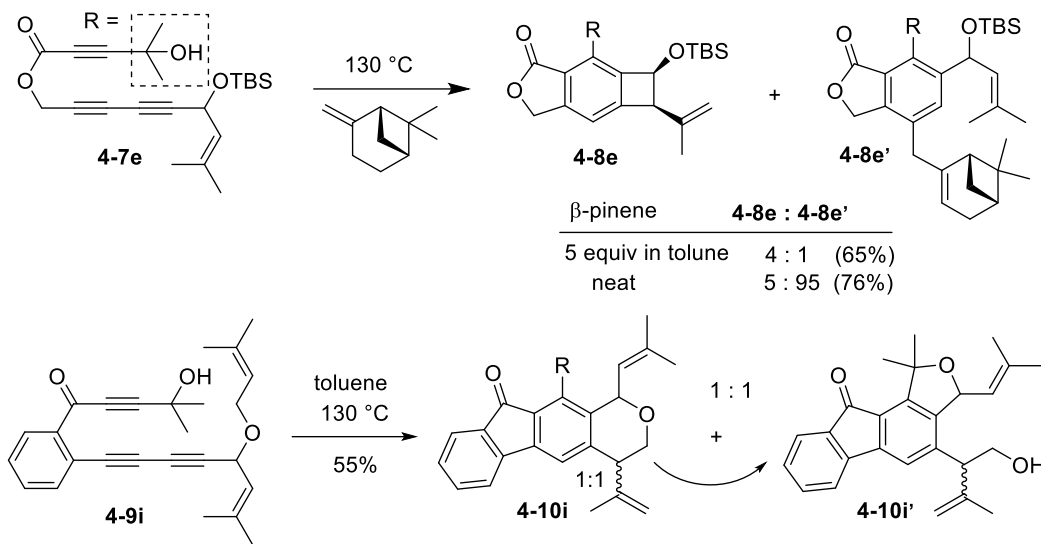
4.2.4. Competition experiments and DFT studies

The competition for intramolecular Alder-ene reactions to form a strained benzocyclobutene versus an intermolecular reaction was examined with triyne **4-7e** (Scheme 4.5). With 5 equivalents of β -pinene, a 4:1 mixture of **4-8e** and **4-8e'** was obtained but the ratio changed to 5:95 in neat β -pinene.¹⁹ An internal competition with triyne **4-9i** provided 6-membered ring product **4-10i** along with its derivative **4-10i'**.²⁰ This indicates that the formation of a 6-membered ring is much more favorable than that of a 4-membered ring via the ene reaction.

Entry	Triynes (4-9) ^a	Benzocyclobutene (4)	Yield (%) ^{b,c}
1	 4-9a	 4-10a	62 (1:1) ^d
2	 4-9b , R = H, R' = Me	 4-10b	72
3	 4-9c , R,R' = (CH ₂) ₄	 4-10c	56
4	 4-9d	 4-10d	42
5	 4-9e , R = H, R' = Me	 4-10e	87 (6:1) ^d
6	 4-9f , R,R' = (CH ₂) ₄	 4-10f	76 (10:1) ^d
7	 4-9g	 4-10g	56 (10:1) ^d
8	 4-9h	 4-10h	87 (1:1) ^d

^aConditions: toluene, 90 °C, 14 h. ^bIsolated yield. ^cDiastereomeric ratio as determined by ¹H NMR of crude. ^dAt 130 °C, 14 h.

Table 4.3. Reactivity of triynes of different tethers



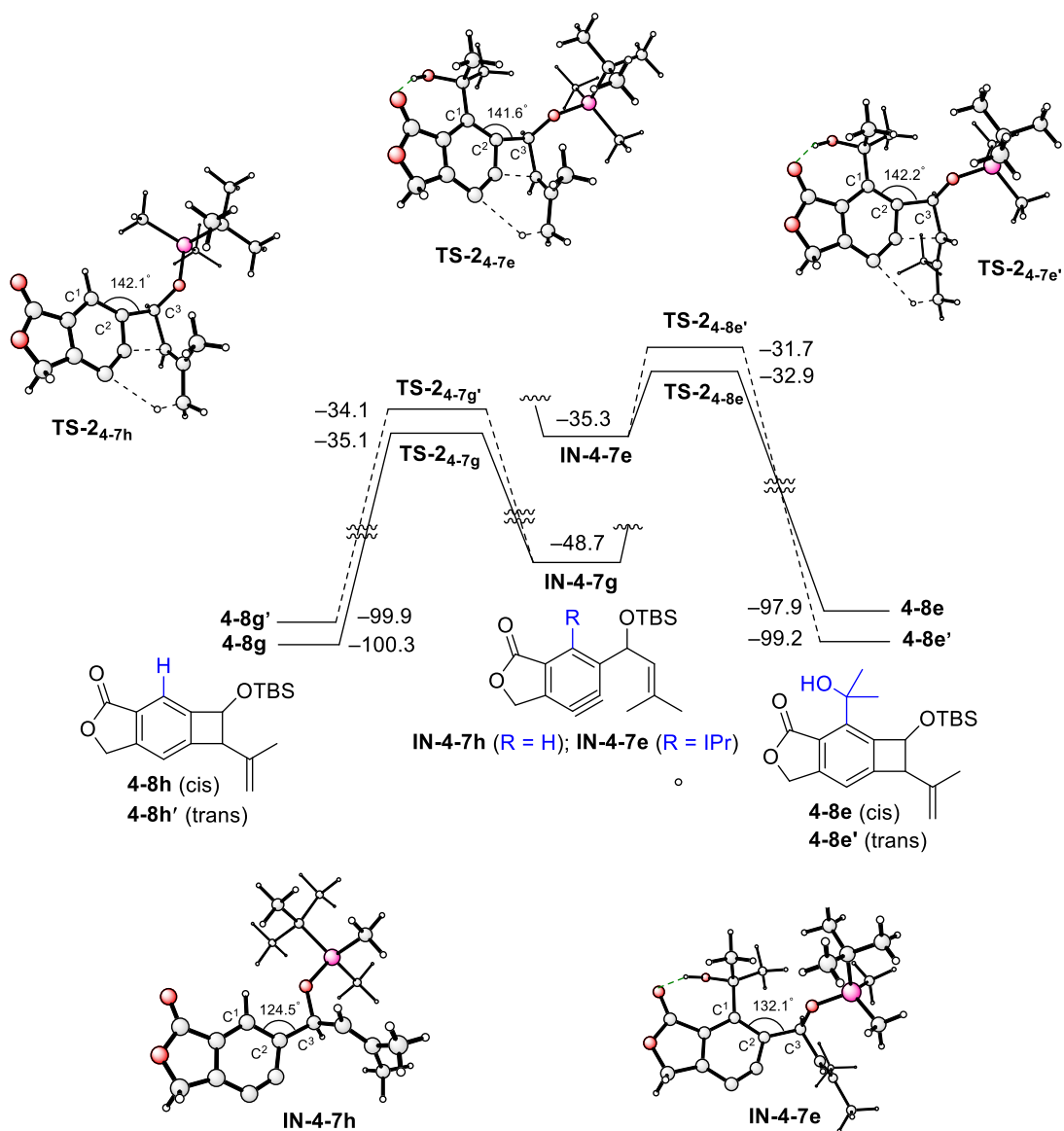
Scheme 4.5. Inter vs. intramolecular Alder-ene reaction

To gain insight into the role of the hydrogen bonding and the unexpected cis-stereoselectivity, the Alder-ene reactions of aryne intermediates **IN-4-7e** and **IN-4-7h** were compared by DFT calculations (**Scheme 4.6**). The more facile Alder-ene reaction of **IN-4-7e** is due to a smaller angle distortion by *ca.* 10° for reaching the transition states **TS-2_{4-7e}** and **TS-2_{4-7e'}**, compared to *ca.* 18° for **IN-4-7h** to reach **TS-2_{4-7h}**. This difference then translates to an activation energy difference of more than 11 kcal mol⁻¹ between these two systems. Although trans-isomer **4-8e'** is more stable than cis-isomer **4-8e** by 1.3 kcal mol⁻¹, the energy of **TS-2_{4-7e}** is lower than that of **TS-2_{4-7e'}** by 1.2 kcal mol⁻¹, which can be attributed to the slightly lower angle distortion in **TS-2_{4-7e}**, leading to the formation of cis-diastereomer **4-8e**.

4.2.5. Reactions of benzocyclobutene derivatives

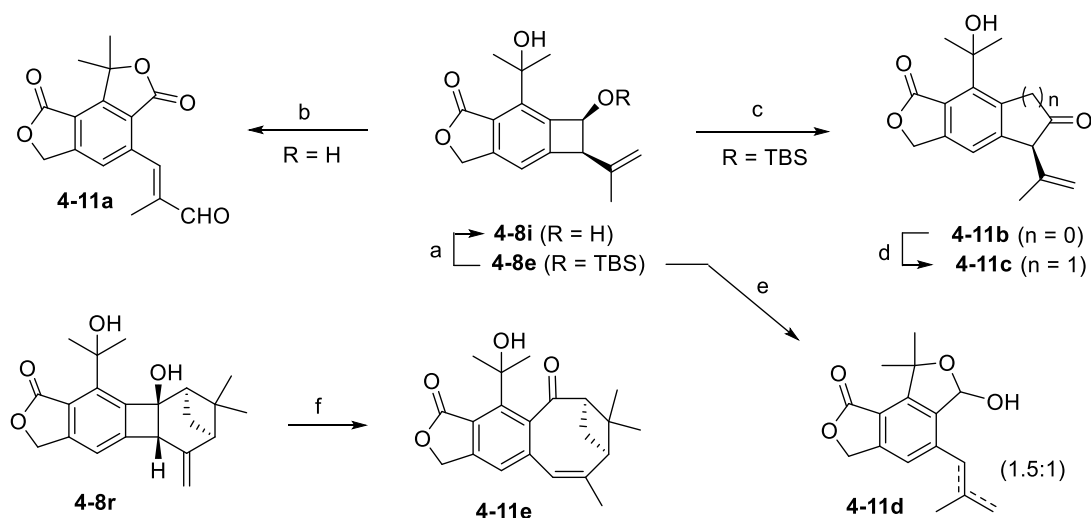
Finally, the benzocyclobutenes generated by Alder-ene reactions could be converted to various other molecular structures via ring expansion or cleavage of the 4-membered ring (**Scheme 4.7**). Oxidation of benzocyclobutenol **4-8l** with MnO₂ resulted in ring opening followed by two independent subsequent allylic oxidations, generating enal **4-11a** in good yield. However, efficient oxidation of **4-8l** to the corresponding ketone **4-11b** could be achieved with Dess–Martin periodinane. One-carbon insertion into **4-11b** afforded

MO6/6-311+G(d,p)//B3LYP/6-31+G* (Energy in kcal/mol)



Scheme 4.6. The energy profiles of Alder-ene reactions and the origin of cis selectivity

4-11c.²¹ Treating silyl ether **4-8e** with TBAF resulted in the ring-opened product **4-11d** as a mixture (1.5:1) of a terminal and an internal alkene. Also, direct ring expansion of the cyclobutanol moiety of **4-8r** cleanly afforded cyclooctenone **4-11e** under basic conditions.



Conditions: (a) 10-camphorsulfonic acid, MeOH–CH₂Cl₂ (1:1), rt, 80%. (b) MnO₂ (excess), CH₂Cl₂, rt, 72%. (c) Dess–Martin periodinane, CH₂Cl₂, rt, 82%. (d) TMSCHN₂, BF₃·Et₂O, CH₂Cl₂, –20 °C, 55%. (e) TBAF, THF, rt, 86%. (f) NaH, THF, 50 °C, 81%.

Scheme 4.7. Reactions of benzocyclobutene derivatives

4.3. Conclusion

In summary, we have explored the Alder-ene reaction of arynes to form benzocyclobutenes, which was affected by installing a bulky substituent next to the ene-donor alkene moiety. It was found that internal hydrogen bonding is crucial not only to facilitate the hexadehydro Diels–Alder reaction to form an aryne intermediate but also to promote its Alder-ene reaction. DFT calculations revealed that the major role of the bulky hydrogen bonding element is to lower the activation barrier by destabilizing the intermediate, which is due to severe bond angle distortion. The transition state leading to the *cis*-isomer is more stable than the *trans*-isomer by 1.2 kcal mol^{–1}, which is the consequence of slightly lower bond angle distortion than the transition state leading to the *trans*-isomer. This reagent-free thermal method to form substituted benzocyclobutene scaffolds would be useful for natural product synthesis and constitute a platform for transition metal-catalyzed transformations.⁴

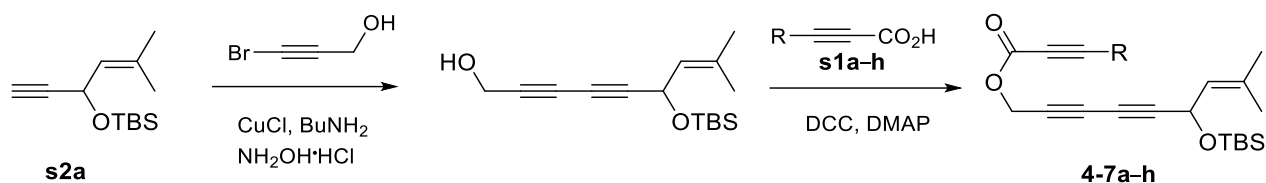
4.4. Experimental Details

4.4.1. General information

Reactions were carried out in oven-dried glassware unless otherwise noted. Compounds were purchased from Aldrich, Acros, TCI America or Oakwood unless otherwise noted. Toluene, dichloromethane, triethylamine and acetonitrile were distilled over calcium hydride (CaH_2) under nitrogen. Tetrahydrofuran was dried over sodiumbenzophenone ketyl. Column chromatography was performed using silica gel 60 Å (32–63 mesh) purchased from Silicycle Inc. Analytical thin layer chromatography (TLC) was performed on 0.25 mm E. Merck precoated silica gel 60 (particle size 0.040–0.063 mm). Yields refer to chromatographically and spectroscopically pure isolated compounds unless otherwise stated. ^1H NMR and ^{13}C NMR spectra were recorded on a Bruker AV–500 spectrometer. ^1H NMR chemical shifts (δ) are reported in parts per million (ppm) downfield of TMS and are referenced relative to the residual protected solvent peak (CDCl_3 (7.26 ppm)). ^{13}C chemical shifts (δ) are reported in parts per million downfield of TMS and are referenced to the carbon resonance of the solvent (CDCl_3 (77.2 ppm)). Multiplicities are indicated by s (singlet), d (doublet), t (triplet), q (quartet), quin (quintet), sext (sextet) or m (multiplet). ^1H NMR signals that fall within a ca. 0.3 ppm range are generally reported as a multiplet, with a range of chemical shift values corresponding to the peak or center of the peak. Coupling constants, J , are reported in Hz (Hertz). Electrospray ionization (ESI) and Electron impact (EI) mass spectra were recorded on a Waters Micromass Q-Tof Ultima and Micromass 70–VSE, respectively in the University of Illinois at Urbana-Champaign.

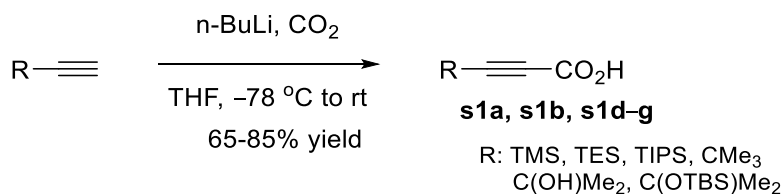
4.4.2. Preparation of substrates

Preparation of triyne 4-7a-h²¹



In a Schlenk flask containing CuCl (80.5 mg, 0.81 mmol) was added 10 mL (30% aqueous BuNH₂ solution) under nitrogen flow. A pinch of NH₂OH·HCl was added until the blue color disappeared. Alkyne **s2a** (700 mg, 3.1 mmol) in CH₂Cl₂ was added at 0 °C to the flask and the solution became yellow. A solution of propargyl alcohol bromide (505 mg, 3.7 mmol) in CH₂Cl₂ was added dropwise at 0 °C. The reaction mixture was stirred for 15 min at room temperature. The nitrogen flow was removed, and the biphasic reaction mixture was transferred to a separatory funnel. Dichloromethane layer was separated and dried over anhydrous Na₂SO₄. After filtration, the organic layer was concentrated and the crude material was purified by column chromatography (SiO₂, hexanes–EtOAc, 5:1) to obtain the diyne (713 mg, 82%) as yellow oil. The diyne (116 mg, 0.5 mmol) was dissolved in CH₂Cl₂ and cooled to 0 °C. The corresponding carboxylic acid (0.6 mmol), DCC (0.75 mmol) and DMAP (0.05 mmol) was added, and the mixture was stirred for 1 h at 0 °C. The precipitate was filtered over a short pad of silica, concentrated, and purified by column chromatography (SiO₂, hexanes–EtOAc, 5:1) to obtain the triyne **4-7a-h** (65–88% yield) as colorless oil.

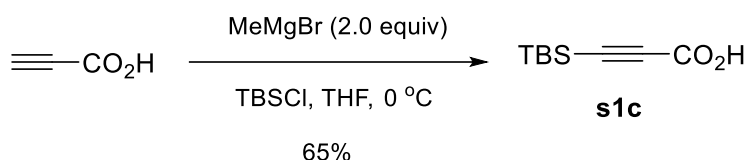
Preparation of carboxylic acids s1a, s1b, s1d–g



Alkyne (5.0–6.0 mmol) was dissolved in anhydrous THF under N₂ and cooled to –78 °C and *n*-BuLi (2.5 M in hexanes) (1.2 equiv) was added dropwise and the mixture was stirred at –78 °C for 45 min. CO₂

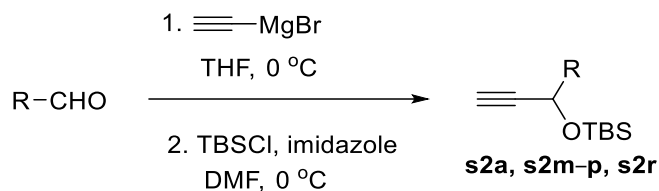
generated from dry ice was dried by passing through a tube containing Drierite was bubbled into the reaction mixture for 30 min at $-78\text{ }^{\circ}\text{C}$. The reaction was stirred at the same temp for another 30 min and then slowly warmed to room temperature. The reaction was quenched by adding 30 mL 1.0 M HCl. Ethyl acetate (30 mL) was added, and the mixture transferred to a separatory funnel. The organic layer was washed with 30 mL water (x1) and 30 mL brine (x2), dried over anhydrous Na_2SO_4 , filtered and concentrated. The carboxylic acid was used directly without further purification. In case of alkyne with free alcohol 2.2 equiv of *n*-BuLi was used.

Preparation of carboxylic acid **s1c**



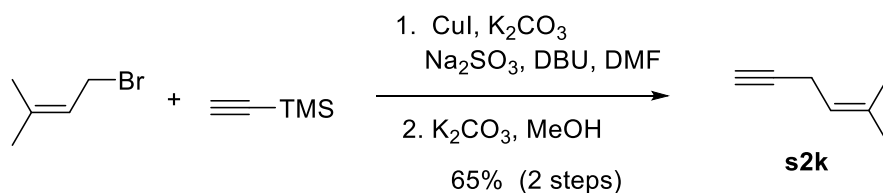
Propiolic acid (500 mg, 7.1 mmol) was dissolved in anhydrous THF under N_2 and cooled to $0\text{ }^{\circ}\text{C}$. MeMgBr (3.0 M in Et_2O , 5.41 mL, 2.2 equiv) was added dropwise and white precipitate was formed due to formation of carboxylate salts. The mixture was stirred at $0\text{ }^{\circ}\text{C}$ for 30 min followed by addition of TBSCl (1.2 g, 1.2 equiv). The mixture was stirred at $0\text{ }^{\circ}\text{C}$ for another 30 min and slowly warmed to room temp. 1.0 M HCl (10 mL) was added to quench the reaction. Ethyl acetate (30 mL) was added, and the mixture was transferred to a separatory funnel. The organic layer was washed with 15 mL water and 15 mL brine (x2), dried over anhydrous Na_2SO_4 , filtered, concentrated, and purified by column chromatography (SiO_2 , hexanes–EtOAc, 3:1) to obtain the carboxylic acid **s1c** (850 mg, 65%) as a white solid.

Preparation of alkyne **s2a**, **s2m-p**, **s2u**



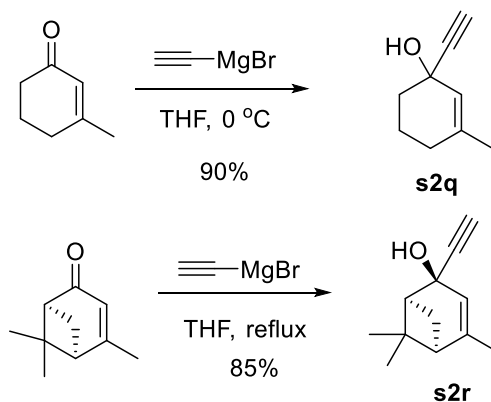
Commercially available aldehydes (prenal, tiglic aldehyde, crotonaldehyde) were used directly for synthesizing **s2a**, **s2m**, and **s2n**. Geranial, neral and but-2-ynal were obtained by oxidation of their corresponding alcohols using MnO_2 and used for synthesizing **s2o**, **s2p**, and **s2u**. The aldehyde (2.0–5.0 mmol) was dissolved in dry THF under N_2 and cooled to $0\text{ }^\circ\text{C}$. Ethynyl magnesium bromide (0.5 M in THF) (1.1 equiv) was added dropwise and stirred for 30 min. The reaction was quenched with NH_4Cl and extracted with EtOAc. The organic layer was washed with water followed by brine, dried over anhydrous Na_2SO_4 , filtered, concentrated and purified by column chromatography (SiO_2 , hexanes–EtOAc, 5:1) to obtain the propargyl alcohols as colorless oils. The propargyl alcohols (2.0–5.0 mmol) was dissolved in DMF (0.5 mL/mmol) and cooled to $0\text{ }^\circ\text{C}$. TBSCl (1.2 equiv) and imidazole (1.4 equiv) was added, and the reaction was stirred for 30 min. The reaction mixture was diluted with hexanes and filtered over silica, concentrated and the alkyne obtained was used for subsequent steps without further purification.

Preparation of alkyne **s2k**



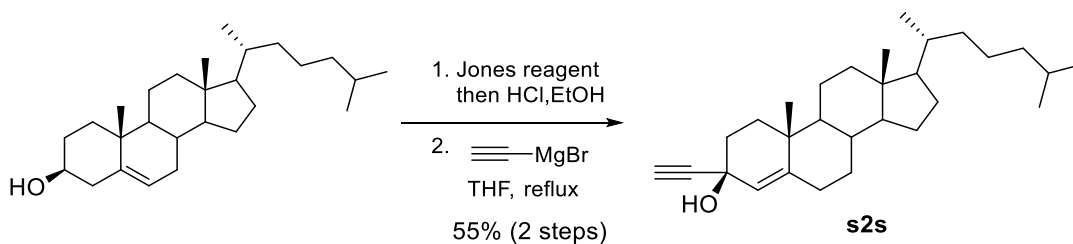
The alkyne **s2k** was synthesized by following literature procedures.²²

Preparation of alkyne **s2q**, **s2r**



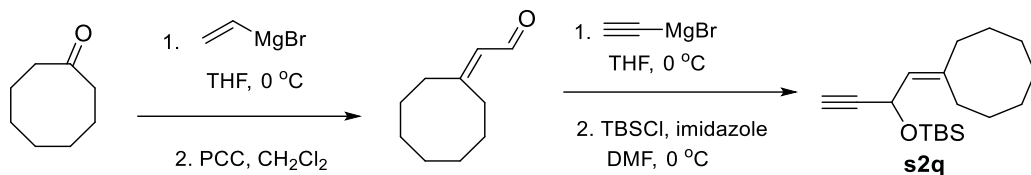
The alkyne **s2q** and **s2r** were prepared by following typical procedure of adding ethynylmagnesium bromide as described above. For **s2r**, reaction conditions involved refluxing under THF for 14 h.

Preparation of alkyne **s2s**



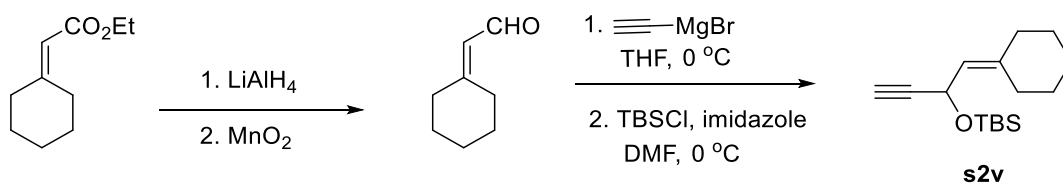
Cholesterol (1.0 g, 2.5mmol) was dissolved in acetone (50 mL) and cooled to 0 °C followed by dropwise addition of Jones reagent (2.7 M) (1.5 mL, 3 mmol). After stirring for 30 min the reaction was quenched by adding 10 mL EtOH and 1 N HCl (10 mL) was added, and the mixture was heated at 50 °C for 15 min. The reaction was cooled, and solvent was removed under reduced pressure. The residue was diluted with EtOAc and washed with satd. NaHCO_3 followed by brine. The organic layer was dried over anhydrous Na_2SO_4 , filtered, concentrated, and purified by column chromatography (SiO_2 , hexanes–EtOAc, 10:1) to give pure 4-cholestan-3-one (750 mg, 74%), which was further converted to **s2s** following method described above. The reaction required 14 h under refluxing THF for complete conversion.

Preparation of alkyne **s2t**



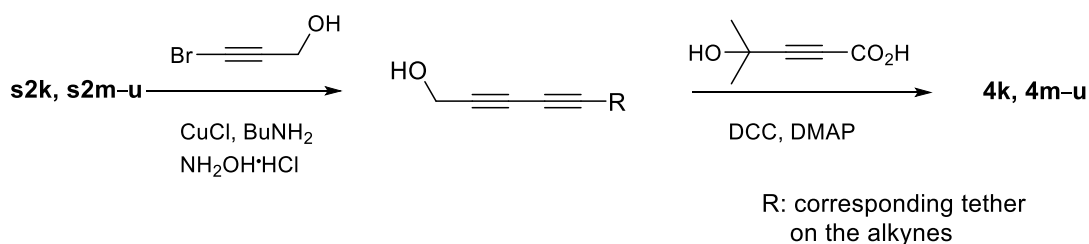
After the preparation of the enal following literature procedures,²³ the enal was converted to **s2t** by the typical procedure described above.

Preparation of alkyne **s2v**



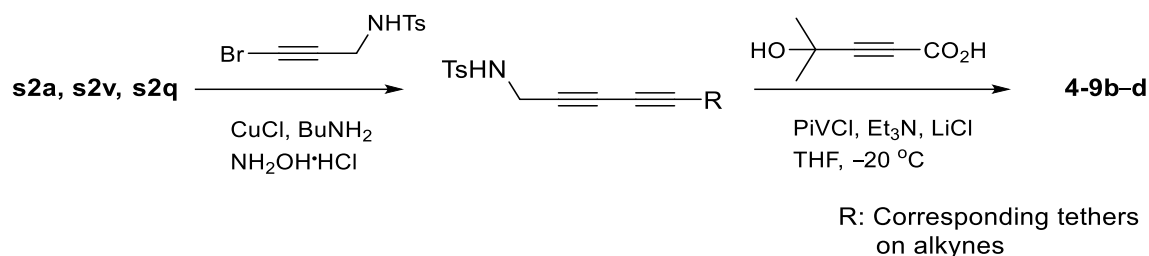
After the preparation of the enal from cyclohexanone (3 steps) following literature procedures,²⁴ the enal was converted to **s2v** by the typical procedure described above.

Preparation of triyne **4-7k, 4-7m-u**



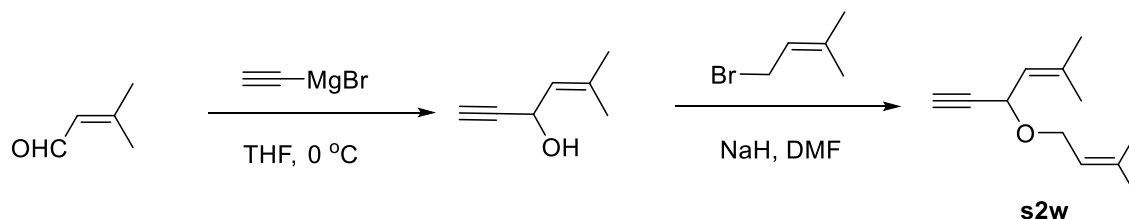
The triynes **4k** and **4m-u** was prepared from the respective alkynes **s2k** and **s2m-u** following the method described above for preparation of related triynes **4a-h**.

Preparation of imide-tethered triyne 4-9b-d²⁵



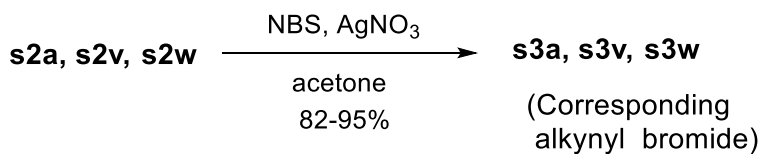
The corresponding diynes were prepared by following typical procedure for a Cadiot–Chodkiewicz coupling described above. The carboxylic acid (1.2 equiv) was dissolved in THF under N₂ and cooled to –20 °C. To it was added pivaloyl chloride (1.4 equiv) followed by Et₃N (2.5 equiv) and, the mixture was stirred for 2 h at –20 °C. To this solution, LiCl (1.5 equiv) and the diyne (0.5–1.5 mmol) were added. The reaction mixture was allowed to warm to room temp and stirred for another 15 min. The mixture was concentrated, and the residue was directly purified through column chromatography. For **4-9b** and **4-9c** (SiO₂, hexanes–EtOAc, 5:1) and for **4-9d** (SiO₂, hexanes–EtOAc, 2:1) was used as eluting solvent in column chromatography.

Preparation of alkyne s2w



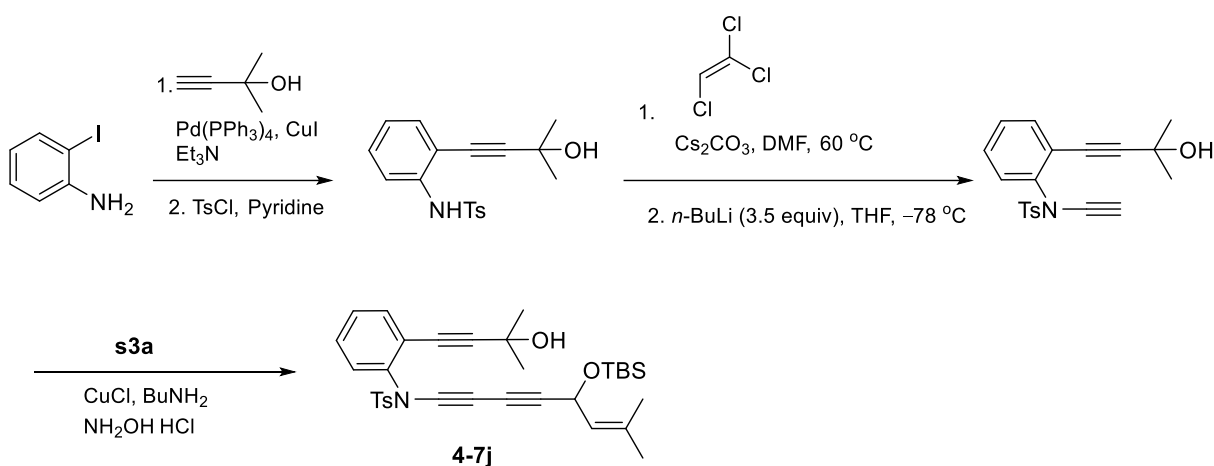
The alkyne **s2w** was prepared by adding ethynyl magnesium bromide as described above followed by a typical Williamson's ether synthesis.

Preparation of alkynyl bromide s3a, s3v and s3w



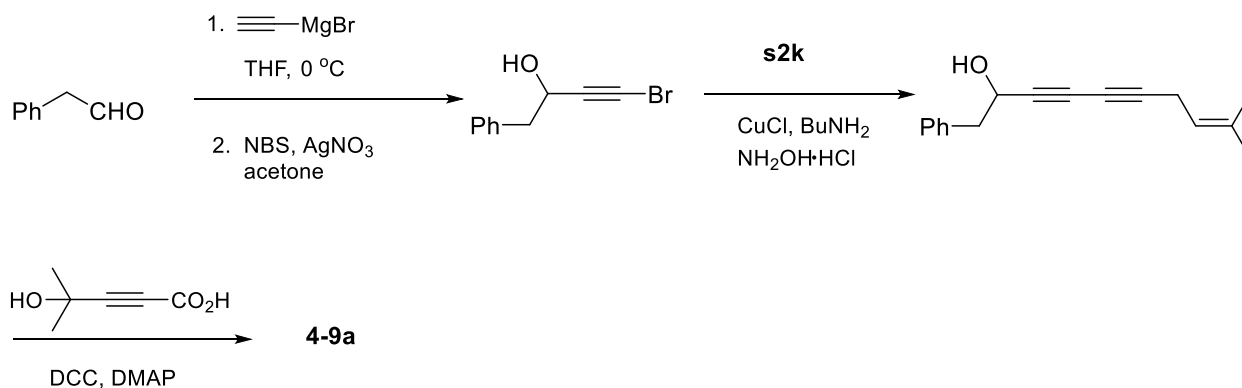
To an acetone solution of alkynes **s2a**, **s2v** and **s2w** (0.5–1.0 mmol) was added AgNO₃ (0.1 equiv) followed by *N*-bromosuccinimide (1.4 equiv) under N₂. The reaction was stirred under dark in a round bottom flask covered with aluminium foil for 2 h. After completion the acetone was removed under reduced pressure. The residue was dissolved in hexanes filtered over silica and concentrated obtaining the corresponding alkynyl bromides **s3a**, **s3v** and **s3w** were obtained as colorless oil (82–95% yield), which were directly used without further purification.

Preparation of triyne 4-7j



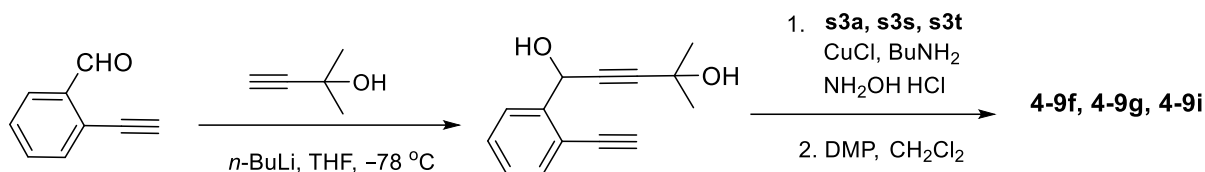
The triyne **4-7j** was synthesized by following literature procedure for related compounds.²⁶

Preparation of triyne 4-9a



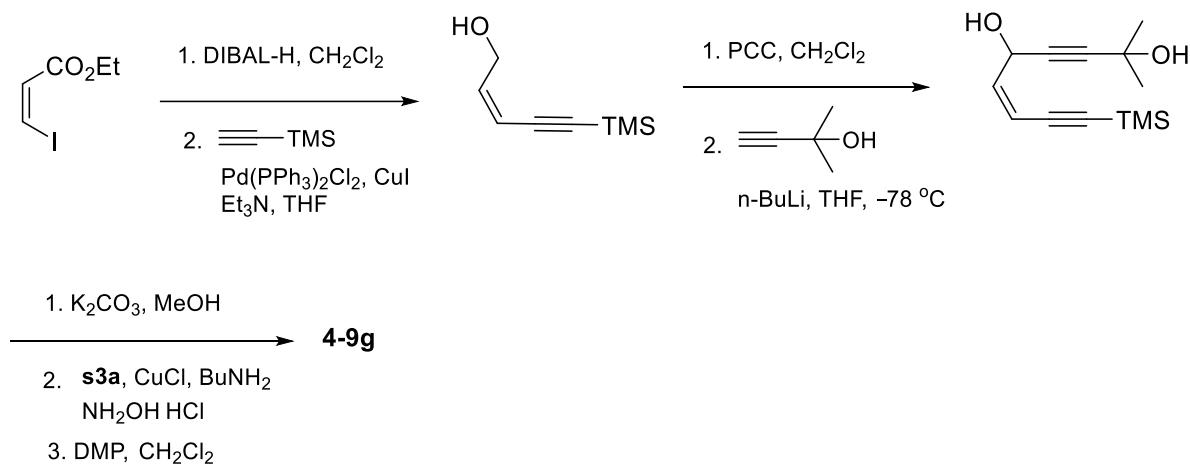
The triyne **4-9a** was synthesized by following the reaction sequence shown above.

Preparation of benzene-tethered triyne 4-9f, 4-9g, 4-9i²⁷



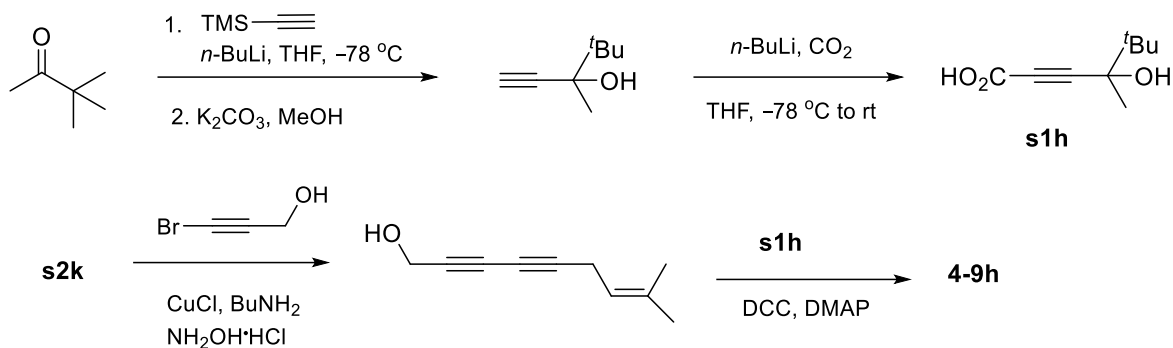
The benzene tethered triynes **4-9f**, **4-9g**, and **4-9i** were synthesized by following literature procedures involving alkynyl anion addition to the aldehyde followed by typical coupling with alkynyl bromides **s3a**, **s3s**, and **s3t** respectively and oxidation using DMP. Oxidation with MnO_2 was also tried but gave significantly low yield.

Preparation of Enone-tethered triyne 4-9g²⁷



The triyne **4-9g** was prepared following literature procedure starting from the vinylic iodide involving the reduction to alcohol using DIBAL-H, a Sonogashira coupling, oxidation to aldehyde, alkynyl anion addition, TMS-deprotection, coupling of alkynyl bromide and DMP oxidation.

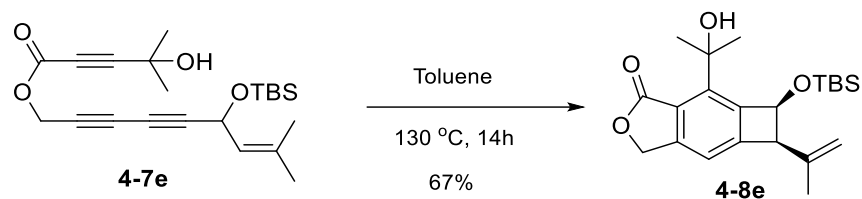
Preparation of 4-9h



The triyne **4-9h** was prepared starting from pinacolone following standard reaction condition described above for synthesizing related triynes.

4.4.3. HDDA reaction to form benzocyclobutenes

Preparation of 4-8e (1.0 mmol scale) via intramolecular Alder-Ene reaction



A toluene solution (0.05 M) of the triyne (400 mg, 1.0 mmol) was heated in a Schlenk tube at 130 °C for 14 h. After completion, the reaction was cooled to room temperature and toluene was removed under reduced pressure. The residue was purified by flash chromatography (SiO₂, hexanes–EtOAc, 6:1) to obtain **4-8e** (268 mg, 67% yield) as white solid with complete *cis*-diastereoselectivity.

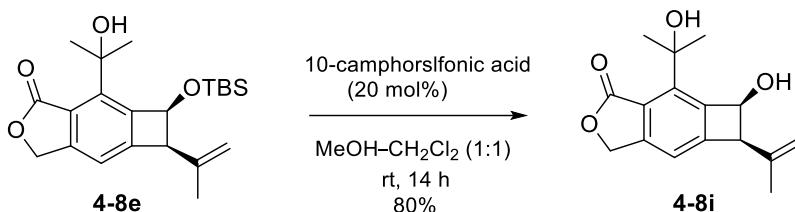
General procedure for Alder-Ene reactions to generate benzocyclobutenes

A toluene solution (0.05 M) of the triyne (0.1–0.3 mmol) was heated in a Schlenk tube at 130 °C for ester-tethered and 90 °C for imide, benzene and enone tether for 14 h. After completion, the reaction was cooled to room temperature and the solvent was removed under reduced pressure. The residue was then purified

by column chromatography. The yield, solvent system used for purification, and physical property of the isolated compounds are given in the characterization data.

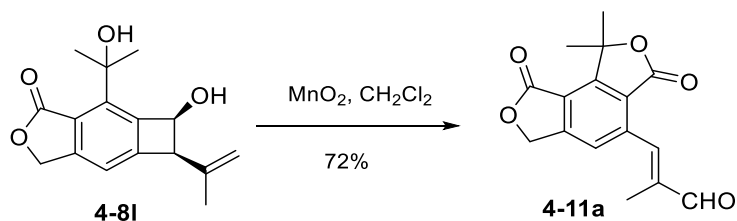
4.4.4. Procedures for reactions of benzocyclobutene derivatives

TBS-deprotection with **4-8e**



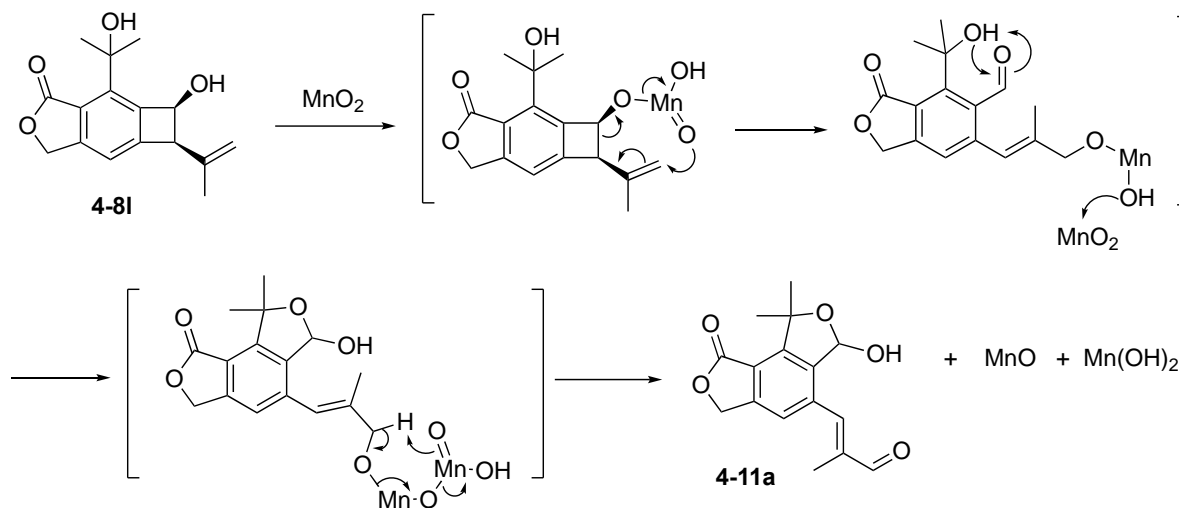
Benzocyclobutene **4-8e** (230 mg, 0.6 mmol) was dissolved in MeOH–CH₂Cl₂ (1:1), and 10-camphorsulfonic acid (30 mg, 0.12 mmol) was added, and the mixture was stirred at rt for 14 h. The solvent was removed under reduced pressure, and the residue was directly purified by flash column chromatography (hexanes–EtOAc, 2:1) to give compound **4-8i** (130 mg, 80 %) as white solid.

MnO₂-mediated ring cleavage and allylic oxidation of **4-8i**

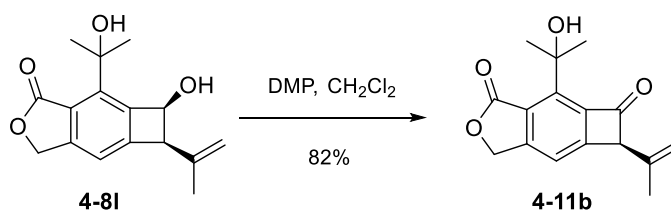


Benzocyclobutenol **4-8i** (30 mg, 0.1 mmol) was dissolved in CH₂Cl₂, and MnO₂ (48 mg, 0.5 mmol) was added and stirred for 15 min. The mixture was filtered over a short pad of celite, concentrated and the residue was purified by column chromatography (SiO₂, hexanes–EtOAc, 5:1 → 2:1) to afford **4-11a** (22 mg, 72%) as white solid.

Mechanism for MnO₂-mediated ring cleavage and allylic oxidation of **4-8l**

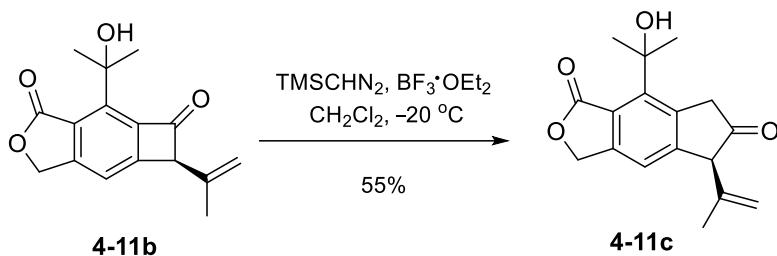


DMP Oxidation of **4-8l**



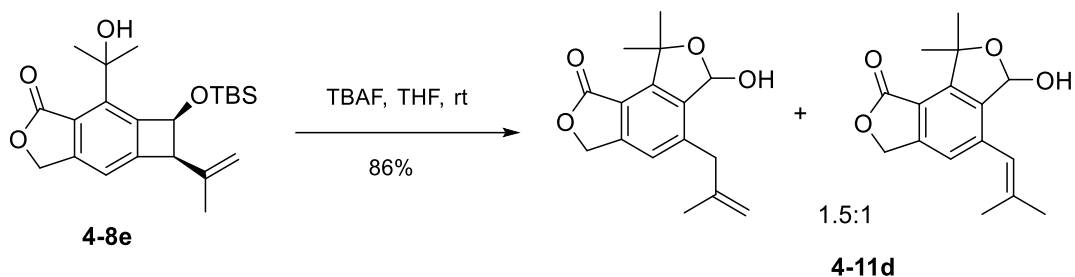
Benzocyclobutenol **4-8l** (65 mg, 0.2 mmol) was dissolved in CH₂Cl₂ and DMP (110 mg, 0.25 mmol) was added and stirred at room temp for 3 h. After completion, Na₂S₂O₃ solution (1 mL), saturated NaHCO₃ (1 mL) and water (1 mL) were added, and the mixture was stirred vigorously until two distinct layers were formed. The mixture was diluted with CH₂Cl₂ and organic layer was separated and washed with water and brine, dried over anhydrous Na₂SO₄, filtered, concentrated and purified by column chromatography (SiO₂, hexanes–EtOAc, 5:1 → 2:1) to give ketone **4-11b** (53 mg, 82%) as white solid.

One-carbon homologation of **4-11b**



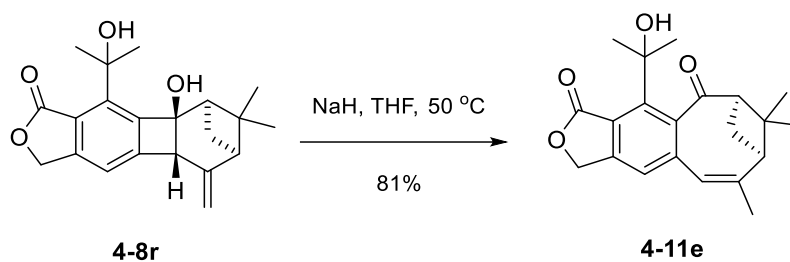
Benzocyclobutenone **4-11b** (20 mg, 0.06 mmol) was dissolved in dry CH_2Cl_2 under N_2 and cooled $-20\text{ }^\circ\text{C}$. TMSCHN_2 (2.0 M in hexanes, 0.04 mL, 0.07 mmol) and $\text{BF}_3\cdot\text{OEt}_2$ (0.01 mL) were added dropwise. The mixture was stirred at $-20\text{ }^\circ\text{C}$ for 20 min. After completion, the reaction was quenched with saturated NH_4Cl and extracted with CH_2Cl_2 . The organic layer was washed with water and brine, dried over anhydrous Na_2SO_4 , filtered, concentrated, and purified by column chromatography (SiO_2 , hexanes– EtOAc , 5:1 \rightarrow 3:1) to give ketone **4-11c** (12 mg, 55%) as colorless oil.

TBAF-induced ring cleavage of **4-8e**



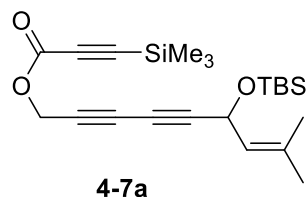
To a THF solution of **4-8e** (60 mg, 0.15 mmol) was added TBAF (1.0 M in THF) (0.18 mL) and the mixture was stirred for 20 min at room temperature. The reaction was quenched with satd. NH_4Cl and extracted with EtOAc . The organic layer was washed with water (x1) and brine (x1), dried over anhydrous Na_2SO_4 , filtered, concentrated, and purified by column chromatography (gradient elution, hexanes– EtOAc , 5:1 to 3:1) to give a mixture of isomeric alkenes **4-11d** (35 mg, 86%) as colorless oil.

Ring expansion of **4-8r**

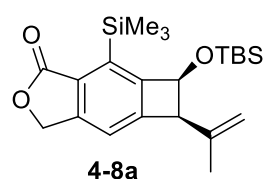


To a THF solution of **4-8r** (30 mg, 0.10 mmol) was added NaH (60% in mineral oil, 3 mg, 0.12 mmol) under N₂ and the mixture was stirred for 30 min at 50 °C. The reaction was filtered over a short pad of celite, concentrated and purified by column chromatography (hexanes–EtOAc, 4:1) to give a mixture of isomeric alkenes **4-11e** (35 mg, 81%) as colorless oil.

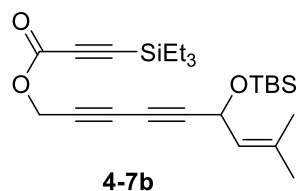
4.4.5. Characterization data



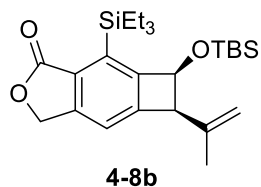
4-7a: colorless oil; $^1\text{H NMR}$ (CDCl_3 , 500 MHz): δ 5.27 (d, J = 8.2 Hz, 1H), 5.08 (d, J = 8.2 Hz, 1H), 4.81 (s, 2H), 1.72 (s, 3H), 1.67 (s, 3H), 0.89 (s, 9H), 0.25 (s, 9H), 0.12 (s, 3H), 0.10 (s, 3H); $^{13}\text{C NMR}$ (CDCl_3 , 500 MHz): δ 151.9, 135.3, 124.6, 95.9, 93.5, 81.4, 71.8, 71.7, 67.4, 60.4, 53.6, 25.7, 18.2, -0.95 , -4.5 , -4.7 ; **HRMS** (ESI) calcd for $\text{C}_{22}\text{H}_{34}\text{O}_3\text{NaSi}$ $[\text{M}+\text{Na}]^+$ 425.1944, found 425.1964.



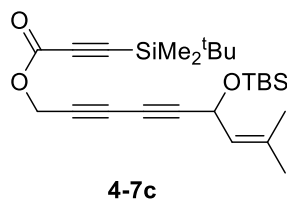
4-7a: white solid; 25 mg (45% yield, 10:1 *dr*); Purification: Flash Chromatography (SiO_2 , hexanes–EtOAc, 50:1 \rightarrow 20:1); $^1\text{H NMR}$ (CDCl_3 , 500 MHz): δ 7.17 (s, 1H), 5.29–5.21 (m, 2H), 5.19 (s, 1H), 4.94 (s, 1H), 4.89 (s, 1H), 3.80 (s, 1H), 1.77 (s, 3H), 0.91 (s, 9H), 0.43 (s, 9H), 0.17 (s, 3H), 0.12 (s, 3H); $^{13}\text{C NMR}$ (CDCl_3 , 500 MHz): δ 153.9, 150.6, 147.9, 142.7, 138.8, 129.6, 119.9, 117.3, 112.8, 76.3, 69.4, 59.7, 25.9, 20.7, 17.9, -0.28 , -3.4 , -4.75 ; **HRMS** (ESI) calcd for $\text{C}_{22}\text{H}_{34}\text{O}_3\text{NaSi}$ $[\text{M}+\text{Na}]^+$ 425.1944, found 425.1945.



4-7b: colorless oil; $^1\text{H NMR}$ (CDCl_3 , 500 MHz): δ 5.27 (d, J = 8.1 Hz, 1H), 5.08 (d, J = 8.1 Hz, 1H), 4.81 (s, 2H), 1.72 (s, 3H), 1.66 (s, 3H), 1.01 (t, J = 8.0 Hz, 9H), 0.88 (s, 9H), 0.67 (q, J = 8.0 Hz, 6H), 0.11 (s, 3H), 0.09 (s, 3H); $^{13}\text{C NMR}$ (CDCl_3 , 500 MHz): δ 151.9, 135.2, 124.6, 94.7, 94.1, 81.3, 71.8, 71.7, 67.4, 60.3, 53.6, 25.7, 25.5, 18.2, 7.2, 3.7, -4.5 , -4.6 ; **HRMS** (ESI) calcd for $\text{C}_{25}\text{H}_{40}\text{O}_3\text{NaSi}_2$ $[\text{M}+\text{Na}]^+$ 467.2414, found 467.2403.

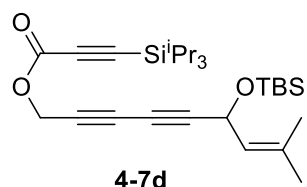


4-8b: white solid; 32 mg (48% yield, 7:1 *dr*); Purification: Flash Chromatography (SiO_2 , hexanes–EtOAc, 50:1 \rightarrow 20:1); $^1\text{H NMR}$ (CDCl_3 , 500 MHz): δ 7.16 (s, 1H), 5.28–5.19 (m, 2H), 5.17 (s, 1H), 4.95 (s, 1H), 4.91 (s, 1H), 3.79 (s, 1H), 1.70 (s, 3H), 1.11–0.91 (m, 6H), 0.94–0.86 (m, 18H), 0.20 (s, 3H), 0.15 (s, 3H); $^{13}\text{C NMR}$ (CDCl_3 , 500 MHz): δ 171.9, 155.2, 150.7, 148.1, 142.6, 136.8, 129.9, 123.5, 119.9, 117.1, 113.1, 76.1, 68.4, 59.8, 25.8, 7.6, 3.0, -3.5 , -5.1 ; **HRMS** (ESI) calcd for $\text{C}_{25}\text{H}_{40}\text{O}_3\text{NaSi}_2$ $[\text{M}+\text{Na}]^+$ 467.2414, found 467.2398.



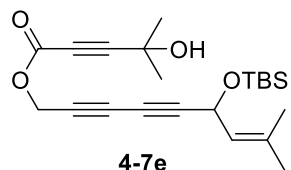
4-7c

4-7c: colorless oil; $^1\text{H NMR}$ (CDCl_3 , 500 MHz): δ 5.26 (dt, $J = 1.5, 8.5$ Hz, 1H), 5.08 (d, $J = 8.0$ Hz, 1H), 4.80 (s, 2H), 1.72 (s, 3H), 1.68 (s, 3H), 0.96 (s, 9H), 0.88 (s, 9H), 0.18 (s, 6H), 0.11 (s, 3H), 0.09 (s, 3H); $^{13}\text{C NMR}$ (CDCl_3 , 500 MHz): δ 151.8, 135.2, 124.6, 94.6, 94.3, 81.3, 71.8, 67.4, 60.4, 53.6, 25.9, 25.7, 25.5, 18.2, 16.5, -4.5, -4.7, -5.3; **HRMS** (ESI) calcd for $\text{C}_{25}\text{H}_{40}\text{O}_3\text{NaSi}_2$ $[\text{M}+\text{Na}]^+$ 467.2414, found 467.2415.



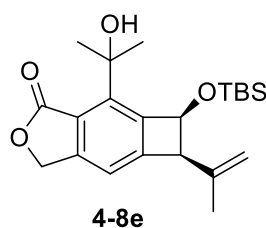
4-7d

4-7d: colorless oil; $^1\text{H NMR}$ (CDCl_3 , 500 MHz): δ 5.27 (d, $J = 7.5$ Hz, 1H), 5.08 (d, $J = 8.0$ Hz, 1H), 4.81 (s, 2H), 1.72 (s, 3H), 1.66 (s, 3H), 1.34–1.26 (m, 3H), 1.10 (s, 18H), 0.88 (s, 9H), 0.11 (s, 3H), 0.10 (s, 3H); $^{13}\text{C NMR}$ (CDCl_3 , 500 MHz): δ 151.9, 135.2, 124.6, 95.6, 93.3, 81.3, 71.9, 71.7, 67.5, 60.4, 53.5, 25.7, 25.5, 18.4, 10.9, -4.7, -4.5; **HRMS** (ESI) calcd for $\text{C}_{28}\text{H}_{46}\text{O}_3\text{NaSi}_2$ $[\text{M}+\text{Na}]^+$ 509.2883, found 509.2891.



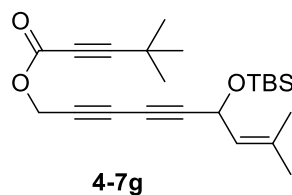
4-7e

4-7e: colorless oil; $^1\text{H NMR}$ (CDCl_3 , 500 MHz): δ 5.26 (d, $J = 8.4$ Hz, 1H), 5.08 (d, $J = 7.1$ Hz, 1H), 4.81 (s, 2H), 2.5 (br s, 1H, OH), 1.71 (s, 3H), 1.65 (s, 3H), 1.55 (s, 6H), 0.87 (s, 9H), 0.10 (s, 3H), 0.09 (s, 3H); $^{13}\text{C NMR}$ (CDCl_3 , 500 MHz): δ 152.5, 135.3, 124.6, 92.7, 81.4, 73.2, 71.9, 71.7, 67.4, 64.9, 60.3, 53.7, 30.4, 25.7, 25.5, 18.2, -4.7, -4.5; **HRMS** (ESI) calcd for $\text{C}_{22}\text{H}_{33}\text{O}_4\text{Si}$ $[\text{M}+\text{H}]^+$ 389.2148, found 389.2132.

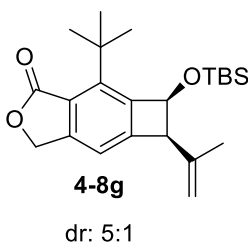


4-8e

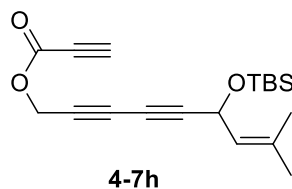
4-8e: white solid; 268 mg (67% yield); Purification: Flash Chromatography (SiO_2 , hexanes–EtOAc, 6:1); $^1\text{H NMR}$ (CDCl_3 , 500 MHz): δ 7.10 (s, 1H), 6.14 (s, 1H, OH), 5.36–5.24 (m, 2H), 5.22 (s, 1H), 4.96 (s, 1H), 4.90 (s, 1H), 3.78 (s, 1H), 1.79 (s, 3H), 1.71 (s, 3H), 1.67 (s, 3H), 0.91 (s, 9H), 0.18 (s, 3H), 0.14 (s, 3H); $^{13}\text{C NMR}$ (CDCl_3 , 500 MHz): δ 173.5, 152.9, 150.5, 148.3, 143.3, 141.9, 121.4, 115.7, 113.7, 75.5, 72.3, 70.1, 59.9, 30.9, 28.5, 25.8, 20.3, 17.8, -3.7, -5.3; **HRMS** (ESI) calcd for $\text{C}_{22}\text{H}_{33}\text{O}_4\text{Si}$ $[\text{M}+\text{H}]^+$ 389.2148, found 389.2158.



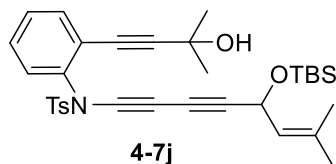
4-7g: colorless oil; $^1\text{H NMR}$ (CDCl_3 , 500 MHz): δ 5.26 (d, $J = 8.7$ Hz, 1H), 5.08 (d, $J = 8.1$ Hz, 1H), 4.79 (s, 2H), 2.5 (br s, 1H, OH), 1.71 (s, 3H), 1.65 (s, 3H), 1.28 (s, 9H), 0.88 (s, 9H), 0.11 (s, 3H), 0.09 (s, 3H) $^{13}\text{C NMR}$ (CDCl_3 , 500 MHz): δ 152.9, 135.2, 124.7, 98.3, 81.2, 72.0, 71.6, 67.5, 60.4, 53.4, 30.0, 29.8, 27.6, 25.8, 25.5, 18.2, -4.5, -4.7; **HRMS** (ESI) calcd for $\text{C}_{23}\text{H}_{34}\text{O}_3\text{NaSi}$ $[\text{M}+\text{Na}]^+$ 409.2175, found 409.2187.



4-8g: colorless oil; 22 mg (49% yield, 5:1 dr); Purification: Flash Chromatography (SiO_2 , hexanes–EtOAc, 20:1 \rightarrow 10:1); $^1\text{H NMR}$ (CDCl_3 , 500 MHz) (for major diastereomer): δ 7.02 (s, 1H), 5.22 (s, 1H), 5.20–5.17 (m, 2H), 4.95 (s, 1H), 4.90 (s, 1H), 3.75 (s, 1H), 1.73 (s, 3H), 1.59 (s, 9H), 0.92 (s, 9H), 0.15 (s, 3H), 0.13 (s, 3H); $^{13}\text{C NMR}$ (CDCl_3 , 500 MHz) (all discernable signals for both : δ 170.6, 152.7, 151.0, 150.8, 144.6, 142.5, 122.5, 116.5, 114.8, 114.5, 113.1, 76.6, 75.9, 68.3, 68.2, 59.4, 56.3, 36.3, 30.6, 30.2, 25.9, 25.8, 20.4, 17.9, -3.7, -5.1; **HRMS** (ESI) calcd for $\text{C}_{23}\text{H}_{35}\text{O}_3\text{Si}$ $[\text{M}+\text{H}]^+$ 387.2355, found 387.2354.

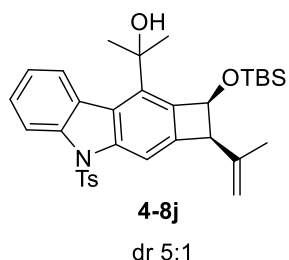


4-7h: colorless oil; $^1\text{H NMR}$ (CDCl_3 , 500 MHz): δ 5.27 (dt, $J = 1.6, 8.3$ Hz, 1H), 5.09 (d, $J = 8.5$ Hz, 1H), 4.84 (s, 2H), 2.95 (s, 1H), 1.72 (s, 3H), 1.67 (s, 3H), 0.89 (s, 9H), 0.12 (s, 3H), 0.10 (s, 3H); $^{13}\text{C NMR}$ (CDCl_3 , 500 MHz): δ 151.8, 135.3, 124.6, 81.5, 76.1, 73.8, 72.1, 71.4, 67.4, 60.4, 53.9, 25.8, 25.4, 18.2, -4.5, -4.7; **HRMS** (ESI) calcd for $\text{C}_{19}\text{H}_{26}\text{O}_3\text{NaSi}$ $[\text{M}+\text{Na}]^+$ 353.1549, found 353.1554.

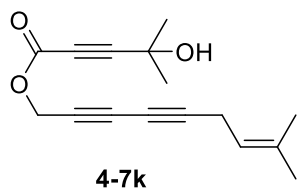


4-7j: yellow oil; $^1\text{H NMR}$ (CDCl_3 , 500 MHz): δ 7.68 (d, $J = 8.1$ Hz, 2H), 7.43–7.38 (m, 1H), 7.35–7.28 (m, 2H), 7.27–7.23 (m, 1H), 5.26 (d, $J = 8.1$ Hz, 1H), 5.11 (d, $J = 9.22$ Hz, 1H), 2.45 (s, 1H), 2.04 (br s, 1H, OH), 1.70 (s, 3H), 1.64 (s, 3H), 1.47 (s, 6H), 0.88 (s, 9H), 0.10 (s, 3H), 0.08 (s, 3H); $^{13}\text{C NMR}$ (CDCl_3 , 500 MHz): δ 145.3, 138.2, 134.5, 134.4, 133.4, 129.9, 129.2, 128.9, 128.4, 125.1, 122.4, 100.7, 84.1, 77.4, 70.5, 68.1,

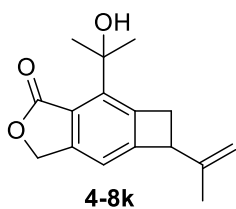
60.7, 58.3, 30.9, 25.8, 25.5, 21.7, 18.2, -4.4, -4.6; **HRMS** (ESI) calcd for $C_{33}H_{41}NO_4NaSSi$ $[M+Na]^+$ 598.2423, found 598.2411.



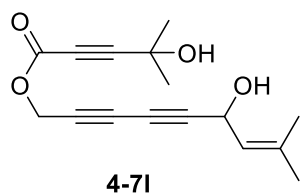
4-8j: yellow solid; 11 mg (28% yield, 5:1 dr); Purification: Flash Chromatography (SiO_2 , hexanes–EtOAc, 10:1); **1H NMR** ($CDCl_3$, 500 MHz) (for major diastereomer): δ 8.45 (d, $J = 7.9$ Hz, 2H), 8.16 (s, 1H), 7.66 (d, $J = 8.4$ Hz, 2H), 7.45 (t, $J = 8.1$ Hz, 1H), 7.35 (t, $J = 7.6$ Hz, 1H), 7.11 (d, $J = 8.0$ Hz, 2H), 5.34–5.32 (m, 1H), 5.01–4.98 (m, 2H), 3.92 (s, 1H), 1.90 (s, 3H), 1.85 (s, 3H), 1.76 (s, 3H), 0.95 (s, 9H), 0.22 (s, 3H), 0.19 (s, 3H); **^{13}C NMR** ($CDCl_3$, 500 MHz) (all discernable signals for both isomers): δ 144.9, 143.4, 143.0, 141.3, 140.9, 138.4, 137.7, 135.0, 129.7, 129.6, 126.6, 126.3, 126.0, 125.5, 123.2, 116.1, 114.8, 113.2, 109.5, 76.0, 73.4, 59.6, 57.2, 31.2, 29.7, 28.2, 25.8, 25.9, 21.5, 20.0, -3.5, -5.1; **HRMS** (ESI) calcd for $C_{33}H_{41}NO_4NaSSi$ $[M+Na]^+$ 598.2423, found 598.2419.



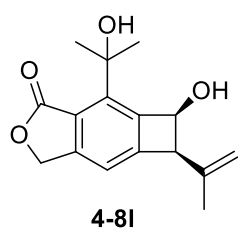
4-7k: colorless oil; **1H NMR** ($CDCl_3$, 500 MHz): δ 5.16–5.09 (m, 1H), 4.79 (s, 2H), 2.97–2.92 (m, 2H), 1.70 (s, 3H), 1.61 (s, 3H), 1.55 (s, 6H); **^{13}C NMR** ($CDCl_3$, 500 MHz): δ 152.6, 135.4, 116.6, 92.6, 81.0, 73.2, 68.3, 65.0, 63.6, 53.9, 30.4, 25.4, 18.3, 17.7; **HRMS** (ESI) calcd for $C_{16}H_{18}O_3Na$ $[M+Na]^+$ 281.1154, found 281.1153.



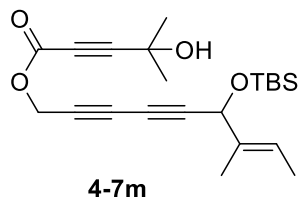
4-8k: white solid; 32 mg (72% yield); Purification: Flash Chromatography (SiO_2 , hexanes–EtOAc, 6:1); **1H NMR** ($CDCl_3$, 500 MHz): δ 7.11 (s, 1H), 6.31 (s, 1H, OH), 5.32 (s, 2H), 4.85 (s, 1H), 4.83 (s, 1H), 4.02–3.97 (m, 1H), 3.58 (dd, $J = 8.3, 5.5$ Hz, 1H), 3.15–3.11 (m, 1H), 1.79 (s, 3H), 1.64 (s, 3H), 1.63 (s, 3H); **^{13}C NMR** ($CDCl_3$, 500 MHz): δ 174.1, 155.5, 148.9, 146.0, 143.9, 140.4, 121.2, 115.3, 110.9, 71.9, 70.3, 47.6, 38.0, 30.2, 30.1, 20.4; **HRMS** (ESI) calcd for $C_{16}H_{18}O_3Na$ $[M+Na]^+$ 281.1154, found 281.1152.



4-7l: colorless oil; $^1\text{H NMR}$ (CDCl_3 , 500 MHz): δ 5.37–5.27 (m, 1H), 5.14–5.08 (d, J = 8.3 Hz, 1H), 4.82 (s, 2H), 1.75 (s, 3H), 2.33 (br s, 1H, OH), 2.04 (br s, 1H, OH), 1.71 (s, 3H), 1.66 (s, 6H); $^{13}\text{C NMR}$ (CDCl_3 , 500 MHz): δ 152.5, 138.4, 123.2, 92.7, 80.6, 73.2, 72.2, 71.5, 68.1, 65.1, 59.4, 53.7, 30.4, 25.6, 18.2; **HRMS** (ESI) calcd for $\text{C}_{16}\text{H}_{18}\text{O}_4\text{Na}$ $[\text{M}+\text{Na}]^+$ 297.1103, found 297.1096.

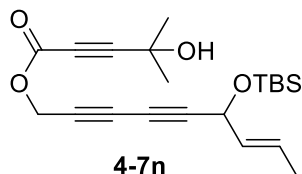


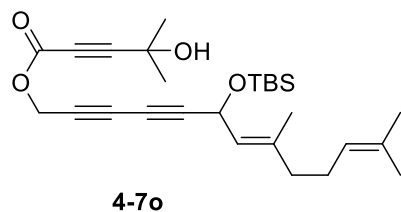
4-8l: white solid; 15 mg (30% yield); Purification: Flash Chromatography (SiO_2 , hexanes–EtOAc, 2:1) $^1\text{H NMR}$ (CDCl_3 , 500 MHz): δ 7.18 (s, 1H), 5.57 (br s, 1H, OH), 5.37–5.27 (m, 2H), 4.99 (s, 1H), 4.87 (s, 1H), 4.75 (s, 1H), 3.85 (br s, 1H, OH), 3.77 (s, 1H), 1.86 (s, 3H), 1.75 (s, 3H), 1.69 (s, 3H); $^{13}\text{C NMR}$ (CDCl_3 , 500 MHz): δ 172.9, 152.1, 150.6, 147.6, 143.3, 142.4, 121.1, 116.5, 111.4, 76.8, 72.8, 69.9, 59.4, 30.5, 29.3, 21.2; **HRMS** (ESI) calcd for $\text{C}_{16}\text{H}_{19}\text{O}_4$ $[\text{M}+\text{H}]^+$ 275.1283, found 275.1283.



4-7m: colorless oil; $^1\text{H NMR}$ (CDCl_3 , 500 MHz): δ 5.62–5.53 (m, 1H), 4.82 (s, 2H), 4.75 (s, 1H), 1.67 (s, 3H), 1.61 (d, J = 6.3 Hz, 3H), 1.56 (s, 6H), 0.89 (s, 9H), 0.11 (s, 3H), 0.08 (s, 3H); $^{13}\text{C NMR}$ (CDCl_3 , 500 MHz): δ 152.0, 134.6, 121.8, 92.7, 80.9, 73.2, 71.8, 71.5, 68.7, 68.2, 65.0, 53.7, 30.4, 25.7, 18.2, 13.2, 11.8, –4.70, –5.02; **HRMS** (ESI) calcd for $\text{C}_{22}\text{H}_{32}\text{O}_4\text{NaSi}$ $[\text{M}+\text{Na}]^+$ 411.1968, found 411.1973.

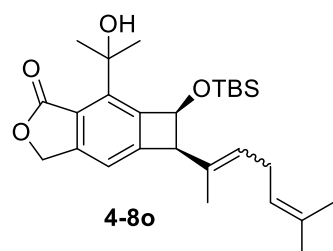
4-7n: colorless oil; $^1\text{H NMR}$ (CDCl_3 , 500 MHz): δ 5.81–5.72 (m, 1H), 5.52–5.45 (m, 1H), 4.86 (d, J = 5.6 Hz, 1H), 4.81 (s, 2H), 2.46 (s, 1H, OH), 1.70 (d, J = 6.5 Hz, 3H), 1.56 (s, 6H), 0.89 (s, 9H), 0.11 (s, 3H), 0.10 (s, 3H); $^{13}\text{C NMR}$ (CDCl_3 , 500 MHz): δ 152.5, 129.8, 127.9, 92.7, 80.5, 73.2, 71.8, 71.7, 68.6, 65.0, 63.8, 53.7, 30.4, 25.7, 18.3, 17.4, –4.6, –4.8; **HRMS** (ESI) calcd for $\text{C}_{21}\text{H}_{30}\text{O}_4\text{NaSi}$ $[\text{M}+\text{Na}]^+$ 397.1811, found 397.1806.





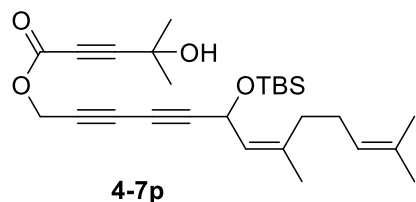
4-7o: colorless oil; $^1\text{H NMR}$ (CDCl_3 , 500 MHz): δ 5.28–5.24 (m, 1H), 5.11–5.03 (m, 1H), 4.81 (s, 2H), 2.38 (s, 1H, OH), 2.12–2.05 (m, 2H), 2.04–1.98 (m, 2H), 1.67 (s, 3H), 1.65 (s, 3H), 1.59 (s, 3H), 1.56 (s, 6H), 0.88 (s, 9H), 0.1 (s, 3H), 0.09 (s, 3H) $^{13}\text{C NMR}$ (CDCl_3 , 500 MHz): δ

152.5, 138.5, 131.9, 124.5, 123.6, 92.7, 81.4, 73.2, 71.9, 71.6, 67.3, 65.0, 60.4, 53.7, 39.2, 30.2, 26.1, 25.74, 25.67, 18.2, 17.7, 16.6, –4.5, –4.7; **HRMS** (ESI) calcd for $\text{C}_{27}\text{H}_{40}\text{O}_4\text{NaSi}$ $[\text{M}+\text{Na}]^+$ 479.2594, found 479.2590.



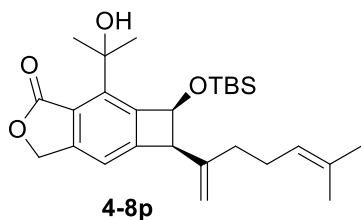
4-8o: white solid; 32 mg (67% yield, 2.5:1 E/Z); Purification: Flash Chromatography (SiO_2 , hexanes–EtOAc, 10:1 \rightarrow 6:1). $^1\text{H NMR}$ (CDCl_3 , 500 MHz) **Major isomer:** δ 7.02 (s, 1H), 6.13 (s, 1H, OH), 5.39 (t, J = 7.4 Hz, 1H), 5.33 (s, 1H), 5.32–5.28 (m, 2H), 5.14 (t, J = 6.1 Hz, 1H), 4.21 (s,

1H), 2.80–2.72 (m, 2H), 1.80 (s, 3H), 1.73 (s, 3H), 1.68 (s, 3H), 1.65 (s, 3H), 1.58 (s, 3H), 0.93 (s, 9H), 0.17 (s, 3H), 0.12 (s, 3H); **Minor isomer:** 7.09 (s, 1H), 6.13 (s, 1H), 5.39 (t, J = 7.4 Hz, 1H), 5.33 (s, 1H), 5.32–5.28 (m, 2H), 5.14 (t, J = 6.1 Hz, 1H, OH), 3.73 (s, 1H), 2.98–2.87 (m, 2H), 1.80 (s, 3H), 1.70 (s, 3H), 1.68 (s, 3H), 1.64 (s, 3H), 1.57 (s, 3H), 0.92 (s, 9H), 0.17 (s, 3H), 0.13 (s, 3H) $^{13}\text{C NMR}$ (CDCl_3 , 500 MHz) (all discernable signals for both isomers): δ 173.4, 153.5, 150.6, 148.1, 143.5, 132.2, 131.3, 130.9, 127.7, 122.5, 122.2, 121.3, 115.7, 75.4, 73.8, 72.3, 70.0, 61.5, 54.4, 31.0, 28.7, 28.6, 27.2, 27.0, 25.8, 25.7, 19.8, 17.8, 13.8, –3.7, –4.3, –5.2, –5.3; **HRMS** (ESI) calcd for $\text{C}_{27}\text{H}_{41}\text{O}_4\text{Si}$ $[\text{M}+\text{H}]^+$ 457.2774, found 457.2779.

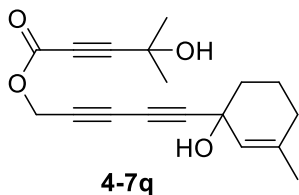


4-7p: Colorless oil $^1\text{H NMR}$ (CDCl_3 , 500 MHz): δ 5.27 (d, J = 8.6 Hz, 1H), 5.12–5.06 (m, 2H), 4.81 (s, 2H), 2.38 (s, 1H, OH), 2.13–1.96 (m, 4H), 1.72 (s, 3H), 1.69 (s, 3H), 1.61 (s, 3H), 1.56 (s, 6H), 0.88 (s, 9H), 0.10 (s, 3H), 0.09 (s, 3H); $^{13}\text{C NMR}$ (CDCl_3 , 500 MHz): δ 152.5,

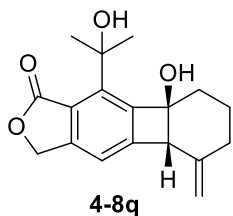
138.7, 132.4, 125.1, 123.5, 92.6, 81.5, 73.2, 71.9, 71.6, 67.4, 65.0, 60.1, 53.7, 32.5, 30.6, 30.4, 26.3, 25.7, 23.2, 18.2, 17.7, –4.4, –4.6; **HRMS** (ESI) calcd for $\text{C}_{27}\text{H}_{40}\text{O}_4\text{NaSi}$ $[\text{M}+\text{Na}]^+$ 479.2594, found 479.2601.



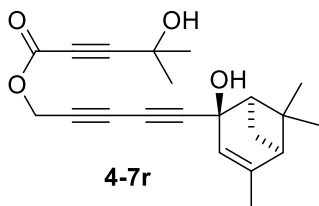
4-8p: white solid; 28 mg (62% yield); Flash Chromatography (SiO₂, hexanes–EtOAc, 10:1 → 6:1) **¹H NMR** (CDCl₃, 500 MHz): δ 7.09 (s, 1H), 6.12 (s, 1H, OH), 5.35–5.26 (m, 2H), 5.04 (s, 1H), 5.11–5.05 (m, 1H), 4.99 (s, 1H), 4.95 (s, 1H), 3.79 (s, 1H), 2.23–2.09 (m, 2H), 2.07–1.98 (m, 2H), 1.80 (s, 3H), 1.68 (s, 6H), 1.59 (s, 3H), 0.92 (s, 9H), 0.18 (s, 3H), 0.14 (s, 3H); **¹³C NMR** (CDCl₃, 500 MHz): δ 173.4, 153.3, 150.4, 148.4, 146.1, 143.4, 132.2, 123.4, 121.4, 115.6, 112.1, 75.9, 72.3, 70.0, 59.4, 34.0, 30.9, 28.6, 26.5, 25.8, 25.6, 17.7, –3.7, –5.2; **HRMS** (ESI) calcd for C₂₇H₄₁O₄Si [M+H]⁺ 457.2774, found 457.2779.



4-7q: colorless oil; **¹H NMR** (CDCl₃, 500 MHz): δ 5.73 (s, 1H), 4.81 (s, 2H), 1.98–1.86 (m, 3H), 1.85–1.71 (m, 3H), 1.69 (s, 3H), 1.56 (s, 6H); **¹³C NMR** (CDCl₃, 500 MHz): δ 152.5, 139.5, 123.7, 92.8, 83.9, 73.1, 72.3, 71.6, 67.0, 66.3, 64.9, 53.7, 37.2, 30.4, 29.6, 23.4, 19.2; **HRMS** (ESI) calcd for C₁₈H₂₀O₄Na [M+Na]⁺ 323.1259, found 323.1257.



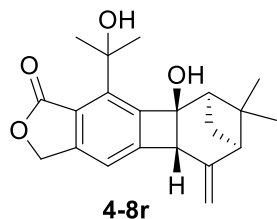
4-8q: white solid; 22 mg (56% yield); Flash Chromatography (SiO₂, hexanes–EtOAc, 4:1 → 2:1); **¹H NMR** (CDCl₃, 500 MHz): δ 7.15 (s, 1H), 5.26 (s, 2H), 5.02 (s, 1H), 4.93 (s, 1H), 3.87 (s, 1H), 3.51 (br s, 1H, OH), 2.20–2.12 (m, 2H), 1.96–1.88 (m, 2H), 1.78 (s, 6H), 1.72–1.64 (m, 2H); **¹³C NMR** (CDCl₃, 500 MHz): δ 184.2, 152.7, 150.5, 147.0, 145.7, 144.5, 120.8, 115.6, 112.5, 81.5, 73.1, 69.4, 57.6, 34.8, 30.5, 30.1, 28.5, 19.0; **HRMS** (ESI) calcd for C₁₈H₂₀O₄Na [M+Na]⁺ 323.1259, found 323.1268.



4-7r: yellow oil; **¹H NMR** (CDCl₃, 500 MHz): δ 5.29 (s, 1H), 4.79 (s, 2H), 3.11 (br s, 1H, OH), 2.55 (br s, 1H, OH), 2.52–2.47 (m, 1H), 2.33–2.28 (m, 1H), 1.98–1.95 (m, 1H), 1.71 (s, 3H), 1.59 (d, *J* = 9.0 Hz, 1H), 1.53 (s, 6H), 1.33 (s, 3H), 1.00 (s, 3H); **¹³C NMR** (CDCl₃, 500 MHz): δ 152.6, 148.6,

118.7, 93.1, 83.7, 73.1, 72.9, 72.3, 71.7, 67.1, 64.9, 53.7, 52.5, 47.6, 42.0, 36.3, 30.4, 26.9, 22.9, 22.6;

HRMS (ESI) calcd for $C_{21}H_{24}O_4Na$ $[M+Na]^+$ 363.1572, found 363.1576.



4-8r: pale-yellow solid; 50 mg (68% yield); Purification: Flash Chromatography

(SiO_2 , hexanes–EtOAc, 4:1 \rightarrow 2:1) **1H NMR** ($CDCl_3$, 500 MHz): δ 7.15 (s, 1H),

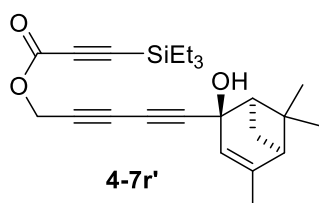
5.25 (s, 2H), 4.97 (s, 1H), 4.85 (s, 1H), 4.01 (s, 1H), 3.48 (br s, 1H, OH), 2.6–

2.52 (m, 2H), 2.25–2.17 (m, 2H), 1.73 (s, 6H), 1.38 (s, 3H), 1.06 (s, 3H), 0.57–

0.52 (m, 1H); **^{13}C NMR** ($CDCl_3$, 500 MHz): δ 172.1, 155.5, 150.5, 149.1, 146.8, 144.8, 120.7, 113.9, 109.1,

83.9, 72.9, 69.4, 53.5, 53.3, 48.9, 41.3, 30.5, 30.3, 27.6, 26.9, 23.9; **HRMS** (ESI) calcd for $C_{21}H_{25}O_4$

$[M+H]^+$ 341.1766, found 341.1762.



4-7r': yellow oil; **1H NMR** ($CDCl_3$, 500 MHz): δ 5.28 (s, 1H), 4.79 (s, 2H),

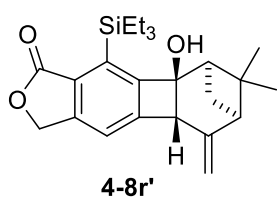
2.54–2.48 (m, 1H), 2.35–2.30 (m, 1H), 2.19 (br s, 1H, OH), 2.01–1.97 (m,

1H), 1.73 (d, J = 1.3 Hz, 3H), 1.61 (d, J = 9.6 Hz, 1H), 1.34 (s, 1H), 1.03–

0.95 (m, 12H), 0.66 (q, J = 7.8 Hz, 6H); **^{13}C NMR** ($CDCl_3$, 500 MHz): δ

151.8, 148.5, 118.8, 94.7, 94.1, 83.5, 72.9, 72.4, 71.6, 67.2, 53.5, 52.6, 47.6, 41.6, 36.3, 26.9, 23.0, 22.6,

7.2, 3.7; **HRMS** (ESI) calcd for $C_{24}H_{32}O_4NaSi$ $[M+Na]^+$ 419.2018, found 419.2013.



4-8r': pale-yellow solid; 42 mg (46% yield); Purification: Flash Chromatography

(SiO_2 , hexanes–EtOAc, 10:1 \rightarrow 5:1) **1H NMR** ($CDCl_3$, 500 MHz): δ 7.22 (s,

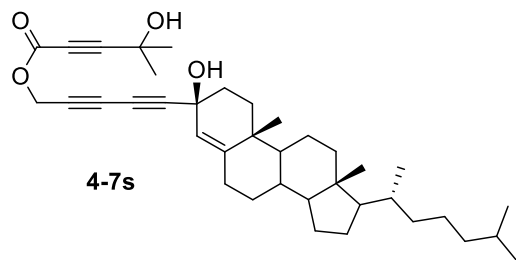
1H), 5.23 (s, 2H), 4.95 (s, 1H), 4.84 (s, 1H), 3.97 (s, 1H), 2.63–2.51 (m, 2H), 2.40

(s, 1H, OH), 2.21–2.13 (m, 1H), 1.40 (s, 3H), 1.13–1.04 (m, 3H), 1.08 (s, 3H),

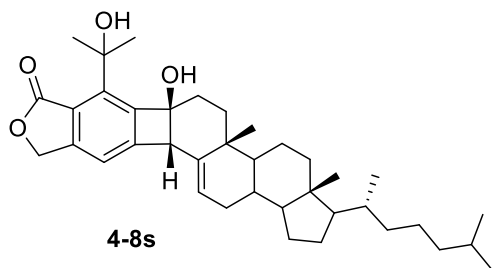
1.02–0.93 (m, 3H), 0.89–0.83 (m, 9H), 0.49 (d, J = 10.9, 1H); **^{13}C NMR** ($CDCl_3$, 500 MHz): δ 171.8, 156.5,

152.9, 149.4, 148.5, 136.4, 130.0, 128.6, 115.5, 108.8, 84.9, 69.1, 54.3, 53.3, 48.6, 41.3, 27.5, 27.0, 23.9,

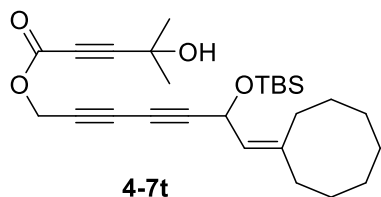
7.7, 3.1; **HRMS** (ESI) calcd for $C_{24}H_{32}O_4NaSi$ $[M+Na]^+$ 419.2018, found 419.2018.



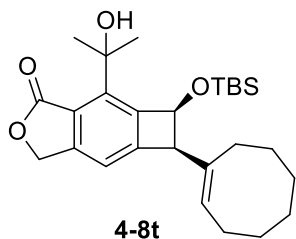
4-7s: ^1H NMR (CDCl_3 , 500 MHz): δ 5.23 (s, 1H), 4.82 (s, 2H), 2.60 (br s, 1H, OH), 2.46 (br s, 1H, OH), 2.18–2.11 (m, 1H), 2.04–1.95 (m, 3H), 1.95–1.88 (m, 1H), 1.86–1.76 (m, 3H), 1.64–1.65 (m, 4H), 1.57 (d, $J = 3.3$ Hz, 1H), 1.56 (s, 6H), 1.38–1.28 (m, 6H), 1.26–1.21 (m, 3H), 1.16–1.03 (m, 6H), 1.02 (s, 3H), 0.89 (d, $J = 6.6$ Hz, 3H), 0.85 (dd, $J = 1.9, 4.7$ Hz, 6H), 0.66 (s, 3H); ^{13}C NMR (CDCl_3 , 500 MHz): δ 152.6, 148.9, 121.8, 92.9, 83.6, 73.1, 72.3, 71.8, 67.4, 67.3, 64.9, 56.2, 55.9, 53.9, 53.7, 42.5, 39.7, 39.5, 37.5, 36.2, 35.8, 34.8, 34.5, 33.9, 32.6, 32.1, 30.6, 30.5, 30.4, 28.2, 28.0, 24.2, 23.8, 23.3, 22.8, 22.5, 21.1, 18.7, 18.5, 11.9; **HRMS** (ESI) calcd for $\text{C}_{38}\text{H}_{54}\text{O}_4\text{Na}$ $[\text{M}+\text{Na}]^+$ 597.3920, found 597.3923.



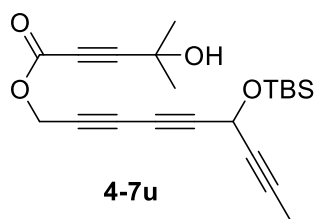
4-8s: white solid; 12 mg (42% yield); Purification: Flash Chromatography (SiO_2 , hexanes–EtOAc, 5:1 \rightarrow 3:1); ^1H NMR (CDCl_3 , 500 MHz): δ 7.23 (s, 1H), 5.58–5.53 (m, 1H), 3.90 (s, 1H), 2.8–1.94 (m, 3H), 1.76 (d, $J = 4.8$ Hz, 6H), 1.71–1.64 (m, 3H), 1.55–1.48 (m, 7H), 1.42–1.24 (m, 6H), 1.15 (s, 3H), 1.13–1.05 (m, 6H), 1.02–0.95 (m, 3H), 0.91 (d, $J = 6.4$ Hz, 3H), 0.86 (dd, $J = 2.6, 4.5$ Hz, 6H), 0.71 (s, 3H); ^{13}C NMR (CDCl_3 , 500 MHz): δ 172.2, 153.8, 150.2, 146.9, 141.4, 130.2, 128.5, 122.1, 117.0, 81.5, 72.8, 69.4, 56.9, 56.1, 53.9, 48.2, 42.5, 39.9, 39.5, 36.7, 36.2, 35.8, 32.9, 32.6, 32.2, 31.3, 30.5, 30.3, 28.3, 28.0, 24.1, 23.8, 22.8, 22.7, 22.5, 21.5, 18.7, 12.0; **HRMS** (ESI) calcd for $\text{C}_{38}\text{H}_{55}\text{O}_4$ $[\text{M}+\text{H}]^+$ 575.4100, found 575.4088.



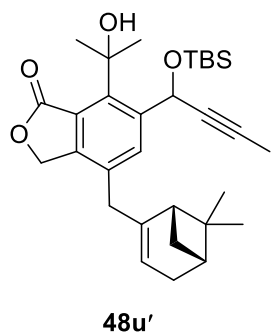
4-7t: colorless oil; ^1H NMR (CDCl_3 , 500 MHz): δ 5.26 (d, $J = 8.2$ Hz, 1H), 5.13 (d, $J = 8.1$ Hz, 1H), 4.82 (s, 2H), 2.32 (s, 1H, OH), 2.26–2.18 (m, 1H), 2.18–2.10 (m, 3H), 1.72–1.58 (m, 4H), 1.56 (s, 6H), 1.52–1.39 (m, 6H), 0.88 (s, 9H), 0.12 (s, 3H), 0.10 (s, 3H); ^{13}C NMR (CDCl_3 , 500 MHz): δ 152.5, 144.8, 124.4, 92.6, 81.4, 73.2, 71.9, 71.5, 67.5, 65.0, 60.1, 53.8, 36.9, 30.4, 29.5, 27.1, 27.0, 26.4, 25.7, 25.5, 18.2, –4.4, –4.6; **HRMS** (ESI) calcd for $\text{C}_{27}\text{H}_{40}\text{O}_4\text{NaSi}$ $[\text{M}+\text{Na}]^+$ 479.2594, found 479.2602.



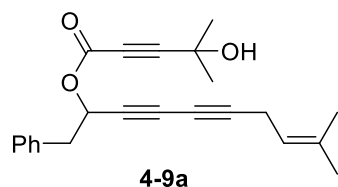
4-8t: white solid; 37 mg (69% yield); Purification: Flash Chromatography (SiO₂, hexanes–EtOAc, 10:1 → 6:1); **¹H NMR** (CDCl₃, 500 MHz): δ 7.08 (s, 1H), 6.17 (s, 1H, OH), 5.59 (t, *J* = 8.2 Hz, 1H), 5.35–5.25 (m, 2H), 5.21 (s, 1H), 3.75 (s, 1H), 2.19–2.13 (m, 2H), 2.13–2.07 (m, 2H), 1.80 (s, 3H), 1.67 (s, 3H), 1.62–1.59 (m, 1H), 1.57–1.45 (m, 7H), 0.92 (s, 9H), 0.17 (s, 3H), 0.12 (s, 3H); **¹³C NMR** (CDCl₃, 500 MHz): δ 173.5, 154.1, 150.3, 148.2, 143.5, 137.5, 128.3, 121.3, 115.9, 76.0, 72.3, 70.0, 60.7, 30.9, 30.1, 29.2, 28.5, 27.3, 26.4, 26.2, 26.2, 25.8, 17.9, –3.5, –5.2; **HRMS** (ESI) calcd for C₂₇H₄₀O₄NaSi [M+Na]⁺ 479.2594, found 479.2601.



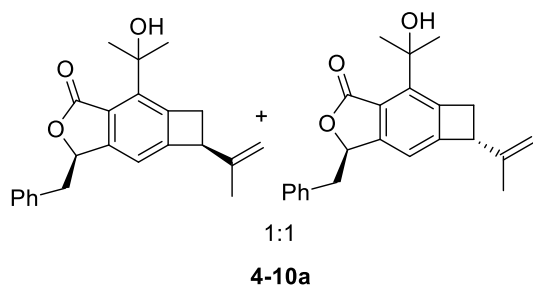
4-7u: yellow oil; **¹H NMR** (CDCl₃, 500 MHz): δ 5.20–5.16 (m, 1H), 4.81 (s, 2H), 2.53 (s, 1H, OH), 1.83 (d, *J* = 2.2 Hz, 3H), 1.55 (s, 6H), 0.89 (s, 9H), 0.15 (s, 3H), 0.14 (s, 3H); **¹³C NMR** (CDCl₃, 500 MHz): δ 152.5, 92.8, 81.4, 78.1, 75.9, 73.1, 72.4, 71.4, 66.8, 65.0, 53.6, 53.4, 30.4, 25.6, 18.2, 3.6, –4.6; **HRMS** (ESI) calcd for C₂₁H₂₈O₄NaSi [M+Na]⁺ 395.1655, found 395.1664.



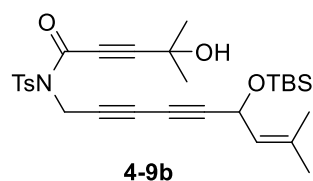
4-8u': pale-yellow oil; 35 mg (76% yield, 1:1 diastereomeric mixture); Purification: Flash Chromatography (SiO₂, hexanes–EtOAc, 3:1); **¹H NMR** (CDCl₃, 500 MHz): δ 7.96 (s, 1H), 6.31 (s, 1H), 6.12–6.08 (m, 1H), 5.22 (s, 2H), 3.32–3.14 (m, 2H), 2.36–2.29 (m, 1H), 2.29–2.15 (m, 1H), 2.11–2.04 (m, 1H), 2.02–1.95 (m, 1H), 1.84 (s, 3H), 1.81 (s, 3H), 1.80 (s, 3H), 1.25–1.17 (m, 1H), 1.22 (s, 3H), 1.12 (dd, *J* = 9, 17 Hz, 1H), 0.89 (s, 9H), 0.75 (s, 3H), 0.18 (s, 3H), 0.11–0.07 (m, 3H); **¹³C NMR** (CDCl₃, 500 MHz) (all discernable signal for both isomer): δ 173.9, 147.8, 146.5, 146.4, 144.7, 144.5, 141.6, 136.2, 136.1, 131.8, 122.8, 118.9, 118.8, 82.7, 82.6, 81.0, 74.0, 68.3, 45.7, 45.5, 40.6, 40.5, 39.4, 39.2, 38.1, 31.7, 31.3, 26.1, 25.7, 20.8, 18.2, 3.7, –4.3, –4.8; **HRMS** (ESI) calcd for C₃₁H₄₅O₄Si [M+H]⁺ 509.3087, found 509.3075.



4-9a: yellow oil; $^1\text{H NMR}$ (CDCl_3 , 500 MHz): δ 7.34–7.28 (m, 2H), 7.28–7.22 (m, 3H), 5.60 (t, $J = 5.4$ Hz, 1H), 5.15–5.09 (m, 1H), 3.15–3.04 (m, 2H), 2.96 (d, $J = 5.0$ Hz, 2H), 2.40 (br s, 1H, OH), 1.71 (s, 3H), 1.62 (s, 3H), 1.56 (s, 6H); $^{13}\text{C NMR}$ (CDCl_3 , 500 MHz): δ 152.2, 135.0, 129.6, 128.5, 127.3, 116.7, 92.4, 81.1, 73.5, 72.2, 71.3, 66.7, 65.0, 63.7, 40.9, 30.5, 25.5, 23.9, 18.4, 17.7; **HRMS** (ESI) calcd for $\text{C}_{23}\text{H}_{24}\text{O}_3\text{Na}$ $[\text{M}+\text{Na}]^+$ 371.1623, found 371.1609.

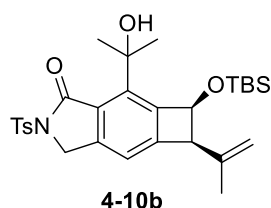


4-10a: 62% total yield; Column Chromatography (SiO_2 , hexanes–EtOAc, 10:1 \rightarrow 6:1); **Diastereomer 1:** white solid; 16 mg; $^1\text{H NMR}$ (CDCl_3 , 500 MHz): δ 7.32–7.26 (m, 2H), 7.27–7.24 (m, 1H), 7.23–7.19 (m, 2H), 6.88 (s, 1H, OH), 6.32 (s, 1H), 5.71–5.63 (m, 1H), 4.83 (s, 1H), 4.79 (s, 1H), 4.00–3.96 (m, 1H), 3.57 (dd, $J = 6.0, 8.5$ Hz, 1H), 3.18 (d, $J = 6.3$ Hz, 2H), 3.10 (d, $J = 13.5$ Hz, 1H), 1.76 (s, 3H), 1.61 (s, 3H), 1.57 (s, 3H); $^{13}\text{C NMR}$ (CDCl_3 , 500 MHz): δ 173.1, 155.2, 151.7, 145.9, 143.9, 140.5, 135.1, 129.6, 128.6, 127.2, 115.4, 110.9, 81.7, 71.8, 47.7, 41.3, 38.0, 30.1, 30.0, 20.3; **HRMS** (ESI) calcd for $\text{C}_{23}\text{H}_{24}\text{O}_3\text{Na}$ $[\text{M}+\text{Na}]^+$ 371.1623, found 371.1618. **Diastereomer 2:** white solid; 16 mg; $^1\text{H NMR}$ (CDCl_3 , 500 MHz): δ 7.30–7.22 (m, 2H), 7.18 (d, $J = 7.3$ Hz, 2H), 6.70 (s, 1H), 6.31 (s, 1H, OH), 5.65 (t, $J = 6.2$ Hz, 1H), 4.86 (s, 1H), 4.79 (s, 1H), 3.94–3.90 (m, 1H), 3.55 (dd, $J = 5.6, 8.4$ Hz, 1H), 3.30 (dd, $J = 8.1, 5.3$ Hz, 2H), 3.15–3.03 (m, 2H), 1.77 (s, 3H), 1.59 (s, 3H), 1.56 (s, 3H); $^{13}\text{C NMR}$ (CDCl_3 , 500 MHz): δ 173.1, 154.9, 151.5, 145.8, 144.1, 140.4, 134.8, 129.7, 128.5, 127.3, 115.7, 110.8, 81.5, 71.8, 47.6, 41.2, 38.1, 30.1, 30.0, 20.3; **HRMS** (ESI) calcd for $\text{C}_{23}\text{H}_{24}\text{O}_3\text{Na}$ $[\text{M}+\text{Na}]^+$ 371.1623, found 371.1627. All attempts to confirm to assign stereochemistry to each diastereomers by nOe failed.



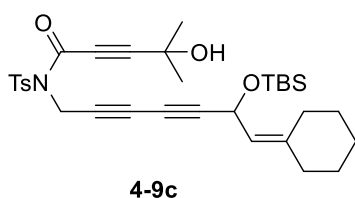
4-9b: colorless oil; $^1\text{H NMR}$ (CDCl_3 , 500 MHz): δ 7.97 (d, $J = 8.1$ Hz, 2H), 7.34 (d, $J = 8.1$ Hz, 2H), 5.27 (d, $J = 7.2$ Hz, 1H), 5.08 (d, $J = 8.1$ Hz, 1H), 4.94 (s, 2H), 2.44 (s, 3H), 1.74 (s, 3H), 1.68 (s, 3H), 1.54 (s, 6H), 0.90 (s, 9H),

0.12 (s, 3H), 0.11 (s, 3H); ^{13}C NMR (CDCl_3 , 500 MHz): δ 151.4, 145.6, 135.3, 135.1, 129.6, 128.9, 124.7, 99.1, 80.4, 74.5, 73.1, 69.4, 67.5, 65.2, 60.4, 36.9, 30.2, 25.8, 25.6, 21.7, 18.2, -4.5, -4.6; **HRMS** (ESI) calcd for $\text{C}_{29}\text{H}_{39}\text{NO}_5\text{NaSiS}$ $[\text{M}+\text{Na}]^+$ 564.2216, found 564.2231.



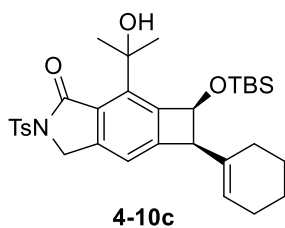
4-10b: white solid; 46 mg (72% yield); Purification: Flash Chromatography (SiO_2 , hexanes–EtOAc, 4:1); ^1H NMR (CDCl_3 , 500 MHz): δ 7.98 (d, J = 8.2 Hz, 2H), 7.32 (d, J = 8.1 Hz, 2H), 7.10 (s, 1H), 6.26 (s, 1H, OH), 5.18 (s, 1H), 4.93 (s, 1H), 4.98 (s, 1H), 4.87 (s, 2H), 3.75 (s, 1H), 2.41 (s, 3H), 1.73 (s, 3H), 1.68 (s, 3H),

1.60 (s, 3H), 0.89 (s, 9H), 0.15 (s, 3H), 0.12 (s, 3H); ^{13}C NMR (CDCl_3 , 500 MHz): δ 168.9, 152.5, 148.2, 145.5, 145.1, 143.2, 141.9, 134.8, 129.8, 125.9, 117.2, 113.6, 75.8, 72.1, 60.1, 50.0, 31.0, 28.5, 25.7, 21.7, 20.3, 17.8, -3.7, -5.3; **HRMS** (ESI) calcd for $\text{C}_{29}\text{H}_{40}\text{NO}_5\text{SiS}$ $[\text{M}+\text{H}]^+$ 542.2396, found 542.2385.



4-9c: yellow oil; ^1H NMR (CDCl_3 , 500 MHz): δ 7.97 (d, J = 8.1 Hz, 2H), 7.34 (d, J = 8.2 Hz, 2H), 5.23 (d, J = 7.2 Hz, 1H), 5.15 (d, J = 8.1 Hz, 1H), 4.84 (s, 2H), 2.44 (s, 3H), 2.30 (br s, 1H), 2.18–2.12 (m, 2H), 2.12–2.06 (m, 2H), 1.60–1.51 (m, 6H), 1.59–1.51 (m, 6H), 0.93–0.87 (m, 9H), 0.14–0.08

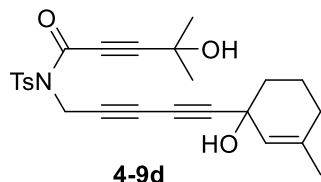
(m, 6H); ^{13}C NMR (CDCl_3 , 500 MHz): δ 151.4, 145.6, 143.0, 135.1, 129.6, 128.9, 121.4, 99.1, 80.7, 74.5, 73.1, 69.4, 67.3, 65.2, 59.5, 36.7, 30.2, 29.3, 28.1, 27.4, 26.5, 25.8, 21.7, 18.2, -4.4, -4.6; **HRMS** (ESI) calcd for $\text{C}_{32}\text{H}_{43}\text{NO}_5\text{NaSiS}$ $[\text{M}+\text{Na}]^+$ 604.2529, found 604.2541.



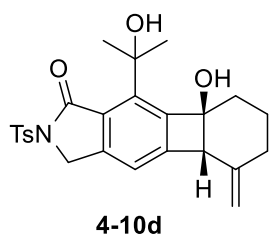
4-10c: white solid; 28 mg (56% yield); Purification: Flash Chromatography (SiO_2 , hexanes–EtOAc, 4:1); ^1H NMR (CDCl_3 , 500 MHz): δ 7.98 (d, J = 8.1 Hz, 2H), 7.32 (d, J = 8.2 Hz, 2H), 7.08 (s, 1H), 6.25 (s, 1H, OH), 5.59 (s, 1H), 5.15 (s, 1H), 4.91–4.81 (m, 2H), 3.66 (s, 1H), 2.42 (s, 3H), 1.88–1.77 (m, 2H),

1.73 (s, 3H), 1.64–1.53 (m, 9H), 0.89 (s, 9H), 0.14 (s, 3H), 0.11 (s, 3H); ^{13}C NMR (CDCl_3 , 500 MHz): δ 168.8, 153.0, 148.0, 145.5, 144.9, 143.4, 134.8, 134.6, 129.8, 128.3, 125.7, 125.0, 117.2, 75.7, 72.1, 60.4,

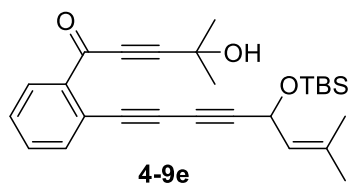
50.0, 31.0, 28.6, 26.4, 25.8, 25.2, 22.7, 22.3, 21.7, 17.9, -3.7, -5.2; **HRMS** (ESI) calcd for C₃₂H₄₄NO₅SiS [M+H]⁺ 582.2709, found 582.2723.



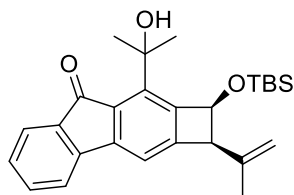
4-9d: colorless oil; **¹H NMR** (CDCl₃, 500 MHz): δ 7.95 (d, *J* = 8.2 Hz, 2H), 7.33 (d, *J* = 8.1 Hz, 2H), 5.43 (s, 1H), 4.81 (s, 2H), 3.05 (br s, 1H), 2.43 (s, 3H), 1.97–1.89 (m, 3H), 1.86–1.74 (m, 3H), 1.69 (s, 3H), 1.52 (s, 6H); **¹³C NMR** (CDCl₃, 500 MHz): δ 151.4, 145.6, 139.5, 135.1, 129.6, 128.9, 123.8, 99.3, 82.9, 74.4, 73.8, 69.2, 67.1, 66.3, 65.2, 37.2, 36.9, 30.2, 29.7, 23.5, 21.7, 19.2; **HRMS** (ESI) calcd for C₂₅H₂₇NO₅NaS [M+Na]⁺ 476.1521, found 476.1519.



4-10d: white solid; 23 mg (42% yield); Purification: Flash Chromatography (SiO₂, hexanes–EtOAc, 4:1); **¹H NMR** (CDCl₃, 500 MHz): δ 8.00 (d, *J* = 7.5 Hz, 2H), 7.34 (d, *J* = 7.6, 2H), 7.13 (s, 1H), 5.00 (s, 1H), 4.91 (s, 1H), 4.84 (s, 2H), 3.83 (s, 1H), 3.19 (s, 1H, OH), 2.43 (s, 3H), 2.30–2.22 (m, 1H), 2.18–2.07 (m, 2H), 1.94–1.85 (m, 1H), 1.70 (s, 3H), 1.69 (s, 3H), 1.66–1.61 (m, 2H); **¹³C NMR** (CDCl₃, 500 MHz): δ 167.6, 152.2, 145.6, 145.4, 145.1, 144.1, 139.6, 135.1, 129.8, 128.3, 128.0, 117.1, 112.5, 109.9, 109.6, 81.9, 58.0, 49.5, 34.7, 30.5, 28.4, 21.7, 19.0; **HRMS** (ESI) calcd for C₂₇H₂₆NO₅S [M+H]⁺ 476.1532, found 476.1531.

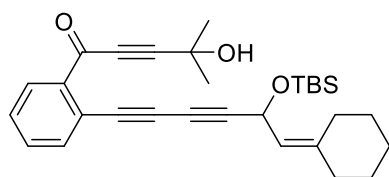


4-9e: yellow oil; **¹H NMR** (CDCl₃, 500 MHz): δ 8.00 (d, *J* = 8.1 Hz, 1H), 7.60 (d, *J* = 8.2 Hz, 1H), 7.49 (t, *J* = 6.3 Hz, 1H), 7.43 (t, *J* = 6.5 Hz, 1H), 5.33–5.28 (m, 1H), 5.18 (d, *J* = 8.3 Hz, 1H), 2.44 (br s, 1H, OH), 1.73 (s, 3H), 1.69 (s, 3H), 1.64 (s, 6H), 0.90 (s, 9H), 0.14 (s, 3H), 0.12 (s, 3H); **¹³C NMR** (CDCl₃, 500 MHz): δ 176.7, 139.0, 135.6, 135.0, 132.6, 131.2, 128.8, 124.8, 121.7, 98.9, 86.0, 80.9, 79.9, 76.3, 68.7, 65.3, 60.7, 30.6, 25.8, 25.6, 18.3, -4.5, -4.6; **HRMS** (ESI) calcd for C₂₇H₃₅O₃Si [M+NH]⁺ 435.2355, found 435.2362.



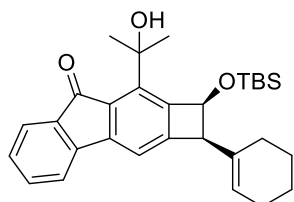
4-10e

4-10e: yellow solid; 42 mg (87% yield, 6:1 *dr*); Purification: Flash Chromatography (SiO₂, hexanes–EtOAc, 10:1); **Major diastereomer:** ¹H NMR (CDCl₃, 500 MHz): δ 7.59 (d, *J* = 7.3 Hz, 1H), 7.47–7.40 (m, 2H), 7.27–7.23 (m, 2H), 7.18 (s, 1H), 6.26 (s, 1H, OH), 5.17 (s, 1H), 4.96 (s, 1H), 4.93 (s, 1H), 3.72 (s, 1H), 1.76 (s, 3H), 1.74 (s, 3H), 1.63 (s, 3H), 0.92 (s, 9H), 0.17 (s, 3H), 0.15 (s, 3H); ¹³C NMR (CDCl₃, 500 MHz): δ 196.7, 153.7, 149.3, 148.6, 144.2, 143.9, 142.3, 135.1, 133.5, 129.2, 124.6, 119.8, 116.5, 114.6, 113.5, 75.9, 72.3, 59.9, 30.5, 28.3, 25.8, 20.3, 17.9, –3.6, –5.2; **HRMS** (ESI) calcd for C₂₇H₃₅O₃Si [M+H]⁺ 435.2355, found 435.2341.



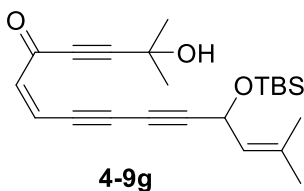
4-9f

4-9f: yellow oil; ¹H NMR (CDCl₃, 500 MHz): δ 8.00 (d, *J* = 7.3 Hz, 1H), 7.61 (d, *J* = 7.8 Hz, 1H), 7.50 (t, *J* = 6.8 Hz, 1H), 7.44 (t, *J* = 7.6 Hz, 1H), 5.26 (s, 2H), 2.30 (s, 1H, OH), 2.21–2.14 (m, 2H), 2.13–2.07 (m, 2H), 1.64 (s, 6H), 1.61–1.49 (m, 6H), 0.90 (s, 9H), 0.14 (s, 3H), 0.12 (s, 3H); ¹³C NMR (CDCl₃, 500 MHz): δ 176.7, 142.8, 139.1, 135.7, 132.6, 131.1, 128.8, 121.5, 98.9, 86.4, 81.0, 76.3, 68.5, 65.3, 59.8, 36.8, 30.7, 29.4, 28.1, 27.4, 26.5, 25.8, 18.3, –4.4, –4.6; **HRMS** (ESI) calcd for C₃₀H₃₈O₃NaSi [M+Na]⁺ 497.2488, found 497.2493.

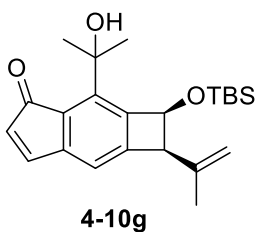


4-10f

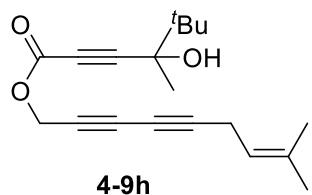
4-10f: yellow solid; 36 mg (76% yield, 10:1 *dr*); Purification: Flash Chromatography (SiO₂, hexanes–EtOAc, 10:1); **Major diastereomer:** ¹H NMR (CDCl₃, 500 MHz): δ 7.56 (d, *J* = 7.2 Hz, 1H), 7.47–7.39 (m, 2H), 7.27–7.23 (m, 1H), 7.18 (s, 1H), 6.27 (s, 1H, OH), 5.95 (s, 1H), 5.15–5.13 (m, 1H), 3.63 (s, 1H), 2.11–2.04 (m, 2H), 1.95–1.89 (m, 2H), 1.76 (s, 3H), 1.63 (s, 3H), 1.65–1.58 (m, 4H), 0.92 (s, 9H), 0.17 (s, 3H), 0.14 (s, 3H); ¹³C NMR (CDCl₃, 500 MHz): δ 196.8, 154.3, 149.2, 148.5, 144.3, 144.1, 135.1, 134.8, 133.6, 129.8, 129.2, 124.8, 124.5, 119.8, 114.7, 75.9, 72.4, 60.3, 30.5, 28.3, 26.4, 25.8, 25.3, 22.8, 22.4, 17.9 –3.7, –5.1; **HRMS** (ESI) calcd for C₃₀H₃₉O₃Si [M+H]⁺ 475.2668, found 475.2658.



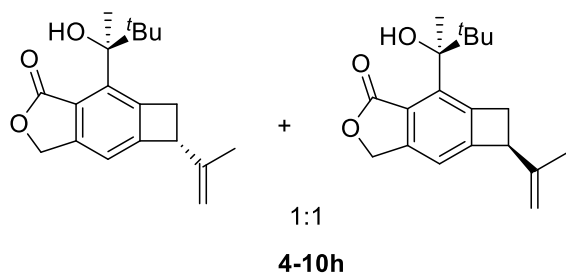
4-9g: yellow oil; $^1\text{H NMR}$ (CDCl_3 , 500 MHz): δ 6.44 (d, $J = 11.9$ Hz, 1H), 6.35 (d, $J = 11.6$ Hz, 1H), 5.27 (d, $J = 7.6$ Hz, 1H), 5.17 (d, $J = 8.3$ Hz, 1H), 2.20 (s, 1H, OH), 1.73 (s, 3H), 1.68 (s, 3H), 1.60 (s, 6H), 0.89 (s, 9H), 0.11 (s, 3H), 0.10 (s, 3H); $^{13}\text{C NMR}$ (CDCl_3 , 500 MHz): δ 174.7, 139.7, 135.5, 124.4, 121.9, 98.0, 89.9, 86.9, 81.4, 74.6, 68.2, 65.2, 60.7, 30.6, 25.7, 25.6, 18.3, -4.6 , -4.7 ; **HRMS** (ESI) calcd for $\text{C}_{23}\text{H}_{32}\text{O}_3\text{NaSi}$ $[\text{M}+\text{Na}]^+$ 407.2018, found 407.2008.



4-10g: yellow oil; 36 mg (56% yield, 10:1 *dr*); Purification: Flash Chromatography (SiO_2 , hexanes–EtOAc, 10:1); The major diastereomer could be completely separated from minor; $^1\text{H NMR}$ (CDCl_3 , 500 MHz): δ 7.44 (d, $J = 5.8$ Hz, 1H), 6.71 (s, 1H, OH), 5.87 (s, 1H), 5.81 (d, $J = 5.8$ Hz, 1H), 5.09 (s, 1H), 4.84 (s, 1H), 4.89 (s, 1H), 3.65 (s, 1H), 1.70 (s, 6H), 1.58 (s, 3H), 0.92 (s, 9H), 0.16 (s, 3H), 0.14 (s, 3H); $^{13}\text{C NMR}$ (CDCl_3 , 500 MHz): δ 201.2, 152.3, 150.5, 148.3, 148.2, 144.3, 142.3, 126.7, 125.8, 117.4, 113.4, 75.8, 72.3, 59.8, 30.4, 28.1, 25.8, 20.2, 17.9, -3.7 , -5.2 ; **HRMS** (ESI) calcd for $\text{C}_{23}\text{H}_{32}\text{O}_3\text{NaSi}$ $[\text{M}+\text{Na}]^+$ 407.2018, found 407.2008.

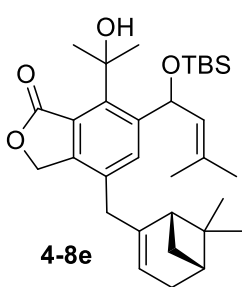


4-9h: colorless oil; $^1\text{H NMR}$ (CDCl_3 , 500 MHz): δ 5.13 (t, $J = 7.3$ Hz, 1H), 4.79 (s, 2H), 2.96 (d, $J = 6.8$ Hz, 1H), 2.11 (br s, 1H, OH), 1.70 (s, 3H), 1.62 (s, 3H), 1.48 (s, 3H), 1.05 (s, 9H); $^{13}\text{C NMR}$ (CDCl_3 , 500 MHz): δ 152.5, 135.4, 116.7, 92.2, 80.9, 75.2, 74.1, 72.5, 68.4, 63.7, 53.8, 38.3, 25.5, 24.9, 24.1, 18.4, 17.7; **HRMS** (ESI) calcd for $\text{C}_{19}\text{H}_{25}\text{O}_3$ $[\text{M}+\text{H}]^+$ 301.1804, found 301.1816.



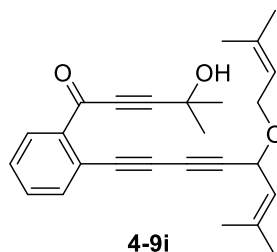
4-10h: 87% total yield; Purification: Column Chromatography (SiO₂, hexanes–EtOAc, 10:1 → 6:1);
Diastereomer 1: white solid; 18 mg; ¹H NMR (CDCl₃, 500 MHz): δ 7.17 (s, 1H, OH), 7.12 (s, 1H), 5.31 (s, 2H), 4.84 (d, *J* = 7.1 Hz, 2H), 3.99–3.95 (m, 1H), 3.58 (dd, *J* =

5.6, 8.3 Hz, 1H), 3.21 (dd, *J* = 2.6, 11.3 Hz), 1.77 (s, 3H), 1.60 (s, 3H), 0.97 (s, 9H); ¹³C NMR (CDCl₃, 500 MHz): δ 174.3, 154.5, 148.3, 145.4, 144.0, 143.5, 122.9, 115.1, 111.0, 80.9, 69.9, 46.8, 41.7, 39.5, 25.7, 24.4, 20.2. **HRMS** (ESI) calcd for C₁₉H₂₅O₃ [M+H]⁺ 301.1804, found 301.1807. **Diastereomer 2:** white solid; 20 mg; ¹H NMR (CDCl₃, 500 MHz): δ 7.17 (s, 1H, OH), 7.11 (s, 1H), 5.35–5.27 (m, 2H), 4.86–4.81 (m, 2H), 3.99–3.95 (m, 1H), 3.67 (dd, *J* = 5.8, 7.9 Hz, 1H), 3.13 (dd, *J* = 2.8, 11.2 Hz), 1.77 (s, 3H), 1.59 (s, 3H), 0.97 (s, 9H); ¹³C NMR (CDCl₃, 500 MHz): δ 174.3, 154.6, 148.3, 145.4, 144.2, 143.7, 122.9, 115.1, 111.0, 80.8, 69.9, 46.8, 41.8, 39.2, 25.8, 24.4, 20.2; **HRMS** (ESI) calcd for C₁₉H₂₅O₃ [M+H]⁺ 301.1804, found 301.1801. All attempts to confirm to assign stereochemistry to each diastereomers by nOe failed.

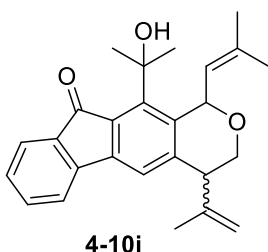


4-8e': colorless oil; 24 mg (76% yield, 1:1 diastereomeric mixture); Purification: Flash Chromatography (SiO₂, hexanes–EtOAc, 4:1); ¹H NMR (both isomers) (CDCl₃, 500 MHz): δ 7.79 (s, 1H), 7.60 (s, 1H), 6.39 (s, 2H), 6.36 (s, 2H), 6.02 (d, *J* = 4.4 Hz, 1H), 6.00 (d, *J* = 4.5 Hz, 2H), 5.21–5.19 (m, 4H), 3.29–3.17 (m, 4H), 2.37–2.31 (m, 2H), 2.27–2.18 (m, 4H), 2.11–2.06 (m, 2H), 2.00–1.95 (m, 2H), 1.86

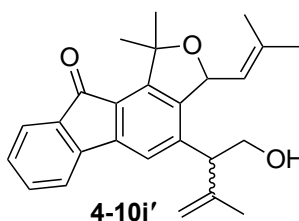
(s, 6H), 1.78 (s, 6H), 1.73–1.68 (m, 12H), 1.23 (s, 6H), 1.14–1.09 (m, 2H), 0.84 (s, 18H), 0.76 (s, 3H), 0.75 (s, 3H), 0.09–0.06 (m, 6H), –0.10 (s, 3H), –0.12 (s, 3H); ¹³C NMR (CDCl₃, 500 MHz) (all discernable signal for both isomer): δ 174.0, 147.0, 147.4, 147.2, 147.1, 144.7, 144.5, 144.3, 144.2, 137.0, 136.9, 134.1, 131.5, 129.5, 129.4, 122.8, 122.7, 119.0, 118.7, 111.4, 73.6, 68.8, 68.6, 68.3, 68.2, 45.8, 45.6, 40.6, 40.5, 39.4, 39.2, 38.1, 31.7, 31.4, 31.3, 31.2, 26.2, 25.9, 25.8, 20.9, 20.8, 19.0, 18.1, –4.1, –4.3, –4.4; ; **HRMS** (ESI) calcd for C₃₂H₄₈O₄NaSi [M+Na]⁺ 547.3220, found 547.3197.



4-9i: yellow oil; $^1\text{H NMR}$ (CDCl_3 , 500 MHz): δ 8.01 (d, J = 7.6 Hz, 1H), 7.61 (d, J = 7.8 Hz, 1H), 7.51 (t, J = 7.4 Hz, 1H), 7.45 (t, J = 7.5, 1H), 5.38 (m, 2H), 4.90 (d, J = 8.6 Hz, 1H), 4.18 (dd, J = 6.8, 4.7 Hz, 1H), 4.02 (dd, J = 7.4, 3.6 Hz, 1H), 1.76 (s, 3H), 1.75 (s, 3H), 1.71 (s, 6H), 1.64 (s, 6H); $^{13}\text{C NMR}$ (CDCl_3 , 500 MHz): δ 176.6, 139.1, 138.3, 135.7, 132.6, 131.3, 128.9, 121.8, 121.6, 120.4, 98.8, 84.2, 80.9, 79.7, 76.2, 70.0, 65.6, 65.3, 64.7, 30.6, 26.1, 25.8, 25.7, 18.4, 18.2; **HRMS** (ESI) calcd for $\text{C}_{26}\text{H}_{29}\text{O}_3$ $[\text{M}+\text{H}]^+$ 389.2117, found 389.2121.

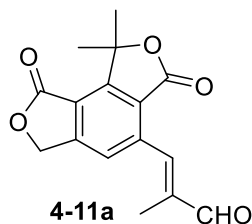


4-10i: yellow oil; 24 mg (28% yield, 1:1 diastereomeric mixture); formed along with **4i'**; Purification: Column Chromatography (SiO_2 , hexanes–EtOAc, 20:1 \rightarrow 10:1); $^1\text{H NMR}$ (CDCl_3 , 500 MHz): δ 7.60 (d, J = 7.8 Hz, 2H), 7.48 (t, J = 6.7 Hz, 1H), 7.31 (s, 1H), 7.29–7.26 (m, 2H), 7.24 (s, 1H), 6.06 (d, J = 6.9 Hz, 1H), 6.01 (d, J = 9.6 Hz, 1H), 5.25–5.19 (m, 2H), 5.13 (s, 1H), 5.00–4.98 (m, 1H), 4.96 (s, 1H), 4.87 (s, 1H), 4.14–4.09 (m, 1H), 4.02–3.96 (m, 1H), 3.83–3.77 (m, 1H), 3.67–3.56 (m, 3H), 1.93–1.90 (m, 3H), 1.87 (s, 3H), 1.80–1.77 (m, 9H), 1.71–1.68 (m, 6H), 1.64 (s, 6H), 1.58 (s, 1H); $^{13}\text{C NMR}$ (CDCl_3 , 500 MHz): δ 196.9, 193.1, 146.5, 147.6, 146.1, 145.9, 144.6, 144.2, 143.8, 143.1, 142.5, 140.2, 139.5, 136.7, 135.0, 134.5, 134.2, 133.9, 129.1, 126.7, 126.2, 124.7, 120.6, 120.1, 119.6, 118.2, 115.1, 111.9, 85.9, 78.2, 74.5, 71.1, 64.8, 63.1, 49.5, 48.1, 30.5, 30.1, 28.5, 27.1, 26.0, 23.2, 19.9, 18.8, 18.0; **HRMS** (ESI) calcd for $\text{C}_{26}\text{H}_{29}\text{O}_3$ $[\text{M}+\text{H}]^+$ 389.2117, found 389.2123.



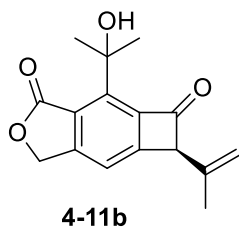
4-10i': yellow oil; 24 mg (28% yield); formed along with **4i**; Purification: Column Chromatography (SiO_2 , hexanes–EtOAc, 20:1 \rightarrow 10:1); $^1\text{H NMR}$ (CDCl_3 , 500 MHz): δ 7.60 (d, J = 7.2 Hz, 1H), 7.46–7.43 (m, 2H), 7.27–7.23 (m, 2H), 6.06 (d, J = 6.6 Hz, 1H), 5.25 (d, J = 6.7 Hz, 1H), 5.04 (s, 1H), 4.91 (s, 1H), 3.97 (dd, J = 3.8, 6.8 Hz, 1H), 3.79–3.72 (m, 2H), 1.88 (s, 3H), 1.79 (s, 3H), 1.78 (s, 3H), 1.72 (s, 3H), 1.66 (s, 3H); $^{13}\text{C NMR}$ (CDCl_3 , 500 MHz): δ 196.8, 151.6, 145.2, 144.6, 144.3, 143.2, 139.9,

139.3, 135.0, 133.9, 130.6, 129.1, 127.2, 124.7, 120.7, 119.6, 116.0, 74.7, 71.1, 62.7, 48.6, 30.7, 30.4, 25.6, 20.1, 18.8; **HRMS** (ESI) calcd for $C_{26}H_{29}O_3$ $[M+H]^+$ 389.2117, found 389.2131.



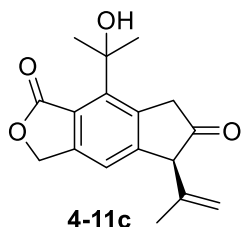
4-11a: white solid; 22 mg (72% yield); Purification: Flash Chromatography (SiO_2 , hexanes–EtOAc 5:1 \rightarrow 2:1); **1H NMR** ($CDCl_3$, 500 MHz): δ 9.76 (s, 1H), 8.27 (s, 1H), 7.69 (s, 1H), 5.51 (s, 1H), 5.29 (s, 1H), 2.06 (s, 3H), 1.89 (s, 6H); **^{13}C NMR** ($CDCl_3$, 500 MHz): δ 194.8, 167.8, 167.6, 155.2, 152.8, 142.8, 141.2, 140.7, 125.4,

123.1, 120.2, 85.7, 70.3, 25.7, 11.3; **HRMS** (ESI) calcd for $C_{16}H_{15}O_3$ $[M+H]^+$ 389.2117, found 389.2131.



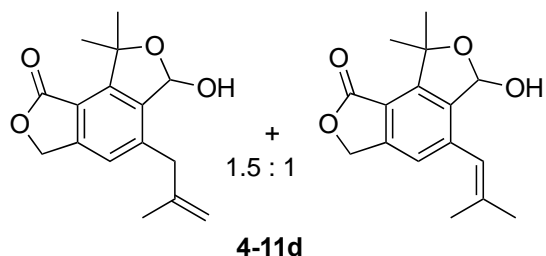
4-11b: white solid; 53 mg (82% yield); Purification: Flash Chromatography (SiO_2 , hexanes–EtOAc, 5:1 \rightarrow 2:1); **1H NMR** ($CDCl_3$, 500 MHz): δ 7.53 (s, 1H), 6.11 (s, 1H), 5.43 (s, 2H), 5.00 (s, 1H), 4.81 (s, 1H), 4.73 (s, 1H), 1.85 (s, 3H), 1.78 (s, 3H), 1.77 (s, 3H); **^{13}C NMR** ($CDCl_3$, 500 MHz): δ 186.3, 172.3, 159.7, 155.3, 150.9,

145.4, 139.7, 123.8, 116.3, 113.4, 72.1, 70.1, 69.0, 30.2, 30.1, 21.3; **HRMS** (ESI) calcd for $C_{16}H_{17}O_4$ $[M+H]^+$ 273.1127, found 273.1133.



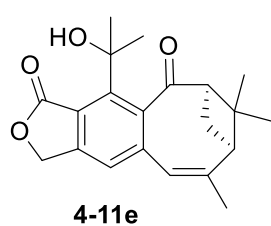
4-11c: colorless oil; 12 mg (55% yield); Purification: Flash Chromatography (SiO_2 , hexanes–EtOAc, 5:1 \rightarrow 3:1); **1H NMR** ($CDCl_3$, 500 MHz): δ 7.50 (s, 1H), 5.32 (s, 2H), 4.98 (s, 1H), 4.82 (s, 1H), 4.70 (s, 1H), 3.31 (s, 2H), 1.87 (s, 3H), 1.80 (s, 3H), 1.79 (s, 3H); **^{13}C NMR** ($CDCl_3$, 500 MHz): δ 185.6, 168.3, 159.3,

155.3, 149.4, 147.1, 140.2, 123.5, 116.3, 113.0, 77.0, 68.8, 68.3, 50.4, 25.2, 24.9, 21.4; **HRMS** (ESI) calcd for $C_{17}H_{18}O_4Na$ $[M+H]^+$ 273.1127, found 273.1133.



4-11d: colorless oil; 35 mg (86% yield, inseparable mixture (1.5:1) of isomeric alkenes); Purification: Flash Chromatography (SiO₂, hexanes–EtOAc, 5:1 → 3:1); ¹H NMR (CDCl₃, 500 MHz): **Major isomer:** δ 7.24 (s, 1H), 6.54 (d, *J* = 5.7 Hz, 1H), 5.31 (s, 2H), 4.91 (s, 1H),

4.69 (s, 1H), 3.88 (d, *J* = 5.6 Hz, 1H, OH), 3.66 (d, *J* = 15.4 Hz, 1H), 3.45 (d, *J* = 15.7, 1H), 1.79 (s, 3H), 1.72 (s, 3H), 1.70 (s, 3H); **Minor isomer:** δ 7.28 (s, 1H), 6.48 (s, 1H), 6.46 (d, *J* = 5.2 Hz, 1H), 5.33 (s, 2H), 3.76 (d, *J* = 5.1 Hz, 1H, OH), 1.96 (s, 3H), 1.88 (s, 3H), 1.79 (s, 3H), 1.69 (s, 3H); ¹³C NMR (CDCl₃, 500 MHz) (all discernable signal for both isomer): δ 169.5, 169.4, 149.5, 149.1, 147.2, 146.9, 142.1, 143.7, 139.3, 138.6, 122.4, 121.6, 120.6, 117.4, 113.6, 99.1, 98.8, 87.1, 87.0, 69.9, 69.8, 40.6, 29.3, 27.5, 27.1, 22.5, 20.0; **HRMS** (ESI) calcd for C₁₆H₁₉O₄ [M+H]⁺ 275.1283, found 275.1281.



4-11e: colorless oil; 35 mg (81% yield); Purification: Flash Chromatography (SiO₂, hexanes–EtOAc, 4:1); ¹H NMR (CDCl₃, 500 MHz): δ 7.23 (s, 1H), 7.22 (s, 1H), 6.11 (s, 2H), 2.94–2.88 (m, 2H), 2.87–2.82 (m, 2H), 2.65–2.59 (m, 1H), 2.25 (d, *J* = 10.8 Hz, 1H), 2.00 (s, 3H), 1.68 (s, 3H), 1.67 (s, 3H), 1.56 (s, 3H),

1.44 (s, 3H); ¹³C NMR (CDCl₃, 500 MHz): δ 201.0, 173.5, 165.9, 150.9, 148.7, 140.8, 131.4, 127.7, 122.3, 121.4, 71.9, 50.5, 39.9, 30.2, 29.9, 27.3, 26.6, 22.0, 21.8; **HRMS** (ESI) calcd for C₂₁H₂₅O₄ [M+H]⁺ 341.1753, found 371.1766.

4.4.6. Computational details

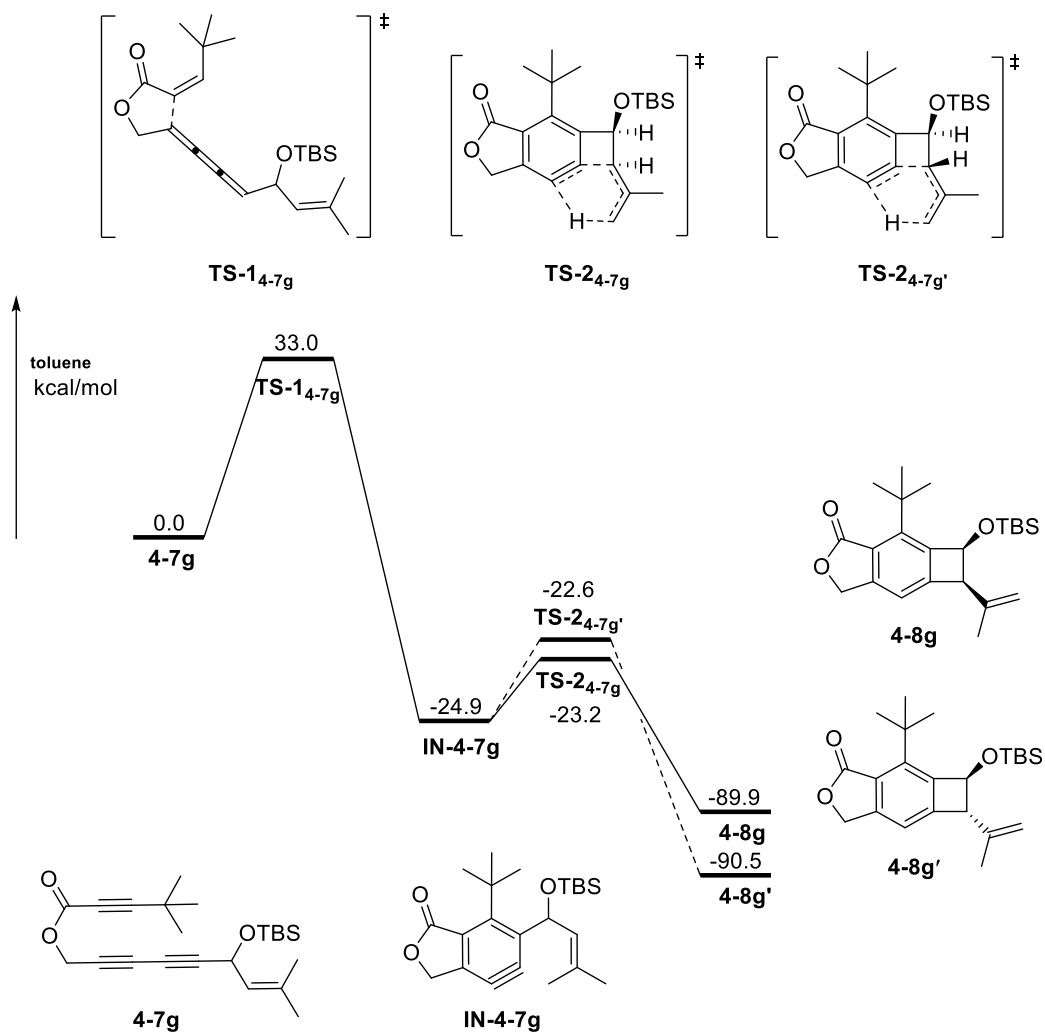
All DFT calculations were carried out with the Gaussian 09 suite of computational programs.^[1] The geometries of all stationary points were optimized using the B3LYP hybrid functional^[2] at the basis set level of 6-31G(d). Frequencies were analytically computed at the same level of theory to obtain the free energies and to confirm whether the structures are minima (no imaginary frequency) or transition states (only one imaginary frequency). The solvent effect of toluene was evaluated by using the SMD polarizable continuum model by carrying out single point calculations at the M06/6-311++G(d,p) level.^[3] All transition state structures were confirmed to connect the proposed reactants and products by intrinsic reaction coordinate (IRC) calculations. The energies given in the text are Gibbs free energies corrected with solvation effects. All these are relative to the energies of the corresponding substrate.

[1] Gaussian 09, Revision A.01, M. J. Frisch, G. W. Trucks, H. B. Schlegel, G. E. Scuseria, M. A. Robb, J. R. Cheeseman, G. Scalmani, V. Barone, B. Mennucci, G. A. Petersson, H. Nakatsuji, M. Caricato, X. Li, H. P. Hratchian, A. F. Izmaylov, J. Bloino, G. Zheng, J. L. Sonnenberg, M. Hada, M. Ehara, K. Toyota, R. Fukuda, J. Hasegawa, M. Ishida, T. Nakajima, Y. Honda, O. Kitao, H. Nakai, T. Vreven, J. A. Montgomery, Jr., J. E. Peralta, F. Ogliaro, M. Bearpark, J. J. Heyd, E. Brothers, K. N. Kudin, V. N. Staroverov, R. Kobayashi, J. Normand, K. Raghavachari, A. Rendell, J. C. Burant, S. S. Iyengar, J. Tomasi, M. Cossi, N. Rega, J. M. Millam, M. Klene, J. E. Knox, J. B. Cross, V. Bakken, C. Adamo, J. Jaramillo, R. Gomperts, R. E. Stratmann, O. Yazyev, A. J. Austin, R. Cammi, C. Pomelli, J. W. Ochterski, R. L. Martin, K. Morokuma, V. G. Zakrzewski, G. A. Voth, P. Salvador, J. J. Dannenberg, S. Dapprich, A. D. Daniels, Ö. Farkas, J. B. Foresman, J. V. Ortiz, J. Cioslowski, D. J. Fox, Gaussian, Inc., Wallingford CT, **2009**.

[2] (a) Becke, A. D. *J. Chem. Phys.* **1993**, 98, 5648. (b) Becke, A. D. *J. Chem. Phys.* **1993**, 98, 1372. (c) Lee, C.; Yang, W.; Parr, R. G. *Phys. Rev. B* **1988**, 37, 785.

[3] (a) Zhao, Y.; Truhlar, D. G. *Theor. Chem. Acc.* **2008**, 120, 215. (b) Zhao, Y.; Truhlar, D. G. *Acc. Chem. Res.* **2008**, 41, 157.

Reaction profile for 4-7g (*t*-butyl substituted substrate)



Calculated Energy Values

Table S1. Energies (in Hartree) calculated at SMD-M06/6-311++G(d,p)//B3LYP/6-31G(d)

Species	E ₀ ^a	H ₂₉₈ ^b	G ₂₉₈ ^c	E ^d	G _{Sol} ^e
4-7e	-1447.365375	-1447.329308	-1447.439061	-1447.330252	-1447.39734543
TS-1_{4-7e}	-1447.325627	-1447.290548	-1447.396384	-1447.291492	-1447.34114204
IN-4-7e	-1447.433618	-1447.401206	-1447.495928	-1447.402150	-1447.46500117
TS-2_{4-7e}	-1447.422274	-1447.390901	-1447.484143	-1447.391845	-1447.46068623
4-8e	-1447.537567	-1447.506475	-1447.597295	-1447.507419	-1447.57016603
TS-2_{4-7e'}	-1447.424417	-1447.392854	-1447.485024	-1447.393798	-1447.45956518
4-8e'	-1447.541054	-1447.509590	-1447.602361	-1447.510535	-1447.57001507
4-7h	-1254.289172	-1254.258565	-1254.355942	-1254.259509	-1254.28800903
TS-1_{4-7h}	-1254.247490	-1254.217869	-1254.309956	-1254.218813	-1254.24141752
IN-4-7h	-1254.380471	-1254.352562	-1254.439719	-1254.353506	-1254.37803205
TS-2_{4-7h}	-1254.352709	-1254.326015	-1254.410066	-1254.326959	-1254.35756375
4-8h	-1254.468509	-1254.442058	-1254.524947	-1254.443002	-1254.46612864
TS-2_{4-7h'}	-1254.353525	-1254.326896	-1254.409497	-1254.327841	-1254.35719017
4-8h'	-1254.470143	-1254.443661	-1254.526190	-1254.444606	-1254.46600106
IN-4-7e-1	-1447.437869	-1447.405392	-1447.499792	-1447.406337	-1447.46448820
TS-2_{4-7e-1}	-1447.423750	-1447.392393	-1447.483469	-1447.393337	-1447.45787739
TS-2_{4-7e'-1}	-1447.425236	-1447.393828	-1447.484677	-1447.394772	-1447.45813213
4-8e-1	-1447.539281	-1447.508081	-1447.598921	-1447.509025	-1447.56636819
4-8e'-1	-1447.541852	-1447.510608	-1447.601546	-1447.511552	-1447.56749431

Species	E ₀ ^a	H ₂₉₈ ^b	G ₂₉₈ ^c	E ^d	G _{Sol} ^e
4-7g	-1411.446725	-1411.410458	-1411.520813	-1411.411402	-1411.47246507
TS-2_{4-7g}	-1411.487610	-1411.455751	-1411.549598	-1411.456696	-1411.52564579
4-8g	-1411.604476	-1411.572764	-1411.665136	-1411.573708	-1411.63660189
TS-2_{4-7g'}	-1411.489703	-1411.457561	-1411.551098	-1411.458505	-1411.52461829
4-8g'	-1411.607558	-1411.575653	-1411.669046	-1411.576598	-1411.63655990

^a Sum of electronic and zero-point energies

^b Sum of electronic and thermal enthalpies

^c Sum of electronic and thermal free energies

^d Electronic energies

^e Single point energies in solution

4.5. Note

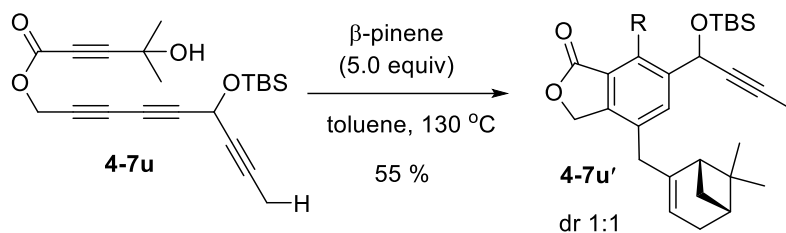
Computational study for this work has been carried out by Yongjia Lin and Prof. Yuanzhi Xia from Wenzhou, University in China.

4.6. References

1. (a) Mehta, G.; Kotha, S. *Tetrahedron* **2001**, *57*, 625. (b) Sadana, A. K.; Saini, R. K.; Billups, W. E. *Chem. Rev.* **2003**, *103*, 1539. (c) Oppolzer, W. A. *Synthesis* **1978**, 793. (b) Charlton, J. L.; Alauddin, M. M. *Tetrahedron* **1987**, *43*, 2873. (d) Nemoto, H.; Fukumoto, K. *Tetrahedron* **1998**, *54*, 5425.
2. (a) Dobish, J. N.; Hamilton, S. K.; Harth, E. *Polym. Chem.* **2012**, *3*, 857. (b) Hayes, C. O.; Chen, P.-h.; Thedford, R. P.; Ellison, C. J.; Dong, G.; Willson, C. G. *Macromolecules* **2016**, *49*, 3706.
3. (a) Graf-Christophe, S.; Kuehm-Caubère, C.; Renard, P.; Pfeiffer, B.; Pierré, A.; Léonce, S.; Caubère, P. *Bioorg. Med. Chem. Lett.* **2000**, *10*, 2589. (b) Yu, D.-Y.; Matsuya, Y.; Zhao, Q.-L.; Ahmed, K.; Wei, Z.-L.; Hori, T.; Nemoto, H.; Kondo, T. *Apoptosis* **2008**, *13*, 448. (c) Tsotinis, A.; Afroudakis, P. A.; Garratt, P. J.; Bocianowska-Zbrog, A.; Sugden, D. *ChemMedChem* **2014**,

- 9, 2238. (d) Zhang, C.; Li, F.; Yu, Y.; Huang, A.; He, P.; Lei, M.; Wang, J.; Huang, L.; Liu, Z.; Liu, J.; Wei, Y. *J. Med. Chem.* **2017**, *60*, 3618.
4. (a) Xu, T.; Ko, H. M.; Savage, N. A.; Dong, G. *J. Am. Chem. Soc.* **2012**, *134*, 20005. (b) Xia, Y.; Liu, Z.; Liu, Z.; Ge, R.; Ye, F.; Hossain, M.; Zhang, Y.; Wang, J. *J. Am. Chem. Soc.* **2014**, *136*, 3013. (c) Chen, P.-h.; Xu, T.; Dong, G. *Angew. Chem., Int. Ed.* **2014**, *53*, 1674. (d) Xu, T.; Savage, N. A.; Dong, G. *Angew. Chem., Int. Ed.* **2014**, *53*, 1891. (e) Xu, T.; Dong, G. *Angew. Chem., Int. Ed.* **2014**, *53*, 10733. (f) Yu, J.; Yan, H.; Zhu, C. *Angew. Chem., Int. Ed.* **2016**, *55*, 1143. (g) Juliá-Hernandez, F.; Ziadi, A.; Nishimura, A.; Martin, R. *Angew. Chem., Int. Ed.* **2015**, *54*, 9537. (h) Deng, L.; Xu, T.; Li, H.; Dong, G. *J. Am. Chem. Soc.* **2016**, *138*, 369. (i) Bender, M.; Turnbull, B. W. H.; Ambler, B. R.; Krische, M. J. *Science* **2017**, *357*, 779.
5. Vollhardt, K. P. C. *Angew. Chem., Int. Ed.* **1984**, *23*, 539.
6. (a) Hosoya, T.; Kuriyama, Y.; Suzuki, K. *Synlett* **1995**, *1995*, 177. (b) Hosoya, T.; Hamura, T.; Kuriyama, Y.; Miyamoto, M.; Matsumoto, T.; Suzuki, K. *Synlett* **2000**, 520. (c) Maurin, P.; IbrahimOuali, M.; Santelli, M. *Tetrahedron Lett.* **2001**, *42*, 8147. (d) Hamura, T.; Hosoya, T.; Yamaguchi, H.; Kuriyama, Y.; Tanabe, M.; Miyamoto, M.; Yasui, Y.; Matsumoto, T.; Suzuki, K. *Helv. Chim. Acta* **2002**, *85*, 3589. (e) Hamura, T.; Ibusuki, Y.; Sato, K.; Matsumoto, T.; Osamura, Y.; Suzuki, K. *Org. Lett.* **2003**, *5*, 3551. (f) Bronner, S. M.; Bahnck, K. B.; Garg, N. K. *Org. Lett.* **2009**, *11*, 1007. (g) Chen, P. H.; Savage, N. A.; Dong, G. *Tetrahedron* **2014**, *70*, 4135. (h) Kasamatsu, K.; Yoshimura, T.; Mandi, A.; Taniguchi, T.; Monde, K.; Furuta, T.; Kawabata, T. *Org. Lett.* **2017**, *19*, 352.
7. Yedulla, V. R.; Pradhan, P.; Yang, L.; Lakshman, M. K. *Eur. J. Org. Chem.* **2015**, *4*, 750.
8. (a) Hedaya, E.; Kent, M. E. *J. Am. Chem. Soc.* **1970**, *92*, 2149. (b) Spangler, R. J.; Kim, J. H. *Tetrahedron Lett.* **1972**, *13*, 1249. (c) Mamer, O. A.; Lossing, F. P.; Hedaya, E.; Kent, M. E. *Can. J. Chem.* **1970**, *48*, 3606.

9. Iwao, M. *J. Org. Chem.* **1990**, *55*, 3622.
10. Dhawan, K. L.; Gowland, B. D.; Durst, T. *J. Org. Chem.* **1980**, *45*, 922.
11. Aidhen, I. S.; Ahuja, J. R. *Tetrahedron Lett.* **1992**, *33*, 5431.
12. Chaumontet, M.; Piccardi, R.; Audic, N.; Hitce, J.; Peglion, J.-L.; Clot, E.; Baudoin, O. *J. Am. Chem. Soc.* **2008**, *130*, 15157.
13. (a) Álvarez-Bercedo, P.; Flores-Gaspar, A.; Correa, A.; Martin, R. *J. Am. Chem. Soc.* **2010**, *132*, 466. (b) Flores-Gaspar, A.; Gutierrez-Bonet, Á.; Martin, R. *Org. Lett.* **2012**, *14*, 5234.
14. (a) Yoshioka, M.; Arai, M.; Nishizawa, K.; Hasegawa, T. *J. Chem. Soc., Chem. Commun.* **1990**, 374. (b) Yoshioka, M.; Momose, S.; Nishizawa, K.; Hasegawa, T. *J. Chem. Soc., Perkin Trans. 1* **1992**, 499.
15. Yano, T.; Kawasaki, T.; Yuhki, T.; Ishida, N.; Murakami, M. *Org. Lett.* **2018**, *20*, 1224.
16. (a) Candito, D. A.; Panteleev, J.; Lautens, M. *J. Am. Chem. Soc.* **2011**, *133*, 14200. (b) Candito, D. A.; Dobrovolsky, D.; Lautens, M. *J. Am. Chem. Soc.* **2012**, *134*, 15572. (c) Karmakar, R.; Mamidipalli, P.; Yun, S. Y.; Lee, D. *Org. Lett.* **2013**, *15*, 1938.
17. (a) Ghosh, S. K.; Sarkar, T. K. *Tetrahedron Lett.* **1986**, *27*, 525. (b) Narasaka, K.; Hayashi, Y.; Shimada, S. *Chem. Lett.* **1988**, *17*, 1609. A general review on gem-dimethyl effect: (c) M. E. Jung and G. Piizzi, *Chem. Rev.* **2005**, *105*, 1735.
18. Mikami, K.; Shimizu, M. *Chem. Rev.* **1992**, *92*, 1021.
19. In presence of 5.0 equiv. of β -pinene **4-7u** formed **4-7u'** by an intermolecular Alder-ene reaction in 55% yield as a 1:1 mixture of diastereomers. This result clearly shows that the formation of arylene intermediate from this substrate is not a problem.



20. The secondary product **4-7i'** is assumed to be generated from **4-7i** via a thermal benzylic alkoxy exchange reaction.

21. Karmakar, R.; Yun, S. Y.; Chen, J.; Xia, Y.; Lee, D. *Angew. Chem., Int. Ed.* **2015**, *54*, 6582.

22. Bieber, L. W.; da Silva, M. F. *Tetrahedron Lett.* **2007**, *48*, 7088.

23. Dauben, W. G.; Mincho, D. *J. Org. Chem.* **1977**, *42*, 682.

24. Fotiadou, A. D.; Zografos, A. F. *Org. Lett.* **2012**, *14*, 5664.

25. Ho, G.-J.; Marthe, D. J. *J. Org. Chem.* **1995**, *60*, 2271.

26. Wang, T.; Hoye, T. R. *J. Am. Chem. Soc.* **2016**, *138*, 13870.

27. Hoye, T. R.; Baire, B.; Niu, D.; Willoughby, D. P. H.; Woods, B. P. *Nature* **2012**, *490*, 208.

CHAPTER 5

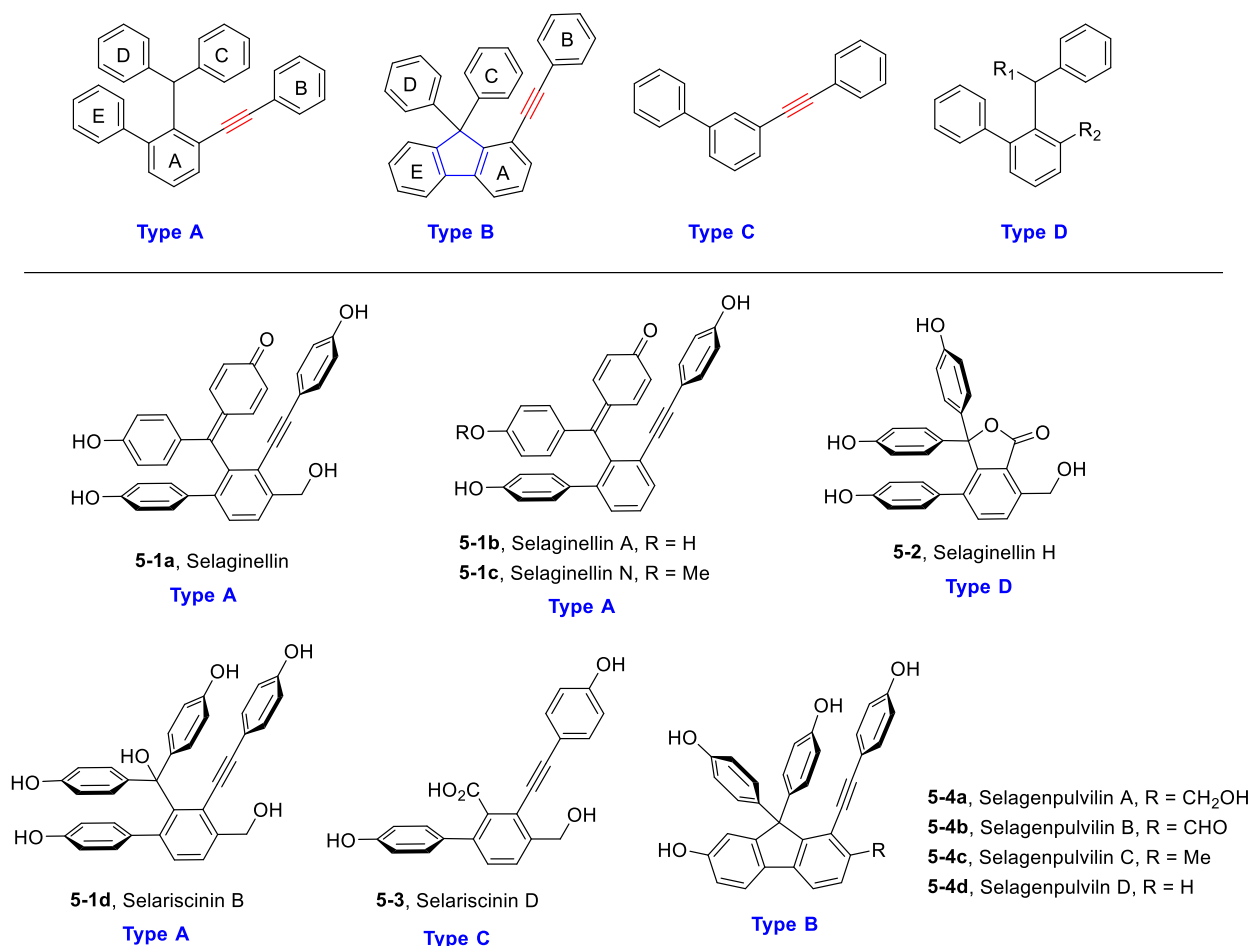
Diversity-Oriented Synthesis of Bioactive Natural Products of the *Selaginella* Family

5.1. Introduction

The versatile reactivity of arynes have find many applications in total synthesis of various natural products over last two decades.¹ The Kobayashi method is a mild and efficient protocol for aryne generation although it has low atom-economy, and the synthesis of complex aromatic architectures by this method is often problematic due to difficulty in the preparation of the corresponding precursors.² On the other hand, the hexadehydro Diels-Alder (HDDA) reaction is a highly atom economic, reagent free approach and can lead to complex aromatic skeletons relatively easily from simple multiyne precursors.³ Since its resurgence, the HDDA reaction has found its applications in the total synthesis of various natural products.⁴ Alkynyl polyphenolic natural products isolated from plants of the genus *Selaginella* including selaginellins and selaginpulvilins have unique aromatic architectures and wide biological activities.⁵ Recently, the Lee group utilized the HDDA reaction to construct the fluorene core of selaginpulvillin C and D and achieved the first total synthesis.⁶ In this chapter a new approach for diversity-oriented synthesis of different natural products of the *Selaginella* genus involving the HDDA reaction is described.

5.1.1. Alkynyl phenol natural products from the genus *Selaginella*

In the last decade, novel natural pigments containing a series of unusual alkynyl phenols were isolated from the genus *Selaginella*, mainly *S. tamariscina* and *S. pulvinata*. These two species were used in traditional Chinese medicine for treatment of dysmenorrhea, abdominal mass, and traumatic injury.⁷ Pharmacological investigations of the genus *Selaginella* revealed its anticancer, antiviral, antioxidant, and anti-inflammatory activities.⁸ To date about 61 naturally occurring selaginellins have been reported. Based on their structural features and the nature of the biosynthetic pathways, the naturally occurring selaginellins can be classified into four groups (**Scheme 5.1**). Types A and B have relatively complex frameworks and comprise a large proportion of selaginellins, while types C and D are considered as the smaller precursors in the biosynthetic route to Type A. Type A selaginellins possesses a 2-benzhydryl-3-phenylethynyl-1,10-biphenyl skeleton featuring a *p*-quinone methide and alkynyl phenol functionalities.⁹ This class undergoes phenol-quinone tautomerism thereby making their structural determination challenging.

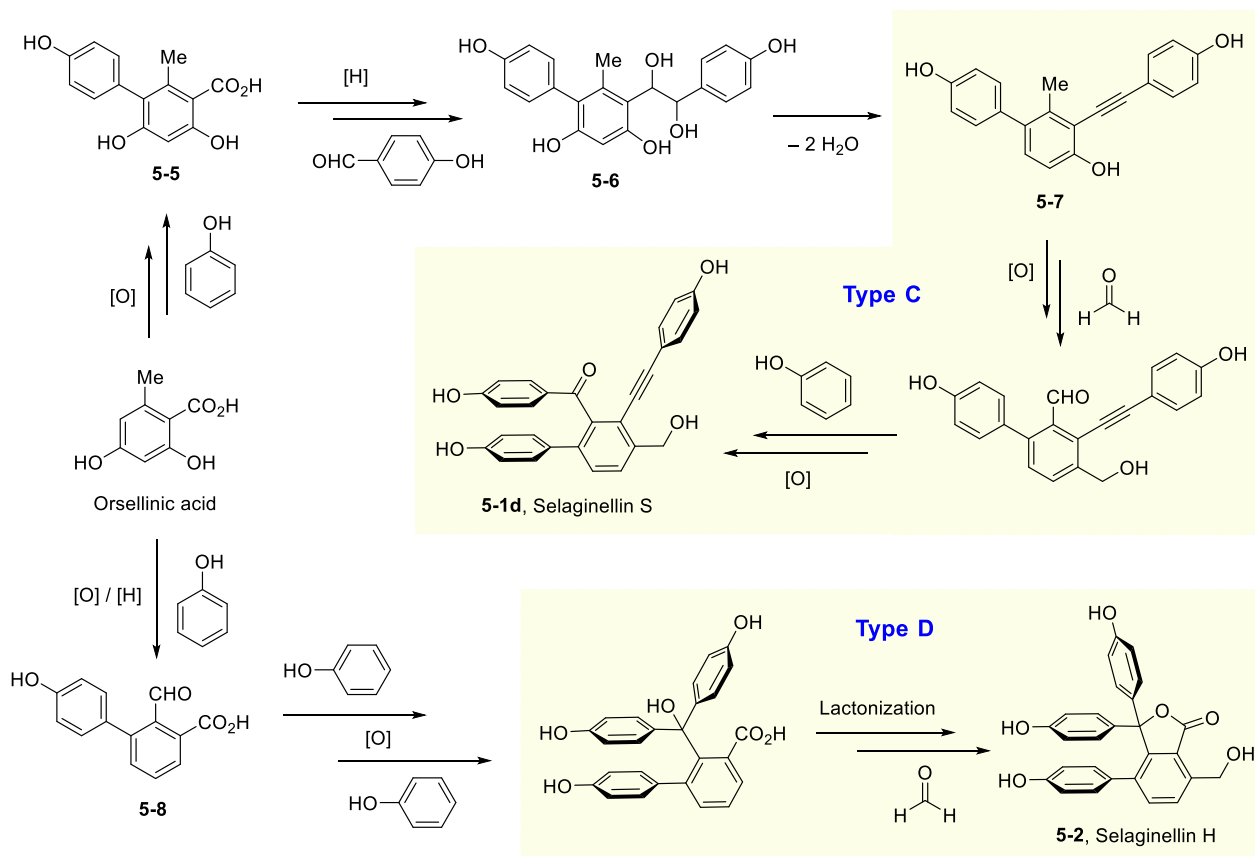


Scheme 5.1. Different classes of natural products from the genus *Selaginella*

The natural products belonging to this category involves selaginellin, selaginellin A–J, M–R and T–X,¹⁰ selariscinin A–C,¹¹ diselaginellin A, B¹² and selariscin A, B.¹³ Type B involves compounds with a 9,9-diphenyl-1-(phenylethynyl)- 9*H*-fluorene skeleton. The natural products in this category includes selagenpulvilin A–T.¹⁴ Type C selaginellins are considered to be the intermediates in the biosynthetic pathway leading to the skeleton of Type A with a trimmed C and/or D ring skeleton. The natural products belonging to this category includes selaginellin K, L, Y, Z, S and selariscinin D.¹⁵ Type D on the other hand contains selaginellins, which are smaller size precursors of Type A devoid of the alkynyl phenol moiety. The natural products belonging to this category includes selaginellin H and selaphenin C.¹⁶

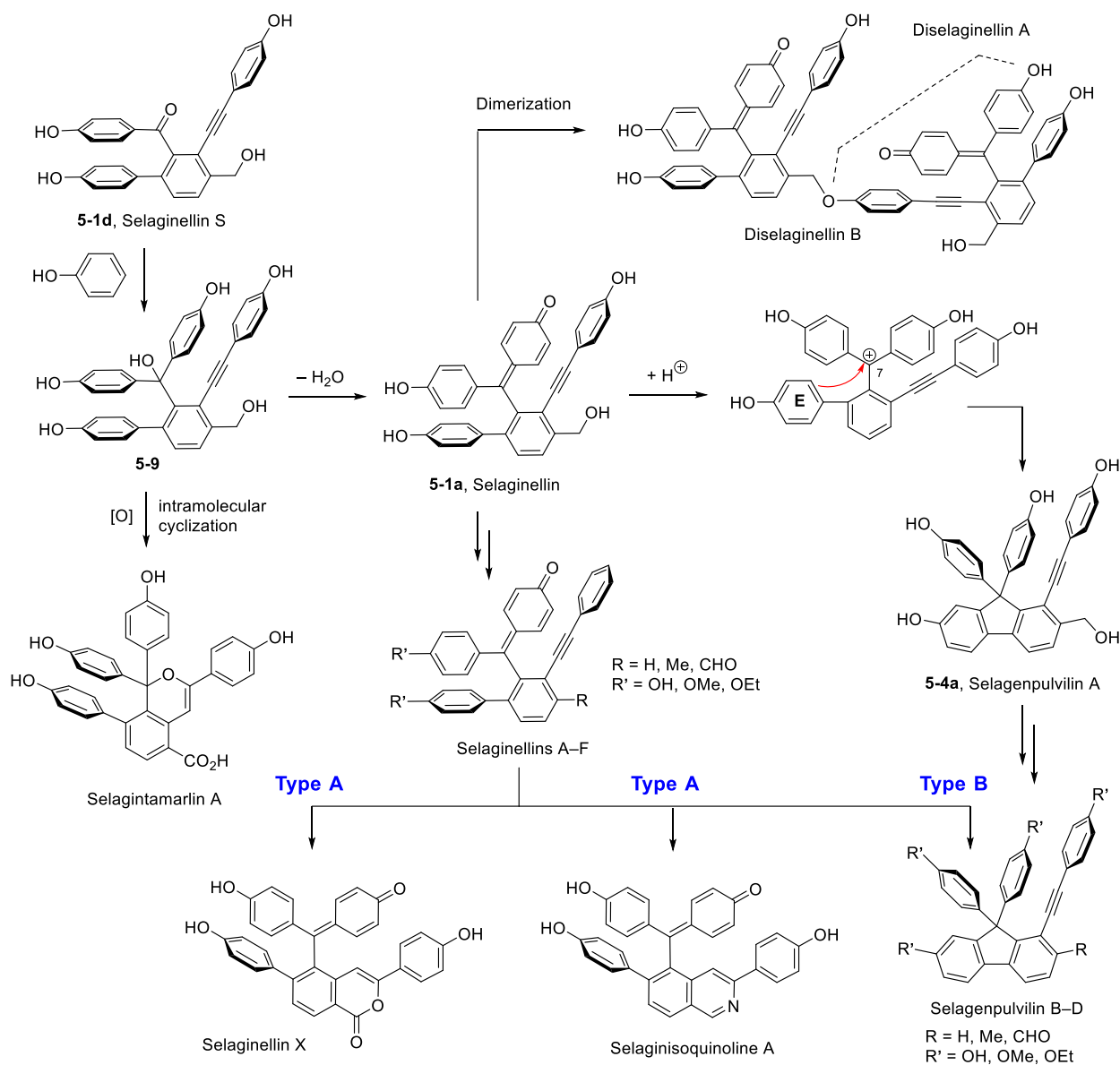
5.1.2. Biosynthesis and biological activity

The biogenesis of the different classes of selaginellins¹⁷ commences from orsellinic acid, which is in turn formed from the condensation of three molecules of malonyl-CoA and a molecule of acetyl-CoA.¹⁸ It is proposed that orsellinic acid is oxidized to a radical cation and then coupled with a 2,5-cyclohexadienone anion to generate a key intermediate **5-5** (Scheme 5.2). The carboxylic acid moiety in **5-5** is reduced to the corresponding formyl group followed by benzoin condensation with *p*-hydroxy benzaldehyde to afford a vicinal diol intermediate **5-6**. This diol intermediate undergoes dehydration to form **5-7** followed by a series of oxidative modifications to produce various selaginellins of Type C. In another pathway, the intermediate **5-5** undergoes a series of modifications especially free radical couplings via the intermediacy of **5-8** to form selaginellins of Type D.



Scheme 5.2. Biosynthetic routes to Type C and D selaginellins

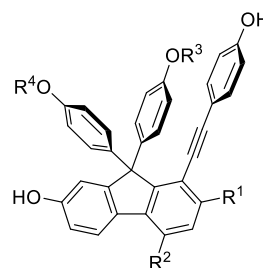
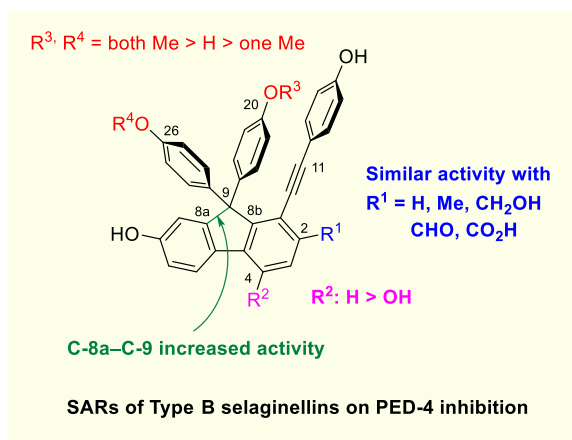
The biogenesis of Type A selaginellins commences from the precursor, selaginellin S (**5-1d**), which couples with phenol to form a tertiary alcohol intermediate **5-9** (Scheme 5.3). This intermediate undergoes oxidation and cyclization to generate selagintamarlin A, and dehydration to generate selaginellin **5-1a**, which is a key intermediate leading to different natural products of Type A and B. Dimerization of **5-1a** via the benzylic hydroxyl group with two different phenolic moieties generates diselaginellin A and B, while acid-catalyzed Friedel-Crafts alkylation at C-8a and C-9 produces a fluorene core-containing Type B



Scheme 5.3. Biosynthetic routes to Type A and B selaginellins

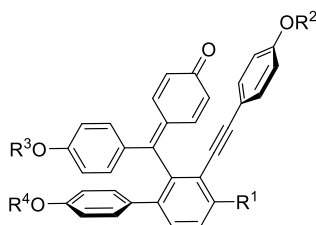
selaginpulvilin A **5-4a**.^{14a} Selaginellin **5-1a** also can generate selaginellins A–F, from which other Type A and Type B selaginellins including selaginellin X, selaginisquinolin A, and selaginpulvilin B–D can be generated through a series of redox reactions, alkylations and intramolecular cyclizations.

A wide structural variety of the *selaginella* genus show diverse pharmacological effects such as promoting blood circulation, pain relief and inducing diuresis to reduce edema, and thus attracted considerable interests from medicinal chemists over the last decades. The biological activities of these alkynyl phenol compounds have been demonstrated to bring hypoglycemic,^{14a} anti-inflammatory,^{14a} antioxidant,^{19b} cardiovascular protection,^{19c} anticancer,^{19d,e} and neuroprotective effects.^{19f} Different members of the selaginellin family have been reported to show remarkable inhibitory activity against phosphodiesterase-4 (PDE-4) (**Scheme 5.4**). Phosphodiesterases are a family of enzymes that catalyze the

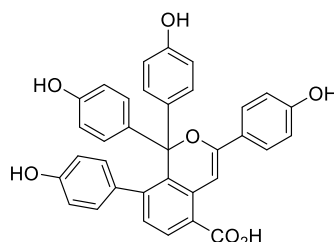


Selaginpulvilin A, $R^1 = \text{CH}_2\text{OH}$, $R^2 = R^3 = R^4 = \text{H}$, $\text{IC}_{50} = 0.24 \mu\text{M}$
 Selaginpulvilin B, $R^1 = \text{CHO}$, $R^2 = R^3 = R^4 = \text{H}$, $\text{IC}_{50} = 0.11 \mu\text{M}$
 Selaginpulvilin C, $R^1 = \text{Me}$, $R^2 = R^3 = R^4 = \text{H}$, $\text{IC}_{50} = 0.18 \mu\text{M}$
 Selaginpulvilin G, $R^1 = \text{CH}_2\text{OH}$, $R^2 = \text{OH}$, $R^3 = R^4 = \text{H}$, $\text{IC}_{50} = 0.41 \mu\text{M}$
 Selaginpulvilin K, $R^1 = \text{CH}_2\text{OH}$, $R^2 = \text{H}$, $R^3 = R^4 = \text{Me}$, $\text{IC}_{50} = 0.011 \mu\text{M}$
 Selaginpulvilin S, $R^1 = \text{CH}_2\text{OH}$, $R^2 = R^3 = \text{H}$, $R^4 = \text{Me}$, $\text{IC}_{50} = 32.1 \mu\text{M}$

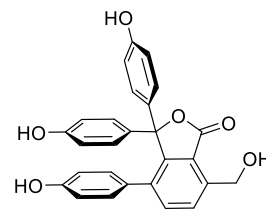
Positive Control: Rolipram $\text{IC}_{50} = 0.54 \mu\text{M}$



Selaginellin, $R^1 = \text{CH}_2\text{OH}$, $R^2 = R^3 = R^4 = \text{H}$, $\text{IC}_{50} = 0.97 \mu\text{M}$
 Selaginellin A, $R^1 = \text{H}$, $R^2 = R^3 = R^4 = \text{H}$, $\text{IC}_{50} = 1.42 \mu\text{M}$
 Selaginellin B, $R^1 = \text{Me}$, $R^2 = R^3 = R^4 = \text{H}$, $\text{IC}_{50} = 1.68 \mu\text{M}$
 Selaginellin N, $R^1 = \text{H}$, $R^2 = \text{H}$, $R^3 = \text{Me}$, $R^4 = \text{H}$, $\text{IC}_{50} = 0.22 \mu\text{M}$



Selagintamarlin A, $\text{IC}_{50} = 0.04 \mu\text{M}$



Selaginellin H, $\text{IC}_{50} = 5.13 \mu\text{M}$

Scheme 5.4. PDE-4 inhibitory activities of selaginellins and selaginpulvilins

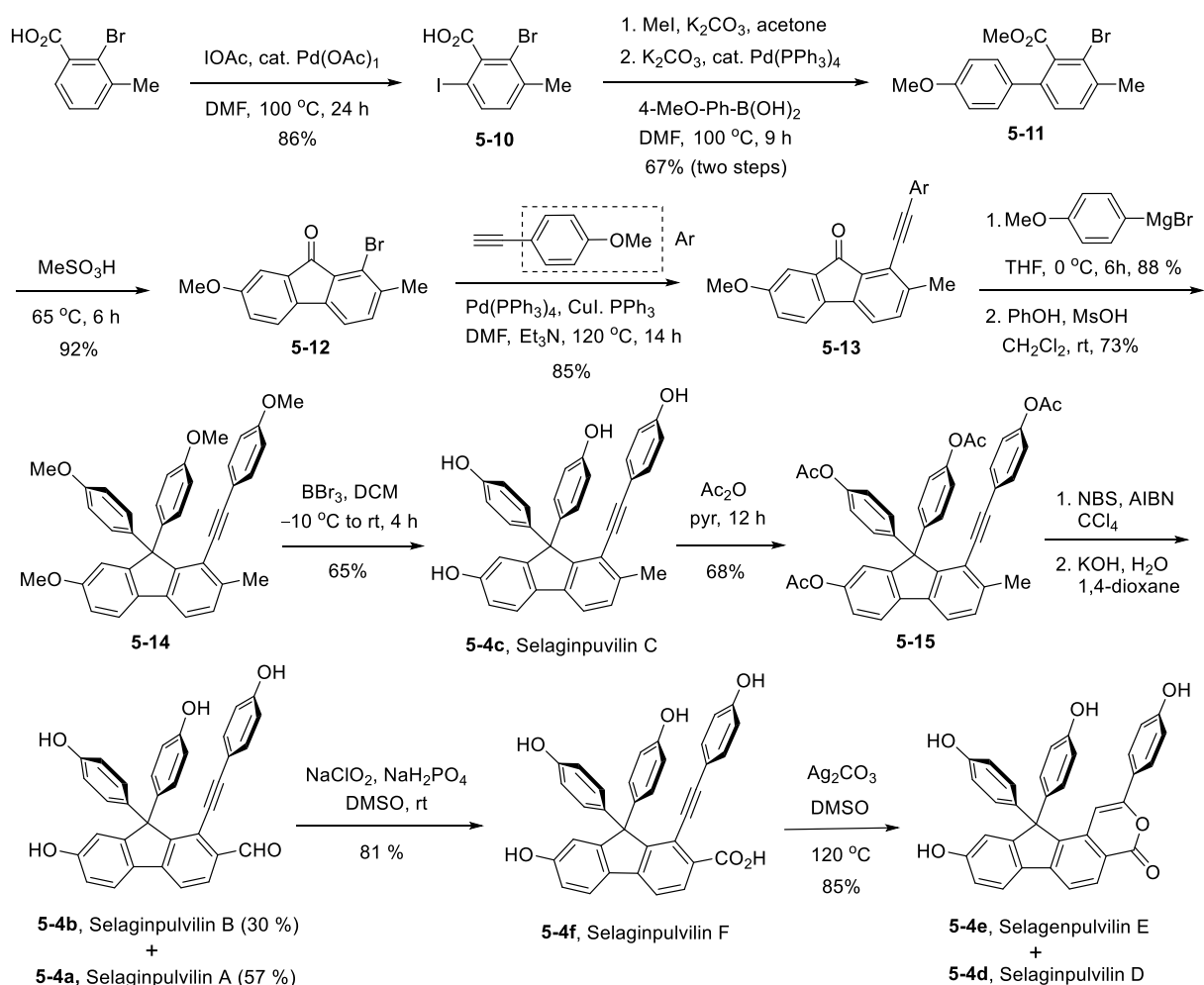
hydrolysis of the second messengers such as cyclic adenosine monophosphate (cAMP) and guanosine monophosphate (cGMP), and thus are a promising therapeutic target of high interest for inflammatory, and respiratory diseases.²⁰ Although several PDE-4 inhibitors are known over the decades roflumilast is the sole inhibitor recently approved for the treatment of chronic obstructive pulmonary disease (COPD).²¹ In recent years, the groups of Yin, Wang, and Sun have extensively studied the PDE-4 inhibition of various selaginellins. Structure-activity relationships of selaginellins shows that the presence of a fluorene core as in type B selaginellins enhances the inhibitory activity to a great extent. Changing the nature of substituent R¹ at C-2 does not significantly changes the inhibition activity. The presence of an OH group at C-4 position reduces the inhibition activity. The methylation of both hydroxy groups at C-20 and C-26 increases the inhibition activity to a great extent while methylation of a single OH at these position decreases the activity. Thus, among the Type B selaginellins, selaginpulvin K shows the highest inhibitory activity with 50-fold stronger than the positive control Rolipram making it the most active natural PDE-4 inhibitors discovered to date (IC₅₀ = 0.011 μ M). Type A selaginellins also show decent PDE-4 inhibitory activity with IC₅₀ values ranging from 0.04–13.7 mM with highest activity for selagintamarlin A. Selaginellins have been reported to show cytotoxic activity against U251, HeLa, MCF-7 and BCG-823 tumor cell lines.^{17a,19d} The Wang group demonstrated decent antimicrobial activities of selaginellins against *S. aureus* and *C. albicans*.^{12d,16a} In 2015, The Woo group demonstrated the inhibitory activity of selaginellins against protein tyrosine phosphatase 1B (PTP1B), which can be a potential target for the treatment of type 2 diabetes.¹¹

5.1.3. Previous syntheses

The isolation of a variety of alkynyl phenol natural products from the *selaginella* genus and their diverse biological activities have attracted attention from many synthetic chemists to pursue a total synthesis. Synthetic attempts were mostly made for Type B selaginellins or the selaginpulvillins while attempts to synthesize the other classes of selaginellins are rare. There are two main strategies reported to construct the fluorene core of selaginpulvillins so far. The first strategy is based on coupling of two arene building blocks to construct a biphenyl carboxylic acid followed by intramolecular Friedel-Crafts acylation.

The second strategy relies on a hexa- or tetrahydro Diels-Alder reaction to directly install the fluorenone core onto which the *gem*-diphenol substituents are installed through Friedel-Crafts arylation.

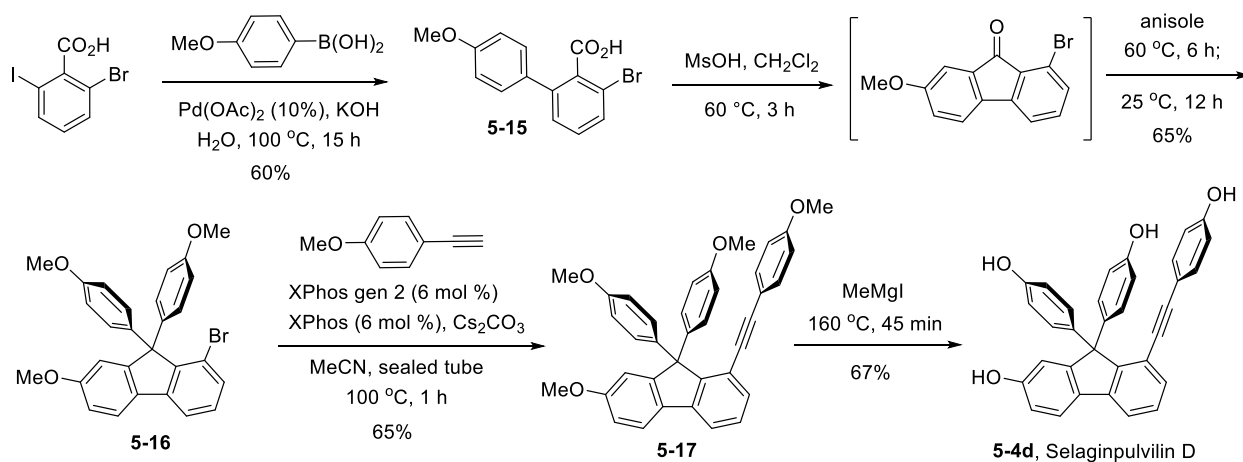
Yin's synthesis of selaginpulvillin A-F: After successful isolation of a variety of selaginpulvillins, Yin's group resorted to the total synthesis of selaginpulvillin A–F to establish the structural identity of this newly discovered class of compounds (**Scheme 5.5**).^{14b} The synthesis commenced with the iodination of 2-bromo-3-methylbenzoic acid through Pd^{II}-catalyzed C–H functionalization using IOAc (generated in-situ from PhI(OAc)₂ and I₂) to form **5-10**. Forming methyl ester of **5-10** followed by a Suzuki coupling with 4-methoxyphenyl boronic acid provided biphenyl carboxylate **5-11**, which was treated with methanesulfonic



Scheme 5.5. Yin's total synthesis of Selaginpulvillin A–F

acid (MsOH) to promote an intramolecular Friedel-Crafts acylation to generate fluorenone **5-12**. Sonogashira coupling of **5-12** with 4-ethynyl anisole was carried out first to obtain 4-methoxyphenyl alkyne-containing fluorenone **5-13**. It was found that if the diaryl substituents were installed first at C-9, the subsequent Sonogashira coupling became inefficient due to the steric hindrance imposed by the diaryl moiety. Treating compound **5-13** with 4-methoxyphenylmagnesium bromide followed by Friedel-Crafts arylation with anisole afforded 9,9-diaryl fluorene **5-14**. Finally, four-fold demethylation of **5-14** with BBr₃ led to completion of synthesis of selaginpulvin C (**5-4c**) in 65% yield. For the synthesis of other selaginpulvins, selaginpulvin C (**5-4c**) was converted to the corresponding tetra-acetate **5-15**, which served as a common precursor. Compound **5-15** was subjected to a benzylic bromination (NBS, AIBN, CCl₄) followed by removal of acetates (KOH, 1,4-dioxane/H₂O) to provide a mixture of selaginpulvin A (**5-4a**) and selaginpulvin B (**5-4b**). Oxidation of the formyl group (NaClO₂, NaH₂PO₄, DMSO, rt) in selaginpulvin B (**5-4b**) gave selaginpulvin F (**5-4f**), decarboxylation of which (conc. HCl) afforded selaginpulvin D (**5-4d**). On the other hand, cyclization of the carboxylic acid onto the alkynyl moiety in selaginpulvin F (Ag₂CO₃, DMSO, 120 °C) generated selaginpulvin E (**5-4e**).

Sherburn's four-step synthesis of selaginpulvin D: Sherburn and a co-worker developed a synthetic approach to construct the fluorenone core of selaginpulvin by intramolecular Friedel-Crafts arylation of biphenyl carboxylic acid derivative (**Scheme 5.6**).²² The merit of this synthetic approach includes only 4-step operations starting from readily available building blocks. The synthesis commenced with a Suzuki-Miyaura coupling between 2-bromo-6-iodobenzoic acid with 4-methoxyphenylboronic acid in an aqueous medium to generate disubstituted 2-phenylbenzoic acid **5-15**. Using bromiodoarene was necessary to give a selective single cross-coupling product since the corresponding diiodide gave a 2-fold coupling product. In the next step, a consecutive intramolecular Friedel-Crafts acylation followed by double arylation generated 9,9-diarylfluorene **5-16** in 65% yield. This one-pot reaction was achieved by warming up the crude product of **5-15** with MsOH and subsequently adding anisole to the reaction mixture. The Sonogashira coupling with **5-16** to install 1-arylethynyl functionality with a sterically congested bromide

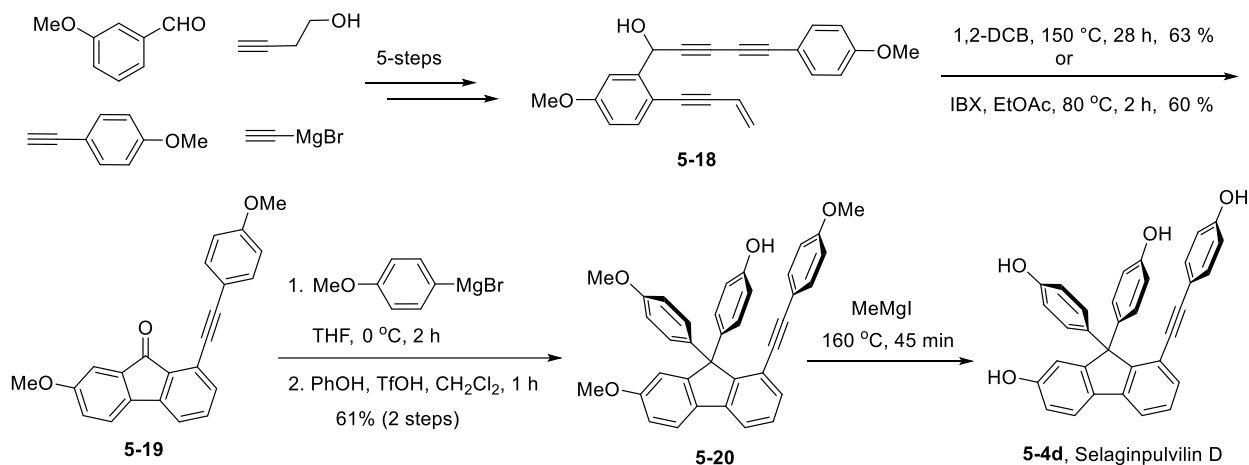


Scheme 5.6. Sherburn's four step synthesis of selaginpulvilin D

was challenging. Among catalyst examined, only Buchwald's second-generation Xphos precatalyst²³ with high concentration of the alkyne provided the desired product **5-17**, and with low concentration an intramolecular Mizoroki-Heck by-product was accompanied.²⁴ Finally, the global demethylation of **28** (MeMgI , neat, 160°C) provided selaginpulvilin D (**5-4d**).²⁵ For this demethylation, other conventional reagents (BBr_3 , RSH/AlCl_3) were ineffective or afforded a mixture of by-products of the alkyne participation. Even though this synthetic route involves only 4-step operations and high overall yield (17.1 %) it lacks flexibility to generate other derivatives of selaginpulvilins.

Baire's synthesis of selaginpulvilins: Baire and co-workers adopted the enyne-alkyne tetradehydro Diels-Alder (TDDA) reaction²⁶ as a key-step to construct the fluorene skeleton of selaginpulvilins. The synthesis of the enyne-triynes precursor **5-18** can be prepared in 5-steps from commercially available starting materials (**Scheme 5.7**).²⁷ Heating enyne-triynes **5-18** in *o*-dichlorobenzene at 150°C afforded fluorenone **5-19** in 63% yield via in situ autooxidation. To improve the efficiency of the TDDA reaction, the alcohol **5-18** was subjected to in situ oxidation (IBX , EtOAc , 80°C , 2 h), which provided fluorenone **5-19** in 60% yield. The synthesis was completed by treating fluorenone **5-19** with *p*-anisylmagnesium bromide to generate the corresponding tertiary alcohol, which was further treated with phenol and catalytic TfOH to

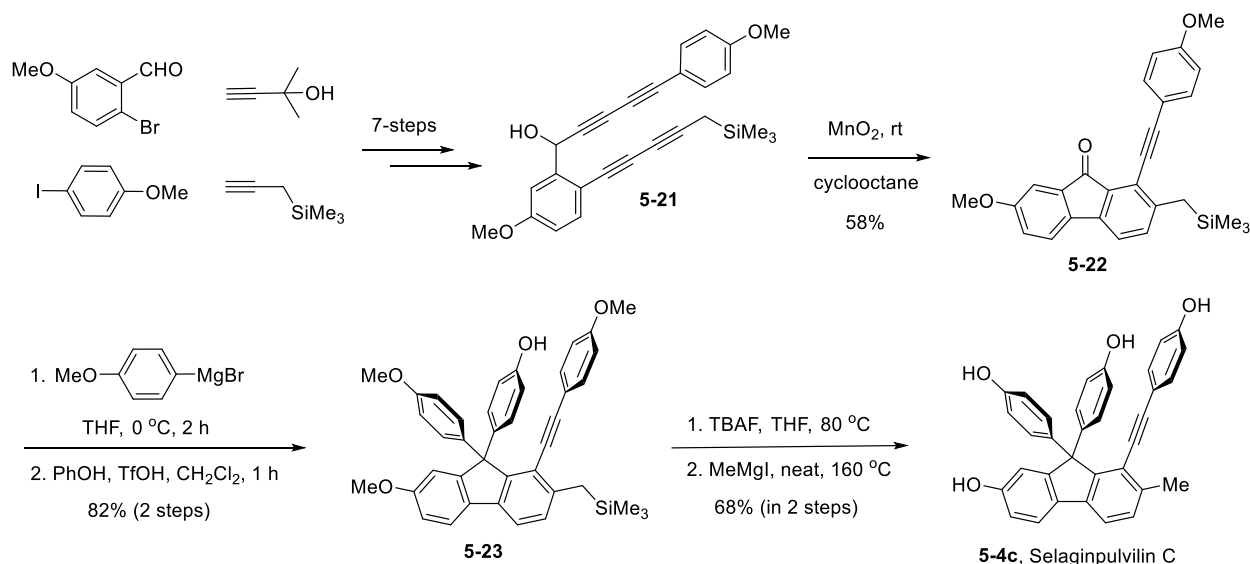
provide a penultimate intermediate **5-20** in 61% yield. Finally, global demethylations of **5-20** under previously reported conditions²⁵ led to selaginpulvin D. Baire's synthesis relying on an enyne-alkyne tetrahydro Diels-Alder (TDDA) reaction as a key strategy led to a formal total synthesis of selaginpulvin D in 10.5% overall yield via 9 linear steps from *m*-anisaldehyde. Baire's group also achieved the synthesis of selaginpulvin A and C by using the same strategy.²⁷



Scheme 5.7. Baire's synthesis of selaginpulvin D (TDDA approach)

Lee's synthesis of selaginpulvinols: Lee and coworker reported the first total synthesis of selaginpulvin C and D by adopting a tetrayne hexadehydro Diels-Alder (HDDA) reaction as a key step to construct the fluorene skeleton (**Scheme 5.8**).⁶ For synthesis of selaginpulvin C, tetrayne **5-21** was synthesized in 7-steps from commercially available starting materials. For synthesis of selaginpulvin D an analogous tetrayne with a trimethylsilyl substituent on the alkyne was employed. The tetrayne **5-21** was subjected to oxidation condition with MnO₂. Upon oxidation of the 2° allylic alcohol to the ketone, spontaneously HDDA cyclization occurred to generate an aryne intermediate, which underwent hydrogenation in presence of cyclooctane (H-donor) to generate fluorenone **5-22** as the single isomer.²⁸ Treating fluorenone **5-22** with *p*-methoxyphenylmagnesium bromide followed by Friedel-Crafts arylation using PhOH in presence of BF₃•OEt₂ provided diarylfluorene **5-23** in 82% yield over two steps. Removal

of the trimethylsilyl group and global demethylation with MeMgI in neat conditions afforded selaginpulvilin C (**5-4c**) in 68% yield over two steps.

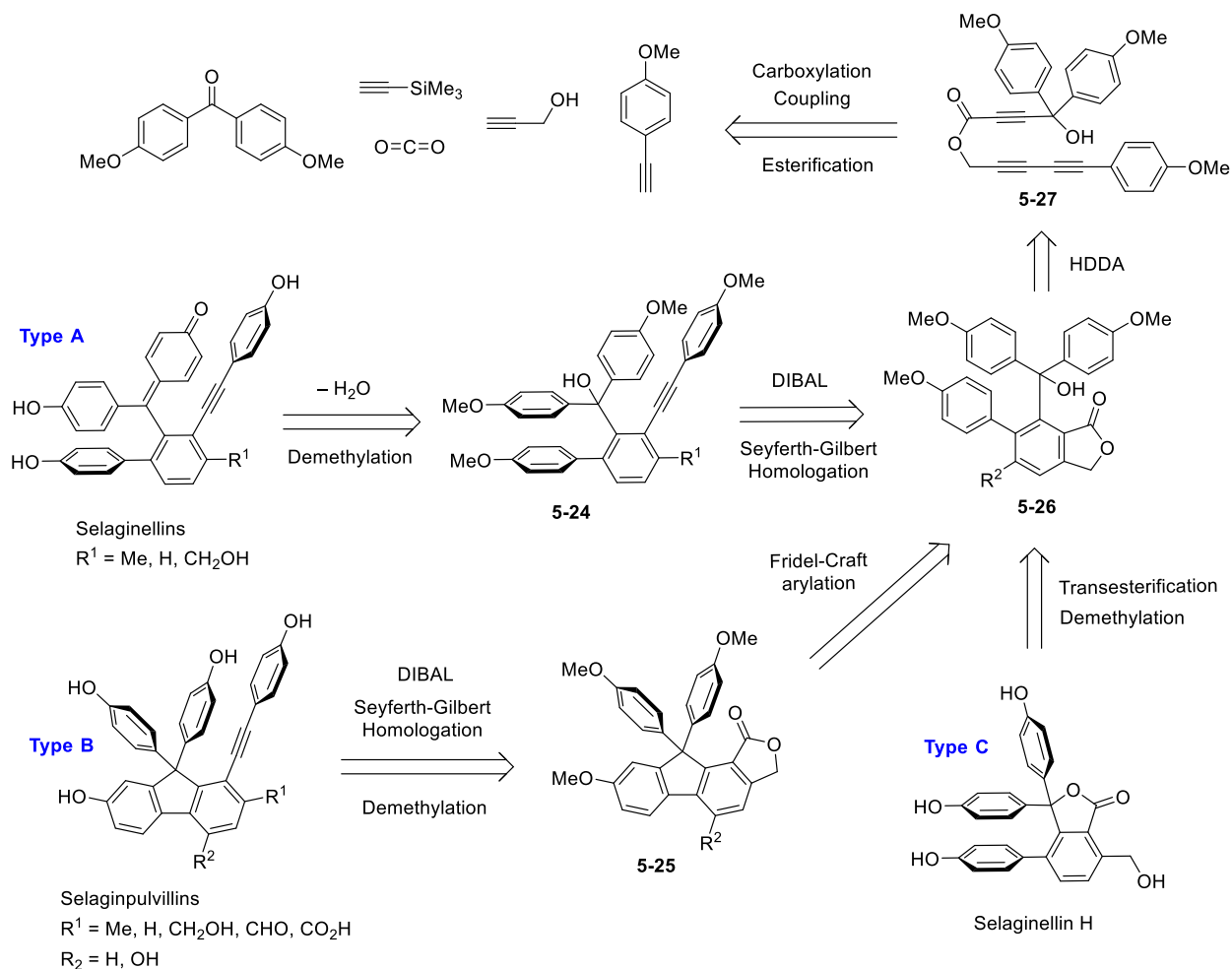


Scheme 5.8. Lee's synthesis of selaginpulvilin C (HDDA approach)

5.2. Diversity-Oriented Approach to Various Natural Products of the *Selaginella* Family

The previous synthetic attempts are mostly restricted for the synthesis of Type B selaginellins, the selaginpulvillins. Two general approaches for synthesis of the fluorene core involves intramolecular Friedel-Craft acylation and cycloaddition (HDDA or TDDA) strategies. Even though the Friedel-Crafts acylation approach has a merit of a shorter overall sequence to a specific target it has limited flexibility for synthesis of other related targets and analogs in comparison to cycloaddition-based approach which can bring flexibility in the fluorene skeleton.²⁹ Considering the significant biological activities of the other types of selaginellins, we resorted to a unified diversity-oriented approach to get access to different classes of selaginellins employing a common intermediate **5-26** (Scheme 5.9). This approach is inspired by the biosynthetic route, in which the fluorene **5-25** core of the selaginpulvilins (Type B) can be constructed by intramolecular Friedel-Craft arylation followed by various homologation, oxidation and reduction

sequences. Also, the same intermediate **5-26** can be converted to selaginellin H (Type C) via transesterification and deprotection and to Type A selaginellins as well via various functional group transformations including Seyferth-Gilbert homologation to introduce the alkyne moiety. The intermediate **5-26** in turn is envisioned to be accessed from the triyne **5-27** through HDDA reaction and the identity of



Scheme 5.9. Diversity-oriented approach to various natural products of the *Selaginella* family

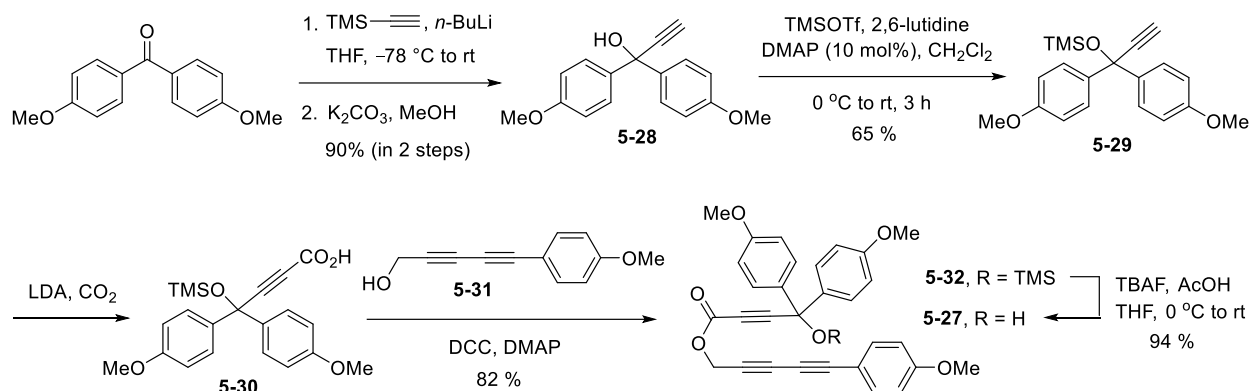
R₂ can also be determined by the trapping agents that react with the aryne intermediate such as MeOH or cyclooctane. The propiolate-tethered triyne **5-27** can be accessed from commercially available building blocks 4,4'-dimethoxybenzophenone, propargyl alcohol, 4-ethynylanisole, trimethylsilyl acetylene, and

carbon dioxide. Thus, this HDDA-based strategy would be flexible to readily get access to different members of selaginellins and selaginpuvilines and their congeners.

5.3. Results and Discussions

5.3.1. Total synthesis of selaginellin H

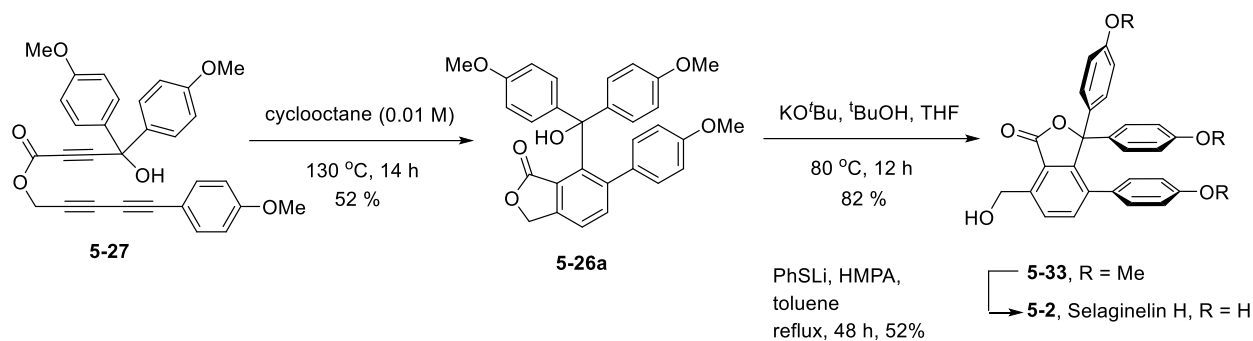
Following the envisioned diversity-oriented approach, we commenced the synthesis of selaginellin H, a Type C selaginellin, from commercially available 4,4'-dimethoxybenzophenone (**Scheme 5.10**). The benzophenone was subjected to nucleophilic addition with lithiated trimethylsilyl acetylene followed by removal of the TMS group with K_2CO_3 in MeOH to generate the tertiary propargylic alcohol **5-28**. An initial attempt to convert **5-28** directly to the corresponding alkynyl carboxylic acid failed as the carboxylic acid readily decomposition during concentration possibly because of the presence of the acid sensitive tertiary alcohol moiety. On concentration this carboxylic acid was found to form brightly colored material and readily decomposed. Changing the substituents on the aromatic rings with less electron-donating group such as silyloxy or pivaloyl group did not significantly increase the stability of the carboxylic acid. Thus, we decided to protect the 3° alcohol as a silyl ether, thus **5-28** was treated with TMSOTf and 2,6-lutidine to generate **5-29**.³⁰ Gratifyingly, the carboxylic acid **5-30** could be obtained by treating **5-29** with LDA followed by trapping with CO_2 . Although carboxylic acid **5-30** is relatively stable to be used for the next step it still tends to decompose on standing, thus it should be used for the next step without any further purification. In the next step, the carboxylic acid **5-30** was subjected to Steglich esterification³¹ with the diyne alcohol **5-31** to form the triyne **5-32** in 82% yield. Based on our previous study in Chapter 4, it was



Scheme 5.10. Synthesis of the triyne intermediate 5-27

expected that the silyl protected 3° alcohol in triyne **5-32** will not promote HDDA reaction due to the lack of hydrogen bonding and increased steric hindrance. Indeed, triyne **5-32** was found to be inert upon heating up to 150 °C. Thus, the silyl protecting group was deprotected using TBAF buffered with acetic acid to generate the triyne **5-27**.³²

With the triyne **5-27** in hand, we explored HDDA cycloaddition in the presence of various hydrogen donors but only cyclooctane (0.01 M) behaved as a suitable hydrogen source to trap the aryne intermediate to generate hydrogenated product **5-26a** in 52% yield (Scheme 5.11).²⁸ Treatment of **5-26a** with KO^tBu cleanly promote transesterification to generate **5-33**, trimethoxy selaginellin H, in 82% yield. Deprotection of the three methoxy group in presence of the lactone moiety was quite challenging. Lewis-acid mediated deprotection with BBr₃³³ mostly lead to transesterification back to **5-26a**. Nucleophilic methods such as Et₂NCH₂CH₂SH, *t*-BuONa,³⁴ in refluxing DMF or neat MeMgI at 160 °C²⁵ also failed to generate the desired deprotected product. Finally, refluxing **5-33** with PhSLi in HMPA³⁵ for 48 h gave selaginellin H, **5-2** in 52% yield. Thus, a total synthesis of selaginellin H^{16a} was achieved in 8 linear sequence from 4,4'-dimethoxybenzophenone (longest linear sequence) in 9.9 % overall yield.

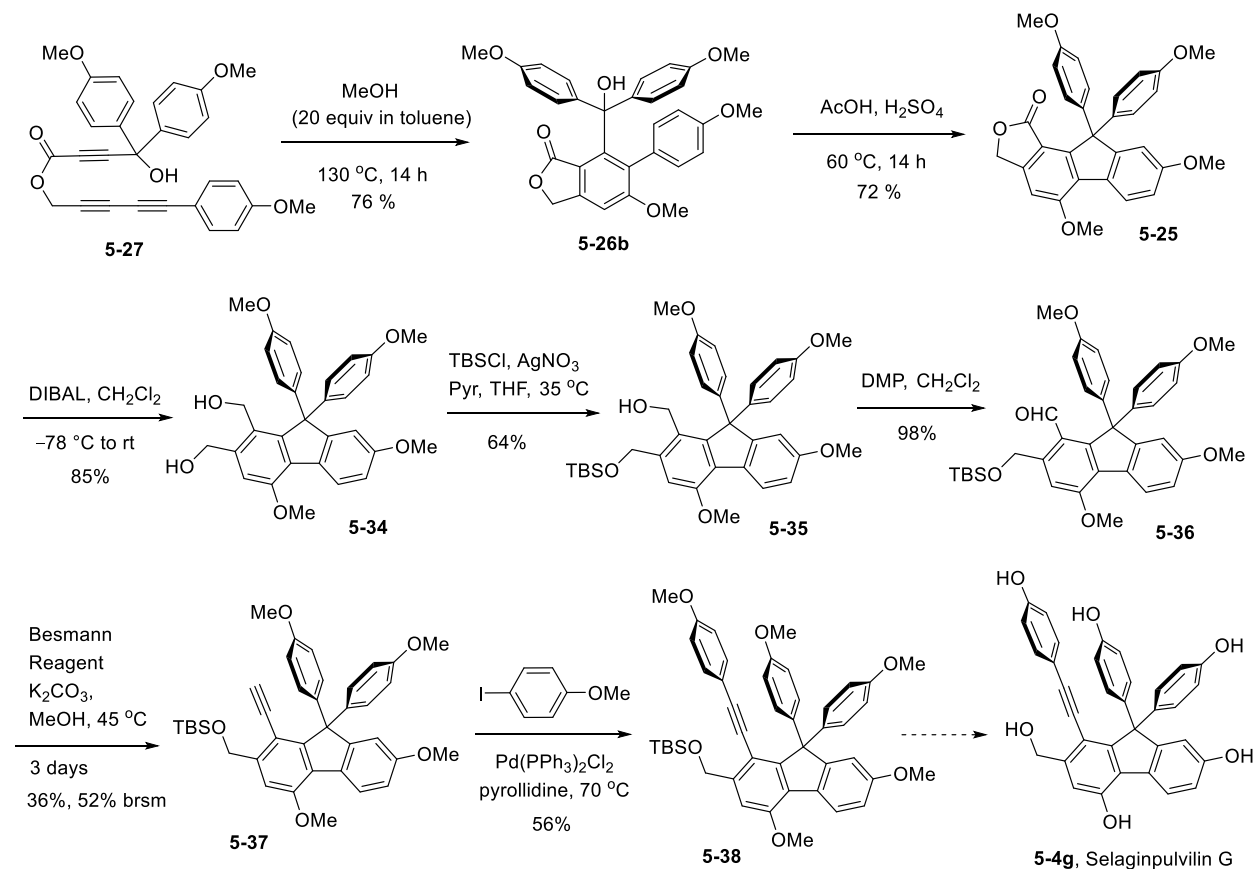


Scheme 5.11. Completion of synthesis of selaginellin H

5.3.2. Synthetic progress to selaginpulvilin G

This new approach for the diversity-oriented synthesis of different types of selaginellins also allows functionalization of C-4 of selaginpulvilins, which is not easily attainable by the previous synthetic approaches. Selaginpulvilin G is a Type B selaginellin natural product that contain an additional hydroxy group at C-4 position compared to other selaginpulvilins. We envisioned that trapping the aryne intermediate generated from the HDDA cycloaddition of **5-27** with methanol can install a methoxy group at the C-4 position provided the addition is regioselective (**Scheme 5.12**). Gratifyingly, the HDDA reaction of **5-27** in the presence of MeOH proceeded smoothly to generate the **5-26b** in 76% yield as a single regioisomer³⁶ confirmed by nOe experiments. It is critical to perform the reaction in toluene with 20 equivalents of MeOH because if the reaction is carried out in MeOH in higher amount or as a solvent methanolysis of the propiolate-tethered triyne **5-27** readily occurred and thus formed product **5-26b** in much lower yield. The acid-catalyzed intramolecular Friedel-Crafts reaction to construct the fluorene core proceeded efficiently with catalytic conc. H₂SO₄ in acetic acid to generate fluorene **5-25** in 72% yield.³⁷ The next goal involves the introduction of the aryl alkyne moiety which involves a series of oxidation,

reduction followed by a Seyferth-Gilbert olefination. Accordingly, the lactone moiety of **5-25** was reduced



Scheme 5.12. Synthetic progress to selaginpulvin G

with DIBAL to generate diol **5-34**, which was subjected to silylation conditions (TBSCl, AgNO₃, pyridine), which promoted mono-silylation of the sterically less-hindered alcohol selectively to provide the mono TBS-protected compound **5-35** in 64% yield.³⁸ The primary alcohol in **5-35** was then subjected to oxidation with DMP to form the corresponding aldehyde **5-36** in 98% yield. The Seyferth-Gilbert homologation of the sterically hindered aldehyde proved to be extremely difficult. The reaction required heating at 50 °C for 3 days, and addition of excess Bestmann reagent at intervals.³⁹ Even after long reaction time and addition of excess reagents, the reaction provided 60 % conversion with 36% yield of the homologated product **5-37**. The Sonogashira coupling of terminal alkyne **5-37** with 4-iodoanisole in the presence of Pd(PPh₃)₂Cl₂ catalyst and pyrrolidine solvent provide compound **5-38** in 56% yield.⁴⁰ It is critical to employ the copper-free conditions to prevent the formation of dimeric byproduct, which is the result of Glaser coupling of the

terminal alkyne. Compound **5-38** is a protected form of selaginpulvin G and a global deprotection of **5-38** would lead to the formation of selaginpulvin G. Unlike the case of successful deprotection in other selaginpulvin syntheses, the global deprotection with MeMgI failed. In the future, further investigations are needed to improve the efficiency for the synthesis of alkyne **5-37** and to find optimum conditions for the global deprotection of **5-38** to complete the total synthesis of selaginpulvin G.

5.4. Conclusion

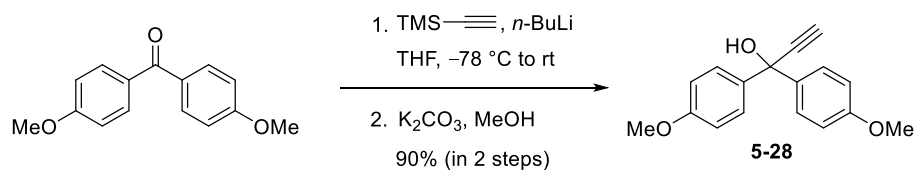
In conclusion, we have developed a diversity-oriented strategy to get access to different members of selaginellins and selaginpuvilins from a common intermediate. Our strategy gives flexibility for introducing structural variations at different stages of the synthesis thereby allowing access to the synthesis of different classes of natural products of the selaginella family apart from giving access to non-natural congeners. A propiolate-tethered triyne containing a *gem*-diaryl alcohol was subjected to HDDA cycloaddition and the aryne was trapped with methanol or cyclooctane depending on the structural requirement of the target natural product. Mimicking the proposed biosynthetic pathways, the products obtained from the HDDA reaction not only can be used for the construction of Type B selagellins but also for the construction of the fluorene-containing selaginpulin skeletons by acid-catalyzed Friedel-Crafts reaction. Relying on this strategy, we accomplished the first total synthesis of selaginellin H, a Type C selaginellin and have made significant progress towards the synthesis of selaginpulvin G. In particular, the current approach allows an easy access to the selaginpulvin G skeleton that contains an additional hydroxy group at a unique position, which is difficult to be installed by other methods. The prowess of this diversity-oriented strategy will allow the synthesis of various natural products and non-natural analogs of selaginella family, which facilitate the structure-activity relationship to discover their new pharmacological properties.

5.5. Experimental Details

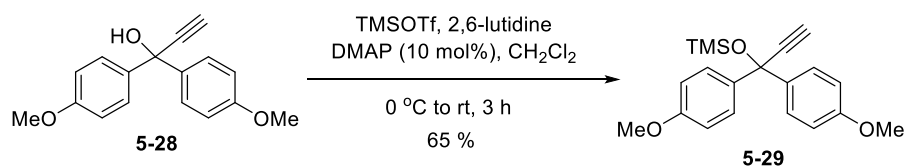
5.5.1. General information

Reactions were carried out in oven-dried glassware unless otherwise noted. Compounds were purchased from Aldrich, Acros, TCI America or Oakwood unless otherwise noted. Toluene, dichloromethane, triethylamine and acetonitrile were distilled over calcium hydride (CaH_2) under nitrogen. Tetrahydrofuran was dried over sodiumbenzophenone ketyl. Column chromatography was performed using silica gel 60 Å (32–63 mesh) purchased from Silicycle Inc. Analytical thin layer chromatography (TLC) was performed on 0.25 mm E. Merck precoated silica gel 60 (particle size 0.040–0.063 mm). Yields refer to chromatographically and spectroscopically pure isolated compounds unless otherwise stated. ^1H NMR and ^{13}C NMR spectra were recorded on a Bruker AV–500 spectrometer. ^1H NMR chemical shifts (δ) are reported in parts per million (ppm) downfield of TMS and are referenced relative to the residual protected solvent peak (CDCl_3 (7.26 ppm) or CD_3OD (3.31 ppm)). ^{13}C chemical shifts (δ) are reported in parts per million downfield of TMS and are referenced to the carbon resonance of the solvent (CDCl_3 (77.2 ppm) or CD_3OD (49.1 ppm)). Multiplicities are indicated by s (singlet), d (doublet), t (triplet), q (quartet), quin (quintet), sext (sextet) or m (multiplet). ^1H NMR signals that fall within a ca. 0.3 ppm range are generally reported as a multiplet, with a range of chemical shift values corresponding to the peak or center of the peak. Coupling constants, J , are reported in Hz (Hertz). Electrospray ionization (ESI) and Electron impact (EI) mass spectra were recorded on a Waters Micromass Q-ToF Ultima and Micromass 70–VSE, respectively in the University of Illinois at Urbana-Champaign.

5.5.2. Experimental procedures and characterization data

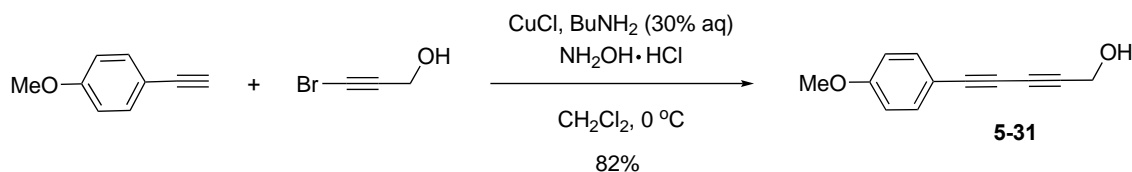


In a 250 mL round-bottomed flask was taken trimethylsilyl acetylene (2.43 g, 24.7 mmol) in anhydrous THF (100 mL) and cooled to $-78\text{ }^{\circ}\text{C}$. *n*-BuLi (8.6 mL, 21.4 mmol, 2.5 M in hexanes) was added dropwise and the mixture was stirred at $-78\text{ }^{\circ}\text{C}$ for 30 min. 4,4'-Dimethoxybenzophenone (4 g, 16.5 mmol) was added, and mixture was stirred at $-78\text{ }^{\circ}\text{C}$ for 1 h followed by warming to room temperature over 1 h. The reaction was quenched with sat. NH_4Cl solution (100 mL) and was extracted with EtOAc (100 mL x 2). The combined organic layers were washed with brine (100 mL x 2), dried over anhydrous MgSO_4 , filtered and concentrated. The crude product was dissolved in MeOH (60 mL) followed by addition of K_2CO_3 (1.12 g, 8.1 mmol) and stirred at room temperature for 3 h. After completion, MeOH was evaporated, and the mixture was extracted with EtOAc (50 mL x 2). The combined organic layers were washed with brine (100 mL x 2), dried over anhydrous Na_2SO_4 , filtered, concentrated, and purified by column chromatography (SiO_2 , hexanes–EtOAc, 10:1 \rightarrow 6:1) to obtain analytically pure propargyl alcohol **5-28** as pale-yellow solid (3.9 g, 90% yield over 2 steps). **^1H NMR** (500 MHz, CDCl_3) δ 7.50 (d, $J = 8.8\text{ Hz}$, 4H), 6.86 (d, $J = 8.8\text{ Hz}$, 4H), 3.79 (s, 6H), 2.97 (br s, 1H), 2.86 (s, 1H); **^{13}C NMR** (125 MHz, CDCl_3) δ 159.14, 137.05, 127.39, 113.59, 86.89, 75.13, 73.65, 55.32; **HRMS** (ESI) calcd for $\text{C}_{17}\text{H}_{17}\text{O}_3$ $[\text{M}+\text{H}]^+$ 269.1178, found 269.1188.

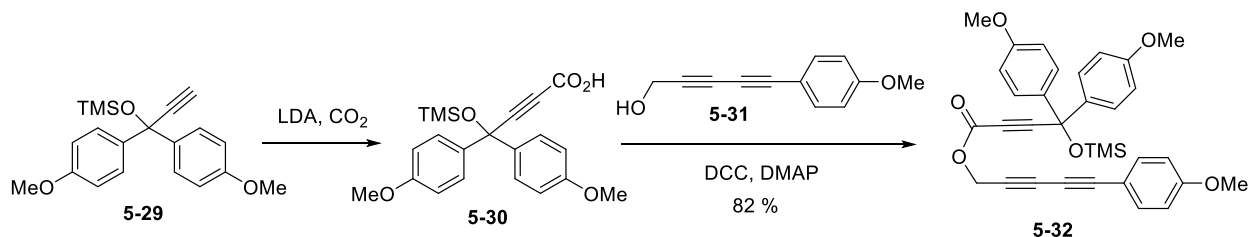


A solution of the propargyl alcohol **5-28** (2.31 g, 8.6 mmol) in dry CH_2Cl_2 (60 mL) is cooled to $0\text{ }^{\circ}\text{C}$ followed by addition of 2,6-lutidine (1.99 mL, 17.2 mmol), TMSOTf (2.34 mL, 12.9 mmol) and DMAP (51.4 mg, 0.86 mmol) sequentially. The mixture was warmed to room temperature and stirred for 3 h. After completion, the reaction was quenched with sat. NaHCO_3 solution (40 mL). The mixture was extracted with CH_2Cl_2 (50 mL x 2) and the combined organic layers were washed with brine (50 mL x 2). The CH_2Cl_2 layer was dried over anhydrous Na_2SO_4 , filtered, concentrated, and purified by column chromatography (SiO_2 , hexanes–EtOAc, 20:1 \rightarrow 10:1) to obtain analytically pure propargylic silyl ether **5-29** as yellow oil

(1.9 g, 65% yield). **¹H NMR** (500 MHz, CDCl₃) δ 7.54 (d, *J* = 8.8 Hz, 4H), 6.89 (d, *J* = 8.8 Hz, 4H), 3.81 (s, 6H), 2.93 (s, 1H), 0.20 (s, 9H); **¹³C NMR** (125 MHz, CDCl₃) δ 158.86, 138.83, 127.39, 113.32, 87.02, 76.44, 74.89, 55.24, 1.69; **HRMS** (ESI) calcd for C₂₀H₂₄O₃NaSi [M+Na]⁺ 363.1409, found 363.1188.

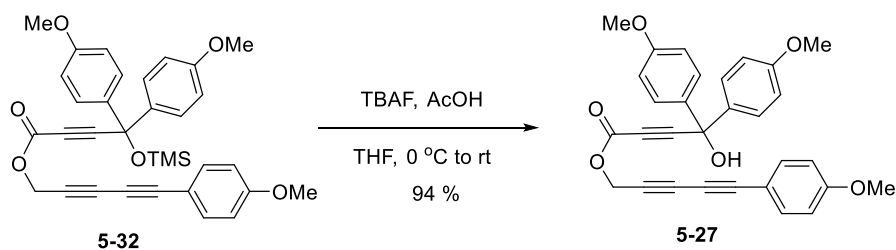


In a Schlenk flask containing CuCl (449.5 mg, 4.5 mmol) was added 30% aqueous BuNH₂ solution (15 mL) under nitrogen flow. A pinch of NH₂OH·HCl was added until the blue color disappeared. 4-Ethynylanisole (2 g, 15.3 mmol) in CH₂Cl₂ was added at 0 °C to the flask and the solution became yellow. A solution of 3-bromoprop-2-yn-1-ol (2.55 g, 18.2 mmol) in CH₂Cl₂ was added dropwise at 0 °C. The reaction mixture was stirred for 15 min at room temperature and the biphasic reaction mixture was transferred to a separatory funnel. The CH₂Cl₂ layer was separated and dried over anhydrous Na₂SO₄. After filtration, the organic layer was concentrated, and the crude material was purified by column chromatography (SiO₂, hexanes–EtOAc, 10:1 → 3:1) to obtain pure diyne **5-31** in 82% yield as yellow solid. **¹H NMR** (501 MHz, CDCl₃) δ 7.43 (d, *J* = 8.8 Hz, 2H), 6.84 (d, *J* = 8.8 Hz, 2H), 4.41 (s, 2H), 3.82 (s, 3H), 1.76 (br s, 1H); **¹³C NMR** (125 MHz, CDCl₃) δ 160.48, 134.26, 114.17, 113.30, 79.88, 78.88, 72.02, 70.76, 55.36, 51.74; **HRMS** (ESI) calcd for C₁₂H₁₁O₂ [M+H]⁺ 187.0759, found 187.0765.



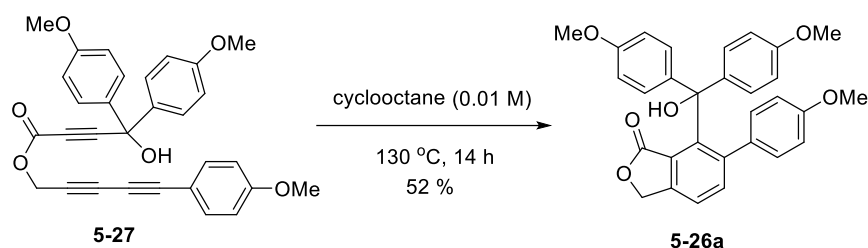
n-BuLi (4.57 mL, 11.4 mmol, 2.5M in hexanes) was added dropwise to a solution of diisopropylamine (1.86 mL, 13.1 mmol) in THF (80 mL) at –78 °C and stirred for 30 min. Alkyne **5-29** (2.94 g, 8.6 mmol)

in THF (20 mL) was added to the LDA solution at $-78\text{ }^{\circ}\text{C}$ and stirred for 45 min. CO_2 (generated from dry ice) was bubbled into the reaction mixture at $-78\text{ }^{\circ}\text{C}$ for 30 min and the reaction mixture was stirred at the same temperature for another 30 min before warming to room temperature. After completion (monitored by TLC) the reaction was cooled to $0\text{ }^{\circ}\text{C}$ and quenched carefully with 1 N HCl (16 mL) followed by water (100 mL). The mixture was extracted with EtOAc (50 mL x 2) and the combined organic layers were washed with brine (50 mL x 2). The organic layer was dried over anhydrous Na_2SO_4 , filtered and concentrated very carefully (the product tends to decompose on concentration). The crude carboxylic acid was immediately dissolved in CH_2Cl_2 and cooled to $0\text{ }^{\circ}\text{C}$ followed by addition of the diyne alcohol **5-31** (1.19 g, 6.4 mmol), DCC (1.91 g, 9.25 mmol) and DMAP (72.7 mg, 0.59 mmol). After completion (monitored by TLC) the reaction mixture was filtered through a short pad of silica, concentrated, and purified by column chromatography (SiO_2 , hexanes–EtOAc, 10:1 \rightarrow 6:1) to obtain analytically pure triyne **5-32** as dark yellow oil (1.7 g, 72% yield over 2 steps). $^1\text{H NMR}$ (500 MHz, CDCl_3) δ 7.55 – 7.29 (m, 6H), 6.99 – 6.69 (m, 6H), 4.93 (s, 2H), 3.80 (s, 3H), 3.79 (s, 6H), 0.16 (s, 9H); $^{13}\text{C NMR}$ (125 MHz, CDCl_3) δ 160.72, 159.22, 152.49, 137.08, 134.41, 127.50, 114.25, 113.54, 112.90, 91.04, 79.67, 78.72, 74.99, 74.56, 72.41, 71.94, 55.35, 55.26, 53.99, 1.49; **HRMS** (ESI) calcd for $\text{C}_{33}\text{H}_{32}\text{O}_6\text{NaSi}$ $[\text{M}+\text{Na}]^+$ 575.1866, found 575.1849.

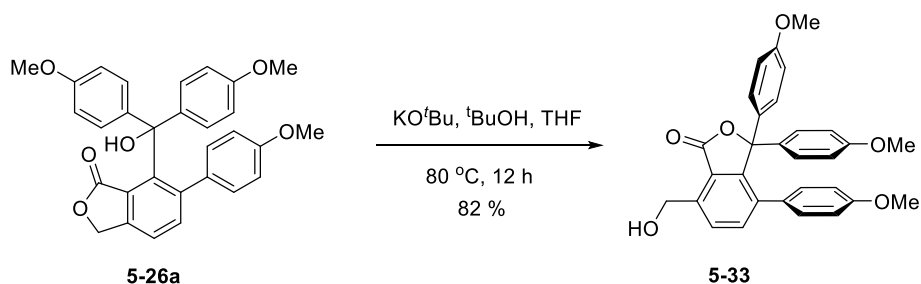


Triyne **5-32** (1.72 g, 3.1 mmol) was dissolved in 20 mL THF and cooled to $0\text{ }^{\circ}\text{C}$ followed by dropwise addition of a mixture of TBAF (4.66 mL, 1 M in THF) and acetic acid (0.36 mL in 5 mL THF). The reaction was warmed to room temperature and stirred for 2 h. After completion, the reaction was quenched with sat. NH_4Cl solution and extracted with EtOAc. The organic layer was dried over anhydrous Na_2SO_4 , filtered,

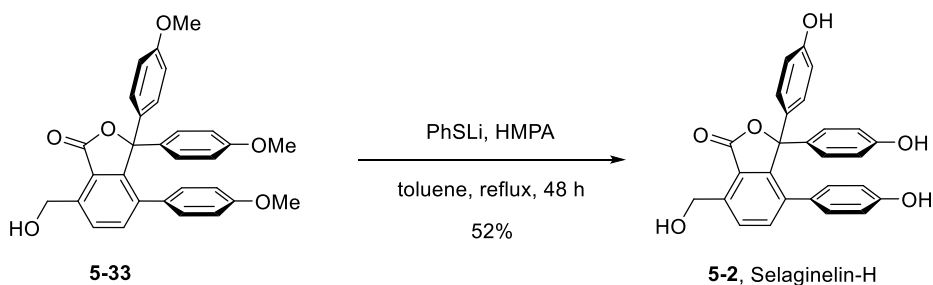
concentrated, and purified by column chromatography (SiO₂, hexanes–EtOAc, 10:1 → 3:1) to obtain analytically pure triyne **5-27** as yellow solid (1.38 g, 94% yield). ¹H NMR (500 MHz, CDCl₃) δ 7.54 – 7.27 (m, 6H), 6.98 – 6.68 (m, 6H), 4.90 (s, 2H), 3.79 (s, 3H), 3.78 (s, 6H), 3.45 (s, 1H); ¹³C NMR (125 MHz, CDCl₃) δ 160.65, 159.44, 152.57, 135.51, 134.41, 127.51, 114.25, 113.80, 112.90, 90.78, 79.71, 77.31, 74.46, 73.72, 72.49, 71.89, 55.38, 55.33, 54.08; HRMS (ESI) calcd for C₃₀H₂₄O₆Na [M+Na]⁺ 503.1471, found 503.1465.



Triyne **5-27** (250 mg, 0.52 mmol) was dissolved in toluene (5 mL) and cyclooctane (45 mL) transferred to a Schlenk tube, degassed, and refilled with argon by freeze, pump, and thaw method (cycle of 3). The reaction mixture was then heated in an oil bath at 130 °C for 14 h. The reaction was cooled, concentrated and the residue was purified by column chromatography (SiO₂, hexanes–EtOAc, 10:1 → 3:1→2:1) to obtain compound **5-26a** as yellow solid (130 mg, 52% yield). ¹H NMR (500 MHz, CDCl₃) δ 7.52 (s, 1H), 7.39 (d, *J* = 7.8 Hz, 1H), 7.32 (d, *J* = 7.8 Hz, 1H), 6.92 (d, *J* = 8.3 Hz, 4H), 6.58 (d, *J* = 8.6 Hz, 4H), 6.50 (d, *J* = 8.4 Hz, 2H), 6.38 (d, *J* = 8.5 Hz, 2H), 5.40 (s, 2H), 3.75 (s, 6H), 3.70 (s, 3H); ¹³C NMR (125 MHz, CDCl₃) δ 173.75, 158.31, 157.59, 149.64, 148.25, 143.64, 139.78, 138.74, 134.61, 132.06, 129.98, 129.38, 125.17, 120.04, 112.61, 81.88, 69.40, 55.23, 55.17; HRMS (ESI) calcd for C₃₀H₂₆O₆Na [M+Na]⁺ 505.1627, found 505.1615.

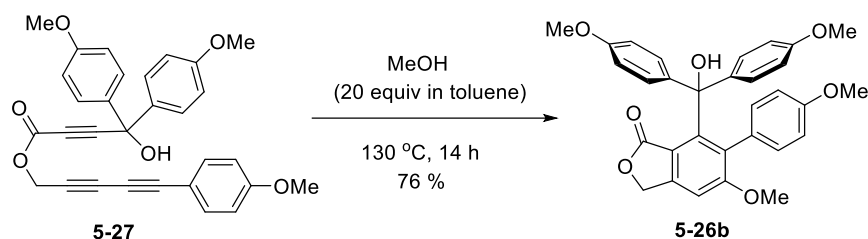


Lactone **5-26a** (85 mg, 0.17 mmol) was dissolved in a mixture of THF (3 mL) and *t*-BuOH (3 mL) and KO*t*-Bu (34.5 mg, 0.25 mmol) was added under nitrogen. The reaction mixture was transferred to a Schlenk tube, degassed, and refilled with argon by freeze, pump, and thaw method (cycle of 3). The reaction mixture was then heated in an oil bath at 80 °C for 12 h. The reaction was quenched with satd. NH₄Cl and extracted with EtOAc. The organic layer was dried over anhydrous Na₂SO₄, filtered, concentrated, and purified by column chromatography (SiO₂, hexanes–EtOAc, 10:1 → 3:1 → 2:1) to obtain compound **5-33** as yellow solid (69.7 mg, 82% yield). **¹H NMR** (500 MHz, CDCl₃) δ 7.50 (d, *J* = 7.6 Hz, 1H), 7.39 (d, *J* = 7.6 Hz, 1H), 6.93 (d, *J* = 8.9 Hz, 4H), 6.71 (d, *J* = 8.8 Hz, 4H), 6.58 (d, *J* = 8.7 Hz, 2H), 6.51 (d, *J* = 8.7 Hz, 2H), 5.05 (d, *J* = 5.7 Hz, 2H), 4.28 (t, *J* = 6.54, 1H), 3.78 (s, 5H), 3.75 (s, 3H); **¹³C NMR** (125 MHz, CDCl₃) δ 171.40, 159.70, 158.98, 151.40, 141.31, 138.53, 137.67, 131.01, 130.71, 130.35, 130.16, 129.02, 124.08, 113.19, 113.02, 94.27, 62.75, 55.33, 55.25; **HRMS** (ESI) calcd for C₃₀H₂₇O₆ [M+H]⁺ 483.1808, found 483.1808.

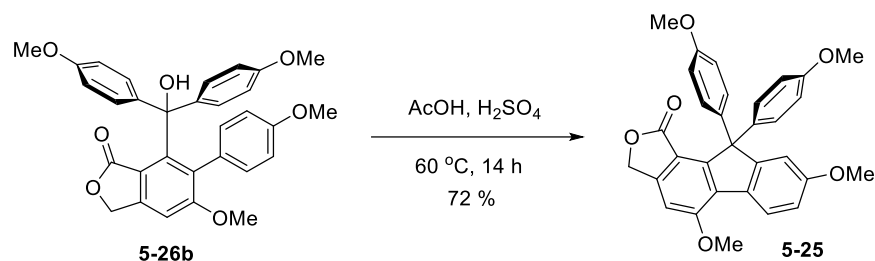


A round-bottomed flask was charged with PhSH (24 mL, 0.24 mmol) in (2 mL) toluene at 0 °C followed by dropwise addition of *n*-BuLi (96 mL, 0.24 mmol, 2.5 M in hexanes). The white precipitate was stirred for 15 min followed by addition of HMPA (0.21 mL, 1.2 mmol) when the reaction mixture became clear. A solution of **5-33** (11.6 mg, 0.024 mmol) in toluene (0.5 mL) was added, and the mixture was refluxed (130 °C) for 48 h. The reaction mixture was cooled followed by addition of EtOAc (5 mL) followed by extraction of organic layer with 1 M NaOH (5 mL x 2). The combined NaOH layer was extracted with EtOAc (5 mL x 2) to remove HMPA. The dark violet NaOH layer was carefully acidified with 6 M HCl (4 mL) when a thick white precipitate was formed. The mixture was extracted with EtOAc (5 mL x 3) and the

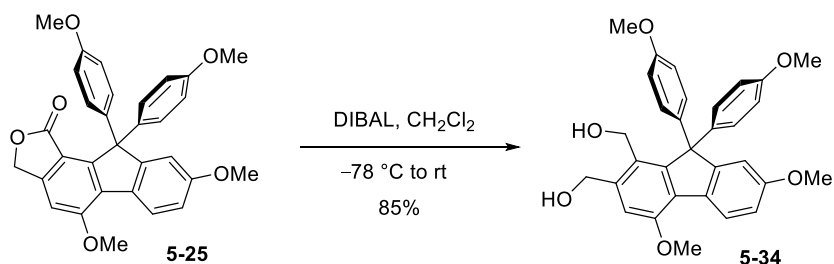
combined organic layers were dried over anhydrous Na₂SO₄, filtered, concentrated, and purified by column chromatography (SiO₂, hexanes–EtOAc, 3:1 → 1:1 → 1:2) to obtain Selaginellin H (**5-2**) as white solid (5.3 mg, 52% yield). ¹H NMR (500 MHz, MeOD) δ 7.76 (d, *J* = 7.5 Hz, 1H), 7.46 (d, *J* = 7.6 Hz, 1H), 6.81 (d, *J* = 8.2 Hz, 4H), 6.62 (d, *J* = 8.1 Hz, 4H), 6.50 – 6.43 (m, 4H), 5.18 (s, 2H); ¹³C NMR (125 MHz, MeOD) δ 170.63, 157.47, 156.64, 151.08, 141.60, 138.17, 137.50, 130.54, 130.01, 129.83, 129.45, 127.34, 122.03, 114.15, 113.94, 93.64, 59.30; HRMS (ESI) calcd for C₂₇H₂₀O₆Na [M+Na]⁺ 463.1158, found 463.1149.



Triyne **5-27** (340 mg, 0.71 mmol) was dissolved in toluene (15 mL) followed by addition of MeOH (450 mg, 14.2 mmol) and transferred to a Schlenk tube, degassed, and refilled with argon by freeze, pump, and thaw method (cycle of 3). The reaction mixture was then heated in an oil bath at 130 °C for 14 h. The reaction was cooled, concentrated and the residue was purified by column chromatography (SiO₂, hexanes–EtOAc, 3:1 → 2:1 → 1:1) to obtain compound **5-26b** as yellow solid (276 mg, 76% yield). ¹H NMR (500 MHz, CDCl₃) δ 7.76 (s, 1H), 6.92 (s, 1H), 6.88 (d, *J* = 8.1 Hz, 4H), 6.57 (d, *J* = 8.4 Hz, 4H), 6.36 (t, *J* = 6.5 Hz, 4H), 5.33 (s, 2H), 3.75 (s, 6H), 3.70 (s, 6H); ¹³C NMR (125 MHz, CDCl₃) δ 173.91, 163.65, 158.16, 157.40, 151.02, 150.95, 139.05, 133.39, 130.44, 129.80, 128.47, 116.80, 112.57, 101.81, 82.05, 69.30, 56.35, 55.17, 55.07; HRMS (ESI) calcd for C₃₁H₂₇O₇Na [M+Na]⁺ 535.1733, found 535.1737.

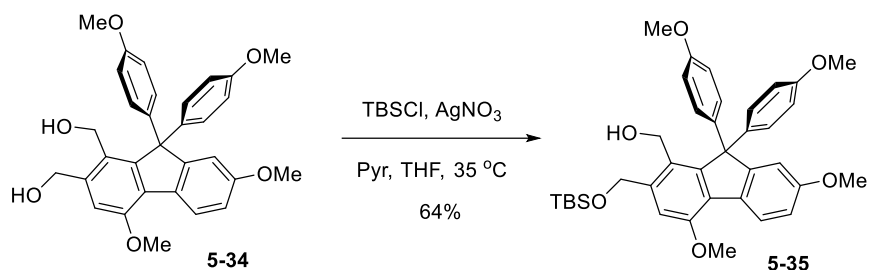


Lactone **5-26b** (268 mg, 0.52 mmol) was dissolved in glacial AcOH (10 mL), cooled to 0 °C followed by addition of conc. H₂SO₄ (20 mL). The mixture was then heated at 60 °C for 14 h. After completion, the mixture was poured carefully to satd. NaHCO₃ solution (50 mL). The mixture was extracted with EtOAc (20 mL x 2) and the combined organic layers were washed with NaHCO₃ (10 mL x 3) and brine (10 mL). The organic layers were dried over anhydrous Na₂SO₄, filtered, concentrated, and purified by column chromatography (SiO₂, hexanes–EtOAc, 3:1 → 2:1 → 1:1) to obtain fluorene **5-25** as yellow solid (185.2 mg, 72% yield). ¹H NMR (500 MHz, CDCl₃) δ 8.05 (d, *J* = 8.4 Hz, 1H), 7.27 (d, *J* = 8.1 Hz, 4H), 6.87 (d, *J* = 8.4 Hz, 1H), 6.84 (s, 1H), 6.80 (s, 1H), 6.74 (d, *J* = 8.3 Hz, 4H), 5.17 (s, 2H), 4.08 (s, 3H), 3.74 (s, 9H); ¹³C NMR (125 MHz, CDCl₃) δ 168.61, 160.03, 159.89, 158.37, 155.35, 152.85, 148.77, 134.91, 130.32, 130.28, 129.65, 124.59, 114.55, 113.24, 113.04, 110.94, 102.68, 68.87, 65.11, 55.91, 55.39, 55.12; HRMS (ESI) calcd for C₃₁H₂₇O₆ [M+Na]⁺ 495.1784, found 495.1788.

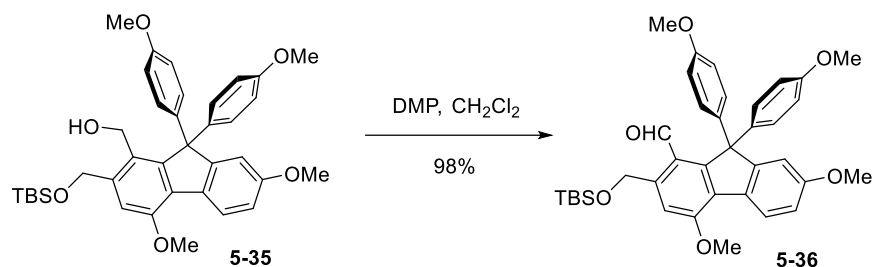


Lactone **5-25** (160.7 mg, 0.32 mmol) was dissolved in dry CH₂Cl₂ (10 mL) and cooled to –78 °C followed by dropwise addition of DIBAL (0.97 mL, 0.96 mmol, 1 M in CH₂Cl₂). The mixture was stirred at –78 °C for 1 h followed by warming to room temperature and stirred for additional 1 h. After completion, the reaction was quenched with satd. NH₄Cl solution and extracted with CH₂Cl₂. The CH₂Cl₂ layer was dried

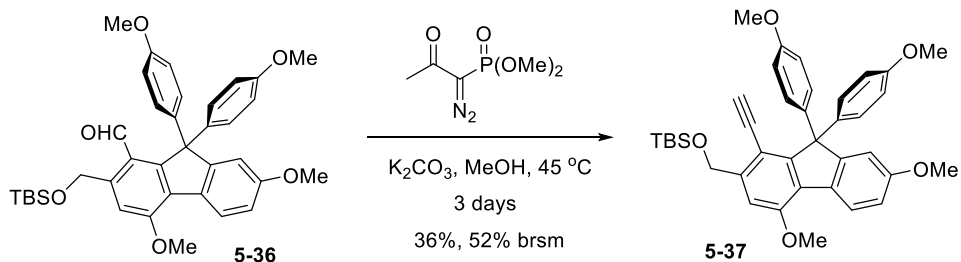
over anhydrous Na_2SO_4 , filtered, concentrated, and purified by column chromatography (SiO_2 , hexanes–EtOAc, 3:1 \rightarrow 1:1 \rightarrow 1:2) to obtain compound **5-34** as white solid (135.6 mg, 85%). **^1H NMR** (500 MHz, CDCl_3) δ 8.02 (d, $J = 8.1$ Hz, 1H), 7.22 (d, $J = 8.8$ Hz, 4H), 7.02 (s, 1H), 6.86 – 6.76 (m, 6H), 4.69 (s, 2H), 4.53 (s, 2H), 4.04 (s, 3H), 3.75 (s, 6H), 3.73 (s, 3H); **^{13}C NMR** (125 MHz, CDCl_3) δ 159.38, 158.37, 155.99, 154.97, 152.23, 141.57, 135.22, 131.21, 129.53, 127.96, 127.86, 124.60, 113.87, 112.58, 112.45, 110.61, 64.51, 64.41, 58.74, 55.47, 55.39, 55.24; **HRMS** (ESI) calcd for $\text{C}_{31}\text{H}_{30}\text{O}_6\text{Na}$ $[\text{M}+\text{Na}]^+$ 521.1940, found 521.1929.



Diol **5-34** (125.2 mg, 0.25 mmol) was dissolved in dry THF (5 mL) followed by addition of pyridine (0.1 mL, 1.25 mmol) and AgNO₃ (50.9 mg, 0.3 mmol) and stirred at room temperature. After 30 min, TBSCl (45.6 mg, 0.3 mmol) was added when a cloudy mixture was formed. The reaction was heated at 35 °C for 14 h and reaction progress was monitored through TLC. After completion, the reaction was quenched with satd. NaHCO₃ and extracted with EtOAc. The organic layer was dried over anhydrous Na₂SO₄, filtered, concentrated, and purified by column chromatography (SiO₂, hexanes–EtOAc, 20:1 → 10:1 → 6:1) to obtain compound **5-35** as colorless oil (98 mg, 64%). ¹H NMR (500 MHz, CDCl₃) δ 7.99 (d, *J* = 8.0 Hz, 1H), 7.24 – 7.20 (m, 5H), 6.86 – 6.71 (m, 6H), 4.88 (s, 2H), 4.39 (s, 2H), 4.04 (s, 3H), 3.75 (s, 6H), 3.72 (s, 3H), 0.96 (s, 9H), 0.13 (s, 6H); ¹³C NMR (125 MHz, CDCl₃) δ 159.13, 158.28, 156.00, 154.83, 151.76, 141.50, 135.45, 131.44, 129.62, 126.88, 126.70, 124.27, 113.72, 112.46, 110.60, 109.73, 64.38, 62.66, 58.04, 55.38, 55.30, 55.22, 25.95, 18.34, -5.18; ; HRMS (ESI) calcd for C₃₇H₄₄O₆NaSi [M+Na]⁺ 635.2805, found 635.2789.

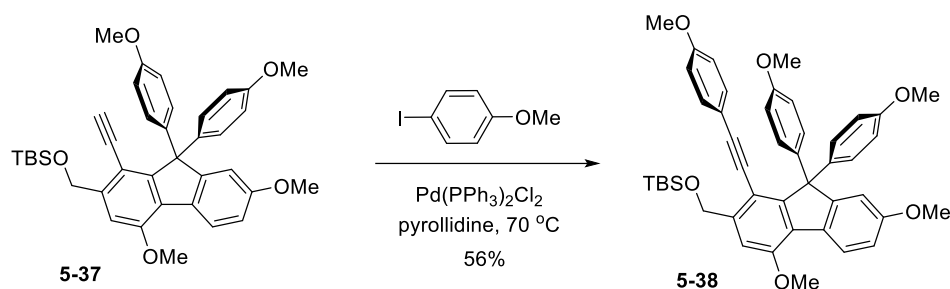


Alcohol **5-35** (100 mg, 0.16 mmol) was dissolved in CH_2Cl_2 (5 mL) followed by addition of DMP (138.5 mg, 0.32 mmol). The cloudy reaction mixture was stirred at room temperature for 2 h. The reaction was diluted with CH_2Cl_2 (5 mL) followed by quenching with satd. NaHCO_3 (5 mL) solution and satd. $\text{Na}_2\text{S}_2\text{O}_3$ solution (5 mL) and the mixture was vigorously stirred until two clear layers could be separated. The organic layers were separated, dried over anhydrous Na_2SO_4 , filtered, concentrated, and purified by column chromatography (SiO_2 , hexanes–EtOAc, 10:1 \rightarrow 6:1) to obtain aldehyde **5-36** as colorless oil (95 mg, 64%). **^1H NMR** (500 MHz, CDCl_3) δ 10.23 (s, 1H), 8.01 (d, J = 8.4 Hz, 1H), 7.59 (s, 1H), 7.19 (d, J = 8.9 Hz, 4H), 6.84 (dd, J = 8.5, 2.2 Hz, 1H), 6.79 (d, J = 2.1 Hz, 1H), 6.75 (d, J = 8.9 Hz, 4H), 5.07 (s, 2H), 4.11 (s, 3H), 3.74 (s, 6H), 3.73 (s, 3H), 1.00 (s, 9H), 0.14 (s, 6H); **^{13}C NMR** (125 MHz, CDCl_3) δ 191.91, 159.52, 158.95, 158.35, 157.55, 156.06, 146.64, 135.52, 130.07, 129.57, 127.23, 124.24, 121.66, 113.83, 112.67, 110.68, 108.07, 64.92, 63.83, 55.55, 55.40, 55.22, 25.99, 18.31, -5.28; ; **HRMS** (ESI) calcd for $\text{C}_{37}\text{H}_{42}\text{O}_6\text{NaSi}$ $[\text{M}+\text{Na}]^+$ 633.2648, found 633.2650.



Aldehyde **5-36** (40 mg, 0.065 mmol) was dissolved in MeOH (5 mL) followed by addition of Bestmann reagent (62 mg, 0.325 mmol) and K_2CO_3 (67.4 mg, 0.49 mmol). The mixture was heated at 50°C for 3 days during which were further added Bestmann reagent (25 mg, 0.13 mmol) and K_2CO_3 (27 mg, 0.19 mmol) at

every 16 h interval. The reaction mixture was concentrated to remove MeOH and extracted with EtOAc and H₂O. The organic layer was separated, dried over anhydrous Na₂SO₄, filtered, concentrated, and purified by column chromatography (SiO₂, hexanes–EtOAc, 20:1→10:1 →6:1) to obtain alkyne **5-37** as colorless oil (14 mg, 36%, 52% brsm). **¹H NMR** (500 MHz, CDCl₃) δ 7.98 (d, *J* = 8.5 Hz, 1H), 7.23 – 7.17 (m, 5H), 6.82 (dd, *J* = 8.4, 2.3 Hz, 1H), 6.78 (d, *J* = 2.1 Hz, 1H), 6.75 – 6.70 (m, 4H), 4.85 (s, 2H), 4.04 (s, 3H), 3.75 (s, 6H), 3.73 (s, 3H), 3.18 (s, 1H), 0.97 (s, 9H), 0.11 (s, 6H); **¹³C NMR** (125 MHz, CDCl₃) δ 159.25, 158.10, 155.55, 155.36, 154.28, 145.13, 134.71, 131.06, 130.35, 127.08, 124.21, 112.86, 112.68, 110.79, 108.42, 107.53, 87.66, 79.28, 63.28, 55.33, 55.12, 29.71, 25.94, -5.26; **HRMS** (ESI) calcd for C₃₈H₄₃O₅Si [M+H]⁺ 607.2880, found 607.2884.



mmol) was dissolved in pyrrolidine (0.5 mL) and transferred to a Schlenk tube. The Schlenk tube was then degassed, and refilled with argon by freeze, pump, and thaw method (cycle of 3). The reaction mixture was then heated in an oil bath at 80 °C for 48 h. After completion, the reaction was quenched with NH₄Cl and extracted with EtOAc. The organic layer was separated, dried over anhydrous Na₂SO₄, filtered, concentrated, and purified by column chromatography (SiO₂, hexanes–EtOAc, 10:1 → 6:1) to obtain alkyne **5-38** as white solid (6.3 mg, 56% yield). **¹H NMR** (500 MHz, CDCl₃) δ 8.01 (d, *J* = 8.4 Hz, 1H), 7.25 – 7.18 (m, 5H), 6.93 (d, *J* = 8.6 Hz, 2H), 6.84 (dd, *J* = 8.5, 2.3 Hz, 1H), 6.82 – 6.76 (m, 3H), 6.75 – 6.68 (m, 4H), 4.93 (s, 2H), 4.04 (s, 3H), 3.81 (s, 3H), 3.74 (s, 3H), 3.73 (s, 6H), 0.97 (s, 9H), 0.12 (s, 6H); **¹³C NMR**

(125 MHz, CDCl₃) δ 159.29, 159.20, 158.10, 155.14, 155.12, 153.68, 143.85, 134.93, 132.30, 131.46, 130.26, 126.99, 124.22, 116.04, 113.91, 112.91, 112.72, 110.83, 109.80, 107.62, 99.36, 84.78, 63.43, 55.37, 55.35, 55.31, 55.20, 25.96, -5.21; **HRMS** (ESI) calcd for C₄₅H₄₉O₆Si [M+H]⁺ 607.2880, found 607.2884.

5.6. References

1. Reviews on application of arynes in natural product synthesis: (a) Tadross, P. M.; Stoltz B. M. *Chem. Rev.* **2012**, *41*, 3550–3577. (b) Gampe, C. M.; Carreira, E. M. *Angew. Chem., Int. Ed.* **2012**, *51*, 3766–3778.
2. Himeshima, Y.; Sonada, T.; Kobayashi, H. *Chem. Lett.* **1983**, *12*, 1211–1214.
3. (a) Hoye, T. R.; Baire, B.; Niu, D. Willoughby, P. H.; Woods, B. P. *Nature* **2012**, *490*, 208–212. For reviews: (b) Holden, C.; Greaney, M. F. *Angew. Chem., Int. Ed.* **2014**, *53*, 5746–5749; (c) Diamond, O. J.; Marder, T. B. *Org. Chem. Front.* **2017**, *4*, 891–910. (d) Fluegel, L. L.; Hoye, T. R. *Chem. Rev.* **2021**, *121*, 2413–2444.
4. (a) Karmakar, R.; Wang, K. P.; Yun, S. Y.; Mamidipalli, P.; Lee, D. *Org. Biomol. Chem.* **2016**, *14*, 4782–4788. (b) Wang, T.; Hoye, T. R. *J. Am. Chem. Soc.* **2016**, *138*, 13870–13873.
5. Li, W.; Tang, G. H.; Yin, S. *Nat. Prod. Rep.* **2021**, Article Asap DOI: 10.1039/d0np00065e
6. Karmakar, R.; Lee, D. *Org. Lett.* **2016**, *18*, 6105–6107.
7. State Administration of Traditional Chinese Medicine of the People's Republic of China. *Chinese Materia Medica (Zhong Hua Ben Cao)*; Editorial Board of 'Zhong Hua Ben Cao'; Shanghai Scientific and Technical Publishers: Shanghai, 1999; Vol. 4, pp 387–389.
8. Xie, Y.; Xu, K. P.; Zou, Z. X.; Tan, G. S. *Cent. South Pharm.* **2017**, *15*, 129–142.
9. Zhang, L. P.; Liang, Y. M.; Wei, X. C.; Cheng, D. L. *J. Org. Chem.* **2007**, *72*, 3921–3924.
10. (a) Cheng, X. L.; Ma, S. C.; Yu, J. D.; Yang, S. Y.; Xiao, X. Y.; Hu, J. Y.; Lu, Y.; Shaw, P. C.; But, P. P.-H.; Lin, R. C. *Chem. Pharm. Bull.* **2008**, *56*, 982–984. (b) Tan, G. S.; Xu, K. P.; Li, F. S.; Wang, C. J.; Li, T. Y.; Hu, C. P.; Shen, J.; Zhou, Y. J.; Li, Y. J. *J. Asian Nat. Prod. Res.* **2009**, *11*, 1001–1004. (c) Cao, Y.; Chen, J. J.; Tan, N. H.; Oberer, L.; Wagner, T.; Wu, Y. P.; Zeng, G. Z.; Yan, H.; Wang, Q. *Bioorg. Med. Chem. Lett.* **2010**, *20*, 2456–2460. (d) Xu, K. P.; Zou, H.; Tan, Q.; Li, F. S.; Liu, J. F.; Xiang, H. L.; Zou, Z. X.; Long, H. P.; Li, Y. J.; Tan, G. S. *J. Asian Nat. Prod. Res.* **2011**, *13*, 93–96. (e) Xu, K. P.; Zou, H.; Liu, G. R.; Long, H. P.; Li, J.; Li, F. S.; Zou, Z. X.; Kuang, J. W.; Xie, X.; Tan, G. S. *J. Asian Nat. Prod. Res.* **2011**, *13*, 1051–1055. (f) Zhang,

- G. G.; Jing, Y.; Zhang, H. M.; Ma, E. L.; Guan, J.; Xue, F. N.; Liu, H. X.; Sun, X. Y. *Planta Med.* **2012**, *78*, 390–392. (g) Yang, C.; Shao, Y. T.; Li, K.; Xia, W. J. *Beilstein J. Org. Chem.*, **2012**, *8*, 1884–1889. (h) Cao, Y.; Yao, Y.; Huang, X. J.; Oberer, L.; Wagner, T.; Guo, J. M.; Gu, W.; Liu, W. D.; Lv, G. X.; Shen, Y. N.; Duan, J. A. *Tetrahedron*, **2015**, *71*, 1581–1587.
11. Nguyen, P. H.; Zhao, B. T.; Ali, M. Y.; Choi, J. S.; Rhyu, D. Y.; Min, B. S.; Woo, M. H. *J. Nat. Prod.* **2015**, *78*, 34–42.
12. Cao, Y.; Zhao, M.; Zhu, Y.; Zhu, Z. H.; Oberer, L.; Duan, J. A. *J. Nat. Prod.* **2017**, *80*, 3151–3158.
13. Woo, S.; Kang, K. B.; Kim, J.; Sung, S. H. *J. Nat. Prod.* **2019**, *82*, 1820–1830.
14. (a) Liu, X.; Luo, H.-B.; Huang, Y.-Y.; Bao, J.-M.; Tang, G.-H.; Chen, Y.-Y.; Wang, J.; Yin, S. *Org. Lett.* **2014**, *16*, 282–285. (b) Zhang, J.-S.; Liu, X.; Weng, J.; Guo, Y.-Q.; Li, Y.-Q.; Ahmed, A.; Tang, G.-H.; Yin, S. *Org. Chem. Front.* **2017**, *4*, 170–177.
15. (a) Xu, K. P.; Zou, H.; Li, F. S.; Xiang, H. L.; Zou, Z. X.; Long, H. P.; Li, J.; Luo, Y. J.; Li, Y. J.; Tan, G. S. *J. Asian Nat. Prod. Res.* **2011**, *13*, 356–360. (b) Xu, K. P.; Li, J.; Zhu, G. Z.; He, X. A.; Li, F. S.; Zou, Z. X.; Tan, L. H.; Cheng, F.; Tan, G. S. *J. Asian Nat. Prod. Res.* **2015**, *17*, 819–822.
16. (a) Cao, Y.; Chen, J. J.; Tan, N. H.; Wu, Y. P.; Yang, J.; Wang, Q. *Magn. Reson. Chem.* **2010**, *48*, 656–659. (b) Wang, C. G.; Yao, W. N.; Zhang, B.; Hua, J.; Liang, D.; Wang, H. S. *Bioorg. Med. Chem. Lett.* **2018**, *28*, 2413–2417.
17. (a) Cao, Y.; Yao, Y.; Huang, X. J.; Oberer, L.; Wagner, T.; Guo, J. M.; Gu, W.; Liu, W. D.; Lv, G. X.; Shen, Y. N.; Duan, J. A. *Tetrahedron* **2015**, *71*, 1581–1587. (b) Yao, W. N.; Huang, R. Z.; Hua, J.; Zhang, B.; Wang, C. G.; Liang, D.; Wang, H. S. *ACS Omega*, **2017**, *2*, 2178–2183. (c) Zhu, Q. F.; Bao, Y.; Zhang, Z. J.; Su, J.; Shao, L. D.; Zhao, Q. S. *R. Soc. Open Sci.* **2017**, *4*, 170352–170359. (d) Cao, Y.; Zhao, M.; Zhu, Y.; Zhu, Z. H.; Oberer, L.; Duan, J. A. *J. Nat. Prod.* **2017**, *80*, 3151–3158. (e) Shi, S. P.; Wang, Y. Z.; Zheng, X. K.; Feng, W. S.; Tu, P. F. *Biochem. Syst. Ecol.* **2012**, *45*, 151–154.
18. Abe, I.; Morita, H. *Nat. Prod. Rep.* **2010**, *27*, 809–838.

19. (a) Nguyen, P.; Zhao, B.; Ali, M. Y.; Choi, J.; Rhyu, D.; Min, B.; Woo, M. *J. Nat. Prod.* **2014**, *78*, 34–42. (b) Wang, C.; Hu, C.; Xu, K.; Tan, G.; Li, Y. *J. Cardiovasc. Pharmacol.* **2010**, *55*, 560–566. (c) Kim, J.; Cho, C.; Tai, B.; Yang, S.; Choi, G.; Kang, J.; Kim, Y. *Molecules* **2015**, *20*, 21405–21414. (d) Zhang, G. G.; Ying, J.; Zhang, H. M.; Ma E. L.; Sun, X. Y. *Planta Med.* **2012**, *78*, 390–392. (e) Wang, S.; Liu, L.; Guo, X.; Li, G.; Wang, X.; Dong, H.; Li, Y.; Zhao, W. *RSC Adv.* **2019**, *9*, 13878–13886. (f) Wang, C.; Hu, C.; Xu, K.; Yuan, Q.; Li, F.; Zou, H.; Tan, G.; Li, Y. *Naunyn-Schmiedeberg's Arch. Pharmacol.* **2010**, *381*, 73–81.
20. (a) Bender, A. T.; Beavo, J. A. *Pharmacol. Rev.* **2006**, *58*, 488–520. (b) Burgin, A. B.; Magnusson, O. T.; Singh, J.; Witte, P.; Staker, B. L.; Bjornsson, J. M.; Thorsteinsdottir, M.; Hrafnisdottir, S.; Hagen, T.; Kiselyov, A. S.; Stewart, L. J.; Gurney, M. E. *Nat. Biotechnol.* **2010**, *28*, 63–72.
21. Fabbri, L. M.; Beghe, B.; Yasothan, U.; Kirkpatrick, P. *Nat. Rev. Drug Discovery* **2010**, *9*, 761–762.
22. Sowden, M. J.; Sherburn, M. S. *Org. Lett.* **2017**, *19*, 636–637.
23. Shu, W.; Buchwald, S. L. *Chem. Sci.* **2011**, *2*, 2321–2325.
24. Ames, D. E.; Opalko, A. *Tetrahedron* **1984**, *40*, 1919–1925.
25. (a) Mechoulam, R.; Braun, P.; Gaoni, Y. *J. Am. Chem. Soc.* **1972**, *94*, 6159–6165. (b) Hoye, T. R.; Humpal, P. E.; Moon, B. *J. Am. Chem. Soc.* **2000**, *122*, 4982–4983.
26. (a) Wills, M. S. B.; Danheiser, R. L.; *J. Am. Chem. Soc.* **1998**, *120*, 9378–9379. (b) Dunetz, J. R.; Danheiser, R. L.; *J. Am. Chem. Soc.* **2005**, *127*, 5776–5777. (c) Wessig, P.; Müller, G. *Chem. Rev.* **2008**, *108*, 2051–2063. (d) Chinta, B. S.; Baire, B. *Eur. J. Org. Chem.* **2017**, *2017*, 3381–3335.
27. (a) Chinta, B. S.; Baire, B. *Org. Biomol. Chem.* **2017**, *15*, 5908–5911. (b) Chinta, B. S.; Baire, B. *Org. Biomol. Chem.* **2017**, *16*, 262–265.
28. Niu, D.; Willoughby, P. H.; Baire, B.; Woods, B. P.; Hoye, T. R. *Nature* **2013**, *501*, 531–534.
29. A review on the synthesis of fluorenone and fluorene-containing natural products: Shi, Y.; Gao, S. *Tetrahedron* **2016**, *72*, 1717–1735.
30. Hanessian, S.; Pan, J.; Carnell, A.; Bouchard, H.; Lesage, L. *J. Org. Chem.* **1997**, *62*, 465–473.

31. Neises, B.; Steglich, W. *Angew. Chem., Int. Ed.* **1978**, *17*, 522–524.
32. Hayward, C. M.; Yohannes, D.; Danishefsky, S. J. *J. Am. Chem. Soc.* **1993**, *115*, 9345–9346.
33. Vickery, E. H.; Pahler, L. F.; Eisenbraun, E. J. *J. Org. Chem.* **1979**, *44*, 4444–4446.
34. Magano, J.; Chen, M. H.; Clark, J. D.; Nussbaumer, T. *J. Org. Chem.* **2006**, *71*, 7103–7105.
35. Tanaka, T.; Mikamiyama, H.; Maeda, K.; Iwata, C. *J. Org. Chem.* **1998**, *63*, 9782–9793.
36. Karmakar, R.; Yun, S. Y.; Wang, K. P.; Lee, D. *Org. Lett.* **2014**, *16*, 6–9.
37. Hart, H.; Sedor, E. A. *J. Am. Chem. Soc.* **1967**, *89*, 2342–2347.
38. Dong, S.; Paquette, L. A. *J. Org. Chem.* **2005**, *70*, 1580–1596.
39. Müller, S.; Liepold, B.; Roth, G. J.; Bestmann, H. J. *Synlett* **1996**, 521–522.
40. Gu, Z.; Li, Z.; Liu, Z.; Wang, Y.; Liu, C.; Xiang, J. *Catal. Commun.* **2008**, *9*, 2154–2157.

CHAPTER 6

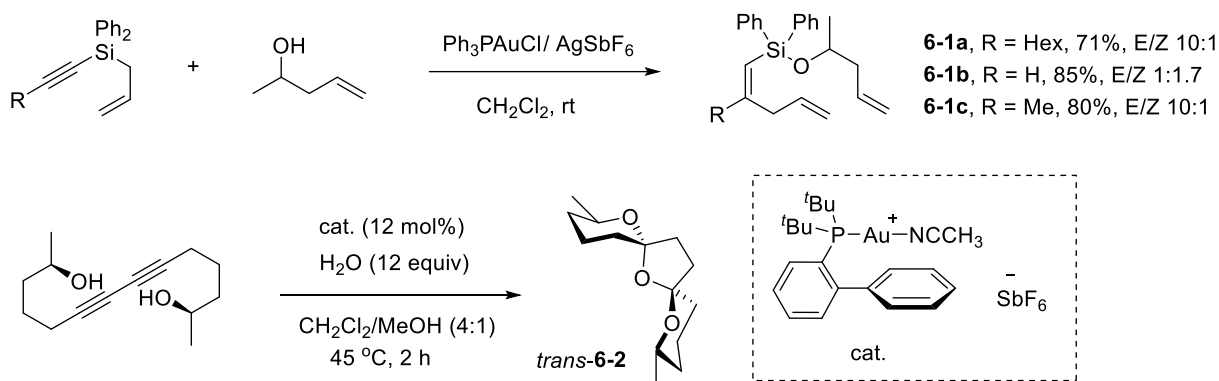
Metal-Catalyzed Reactions of Multiynes

6. Metal-Catalyzed Reactions of Multiynes

The thermal reactions of multiynes involve a wide range of cycloaddition and cyclization reactions that find applications especially in the synthesis of compounds with aromatic rings. One of the most prominent of these is the hexadehydro Diels-Alder reaction, a mild and reagent-free process for aryne generation, that allows for the synthesis of various highly substituted aromatic compounds and the discovery of new aryne chemistry.¹ Transition metal-catalyzed reactions of a multiynes are also versatile tool for the formation of various unsaturated cyclic molecular frameworks. Electrophilic transition metals such as gold and platinum complexes can activate multiynes to form of alkynyl metal carbene species, which can display various metal-carbenoid reactivities including metallotropic shifts and cyclopropanation. Ruthenium-alkylidene complexes serve as powerful initiators for olefin metathesis reactions, which can be extended to tandem metathesis-based processes with multiynes.² The metathesis processes of multiynes find extensive applications in polymer chemistry and total synthesis of natural products. Also, complexes of osmium and ruthenium can interact with multiynes to form unique metallaaromatic complexes.⁴²

6.1. Platinum and Gold-Catalyzed Reaction

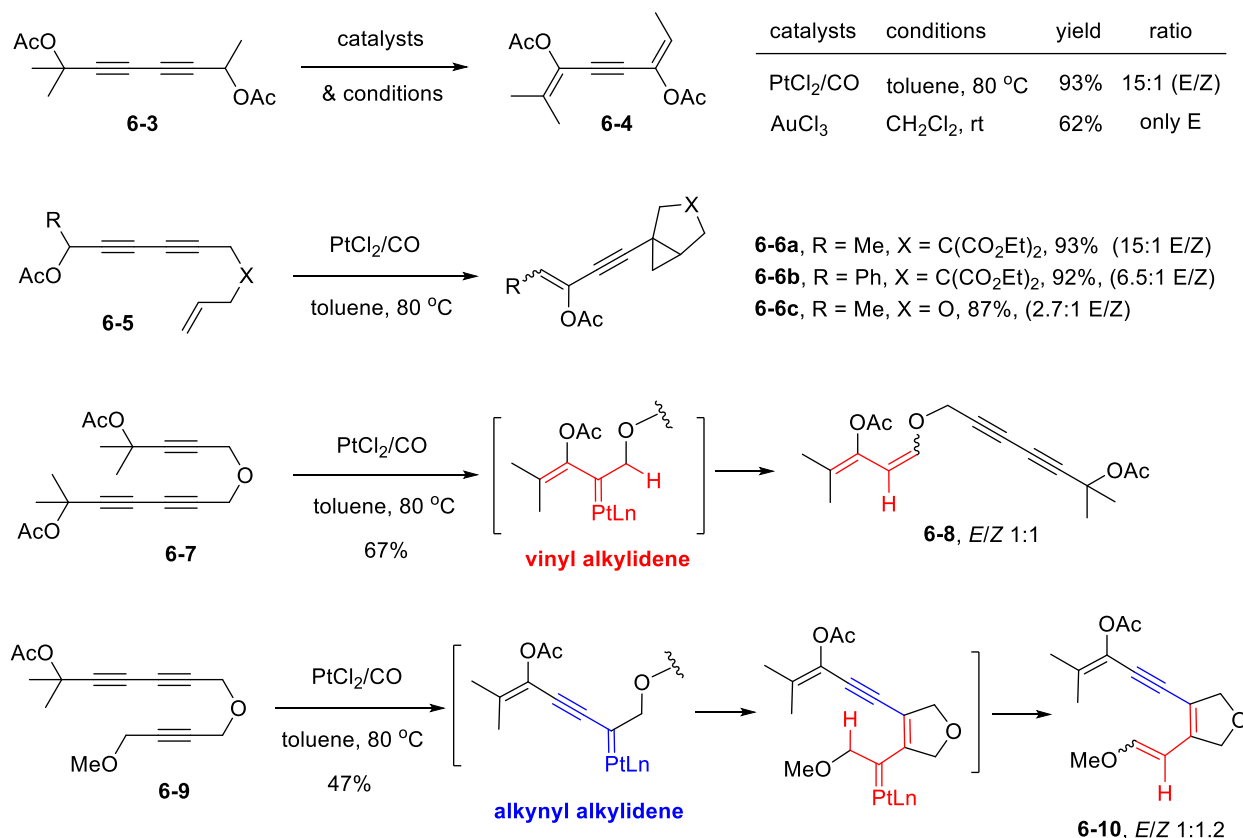
Electrophilic transition metal complexes of Pt and Au interacts with multiynes to promote formation of various cyclic molecular frameworks. The Lee group examined a gold-catalyzed tandem intramolecular



Scheme 6.1. Gold-catalyzed transformations of multiynes

allyl transfer reaction induced by an alcoholysis of allyl silanes, which generates various alkoxy vinyl silanes **6-1a-c** in high *Z/E*-selectivity (**Scheme 6.1**).³ Lee and coworkers demonstrated an efficient one-step synthesis of 5-5-5, 5-5-6 and 6-5-6 bis-spiroketal from 4,6-diyne-1,n-diols and 5,7-diyne-1,n-diols catalyzed by a π -philic Lewis acid ($\text{Ph}_3\text{PAuCl}/\text{AgOTf}$).⁴ Generally, most substrates generate a mixture of *cis*- and *trans*-bis-spiroketal and they can undergo interconversion to reach an equilibrium composition except for **6-2**, which forms exclusively a *trans*-isomer.

The Lee group demonstrated that 1,3-diynes possessing propargylic heteroatom substituents provide functionalized 1,5-dien-3-yne when catalyzed by Pt- and Au-complexes (**Scheme 6.2**).⁵ These transformations involve formation of metal-carbenoid intermediates followed by metallotropic [1,3] shift.



Scheme 6.2. Platinum-catalyzed bond-reorganization of multiynes

While Pt-catalyzed conditions provided higher yield of **6-4** from diyne **6-3** the corresponding Au-catalyzed conditions turned out to be more stereoselective to generate only *E*-isomer (**Scheme 6.2**).⁷ The reaction of 1,3-diyne **6-5** having a tethered alkene on one side is initiated by preferential participation of the acetate to generate a Pt-carbenoid, which undergoes a metallotropic [1,3] shift followed by termination through a cyclopropanation reaction with the alkene, leading to cyclopropane products **6-6a–c**.⁶ While vinyl Pt-carbenoid formed from **6-7** undergo [1,2]-H shift to generate vinyl ether **6-8** an alkynyl Pt-carbenoid formed from **6-9** preferentially undergoes an addition reaction with a tethered alkyne to form a vinyl Pt-carbenoid, which then undergo [1,2]-H shift to generate vinyl ether **6-10**.

6.2. Ruthenium-Catalyzed Reaction: Enyne metathesis

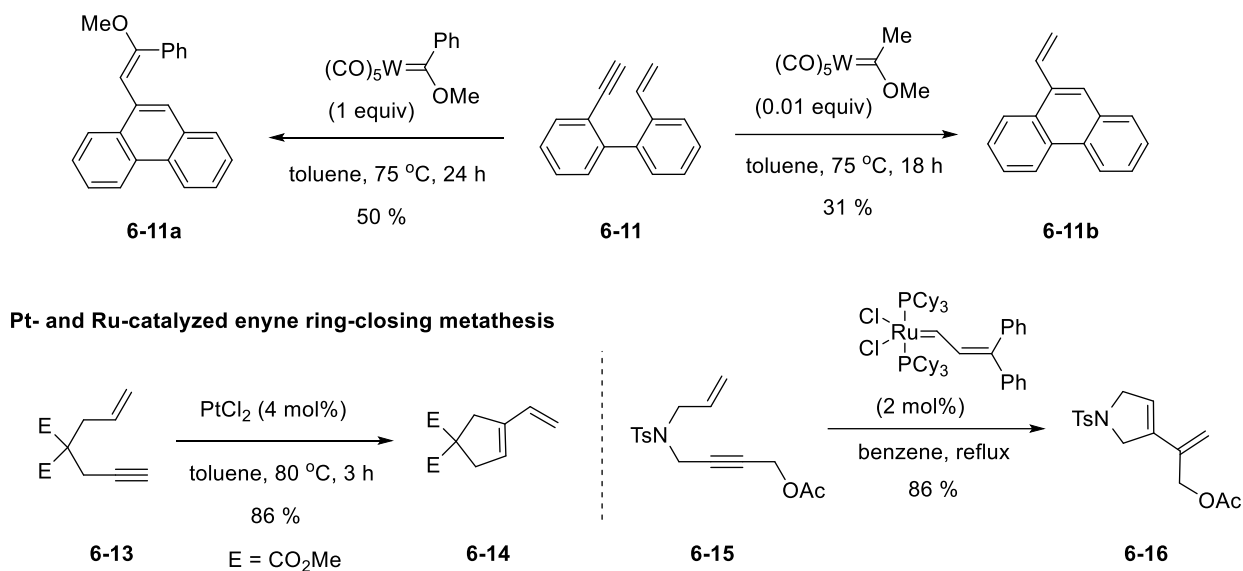
6.2.1. Historical background and mechanisms

Olefin metathesis is a powerful and atom-economical synthetic tool⁸ for the construction of carbon–carbon double bond and its paramount impacts in many areas of research in academia and industry⁹ have been recognized by the 2005 Nobel Prize. In 1971, Chauvin proposed a mechanism for the olefin metathesis process in which a propagating metal-carbene species reacts with an alkene via [2+2] cycloaddition to form metallacyclobutane intermediate.¹⁰ After this proposal, extensive investigations have been devoted to the developments of catalytically active metathesis initiators, and the first major breakthroughs came in the early 1990s from the groups of Schrock¹¹ and Grubbs¹² that independently developed the molybdenum and ruthenium-based metathesis initiators, respectively. Depending on the type of π -systems involved in the events of metathesis, it can be classified into three major categories: diene, enyne, and diyne metathesis.¹³ Based on the structural change involved in the metathesis process, these metathesis events are further categorized into different classes and the most general three major classes are cross metathesis (CM)¹⁴, ring-closing metathesis (RCM)¹⁵, and ring-opening metathesis (ROM)¹⁶.

Among diene, enyne, and diyne metathesis, enyne metathesis is the most atom-economical process that can generate conjugated 1,3-diene via a formal addition reaction between an alkene and alkyne in both inter and intramolecular manners.¹⁷ In 1985 Katz and coworkers reported the first example of enyne ring-

closing metathesis in the presence of two different Fischer-type tungsten complexes (**Scheme 6.3**).¹⁸ In this intramolecular enyne metathesis, enyne **6-11** was converted to compounds **6-11a** in the presence of stoichiometric whereas **6-11b** was generated with a catalytic amount of a closely related tungsten complex. The proposed mechanism involves a metallocyclobutene formation from the alkyne and the tungsten-carbene complex followed by its subsequent metathesis with the vinyl group.

Examples of early enyne metathesis

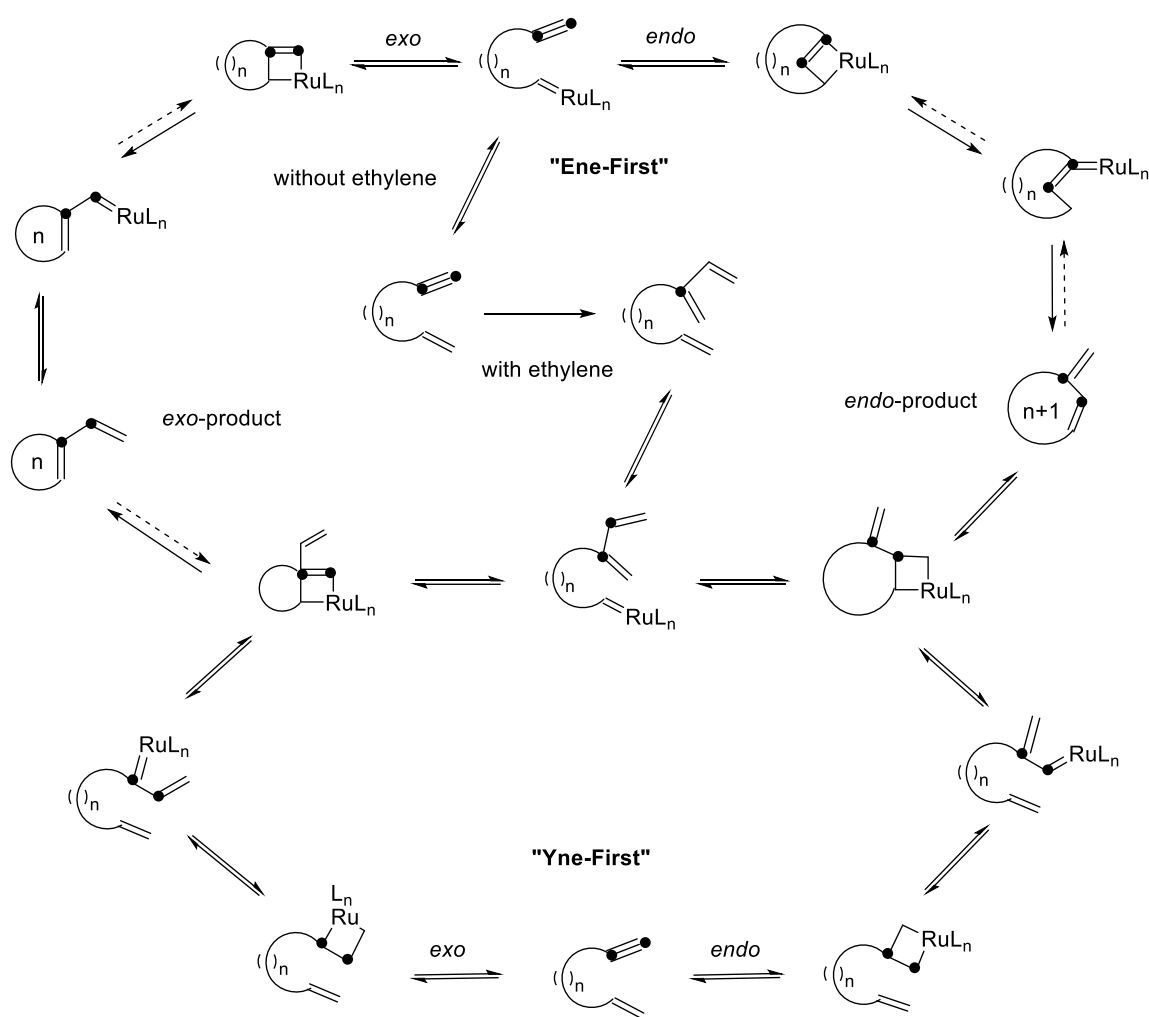


Scheme 6.3. Earlier reports on enyne metathesis

Murai reported a platinum-catalyzed enyne ring-closing metathesis. In this study, the 1,6-enyne **6-13** was treated with a catalytic amount of PtCl_2 to generate 1-vinylcyclopentene **6-14** in high yield. The suggested mechanism for this transformation involves non-classical carbocations.¹⁹ The first ruthenium-catalyzed enyne metathesis was reported by Mori and Kinoshita.²⁰ Enyne **6-15** upon treatment with a catalytic amount of ruthenium-alkylidene complex (2 mol%) efficiently provided diene **6-16** in 86% yield.

Compared to the ring-closing metathesis of dienes and diynes, which generate only one product regardless of the initiation events, ring-closing metathesis of enynes potentially lead to two different products through three different initiation events of “Ene-First” and “Yne-First” pathways (**Scheme 6.4**). Although these pathways involve unique propagating alkylidene species, only two distinct RCM products

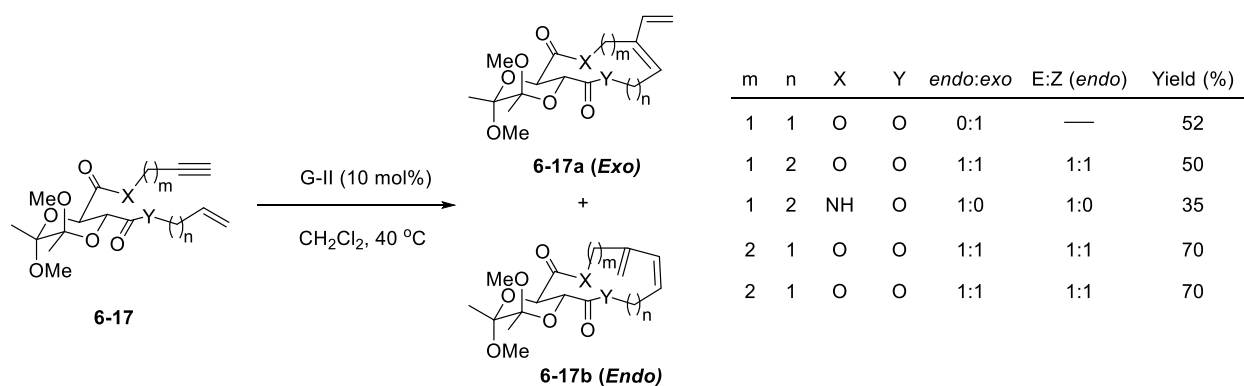
are observed (1,2-substituted or 1,3-substituted dienes) via isomeric vinyl ruthenium alkylidene intermediates. Mori and coworkers observed the formation of *endo*-RCM products when disubstituted alkenes are present in the substrate.²¹ Hoveyda and coworkers also demonstrated that enyne metathesis catalyzed by group VI metals (W, Mo) generally initiates at the alkyne counterpart. Although computational studies did not show any preference for either “Ene-First” and “Yne-First” mechanism, yet it showed the preferential formation of either *endo*- or *exo*-product depending on the nature of substituents.²²



Scheme 6.4. Possible mechanism for enyne RCM

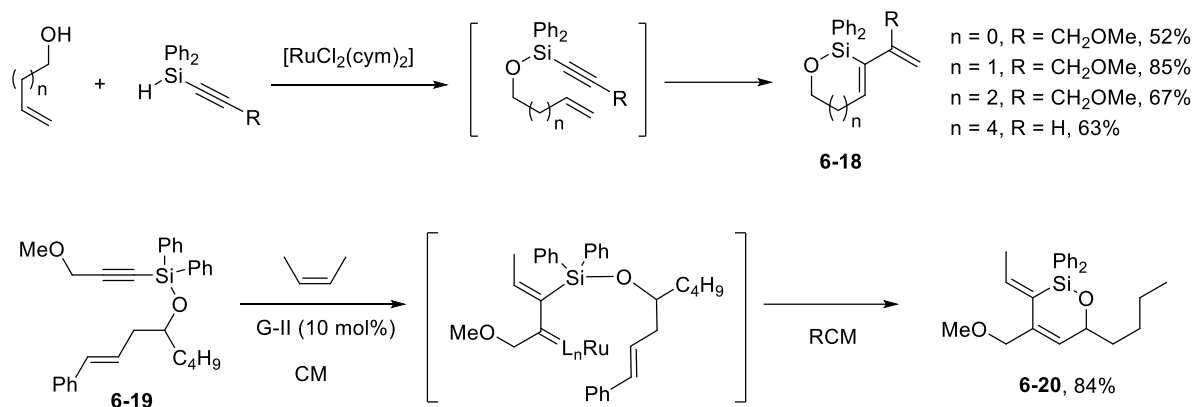
6.2.2. *Exo/endo*-mode selectivity

Lee and Hansen carried out extensive studies to probe into the *exo/endo*-mode selectivity for enyne metathesis. The definition of *exo/endo*-mode is based on the position of the carbon–carbon bond derived from the triple bond of the alkyne in the final product. Thus, an *exo*-mode RCM gives a product where the original C–C bond is in an exocyclic position, whereas an *endo*-mode RCM gives a product with the original C–C bond in an endocyclic position. Consequently, the ring formed from an *endo*-mode cyclization is one-carbon larger than the corresponding *exo*-mode products. Previous studies indicates that the *exo/endo*-mode selectivity depends on the ring size; for example, small- to medium-sized rings (6-9-membered rings) are formed via *exo*-mode ring closure²³ whereas larger rings are formed via *endo*-mode ring closure.²⁴ To study the general selectivity feature, Lee and Hansen studied the macrocyclic enyne metathesis to form 10–15-membered rings using tartarate-tethered enynes (**Scheme 6.5**).²⁵ It was observed that for the formation of 10-membered ring the *exo*-mode was favored exclusively. For an 11-membered ring, a 1:1 mixture of products were generated through both the *exo*- and the *endo*-mode closure. For 12- to 15-membered rings, the reaction occurred exclusively through the *endo*-mode. The selectivity also depends on the nature of the tether. For instance, an amide tether in the enyne substrate provided an 11-membered ring with exclusive *endo*-selectivity. Under ethylene atmosphere, however, the substrates that inherently form *exo*-products was diverted to react through the *endo*-mode.



Scheme 6.5. *Exo/endo*-mode selectivity in the enyne RCM of tartrate-tethered enynes

Lee and coworkers also developed silicon-tethered enyne metathesis substrates that display exclusive *exo*-mode selectivity. For this system, the *endo*-mode RCM is disfavored due to the formation of the sterically hindered silicon-substituted alkylidene intermediate. Various silyloxy-tethered enynes obtained from $[\text{RuCl}_2(p\text{-cymene})]_2$ -catalyzed silylation of alcohols with alkynyl silanes underwent smooth enyne RCM to generate products **6-18** possessing *Z*-stereochemistry of the endocyclic double-bonds regardless of the tether size.²⁶ The reactivity of this silicon-tethered system could be modulated to give *endo*-mode product through a tandem CM/RCM procedure. For example, the silyloxy-tethered enyne **6-19** undergoes CM in the presence of *cis*-butene to form a ruthenium alkylidene intermediate that undergoes RCM to form **6-20** in 84 % (Scheme 6.6).²⁷

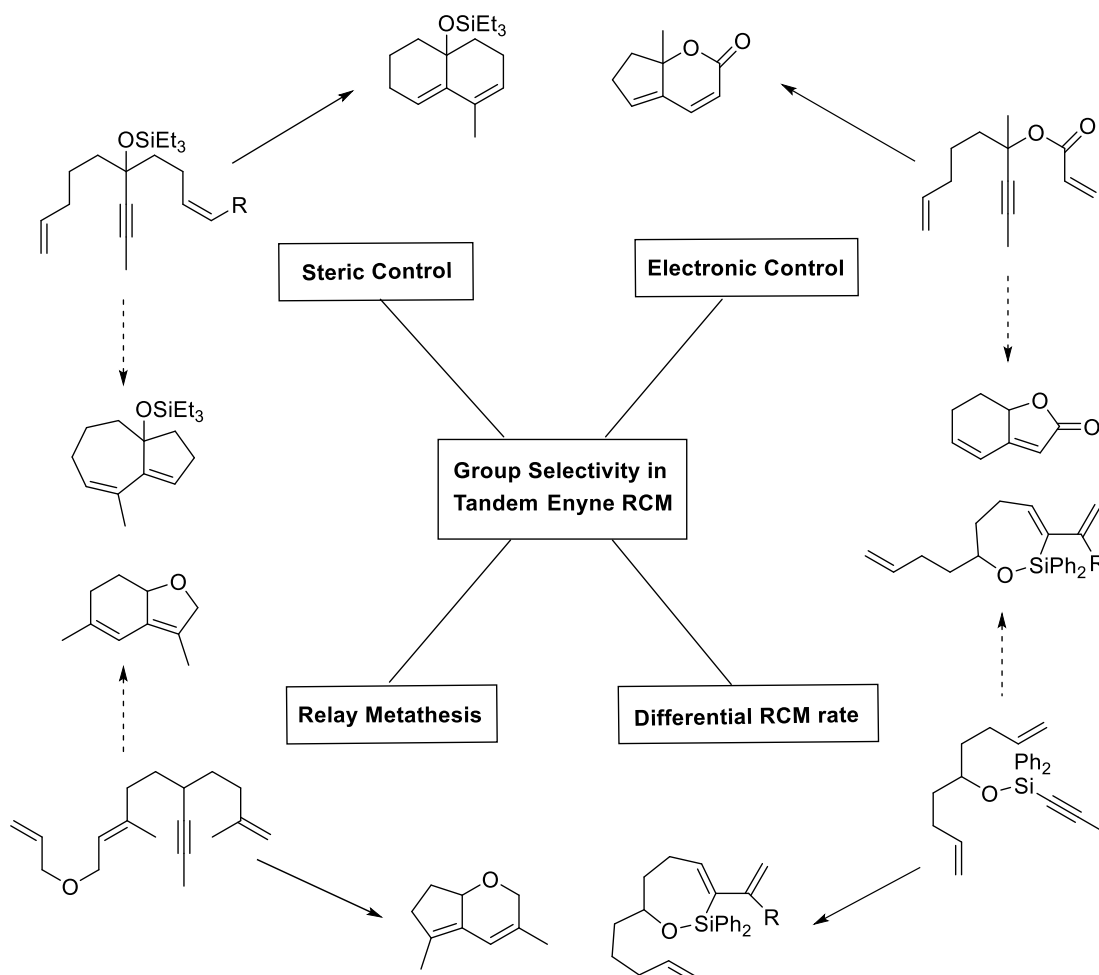


Scheme 6.6. *Exo/endo*-mode selectivity in the RCM with silicon-tethered enynes

6.2.3. Group selectivity in tandem enyne metathesis

Group-selective transformations break local or molecular symmetry by the selective conversion of one of the enantiotopic or diastereotopic functionalities.²⁸ Relying on the reversible nature of the diene metathesis process, several examples of group-selective metathesis reactions have been reported.²⁹ On the other hand, not all steps of enyne metathesis are reversible, therefore the selectivity might depend on the site of initiation. In the case of dienynes, differentiation of two alkenyl groups in similar steric and electronic environments is difficult. To overcome this difficulty several strategies are implemented relying on steric bulk, electronic variation, relay metathesis, and ring-closure kinetics to exert control over the reaction

pathways.³⁰ Group selective tandem enyne RCM relies on controlling the site of initiation by modifying the reactivity of the alkene or alkyne moieties with steric and stereoelectronic factors.³¹ Although the introduction of the biasing elements is proven successful in many cases, it might reduce the reaction scope because extra efforts are need to install the biasing elements (**Scheme 6.7**).



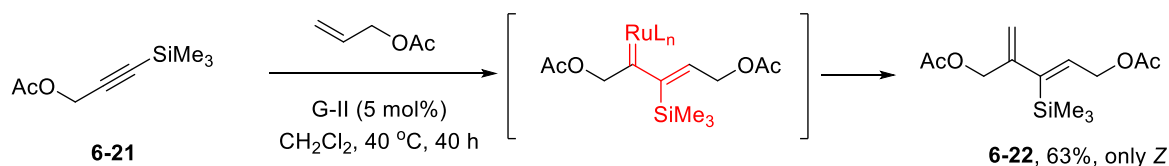
Scheme 6.7. Group selectivity in tandem enyne metathesis

6.2.4. Enyne cross metathesis

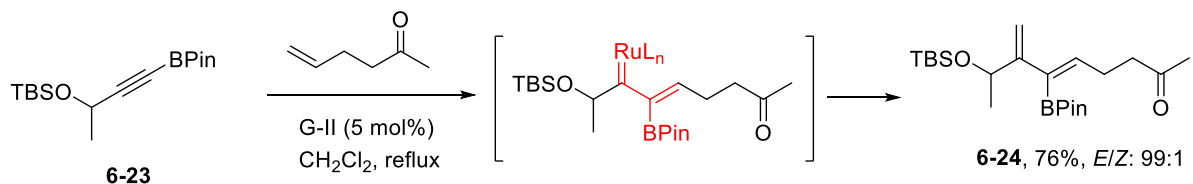
Application of enyne CM has been limited due to its poor regio- and stereoselectivity. The issue of chemoselectivity due to competition between homo- and hetero-coupled products further complicated the enyne CM. This problem could be overcome by confining the reaction pairs to an internal alkyne and

terminal alkenes.³² The Lee group envisioned implementing the known steric and stereoelectronic biasing effect of silyl functionality in RCM reactions to the corresponding CM of silylated alkynes. It was observed that TMS-substituted alkyne **6-21** underwent enyne CM with allyl acetate to form diene product **6-22** as an exclusive *Z*-isomer although the reaction takes a very long time of 40 h (**Scheme 6.8**).³³ A strong directing effect of boronate can be also implemented for a general and stereocontrolled synthesis of vinyl boronates.

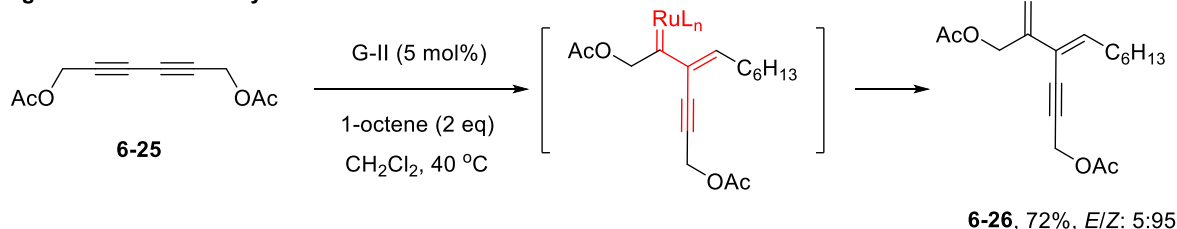
Z-selectivity in Silylated Alkynes



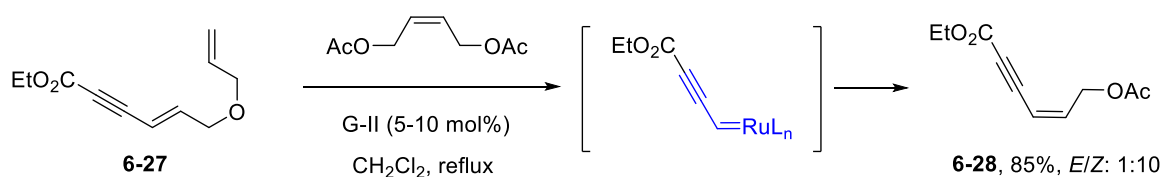
E-selectivity in Borylated Alkynes



Regioselective CM of Diynes



Relay CM of Conjugated Enynes



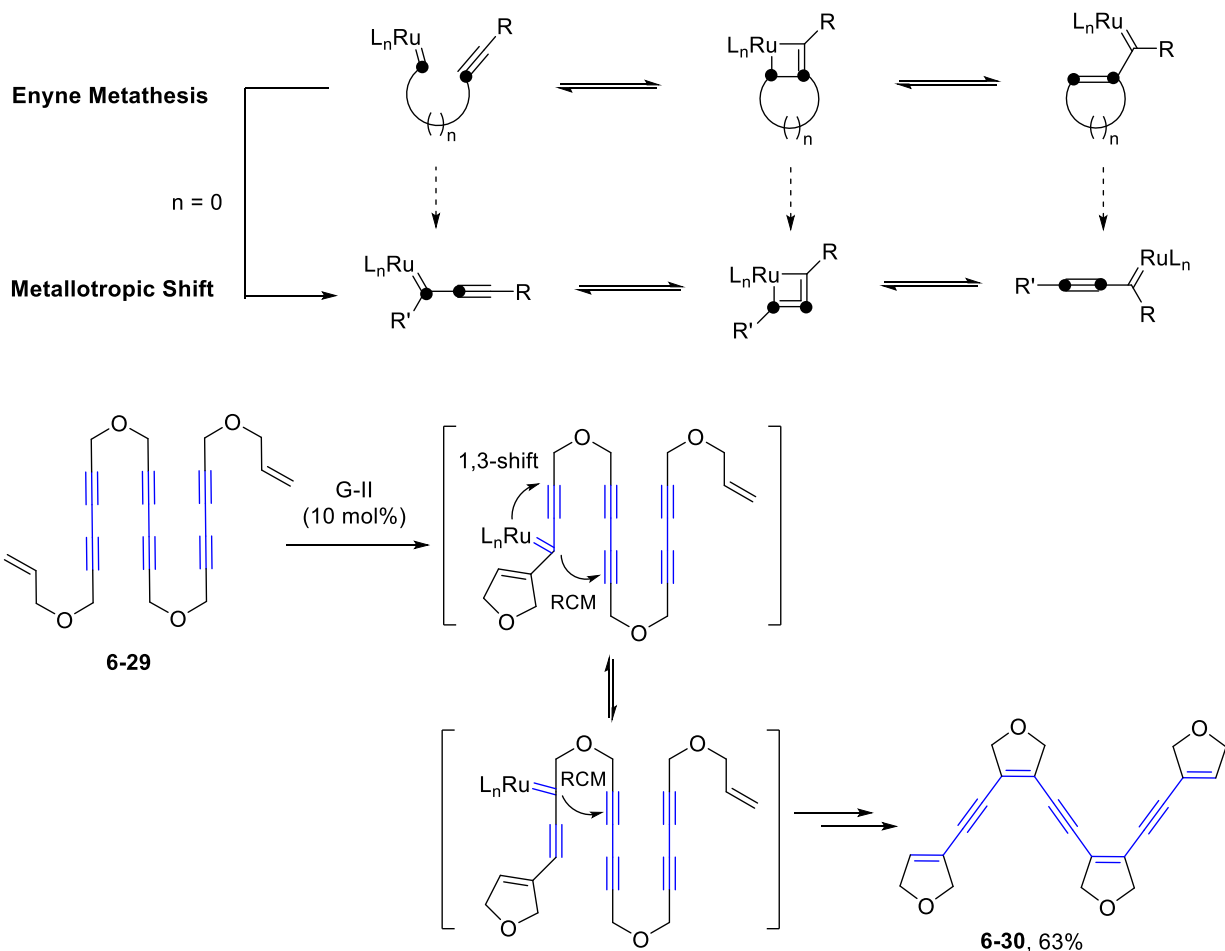
Scheme 6.8. Regio- and stereoselectivity in enyne cross metathesis

The CM between a borylated alkyne **6-23** and hex-5-en-2-one proceeds smoothly to form vinyl boronate **6-24** with high *E*-selectivity.³⁴ The stereoselectivity depends mainly on the nature of the alkene and in some

cases favors *Z*-selectivity. In a similar manner as silyl and boryl substituents, an alkynyl substituent can also help in controlling the regio- and stereoselectivity in enyne CM reactions. Thus, diyne **6-25** undergoes enyne CM smoothly with 1-octene to generate the 1,3-diene **6-26** in high yield and *Z*-selectivity.³⁵ A relay metathesis strategy was implemented to achieve the desired site selectivity in the CM of conjugated enynes. For example, enyne **6-27** containing a relay-tether generated the conjugated alkynyl alkylidene after the extrusion of dihydrofuran, which then undergoes CM with the external alkene to form the product **6-28** in high yield and as a 1:20 *E/Z* mixture.³⁶

6.2.5. Metallotropic [1,3]-shift

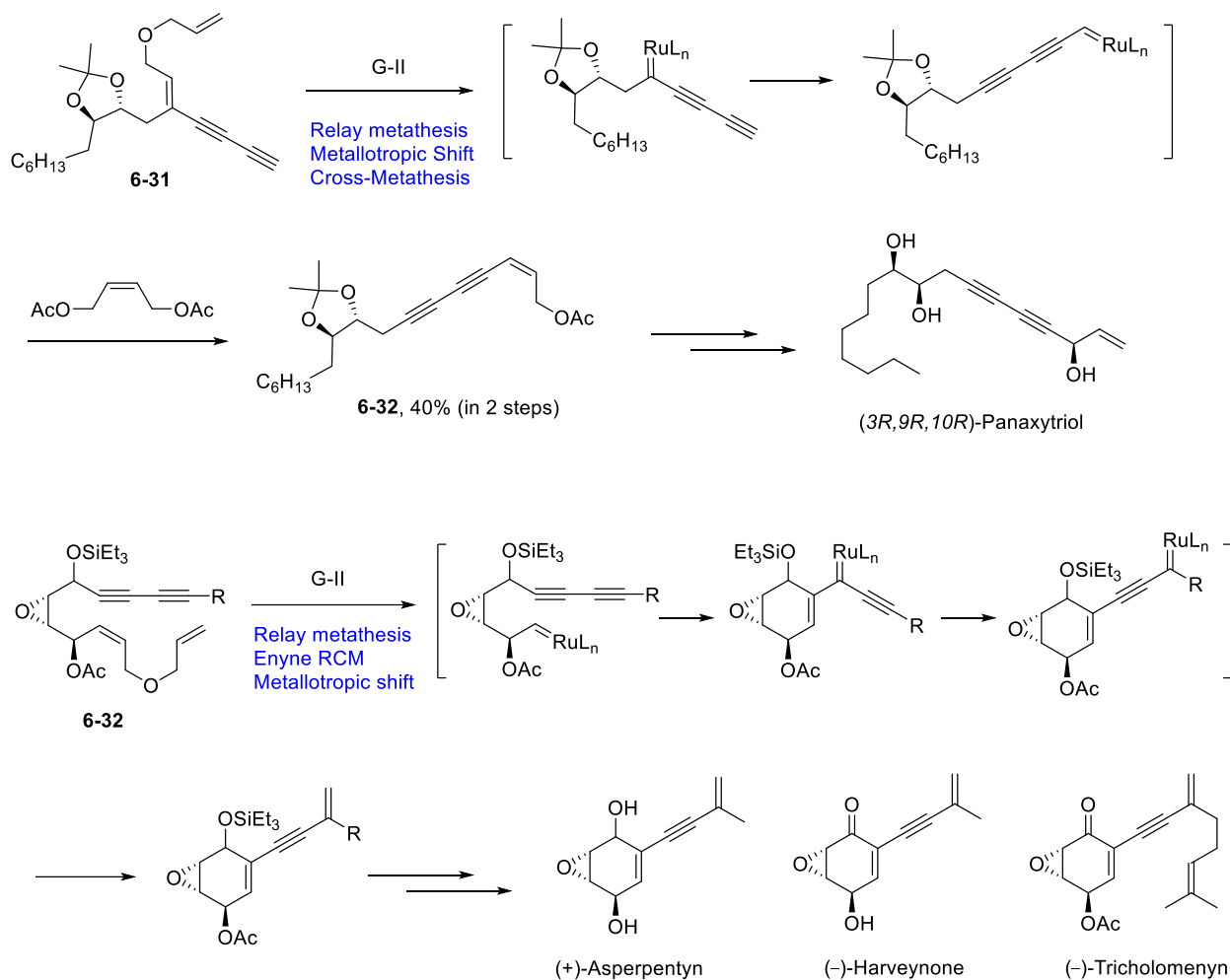
Alkynyl carbenes are known to undergo bond rearrangement/ shift to generate an isomeric carbene intermediate for a long time. The development of transition metal-based strategies provided easy access to alkynyl metal carbenes and permitted the study of this unique carbene [1,3]-shift across triple bonds which is termed as metallotropic [1,3]-shift. This phenomenon is often encountered in the enyne metathesis of multiynes which affects the structure of the product formed. Conceptually, metallotropic [1,3]-shift is closely related to enyne metathesis. If the tether length between the ruthenium alkylidene-carbene and the alkyne in an enyne metathesis is reduced to zero we end up with an alkynyl ruthenium carbene intermediate which can undergo [1,3]-shift across the triple bonds through a mechanistically related process (**Scheme 6.9**).³⁷ In the case of multiynes the RCM event is generally followed by metallotropic [1,3]-shift leading to the formation of interesting products. Lee and Kim designed a substrate **6-29** that can undergo repetitive ring-closing metathesis–metallotropic [1,3]-shift (M & M) process, which leads to the formation of oligoenyne **6-30** in 63% yield. This method was powerful enough to synthesize a wide variety of oligoenynes and can remarkably form a maximum of five new triple bonds and four new double bonds in a single operation.³⁸



Scheme 6.9. Metathesis and metallotropic [1,3]-shift

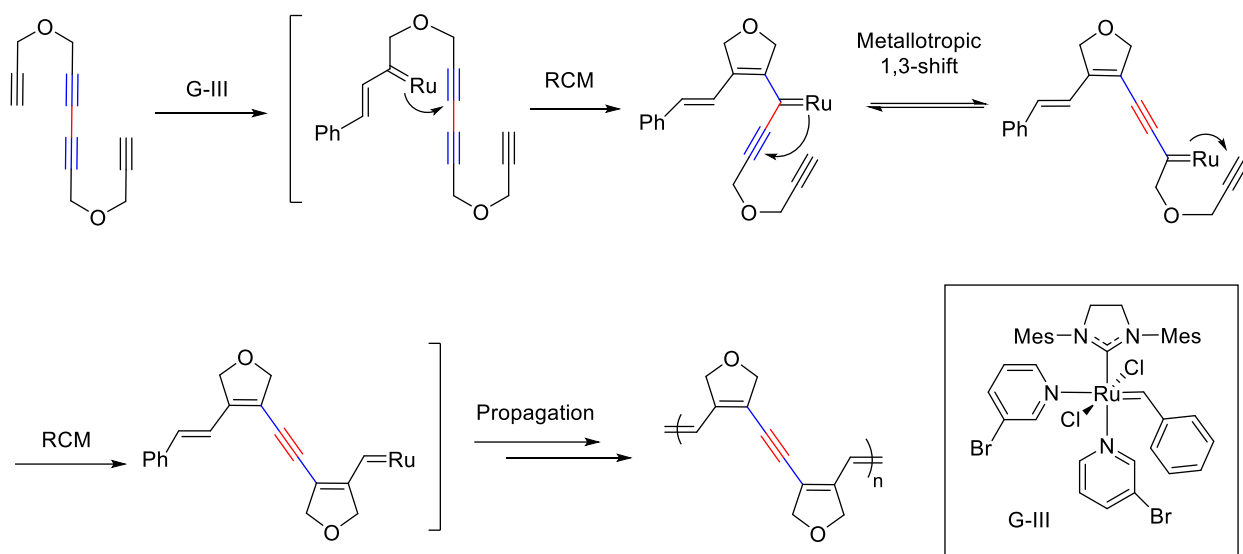
6.3. Metathesis and Metallotropy: Applications in Total Synthesis and Polymer Chemistry

The combination of metathesis and metallotropy (M & M) has been used in the total synthesis of various natural products. Lee and coworkers applied this strategy for the total synthesis of (3*R*,9*R*,10*R*)-panaxytriol (**Scheme 6.10**).³⁹ The key step involves a tandem relay metathesis, metallotropic shift, and cross-metathesis sequence with diyne **6-31** to form compound **6-32**. Compound **6-32** could be further converted to the target molecule after standard reaction sequences. The Lee group also demonstrated the utility of the tandem sequence in the synthesis of (+)-asperpentyn, (–)-harveynone, and (–)-tricholomenyn from the intermediate **6-32** initiated by relay metathesis.⁴⁰



Scheme 6.10. Metathesis and metallotropy – applications in total synthesis

Recently, Choi and coworkers applied the M & M strategy to the synthesis of novel conjugated polymers. Polymerization of 1,3-diyne-containing tetrayne monomers with a Ru-based initiator provided well-defined polyenynes via sequential cascade M & M polymerization (**Scheme 6.11**).⁴¹ The reaction was smoothly catalyzed by the Grubbs third-generation complex that has been extensively exploited for metathesis polymerization reactions. Even exotic monomers such as hexaynes effectively underwent living cascade polymerization via five independent sequences of the intramolecular transformations to give new conjugated polyenynes consisting of four double bonds and two triple bonds in the repeat unit.



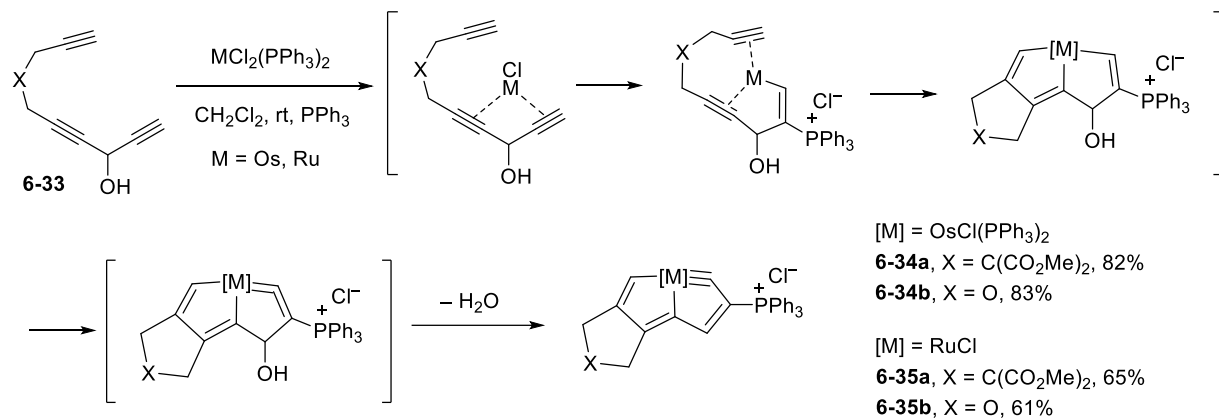
Scheme 6.11. Metathesis and metallotropy – applications in polymer chemistry

6.4. Metal Complexes with Multiynes

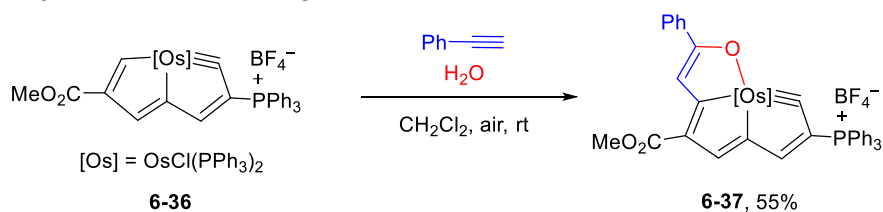
The formation of metal–carbon bonds is one of the most important issues in organometallic chemistry. Chelation of a polydentate ligand to a metal via several metal–carbon bonds is rare. In metallabenzenes or metallabenzynes, metals are coordinated through two metal–carbon bonds. With the recent development in metallaaromatics, it is possible to achieve polydentate chelation (**Scheme 6.12**).⁴² For example, triyne **6-33** reacts with the commercially available osmium complex $\text{OsCl}_2(\text{PPh}_3)_3$ and PPh_3 at room temperature in air to form osmapentalyne **6-34a, b** in high yield.⁴³ Similar reactivity is observed with $\text{RuCl}_2(\text{PPh}_3)_2$ which leads to the formation of a ruthenapentalyne **6-35a, b**.⁴⁴ Metallapentalyne can be viewed as a 7-carbon (7C) chain coordinated to a metal via three metal–carbon bonds. Although metallapentalynes contain a metal–carbon triple bond in a five-membered ring with the bond angle around the carbyne carbon is only 129.5° they exhibit excellent stability to air, moisture, and heat. Further increase in the number of bonds coordinated with the metal center could be achieved by synthesis of tricyclic and tetracyclic metallaaromatic frameworks. Osmapentalyne **6-36** can react with phenyl acetylene and water at

room temperature under air to generate α -metallapentalenofuran **6-37** where the osmium center is shared

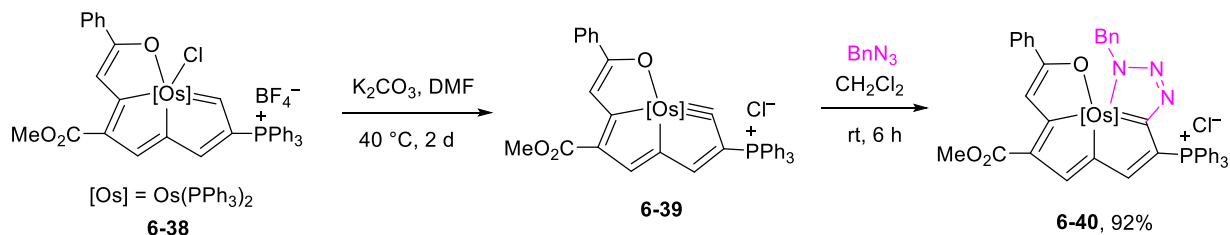
Metallapetalyne



Tricyclic Aromatics with Bridged Metal



Tetracyclic Aromatics with Bridged Metal



Scheme 6.12. Metal complexes with multiynes

by three-fused five-membered rings with a seven-coordinated pentagonal bipyramidal geometry.⁴⁵ Tricyclic complex **6-38** can be converted to α -metallapentalenofuran **6-39**, which undergoes a novel metallaclick reaction with benzyl azide to form a tetracyclic metallaaromatic complex **6-40**.⁴⁶

6.5. Summary

In summary, various transition metal complexes show their unique reactivity with multiynes to form various cyclic unsaturated frameworks. For instance, electrophilic transition metal complexes of platinum and gold can react with multiynes to form alkynyl metal-carbene species, which can provide various products derived from characteristic metal-carbenoid reactivity. Enyne metathesis is a prominent metathesis event that is usually catalyzed by ruthenium alkylidene-carbene to form 1,3-dienes. Enyne metathesis of multiynes provides a powerful tool to address various reactivity and selectivity problems including *exo/endo* mode selectivity, group selectivity, and regio- and stereoselectivity. The sequential metathesis process combined with metallotropy has a tremendous application potential for the efficient preparation of oligoenynes, total synthesis of natural products, and polymer chemistry. Metal complexes of osmium and ruthenium react with multiynes to form unique metallaaromatic complexes with polydentate metal chelation.

6.6. References

1. (a) Diamond, O. J.; Marder, T. B. *Org. Chem. Front.* **2017**, *4*, 891. (b) Fluegel, L. L.; Hoye, T. R. *Chem. Rev.* **2021**, *121*, 2413.
2. (a) Vougioukalakis, G. C.; Grubbs, R. H. *Chem. Rev.* **2010**, *110*, 1746. (b) Ogba, O. M.; Warner, N. C.; O'Leary, D. J.; Grubbs, R. H. *Chem. Soc. Rev.* **2018**, *47*, 4510.
3. Park, S.; Lee, D. *J. Am. Chem. Soc.* **2006**, *128*, 10664.
4. Volchkov, I.; Sharma, K.; Cho, E. J.; Lee, D. *Chem. Asian J.* **2011**, *6*, 1961.
5. Cho, E. J.; Kim, M.; Lee, D. *Eur. J. Org. Chem.* **2006**, *2006*, 3074.
6. Cho, E. J.; Kim, M.; Lee, D. *Org. Lett.* **2006**, *8*, 5413.
7. (a) Cho, E. J.; Lee, D. *Adv. Synth. Cat.* **2008**, *350*, 2719. (b) Huang, G.; Xie, K.; Lee, D.; Xia, Y. *Org. Lett.* **2012**, *14*, 3850.
8. (a) Fürstner, A. *Angew. Chem., Int. Ed.* **2000**, *39*, 3012. (b) Fürstner, A. *Science* **2013**, *341*, 1229713. (c) Hoveyda, A. H.; Zhugralin, A. R. *Nature* **2007**, *450*, 243.
9. (a) Mol, J. C. *J. Mol. Catal. A: Chem.* **2004**, *213*, 39. (b) Grubbs, R. H. *Angew. Chem., Int. Ed.* **2006**, *45*, 3760. (c) Clavier, H.; Grela, K.; Kirschning, A.; Mauduit, M.; Nolan, S. P. *Angew. Chem., Int. Ed.* **2007**, *46*, 6786. (d) Higman, C. S.; Lummiss, J. A. M.; Fogg, D. E. *Angew. Chem., Int. Ed.* **2016**, *55*, 3552.
10. Hérisson, J.-L.; Chauvin, Y. *Makromol. Chem.* **1971**, *141*, 161.
11. Bazan, G. C.; Oskam, J. H.; Cho, H.-N.; Park, L. Y.; Schrock, R. R. *J. Am. Chem. Soc.* **1991**, *113*, 6899.
12. Nguyen, S. T.; Johnson, L. K.; Grubbs, R. H.; Ziller, J. W. *J. Am. Chem. Soc.* **1992**, *114*, 3974.
13. Grubbs, R. H., Ed. *Handbook of Metathesis*; Wiley-VCH: Weinheim, Germany, 2003.

14. (a) Chatterjee, A. K.; Morgan, J. P.; Scholl, M.; Grubbs, R. H. *J. Am. Chem. Soc.* **2000**, *122*, 3783. (b) Chatterjee, A. K.; Choi, T. L.; Sanders, D. P.; Grubbs, R. H. *J. Am. Chem. Soc.* **2003**, *125*, 11360.
15. (a) Grubbs, R. H.; Miller, S. J.; Fu, G. C. *Acc. Chem. Res.* **1995**, *28*, 446. (b) Deiters, A.; Martin, S. F. *Chem. Rev.* **2004**, *104*, 2199.
16. (a) Bielawski, C. W.; Grubbs, R. H. *Angew. Chem., Int. Ed.* **2000**, *39*, 2903. (b) Slugovc, C. *Macromol. Rapid Commun.* **2004**, *25*, 1283. (c) Bielawski, C. W.; Grubbs, R. H. *Prog. Polym. Sci.* **2007**, *32*, 1.
17. (a) Diver, S. T.; Giessert, A. J. *Chem. Rev.* **2004**, *104*, 1317. (b) Diver, S. T. *Coord. Chem. Rev.* **2007**, *251*, 671. (c) Hansen, E. C.; Lee, D. *Acc. Chem. Res.* **2006**, *39*, 509.
18. (a) Katz, T. J.; Sivavec, T. M. *Tetrahedron Lett.* **1985**, *26*, 2159. (b) Katz, T. J.; Sivavec, T. M. *J. Am. Chem. Soc.* **1985**, *107*, 737.
19. (a) Chatani, N.; Furukawa, N.; Sakurai, H.; Murai, S. *Organometallics* **1996**, *15*, 901. (b) Fürstner, A.; Szillat, H.; Gabor, B.; Mynott, R. *J. Am. Chem. Soc.* **1998**, *120*, 8305.
20. Kinoshita, A.; Mori, M. *Synlett* **1994**, 1020.
21. (a) Kitamura, T.; Sato, Y.; Mori, M. *Chem. Commun.* **2001**, 1258. (b) Kitamura, T.; Sato, Y.; Mori, M. *Adv. Synth. Catal.* **2002**, *344*, 678.
22. For a recent mechanistic study of enyne metathesis, see: (a) Lippsteau, J. J.; Straub, B. F.; *J. Am. Chem. Soc.* **2005**, *127*, 7444. (b) Galan, B. R.; Giessert, A. J.; Keister, J. B.; Diver, S. T. *J. Am. Chem. Soc.* **2005**, *127*, 5762. (c) Giessert, A. J.; Diver, S. T. *Org. Lett.* **2005**, *7*, 351. (d) Lloyd-Jones, G. C.; Margue, R. G.; de Vries, J. G. *Angew. Chem., Int. Ed.* **2005**, *44*, 7442. (e) Dieltiens, N.; Moonen, K.; Stevens, C. V. *Chem. Eur. J.* **2007**, *13*, 203. (f) Marshall, J. E.; Keister,

- J. B.; Diver, S. T. *Organometallics* **2011**, *30*, 1319. (g) NuÇez-Zarur, F.; Solans-Monfort, X.; Rodriguez-Santiago, L.; Pleixats *Chem. Eur. J.* **2011**, *17*, 7506.
23. Kitamura, T.; Sato, Y.; Mori, M. *Adv. Synth. Catal.* **2002**, *344*, 678.
24. Morales, C. A.; Layton, M. E.; Shair, M. D. *Proc. Natl. Acad. Sci. U.S.A.* **2004**, *101*, 12036.
25. Hansen, E.; Lee, D. *J. Am. Chem. Soc.* **2004**, *126*, 15074.
26. Miller, R. L.; Maifeld, S. V.; Lee, D. *Org. Lett.* **2004**, *6*, 2773.
27. Park, S.; Kim, M.; Lee, D. *J. Am. Chem. Soc.* **2005**, *127*, 9410.
28. Hoffmann, R. W. *Synthesis* **2004**, 2075. (b) Magnuson, S. *Tetrahedron* **1995**, *51*, 2167.
29. Lautens, M.; Hughes, G. *Angew. Chem., Int. Ed.* **1999**, *38*, 129.
30. Maifeld, S. A.; Lee, D. *Chem.–Eur. J.* **2005**, *11*, 6118.
31. Grubbs, R. H.; Bowden, N. B.; Zuercher, W. J.; Kim, S.-H. *J. Org. Chem.* **1996**, *61*, 1073.
32. Stragies, R.; Schuster, M.; Blechert, S. *Angew. Chem., Int. Ed.* **1997**, *36*, 2518.
33. Kim, M.; Park, S.; Maifeld, S. A.; Lee, D. *J. Am. Chem. Soc.* **2004**, *126*, 10242.
34. Kim, M.; Lee, D. *Org. Lett.* **2005**, *7*, 1865.
35. Kim, M.; Miller, R. L.; Lee, D. *J. Am. Chem. Soc.* **2005**, *127*, 12818.
36. Hansen, E.; Lee, D. *Org. Lett.* **2004**, *6*, 2035.
37. Lee, D., & Kim, M. *Org. Biomol. Chem.* **2007**, *5*, 3418.
38. Kim, M.; Lee, D. *J. Am. Chem. Soc.* **2005**, *127*, 18024.
39. Cho, E. J.; Lee, D. *Org. Lett.* **2008**, *10*, 257.
40. Li, J.; Park, S.; Miller, R. L.; Lee, D. *Org. Lett.* **2009**, *11*, 571.

41. Kang, C.; Kwon, S.; Sung, J. C.; Kim, J.; Baik, M. H.; Choi, T. L. *J. Am. Chem. Soc.* **2018**, *140*, 16320.
42. Zhu, C.; Xia, H. *Acc. Chem. Res.* **2018**, *51*, 1691.
43. Zhuo, Q.; Lin, J.; Hua, Y.; Zhou, X.; Shao, Y.; Chen, S.; Chen, Z.; Zhu, J.; Zhang, H.; Xia, H. *Nat. Commun.* **2017**, *8*, 1912.
44. Zhuo, Q.; Zhang, H.; Hua, Y.; Kang, H.; Zhou, X.; Lin, X.; Chen, Z.; Lin, J.; Zhuo, K.; Xia, H. *Sci. Adv.* **2018**, *4*, eaat0336.
45. Lu, Z.; Zhu, C.; Cai, Y.; Zhu, J.; Hua, Y.; Chen, Z.; Chen, J.; Xia, H. *Chem.–Eur. J.* **2017**, *23*, 6426.
46. Lu, Z.; Zhu, Q.; Cai, Y.; Chen, Z.; Zhuo, K.; Zhu, J.; Zhang, H.; Xia, H. *Sci. Adv.* **2020**, *6*, eaay2535.

CHAPTER 7

Alkene-Chelated Ruthenium Alkylidenes: A Missing Link to New Catalysts

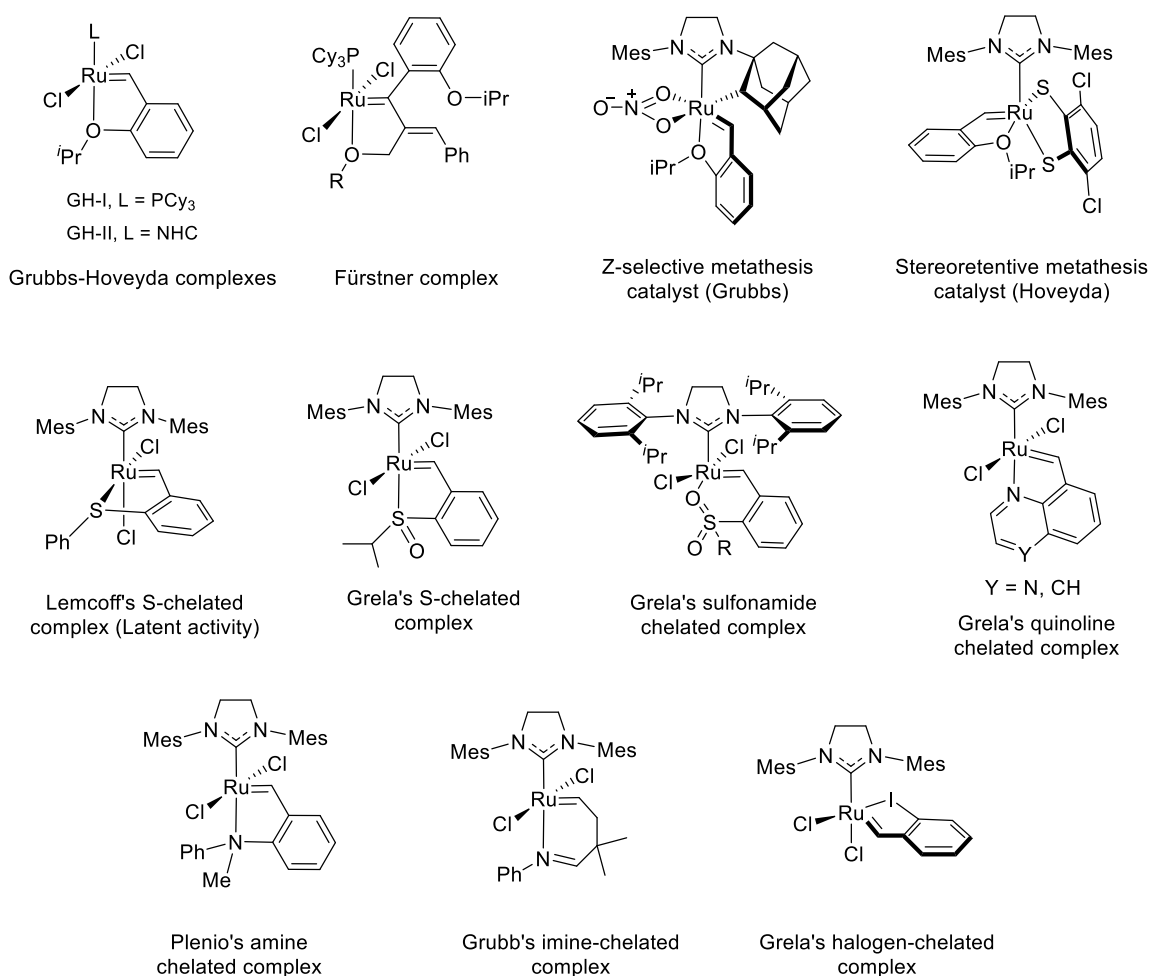
7.1. Introduction*

Olefin metathesis is a powerful and atom-economical synthetic tool¹ for the construction of carbon–carbon double bond and its paramount impacts in many areas of research in academia and industry² have been recognized by the 2005 Nobel Prize. The ruthenium-alkylidene carbene complexes, known as the Grubbs catalyst (G-I and G-II),³ are standard metathesis catalysts and have found broad application in synthetic chemistry particularly natural product synthesis⁴ and polymer chemistry. The relatively high stability and compatibility with various polar functional groups make the Grubbs catalyst as the favorable choice. Even in the presence of Lewis basic polar functional groups, the preferred coordination of an alkene or alkyne to the coordinatively unsaturated ruthenium metal center can be realized for productive metathesis. However, too strong coordination events at any intermediate stage may halt the catalytic cycle leading to unproductive metathesis, which leads to the isolation of various heteroatom-chelated ruthenium complexes that can be further developed as novel metathesis catalysts. Certain heteroatom-chelated ruthenium alkylidene complexes can show interesting properties including high catalyst recoverability and latent catalytic activity and thus can serve as a platform for novel catalyst development.

7.1.1. Heteroatom-chelated ruthenium alkylidenes

The most popular heteroatom-chelated ruthenium alkylidenes is the Hoveyda-Grubbs complex (GH-I and GH-II).⁵ The Hoveyda-Grubbs complex forms the earliest member of heteroatom-chelated ruthenium complexes where the ruthenium center is chelated to a 2-isopropoxy phenyl group (**Scheme 7.1**). The Hoveyda-Grubbs complex shows appreciable activity and is exceptionally robust. This class of catalysts is recyclable, and the recycled catalyst has no significant loss in activity upon reuse. These properties make **GH-II** an extremely popular olefin metathesis catalyst for large scale industrial applications. Introducing

*This chapter has been reprinted (adapted) with permission from Gupta, S.; Sabbasani, V. R.; Su, S.; Wink, D. J.; Lee, D. “Alkene-Chelated Ruthenium Alkylidenes: A Missing Link to New Catalysts” *ACS Catal.* **2021**, *11*, 1977–1987. Copyright 2021, American Chemical Society.



Scheme 7.1. Heteroatom-chelated ruthenium alkylidene

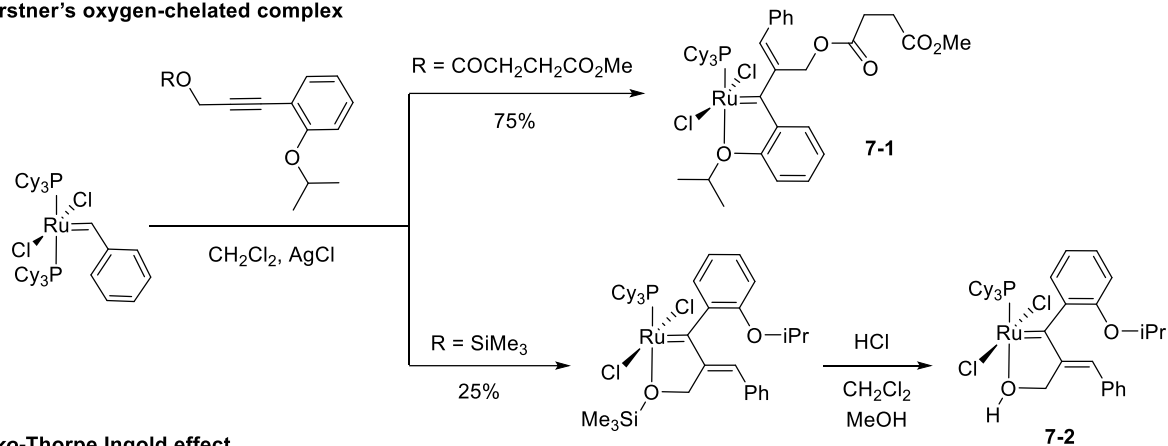
electronic and steric perturbations in **GH-II** can further enhance the catalytic activity; for example, a nitro group in the nitro-Grela catalyst⁶ or a phenyl substituent *ortho* to the chelated oxygen as in the Blechart catalyst.⁷ Hoveyda and coworkers also developed dendritic Ru-based complexes with excellent recyclability features for a wide range of metathesis processes.⁸ Fürstner and coworkers investigated the synthesis and catalytic activity of a series of bidentate η^1 -vinylcarbene ruthenium complexes derived from the enyne metathesis of phenylacetylene derivatives bearing an isopropoxy substituent at their *ortho* position.⁹ Grubbs and coworkers reported a C–H activated ruthenium catalyst for *Z*-selective olefin metathesis. This catalyst is chelated to a unique nitrato ligand, which improves its metathesis activity and selectivity.¹⁰ In 2013, Hoveyda and coworkers developed a Ru-based *Z*-selective olefin metathesis complex

containing a dithiolate ligand. These catalysts have high efficiency and exceptional Z-selectivity (>98:2 Z:E) in the ROMP and ring-opening/cross metathesis process.¹¹ Additionally, these catalysts need low catalyst loading of 0.002 mol% and have a high turnover number thereby increasing their utility in industrial processes. Other sulfur chelated ruthenium complexes developed involves Lemcoff's latent sulfur chelated ruthenium catalysts where steric perturbations can regulate catalytic activities at different temperatures¹² and Grela's sulfoxide chelated ruthenium-based olefin metathesis initiator.¹³ Grela reported six-membered chelates where the Ru is chelated to sulfonyl oxygens.¹⁴ Proper tuning of the electronic and steric factors of the benzylidene part has a direct impact on the stability and catalytic activity of these complexes. Several nitrogen chelated Ru-alkylidene complexes have also been reported. These involve Grela's quinoline or quinoxaline chelated complexes¹⁵, Plenio's secondary amine chelated complexes which are fast initiators even at low catalyst loading¹⁶ and Grubbs's imine chelated latent metathesis catalyst.¹⁷ Grela and coworkers reported a unique type of ruthenium complex with a rare ruthenium-halogen interaction.¹⁸ These complexes could be easily synthesized, have excellent stability, and shows a significant acceleration of the reaction rate at elevated temperature.

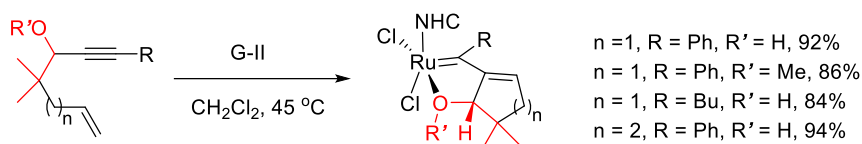
Same as in diene metathesis, ruthenium-alkylidene intermediate in enyne metathesis can coordinate with polar functional groups to arrest the catalytic cycle either temporarily or permanently. It is crucial to understand the structure and dynamics of the trapped ruthenium alkylidene species to minimize non-productive metathesis events and design substrates that avoid these problems. Fürstner and coworkers isolated ether and hydroxy-chelated ruthenium complexes while studying enyne metathesis of phenylacetylene derivatives bearing an isopropoxy substituent at their ortho position (**Scheme 7.2**).⁹ Both terminal and non-terminal phenylacetylenes reacted similarly, generating novel oxygen-chelated complexes. The enyne metathesis of internal alkyne having a methyl succinate moiety with **G-II** generated complex **7-1**. On the other hand, the alkyne with a trimethylsilyl moiety formed a complex where the ruthenium is chelated to the silyl ether. This complex on desilylation formed a hydroxy-chelated ruthenium

complex **7-2**. Lee and coworkers developed an enyne metathesis-based approach to hydroxy- and ether-chelated ruthenium-alkylidenes where the *exo*- and *endo*-Thorpe Ingold effect plays an important role.¹⁹

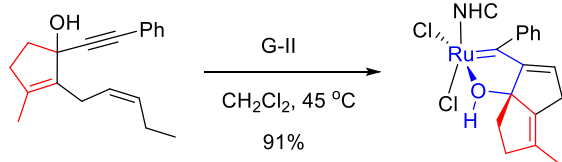
Fürstner's oxygen-chelated complex



Exo-Thorpe Ingold effect

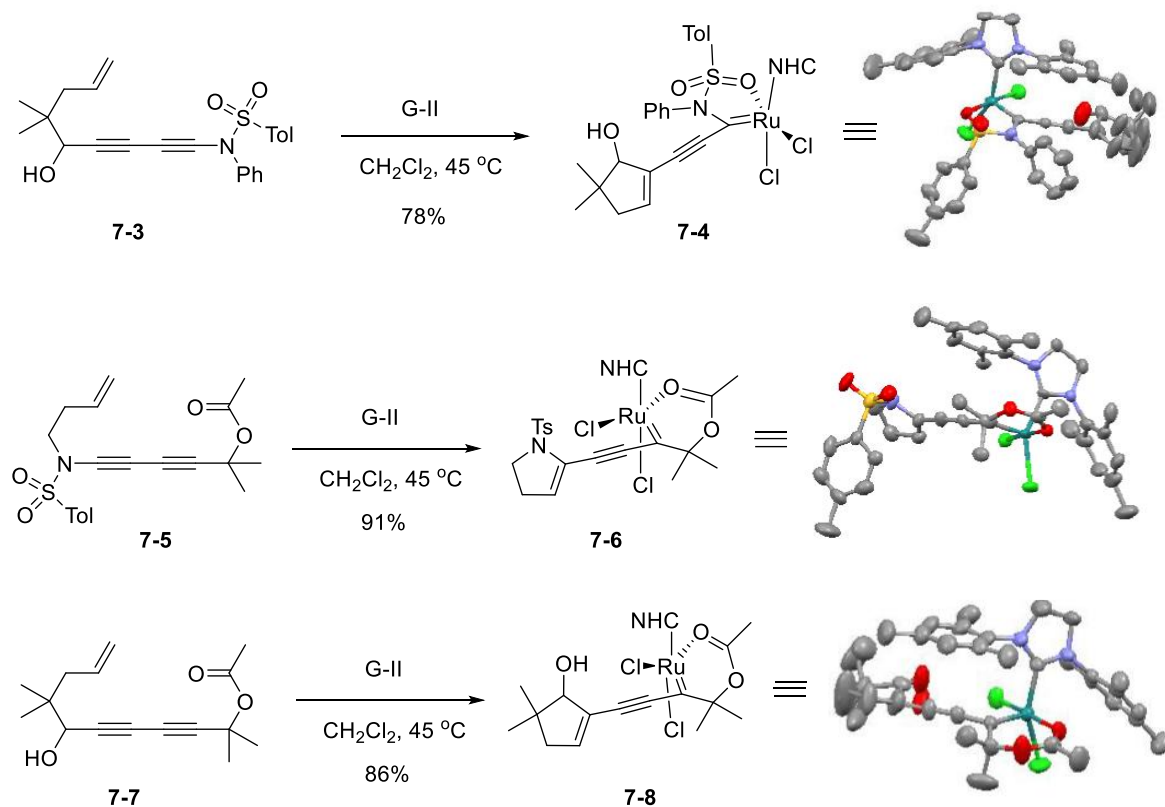


Endo-Thorpe Ingold effect



Scheme 7.2. Enyne metathesis approach to hydroxy- and ether-chelated ruthenium alkylidenes

These complexes have a *cis* disposition of the chloride ligands and display metathesis activity at elevated temperatures. Lee and coworkers also synthesized several sulfonamide- and acetate-chelated ruthenium complexes via enyne metathesis which also have a *cis*-disposition of the chloride ligands.²⁰ Substrate **7-3** which has the possibility to form either hydroxy-chelate or acetate-chelate, undergoes enyne metathesis followed by metallotropic-[1,3] shift to form acetate-chelate **7-4** exclusively. Similarly, substrate **7-5** forms acetate-chelate **7-6** preferentially over the sulfonamide-chelate, and substrate **7-7** forms the acetate-chelate **7-8** preferentially over the hydroxy-chelate (**Scheme 7.3**).

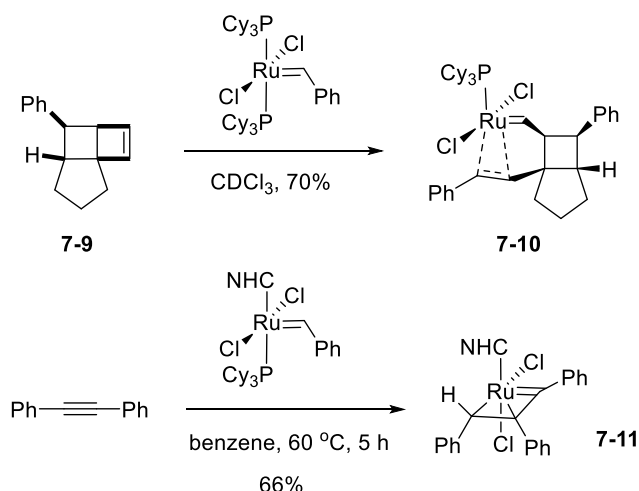


Scheme 7.3. Enyne metathesis approach to oxygen-chelated ruthenium alkylidenes

7.1.2. Previous alkene- and alkyne-chelated ruthenium alkylidenes

In comparison with numerous heteroatom-chelated ruthenium-alkylidenes, the corresponding alkene and alkyne-chelated ruthenium alkylidene complexes are only sporadically reported in the literature. The reason for the paucity of these complexes lies in the fact that chelation to alkene and alkyne is a part of crucial step in every productive metathesis. Thus, for the stabilization of alkene- and alkyne-chelates, additional structural features are required which prevents the termination of the chelates to the metathesis products. The first alkene-chelated ruthenium alkylidene **7-10** was isolated by Snapper and coworkers in the ring-opening metathesis of cyclobutene **7-9** with a stoichiometric amount of **G-I**.²¹ X-ray crystallographic structure of **7-10** indicates that the alkene chelated to the metal center is *trans* to the PCy_3 ligand, which is also called bottom-bound alkene-chelated ruthenium alkylidene (**Scheme 7.4**). The newly

generated bottom-bound complex **7-10** can re-enter into the catalytic cycle. In 2001, Grubbs and coworkers reported η^3 -vinylcarbene complexes derived from **G-II**.²² An excess amount of diphenyl acetylene reacted with **G-II** to afford phosphine-free complex **7-11**. The crystal structure of **7-11** shows that the chelated alkene is *cis* to the *N*-heterocyclic (NHC) ligand. The newly generated η^3 -vinylcarbene complex **7-11** was found to be metathesis inactive.

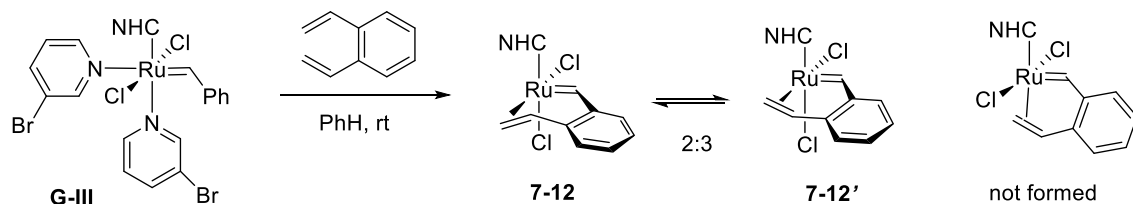


Scheme 7.4. Alkene-chelated ruthenium alkylidenes: Snapper's and Grubbs'

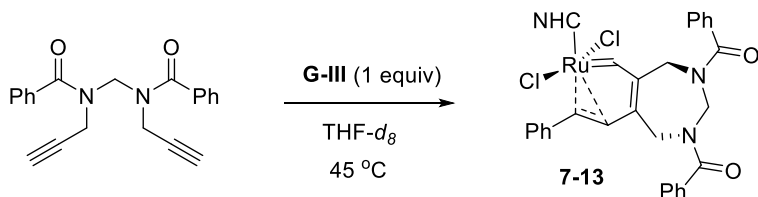
In 2006, Grubbs and coworkers observed that the reaction of Grubbs third-generation complex **G-III** with *ortho*-divinyl benzene afforded a mixture of two alkene-chelated ruthenium alkylidenes.²³ The X-ray crystallographic structure of the minor isomer shows that the chelated alkene is *cis* to the NHC ligand (side-bound). Careful NMR analysis revealed that both complexes **7-12** and **7-12'** are side-bound and have an equilibrium ratio of 2:3. It is interesting to note that no bottom-bound complex similar to Snapper's was observed (**Scheme 7.5**). Recently Choi and coworkers isolated an alkene chelate **7-13** from cyclopolymerization of 1,8-nonadiyne with **G-III** or **GH-II**.²⁴ This complex is a bottom-bound complex where the chelated alkene and the NHC ligand are *trans* to each other. While studying enyne metathesis and metallotropic-[1,3] shift with triynes, Lee and coworkers discovered alkyne chelated ruthenium alkylidenes **7-14a**.²⁵ This alkyne chelate is also a bottom-bound complex with the chelated alkyne and the NHC ligand at *trans* orientation. The presence of a *gem*-dimethyl substituent with an optimum tether length

promote the formation of alkyne chelate devoid of any metathesis by-product. A six-membered ring is crucial to stabilize the complex, thus in the case of complexes with a five-membered ring, a mixture of alkyne chelates **7-14a** and metathesis product **7-14b** in a varying ratio depending on the reaction time.

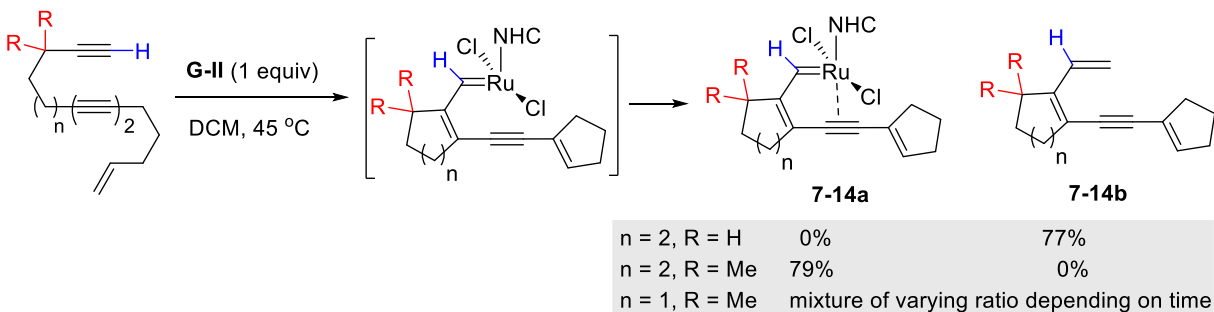
Grubbs's alkene-chelated complex



Choi's alkene-chelated complex



Lee's alkyne-chelated complex



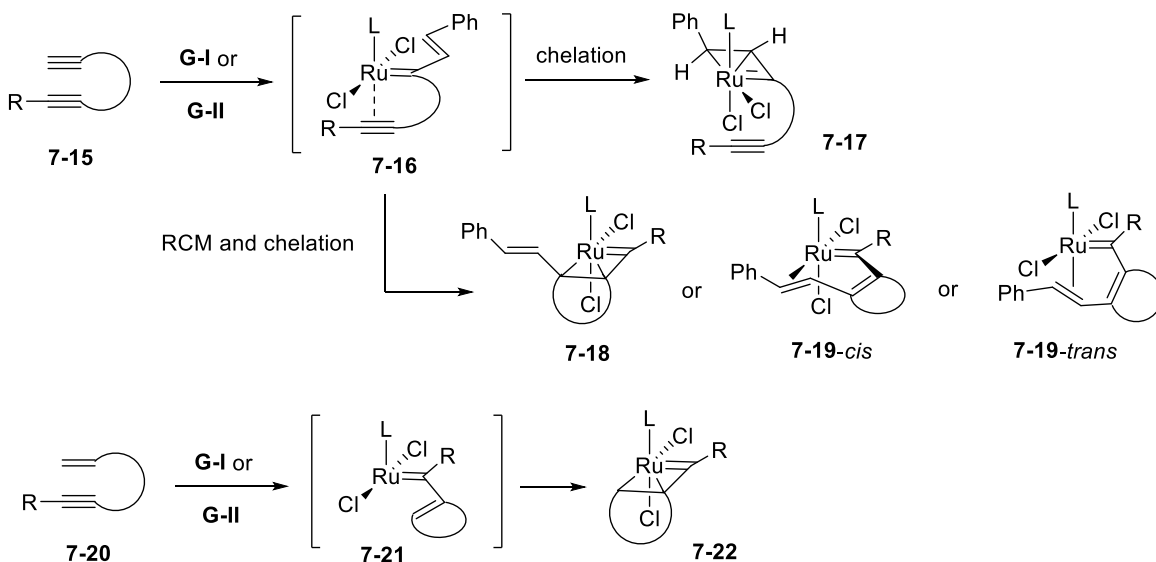
Scheme 7.5. Alkene and alkyne-chelated ruthenium alkylidenes

7.2. Results and Discussions

7.2.1. Enyne metathesis-based design to ruthenium alkylidenes

Because of the paucity of π -chelated ruthenium alkylidene complexes, it is difficult to generalize the preferred chelation mode of the tethered alkene or alkyne to the ruthenium center, which calls for further investigations. We expect that the preference for different chelation modes should depend on the combined steric and electronic effects of the ligand environment on the metal center.²⁶ We envisioned that the RCM

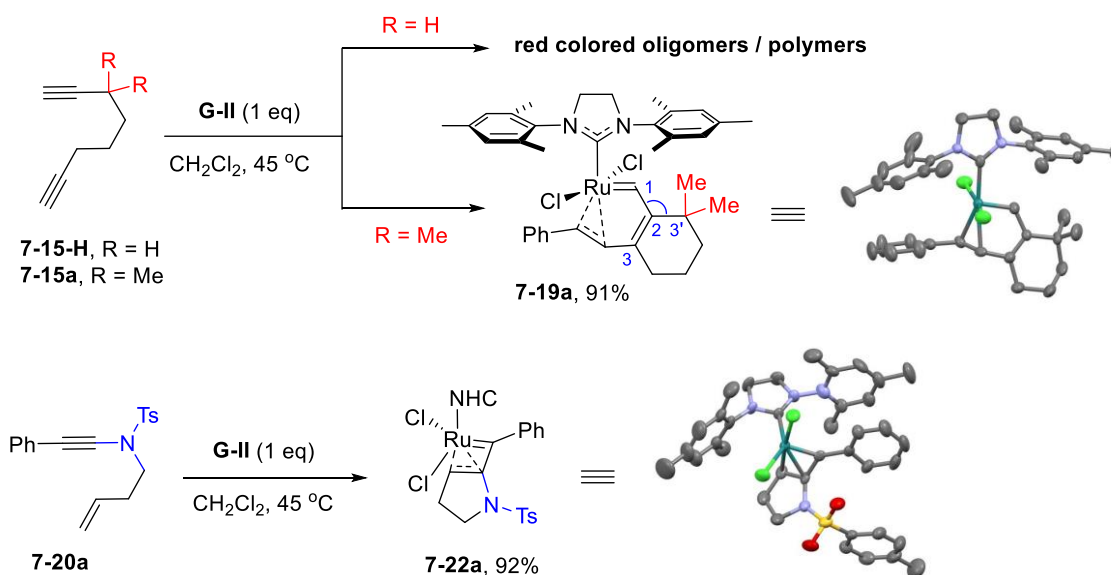
of 1,n-diyne **7-15** would provide an ideal platform for systematic exploration of the chelation behavior of structurally differentiated ruthenium alkylidenes (**Scheme 7.6**). It is expected that the CM between the terminal alkyne moieties of **7-15** and a ruthenium alkylidene initiator **G-I** or **G-II** would generate styryl-substituted alkylidene **7-16**.²⁷ If the styryl chelation is preferred to the subsequent ring closure, complex **7-16** would be arrested to generate η^3 -vinyl chelate **7-17**, whereas if the ring closure of **7-16** is favored, either η^3 -vinyl chelate **7-18** or 1,5-chelate **7-19-cis/trans** would be generated wherein formation of the latter should be more favorable due to a geometric constraint.²⁸ On the other hand, RCM of 1,n-enyne **7-20** would generate an alkylidene **7-21**, which may form η^3 -vinyl chelate **7-22**.²² The prerequisite for formation of these alkene-chelates is a rapid initiation by a stoichiometric initiator and a strong intramolecular interaction of the metal center with a newly formed double bond such that the next catalytic cycle is halted.



Scheme 7.6. Alkene-chelated ruthenium alkylidenes generated through enyne RCM

In this study, we focused our exploration on identifying general structural elements that strongly stabilize alkene-chelates. We found that the RCM of diyne **7-15-H** with **G-II** provided only polymerized material while RCM of **7-15a** led to formation of **7-19a**, which is believed to be the consequence of the *exo*-Thorpe-Ingold effect exerted by a *gem*-dialkyl moiety, which effectively promote the alkene-chelation

(Scheme 7.7).^{19,29} This outcome clearly indicates that 6-membered ring chelate of type **7-19-*trans*** containing a *trans*-relationship between *N*-heterocyclic carbene (NHC) ligand and the chelated alkene is most favorable. This ligand disposition is similar to that of chelate **7-13**, which does not contain a *gem*-dimethyl group. In the RCM of ynamide-tethered enyne **7-20a**, the electron-rich nature of an enamide moiety of the intermediate facilitates formation of η^3 -vinyl alkylidene **7-22a**.³⁰ These steric and electronic controlling structural elements were exploited for preparation of other related alkene-chelated complexes. The stability and reactivity profiles of these complexes were found to be finely tunable, which is reflected in their catalytic performances in RCM, CM, and ROMP reactions.

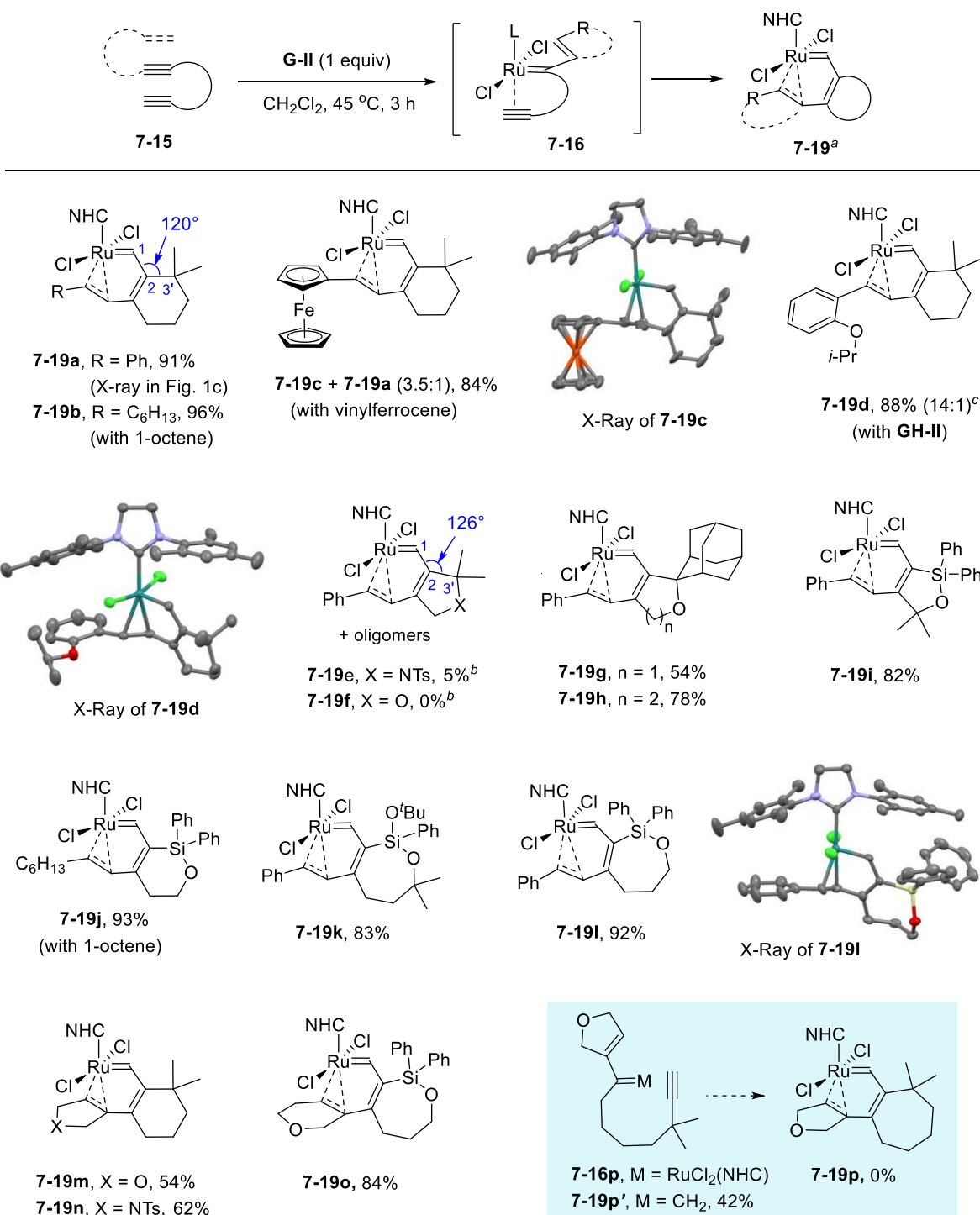


Scheme 7.7. Steric and electronic factors stabilizing alkene-chelates

7.2.2. 1,5-Alkene chelates

7.2.2.1. Tandem RCM–CM approach with 1,*n*-diynes: The contrasting behavior of 1,7-diynes **7-15-H** and **7-15a** implies that the *gem*-dimethyl group at the propargylic carbon of **7-15a** is crucial for promoting formation of alkene-chelate **7-19a** (Scheme 7.6). The structural characteristics of **7-19a** suggest that the *gem*-dimethyl group should not only restrict the rotation of the C1–C2 bond but also force the metal center to be oriented toward the styryl group at the β -position. Although we expected that the *gem*-dimethyl

group-based steric effect, the *exo*-Thorpe-Ingold effect, should be a dominating factor to stabilize the alkene-chelation in **7-19a** the overall stability is likely to depend on other structural factors. To identify stabilizing and destabilizing structural elements for alkene-chelated ruthenium complexes, we explored the reaction of various 1,n-diynes with **G-II** in CH₂Cl₂ at 45 °C (**Table 7.1**). In the presence of 1-octene (3 equiv), treating **7-15a** with **G-II** generated a hexyl group-incorporated alkene-chelate **7-19b** in 96% yield. This implies that the reaction of **G-II** with 1-octene is faster than that with diyne **7-15a**. However, with vinyl ferrocene (3 equiv) under otherwise identical conditions, ferrocene-containing complex **7-19c** was obtained along with **7-19a** in a 3.5:1 ratio (84% yield).³¹ X-ray-crystallographic data of **7-19c** shows replacing the phenyl group in **7-19a** with a ferrocenyl group does not perturb the original structure. With the Grubbs-Hoveyda second-generation complex (**GH-II**), the diyne **a** formed chelate **7-19d** in 88% yield (*E:Z* = 14:1) where the isopropoxy ether does not interact with the metal center. Treating 1,6-diynes containing a *gem*-dimethyl group with **G-II**, however, generated mostly oligomers from which alkene-chelate **7-19e** was isolated only in 5% yield and none of **7-19f** was obtained. The enlarged bond angle between the carbenic carbon and the *gem*-dimethylated carbon of the fused 5-membered ring (126°) compared to the corresponding 6-membered ring-fused chelate (120°) may weaken the *exo*-Thorpe-Ingold effect. We surmised that replacement of the *gem*-dimethyl group in **7-19f** with a bulkier substituent such as an adamantyl moiety would reconstitute the proper steric effect.³² Indeed, an adamantyl substituted alkene-chelate **7-19g** was isolated in 54% yield, and the corresponding 6-membered ring-fused alkene-chelate **7-19h** was obtained in much higher yield (78%). Replacing the *gem*-dimethyl carbon moiety with a diphenylsilyl group along with an additional *gem*-dimethyl group in the 5-membered ring turned out to be more effective to promote alkene chelation to provide **7-19i** in 82% yield. From silyl ether-tethered 1,7- and 1,8-diynes, 6- and 7-membered cyclic silyl ether-fused chelate **7-19j–7-19l** were generated efficiently.³³ The RCM initiated from an alkene tethered to 1,n-diynes followed by tandem enyne RCM provided ruthenium alkylidenes **7-19m–7-19o** that contain a chelated trisubstituted cyclic alkene. Unexpectedly, however, the all-carbon *gem*-dimethyl-containing intermediate **7-16p** did not undergo the 7-membered ring forming RCM to generate **7-19p** instead it terminates with methylene transfer to provide **7-19p'** as the final

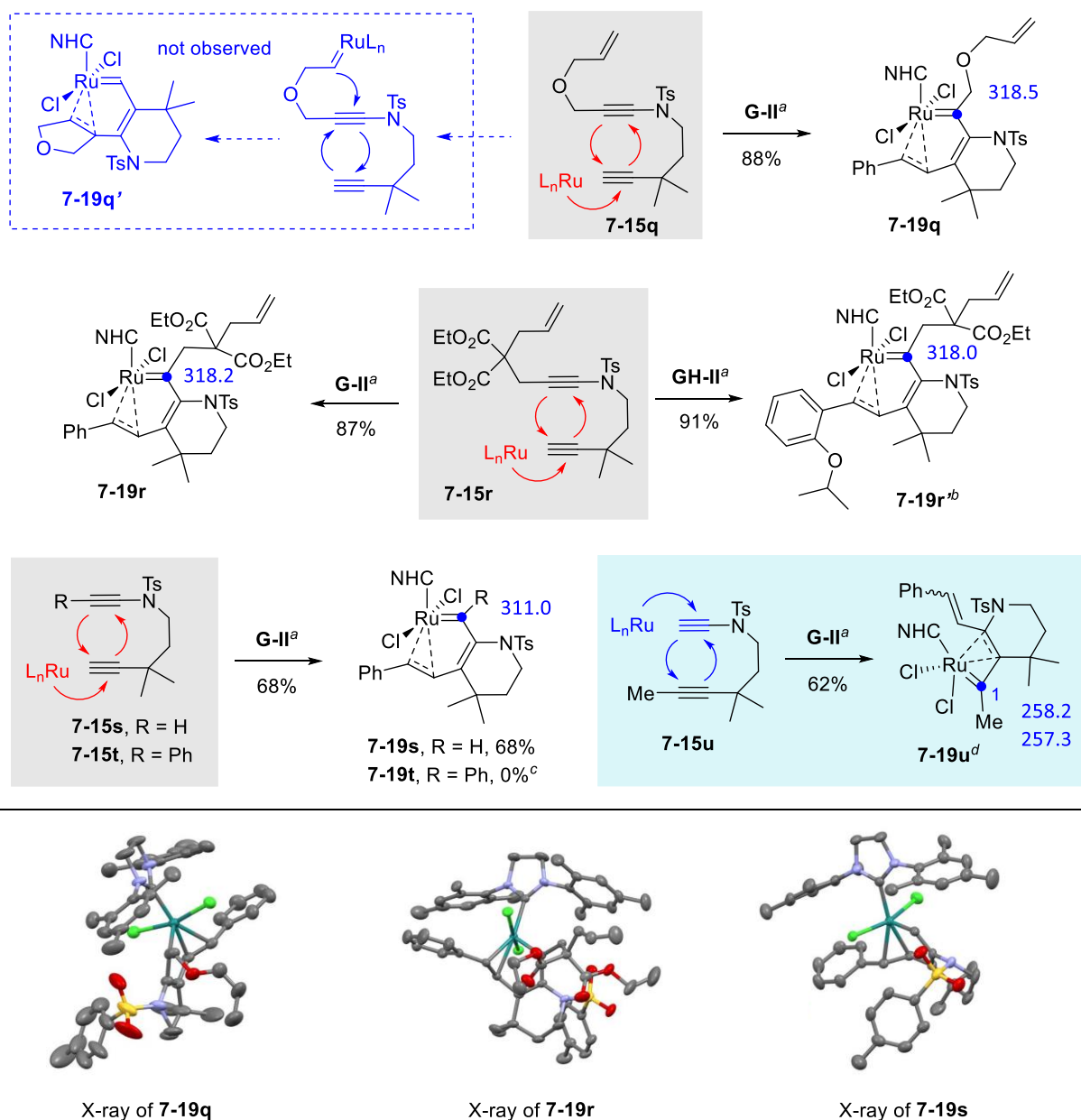


^a Isolated yield. ^b Mostly oligomers formed. ^c *E*:*Z* ratio

Table 7.1. Tandem CM-RCM of 1, *n*-diynes to generate 1,5-alkene-chelates

product. This is in stark contrast to the formation of **7-19o** linked with a diphenylsilyl tethered system, which clearly shows that the diphenylsilyl moiety plays a dual role as a *gem*-dialkyl surrogate to exert the *exo*-Thorpe-Ingold effect and as a promotor of RCM through the Thorpe-Ingold effect.³⁴

7.2.2.2. RCM approach from ynamide-tethered 1,7-diynes: To examine the electronic effect on the alkene to chelate with ruthenium center, an ynamide tether is introduced to 1,*n*-diynes such that after RCM an enamide moiety would be installed in the final ruthenium alkylidene product (**Scheme 7.8**). According to a common reactivity, it is expected that an alkene-tethered 1,7-endiyne **7-15q** should initiate a tandem RCM from the alkene to generate chelate **7-19q'**. In contrast, an initiation at the sterically most hindered neopentynyl site followed by RCM and chelation of the propagating ruthenium alkylidene with the styryl moiety provided **7-19q** in 88% yield. This unique mode of initiation at the alkyne of a neopentynyl nature is unprecedented, which may involve unusual chelation of ruthenium alkylidene between the two alkynes. Also, it is surprising that the tethered alkene remains intact without participating in RCM. Similarly, treatment of allylmalonyl tethered diyne **7-15r** with **G-II** and **GH-II** generated alkene-chelates **7-19r** and **7-19r'** in 87 and 91% yield respectively, while **G-I** failed to undergo an initiation. With 1,7-diyne **7-15s** containing two terminal alkynes, the initiation occurred favorably at the more sterically hindered neopentynyl alkyne over the terminal ynamide, generating chelate **7-19s** (68%), while structurally similar diyne **7-15t** containing a phenyl substituent only decomposed under the same conditions. On the other hand, 1,7-diyne **7-15u** containing a terminal ynamide and a methyl group on the other alkyne underwent initiation at the terminal ynamide to provide η^3 -vinyl alkylidene complex **7-19u** in 62% yield (*E/Z* = 4:1). Complex **7-19u** displays the ¹³C-signals at 258.2 and 257.3 ppm (*E/Z* mixture) for the carbenic carbon C1, which corresponds to the ¹³C-signal range of η^3 -chelated carbenes (230–285 ppm), whereas 1,5-chelates **7-19q–7-19s** display the carbenic ¹³C-signals higher than 310 ppm. Formation of η^3 -chelate from **7-15u** can be justified by an alternative initiation from the terminal ynamide to form the corresponding enamide moiety where the connectivity of the *N*-Ts is optimally disposed to provide an electronic driving force for the chelation similar to that in **7-22** in **Table 7.2**.

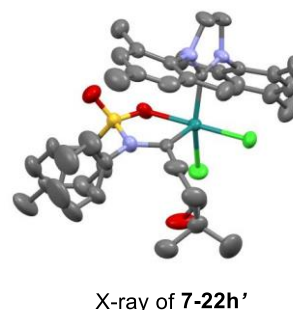
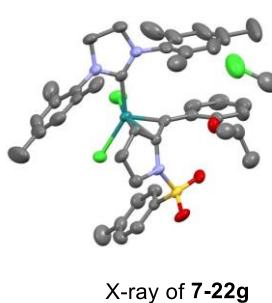
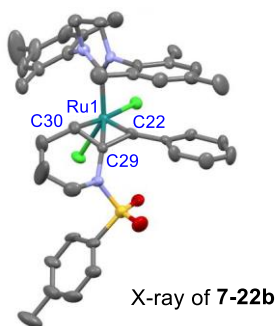
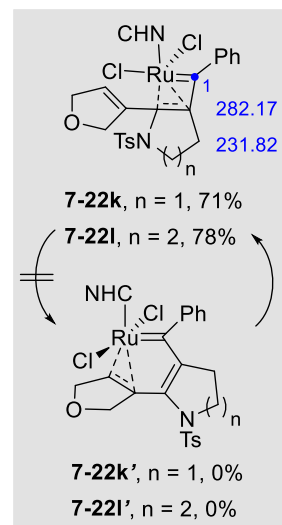
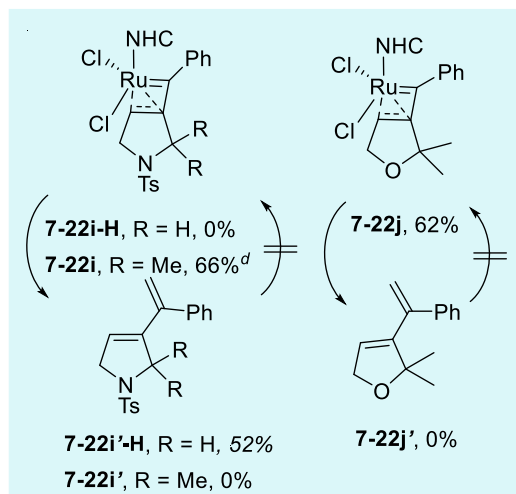
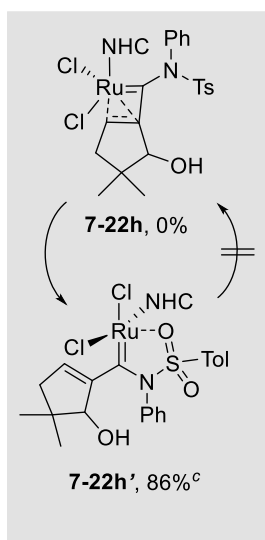
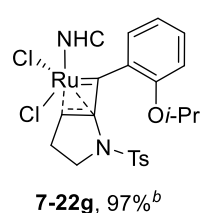
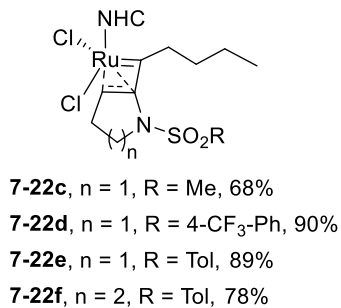
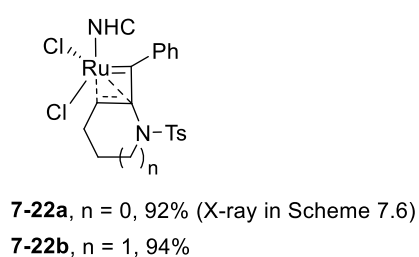
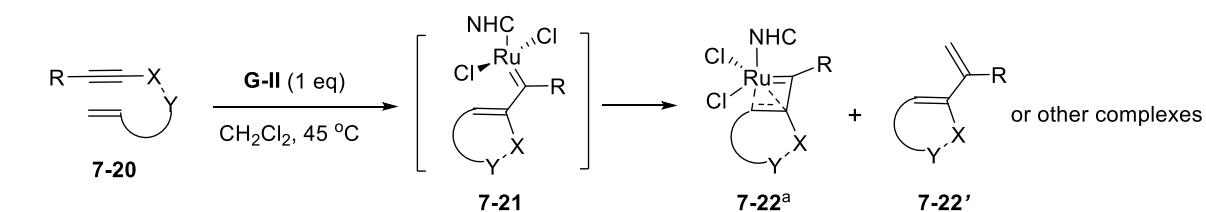


Scheme 7.8. Unusual mode of RCM of ynamide-tethered 1,7-diynes to generate alkene-chelates

^a **G-II** or **GH-II** (0.8 equiv), CH_2Cl_2 , 45 °C (reported yields are isolated yields). ^b The structure was confirmed by X-ray crystallography. ^c Decomposition of the starting material. ^d Mixture of *E*:*Z* isomer (4:1) and each isomer displays the carbenic ^{13}C -signals at 258.2 and 257.3 ppm. The differently colored arrow represents the propagation of the ruthenium alkylidene along the π -bonds with red-colored arrow representing the initiation from the more hindered alkyne while the blue arrow indicating initiation from the electron-rich ynamide.

7.2.3. η^3 -Vinyl alkylidene chelates

7.2.3.1. RCM of 1,n-enynes: Although we expected that a relatively electron-rich enamide might chelate with the ruthenium center to form a η^3 -vinyl alkylidene, complexes **7-19q–7-19s** in **Scheme 7.8** chelated with the distal alkene most likely due to the favorable geometry of forming 1,5-chelates over strained η^3 -vinyl alkylidenes. We suspect that, by removing this distal alkene, the ruthenium center would interact with the proximal enamide. With this hypothesis in mind, we explored the reaction of various 1,n-enynes containing an ynamide tether (**Table 7.2**).³⁵ Gratifyingly, treating 1,6- and 1,7-enyne containing a sulfonamide tether with **G-II** generated alkylidene chelates **7-22a** and **7-22b** in 92 and 94% yield, respectively. The X-ray crystallographic analysis of these complexes confirmed the η^3 -vinyl chelation where the two chloride ligands are in a cis relationship. The true η^3 -chelation mode of the complex **7-22b** can be confirmed from its X-ray structure which shows delocalized bonding between C22, C29 and C30. The C29–C30 bond length is 1.395 Å which is somewhat longer than typical C=C bonds (~1.35 Å) and the C22–C29 bond length is 1.44 Å which is shorter than typical C–C bonds (~1.55 Å). X-ray structures of other complexes of this type also shows true η^3 -chelation mode (see section 7.4.5). Subtle electronic and structural changes including the tether size, nature of sulfonamide and the substituent on the alkyne were tolerant and η^3 -vinyl chelates **7-22c–7-22f** were obtained in high yields. To examine the possibility of competing chelation by an enamide and an ether functionality, a 2-isopropoxyphenyl-substituted enynamide was employed with a prediction of forming a 5-membered ring chelate by the isopropoxy group. However, the obtained complex was η^3 -vinyl chelate **7-22g**, proved by X-ray crystal structure analysis. Whereas the expected oxygen-chelation was established by installing a terminal ynamide such that sulfonamide oxygen-chelated structure **7-22h'** was indeed isolated rather than alkene-chelate **7-22h**. When there is no electronic driving force, *exo*-Thorpe Ingold effect by a *gem*-dimethyl moiety can be resorted to promote chelation. For example, without a *gem*-dimethyl group on the propargylic site, metathesis product **7-22i'-H** (52% yield) was generated devoid of η^3 -vinyl chelate **7-22i-H**, whereas the corresponding *gem*-dimethyl-containing substrate provided η^3 -vinyl chelate **7-22i** in 66% yield without forming metathesis



^a Isolated yield. ^b The η^3 -vinyl chelation was confirmed by X-ray crystallographic analysis. ^c Two chlorides are in a cis relationship. ^d 82% yield based on recovered starting material.

Table 7.2. RCM 1,n-enynes to form η^3 -vinyl alkylidene chelates

product **7-22i'**. The presence of *gem*-dimethyl group in **7-22i** prevents further [2 + 2] cycloaddition as the incipient ruthenacyclobutane is destabilized by the unfavorable syn-pentane interaction by the *gem*-dimethyl group, thus no metathesis product is formed in this case. A similar complex **7-22j** was formed from a propargylic ether tethered enyne in 62% yield devoid of any metathesis product. Finally, competition between η^3 -vinyl chelation and 1,5-chelation showed a preference for η^3 -vinyl chelates in **7-22k** and **7-22l** over 1,5-chelates **7-22k'** and **7-22l'**, and this assignment is supported by the ^{13}C NMR signals of the carbenic C1 carbon at 282.17 and 231.82 ppm respectively.

7.2.3.2. Heteroatom substituent effect: The favorable interaction of the ruthenium center to form η^3 -vinyl chelates with an enamide generated through RCM of ynamide prompted us to explore chelation behavior of other electron-rich heterocycles such as pyrrole, furan, thiophene and indole.³⁶ Toward this goal, we employed enyne RCM of **7-20m–7-20v** that contain preformed respective heteroaromatic systems (Table 7.3). Treating 2-allyloxypropynyl pyrrole derivative **7-20m** gave predominately alkene-chelated complex **7-22m** in 95% yield where a minor sulfonamide-chelate exists in a 3:1 ratio. On the other hand, the corresponding furan and thiophene derivatives **7-20n** and **7-20o** gave only metathesis products **7-22n'** and **7-22o'**. As opposed to 2-pyrrole derivative **7-20m**, the corresponding 2-alkynyl indole derivatives **7-20p** and **7-20q** did not provide alkene-chelates, but only oxygen-chelates **7-22p'** and **7-22q'** were formed with an acetyl and a sulfonyl group, respectively. This drastic change in chelation behavior can be attributed to the reduced electron density of the enamide moiety of an indole ring compared to pyrrole thereby the alkene-chelation is superseded by oxygen chelation. By removing the possibility of oxygen chelation with geometrical constraints, only η^3 -vinyl chelates **7-22r–7-22t** were obtained. The electron-withdrawing *p*-toluenesulfonyl and acetyl groups of **7-22r** and **7-22s** increase the lability of these complexes, which thus turn over to the metathesis products **7-22r'** and **7-22s'** in significant amounts compared to a methyl group-containing complex **7-22t**. An ynamide-tethered alkynyl indole **7-20v** was designed to examine the competition of ruthenium chelation between two similar enamide moieties of dihydropyrrole and indole.

As expected, chelation occurred with the more electron-rich dihydropyrrole to form η^3 -vinyl complex **7-22v** without **7-22v'**, whose structure was unambiguously confirmed by X-ray crystallographic analysis.

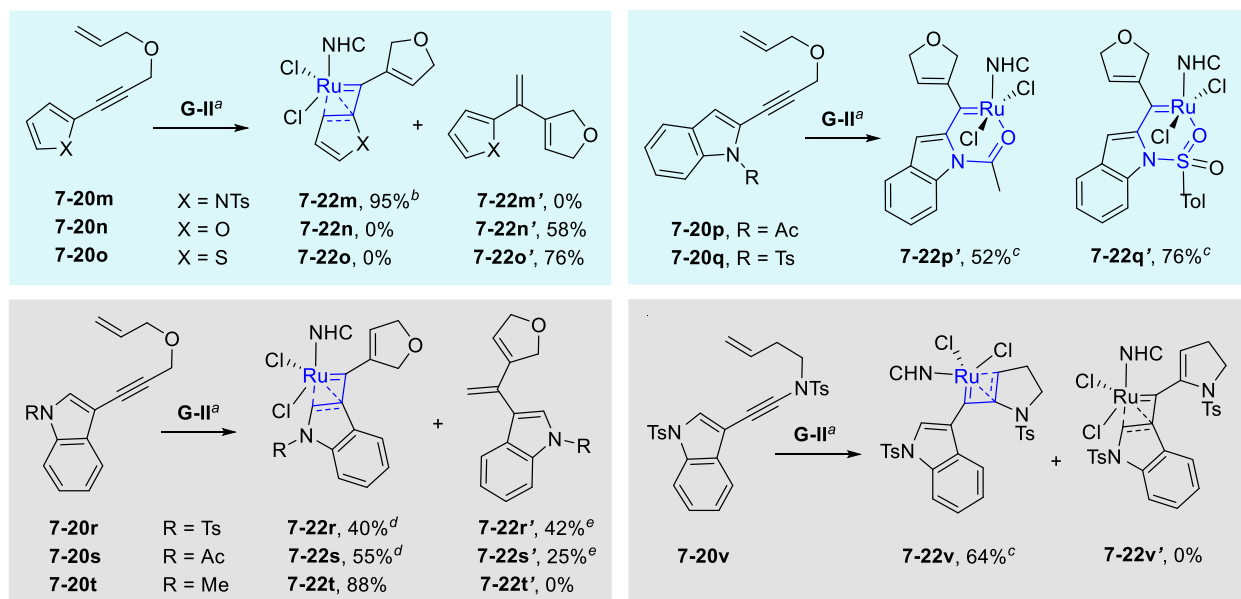


Table 7.3. Heteroatom substituent effect on the formation of η^3 -vinyl alkylidene complexes. ^a **G-II**

(0.8 equiv), CH₂Cl₂, 45 °C (reported yields are isolated yields). ^b Inseparable mixture of alkene- and sulfonamide-chelate in a 3:1 ratio. ^c Confirmed by X-ray crystallographic analysis. ^d The reaction was performed at 35 °C for 1 h. ^e NMR yields measured using internal standards.

7.2.4. Catalytic activity studies

7.2.4.1. Structure-Activity relationships: Having developed structurally diverse 1,5-alkene-chelates and η^3 -vinyl chelates, we investigated the catalytic activities of these complexes for different metathesis process.³⁷ First we tested the catalytic activity of a variety of complexes for RCM reaction of dimethyl diallylmalonate to establish a structure activity relationship. In general, the *trans*-1,5-alkene-chelated complexes fused with a 5-membered ring such as **7-19g** and **7-19i** are active at ambient temperature (30 °C) but the corresponding 6- or 7-membered ring-fused chelates **7-19h** and **7-19l** showed latent behaviors, inert at room temperature up to 45 °C but became active at higher temperature.³⁸ In comparison, η^3 -vinyl chelates **7-22a–7-22f** are highly active at ambient temperature whereas η^3 -vinyl chelate **7-11** was

inactive for metathesis under otherwise identical conditions.¹⁷ The catalytic activities of the latent 1,5-chelates were found to change drastically with variation in the tethering group (for details, see section 7.4.3). For instance, in the RCM of dimethyl diallylmalonate catalyzed by these latent chelates at 80 °C in C₆D₆, complex **7-19b** containing a *gem*-dimethyl group on the fused 6-membered ring is less active (12% conversion) than the corresponding adamantyl-containing complex **7-19h** (57% conversion), yet 7-membered ring-fused complex **7-19i** containing a diphenylsilyl group is much more reactive (99.1% conversion). The reactivity of the complexes are also significantly affected by the substituent on the carbenic carbon. Increasing the steric bulk of the substituent at the carbenic carbon decreases the reactivity significantly, thus η^3 -vinyl chelate **7-22a** with a smaller butyl substituent³⁹ is much reactive than **7-22b** with a larger phenyl group (3 min vs. 13 min for complete conversion at 45 °C). Sometimes the presence of an alternate chelating group may shut the catalytic activity completely, for example **7-19g** with an ortho-isopropoxyphenyl substituent is catalytically inactive presumably due to a constant shuttling between the alkene-chelate and oxygen.

Another important factor affecting the catalytic activity of η^3 -vinyl chelates is the size of the fused ring, thus 6-membered ring-fused complexes **7-22b** (99% conversion in 3 min, 45 °C) is more reactive than the corresponding 5-membered ring congener **7-22a** (96% conversion in 13 min, 45 °C). This reactivity difference can be justified by the structural difference in **7-22a** and **7-22b** revealed by their X-ray structures (Figure 7.1).

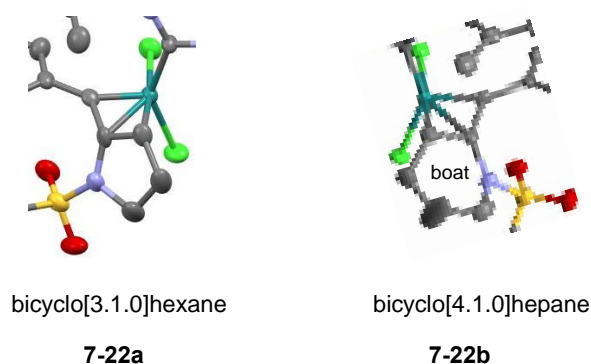


Figure 7.1. Partial structure of **7-22a** and **7-22b** from X-ray

While the 5-membered ring of the bicyclo[3.1.0]hexane substructure in **7-22a** is unstrained, the 6-membered ring of the bicyclo[4.1.0]heptane moiety in **7-22b** is highly distorted to assume a boat conformation. Thus, the barrier for dissociation of the chelated alkene in **7-22b** should be lower than **7-22a**. Catalytic activity of oxygen chelated complexes like **7-22p'** and **7-22q'** for RCM reactions were also tested, while acetate chelate **7-22p'** did not show any activity, the corresponding sulfonamide chelate **7-22q'** was catalytically active at 45 °C (for kinetic profile, see section 7.4.4).

7.2.4.2. Benchmarking catalytic activity: After establishing a reactivity trend for the different types of alkene-chelates, we selected a subset of relatively more active complexes to benchmark their catalytic activity for various metathesis process with respect to standard metathesis catalysts. Accordingly, the reaction profile of these complexes was studied for RCM of dimethyl diallylmalonate and dimethyl allylmethylmalonate⁴⁰, CM of terminal alkene with acrylate⁴¹, ROMP of 1,5-cyclooctadiene⁴² (**Figure 7.2**), and kinetic parameters including rate constants (k_{obs} , k_{rel}) and half-lives ($t_{1/2}$) were determined with reference to **G-II** (**Table 7.4**). Among the tested for the RCM, **7-19g** (k_{rel} = 9.64, 97.7% conversion) and **7-22f** (k_{rel} = 11.48, 98.6% conversion) showed the best performance. The kinetics for RCM of dimethyl diallylmalonate was also studied in CD₂Cl₂ to compare with previously reported conditions.³⁷ In CD₂Cl₂ there was a great rate enhancement for standard metathesis catalysts like **G-II** and **G-III** while the alkene-chelates demonstrated superior activity in both CD₂Cl₂ and CDCl₃. More specifically alkene-chelates **13c**, **7-22d**, **7-22e** and **7-22i** showed an enhancement in rate while **7-19g** and **7-22f** showed a decrease in rate in CD₂Cl₂ compared to CDCl₃. In the RCM of dimethyl allylmethylmalonate, catalysts **7-22c** (k_{rel} = 5.43, 97.0% conversion) and **7-22e** (k_{rel} = 4.14, 97.7% conversion) achieved near full conversion although their k_{rel} are lower than **7-19g** (k_{rel} = 6.15, 93.5% conversion) and **7-22f** (k_{rel} = 7.61, 87% conversion). In CM of 5-hexenyl acetate with methacrylate, complexes **7-19g**, **7-22c**, and **7-22e** initiated the reaction with higher rate than **G-II** but the reactions slowed down and resulted in 63–82% conversion while the conversion with **G-II** was 94%. In ROMP of 1,5- cyclooctadiene, **7-22e** (k_{rel} = 1.38, 98% conversion) and **7-22f** (k_{rel} = 1.66, 99% conversion) provided near full conversion with slightly higher rate compared to **G-II**.

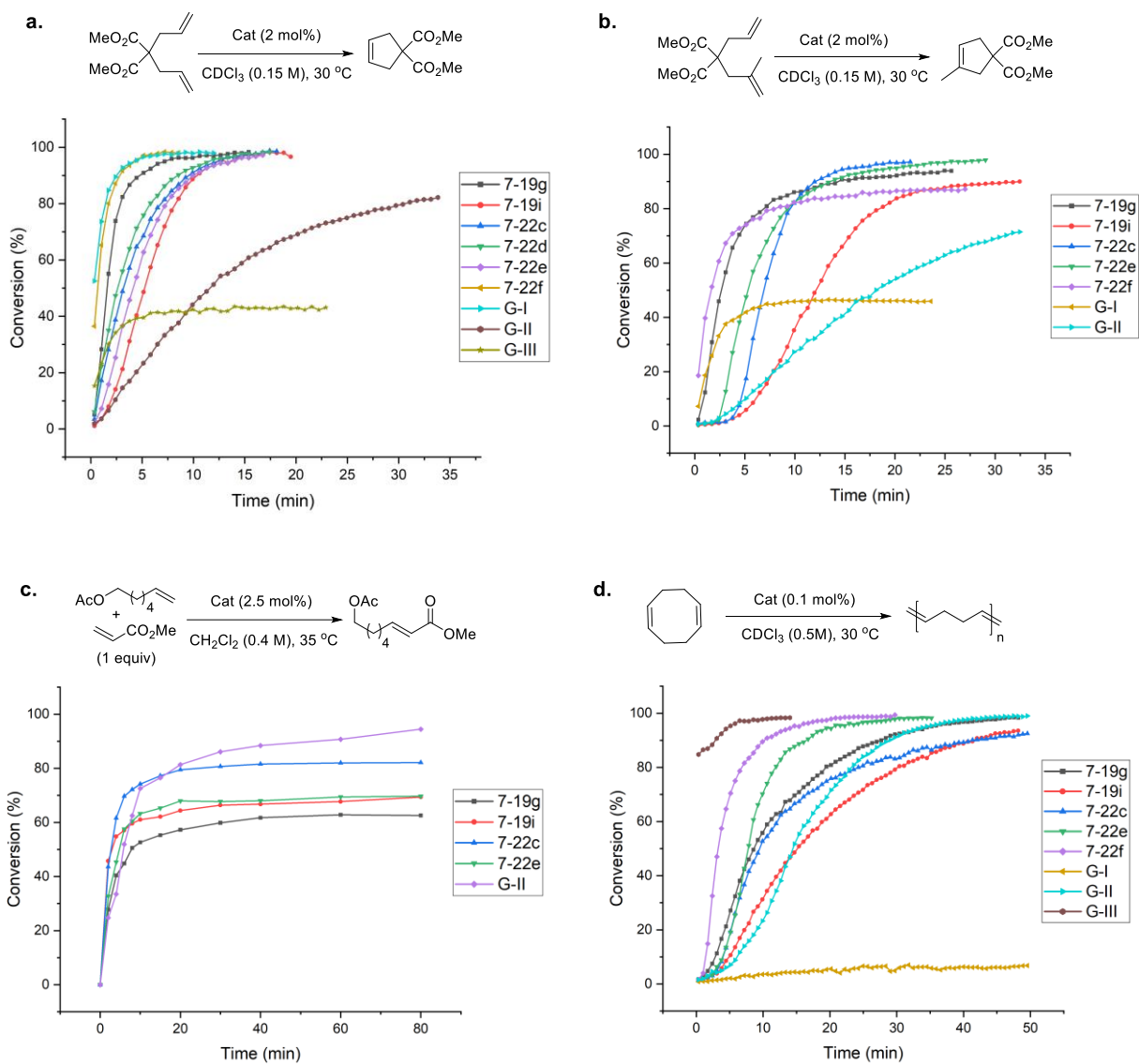


Figure 7.2. Catalytic activities of alkene-chelated ruthenium alkylidene complexes

Kinetic profile for each reaction was obtained by NMR spectroscopy (Bruker's pseudo 2D kinetics method) by equilibrating the NMR probe at requisite temperature. Each data point represents the average of three runs of individual experiment except for CM experiments where two runs were performed. **a.** RCM profiles of dimethyl diallylmalonate at 30 °C in CDCl_3 (0.15 M). **b.** RCM profiles of dimethyl allylmethylmalonate at 30 °C in CDCl_3 (0.15 M). **c.** CM profiles of 5-hexenyl acetate with methyl acrylate at 35 °C in CH_2Cl_2 (0.4 M). **d.** ROMP profiles of 1,5-cyclooctadiene at 30 °C in CDCl_3 (0.5 M).

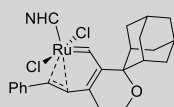
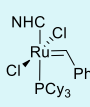
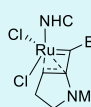
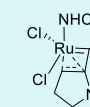
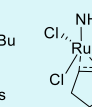
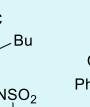
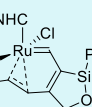
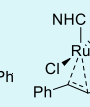
Latent Catalyst ^a	Active Catalyst							
 7-19h	 G-II	 7-22c	 7-22e	 7-22d	 7-19i	 7-19g	 7-22f	
RCM (disubstituted olefin)								
k_{rel} (CDCl ₃) ^b (no initiation)	0	1.00	4.80	4.64	4.76	5.50	9.64	11.48
k_{rel} (CD ₂ Cl ₂) ^{b, c}		1.00	3.74	3.48	3.83	3.63	3.57	5.98
RCM (trisubstituted olefin)								
k_{rel} (CDCl ₃) ^b		1.00	5.43	4.14		3.13	6.15	7.61
ROMP								
k_{rel} (CDCl ₃) ^b		1.00	0.42	1.35		0.75	0.52	1.66

Table 7.4. Reactivity order of selected alkene-chelates for different metathesis process. ^aLatent catalysts involves the 1,5-chelates with six or seven membered rings. These complexes do not show catalytic activity at room temperature and is only active at higher temperature. ^b k_{rel} value represents the rate constant for a particular complex with respect to G-II for different metathesis process. ^c k_{rel} value for RCM of dimethyl diallylmalonate was also determined in CD₂Cl₂ for comparison with previously reported data.³⁷

Overall, these two different classes of alkene-chelated ruthenium alkylidenes, 1,5-alkene chelates and η^3 -vinyl chelates, if they have right combinations of structural elements, can display efficient metathesis activity in different types of metathesis reactions with consistency. This compares favorably with the behaviors of typical Grubbs-type metathesis catalysts. For example, **G-III** is an excellent catalyst for ROMP but shows relatively low reactivity toward RCM reactions (**Figure 7.2a,d**).⁴³

7.3. Conclusion

We have developed a general approach to promote the formation of alkene-chelated ruthenium alkylidenes relying on ring-closing enyne metathesis of 1,n-diynes and 1,n-enynes. Because of the tandem nature of enyne metathesis to form these complexes, steric and electronic variation can be easily introduced to engineer the stability and catalytic activities of these new complexes. The crucial structural element that facilitates 1,5-alkene chelation is the *exo*-Thorpe-Ingold effect of a *gem*-dialkyl substituent. On the other hand, the driving force for formation of geometrically constrained η^3 -vinyl alkylidene is provided by an electronic activation on the chelating alkene. The stability and reactivity of these alkene-chelated complexes can be modulated not only by these crucial structural elements but also by other auxiliaries. For example, 5-membered ring-fused 1,5-chelates are more reactive than the corresponding 6- and 7-membered ring-fused congeners. In general, η^3 -vinyl alkylidenes and 1,5-chelates fused with a 5-membered ring display superior catalytic activity in RCM, CM and ROMP reactions compared to other alkene-chelates. Another meritorious feature of these new alkene-chelated ruthenium alkylidenes is their consistency in performing different types of metathesis processes. The versatility of catalysts⁴⁴ for different types of reactions, which many standard metathesis catalysts lack, is an important goal in developing new catalysts. Thus, these alkene-chelated ruthenium alkylidene complexes might provide a sustainable platform to further develop catalysts of enhanced catalytic activity and versatility. This study not only demonstrated the possibility of generating novel alkene-chelates by exploiting non-productive coordination events in enyne metathesis but also discovered new metathesis catalysts with high activity, which might find broad utility in organic synthesis and polymer chemistry.

7.4. Experimental Details

7.4.1. General information

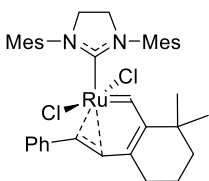
All Reactions were carried out in oven-dried glassware under inert atmosphere unless otherwise noted. All organometallic reactions were performed under argon using glovebox and standard Schlenk techniques. All reagents and compounds were purchased from Sigma-Aldrich, Acros, TCI America or Oakwood and used as received, unless otherwise noted. Grubbs 2nd generation catalyst was purchased from Aldrich and CAPOT Chemicals (Sanghai, China) and used without any further purification. Toluene, dichloromethane, triethylamine, and acetonitrile were distilled over calcium hydride (CaH₂) under nitrogen. Tetrahydrofuran was dried over sodium benzophenone ketyl. Column chromatography was performed using silica gel 60 Å (32–63 mesh) purchased from Silicycle Inc. Analytical thin layer chromatography (TLC) was performed on 0.25 mm E. Merck precoated silica gel 60 (particle size 0.040–0.063 mm). Yields refer to chromatographically and spectroscopically pure isolated compounds unless otherwise stated. ¹H NMR and ¹³C NMR spectra were recorded on a Bruker AV–500 spectrometer. ¹H NMR chemical shifts (δ) are reported in parts per million (ppm) downfield of TMS and are referenced relative to the residual solvent peak (CDCl₃ (7.26 ppm)). ¹³C chemical shifts (δ) are reported in parts per million downfield of TMS and are referenced to the carbon resonance of the solvent (CDCl₃ (77.02 ppm)). Multiplicities are indicated by s (singlet), d (doublet), t (triplet), q (quartet), p (quintet), h (sextet), dd (doublet of doublet), dt (doublet of triplet), m (multiplet) and so on. ¹H NMR signals that fall within a ca. 0.3 ppm range are generally reported as a multiplet, with a range of chemical shift values corresponding to the peak or center of the peak. Coupling constants, *J*, are reported in Hz (Hertz). Electrospray ionization (ESI) and Electron impact (EI) mass spectra were recorded on a Waters Micromass Q-Tof Ultima and Micromass 70–VSE, respectively in the University of Illinois at Urbana-Champaign.

7.4.2. General procedure for alkene-chelate formation

A Schlenk tube was charged with the 1,n-diyne/endiynes or 1,n-enynes (0.07 mmol), **G-II** catalyst (50 mg, 0.06 mmol) and dry CH₂Cl₂ (5 mL, 0.015 M) inside a glove box. The Schlenk tube was taken out, degassed, and refilled with argon by freeze, pump, and thaw process (three cycles). The reaction mixture was then heated at 45 °C for 3 h. After completion, the reaction mixture was concentrated, and the residue was quickly purified by flash chromatography under N₂. Details of physical appearance, yield, amount of complex prepared, solvent system used for purification and characterization data for each complex is provided underneath.

Stability and storage of the complexes: Most of the complexes are stored in normal glass vials in freezer (–20 °C) under neat conditions and remains good for few months. The complexes are not stored in solution which might lead to quicker degradation. Some complexes like **7-19u**, **7-22f**, **7-22k**, **7-22l** and **7-22t** are relatively less stable and are stored in glove box freezer.

7.4.3. Characterization data of alkene-chelate



7-19a

E:Z = 3:1

7-19a: 91% yield; *E/Z*-mixture in a 3:1 ratio; red solid; 57 mg obtained; Purification:

Flash Chromatography (SiO₂, hexanes–EtOAc, 10:1 → 4:1); **¹H NMR** (500 MHz,

CDCl₃) **E-isomer:** δ 16.56 (s, 1H), 7.20 (t, *J* = 7.1 Hz, 1H), 7.12–7.02 (m, 4H), 7.01–

6.96 (m, 2H), 6.55 (s, 2H), 5.41 (d, *J* = 13.0 Hz, 1H), 4.48 (d, *J* = 13.0 Hz, 1H), 4.04–

3.85 (m, 4H), 2.54–2.41 (m, 6H), 2.32 (s, 3H), 2.29–2.24 (m, 6H), 2.23 (s, 3H), 1.70–

1.59 (m, 3H), 1.35–1.28 (m, 3H), 0.71 (s, 6H); **Z-isomer:** δ 15.31 (s, 1H), 7.20 (t, *J* = 7.1 Hz, 1H), 7.12–

7.02 (m, 4H), 6.99 (s, 1H), 6.83 (s, 1H), 6.79 (s, 1H), 6.41 (s, 1H), 5.70 (d, *J* = 13.2 Hz, 1H), 4.26 (d, *J* =

13.2 Hz, 1H), 4.18–4.05 (m, 2H), 4.04–3.85 (m, 2H), 2.82 (s, 3H), 2.32 (s, 3H), 2.26 (s, 3H), 2.39 (s, 3H),

2.11 (s, 3H), 2.03 (s, 3H), 1.54–1.49 (m, 2H), 1.43–1.37 (m, 2H), 1.35–1.30 (m, 2H), 0.98 (s, 3H), 0.91 (s,

3H); **¹³C NMR** (125 MHz, CDCl₃) δ (all discernable signals for both isomers) 313.52, 312.68, 207.22,

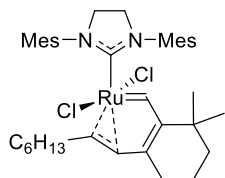
207.13, 167.90, 167.03, 160.43, 158.24, 138.42, 138.19, 137.78, 137.69, 137.63, 137.51, 137.28, 137.13,

137.07, 135.26, 134.78, 134.06, 129.99, 129.94, 129.72, 129.49, 129.17, 128.97, 128.63, 128.55, 126.56,

126.38, 126.21, 123.31, 122.42, 107.65, 106.77, 52.24, 51.85, 51.72, 51.57, 38.35, 38.13, 37.90, 34.50,

33.55, 28.58, 28.24, 27.43, 27.18, 21.15, 21.02, 20.97, 19.93, 19.74, 19.55, 19.33, 19.24, 18.82, 18.58,

18.43; **HRMS (ESI)** calcd for C₃₈H₄₆N₂Cl₂Ru [M]⁺ 702.2076 found, 702.2083.



7-19b

7-19b: 96% yield, only *E*-isomer; red solid; 50 mg obtained; Purification: Flash

Chromatography (SiO₂, hexanes–EtOAc, 10:1 → 5:1); **¹H NMR** (500 MHz, CDCl₃)

δ 16.53 (s, 1H), 6.96 (s, 2H), 6.92 (s, 2H), 4.79 (d, *J* = 12.9 Hz, 1H), 4.10 (s, 4H), 3.73

(dt, *J* = 13.5, 6.9 Hz, 1H), 2.57 (s, 6H), 2.55–2.37 (m, 6H), 2.29 (s, 3H), 2.27 (s, 3H),

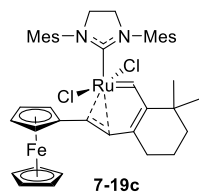
1.60–1.54 (m, 2H), 1.32–1.21 (m, 5H), 1.21–1.07 (m, 6H), 0.96–0.81 (m, 6H), 0.64 (s, 6H); **¹³C NMR** (125

MHz, CDCl₃) δ 311.05, 208.33, 167.21, 158.12, 139.20, 138.77, 138.46, 137.58, 136.89, 133.84, 129.77,

129.24, 128.00, 113.13, 52.28, 51.15, 38.18, 33.98, 33.47, 31.66, 30.72, 30.60, 29.10, 28.64, 22.68, 21.02,

20.95, 20.56, 18.69, 18.57, 14.10; **HRMS (ESI)** calcd for C₃₈H₅₃N₂Ru [M – 2Cl – H]⁺ 639.3247 found,

639.3285.

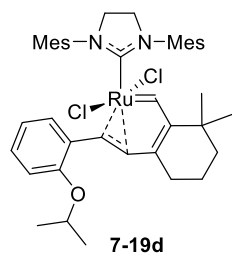


7-19c: 84% yield; 3.5:1 mixture with **7-19a**; red solid; 31.6 mg obtained; Purification:

Flash Chromatography (SiO₂, hexanes–EtOAc, 10:1 → 5:1 → 3:1); ¹H NMR (500 MHz,

CDCl₃) δ 16.51 (s, 1H), 6.97 (bs, 2H), 6.65 (s, 2H), 5.01 (d, *J* = 13.0 Hz, 1H), 4.47 (d, *J* = 13.0 Hz, 1H), 4.09–3.97 (m, 13 H), 2.65–2.21 (m, 18H), 1.65 (m, 2H), 1.54 (m, 2H),

1.34 (m, 2H), 0.70 (s, 6H); ¹³C NMR (125 MHz, CDCl₃) δ 312.2, 208.0, 167.0, 159.2, 138.4, 137.7, 137.6, 137.2, 134.3, 130.0, 129.9, 129.7, 129.5, 128.6, 126.6, 121.0, 108.4, 69.1, 52.2, 51.7, 38.4, 34.9, 21.2, 21.0, 20.0, 18.8, 18.7; **HRMS (ESI)** calcd for C₄₂H₅₀N₂Cl₂FeRu [M]⁺ 810.1738, found 810.1743.

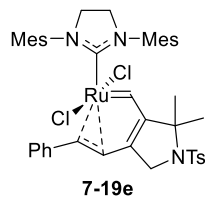


7-19d: 88% yield; *E/Z*-mixture in 14:1 ratio; red solid; 55 mg obtained; Purification:

Flash Chromatography (SiO₂, hexanes–EtOAc, 10:1 → 4:1); ¹H NMR (500 MHz,

CDCl₃) δ 16.65 (s, 1H), 7.15 (d, *J* = 7.1 Hz, 1H), 7.08 (t, *J* = 7.8 Hz, 1H), 6.98 (s, 2H), 6.68 (d, *J* = 8.2 Hz, 1H), 6.62 (s, 2H), 6.54 (t, *J* = 7.4 Hz, 1H), 5.22–5.21 (m,

2H), 4.41–4.38 (m, 1H), 4.02–3.95 (m, 4H), 2.49 (s, 6H), 2.32 (s, 3H), 2.30 (s, 6H), 2.26 (s, 3H), 1.72–1.63 (m, 4H), 1.36–1.33 (m, 2H), 1.24 (s, 3H), 1.23 (s, 3H), 0.71 (s, 6H); ^{13}C NMR (125 MHz, CDCl_3) δ 312.2, 212.3, 207.5, 166.9, 160.6, 154.8, 138.3, 137.9, 137.5, 137.3, 134.6, 130.0, 129.7, 127.5, 126.7, 126.4, 125.1, 121.3, 113.5, 102.0, 70.2, 52.3, 51.9, 38.5, 34.7, 33.6, 28.7, 22.0, 21.2, 21.0, 19.9, 18.9, 18.7; **HRMS** (**ESI**) calcd for $\text{C}_{41}\text{H}_{52}\text{Cl}_2\text{N}_2\text{ORu} [\text{M}]^+$ 760.2495, found 760.2486.

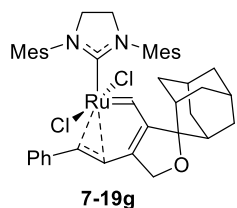


7-19e: 5% yield; greenish yellow solid; 3 mg obtained; Purification: Flash

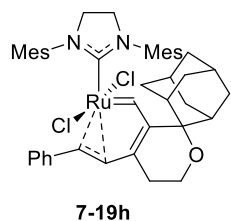
Chromatography (SiO₂, hexanes–EtOAc, 10:1 → 3:1 → 1:1); ¹H NMR (500 MHz,

CDCl₃) δ 16.16 (s, 1H), 7.69 (d, *J* = 8.0 Hz, 2H), 7.26–7.20 (m, 3H), 7.14 (d, *J* = 7.6 Hz, 2H), 7.03–6.74 (m, 2H), 6.63–6.40 (m, 2H), 5.35 (d, *J* = 14.0 Hz, 1H), 5.06

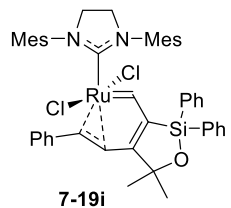
(d, $J = 14.0$ Hz, 1H), 4.09–3.74 (m, 4H), 3.13 (s, 2H), 2.69–2.01 (m, 21H), 1.29 (s, 6H); ^{13}C NMR (125 MHz, CDCl_3) δ 297.04, 203.16, 170.77, 149.02, 143.21, 137.69, 137.64, 133.26, 129.66, 129.56, 129.06, 128.64, 127.55, 127.39, 127.27, 126.66, 124.32, 114.27, 69.35, 57.77, 51.83, 35.64, 35.16, 27.85, 27.00, 26.91, 26.63, 26.36, 26.17, 21.48, 21.05, 19.63, 18.68.; HRMS (ESI) calcd for CHO $[\text{M}+\text{H}]^+$; **HRMS (ESI)** calcd for $\text{C}_{43}\text{H}_{48}\text{N}_3\text{O}_2\text{SCL}_2\text{Ru}$ $[\text{M}-\text{H}]^+$ 842.1882, found 842.1920.



7-19g: 54% yield; yellowish brown solid; 42 mg obtained; Purification: Flash Chromatography (SiO₂, hexanes–EtOAc, 20:1 → 10:1); **¹H NMR** (500 MHz, CDCl₃) δ 17.13 (s, 1H), 7.30–7.25 (m, 1H), 7.16 (d, *J* = 7.7 Hz, 2H), 7.09 (t, *J* = 7.7 Hz, 2H), 6.94 (s, 2H), 6.51 (s, 2H), 5.29–4.95 (m, 2H), 3.97–3.84 (m, 4H), 3.63 (s, 2H), 2.48 (s, 6H), 2.33–2.09 (m, 12H), 2.14 (d, *J* = 12.7 Hz, 2H), 1.86–1.71 (m, 4H), 1.69–1.63 (m, 2H), 1.53–1.36 (m, 4H), 0.97 (d, *J* = 13.3 Hz, 2H); **¹³C NMR** (125 MHz, CDCl₃) δ 300.81, 204.15, 172.30, 164.64, 138.28, 137.78, 137.08, 136.81, 134.43, 133.69, 130.21, 129.59, 128.65, 127.38, 126.79, 117.04, 112.03, 92.25, 75.15, 53.07, 51.55, 38.23, 37.67, 34.12, 33.32, 27.10, 27.01, 26.92, 26.69, 26.38, 26.18, 21.18, 19.77, 18.79; **HRMS (ESI)** calcd for C₄₃H₄₉N₂ORu [M – 2Cl – H]⁺ 711.2888, found 711.2900.

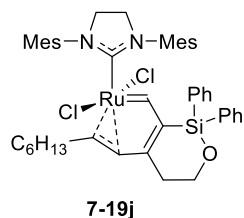


7-19h: 78% yield; yellowish brown solid; 58 mg obtained; Purification: Flash Chromatography (SiO₂, hexanes–EtOAc, 10:1 → 4:1); **¹H NMR** (500 MHz, CDCl₃) δ 16.89 (s, 1H), 7.22 (t, *J* = 7.3 Hz, 1H), 7.13–7.00 (m, 5H), 6.84 (s, 1H), 6.55 (s, 1H), 6.41 (s, 1H), 5.24 (d, *J* = 12.3 Hz, 1H), 4.71 (d, *J* = 12.3 Hz, 1H), 4.05–3.69 (m, 6H), 2.79 (s, 3H), 2.42 (s, 3H), 2.33–2.05 (m, 14H), 1.80–1.68 (m, 3H), 1.66 (s, 2H), 1.64–1.53 (m, 2H), 1.52–1.31 (m, 6H), 1.11 (d, *J* = 13.2 Hz, 1H); **¹³C NMR** (125 MHz, CDCl₃) δ 300.81, 204.15, 172.30, 164.64, 138.28, 137.78, 137.08, 136.81, 134.43, 133.69, 130.21, 129.59, 128.65, 127.38, 126.79, 117.04, 112.03, 92.25, 75.15, 53.07, 51.55, 38.23, 37.67, 34.12, 33.32, 27.10, 27.01, 26.92, 26.69, 26.38, 26.18, 21.18, 19.77, 18.79; **HRMS (ESI)** calcd for C₄₄H₅₁N₂ORu [M – 2Cl – H]⁺ 725.3045, found 725.3053.



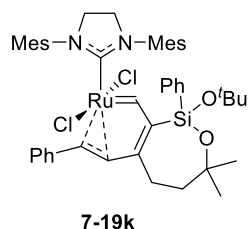
7-19i: 82% yield; red solid; 44 mg obtained; Purification: Flash Chromatography (SiO₂, hexanes–EtOAc, 10:1 → 4:1); **¹H NMR** (500 MHz, CDCl₃) δ 16.02 (s, 1H), 7.51–7.49 (m, 2H), 7.42 (m, 8H), 7.23 (t, *J* = 7.0 Hz, 1H), 7.09–7.03 (m, 4H), 6.94 (s, 2H), 6.26 (bs, 2H), 5.77 (d, *J* = 13.5 Hz, 1H), 4.79 (d, *J* = 13.5 Hz, 1H), 4.02–3.99 (m, 4H), 2.32 (s, 9H), 2.21 (s, 6H), 2.01 (s, 3H), 1.53 (s, 6H); **¹³C NMR** (125 MHz, CDCl₃) δ 311.9, 204.9, 182.6, 159.8, 138.0, 137.9, 137.2, 137.0, 135.1, 134.3, 133.6, 130.6, 129.8, 129.4, 128.8, 128.0, 126.9,

126.3, 123.7, 107.8, 86.2, 51.8, 51.6, 28.2, 21.3, 21.1, 19.7, 18.8; **HRMS (ESI)** calcd for $C_{47}H_{49}N_2OSiRu$ $[M - 2Cl - H]^+$ 787.2652, found 787.2637.



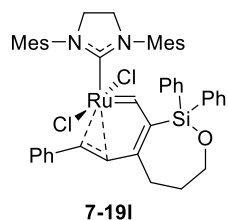
7-19j: 93% yield; red solid; 43 mg obtained; Purification: Flash Chromatography (SiO₂, hexanes–EtOAc, 10:1 → 4:1); **¹H NMR** (500 MHz, CDCl₃) δ 16.43 (s, 1H), 7.47 (t, *J* = 7.4 Hz, 2H), 7.37 (t, *J* = 7.4 Hz, 4H), 7.31 (d, *J* = 7.1 Hz, 4H), 6.94 (s, 2H), 6.20 (s, 2H), 5.07 (d, *J* = 13.0 Hz, 1H), 4.09–4.05 (m, 4H), 3.97–3.86 (m, 3H),

2.56 (s, 6H), 2.34 (s, 3H), 2.30 (s, 6H), 2.02 (t, *J* = 4.9 Hz, 2H), 1.73 (s, 3H), 1.60 (m, 2H), 1.28–1.12 (m, 8H), 0.88 (t, *J* = 7.2 Hz, 3H); **¹³C NMR** (125 MHz, CDCl₃) δ 312.2, 206.7, 171.7, 155.8, 139.3, 138.9, 138.1, 136.9, 136.4, 135.2, 133.7, 133.4, 131.7, 130.4, 130.0, 129.5, 129.4, 127.0, 112.7, 60.6, 52.3, 51.1, 37.9, 31.7, 30.8, 30.7, 29.1, 27.8, 26.3, 22.7, 20.9, 20.6, 18.8, 14.2; **HRMS (ESI)** calcd for $C_{46}H_{55}N_2OSiRu$ $[M - 2Cl - H]^+$ 781.3122, found 781.3052.



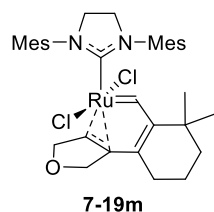
7-19k: 83% yield; red solid; 44 mg obtained; Purification: Flash Chromatography (SiO₂, hexanes–EtOAc, 10:1 → 4:1 → 2:1); **¹H NMR** (500 MHz, CDCl₃) δ 16.07 (s, 1H), 7.45–7.37 (m, 5H), 7.21–7.19 (m, 1H), 7.06–7.03 (m, 4H), 6.86 (s, 2H), 6.35 (s, 1H), 5.67 (d, *J* = 12.6 Hz, 1H), 5.22 (s, 1H), 4.45 (d, *J* = 12.6 Hz, 1H),

4.04–3.86 (m, 4H), 2.74 (s, 3H), 2.44 (s, 3H), 2.30 (s, 3H), 1.98 (s, 3H), 1.87 (s, 3H), 1.83 (s, 3H), 1.78 (m, 2H), 1.38 (m, 5H), 1.21 (s, 9H), 1.13 (s, 3H); **¹³C NMR** (125 MHz, CDCl₃) δ 317.5, 206.4, 179.4, 158.4, 138.6, 138.3, 138.1, 137.6, 137.2, 136.0, 135.6, 134.6, 134.1, 130.2, 129.9, 129.7, 129.4, 129.1, 128.7, 127.4, 126.4, 126.2, 125.7, 104.9, 74.1, 73.5, 51.8, 40.2, 35.5, 31.8, 31.7, 31.5, 31.3, 31.2, 28.2, 27.7, 26.6, 21.2, 21.1, 20.1, 19.3, 19.2, 18.4; **HRMS (ESI)** calcd for $C_{47}H_{58}Cl_1N_2O_2RuSi$ $[M - Cl]^+$ 847.2994, found 847.2999

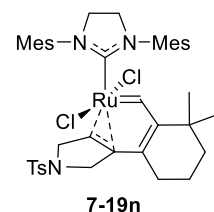


7-19l: 92% yield; red solid; 47 mg obtained; Purification: Flash Chromatography (SiO₂, hexanes–EtOAc, 10:1 → 4:1); **¹H NMR** (500 MHz, CDCl₃) δ 16.38 (s, 1H), 7.50 (t, *J* = 7.2 Hz, 2H), 7.42 (t, *J* = 7.3 Hz, 4H), 7.35 (d, *J* = 7.0 Hz, 4H), 7.24–7.23 (m, 1H), 7.18 (d, *J* = 7.6 Hz, 2H), 7.09 (t, *J* = 7.53 Hz, 2H), 6.55 (bs, 2H), 6.05 (bs,

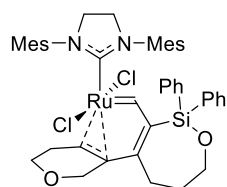
2H), 5.67 (d, $J = 12.7$ Hz, 1H), 4.91 (d, $J = 12.7$ Hz, 1H), 3.92 (bm, 6H), 2.29–2.24 (m, 17H), 1.94–1.77 (m, 2H), 1.46 (s, 3H); ^{13}C NMR (125 MHz, CDCl_3) δ 315.1, 206.2, 181.2, 157.5, 137.8, 137.8, 136.3, 135.3, 135.1, 134.6, 133.9, 133.9, 130.2, 129.8, 129.5, 128.7, 128.3, 128.1, 128.0, 126.8, 126.6, 109.5, 65.3, 52.3, 51.7, 37.6, 28.9, 26.4, 26.2, 21.2, 20.5, 20.0, 19.9, 18.7; **HRMS (ESI)** calcd for $\text{C}_{47}\text{H}_{50}\text{Cl}_1\text{N}_2\text{OSiRu}$ $[\text{M} - \text{Cl}]^+$ 823.2419, found 823.2413.



7-19m: 54% yield; red solid; 28.5 mg obtained; Purification: Flash Chromatography (SiO_2 , hexanes–EtOAc, 10:1 \rightarrow 4:1 \rightarrow 2:1); ^1H NMR (500 MHz, CDCl_3) δ 16.13 (s, 1H), 7.07 (s, 1H), 6.93 (s, 1H), 6.90 (s, 1H), 6.78 (s, 1H), 5.48 (d, $J = 10.0$ Hz, 1H), 4.59 (d, $J = 10.0$ Hz, 1H), 4.20–4.07 (m, 5H), 3.71 (d, $J = 11.9$ Hz, 1H), 2.97 (s, 3H), 2.75 (d, $J = 11.9$ Hz, 1H), 2.65 (s, 3H), 2.51 (m, 3H), 2.27 (s, 3H), 2.26 (s, 3H), 2.22 (s, 3H), 1.63–1.54 (m, 3H), 1.43–1.41 (m, 1H), 1.31–1.20 (m, 2H), 0.86 (s, 3H), 0.36 (s, 3H); ^{13}C NMR (125 MHz, CDCl_3) δ 303.1, 207.2, 167.6, 160.7, 139.2, 139.0, 138.4, 138.2, 137.6, 137.5, 136.4, 133.1, 130.0, 129.3, 129.2, 127.5, 104.9, 73.5, 72.8, 52.1, 51.5, 38.2, 33.7, 33.1, 30.0, 28.2, 21.0, 20.9, 20.6, 20.4, 19.3, 18.7, 18.3; **HRMS (ESI)** calcd for $\text{C}_{34}\text{H}_{43}\text{N}_2\text{ORu}$ $[\text{M} - 2\text{Cl} - \text{H}]^+$ 597.2413 found, 597.2411.



7-19n: 62% yield; red solid; 38 mg obtained; Purification: Flash Chromatography (SiO_2 , hexanes–EtOAc, 10:1 \rightarrow 4:1 \rightarrow 1:1); ^1H NMR (500 MHz, CDCl_3) δ 16.10 (s, 1H), 7.68 (d, $J = 7.9$ Hz, 2H), 7.32 (d, $J = 7.9$ Hz, 2H), 7.10 (s, 1H), 7.06 (s, 1H), 6.96 (s, 1H), 6.77 (s, 1H), 5.00 (d, $J = 10.9$ Hz, 1H), 4.23–4.17 (m, 1H), 4.17–4.14 (m, 1H), 4.13–4.10 (m, 1H), 4.09–4.05 (m, 2H), 4.02–3.99 (m, 1H), 3.81 (d, $J = 10.9$ Hz, 1H), 3.05 (d, $J = 12.9$ Hz, 1H), 2.95 (s, 3H), 2.64 (s, 3H), 2.58 (s, 3H), 2.45–2.39 (m, 5H), 2.32 (s, 3H), 2.25 (s, 3H), 2.19 (s, 3H), 1.49–1.42 (m, 2H), 1.16 (dd, $J = 23.5, 10.8$ Hz, 2H), 0.78 (s, 3H), 0.34 (s, 3H); ^{13}C NMR (125 MHz, CDCl_3) δ 303.68, 205.95, 167.30, 160.78, 143.40, 139.65, 138.40, 137.96, 137.54, 137.48, 136.47, 132.91, 132.60, 130.49, 130.08, 129.62, 129.56, 129.39, 128.25, 124.36, 53.57, 53.17, 52.08, 51.65, 38.07, 33.62, 33.04, 29.83, 27.83, 21.55, 21.09, 20.89, 20.36, 20.18, 19.28, 18.63, 18.06; **HRMS (ESI)** calcd for $\text{C}_{41}\text{H}_{52}\text{N}_3\text{O}_2\text{SCl}_2\text{Ru}$ $[\text{M} + \text{H}]^+$ 822.2195, found 822.2194.



7-19o

7-19o: 84% yield; red solid; 42 mg obtained; Purification: Flash Chromatography

(SiO₂, hexanes–EtOAc, 10:1 → 4:1 → 1:1); **¹H NMR** (500 MHz, CDCl₃) δ 16.51 (s, 1H), 7.50–7.44 (m, 2H), 7.41–7.34 (m, 5H), 7.31–7.30 (m, 2H), 6.97 (s, 1H), 6.87

(s, 1H), 6.30 (s, 1H), 5.89 (s, 1H), 5.45 (d, *J* = 14.4 Hz, 1H), 4.60 (d, *J* = 3.4 Hz, 1H),

4.52 (d, *J* = 14.4 Hz, 1H), 4.16–3.98 (m, 4H), 3.90–3.79 (m, 3H), 3.29 (td, *J* = 11.0, 5.4 Hz, 1H), 3.05–3.00

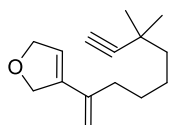
(m, 1H), 2.62 (s, 3H), 2.59 (s, 3H), 2.45 (s, 3H), 2.27 (s, 3H), 2.22 (s, 3H), 2.10–1.90 (m, 4H), 1.66–1.57

(m, 2H), 1.53 (m, 3H); **¹³C NMR** (125 MHz, CDCl₃) δ 309.8, 205.0, 177.6, 155.6, 139.7, 139.2, 138.9,

137.7, 136.6, 136.2, 135.6, 135.2, 135.0, 134.5, 133.4, 132.7, 130.2, 130.1, 129.9, 129.1, 127.0, 102.7, 63.7,

62.8, 52.4, 51.0, 34.2, 27.9, 24.7, 21.0, 20.7, 20.6, 20.5, 18.9, 18.7; **HRMS (ESI)** calcd for C₄₄H₄₉N₂O₂RuSi

[*M* – 2Cl – H]⁺ 767.2601, found 767.2575.



7-19p'

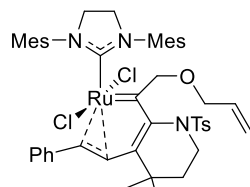
7-19p': 42% yield; colorless oil; 8 mg obtained; Purification: Flash Chromatography

(SiO₂, hexanes–EtOAc, 50:1 → 20:1); **¹H NMR** (500 MHz, CDCl₃) δ 5.84 (s, 1H), 5.00

(s, 1H), 4.77–4.70 (m, 5H), 2.30 (t, *J* = 7.0, 2H), 2.08 (s, 1H), 1.52–1.41 (m, 6H), 1.21

(s, 6H); **¹³C NMR** (125 MHz, CDCl₃) δ 140.7, 121.5, 118.6, 112.9, 92.0, 76.6, 75.3, 67.7, 43.0, 34.1, 31.0,

29.7, 29.2, 28.9, 25.2; **LRMS (ESI)** calcd for C₁₅H₂₀OLi [*M* – 2H + Li]⁺ 223.2, found, 223.2.



7-19q

7-19q: 88% yield; red solid; 61 mg obtained; Purification: Flash Chromatography

(SiO₂, hexanes–EtOAc, 10:1 → 4:1 → CH₂Cl₂–EtOAc, 1:1); **¹H NMR** (500 MHz,

CDCl₃) δ 7.86 (d, *J* = 8.0 Hz, 2H), 7.29 (d, *J* = 8.0 Hz, 2H), 7.23 (t, *J* = 7.3 Hz, 1H),

7.07 (t, *J* = 7.6 Hz, 2H), 7.00 (bs, 1H), 6.93 (m, 4H), 6.33 (s, 1H), 5.82 (m, 1H),

5.71 (d, *J* = 13.4 Hz, 1H), 5.21 (s, 1H), 5.18 (s, 1H), 5.08 (m, 1H), 4.10–3.71 (m, 8H), 2.97 (dd, *J* = 20.3,

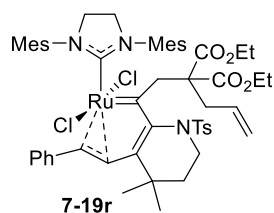
7.9 Hz, 1H), 2.85 (s, 3H), 2.58 (d, *J* = 15.0 Hz, 1H), 2.46 (s, 3H), 2.39 (s, 3H), 2.32 (s, 6H), 2.11 (s, 3H),

1.83 (s, 3H), (d, *J* = 13.8 Hz, 1H), 0.85 (s, 6H), 0.81 (d, *J* = 3.7 Hz, 1H); **¹³C NMR** (125 MHz, CDCl₃) δ

318.5, 205.7, 162.6, 155.4, 143.3, 139.1, 138.0, 137.7, 137.2, 136.7, 136.1, 135.8, 133.9, 131.7, 131.0,

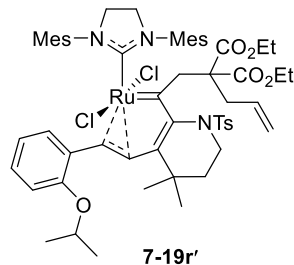
129.6, 129.4, 129.3, 128.8, 128.5, 127.1, 127.0, 115.2, 105.0, 98.7, 85.5, 72.2, 52.5, 52.3 44.5, 36.8, 34.1,

30.7, 26.4, 21.6, 21.2, 20.4, 19.1, 18.9, 18.8; **HRMS (ESI)** calcd for $C_{48}H_{57}N_3O_3SClRu [M - Cl]^+$ 892.2847 found, 892.2845.



7-19r: 87% yield; red solid; 56 mg obtained; Purification: Flash Chromatography (SiO₂, hexanes–EtOAc, 10:1 → 4:1 → CH₂Cl₂–EtOAc, 1:1); **¹H NMR** (500 MHz, CDCl₃) δ 7.92 (d, *J* = 7.1 Hz, 2H), 7.29 (d, *J* = 7.9 Hz, 2H), 7.19 (t, *J* = 7.2 Hz, 1H), 7.04–7.00 (m, 4H), 6.92 (d, *J* = 7.7 Hz, 2H), 6.84 (s, 1H), 6.21 (s, 1H),

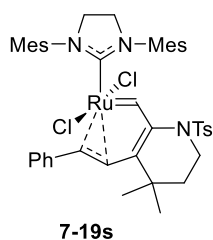
5.90–5.81 (m, 1H), 5.66 (d, *J* = 13.2 Hz, 1H), 5.04–4.97 (m, 2H), 4.42 (d, *J* = 15.9 Hz, 1H), 4.27–4.16 (m, 3H), 4.05–3.93 (m, 5H), 3.74–3.73 (m, 1H), 3.63 (d, *J* = 14.6 Hz, 1H), 3.25–3.18 (m, 1H), 2.66 (s, 3H), 2.69–2.67 (m, 1H), 2.46 (s, 3H), 2.40 (s, 3H), 2.38 (s, 3H), 2.30–2.27 (m, 4H), 2.20 (s, 3H), 2.10–2.07 (m, 1H), 1.98 (s, 3H), 1.31–1.24 (m, 6H), 0.91 (s, 3H), 0.83 (bm, 2H), 0.71 (s, 3H); **¹³C NMR** (125 MHz, CDCl₃) δ 318.2, 205.0, 171.1, 169.4, 163.7, 155.9, 143.3, 138.6, 137.7, 137.6, 137.3, 137.0, 136.9, 136.2, 135.5, 133.9, 131.6, 130.7, 129.8, 129.4, 129.3, 128.5, 126.9, 126.6, 117.5, 104.0, 96.2, 61.7, 60.8, 60.7, 55.3, 53.0, 52.1, 45.1, 42.2, 37.2, 33.2, 30.4, 26.0, 21.5, 21.3, 20.5, 19.2, 18.8, 14.1, 13.9; **HRMS (ESI)** calcd for $C_{55}H_{67}N_3O_6SCl_2Ru [M]^+$ 1069.3166 found, 1069.3180.



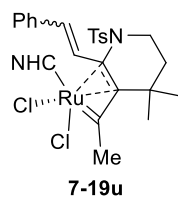
7-19r': 91% yield; red solid; 61 mg obtained; Purification: Flash Chromatography (SiO₂, hexanes–EtOAc, 10:1 → 4:1 → CH₂Cl₂–EtOAc, 1:1); **¹H NMR** (500 MHz, CDCl₃) δ 7.95 (d, *J* = 7.2 Hz, 2H), 7.29 (d, *J* = 8.1 Hz, 2H), 7.04–7.00 (m, 1H), 6.96 (d, *J* = 2.8 Hz, 2H), 6.90 (s, 1H), 6.67 (d, *J* = 8.2 Hz, 1H), 6.54 (d, *J* = 7.5 Hz, 1H), 6.44 (s, 1H), 6.41 (t, *J* = 7.5 Hz, 1H), 5.84 (dtd, *J*

= 17.2, 9.5, 5.2 Hz, 1H), 5.75 (d, *J* = 13.3 Hz, 1H), 4.99 (d, *J* = 16.8 Hz, 1H), 4.92 (dd, *J* = 1.9 Hz, 10.1 Hz, 1H), 4.77–4.73 (m, 2H), 4.37–4.30 (m, 1H), 4.20–4.11 (m, 4H), 3.99–3.93 (m, 3H), 3.76–3.72 (m, 1H), 3.68–3.61 (m, 1H), 3.19–3.11 (m, 1H), 2.89 (s, 3H), 2.53 (s, 3H), 2.39–2.34 (m, 2H), 2.38 (s, 3H), 2.36 (s, 3H), 2.30 (s, 3H), 2.28–2.23 (m, 1H), 2.21 (m, 3H), 2.13 (s, 3H), 1.93 (d, *J* = 16.2 Hz, 1H), 1.29 (t, *J* = 7.1 Hz, 3H), 1.26–1.20 (m, 6H), 1.12 (d, *J* = 6.1 Hz, 3H), 0.85–0.78 (m, 2H), 0.91 (s, 3H), 0.68 (s, 3H); **¹³C NMR** (125 MHz, CDCl₃) δ 318.0, 205.1, 171.0, 170.2, 163.2, 156.2, 155.7, 143.3, 138.6, 138.1, 137.6,

137.2, 136.9, 136.7, 135.7, 135.0, 131.5, 130.8, 129.9, 129.5, 129.4, 128.1, 126.3, 121.1, 117.4, 113.7, 107.4, 94.1, 70.6, 61.2, 60.5, 56.7, 53.0, 52.5, 45.3, 40.5, 36.9, 33.0, 30.4, 26.0, 22.5, 22.0, 21.5, 21.3, 20.5, 19.7, 19.5, 18.9, 14.2, 13.8; **HRMS (ESI)** calcd for $C_{58}H_{73}Cl_2N_3O_7RuS$ $[M - H]^+$ 1126.3506, found 1126.3564.

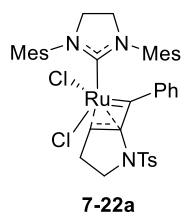


7-19s: 68% yield; red solid; 35 mg obtained; Purification: Flash Chromatography (SiO_2 , hexanes–EtOAc, 10:1 \rightarrow 4:1 \rightarrow CH_2Cl_2 –EtOAc, 1:1); **1H NMR** (500 MHz, $CDCl_3$) δ 16.34 (s, 1H), 7.48 (d, J = 8.1 Hz, 2H), 7.27–7.25 (m, 2H), 7.20–7.17 (m, 4H), 7.11 (t, J = 7.6 Hz, 2H), 6.89 (s, 1H), 6.55 (s, 1H), 6.52 (s, 1H), 5.23 (d, J = 13.2 Hz, 1H), 4.72 (d, J = 13.2 Hz, 1H), 4.11–3.91 (m, 4H), 3.74 (td, J = 3.9 Hz, J = 14.4 Hz, 1H), 3.26–3.20 (m, 1H), 2.77 (s, 3H), 2.37 (s, 3H), 2.33 (s, 6H), 2.28 (s, 3H), 2.25 (s, 3H), 2.21 (s, 3H), 1.10 (s, 3H), 1.04–1.01 (m, 1H), 0.78–0.72 (m, 1H), 0.51 (s, 3H); **^{13}C NMR** (125 MHz, $CDCl_3$) δ 311.0, 205.6, 159.8, 152.2, 143.5, 138.7, 138.2, 137.7, 137.2, 137.1, 136.3, 136.1, 135.5, 134.7, 134.2, 131.0, 129.5, 129.4, 129.3, 128.6, 128.5, 127.3, 126.9, 115.2, 112.9, 52.4, 51.8, 44.1, 37.3, 33.8, 27.7, 27.2, 21.6, 21.2, 19.86, 19.81, 19.1, 18.7; **HRMS (ESI)** calcd for $C_{44}H_{51}N_3O_2SClRu$ $[M - Cl]^+$ 822.2429, found 822.2429.



7-19u: 62% yield; mixture of *E/Z*-isomers in a 4:1 ratio; red solid; 40 mg obtained; Purification: Flash Chromatography Chromatography (SiO_2 , hexanes–EtOAc, 10:1 \rightarrow 4:1 \rightarrow CH_2Cl_2 –EtOAc, 1:1); **1H NMR** (500 MHz, $CDCl_3$) ***E* isomer:** δ 8.23 (d, J = 8.1 Hz, 2H), 7.56 (d, J = 15.6 Hz, 1H), 7.34 (d, J = 7.2 Hz, 2H), 7.29–7.21 (m, 5H), 7.06 (s, 2H), 6.94 (s, 1H), 6.70 (s, 1H), 5.36 (d, J = 15.6 Hz, 1H), 4.21–4.01 (m, 4H), 3.66–3.53 (m, 1H), 3.33–3.23 (m, 1H), 2.57 (s, 3H), 2.44 (s, 3H), 2.38 (s, 3H), 2.36 (s, 3H), 2.32 (s, 6H), 2.19 (s, 3H), 1.77 (s, 3H), 1.44 (td, J = 13.2, 4.3 Hz, 1H), 0.89 (s, 3H), 0.80 (s, 3H), 0.45–0.34 (m, 1H); ***Z* isomer:** δ 8.16 (d, J = 8.0 Hz, 2H), 7.41 (d, J = 7.7 Hz, 2H), 7.29–7.20 (m, 4H), 7.09 (s, 1H), 7.06–7.04 (m, 1H), 7.04 (s, 1H), 7.02 (s, 1H), 6.92 (s, 1H), 6.05 (d, J = 13.1 Hz, 1H), 4.55 (d, J = 13.1 Hz, 1H), 4.39–4.22 (m, 4H), 3.39–3.32 (m, 1H), 2.97–2.86 (m, 1H), 2.67 (s, 3H), 2.63 (s, 3H), 2.57 (s, 3H), 2.37–2.34 (m, 9H), 2.26 (s, 3H), 1.73 (s, 3H), 1.67–1.54 (m, 2H), 0.98 (s, 3H), 0.84 (s, 3H); **^{13}C NMR** (125 MHz, $CDCl_3$) (all discernable peaks for both

isomers) δ 258.18, 257.30, 217.17, 214.30, 146.29, 146.11, 140.37, 140.12, 140.04, 139.75, 139.41, 138.99, 138.31, 137.85, 137.80, 137.28, 137.23, 136.80, 136.41, 136.36, 133.37, 131.44, 131.20, 130.62, 130.47, 130.38, 130.12, 130.11, 129.94, 129.87, 129.73, 129.65, 129.59, 128.86, 128.56, 128.25, 128.10, 127.32, 127.12, 84.53, 84.13, 76.53, 76.10, 52.20, 52.13, 51.16, 50.97, 46.96, 46.74, 40.09, 39.54, 29.71, 29.45, 29.39, 29.21, 29.19, 28.66, 21.79, 21.38, 21.34, 21.10, 21.05, 20.13, 20.02, 19.38, 19.29, 18.77, 18.55, 18.48, 3.58, 3.54; **HRMS (ESI)** calcd for $C_{45}H_{52}N_3O_2SRu$ $[M - 2Cl - H]^+$ 800.2824, found 800.2814.

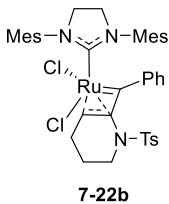


7-22a: 92% yield; green solid; 48 mg obtained; Purification: Flash Chromatography

(SiO_2 , hexanes–EtOAc, 10:1 \rightarrow 4:1 \rightarrow CH_2Cl_2 –EtOAc, 1:1); **1H NMR** (500 MHz, $CDCl_3$) δ 8.33–7.56 (d, J = 8.0 Hz, 2H), 7.54 (t, J = 7.5 Hz, 1H), 7.14 (t, J = 7.7 Hz, 2H),

7.03 (s, 1H), 7.00 (s, 1H), 6.95 (d, J = 8.1 Hz, 2H), 6.88 (d, J = 7.9 Hz, 2H), 6.28 (s, 1H),

6.08 (s, 1H), 4.25–4.16 (m, 1H), 4.07–3.93 (m, 2H), 3.87–3.58 (m, 3H), 3.54 (d, J = 5.1 Hz, 1H), 2.62 (s, 3H), 2.61 (s, 3H), 2.41–2.34 (m, 1H), 2.30 (s, 3H), 2.29 (s, 3H), 2.19 (s, 3H), 1.94 (s, 3H), 1.80–1.70 (m, 1H), 1.69 (s, 3H); **^{13}C NMR** (125 MHz, $CDCl_3$) δ 266.91, 209.92, 144.30, 143.58, 140.48, 139.82, 138.37, 136.96, 135.61, 133.43, 131.05, 130.07, 129.82, 129.44, 129.23, 128.96, 128.85, 128.62, 128.26, 127.92, 114.89, 104.90, 52.88, 52.17, 51.77, 51.60, 27.93, 21.59, 21.25, 20.93, 20.58, 18.98, 18.77, 17.71; **HRMS (ESI)** calcd for $C_{39}H_{42}N_3O_2RuS$ $[M - 2Cl - H]^+$ 718.2036, found 718.2075.



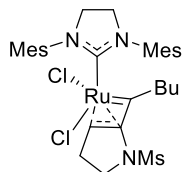
7-22b: 94% yield; green solid; 45 mg obtained; Purification: Flash Chromatography

(SiO_2 , hexanes–EtOAc, 10:1 \rightarrow 4:1 \rightarrow CH_2Cl_2 –EtOAc, 1:1); **1H NMR** (500 MHz, $CDCl_3$) δ 7.64 (d, J = 8.1 Hz, 2H), 7.18 (d, J = 8.1 Hz, 2H), 7.16–7.08 (m, 2H), 7.07–

7.01 (m, 4H), 6.99 (s, 2H), 6.95 (s, 1H), 6.08 (t, J = 4.5 Hz, 1H), 4.30 (q, J = 11.1 Hz,

1H), 4.23–4.12 (m, 2H), 4.11–4.03 (m, 1H), 3.96 (q, J = 11.1 Hz, 1H), 3.85–3.74 (m, 1H), 3.54–3.27 (m, 1H), 3.01–2.88 (m, 1H), 2.57 (s, 3H), 2.48 (s, 3H), 2.41 (s, 3H), 2.35 (s, 3H), 2.32 (s, 3H), 2.30 (s, 3H), 1.98 (s, 3H), 1.28–1.24 (m, 1H), 0.67 (ddd, J = 24.7, 13.2, 5.4 Hz, 1H); **^{13}C NMR** (125 MHz, $CDCl_3$) δ 280.76, 215.28, 160.37, 154.46, 145.04, 140.66, 140.22, 139.15, 138.34, 137.77, 136.78, 136.58, 133.78, 130.44, 130.36, 130.06, 129.60, 129.52, 128.49, 128.39, 126.26, 125.60, 122.18, 52.08, 51.29, 45.78, 23.42,

21.67, 21.33, 21.14, 20.60, 19.36, 19.09, 18.75, 17.17; **HRMS (ESI)** calcd for $C_{40}H_{45}N_3O_2SClRu$ $[M - Cl]^+$ 768.1959, found 768.1977.



7-22c

7-22c: 68% yield; green solid; 35 mg obtained; Purification: Flash Chromatography

(SiO_2 , hexanes–EtOAc, 10:1 \rightarrow 4:1 \rightarrow CH_2Cl_2 –EtOAc, 1:1); **1H NMR** (500 MHz, $CDCl_3$)

δ 7.05 (s, 1H), 7.03 (s, 1H), 6.89 (s, 1H), 6.83 (s, 1H), 5.98 (t, J = 3.6 Hz, 1H), 4.26–4.14

(m, 2H), 4.10–3.97 (m, 2H), 3.80 (td, J = 11.2, 6.2 Hz, 1H), 3.63 (td, J = 11.1, 8.1 Hz,

1H), 2.76 (s, 3H), 2.51 (s, 3H), 2.39 (s, 3H), 2.34 (s, 3H), 2.29 (s, 6H), 2.17 (s, 3H), 2.13–2.04 (m, 2H),

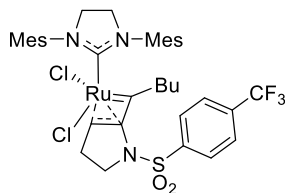
1.72–1.56 (m, 1H), 1.43–1.18 (m, 4H), 1.18–1.09 (m, 1H), 0.79 (t, J = 7.3 Hz, 3H); **^{13}C NMR** (125 MHz,

$CDCl_3$) δ 284.23, 216.99, 159.24, 139.90, 139.80, 138.46, 138.01, 137.93, 137.21, 136.35, 131.87, 130.29,

129.58, 129.49, 128.52, 103.64, 58.07, 51.58, 51.47, 48.64, 34.50, 29.44, 28.25, 22.96, 21.32, 21.12, 20.33,

18.63, 18.45, 18.19, 13.66; **HRMS (ESI)** calcd for $C_{31}H_{42}N_3O_2SRu$ $[M - 2Cl-H]^+$ 622.2041, found

622.2049.



7-22d

7-22d: 90% yield; green solid; 54 mg obtained; Purification: Flash

Chromatography (SiO_2 , hexanes–EtOAc, 10:1 \rightarrow 4:1 \rightarrow CH_2Cl_2 –EtOAc, 1:1);

1H NMR (500 MHz, $CDCl_3$) δ 7.87 (d, J = 8.3 Hz, 2H), 7.65 (d, J = 8.4 Hz, 2H),

7.11–7.06 (m, 1H), 7.02–6.97 (m, 1H), 6.91 (s, 1H), 6.87 (s, 1H), 6.10 (t, J = 3.6

Hz, 1H), 4.42–4.31 (m, 1H), 4.30–4.21 (m, 2H), 4.16 (td, J = 10.5, 5.2 Hz, 1H), 4.09–4.00 (m, 1H), 3.75

(td, J = 11.4, 8.7 Hz, 1H), 3.43 (td, J = 11.3, 5.0 Hz, 1H), 2.49 (s, 6H), 2.44 (s, 3H), 2.33–2.26 (m, 3H),

2.31 (s, 3H), 2.29 (s, 3H), 2.19 (s, 3H), 1.41–1.23 (m, 2H), 1.14 (ddt, J = 19.6, 11.1, 3.8 Hz, 2H), 0.86 (t, J

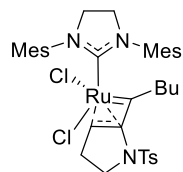
= 7.3 Hz, 3H); **^{13}C NMR** (125 MHz, $CDCl_3$) δ 284.31, 216.56, 156.32, 140.10, 139.96, 138.85, 137.97,

137.77, 137.15, 136.96, 136.39, 131.30, 130.42, 129.70, 129.66, 129.20, 128.54, 128.50, 126.27, 126.23,

106.43, 57.61, 51.81, 51.27, 48.38, 29.29, 28.06, 23.07, 21.29, 21.10, 20.39, 18.87, 18.64, 18.48, 13.64; **^{19}F**

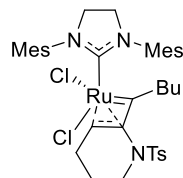
NMR (376 MHz, $CDCl_3$) δ -63.86; **HRMS (ESI)** calcd for $C_{37}H_{43}N_3O_2SRuF_3$ $[M - 2Cl - H]^+$ 822.2429,

found 822.2429.



7-22e

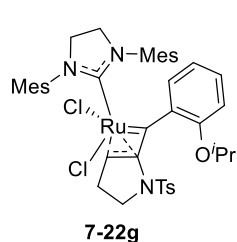
7-22e: 89% yield; green solid; 41 mg obtained; Purification: Flash Chromatography (SiO₂, hexanes–EtOAc, 10:1 → 4:1 → CH₂Cl₂–EtOAc, 1:1); **¹H NMR** (500 MHz, CDCl₃) δ 7.57 (d, *J* = 8.0 Hz, 2H), 7.15 (d, *J* = 8.1 Hz, 2H), 7.08 (s, 1H), 7.00 (s, 1H), 6.90 (s, 1H), 6.86 (s, 1H), 6.04 (t, *J* = 3.5 Hz, 1H), 4.39–4.31 (m, 1H), 4.28–4.19 (m, 1H), 4.14 (td, *J* = 10.6, 4.8 Hz, 1H), 4.02 (q, *J* = 11.2 Hz, 1H), 3.67 (td, *J* = 11.3, 8.7 Hz, 1H), 3.43 (td, *J* = 11.3, 4.9 Hz, 1H), 2.49 (s, 6H), 2.45 (s, 3H), 2.33–2.25 (m, 13H), 2.19 (s, 3H), 1.33 (tq, *J* = 13.6, 6.8 Hz, 2H), 1.21–1.13 (m, 1H), 1.12–1.03 (ddt, *J* = 15.5, 10.4, 4.8 Hz, 1H), 0.86 (t, *J* = 7.4 Hz, 3H); **¹³C NMR** (126 MHz, CDCl₃) δ 285.42, 217.14, 156.56, 144.94, 139.94, 139.89, 138.79, 137.95, 137.80, 137.15, 136.47, 131.50, 130.64, 130.34, 129.69, 129.57, 129.39, 128.65, 128.55, 106.00, 57.48, 51.81, 51.21, 48.21, 29.34, 28.05, 23.11, 21.58, 21.30, 21.09, 20.40, 18.93, 18.69, 18.53, 13.68; **HRMS (ESI)** calcd for C₃₇H₄₆N₃O₂SRu [M – 2Cl – H]⁺ 698.2354, found 698.2364.



7-22f

7-22f: 78% yield; green solid; 38 mg obtained; Purification: Flash Chromatography (SiO₂, hexanes–EtOAc, 10:1 → 4:1 → CH₂Cl₂–EtOAc, 1:1); The ¹H NMR for this complex at 298K gave broad signals due to fluxionality in the complex but sharper NMR with distinct signals was obtained at 253 K; **¹H NMR** (400 MHz, CDCl₃, 253 K) δ 7.45 (d, *J* = 8.1 Hz, 2H), 7.15 (s, 1H), 7.07–7.02 (m, 3H), 6.91 (s, 1H), 6.82 (s, 1H), 5.49 (t, *J* = 4.4 Hz, 1H), 4.54 (d, *J* = 13.3 Hz, 1H), 4.32–4.08 (m, 1H), 4.07–3.78 (m, 4H), 3.62 (t, *J* = 12.6 Hz, 1H), 3.32 (t, *J* = 12.9 Hz, 1H), 2.90 (s, 3H), 2.46 (s, 6H), 2.34 (s, 3H), 2.30 (s, 3H), 2.27 (s, 3H), 2.00–1.89 (m, 2H), 1.94 (s, 3H), 1.88–1.73 (m, 2H), 1.51–1.23 (m, 4H), 0.48 (t, *J* = 6.7 Hz, 3H); **¹³C NMR** (125 MHz, CDCl₃, 298K) δ 318.00, 210.60, 154.36, 145.04, 143.94, 139.37, 138.37, 138.16, 137.07, 135.16, 133.68, 130.33, 129.89, 129.83, 129.68, 129.38, 129.28, 128.93, 128.53, 127.98, 112.35, 99.26, 65.16, 52.89, 50.79, 46.62, 28.13, 25.14, 23.31, 22.48, 21.79, 21.46, 21.27, 21.04, 18.67, 13.43; **HRMS (ESI)** calcd for C₃₈H₄₈N₃O₂SRu [M – 2Cl – H]⁺ 712.2511, found 712.2493. (The reason for the unusual downfield shift of the carbene signal comparable to that of *trans*-1,5-chelate might be due to combined effects of the presence of alkyl substituent

(Bu group) and a 6-membered ring. These two factors usually make the carbene signal downfield shifted for h^3 -vinyl alkylidene complexes, for example **13a** vs. **13b** and **13a** vs. **13e**).



7-22g: 97% yield; green solid; 58 mg obtained; Purification: Flash Chromatography

(SiO₂, hexanes–EtOAc, 10:1 → 4:1 → CH₂Cl₂–EtOAc, 1:1); **¹H NMR** (500 MHz,

CDCl₃) δ 9.11 (dd, *J* = 7.8, 1.8 Hz, 1H), 7.57–7.43 (m, 1H), 7.08 (d, *J* = 8.1 Hz, 2H),

7.01–6.84 (m, 4H), 6.81 (t, *J* = 7.5 Hz, 1H), 6.60 (d, *J* = 8.4 Hz, 1H), 6.30 (s, 1H),

6.28 (s, 1H), 4.57 (p, *J* = 6.1 Hz, 1H), 4.24 (q, *J* = 10.6 Hz, 1H), 4.03–3.91 (m, 1H), 3.84–3.78 (m, 2H),

3.42 (dt, *J* = 11.9, 8.5 Hz, 1H), 3.27 (d, *J* = 5.3 Hz, 1H), 2.67 (s, 3H), 2.53 (s, 3H), 2.52 (s, 3H), 2.26 (s,

3H), 2.23–2.16 (m, 1H) 2.20 (s, 4H), 1.94 (s, 3H), 1.70 (s, 3H), 1.67–1.60 (m, 1H), 1.59 (d, *J* = 6.0 Hz,

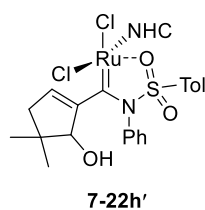
3H), 1.55 (d, *J* = 6.0 Hz, 3H); **¹³C NMR** (125 MHz, CDCl₃) δ 261.11, 209.89, 143.44, 140.36, 139.91,

137.65, 137.32, 136.96, 135.71, 135.43, 134.35, 133.95, 133.20, 132.42, 131.43, 131.03, 130.02, 129.11,

129.00, 128.94, 121.01, 111.64, 108.77, 71.52, 52.73, 51.49, 51.16, 46.35, 27.12, 22.91, 22.26, 21.66,

21.28, 20.99, 20.63, 19.25, 18.69, 17.95; **HRMS (ESI)** calcd for C₄₂H₄₉N₃O₃SClRu [M – Cl]⁺ 812.2227,

found 812.2250.



7-22h': 86% yield; green solid; 44 mg obtained; Purification: Flash Chromatography

(SiO₂, hexanes–EtOAc, 10:1 → 4:1 → CH₂Cl₂–EtOAc, 1:1); **¹H NMR** (500 MHz,

CDCl₃) δ 7.76 (d, *J* = 8.2 Hz, 2H), 7.22–7.14 (m, 3H), 7.10–7.02 (m, 4H), 6.86–6.82 (m,

2H), 6.86–6.57 (m, 2H), 5.53 (d, *J* = 2.0 Hz, 1H), 4.31–4.04 (m, 4H), 3.90 (s, 1H), 3.62

(d, *J* = 4.2 Hz, 1H), 2.59 (s, 3H), 2.56 (s, 3H), 2.42 (s, 3H), 2.36 (s, 3H), 2.34 (s, 3H), 2.29 (s, 3H), 2.24 (s,

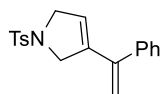
3H), 1.79 (d, *J* = 16.6 Hz, 1H), 1.38 (d, *J* = 16.4 Hz, 1H), 0.96 (s, 3H), 0.46 (s, 3H); **¹³C NMR** (125 MHz,

CDCl₃) δ 262.6, 214.7, 153.9, 146.2, 140.5, 139.0, 138.4, 138.3, 137.2, 137.0, 136.3, 132.9, 130.6, 130.5,

130.0, 129.9, 129.7, 129.3, 129.1, 128.5, 127.8, 122.1, 88.1, 52.7, 51.1, 47.2, 41.7, 27.7, 23.5, 21.8, 21.4,

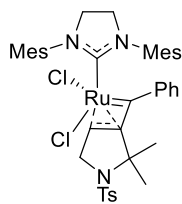
21.1, 20.5, 19.2, 19.0, 18.7; **HRMS (ESI)** calcd for C₄₃H₅₀N₃O₄RuS [M – 2Cl + H + CO]⁺ 806.2560 found,

806.2483.



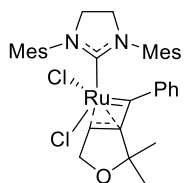
7-22i'-H

7-22i'-H: 52% yield; pale-yellow oil; Purification: Flash Chromatography (SiO₂, hexanes–EtOAc, 10:1 → 7:1); **¹H NMR** (500 MHz, CDCl₃) δ 7.76 (d, *J* = 8.0 Hz, 2H), 7.35 (d, *J* = 8.0 Hz, 2H), 7.32–7.28 (m, 3H), 7.23–7.18 (m, 2H), 5.46 (s, 1H), 5.17 (s, 1H), 5.07 (s, 1H), 4.35 (s, 2H), 4.20 (d, *J* = 3.2 Hz, 2H), 2.44 (s, 3H); **¹³C NMR** (125 MHz, CDCl₃) δ 143.57, 143.01, 140.06, 138.35, 134.21, 129.86, 128.50, 128.22, 127.83, 127.53, 124.03, 115.95, 55.58, 54.71, 21.56; **HRMS (ESI)** calcd for C₁₉H₂₀NO₂S [M + H]⁺ 326.1215, found 326.1227.



7-22i

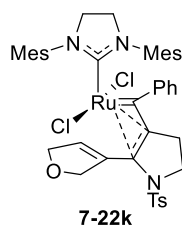
7-22i: 66% yield; green solid; 35 mg obtained; Purification: Flash Chromatography (SiO₂, hexanes–EtOAc, 10:1 → 4:1 → CH₂Cl₂–EtOAc, 1:1); **¹H NMR** (500 MHz, CDCl₃) δ 9.13–8.90 (m, 1H), 7.61 (d, *J* = 7.9 Hz, 2H), 7.55 (t, *J* = 7.6 Hz, 1H), 7.24–7.12 (m, 3H), 7.09 (d, *J* = 7.9 Hz, 2H), 6.98 (s, 1H), 6.95 (s, 1H), 6.20 (s, 1H), 6.18 (s, 1H), 4.39–4.30 (m, 1H), 4.25 (q, *J* = 10.7 Hz, 1H), 4.15–4.04 (m, 1H), 3.90 (dd, *J* = 13.3, 3.8 Hz, 1H), 3.86–3.73 (m, 2H), 2.67 (d, *J* = 13.3 Hz, 1H), 2.62 (s, 3H), 2.57 (s, 3H), 2.37 (s, 3H), 2.31 (s, 3H), 2.22 (s, 3H), 2.01 (s, 3H), 1.85 (s, 3H), 1.56 (s, 3H), 1.00 (s, 3H); **¹³C NMR** (125 MHz, CDCl₃) δ 272.81, 208.75, 142.72, 142.10, 140.08, 139.33, 138.32, 137.58, 137.27, 134.77, 134.44, 133.76, 132.59, 130.99, 130.27, 130.09, 129.05, 128.89, 128.76, 127.76, 123.72, 94.22, 66.04, 58.64, 52.82, 52.48, 51.86, 32.19, 22.32, 21.53, 20.95, 20.84, 20.59, 19.10, 19.02, 17.39; **HRMS (ESI)** calcd for C₄₁H₄₈N₃O₂SRu [M – 2Cl + H]⁺ 748.2511, found 748.2504.



7-22j

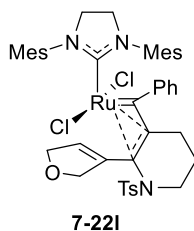
7-22j: 62% yield; green solid; 35 mg obtained; Purification: Flash Chromatography (SiO₂, hexanes–EtOAc, 10:1 → 4:1 → CH₂Cl₂–EtOAc, 1:1); **¹H NMR** (500 MHz, CDCl₃) δ 9.64 – 8.71 (m, 1H), 7.57 (t, *J* = 7.4 Hz, 1H), 7.40 – 7.11 (m, 3H), 7.08 (s, 1H), 7.04 (s, 1H), 6.32 (s, 1H), 6.08 (s, 1H), 4.51 (s, 1H), 4.32 – 4.10 (m, 3H), 3.88 (q, *J* = 10.9 Hz, 1H), 3.76 (q, *J* = 11.2 Hz, 1H), 3.69 (d, *J* = 12.9 Hz, 1H), 2.76 (s, 3H), 2.58 (s, 3H), 2.31 (s, 6H), 1.86 (s, 3H), 1.76 (s, 3H), 1.62 (s, 3H), 0.77 (s, 3H); **¹³C NMR** (125 MHz, CDCl₃) δ 271.77, 211.35, 141.59, 140.16, 139.33, 138.43, 137.64, 135.17, 134.89, 134.20, 132.64, 131.00, 130.43, 130.08, 129.36, 128.77, 91.14,

81.19, 70.99, 66.09, 52.30, 52.23, 29.72, 22.90, 21.20, 20.82, 20.51, 19.24, 19.01, 17.75; **HRMS (ESI)** calcd for $C_{34}H_{40}N_2OClRu$ $[M - Cl]^+$ 629.1873, found 629.1879.



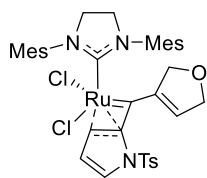
7-22k: 71% yield; yellow-brown solid; 34 mg obtained; Purification: Flash Chromatography (SiO_2 , hexanes–EtOAc, 10:1 \rightarrow 4:1 \rightarrow CH_2Cl_2 –EtOAc, 1:1); **1H NMR** (500 MHz, $CDCl_3$) δ 7.65 (d, J = 7.9 Hz, 2H), 7.28 (d, J = 8.2 Hz, 2H), 7.14–7.06 (m, 2H), 6.95 (dd, J = 16.6, 9.0 Hz, 3H), 6.86 (s, 1H), 6.45 (s, 1H), 6.29 (s, 1H), 6.27 (s, 1H),

4.92 (d, J = 12.0 Hz, 1H), 4.67 (s, 1H), 4.49 (d, J = 12.2 Hz, 1H), 4.22 (d, J = 18.3 Hz, 1H), 4.04–3.87 (m, 4H), 3.79 (dt, J = 16.5, 9.0 Hz, 2H), 3.38 (q, J = 11.5 Hz, 1H), 2.77 (s, 3H), 2.62 (s, 3H), 2.49–2.40 (m, 4H), 2.34 (s, 3H), 2.30 (s, 3H), 2.24 (s, 3H), 1.81 (s, 3H), 1.50 (d, J = 18.3 Hz, 1H); **^{13}C NMR** (125 MHz, $CDCl_3$) δ 282.17, 203.93, 169.24, 144.91, 139.18, 139.02, 138.86, 138.26, 138.13, 137.39, 136.65, 134.59, 134.22, 133.17, 130.94, 130.21, 129.91, 129.38, 128.80, 128.17, 127.64, 125.57, 112.24, 96.11, 87.55, 69.76, 53.10, 52.84, 51.91, 26.84, 21.74, 21.19, 21.12, 20.51, 19.25, 19.08, 18.75; **HRMS (ESI)** calcd for $C_{43}H_{46}N_3O_3SRu$ $[M - 2Cl - H]^+$ 786.2298 found, 786.2277.



7-22l: 78% yield; yellow-brown solid; 44 mg obtained; Purification: Flash Chromatography (SiO_2 , hexanes–EtOAc, 10:1 \rightarrow 4:1 \rightarrow CH_2Cl_2 –EtOAc, 1:1); **1H NMR** (500 MHz, $CDCl_3$) δ 7.72 (d, J = 8.1 Hz, 2H), 7.47 (d, J = 7.3 Hz, 2H), 7.37–7.33 (m, 3H), 7.29–7.27 (m, 2H), 7.11 (s, 1H), 7.06 (s, 1H), 6.98 (s, 1H), 6.83 (s, 1H),

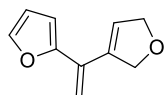
4.64–4.57 (m, 2H), 4.38–4.26 (m, 1H), 4.20–3.98 (m, 4H), 3.96 (s, 1H), 3.65 (td, J = 13.7, 4.3 Hz, 1H), 3.09 (dt, J = 14.9, 7.6 Hz, 1H), 2.82 (d, J = 12.3 Hz, 1H), 2.70 (s, 3H), 2.64 (s, 3H), 2.63–2.60 (m, 1H), 2.57 (s, 3H), 2.53–2.48 (m, 1H), 2.41 (s, 3H), 2.35–2.28 (m, 5H), 2.22 (s, 3H), 1.46 (s, 3H); **^{13}C NMR** (125 MHz, $CDCl_3$) δ 231.82, 207.22, 146.67, 139.87, 138.86, 137.82, 137.62, 134.92, 134.89, 134.27, 133.99, 131.65, 131.48, 131.02, 130.63, 129.96, 129.77, 128.47, 128.40, 127.67, 124.12, 116.89, 89.55, 80.97, 75.90, 73.61, 67.03, 66.06, 52.18, 52.13, 52.09, 26.66, 21.79, 21.08, 20.91, 20.72, 19.73, 18.82, 17.32, 17.18; **HRMS (ESI)** calcd for $C_{44}H_{48}N_3O_3SRu$ $[M - 2Cl - H]^+$ 800.2460, found 800.2452.



7-22m

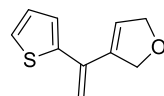
7-22m: This compound was obtained as a 3:1 mixture with sulfonamide chelate byproduct; 95% yield; green solid; 62 mg obtained; Purification: Flash Chromatography (SiO₂, hexanes–EtOAc, 10:1 → 4:1 → CH₂Cl₂–EtOAc, 1:1); **¹H NMR** (500 MHz, CDCl₃) δ (the spectral description for only the alkene chelate is given)

8.62 (dd, *J* = 4.0, 1.7 Hz, 1H), 7.38 (dd, *J* = 3.2, 1.7 Hz, 1H), 7.25–7.18 (m, 4H), 7.11 (s, 1H), 7.05 (d, *J* = 5.4 Hz, 2H), 6.57 (s, 1H), 6.51 (s, 1H), 6.30 (t, *J* = 3.5 Hz, 1H), 4.24–4.09 (m, 3H), 4.00–3.87 (m, 5H), 2.69 (s, 3H), 2.61 (s, 3H), 2.56 (s, 3H), 2.36 (s, 3H), 2.30 (s, 3H), 2.06 (s, 3H), 1.70 (s, 3H); **¹³C NMR** (125 MHz, CDCl₃) δ (all discernable signals for product and byproduct) 249.76, 209.16, 146.39, 145.41, 140.97, 140.52, 140.29, 139.13, 138.20, 137.46, 137.34, 136.86, 135.65, 135.12, 134.98, 134.26, 132.66, 131.21, 130.57, 130.40, 130.07, 129.96, 129.71, 129.47, 129.39, 129.28, 127.46, 125.06, 124.78, 124.41, 118.87, 117.44, 112.05, 109.06, 88.15, 76.88, 76.64, 74.20, 66.46, 63.51, 52.50, 51.91, 51.30, 51.24, 26.49, 26.37, 26.16, 26.03, 21.57, 21.16, 20.90, 20.65, 19.26, 18.99, 18.96, 18.87, 18.83, 17.56; **HRMS (ESI)** calcd for C₃₇H₄₂N₃O₃SRu [M – 2Cl + H]⁺ 710.1990 found, 710.1965.



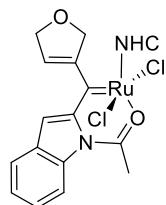
7-22n'

7-22n': 58% yield; colorless oil; 10 mg obtained; Purification: Flash Chromatography (SiO₂, hexanes–EtOAc, 40:1 → 20:1); **¹H NMR** (500 MHz, CDCl₃) δ 7.42 (d, *J* = 1.9 Hz, 1H), 6.46 (d, *J* = 3.2 Hz, 1H), 6.42 (dd, *J* = 3.5, 1.8 Hz, 1H), 6.22–6.17 (m, 1H), 5.60 (s, 1H), 5.02 (s, 1H), 4.89–4.84 (m, 2H), 4.84–4.78 (m, 2H); **¹³C NMR** (125 MHz, CDCl₃) δ 143.17, 142.02, 136.25, 131.06, 124.84, 113.18, 111.08, 107.89, 76.88, 75.75; **LRMS (EI)** calcd for C₁₀H₁₀O₂ [M]⁺ 162.0, found 162.0.



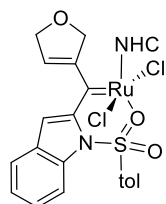
7-22o'

7-22o': 76% yield; yellow oil; 16 mg obtained; Purification: Flash Chromatography (SiO₂, hexanes–EtOAc, 40:1 → 20:1); **¹H NMR** (500 MHz, CDCl₃) δ 7.25 (d, *J* = 5.5 Hz, 1H), 7.12 (d, *J* = 3.5 Hz, 1H), 7.03 (d, *J* = 4.3 Hz, 1H), 6.09 (s, 1H), 5.40 (s, 1H), 5.00 (s, 1H), 4.87 (d, *J* = 5.0 Hz, 2H), 4.81 (d, *J* = 4.6 Hz, 2H); **¹³C NMR** (125 MHz, CDCl₃) δ 143.17, 142.02, 136.25, 131.06, 124.84, 113.18, 111.08, 107.89, 76.88, 75.75; **LRMS (EI)** calcd for C₁₀H₁₀OS [M]⁺ 178.0, found 178.0.



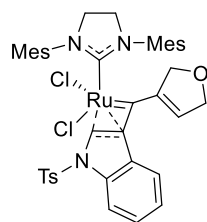
7-22p'

7-22p': 52% yield; green solid; 36 mg obtained; Purification: Flash Chromatography (SiO₂, hexanes–EtOAc, 10:1 → 4:1 → CH₂Cl₂–EtOAc, 1:1); **¹H NMR** (500 MHz, CDCl₃) δ 7.79 (d, *J* = 7.7 Hz, 1H), 7.71 (d, *J* = 7.5 Hz, 1H), 7.67 (d, *J* = 8.4 Hz, 1H), 7.42 (t, *J* = 7.5 Hz, 1H), 7.20 (s, 1H), 7.11 (s, 1H), 6.89 (s, 1H), 6.84 (s, 1H), 5.52–5.32 (m, 3H), 4.76 (s, 1H), 4.66 (d, *J* = 13.5 Hz, 2H), 4.31–4.07 (m, 2H), 3.87 (d, *J* = 11.0 Hz, 2H), 3.02 (s, 3H), 2.65 (s, 3H), 2.49 (s, 3H), 2.38 (s, 3H), 2.14 (s, 3H), 2.04 (s, 3H), 1.70 (s, 3H); **¹³C NMR** (125 MHz, CDCl₃) δ 216.06, 177.22, 159.29, 144.37, 140.39, 138.00, 136.75, 135.54, 133.92, 132.15, 130.80, 129.80, 129.69, 128.22, 126.67, 126.05, 123.86, 115.64, 113.09, 101.04, 76.93, 51.59, 50.74, 26.86, 26.38, 21.37, 20.96, 20.40, 18.85, 18.62, 17.04; **HRMS (ESI)** calcd for C₃₆H₃₉N₃O₂ClRu [M – Cl]⁺ 682.1774 found, 682.1782.



7-22q'

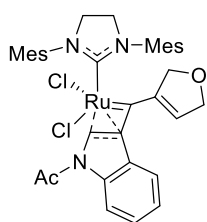
7-22q': 76% yield; green solid; 41 mg obtained; Purification: Flash Chromatography (SiO₂, hexanes–EtOAc, 10:1 → 4:1 → CH₂Cl₂–EtOAc, 1:1); **¹H NMR** (500 MHz, CDCl₃) δ 7.97 (d, *J* = 8.4 Hz, 1H), 7.70 (t, *J* = 7.9 Hz, 1H), 7.61 (d, *J* = 7.7 Hz, 1H), 7.51 (d, *J* = 8.0 Hz, 2H), 7.33–7.25 (m, 1H), 7.21 (s, 1H), 7.13 (s, 1H), 7.06 (s, 1H), 6.96 (d, *J* = 8.1 Hz, 2H), 6.75 (s, 1H), 5.62–5.47 (m, 2H), 5.36 (s, 1H), 4.84–4.67 (m, 2H), 4.59 (t, *J* = 8.3 Hz, 1H), 4.38–4.24 (m, 2H), 4.15 (td, *J* = 11.3, 5.8 Hz, 1H), 3.98 (q, *J* = 11.2 Hz, 1H), 2.57 (s, 3H), 2.46 (s, 3H), 2.35 (s, 3H), 2.24 (s, 3H), 2.15 (s, 3H), 2.09 (s, 3H), 1.97 (s, 3H); **¹³C NMR** (125 MHz, CDCl₃) δ 259.98, 213.79, 160.53, 155.56, 146.18, 140.69, 140.51, 138.05, 137.59, 137.40, 137.17, 135.73, 132.78, 131.13, 130.56, 130.15, 129.84, 129.63, 129.08, 128.50, 127.54, 126.78, 126.52, 125.21, 122.66, 116.50, 113.01, 105.24, 76.91, 76.70, 51.25, 51.21, 21.54, 21.37, 20.93, 20.44, 18.89, 18.54; **HRMS (ESI)** calcd for C₄₁H₄₃N₃O₃SClRu [M – Cl]⁺ 794.1757 found, 794.1763.



7-22r

7-22r: The reaction was performed at 35 °C for 1 h. This compound was isolated in 40% yield alongwith 42% (NMR yield) metathesis product; green solid; 38 mg obtained; Purification: Flash Chromatography (SiO₂, hexanes–EtOAc, 10:1 → 4:1 → CH₂Cl₂–EtOAc, 1:1); The ¹H NMR for this complex at 298K gave broad signals due to fluxionality in the complex but sharper NMR with distinct signals was obtained at

253K; **¹H NMR** (400 MHz, CDCl₃, 253K) δ 9.43 (s, 1H), 8.05–7.76 (m, 3H), 7.44–7.36 (m, 3H), 7.32 (d, *J* = 8.1 Hz, 2H), 7.13 (s, 1H), 7.12 (s, 1H), 6.49 (s, 1H), 5.76 (s, 1H), 4.61–4.51 (m, 2H), 4.46 (s, 1H), 4.27 (td, *J* = 30.9, 28.1, 9.8 Hz, 3H), 3.88 (d, *J* = 12.3 Hz, 3H), 2.70 (s, 3H), 2.66 (s, 3H), 2.57 (s, 3H), 2.37 (s, 3H), 2.33 (s, 3H), 1.65 (s, 3H), 1.50 (s, 3H); **¹³C NMR** (125 MHz, CDCl₃) δ 255.26, 210.56, 146.23, 140.64, 139.60, 138.64, 137.50, 137.05, 135.60, 134.26, 134.18, 131.19, 130.61, 130.47, 130.17, 129.43, 128.88, 127.62, 125.30, 124.37, 119.83, 113.59, 74.44, 68.79, 66.78, 52.36, 51.84, 21.71, 21.23, 20.50, 20.27, 19.10, 18.94, 17.65; **HRMS (ESI)** calcd for C₄₁H₄₄N₃O₃SRu [M – 2Cl + H]⁺ 760.2147 found, 760.2112.



7-22s

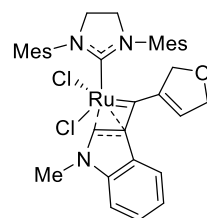
7-22s: The reaction was performed at 35 °C for 1 h. This compound was isolated in 55% yield along with 25% (NMR yield) metathesis product; green solid; 40 mg obtained;

Purification: Flash Chromatography (SiO₂, hexanes–EtOAc, 10:1 → 4:1 → CH₂Cl₂–

EtOAc, 1:1); **¹H NMR** (500 MHz, CDCl₃) δ 9.39 (s, 1H), 8.43 (d, *J* = 7.7 Hz, 1H),

7.58–7.44 (m, 1H), 7.44–7.33 (m, 2H), 7.12 (d, *J* = 8.4 Hz, 2H), 6.52 (s, 1H), 5.65 (s,

1H), 4.64 (d, *J* = 12.4 Hz, 1H), 4.49 (s, 1H), 4.47–4.39 (m, 2H), 4.35 (q, *J* = 11.1 Hz, 1H), 4.18 (q, *J* = 10.5 Hz, 1H), 3.89 (p, *J* = 9.5, 8.1 Hz, 2H), 3.64 (d, *J* = 11.7 Hz, 1H), 2.73 (s, 3H), 2.70 (s, 3H), 2.67 (s, 3H), 2.58 (s, 3H), 2.34 (s, 3H), 1.53 (d, *J* = 6.1 Hz, 6H); **¹³C NMR** (125 MHz, CDCl₃) δ 256.60, 209.38, 169.47, 140.75, 138.94, 138.60, 137.27, 137.07, 135.25, 135.10, 134.40, 131.63, 131.44, 129.99, 129.55, 129.03, 128.85, 126.08, 125.05, 123.02, 118.91, 117.02, 74.43, 68.69, 66.33, 52.38, 51.76, 23.75, 21.22, 20.41, 20.31, 19.32, 19.04, 17.31; **HRMS (ESI)** calcd for C₃₆H₃₈N₃O₂Ru [M – 2Cl – H]⁺ 646.2008 found, 646.1986.



7-22t

7-22t: 88% yield; red solid; 55 mg obtained; Purification: Flash Chromatography (SiO₂,

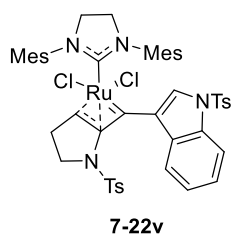
hexanes–EtOAc, 10:1 → 4:1 → CH₂Cl₂–EtOAc, 1:1); **¹H NMR** (500 MHz, CDCl₃) δ

8.88 (s, 1H), 7.45 (d, *J* = 7.5 Hz, 1H), 7.35–7.26 (m, 3H), 7.11 (s, 1H), 7.07 (s, 1H),

6.42 (s, 1H), 5.73 (s, 1H), 4.65–4.54 (m, 1H), 4.47 (d, *J* = 11.4 Hz, 1H), 4.39 (d, *J* =

11.9 Hz, 1H), 4.36–4.22 (m, 2H), 4.20–4.06 (m, 1H), 3.91–3.82 (m, 1H), 3.78 (d, *J* = 10.8 Hz, 2H), 3.73 (s, 3H), 2.71 (s, 3H), 2.67 (s, 3H), 2.56 (s, 3H), 2.33 (s, 3H), 1.62 (s, 3H), 1.47 (s, 3H); **¹³C NMR** (125

MHz, CDCl₃) δ 250.51, 211.56, 144.52, 140.16, 139.10, 137.85, 137.41, 136.34, 135.41, 135.33, 134.83, 132.34, 131.17, 129.76, 129.49, 128.76, 128.35, 127.97, 123.44, 123.14, 121.07, 119.59, 110.04, 74.62, 67.07, 66.89, 52.36, 51.80, 34.05, 21.22, 20.46, 20.34, 19.30, 19.10, 17.56; **HRMS (ESI)** calcd for C₃₅H₄₀N₃ORu [M – 2Cl + H]⁺ 620.2215 found, 620.2184.

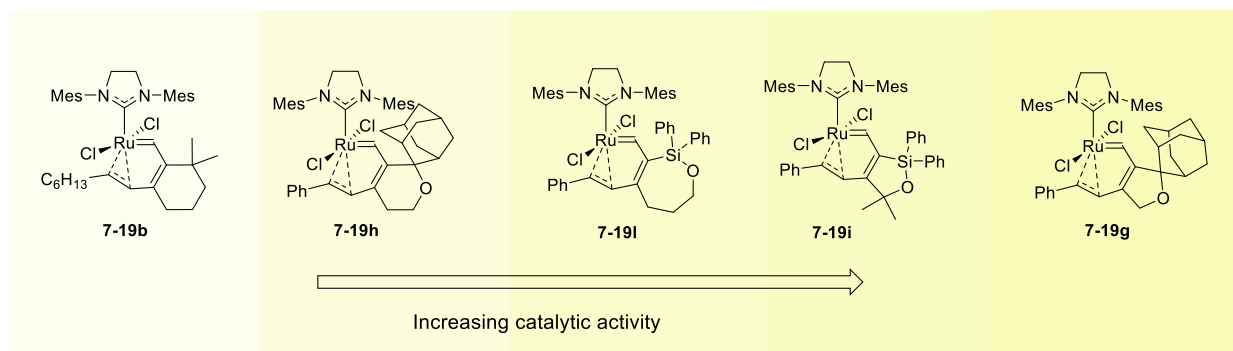


7-22v: 64% yield; green solid; 40 mg obtained; Purification: Flash Chromatography (SiO₂, hexanes–EtOAc, 10:1 → 4:1 → CH₂Cl₂–EtOAc, 1:1); **¹H NMR** (500 MHz, CDCl₃) δ 9.65 (s, 1H), 7.96–7.70 (m, 3H), 7.55 (s, 1H), 7.34–7.25 (m, 3H), 7.20–7.13 (m, 2H), 7.06–6.98 (m, 2H), 6.97–6.84 (m, 3H), 6.50 (s, 1H), 6.30 (s, 1H), 5.60 (s, 1H), 4.26–4.17 (m, 1H), 3.82–3.67 (m, 4H), 3.48–3.37 (m, 1H), 2.67 (s, 3H), 2.59–2.51 (m, 6H), 2.28–2.20 (m, 9H), 1.96–1.86 (m, 2H), 1.72 (s, 3H), 1.55 (s, 3H); **¹³C NMR** (125 MHz, CDCl₃) δ 250.97, 207.46, 145.42, 143.59, 140.76, 139.95, 138.24, 136.58, 135.95, 135.19, 134.69, 134.31, 133.82, 133.22, 131.18, 130.12, 129.71, 129.22, 128.83, 128.57, 128.05, 127.69, 126.95, 124.91, 123.34, 122.22, 113.15, 111.83, 105.80, 53.18, 51.36, 51.15, 49.27, 27.51, 21.68, 21.53, 21.29, 20.81, 20.48, 19.01, 18.72, 17.64; **HRMS (ESI)** calcd for C₄₈H₅₁N₄O₄S₂Ru [M – 2Cl + H]⁺ 913.2395 found, 913.2360.

7.4.4. Catalytic activity studies³⁷

Different types of alkene-chelates were tested for their RCM activity on dimethyl diallylmalonate. Based on their reactivity, the structure-activity relationships of these catalysts were established and various factors affecting the catalytic activity were determined. The general trend of catalytic activities for the *trans*-1,5-chelates and η^3 -vinyl chelates along with the factors affecting catalytic activity is enlisted below. The kinetic data (raw data and plot) for catalytic activities of η^3 -vinyl chelates and *trans*-1,5-chelates are also provided in the subsections underneath.

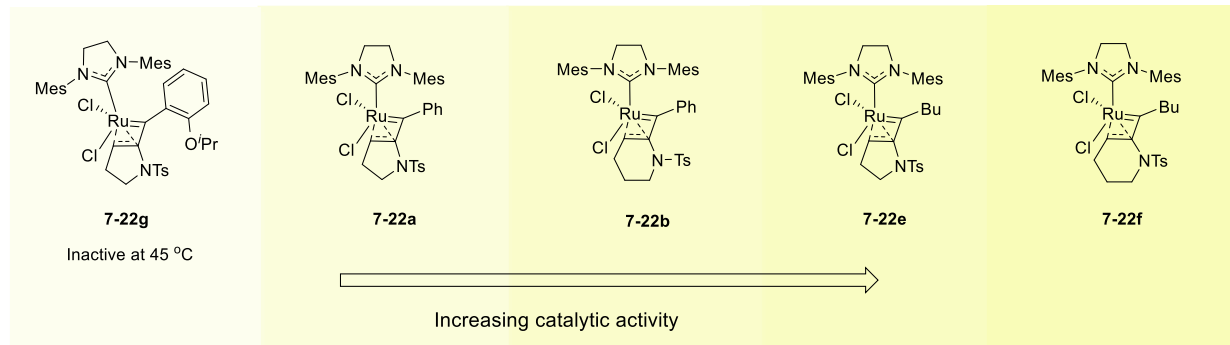
Reactivity trends for *trans*-1,5-chelates



Factors affecting catalytic-activity of *trans*-1,5-chelates:

- 1,5-chelates associated with 5-membered ring like **7-19i** and **7-19g** are highly reactive and are metathesis active at room temperature while complexes associated with 6 or 7-membered rings like **7-19b**, **7-19h** and **7-19l** are inactive at room temperature and show catalytic activity at higher temperature (60 °C or higher).
- Catalytic activity increases drastically with variation in the tethering group. For instance, in the RCM of dimethyl diallylmalonate catalyzed by these latent chelates at 80 °C in C₆D₆, complex **b** containing a *gem*-dimethyl group on the fused 6-membered ring is much less active (12% conversion) than the corresponding adamantyl-containing complex **7-19h** (57% conversion), yet 7-membered ring-fused complex **7-19l** containing a diphenylsilyl group is much more reactive (99.1% conversion).

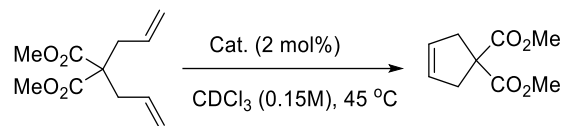
Reactivity trends for η^3 -vinyl chelates



Factors affecting catalytic-activity of η^3 -vinyl chelates:

- The η^3 -vinyl chelates are generally highly active catalysts reactive at room temperature. The catalytic activity depends on the substituent on the carbenic carbon. The lesser is the steric hindrance by the substituent the more is the catalytic-activity due to easier [2+2] cycloaddition with the substrate alkene. Thus, butyl substituted catalysts like **7-22e** and **7-22f** are more reactive than phenyl substituted congeners **7-22a** and **7-22b**.
- Size of the fused ring also affects the catalytic activity. Six-membered ring fused complexes like **13b** and **13f** are more reactive than their 5-membered ring congeners like **13a** and **13e**. The reason for higher reactivity of six-membered fused complexes lies to the fact that the six-membered ring of the bicyclo[4.1.0]heptane moiety is highly distorted to assume a boat conformation (revealed from X-ray structure) thereby having a lower dissociation barrier.
- Interestingly complex **13g** is catalytically inactive. The reason could be the presence of an alternate chelation site which is the 2-isopropoxy group. The free Ru-alkylidene might form a continuous equilibrium between the alkene-chelate and the oxygen-chelate and renders the complex inactive.

Catalytic activities of η^3 -vinyl chelates for RCM reaction of dimethyldiallyl malonate at 45 °C



An NMR tube with a screw-cap septum top was charged inside a glovebox with catalyst stock solution (0.1 M, 24 μ L, 2.4 mmol, 2 mol%) in 0.3 mL of CDCl₃. The NMR tube was degassed by freeze, pump, thaw method (x 3) and refilled with argon. The sample was equilibrated at 45 °C in the NMR probe before dimethyl diallyl malonate (25 mg, 0.12 mmol) solution in 0.5 mL of CDCl₃ was added via a syringe. Data points were collected over an appropriate time interval using the Bruker pseudo 2D kinetics method. The conversion of the product was determined by comparing the ratio of the integrals of the methylene protons in the starting material, δ 2.67–2.57 (m), with those of the product, δ 3.02 (s). Three independent experiments were performed for each complex and mean conversion was determined. The conversion versus time graph was plotted for different complexes to have a comparison of their reactivities.

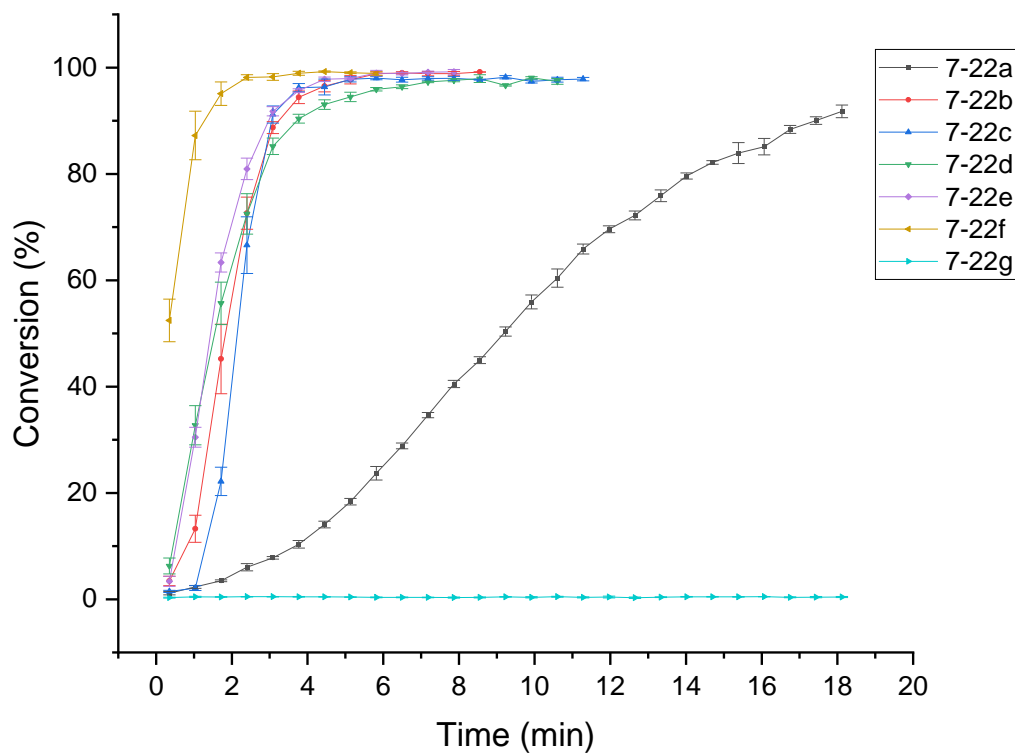
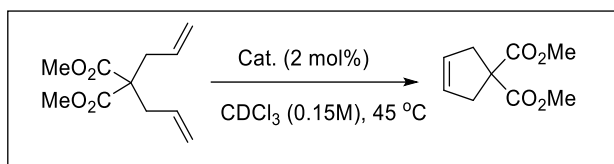


Fig. S1. Kinetic profile for RCM reactions to disubstituted olefins using η^3 -vinyl chelates as catalysts at 45 °C. Each data point represents the average of three independent experiments. Error bar represents standard error of the triplicate experiments.

Comparison of RCM activity of oxygen chelates 13p' and 13q' with alkene chelates

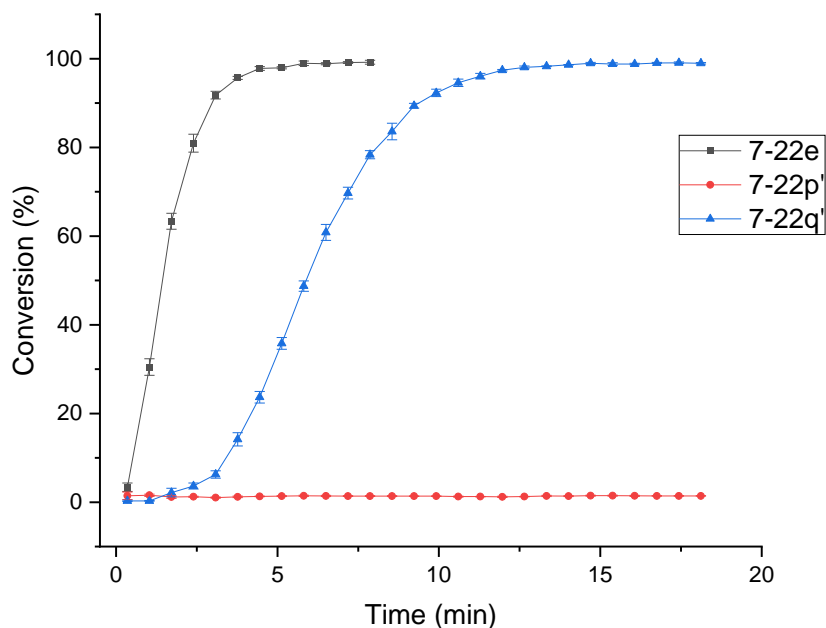
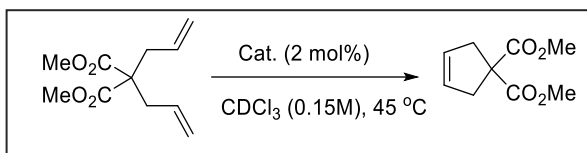
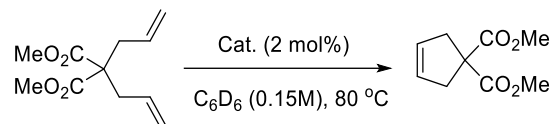


Fig. S2. Kinetic profile for RCM reactions to disubstituted olefins using oxygen-chelated complexes and its comparison with a h^3 -vinyl chelate **7-22e**. The error bar represents the standard error for the triplicate experiments.

Notes: The acetamide chelated complex **7-22p'** did not show any catalytic activity at 45°C compared to the sulfonamide chelated complex **7-22q'** which showed decent catalytic activity. The reason for this might be attributed to the reduced electron-density on the sulfonyl oxygen of **7-22q'** (due to higher electron-withdrawing nature of S) which makes the oxygen chelation weaker thereby increasing the catalytic activity. On the other hand, the acetamide oxygen in **7-22p'** has much higher electron-density as it is connected to a much less electronegative element “carbon”, thus oxygen chelation is much stronger, and

no catalytic activity is observed at 45 °C. The catalytic activity of **7-22p'** was also tested at higher temperature (60 °C) but lead to less than 5% conversion after 20 h.

Catalytic activities of *trans*-1,5-chelate for RCM reaction of dimethyl diallylmalonate at 80 °C



An NMR tube with a screw-cap septum top was charged inside a glovebox with catalyst stock solution (0.1 M, 24 μ L, 2.4 mmol, 2 mol%) in 0.3 mL of C₆D₆ and a solution of dimethyl diallylmalonate (25 mg, 0.12 mmol) in 0.5 mL of C₆D₆. The NMR tube was degassed by freeze, pump, thaw method (x 3) and refilled with argon. An initial NMR was taken to get the initial conversion which is zero at room temperature (as these complexes are latent at room temperature). The NMR tube was heated in an oil bath at 80 °C. The NMR tube was removed at regular intervals and cooled immediately in an ice-bath and ¹H NMR was taken to determine the conversion. The conversion of the product was determined by comparing the ratio of the integrals of the methylene protons in the starting material, δ 2.63 (d), with those of the product, δ 3.02 (s). Three independent experiments were performed for each complex and mean conversion was determined. The conversion versus time graph was plotted for different complexes to have a comparison of their reactivities.

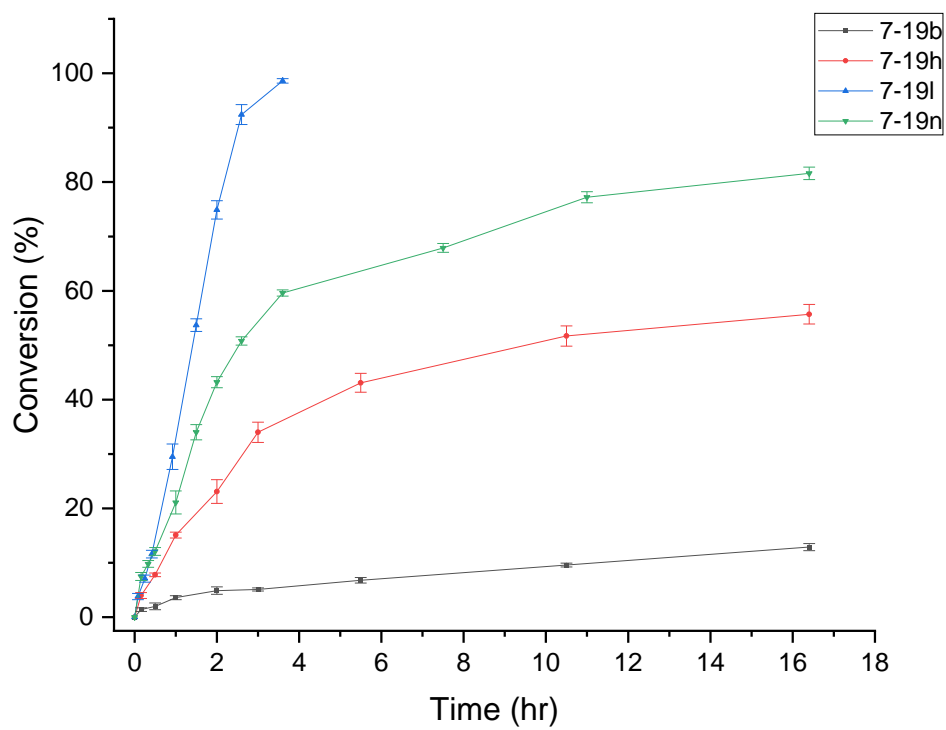
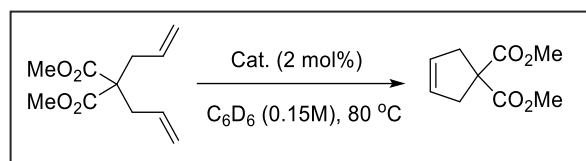


Fig. S3. Kinetic profile for RCM reactions to disubstituted olefins using the latent *trans*-1,5-chelates as catalysts at 80 °C. Each data point represents the average of three independent experiments. Error bar represents standard error of the triplicate experiments.

Catalytic activity for latent 1,5-chelates in CDCl_3 at 60 °C

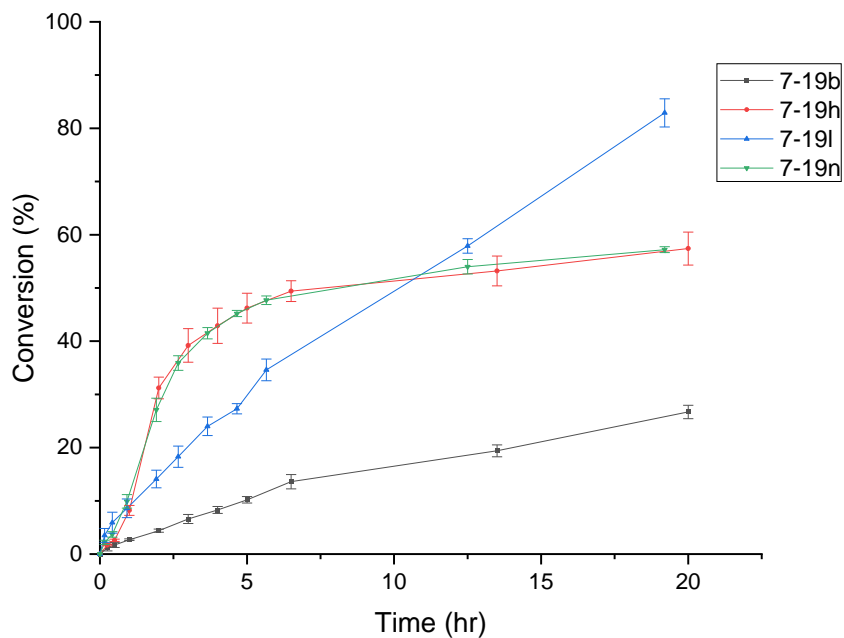
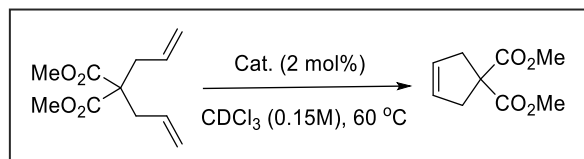


Fig. S4. Kinetic Profile for RCM activity of latent 1,5-chelates in CDCl_3 at 60 °C. Each data point represents the average of three independent experiments. Error bar represents standard error of the triplicate experiments.

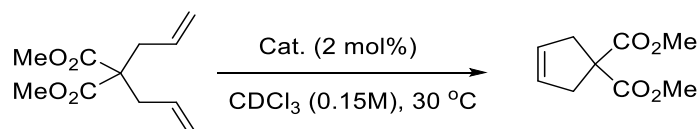
The catalytic activity of the latent 1,5-chelates were also monitored in CDCl_3 to have consistency with other experiments. Since the monitoring was done at 60 °C compared to the one done in C_6D_6 at 80 °C, the net conversion of the complexes is much lower after a period of 20h. However, the relative differences of reactivities of these four complexes did not change much. Although some striking differences can be noticed, for instance in CDCl_3 the complex **7-19l** initiates at a slow rate compared to its initiation in

C₆D₆ although the final conversion is 85%, the highest among the four complexes. The reactivity of **7-19h** and **7-19n** is similar in CDCl₃ although in C₆D₆ the reactivity of **7-19n** is higher than **7-19l**.

Benchmarking catalytic activity

After establishing a structure-activity relationship for different types of alkene-chelates we selected a subset of relatively more active complexes to benchmark their catalytic activity for various metathesis process with respect to standard metathesis catalysts. The kinetics of catalytic activity of the alkene-chelates were studied for different reactions using NMR techniques (Bruker pseudo 2D kinetics method). The experimental details, raw data of conversion with time, plots showing reaction profile and calculations of kinetic parameters like k_{obs} , $t_{1/2}$, and k_{obs} (w.r.t G-II) for various metathesis process are given in the subsections underneath.

Catalytic activities of alkene-chelates for RCM reaction of dimethyl diallylmalonate at 30 °C



An NMR tube with a screw-cap septum top was charged inside a glovebox with catalyst stock solution (0.1 M, 24 μ L, 2.4 mmol, 2 mol%) in 0.3 mL of CDCl₃. The NMR tube was degassed by freeze, pump, thaw method (cycle of 3) and refilled with argon. The sample was equilibrated at 30 °C in the NMR probe before dimethyl diallylmalonate (25 mg, 0.12 mmol) solution in 0.5 mL of CDCl₃ was added via a syringe. Data points were collected over an appropriate time interval using the Bruker pseudo 2D kinetics method. The conversion of the product was determined by comparing the ratio of the integrals of the methylene protons in the starting material, δ 2.67–2.57 (m), with those of the product, δ 3.02 (s). Three independent experiments were performed for each complex and the mean conversion was determined. The conversion versus time graph was plotted for different complexes to have a comparison of their reactivities. Kinetic

parameter k_{obs} was determined from the slope of $\ln([\text{SM}])$ vs time plot, where, $\ln([\text{SM}]) = \ln((100 - \text{avg. conv.}) / 100 * \text{conc. (0.15 M)})$.

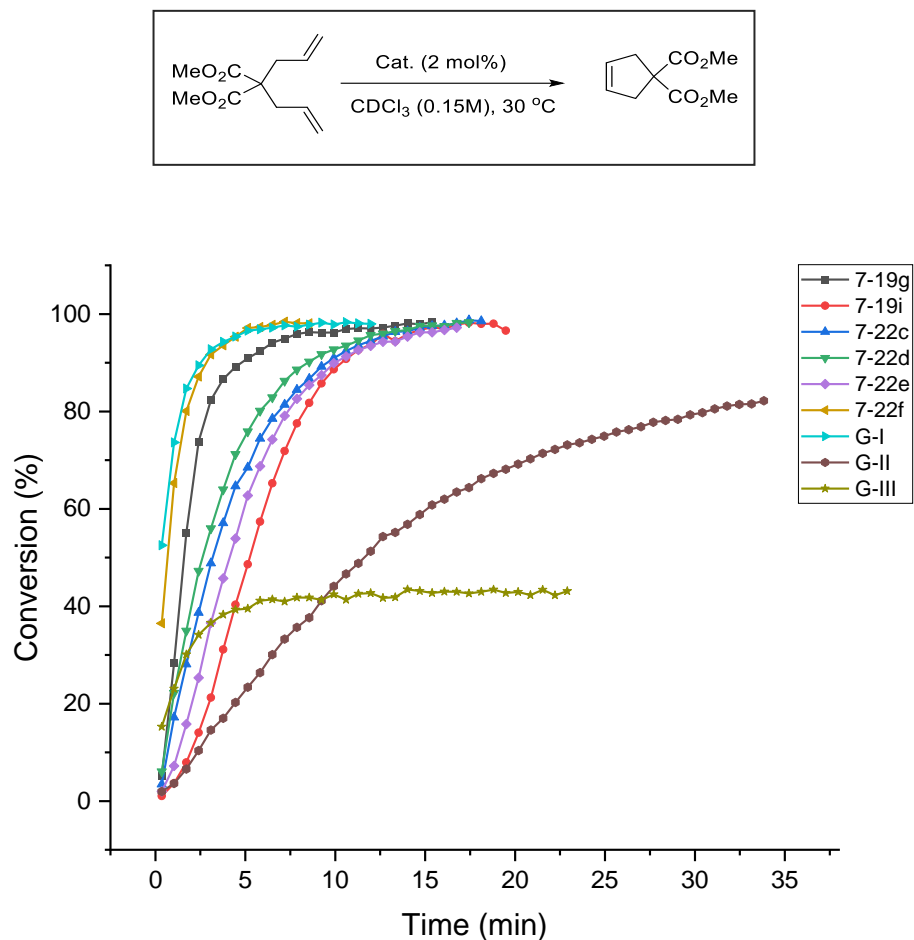


Fig. S5. Kinetic profiles for RCM reactions to disubstituted olefins in CDCl₃ using selected alkene-chelates as catalysts at 30 °C. Each data point represents the average of three independent experiments. Error bar represents standard error of the triplicate experiments.

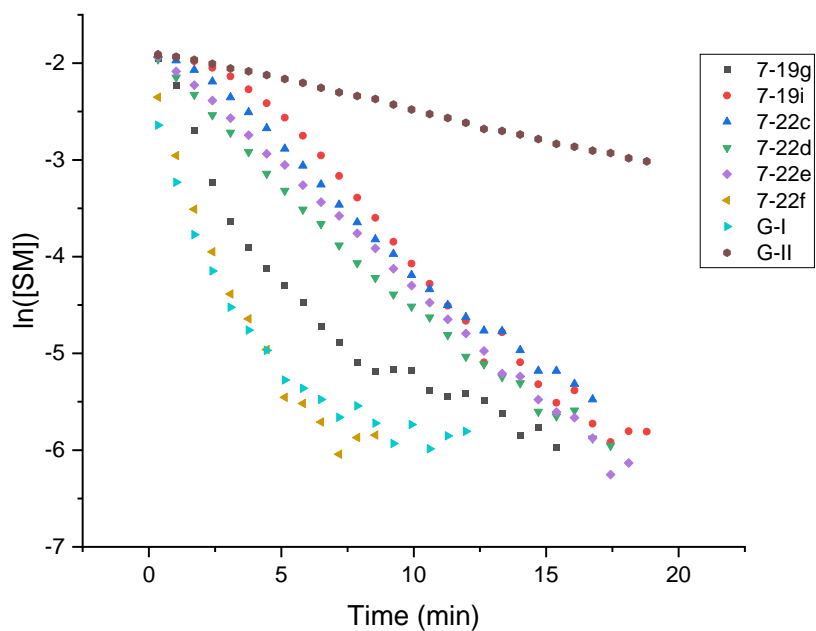
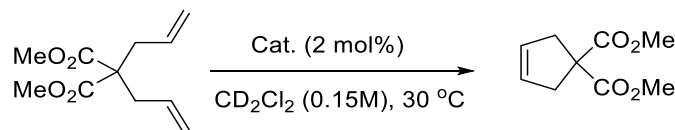


Fig. S6. Log plot of selected alkene-chelates for RCM reaction to disubstituted olefins in CDCl_3 . K_{obs} was determined from the slope of these curves and $t_{1/2}$ values were accordingly determined as $\ln 2/k_{\text{obs}}$

Kinetic parameters (in CDCl_3) of catalysts for RCM to disubstituted alkenes (k_{obs} , $t_{1/2}$ and k_{rel})

Cat.	k_{obs} (10^{-4} s^{-1})	$t_{1/2}$ (s)	k_{rel} (CDCl_3)	Linearity of plot
7-19g	86.8	79.9	9.64	Upto 90% conv.
7-19i	49.5	140.0	5.50	Between 14% to 90% conv.
7-22c	43.2	160.5	4.80	
7-22d	42.8	162.0	4.76	
7-22e	41.8	165.8	4.64	
7-22f	103.3	67.1	11.48	
G-I	88.5	57.2	9.83	
GII	9	770.2	1	

Catalytic activities of alkene-chelates for RCM reaction of dimethyl diallylmalonate at 30 °C in CD₂Cl₂ solvent



An NMR tube with a screw-cap septum top was charged inside a glovebox with catalyst stock solution (0.1 M, 16 μ L, 1.6 mmol, 2 mol%) in 0.2 mL of CD₂Cl₂. The NMR tube was degassed by freeze, pump, thaw method (cycle of 3) and refilled with argon. The sample was equilibrated at 30 °C in the NMR probe before dimethyl diallylmalonate (16.5 mg, 0.078 mmol) solution in 0.3 mL of CD₂Cl₂ was added via a syringe. Data points were collected over an appropriate time interval using the Bruker pseudo 2D kinetics method. The conversion of the product was determined by comparing the ratio of the integrals of the methylene protons in the starting material, δ 2.65–2.61 (m), with those of the product, δ 3.01 (s). Three independent experiments were performed for each complex and the mean conversion was determined. The conversion versus time graph was plotted for different complexes to have a comparison of their reactivities. Kinetic parameter k_{obs} was determined from the slope of $\ln([\text{SM}])$ vs time plot, where, $\ln([\text{SM}]) = \ln((100 - \text{avg. conv.}) / 100 * \text{conc. (0.15 M)})$.

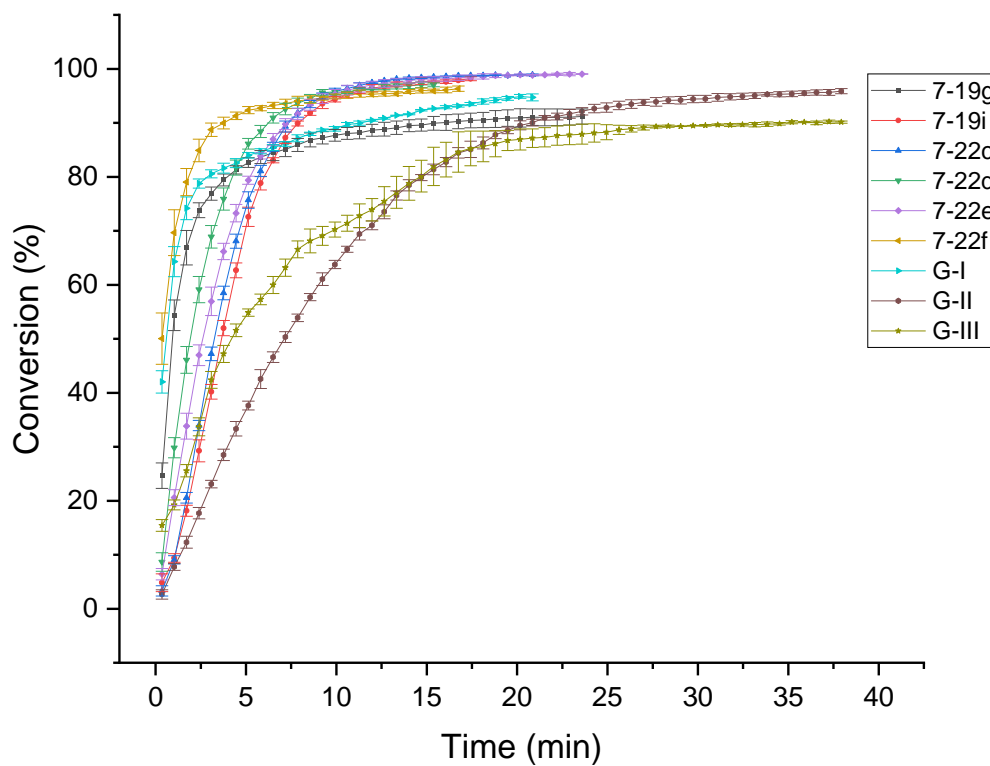
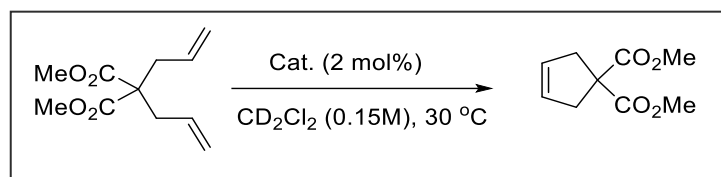


Fig. S7. Kinetic profiles for RCM reactions to disubstituted olefins using selected alkene-chelates as catalysts at 30 °C in CD₂Cl₂. Each data point represents the average of three independent experiments. Error bar represents standard error of the triplicate experiments.

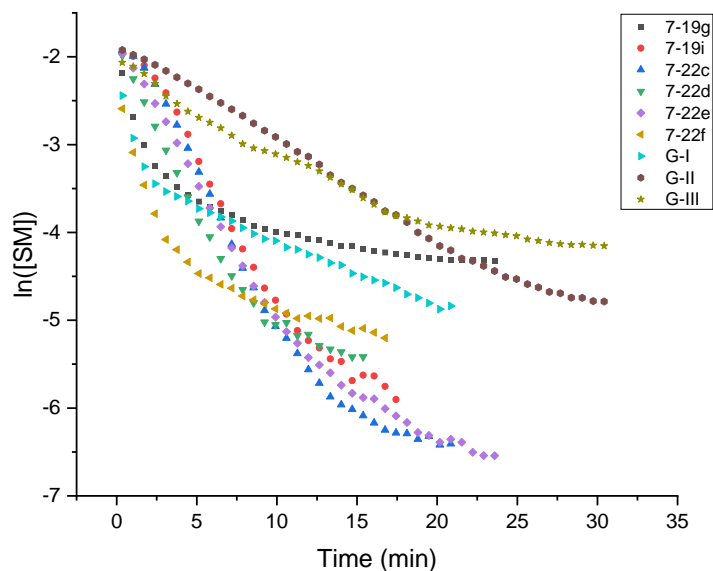


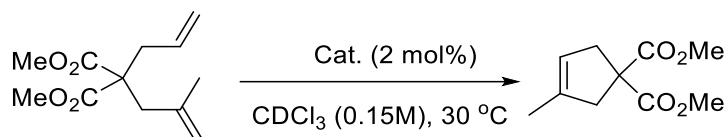
Fig. S8. Log plot of selected alkene-chelates for RCM reaction in CD_2Cl_2 to disubstituted olefins. K_{obs} was determined from the slope of these curves and $t_{1/2}$ values were accordingly determined as $\ln 2/k_{\text{obs}}$

Kinetic parameters (in CD_2Cl_2) of catalysts for RCM to disubstituted alkenes (k_{obs} , $t_{1/2}$ and k_{rel})

Cat.	k_{obs} (10^{-4} s^{-1})	$t_{1/2}$ (s)	k_{rel} (CD_2Cl_2)	Linearity of plot
7-19g	53.5	129.6	3.57	Upto 80% conv.
7-19i	54.6	127.2	3.63	
7-22c	56.1	123.6	3.74	Upto 90% conv.
7-22d	57.5	120.5	3.83	
7-22e	52.2	132.8	3.48	Upto 80% conv.
7-22f	89.7	77.3	5.98	
G-I	66	105.0	4.40	Upto 85% conv.
G-II	15	462.1	1	
G-III	16.3	425.2	1.09	

The kinetics of RCM of dimethyl diallylmalonate was also monitored in CD_2Cl_2 to have a consistency with previously reported experiments (ref. 37). It was found that in CD_2Cl_2 the reactivity of standard metathesis catalysts like **G-II** and **G-III** increases significantly giving higher conversion (95% vs. 82% for **G-II** and 90% vs. 45% for **G-III**) and higher overall rate. For **G-II** there is 1.6 times rate enhancement. For alkene-chelates which showed excellent reactivity in CDCl_3 also showed decent reactivity in CD_2Cl_2 . In CD_2Cl_2 the rate increased for complexes **7-19i**, **7-22c**, **7-22d** and **7-22e** while complexes like **7-19g**, **7-22f** and **G-I** showed a decrease in rate compared to that in CDCl_3 .

Catalytic activities of alkene chelates for RCM reaction of dimethyl allylmethallylmalonate at 30 °C



An NMR tube with a screw-cap septum top was charged inside a glovebox with catalyst stock solution (0.1 M, 22 μL , 2.2 mmol, 2 mol%) in 0.3 mL of CDCl_3 . The NMR tube was degassed by freeze, pump, thaw method (cycle of 3) and refilled with argon. The sample was equilibrated at 30 °C in the NMR probe before dimethyl allylmethallylmalonate (25 mg, 0.11 mmol) solution in 0.5 mL of CDCl_3 was added via a syringe. Data points were collected over an appropriate time interval using the Bruker pseudo 2D kinetics method. The conversion of the product was determined by comparing the ratio of the integrals of the methylene protons in the starting material, δ 2.70 (s), 2.67 (dt), with those of the product, δ 2.97(s), 2.91(m). Three independent experiments were performed for each complex and mean conversion was determined. The conversion versus time graph was plotted for different complexes to have a comparison of their reactivities. Kinetic parameter k_{obs} was determined from the slope of $\ln([\text{SM}])$ vs time plot, where, $\ln([\text{SM}]) = \ln((100 - \text{avg. conv.}) / 100 * \text{conc. (0.15 M)})$.

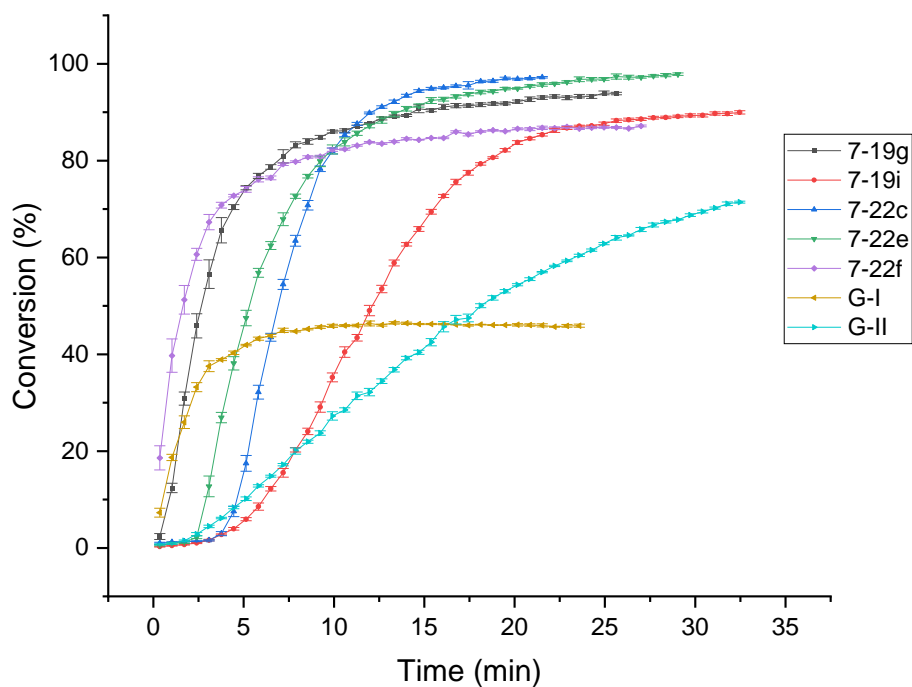
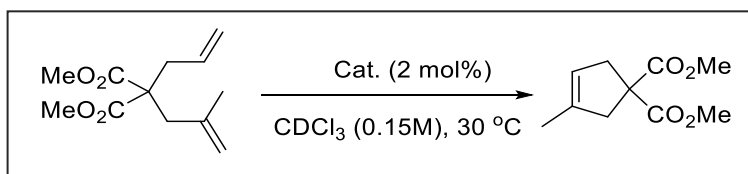


Fig. S9. Kinetic profiles for RCM reactions to trisubstituted olefins using selected alkene-chelates as catalysts at 30 °C. Each data point represents the average of three independent experiments. Error bar represents standard error of the triplicate experiments.

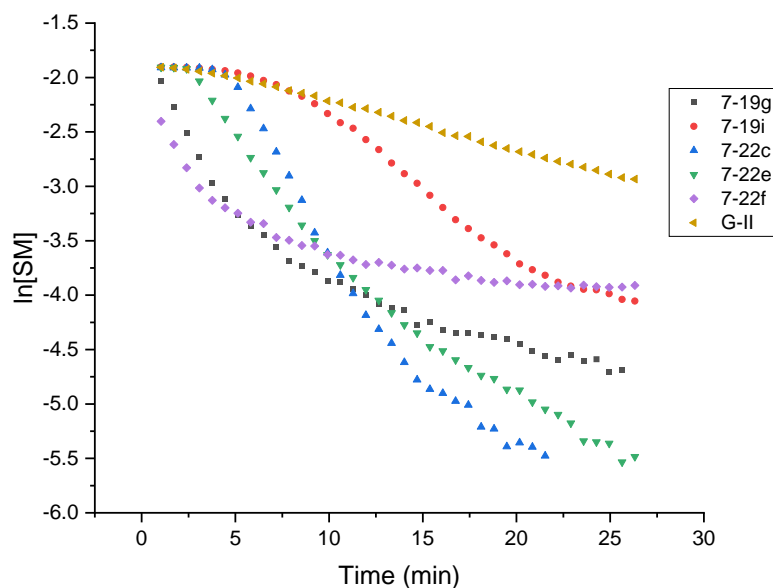
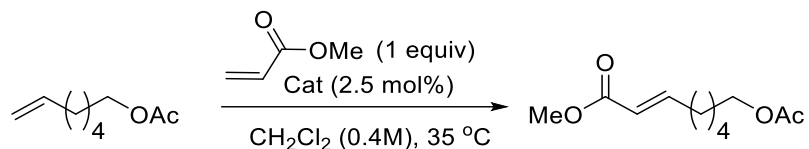


Fig. S10. Log plot of selected alkene-chelates for RCM reaction to trisubstituted olefins. K_{obs} was determined from the slope of these curve and $t_{1/2}$ values were accordingly determined. It is worth noting that for RCM to trisubstituted olefins the fastest catalysts like **13f** and **10g** the log plots are curved which indicates quicker catalytic decomposition which is also well reflected in their low conversion. To determine k_{obs} for these catalysts only the portions of the curve showing linearity is considered.

Kinetic parameters of catalysts for RCM to trisubstituted alkenes (k_{obs} , $t_{1/2}$ and k_{rel})

Cat.	k_{obs} (10^{-4} s^{-1})	$t_{1/2}$ (s)	k_{rel} (CDCl_3)	Linearity of plot
7-19g	44.3	156.5	6.15	Upto 80% conv.
7-19i	22.5	308.1	3.13	Between 12-85% conv.
7-22c	39.1	177.3	5.43	
7-22e	29.8	232.6	4.14	Above 12% conv.
7-22f	54.8	126.5	7.61	
GII	7.2	962.7	1	

Catalytic activities of alkene chelates for CM reaction of 5-hexenyl acetate and methyl acrylate



5-Hexenyl acetate (30 mg, 0.21 mmol) and methyl acrylate (18.1 mg, 0.21 mmol) and internal standard anthracene (18.5 mg, 0.1 mmol) was mixed in 0.4 mL CH_2Cl_2 . The mixture was transferred in a 5 mL septum-topped vial filled with argon and 15 μmol aliquot was removed and diluted with 0.5 mL of CH_2Cl_2 to take the initial nmr. The catalyst stock solution (5.25 μmol , 104 μL , 0.05 M in CH_2Cl_2) was added and the reaction mixture was heated at 35 °C. An aliquot (15 μL) was removed from the vial at desired time interval and diluted with 0.5 mL of CDCl_3 in an NMR tube which was kept at -78°C until NMR was taken. Attempts to monitor this reaction in an NMR tube resulted to incomplete conversions due to ethylene build-up. All conversions were determined relative to anthracene which was the internal standard. The internal standard singlet at 8.43 ppm was given an integration of 1.00 in the spectrum at each time point. The multiplet at 5.05–4.91 ppm (2H; $\text{C}=\text{CH}_2$ of 5-hexenyl acetate) and the doublet of doublets at 6.13 ppm (1H; $J = 17.3, 1.7$ Hz; $\text{cis-C}=\text{CHH}$ of methyl acrylate) were used as peaks to monitor the disappearance of the starting materials. The conversion of the product was determined from the integration of the doublet of triplet at 6.95 ppm (1H; $J = 15.3, 6.9$ Hz; $\text{C}=\text{CHR}$). The experiment was performed twice and the mean % conversion was determined. (Attempt to perform the reaction in CDCl_3 lead to much lower conversion with a maximum of 69 % for G-II).

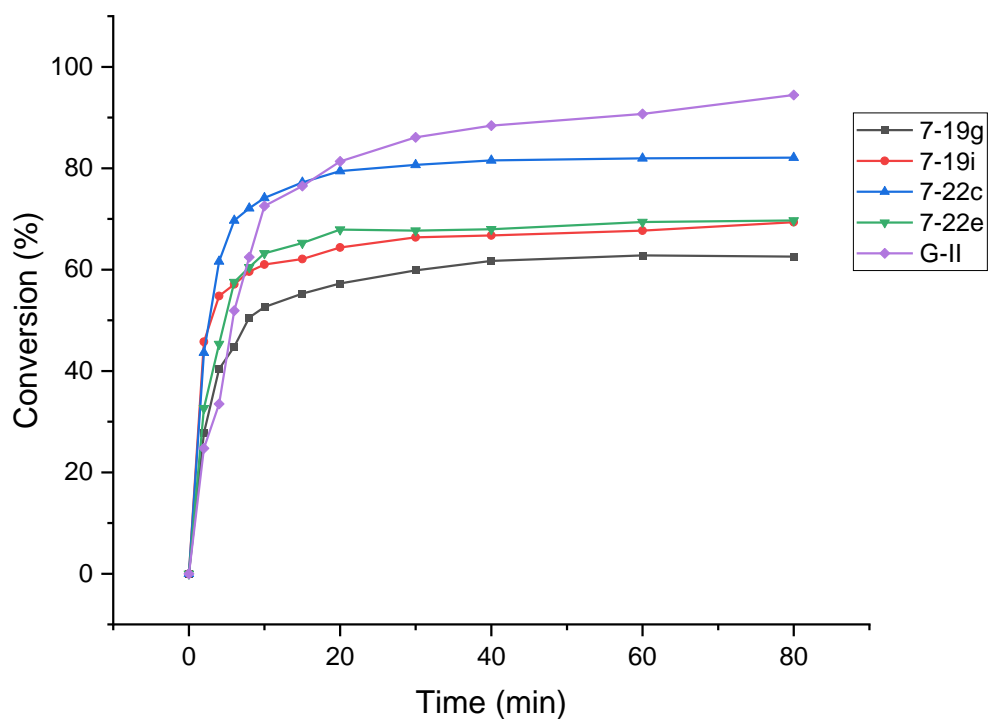
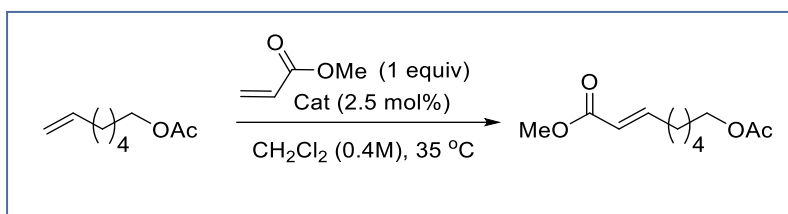
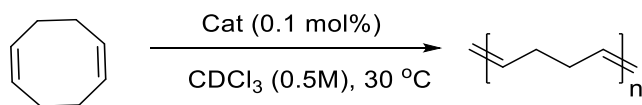


Fig. S11. Kinetic Profile for cross-metathesis of 5-hexenyl acetate with methyl acrylate using active alkene-chelated ruthenium alkylidenes as catalysts. Each data point represents the average of two independent experiments. Error bars represents standard error of the duplicate experiment. The alkene-chelates initiates with a much higher rate compared to **G-II** but slows down leading to lower conversions compared to **G-II**. The low conversion for alkene-chelates can be due to either rapid catalyst decomposition or higher formation of homo metatathesis product from 5-hexenyl acetate which could be indicated by the higher consumption of 5-hexenyl acetate.

Catalytic activities of alkene chelates for ROMP of 1,5-cyclooctadiene



An NMR tube with a screw-cap septum top was charged inside a glovebox with catalyst stock solution (0.01 M, 27 μL , 0.1 mol%) in 0.3 mL of CDCl₃. The NMR tube was degassed by freeze, pump, thaw method (cycle of 3) and refilled with argon. The sample was equilibrated at 30 °C in the NMR probe before 1,5-cyclooctadiene (30 mg, 0.27 mmol) solution in 0.5 mL of CDCl₃ was added via a syringe. Data points were collected over an appropriate time interval using the Bruker pseudo 2D kinetics method. The conversion of the polymer was determined by comparing the ratio of the integrals of the methylene protons in the starting material, δ 5.61–5.51 (m), with those of the polymer, δ 5.45–5.34 (br m). Three independent experiments were performed for each complex and mean conversion was determined. The conversion versus time graph was plotted for different complexes to have a comparison of their reactivities. The kinetic parameter k_{obs} was determined from the slope of $\ln([\text{SM}])$ vs time plot, where, $\ln([\text{SM}]) = \ln((100 - \text{avg. conv.}) / 100 * \text{conc. (0.5 M)})$.

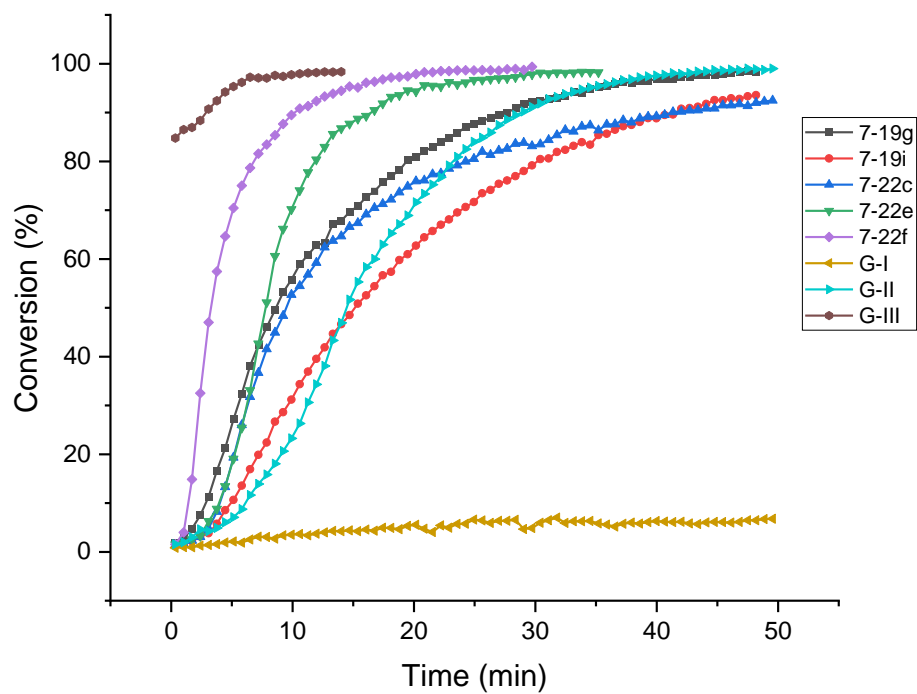
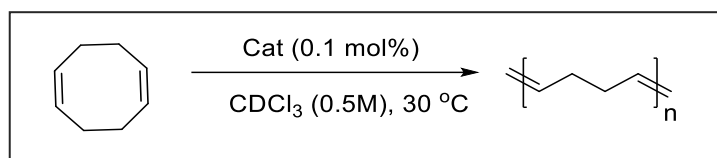


Fig. S12. Kinetic profiles for ROMP reaction of 1,5-cyclooctadiene using selected alkene-chelates as catalysts at 30 °C. Each data point represents the average of three independent experiments. Error bar represents standard error of the triplicate experiments.

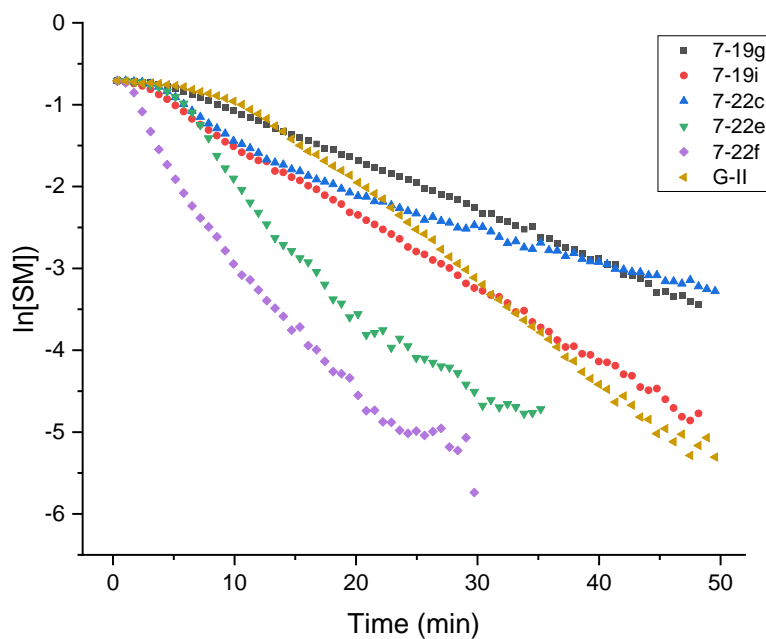


Fig. S13. Log plot of selected alkene-chelates for ROMP reaction of 1,5-cyclooctadiene. K_{obs} was determined from the slope of these curves and $t_{1/2}$ values were accordingly determined.

Kinetic parameters of catalysts for ROMP of 1,5-cyclooctadiene (k_{obs} , $t_{1/2}$ and k_{rel})

Cat.	k_{obs} (10^{-4} s^{-1})	$t_{1/2}$ (s)	k_{rel}	Linearity of plot
7-19g	10.2	679.6	0.52	
7-19i	14.8	468.3	0.75	
7-22c	8.2	845.3	0.42	Above 13% conv.
7-22e	26.5	261.6	1.35	Above 33% conv.
7-22f	32.7	212.0	1.66	
GII	19.7	351.9	1	Above 26% conv.

Note: With **G-III**, 86.5% conversion was achieved within first 35s hence, log plot cannot be obtained and k_{obs} was not determined.

7.4.5. X-ray crystallographic data

All X-Ray data can be obtained free of charge from The Cambridge Crystallographic Data Centre via www.ccdc.cam.ac.uk/data_request/cif.

Summary of Xray-Crystallographic data

Crystal data	Compound 7-19a	Compound 7-19c	Compound 7-19d
CCDC Deposition	2018298	2021743	2018914
Chemical formula	$C_{38}H_{46}Cl_2N_2Ru$	$C_{42}H_{44}Cl_2FeN_2Ru$	$C_{41}H_{52}Cl_2N_2ORu$
M_r	702.74	804.61	760.81
Crystal system, space group	Monoclinic, $P2_1$	Triclinic, $P-1$	Triclinic, $P-1$
Temperature (K)	200	200	200
a, b, c (Å)	11.9816 (10), 10.5576 (7), 13.8098 (12)	12.269 (4), 13.206 (4), 13.740 (4)	10.2526 (9), 12.9230 (13), 14.9304 (15)
α, β, γ (°)	90, 93.972 (3), 90	103.978 (8), 96.479 (9), 116.864 (7)	75.270 (3), 77.074 (3), 87.610 (3)
V (Å ³)	1742.7 (2)	1862.7 (10)	1864.5 (3)
Z	2	2	2
Radiation type	Mo $K\alpha$	Mo $K\alpha$	Mo $K\alpha$
μ (mm ⁻¹)	0.63	0.97	0.60
Crystal size (mm)	0.60 × 0.32 × 0.16	0.60 × 0.22 × 0.20	0.6 × 0.32 × 0.2
Diffractometer	Bruker SMART X2S	Bruker X2S	Bruker SMART X2S
Absorption correction	Multi-scan	Multi-scan	Multi-Scan
T_{min}, T_{max}	0.64, 0.91	0.594, 0.830	0.71, 0.89
No. of measured, independent and observed [$I > 2\sigma(I)$] reflections	17704, 5926, 5252	23566, 6332, 5072	33272, 6550, 5893
R_{int}	0.060	0.108	0.043
$(\sin \theta/\lambda)_{max}$ (Å ⁻¹)	0.596	0.596	0.598
$R[F^2 > 2\sigma(F^2)], wR(F^2),$ S	0.036, 0.115, 0.60	0.152, 0.391, 2.54	0.035, 0.107, 1.09
No. of reflections	5926	6332	6550
No. of parameters	396	460	434
No. of restraints	1	0	0
H-atom treatment	H-atom parameters constrained	H-atom parameters constrained	H-atom parameters constrained
$\Delta\rho_{max}, \Delta\rho_{min}$ (e Å ⁻³)	0.45, -0.59	2.78, -3.89	0.81, -0.62
Absolute structure parameter	-0.02 (2)	N/A	N/A

Crystal data	Compound 7-19l	Compound 7-19q	Compound 7-19r
CCDC Deposition	2018302	2018588	2018303
Chemical formula	C ₄₈ H ₅₂ Cl ₄ N ₂ ORuSi	C ₄₈ H ₅₇ Cl ₂ N ₃ O ₃ RuS	C ₅₅ H ₆₇ Cl ₂ N ₃ O ₆ RuS
M_r	943.87	927.99	1070.14
Crystal system, space group	Orthorhombic, $Pna2_1$	Monoclinic, $P2_1/c$	Triclinic, $P-1$
Temperature (K)	200	200	200
a, b, c (Å)	15.2754 (16), 28.119 (3), 10.4160 (9)	12.6853 (18), 12.842 (2), 32.754 (5)	11.0039 (7), 12.6857 (9), 20.6490 (15)
α, β, γ (°)	90, 90, 90	90, 96.636 (4), 90	101.995 (2), 101.394 (2), 106.335 (2)
V (Å ³)	4474.0 (8)	5299.8 (13)	2603.1 (3)
Z	4	4	2
Radiation type	Mo $K\alpha$	Mo $K\alpha$	Mo $K\alpha$
μ (mm ⁻¹)	0.65	0.47	0.50
Crystal size (mm)	0.44 × 0.40 × 0.07	0.46 × 0.4 × 0.31	0.40 × 0.31 × 0.29
Diffractometer	Bruker <i>SMART</i> X2S	Bruker APEX-II CCD	Bruker <i>SMART</i> X2S
Absorption correction	Multi-scan	Multi-scan	Multi-scan
T_{\min}, T_{\max}	0.71, 0.96	0.534, 0.867	0.74, 0.87
No. of measured, independent and observed [$I > 2\sigma(I)$] reflections	78579, 7870, 7294	54576, 9368, 8058	43746, 7950, 7272
R_{int}	0.076	0.058	0.038
$(\sin \theta/\lambda)_{\text{max}}$ (Å ⁻¹)	0.596	0.596	0.568
$R[F^2 > 2\sigma(F^2)]$, $wR(F^2)$, S	0.041, 0.128, 1.01	0.054, 0.133, 1.10	0.029, 0.102, 1.16
No. of reflections	7870	9368	7950
No. of parameters	520	532	624
No. of restraints	1	0	0
H-atom treatment	H-atom parameters constrained	H-atom parameters constrained	H-atom parameters constrained
$\Delta\rho_{\text{max}}, \Delta\rho_{\text{min}}$ (e Å ⁻³)	1.70, -0.54	0.59, -1.09	0.94, -0.76
Absolute structure parameter	-0.036 (14)	N/A	N/A

Crystal data	Compound 7-19r'	Compound 7-19s	Compound 7-22a
CCDC Deposition	2018594	2018596	2018283
Chemical formula	C ₅₉ H ₇₅ Cl ₄ N ₃ O ₇ RuS	C ₄₆ H ₅₅ Cl ₆ N ₃ O ₂ RuS	C ₄₀ H ₄₅ Cl ₄ N ₃ O ₂ RuS
M_r	1213.15	1027.76	874.72
Crystal system, space group	Triclinic, $P-1$	Monoclinic, $P2_1/n$	Monoclinic, $P2_1/c$
Temperature (K)	200	200	300
a, b, c (Å)	12.580 (3), 13.814 (4), 19.537 (5)	15.3127 (15), 13.8064 (11), 22.985 (2)	8.471 (2), 26.951 (8), 18.341 (6)
α, β, γ (°)	90.610 (9), 105.904 (8), 113.609 (8)	90, 91.300 (3), 90	90, 97.843 (9), 90
V (Å ³)	2963.8 (13)	4858.1 (8)	4148 (2)
Z	2	4	4
Radiation type	Mo $K\alpha$	Mo $K\alpha$	Mo $K\alpha$
μ (mm ⁻¹)	0.53	0.74	0.72
Crystal size (mm)	0.60 × 0.38 × 0.16	0.60 × 0.53 × 0.07	0.60 × 0.20 × 0.20
Diffractometer	Bruker <i>SMART</i> X2S	Bruker <i>SMART</i> X2S	Bruker <i>SMART</i> X2S
Absorption correction	Multi-scan	Multi-scan	Multi-scan
T_{\min}, T_{\max}	0.49, 0.92	0.63, 0.95	0.67, 0.87
No. of measured, independent and observed [$I > 2\sigma(I)$] reflections	60461, 12790, 8360	81174, 8620, 6868	17685, 7945, 7945
R_{int}	0.169	0.124	0.134
$(\sin \theta/\lambda)_{\max}$ (Å ⁻¹)	0.641	0.598	0.625
$R[F^2 > 2\sigma(F^2)]$, $wR(F^2)$, S	0.087, 0.242, 1.20	0.053, 0.170, 1.09	0.134, 0.325, 1.25
No. of reflections	12790	8620	7945
No. of parameters	689	541	468
No. of restraints	0	0	146
H-atom treatment	H-atom parameters constrained	H-atom parameters constrained	H-atom parameters constrained
$\Delta\rho_{\max}, \Delta\rho_{\min}$ (e Å ⁻³)	1.45, -1.68	3.03, -0.77	2.28, -2.31
Absolute structure parameter	N/A	N/A	N/A

Crystal data	Compound 7-22b	Compound 7-22g	Compound 7-22h'
CCDC Deposition	2018831	2018917	2021918
Chemical formula	<u>C₄₁H₄₇Cl₄N₃O₂RuS</u>	<u>C₄₃H₅₁Cl₄N₃O₃RuS</u>	<u>C₄₃H₅₁Cl₄N₃O₃RuS</u>
M_r	<u>888.74</u>	<u>932.80</u>	<u>932.80</u>
Crystal system, space group	<u>Orthorhombic, <i>Pbca</i></u>	<u>Monoclinic, <i>P2₁/n</i></u>	<u>Monoclinic, <i>P2₁/n</i></u>
Temperature (K)	<u>200</u>	<u>296</u>	<u>300</u>
a, b, c (Å)	<u>21.747 (7), 16.485 (5), 23.171 (8)</u>	<u>13.6581 (8), 10.7783 (6), 30.3452 (16)</u>	<u>13.3662 (8), 19.3514 (12), 18.2778 (11)</u>
α, β, γ (°)	90, 90, 90	90, <u>96.306 (1), 90</u>	90, <u>107.451 (2), 90</u>
V (Å ³)	<u>8307 (5)</u>	<u>4440.1 (4)</u>	<u>4510.0 (5)</u>
Z	<u>8</u>	<u>4</u>	<u>4</u>
Radiation type	<u>Mo $K\alpha$</u>	<u>Mo $K\alpha$</u>	<u>Mo $K\alpha$</u>
μ (mm ⁻¹)	<u>0.72</u>	<u>0.68</u>	<u>0.67</u>
Crystal size (mm)	<u>0.60 × 0.26 × 0.05</u>	<u>0.25 × 0.18 × 0.10</u>	<u>0.40 × 0.40 × 0.40</u>
Diffractometer	<u>Bruker <i>SMART</i> X2S</u>	<u>CCD</u>	<u>Bruker <i>SMART</i> X2S</u>
Absorption correction	<u>Multi-scan</u>	<u>Multi-scan</u>	<u>Multi-scan</u>
T_{\min}, T_{\max}	<u>0.67, 0.96</u>	<u>0.850, 0.934</u>	<u>0.775, 0.775</u>
No. of measured, independent and observed [$I > 2\sigma(I)$] reflections	<u>36892, 9861, 4758</u>	<u>37672, 7129, 5696</u>	<u>92644, 9210, 7407</u>
R_{int}	<u>0.305</u>	<u>0.038</u>	<u>0.050</u>
$(\sin \theta/\lambda)_{\max}$ (Å ⁻¹)	0.658	0.578	0.625
$R[F^2 > 2\sigma(F^2)]$, $wR(F^2)$, S	<u>0.092, 0.237, 1.01</u>	<u>0.045, 0.134, 0.99</u>	<u>0.058, 0.190, 1.35</u>
No. of reflections	<u>9861</u>	<u>7129</u>	<u>9210</u>
No. of parameters	<u>476</u>	<u>509</u>	<u>506</u>
No. of restraints	0	0	<u>155</u>
H-atom treatment	<u>H-atom parameters constrained</u>	<u>H-atom parameters constrained</u>	<u>H-atom parameters constrained</u>
$\Delta\rho_{\max}, \Delta\rho_{\min}$ (e Å ⁻³)	<u>1.06, -0.84</u>	<u>0.50, -1.08</u>	<u>2.14, -0.96</u>
Absolute structure parameter	N/A	N/A	N/A

Crystal data	Compound 7-22p'	Compound 7-22q'	Compound 7-22v
CCDC Deposition	2019504	2019503	2019480
Chemical formula	<u>C₇₅H₇₈Cl₁₀N₆O₄Ru₂</u>	<u>C₄₁H₄₂Cl₂N₃O₃RuS</u>	<u>C₄₈H₅₁Cl₂N₄O₄RuS₂</u>
M_r	<u>1684.07</u>	<u>828.81</u>	<u>984.02</u>
Crystal system, space group	<u>Monoclinic, $P2_1/n$</u>	<u>Monoclinic, $P2_1/c$</u>	<u>Monoclinic, $P2_1/n$</u>
Temperature (K)	<u>296</u>	<u>296</u>	<u>296</u>
a, b, c (Å)	<u>19.5436 (12),</u> <u>16.2686 (10),</u> <u>25.2292 (14)</u>	<u>10.9001 (7),</u> <u>16.3943 (10),</u> <u>21.6403 (14)</u>	<u>11.6701 (9), 29.6716 (19),</u> <u>13.7738 (10)</u>
α, β, γ (°)	90, <u>92.134 (2), 90</u>	90, <u>98.664 (2), 90</u>	90, <u>93.446 (2), 90</u>
V (Å ³)	<u>8016.0 (8)</u>	<u>3823.0 (4)</u>	<u>4760.8 (6)</u>
Z	<u>4</u>	<u>4</u>	<u>4</u>
Radiation type	<u>Mo $K\alpha$</u>	<u>Mo $K\alpha$</u>	<u>Mo $K\alpha$</u>
μ (mm ⁻¹)	<u>0.76</u>	<u>0.65</u>	<u>0.58</u>
Crystal size (mm)	<u>0.54 × 0.33 × 0.07</u>	<u>0.35 × 0.20 × 0.10</u>	<u>0.38 × 0.18 × 0.04</u>
Diffractometer	<u>CCD</u>	<u>CCD</u>	<u>CCD</u> <u>diffractometer</u>
Absorption correction	<u>Multi-scan</u>	<u>Multi-scan</u>	<u>Multi-scan</u> <u>SADABS</u>
T_{\min}, T_{\max}	<u>0.686, 0.950</u>	<u>0.805, 0.938</u>	<u>0.810, 0.976</u>
No. of measured, independent and observed [$I > 2\sigma(I)$] reflections	<u>60908, 12846,</u> <u>8422</u>	<u>47856, 6063, 4182</u>	<u>17303, 7347, 4976</u>
R_{int}	<u>0.084</u>	<u>0.100</u>	<u>0.040</u>
$(\sin \theta/\lambda)_{\text{max}}$ (Å ⁻¹)	<u>0.578</u>	<u>0.575</u>	<u>0.575</u>
$R[F^2 > 2\sigma(F^2)],$ $wR(F^2), S$	<u>0.148, 0.325, 1.88</u>	<u>0.050, 0.142, 0.90</u>	<u>0.071, 0.184, 1.13</u>
No. of reflections	<u>12846</u>	<u>6063</u>	<u>7347</u>
No. of parameters	<u>874</u>	<u>467</u>	<u>558</u>
No. of restraints	0	0	0
H-atom treatment	<u>H atoms treated by</u> <u>a mixture of</u> <u>independent and</u> <u>constrained</u> <u>refinement</u>	<u>H-atom parameters</u> <u>constrained</u>	<u>H-atom parameters</u> <u>constrained</u>
$\Delta\rho_{\text{max}}, \Delta\rho_{\text{min}}$ (e Å ⁻³)	<u>1.93, -1.20</u>	<u>0.60, -0.68</u>	<u>0.49, -0.90</u>
Absolute structure parameter	N/A	N/A	N/A

Crystal structure of 7-19a

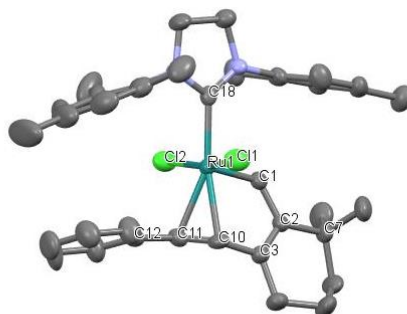


Fig. S14. Molecular Structure of **7-19a** (CCDC 2018298) showing 50% thermal probability ellipsoids. Hydrogen atoms are not shown for clarity. Selected bond distances [\AA]: Ru1-Cl1 2.360(2), Ru1-Cl2 2.385(2), Ru1-C1 1.846(6), Ru1-C10 2.302(7), Ru1-C11 2.277(7), Ru1-C18 2.106(7), C1-C2 1.42 (1), C10-C11 1.37(1), C11-C12 1.46(1). Selected bond angles [$^\circ$]: Cl1-Ru1-Cl2 166.59(7), Cl1-Ru1-C1 101.2(2), Cl1-Ru1-C18 87.2(2), C1-Ru1-C10 78.8(2), Ru1-C1-C2 123.7(5), C10-Ru1-C11 34.7(3), Ru1-C11-C10 73.7(4), Ru1-C10-C11 71.6(4), Ru1-C11-C12 109.3(5), C1-C2-C7 122.1 (6).

Crystal structure of 7-19c

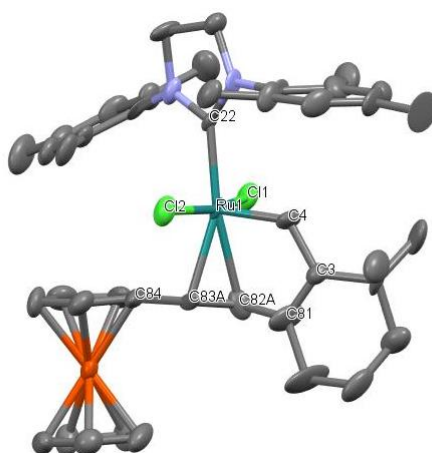


Fig. S15. Molecular Structure of **7-19c** (CCDC 2021743) showing 50% thermal probability ellipsoids. Hydrogen atoms are not shown for clarity. Selected bond distances [\AA]: Ru1-Cl1 2.360(5), Ru1-Cl2

2.372(5), Ru1-C4 1.86(1), Ru1-C22 2.08(1), Ru1-C82A 2.35(3), Ru1-C83A 2.25(3), C82A-C83A 1.32(6), C83A-C84 1.65(4), C3-C4 1.43(2). Selected bond angles [°]: Cl1-Ru1-Cl2 165.7(1), Cl1-Ru1-C4 97.6(5), Cl1-Ru1-C22 87.3(4), C4-Ru1-C82A 76.0(9), Ru1-C4-C3 124(1), C82A-Ru1-C83A 33(1), Ru1-C82A-C83A 69(2), Ru1-C83A-C82A 77(2), Ru1-C83A-C84 109.3(5), C4-C3-C5 123(1).

Crystal structure of 7-19d

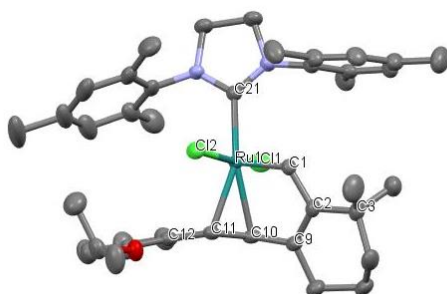


Fig. S16. Molecular Structure of **7-19d** (CCDC 2018914) showing 50% thermal probability ellipsoids. Hydrogen atoms are not shown for clarity. Selected bond distances [Å]: Ru1-Cl1 2.374(9), Ru1-Cl2 2.368(7), Ru1-C1 1.840(3), Ru1-C10 2.307(3), Ru1-C11 2.282(3), Ru1-C21 2.804(3), C1-C2 1.436(4), C10-C11 1.379(3), C11-C12 1.474(4). Selected bond angles [°]: Cl1-Ru1-Cl2 164.90(3), Cl1-Ru1-C1 102.02(9), Cl1-Ru1-C21 83.76(8), C1-Ru1-C10 78.4(1), Ru1-C1-C2 123.3(2) C10-Ru1-C11 35.0(1), Ru1-C11-C10 73.5(2), Ru1-C10-C11 71.5(2), Ru1-C11-C12 108.7(2), C1-C2-C3 121.6(2).

Crystal structure of 7-19l

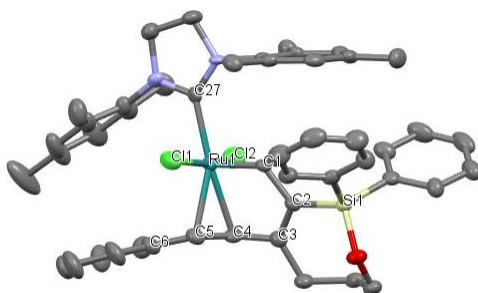


Fig. S17. Molecular Structure of **7-19l** (CCDC 2018302) showing 50% thermal probability ellipsoids. Hydrogen atoms are not shown for clarity. Selected bond distances [\AA]: Ru1-Cl1 2.395(2), Ru1-Cl2 2.354(2), Ru1-C1 1.848(5), Ru1-C4 2.295(7), Ru1-C5 2.225(7), Ru1-C27 2.109(6), C1-C2 1.446(9), C4-C5 1.36(1), C5-C6 1.48(1). Selected bond angles [$^\circ$]: Cl1-Ru1-Cl2 166.93(7), Cl1-Ru1-C1 89.4(2), Cl1-Ru1-C27 82.0(2), C1-Ru1-C4 78.7(4), Ru1-C1-C2 123.4(5), C4-Ru1-C5 35.0(3), Ru1-C5-C4 75.3(4), Ru1-C4-C5 69.7(4), Ru1-C5-C6 107.8(5), C1-C2-Si1 120.8(4).

Crystal structure of 7-19q

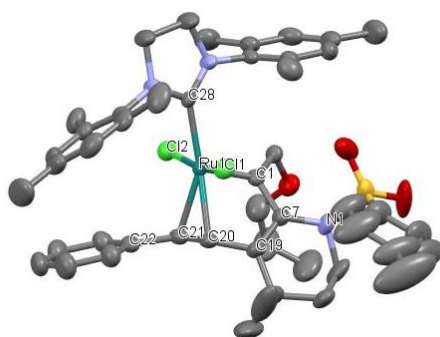


Fig. S18. Molecular Structure of **7-19q** (CCDC 2018588) showing 50% thermal probability ellipsoids. Hydrogen atoms are not shown for clarity. Selected bond distances [\AA]: Ru1-Cl1 2.380(1), Ru1-Cl2 1.866(1), Ru1-C1 1.866(4), Ru1-C20 2.234(4), Ru1-C21 2.243(4), Ru1-C28 2.119(4), C1-C7 1.467(5), C20-C21 1.379(5), C21-C22 1.484(5). Selected bond angles [$^\circ$]: Cl1-Ru1-Cl2 166.16(4), Cl1-Ru1-C1 96.1(1), Cl1-Ru1-C28 85.1(1), C1-Ru1-C20 79.5(4), Ru1-C1-C7 117.2(3), C20-Ru1-C21 35.9(1), Ru1-C20-C21 72.4(2), Ru1-C21-C20 71.7(2), Ru1-C21-C22 112.8(2), C1-C7-N1 122.7(3).

Crystal structure of 7-19r

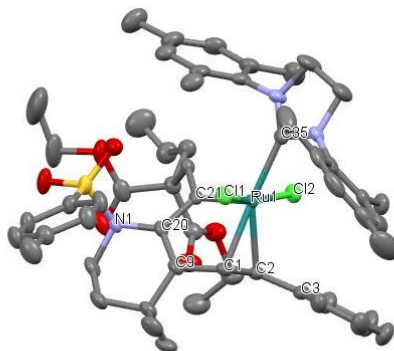


Fig. S19. Molecular Structure of **7-19r** (CCDC 2018303) showing 50% thermal probability ellipsoids. Hydrogen atoms are not shown for clarity. Selected bond distances [Å]: Ru1-Cl1 2.3772(7), Ru1-Cl2 2.4161(1), Ru1-C1 2.219(2), Ru1-C2 2.230(3), Ru1-C21 1.877(4), Ru1-C35 2.152(2), C1-C2 1.388(4), C2-C3 1.479(4), C20-C21 1.462(3). Selected bond angles [°]: Cl1-Ru1-Cl2 165.59(3), Cl1-Ru1-C21 97.11(8), Cl1-Ru1-C35 84.92(8), C1-Ru1-C21 79.5(1), C1-Ru1-C2 36.4(1), Ru1-C1-C2 72.2(2), Ru1-C2-C1 71.4(2), Ru1-C2-C3 113.1 (2), Ru1-C21-C20 116.4(2), C21-C20-N1 120.9(2).

Crystal structure of 7-19r'

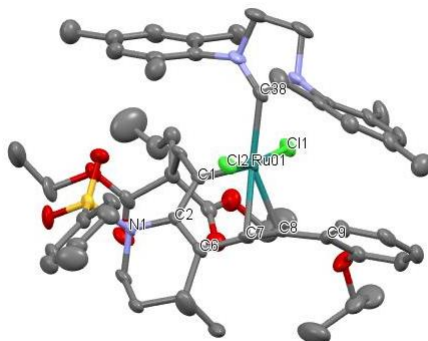


Fig. S20. Molecular Structure of **7-19r'** (CCDC 2018594) showing 50% thermal probability ellipsoids. Hydrogen atoms are not shown for clarity. Selected bond distances [Å]: Ru01-Cl1 2.410(1), Ru01-Cl2

2.369(1), Ru01-C1 1.876(6), Ru01-C7 2.223(7), Ru01-C8 2.229(8), Ru01-C38 2.159(7), C1-C2 1.461(9), C7-C8 1.399(9), C8-C9 1.48(1). Selected bond angles [°]: Cl1-Ru01-Cl2 165.07(6), Cl1-Ru01-C1 99.1(2), Cl1-Ru01-C38 82.4(2), C1-Ru01-C7 79.4(3), C7-Ru01-C8 36.6(2), Ru01-C1-C2 117.0(4), Ru01-C7-C8 71.9(4), Ru01-C8-C7 71.5(4), Ru01-C8-C9 112.3(5), C1-C2-N1 121.7(5).

Crystal structure of 7-19s

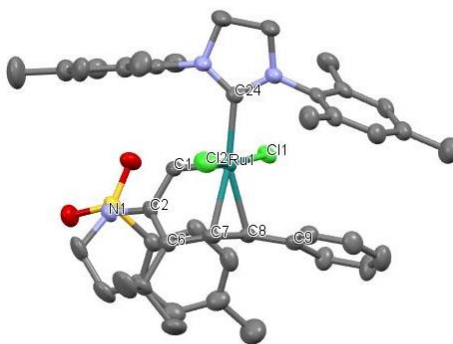


Fig. S21. Molecular Structure of **7-19s** (CCDC 2018596) showing 50% thermal probability ellipsoids. Hydrogen atoms are not shown for clarity. Selected bond distances [Å]: Ru1-Cl1 2.392(1), Ru1-Cl2 2.351(1), Ru1-C1 1.844(5), Ru1-C7 2.263(4), Ru1-C8 2.2250(4), Ru1-C24 2.103(4), C1-C2 1.431(6), C7-C8 1.363(6), C8-C9 1.477(6). Selected bond angles [°]: Cl1-Ru1-Cl2 165.30(4), Cl1-Ru1-C1 92.4(1), Cl1-Ru1-C24 86.4(1), C1-Ru1-C7 79.0(2), C7-Ru1-C8 35.2(2), Ru1-C1-C2 121.6(3), Ru1-C7-C8 71.9(2), Ru1-C8-C7 73.0(2), Ru1-C8-C9 109.2(3), C1-C2-N1 120.6(4).

Crystal structure of 7-22a

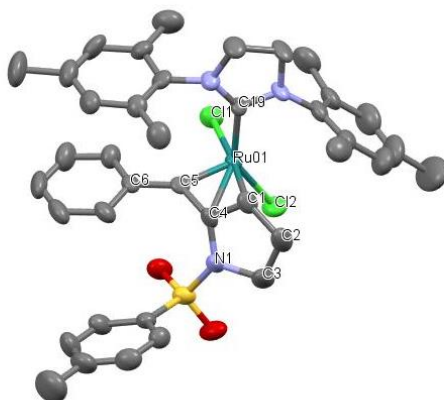


Fig. S22. Molecular Structure of **7-22a** (CCDC 2018283) showing 50% thermal probability ellipsoids. Hydrogen atoms are not shown for clarity. Selected bond distances [Å]: Ru1-Cl1 2.380(4), Ru1-Cl2 2.347(4), Ru1-C1 2.27(1), Ru1-C4 2.18(1), Ru1-C5 1.84(1), Ru1-C19 2.04(), C1-C4 1.39(2), C4-C5 1.44(2), C4-N1 1.41(2), C5-C6 1.47(2) Selected bond angles [°]: Cl1-Ru1-Cl2 87.6(1), Cl1-Ru1-C5 103.1(4), Cl1-Ru1-C19 92.7(4), C4-Ru1-C5 40.9(5), C4-Ru1-C1 36.3(5), Ru1-C1-C4 71.4(8), Ru1-C5-C4 82.6(8), Ru1-C5-C6 144(2), C1-C2-C3 105(1), N1-C4-C1 109(1).

Crystal structure of 7-22b

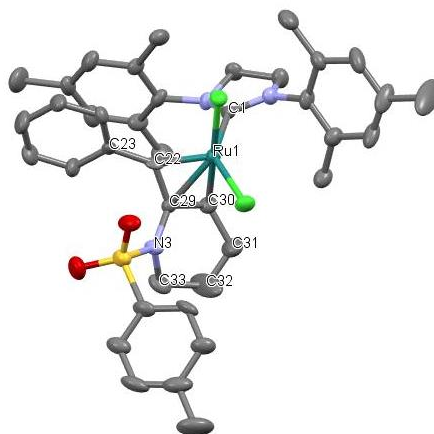


Fig. S23. Molecular Structure of **7-22b** (CCDC 2018831) showing 50% thermal probability ellipsoids. Hydrogen atoms are not shown for clarity. Selected bond distances [Å]: Ru1-Cl1 2.380(2), Ru1-Cl2 2.356(2), Ru1-C1 2.024(7), Ru1-C22 1.838(7), Ru1-C29 2.219(7), Ru1-C30 2.282(7), C22-C29 1.44(1), C29-C30 1.395(9), C22-C23 1.459(9), C29-N3 1.404(8). Selected bond angles [°]: Cl1-Ru1-Cl2 86.97(6), Cl1-Ru1-C1 97.0(3), Cl1-Ru1-C22 108.1(2), C22-Ru1-C29 40.3(3), C29-Ru1-C30 36.1(2), Ru1-C22-C29 84.2(4), Ru1-C30-C29 69.5(4), Ru1-C22-C23 143.9(5), C30-C31-C32 115.8(9), N3-C29-C30 124.4(6).

Crystal structure of 7-22g

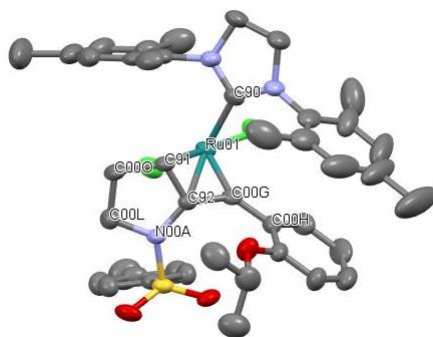


Fig. S24. Molecular structure of **7-22g** (CCDC 2018917) showing 50% thermal probability ellipsoids. Hydrogen atoms are not shown for clarity. Selected bond distances [Å]: Ru01-Cl03 2.349(1), Ru01-Cl04 2.396(1), Ru01-C90 2.039(7), Ru01-C91 2.237(4), Ru01-C92 2.169(3), Ru01-C00G 1.842(3), C91-C92 1.400(5), C92-C00G 1.436(5), C00G-C00H 1.451(5), C92-N00A 1.415(4). Selected bond angles [°]: Cl03-Ru01-Cl04 88.28(4), Cl04-Ru01-C00G 105.2(1), Cl04-Ru1-C90 86.98(9), C91-Ru01-C92 37.0(1), C92-Ru01-C00G 40.9(1), Ru01-C91-C92 68.9(2), Ru01-C00G-C92 81.9(2), Ru01-C00G-C00H 132.9(3), C91-C00O-C00L 104.3(3), N00A-C92-C91 108.9(3).

Crystal structure of 7-22h'

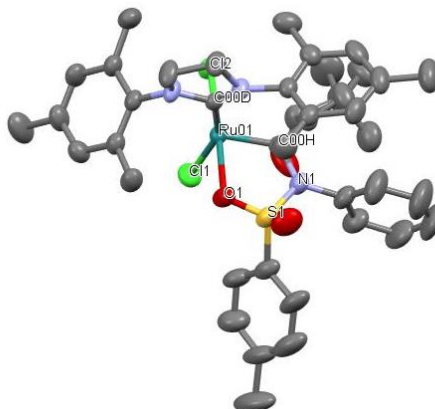


Fig. S25. Molecular Structure of **7-22h'** (CCDC 2021918) showing 50% thermal probability ellipsoids. Hydrogen atoms are not shown for clarity. Selected bond distances [\AA]: Ru01-Cl1 2.415(1), Ru01-Cl2 2.343(1), Ru01-C00D 2.019(3), Ru01-O1 2.172(3), Ru01-C00H 1.848(4), Ru01-C00G 1.842(3), S1-O1 1.454(5). Selected bond angles [$^\circ$]: Cl1-Ru01-Cl2 89.85(4), Cl1-Ru01-C00D 154.8(1), Cl1-Ru1-C00H 99.3(1), O1-Ru01-C00H 81.4(1), Ru01-O1-S1 117.3(2), O1-S1-N1 103.0(2), Ru01-C00H-N1 120.8(3).

Crystal structure of 7-22p'

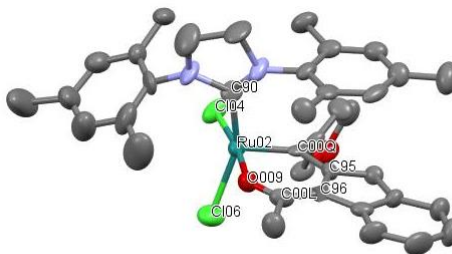


Fig. S26. Molecular Structure of **13p'** (CCDC 2019504) showing 50% thermal probability ellipsoids. Hydrogen atoms are not shown for clarity. Selected bond distances [\AA]: Ru02-Cl04 2.363(3), Ru01-Cl06 2.374(4), Ru02-C90 2.02(2), Ru02-O009 2.086(8), Ru02-C00Q 1.86(1), C00Q-C95 1.44(2), O009-C00L 1.24(2). Selected bond angles [$^\circ$]: Cl04-Ru02-Cl06 90.5(1), Cl04-Ru02-C90 92.8(4), Cl04-Ru02-C00Q

98.6(3), C00Q-Ru02-O009 88.6(4), Ru02-O009-C00L 124(1), Ru02-C00Q-C95 125.0(8), O009-C00L-C96 123(1).

Crystal structure of 7-22q'

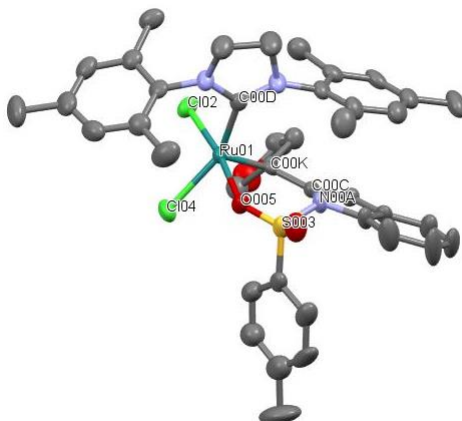


Fig. S27. Molecular Structure of **7-22q'** (CCDC 2019503) showing 50% thermal probability ellipsoids. Hydrogen atoms are not shown for clarity. Selected bond distances [Å]: Ru02-Cl02 2.328(1), Ru01-Cl04 2.360(2), Ru01-C00D 2.034(4), Ru01-C00K 1.856(5), Ru01-O005 2.170(3), S003-O005 1.439(4), C00C-C00K 1.455(6) Selected bond angles [°]: Cl02-Ru01-Cl04 90.33(5), Cl02-Ru01-C00D 90.5(1), Cl02-Ru01-C00K 96.9(1), C00K-Ru01-O005 88.8(2), Ru01-C00K-C00C 127.4(3), Ru01-O005-S003 135.4(2), O005-S003-N00A 105.4(2).

Crystal structure of 7-22v

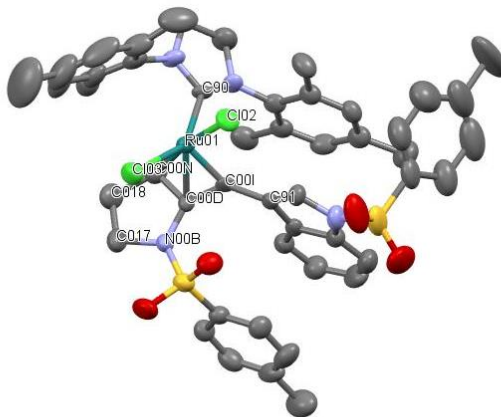


Fig. S28. Molecular Structure of **7-22v** (CCDC 2019480) showing 50% thermal probability ellipsoids. Hydrogen atoms are not shown for clarity. Selected bond distances [Å]: Ru01-C02 2.418(2), Ru01-Cl04 2.359(2), Ru01-C90 2.0416(6), Ru01-C00D 2.173(7), Ru01-C00I 1.827(6), Ru01-C00N 2.250(7), C00D-C00I 1.400(5), C00D-C00N 1.436(5), C00D-N00B 1.409(9), C00I-C91 1.437(8). Selected bond angles [°]: Cl02-Ru01-Cl03 87.8(6), Cl02-Ru01-C90 95.8(2), Cl02-Ru01-C00I 99.1(2), C00I-Ru01-C00D 40.8(2), C00D-Ru01-C00I 37.0(2), Ru01-C00I-C00D 82.7(4), Ru01-C00N-C00D 68.5(4), Ru01-C00I-C91 143.8(5), C00N-C018-C017 106.0(7), N00B-C00D-C00N 110.0(5).

7.5. Note

A part of this work was performed by Dr. Venkata R. Sabbasani and Mr. Siyuan Su. The X-ray crystallographic data was obtained by Prof. Donald J. Wink.

7.6. References

1. (a) Fürstner, A. *Angew. Chem., Int. Ed.* **2000**, *39*, 3012. (b) Fürstner, A. *Science* **2013**, *341*, 1229713. (c) Hoveyda, A. H.; Zhugralin, A. R. *Nature* **2007**, *450*, 243.
2. (a) Mol, J. C. *J. Mol. Catal. A: Chem.* **2004**, *213*, 39. (b) Grubbs, R. H. *Angew. Chem., Int. Ed.* **2006**, *45*, 3760. (c) Clavier, H.; Grela, K.; Kirschning, A.; Mauduit, M.; Nolan, S. P. *Angew. Chem., Int. Ed.* **2007**, *46*, 6786. (d) Higman, C. S.; Lummiss, J. A. M.; Fogg, D. E. *Angew. Chem., Int. Ed.* **2016**, *55*, 3552.
3. (a) Vougioukalakis, G. C.; Grubbs, R. H. *Chem. Rev.* **2010**, *110*, 1746. (b) Ogba, O. M.; Warner, N. C.; O'Leary, D. J.; Grubbs, R. H. *Chem. Soc. Rev.* **2018**, *47*, 4510.
4. (a) Mori, M. *Adv. Synth. Catal.* **2007**, *349*, 121. (b) Grubbs, R. H. *Metathesis in natural product synthesis: strategies, substrates and catalysts*; John Wiley & Sons: 2011. (c) Prunet, J. *Eur. J. Org. Chem.* **2011**, *2011*, 3634. (d) Werrel, S.; Walker, J. C. L.; Donohoe, T. J. Application of *Tetrahedron Lett.* **2015**, *56*, 5261.
5. (a) Harrity, J. P. A.; Visser, M. S.; Gleason, J. D.; Hoveyda, A. H. *J. Am. Chem. Soc.* **1997**, *119*, 1488. (b) Kingsbury, J. S.; Harrity, J. P. A.; Bonitatebus, P. J.; Hoveyda, A. H. *J. Am. Chem. Soc.* **1999**, *121*, 791–799.
6. Michrowska, A.; Bujok, R.; Harutyunyan, S.; Sashuk, V.; Dolgonos, G.; Grela, K. *J. Am. Chem. Soc.* **2004**, *126*, 9318.
7. Wakamatsu, H.; Blechert, S. *Angew. Chem., Int. Ed.* **2002**, *114*, 2509.
8. Garber, S. B.; Kingsbury, J. S.; Gray, B. L.; Hoveyda, A. H. *J. Am. Chem. Soc.* **2000**, *122*, 8168.
9. Fürstner, A.; Davies, P. W.; Lehmann, C. W. *Organometallics* **2005**, *24*, 4065.

10. Keitz, B. K.; Endo, K.; Patel, P. R.; Herbert, M. B.; Grubbs, R. H. *J. Am. Chem. Soc.* **2012**, *134*, 693.
11. Khan, R. K. M.; Torker, S.; Hoveyda, A. H. *J. Am. Chem. Soc.* **2013**, *135*, 10258.
12. (a) Kost, T.; Sigalov, M.; Goldberg, I.; Ben-Asuly, A.; Lemcoff, N. G. *J. Organomet. Chem.* **2008**, *693*, 2200. (b) Ivry, E.; Nechmad, N. B.; Baranov, M.; Goldberg, I.; Lemcoff, N. G. *Inorg. Chem.* **2018**, *57*, 15592. (c) Nechmad, N. B.; Lemcoff, N. G. *Synlett* **2020**, DOI: 10.1055/s-0040-1707231.
13. Szadkowska, A.; Makal, A.; Woźniak, K.; Kadyrov, R.; Grela, K. *Organometallics* **2009**, *28*, 2693.
14. Szadkowska, M.; Zukowska, K.; Pazio, A. E.; Wozniak, K.; Kadyrov, R.; Grela, K. *Organometallics* **2011**, *30*, 1130.
15. Barbasiewicz, M.; Szadkowska, A.; Bujok, R.; Grela, K. *Organometallics* **2006**, *25*, 3599.
16. Peeck, L. H.; Savka, R. D.; Plenio, H. *Chem. Eur. J.* **2012**, *18*, 12845–12853.
17. Hejl, A.; Day, M. W.; Grubbs, R. H. *Organometallics* **2006**, *25*, 6149.
18. Barbasiewicz, M.; Michalak, M.; Grela, K. *Chem. Eur. J.* **2012**, *18*, 14237.
19. Sabbasani, V. R.; Gupta, S.; Yun, S. Y.; Lee, D. *Org. Chem. Front.* **2018**, *5*, 1532.
20. Sabbasani, V. R.; Yun, S. Y.; Lee, D. *Org. Chem. Front.* **2016**, *3*, 939.
21. Tallarico, J. A.; Bonitatebus, P. J.; Snapper, M. L. *J. Am. Chem. Soc.* **1997**, *119*, 7157.
22. Trnka, T. M.; Day, M. W.; Grubbs, R. H. *Organometallics* **2001**, *20*, 3845.
23. Anderson, D. R.; Hickstein, D. D.; O'Leary, D. J.; Grubbs, R. H. *J. Am. Chem. Soc.* **2006**, *128*, 8386–8387.

24. Song, J. A.; Park, B.; Kim, S.; Kang, C.; Lee, D.; Baik, M. H.; Grubbs, R. H.; Choi, T. L. *J. Am. Chem. Soc.* **2019**, *141*, 10039.
25. Wang, K. P.; Yun, S. Y.; Lee, D.; Wink, D. J. *J. Am. Chem. Soc.* **2009**, *131*, 15114.
26. (a) Benitez, D.; Tkatchouk, E.; Goddard III, W. A. *Chem. Commun.* **2008**, *46*, 6194. (b) Diesendruck, C. E.; Tzur, E.; Ben-Asuly, A.; Goldberg, I.; Straub, B. F.; Lemcoff, N. G. *Inorg. Chem.* **2009**, *48*, 10819. (c) Pump, E.; Poater, A.; Zirngast, M.; Torvisco, A.; Fischer, R.; Cavallo, L.; Slugovc, C. *Organometallics* **2012**, *33*, 2806. (d) Pump, E.; Cavallo, L.; Slugovc, C. *Monatsh. Chem.* **2015**, *146*, 1131.
27. (a) Diver, S. T.; Giessert, A. J. *Chem. Rev.* **2004**, *104*, 1317. (b) Diver, S. T. *Coord. Chem. Rev.* **2007**, *251*, 671. (c) Hansen, E. C.; Lee, D. *Acc. Chem. Res.* **2006**, *39*, 509.
28. (a) Anderson, D. R.; O'Leary, D. J.; Grubbs, R. H. *Chem. Eur. J.* **2008**, *14*, 7536. (b) Stewart, I. C.; Benitez, D.; O'Leary, D. J.; Tkatchouk, E.; Day, M. W.; Goddard III, W. A.; Grubbs, R. H. *J. Am. Chem. Soc.* **2009**, *131*, 1931.
29. (a) Jung, M. E.; Piizzi, G. *Chem. Rev.* **2005**, *105*, 1735. (b) Forbes, M. D.; Patton, J. T.; Myers, T. L.; Maynard, H. D.; Smith Jr, D. W.; Schulz, G. R.; Wagener, K. B. *J. Am. Chem. Soc.* **1992**, *114*, 10978. (c) Kirkland, T. A.; Grubbs, R. H. *J. Org. Chem.* **1997**, *62*, 7310. (d) Urbina-Blanco, C. A.; Skibiński, M.; O'Hagan, D.; Nolan, S. P. *Chem. Commun.* **2013**, *49*, 7201.
30. Mori, M.; Wakamatsu, H.; Saito, N.; Sato, Y.; Narita, R.; Sato, Y.; Fujita, R. *Tetrahedron* **2006**, *62*, 3872.
31. Maishal, T. K.; Sarkar, A. *Synlett* **2002**, 1925.
32. Salvio, R.; Mandolini, L.; Savelli, C. *J. Org. Chem.* **2013**, *78*, 7259–7263.
33. (a) Miller, R. L.; Maifeld, S. V.; Lee, D. *Org. Lett.* **2004**, *6*, 2773. (b) Park, S.; Kim, M.; Lee, D. *J. Am. Chem. Soc.* **2005**, *127*, 9410. For reviews on silicon tethers: (c) Bols, M.; Skrydstrup, T. *Chem. Rev.* **1995**, *95*, 1253. (d) Gauthier Jr, D. R.; Zandi, K. S.; Shea, K. J. *Tetrahedron* **1998**, *54*, 2289.

34. (a) Kim, Y. J.; Grimm, J. B.; Lee, D. *Tetrahedron Lett.* **2007**, 48, 7961. (b) Luh, T. Y.; Hu, Z. *Dalton Trans.* **2010**, 39, 9185. (c) Čusak, A. *Chem. Eur. J.* **2012**, 18, 5800.
35. Mori and co-workers have demonstrated the enyne metathesis of ynamides in the presence of ethylene at higher temperature. This might be due to arresting of the propagating species through chelation with the enamide moiety in absence of ethylene at low temperature. (a) Saito, N.; Sato, Y.; Mori, M. *Org. Lett.* **2002**, 4, 803. (b) Evano, G.; Coste, A.; Jouvin, K. *Angew. Chem., Int. Ed.* **2010**, 49, 2840.
36. Sadimenko, A. P. *Adv. Heterocycl. Chem.* 2001, 79, 115.
37. Ritter, T.; Hejl, A.; Wenzel, A. G.; Funk, T. W.; Grubbs, R. H. *Organometallics* **2006**, 25, 5740.
38. Hejl, A.; Day, M. W.; Grubbs, R. H. *Organometallics* **2006**, 25, 6149. (b) Kost, T.; Sigalov, M.; Goldberg, I.; Ben-Asuly, A.; Lemcoff, N. G. *J. Organomet. Chem.* 2008, 693, 2200. (c) Ben-Asuly, A.; Tzur, E.; Diesendruck, C. E.; Sigalov, M.; Goldberg, I.; Lemcoff, N. G. *Organometallics* **2008**, 27, 811. (d) Monsaert, S.; Vila, A. L.; Drozdak, R.; Van Der Voort, P.; Verpoort, F. *Chem. Soc. Rev.* **2009**, 38, 3360. (e) Ginzburg, Y.; Anaby, A.; Vidavsky, Y.; Diesendruck, C. E.; Ben-Asuly, A.; Goldberg, I.; Lemcoff, N. G. *Organometallics* **2011**, 30, 3430.
39. Lehman, S. E.; Wagener, K. B. *Organometallics* **2005**, 24, 1477.
40. (a) Grubbs, R. H.; Miller, S. J.; Fu, G. C. *Acc. Chem. Res.* **1995**, 28, 446. (b) Deiters, A.; Martin, S. F. *Chem. Rev.* **2004**, 104, 2199.
41. (a) Chatterjee, A. K.; Morgan, J. P.; Scholl, M.; Grubbs, R. H. *J. Am. Chem. Soc.* **2000**, 122, 3783. (b) Chatterjee, A. K.; Choi, T. L.; Sanders, D. P.; Grubbs, R. H. *J. Am. Chem. Soc.* **2003**, 125, 11360.
42. (a) Bielawski, C. W.; Grubbs, R. H. *Angew. Chem., Int. Ed.* **2000**, 39, 2903. (b) Slugovc, C. *Macromol. Rapid Commun.* **2004**, 25, 1283. (c) Bielawski, C. W.; Grubbs, R. H. *Prog. Polym. Sci.* **2007**, 32, 1. (d) Song, K.; Kim, K.; Hong, D.; Kim, J.; Heo, C. E.; Kim, H. I.; Hong, S. H. *Nat. Commun.* **2019**, 10, 1.

43. (a) Camm, K. D.; Martinez Castro, N.; Liu, Y.; Czechura, P.; Snelgrove, J. L.; Fogg, D. E. *J. Am. Chem. Soc.* **2007**, *129*, 4168. (b) Kang, E. H.; Yu, S. Y.; Lee, I. S.; Park, S. E.; Choi, T. L. *J. Am. Chem. Soc.* **2014**, *136*, 10508. (c) Yasir, M.; Liu, P.; Tennie, I. K.; Kilbinger, A. F. M. *Nat. Chem.* **2019**, *11*, 488.
44. (a) Vehlow, K.; Maechling, S.; Köhler, K.; Blechert, S. *J. Organomet. Chem.* **2006**, *691*, 5267–5277. (b) Dumas, A.; Tarrieu, R.; Vives, T.; Roisnel, T.; Dorcet, V.; Baslé, O.; Mauduit, M. *ACS Catal.* **2018**, *8*, 3257.

CHAPTER 8

Ruthenabenze: A Robust Precatalyst

8.1. Introduction*

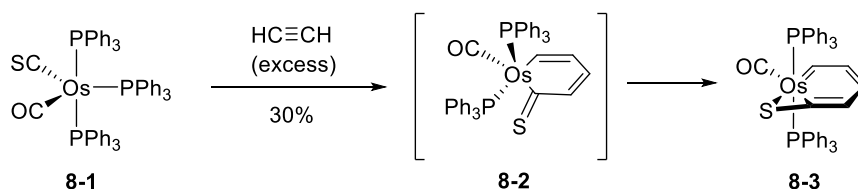
The concept of aromaticity has fascinated chemists for over a century and still draws considerable attention among different branches of chemistry. The archetypical aromatic compound is benzene. Formal replacement of a CH group in benzene by an isolobal hetero atom/ group can give rise to heterocyclic aromatic compounds. Heteroaromatic compounds form a vital constituent in many bioactive natural products and have tremendous application in pharmaceuticals.¹ Similarly replacing the CH group in benzene with isolobal transition metals leads to the formation of a unique class of compounds known as metallabenzene.² These complexes are particularly intriguing as they have the properties of both aromatic compounds and transition metals. In 1979, Thorn and Hoffmann predicted theoretically the possibility of Mn- and Rh-metallabenzenes.³ In 1982, Roper and coworkers synthesized the first stable metallabenzene based on osmium.⁴ After that, this unique class of organometallic compounds has burgeoned significant interests and witnessed rapid theoretical and experimental advances.⁵ One of the main studies involving metallabenzenes generally deals with the structural characterization related to their relative aromaticity compared to the carbon archetype. While different criteria for predicting the aromaticity of metallabenzenes can be used, based on the calculated aromatic stabilization energies (ASEs), metallabenzenes are considered to be aromatic even though the aromatic stabilization is weaker than that of the parent benzene.⁶ Several general synthetic routes have been developed for the synthesis of metallabenzene rings. A vast number of metallabenzenes can be also accessed through ligand modification/ substitutions on simple metallabenzenes.

The earliest synthetic route for the synthesis of metallabenzenes involves coupling of thiocarbonyl ligands with alkynes. This strategy was implemented by Roper and coworkers for the synthesis of the first stable metallabenzene, osmabenzene **8-3**, from the reaction of the osmiumthiocarbonyl complex **8-1** with

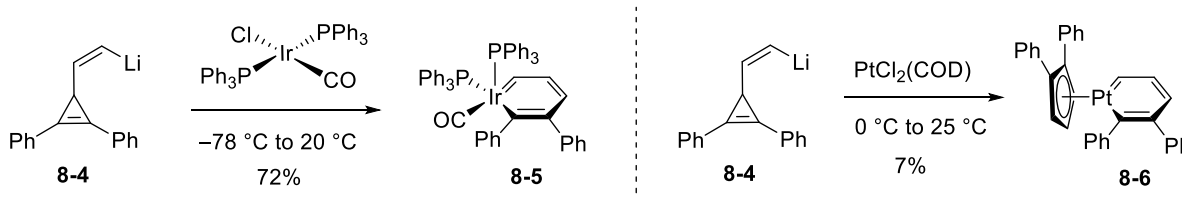
*This chapter has been reprinted (adapted) with permission from Gupta, S.; Su, S.; Zhang, Y.; Liu, P.; Wink, D. J.; Lee, D. "Ruthenabenzene: A Robust Precatalyst" *J. Am. Chem. Soc.* **2021**, *143*, 7490–7500. Copyright 2021, American Chemical Society.

excess of ethyne (**Scheme 8.1**).⁴ Van der boom and coworkers carried out computational studies to probe into the mechanistic details for the transformation of complex **8-1** to **8-3**.⁷ The mechanism involves sequential coordination to two equivalents of acetylene and a migratory insertion of the thiocarbonyl ligand, which leads to the formation of intermediate **8-2** that rearranges to osmabenzene **8-3**. Reactions of lithiated 3-vinyl-1-cyclopropenes with metal halide complexes provide another route to metallabenzenes. Haley and coworkers used this strategy to synthesize the iridabenzene **8-5**, which was produced from the reaction of (Z)-1,2-diphenyl-3-(2-lithioethenyl)-1-cyclopropene, **8-4** with IrCl(CO)(PPh₃)₂.⁸ This methodology was successfully extended by Haley and coworkers to prepare platinabenzenes.⁹ Thus, lithiated vinyl cyclopropene **8-4** reacted with PtCl₂(1,5-COD) to form the platinabenzene **8-6**. Metallacyclohexadienes form a useful starting material for the synthesis of metallabenzenes. In 1989, Bleke and coworkers used this strategy to synthesize the first stable iridabenzene. The reaction of Ir(PEt₃)₃Cl with pentadienyl potassium leads to the formation of the iridacyclohexa-1,3-diene-hydride complex **8-7**. Subsequent

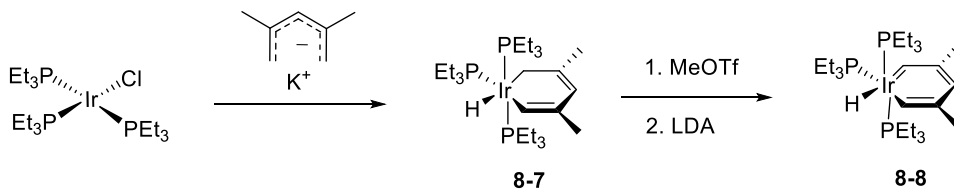
Coupling of thiocarbonyl ligand with alkynes



From lithiated 3-vinyl-1-cyclopropenes



From metallacyclohexadiene

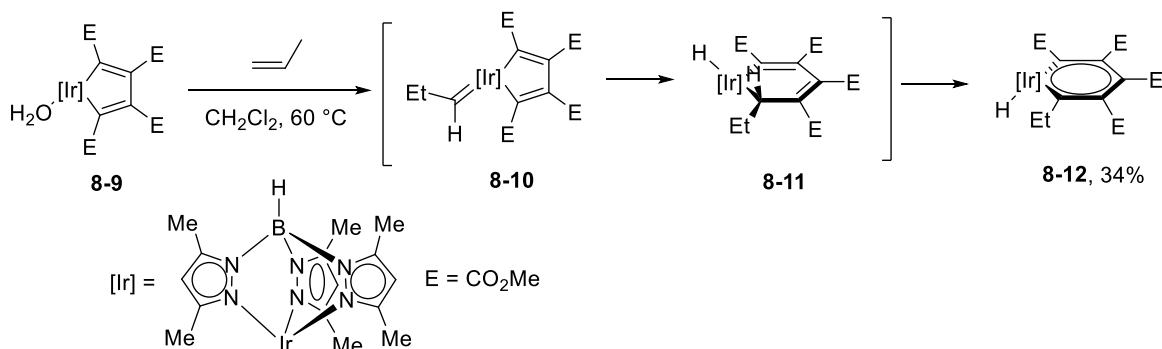


Scheme 8.1. Various synthetic routes to metallabenzenes

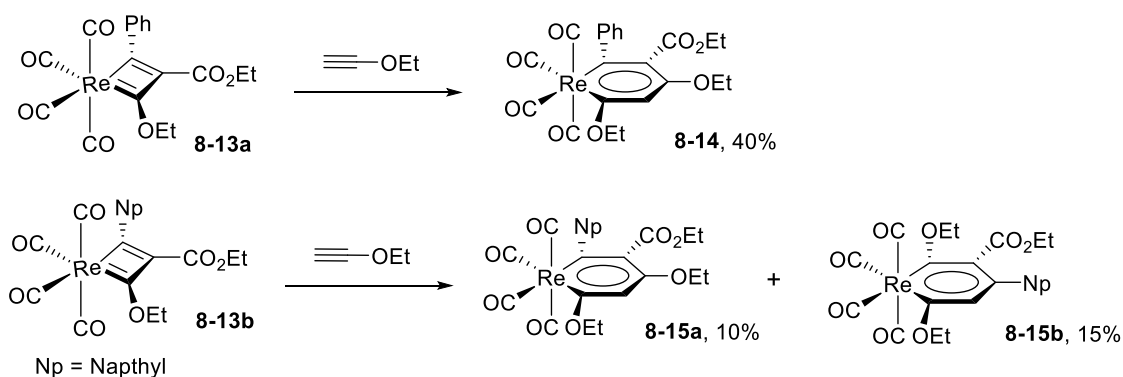
abstraction of metal hydride with methyl triflate followed by deprotonation leads to the formation of iridabenzene **8-8** (Scheme 8.1).¹⁰

Reactions of alkenes with metallacyclopentadienes to form metallabenzenes have been reported for iridium systems. For example, the metallacyclopentadiene complex **8-9** reacted with propene at 60 °C to give the iridabenzene **8-12** (Scheme 8.2).¹¹ The reaction proceeds through the initial coordination of complex **8-9** with alkene followed by isomerization to propylidene species **8-10**, in which the propylidene ligand undergoes carbene migratory insertion to form the iridacyclopentadiene **8-11**. Subsequent α -hydride

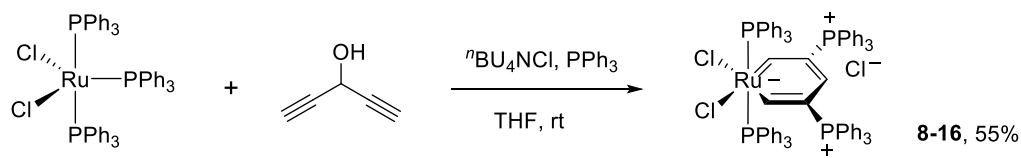
Reactions of alkenes with metallacyclopentadienes



Reactions of alkynes with metallacyclobutadienes



Nucleophilic addition to coordinated alkynes



Scheme 8.2. Various synthetic routes to metallabenzenes

elimination from **8-11** produces iridabenzene **8-12**. Reactions of metallacyclobutadienes with alkynes provide another route to metallabenzenes. This reaction has been used for the synthesis of rhenabenzenes. Treatment of the rhenacyclobutadiene complex **8-13a** with ethyl propiolate gave the rhenabenzene **8-14** in 40% yield. On contrary, when rhenacyclobutadiene complex **8-13b** was used, rhenabenzenes **8-15a** and **8-15b** can be isolated in 10% and 15% yields, respectively.¹² Nucleophilic addition of phosphines to properly functionalized alkynols could give complexes that can be manipulated to give metallabenzenes. This strategy was used by Jia and coworkers for the first synthesis of stable ruthenabenzenes which is also the first example for metallabenzene with second-row transition metals. Treatment of $\text{RuCl}_2(\text{PPh}_3)_3$ with penta-1,4-diyn-3-ol in the presence of PPh_3 at room temperature produced the ruthenabenzene **8-16** in 55% yield.¹³ This complex could even be obtained from the one-pot reaction of RuCl_3 , PPh_3 , and the penta-1,4-diyn-3-ol in CHCl_3 or in a mixed-solvent of ionic liquid and CH_2Cl_2 . Although there has been significant development for new synthetic routes to metallabenzenes, the studies of metallabenzenes are mostly limited to structure and reactivity. The applications of these complexes in catalysis are extremely limited.

8.2. Results and Discussions

8.2.1. Initial design, structural requirements, and substituent effects

Although metallabenzenes have not been developed as catalysts, it has been implicated as transient intermediates in many catalytic processes. For example, Schrock proposed tungstenabenzenes as transient intermediates in alkyne polymerization although they were not isolated and characterized.¹⁴ In recent olefin metathesis area, ruthenium-based Grubbs-type alkylidene complexes (**G-I-G-III**) and their oxygen-chelated congener Grubbs-Hoveyda catalyst (**GH-I/II**) are considered to be the most user-friendly catalysts (**Figure 8.1A**).¹⁵ In terms of the structural characteristics, the oxygen-chelated Grubbs-Hoveyda catalyst¹⁶ can be considered as the ruthenium analog¹⁷ of benzofuran. We envisage that the 5-membered aromatic furan moiety can be expanded to a 6-membered aromatic system¹⁸ to generate a ruthenanaphthalene (or ruthenabenzene) by replacing the lone-pair electron-containing O-atom with a C–C double bond. Based on the similarity between these isolobal analogies¹⁹ of ruthenabenzofuran and ruthenanaphthalene, we predict

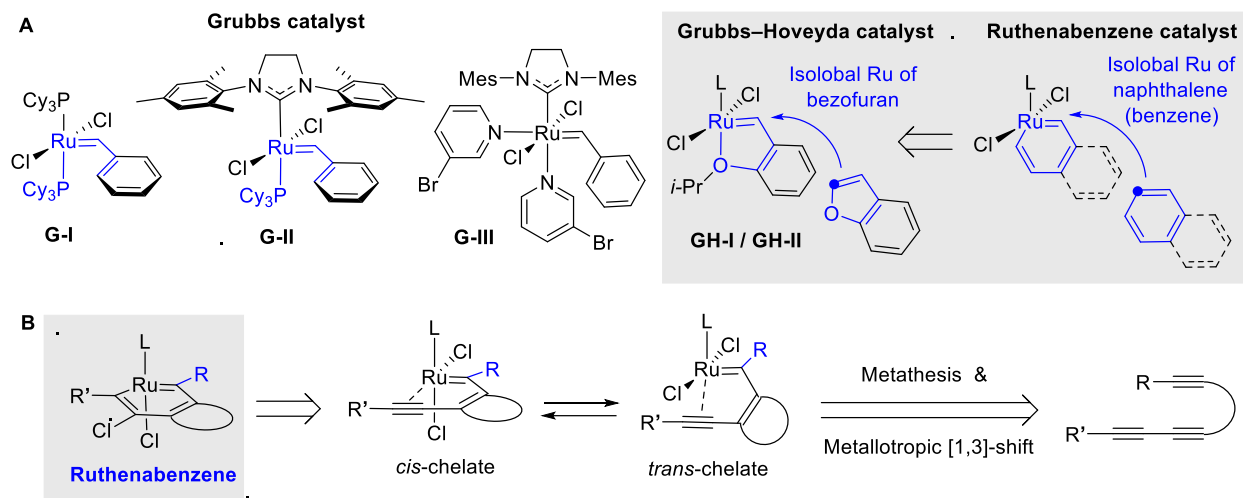
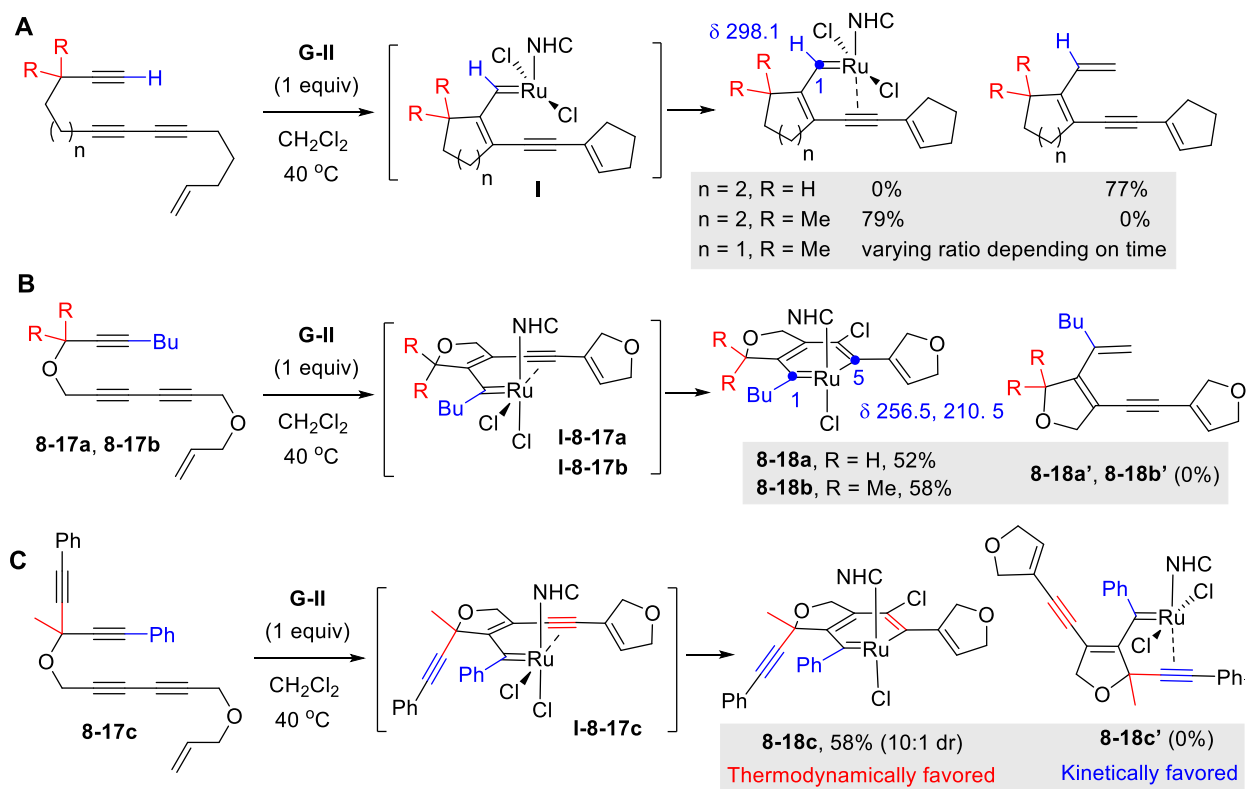


Figure 8.1. A new approach to ruthenabenzenes: (A) Isolobal analogy of the Grubbs-Hoveyda complex and a ruthenabenzene. (B) Ruthenabenzenes from ruthenium alkylidenes generated via enyne metathesis and metallotropic [1,3]-shift.

that the latter compound would be more stable than the ruthenabenzofuran moiety of the Grubbs-Hoveyda catalyst (**GH-I/II**) but it can still engage the ruthenium alkylidene ($\text{Ru}=\text{C}$) moiety to participate in catalytic process. In theory, we envisage that the ruthenabenzene framework^{13, 20} can be generated from the 1,3-enyne-conjugated ruthenium alkylidene upon appropriate alkyne-chelation. In turn, the precursor ruthenium alkylidene can be derived from multiynes via enyne metathesis²¹ and metallotropic [1,3]-shift²² (**Figure 8.1B**). Upon forming the 14-electron ruthenium alkylidene species, the preference for the disposition of the chelated alkyne either *trans* or *cis* relative to the *N*-heterocyclic carbene (NHC)²³ would depend on the substituent *R* on the carbenic carbon and the structure of the fused ring. While in equilibrium, the aligned three π -systems on the alkylidene, ($\text{Ru}=\text{C}$) and the conjugated 1,3-enyne, of the *cis*-chelate might undergo structural reorganization to form the ruthenabenzene core driven by the expected aromatic stabilization.

Previous study shows that the *trans*-chelate is more favorable if the carbenic carbon (C1) is monosubstituted in the 14-electron ruthenium intermediate **I**, and the *trans*-chelates could be isolated if stabilized by a *gem*-dimethyl group (*exo*-Thorpe-Ingold effect) and the size of the fused ring (**Figure 8.2A**).²⁴ These results indicate that the 5-membered ring fused chelate would have lesser chance to be

trapped as a *trans*-chelate, thus the effect of the substituent on the carbenic carbon was examined by employing ene-triynes **8-17a** and **8-17b** (Figure 8.2B). Much to our delight, both the reactions of **8-17a** and **8-17b** with a stoichiometric amount of **G-II** provided ruthenabenzenes **8-18a** and **8-18b** as green solid in 52 and 58% yield, respectively, while none of the corresponding metathesis products **8-18a'** and **8-18b'** were observed. These results clearly indicate that the butyl group on the carbenic carbon (C1) of intermediate **I-8-17a** and **I-8-17b** is crucial for populating the *cis*-chelate that led to ruthenabenzene; while the *gem*-dimethyl group seems to confer only a minimal effect in these reactions. The ^{13}C NMR spectrum of **8-18a** shows two carbene signals at 256.5 and 210.5 ppm, which are significantly shielded compared to the carbene of the *trans*-chelate (298.1 ppm), indicating that the π -bonds in **8-18a** are delocalized such that



both the C1 and C5 carbons share the carbenic nature.²⁵ The competition between kinetically favored *trans*-chelate and thermodynamically favored ruthenabenzene was tested by employing alkene-tethered tetrayne **8-17c**. If the *gem*-dialkyl effect (Thorpe-Ingold effect)²⁶ is large enough to promote strong interaction between the alkyne and the ruthenium center *trans*-chelate **8-18c'** would be generated, otherwise, aromatization of *cis*-chelate **1-8-17c** would provide ruthenabenzene **8-18c**. Indeed, the reaction of **8-17c** with **G-II** provided only ruthenabenzene **8-18c** in 58% yield (10:1 *dr*) (**Figure 8.2C**).

8.2.2. Tolerance of structural variations on the ruthenabenzene framework

Having defined the structural requirements for the formation of ruthenabenzenes, further structural variations were introduced onto the aromatic system (**Figure 8.3**). The electronic effect of heteroatom substituents was examined by introducing an NTs-linked ynamide, which ends up as ruthenaindolines **8-18d** and **8-18e** in 62% and 63% yields, where the phenyl and butyl substituent on the carbenic carbon does not make any difference in the reaction efficiency. Also, by employing **G-I**, the corresponding ruthenabenzene **8-18d-I** was obtained in 82% yield. The X-ray structure of **8-18d** confirms the expected ruthenabenzene framework which is a rare four-ligands containing distorted tetrahedral 14-electron ruthenium alkylidene²⁷ rather than the typical five-ligands containing square pyramidal 16-electron alkylidene. To reconstitute the original square pyramidal ligand geometry around the ruthenium center, an oxygen chelating group²⁸ was introduced in ruthenaindolines **2f**, the X-ray structure of which shows the ruthenabenzene core as a part of a square pyramidal structure geometry where the isopropoxy group chelated to the ruthenium center is *cis* to the NHC ligand.²⁹ A tricyclohexylphosphine ligand-containing complex **8-18f-I** was also obtained in excellent yield by employing **G-I**.

Surprisingly, introducing a 4-nitro group in **8-18f** makes the resulting complex **8-18g** too unstable to be isolated whereas **8-18g-I** could be obtained in 68% yield. Replacing the *ortho*-isopropoxyphenyl group in **8-18f** with an acetoxymethyl group provided the corresponding 6-membered carbonyl group-chelated complex **8-18h** in 94% yield.³⁰ Moving the NTs group to the next position resulted in slightly higher yield of ruthenaisoindolines **8-18i** (71%), **8-18j** (78%), and **8-18k** (89%) where the alkyl groups on the carbenic

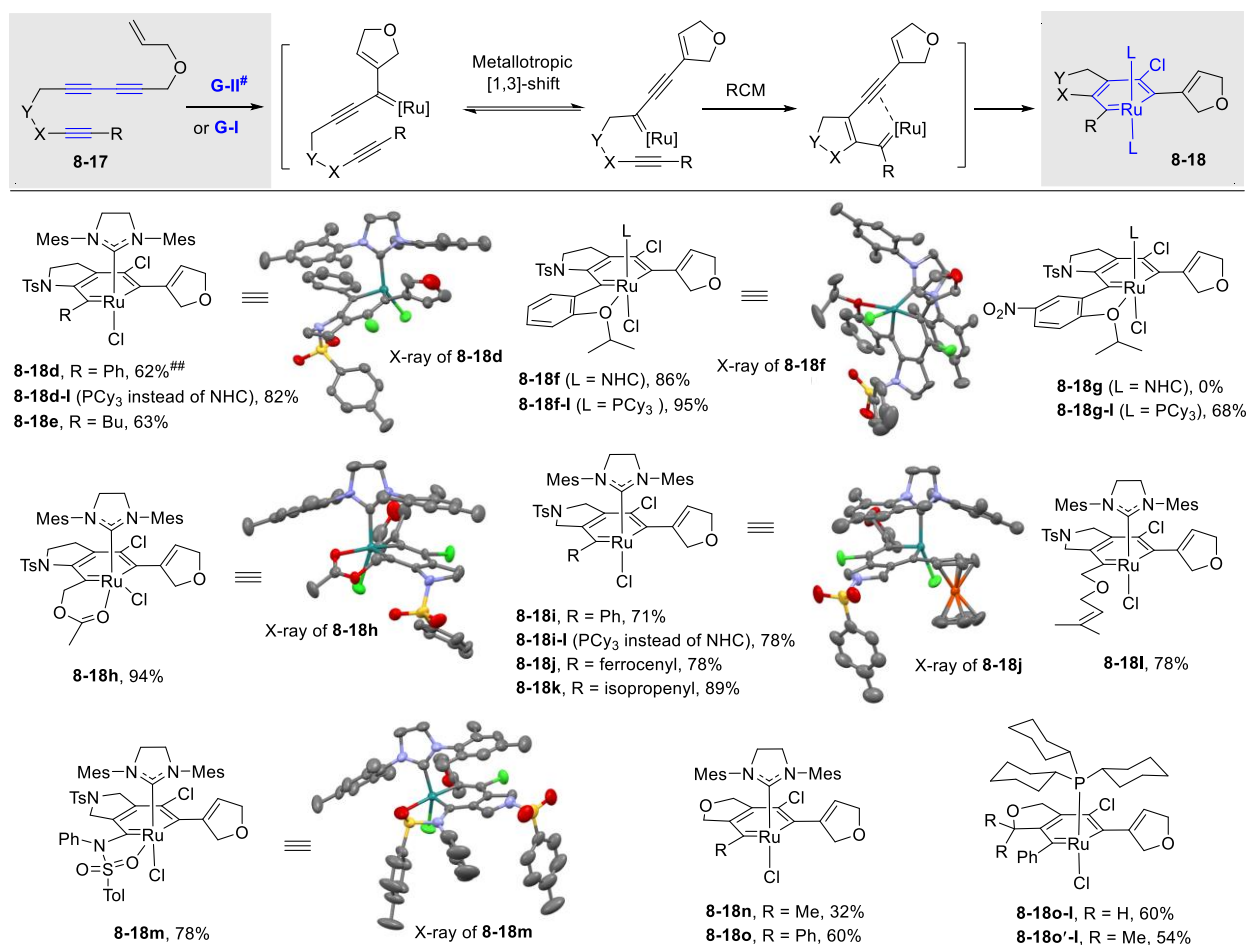


Figure 8.3. Ruthenabenzene formation via ring-closing metathesis (RCM) → metallotropic [1,3]-shift (MTS) → RCM → aromatization sequence with ene-triynes. [#] Reactions conditions: **G-II** or **G-I** (0.8 equiv) in CH₂Cl₂, 45 °C, 3h. ^{##}**8-18d** was also obtained in 68% yield with **G-III** catalyst in CDCl₃, 45 °C, 3 h.

carbon are phenyl, ferrocenyl, and isopropenyl respectively. With **G-I**, the corresponding complex **8-18i-I** was also obtained in 78% yield. The X-ray structure of **8-18j** shows that the bulky ferrocenyl group does not cause any structural perturbation compared with **8-18d**. Surprisingly, **8-18l** was obtained in 78% yield without any accompanied metathesis of the alkylidene intermediate with the prenyl group. This suggests that the ruthenium center of the intermediate alkylidene interacts with the alkyne moiety more favorably than the alkene.^{31,32} When additional NTs group was introduced at the carbenic carbon, the sulphonyl oxygen-chelated complex **8-18m**³³ was obtained and the overall ligand disposition of **8-18m** around the

ruthenium center is quite similar to that of other oxygen-chelates **8-18f** and **8-18h**. Reducing the steric bulk of the substituent either on the tether or on the carbenic carbon decreased the stability of the resultant complexes, thus ruthenadihydroisobenzofuran **8-18n** and **8-18o** containing a methyl and phenyl group were obtained in 32 and 60% yield, respectively. Tricyclohexylphosphine-containing complexes **8-18o-I** and **18o'-I** were obtained in similar yield with **G-I**, which suggests that the effect of *gem*-dimethyl group is only minimal if at all for formation of ruthenabenzenes. The NICS calculations of aromaticity³⁴ for several ruthenabenzenes show that the order of aromaticity (ppm) follows **8-18o-I** (−19.6) < **8-18a** (−20.1) < **8-18o** (−21.2) < **8-18d** (−23.8) < **8-18e** (−24.0). This result suggests the aromaticity of ruthenabenzenes is affected by the ligand on the ruthenium center to a higher extent than the substituent on the carbon framework.

8.2.3. Different mode of initiation and pathway selectivity

In the RCM-initiated formation of ruthenabenzenes, the incorporation of a cyclic alkene such as dihydrofuran at the C5 position is unavoidable. To alleviate this limitation, a cross metathesis (CM)-initiated approach was implemented with terminal 1,3-diyne **8-17p** (Figure 8.4A).³⁵ In this approach, installation of different alkene functionality at the C5 position in ruthenaindolines **8-18pa–8-18pc** could be achieved by employing different terminal alkenes to generate intermediate **I-8-17p**. For example, while **8-18pa** can be obtained directly from **8-17p** and **G-II**, **8-18pb** and **8-18pc** were obtained in the presence of 1-octene and ethylene, respectively. Cross metathesis between **8-18pa** and 1-octene or ethylene did not produce **8-18pb** or **8-18pc**, which suggest that the alkylidene exchange between the catalyst and the alkene happened before the formation of ruthenabenzene. This CM-initiated approach, although effective for diversifying the substituent at C5, provided relatively low yield of the products. To improve the efficiency of delivering the ruthenium alkylidene onto the main frame to generate intermediate **I-8-17r**, a relay metathesis strategy was also designed (Figure 8.4B),³⁶ where intramolecular delivery of the metal center can be achieved by a concomitant removal of the relay tether (dihydrofuran). This strategy allows for installation of an alkyl group at the C5 position, thus generating a methyl group-containing ruthenadihydroisobenzofuran **8-18r** in 67% yield. Another tactic to get access to the 1,3-enynyl ruthenium

alkylidene relies on enediynes, a minimum structural element required for ruthenabenzene formation (**Figure 8.4C**). In this approach, the chelating alkyne is preinstalled with a different terminal substituent, thus providing flexibility at the C5 position. RCM of enetriyne **8-17s** with **G-II** generated an intermediate **I-8-17s**, which provided **8-18s** after a metallotropic [1,3]-shift, while enediyne **1t** with **G-I** delivered **8-18t** through an aromatization of intermediate **I-8-17t**. Finally, tetraynes **8-17u-z** were employed to examine the selectivity for forming different end products from a common precursor, which should depend on the

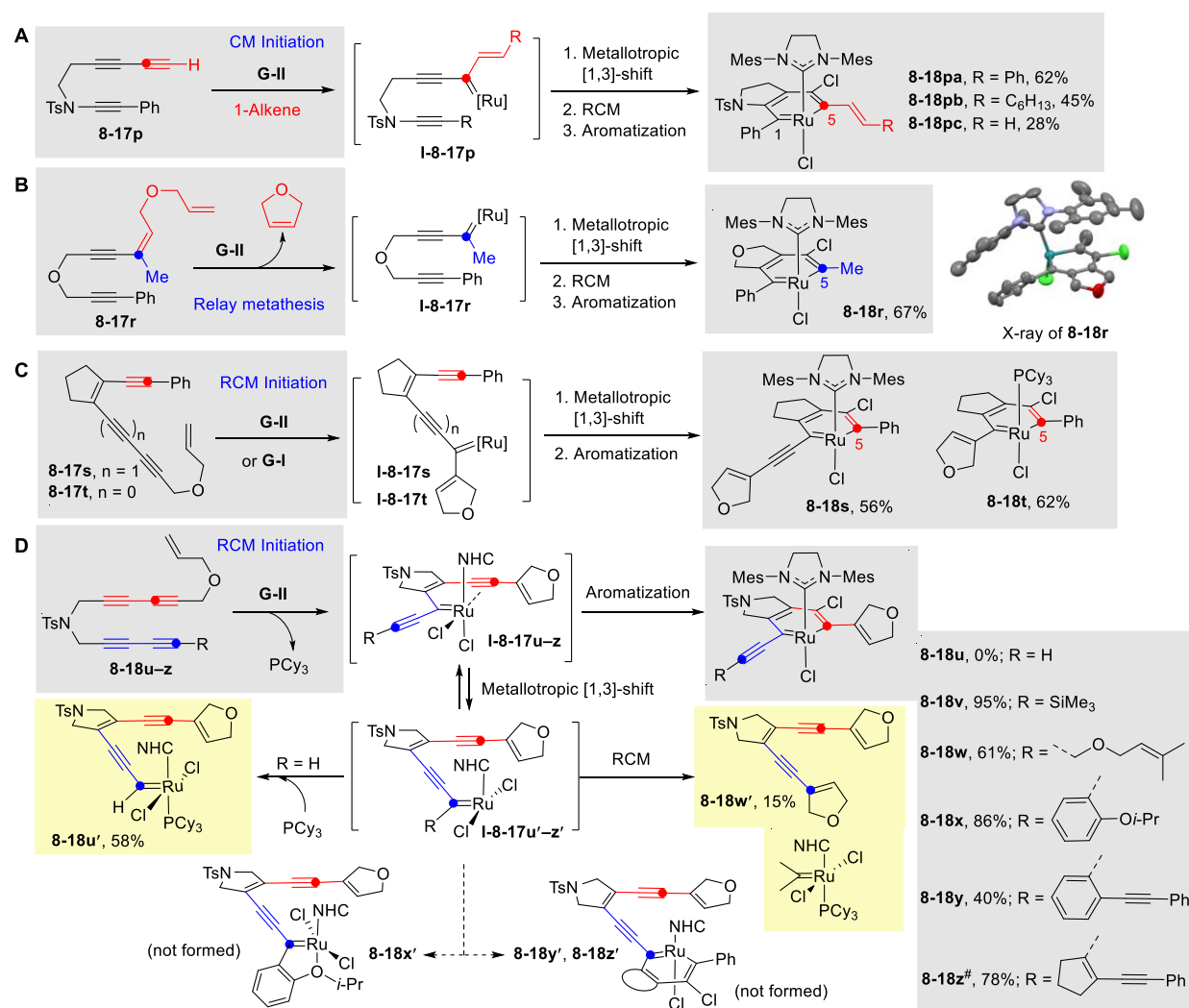


Figure 4. Different modes of initiation and selectivity: (A) Cross metathesis (CM)-initiated pathway. (B) Relay metathesis allows for installation of an alkyl group at the C5 carbenic carbon. (C) RCM-initiated pathway with enediynes and enetriynes. (D) Selectivity between cycloaromatization and metallotropic [1,3]-shift. [#]X-ray crystallographic data of **2z** confirmed the structure.

relative rate of alkyne chelation-induced aromatization versus metallotropic [1,3]-shift from the initially formed alkylidene **I-8-17u-z** (Figure 8.4D). Treatment of terminal tetrayne **8-17u** (R = H) with **G-II** resulted in forming complex **8-18u**³⁷ instead of ruthenabenzene **8-18u**, which suggest that the metallotropic [1,3]-shift of **I-8-17u** to mono-substituted alkylidene **I-8-17u'** should be faster than aromatization in this case. On the other hand, tetrayne **8-17v** (R = SiMe₃) provided ruthenabenzene **8-18v** in 95% yield, which is the consequence of a preferred aromatization of intermediate **I-8-17v** over [1,3]-shift because the silyl group prohibit the [1,3]-shift. A sterically less hindered prenyloxymethyl group-containing tetrayne **8-17w** provided ruthenabenzene **8-18w** in 61% yield along with RCM product **8-18w'** in 15% yield. It is not clear whether the ratio of these products reflect the equilibrium ratio of **I-8-17w** and **I-8-17w'** or their respective rates of aromatization and RCM while the two intermediates rapidly interconvert. Tetrayne **8-17x** containing an *ortho*-isopropoxy phenyl substituent provided ruthenabenzene **8-18x** in 86% yield without forming isopropoxy-chelate **8-18x'**. Considering the possibility of interconversion of **I-8-17x** and **I-8-17x'**, oxygen-chelate **8-18x'** could be formed but the reversible nature of the chelation funnels the equilibrium of these hemilabile species to ruthenabenzene **8-18x**. Both tetraynes **8-17y** and **8-17z** led to the formation of **8-18y** and **8-18z** in 40 and 78% yield, respectively. Even though there is possibility for metallotropic [1,3]-shift of **I-8-17y** and **I-8-17z** to **I-8-17y'** and **I-8-17z'** and generate alternative ruthenabenzene **8-18y'** and **8-18z'** but these were not observed.

8.2.4. Mechanism of ruthenabenzene formation

The mechanisms of cycloaromatization³⁸ of the alkyne-chelated ruthenium alkylidene to form a ruthenabenzene core were investigated using DFT calculations.³⁹ The Ru-alkylidene **Int-I** was used in the calculations as a representative system, which is formed from triyne **8-17d** through a cascade process involving an RCM–metallotropic [1,3]-shift–RCM sequence. Among other possibilities, two most probable pathways for the conversion of **Int-I** to ruthenabenzene **8-18d** were considered (Figure 8.5A). Path A involves the dissociation of a chloride anion to form ion-pair **Int-II** followed by its recombination via nucleometallation (**TS2**) of the π -alkyne complex. Path B proceeds via a *cis-trans* isomerization to form

intermediate **Int-I'** followed by an intramolecular 1,5-Cl shift. The energy profiles of these pathways were computed using the M06⁴⁰/SDD⁴¹-6-311+G(d,p)/SMD(CH₂Cl₂)⁴²//B3LYP-D3(BJ)/SDD-6-31G(d)/SMD(CH₂Cl₂) level of theory (**Figure 8.5B**).

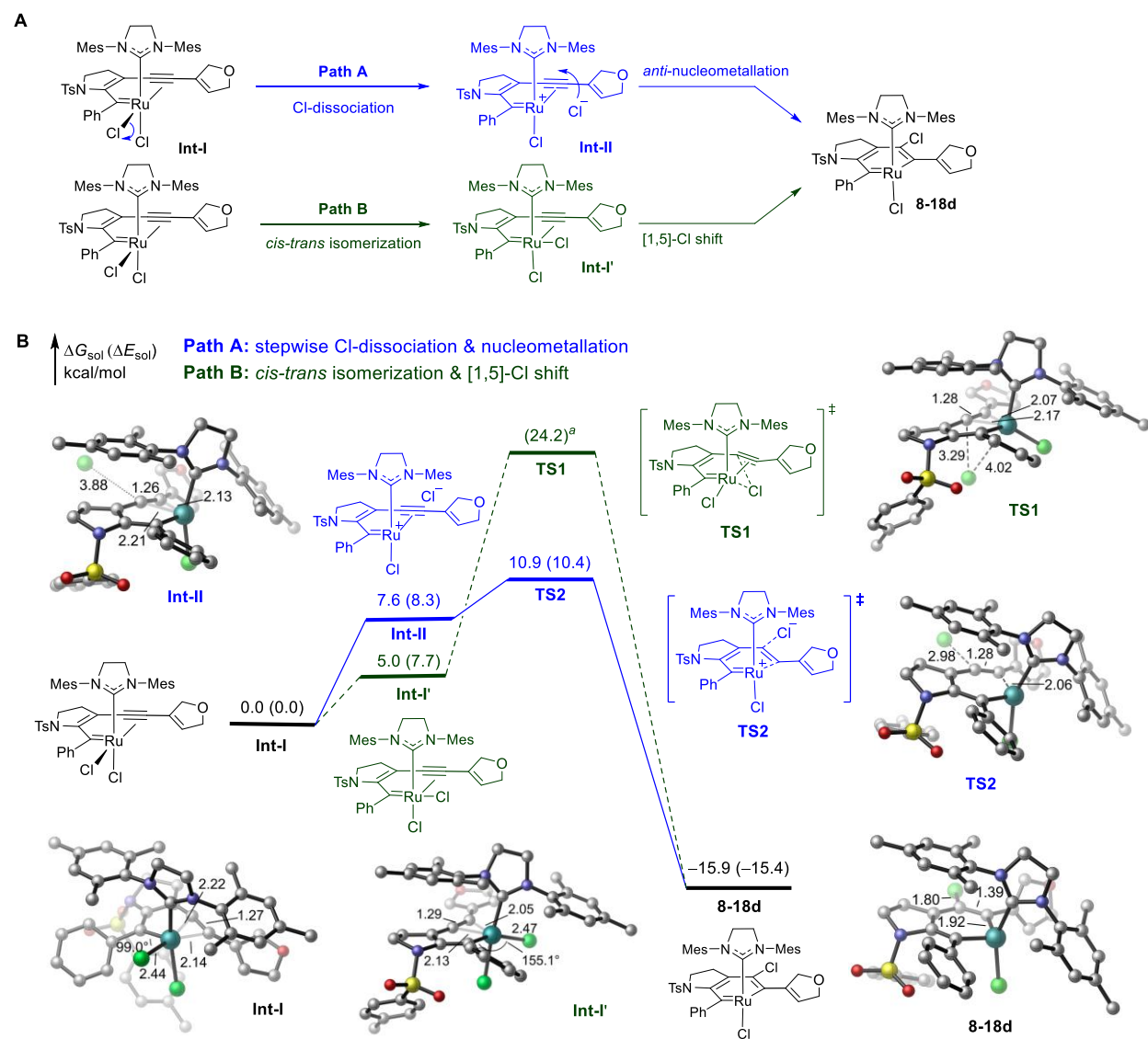


Figure 8.5. Mechanisms of cycloaromatization to form ruthenabenzene: (A) Plausible pathways for ruthenabenzene formation from the ruthenium alkylidene intermediate. (B) Computed energy profiles at the M06/SDD-6-311+G(d,p)/SMD(CH₂Cl₂)//B3LYP-D3(BJ)/SDD-6-31G(d)/SMD(CH₂Cl₂) level of theory. H atoms are omitted in the 3D structures for clarity. ^aThe geometry of **TS1** was optimized using the growing string method (GSM).

In Path A, Cl[−] ion dissociation from **Int-I** to form ion pair **Int-II** is endergonic by 7.6 kcal/mol. The resulting π -alkyne complex with the cationic Ru center is highly reactive towards *anti*-nucleometallation with the Cl[−] ion.⁴⁴ The nucleometallation transition state **TS2** requires an activation free energy of 10.9 kcal/mol with respect to **Int-I** and leads directly to the ruthenabenzene (**8-18d**). Path B involves a *cis-trans* isomerization to place one of the chloride ligands *trans* to the alkylidene to form **Int-I'** ($\Delta G_{\text{sol}} = 5.0$ kcal/mol). The *trans* effect of the alkylidene weakens the Ru–Cl bond in **Int-I'** (the Ru–Cl bond distance is 2.47 Å compared to 2.44 Å in **Int-I**) and promotes the subsequent [1,5]-Cl shift to form **8-18d**. Because the potential energy surface of the [1,5]-Cl shift is nearly flat in the transition state region (see SI for details), the transition state (**TS1**) could not be located using Gaussian after multiple attempts. Therefore, we applied the growing string method (GSM)⁴⁵ to locate this transition state structure and calculate the activation barrier. The GSM calculations indicate the [1,5]-Cl shift is a concerted process via **TS1**, with relatively long bond lengths of the cleaving Ru–Cl bond and the forming C–Cl bond (4.02 Å and 3.29 Å, respectively). The activation energy ($\Delta E_{\text{sol}}^{\ddagger}$) of **TS1** is 24.2 kcal/mol with respect to **Int-I**, which is 13.8 kcal/mol higher than that of **TS2** ($\Delta E_{\text{sol}}^{\ddagger} = 10.4$ kcal/mol). These computational results suggest that Path A involving the stepwise chloride dissociation and nucleometallation is the most favorable pathway to form the ruthenabenzene.

8.2.5. Catalytic activity of ruthenabenzenes

The catalytic activity of ruthenabenzenes was examined by using a standard substrate **8-19a** for RCM reaction to generate **8-20a** (see **Fig. S1**, Section 8.4.4). The relative reactivities of ruthenabenzenes containing different substituents on the carbenic carbons (C1–Ru–C5) and the fused ring were compared. Calculations revealed that these ruthenabenzenes are in fact precatalysts which releases small amount of active alkyne-chelated ruthenium alkylidene species which catalyzes the reaction (see **Figure 8.7**). Since most of these complexes show only latent catalytic behaviors,⁴⁶ the reactions were performed in toluene-d₈ at 70 °C. From their reaction profiles, it is evident that the sterically less hindered oxygen-containing ruthenadihydroisobenzofurans are more reactive than NTs-containing ruthenaindolines and

ruthenaisoindolines; for example, **8-18a** (97% conv. at 70 min) and **8-18o** (99% conv. at 18.3 h) are more reactive than **8-18d** (36% conv. at 45 h), and **8-18i** (30.5% conv. at 42.5 h). Ruthenabenzenes containing an alkyl group at C1 are more reactive than the corresponding phenyl-containing complexes; a butyl-containing **8-18a** is more reactive than a phenyl-containing **8-18o**. Also, NHC and PCy₃ ligands have a significant impact on the catalytic activity; **8-18o** with NHC (99% conv. at 18.3 h) is more reactive than **8-18o-I** with PCy₃ (81% conv. at 43.5 h). As expected, chelated complex **8-18f** showed a slower initial rate than non-chelated congener **8-18d** but gave a higher conversion (56% vs. 36% at 45.0 h) probably because of its higher longevity. After identifying the general reactivity trend of ruthenabenzene-based precatalysts,

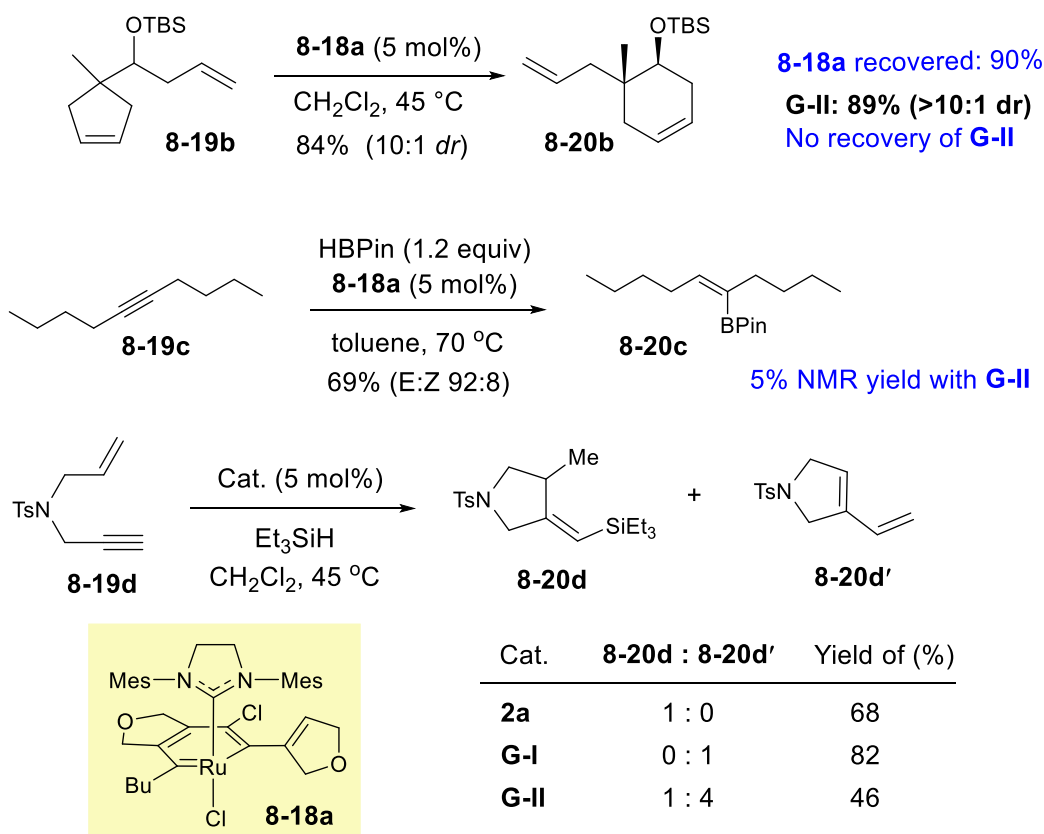


Figure 8.6. Reactivity of ruthenabenzene in various metathetic and non-metathetic reactions

the reactivity of **8-18a**, **8-18n** and **8-18r** were compared with **G-I** and **G-II** at 45 °C in RCM of **8-19a** to generate **8-20a** (see Fig. S2, Section 8.4.4). Because the ruthenium alkylidene moiety is a part of an

aromatic system and in a more sterically congested environment, these ruthenabenzene-based precatalysts showed much lower reaction rates than **G-I** and **G-II**. Thus, while complete conversion was achieved within few minutes by **G-I** and **G-II** catalyst, roughly 45, 17, and 12% conversions were achieved by precatalysts **8-18a**, **8-18n** and **8-18r** respectively after 1 h. It is interesting to note that a sterically less hindered methyl group-containing catalyst **8-18n** turned out to be slightly less active in comparison to **8-18a** with a butyl substituent. RCM of **8-19a** could be promoted effectively with lower catalyst loading (2 mol%) but took longer time. Precatalyst **8-18a** also demonstrated effective cross-metathesis reaction involving allyl benzene and (*Z*)-but-2-ene-1,4-diyl diacetate (see Section 8.4.5).

The catalytic activity for the most active precatalyst was also tested for other processes (**Figure 8.6**). The ring-rearrangement metathesis of cyclopentenyl derivative **8-19b** with catalyst **8-18a** provided cyclohexenyl derivative **8-20b** in 84% yield with 10:1 *dr*, which is nearly the same result as with **G-II** (89% yield, >10:1 *dr*).⁴⁷ A non-metathetic catalytic activity of **8-18a** was also examined for hydroboration⁴⁸ of 5-decyne **8-19c**, which provided *E*-alkenyl boronate **8-20c** in 69% yield while **G-II** was found to be nearly unreactive for this transformation. The catalytic activity of **8-18a** was also examined for hydrosilylative cyclization⁴⁹ of 1,6-enyne **8-19d** in comparison with **G-I** and **G-II** (**Figure 8.6**). Under identical conditions, these catalysts showed significant difference in forming products **8-20d** and **8-20d'**. While precatalyst **8-18a** exclusively provided hydrosilylation/ cyclization product **8-20d** in 68% yield, **G-I** and **G-II** generated enyne metathesis product **8-20d'** as the predominant product. Precatalyst **8-18a** was found to be recoverable,⁵⁰ and its longevity was demonstrated by five rounds of recycling of **8-18a**, with similar efficiency in each cycle for the RCM of dienyl alcohol **8-19e** to **8-20e** (see **Fig. S3**, Section 8.4.6). The robust nature of ruthenabenzenes compared to **G-II** is demonstrated by higher stability of precatalyst **8-18a** under air or ethylene atmosphere (see **Fig. S4** and **S5**, Section 8.4.6).

The recyclability of the precatalyst might have two independent origins. The first path, because of the stable aromatic nature of **8-18a**, involves only a small fraction of the ruthenabenzene precatalyst

entering the Catalytic Cycle I via reversion to alkyne-chelated alkylidene **I-8-17a** (**Figure 8.7**). The other path initiated by direct participation of the ruthenabenzene precatalyst entails the Catalytic Cycle II or III,

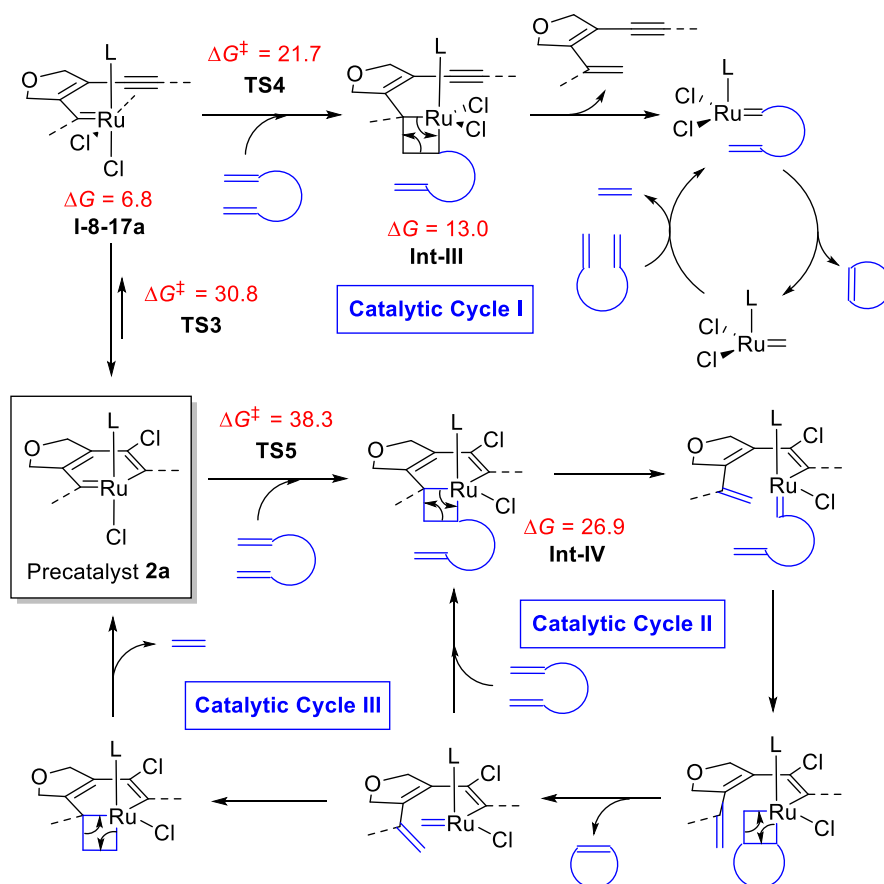


Figure 8.7. Possible catalytic cycles. Computed activation free energies (kcal/mol) of ^areversion of precatalyst **8-18a** to alkyne-chelated alkylidene **I-8-17a** (TS3), ^binitiation by [2+2] cycloaddition of **I-8-17a** with diene (TS4), and ^cinitiation by [2+2] cycloaddition of **8-18a** with diene (TS5). ^dComputed energies for the intermediates (kcal/mol) with respect to **8-18a**.

wherein catalytically active species are constantly regenerated. To gain more insight into these mechanisms, the energy profiles of the different initiation pathways were calculated using DFT (see Section 8.5.7). A direct [2+2] cycloaddition with ruthenabenzene precatalyst **8-18a** to form a dearomatized ruthenacyclobutane intermediate requires very high activation free energy (TS5, $\Delta G^\ddagger = 38.3$ kcal/mol), suggesting both the Catalytic Cycles II and III are less likely operative. On the other hand, the Catalytic

Cycle I requires a lower barrier (**TS4**, $\Delta G^\ddagger = 14.9$ kcal/mol) for the [2+2] cycloaddition by alkyne-chelated alkylidene **I-8-17a** ($\Delta G = 6.8$ kcal/mol) that is generated by ring-opening of the ruthenabenzene (**TS3**, $\Delta G^\ddagger = 30.8$ kcal/mol with respect to **8-18a** in toluene). Involvement of Catalytic Cycle I is further supported by mass analysis of the reaction of 1-octene with **8-18a** wherein the organic component formed from dearomatization of **8-18a** followed by exchange with methylene ($[M + H]^+ = 245.1665$) was detected unambiguously in the crude reaction mixture. The fact that the ruthenabenzene coordinated with NHC ligand shows higher productivity than that with PCy_3 (**8-18o** vs. **8-18o-I**) is an indication of a mechanism similar to the classical **G-I** and **G-II** catalysts, where the trans-disposed chloride and the donor ligands are positioned trans to the Ru-bound alkene and the metallacyclobutane and this geometry only occur for Catalytic Cycle I.

8.3. Conclusion

In conclusion, we have developed an effective method to prepare a diverse array of ruthenabenzenes and explored their structural characteristics and catalytic activities. A tandem enyne metathesis and metallotropic [1,3]-shift process was resorted to form ruthenium alkylidene intermediates, which spontaneously cycloaromatize if an alkyne is appropriately chelated. This approach to form a ruthenabenzene framework is general and tolerant to broad structural variations. The aromatic nature of these complexes was confirmed by spectroscopic and X-ray crystallographic data and the mechanistic pathways for the cycloaromatization process were studied by DFT calculations. As for reactivity, these stable ruthenabenzenes display robust catalytic activity.⁵¹ Even though the ruthenium alkylidene moiety is a part of an aromatic system, it can still show sufficient reactivity for olefin metathesis with increased longevity, which illustrates that metallabenzenes are not only compounds of structural and theoretical interests but also are a novel platform for new catalyst development.

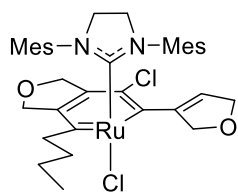
8.4. Experimental Details

8.4.1. General information

All Reactions were carried out in oven-dried glassware under inert atmosphere unless otherwise noted. All organometallic reactions were performed under argon using glove-box and standard Schlenk techniques. All reagents and compounds were purchased from Aldrich, Acros, TCI America or Oakwood and used as received, unless otherwise noted. Grubbs 2nd generation catalyst was purchased from Aldrich and CAPOT Chemicals (Sanghai, China) and used without any further purification. Toluene, dichloromethane, triethylamine and acetonitrile were distilled over calcium hydride (CaH₂) under nitrogen. Tetrahydrofuran was dried over sodium-benzophenone ketyl. Column chromatography was performed using silica gel 60 Å (32–63 mesh) purchased from Silicycle Inc. Analytical thin layer chromatography (TLC) was performed on 0.25 mm E. Merck precoated silica gel 60 (particle size 0.040–0.063 mm). Yields refer to chromatographically and spectroscopically pure isolated compounds unless otherwise stated. ¹H NMR and ¹³C NMR spectra were recorded on a Bruker AV–500 spectrometer. ¹H NMR chemical shifts (δ) are reported in parts per million (ppm) downfield of TMS and are referenced relative to the residual proteated solvent peak (CDCl₃ (7.26 ppm)). ¹³C chemical shifts (δ) are reported in parts per million downfield of TMS and are referenced to the carbon resonance of the solvent (CDCl₃ (77.02 ppm)). Multiplicities are indicated by s (singlet), d (doublet), t (triplet), q (quartet), p (quintet), h (sextet), dd (doublet of doublet), dt (doublet of triplet), m (multiplet) and so on. ¹H NMR signals that fall within a ca. 0.3 ppm range are generally reported as a multiplet, with a range of chemical shift values corresponding to the peak or center of the peak. Coupling constants, *J*, are reported in Hz (Hertz). Electrospray ionization (ESI) and Electron impact (EI) mass spectra were recorded on a Waters Micromass Q-Tof Ultima and Micromass 70–VSE, respectively in the University of Illinois at Urbana-Champaign.

8.4.2. Experimental procedures

8.4.3. Characterization data



8-18a

8-18a: This compound was synthesized in 52% yield as a green solid (65 mg);

Purification: flash chromatography under N₂ (SiO₂, hexanes–EtOAc, 10:1 → 3:1

→1:1); **¹H NMR** (500 MHz, CDCl₃) δ 7.08 – 6.77 (m, 4H), 6.24 (s, 1H), 5.58 – 5.47

(m, 1H), 5.21 (d, *J* = 10.0 Hz, 1H), 4.93 (dq, *J* = 8.9, 2.5 Hz, 1H), 4.76 (d, *J* = 10.0

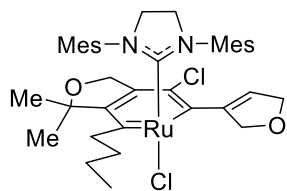
Hz, 1H), 4.68 – 4.53 (m, 2H), 4.30 – 4.17 (m, 2H), 3.78 (d, *J* = 50.4 Hz, 4H), 3.53 (td, *J* = 12.7, 4.5 Hz,

1H), 2.34 (s, 16H), 1.97 – 1.85 (m, 2H), 1.45 (h, *J* = 7.1 Hz, 3H), 1.36 – 1.22 (m, 2H), 0.96 (t, *J* = 7.3 Hz,

3H); **¹³C NMR** (125 MHz, CDCl₃) δ 256.53, 210.47, 207.91, 151.07, 145.25, 139.18, 135.86, 135.62,

133.21, 129.75, 129.30, 129.25, 129.22, 128.26, 112.01, 77.82, 76.65, 75.01, 74.72, 51.35, 46.48, 26.82,

23.59, 21.12, 18.31, 13.66; **HRMS** (ESI) calcd for C₃₆H₄₄N₂O₂ClRu [M-Cl]⁺ 673.2135, found 673.2124.



8-18b

8-18b: This compound was synthesized in 58% yield as a green solid (52 mg);

Purification: flash chromatography under N₂ (SiO₂, hexanes–EtOAc, 10:1 → 3:1

→1:1); **¹H NMR** (500 MHz, CDCl₃) δ 6.95 (s, 4H), 6.24 (s, 1H), 5.52 – 5.36

(m, 1H), 5.06 – 4.89 (m, 1H), 4.66 (d, *J* = 11.4 Hz, 1H), 4.58 (d, *J* = 13.3 Hz,

1H), 4.06 (d, *J* = 15.5 Hz, 1H), 3.98 (d, *J* = 15.5 Hz, 1H), 3.74 (s, 4H), 3.38 – 3.25 (m, 1H), 2.94 – 2.81 (m,

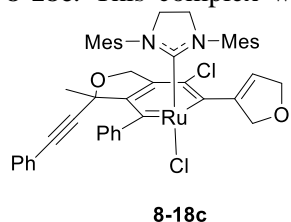
1H), 2.79 – 1.91 (m, 20H), 1.49 (q, *J* = 7.1 Hz, 2H), 1.34 (s, 3H), 1.31 (s, 3H), 0.99 (t, *J* = 7.2 Hz, 3H); **¹³C**

NMR (125 MHz, CDCl₃) δ 254.12, 213.60, 208.45, 152.63, 146.26, 143.02, 129.72, 127.88, 113.04, 88.28,

76.63, 74.94, 73.72, 51.70, 43.11, 30.10, 29.98, 26.94, 24.09, 21.06, 18.43, 13.67; **HRMS** (ESI) calcd for

C₃₈H₄₈N₂O₂ClRu [M-Cl]⁺ 701.2448, found 701.2437.

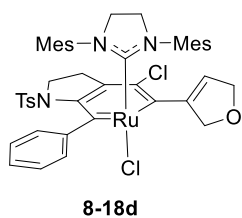
8-18c: This complex was isolated as a 10:1 diastereomeric mixture (green solid, 58% yield, 48 mg);



Purification: flash chromatography under N₂ (SiO₂, hexanes–EtOAc, 10:1 → 3:1

→ 1:1); **¹H NMR** (500 MHz, CDCl₃) Major isomer: δ 7.64 – 7.52 (m, 2H), 7.32 (dt, *J* = 15.7, 8.0 Hz, 3H), 7.23 – 7.09 (m, 5H), 7.05 (s, 1H), 6.87 (s, 1H), 6.79

(s, 1H), 6.77 (s, 1H), 6.53 – 6.44 (m, 1H), 5.51 (dt, *J* = 11.8, 4.0 Hz, 1H), 5.20 – 5.12 (m, 1H), 4.68 – 4.51 (m, 2H), 4.26 – 4.02 (m, 2H), 4.01 – 3.94 (m, 1H), 3.90 (t, *J* = 10.8 Hz, 1H), 3.77 (dt, *J* = 14.9, 6.9 Hz, 1H), 3.68 (t, *J* = 11.2 Hz, 1H), 2.52 (s, 3H), 2.29 (s, 3H), 2.28 (s, 3H), 2.26 (s, 3H), 1.97 (s, 3H), 1.90 (s, 3H), 1.31 (s, 3H); **¹³C NMR** (125 MHz, CDCl₃) (all discernable signals for both isomers) δ 244.35, 217.88, 207.43, 153.13, 147.13, 146.15, 139.99, 139.54, 138.65, 137.30, 137.18, 135.86, 134.74, 133.85, 131.88, 131.49, 131.37, 130.69, 130.43, 130.10, 129.41, 129.22, 128.84, 128.75, 128.43, 127.84, 127.78, 127.68, 127.60, 127.50, 127.40, 123.15, 115.11, 92.86, 84.71, 82.64, 76.49, 75.85, 74.43, 52.14, 51.72, 51.52, 28.48, 21.20, 20.85, 19.49, 18.41, 18.32; **HRMS** (ESI) calcd for C₄₇H₄₆N₂O₂ClRu [M-Cl]⁺ 807.2291, found 807.2301.

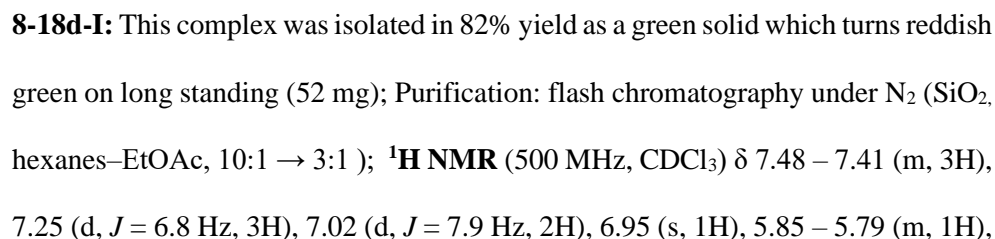


8-18d: This complex was isolated in 62% yield as a green solid (45 mg); Purification:

flash chromatography under N₂ (SiO₂, hexanes–EtOAc, 10:1 → 3:1 → 1:1); **¹H NMR**

(500 MHz, CDCl₃) δ 8.16 – 7.82 (m, 2H), 7.42 (t, *J* = 7.3 Hz, 1H), 7.35 (t, *J* = 7.6 Hz, 2H), 7.13 (s, 1H), 7.04 – 6.96 (m, 3H), 6.83 (s, 1H), 6.81 (s, 1H), 6.71 (s, 1H),

6.67 (s, 1H), 6.50 (s, 1H), 5.41 – 5.32 (m, 1H), 5.07 – 4.98 (m, 1H), 4.86 – 4.75 (m, 1H), 4.73 – 4.61 (m, 1H), 3.95 (ddd, *J* = 18.6, 11.9, 8.0 Hz, 2H), 3.81 – 3.58 (m, 2H), 3.45 (tt, *J* = 12.7, 6.2 Hz, 2H), 2.62 (s, 3H), 2.42 (s, 3H), 2.24 (s, 6H), 1.96 (s, 3H), 1.81 (s, 3H), 1.61 (s, 3H), 1.47 (dd, *J* = 18.2, 8.0 Hz, 1H), 0.72 (ddd, *J* = 19.1, 11.7, 8.0 Hz, 1H); **¹³C NMR** (125 MHz, CDCl₃) δ 235.16, 222.35, 205.90, 149.55, 146.34, 146.21, 143.27, 139.99, 137.78, 137.71, 137.56, 136.21, 136.01, 134.23, 133.52, 131.96, 130.83, 130.12, 128.78, 128.65, 128.47, 128.36, 128.05, 127.90, 127.46, 118.22, 76.88, 73.99, 51.57, 51.21, 49.70, 35.22, 21.43, 21.28, 20.94, 19.76, 18.74, 18.66, 18.40; **HRMS** (ESI) calcd for C₄₅H₄₇N₃O₃SClRu [M-Cl]⁺ 846.2070, found 846.2075.



8-18e

326

Purification: flash chromatography under N₂ (SiO₂, hexanes–EtOAc, 10:1 → 3:1)

→1:1); ¹H NMR (500 MHz, CDCl₃) δ 8.29 (d, *J* = 7.9 Hz, 1H), 7.41 (d, *J* = 7.8

Hz, 2H), 7.33 (t, $J = 7.7$ Hz, 1H), 7.17 – 7.04 (m, 4H), 7.01 (s, 1H), 6.99 (s, 1H),

8-18f-I

green on long standing (64 mg); Purification: flash chromatography under N₂ (SiO₂,

hexanes–EtOAc, 10:1 \rightarrow 3:1); $^1\text{H NMR}$ (500 MHz, CDCl_3) δ 8.29–7.54 (m, 1H),

7.44 (s, 3H), 7.26 (d, $J = 7.7$ Hz, 2H), 7.02 (d, $J = 7.9$ Hz, 2H), 6.95 (s, 1H), 5.86 –

327



Purification: flash chromatography under N₂ (SiO₂, hexanes–EtOAc, 10:1 →

2.9 Hz, 1H), 7.57 (d, $J = 7.9$ Hz, 2H), 7.38 (s, 1H), 7.32 (d, $J = 9.3$ Hz, 1H),

10.9, 4.4 Hz, 2H), 4.05 (ddd, $J = 31.8, 12.9, 8.3$ Hz, 2H), 2.34 (s, 3H), 2.22 (dd, $J = 18.4, 8.0$ Hz, 1H), 1.89

CDCl₃) δ 240.03, 239.94, 230.12, 230.03, 159.35, 155.52, 148.52, 143.86, 141.75, 141.35, 137.88, 133.66,

29.99, 28.74, 27.70, 27.62, 27.44, 27.37, 26.20, 22.80, 21.54, 21.35; ³¹P NMR (203 MHz, CDCl₃) δ 44.62;

8-18h: This complex was isolated in 94% yield as a green solid (66 mg); Purification: flash chromatography



δ 7.31 (d, $J = 7.9$ Hz, 2H), 7.11–6.62 (m, 4H), 6.95 (d, $J = 8.0$ Hz, 2H), 6.88–6.82

(m, 1H), 6.10 (d, $J = 11.3$ Hz, 1H), 5.66–5.52 (m, 1H), 5.19 (d, $J = 11.3$ Hz, 2H),

1H), 2.54–1.82 (m, 24H), 1.28 (dd, $J = 17.0, 8.8$ Hz, 1H), 0.30 (ddd, $J = 19.1, 11.7, 8.4$ Hz, 1H); ¹³C NMR

129.00, 128.73, 128.52, 127.95, 121.23, 76.56, 76.00, 73.07, 51.79, 49.86, 35.62, 22.92, 21.43, 21.03,

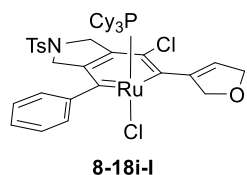
18.90, 18.45; **HRMS** (ESI) calcd for $C_{42}H_{47}N_3O_5SClRu$ $[M-Cl]^+$ 842.1968, found 842.1970.

flash chromatography under N₂ (SiO₂, hexanes–EtOAc, 10:1 → 3:1 → 1:1); ¹H NMR

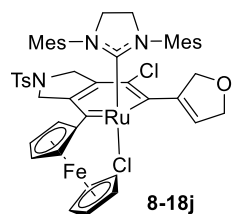
(500 MHz, CDCl₃) δ 7.62 (dd, J = 13.3, 7.8 Hz, 4H), 7.45 (t, J = 7.2 Hz, 1H), 7.38 (t,

$J = 7.4$ Hz, 2H), 7.21 (d, $J = 7.9$ Hz, 2H), 7.07 (s, 1H), 6.86 (s, 1H), 6.81 (d, $J = 4.6$

Hz, 2H), 6.57 (s, 1H), 5.37 (d, $J = 11.6$ Hz, 1H), 5.10 – 5.01 (m, 1H), 4.90 (d, $J = 11.7$ Hz, 1H), 4.70 (d, $J = 14.2$ Hz, 1H), 4.61 (d, $J = 14.1$ Hz, 1H), 4.37 (d, $J = 11.9$ Hz, 1H), 3.95 (q, $J = 10.0$ Hz, 1H), 3.78 (t, $J = 12.9$ Hz, 2H), 3.65 (q, $J = 11.2$ Hz, 2H), 3.54 (d, $J = 16.1$ Hz, 1H), 2.54 (s, 3H), 2.41 (s, 3H), 2.33 (d, $J = 5.3$ Hz, 6H), 1.95 (s, 3H), 1.91 (s, 3H), 1.76 (s, 3H); ^{13}C NMR (125 MHz, CDCl_3) δ 241.74, 216.88, 205.65, 147.07, 146.28, 145.82, 143.57, 140.19, 139.33, 137.27, 137.21, 135.74, 135.26, 133.49, 133.36, 132.81, 131.36, 130.66, 130.33, 129.78, 128.94, 128.63, 128.55, 128.02, 127.43, 126.13, 115.19, 76.57, 74.82, 57.84, 54.86, 51.73, 51.15, 21.47, 21.22, 21.09, 19.50, 18.47, 18.35, 18.04; **HRMS** (ESI) calcd for $\text{C}_{45}\text{H}_{47}\text{N}_3\text{O}_3\text{SClRu} [\text{M}-\text{Cl}]^+$ 846.2070, found 846.2055.

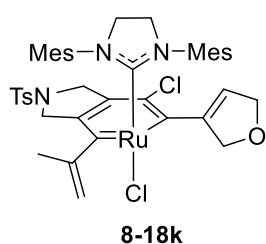


8-18i-I: This complex was isolated in 78% yield as a green solid which turns reddish green on long standing (55 mg); Purification: flash chromatography under N_2 (SiO_2 , hexanes–EtOAc, 10:1 \rightarrow 3:1); ^1H NMR (500 MHz, CDCl_3) δ 7.69 (d, $J = 7.9$ Hz, 2H), 7.63 (d, $J = 6.7$ Hz, 2H), 7.47 – 7.40 (m, 3H), 7.28 (d, $J = 8.0$ Hz, 2H), 6.80 (s, 1H), 5.78 – 5.70 (m, 1H), 5.27 (dd, $J = 12.4, 2.8$ Hz, 1H), 4.91 – 4.82 (m, 1H), 4.78 – 4.62 (m, 2H), 4.52 (d, $J = 12.5$ Hz, 1H), 4.25 (dd, $J = 16.6, 2.8$ Hz, 1H), 3.89 (d, $J = 16.5$ Hz, 1H), 2.38 (s, 3H), 1.72 – 1.66 (m, 5H), 1.65 – 1.50 (m, 11H), 1.49 – 1.38 (m, 3H), 1.00 – 0.89 (m, 11H), 0.78 – 0.68 (m, 3H); ^{13}C NMR (125 MHz, CDCl_3) δ 234.67, 234.60, 216.42, 216.34, 146.31, 145.67, 145.17, 143.74, 134.18, 133.15, 132.28, 129.86, 129.00, 128.42, 127.58, 126.68, 113.58, 76.47, 75.48, 58.53, 55.42, 34.53, 34.34, 29.38, 29.26, 27.30, 27.22, 27.13, 27.04, 26.99, 26.02, 21.52; ^{31}P NMR (203 MHz, CDCl_3) δ 59.08; **HRMS** (ESI) calcd for $\text{C}_{42}\text{H}_{54}\text{NO}_3\text{PSClRu} [\text{M}-\text{Cl}]^+$ 820.2294, found 820.2230.



8-18j: This complex was isolated in 78% yield as a purple solid (62 mg); Purification: flash chromatography under N_2 (SiO_2 , hexanes–EtOAc, 10:1 \rightarrow 3:1 \rightarrow 1:1); ^1H NMR (500 MHz, CDCl_3) δ 7.79 (d, $J = 7.9$ Hz, 2H), 7.24 (d, $J = 8.0$ Hz, 2H), 7.12 (s, 1H), 7.08 (s, 1H), 6.78 (s, 2H), 6.32 (s, 1H), 5.50 – 5.35 (m, 1H), 5.14 (d, $J = 11.1$ Hz, 1H), 5.04 – 4.93 (m, 1H), 4.84 – 4.76 (m, 2H), 4.74 – 4.63 (m, 4H), 4.56 (s, 1H), 4.48 (s, 1H), 3.98 – 3.87 (m,

6H), 3.84 – 3.69 (m, 2H), 3.66 – 3.56 (m, 2H), 2.59 (s, 3H), 2.46 (s, 3H), 2.41 (s, 3H), 2.28 (s, 3H), 2.17 (s, 3H), 1.88 (s, 3H), 1.55 (s, 3H); ^{13}C NMR (125 MHz, CDCl_3) δ 243.62, 213.26, 206.67, 145.33, 145.11, 143.70, 140.02, 139.16, 138.24, 137.19, 135.62, 135.51, 133.94, 133.32, 132.55, 130.63, 130.48, 130.15, 129.95, 128.69, 128.35, 127.25, 126.83, 113.14, 91.03, 76.96, 74.51, 70.70, 70.44, 70.22, 67.27, 57.48, 55.95, 51.61, 50.95, 21.42, 21.13, 19.77, 19.24, 18.39, 18.06; **HRMS** (ESI) calcd for $\text{C}_{49}\text{H}_{52}\text{N}_3\text{O}_3\text{SCl}_2\text{FeRu}$ $[\text{M}+\text{H}]^+$ 990.1499, found 990.1485.

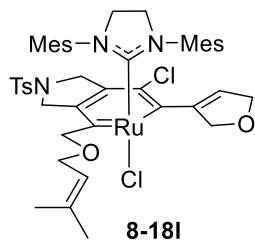


8-18k: This complex was isolated in 89% yield as a green solid (64 mg);

Purification: flash chromatography under N_2 (SiO_2 , hexanes–EtOAc, 10:1 \rightarrow 3:1

\rightarrow 1:1); ^1H NMR (500 MHz, CDCl_3) δ 7.69 (d, J = 8.1 Hz, 2H), 7.28 (d, J = 8.2 Hz, 2H), 7.09 (s, 1H), 7.08 (s, 1H), 6.79 (s, 1H), 6.76 (s, 1H), 6.56 (s, 1H), 5.61

(d, J = 5.8 Hz, 2H), 5.43 – 5.31 (m, 1H), 5.03 (d, J = 11.3 Hz, 1H), 4.73 – 4.62 (m, 2H), 4.59 (d, J = 13.2 Hz, 1H), 4.52 (d, J = 13.5 Hz, 1H), 4.01 – 3.88 (m, 2H), 3.71 (q, J = 10.5 Hz, 1H), 3.64 – 3.53 (m, 2H), 3.36 (d, J = 16.0 Hz, 1H), 2.56 (s, 3H), 2.53 (s, 3H), 2.40 (s, 3H), 2.37 (s, 3H), 2.34 (s, 3H), 2.06 (s, 3H), 1.98 (s, 3H), 1.93 (s, 3H); ^{13}C NMR (125 MHz, CDCl_3) δ 245.85, 215.47, 206.81, 151.55, 146.62, 146.43, 143.71, 140.19, 139.21, 137.69, 137.52, 135.22, 135.07, 133.23, 133.06, 131.88, 130.80, 130.65, 130.36, 129.84, 129.00, 128.59, 128.45, 127.52, 116.00, 114.53, 76.34, 75.88, 57.98, 54.25, 52.06, 51.37, 21.47, 21.20, 21.06, 19.63, 19.53, 18.94, 18.57, 18.40; **HRMS** (ESI) calcd for $\text{C}_{42}\text{H}_{47}\text{N}_3\text{O}_3\text{SClRu}$ $[\text{M}-\text{Cl}]^+$ 810.2070, found 810.2076.



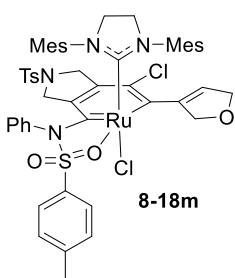
8-18l: This complex was isolated in 78% yield as a green solid (42 mg);

Purification: flash chromatography under N_2 (SiO_2 , hexanes–EtOAc, 10:1 \rightarrow 3:1

\rightarrow 1:1); ^1H NMR (500 MHz, CDCl_3) δ 7.66 (d, J = 8.0 Hz, 2H), 7.27 (d, J = 6.5 Hz, 2H), 7.08 (s, 2H), 6.89 (s, 1H), 6.77 (s, 1H), 6.10 (s, 1H), 5.41 (s, 1H), 5.39 – 5.31

(m, 1H), 4.79 (dd, J = 9.0, 2.5 Hz, 1H), 4.62 (d, J = 11.0 Hz, 1H), 4.58 – 4.47 (m, 2H), 4.32 (d, J = 11.4 Hz, 1H), 4.26 (d, J = 11.1 Hz, 1H), 4.19 (dd, J = 13.0, 7.5 Hz, 1H), 4.12 (dd, J = 13.1, 6.6 Hz, 1H), 3.92 (d,

$J = 15.5$ Hz, 3H), 3.75 (d, $J = 15.9$ Hz, 1H), 3.61 (s, 2H), 3.48 (d, $J = 15.9$ Hz, 1H), 2.78 – 2.12 (m, 18H), 1.82 (s, 3H), 1.70 (s, 6H); ^{13}C NMR (125 MHz, CDCl_3) δ 248.91, 211.11, 207.27, 146.27, 145.38, 143.66, 139.47, 137.52, 133.32, 130.14, 129.89, 128.79, 128.48, 127.44, 126.62, 120.68, 112.91, 86.88, 76.78, 75.27, 67.92, 57.59, 53.93, 51.34, 26.03, 21.46, 21.23, 18.63, 18.20, 18.04, 17.75, 17.59; HRMS (ESI) calcd for $\text{C}_{45}\text{H}_{52}\text{N}_3\text{O}_4\text{SRu} [\text{M}-2\text{Cl}-\text{H}]^+$ 832.2722, found 832.2720.



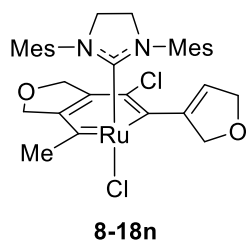
8-18m: This complex was isolated in 78% yield as a green solid (56 mg);

Purification: flash chromatography under N_2 (SiO_2 , hexanes–EtOAc, 10:1 \rightarrow 3:1 \rightarrow

CH_2Cl_2 –EtOAc 1:1); ^1H NMR (500 MHz, CDCl_3) δ 7.74 (d, $J = 7.8$ Hz, 1H), 7.70

(d, $J = 7.9$ Hz, 2H), 7.57 – 7.45 (m, 1H), 7.32 (t, $J = 7.3$ Hz, 1H), 7.17 – 7.04 (m, 4H), 7.00 (s, 1H), 6.96 – 6.89 (m, 3H), 6.87 (s, 1H), 6.81 (s, 1H), 6.73 – 6.66 (m,

1H), 6.34 (d, $J = 2.2$ Hz, 1H), 6.23 – 6.13 (m, 1H), 5.45 – 5.29 (m, 1H), 5.06 – 4.93 (m, 1H), 4.89 – 4.80 (m, 1H), 4.78 – 4.68 (m, 1H), 4.00 – 3.88 (m, 2H), 3.72 – 3.56 (m, 3H), 3.50 (dd, $J = 16.0, 3.2$ Hz, 1H), 3.22 (dd, $J = 16.1, 3.0$ Hz, 1H), 2.74 (s, 3H), 2.73 – 2.67 (m, 1H), 2.47 – 2.36 (m, 9H), 2.32 (s, 3H), 2.23 (s, 6H), 2.20 (s, 3H); ^{13}C NMR (125 MHz, CDCl_3) δ 229.63, 228.69, 208.25, 152.81, 147.13, 145.00, 143.29, 139.82, 139.27, 138.39, 137.50, 135.78, 135.30, 135.18, 134.93, 134.20, 132.17, 131.79, 131.60, 131.13, 129.74, 129.66, 129.49, 129.38, 129.18, 129.12, 128.82, 128.75, 128.60, 127.71, 123.67, 119.04, 113.64, 76.96, 75.88, 57.41, 55.20, 52.62, 52.21, 21.55, 21.41, 21.26, 20.98, 19.43, 18.99, 18.93, 18.42; HRMS (ESI) calcd for $\text{C}_{52}\text{H}_{54}\text{N}_4\text{O}_5\text{S}_2\text{ClRu} [\text{M}-\text{Cl}]^+$ 1015.2268, found 1015.2267.



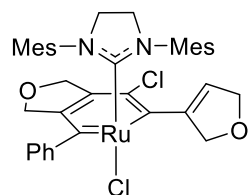
8-18n: This complex was isolated in 32% yield as a green solid (28 mg);

Purification: flash chromatography under N_2 (SiO_2 , hexanes–EtOAc, 10:1 \rightarrow 3:1 \rightarrow

1:1); ^1H NMR (500 MHz, CDCl_3) δ 7.02 – 6.85 (m, 4H), 6.22 – 6.09 (m, 1H), 5.57 – 5.44 (m, 1H), 5.20 (d, $J = 9.9$ Hz, 1H), 5.04 – 4.91 (m, 1H), 4.84 (d, $J = 9.9$ Hz,

1H), 4.72 – 4.54 (m, 2H), 4.33 – 4.13 (m, 2H), 3.89 – 3.69 (m, 4H), 2.54 (s, 3H), 2.38 – 2.11 (m, 18H); ^{13}C NMR (125 MHz, CDCl_3) δ 251.12, 212.30, 207.42, 151.26, 145.18, 139.30, 136.11, 135.86, 133.01,

129.73, 129.26, 127.44, 77.91, 76.65, 75.38, 75.03, 51.32, 33.90, 21.13, 18.28, 18.22; **HRMS** (ESI) calcd for $C_{33}H_{38}N_2O_2ClRu$ $[M-Cl]^+$ 631.1665, found 631.1638.



8-18o

8-18o: This complex was isolated in 60% yield as a green solid (45 mg);

Purification: flash chromatography under N_2 (SiO_2 , hexanes–EtOAc, 10:1 \rightarrow 3:1 \rightarrow

1:1); **1H NMR** (500 MHz, $CDCl_3$) δ 7.67 (d, J = 7.4 Hz, 2H), 7.43 (t, J = 7.3 Hz,

1H), 7.36 (t, J = 7.5 Hz, 2H), 7.10 (s, 1H), 6.91 (s, 1H), 6.80 (s, 2H), 6.62 (s, 1H),

5.49 – 5.40 (m, 1H), 5.37 – 5.31 (m, 1H), 5.15 – 5.08 (m, 1H), 5.07 – 5.01 (m, 1H), 4.77 – 4.70 (m, 1H),

4.64 (dt, J = 13.8, 4.2 Hz, 1H), 4.30 – 4.22 (m, 1H), 4.08 – 4.02 (m, 1H), 3.95 (q, J = 10.7 Hz, 1H), 3.78

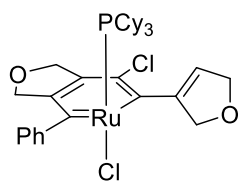
(q, J = 10.6 Hz, 1H), 3.68 (q, J = 10.3 Hz, 1H), 3.64 – 3.53 (m, 1H), 2.58 (s, 3H), 2.36 (s, 3H), 2.34 (s, 3H),

1.97 (s, 3H), 1.83 (s, 3H), 1.82 (s, 3H); **^{13}C NMR** (125 MHz, $CDCl_3$) δ 238.43, 216.19, 206.35, 151.53,

147.56, 146.44, 140.05, 138.60, 137.37, 137.24, 135.93, 135.47, 133.77, 131.76, 130.64, 130.26, 128.97,

128.54, 128.37, 127.96, 127.88, 126.02, 114.54, 77.72, 76.61, 75.87, 74.80, 51.69, 51.13, 21.25, 21.03,

19.30, 18.52, 18.26; **HRMS** (ESI) calcd for $C_{38}H_{40}N_2O_2ClRu$ $[M-Cl]^+$ 693.1822, found 693.1832.



8-18o-I

8-18o-I: This complex was isolated in 60% yield as a green solid which turns

reddish green on long standing (42 mg); Purification: flash chromatography under

N_2 (SiO_2 , hexanes–EtOAc, 10:1 \rightarrow 3:1); **1H NMR** (500 MHz, $CDCl_3$) δ 7.76 –

7.65 (m, 2H), 7.47 – 7.38 (m, 3H), 6.87 (s, 1H), 5.86 – 5.73 (m, 2H), 5.17 (d, J =

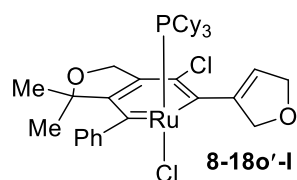
11.5 Hz, 1H), 4.96 – 4.89 (m, 1H), 4.78 – 4.65 (m, 2H), 4.61 (d, J = 15.7 Hz, 1H), 4.51 (d, J = 15.6 Hz,

1H), 1.83 – 1.68 (m, 6H), 1.67 – 1.54 (m, 9H), 1.52 – 1.44 (m, 3H), 1.16 – 0.91 (m, 12H), 0.82 – 0.70 (m,

3H); **^{13}C NMR** (125 MHz, $CDCl_3$) δ 232.52, 232.44, 215.62, 215.54, 151.15, 146.90, 145.38, 138.31,

131.93, 128.83, 128.21, 126.50, 112.75, 78.31, 76.50, 75.96, 75.48, 34.59, 34.41, 29.38, 29.27, 27.40,

27.32, 27.18, 27.10, 26.10; **³¹P NMR** (203 MHz, CDCl₃) δ 58.96; **HRMS** (ESI) calcd for C₃₅H₄₇O₂PClRu [M-Cl]⁺ 667.2046, found 667.2006.



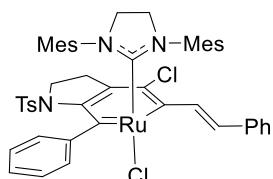
8-18o'-I

8-18o'-I: This complex was isolated in 54% yield as a green solid which turns

reddish green on long standing (44 mg); Purification: flash chromatography

under N₂ (SiO₂, hexanes–EtOAc, 10:1 → 3:1); **¹H NMR** (500 MHz, CDCl₃) δ

7.79 – 7.50 (m, 2H), 7.45 – 7.32 (m, 3H), 6.77 (s, 1H), 5.83 – 5.71 (m, 1H), 4.91 (d, *J* = 9.6 Hz, 1H), 4.79 – 4.62 (m, 2H), 4.40 (s, 2H), 1.96 – 1.38 (m, 24H), 1.17 – 0.97 (m, 9H), 0.90 (s, 3H), 0.78 (s, 3H); **¹³C NMR** (125 MHz, CDCl₃) δ 233.56, 233.48, 218.05, 217.97, 152.48, 146.14, 145.51, 144.60, 130.99, 128.26, 128.06, 113.72, 89.06, 76.51, 75.84, 74.02, 34.30, 30.33, 29.57, 29.41, 28.52, 27.27, 27.19, 27.11, 26.11; **³¹P NMR** (203 MHz, CDCl₃) δ 60.29; **HRMS** (ESI) calcd for C₃₇H₅₁O₂PClRu [M-Cl]⁺ 695.2539, found 695.2306.



8-18pa

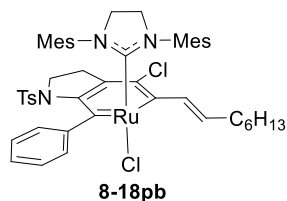
8-18pa: This complex was isolated in 62% yield as a green solid (56 mg);

Purification: flash chromatography under N₂ (SiO₂, hexanes–EtOAc, 10:1 → 3:1

→ 1:1); **¹H NMR** (500 MHz, CDCl₃) δ 7.87 – 7.80 (m, 2H), 7.80 – 7.69 (m, 3H),

7.51 – 7.40 (m, 3H), 7.38 (t, *J* = 7.3 Hz, 1H), 7.36 – 7.29 (m, 2H), 7.28 – 7.25

(m, 1H), 7.09 (s, 1H), 7.05 (d, *J* = 8.0 Hz, 2H), 6.90 (d, *J* = 8.2 Hz, 2H), 6.84 (d, *J* = 7.9 Hz, 2H), 6.63 (s, 1H), 4.09 (dd, *J* = 12.8, 8.1 Hz, 1H), 3.80 (td, *J* = 12.3, 8.0 Hz, 1H), 3.67 (dd, *J* = 11.8, 7.9 Hz, 2H), 3.60 – 3.35 (m, 2H), 2.63 (s, 3H), 2.43 (s, 3H), 2.27 (s, 3H), 2.19 (s, 3H), 2.15 (s, 3H), 1.76 (dd, *J* = 17.9, 7.9 Hz, 1H), 1.67 (s, 3H), 1.38 (s, 3H), 0.84 (ddd, *J* = 19.2, 11.8, 8.4 Hz, 1H); **¹³C NMR** (126 MHz, CDCl₃) δ 232.39, 225.97, 205.22, 148.17, 146.75, 143.16, 139.46, 138.72, 137.98, 137.77, 136.43, 135.62, 135.55, 134.26, 134.09, 133.87, 132.01, 130.66, 130.12, 129.37, 128.96, 128.36, 128.12, 128.09, 127.86, 127.09, 120.49, 51.06, 50.12, 34.93, 21.35, 21.30, 21.14, 19.57, 18.89, 17.09; **HRMS** (ESI) calcd for C₄₉H₄₉N₃O₂SClRu [M-Cl]⁺ 880.2278, found 880.2279.



8-18pb: This complex was isolated in 45% yield as a green solid (42 mg);

Purification: flash chromatography under N₂ (SiO₂, hexanes–EtOAc, 10:1 → 3:1

→ 1:1); ¹H NMR (500 MHz, CDCl₃) δ 7.75 (d, *J* = 7.6 Hz, 2H), 7.41 (t, *J* = 7.5

Hz, 1H), 7.32 – 7.23 (m, 3H), 7.14 (s, 1H), 7.06 (d, *J* = 7.8 Hz, 2H), 6.92 – 6.74

(m, 4H), 6.59 (s, 1H), 6.48 (d, *J* = 16.3 Hz, 1H), 4.11 – 4.01 (m, 1H), 3.90 – 3.77 (m, 1H), 3.76 – 3.65 (m,

2H), 3.61 – 3.50 (m, 1H), 3.43 (t, *J* = 11.8 Hz, 1H), 2.70 (s, 3H), 2.42 (s, 3H), 2.33 – 2.17 (m, 10H), 1.77

(dd, *J* = 17.8, 7.9 Hz, 1H), 1.70 – 1.59 (m, 5H), 1.49 – 1.42 (m, 2H), 1.41 – 1.33 (m, 3H), 1.29 (s, 3H), 0.98

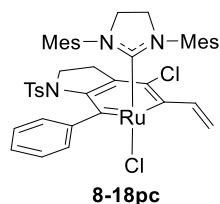
– 0.91 (m, 3H), 0.86 (t, *J* = 9.9 Hz, 2H); ¹³C NMR (125 MHz, CDCl₃) δ 237.48, 224.11, 206.01, 148.26,

146.96, 143.00, 139.67, 139.39, 138.87, 138.70, 137.97, 136.34, 135.55, 135.29, 134.19, 134.08, 132.11,

130.68, 129.97, 129.54, 128.94, 128.24, 128.11, 127.70, 119.11, 51.14, 51.06, 50.15, 35.01, 34.88, 31.77,

29.40, 28.77, 22.72, 21.37, 21.28, 21.09, 19.76, 18.90, 18.86, 16.89, 14.16; HRMS (ESI) calcd for

C₄₉H₅₇N₃O₂SClRu [M-Cl]⁺ 888.2904, found 888.2903.



8-18pc: This complex was isolated in 28% yield as a green solid (24 mg); Purification:

flash chromatography under N₂ (SiO₂, hexanes–EtOAc, 10:1 → 3:1 → 1:1); ¹H NMR

(500 MHz, CDCl₃) δ 7.81 (d, *J* = 7.8 Hz, 2H), 7.43 (t, *J* = 7.3 Hz, 1H), 7.31 (t, *J* = 7.7

Hz, 2H), 7.13 (s, 1H), 7.04 (d, *J* = 7.7 Hz, 2H), 6.90 (s, 1H), 6.89 – 6.70 (m, 4H), 6.61

(s, 1H), 6.36 (dd, *J* = 17.7, 1.9 Hz, 1H), 5.88 – 5.73 (m, 1H), 4.07 (dd, *J* = 12.9, 7.9 Hz, 1H), 3.87 – 3.60

(m, 3H), 3.62 – 3.46 (m, 1H), 3.44 (d, *J* = 11.4 Hz, 1H), 2.66 (s, 3H), 2.42 (s, 3H), 2.23 (s, 3H), 2.21 (s,

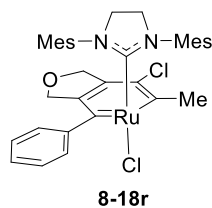
3H), 2.19 (s, 3H), 1.74 (dd, *J* = 17.9, 8.0 Hz, 1H), 1.63 (s, 3H), 1.42 (s, 3H), 0.87 (d, *J* = 10.9 Hz, 1H); ¹³C

NMR (125 MHz, CDCl₃) δ 234.17, 226.89, 205.20, 148.30, 146.74, 145.00, 143.12, 139.62, 138.63,

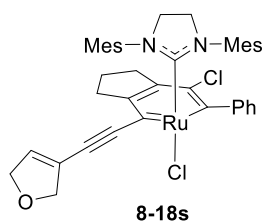
136.46, 135.66, 135.37, 131.97, 130.63, 130.08, 129.35, 128.94, 128.32, 128.14, 127.87, 127.09, 120.22,

119.20, 51.18, 51.03, 50.15, 34.82, 21.36, 21.29, 21.07, 19.77, 18.91, 18.71, 17.23; HRMS (ESI) calcd for

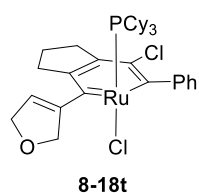
C₄₃H₄₅N₃O₂SClRu [M-Cl]⁺ 804.1964, found 804.1973.



8-18r: This complex was isolated in 67% yield as a green solid (64 mg); Purification: flash chromatography under N₂ (SiO₂, hexanes–EtOAc, 10:1 → 3:1 → 1:1); **¹H NMR** (500 MHz, CDCl₃) δ 7.50 – 7.45 (m, 2H), 7.38 (t, *J* = 7.3 Hz, 1H), 7.28 (t, *J* = 7.5 Hz, 2H), 7.05 – 6.85 (m, 2H), 6.82 (s, 2H), 5.51 (d, *J* = 10.4 Hz, 1H), 5.00 – 4.92 (m, 1H), 4.38 – 4.13 (m, 2H), 3.79 – 3.60 (m, 4H), 2.66 (s, 3H), 2.58 – 1.42 (m, 12H), 2.35 (s, 6H); **¹³C NMR** (125 MHz, CDCl₃) δ 241.11, 229.98, 206.40, 152.06, 147.66, 139.24, 136.48, 129.68, 128.53, 127.56, 125.46, 114.59, 77.20, 75.57, 51.13, 32.59, 29.71, 27.02, 26.92, 26.37, 26.15, 21.21, 18.72, 17.62; **HRMS** (ESI) calcd for C₃₅H₃₈N₂OClRu [M-Cl]⁺ 639.1716, found 639.1703.

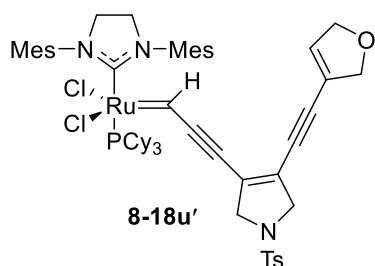


8-18s: This complex was isolated in 56% yield as a green solid (47 mg); Purification: flash chromatography under N₂ (SiO₂, hexanes–EtOAc, 10:1 → 3:1 → 1:1); **¹H NMR** (500 MHz, CDCl₃) δ 7.60 (d, *J* = 7.5 Hz, 2H), 7.37 (d, *J* = 7.4 Hz, 1H), 7.29 (t, *J* = 7.8 Hz, 2H), 7.07 (s, 1H), 6.82 (s, 1H), 6.78 (s, 1H), 6.70 (s, 1H), 6.32 (s, 1H), 4.90 – 4.79 (m, 2H), 4.75 – 4.66 (m, 2H), 3.87 – 3.73 (m, 2H), 3.63 – 3.54 (m, 2H), 3.24 (dt, *J* = 15.7, 8.0 Hz, 1H), 2.88 (s, 3H), 2.74 (dt, *J* = 15.6, 7.7 Hz, 1H), 2.38 – 2.21 (m, 13H), 1.87 (d, *J* = 22.5 Hz, 6H); **¹³C NMR** (125 MHz, CDCl₃) δ 225.60, 206.59, 206.13, 155.78, 148.15, 146.51, 139.57, 138.16, 137.83, 136.73, 136.37, 135.73, 133.96, 131.64, 130.58, 130.10, 129.88, 128.81, 128.39, 128.05, 127.34, 123.90, 118.77, 107.90, 99.95, 76.94, 76.30, 51.85, 50.97, 39.20, 35.36, 22.96, 21.27, 21.05, 19.62, 19.05, 18.18, 17.13; **HRMS** (ESI) calcd for C₄₁H₄₃N₃O₃SClRu [M-Cl+H]⁺ 715.2029, found 715.2012.



8-18t: This complex was isolated in 62% yield as a yellowish-brown solid (44 mg); Purification: flash chromatography under N₂ (SiO₂, hexanes–EtOAc, 10:1 → 3:1); **¹H NMR** (500 MHz, CDCl₃) δ 7.86 – 7.73 (m, 2H), 7.48 – 7.35 (m, 3H), 6.62 (s, 1H), 5.55 – 5.36 (m, 1H), 5.03 – 4.83 (m, 1H), 4.69 (d, *J* = 7.4 Hz, 2H), 3.43 (t, *J* = 7.4 Hz, 2H), 2.63 (dt, *J* = 18.4, 6.5 Hz, 1H), 2.42 (dt, *J* = 17.4, 8.2 Hz, 1H), 2.15 (q, *J* = 8.5, 8.0 Hz, 2H), 1.78 – 1.67

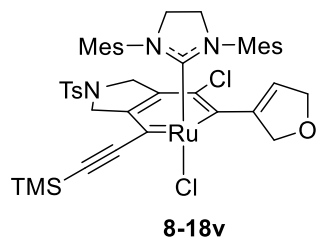
(m, 5H), 1.67 – 1.51 (m, 10H), 1.45 (s, 3H), 1.11 – 0.91 (m, 11H), 0.79 (d, $J = 14.2$ Hz, 4H); ^{13}C NMR (125 MHz, CDCl_3) δ 225.87, 225.79, 221.79, 221.71, 156.61, 147.04, 145.56, 142.70, 129.03, 128.53, 128.09, 127.73, 117.57, 77.03, 75.71, 39.65, 36.33, 35.64, 35.16, 34.66, 34.48, 29.43, 29.26, 27.40, 27.30, 27.20, 26.18, 24.75; ^{31}P NMR (203 MHz, CDCl_3) δ 58.64; **HRMS** (ESI) calcd for $\text{C}_{36}\text{H}_{47}\text{OClRuP}$ [$\text{M}+2\text{H}-\text{Cl}$] $^+$ 663.2097, found 663.2103.



8-18u': This complex was isolated in 58% yield as a yellowish-brown solid (40 mg); Purification: flash chromatography under N_2 (SiO_2 , hexanes–EtOAc, 10:1 \rightarrow 3:1); ^1H NMR (500 MHz, CDCl_3) δ 18.61 (s, 1H), 7.76 (d, $J = 8.0$ Hz, 2H), 7.36 (d, $J = 7.9$ Hz, 2H), 6.96 (s, 2H), 6.71 (s, 2H), 6.41 (s,

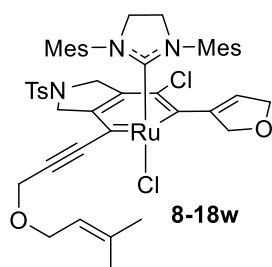
1H), 4.67 (s, 4H), 4.41 (s, 2H), 3.97 (dq, $J = 15.6, 10.0$ Hz, 4H), 3.78 (s, 2H), 2.57 (s, 6H), 2.42 (s, 3H), 2.36 (s, 6H), 2.29 (s, 3H), 2.25–2.16 (m, 3H), 2.14 (s, 3H), 1.54 (s, 9H), 1.48 – 1.37 (m, 6H), 1.02 (dd, $J = 27.6, 11.1$ Hz, 15H); ^{13}C NMR (125 MHz, CDCl_3) δ 253.15, 253.09, 218.51, 217.93, 143.94, 138.94, 138.83, 138.02, 137.68, 137.02, 134.04, 133.76, 133.47, 129.96, 129.86, 129.46, 129.07, 127.66, 121.56, 118.72, 116.40, 115.22, 90.59, 88.06, 76.58, 76.40, 58.10, 55.55, 51.98, 51.54, 31.60, 31.46, 28.64, 27.61, 27.53, 26.30, 21.56, 21.16, 19.69, 18.84; ^{31}P NMR (203 MHz, CDCl_3) δ 27.78; **HRMS** (ESI) calcd for $\text{C}_{59}\text{H}_{78}\text{N}_3\text{O}_3\text{SCl}_2\text{RuP}$ [$\text{M}+2\text{H}$] $^+$ 1111.3992, found 1111.3966.

8-18v: This complex was isolated in 95% yield as a green solid (66 mg); Purification: flash chromatography



under N_2 (SiO_2 , hexanes–EtOAc, 10:1 \rightarrow 3:1 \rightarrow 1:1); ^1H NMR (500 MHz, CDCl_3) δ 7.68 (d, $J = 8.0$ Hz, 2H), 7.30 – 7.26 (m, 2H), 7.12 (s, 1H), 7.07 (s, 1H), 6.90 (s, 1H), 6.71 (s, 1H), 6.25 (s, 1H), 5.59 – 5.45 (m, 1H), 4.99 (d, $J = 11.8$ Hz, 1H), 4.67 – 4.47 (m, 4H), 4.11 – 3.99 (m, 1H), 3.97 – 3.82 (m, 2H), 3.72 – 3.58 (m, 2H), 3.43 (d, $J = 16.0$ Hz, 1H), 2.88 (s, 3H), 2.47 (s, 3H), 2.43 (s, 3H), 2.36 (s, 3H), 2.34

(s, 3H), 2.32 (s, 3H), 1.66 (s, 3H), 0.33 (s, 9H); ^{13}C NMR (125 MHz, CDCl_3) δ 218.53, 207.91, 204.01, 144.84, 144.81, 143.62, 139.95, 139.69, 138.41, 137.11, 136.87, 136.08, 134.82, 133.30, 132.85, 131.88, 130.97, 130.02, 129.90, 129.43, 128.82, 128.24, 127.48, 125.63, 114.28, 110.17, 76.68, 74.83, 58.11, 55.75, 51.62, 51.20, 21.45, 21.27, 19.94, 19.21, 17.93, 17.53, -0.21; **HRMS** (ESI) calcd for $\text{C}_{44}\text{H}_{51}\text{N}_3\text{O}_3\text{SiSClRu}$ $[\text{M}-\text{Cl}]^+$ 866.2152, found 820.2184.



8-18w: This complex was isolated in 61% yield as a green solid (74 mg);

Purification: flash chromatography under N_2 (SiO_2 , hexanes–EtOAc, 10:1 \rightarrow 3:1

\rightarrow 1:1); ^1H NMR (500 MHz, CDCl_3) δ 7.67 (d, J = 8.1 Hz, 2H), 7.26 (d, J = 8.3

Hz, 2H), 7.08 (d, J = 11.3 Hz, 2H), 6.90 (s, 1H), 6.72 (s, 1H), 6.24 (s, 1H), 5.54 –

5.46 (m, 1H), 5.43 (t, J = 7.2 Hz, 1H), 5.03 – 4.94 (m, 1H), 4.68 – 4.52 (m, 4H), 4.40 – 4.27 (m, 2H), 4.19

(d, J = 6.9 Hz, 2H), 4.04 (s, 1H), 3.89 (d, J = 16.3 Hz, 2H), 3.67 (s, 2H), 3.46 (d, J = 16.1 Hz, 1H), 2.87 (s,

3H), 2.41 (d, J = 41.6 Hz, 15H), 1.83 (s, 3H), 1.77 (s, 3H), 1.68 (s, 3H); ^{13}C NMR (125 MHz, CDCl_3) δ

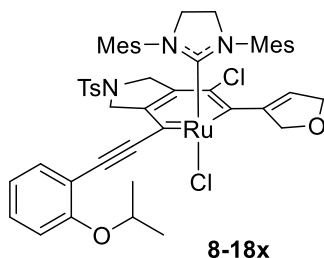
219.64, 207.37, 203.89, 145.08, 144.66, 143.64, 139.95, 138.36, 137.95, 137.11, 136.90, 136.06, 134.88,

133.27, 130.98, 129.88, 129.16, 128.82, 128.28, 127.49, 120.43, 115.81, 114.29, 92.57, 76.73, 74.77, 66.49,

59.26, 58.03, 55.79, 51.60, 51.26, 25.94, 21.46, 21.28, 19.31, 18.81, 18.38, 17.96, 17.54; **HRMS** (ESI)

calcd for $\text{C}_{47}\text{H}_{53}\text{N}_3\text{O}_4\text{SClRu}$ $[\text{M}-\text{Cl}]^+$ 892.2489, found 892.2489. Metathesis product **2w'** was also isolated

in 15% yield whose characterization is reported in literature.²⁷



8-18x: This complex was isolated in 86% yield as a green solid (61 mg);

Purification: flash chromatography under N_2 (SiO_2 , hexanes–EtOAc, 10:1 \rightarrow

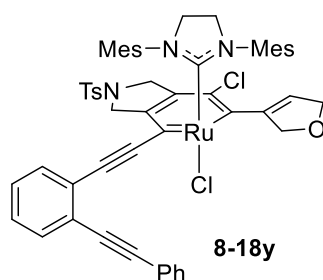
3:1 \rightarrow 1:1); ^1H NMR (500 MHz, CDCl_3) δ 7.67 (d, J = 7.9 Hz, 2H), 7.55 (d,

J = 7.0 Hz, 1H), 7.40 (t, J = 7.4 Hz, 1H), 7.24 (d, J = 8.0 Hz, 2H), 7.13 (s,

1H), 7.08 (s, 1H), 6.96 (dd, J = 19.2, 11.1 Hz, 3H), 6.74 (s, 1H), 6.26 (s, 1H),

5.58 – 5.43 (m, 1H), 4.99 (d, J = 10.7 Hz, 1H), 4.76 (dd, J = 11.9, 6.5 Hz, 2H), 4.68 (d, J = 12.1 Hz, 1H),

4.60 (q, $J = 15.0, 14.2$ Hz, 2H), 4.04 (s, 1H), 3.95 (dd, $J = 16.2, 2.9$ Hz, 1H), 3.87 (s, 1H), 3.66 (s, 2H), 3.52 (d, $J = 16.6$ Hz, 1H), 2.98 (s, 3H), 2.49 (s, 3H), 2.45 (s, 3H), 2.35 (s, 6H), 2.30 (s, 3H), 1.69 (s, 3H), 1.59 (d, $J = 6.0$ Hz, 3H), 1.53 (d, $J = 6.0$ Hz, 3H); ^{13}C NMR (125 MHz, CDCl_3) δ 217.30, 209.09, 204.63, 157.30, 144.82, 144.65, 143.51, 139.85, 139.62, 137.88, 137.16, 136.94, 136.50, 134.90, 133.43, 133.43, 132.81, 132.13, 130.95, 130.44, 130.03, 129.84, 128.97, 128.19, 127.49, 120.44, 116.20, 115.20, 113.83, 113.61, 100.16, 76.73, 74.82, 70.87, 58.21, 56.05, 51.64, 51.23, 22.43, 22.32, 21.44, 21.32, 19.64, 19.04, 17.98, 17.57; **HRMS** (ESI) calcd for $\text{C}_{50}\text{H}_{53}\text{N}_3\text{O}_4\text{SClRu}$ $[\text{M}-\text{Cl}]^+$ 928.2489, found 928.2499.

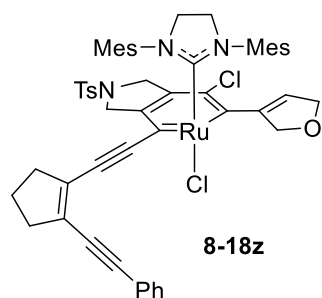


8-18y: This complex was isolated in 40% yield as a green solid (42 mg);

Purification: flash chromatography under N_2 (SiO_2 , hexanes–EtOAc, 10:1 \rightarrow

3:1 \rightarrow 1:1); ^1H NMR (500 MHz, CDCl_3) δ 7.81 (d, $J = 7.5$ Hz, 2H), 7.74 – 7.61 (m, 4H), 7.51 (t, $J = 7.6$ Hz, 2H), 7.47 – 7.36 (m, 3H), 7.21 (d, $J = 7.9$ Hz, 2H), 7.05 (s, 1H), 6.93 (s, 1H), 6.68 (s, 1H), 6.47 (s, 1H), 6.26 (s, 1H),

5.57 – 5.46 (m, 1H), 4.99 (d, $J = 11.4$ Hz, 1H), 4.81 (dd, $J = 11.7, 2.9$ Hz, 1H), 4.75 (d, $J = 11.9$ Hz, 1H), 4.60 (q, $J = 14.3$ Hz, 2H), 3.98 (s, 1H), 3.89 (dd, $J = 16.2, 3.0$ Hz, 1H), 3.75 (s, 1H), 3.58 (s, 2H), 3.47 (d, $J = 16.1$ Hz, 1H), 2.88 (s, 3H), 2.43 (s, 3H), 2.39 – 2.21 (m, 12H), 1.67 (s, 3H); ^{13}C NMR (125 MHz, CDCl_3) δ 218.72, 206.36, 203.87, 144.88, 144.78, 143.52, 139.86, 139.65, 138.23, 137.09, 136.88, 136.30, 134.72, 133.26, 133.14, 132.36, 131.91, 130.97, 129.87, 129.22, 129.01, 128.92, 128.80, 128.73, 128.61, 128.26, 128.16, 127.54, 126.78, 123.82, 123.03, 117.24, 114.29, 99.05, 94.28, 88.38, 74.79, 65.86, 58.19, 55.95, 51.58, 51.14, 21.43, 21.21, 19.53, 18.95, 17.92, 17.50, 15.29; **HRMS** (ESI) calcd for $\text{C}_{55}\text{H}_{51}\text{N}_3\text{O}_3\text{SClRu}$ $[\text{M}-\text{Cl}]^+$ 970.2383, found 970.2389.



8-18z

8-18z: This complex was isolated in 78% yield as a green solid (64 mg);

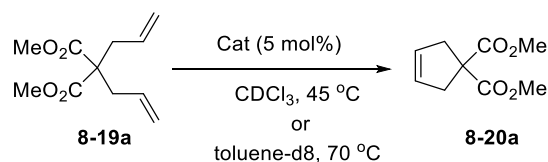
Purification: flash chromatography under N₂ (SiO₂, hexanes–EtOAc, 10:1 →

3:1 → 1:1); **¹H NMR** (500 MHz, CDCl₃) δ 7.70 (d, *J* = 7.5 Hz, 2H), 7.64 (d, *J* = 7.8 Hz, 2H), 7.42 (t, *J* = 7.5 Hz, 2H), 7.39 – 7.33 (m, 1H), 7.20 (d, *J* = 7.9 Hz, 2H), 7.04 (s, 1H), 6.92 (s, 1H), 6.76 (s, 1H), 6.70 (s, 1H), 6.24 (s, 1H),

5.57 – 5.46 (m, 1H), 5.03 – 4.92 (m, 1H), 4.70 (q, *J* = 12.0 Hz, 2H), 4.57 (q, *J* = 15.3, 13.8 Hz, 2H), 4.06 – 3.87 (m, 2H), 3.76 (d, *J* = 12.4 Hz, 1H), 3.60 (s, 2H), 3.46 (d, *J* = 15.8 Hz, 1H), 2.89 (s, 5H), 2.64 (s, 2H), 2.41 (s, 6H), 2.34 (s, 6H), 2.28 (s, 3H), 2.11 (t, *J* = 7.6 Hz, 2H), 1.64 (s, 3H); **¹³C NMR** (125 MHz, CDCl₃) δ 217.93, 206.97, 204.25, 144.82, 144.71, 143.52, 139.72, 137.89, 137.03, 137.01, 136.93, 136.29, 134.79, 133.23, 132.14, 131.07, 130.96, 129.86, 129.71, 129.25, 128.92, 128.74, 128.64, 128.21, 127.52, 123.25, 115.41, 114.06, 102.00, 98.11, 87.05, 76.72, 74.79, 58.20, 55.84, 51.56, 51.13, 38.29, 37.12, 23.36, 21.43, 21.23, 20.04, 19.12, 17.91, 17.50; **HRMS** (ESI) calcd for C₅₄H₅₃N₃O₃SClRu [M-Cl]⁺ 960.2540, found 960.2554.

8.4.4. Kinetic studies for RCM

RCM of dimethyldiallyl malonate



An NMR tube with a screw-cap septum top was charged with dimethyldiallyl malonate (25 mg, 0.12 mmol) solution in 0.8 mL of toluene-d₈ followed by the catalyst stock solution (0.05 M, 0.12 mL, 6 mmol) in a glove box. The NMR tube was then degassed and refilled with argon by freeze, pump thaw process (3 cycles). The reaction was then heated at 70 °C and the conversion was monitored by ¹H NMR spectroscopy at regular time interval. Since the reaction rate at room temperature is extremely slow, the error in conversion during the course of taking nmr can be considered negligible. The conversion to RCM product

was determined by comparing the ratio of the integrals of the methylene protons in the starting material, δ 2.76 (d), with those in the product, δ 3.07 (s). Similarly, reactions were also carried at 45 °C for certain highly active catalysts in CDCl_3 solvent in same concentration and the conversions were determined after specific time interval. Conversion vs time plots were generated using Origin Pro software. For catalysts which are extremely fast like Grubbs-I, Grubbs-II or catalyst **8-18a** at 70 °C the reaction profile was obtained by equilibrating the NMR probe at requisite temperature and using Bruker's 2D kinetics.⁶⁵

Note: Complex **8-18a** underwent complete conversion within 70 min hence its Kinetics was studied using Bruker pseudo 2D kinetic method.

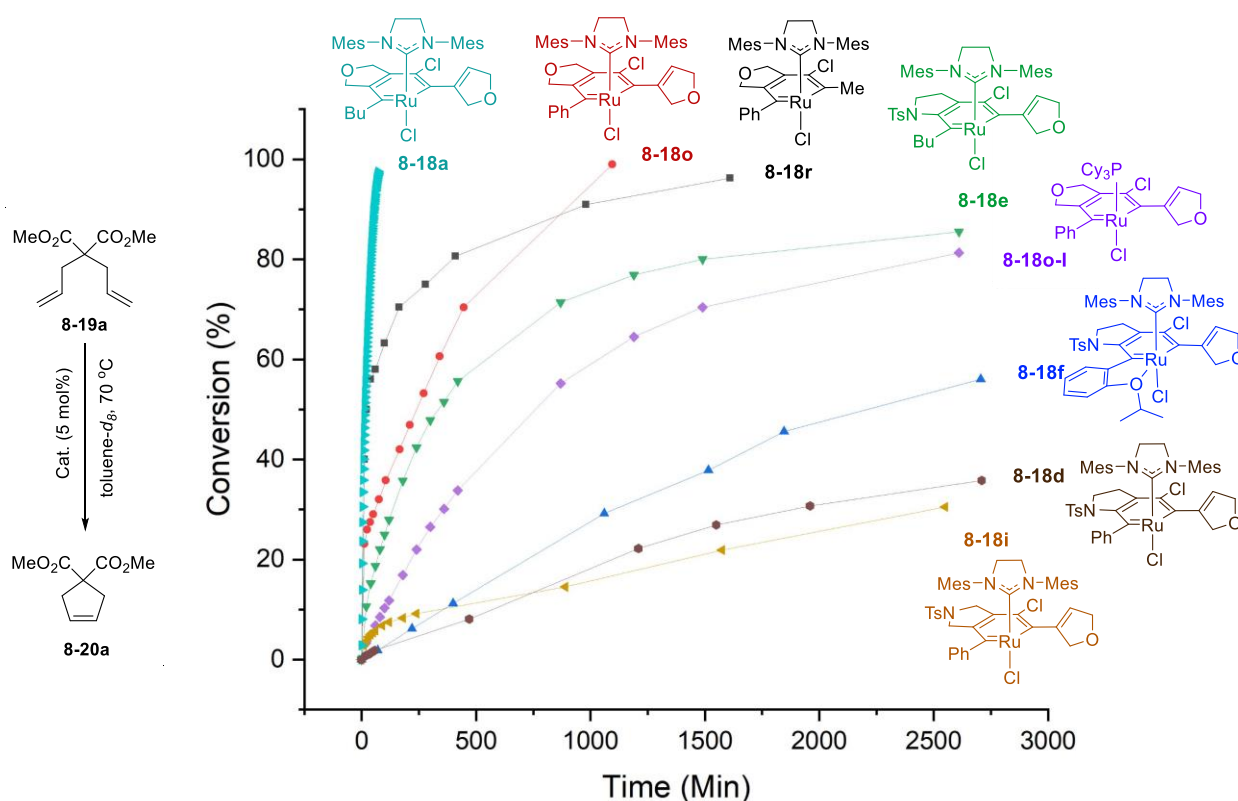


Fig. S1 Conversion vs Time Plot for RCM of dimethyldiallyl malonate at 70 °C in toluene-d₈

Note: **G-I** and **G-II** underwent complete conversion within few minutes using only 1 mol% catalyst hence its Kinetics was studied using Bruker pseudo 2D kinetic method.

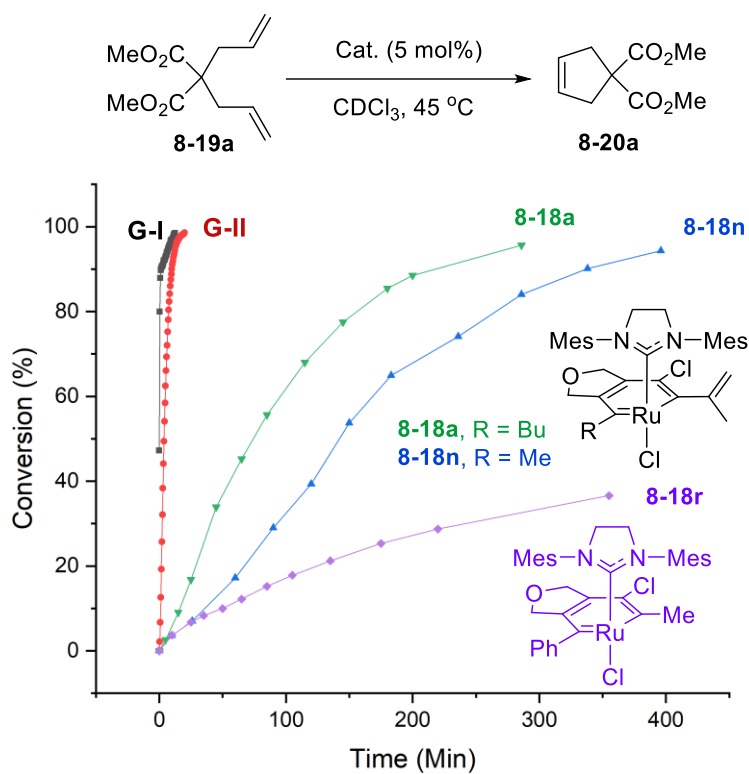
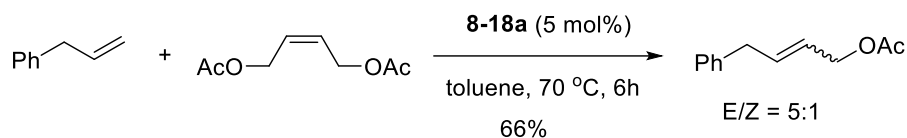


Fig. S2 Conversion vs Time Plot for RCM of dimethyldiallyl malonate at 45 °C in CDCl₃.

Note: The RCM of **8-19a** to **8-20a** was also done using 2 mol% of **8-18a** giving a conversion of 90% after 12 hours at 45 °C and 96% after 5 hours at 70 °C. Thus, with lower catalyst loading the RCM reaction leads to near complete conversion but requires longer reaction time.

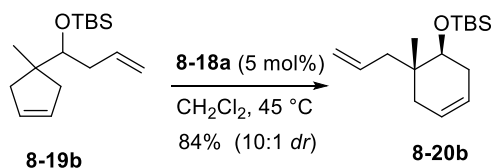
8.4.5. Other reactivities of ruthenabenzenes

Cross Metathesis Reaction catalyzed by **8-18a**



Allylbenzene (20 mg, 0.16 mmol) and (*Z*)-but-2-ene-1,4-diyl diacetate (85.4 mg, 0.56 mmol) was dissolved in 0.6 mL of anhydrous toluene in a screw capped vial followed by addition of **8-18a** (0.16 mL, 8 mmol) from a 0.05 M stock solution in toluene. The mixture was heated under N₂ at 70 °C for 6h. After completion, the reaction mixture was directly loaded on a short column and 4-phenylbut-2-en-1-yl acetate was isolated by flash chromatography (SiO₂, hexanes–EtOAc, 10:1→5:1) in 84% yield as 5:1 E/*Z* mixture. ¹H NMR (500 MHz, CDCl₃) Major isomer: δ 7.31 (t, *J* = 7.4 Hz, 2H), 7.24 – 7.17 (m, 3H), 5.93 (dt, *J* = 14.6, 6.6 Hz, 1H), 5.64 (dt, *J* = 14.9, 6.3 Hz, 1H), 4.55 (d, *J* = 6.2 Hz, 2H), 3.41 (d, *J* = 6.5 Hz, 2H), 2.07 (s, 3H). ¹³C NMR (126 MHz, CDCl₃) (all discernable signals for both isomers) δ 170.86, 139.57, 134.55, 133.47, 128.61, 128.52, 128.39, 126.27, 125.27, 124.26, 64.92, 60.23, 38.66, 33.80, 21.03. The spectroscopic data are consistent with literature report.⁶⁶

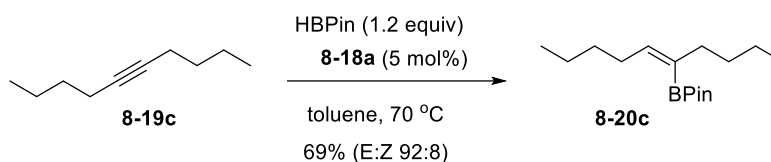
Ring Rearrangement Metathesis (RRM) of dimethyldiallyl malonate



8-19b was synthesized by following literature procedure.⁴⁷ A screw capped vial equipped with a septum was charged with **8-19b** (30 mg, 0.11 mmol) in 1 mL of anhydrous CH₂Cl₂ under argon, followed by addition of **8-18a** (0.11 mL, 5.5 mmol) from a 0.05 M stock solution in CH₂Cl₂. After stirring at 45 °C for 2h, the reaction mixture was directly loaded on a short column and **8-20b** was isolated by flash chromatography (SiO₂, hexanes–EtOAc, 20:1→10:1) in 84% yield with 10:1 diastereomeric ratio

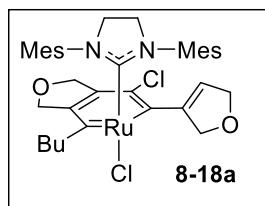
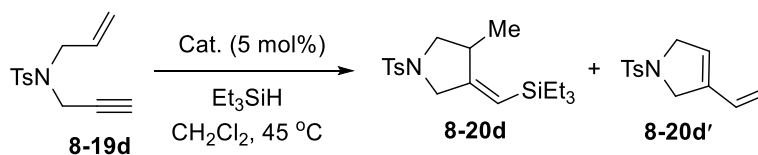
(determined by ^1H NMR). The catalyst **8-18a** was also recovered by flash chromatography (SiO_2 , hexanes–EtOAc, 3:1→1:1) with 90% recoverability. The characterization data for **8-20b** is available in literature.¹⁷

trans-Hydroboration of 5-decyne^{48a}



A screw capped vial equipped with a septum was charged with **8-19c** (20 mg, 0.14 mmol) in 1 mL anhydrous toluene under argon, followed by addition of HBPIn (24.6 mL, 0.17 mmol) and catalyst **8-18a** (0.14 mL, 7 mmol) from a 0.05 M stock solution in toluene. After stirring at 70 °C for 14h, the solvent was removed and the reaction mixture was purified flash chromatography (SiO_2 , hexanes–EtOAc, 20:1→10:1) to obtain the alkenyl boronate as a colorless oil in 69% yield with high E-selectivity (E:Z 92:8). ^1H NMR (500 MHz, CDCl_3) δ 5.97 (t, J = 7.4 Hz, 1H), 2.29 (q, J = 7.0 Hz, 2H), 2.07 (t, J = 7.1 Hz, 2H), 1.38 – 1.18 (m, 20H), 0.88 (q, J = 6.7 Hz, 6H); ^{13}C NMR (125 MHz, CDCl_3) δ 145.87, 82.75, 36.59, 32.62, 32.29, 30.83, 24.80, 22.35, 22.22, 14.06, 13.98; HRMS (ESI) calcd for $\text{C}_{16}\text{H}_{32}\text{O}_2\text{B}$ $[\text{M}+\text{H}]^+$ 267.2495, found 267.2493.

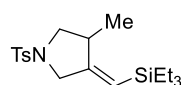
Hydrosilylative Cyclization Vs. Enyne RCM in **8-19d**^{49c}



Cat.	8-20d : 8-20d'	Yield (%)
2a	1 : 0	68
G-I	0 : 1	82
G-II	1 : 4	46

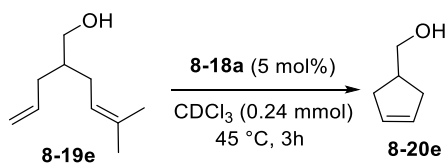
A screw capped vial equipped with a septum was charged with **8-19d** (25 mg, 0.1 mmol), triethylsilane (19.2 mL, 0.12 mmol) in 0.8 mL of CH₂Cl₂ under argon, followed by addition of **8-18a** (0.1 mL, 5 mmol)/ **G-I** (0.1 mL, 5 mmol) or **G-II** (0.1 mL, 5 mmol) from their 0.05 M stock solution in CH₂Cl₂. After stirring at 45 °C for 2h, the reaction mixture was directly loaded on a short column and hydrosilylative cyclization (**8-20d**) and enyne RCM (**8-20d'**) products were isolated by flash chromatography (SiO₂, hexanes–EtOAc, 20:1→10:1) for **4d** and (SiO₂, hexanes–EtOAc, 10:1→3:1) for **8-20d'**.⁶⁷ The ratios of product distribution changes with the type of catalyst used and is shown in the figure above. The yield shown denotes the yield of major product.

8-20d: yellow oil; This compound was isolated in 68% yield as single isomer. ¹H NMR (500 MHz, CDCl₃)

 δ 7.70 (d, *J* = 8.2 Hz, 2H), 7.32 (d, *J* = 8.0 Hz, 2H), 5.24 (q, *J* = 1.8 Hz, 1H), 4.05 (dt, *J* = 14.2, 1.7 Hz, 1H), 3.58 (dd, *J* = 14.1, 1.8 Hz, 1H), 3.25 (dd, *J* = 9.4, 1.5 Hz, 1H), 3.14 (dd, *J* = 9.3, 6.0 Hz, 1H), 2.75 – 2.64 (m, 1H), 2.43 (s, 3H), 1.04 (d, *J* = 7.1 Hz, 3H), 0.88 (t, *J* = 7.9 Hz, 9H), 0.56 (q, *J* = 7.9 Hz, 6H); ¹³C NMR (125 MHz, CDCl₃) δ 158.30, 143.47, 133.25, 129.63, 127.76, 117.86, 55.58, 53.70, 37.86, 21.54, 20.88, 7.45, 4.24; HRMS (ESI) calcd for C₁₉H₃₂NO₂SSi [M+H]⁺ 366.1923, found 366.1912.

8.4.6. Recyclability and degradation experiments

Catalytic Recyclability Experiment^{50c}



The RCM of **8-19e** to **8-20e**⁶⁸ was selected as the platform to study the recyclability of catalyst **8-18a**. A screw capped vial equipped with septum was charged with **8-19e** (63 mg, 0.41 mmol) in 1.71 ml CDCl₃ (0.24 M) under argon, followed by addition of **8-18a** (0.41 mL, 20.5 mmol) from a 0.05 M stock solution in CDCl₃. After stirring for 3h at 45 °C, a portion of reaction mixture was taken to determine conversion

through ^1H NMR (99% for first cycle). The reaction mixture was directly loaded on short pad of silica under N_2 and eluted with 1:1 hexanes–EtOAc to recover the catalyst **8-18a**. The purity of recovered catalyst was confirmed by ^1H NMR and % of catalyst recovered was determined (81% for first cycle). The recovered catalyst was reused for the second round following procedure described above. A total of five cycles were performed with % conversion after 3h being 99%, 97%, 92%, 87% and 70% respectively for each round. The catalytic recoverability varies from 71–81%. A graph is plotted to document the change in % conversion after 3h with respect to the number of cycles. For fifth cycle a conversion up to 90% was achieved after 12 h. The percentage of catalyst recovered was calculated by weighing the isolated recovered catalyst. The percentage of recovered catalyst in a particular round is calculated with respect to the weight of the isolated recovered catalyst of the previous round.

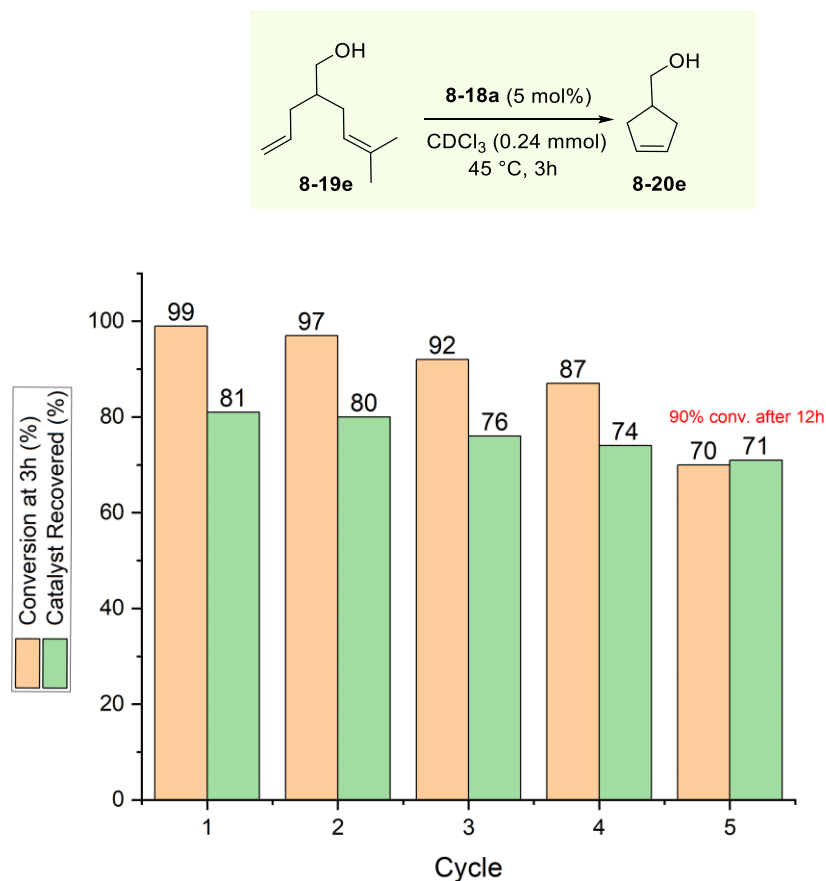


Fig. S3. Plot showing the % conversion of **4e** attained after 3h with each round of recoverability

Decomposition Experiment of G-II, Grubbs-Hoveyda catalyst (GH-II) and complex 8-18a in air⁶⁹

0.4 mL of 0.03 M stock solution of each **G-II**, **GH-II** and complex **8-18a** in CDCl₃ were taken in three NMR tubes followed by addition of 0.1 mL of 0.12 M stock solution of anthracene (internal standard) in CDCl₃. The NMR tubes were heated at 60 °C and the decomposition of the catalyst was monitored by ¹H NMR by calculating the change in concentration of the catalyst with respect to the internal standard. It was found out that both **GH-II** and ruthenabenzene complex **8-18a** are incredibly stable in air and underwent minor decomposition after 20h. On the other hand, **G-II** decomposed by around 90% within 10h due to its reaction with oxygen. A conc. vs time plot was obtained to demonstrate the decomposition of these three catalysts.

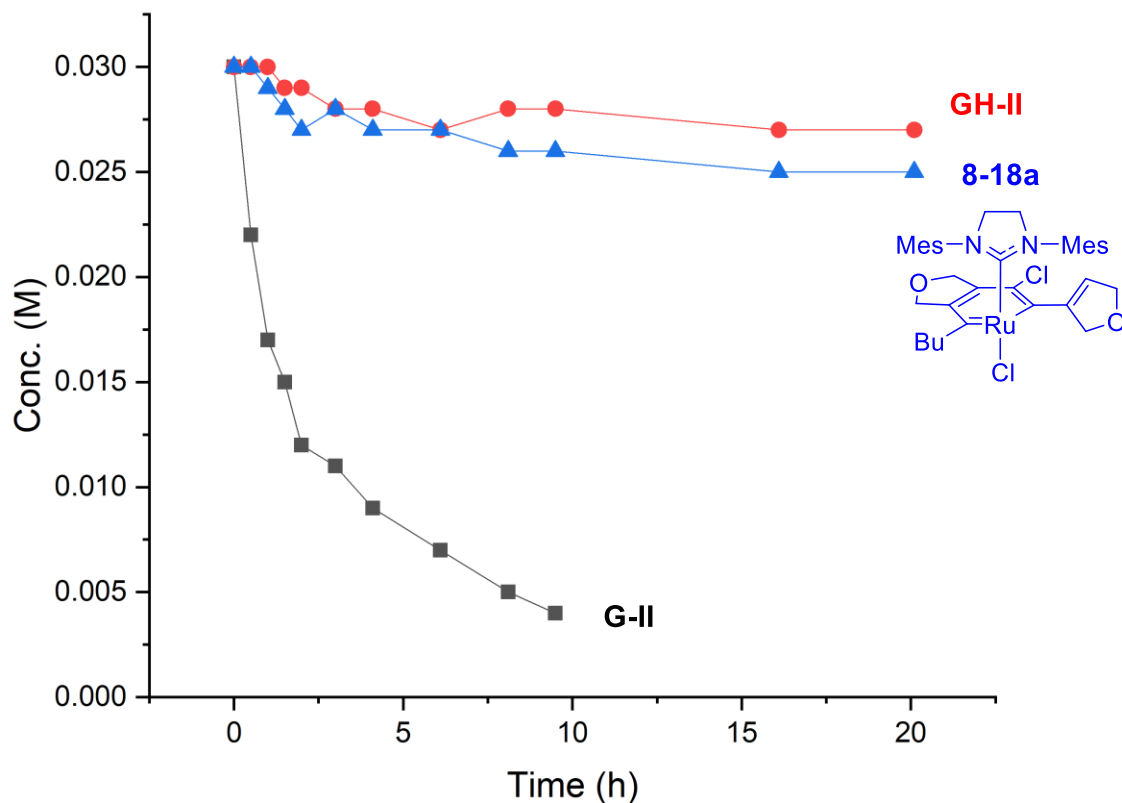


Fig. S4. Decomposition plot for **G-II**, **GH-II** and complex **8-18a** in air at 60 °C

Decomposition Experiment of GH-II and complex 8-18a under ethylene⁷⁰

A stock solution of each **GH-II** (0.03 M, 0.4 mL) and complex **8-18a** in CDCl₃ were taken in three screw capped NMR tubes with septum, followed by addition of a stock solution of anthracene (internal standard, 0.12 M, 0.1 mL) in CDCl₃. The NMR tubes were degassed and refilled with ethylene by freeze pump and thaw process (three cycles). A constant ethylene atmosphere was further maintained by keeping an ethylene balloon throughout the course of the experiment. Each NMR tubes were heated at 60 °C and the decomposition of the catalyst was monitored by ¹H NMR by calculating the change in concentration of the catalyst with respect to the internal standard. It was observed the degradation of ruthenabenzene complex **8-18a** is much slower than the **GH-II** catalyst which might be an indication to the higher stability of the complex compared to **GH-II**.

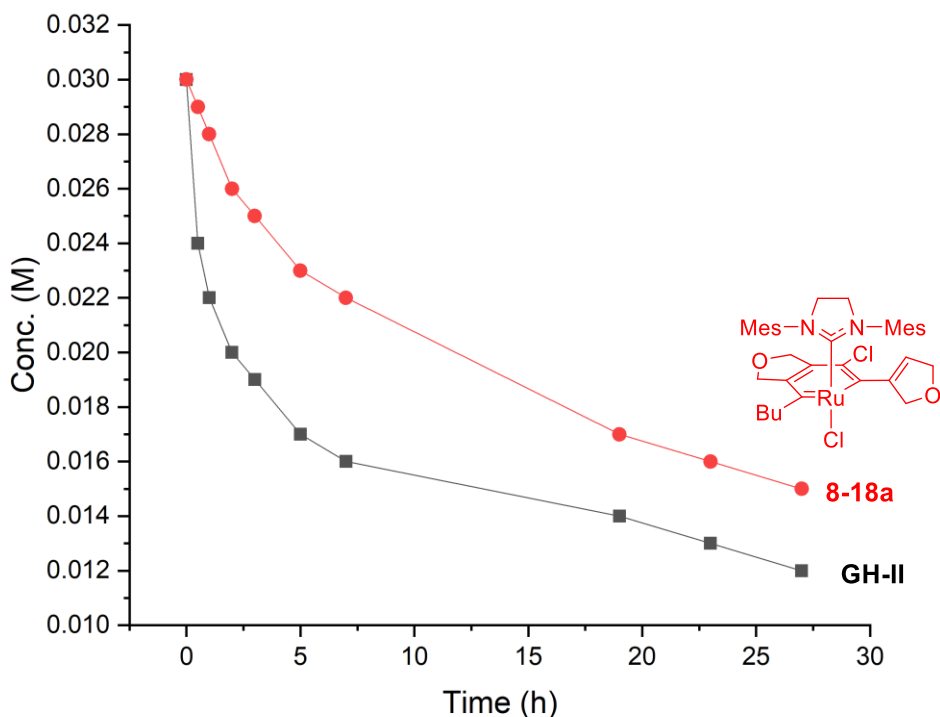


Fig. S5. Decomposition plot for GH-II and complex **8-18a** under ethylene at 60 °C.

8.4.7. Computational studies

Computational methods for the calculations of the mechanisms of ruthenabenzene formation

All density functional theory (DFT) calculations in **Figure 8.5** were carried out using the Gaussian 16 program⁷¹ and Zimmerman's GSM method.⁴⁵ Geometries of intermediates **Int-I**, **Int-I'**, **Int-II**, **2d** and transition states **TS2** were optimized in Gaussian using B3LYP functional with Grimme's DFT-D3(BJ) dispersion correction⁴³ with a mixed basis set of SDD⁴¹ for Ru and 6-31G(d) for other atoms in the dichloromethane solvent phase by using SMD continuum solvation model.⁴² Vibrational frequency calculations were performed for **Int-I**, **Int-I'**, **Int-II**, **TS2** and **8-18d** to confirm if each optimized structure is a local minimum or a transition state structure. Optimized transition state structure **TS2** has only one imaginary (negative) frequency, and all minima have no imaginary frequencies. The M06 functional⁴⁰ with a mixed basis set of SDD for Ru and 6-311+G(d,p) for other atoms was used for single-point energy calculations in the dichloromethane solvent phase by using SMD continuum solvation model. The reported Gibbs free energies and enthalpies include thermal corrections at 298K. The potential energy surface of the cis-trans isomerization and [1,5]-Cl shift pathway (Path B) is nearly flat in the transition state region (see later), therefore transition state structure **TS1** could not be located by using Gaussian after multiple attempts. Growing string method (GSM) was applied to locate this transition state structure. The B3LYP-D3(BJ)/SDD-6-31G(d)/SMD(CH₂Cl₂) level of theory was used in the GSM calculations to locate the transition state structure. The convergence threshold of growing string method was 0.0005. Single point energy of **TS1** was then calculated at the M06/SDD-6-311+G(d,p)/SMD(CH₂Cl₂) level of theory.

Computational methods for the calculations of the catalyst initiation mechanisms of ruthenabenzenes

Because the ruthenabenzene-catalyzed metathesis reactions were performed in toluene, the DFT calculations of the catalyst initiation mechanisms were performed in toluene accordingly. All DFT calculations in **Figure 8.7** and **Figure S7** were carried out using the Gaussian 16 program, with geometries optimized at the B3LYP-D3(BJ)/SDD-6-31G(d) level of theory in the gas phase and single-point energy

calculations at the M06/SDD-6-311+G(d,p) level of theory in toluene solvent using the SMD continuum solvation model. The reported Gibbs free energies and enthalpies include thermal corrections at 298K.

The Nucleus-Independent Chemical Shift (NICS) calculations were performed to evaluate the aromaticity of ruthenabenzenes **8-18a**, **8-18o**, **8-18e**, **8-18o-I** and **8-18d**. Geometries were optimized at the B3LYP-D3(BJ)/SDD-6-31G(d) level in gas phase. NICS values were computed using B3LYP functional with a mixed basis set of SDD for Ru and 6-311+G(d,p) for other atoms. The ghost atoms were placed 1 angstrom above and below the center of the 6-membered ruthenacycle, giving NICS(1)_{zz} and NICS(-1)_{zz} values, respectively. The average of NICS(1)_{zz} and NICS(-1)_{zz}, $\text{NICS} = [\text{NICS}(1)_{zz} + \text{NICS}(-1)_{zz}]/2$, was used as the NICS values to describe the aromaticity of the ruthenabenzenes. More negative value indicates a more aromatic system. All NICS values are in ppm.

Computed potential energy surface of the [1,5]-Cl shift step

The [1,5]-Cl shift transition state that directly connects the intermediate **Int-I'** and ruthenabenzene **8-18d** cannot be located by using Gaussian after multiple attempts. This transition state (**TS1**) was located using Zimmerman's growing string method (GSM) instead. To obtain further insights into this potential pathway, the potential energy surface (PES) was constructed by plotting the electronic energies (E, with respect to **Int-I'** in kcal/mol) obtained from constrained geometry optimizations with fixed C-Cl and Ru-Cl bond distances (Fig. S6). Stationary points **Int-I'**, **TS1**, and **8-18d** are labeled on the surface. The region on the potential energy surface around the [1,5]-chloride shift transition state (**TS1**, located by GSM) is nearly flat, which is consistent with the challenges of locating such transition state using Gaussian. The electronic energy of **TS1** on the PES is approximately 16.0 kcal/mol with respect to **Int-I'**, 23.7 kcal/mol with respect to **Int-I**, which is consistent with the GSM calculations. This activation energy is much higher than that of the nucleometallation TS in the alternative pathway (**TS2**, $\Delta E^\ddagger = 10.4$ kcal/mol with respect to **Int-I**).

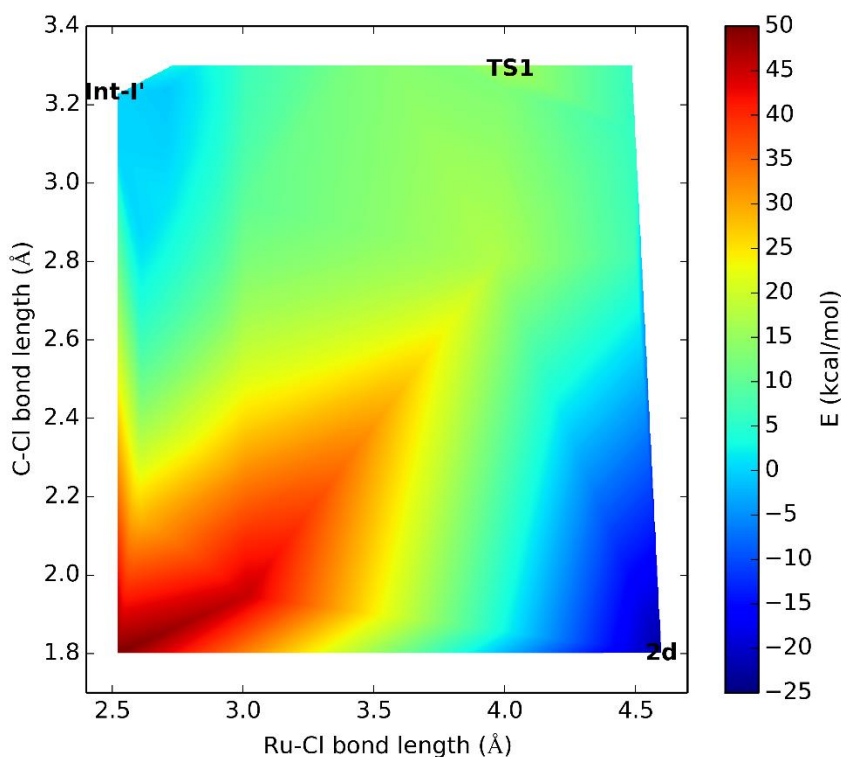


Fig. S6. Potential energy surface of the [1,5]-Cl-shift from **Int-I'** to ruthenabenzene **8-18d**.

Energy profiles of possible mechanisms of catalyst initiation of **8-18a**

We computed two possible catalyst initiation mechanisms of ruthenabenzene **8-18a**. We used propene as a model terminal olefin in the calculations. The [2+2] cycloaddition with the Ru=C bond in the ruthenabenzene (**TS5**) requires a very high activation free energy of 38.3 kcal/mol with respect to **8-18a**. The high barrier of **TS5** is due to the aromaticity of the ruthenabenzene as well as the distortion of the chloride ligand in **8-18a** from the position trans to the NHC to the cis position in **TS5**. The ruthenacyclobutane intermediate (**Int-IV**) is also relatively unstable, 26.9 kcal/mol higher in energy than the starting materials (separated **8-18a** and propene).

On the other hand, the catalyst initiation via the ruthenabenzene ring-opening is more favorable. The ruthenabenzene ring-opening occurs via an E2-type transition state (**TS3**), which is the reverse of the

nucleometallation to form the ruthenabenzene. This process leads to the π -alkyne alkylidene complex **I-8-17a** after the eliminated chloride anion associates to the Ru center. Although the ring-opening is endergonic by 6.8 kcal/mol (see later for reaction energies of ring-opening of other ruthenabenzenes), the resulting π -alkyne alkylidene complex **I-8-17a** is much more reactive than the ruthenabenzene in the [2+2] cycloaddition. The [2+2] cycloaddition with **I-8-17a** takes place via **TS4**, which is only 14.9 kcal/mol with respect to **I-8-17a**. The resulting ruthenacyclobutane **Int-III** is also significantly more stable than **Int-IV**. The rate-determining step in the ring-opening initiation pathway is **TS3**, which requires an activation free energy of 30.8 kcal/mol with respect to **8-18a**, 7.5 kcal/mol lower than that of **TS5** in the direct [2+2] cycloaddition pathway.

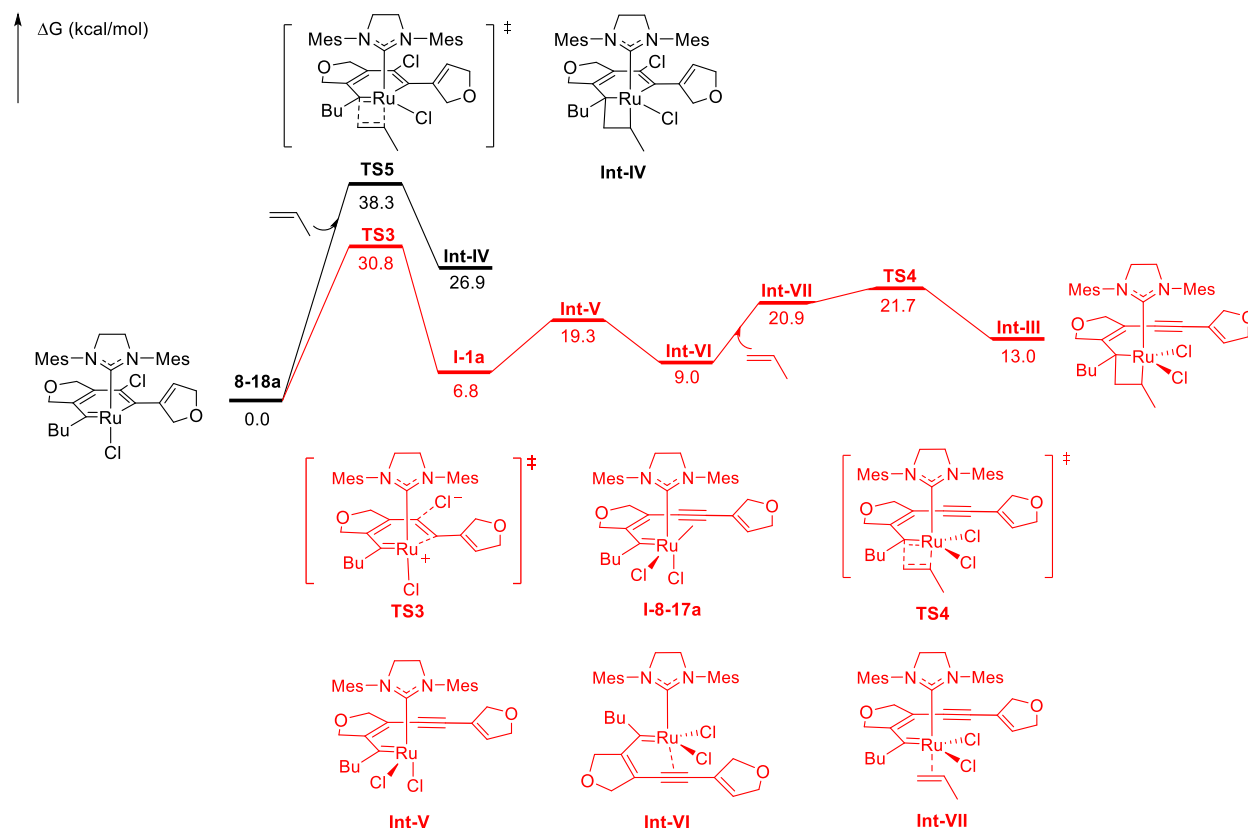


Fig. S7. Energy profiles of possible initiation pathways of ruthenabenzene precatalyst **8-18a**.

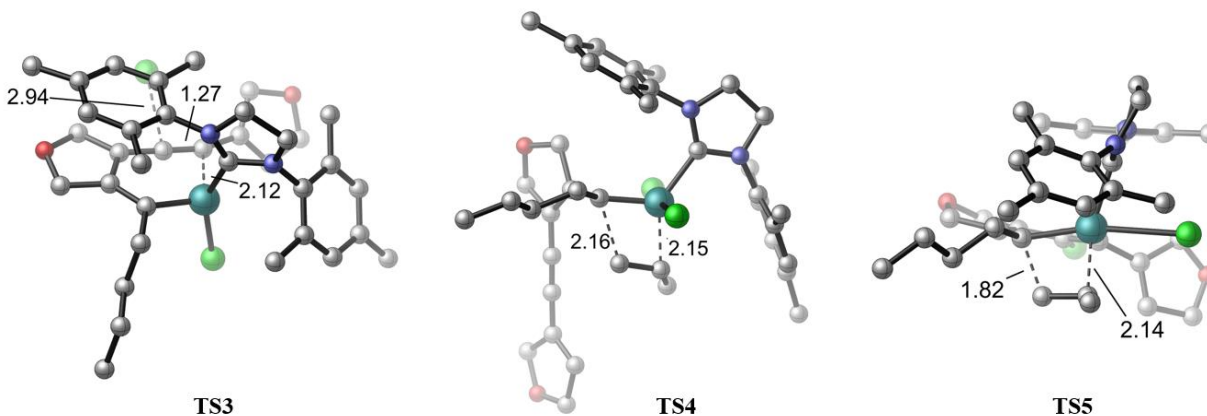
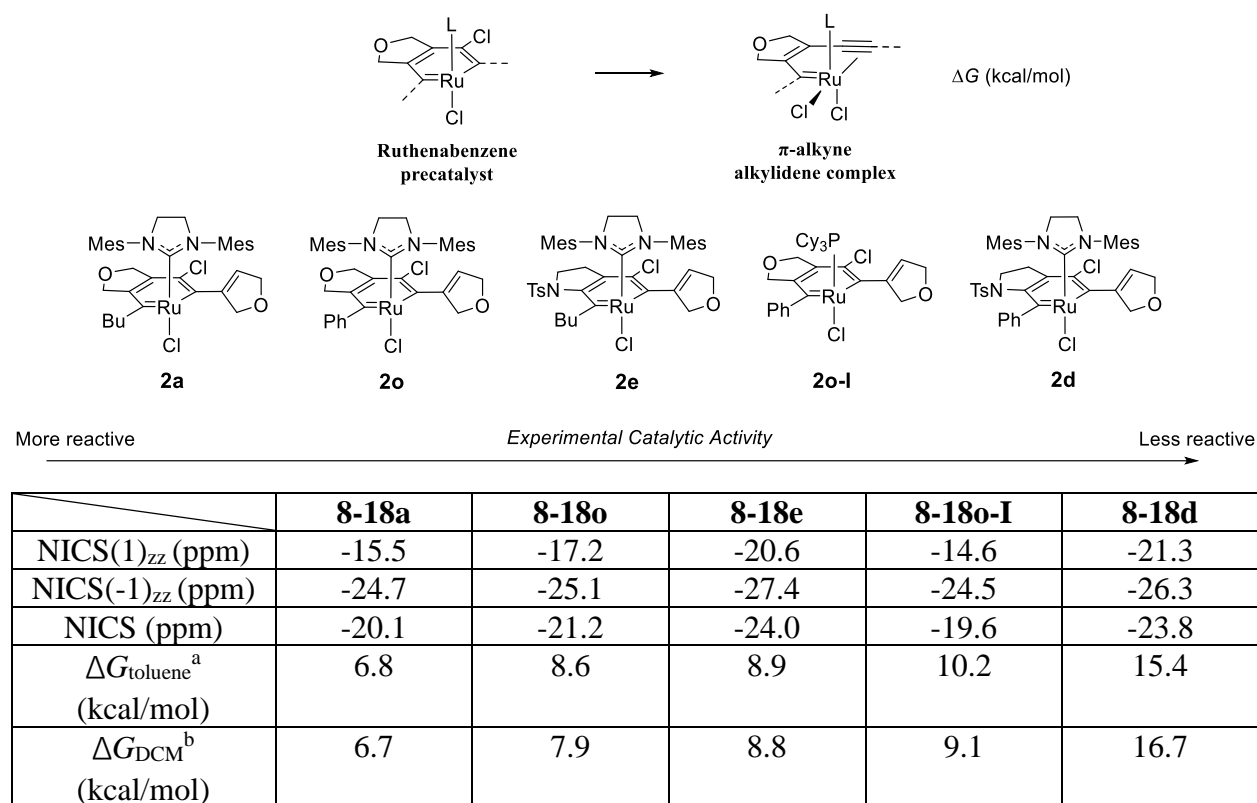


Fig. S8. 3D structures of **TS3**, **TS4**, and **TS5** in the initiation pathways. H atoms are omitted for clarity

Catalytic activity of ruthenabenzenes

To explore the origin of the experimental catalytic activity of ruthenabenzenes, we computed the NICS values, which describe the aromaticity of the ruthenabenzene, and the energy required for the ruthenabenzene ring-opening to form the π -alkyne alkylidene intermediate. The experimental catalytic activity does not have an obvious trend with the computed NICS values of ruthenabenzenes. On the other hand, a good agreement between the experimental catalytic activity trend and the relative free energy of the π -alkyne alkylidene complex. These results suggest that the catalytic activities of ruthenabenzenes are affected by the thermodynamic stability, which does not correlate with the aromaticity. In addition, these results support the catalyst initiation mechanism via ruthenabenzene ring-opening to form the π -alkyne alkylidene complex.

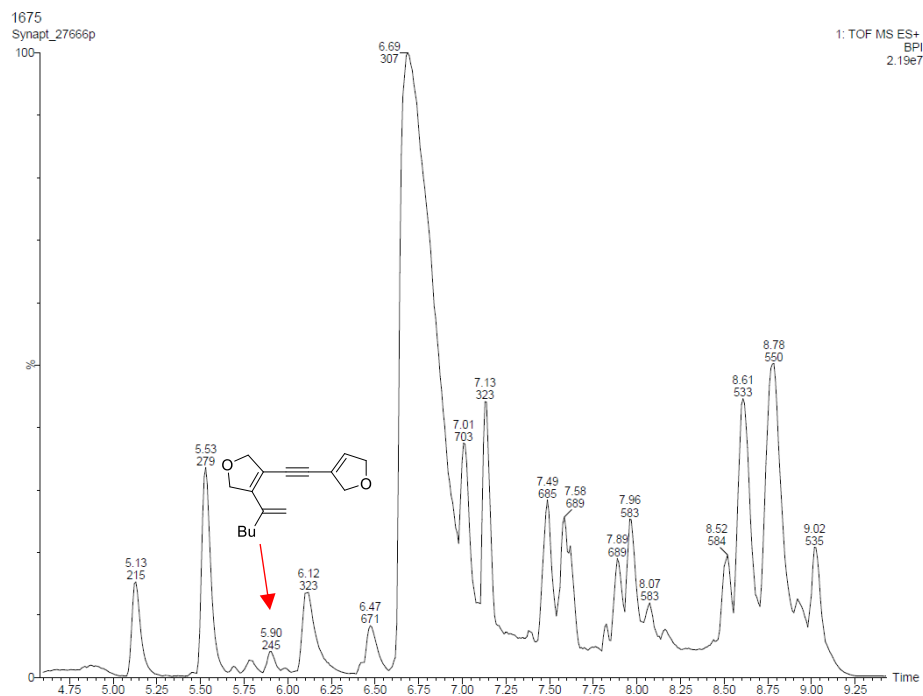


^a Single point energies were computed at the M06/SDD-6-311+G(d,p) level with SMD continuum solvation model in toluene.

^b Single point energies were computed at the M06/SDD-6-311+G(d,p) level with SMD continuum solvation model in dichloromethane.

Mass Spectrometric Evidence in favor of Catalytic Cycle I

The DFT calculations revealed that the catalyst initiation via ruthenabenzene ring-opening (Catalytic Cycle I) is more favorable. To provide an experimental support for this calculation, ruthenabenzene **8-18a** was treated with 3 equiv. of 1-octene in CDCl_3 at 60 °C. The reaction was monitored through NMR spectroscopy and after complete consumption of **8-18a**, the crude reaction mixture was subjected to LCMS analysis. Gratifyingly, the organic component formed from dearomatization of **8-18a** followed by exchange with methylene ($[\text{M} + \text{H}]^+ = 245.1665$) was detected unambiguously in this crude reaction mixture. The detection of this compound in LCMS analysis supports catalyst initiation via ruthenabenzene ring-opening.



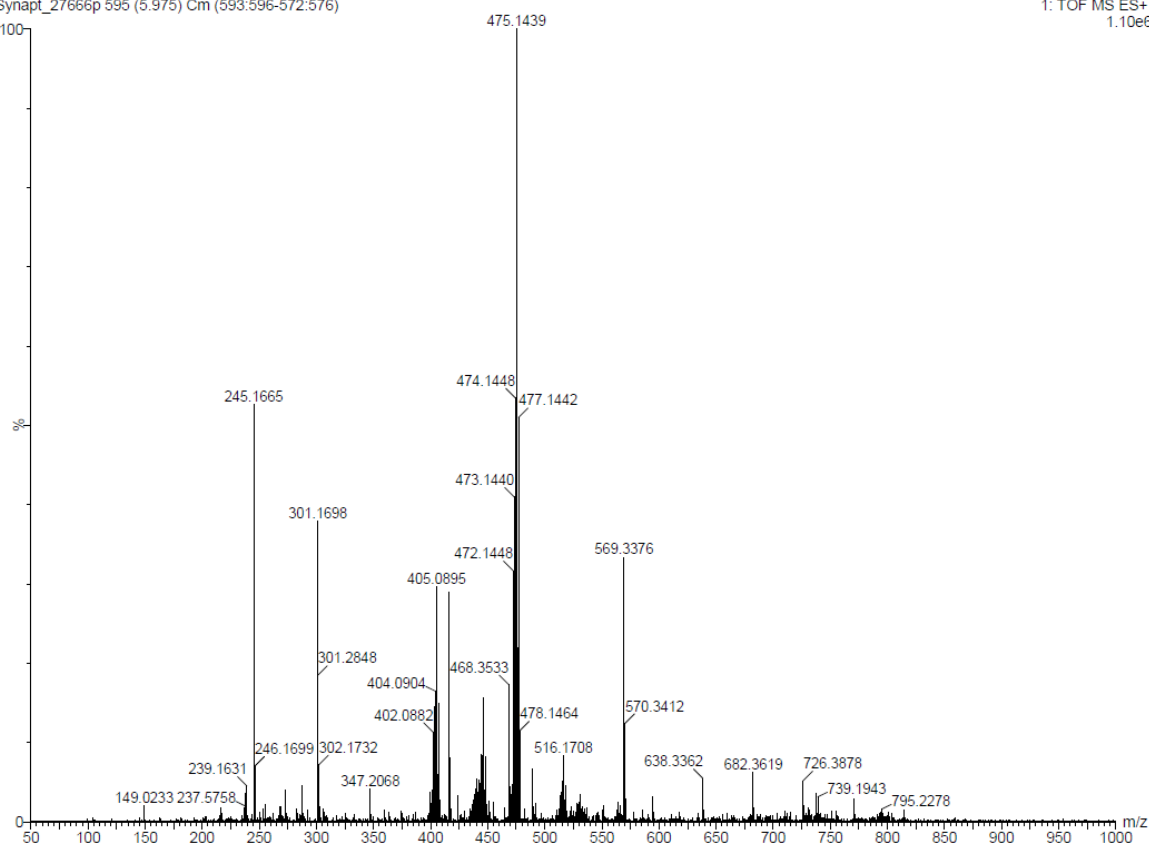
LCMS plot showing the presence of methylene exchanged component.

HRMS analysis and Element Composition report for the methylene exchange component (which could be generated only if Catalytic Cycle I is operating).

Le, Ting; 1675

Synapt_27666p 595 (5.975) Cm (593:596-572:576)

1: TOF MS ES+
1.10e6



Elemental Composition Report

Page 1

Single Mass Analysis

Tolerance = 10.0 PPM / DBE: min = -1.5, max = 50.0

Element prediction: Off

Number of isotope peaks used for i-FIT = 3

Monoisotopic Mass, Even Electron Ions

80 formula(e) evaluated with 1 results within limits (up to 50 closest results for each mass)

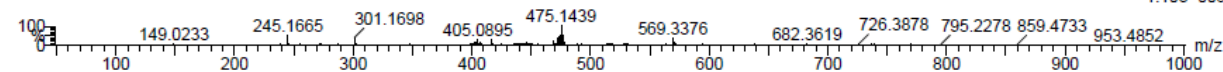
Elements Used:

C: 0-100 H: 0-120 N: 0-3 O: 0-5

Le, Ting; 1675

Synapt_27666p 595 (5.975) Cm (593:596-572:576)

1: TOF MS ES+
1.10e+006



Minimum:

Maximum: 5.0 10.0 -1.5

Mass	Calc. Mass	mDa	PPM	DBE	i-FIT	Norm	Conf(%)	Formula
------	------------	-----	-----	-----	-------	------	---------	---------

245.1665	245.1654	1.1	4.5	6.5	650.6	n/a	n/a	C15 H21 N2 O
----------	----------	-----	-----	-----	-------	-----	-----	--------------

Calculated total energies and thermochemical corrections of the mechanisms of ruthenabenzene formation

	Optimization		
	B3LYP-D3(BJ)/SDD-6-31G(d)/SMD(CH ₂ Cl ₂)		
	SCF energy (a.u.)	Enthalpy (a.u.)	Free energy (a.u.)
Int-I	-3546.799615	-3545.917456	-3546.061586
2d	-3546.833073	-3545.950155	-3546.09574
Int-I'	-3546.7829	-3545.90091	-3546.049265
TS1	-3546.764228	N/A	N/A
Int-II	-3546.790744	-3545.90754	-3546.053787
TS2	-3546.788553	-3545.906259	-3546.049771

	Single point		
	M06/SDD-6-311+G(d,p)/SMD(CH ₂ Cl ₂)		
	SCF energy (a.u.)	Enthalpy (a.u.)	Free energy (a.u.)
Int-I	-3545.469858	-3544.587699	-3544.731829
2d	-3545.494465	-3544.611547	-3544.757132
Int-I'	-3545.457509	-3544.575519	-3544.723874
TS1	-3545.431258	N/A	N/A
Int-II	-3545.45668	-3544.573476	-3544.719723
TS2	-3545.453271	-3544.570977	-3544.714489

Calculated total energies and thermochemical corrections of the catalyst initiation mechanisms of ruthenabenzenes

	Optimization		
	B3LYP-D3(BJ)/SDD-6-31G(d)		
	SCF energy (a.u.)	Enthalpy (a.u.)	Free energy (a.u.)
2o	-2747.634970	-2746.892628	-2747.016347
2o-I	-2869.413482	-2868.611525	-2868.726308
2e	-3472.961461	-3472.043872	-3472.192031
2d	-3546.765502	-3545.88207	-3546.029053
π -alkyne alkylidene complex of 2o	-2747.609462	-2746.867682	-2746.991445
π -alkyne alkylidene complex of 2d	-3546.737402	-3545.854552	-3545.998587
π -alkyne alkylidene complex of 2e	-3472.939471	-3472.022423	-3472.168671
π -alkyne alkylidene complex of 2o-I	-2869.378052	-2868.57697	-2868.693816
Propene	-117.913249	-117.828104	-117.858127
2a	-2673.827736	-2673.05214	-2673.179534
TS5	-2791.705064	-2790.840598	-2790.974462

Int-IV	-2791.725907	-2790.860353	-2790.995748
TS3	-2673.764751	-2672.990972	-2673.118799
I-1a	-2673.808436	-2673.03298	-2673.160518
TS4	-2791.708282	-2790.845511	-2790.988237
Int-III	-2791.7207	-2790.856012	-2790.998692
Int-V	-2673.771094	-2672.995962	-2673.132969
Int-VI	-2673.804559	-2673.028514	-2673.158783
Int-VII	-2791.720619	-2790.856678	-2791.000897

	Single point		
	M06/SDD-6-311+G(d,p)/SMD(Toluene)		
	SCF energy (a.u.)	Enthalpy (a.u.)	Free energy (a.u.)
2o	-2746.552415	-2745.810073	-2745.933792
2o-I	-2868.423418	-2867.621461	-2867.736244
2e	-3471.706941	-3470.789352	-3470.937511
2d	-3545.470536	-3544.587104	-3544.734087
π -alkyne alkylidene complex of 2o	-2746.538088	-2745.796308	-2745.920071
π -alkyne alkylidene complex of 2d	-3545.448327	-3544.565477	-3544.709512
π -alkyne alkylidene complex of 2e	-3471.694179	-3470.777131	-3470.923379
π -alkyne alkylidene complex of 2o-I	-2868.404156	-2867.603074	-2867.71992
Propene	-117.837388	-117.752243	-117.782266
2a	-2672.789624	-2672.014028	-2672.141422
TS5	-2790.593244	-2789.728778	-2789.862642
Int-IV	-2790.611052	-2789.745498	-2789.880893
TS3	-2672.738266	-2671.964487	-2672.092314
I-1a	-2672.778526	-2672.00307	-2672.130608
TS4	-2790.609183	-2789.746412	-2789.889138
Int-III	-2790.625081	-2789.760393	-2789.903073
Int-V	-2672.74879	-2671.973658	-2672.110665
Int-VI	-2672.772808	-2671.996763	-2672.127032
Int-VII	-2790.610052	-2789.746111	-2789.89033

	Single point		
	M06/SDD-6-311+G(d,p)/SMD(CH ₂ Cl ₂)		
	SCF energy (a.u.)	Enthalpy (a.u.)	Free energy (a.u.)
2o	-2746.567899	-2745.825557	-2745.949276
2o-I	-2868.435306	-2867.633349	-2867.748132
2e	-3471.724157	-3470.806568	-3470.954727
2d	-3545.48913	-3544.605698	-3544.752681

π -alkyne alkylidene complex of 2o	-2746.554655	-2745.812875	-2745.936638
π -alkyne alkylidene complex of 2d	-3545.464937	-3544.582087	-3544.726122
π -alkyne alkylidene complex of 2e	-3471.711506	-3470.794458	-3470.940706
π -alkyne alkylidene complex of 2o-I	-2868.417941	-2867.616859	-2867.733705
2a	-2672.805303	-2672.029707	-2672.157101
I-1a	-2672.794394	-2672.018938	-2672.146476

8.4.8. X-ray crystallography data

All X-Ray data can be obtained free of charge from The Cambridge Crystallographic Data Centre via www.ccdc.cam.ac.uk/data_request/cif.

Summary of Xray-Crystallographic data

Crystal data	Compound 2d	Compound 2f	Compound 2h
CCDC Deposition	2050605	2050606	2050607
Chemical formula	C ₄₆ H ₄₉ Cl ₄ N ₃ O ₃ RuS	C ₄₉ H ₅₅ Cl ₄ N ₃ O ₄ RuS	C _{25.50} H ₃₃ ClN _{1.50} O _{2.50} Ru _{0.5} oS _{0.50}
M_r	966.81	1024.89	502.55
Crystal system, space group	Monoclinic, $P2_1/c$	Monoclinic, $P2_1/c$	Triclinic, $P-1$
Temperature (K)	293	293	296
a, b, c (Å)	14.273 (10), 12.308 (9), 25.627 (17)	11.3418 (8), 20.9073 (13), 20.3670 (14)	12.5227 (10), 14.9651 (12), 15.8339 (14)
α, β, γ (°)	94.284 (19)	98.0453 (17)	67.383 (2), 73.518 (2), 79.756 (2)
V (Å ³)	4490 (5)	4782.0 (6)	2618.6 (4)
Z	4	4	4
Radiation type	Mo $K\alpha$	Mo $K\alpha$	Mo $K\alpha$
μ (mm ⁻¹)	0.68	0.64	0.49
Crystal size (mm)	0.46 × 0.18 × 0.17	0.40 × 0.30 × 0.20	0.39 × 0.21 × 0.17
Diffractometer	CCD	CCD	CCD
Absorption correction	Multi-scan SADABS	Multi-scan SADABS	Multi-scan SADABS
T_{\min}, T_{\max}	0.746, 0.894	0.783, 0.882	0.833, 0.922
No. of measured, independent and observed [$I > 2\sigma(I)$] reflections	19865, 6969, 4358	74403, 6906, 5393	30387, 7863, 5684
R_{int}	0.070	0.075	0.064
$(\sin \vartheta/\lambda)_{\max}$ (Å ⁻¹)	0.575	0.560	0.570
$R[F^2 > 2\sigma(F^2)], wR(F^2), S$	0.048, 0.145, 0.85	0.067, 0.180, 1.30	0.074, 0.209, 1.33
No. of reflections	6969	6906	7863
No. of parameters	530	568	534
No. of restraints	0		12
H-atom treatment	H-atom parameters constrained	H-atom parameters constrained	H-atom parameters constrained
$\Delta\rho_{\max}, \Delta\rho_{\min}$ (e Å ⁻³)	0.33, -0.49	1.05, -0.92	1.01, -1.60
Absolute structure parameter	N/A	N/A	N/A

Crystal data	Compound 2j	Compound 2m	Compound 2r	Compound 2z
CCDC Deposition	2050608	2050609	2050611	2050610
Chemical formula	C ₅₀ H ₅₃ Cl ₄ FeN ₃ O ₃ Ru S	C ₁₀₈ H ₁₁₈ Cl ₅ N ₈ O ₁₀ Ru ₂ S ₄	C ₇₃ H ₇₉ Cl ₄ N ₄ O ₂ Ru ₂	C ₅₈ H ₅₉ Cl ₂ N ₃ O ₅ Ru S
M_r	1074.73	2195.73	1388.34	1082.11
Crystal system, space group	Triclinic, <i>P</i> -1	Monoclinic, <i>C2/c</i>	Triclinic, <i>P</i> -1	Monoclinic, <i>C2/c</i>
Temperature (K)	296	296	296	296
a, b, c (Å)	11.1746 (7), 11.2697 (7), 20.8743 (13)	28.2156 (17), 16.4438 (10), 26.215 (2)	8.4178 (6), 19.6542 (14), 20.8266 (15)	23.705 (2), 15.6917 (14), 29.659 (3)
α, β, γ (°)	86.946 (2), 80.392 (2), 67.197 (2)	90, 121.945 (2), 90	100.829 (2), 101.224 (2), 91.050 (2)	90, 99.820 (2), 90
V (Å ³)	2389.2 (3)	10321.1 (13)	3314.2 (4)	10870.6 (17)
Z	2	4	2	8
Radiation type	Mo $K\alpha$	Mo $K\alpha$	Mo $K\alpha$	Mo $K\alpha$
μ (mm ⁻¹)	0.93	0.54	0.67	0.48
Crystal size (mm)	0.40 × 0.40 × 0.30	0.50 × 0.40 × 0.30	0.35 × 0.30 × 0.30	0.49 × 0.33 × 0.11
Diffractometer	CCD	CCD	CCD	CCD
Absorption correction	Multi-scan SADABS	Multi-scan	Multi-scan	Multi-scan
T_{\min}, T_{\max}	0.707, 0.767	0.6506, 0.7451	0.8003, 0.8251	0.800, 0.950
No. of measured, independent and observed [$I > 2\sigma(I)$] reflections	46307, 8125, 7091	87594, 8908, 7001	50156, 10550, 8018	56757, 8135, 4670
R_{int}	0.027	0.045	0.043	0.172
$(\sin \vartheta/\lambda)_{\max}$ (Å ⁻¹)	0.589	0.591	0.577	0.569
$R[F^2 > 2\sigma(F^2)],$ $wR(F^2), S$	0.038, 0.140, 1.12	0.048, 0.168, 1.23	0.0397, 0.1325, 0.937	0.125, 0.286, 1.56
No. of reflections	8125	8908	10550	8135
No. of parameters	575	628	780	640
No. of restraints	0	2	0	0
H-atom treatment	H-atom parameters constrained	H-atom parameters constrained	H-atom parameters constrained	H atoms treated by onstrained refinement
$\Delta\rho_{\max}, \Delta\rho_{\min}$ (e Å ⁻³)	0.76, -0.76	1.17, -0.55	0.46, -0.48	1.21, -1.32
Absolute structure parameter	N/A	N/A	N/A	N/A

Crystal structure of **8-18d**

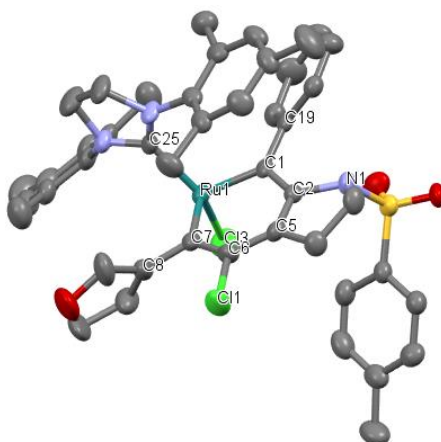


Fig. S9. Molecular Structure of **8-18d** (CCDC 2050605) showing 50% thermal probability ellipsoids. Hydrogen atoms are not shown for clarity. Selected bond distances [\AA]: Ru1-Cl3 2.315(2), Ru1-C1 1.908(5), Ru1-C7 1.917(5), Ru1-C25 2.050(5), Cl1-C6 1.779(5), C1-C2 1.412(7), C2-C5 1.387(7), C5-C6 1.396(7), C6-C7 1.382(8), C7-C8 1.478(7). Selected bond angles [$^\circ$]: Cl3-Ru1-C1 102.2(1), Cl3-Ru1-C7 105.4(2), Cl3-Ru1-C25 145.9(1), C1-Ru1-C7 97.2(2), C1-Ru1-C25 103.4(2), C7-Ru1-C25 93.3(2), Ru1-C1-C2 120.5(4), C1-C2-C5 126.0(4), C2-C5-C6 125.0(4), C5-C6-C7 125.2(5), Ru1-C7-C6 123.4(4), Ru1-C1-C19 118.3(3).

Crystal structure of **8-18f**

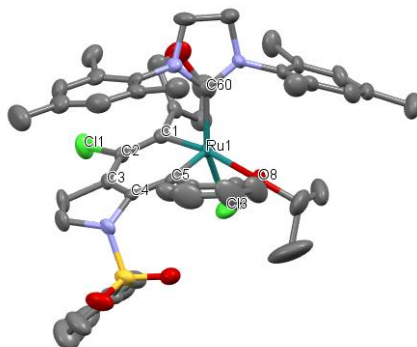


Fig. S10. Molecular Structure of **8-18f** (CCDC 2050606) showing 50% thermal probability ellipsoids. Hydrogen atoms are not shown for clarity. Selected bond distances [\AA]: Ru1-C1 1.919(6), Ru1-Cl3 2.374(2), Ru1-C5 1.886(6), Ru1-O8 2.376(4), Ru1-C60 2.052(6), C1-C2 1.365(8), C2-C3 1.388(9), C3-C4 1.377(9), C4-C5 1.389(8), Cl1-C2 1.769(6). Selected bond angles [$^\circ$]: C1-Ru1-Cl3 89.1(2), C1-Ru1-C5 97.0(2), C1-Ru1-C60 91.1(2), C5-Ru1-O8 77.3(2), C5-Ru1-C60 99.8(2), O8-Ru1-C60 96.9(2), Ru1-C1-C2 122.0(5), C1-C2-C3 125.9(6), C2-C3-C4 124.7(6), C3-C4-C5 125.8(5), Ru1-C5-C4 121.0(4).

Crystal structure of **8-18h**

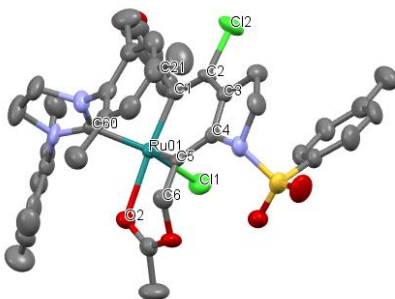


Fig. S11. Molecular Structure of **8-18h** (CCDC 2050607) showing 50% thermal probability ellipsoids. Hydrogen atoms are not shown for clarity. Selected bond distances [\AA]: Ru01-C1 1.951(7), Ru01-Cl1

2.376(2), Ru01-O2 2.269(5), Ru01-C5 1.877(6), Ru01-C60 2.030(7), C1-C2 1.382(8), C2-Cl2 1.781(8), C2-C3 1.39(1), C3-C4 1.39(1), C4-C5 1.423(8), Selected bond angles [°]: C1-Ru01-Cl1 92.1(2), C1-Ru01-C5 96.1(3), C1-Ru01-C60 94.8(3), O2-Ru01-C5 87.0(2), O2-Ru01-C60 91.5(2), C5-Ru01-C60 98.7(3), Ru01-C1-C2 123.0(5), C1-C2-C3 126.1(7), C2-C3-C4 124.1(6), C3-C4-C5 125.5(6), C4-C5-Ru01 123.1(5), C4-C5-C6 119.1(6).

Crystal structure of **8-18j**

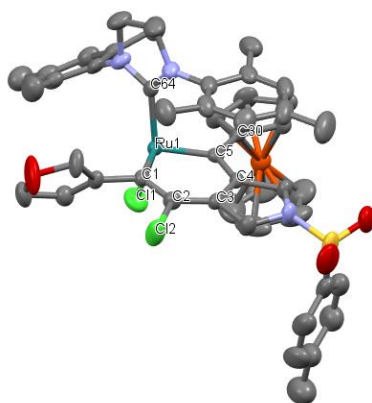


Fig. S12. Molecular Structure of **8-18j** (CCDC 2050608) showing 50% thermal probability ellipsoids. Hydrogen atoms are not shown for clarity. Selected bond distances [Å]: Ru1-C1 1.916(4), Ru1-Cl1 2.327(1), Ru1-C5 1.901(3), Ru1-C64 2.040(3), C1-C2 1.375(5), C2-Cl2 1.767(4), C2-C3 1.398(4), C3-C4 1.385(5), C4-C5 1.404(5), C50-C30 1.463(5). Selected bond angles [°]: C1-Ru1-Cl1 99.2(1), C1-Ru1-C5 97.5(1), C1-Ru1-C64 93.8(1), Cl1-Ru1-C5 97.5(1), Cl1-Ru1-C64 154.0(1), C5-Ru1-C64 99.6(1), Ru1-C1-C2 122.6(3), C1-C2-C3 125.8(3), C2-C3-C4 125.8(3), C3-C4-C5 124.6(3), C4-C5-Ru1 123.3(2), Ru1-C5-C30 113.3(2).

Crystal structure of 8-18m

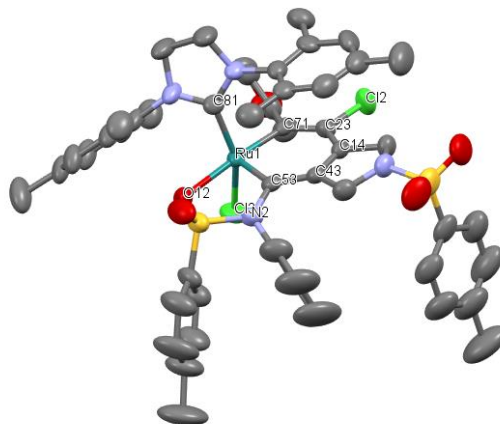


Fig. S13. Molecular Structure of **8-18m** (CCDC 2050609) showing 50% thermal probability ellipsoids. Hydrogen atoms are not shown for clarity. Selected bond distances [\AA]: Ru1-Cl3 2.388(1), Ru1-O12 2.2273(4), Ru1-C53 1.890(3), Ru1-C71 1.948(5), Ru1-C81 2.0838(3), C53-C43 1.425(6), C14-C43 1.374(6), C14-C23 1.396(4), C23-C71 1.376(6), C23-Cl2 1.769(5), C53-N2 1.424(5). Selected bond angles [$^\circ$]: Cl3-Ru1-O12 84.81(9), Cl3-Ru1-C53 102.2(1), Cl3-Ru1-C71 92.2(1), O12-Ru1-C53 83.2(1), C53-Ru1-C81 101.7(2), C71-Ru1-C81 94.5(2), C53-Ru1-C71 94.7(2), Ru1-C53-N2 116.9(3), Ru1-C53-C43 126.3(3), C53-C43-C14 128.4(3), C43-C14-C23 126.2(4), C14-C23-C71 125.4(4), Ru1-C71-C23 124.1(3).

Crystal structure of 8-18r

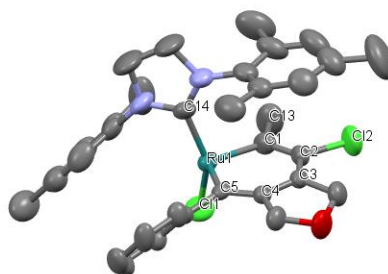


Fig. S14. Molecular Structure of **8-18r** (CCDC 2050611) showing 50% thermal probability ellipsoids. Hydrogen atoms are not shown for clarity. Selected bond distances [Å]: Ru1-Cl1 2.328(1), Ru1-C1 1.904(4), Ru1-C5 1.924(4), Ru1-C14 2.000(4), C2-Cl2 1.774(4), C1-C2 1.379(6), C2-C3 1.374(5), C3-C4 1.385(5), C4-C5 1.388(6), C1-C13 1.485(7). Selected bond angles [°]: Cl1-Ru1-C1 98.2(1), Cl1-Ru1-C5 112.7(1), Cl1-Ru1-C14 146.2(1), C1-Ru1-C5 96.0(2), C1-Ru1-C14 100.4(2), C5-Ru1-C14 93.1(2), Ru1-C1-C2 123.8(3), Ru1-C1-C13 114.6(4), C1-C2-C3 125.7(4), C2-C3-C4 125.7(4), C3-C4-C5 124.7(4), C4-C5-Ru1 123.7(5).

Crystal structure of 8-18z

Fig. S15. Molecular Structure of **8-18z** (CCDC 2050610) showing 50% thermal probability ellipsoids. Hydrogen atoms are not shown for clarity. Selected bond distances [Å]: Ru1-Cl1 2.313(3), Ru1-C1 1.89(1), Ru1-C5 1.91(1), Ru1-C60 1.988(9), C1-C2 1.36(2), C2-C3 1.35(2), C3-C4 1.42(1), C4-C5 1.37(2), C5-C6 1.43(2), C2-Cl2 1.80(1). Selected bond angles [°]: Cl1-Ru1-C1 106.3(3), Cl1-Ru1-C5 104.1(3), Cl1-Ru1-C60 147.5(3), C1-Ru1-C5 93.8(5), C1-Ru1-C60 94.2(4), C5-Ru1-C60 99.3(4), Ru1-C1-C2 124.4(8), C1-C2-C3 128(1), C2-C3-C4 122(1), C3-C4-C5 124(1), C4-C5-Ru1 126.1(8), C6-C5-Ru1 114.5(8).

8.5. Note

A part of this work was performed by Mr. Siyuan Su. The computational study was done by Mr. Yu Zhang and Prof. Peng Liu at University of Pittsburgh. The X-ray crystallographic data was obtained by Prof. Donald J. Wink at University of Illinois, Chicago.

8.6. References

1. (a) Gribble, G. W.; Joule, J. *Progress in heterocyclic chemistry*; Elsevier: 2009. (b) Taylor, A. P.; Robinson, R. P.; Fobian, Y. M.; Blakemore, D. C.; Jones, L. H.; Fadeyi, O. *Org. Biomol. Chem.* 2016, *14*, 6611. (c) Joule, J. A.; Mills, K.; Smith, G. F. *Heterocyclic chemistry*; CRC Press: 2020.
2. (a) Bleeke, J. R. *Chem. Rev.* **2001**, *101*, 1205. (b) Landorf, C. W.; Haley, M. M. *Angew. Chem., Int. Ed.* **2006**, *45*, 3914. (c) Wright, L. J. *Dalton Trans* **2006**, 1821. (d) Dalebrook, A. F.; Wright, L. J. *Adv. Organomet. Chem.* **2012**, *60*, 93. (e) Chen, J.; Jia, G. *Coord. Chem. Rev.* **2013**, *257*, 2491. (f) Frogley, B. J.; Wright, L. J. *Coord. Chem. Rev.* **2014**, *270–271*, 151.
3. Thorn, D. L.; Hoffmann, R. *Nouv. J. Chim.* **1979**, *3*, 39.
4. Elliott, G. P.; Roper, W. R.; Waters, J. M. *J. Chem. Soc., Chem. Commun.* **1982**, *14*, 811.
5. (a) Cao, X.-Y.; Zhao, Q.; Lin, Z.; Xia, H. *Acc. Chem. Res.* **2014**, *47*, 341. (b) Wright, L. J. *Metallabenzenes: An Expert View*; John Wiley & Sons Ltd: Hoboken, NJ, 2017. (c) Frogley, B. J.; Wright, L. J. *Chem. - Eur. J.* **2018**, *24*, 2025. (d) Chen, D.; Hua, Y.; Xia, H. *Chem. Rev.* **2020**, *120*, 12994.
6. (a) Fernández, I.; Frenking, G. *Chem. - Eur. J.* **2007**, *13*, 5873. (b) Fernández, I.; Frenking, G.; Merino, G. *Chem. Soc. Rev.* **2015**, *44*, 6452. (c) Chen, D.; Xie, Q.; Zhu, J. *Acc. Chem. Res.* **2019**, *52*, 1449.

7. Iron, M. A.; Lucassen, A. C. B.; Cohen, H.; van der Boom, M. E.; Martin, J.M. L. *J. Am. Chem. Soc.* **2004**, *126*, 11699.
8. Gilbertson, R. D.; Weakley, T. J. R.; Haley, M. M. *J. Am. Chem. Soc.* **1999**, *121*, 2597.
9. (a) Jacob, V.; Weakley, T. J. R.; Haley, M. M. *Angew. Chem., Int. Ed.* **2002**, *41*, 3470. (b) Jacob, V.; Landorf, C. W.; Zakharov, L. N.; Weakley, T. J. R.; Haley, M. M. *Organometallics* **2009**, *28*, 5183.
10. (a) Bleeker, J. R.; Xie, Y. F.; Peng, W. J.; Chiang, M. *J. Am. Chem. Soc.* **1989**, *111*, 4118. (b) Bleeker, J. R.; Behm, R.; Xie, Y. F.; Chiang, M.; Robinson, K. D.; Beatty, A. M. *Organometallics* **1997**, *16*, 606.
11. Alvarez, A.; Paneque, M.; Poveda, M. L.; Rendón, N. *Angew. Chem., Int. Ed.* **2006**, *45*, 474.
12. Poon, K. C.; Liu, L.; Guo, T.; Li, J.; Sung, H. H. Y.; Williams, I. D.; Lin, Z.; Jia, G. *Angew. Chem., Int. Ed.* **2010**, *49*, 2759.
13. (a) Zhang, H.; Xia, H.; He, G.; Wen, T. B.; Gong, L.; Jia, G. *Angew. Chem., Int. Ed.* **2006**, *45*, 2920. (b) Zhang, H.; Feng, L.; Gong, L.; Wu, L.; He, G.; Wen, T.; Yang, F.; Xia, H. *Organometallics* **2007**, *26*, 2705.
14. Schrock, R. R.; Pedersen, S. F.; Churchill, M. R.; Ziller, J. W. *Organometallics* **1984**, *3*, 1574.
15. (a) Straub, B. F. *Angew. Chem., Int. Ed.* **2005**, *44*, 5974. (b) Vougioukalakis, G. C.; Grubbs, R. H. *Chem. Rev.* **2010**, *110*, 1746. (c) Ogbay, O. M.; Warner, N. C.; O'Leary, D. J.; Grubbs, R. H. *Chem. Soc. Rev.* **2018**, *47*, 4510.
16. (a) Garber, S. B.; Kingsbury, J. S.; Gray, B. L.; Hoveyda, A. H. *J. Am. Chem. Soc.* **2000**, *122*, 8168. (b) Gessler, S.; Randl, S.; Blechert, S. *Tetrahedron Lett.* **2000**, *41*, 9973.

17. (a) Barbasiewicz, M.; Grudzień, K.; Malinska, M. *Organometallics* **2012**, *31*, 3171. (b) Grudzień, K.; Malinska, M.; Barbasiewicz, M. *Organometallics* **2012**, *31*, 3636.
18. (a) Xia, H.; He, G.; Zhang, H.; Wen, T. B.; Sung, H. H. Y.; Williams, I. D.; Jia, G. *J. Am. Chem. Soc.* **2004**, *126*, 6862. (b) Gong, L.; Chen, Z.; Lin, Y.; He, X.; Wen, T. B.; Xu, X.; Xia, H. *Chem. - Eur. J.* **2009**, *15*, 6258. (c) Liu, B.; Xie, H.; Wang, H.; Wu, L.; Zhao, Q.; Chen, J.; Wen, T. B.; Cao, Z.; Xia, H. *Angew. Chem., Int. Ed.* **2009**, *48*, 5461. (d) Ishii, T.; Suzuki, K.; Nakamura, T.; Yamashita, M. *J. Am. Chem. Soc.* **2016**, *138*, 12787.
19. Albright, T. A.; Burdett, J. K.; Whangbo, M. H. The Isolobal Analogy. In *Orbital interactions in chemistry*, 2nd ed.; John Wiley & Sons Ltd: Hoboken, NJ, 2013; pp 616–652.
20. (a) Yamazaki, H.; Aoki, K. *J. Organomet. Chem.* **1976**, *122*, C54. (b) Yang, J.; Jones, W. M.; Dixon, J. K.; Allison, N. T. *J. Am. Chem. Soc.* **1995**, *117*, 9776. (c) Clark, G. R.; O’Neale, T. R.; Roper, W. R.; Tonei, D. M.; Wright, L. J. *Organometallics* **2009**, *28*, 567. (d) Lin, R.; Zhang, H.; Li, S.; Wang, J.; Xia, H. *Chem. - Eur. J.* **2011**, *17*, 4223. (e) Zhuo, Q.; Chen, Z.; Yang, Y.; Zhou, X.; Han, F.; Zhu, J.; Zhang, H.; Xia, H. *Dalton Trans* **2016**, *45*, 913. (d) Wdowik, T.; Samojłowicz, C.; Jawiczuk, M.; Malińska, M.; Woźniak, K.; Grela, K. *Chem. Commun.* **2013**, *49*, 674.
21. (a) Diver, S. T.; Giessert, A. J. *Chem. Rev.* **2004**, *104*, 1317. (b) Diver, S. T. *Coord. Chem. Rev.* **2007**, *251*, 671. (c) Hansen, E. C.; Lee, D. *Acc. Chem. Res.* **2006**, *39*, 509. (d) Li, J.; Lee, D. *Eur. J. Org. Chem.* **2011**, *2011*, 4269.
22. Kim, M.; Lee, D. *J. Am. Chem. Soc.* **2005**, *127*, 18024. (b) Kim, M.; Miller, R. L.; Lee, D. *J. Am. Chem. Soc.* **2005**, *127*, 12818. (c) Lee, D.; Kim, M. *Org. Biomol. Chem.* **2007**, *5*, 3418. (d) Kang, C.; Park, H.; Lee, J. K.; Choi, T. L. *J. Am. Chem. Soc.* **2017**, *139*, 11309.
23. (a) Benitez, D.; Tkatchouk, E.; Goddard III, W. A. *Chem. Commun.* **2008**, *46*, 6194. (b) Diesendruck, C. E.; Tzur, E.; Ben-Asuly, A.; Goldberg, I.; Straub, B. F.; Lemcoff, N. G. *Inorg. Chem.* **2009**, *48*, 10819. (c) Pump, E.; Poater, A.; Zirngast, M.; Torvisco, A.; Fischer, R.; Cavallo,

- L.; Slugovc, C. *Organometallics* **2012**, *33*, 2806. (d) Pump, E.; Cavallo, L.; Slugovc, C. *Monatsh. Chem.* **2015**, *146*, 1131.
24. Wang, K. P.; Yun, S. Y.; Lee, D.; Wink, D. J. *J. Am. Chem. Soc.* **2009**, *131*, 15114.
25. Baya, M.; Esteruelas, M. A.; Gonzalez, A. I.; Lo'pez, A. M.; Oñate, E. *Organometallics* **2005**, *24*, 1225.
26. (a) Jung, M. E.; Piizzi, G. *Chem. Rev.* **2005**, *105*, 1735. (b) Forbes, M. D.; Patton, J. T.; Myers, T. L.; Maynard, H. D.; Smith Jr, D. W.; Schulz, G. R.; Wagener, K. B. *J. Am. Chem. Soc.* **1992**, *114*, 10978. (c) Urbina-Blanco, C. A.; Skibiński, M.; O'Hagan, D.; Nolan, S. P. *Chem. Commun.* **2013**, *49*, 7201. (d) Sabbasani, V. R.; Gupta, S.; Yun, S. Y.; Lee, D. *Org. Chem. Front.* **2018**, *5*, 1532. (e) Gupta, S.; Sabbasani, V. R.; Su, S.; Wink, D. J. Lee, D. *ACS Catal.* **2021**, *11*, 1977.
27. Sanford, M. S.; Henling, L. M.; Day, M. W.; Grubbs, R. H. *Angew. Chem., Int. Ed.* **2000**, *39*, 3451.
28. (a) Fürstner, A.; Thiel, O. R.; Lehmann, C. W. *Organometallics* **2002**, *21*, 331. (b) Wakamatsu, H.; Blechert, S. *Angew. Chem., Int. Ed.* **2002**, *41*, 794. (c) Grela, K.; Harutyunyan, S.; Michrowska, A. *Angew. Chem., Int. Ed.* **2002**, *114*, 4210. (d) Fürstner, A.; Davies, P. W.; Lehmann, C. W. *Organometallics* **2005**, *24*, 4065.
29. Slugovc, C.; Perner, B.; Stelzer, F.; Mereiter, K. *Organometallics* **2004**, *23*, 3622.
30. Sabbasani, V. R.; Yun, S. Y.; Lee, D. *Org. Chem. Front.* **2016**, *3*, 939.
31. Villar, H.; Frings, M.; Bolm, C. *Chem. Soc. Rev.* **2007**, *36*, 55.
32. Lozano-Vila, A. M.; Monsaert, S.; Bajek, A.; Verpoort, F. *Chem. Rev.* **2010**, *110*, 4865.
33. Szadkowska, M.; Zukowska, K.; Pazio, A. E.; Wozniak, K.; Kadyrov, R.; Grela, K. *Organometallics* **2011**, *30*, 1130.

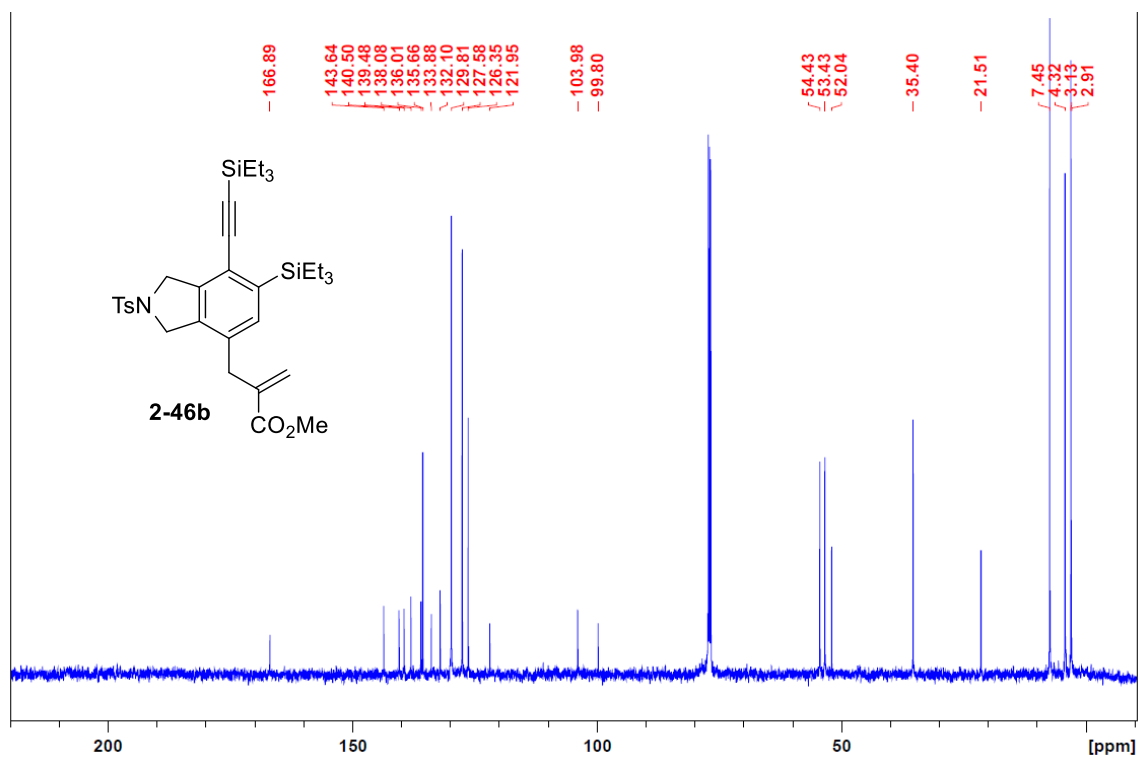
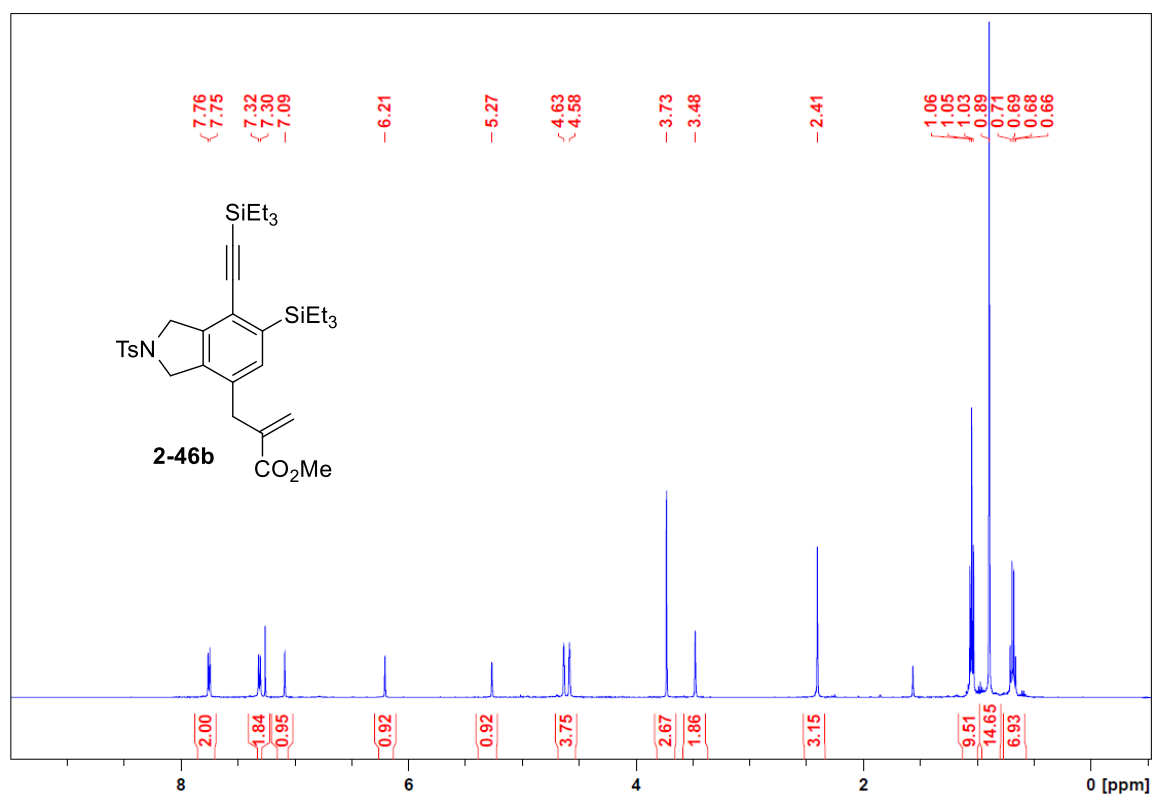
34. (a) Schleyer, P. v. R.; Maerker, C.; Dransfeld, A.; Jiao, H.; Hommes, N. J. R. v. E. *J. Am. Chem. Soc.* **1996**, *118*, 6317. (b) Chen, Z.; Wannere, C. S.; Corminboeuf, C.; Puchta, R.; Schleyer, P. v. R. *Chem. Rev.* **2005**, *105*, 3842. (c) Fallah-Bagher-Shaidaei, H.; Wannere, C. S.; Corminboeuf, C.; Puchta, R.; Schleyer, P. v. R. *Org. Lett.* **2006**, *8*, 863.
35. (a) Lee, H. Y.; Kim, B. G.; Snapper, M. L. *Org. Lett.* **2003**, *5*, 1855. (b) Kim, M.; Park, S.; Maifeld, S. A.; Lee, D. *J. Am. Chem. Soc.* **2004**, *126*, 10242. (c) Yun, S. Y.; Wang, K. P.; Kim, M.; Lee, D. *J. Am. Chem. Soc.* **2010**, *132*, 8840.
36. (a) Hoye, T. R.; Jeffrey, C. S.; Tennakoon, M. A.; Wang, J.; Zhao, H. *J. Am. Chem. Soc.* **2004**, *126*, 10210. (b) Hansen, E. C.; Lee, D. *Org. Lett.* **2004**, *6*, 2035.
37. Yun, S. Y.; Kim, M.; Lee, D.; Wink, D. J. *J. Am. Chem. Soc.* **2009**, *131*, 24.
38. Hitt, D. M.; O'Connor, M. J. *Chem. Rev.* **2011**, *111*, 7904.
39. (a) Iron, M. A.; Martin, J. M.; Van der Boom, M. E. *J. Am. Chem. Soc.* **2003**, *125*, 13020. (b) Fan, J.; Wang, X.; Zhu, J. *Organometallics* **2014**, *33*, 2336. (c) Zhu, C.; Zhou, X.; Xing, H.; An, K.; Zhu, J.; Xia, H. *Angew. Chem., Int. Ed.* **2015**, *54*, 3102.
40. Zhao, Y.; Truhlar, D. G. *Theor. Chem. Acc.* **2007**, *120*, 215.
41. Roy, L. E.; Hay, P. J.; Martin, R. L. *J. Chem. Theory Comput.* **2008**, *4*, 1029.
42. Marenich, A. V.; Cramer, C. J.; Truhlar, D. G. *J. Phys. Chem. B* **2009**, *113*, 6378.
43. (a) Becke, A. D. *J. Chem. Phys.* **1993**, *98*, 5648. (b) Lee, C.; Yang, W.; Parr, R. G. *Phys. Rev. B: Condens. Matter Mater. Phys.* **1988**, *37*, 785. (c) Grimme, S.; Ehrlich, S.; Goerigk, L. *J. Comput. Chem.* **2011**, *32*, 1456.
44. Trost, B. M.; Pinkerton, A. B. *J. Am. Chem. Soc.* **1999**, *121*, 1988.

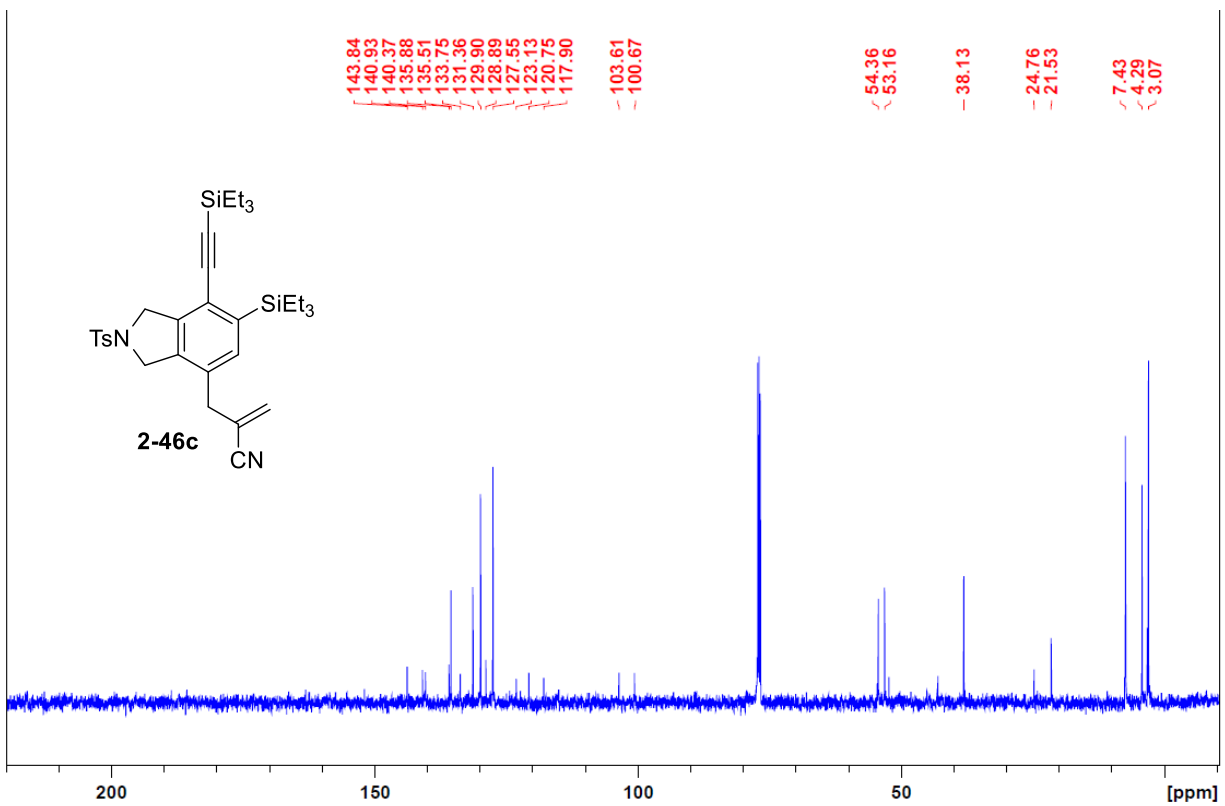
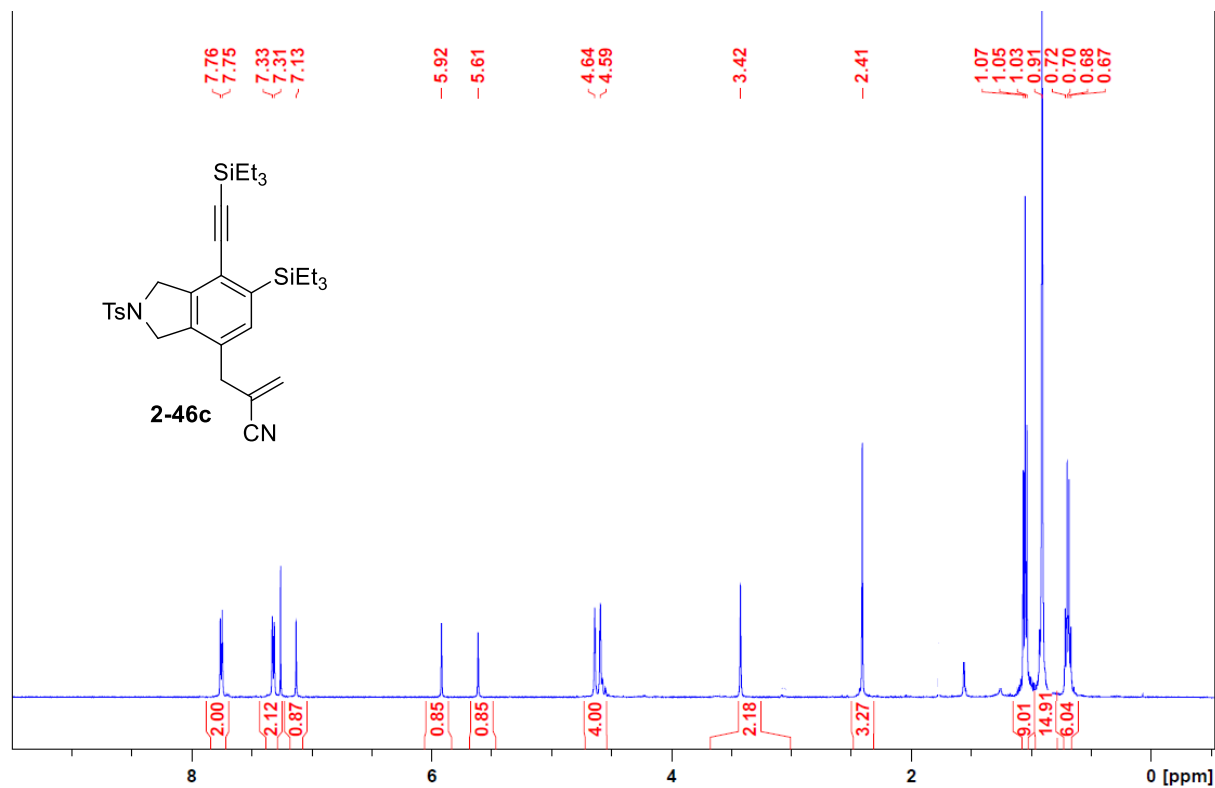
45. (a) Zimmerman, P. M. *Journal of Chemical Physics*. **2013**, *138*, 184102. (b) Zimmerman, P. M. *J. Chem. Theory Comput.* **2013**, *9*, 3043. (c) Zimmerman, P. M. *Journal of Computational Chemistry* **2015**, *36*, 601. (d) Jafari, M.; Zimmerman, P. M. *Journal of Computational Chemistry* **2017**, *38*, 645. (e) Roessler, A. G.; Zimmerman, P. M. *J. Phys. Chem. C* **2018**, *122*, 6996. (f) Aldaz, C.; Kammeraad, J.; Zimmerman, P. M. *Phys. Chem. Chem. Phys.* **2018**, *20*, 27394.
46. (a) Hejl, A.; Day, M. W.; Grubbs, R. H. *Organometallics* **2006**, *25*, 6149. (b) Kost, T.; Sigalov, M.; Goldberg, I.; Ben-Asuly, A.; Lemcoff, N. G. *J. Organomet. Chem.* **2008**, *693*, 2200. (c) Ben-Asuly, A.; Tzur, E.; Diesendruck, C. E.; Sigalov, M.; Goldberg, I.; Lemcoff, N. G. *Organometallics* **2008**, *27*, 811. (d) Monsaert, S.; Vila, A. L.; Drozdak, R.; Van Der Voort, P.; Verpoort, F. *Chem. Soc. Rev.* **2009**, *38*, 3360. (e) Ginzburg, Y.; Anaby, A.; Vidavsky, Y.; Diesendruck, C. E.; Ben-Asuly, A.; Goldberg, I.; Lemcoff, N. G. *Organometallics* **2011**, *30*, 3430.
47. Li, J.; Lee, D. *Chem. Sci.* **2012**, *3*, 3296.
48. (a) Sundararaju, B.; Fürstner, A. *Angew. Chem., Int. Ed.* **2013**, *52*, 14050. (b) Song, L. J.; Wang, T.; Zhang, X.; Chung, L. W.; Wu, Y. D. *ACS Catal.* **2017**, *7*, 1361.
49. (a) Wang, X.; Chakrapani, H.; Madine, J. W.; Keyerleber, M. A.; Widenhoefer, R. A. *J. Org. Chem.* **2002**, *67*, 2778. (b) Chakrapani, H.; Liu, C.; Widenhoefer, R. A. *Org. Lett.* **2003**, *5*, 157.
50. (a) Kingsbury, J. S.; Harrity, J. P.; Bonitatebus, P. J.; Hoveyda, A. H. *J. Am. Chem. Soc.* **1999**, *121*, 791. (b) Jafarpour, L.; Nolan, S. P. *Org. Lett.* **2000**, *2*, 4075. (c) Connon, S. J.; Dunne, A. M.; Blechert, S. *Angew. Chem., Int. Ed.* **2002**, *41*, 3835. (d) Van Veldhuizen, J. J.; Garber, S. B.; Kingsbury, J. S.; Hoveyda, A. H. *J. Am. Chem. Soc.* **2002**, *124*, 4954.
51. Opstal, T.; Verpoort, F. *J. Mol. Catal. A: Chem.* **2003**, *200*, 49. (b) Audic, N.; Clavier H.; Mauduit, M.; Guillemin, J. C. *J. Am. Chem. Soc.* **2003**, *125*, 9248. (c) Occhipinti, G.; Koudriavtsev, V.; Törnroos, K. W.; Jensen, V. R. *Dalton Trans* **2014**, *43*, 11106.

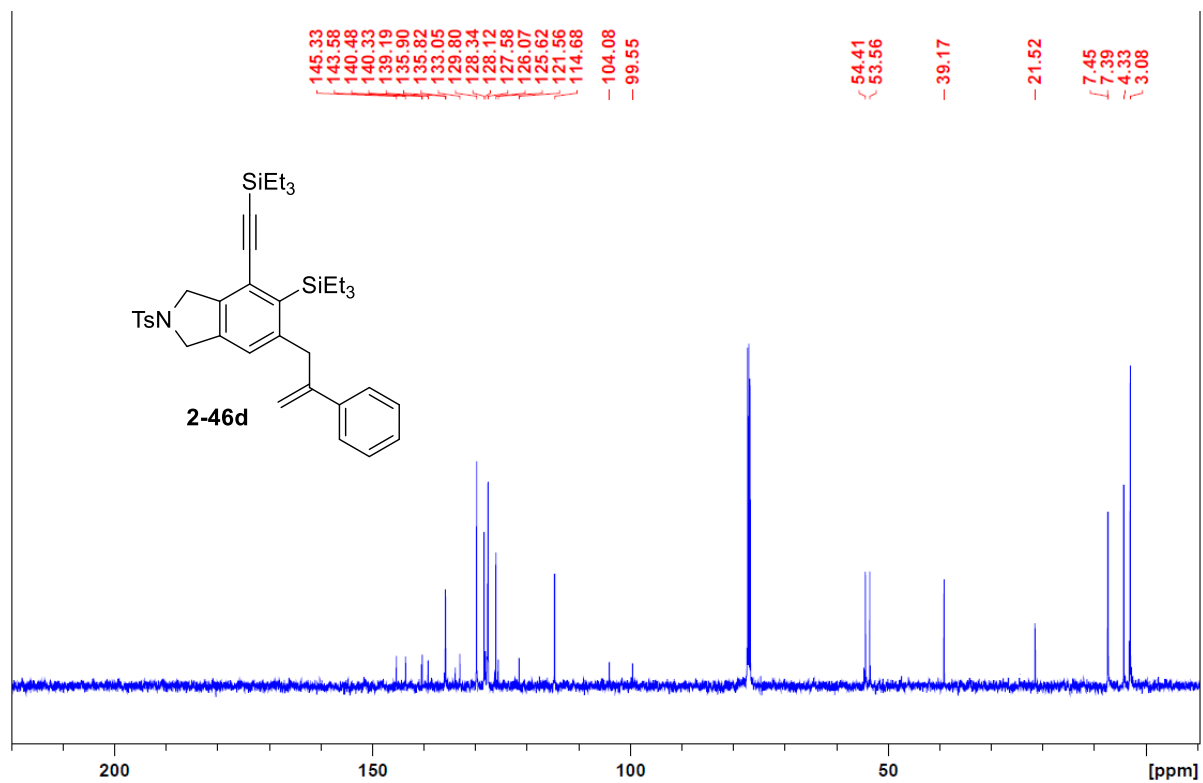
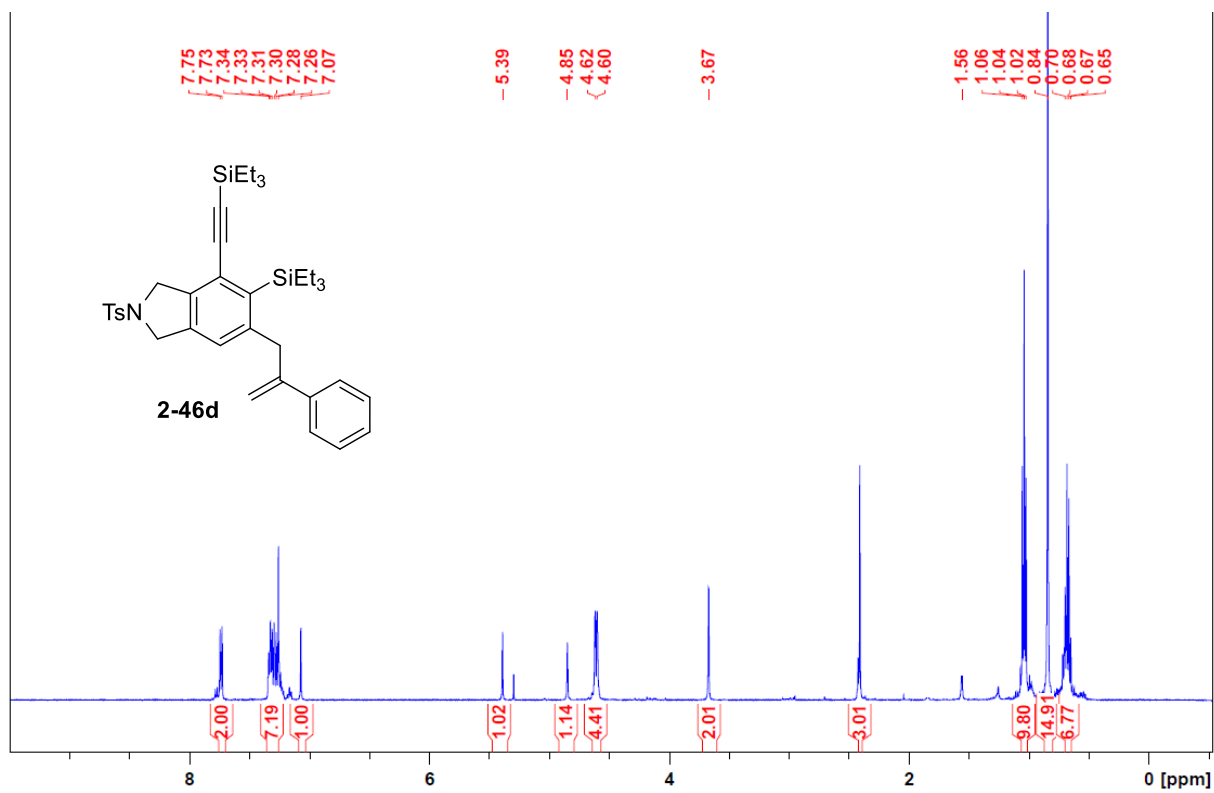
52. Cadiot, P.; Chodkiewicz, W. in *Chemistry of Acetylenes*, H. G. Viehe, Ed. (Marcel Dekker, New York, 1969), pp. 597.
53. Mitsunobu, O. *Synthesis* **1981**, *1*, 1.
54. Sonogashira, K. *J. Organomet. Chem.* **2002**, *653*, 46.
55. Ratovelomanana, V.; Rollin, Y.; Gébéhenne, C.; Gosmini, C.; Périchon, J. *Tetrahedron Lett.* **1994**, *35*, 4777.
56. Marshall, J. A.; Bartley, G. S. *J. Org. Chem.* **1994**, *59*, 7169.
57. Zhang, Y.; Hsung, R. P.; Tracey, M. R.; Kurtz, K. C.; Vera, E. L. *Org. Lett.* **2004**, *6*, 1151.
58. Alfonzo, E.; Alfonso, F. S.; Beeler, A. B. *Org. Lett.* **2017**, *19*, 2989.
59. Dyadchenko, V. P.; Dyadchenko, M. A.; Okulov, V. N.; Lemenovskii, D. A. *J. Organomet. Chem.* **2011**, *696*, 468.
60. Kern, N.; Blanc, A.; Miaskiewicz, S.; Robinette, M.; Meibel, J. M.; Pale, P. *J. Org. Chem.* **2012**, *77*, 4323.
61. Bernar, I.; Blanco-Ania, D.; Stok, S. J.; Sotorríos, L. Gómez-Bengoa, E.; Rutjes, F. P. *Eur. J. Org. Chem.* **2018**, *2018*, 5435.
62. Karmakar, R.; Yun, S. Y.; Chen, J.; Xia, Y.; Lee, D. *Angew. Chem., Int. Ed.* **2015**, *54*, 6582.
63. Hayashi, Y.; Shoji, M.; Ishikawa, H.; Yamaguchi, H.; Tamura, T.; Imai, T.; Nishigaya, Y. Takabe, K.; Kakeya, H.; Osada, H. *Angew. Chem., Int. Ed.* **2008**, *47*, 6657.
64. Salem, B.; Delort, E.; Klotz, P.; Suffert, J. *Org. Lett.* **2003**, *5*, 2307.
65. Ritter, T.; Hejl, A.; Wenzel, A. G.; Funk, T. W.; Grubbs, R. H. *Organometallics* **2006**, *25*, 5740.
66. Henderson, W. H.; Check, C. T.; Proust, N.; Stambuli, J. P. *Org. Lett.* **2010**, *12*, 824.

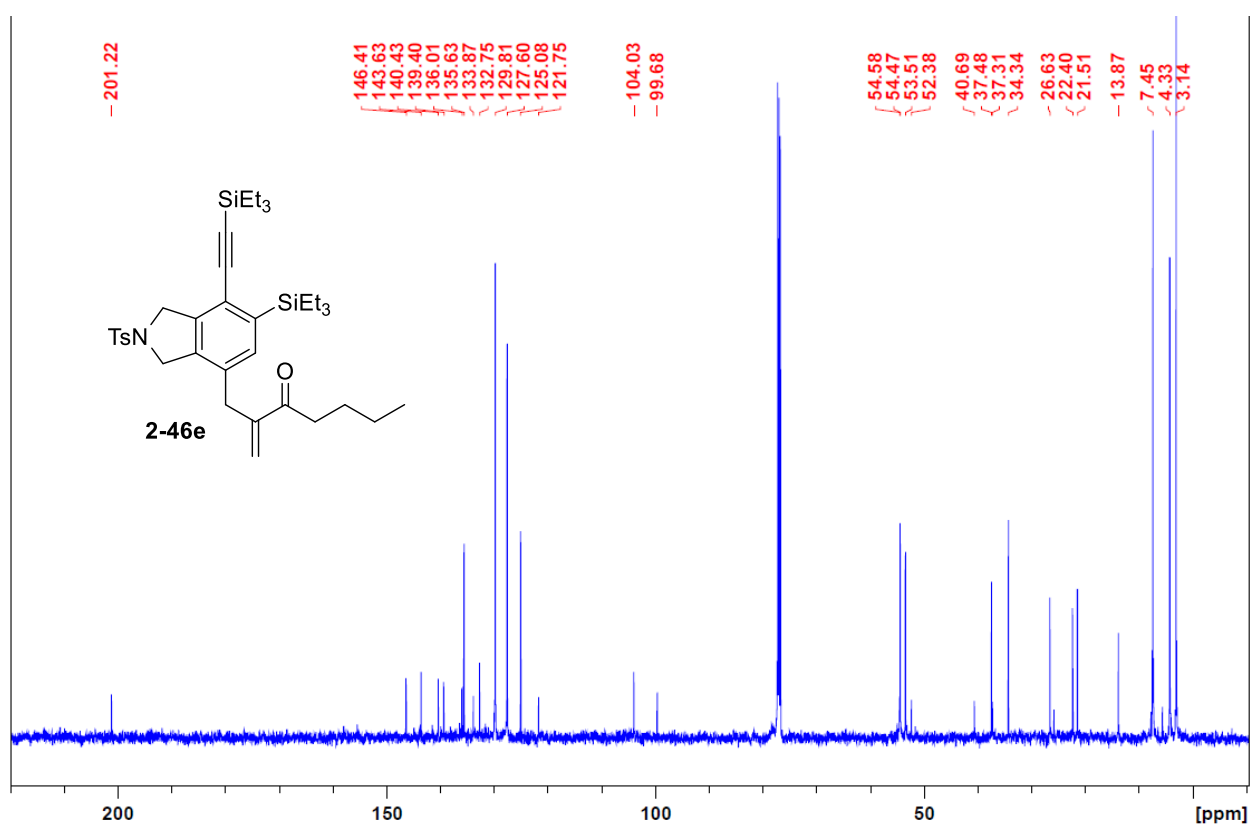
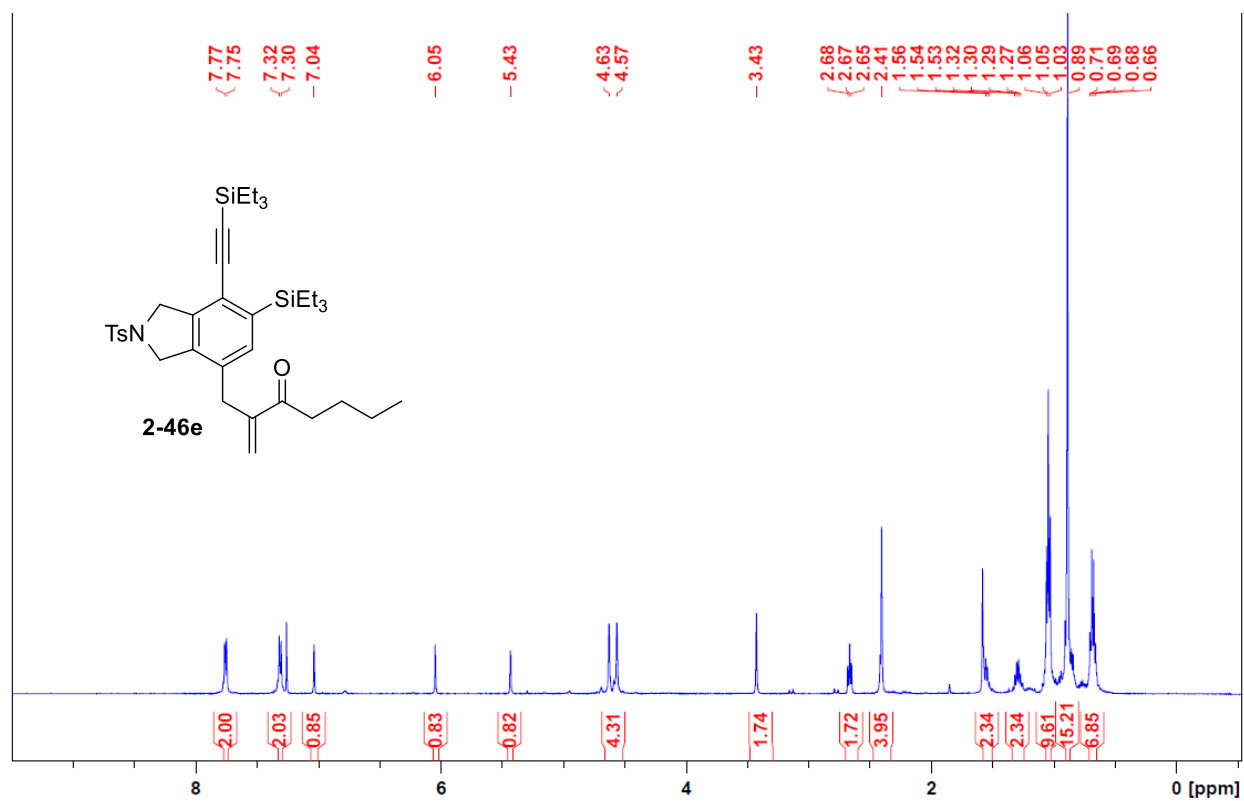
67. Mori, M.; Sakakibara, N.; Kinoshita, A. *J. Org. Chem.* **1998**, *63*, 6082.
68. Kan, T.; Kawamoto, Y.; Asakawa, T.; Furuta, T.; Fukuyama, T. *Org. Lett.* **2008**, *10*, 169.
69. Dinger, M. B.; Mol, J. C. *Eur. J. Inorg. Chem.* **2003**, *2003*, 2827.
70. Hong, S. H.; Wenzel, A. G.; Salguero, T. T.; Day, M. W.; Grubbs, R. H. *J. Am. Chem. Soc.* **2007**, *129*, 7961.
71. Frisch, M. J *et al.* Gaussian 16 Rev. B.01, Wallingford, CT, 2016.

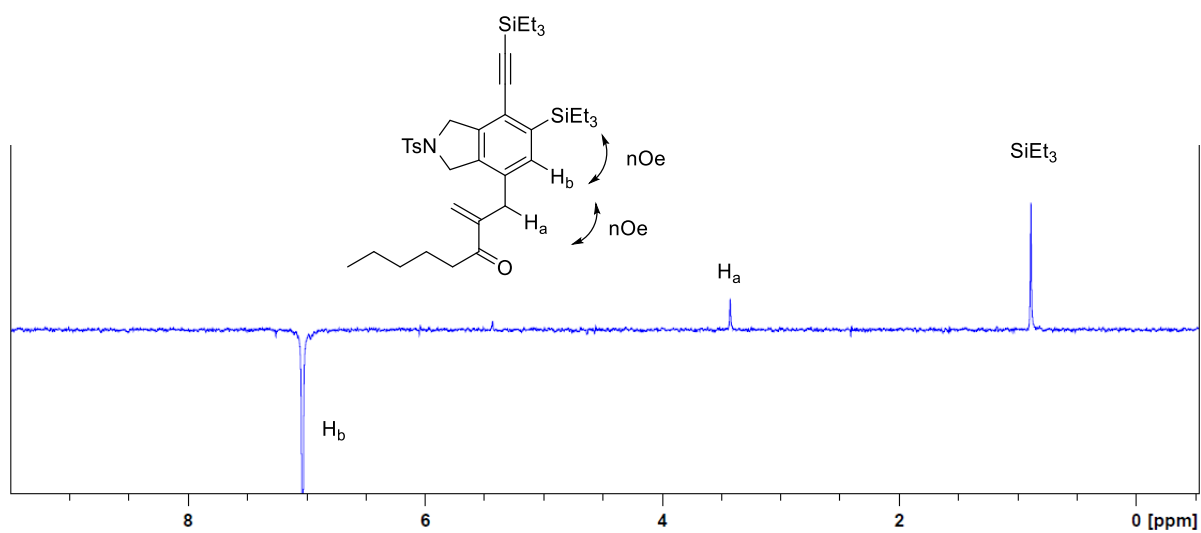
Appendix I
Selected NMR Spectra for Chapter 2

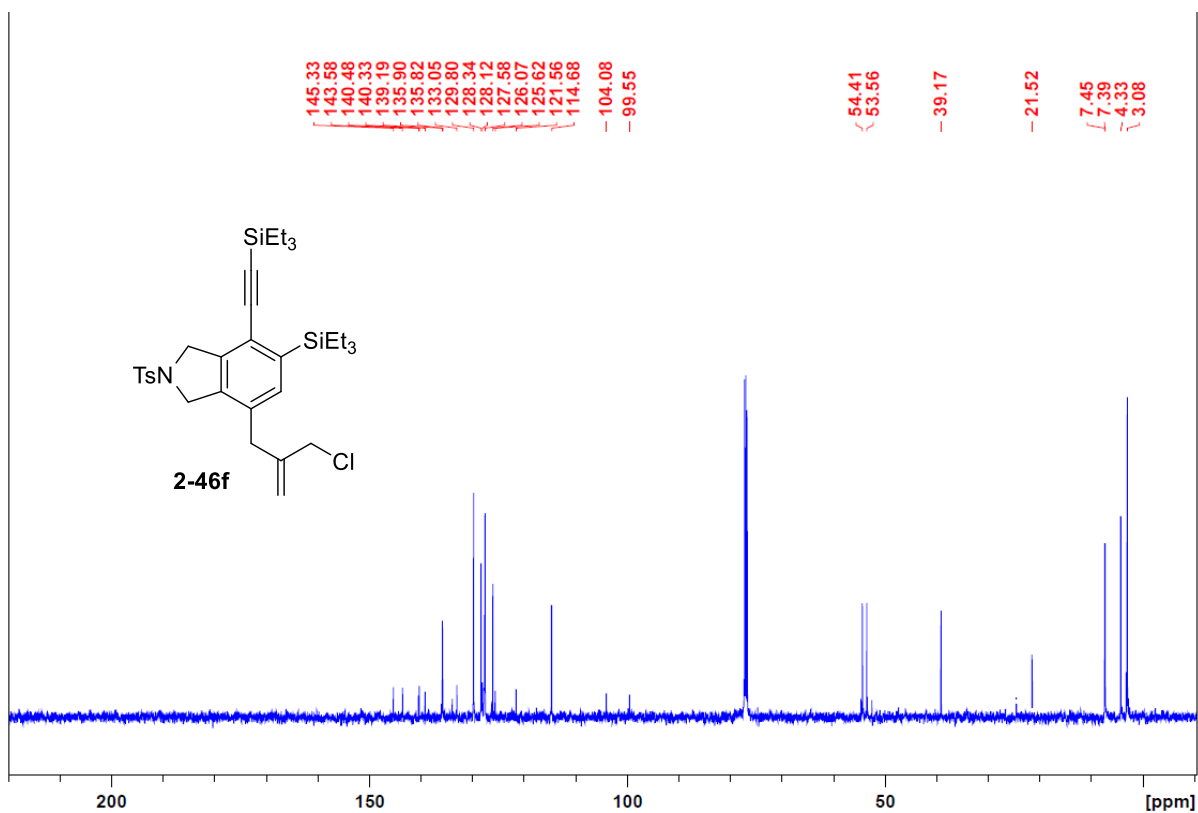
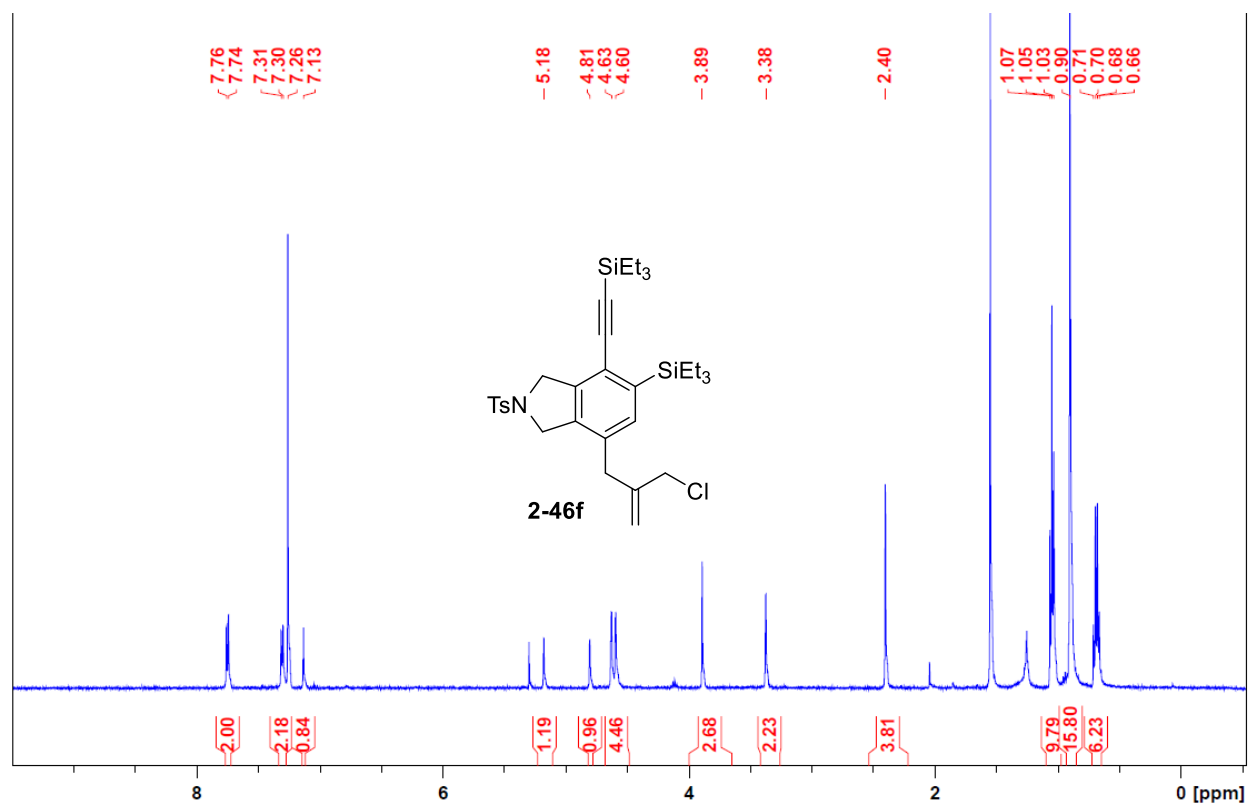


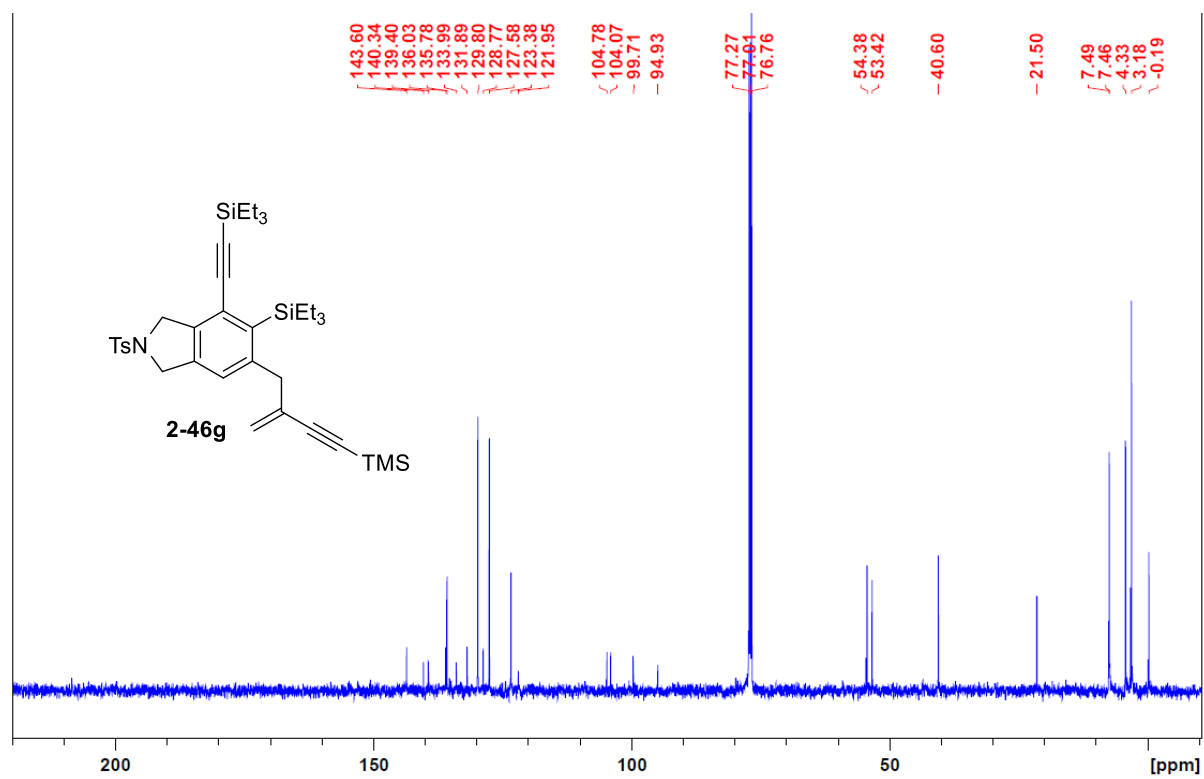
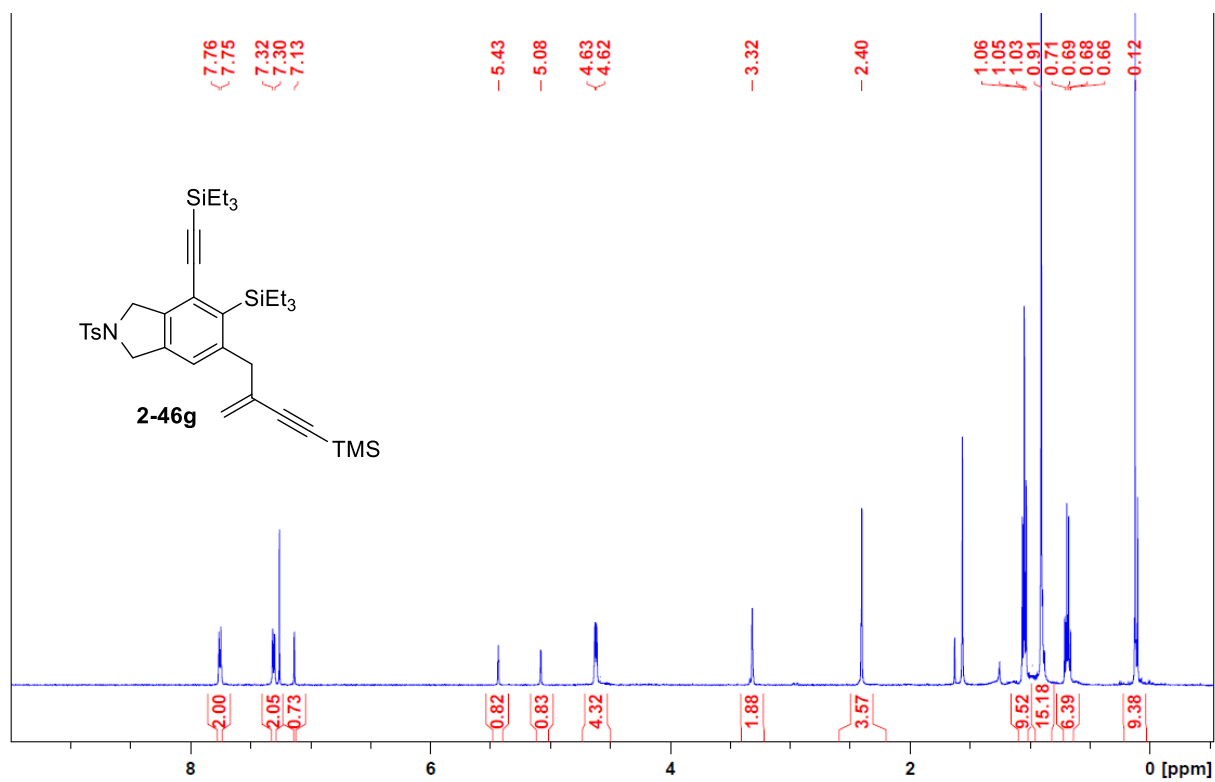


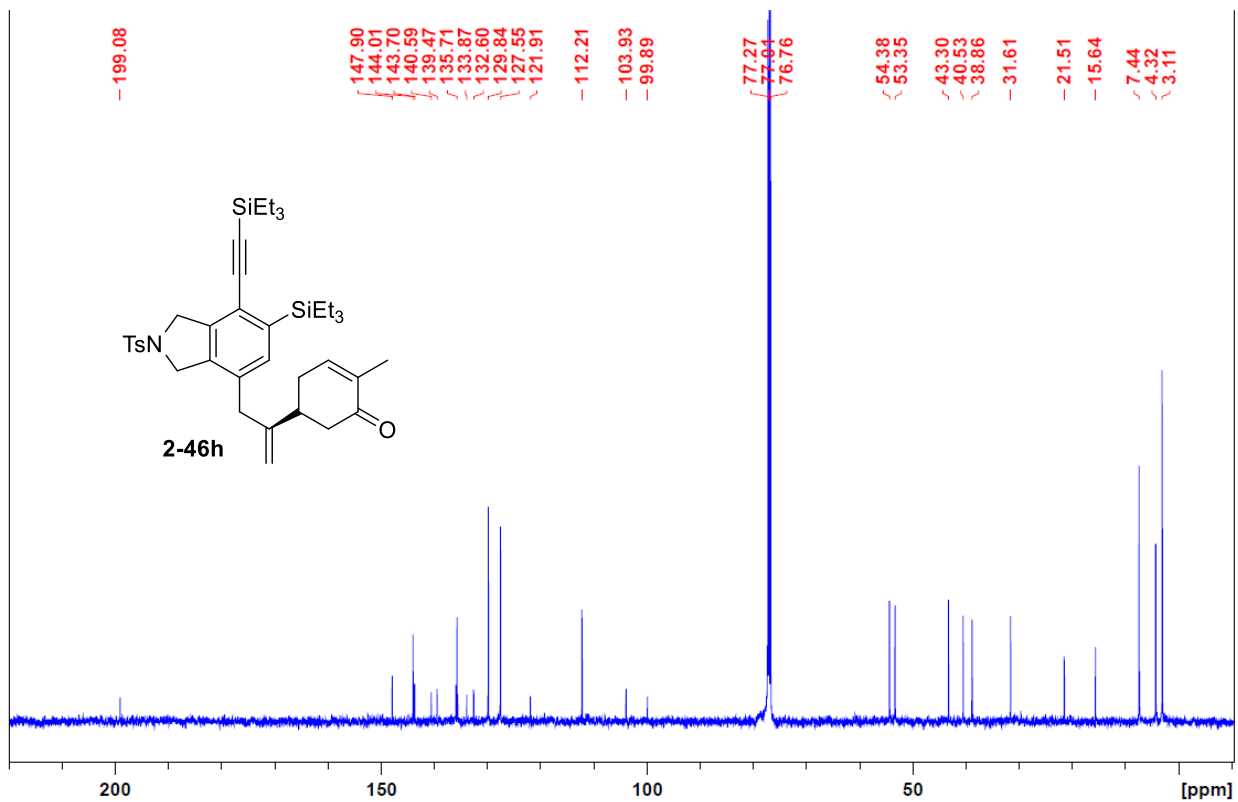
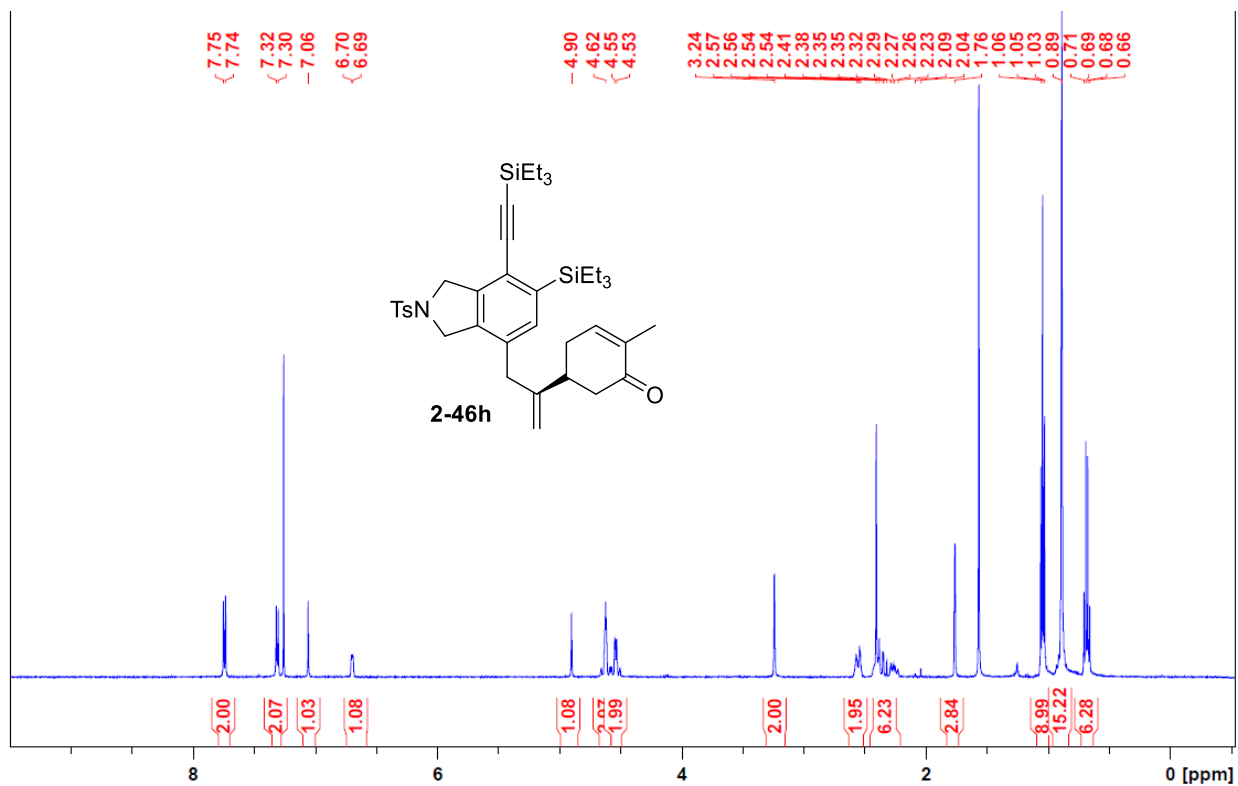


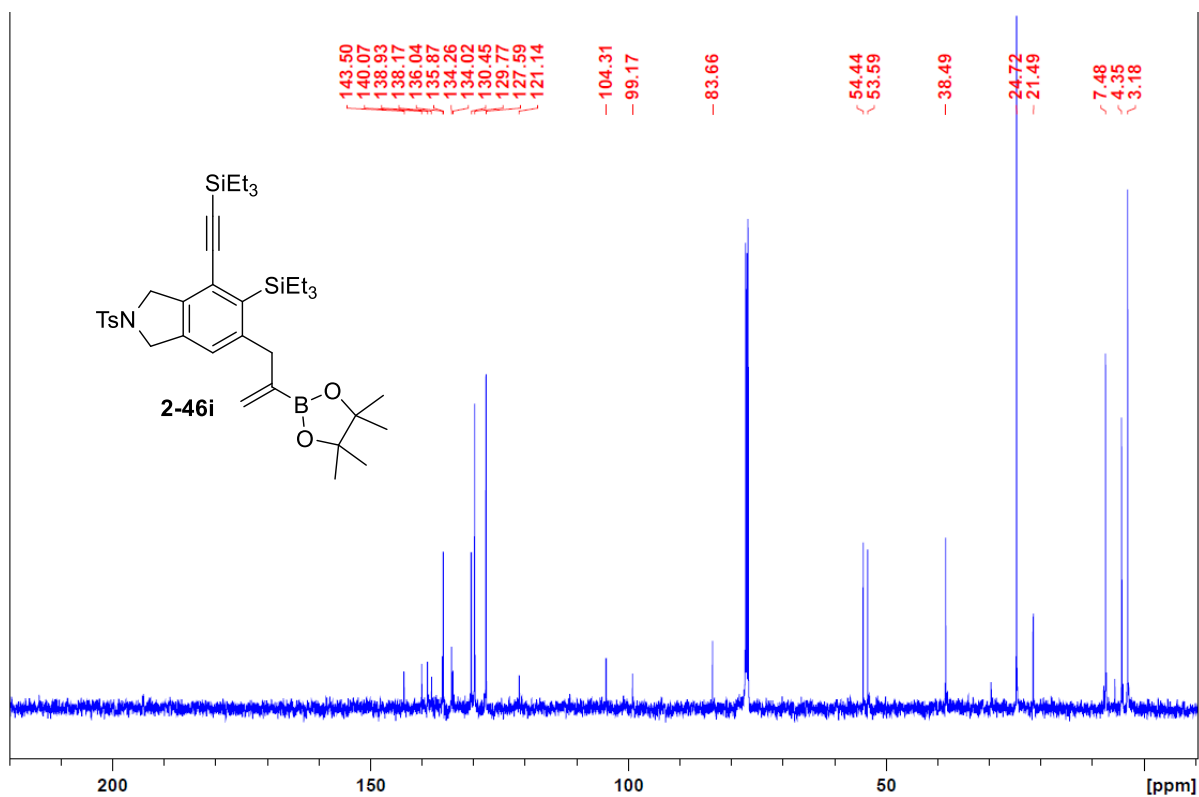
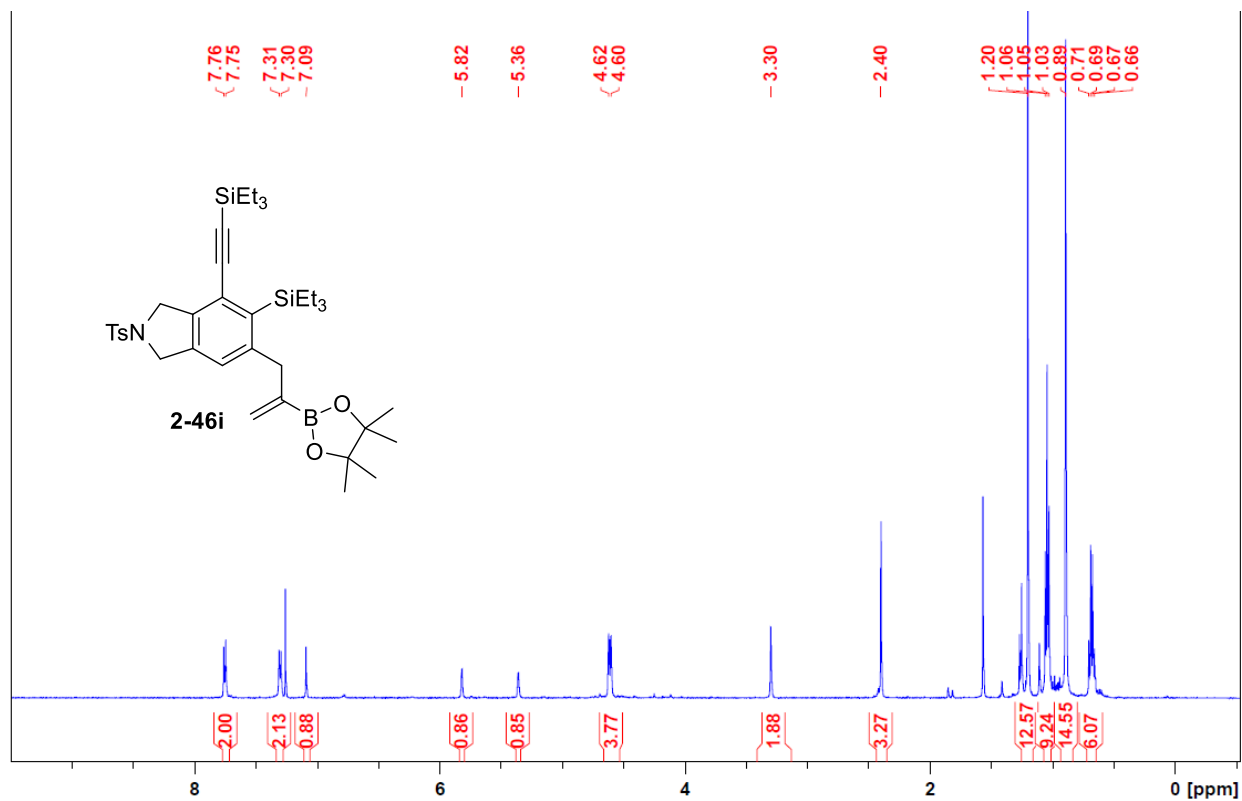


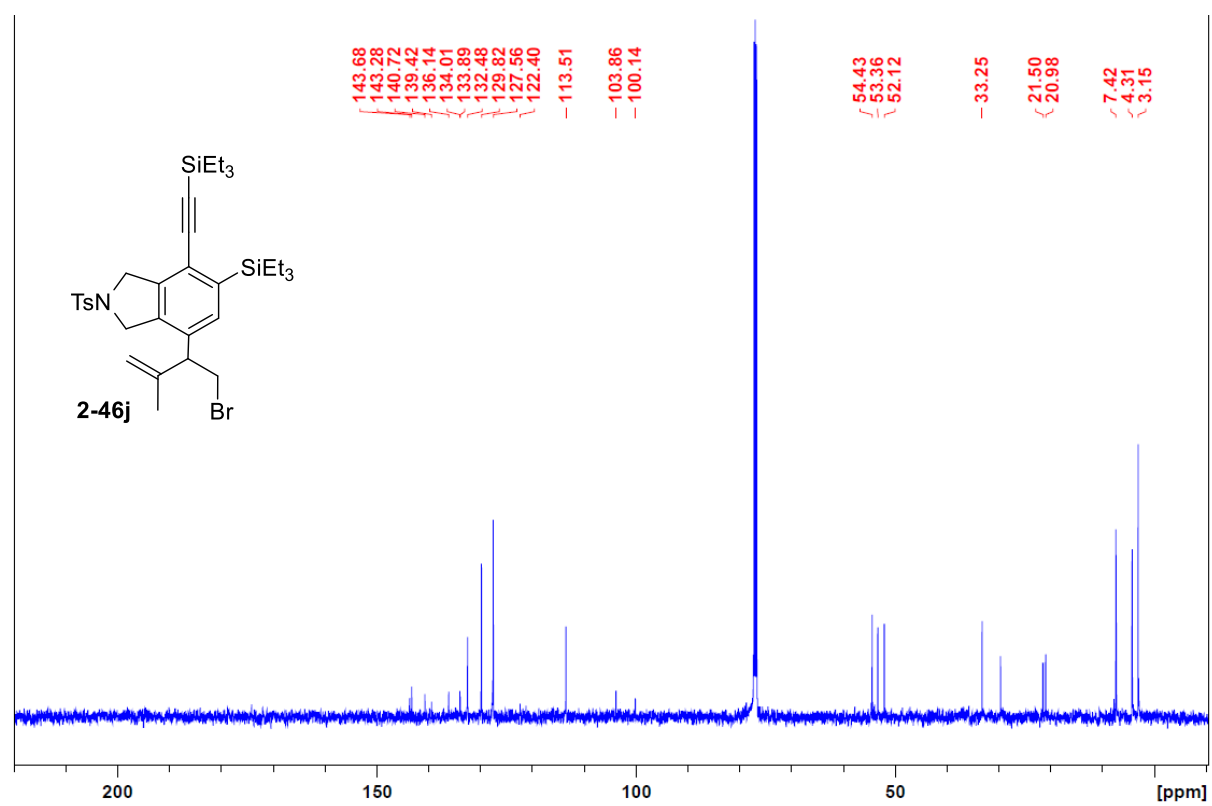
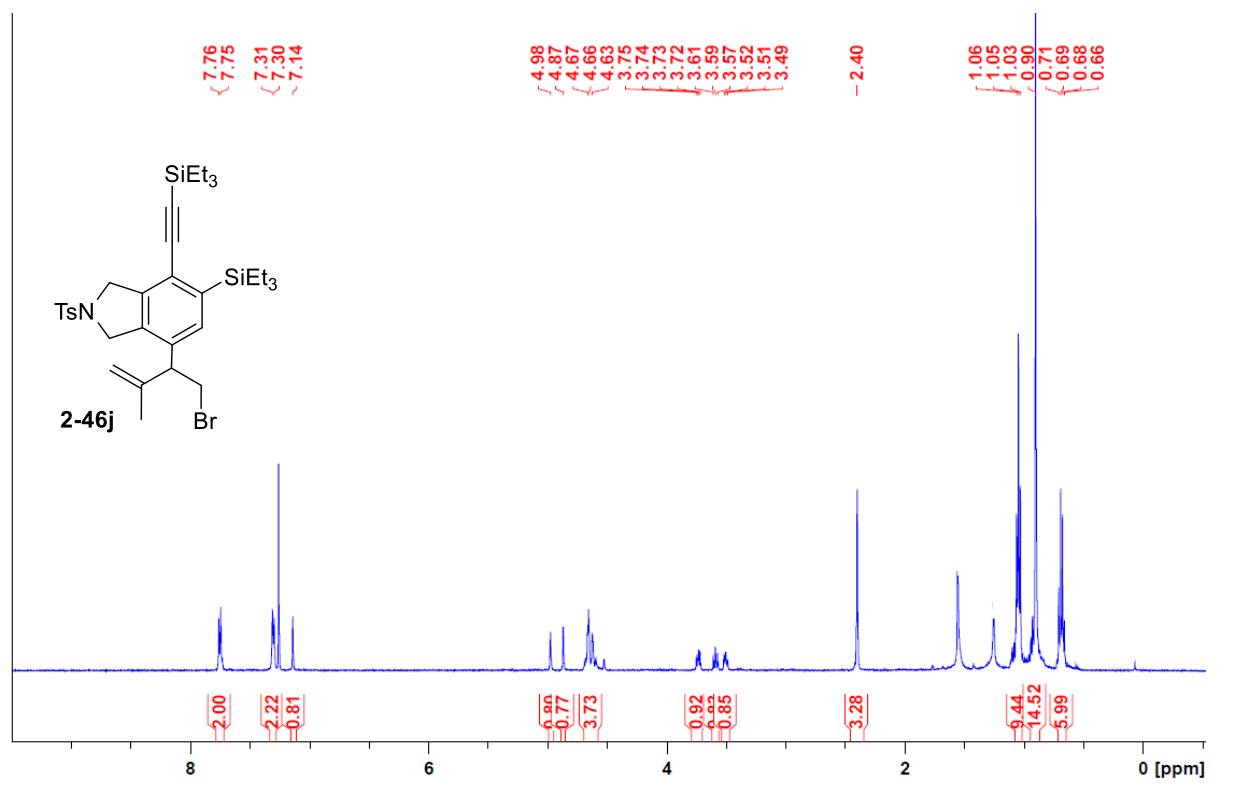


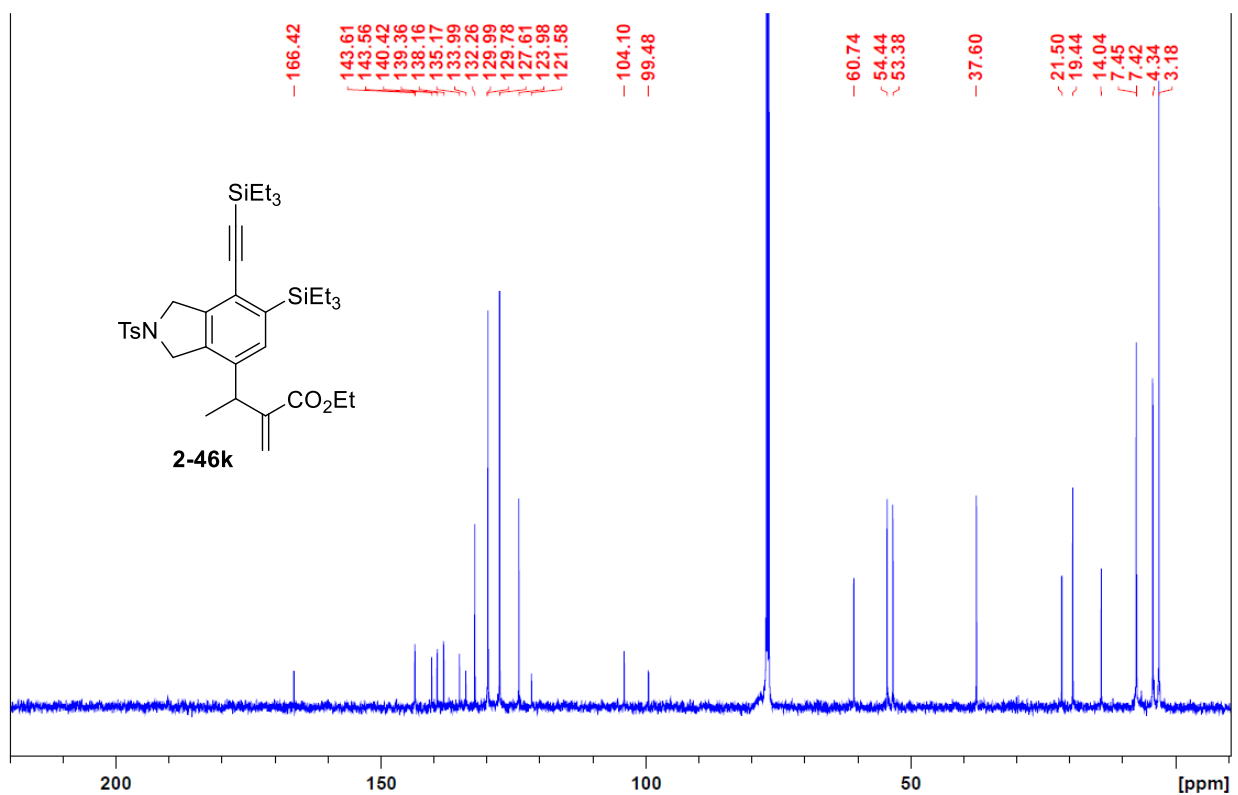
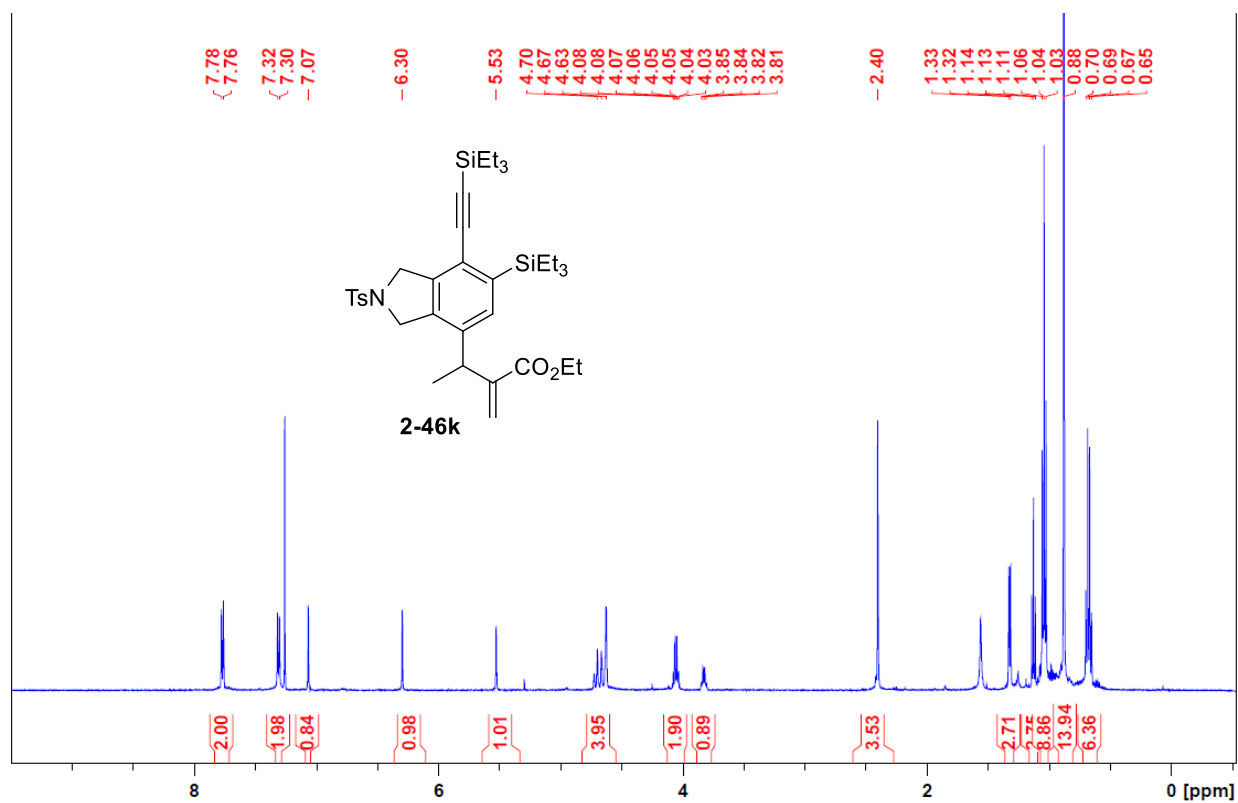


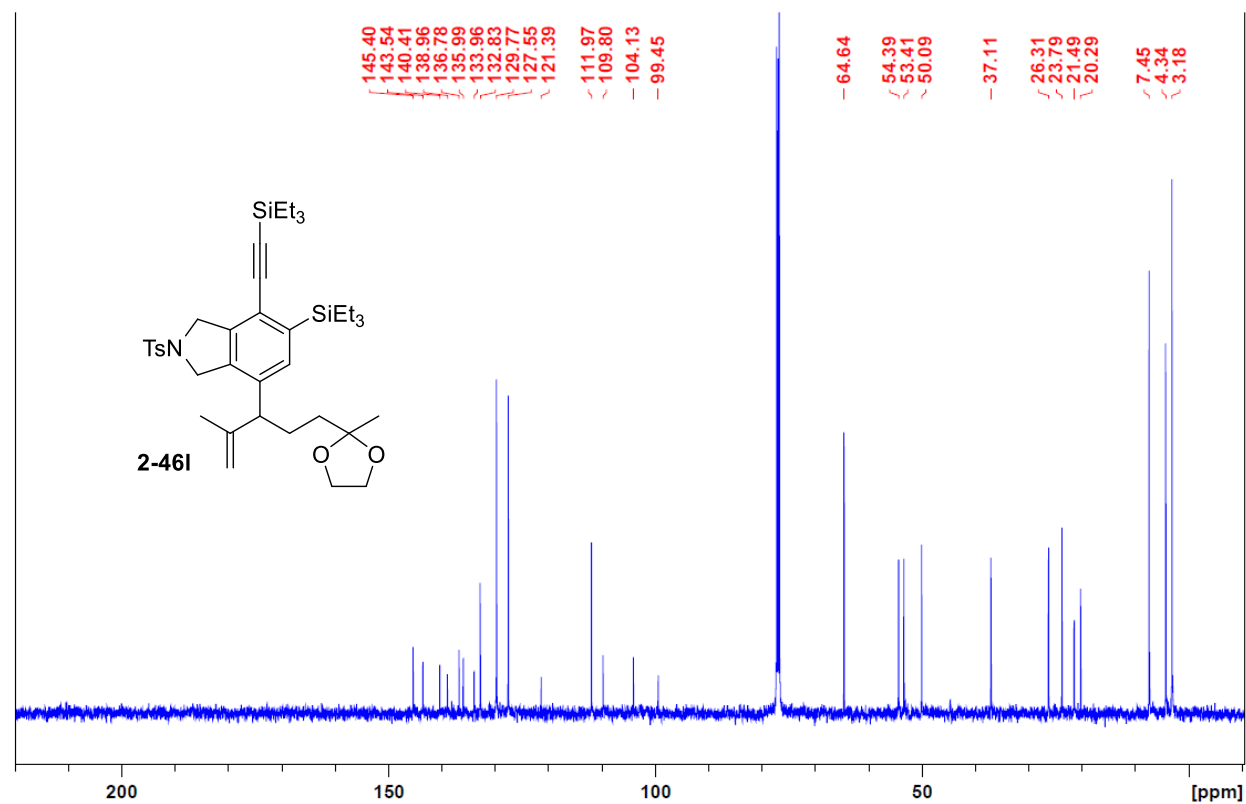
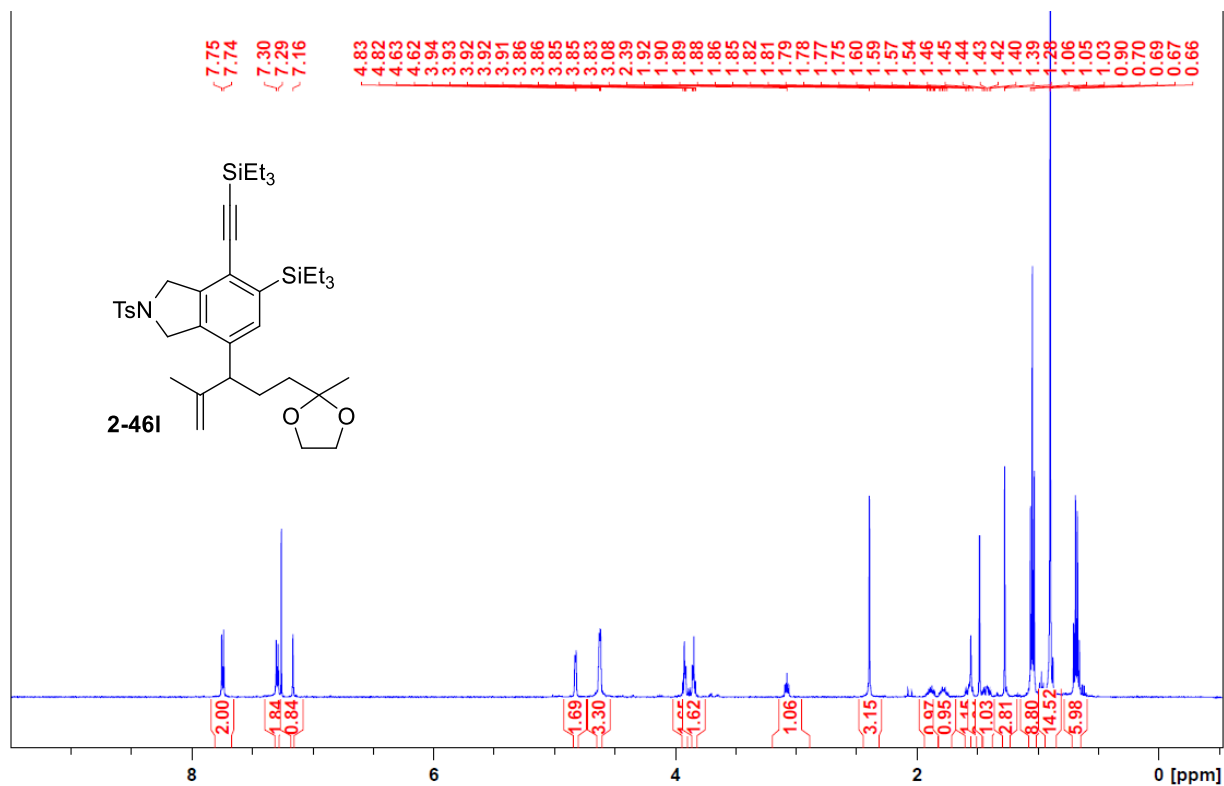


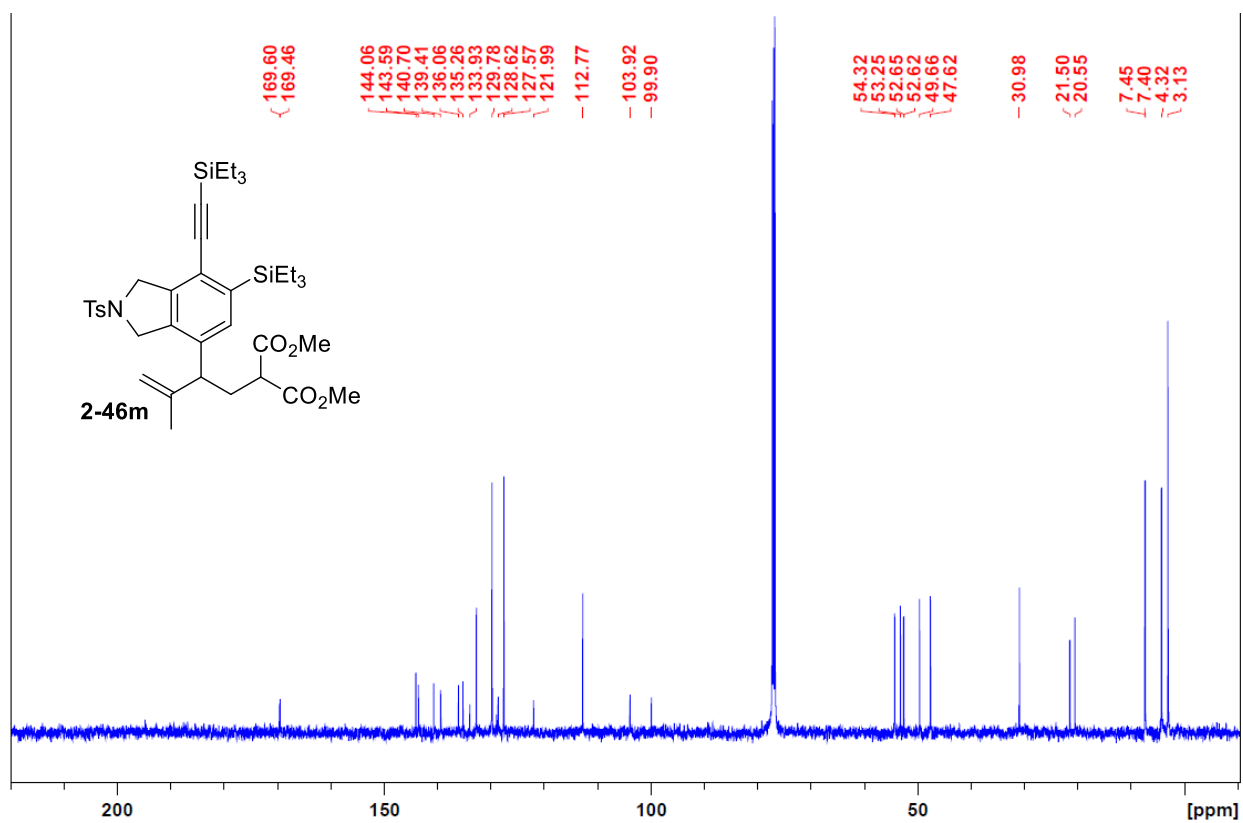
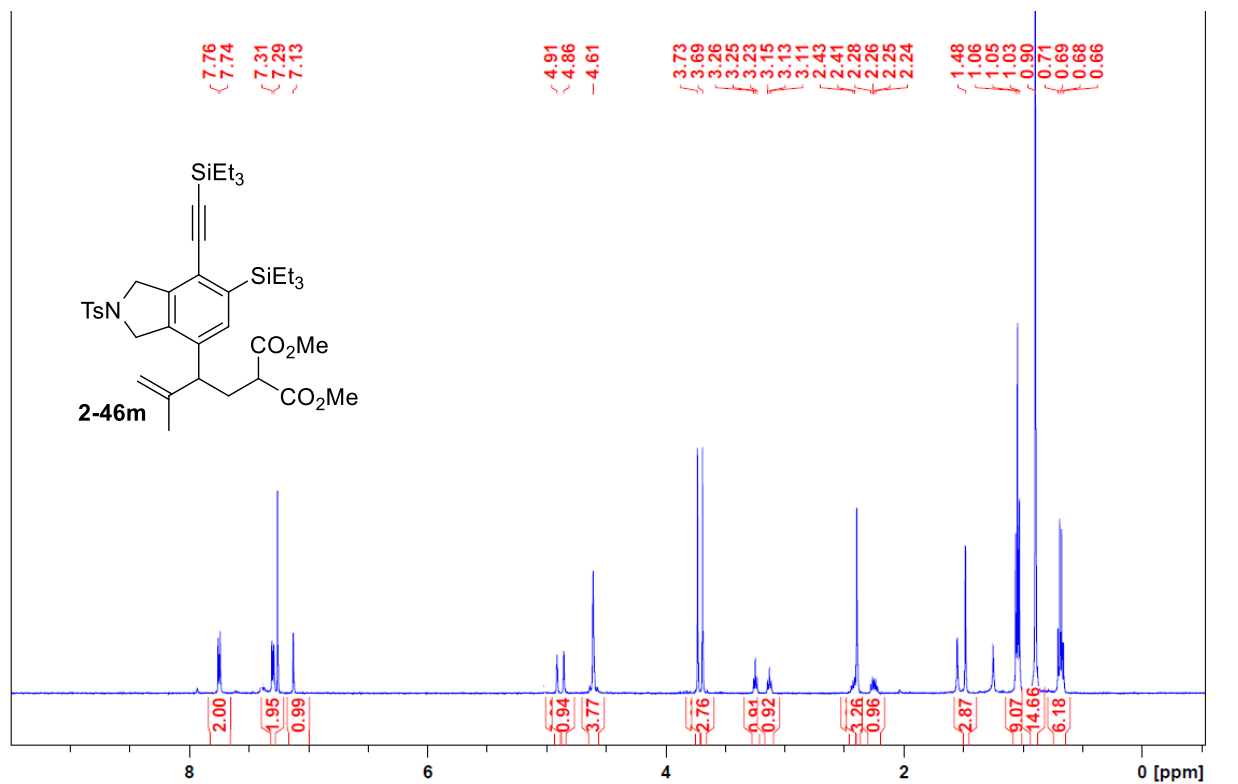


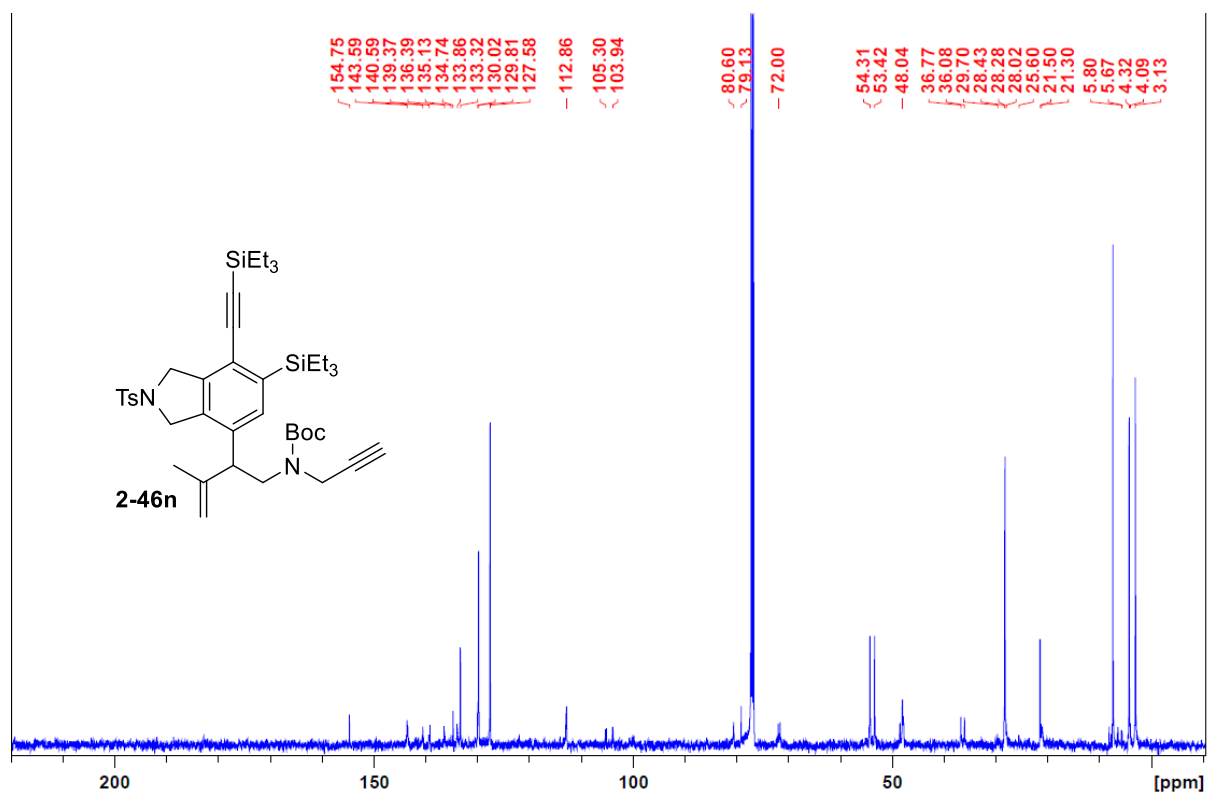
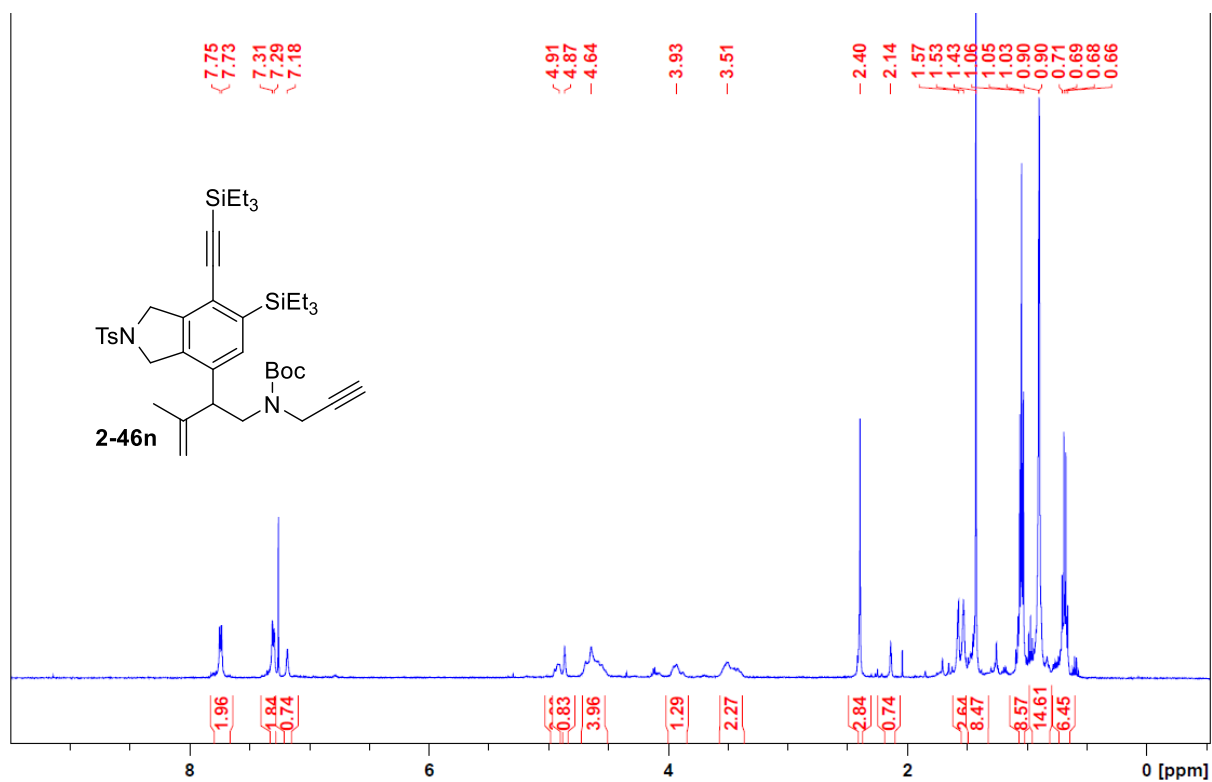


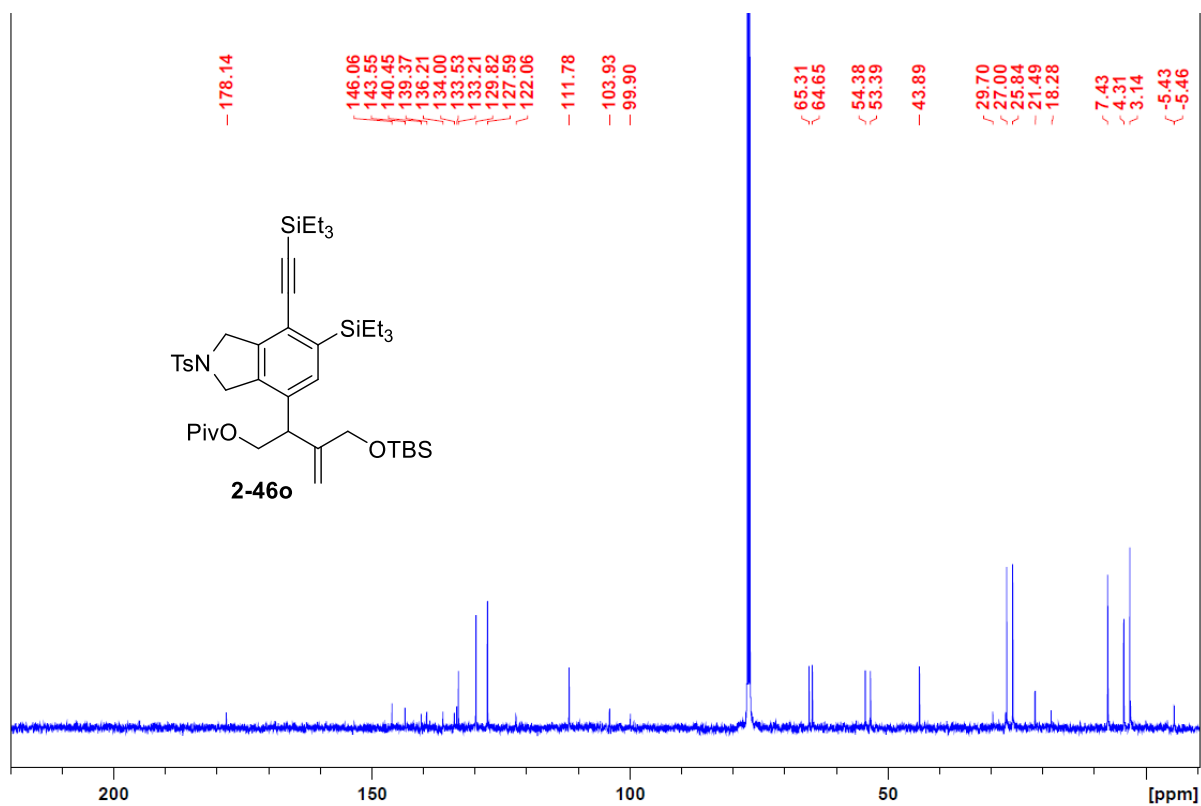
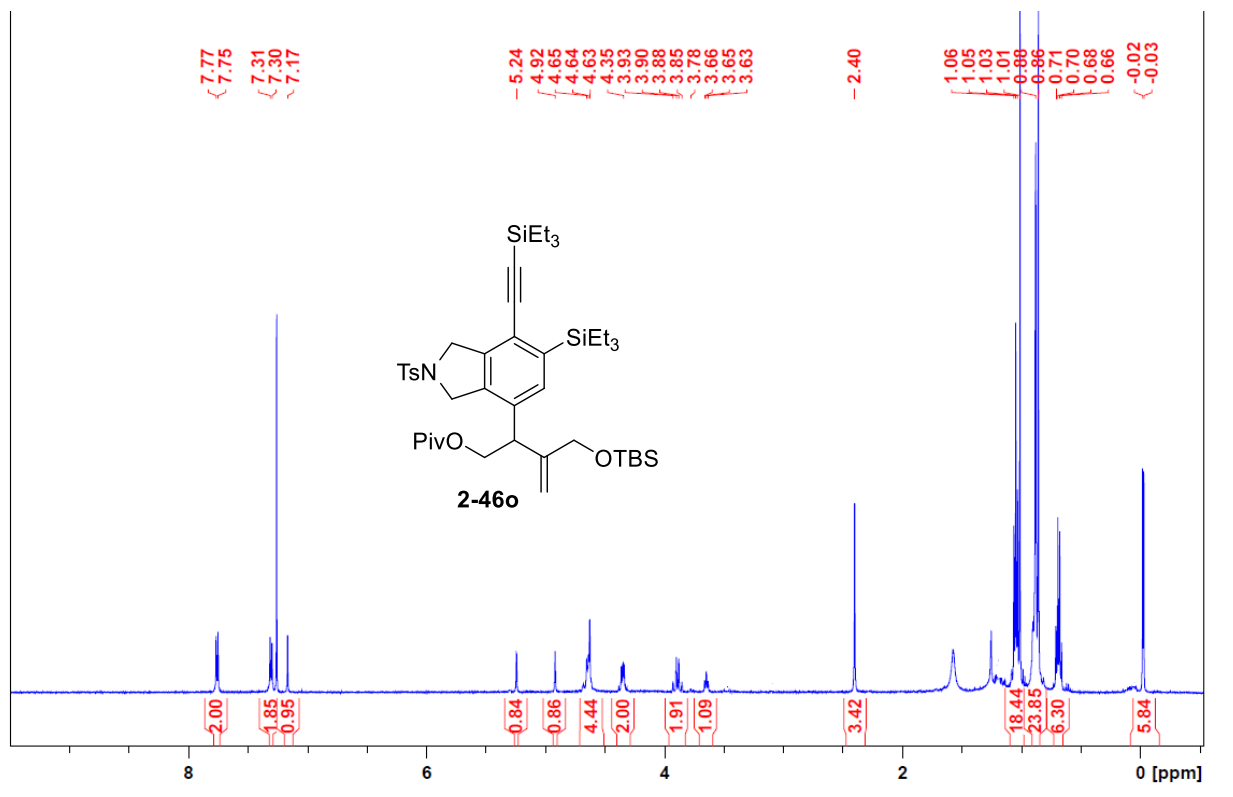


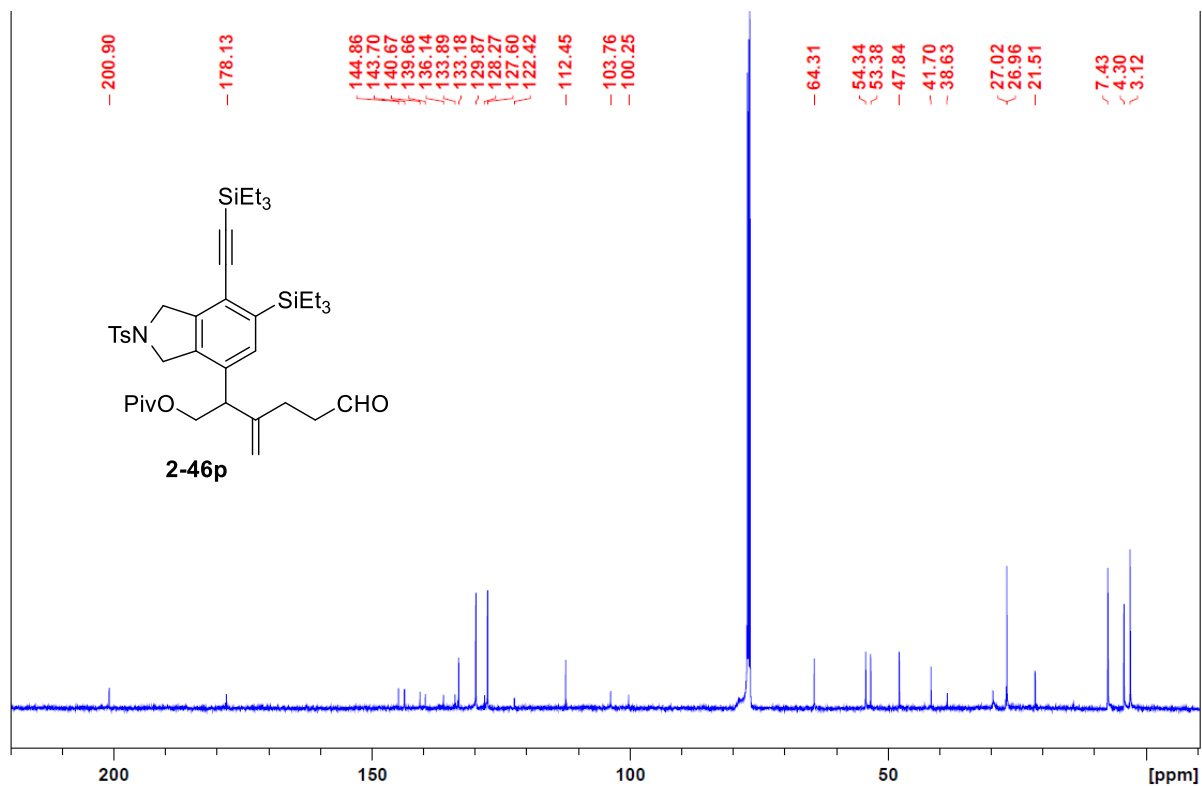
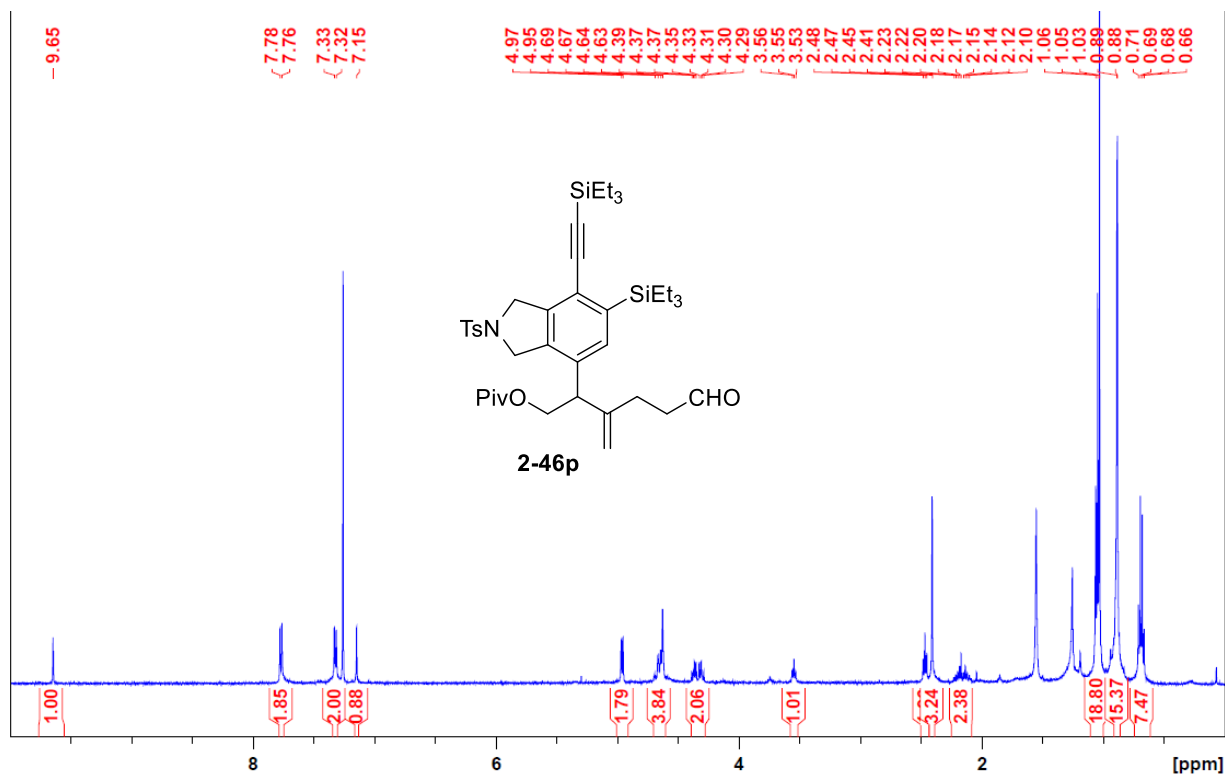


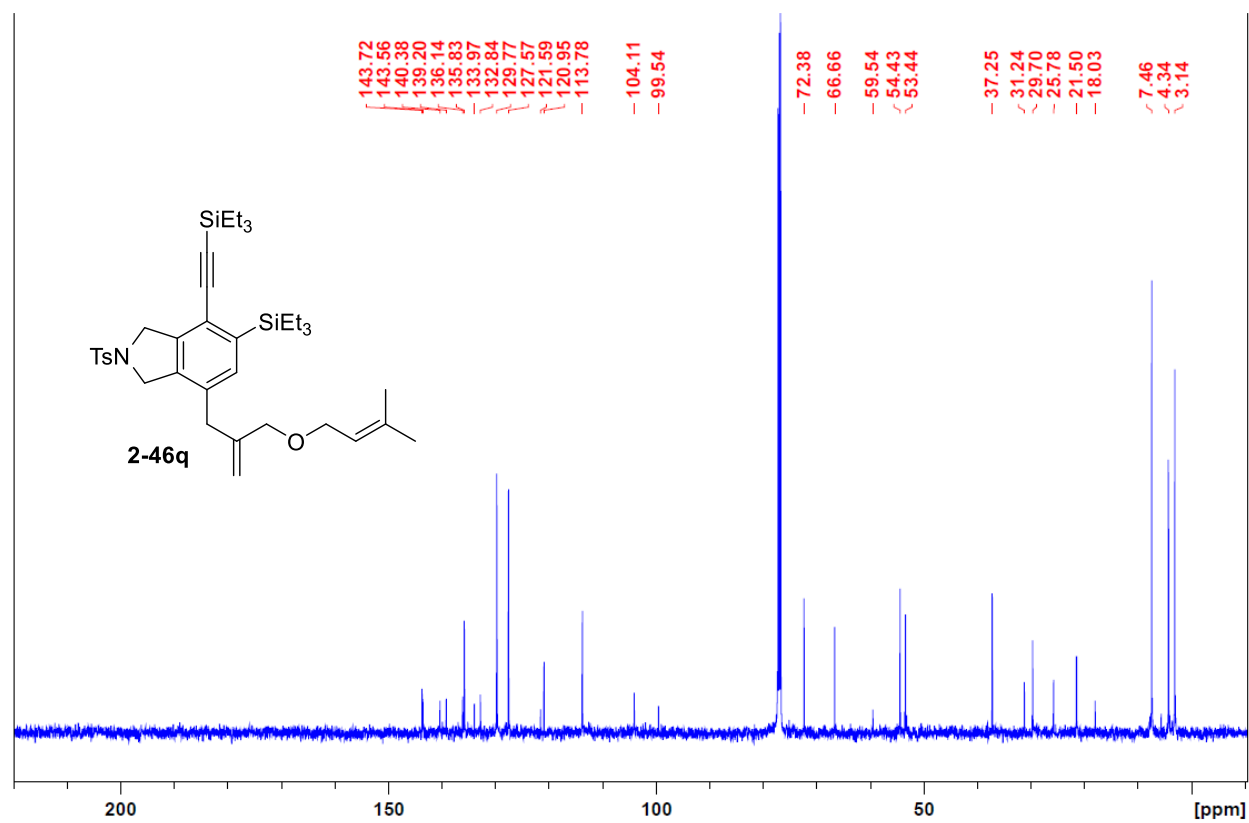
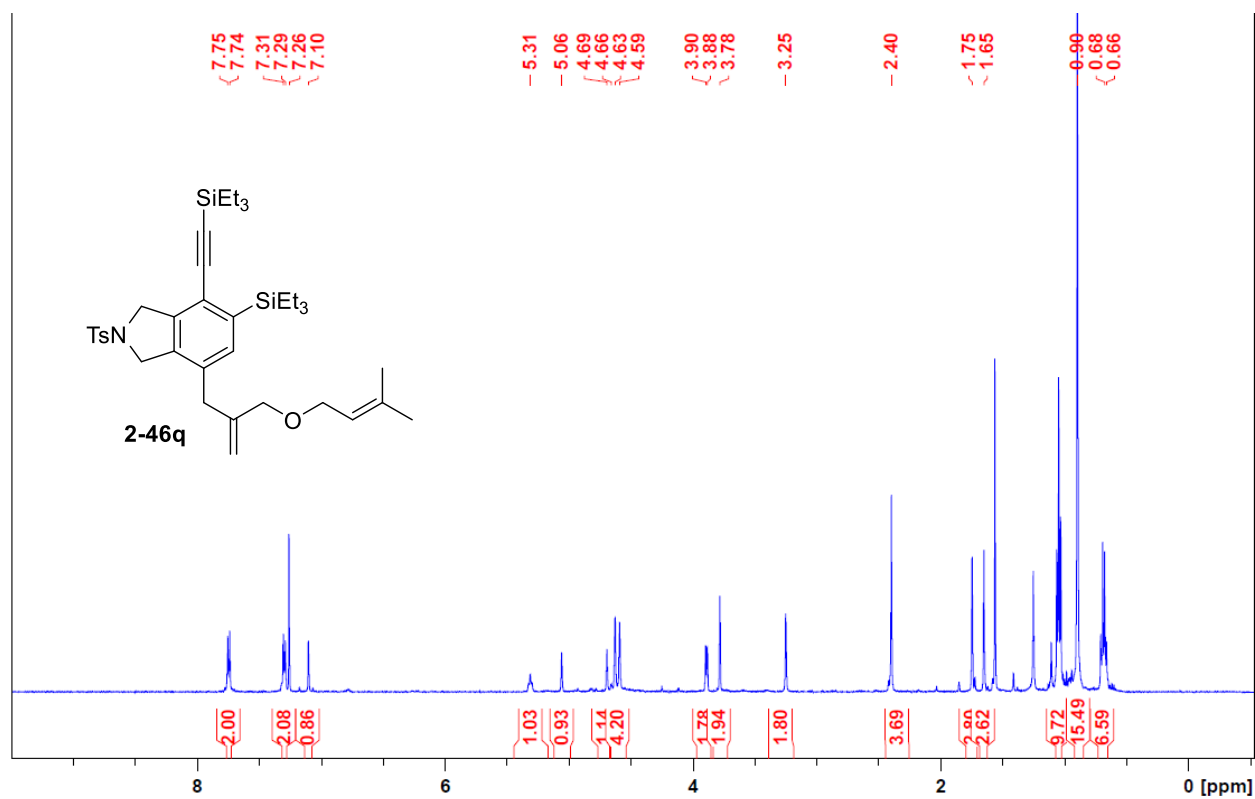


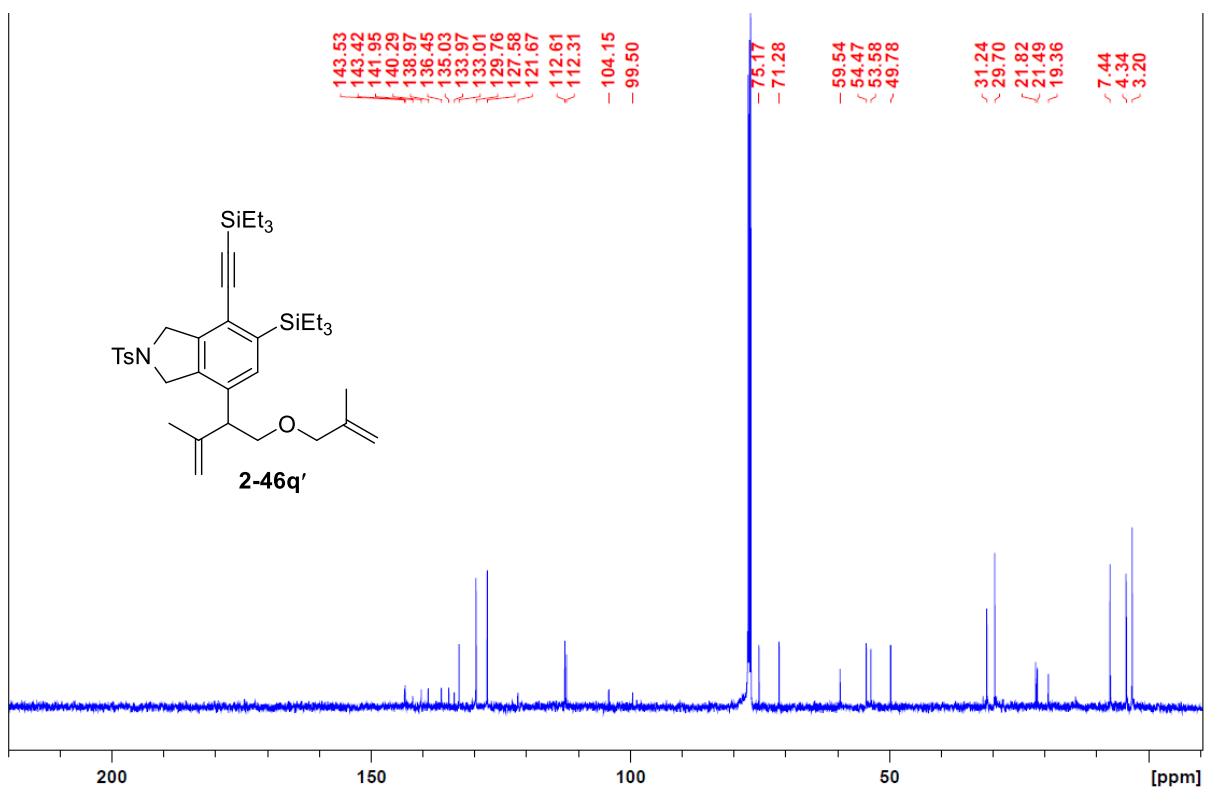
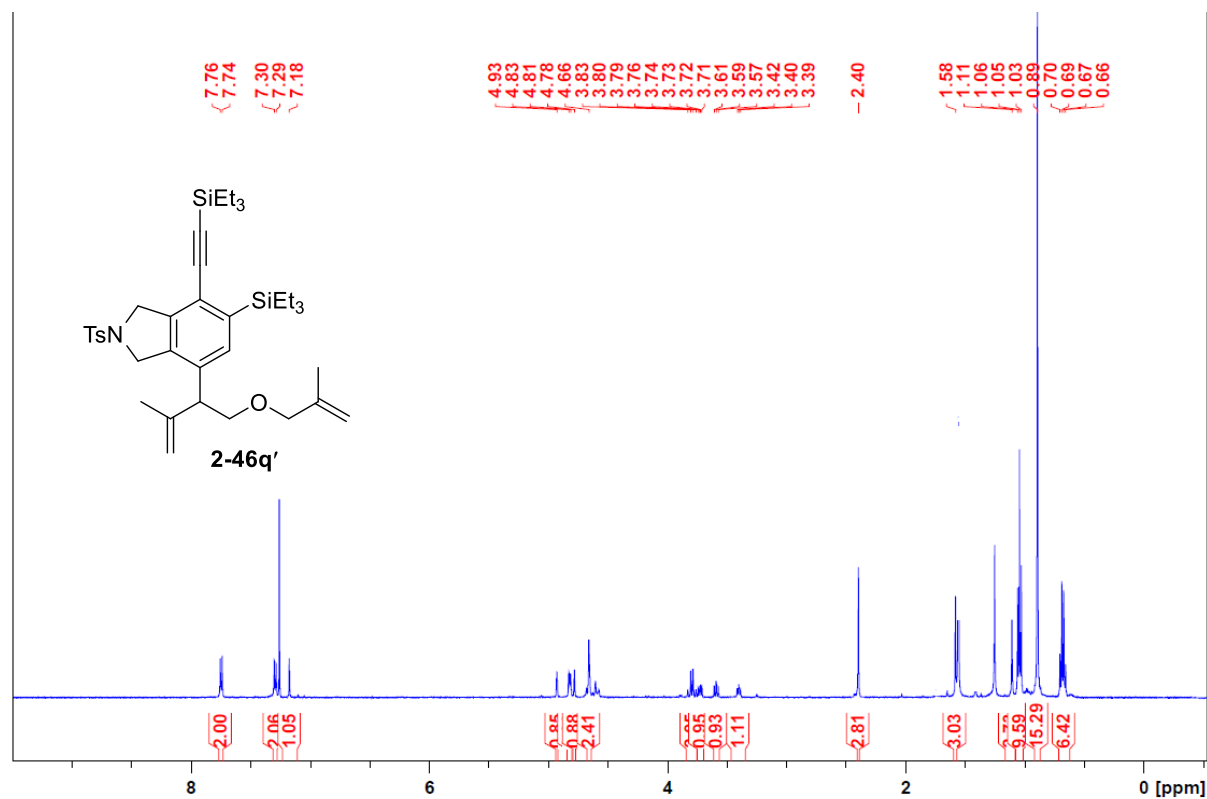


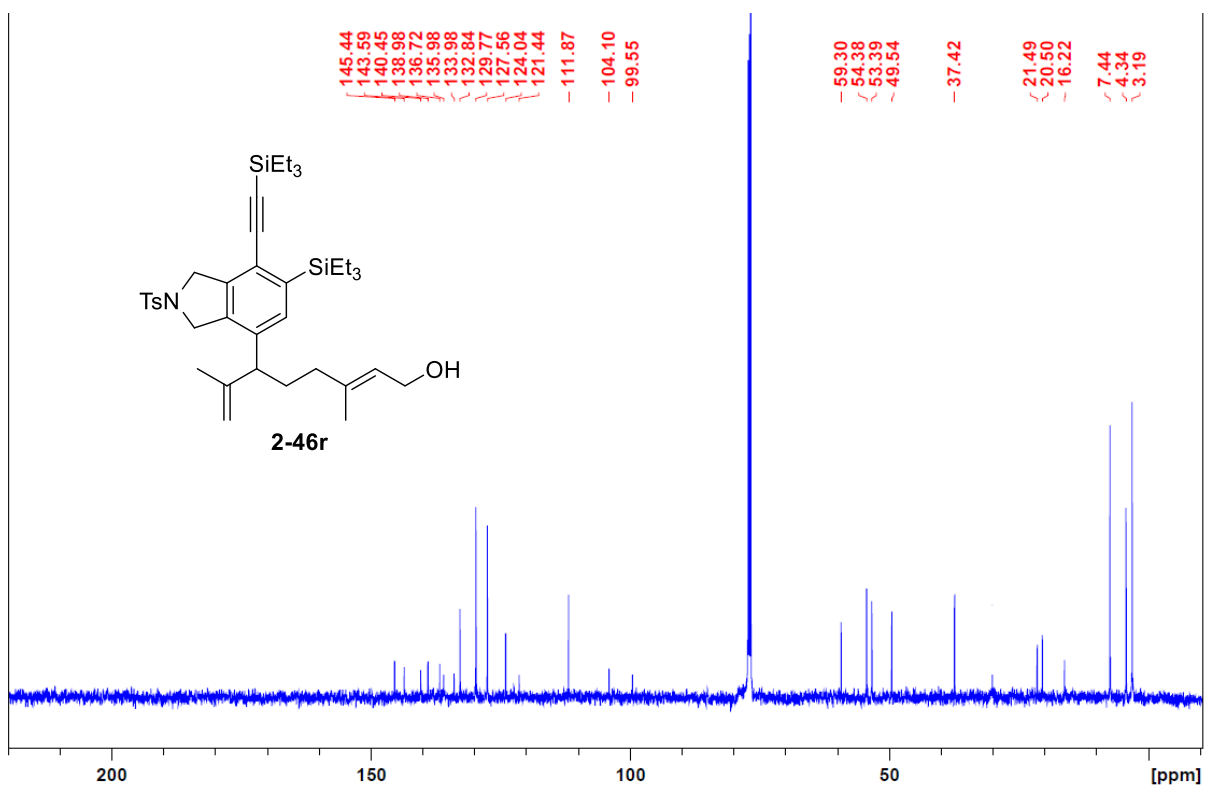
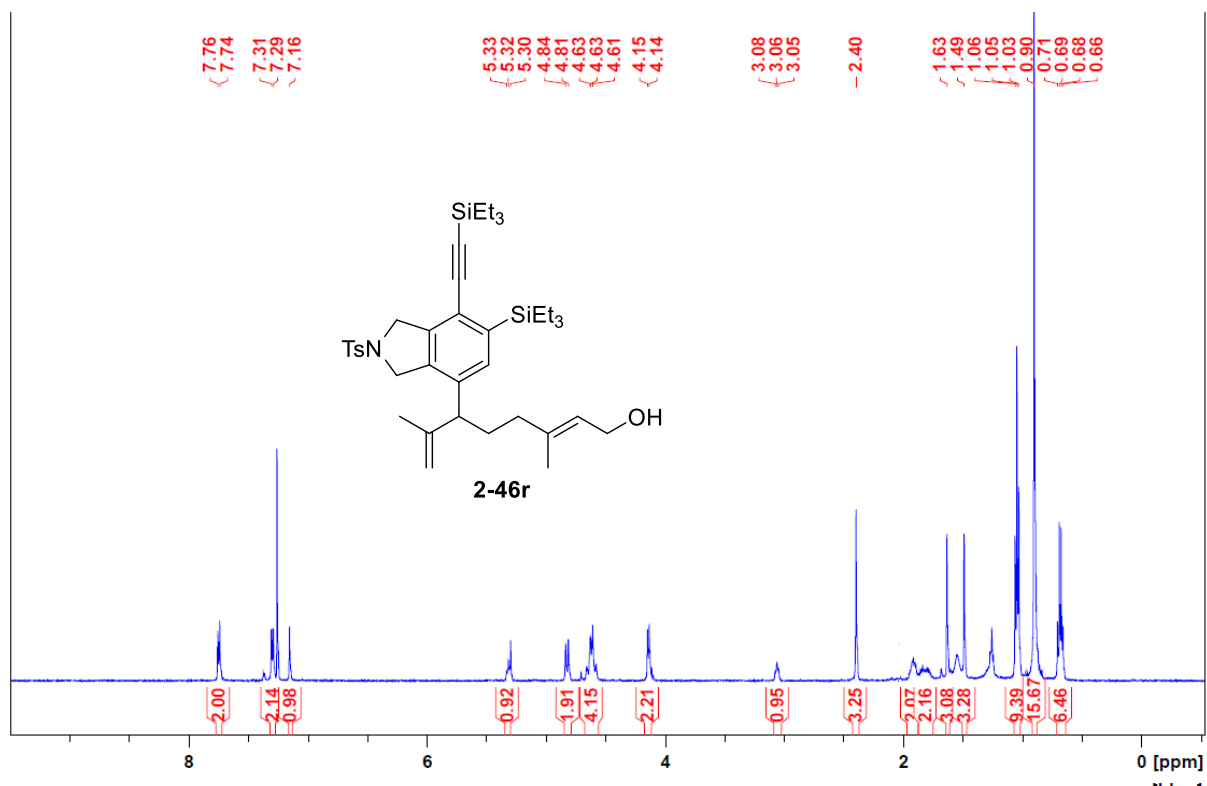


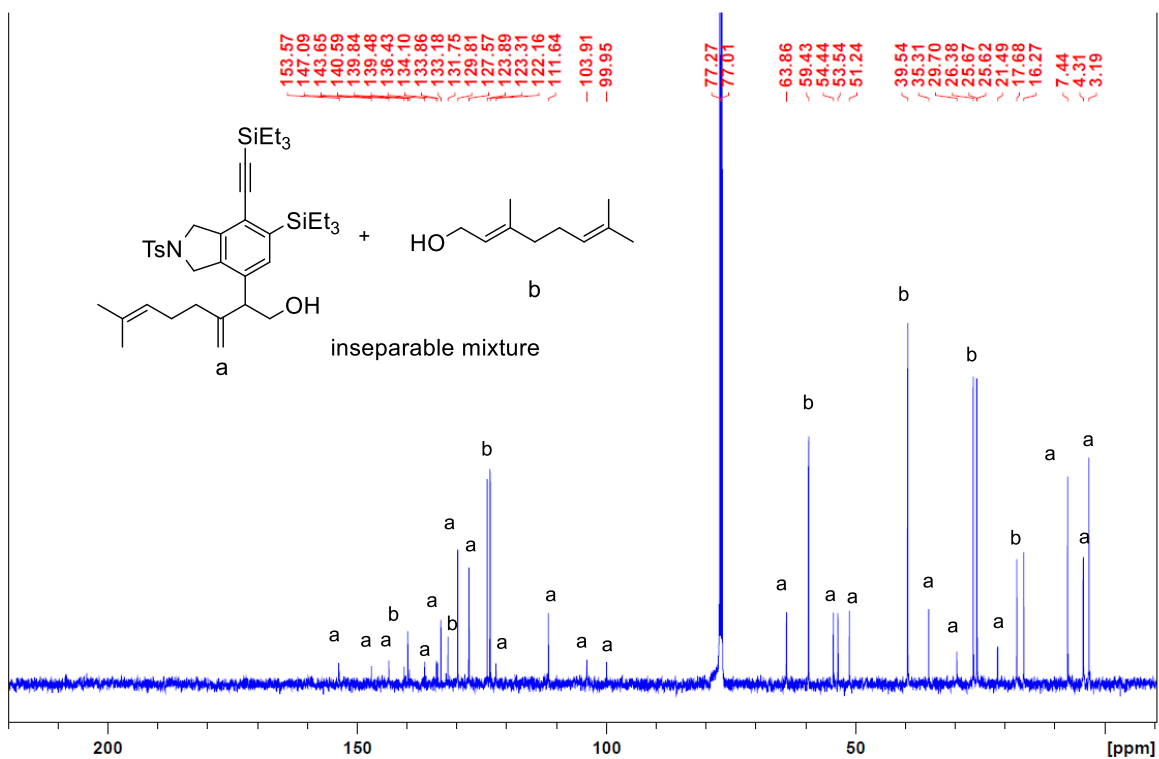
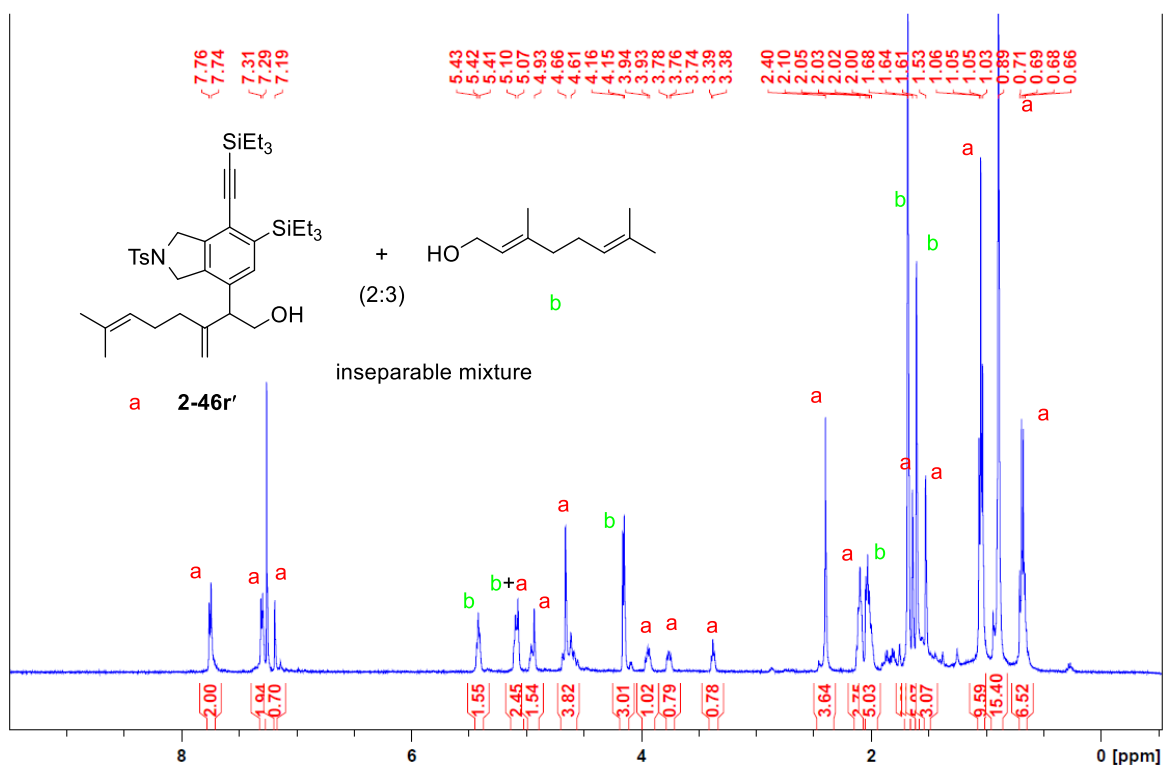


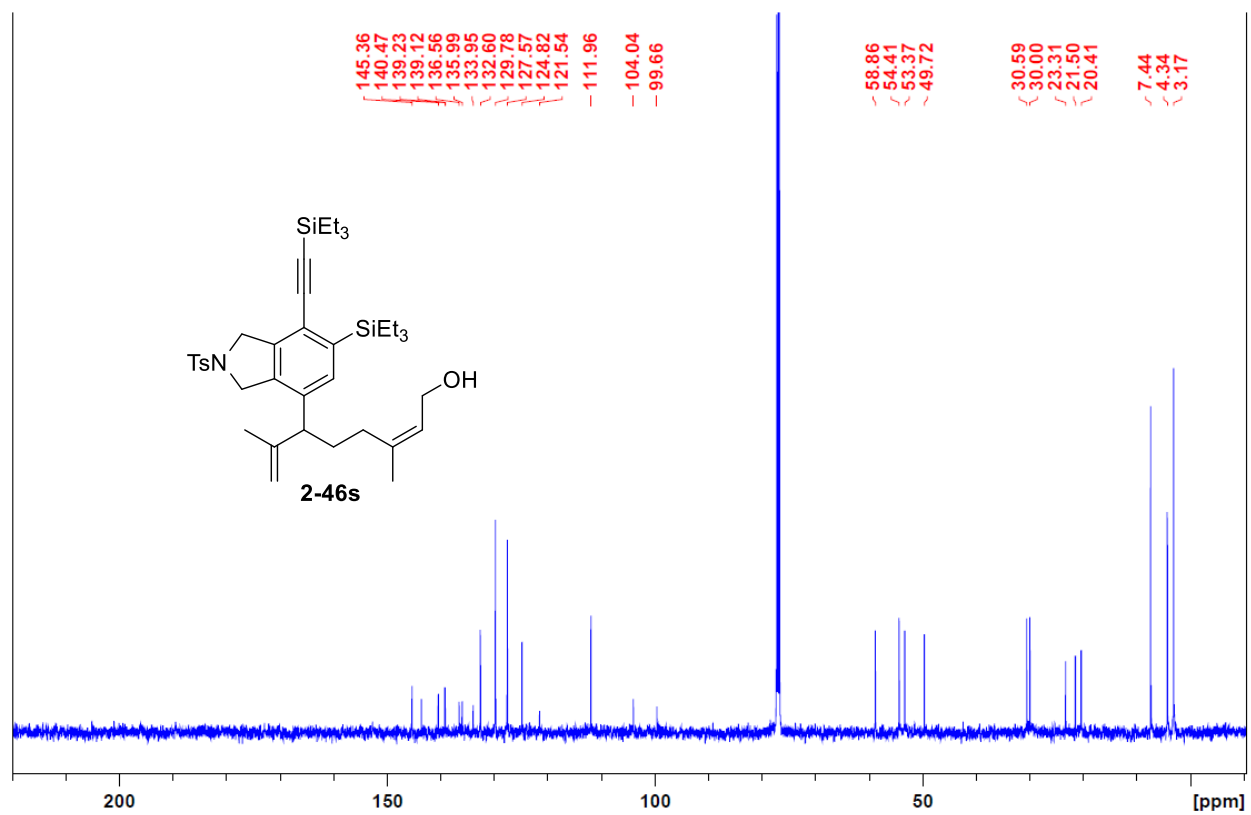
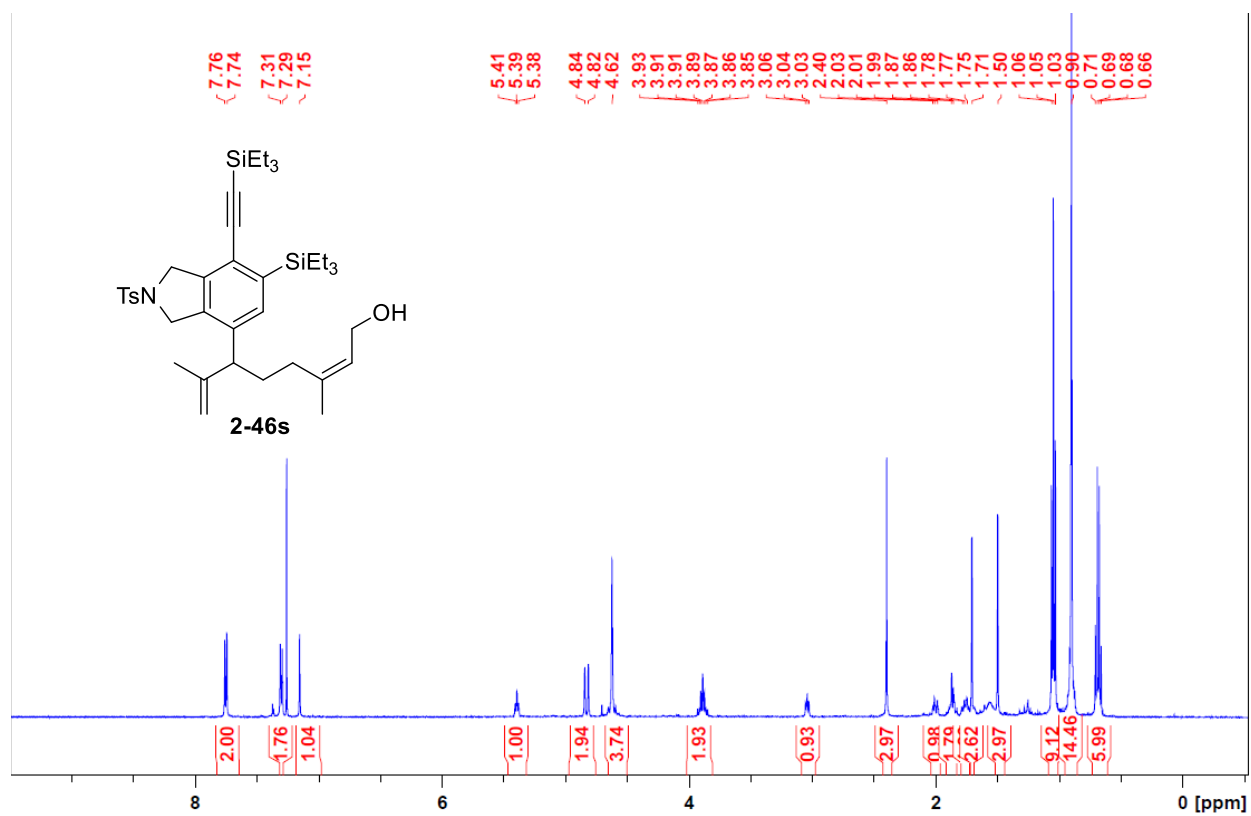


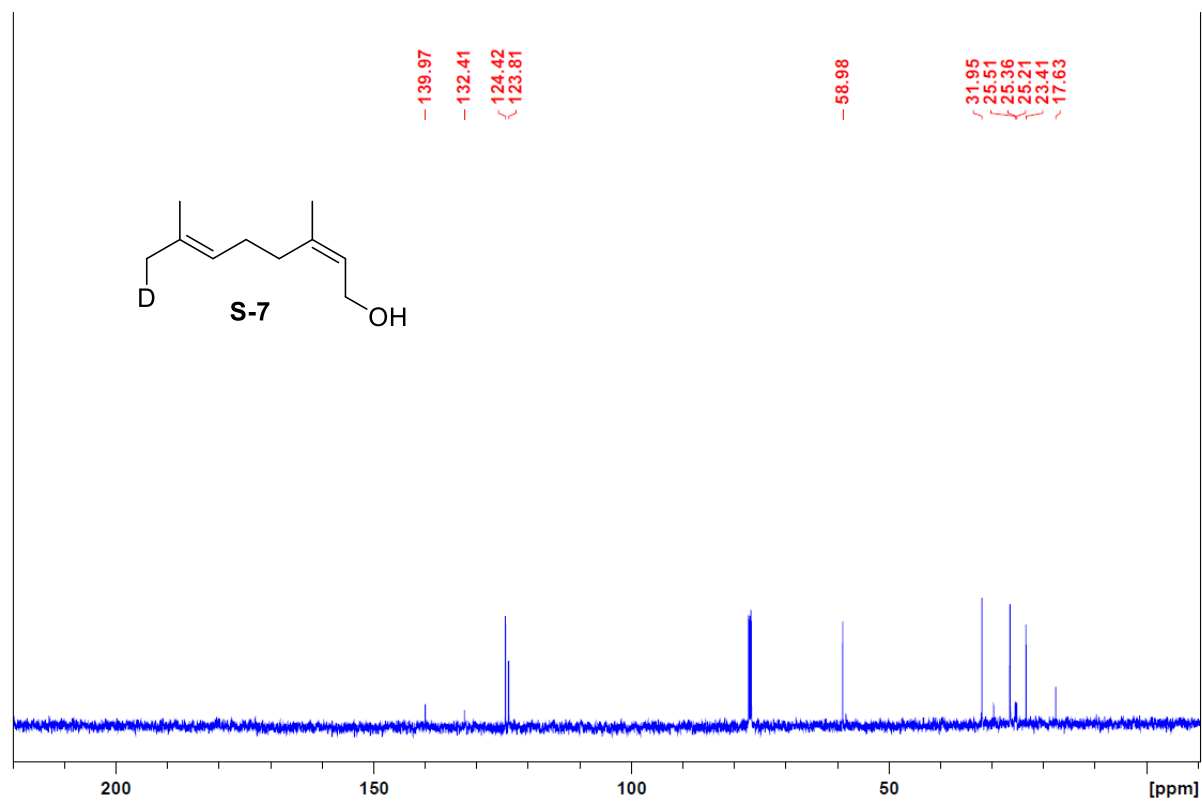
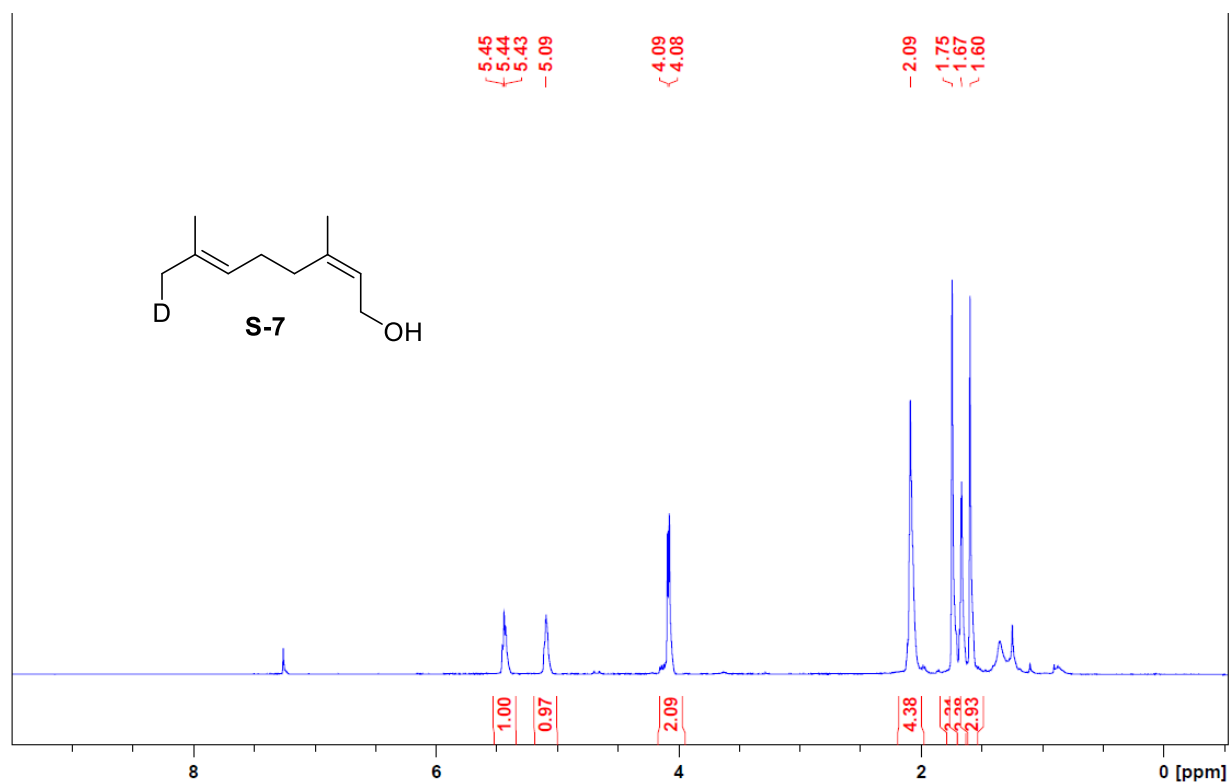


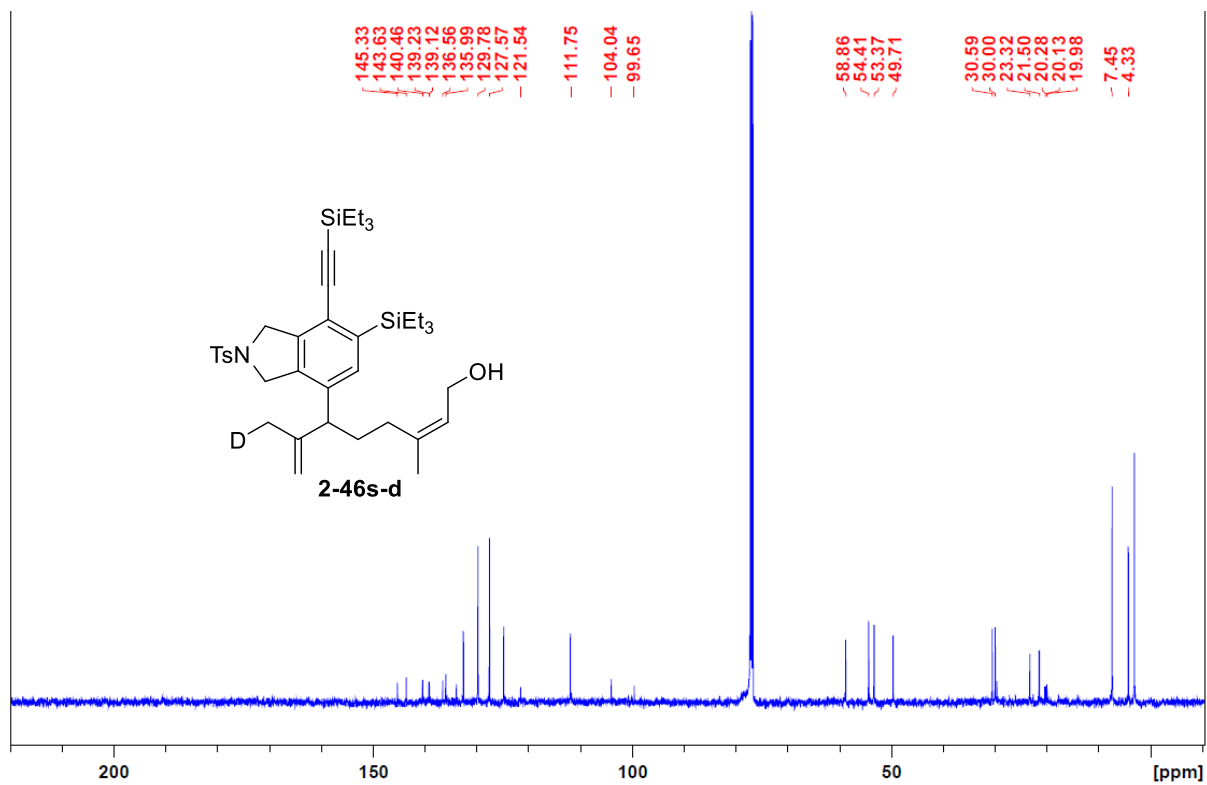
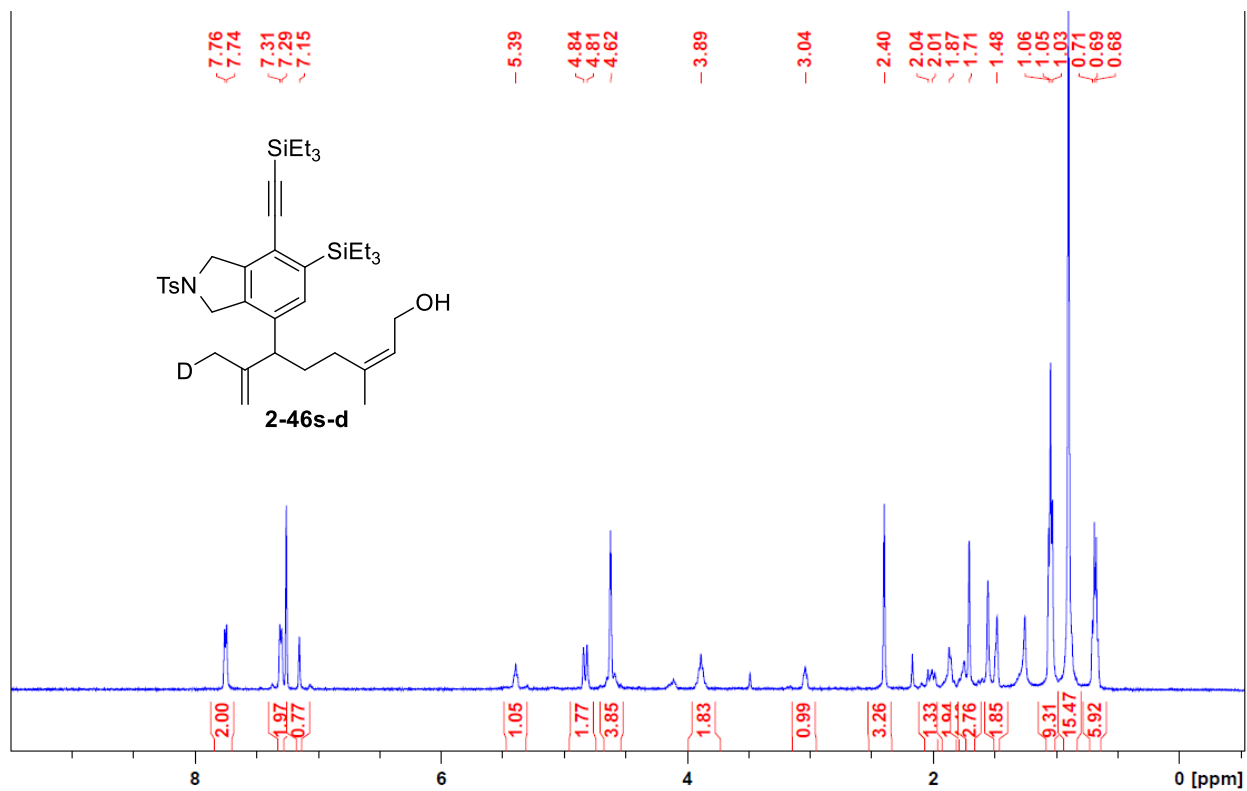


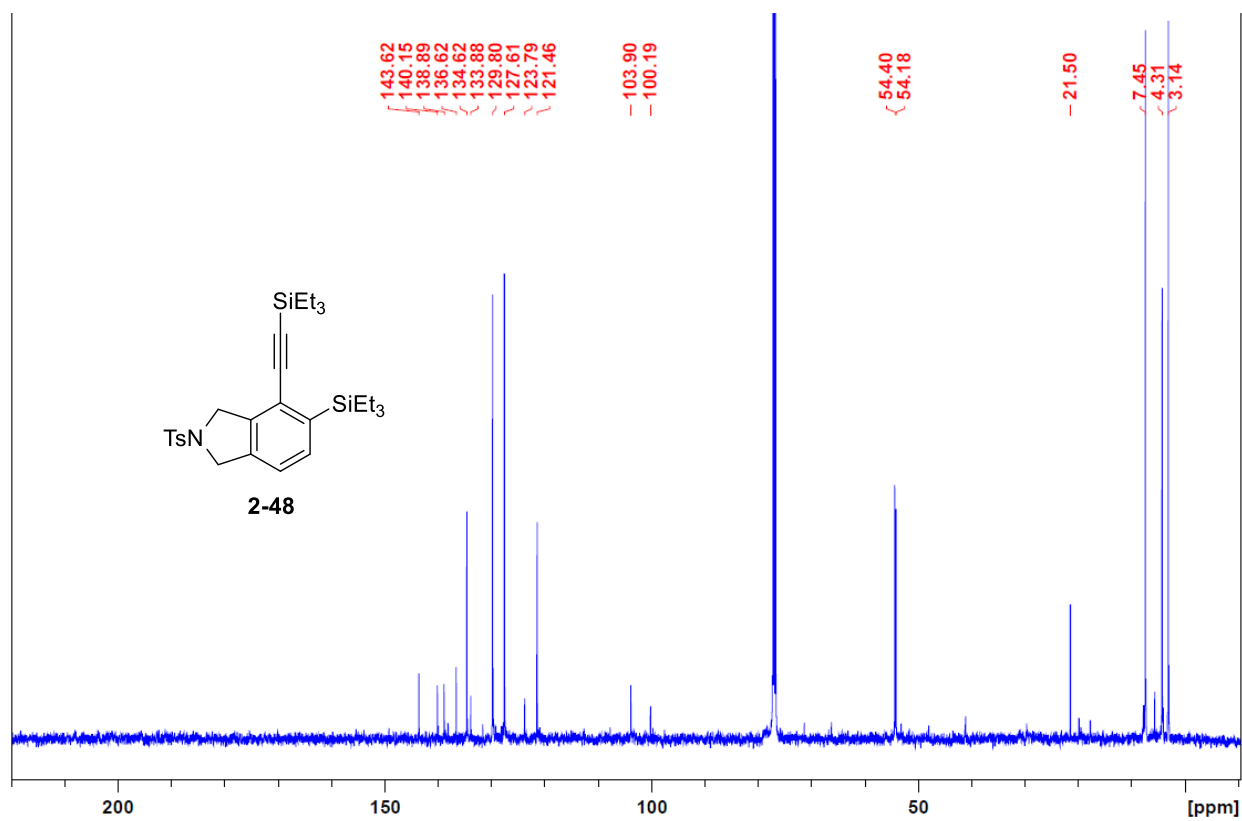
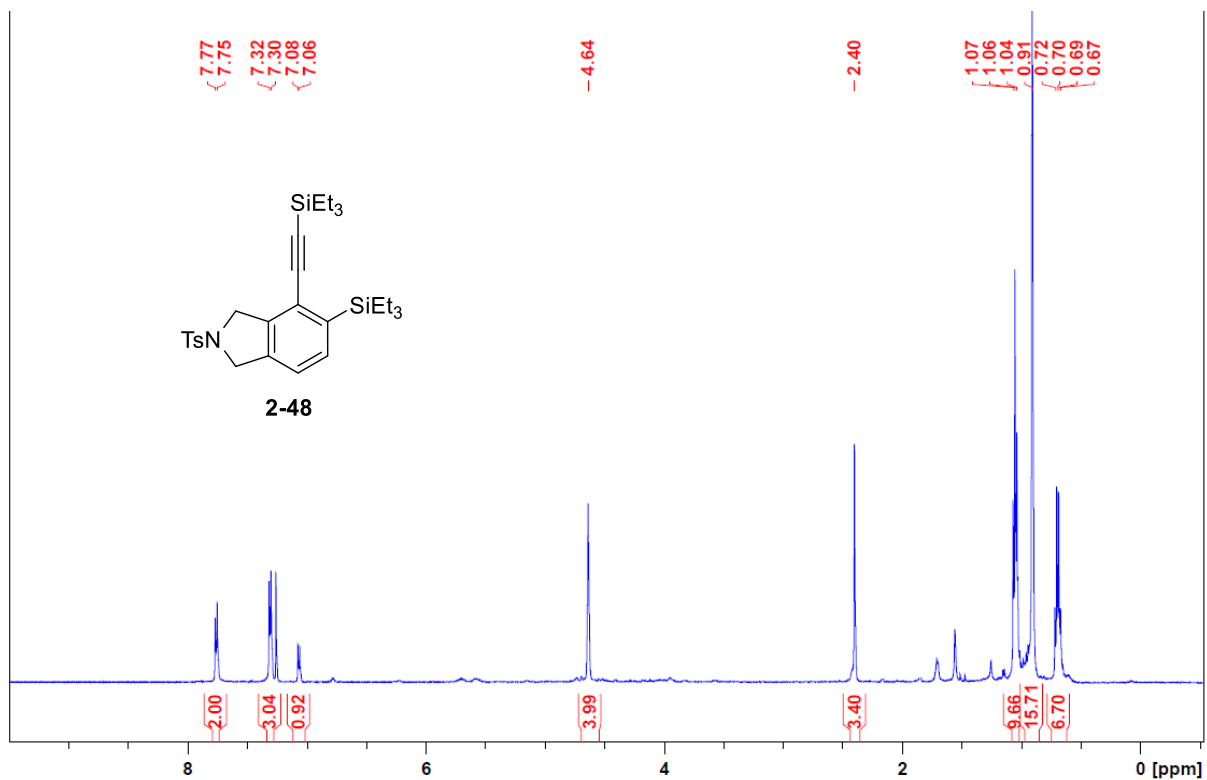


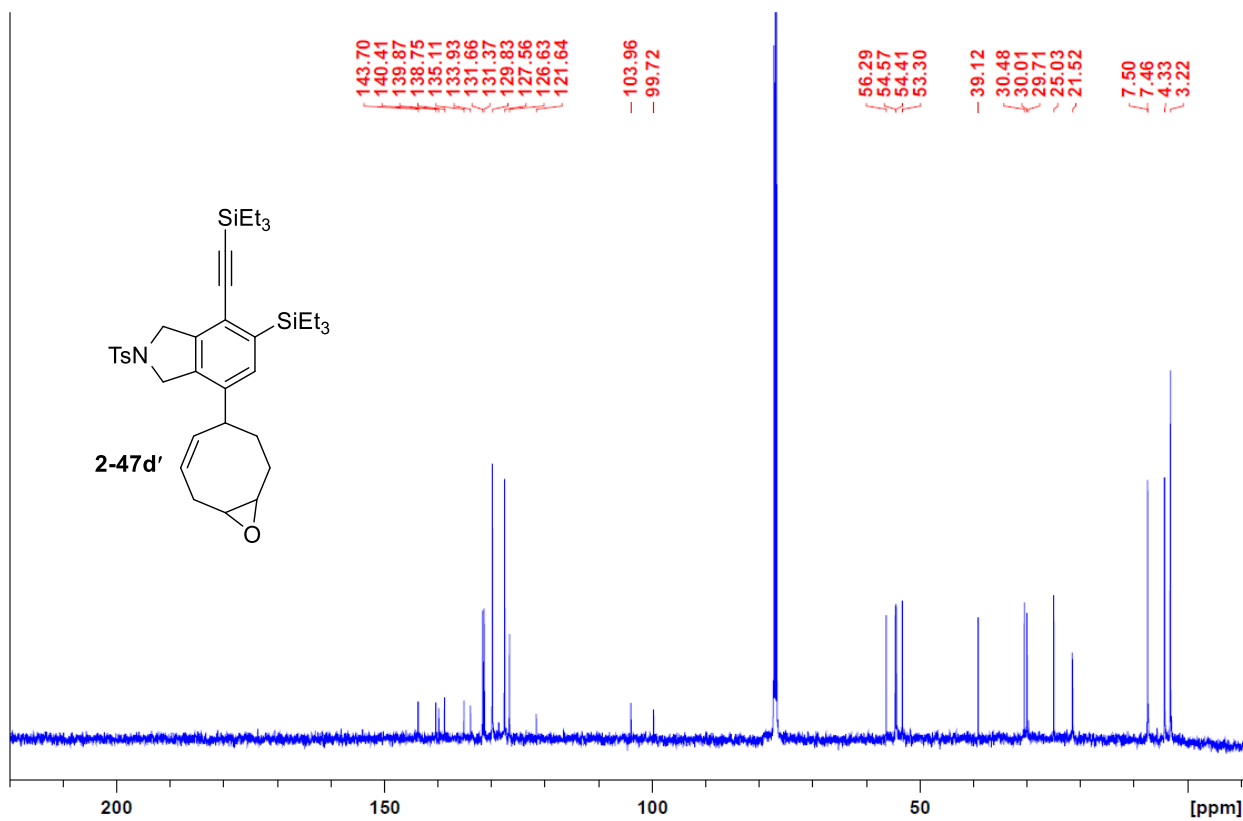
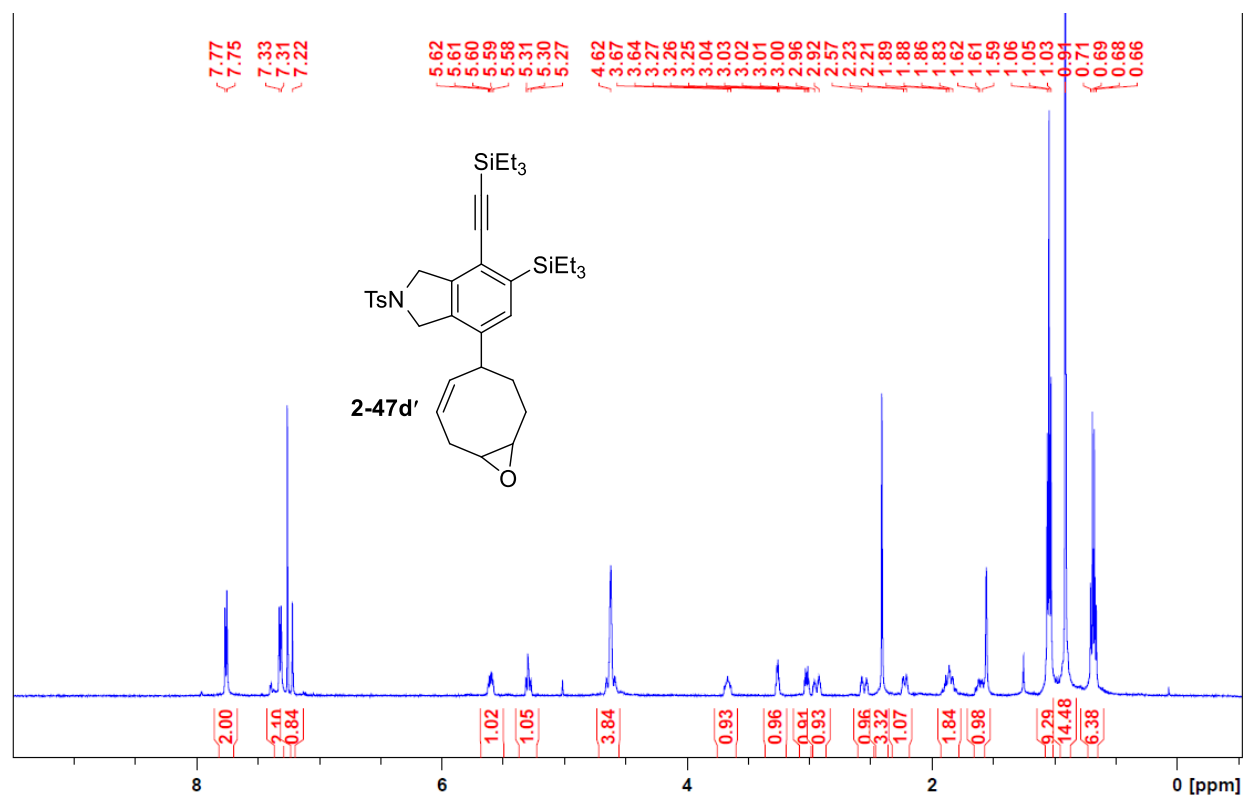


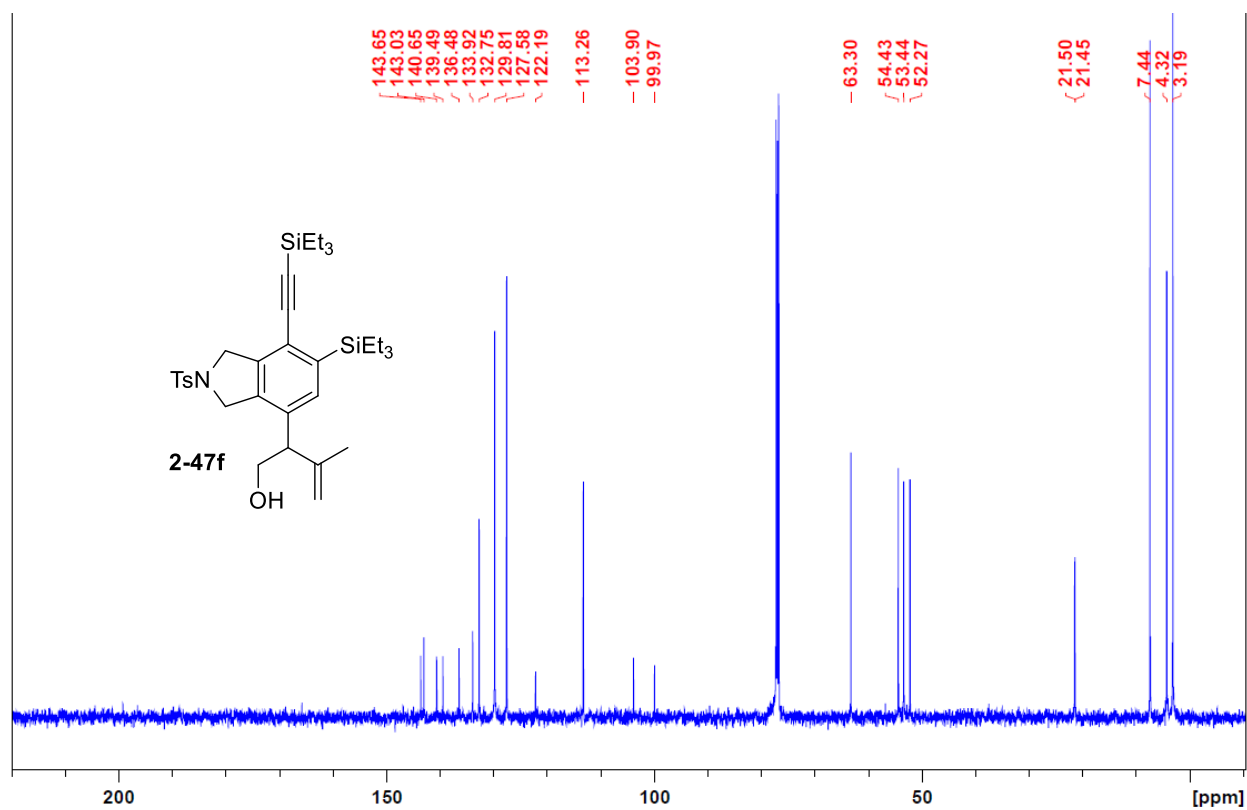
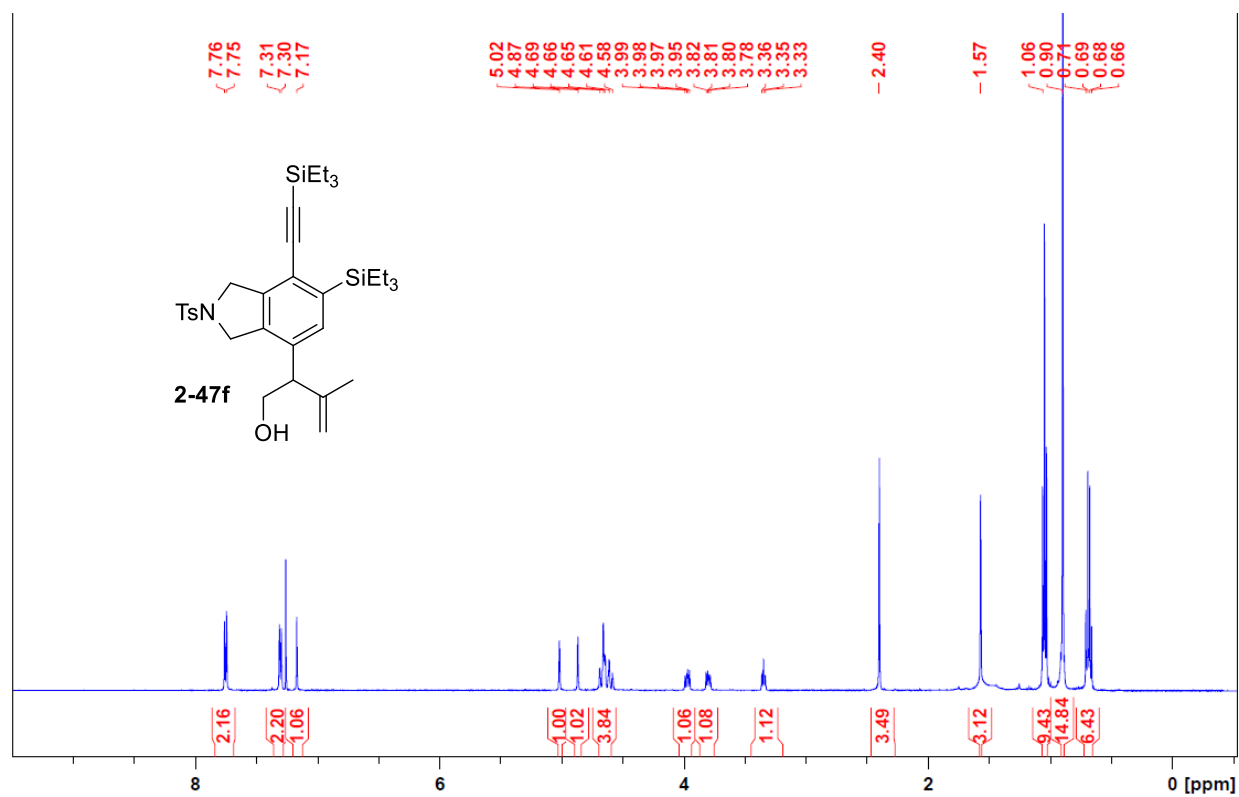


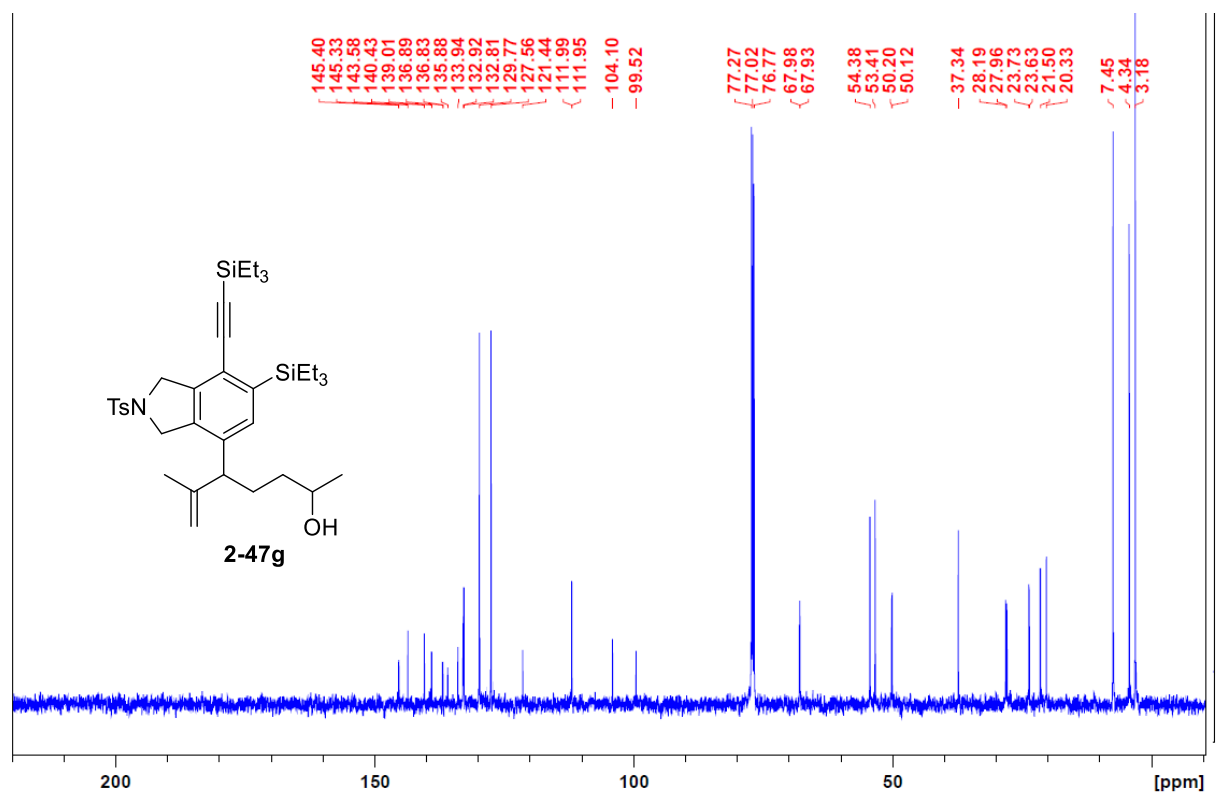
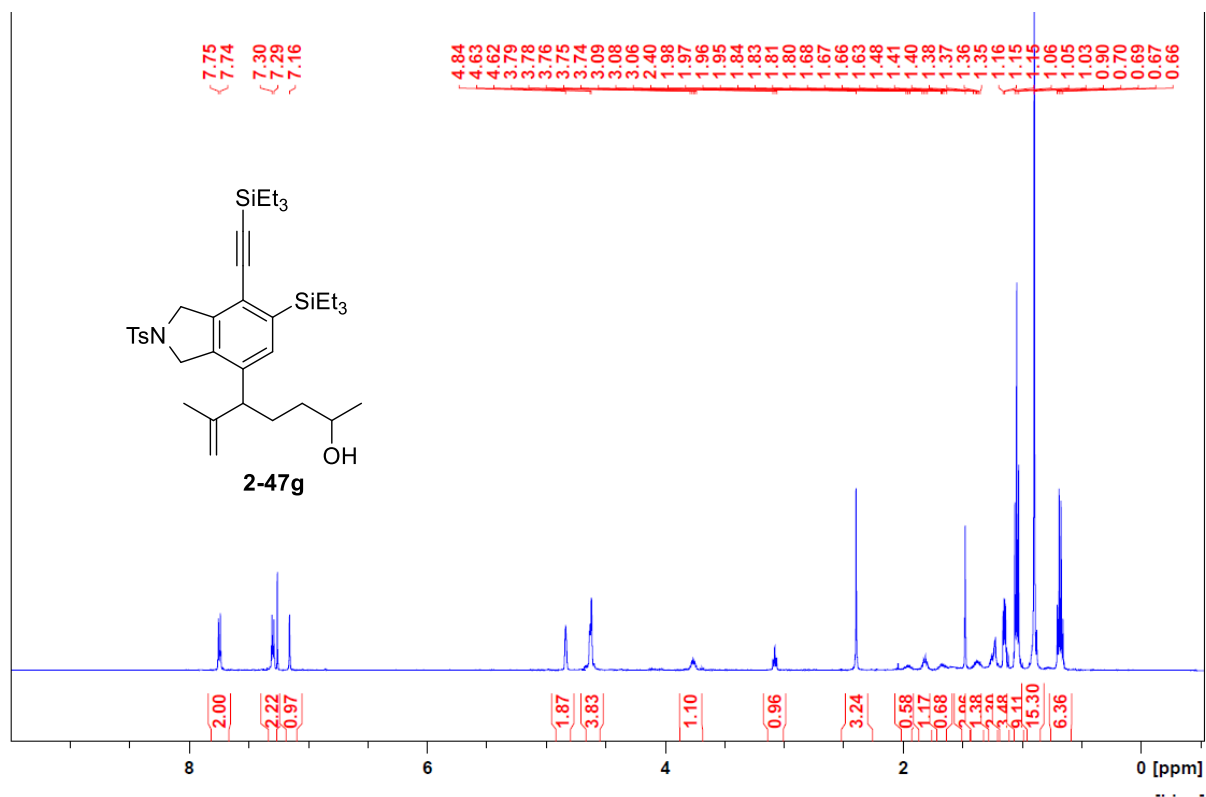


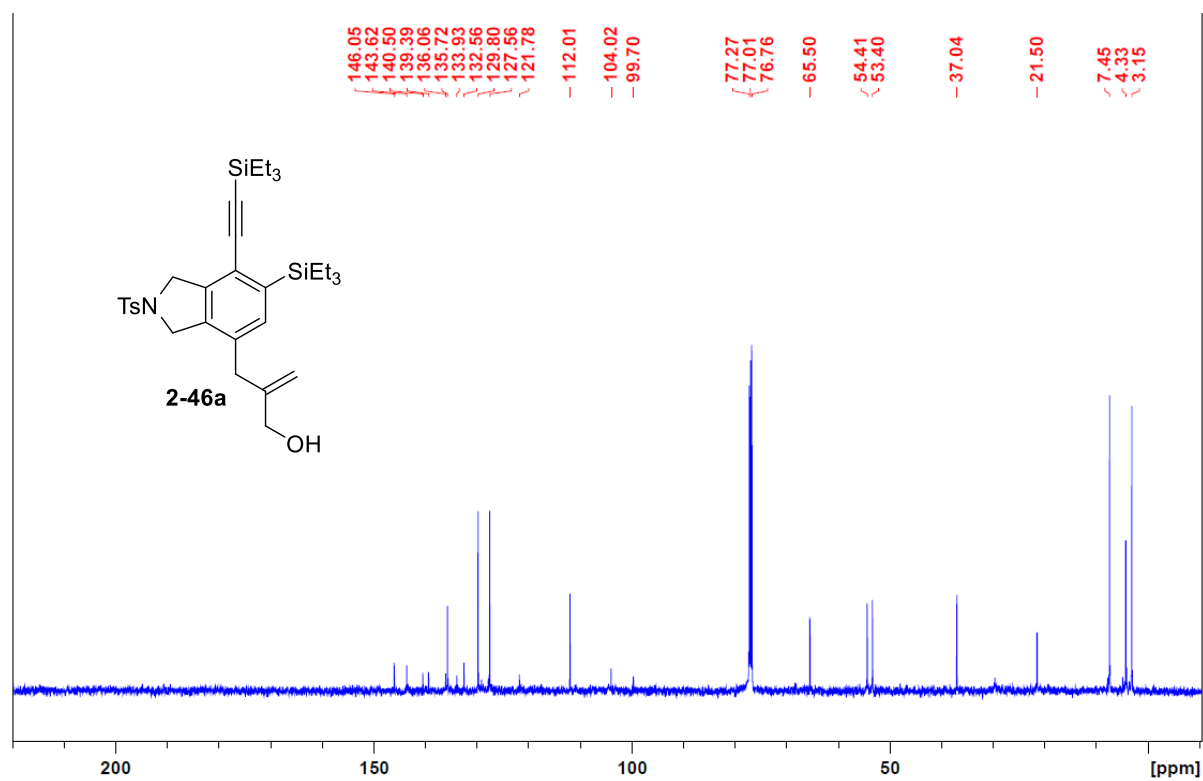
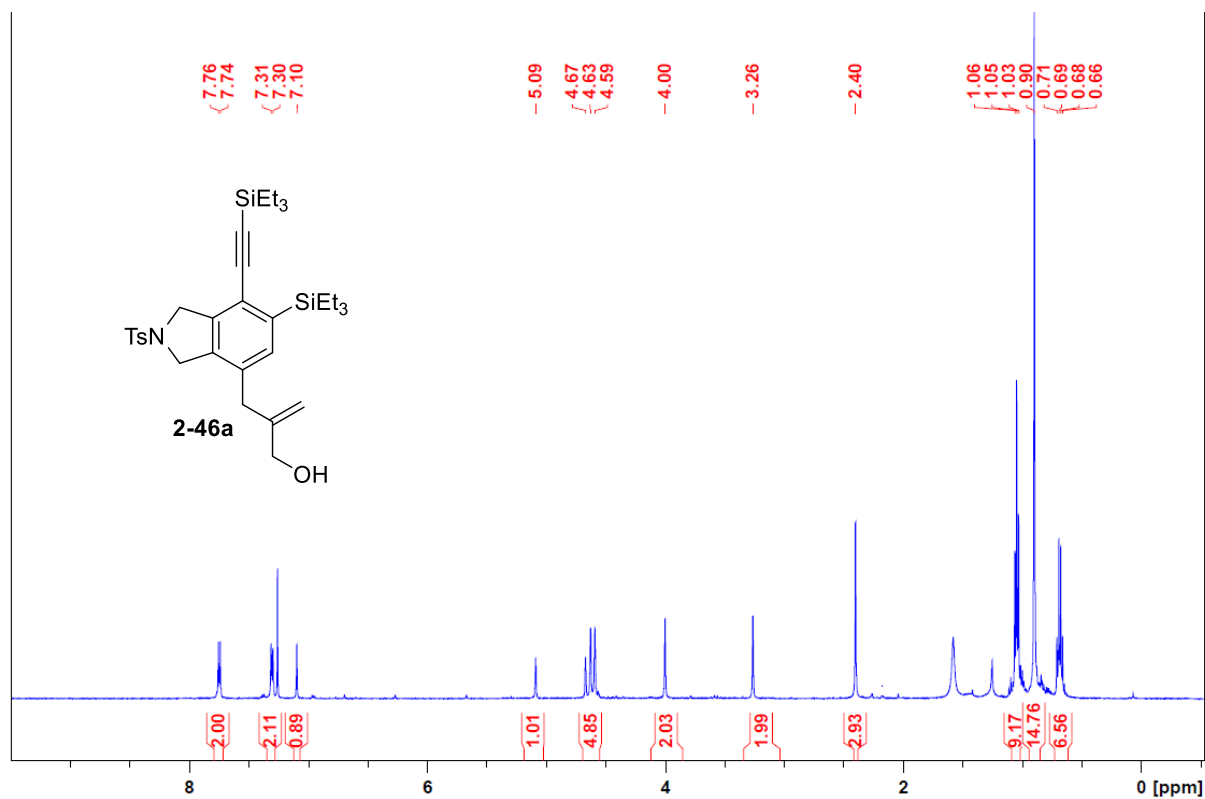


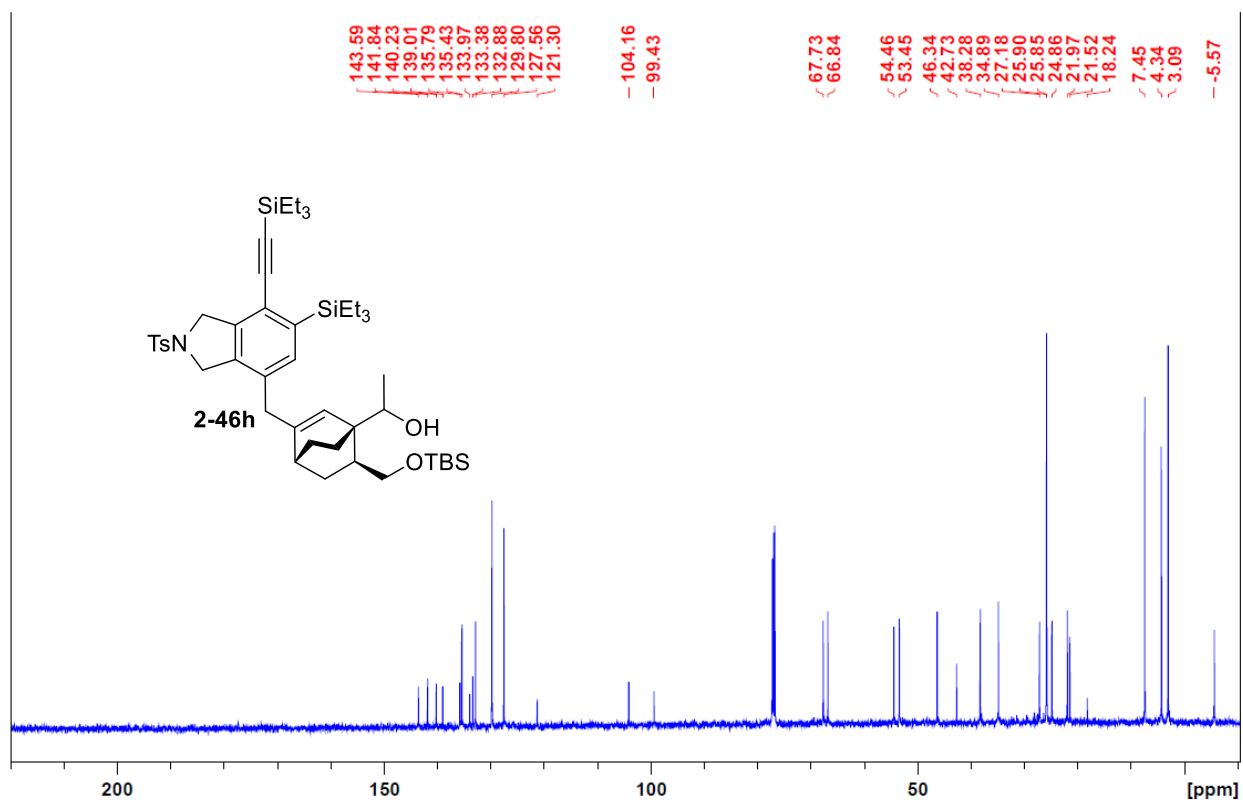
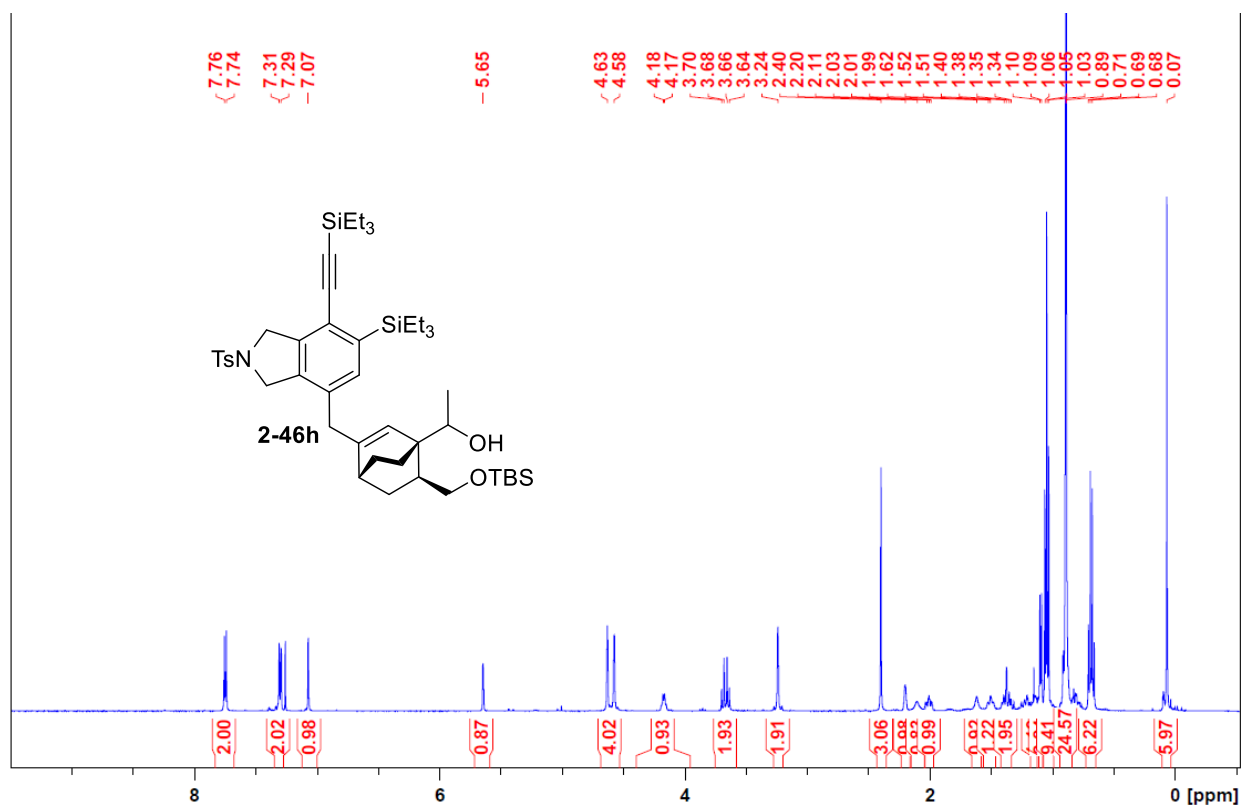


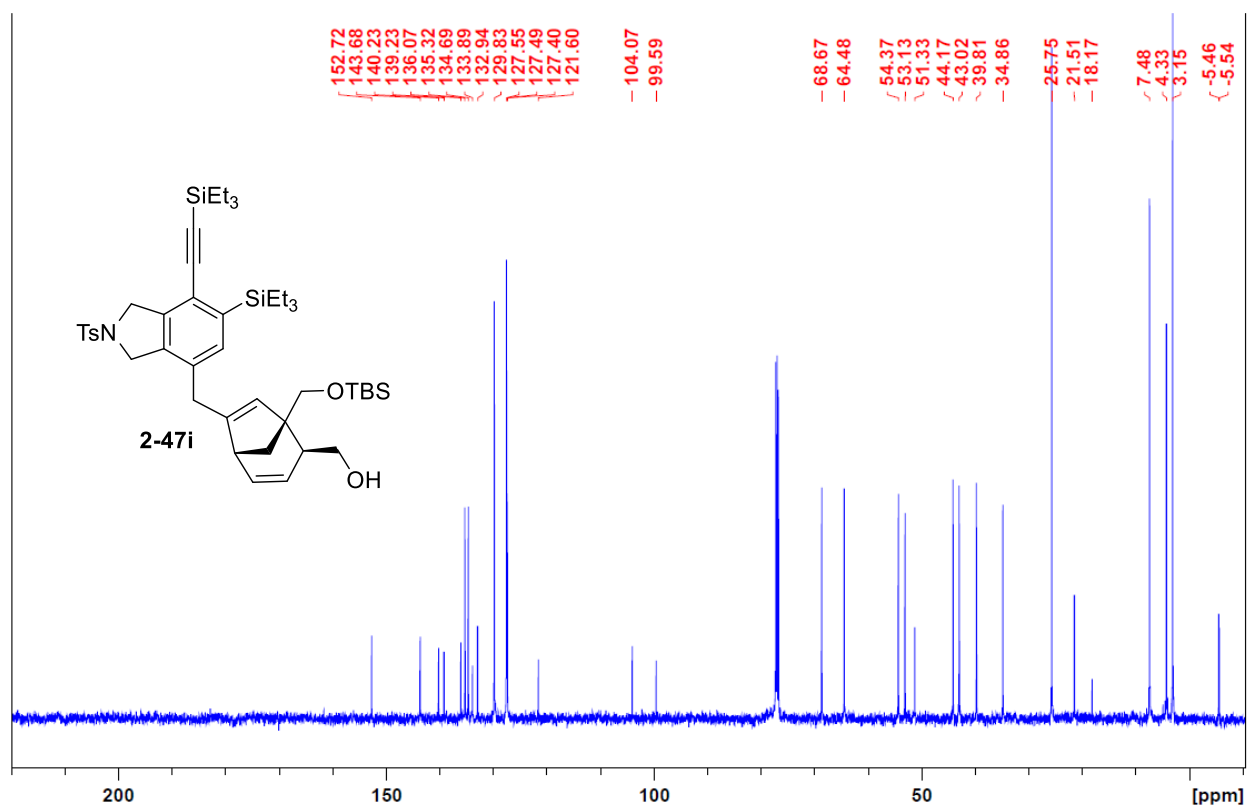
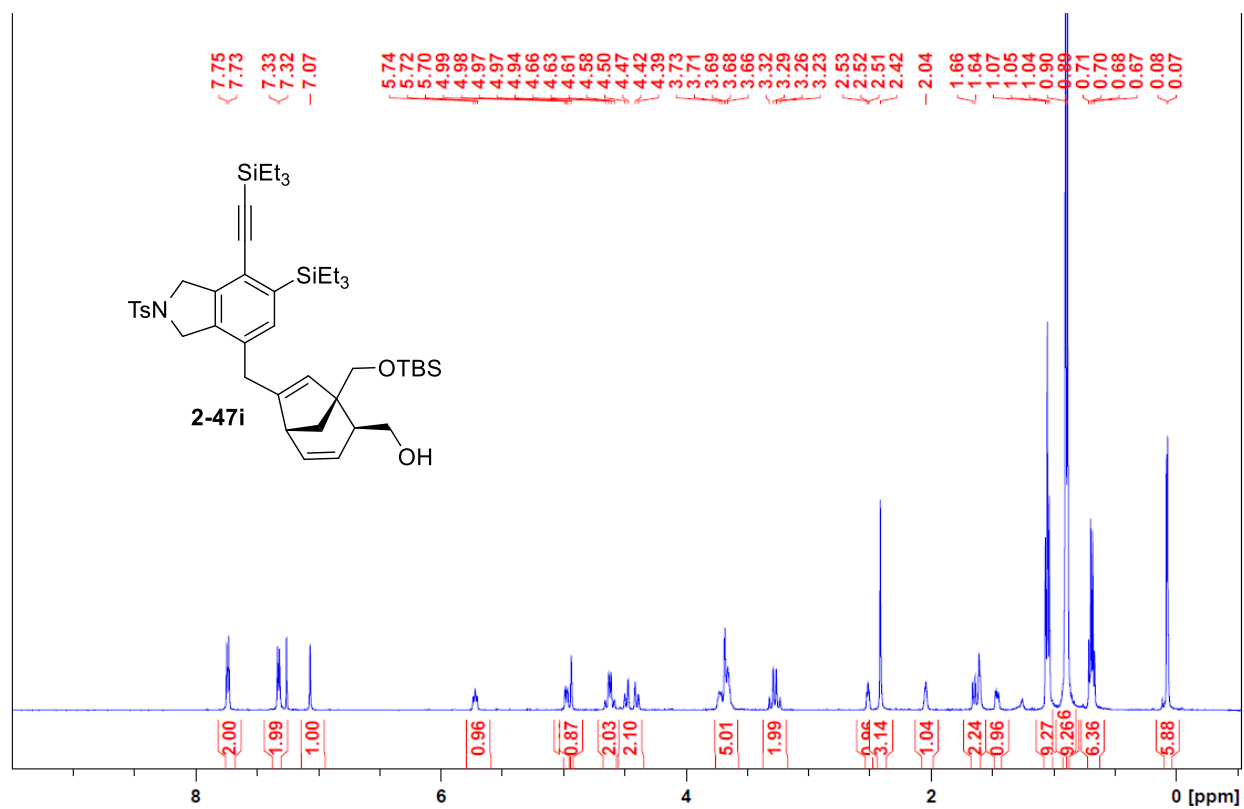


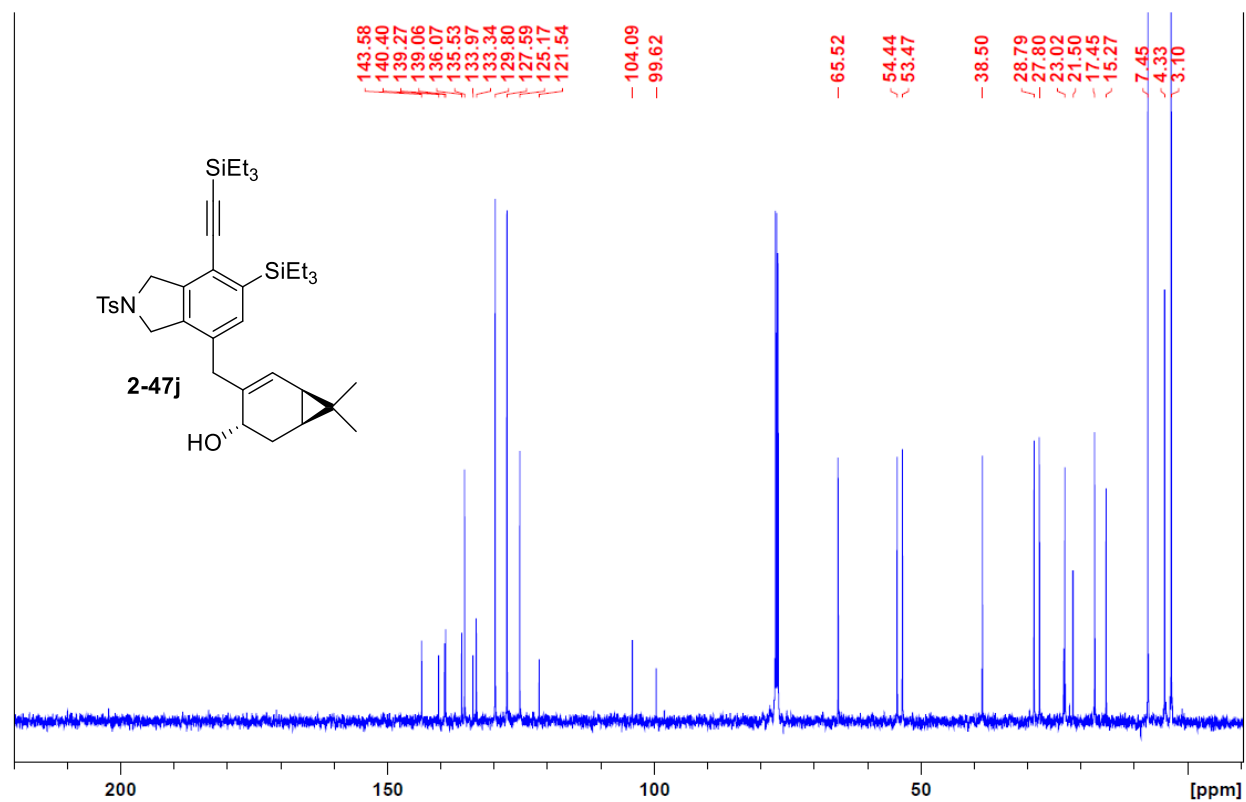
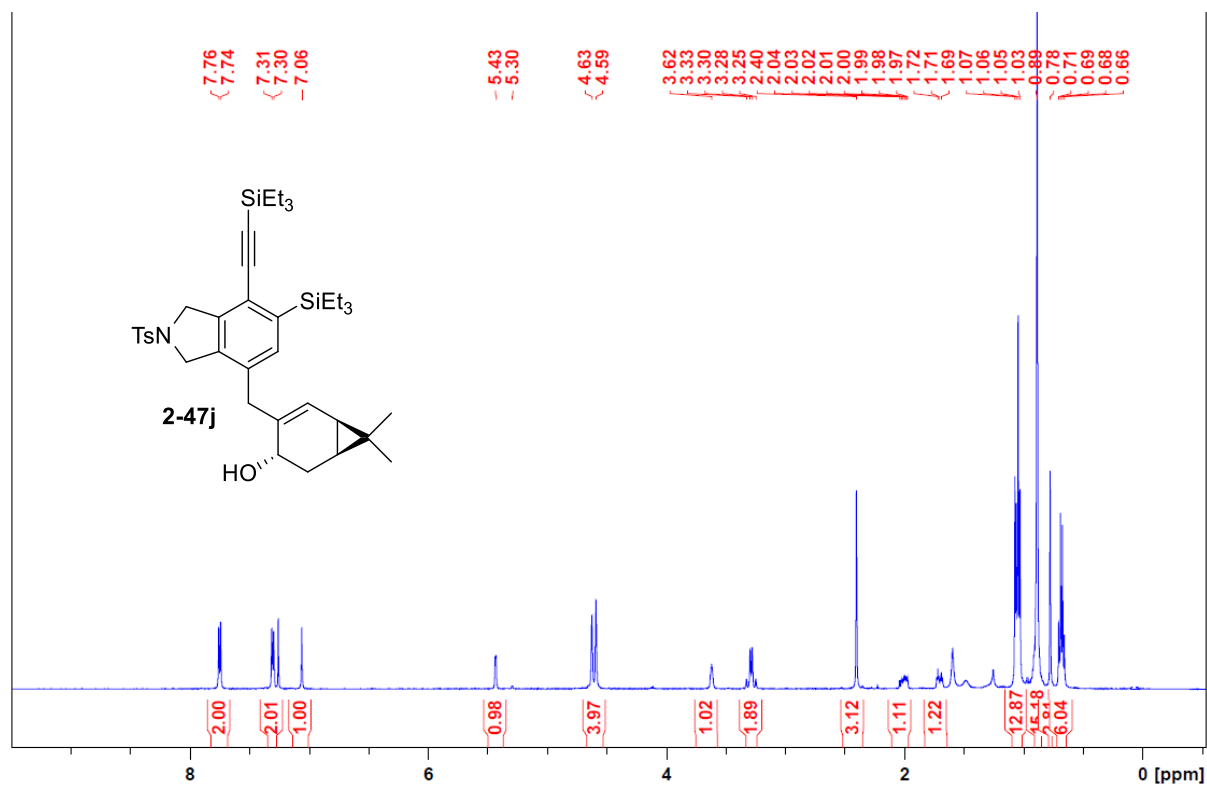


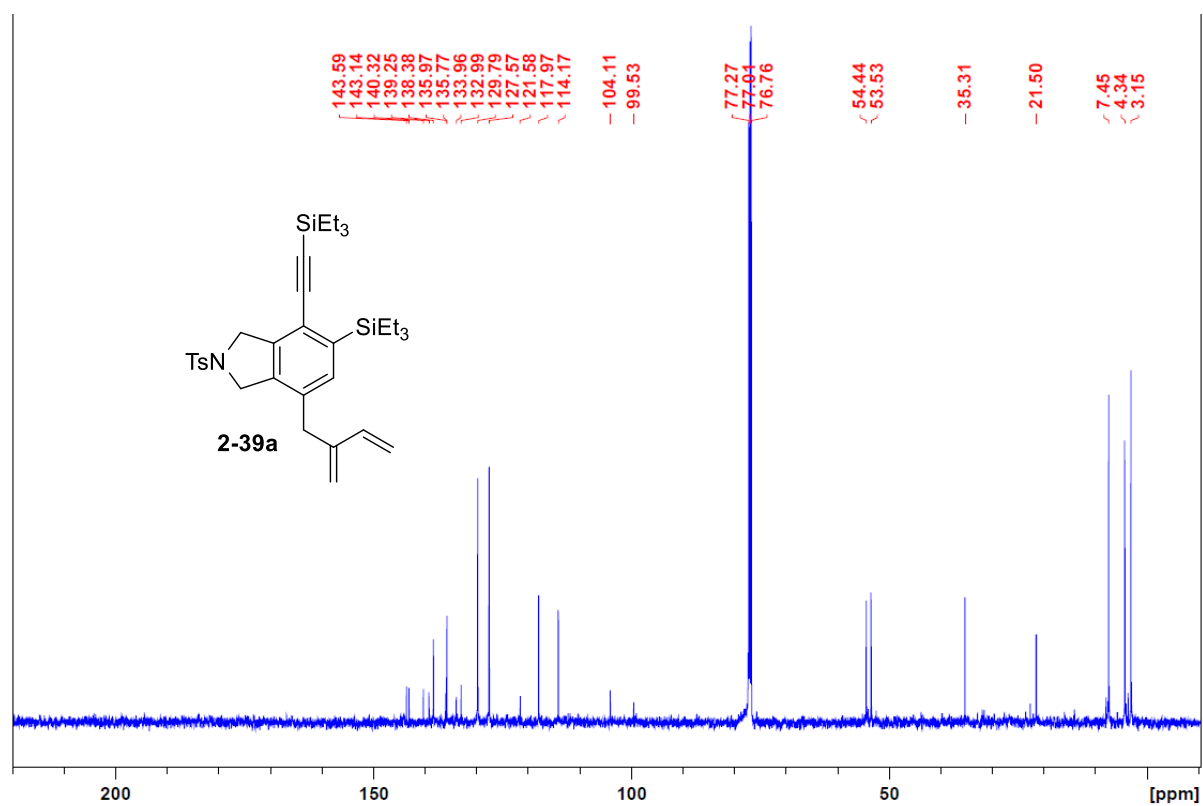
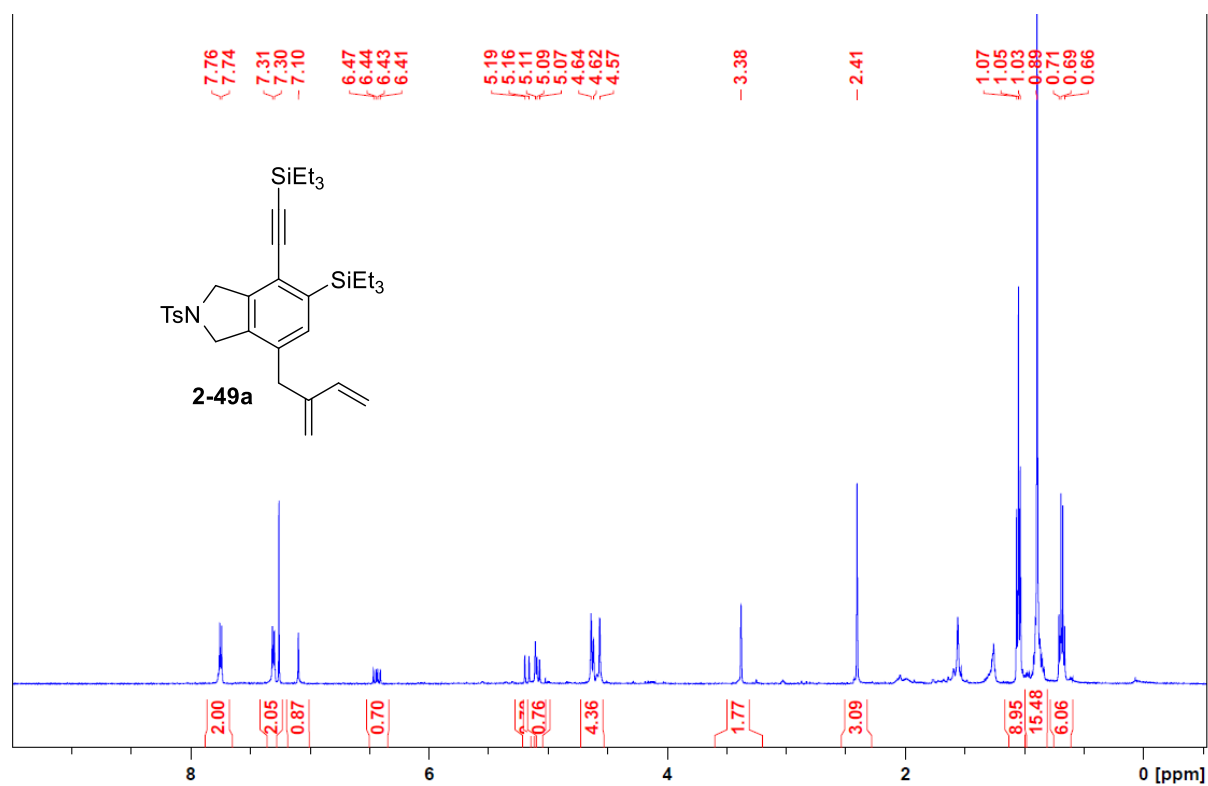


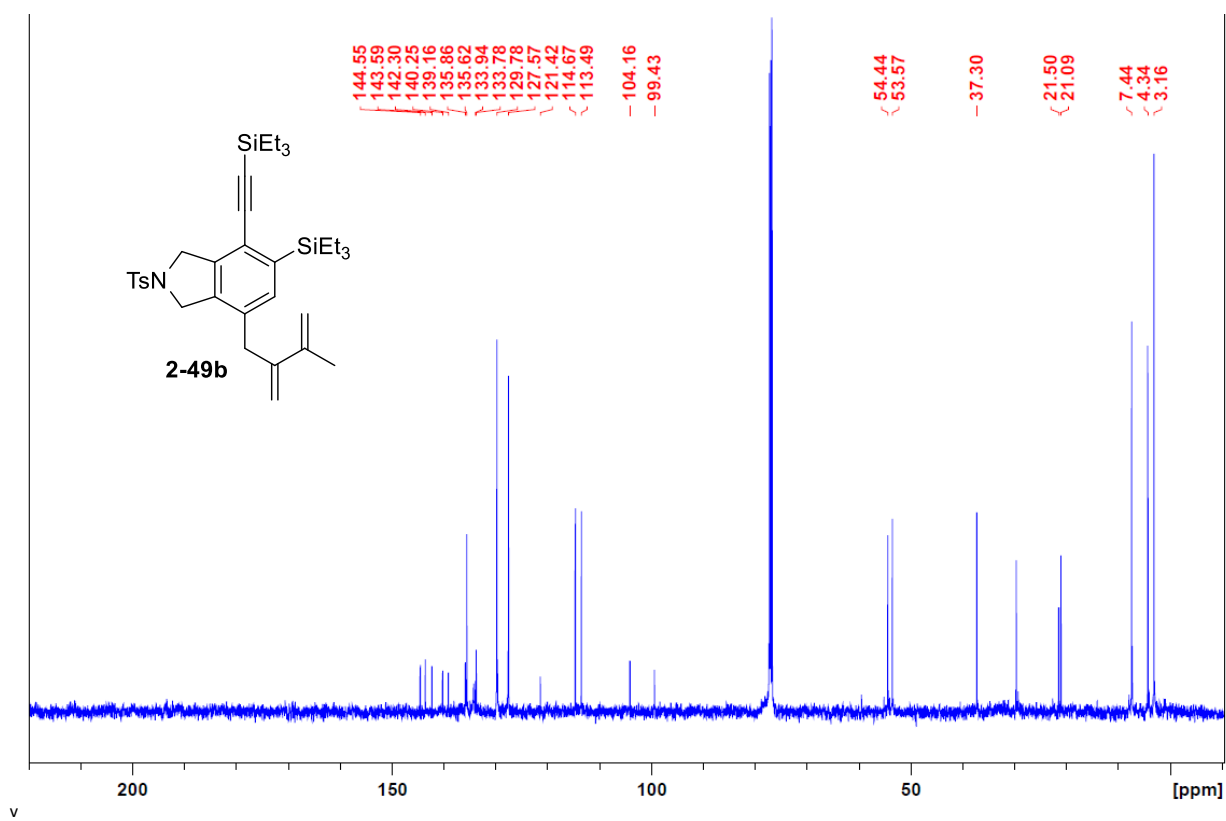
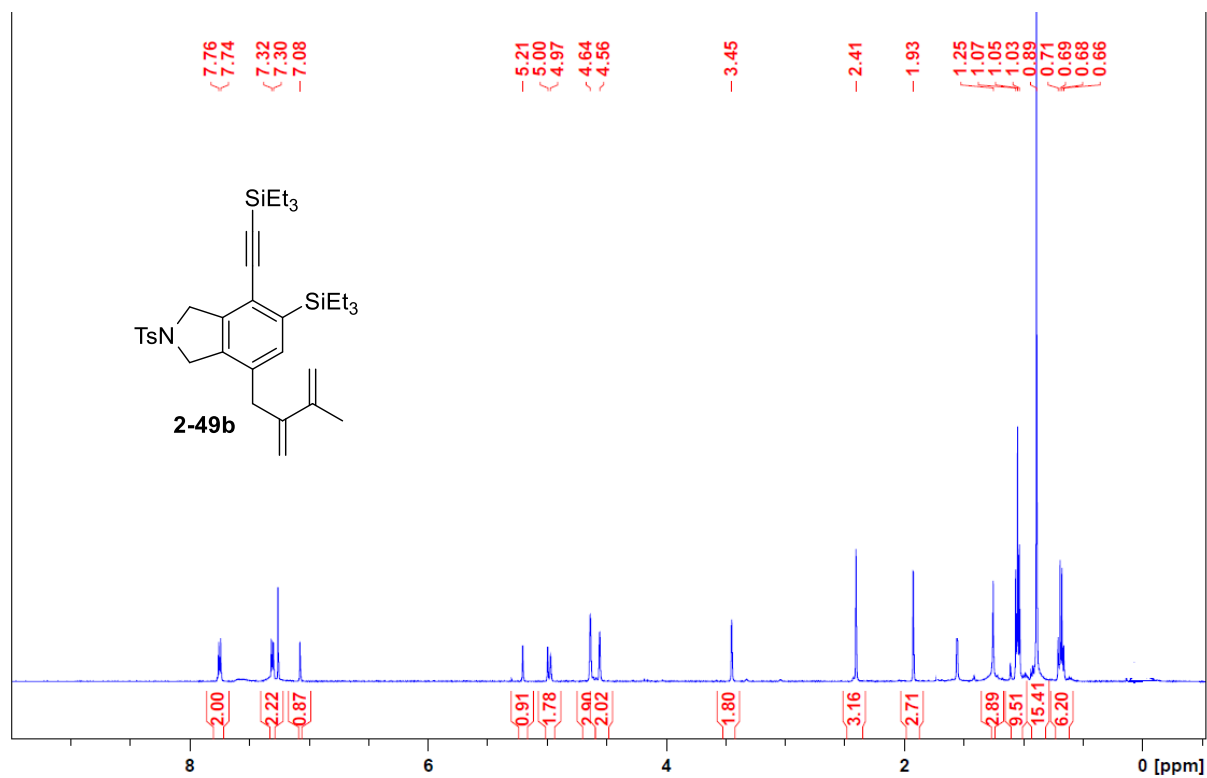


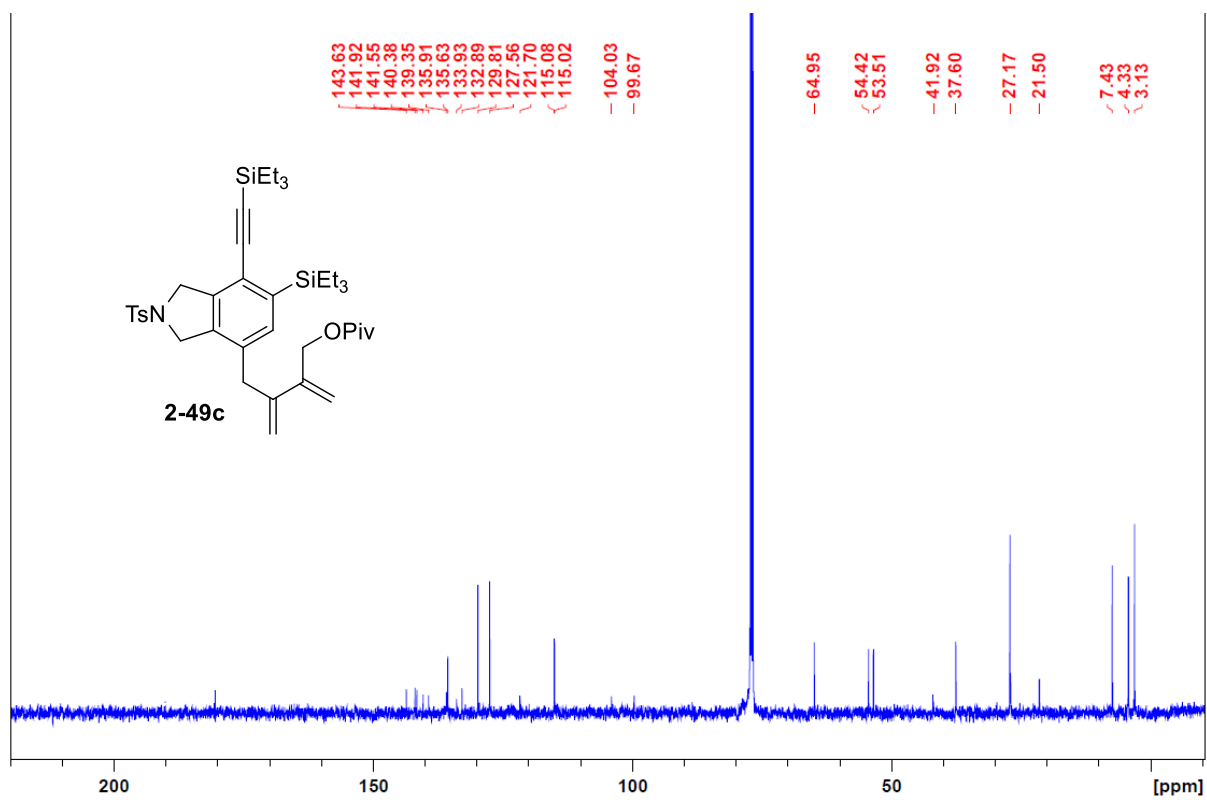
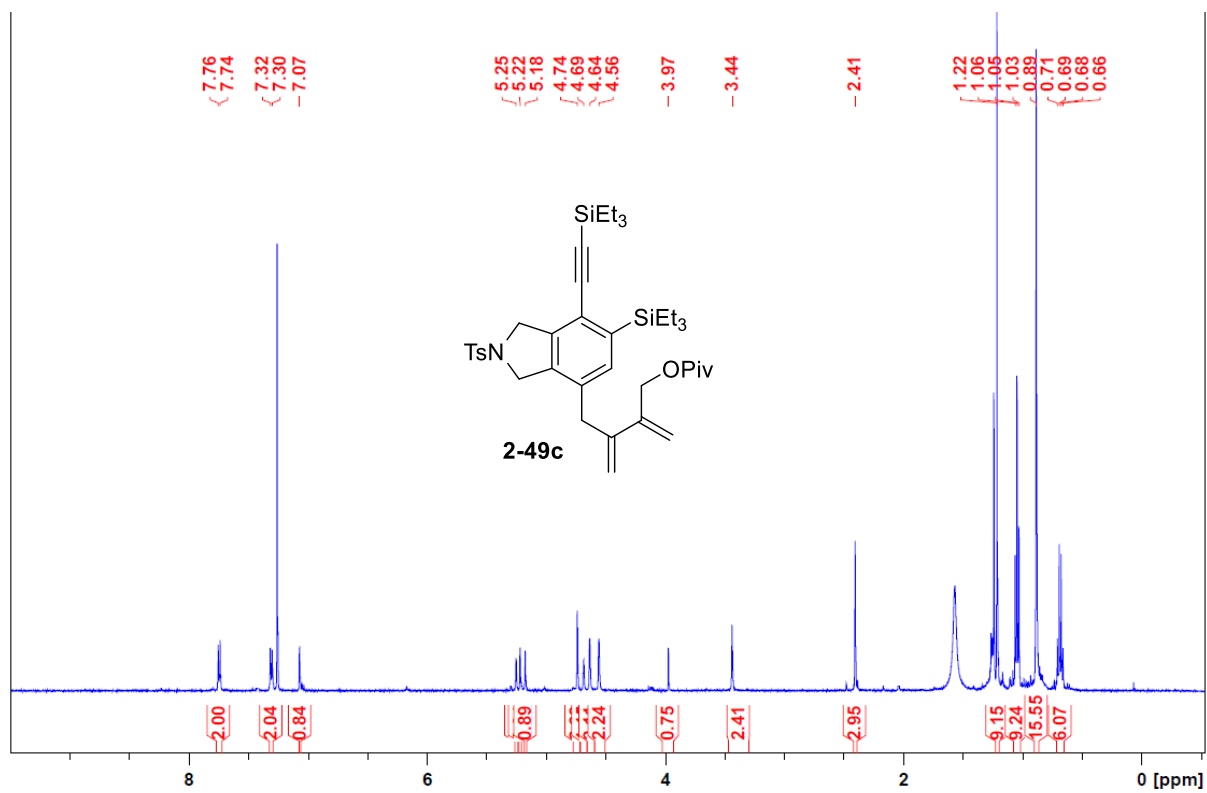


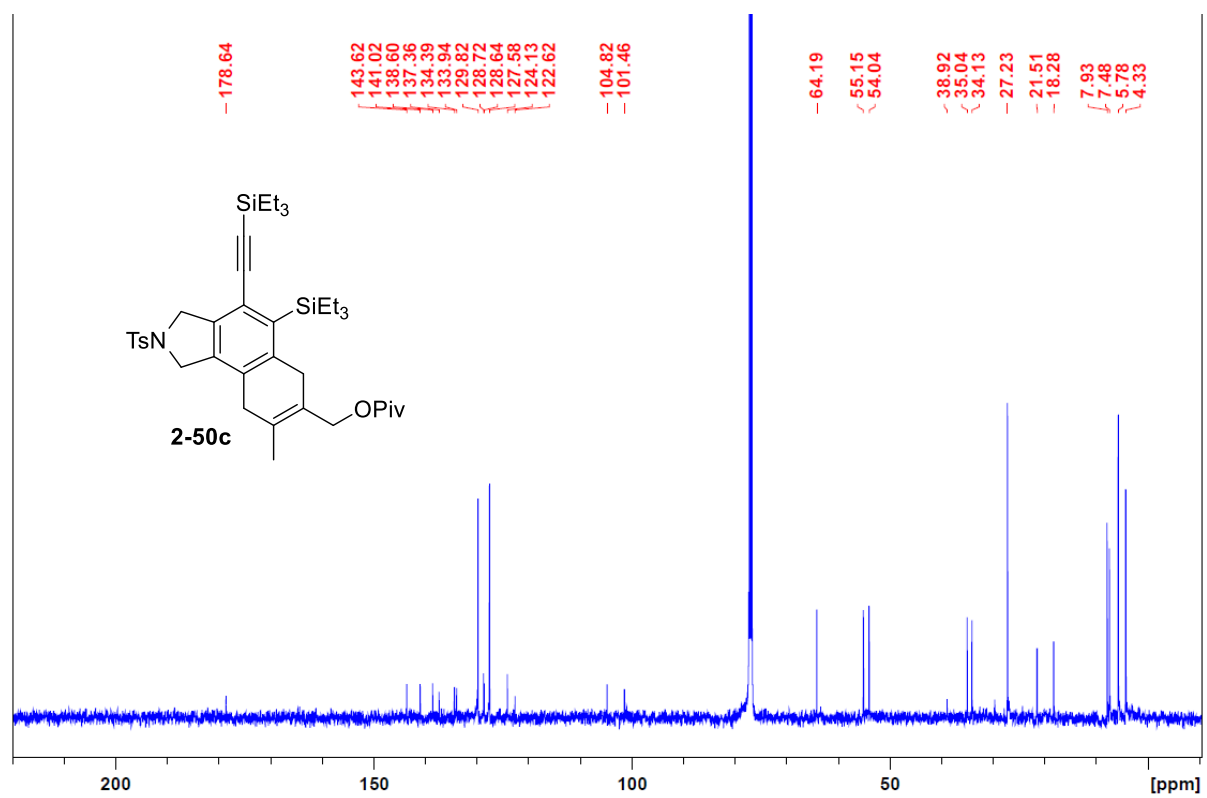
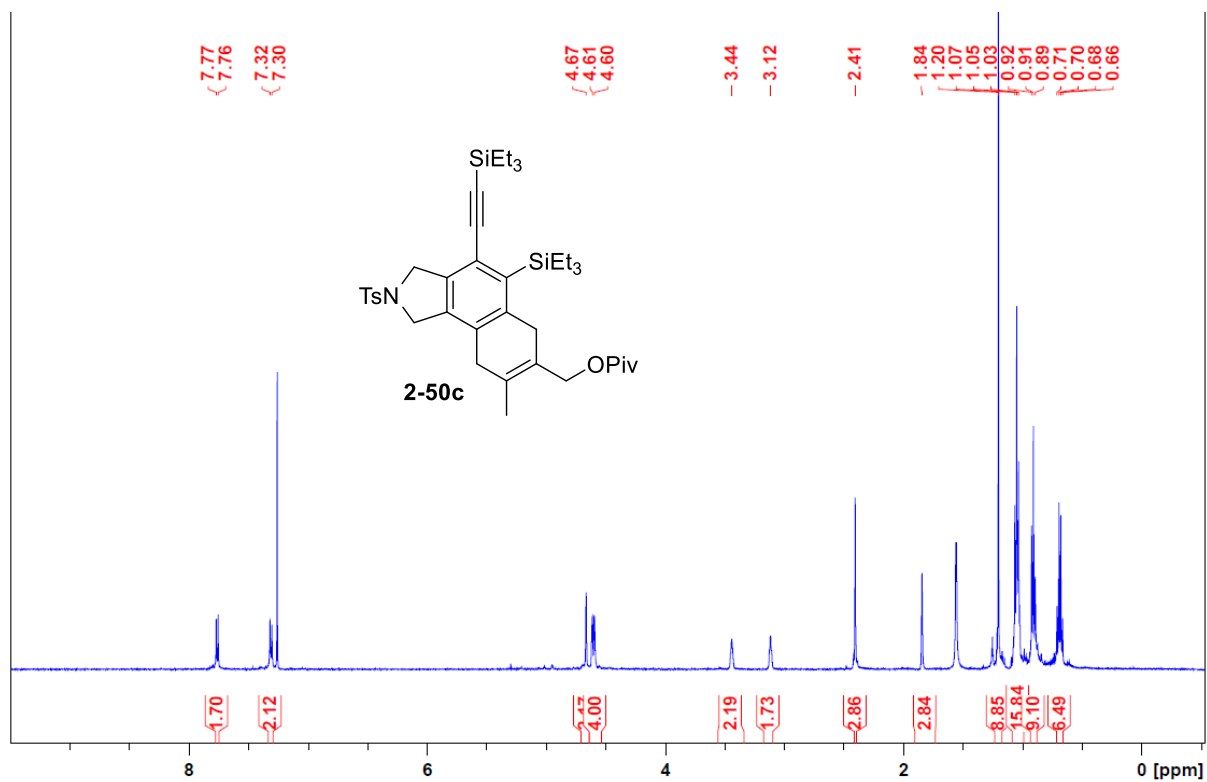


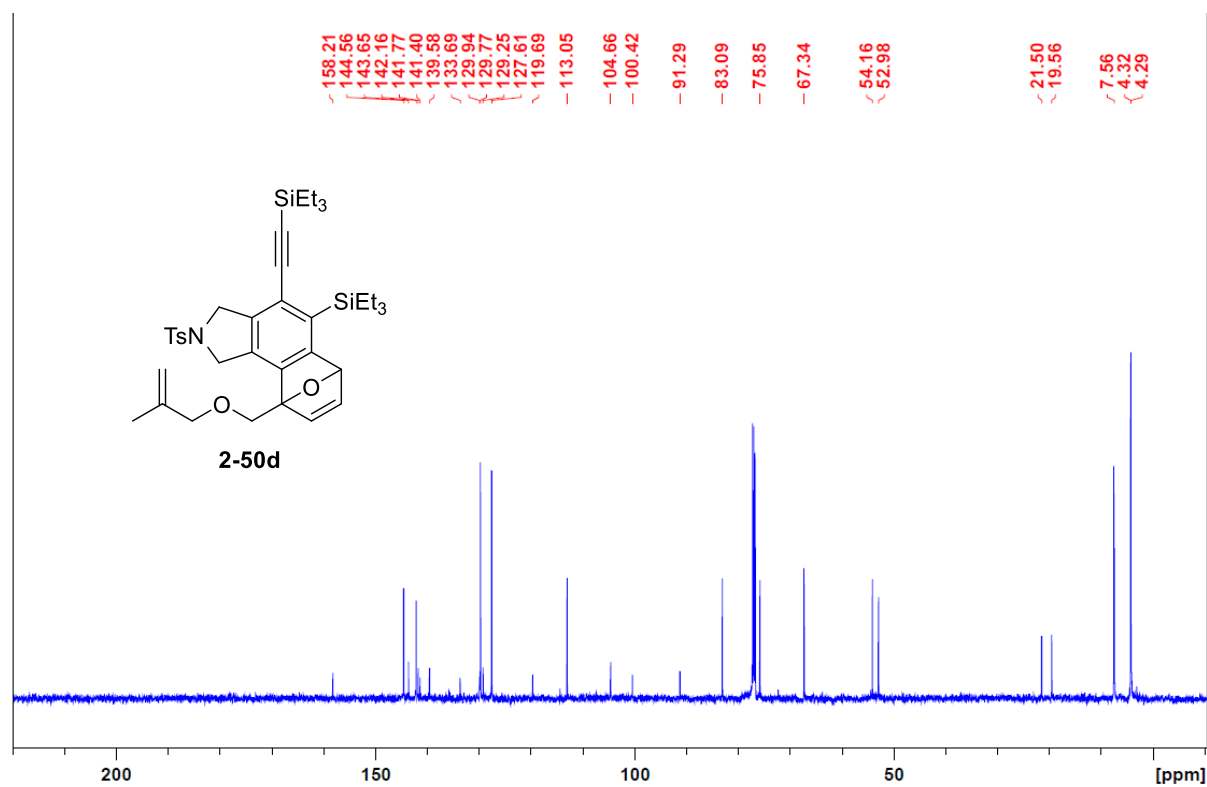
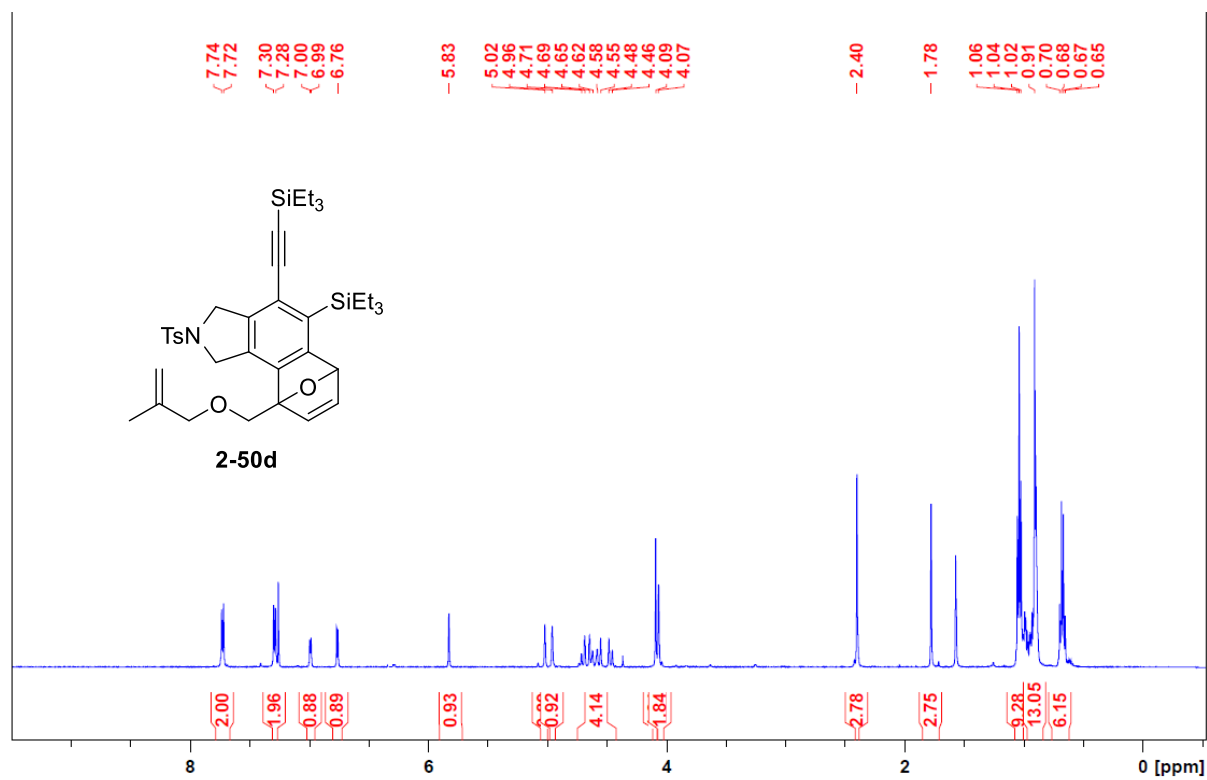


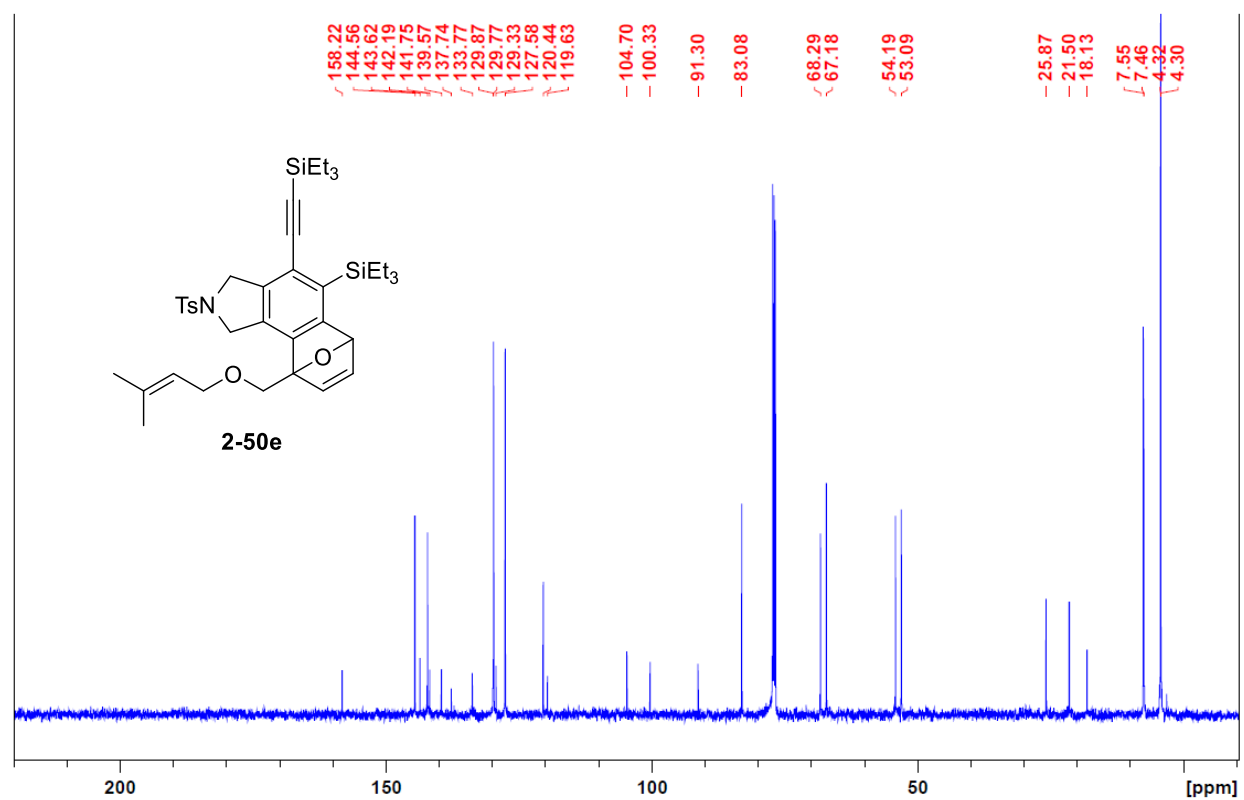
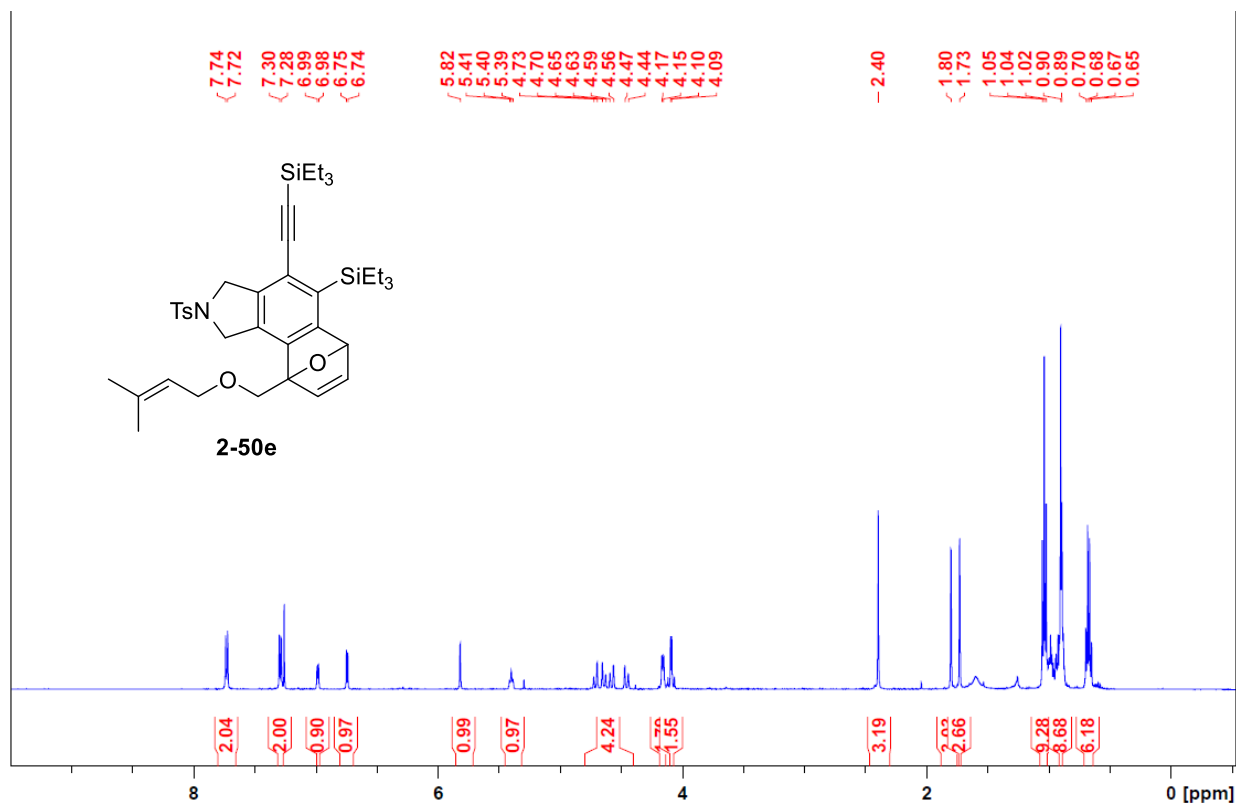


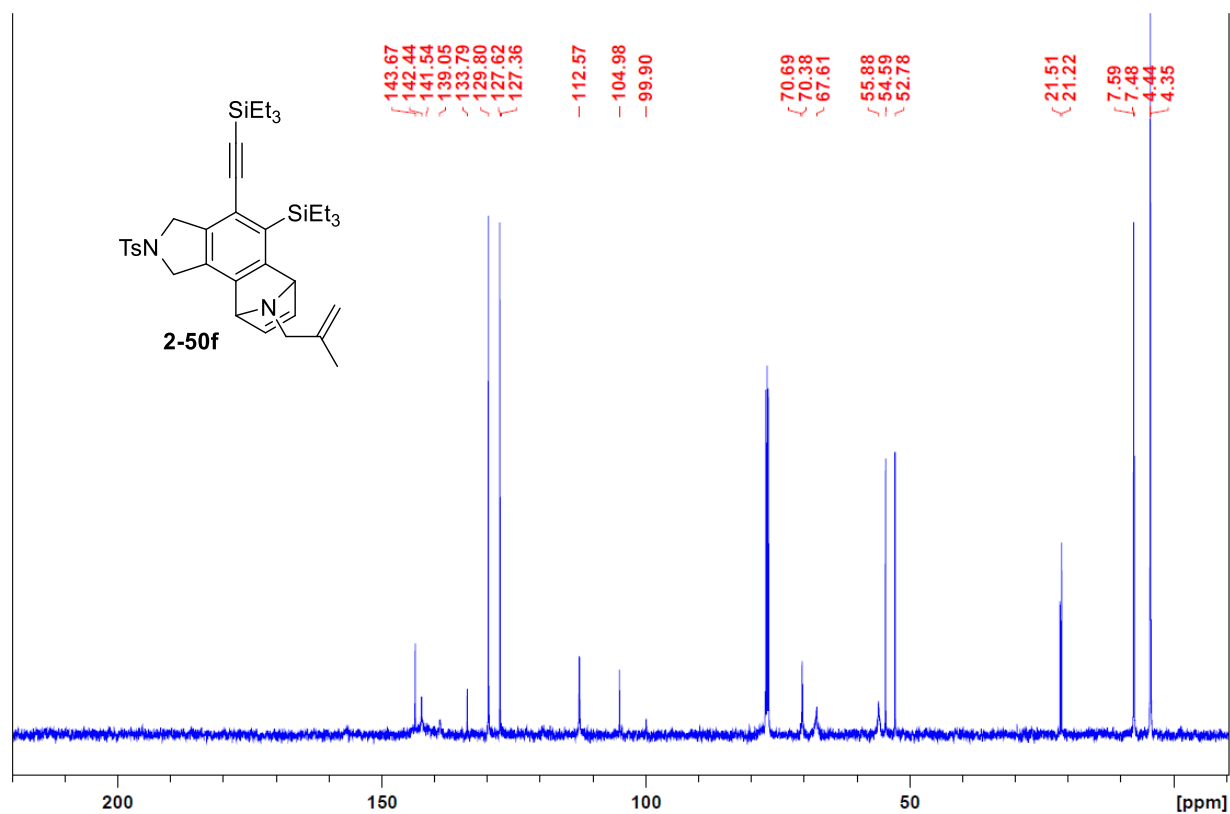
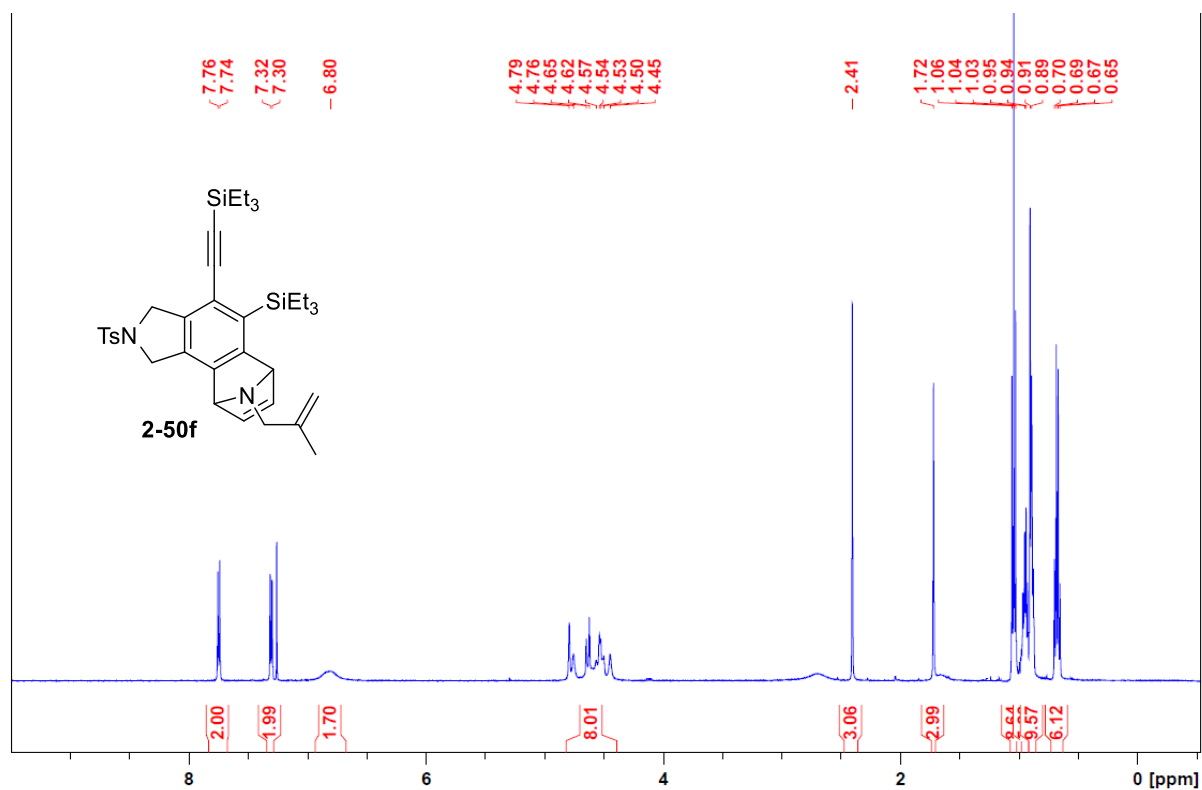


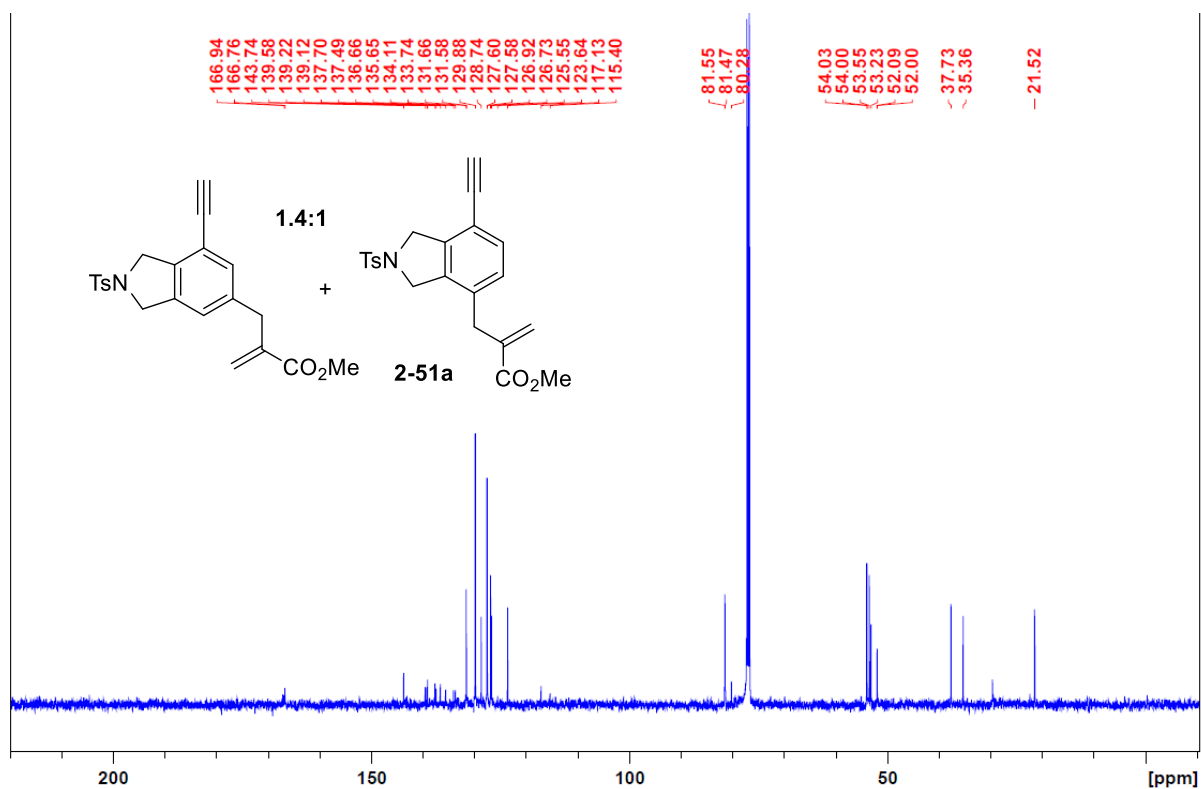
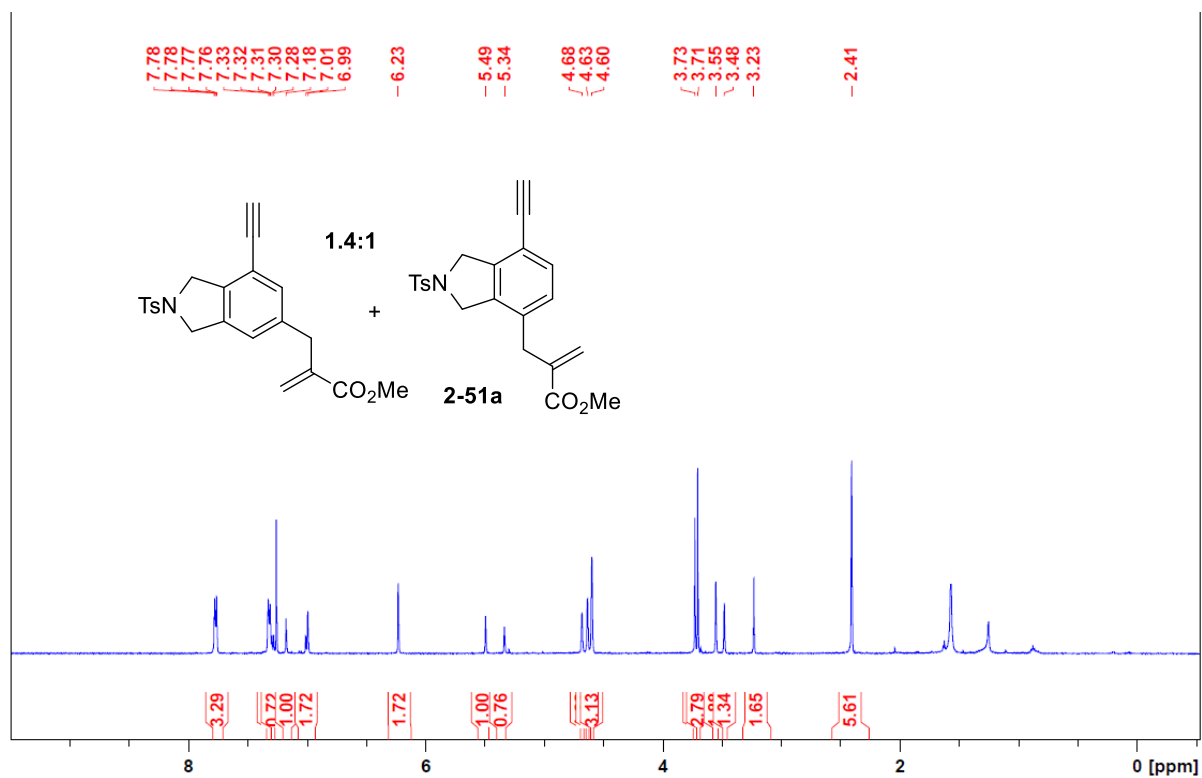


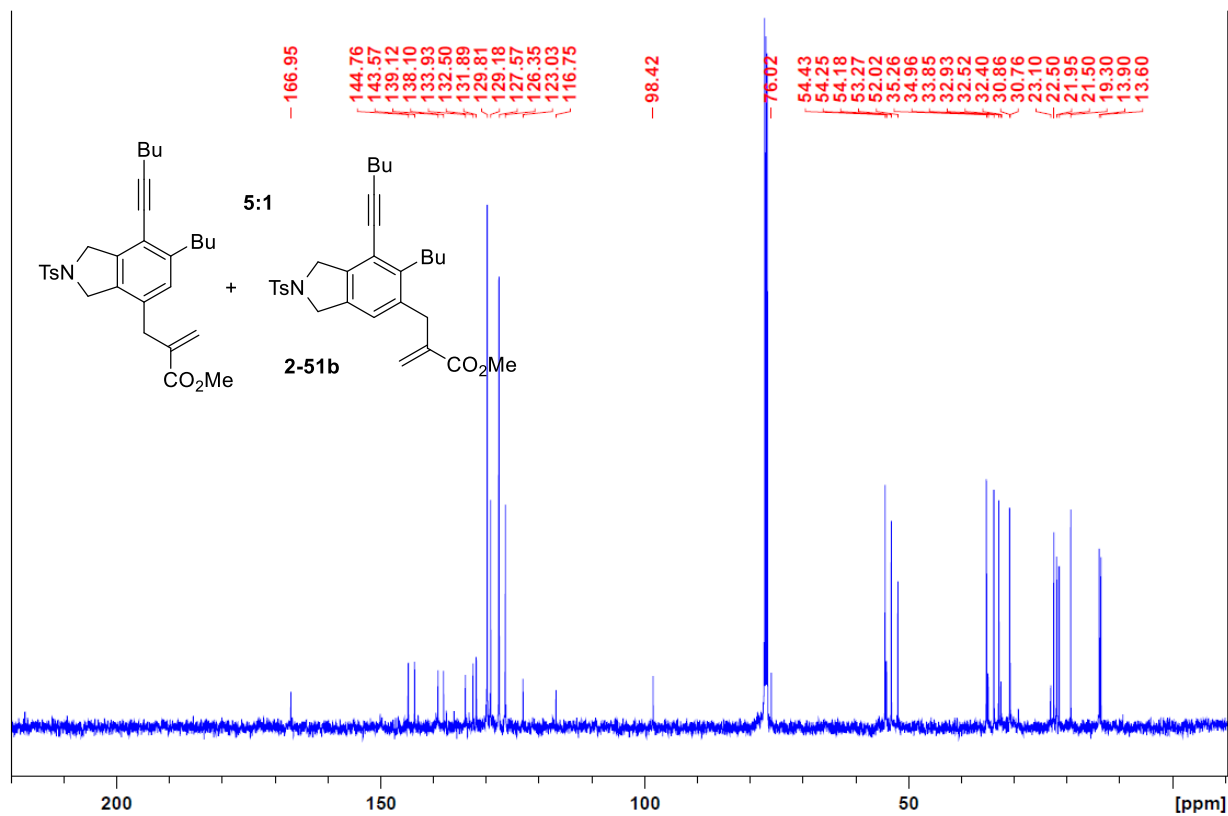
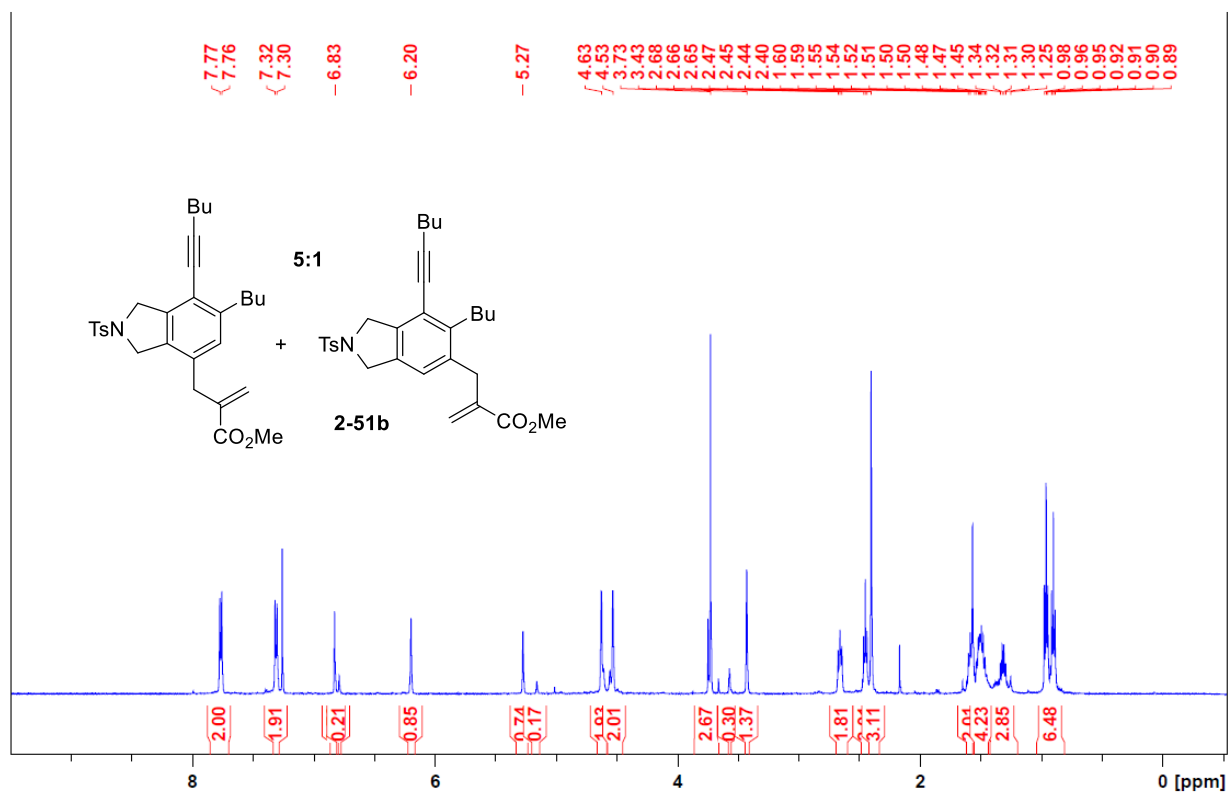


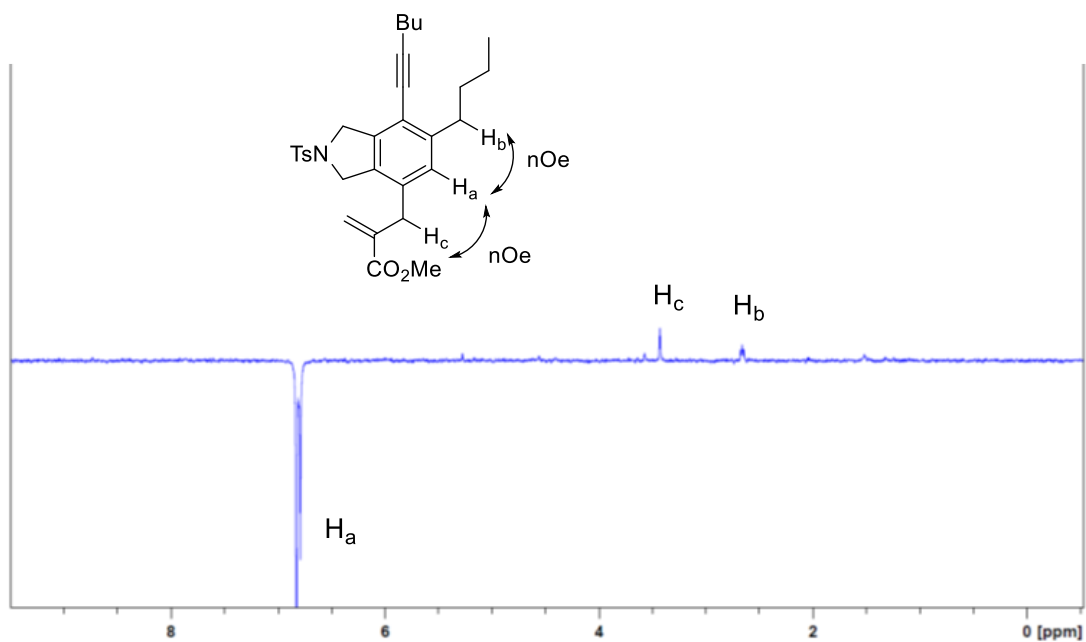


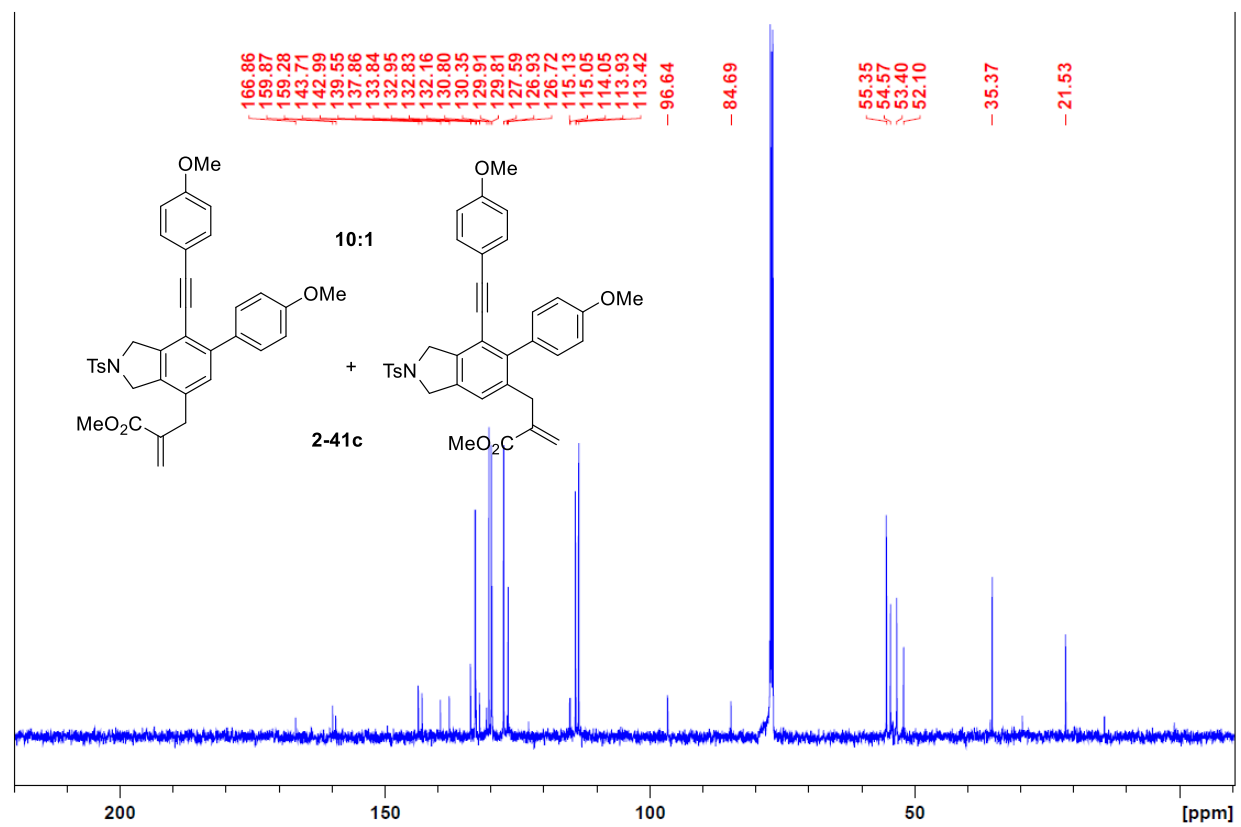
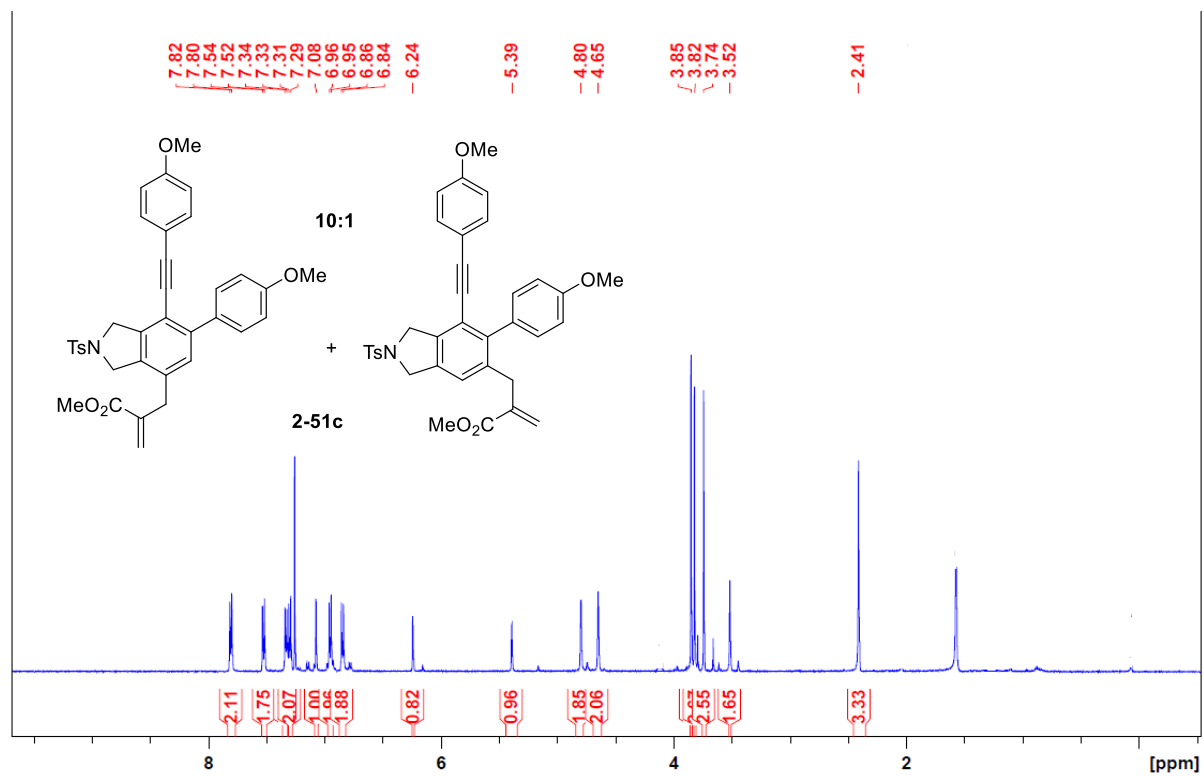


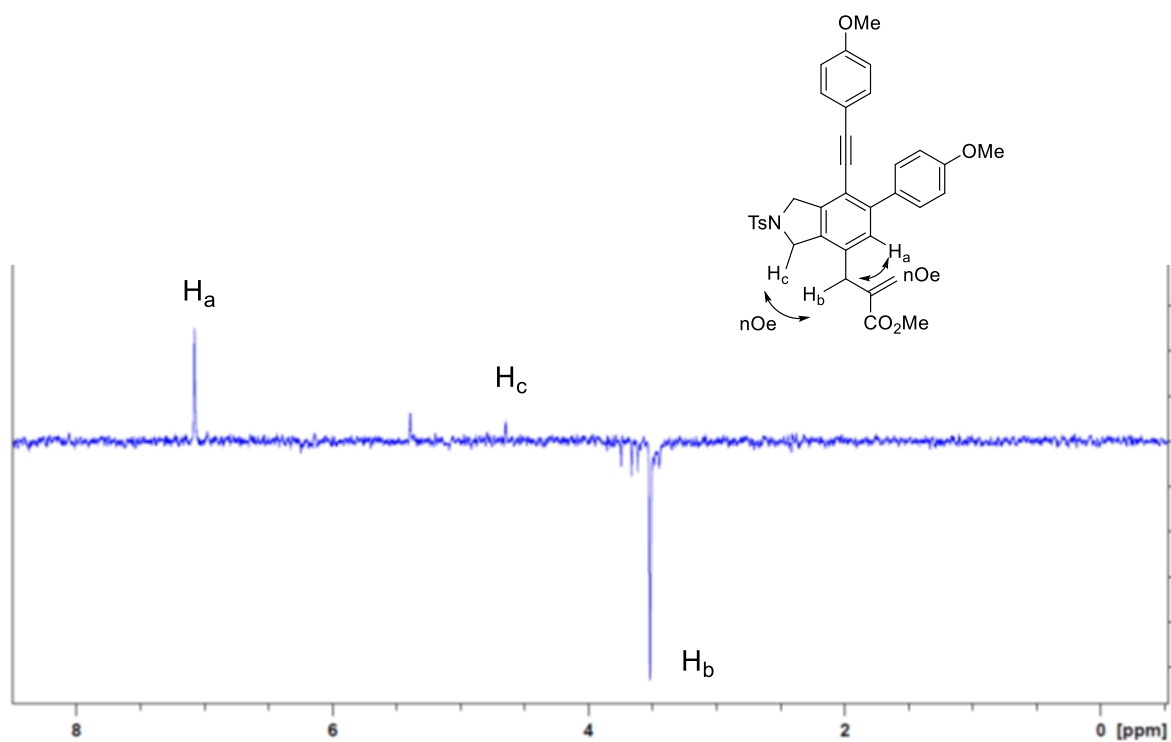


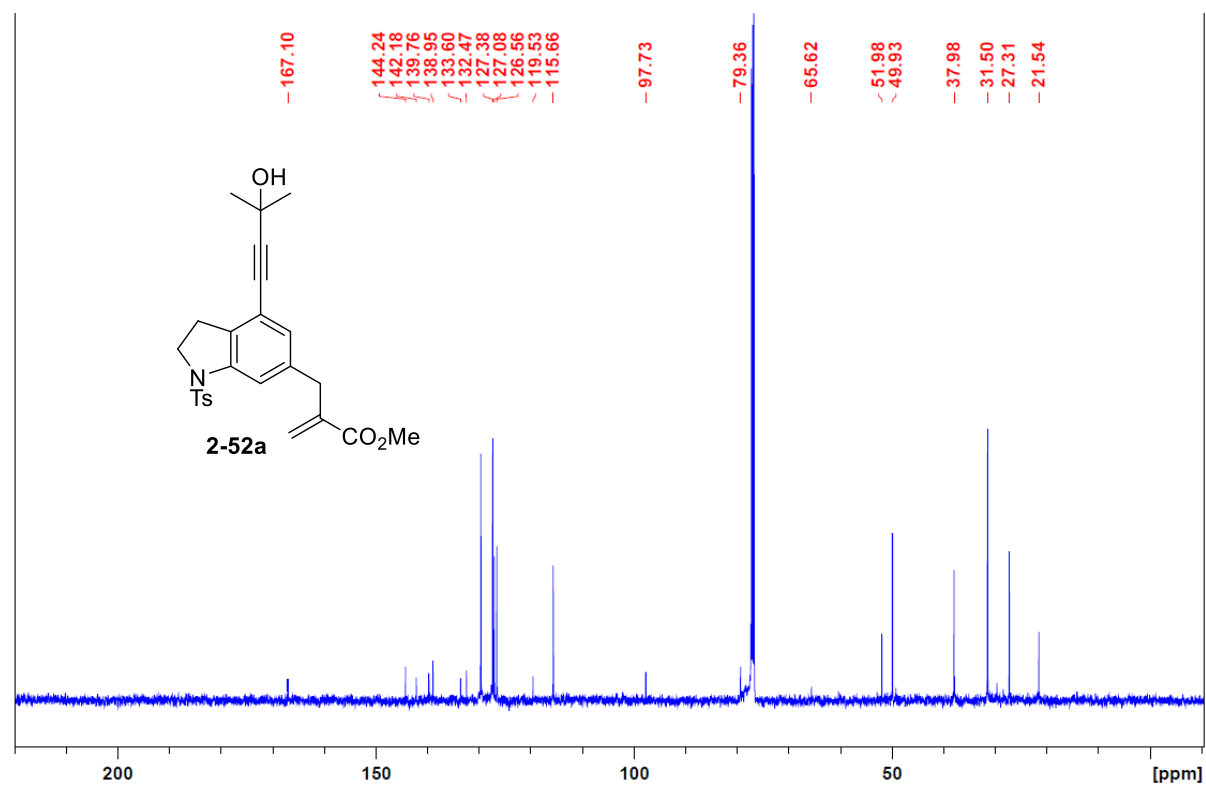
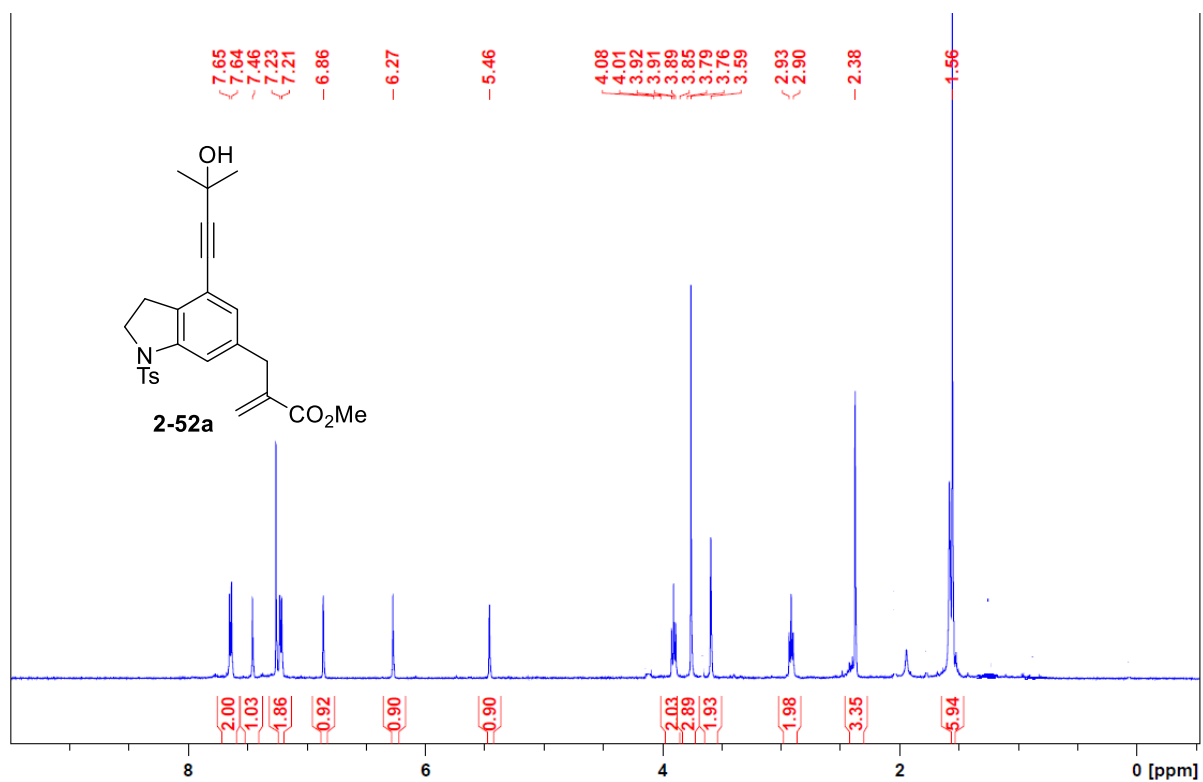


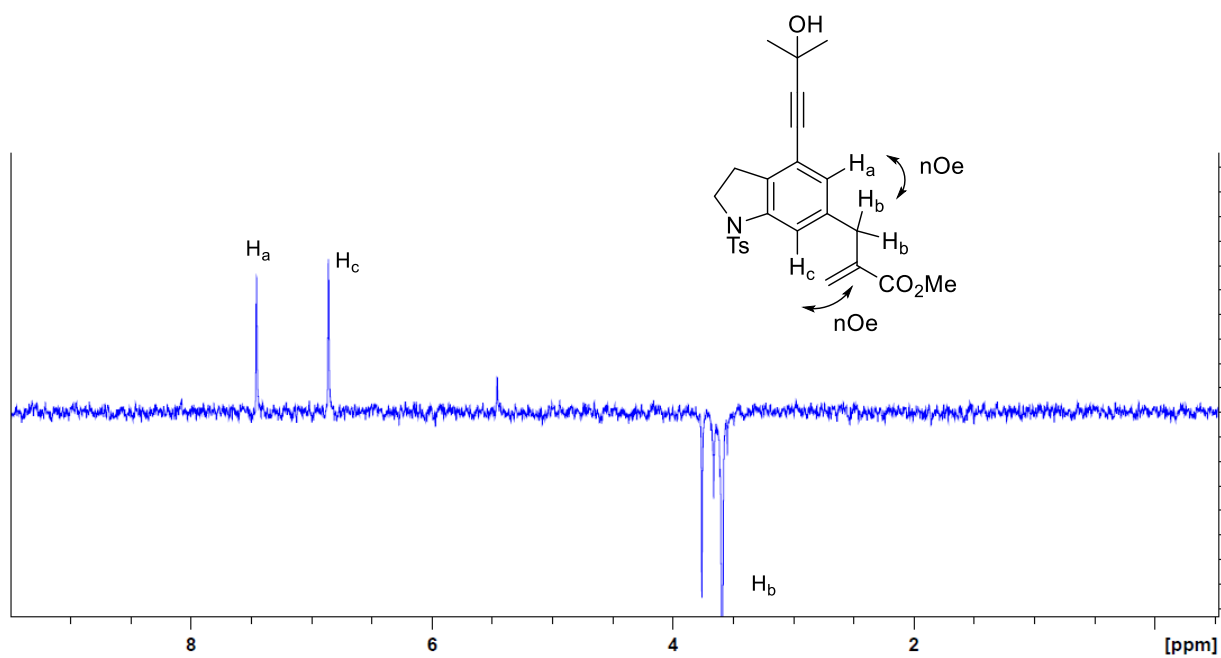


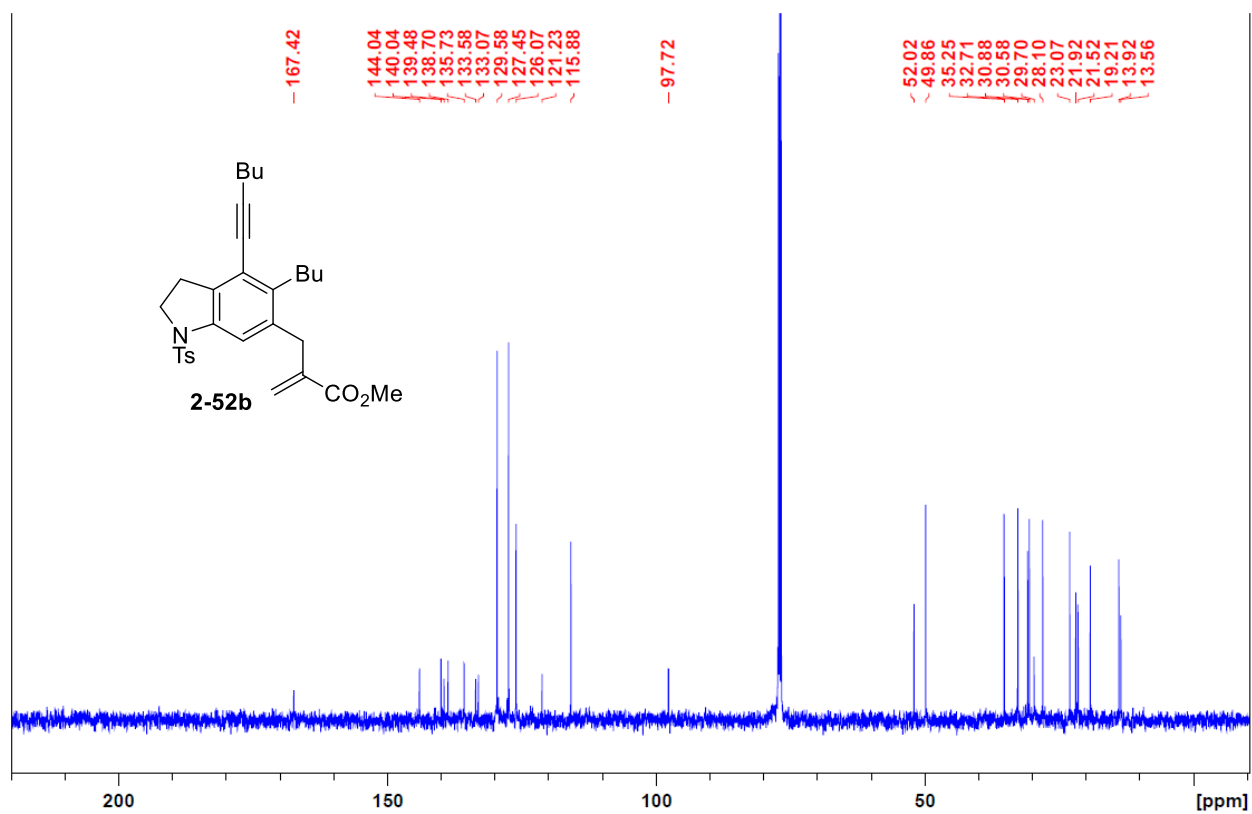
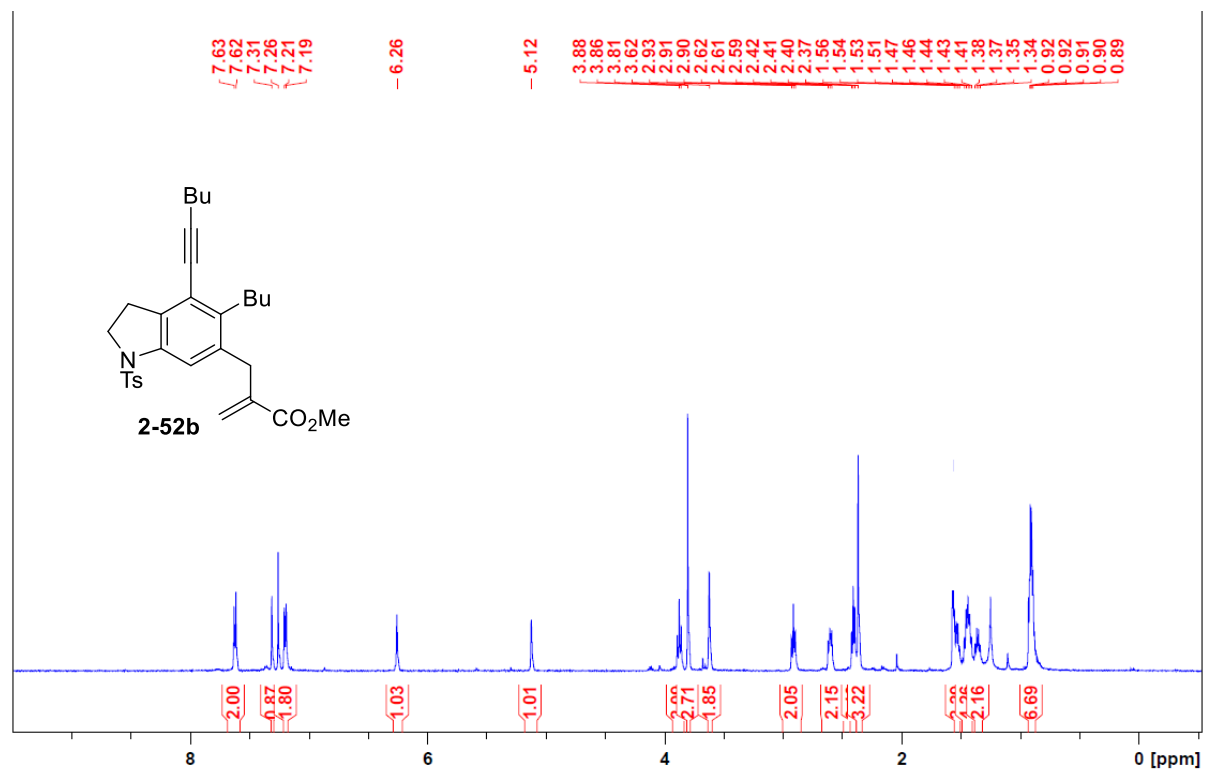


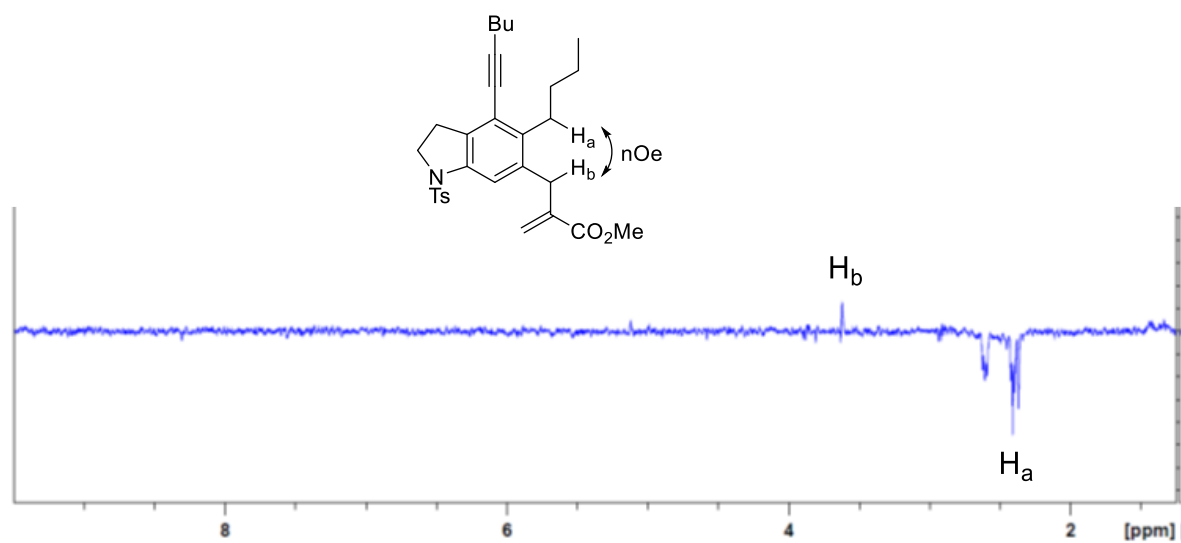


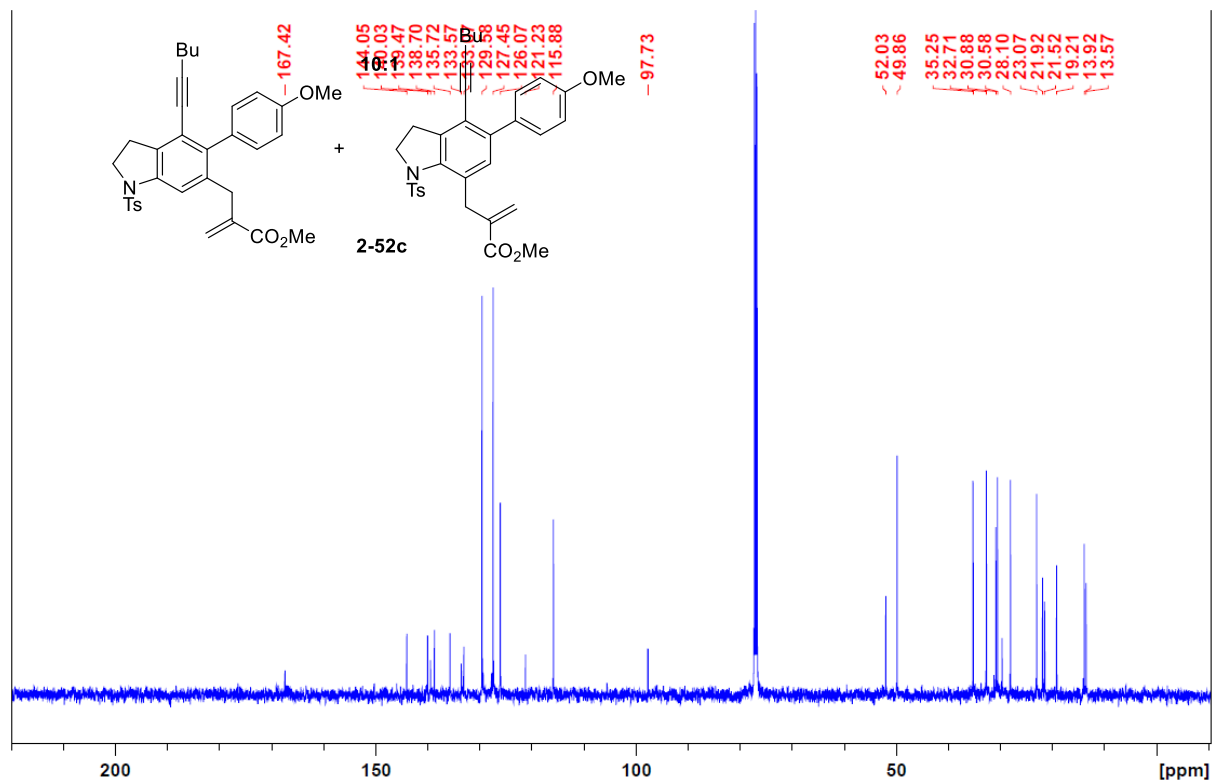
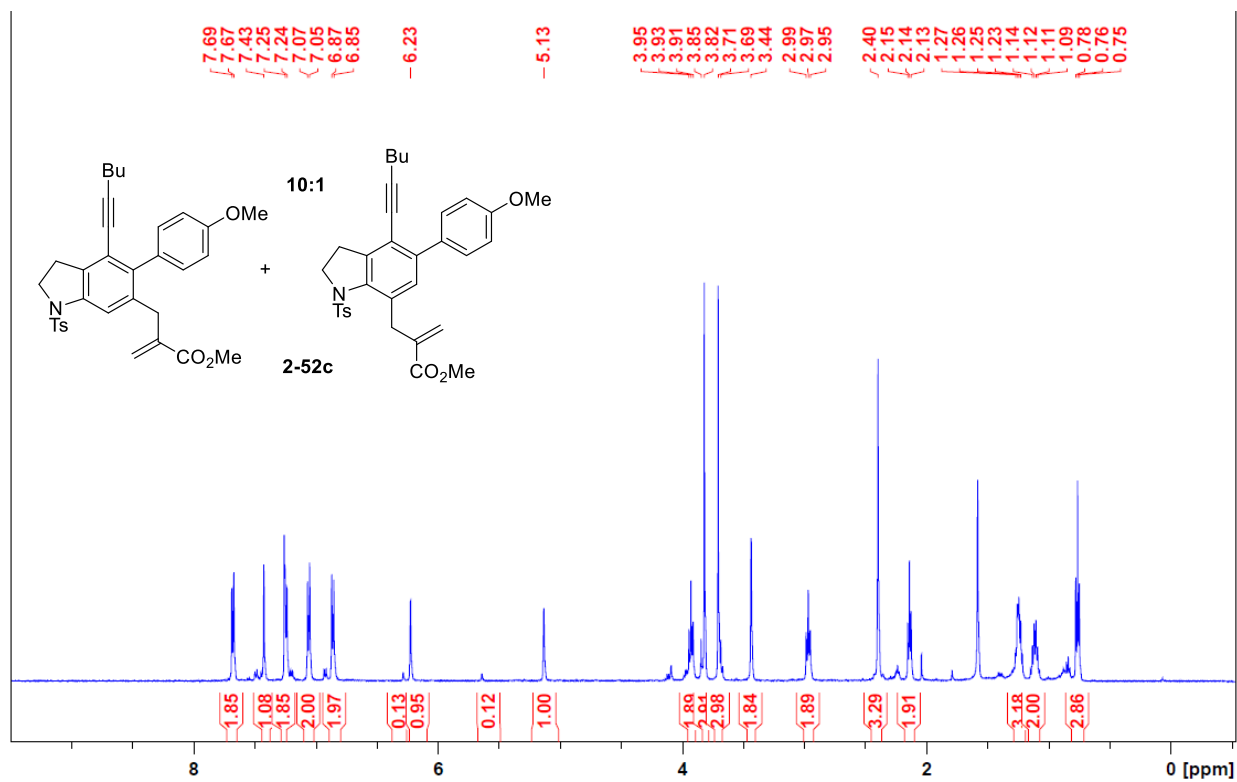


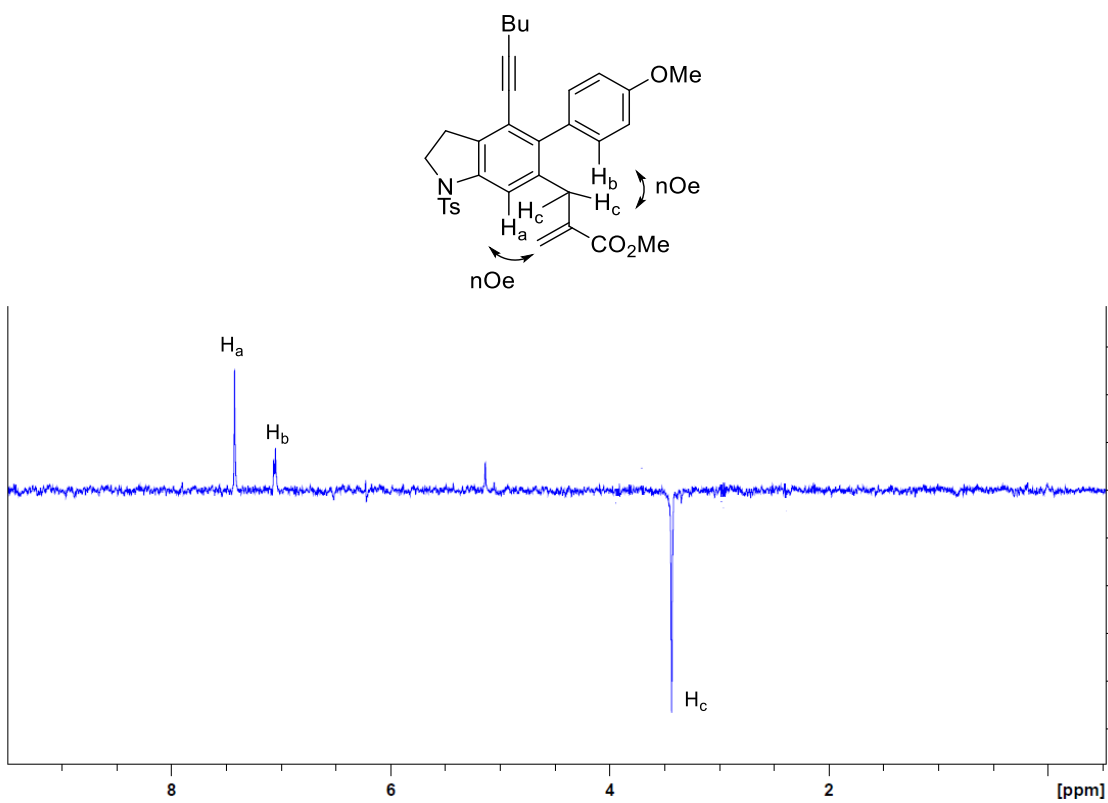


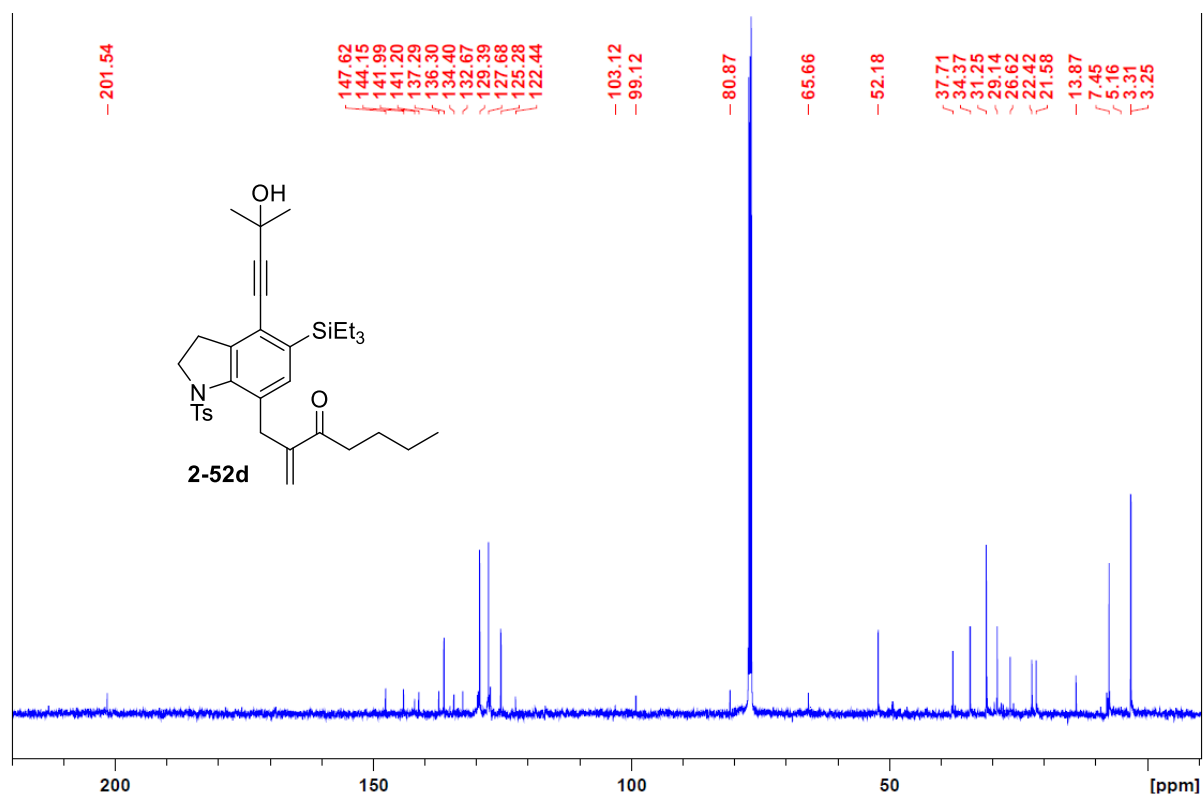
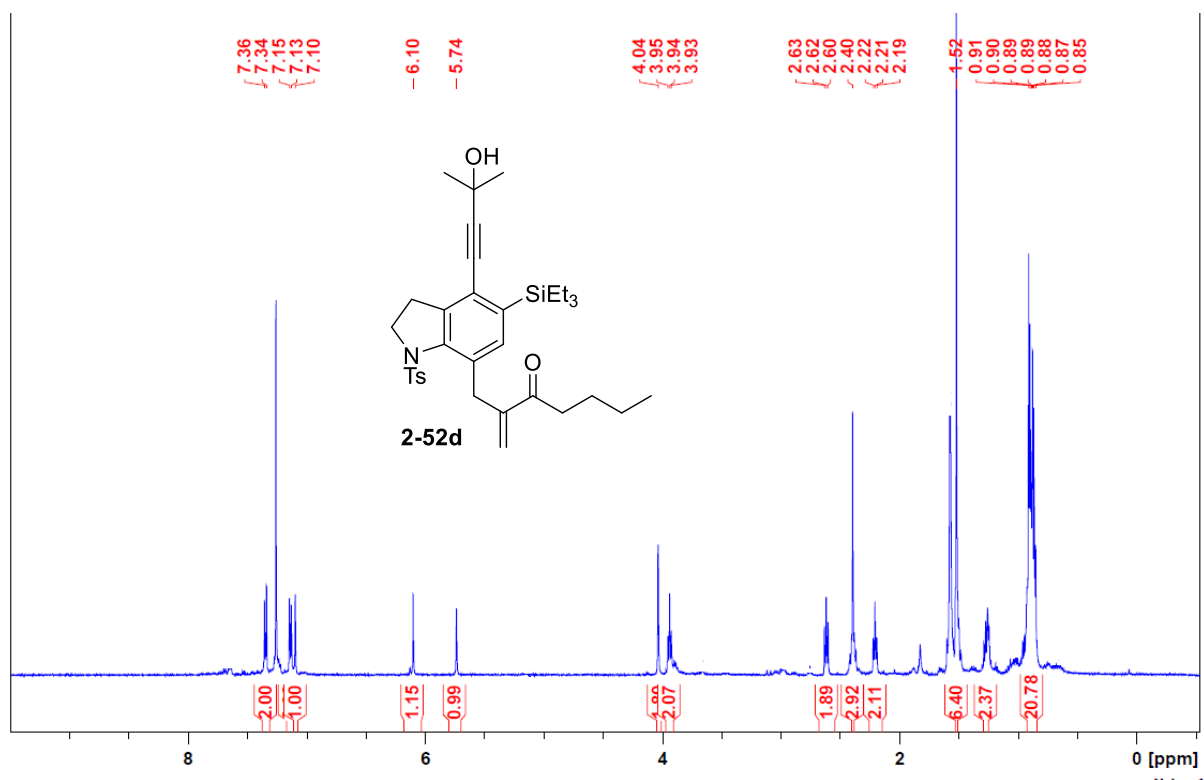


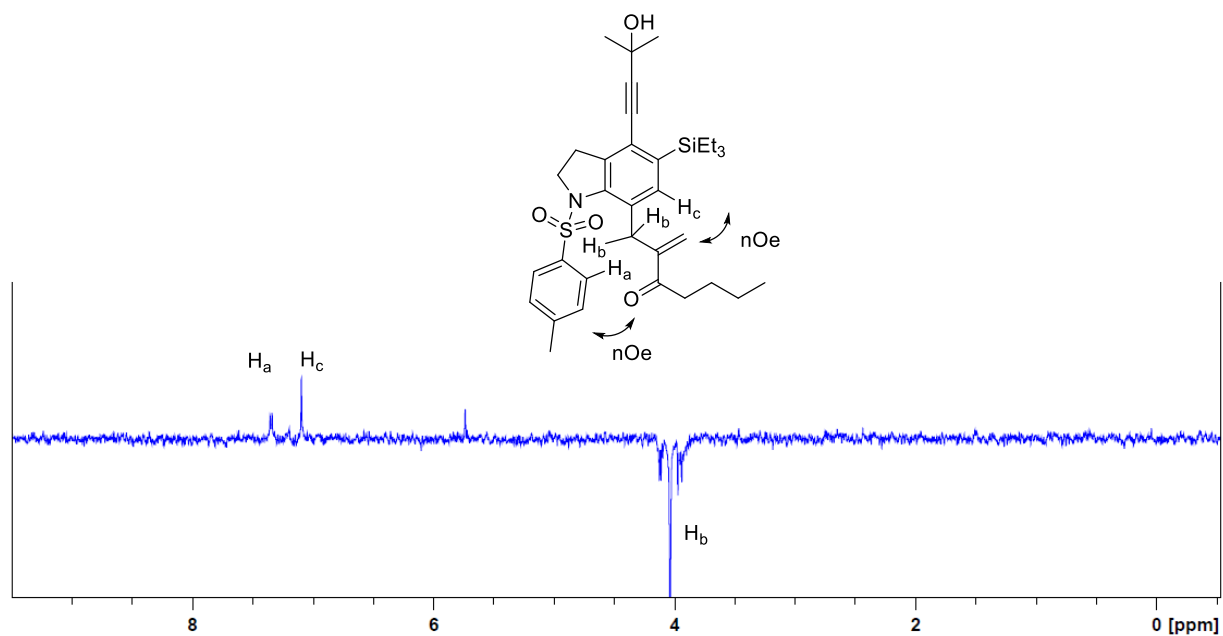


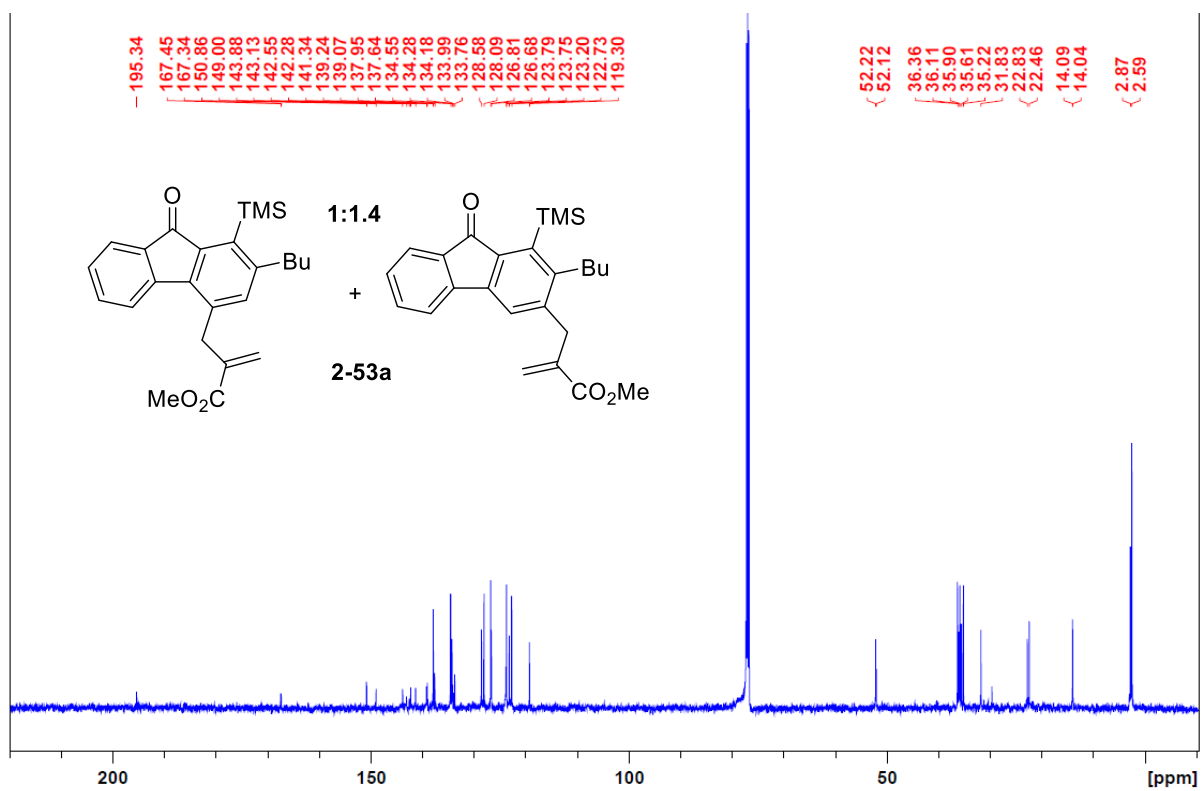
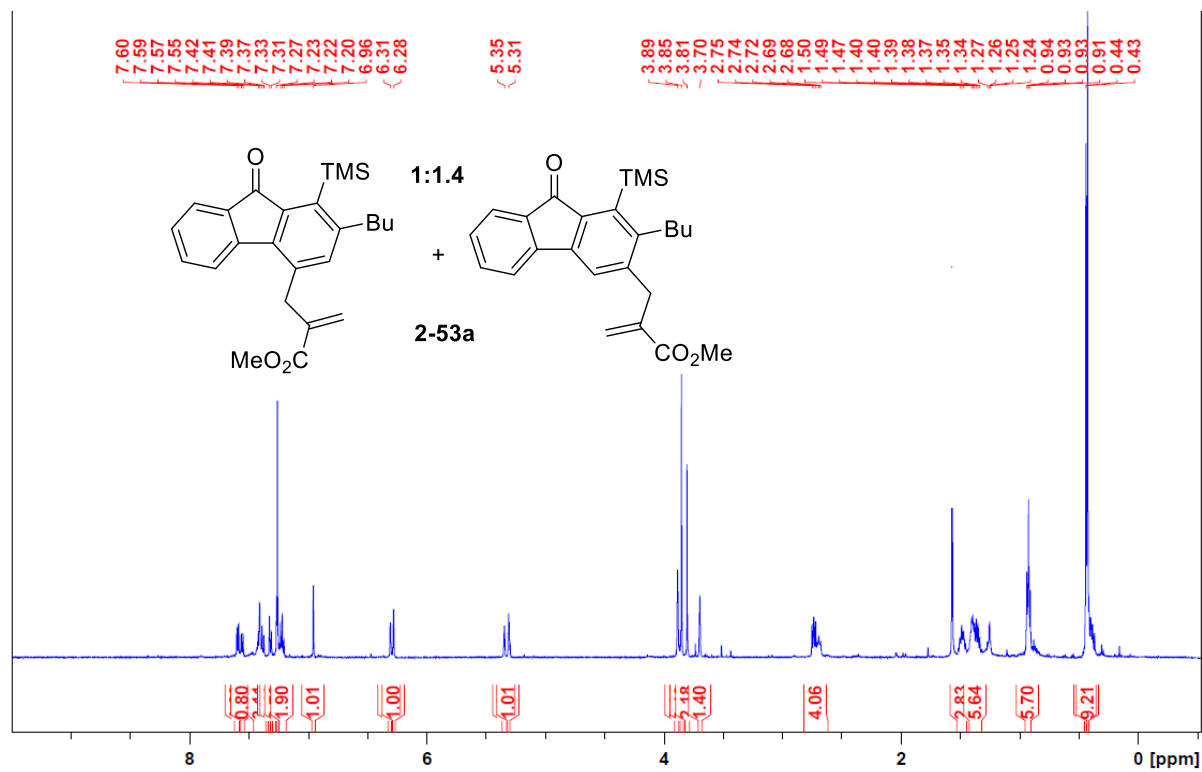


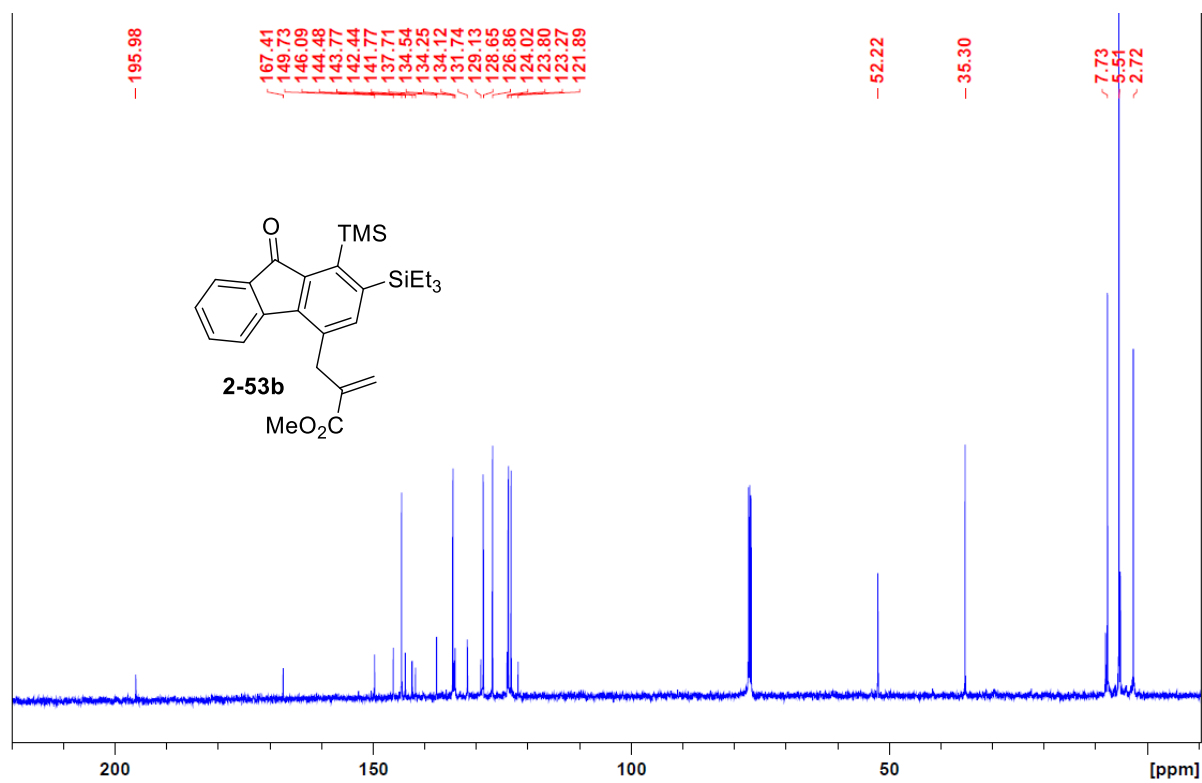
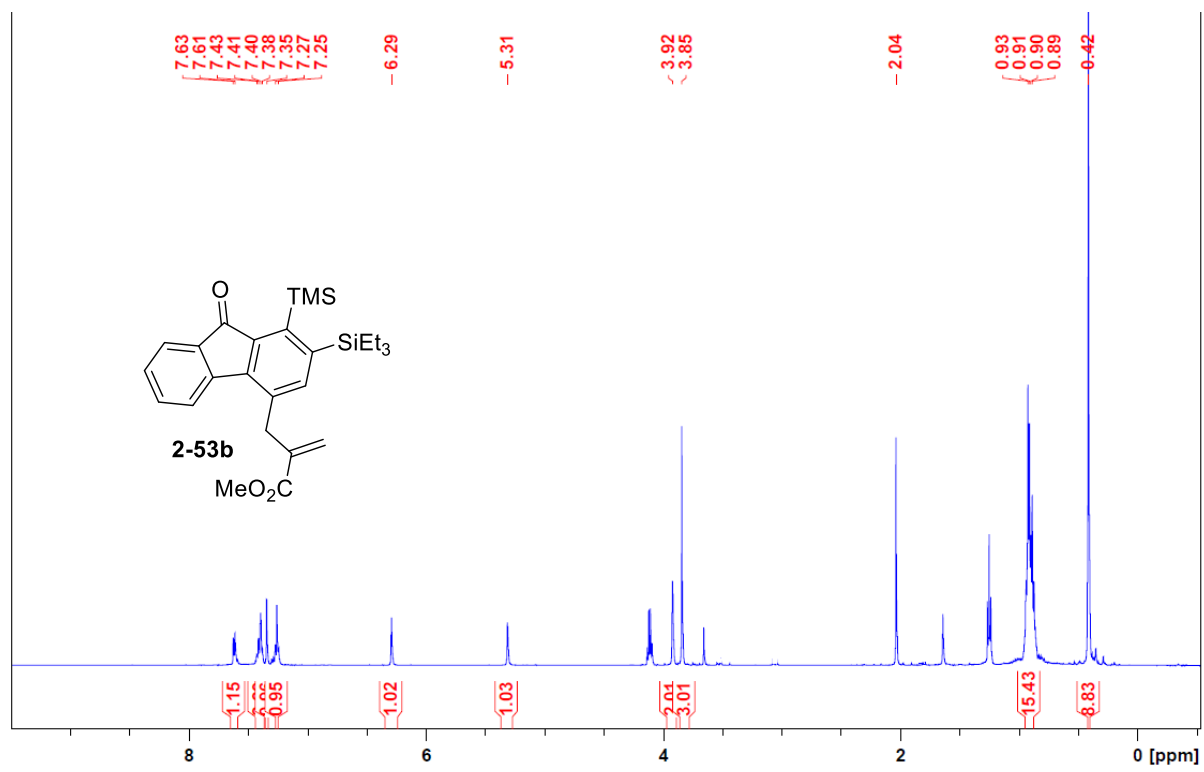


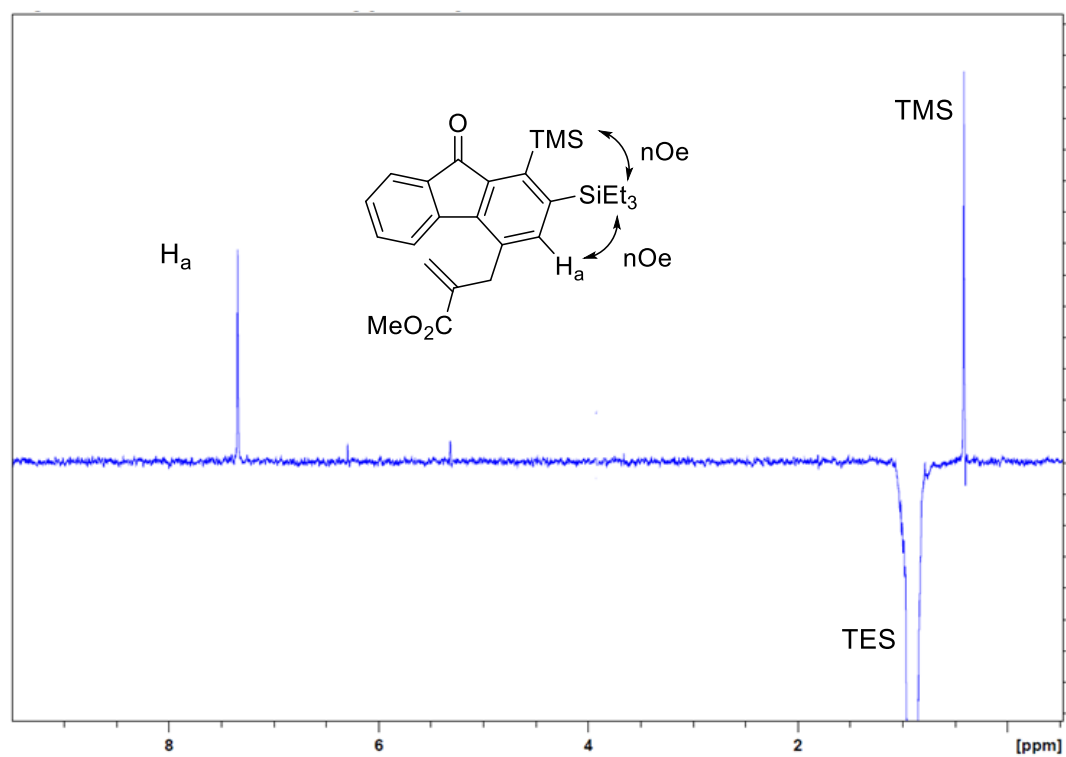


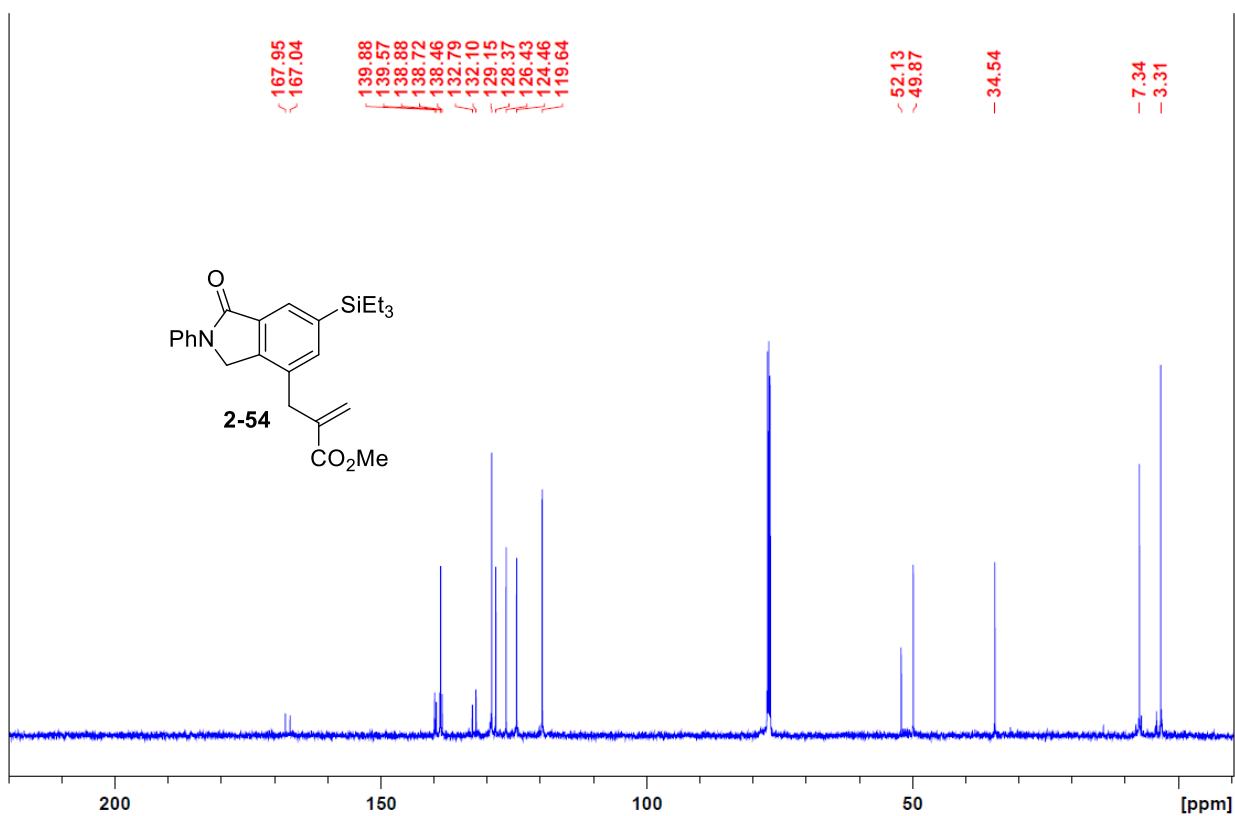
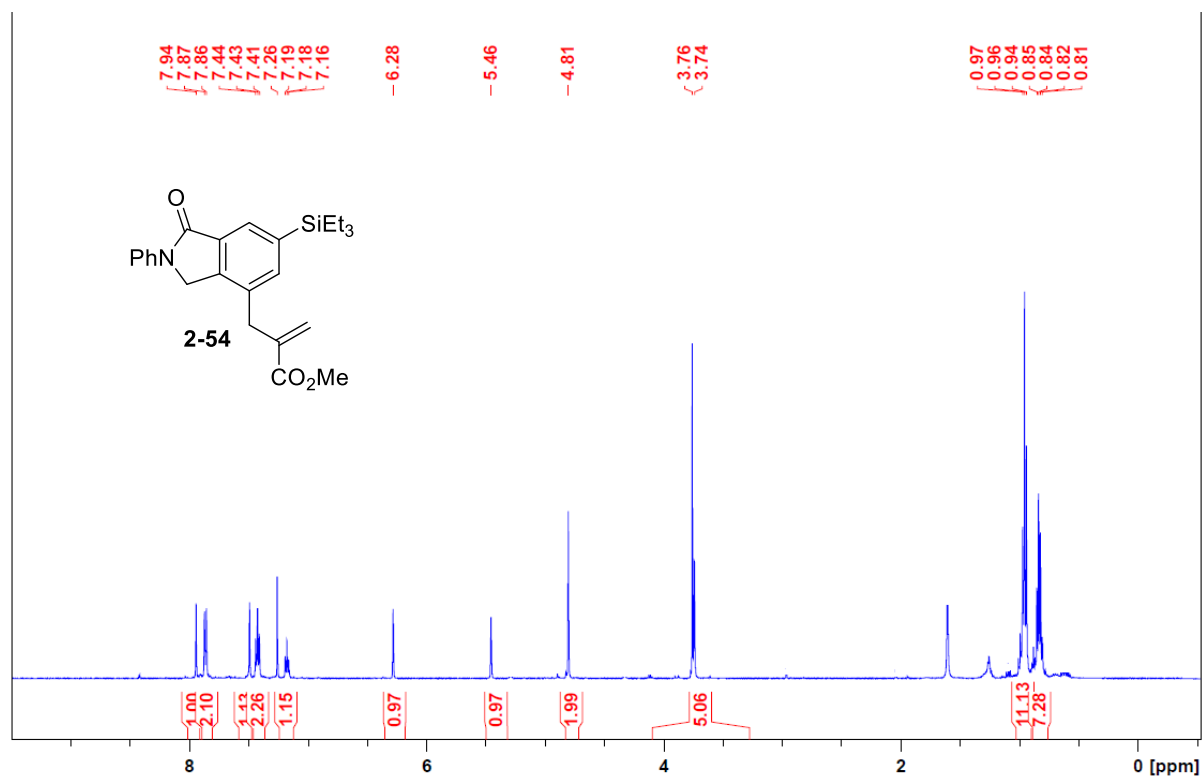


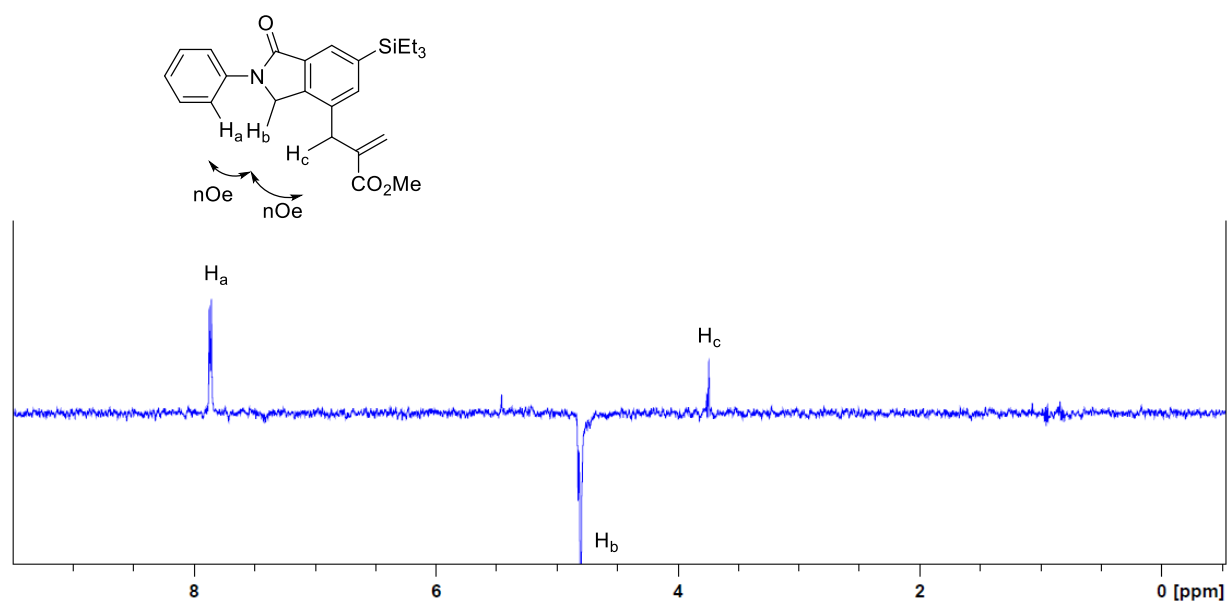


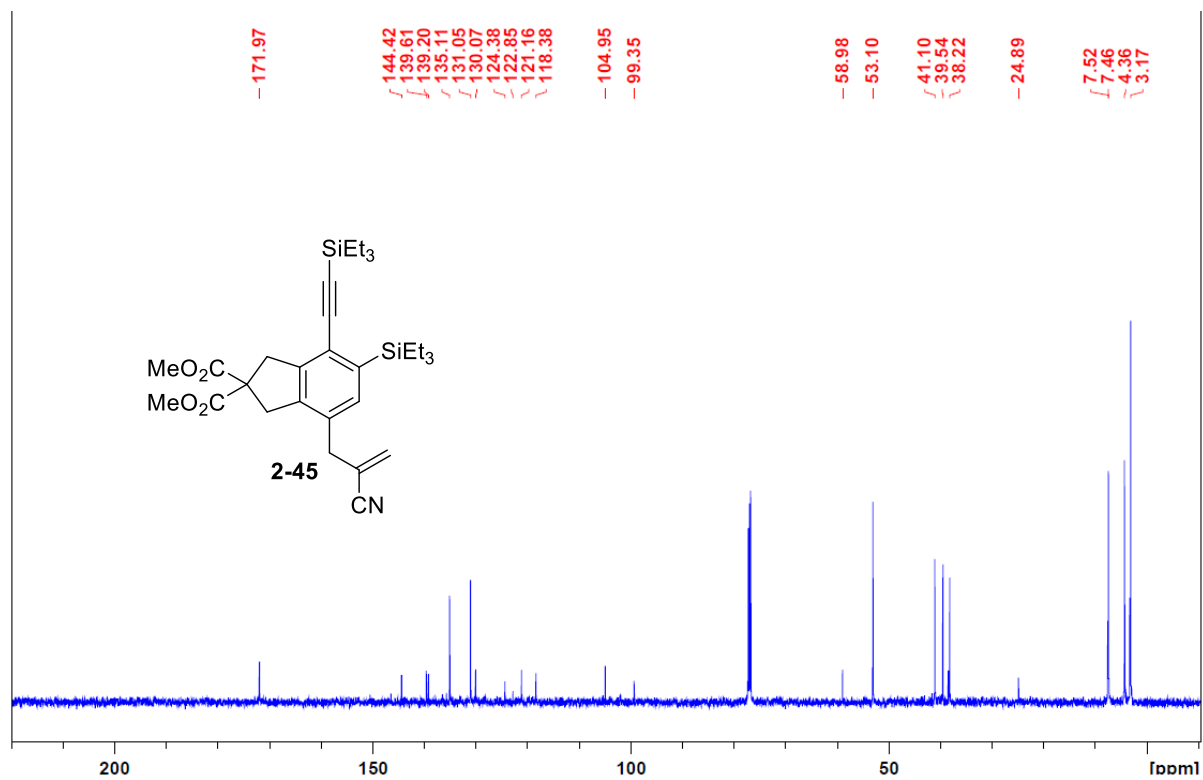
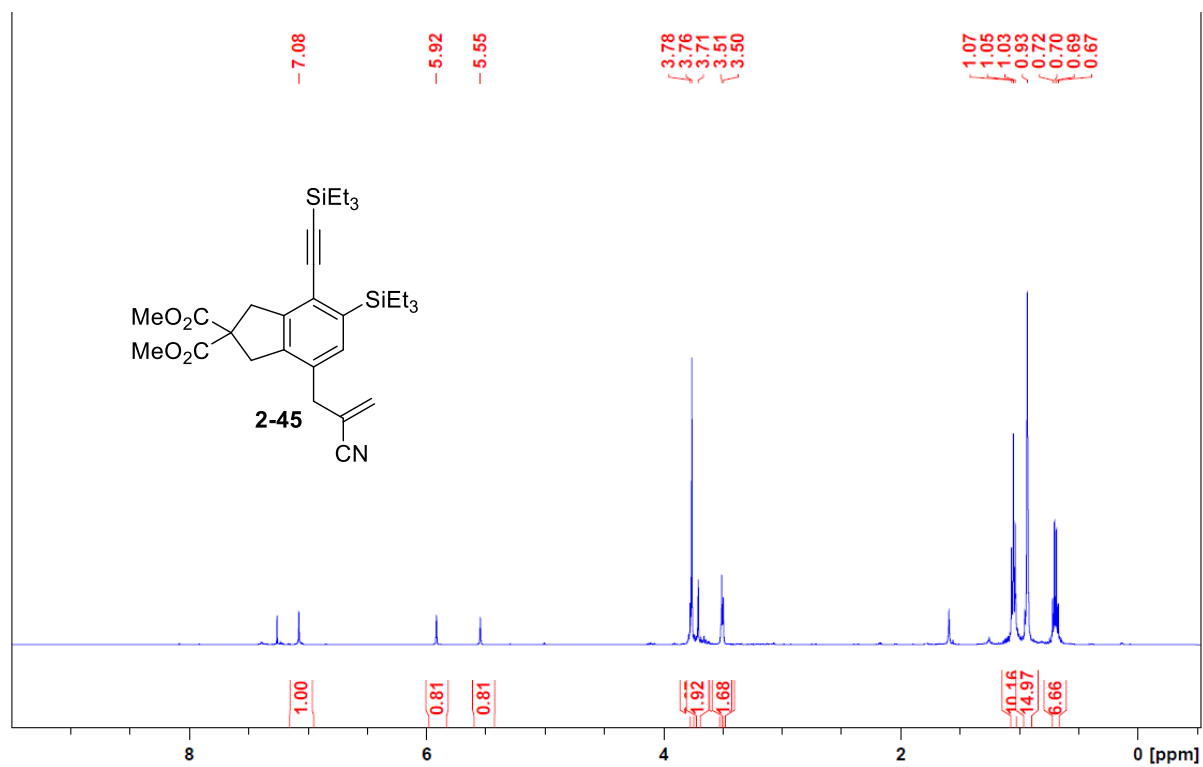


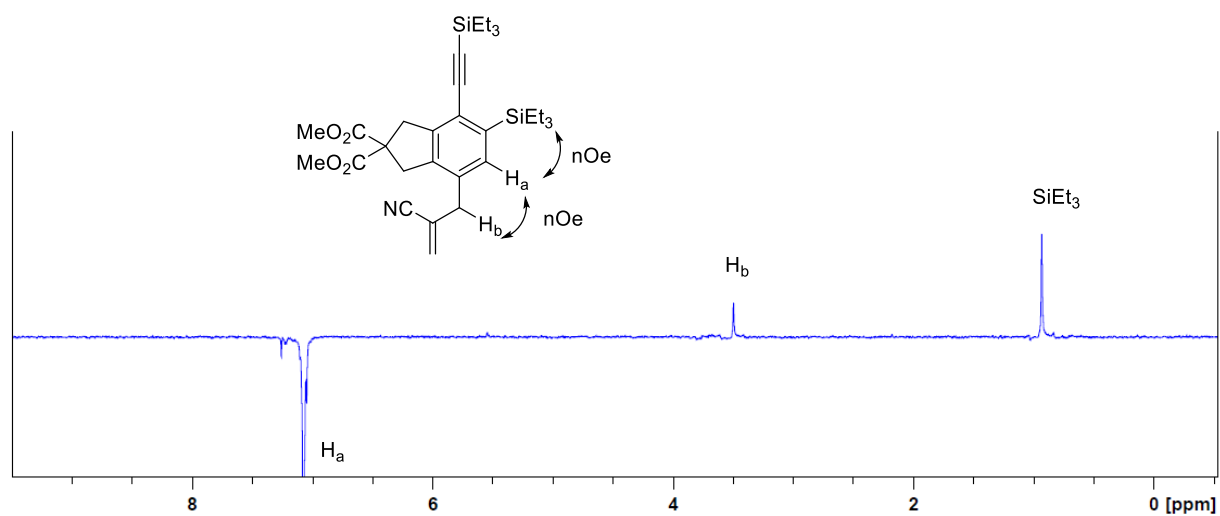




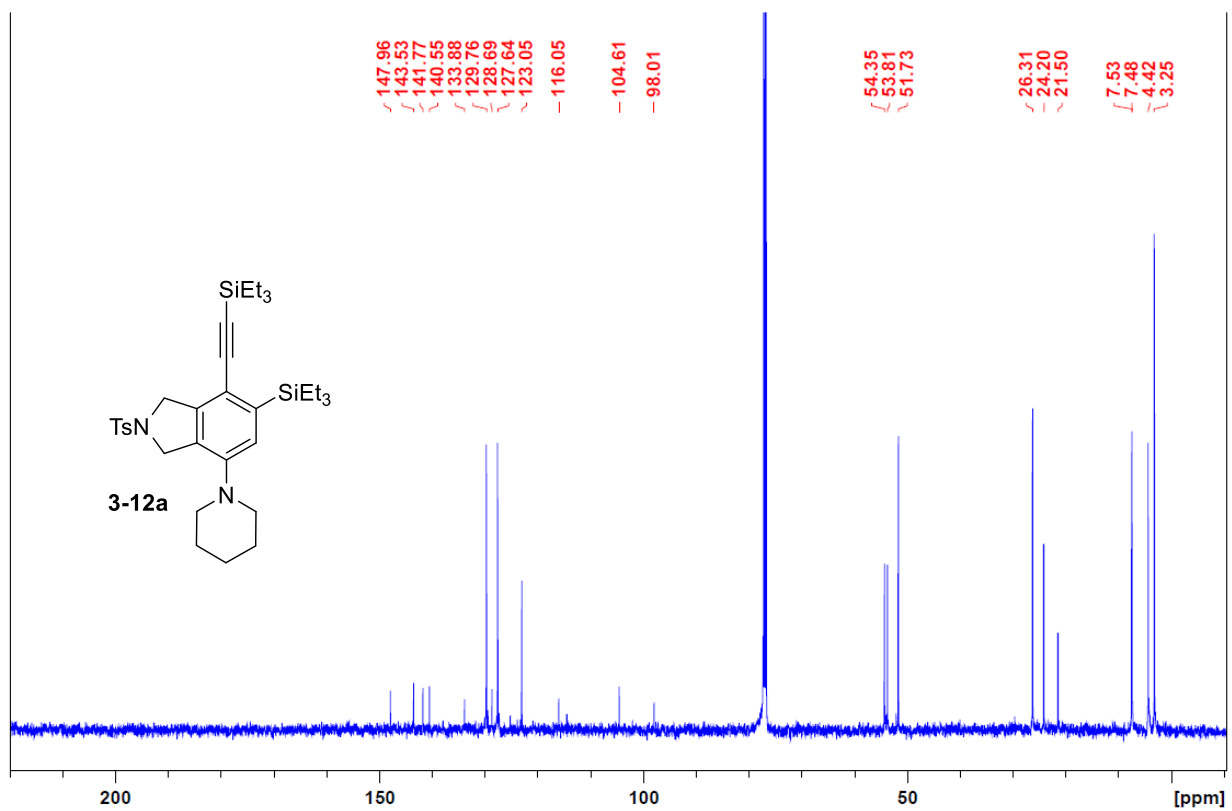
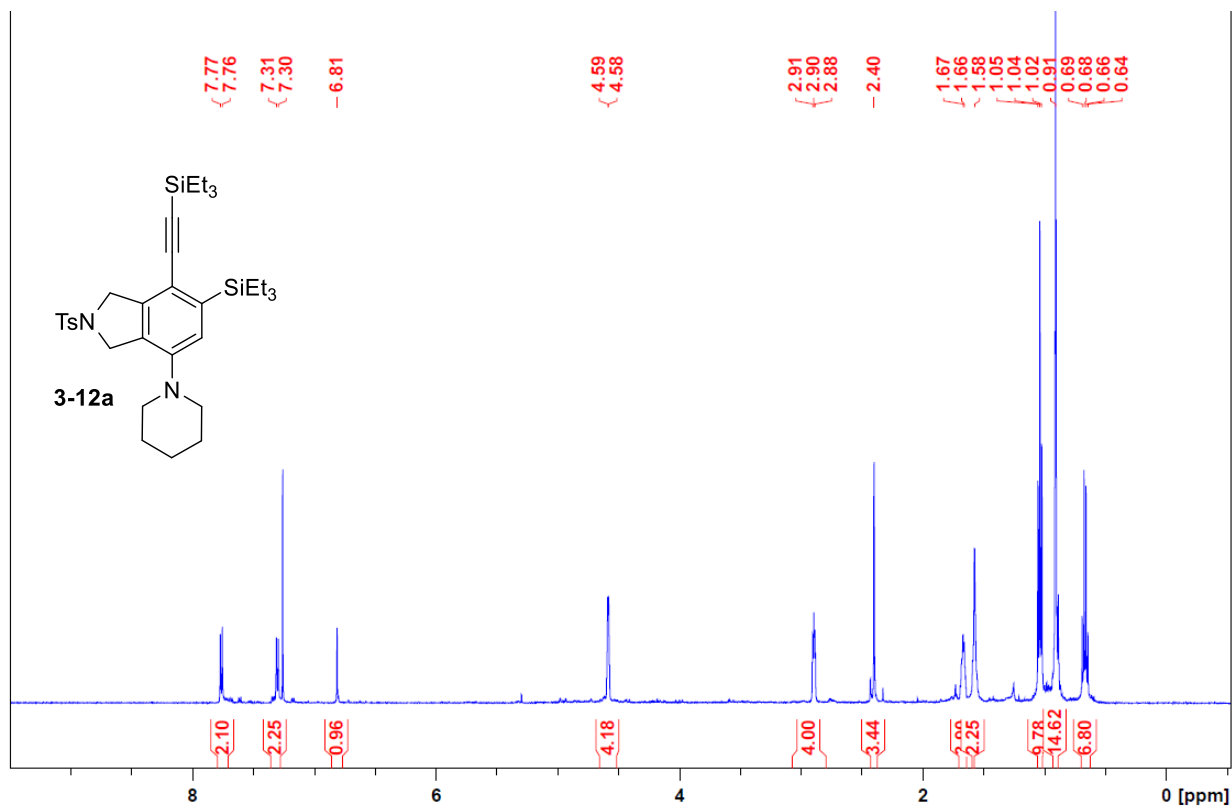


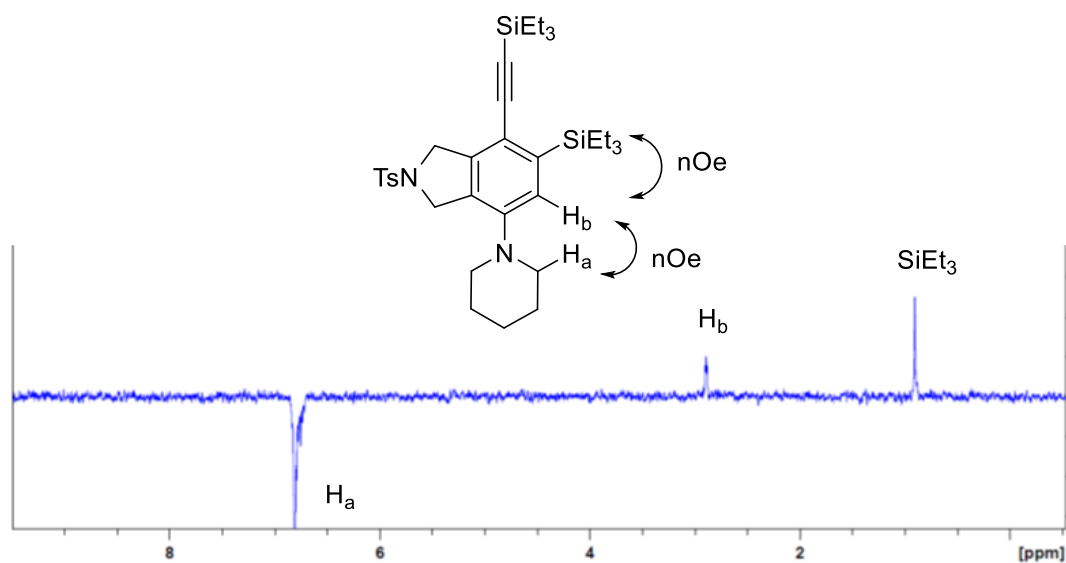


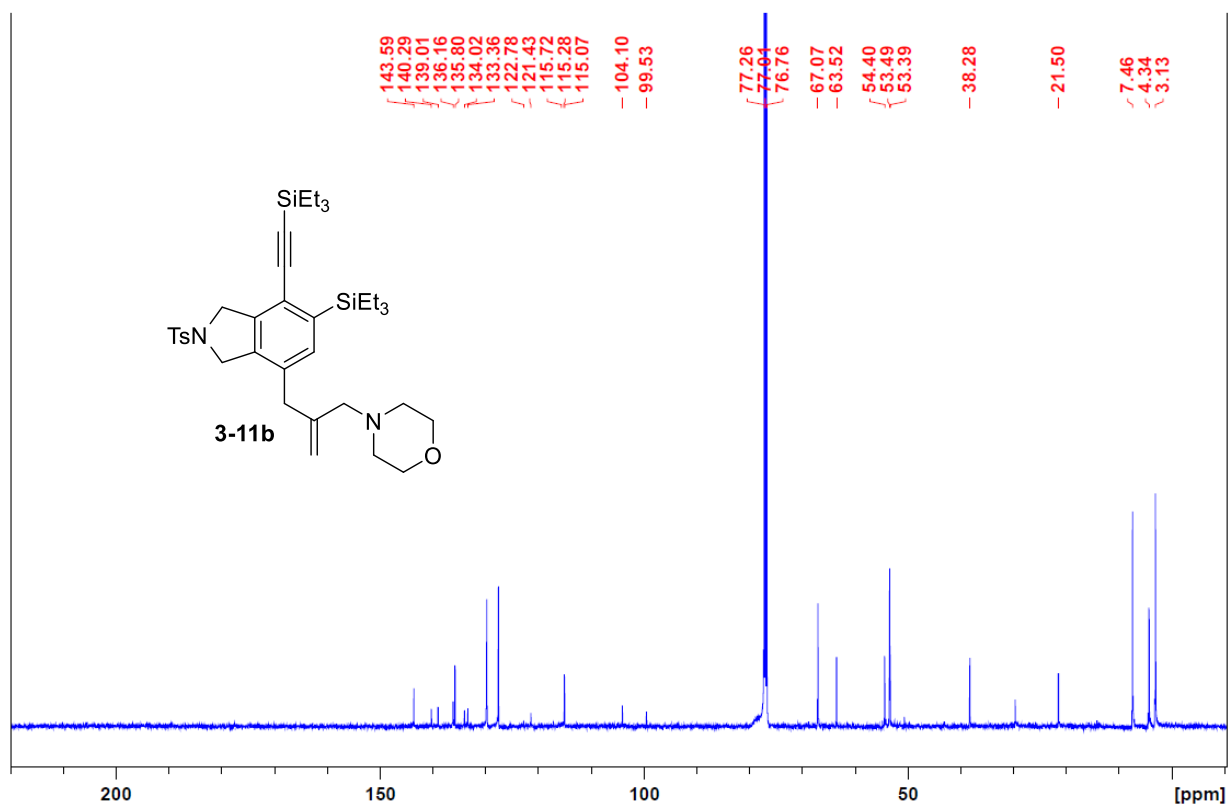
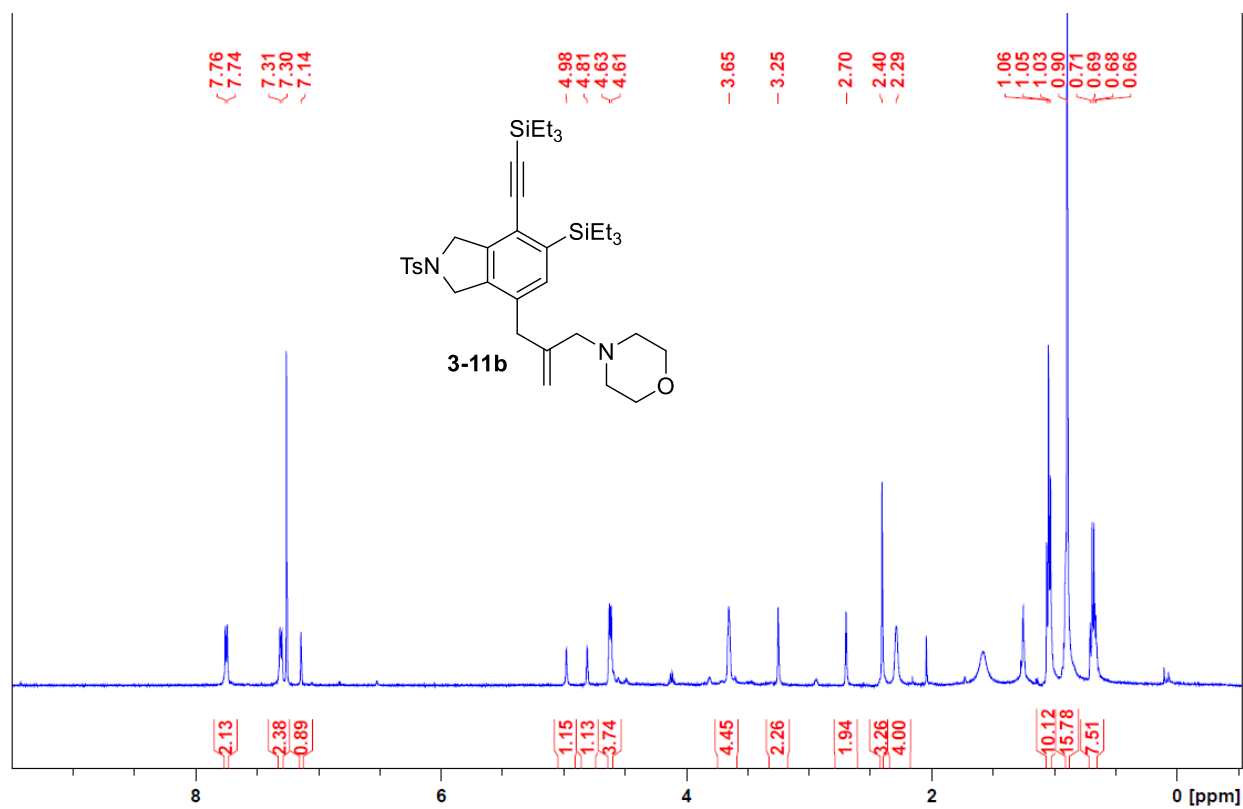


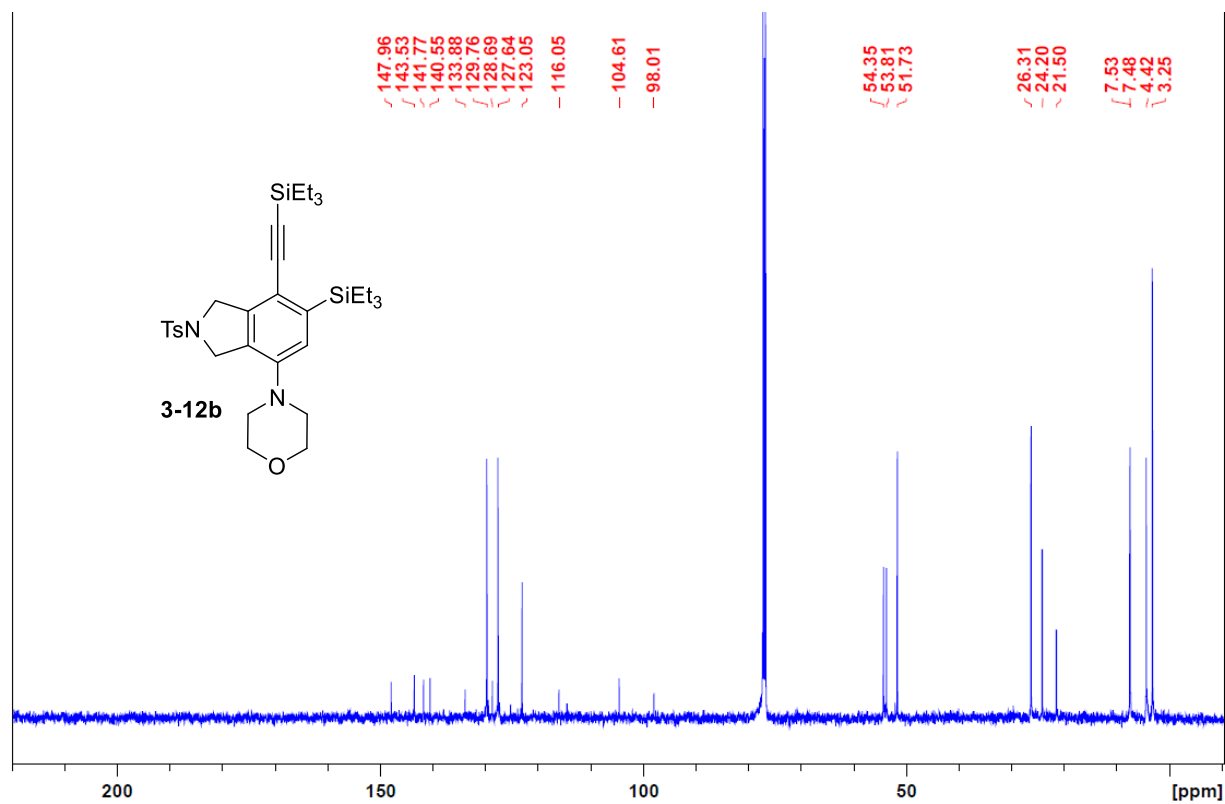
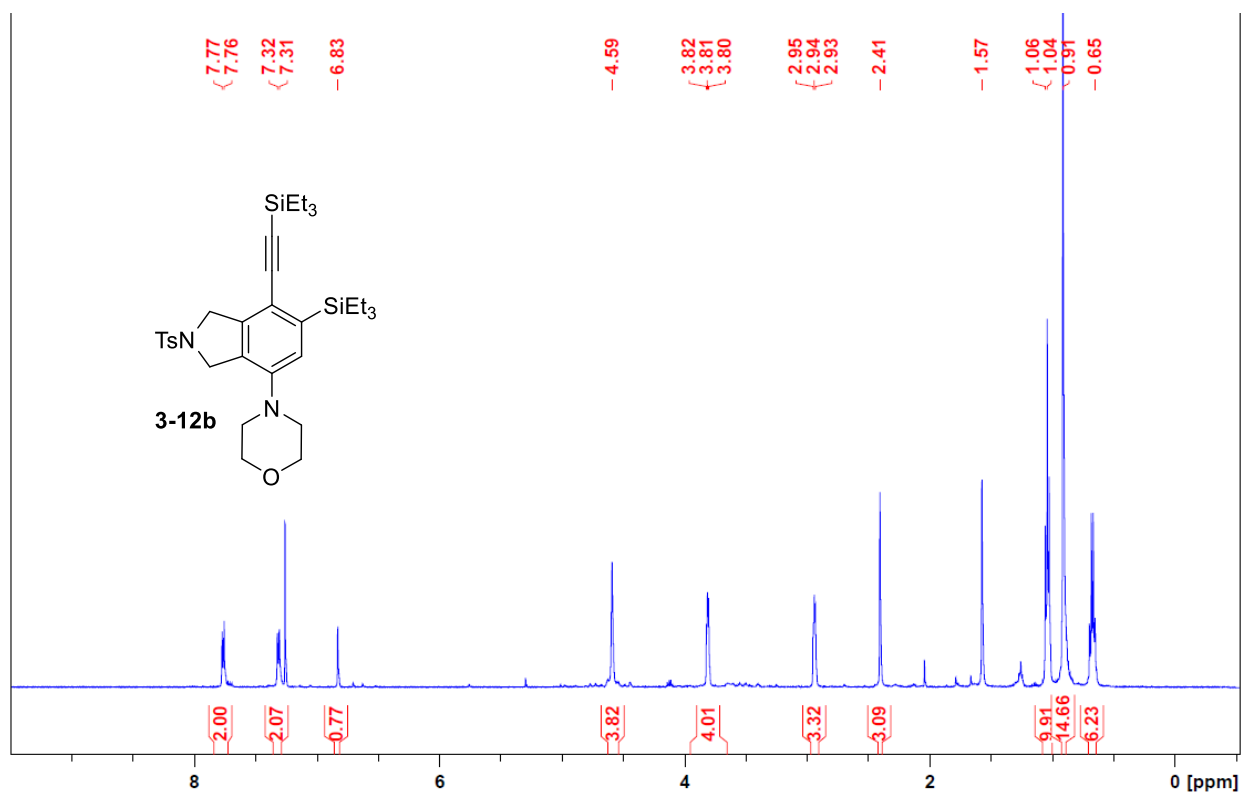


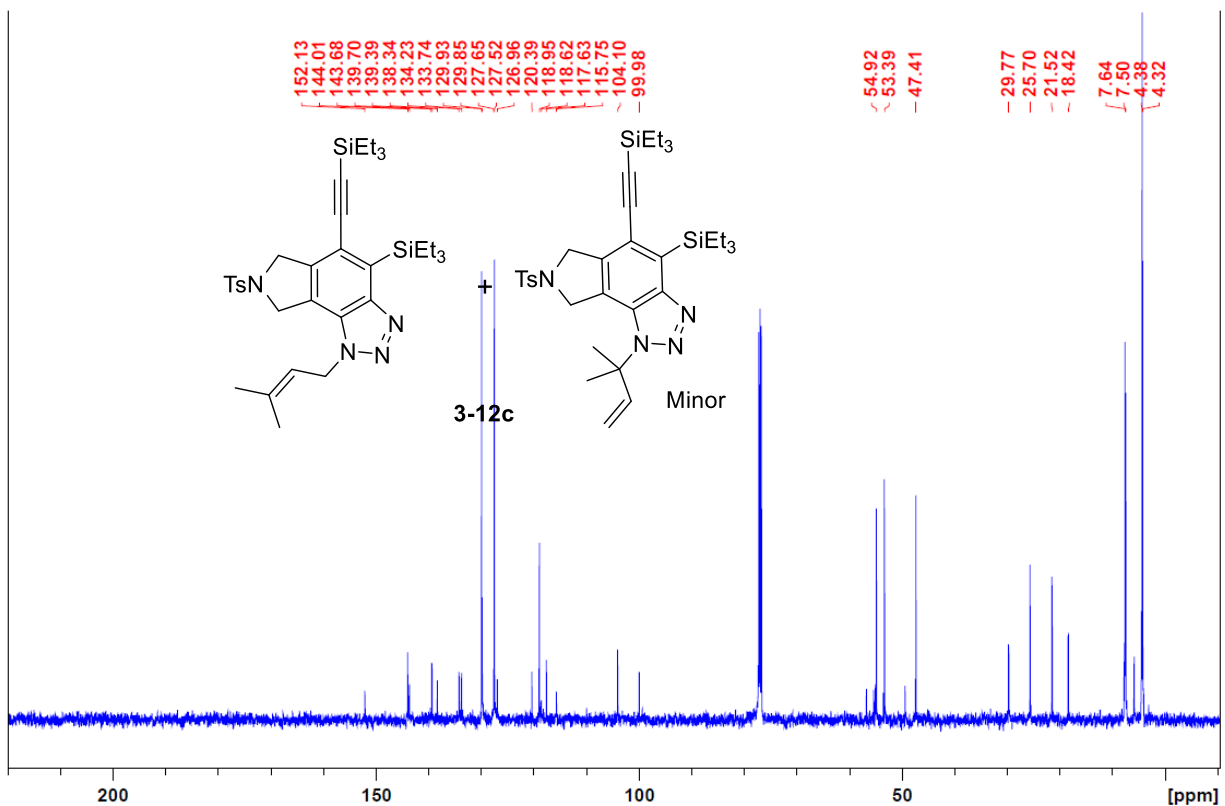
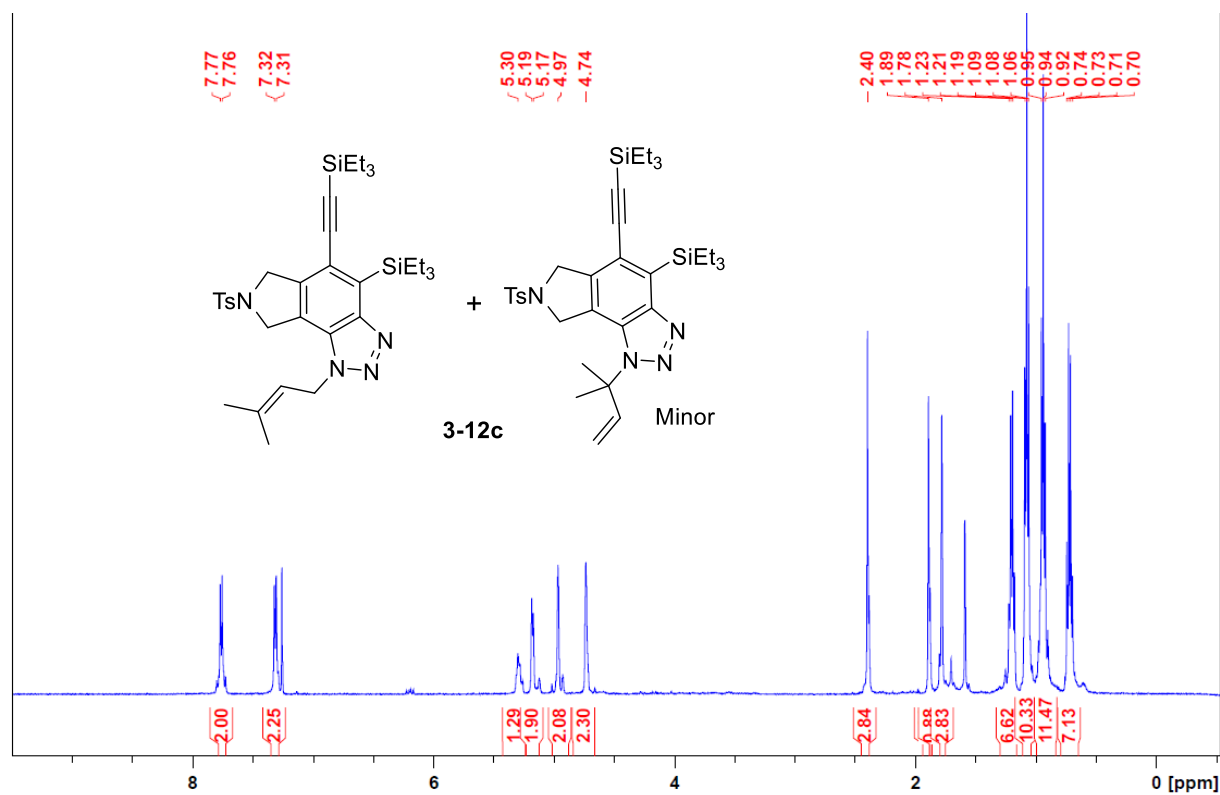
Appendix II
Selected NMR Spectra for Chapter 3

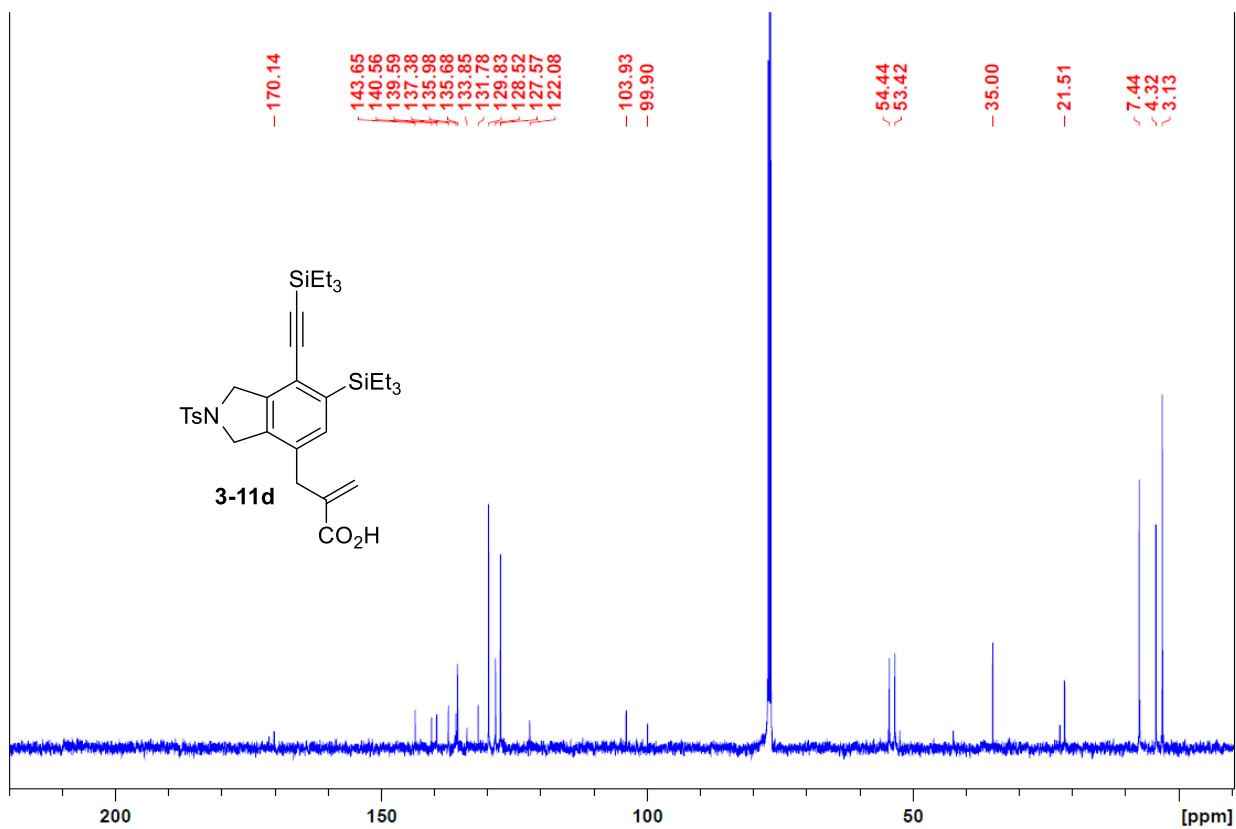
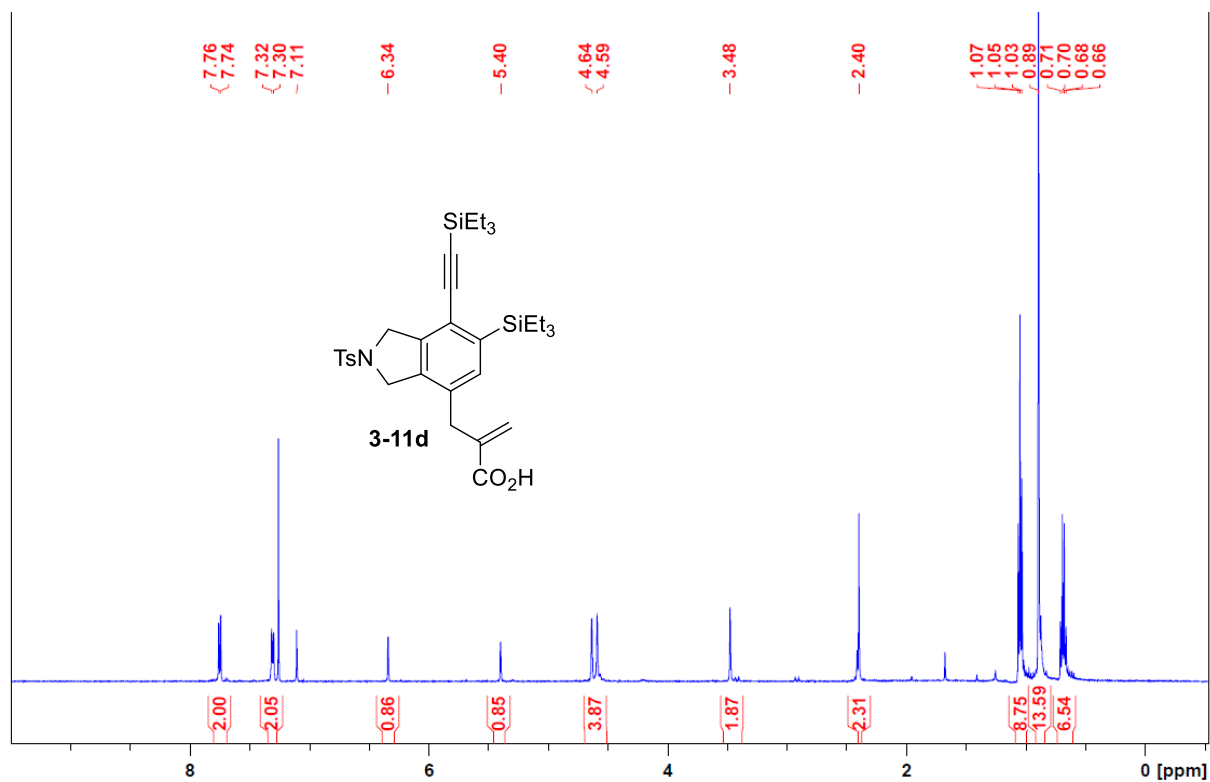


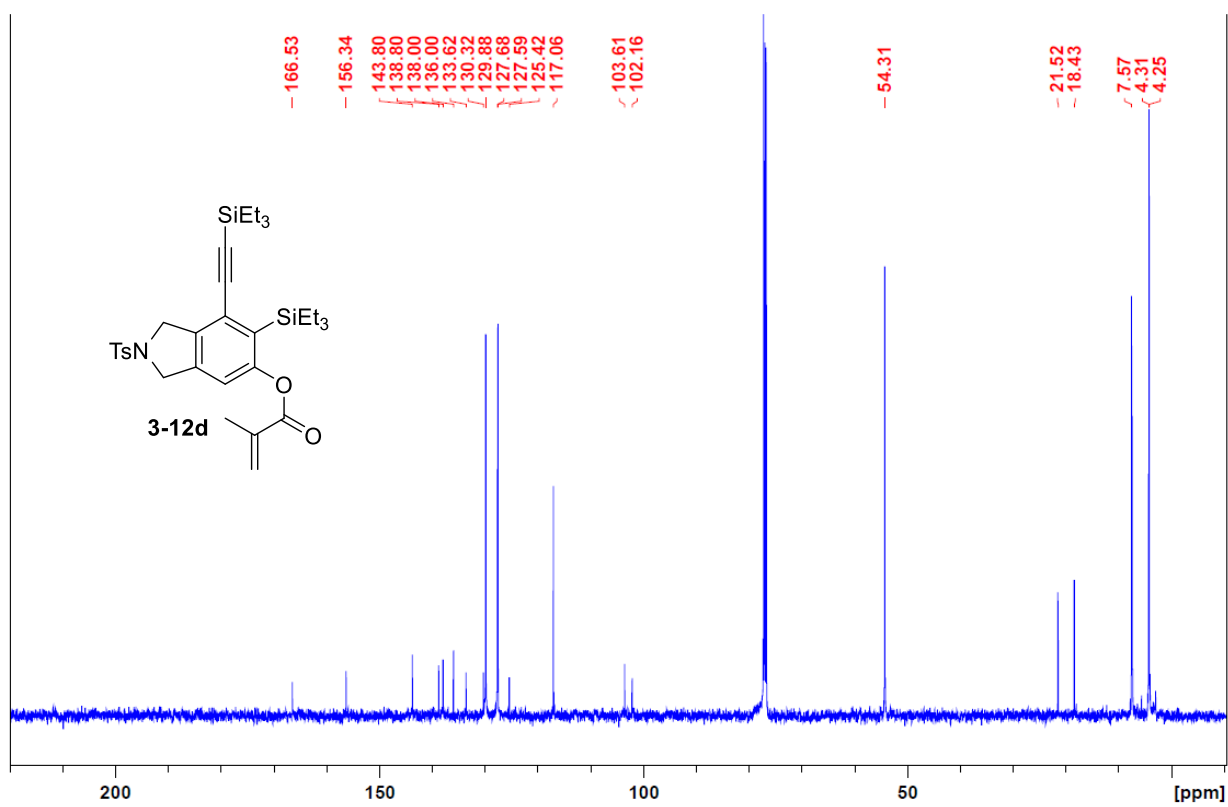
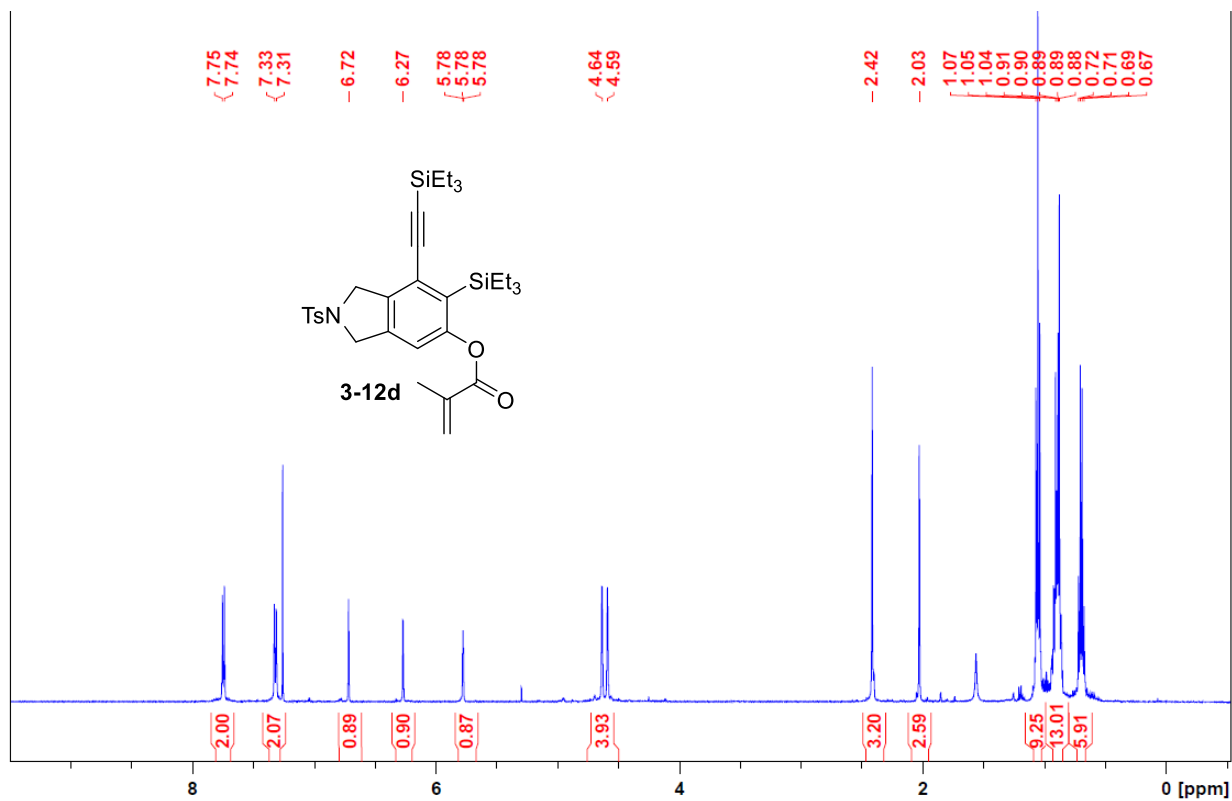


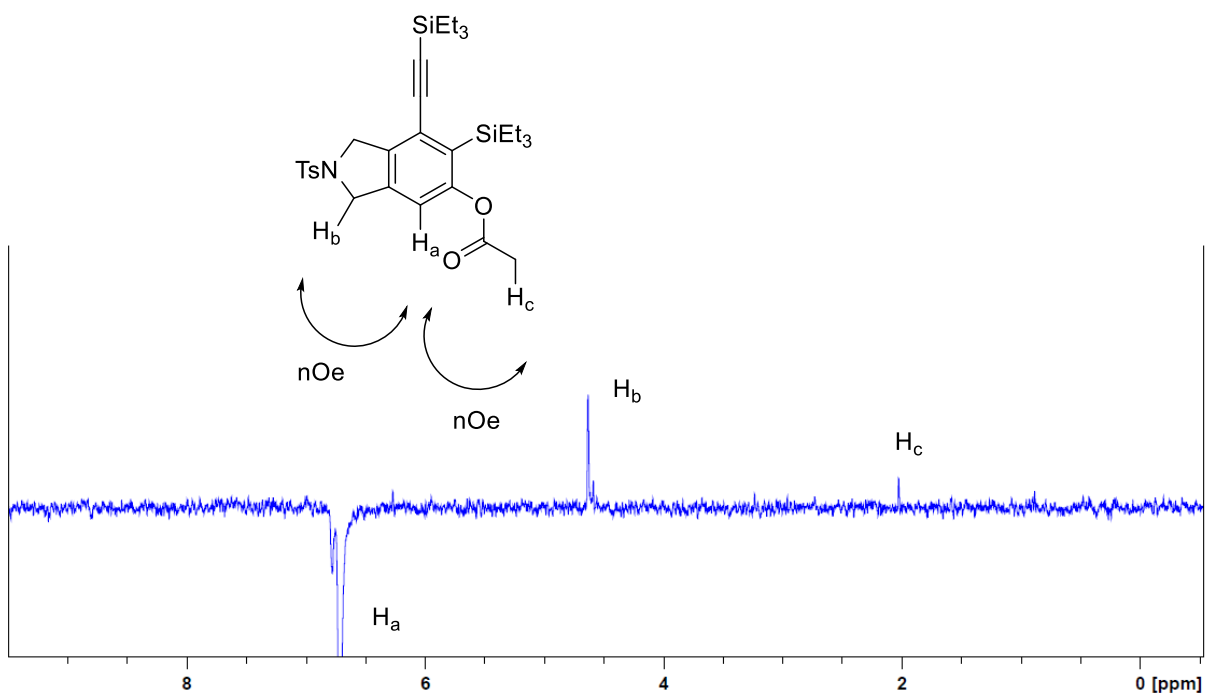


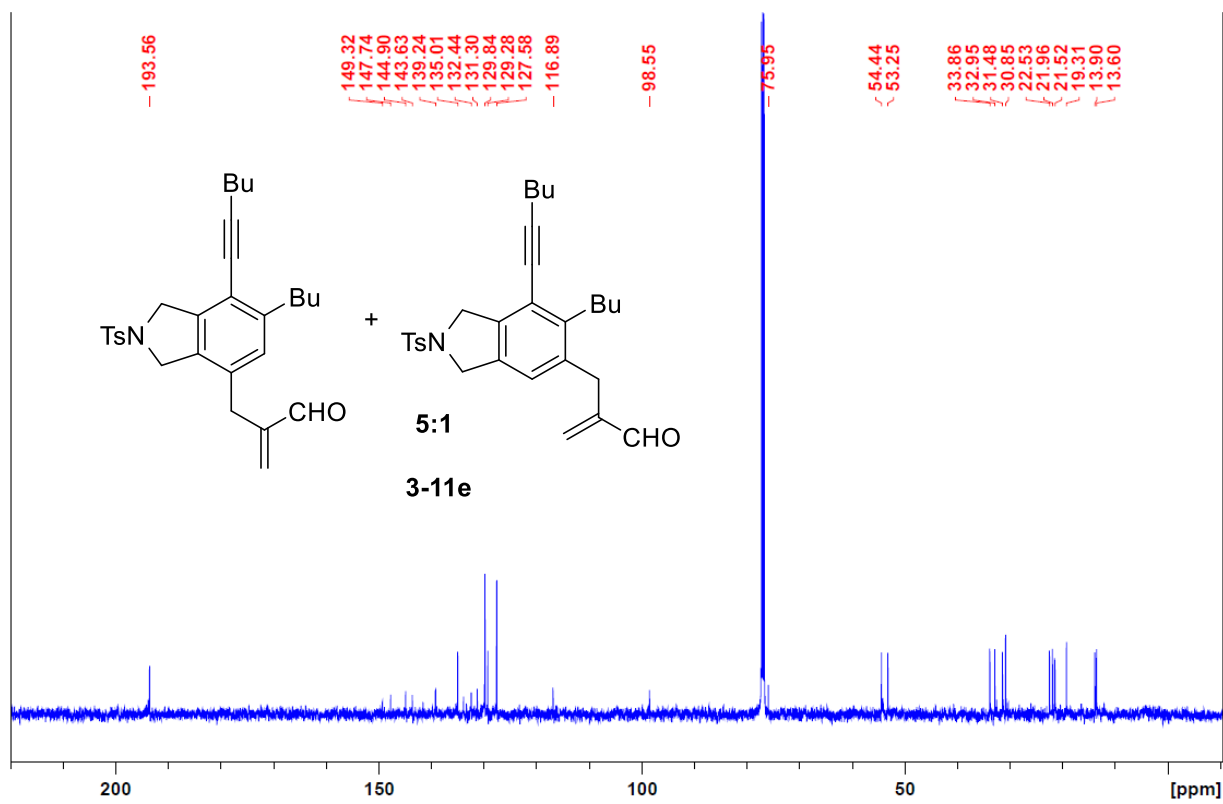
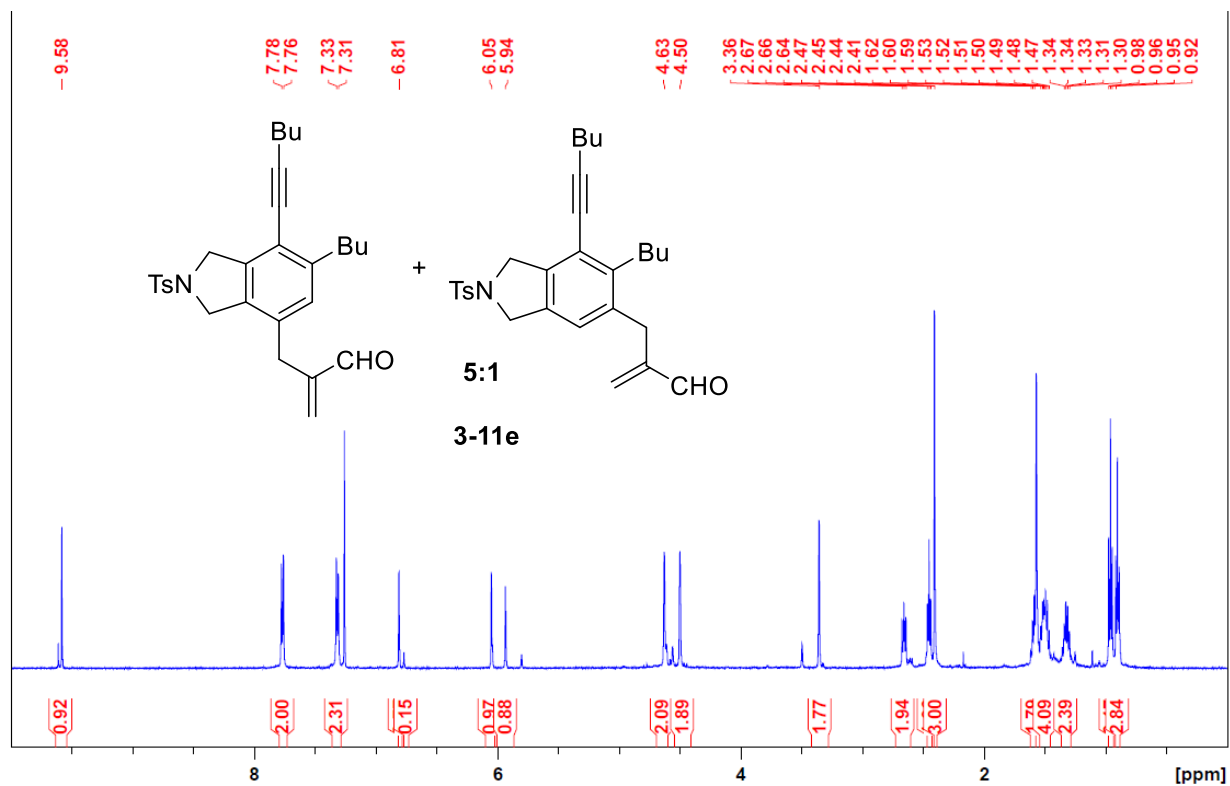


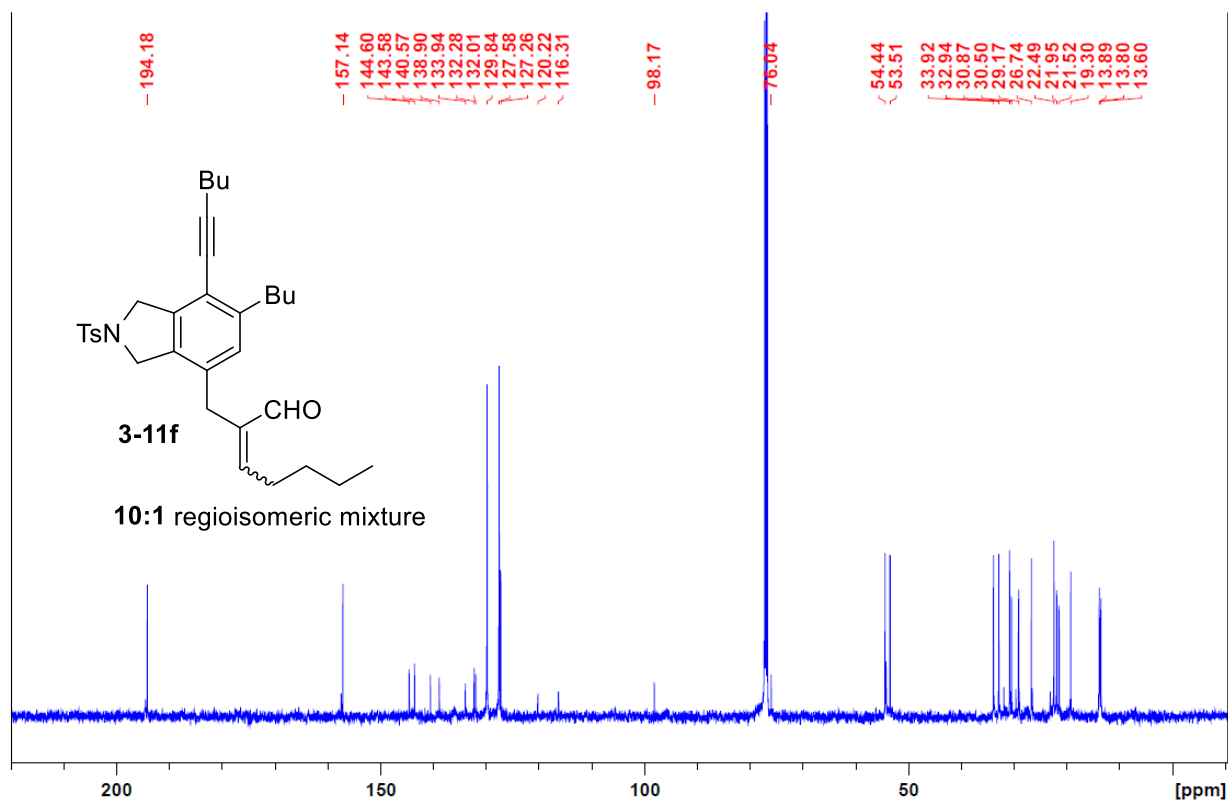
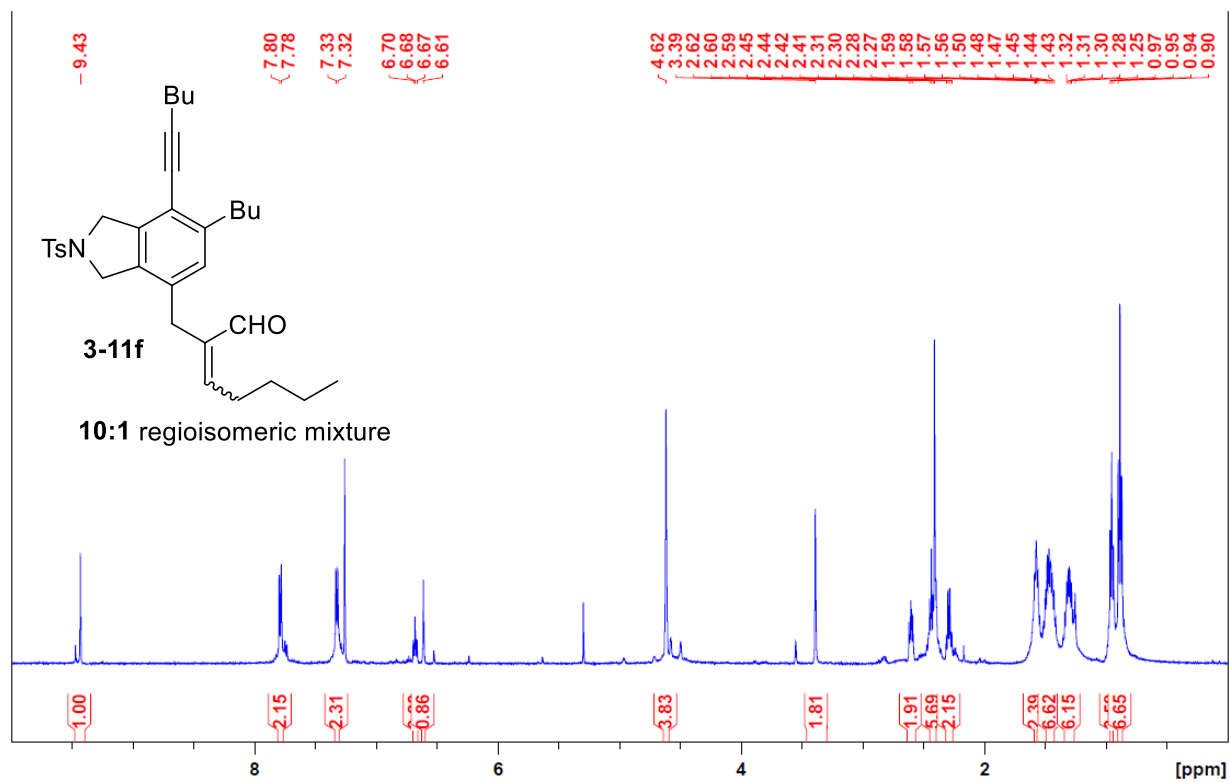


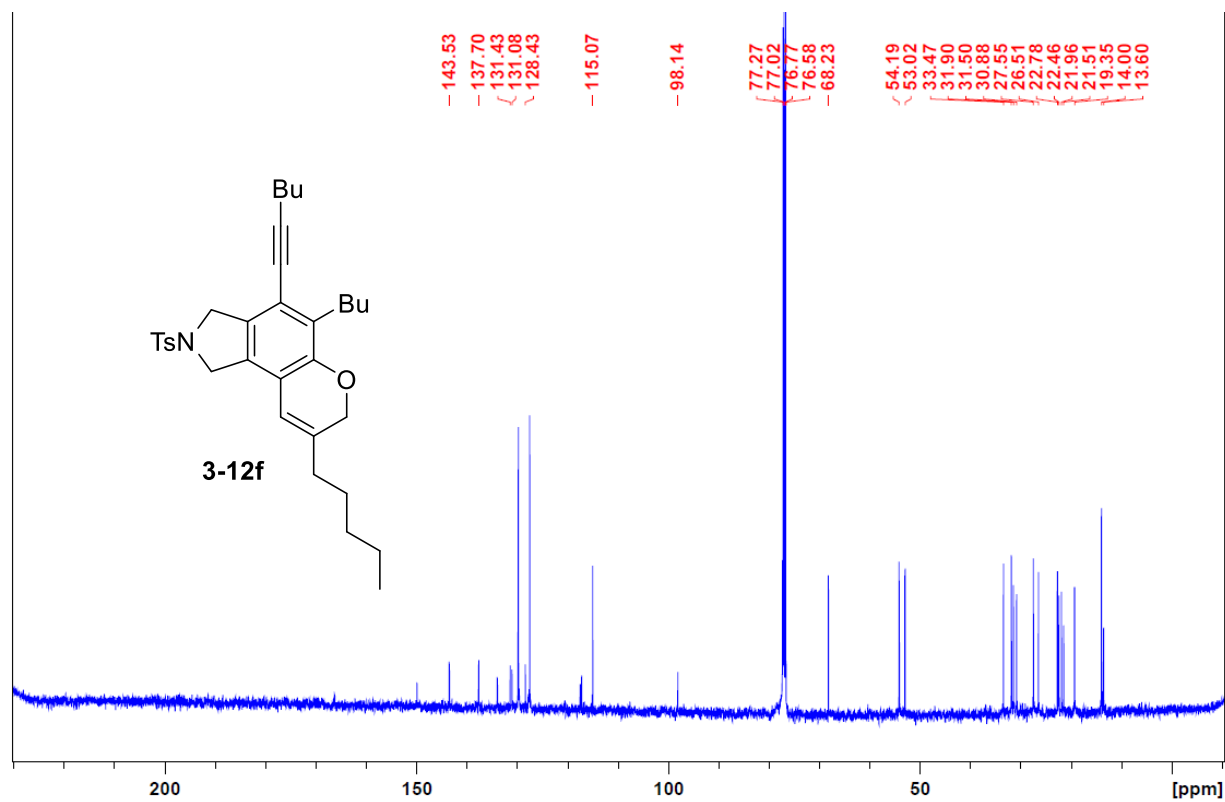
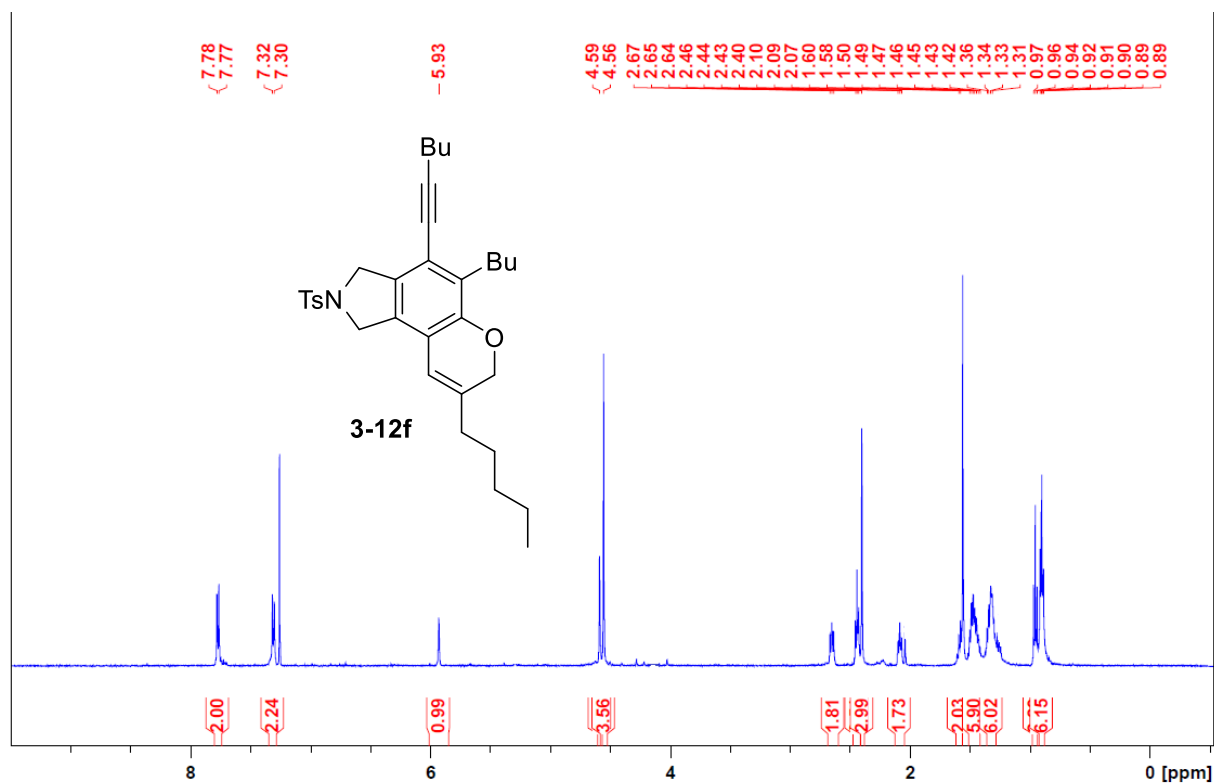


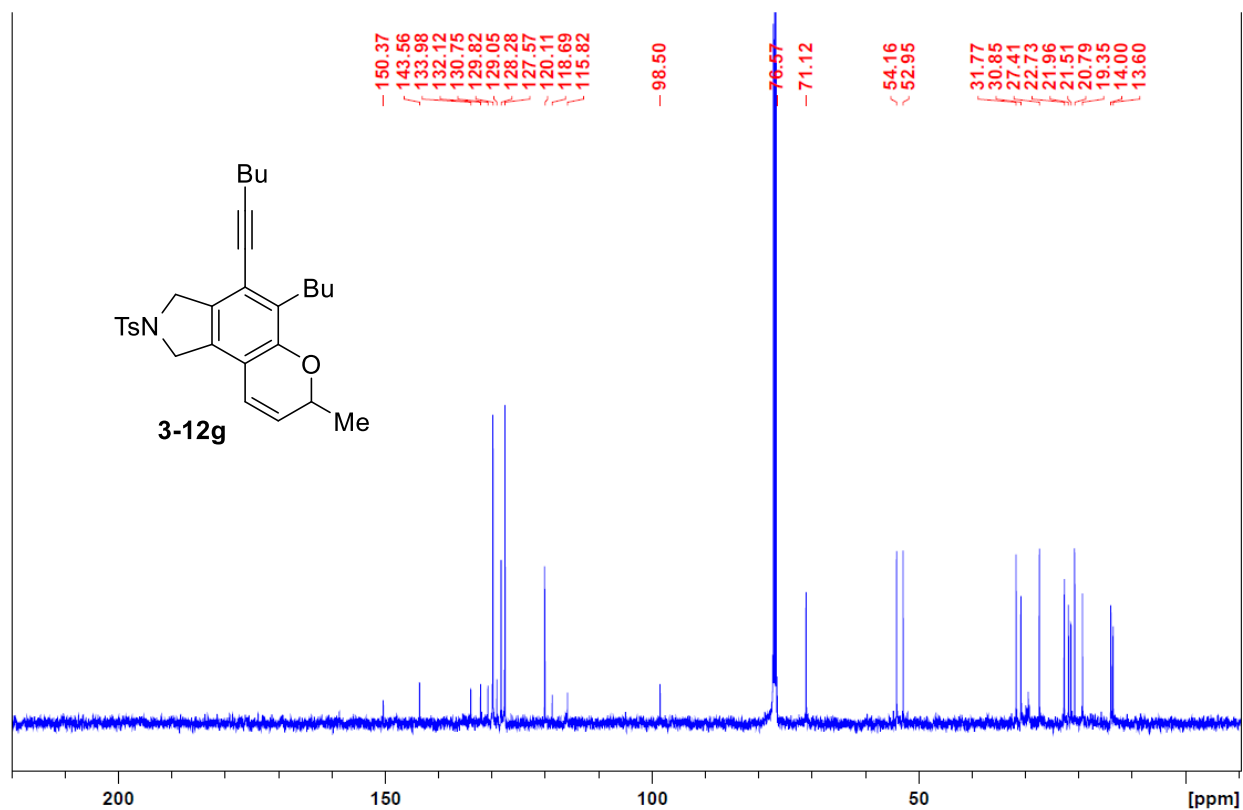
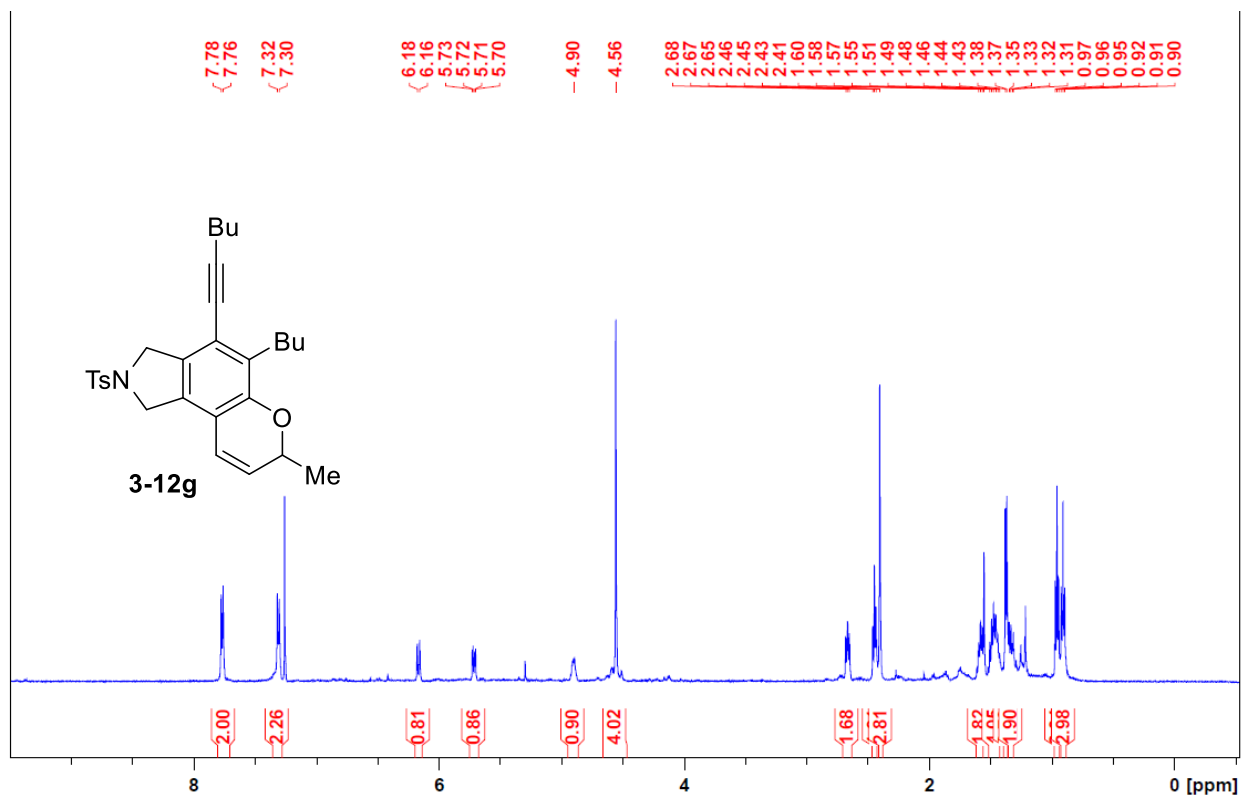


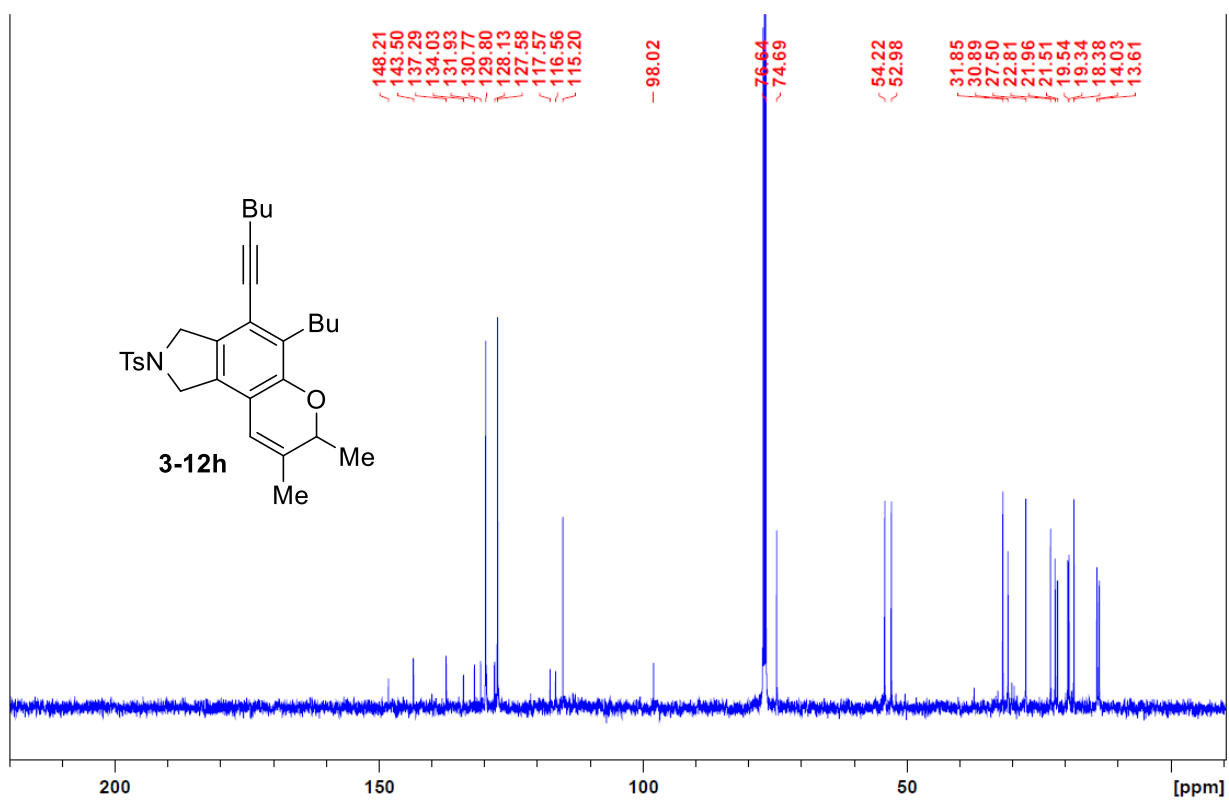
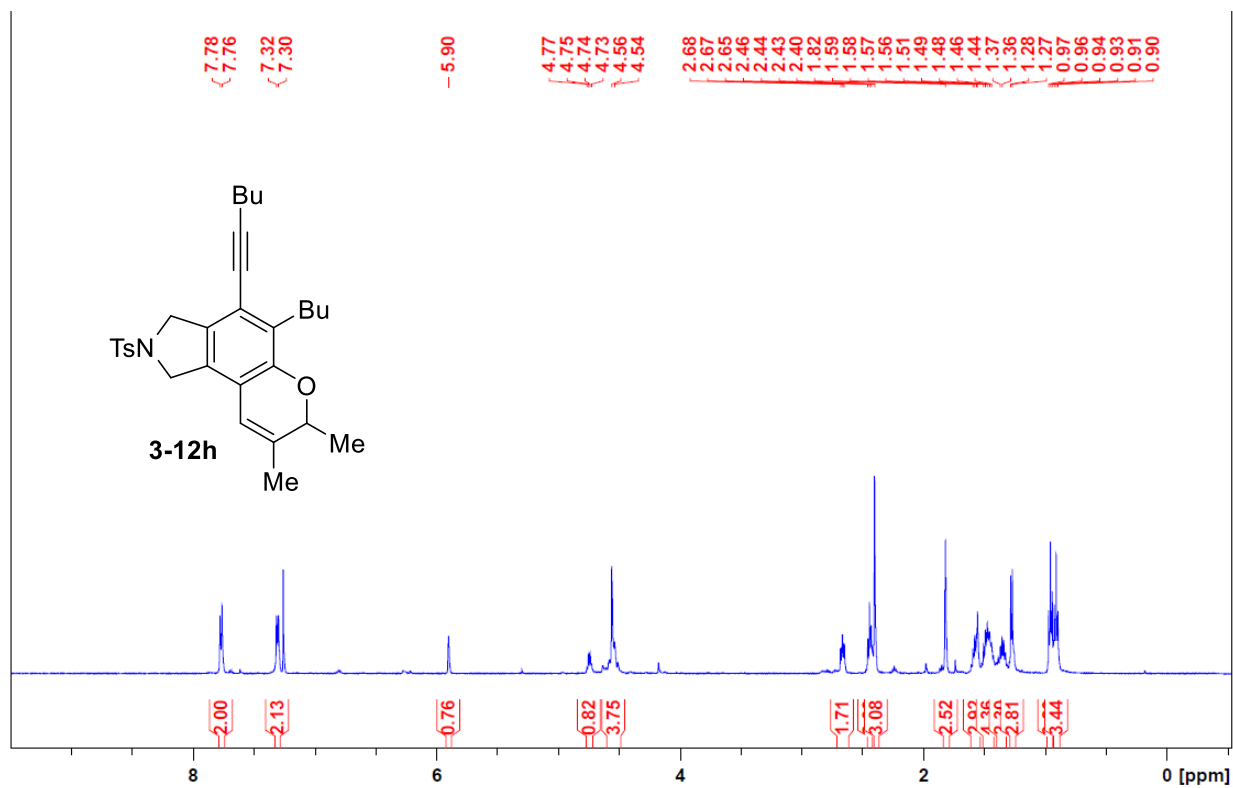


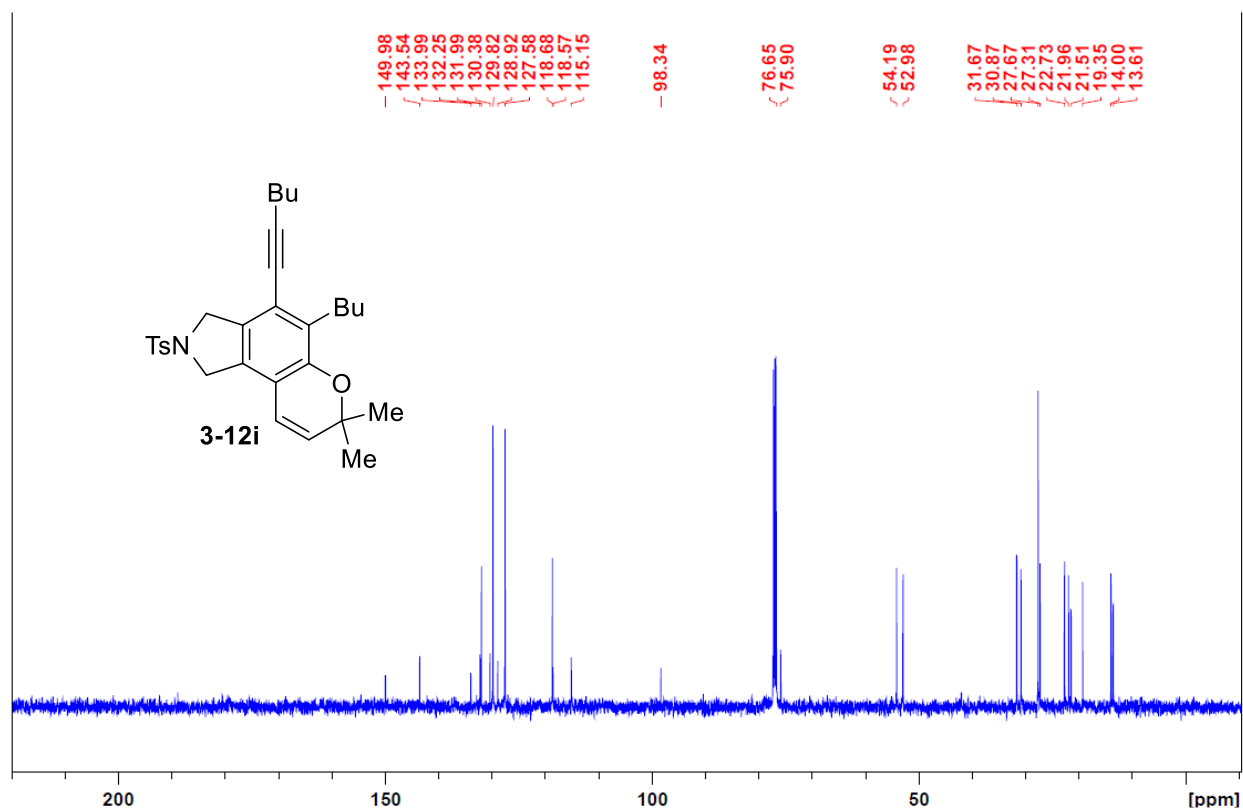
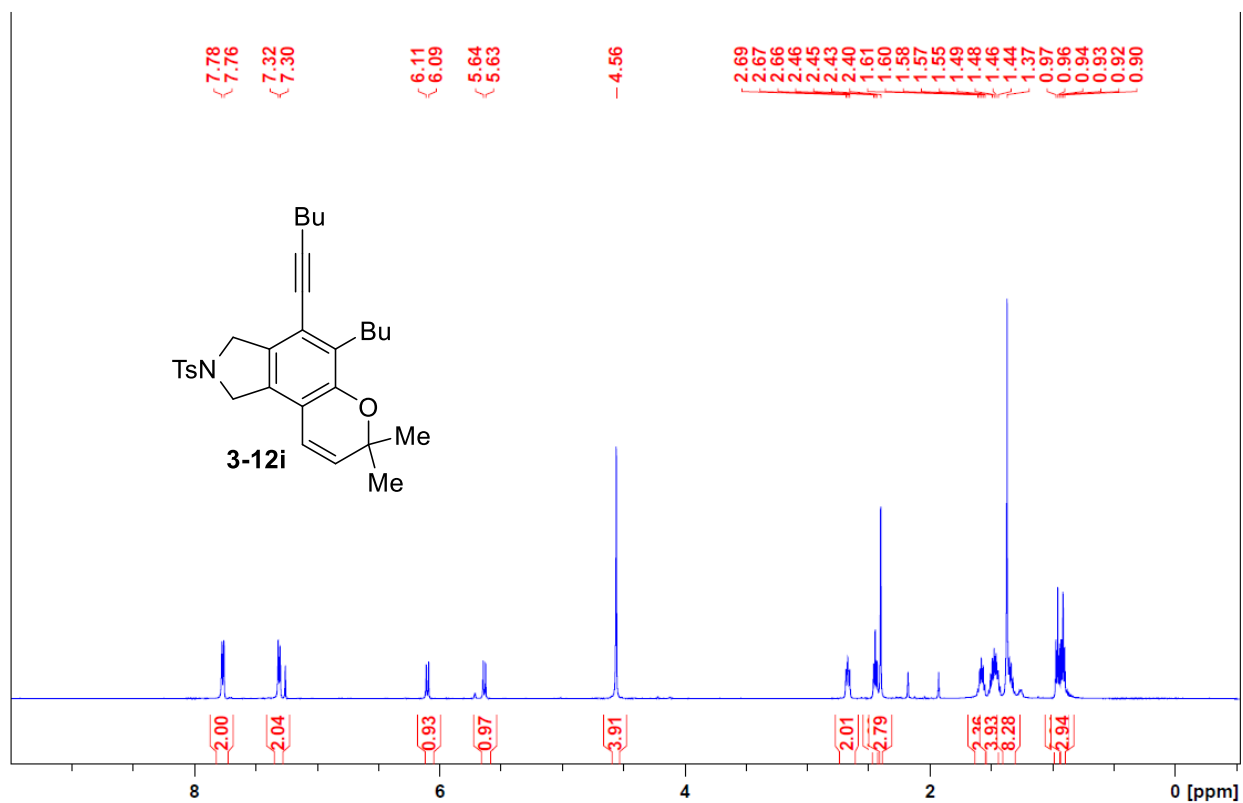


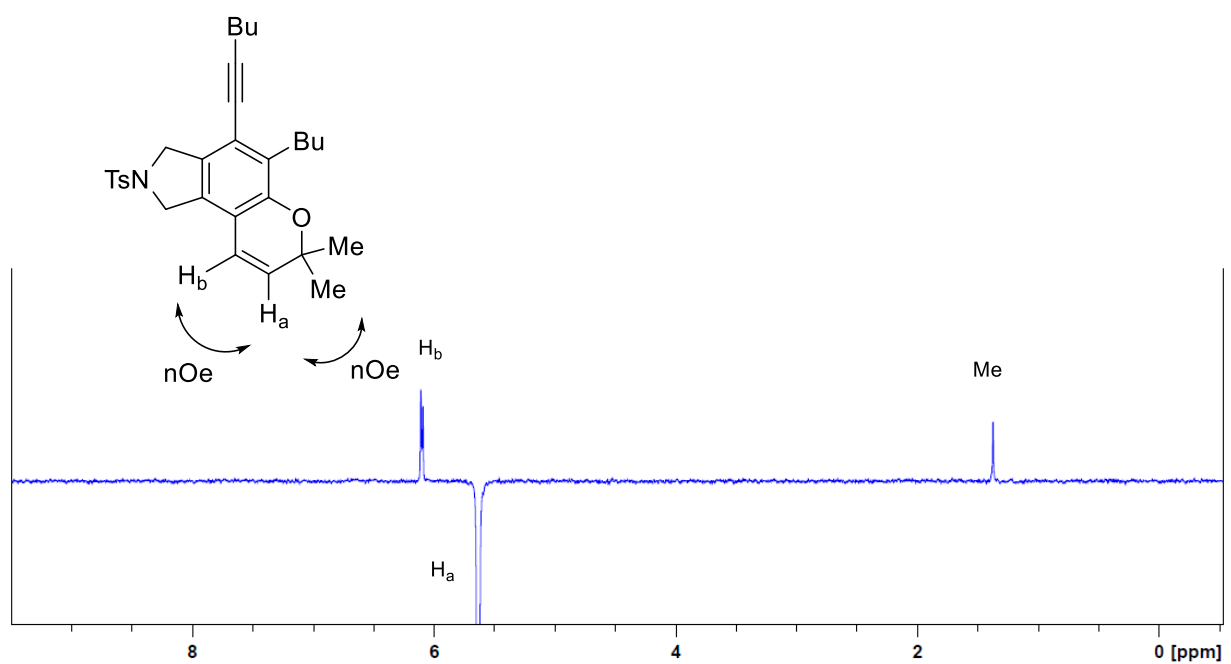
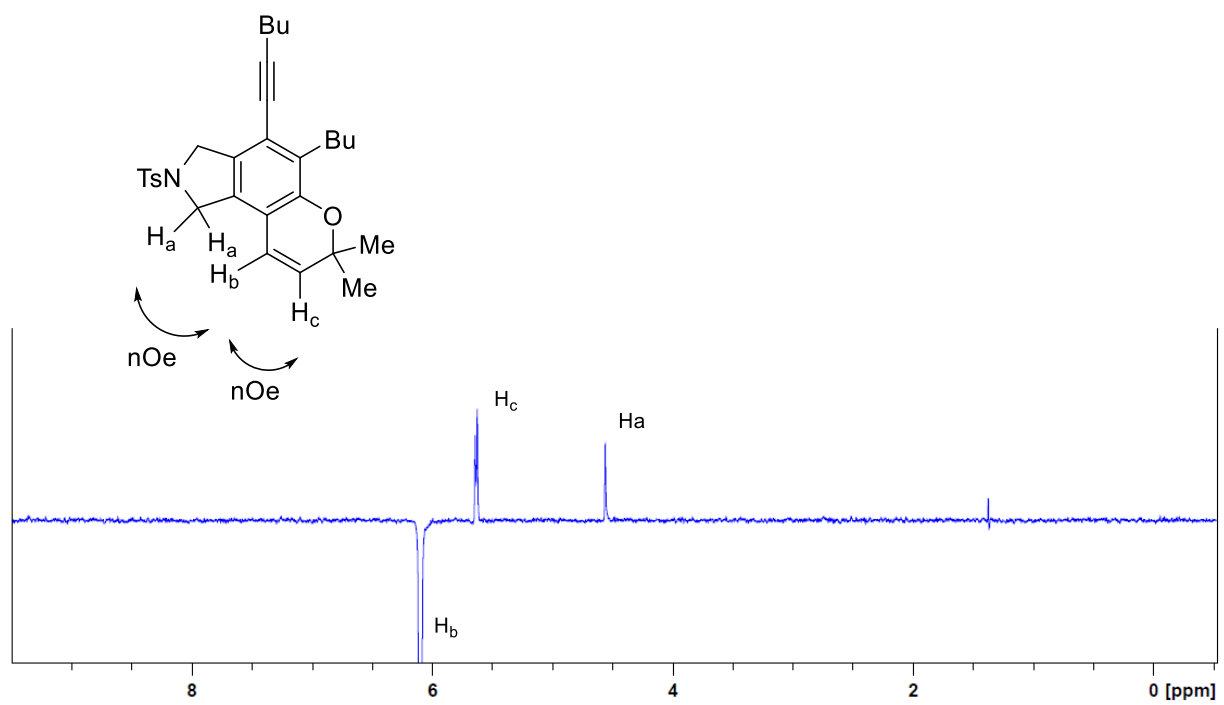


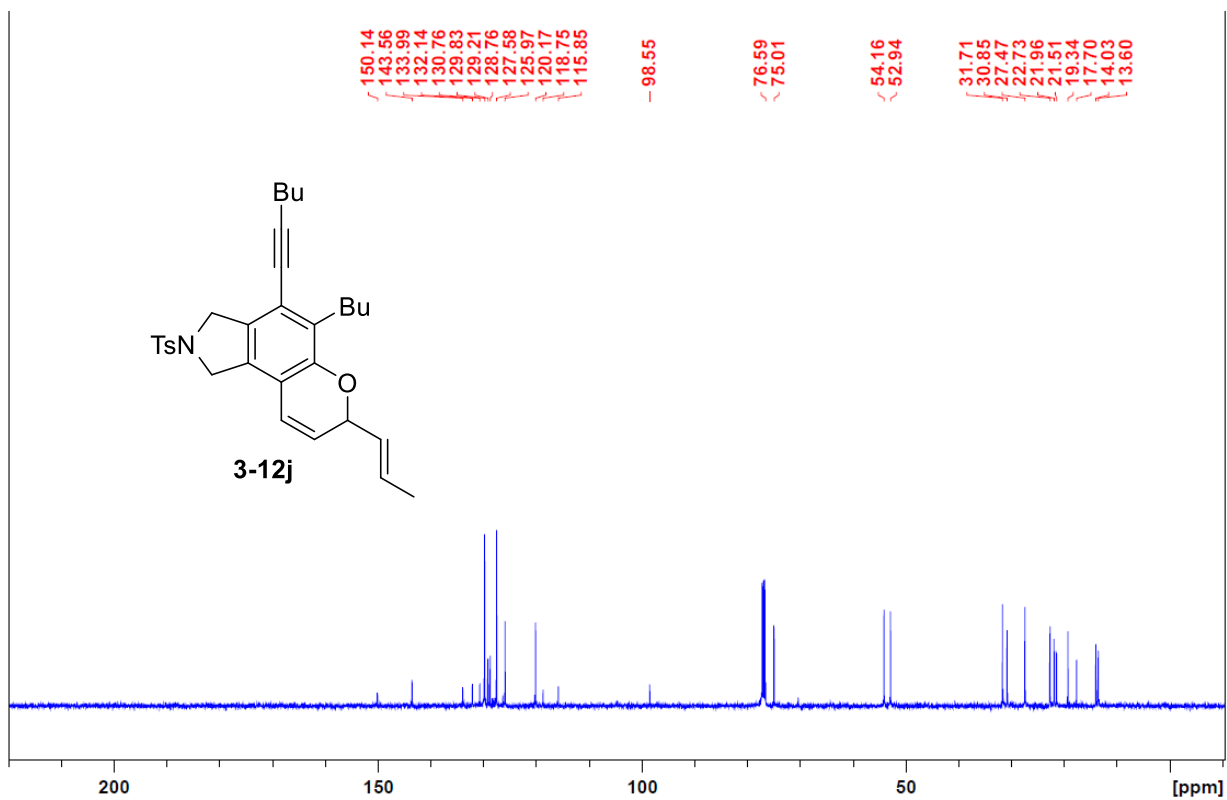
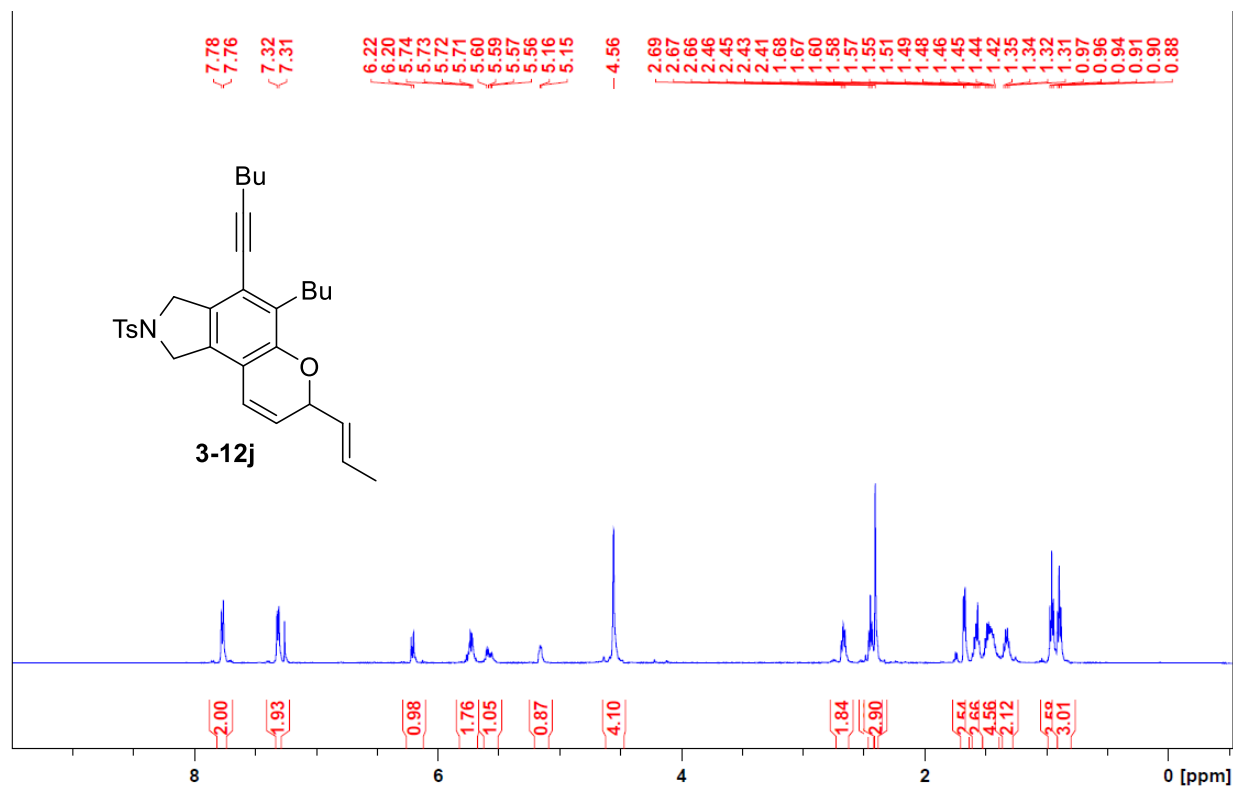


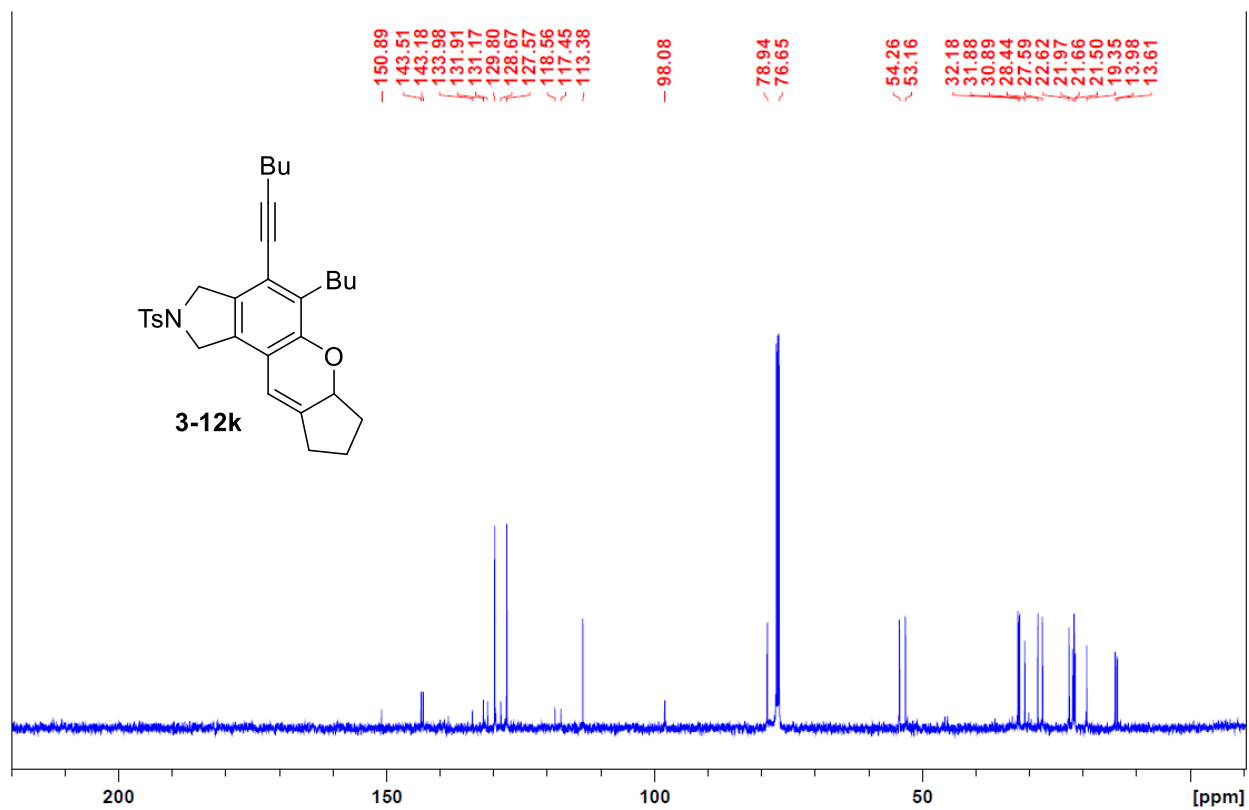
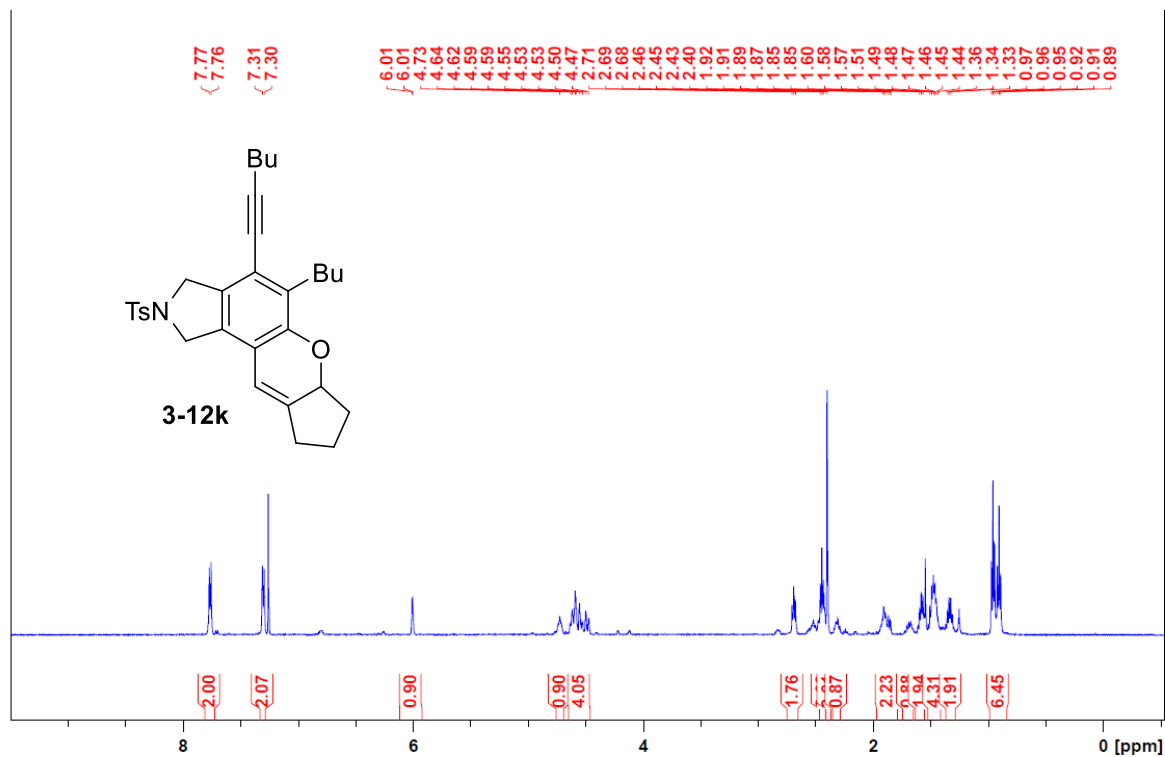


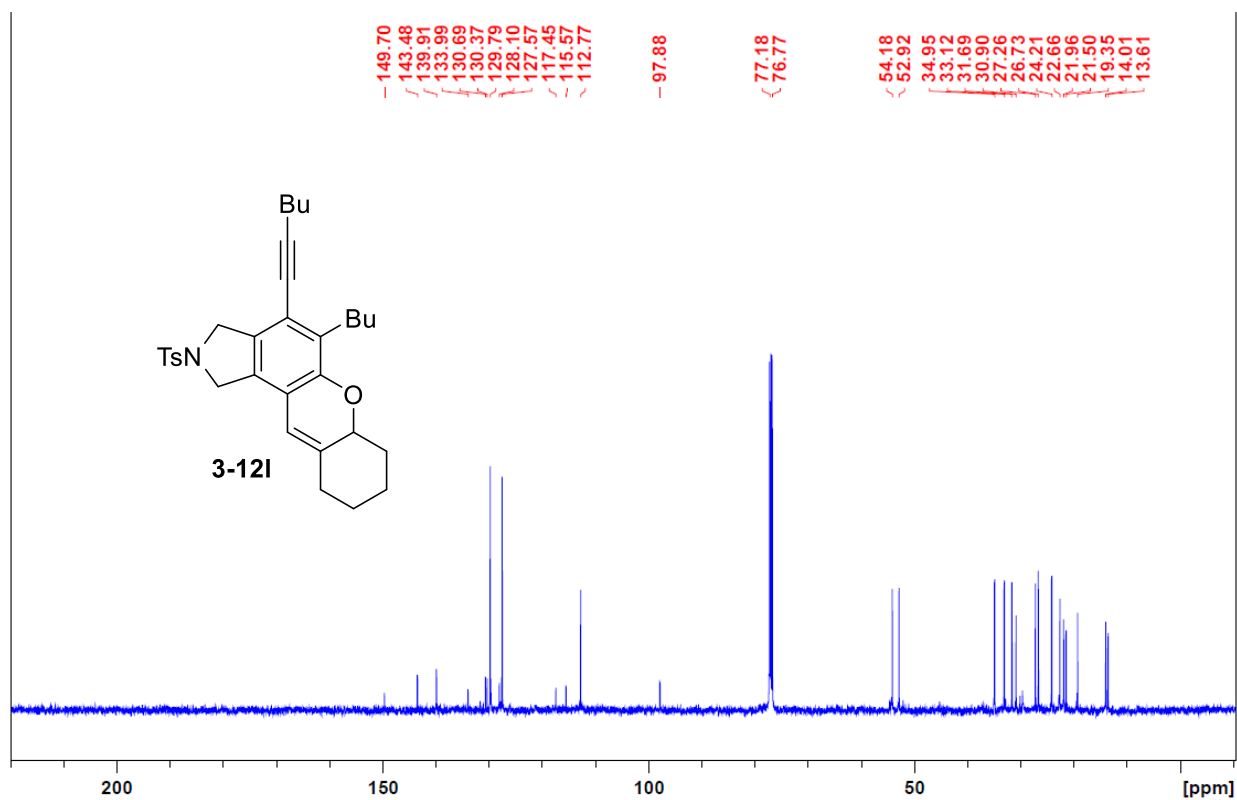
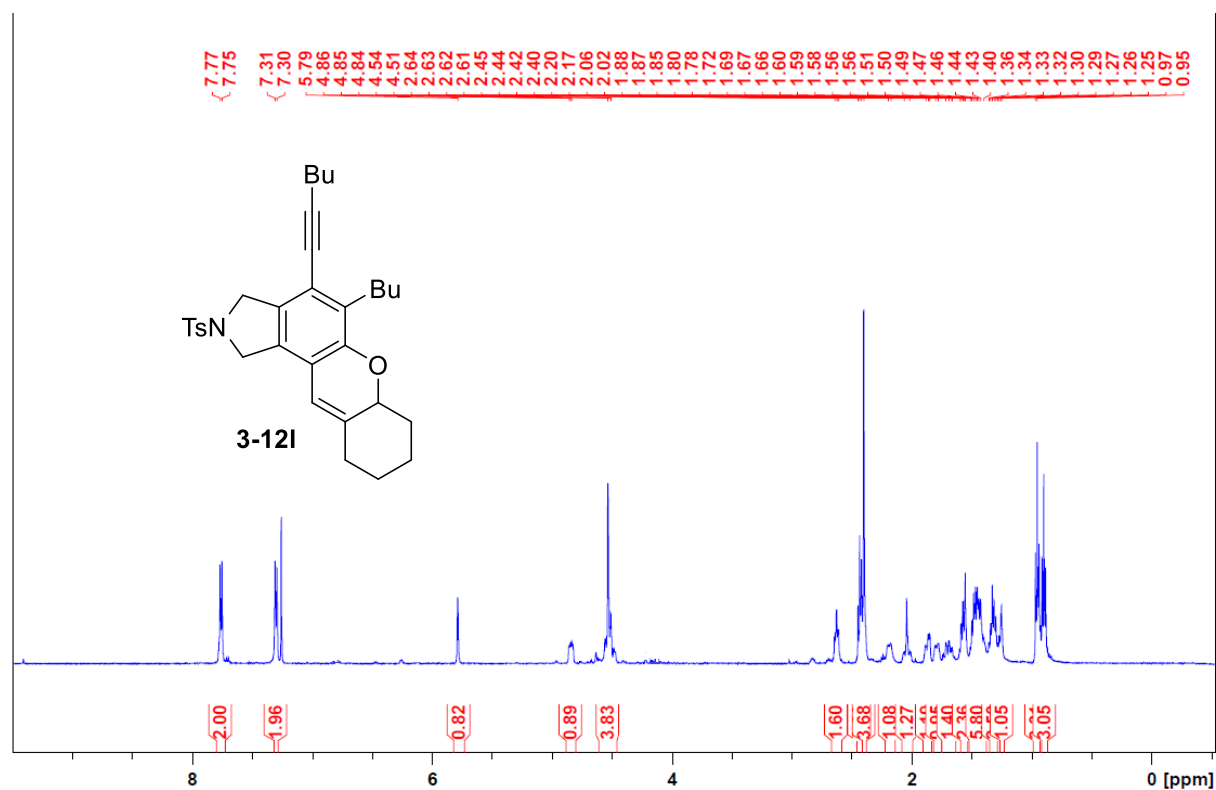


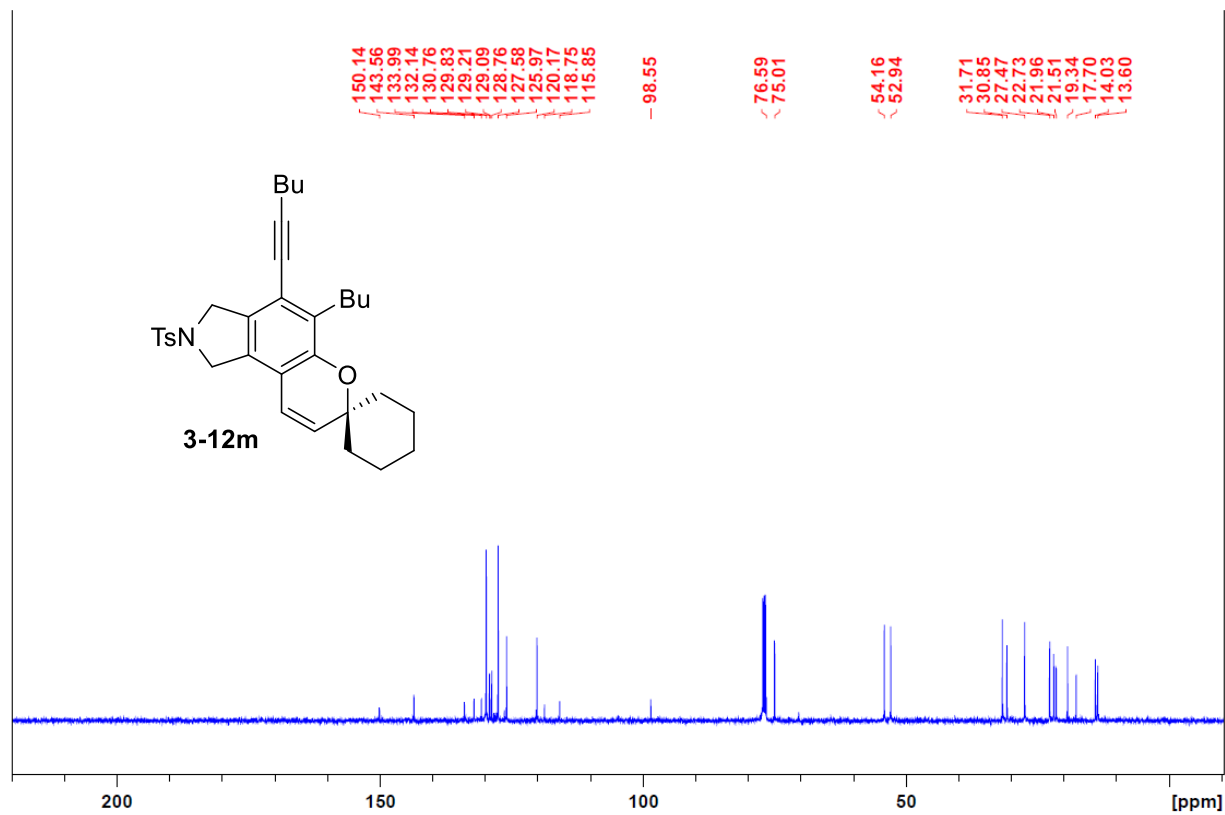
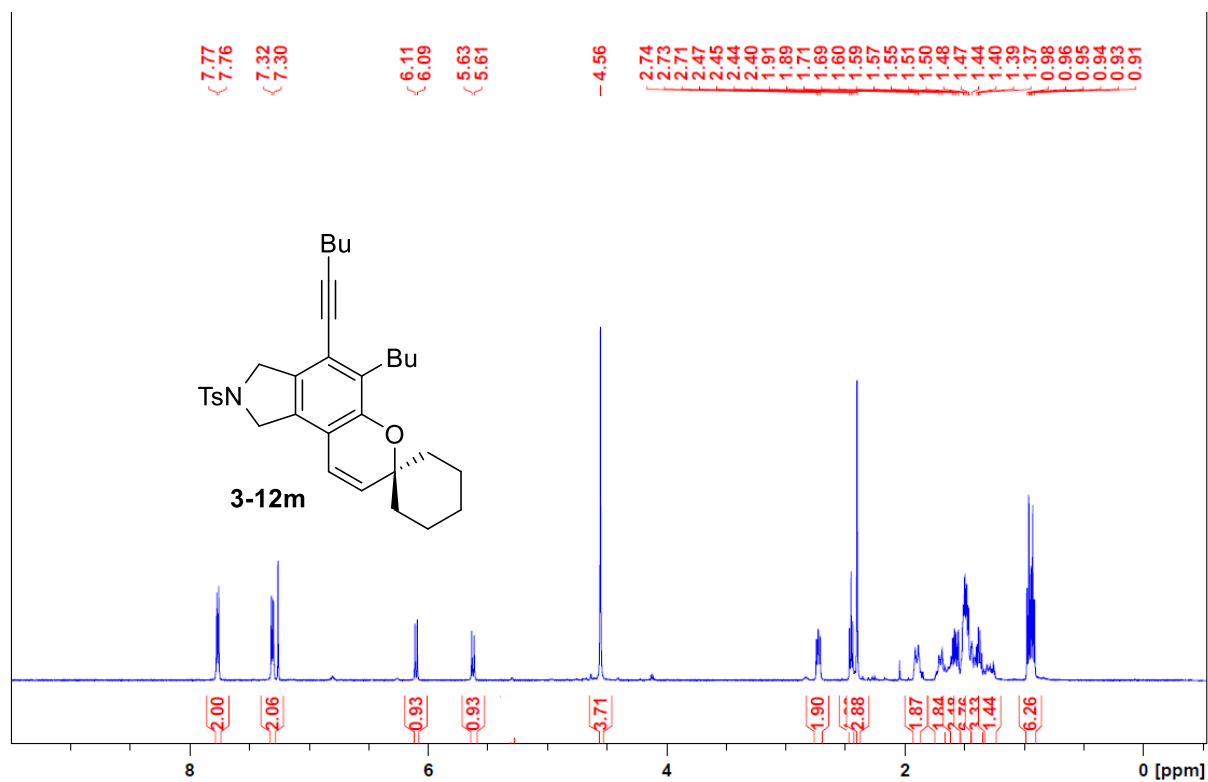


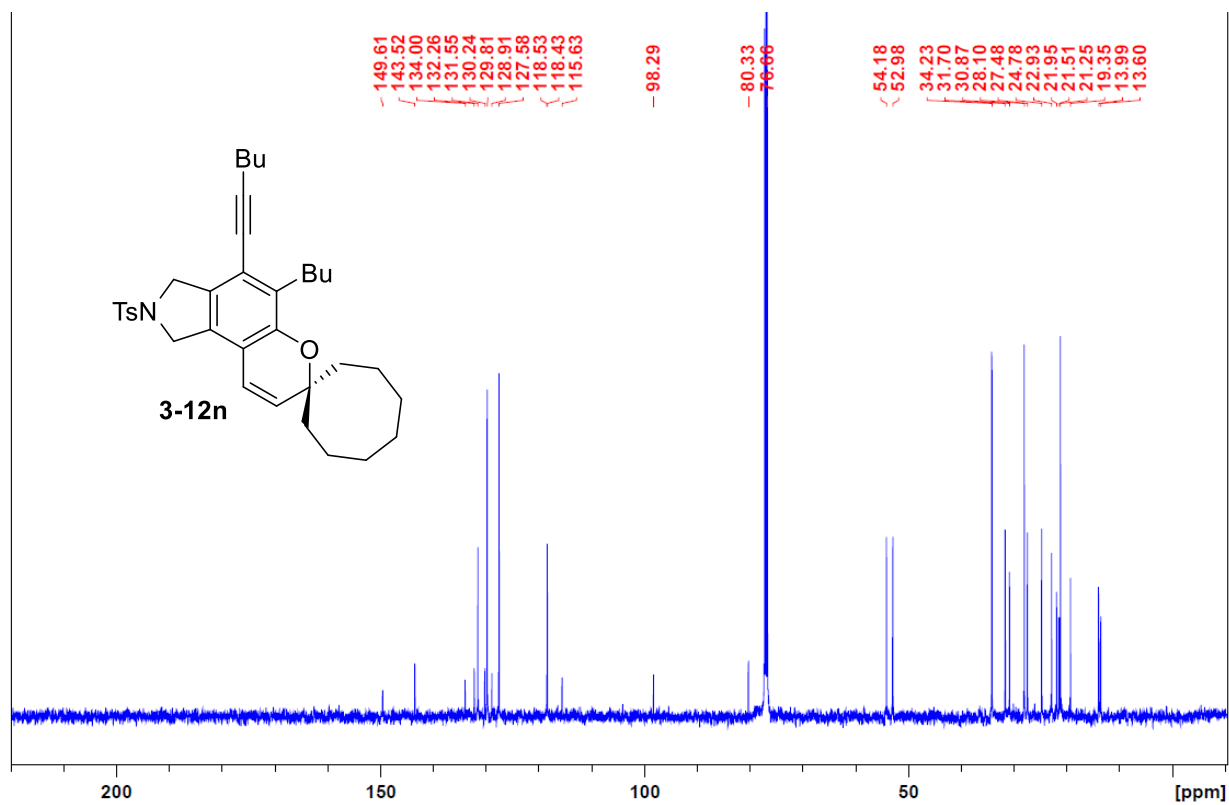
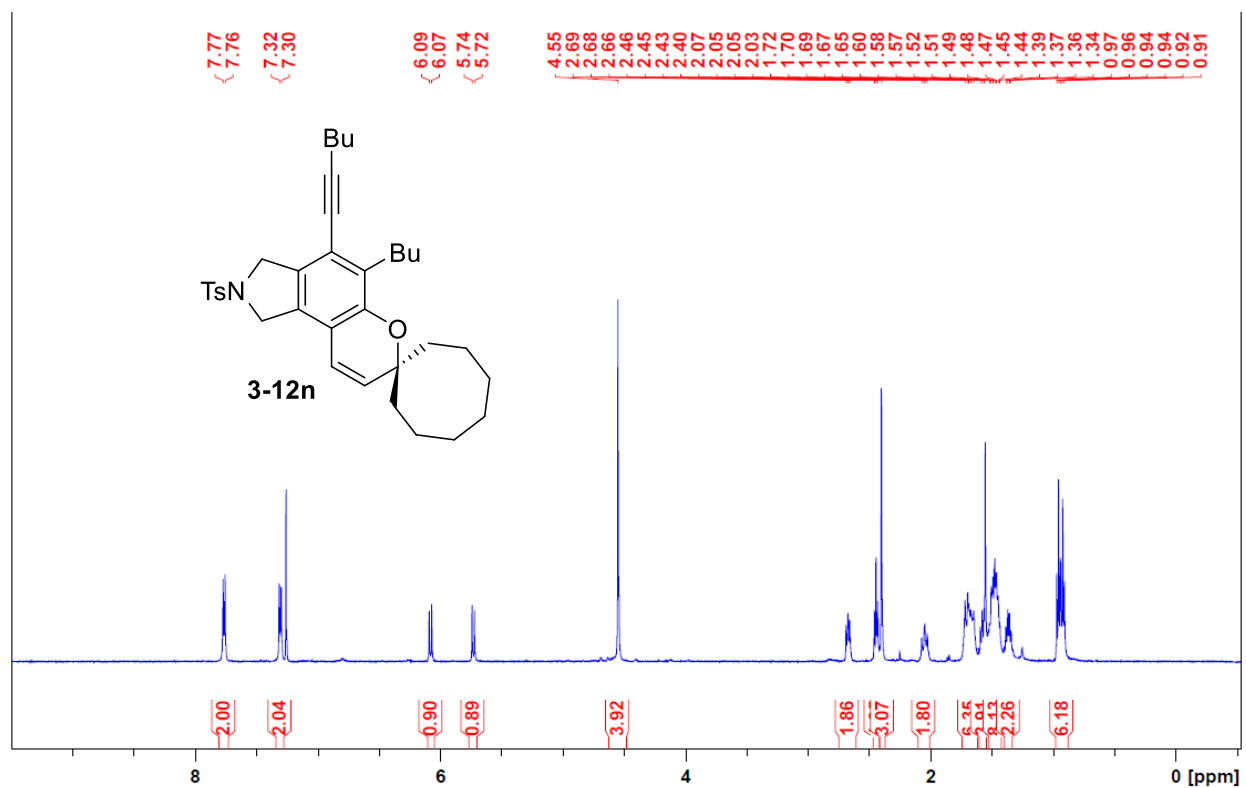


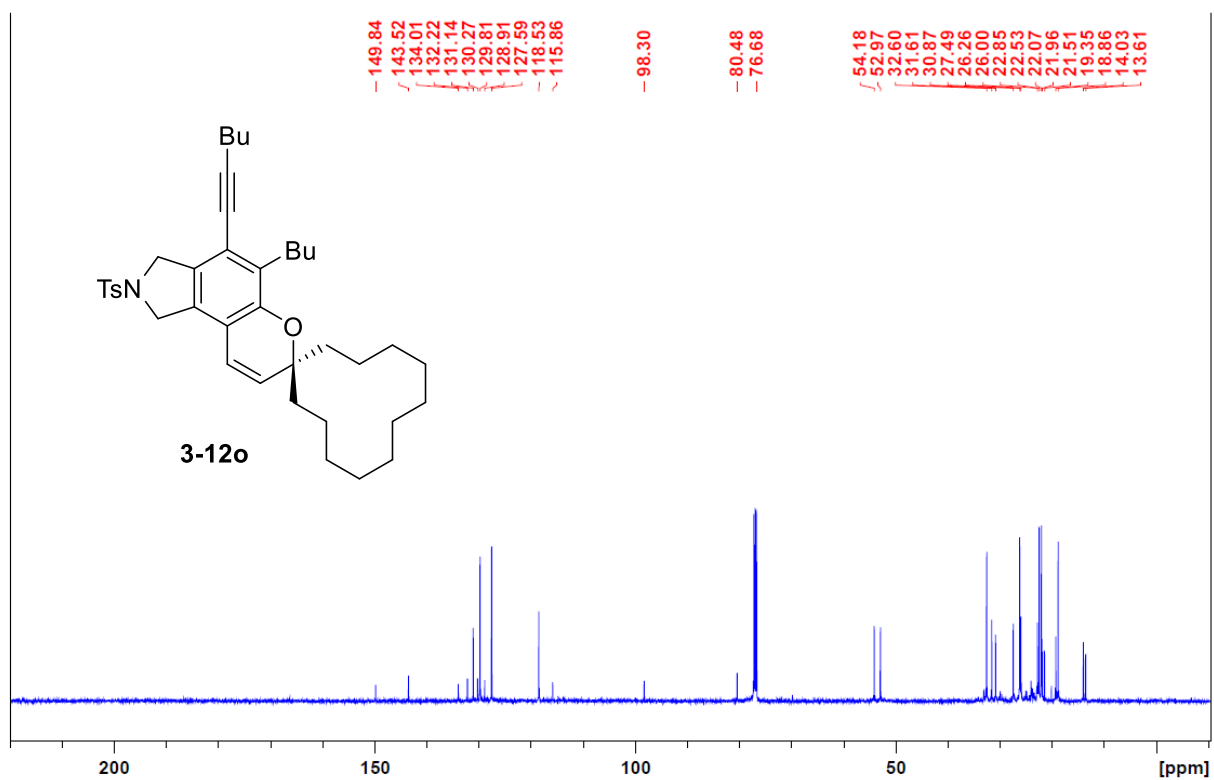
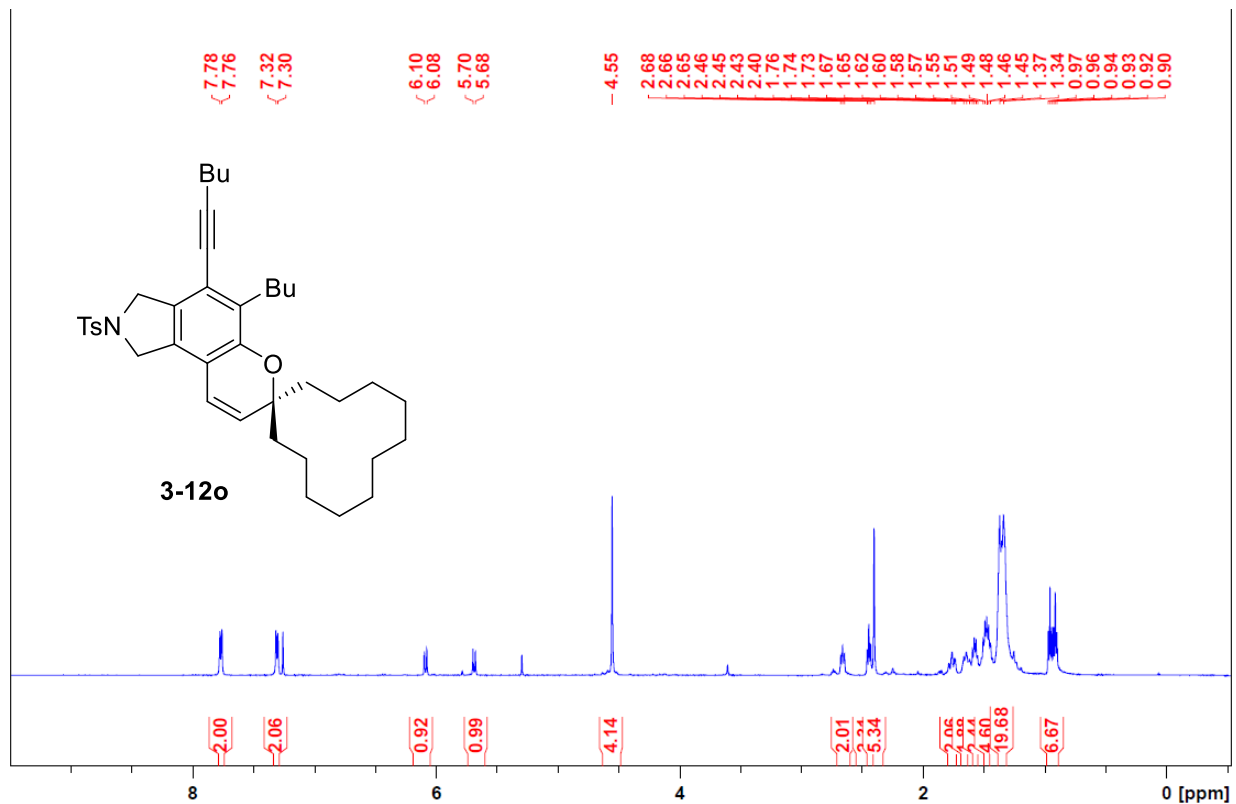


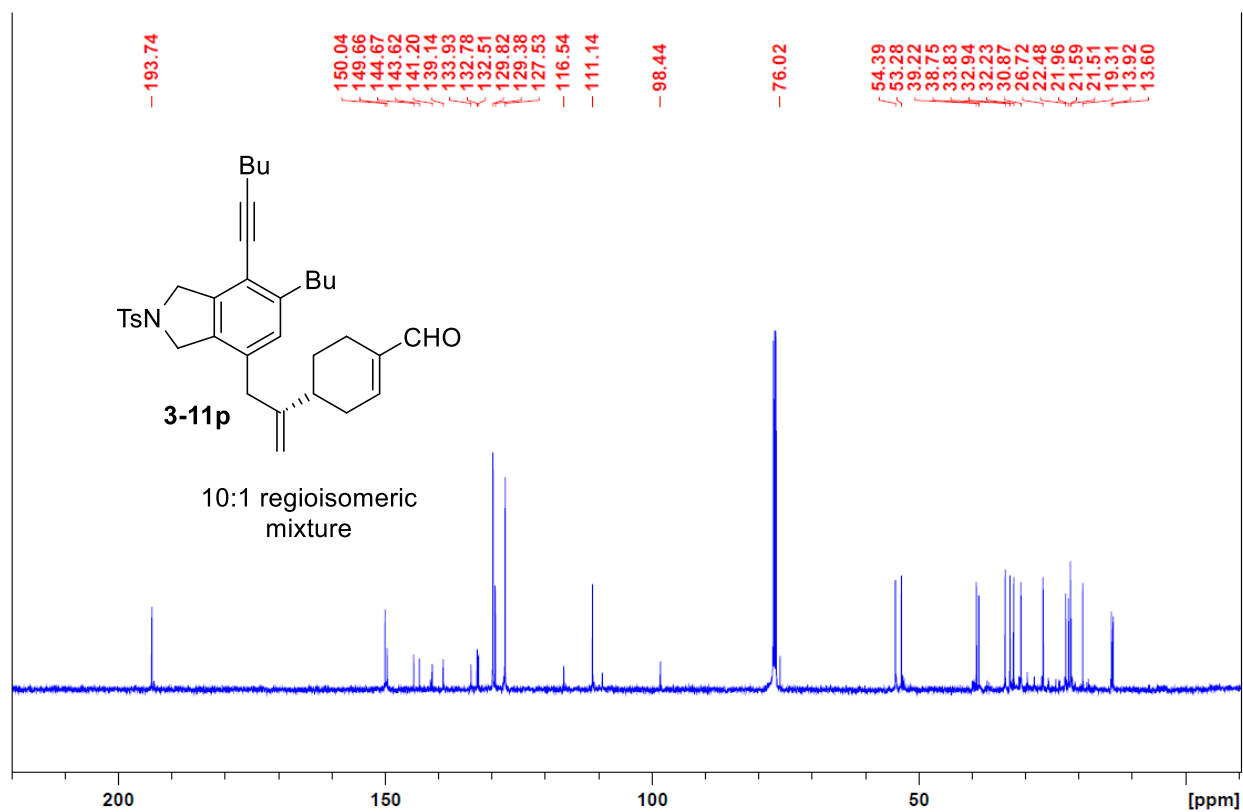
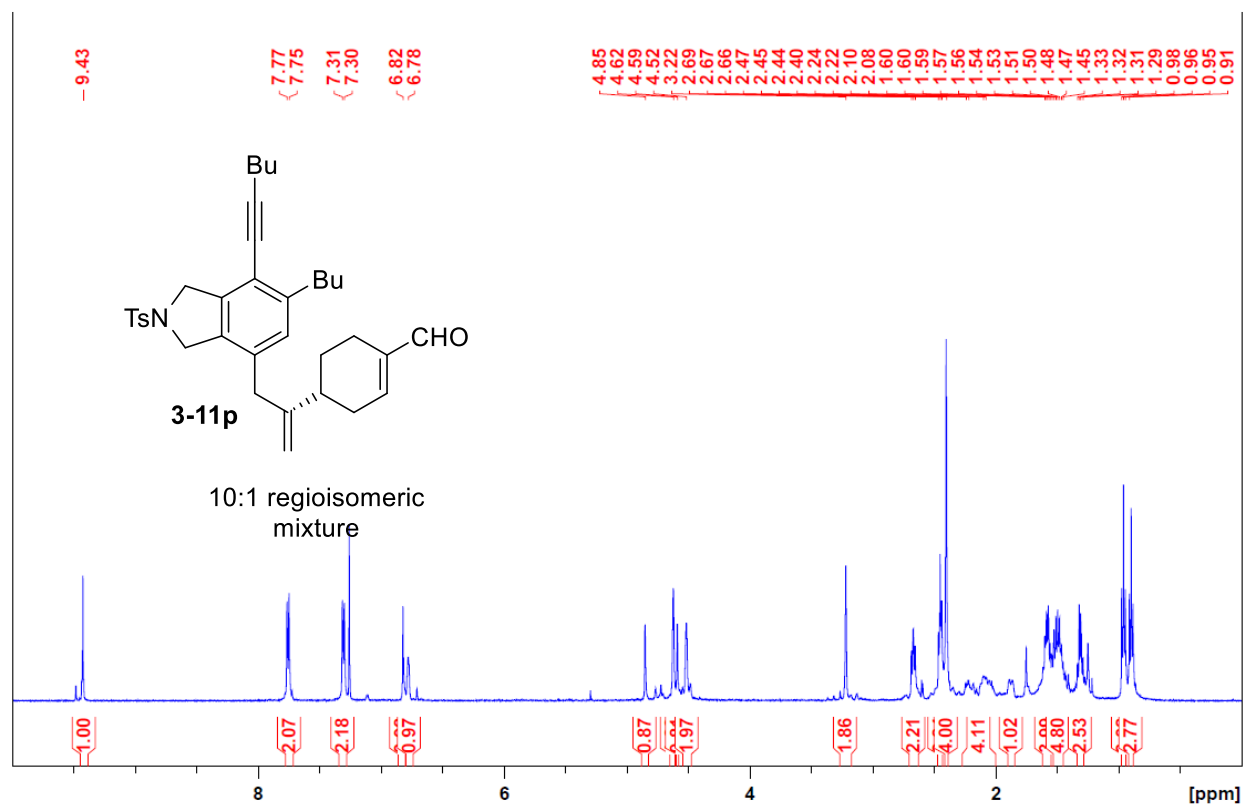


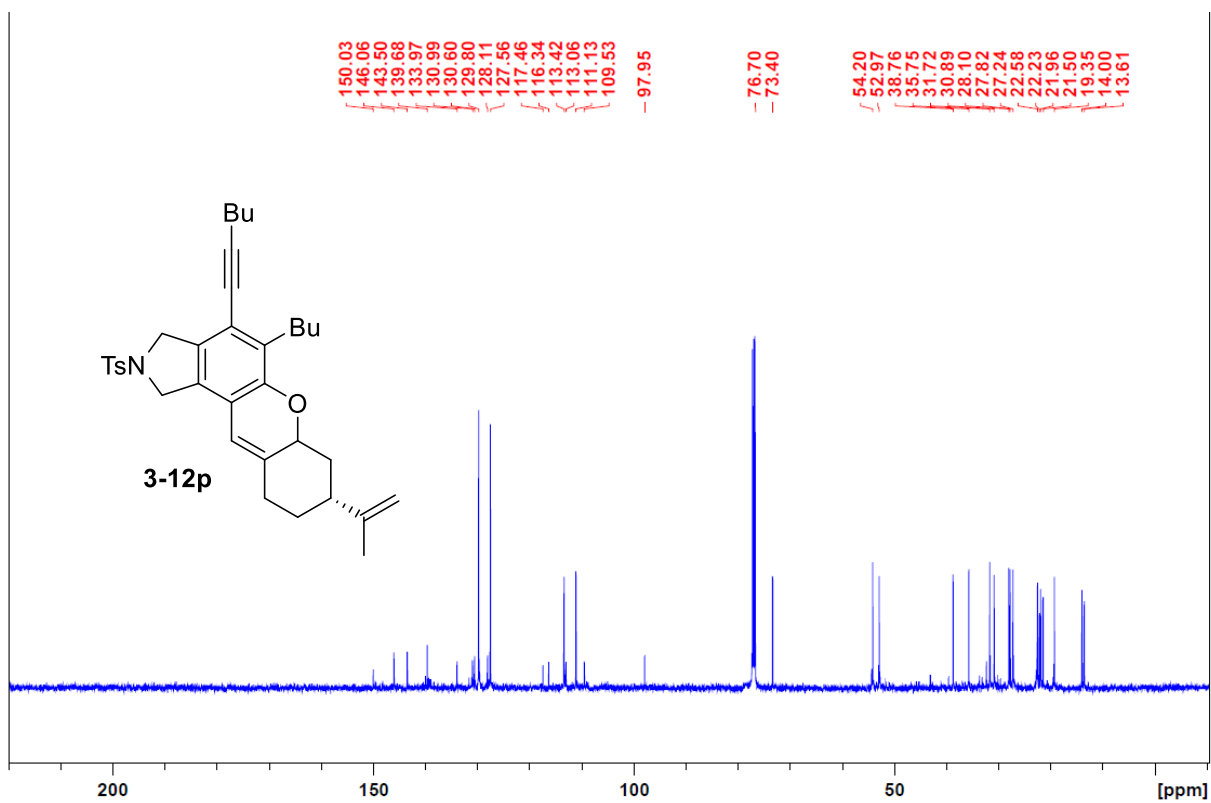
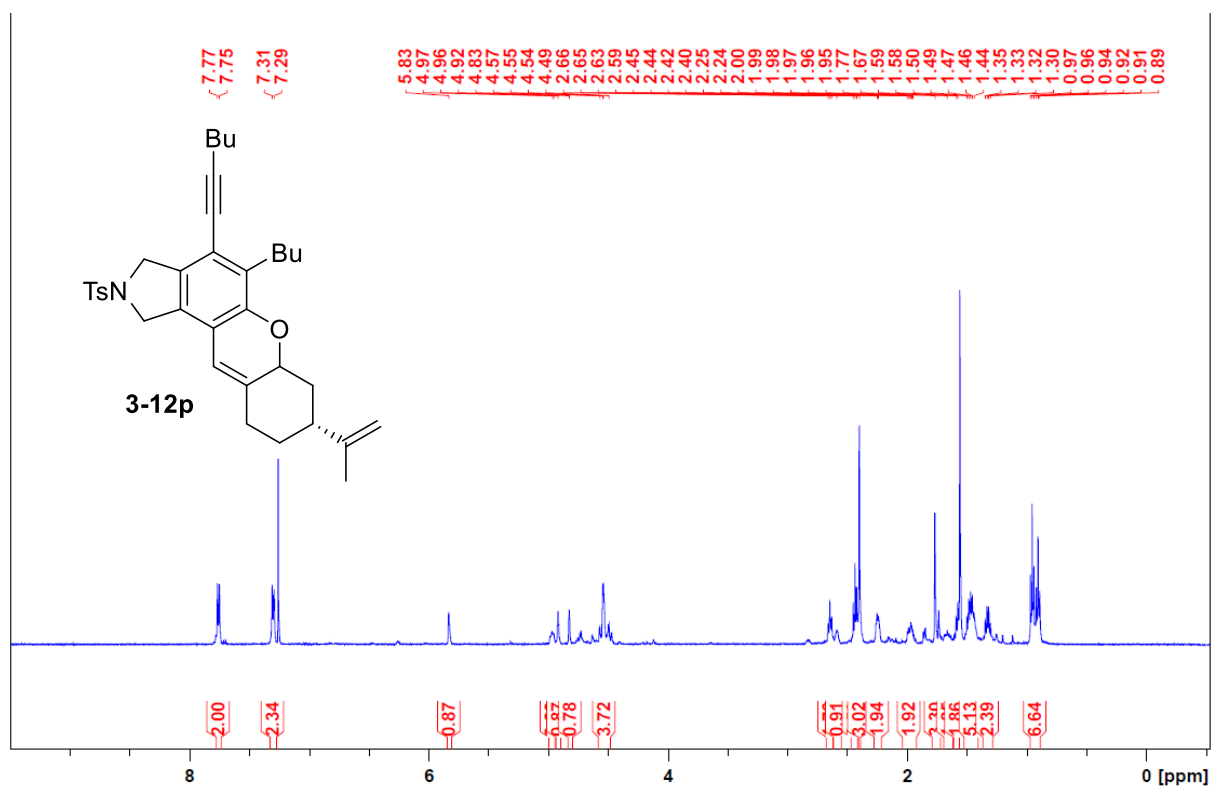


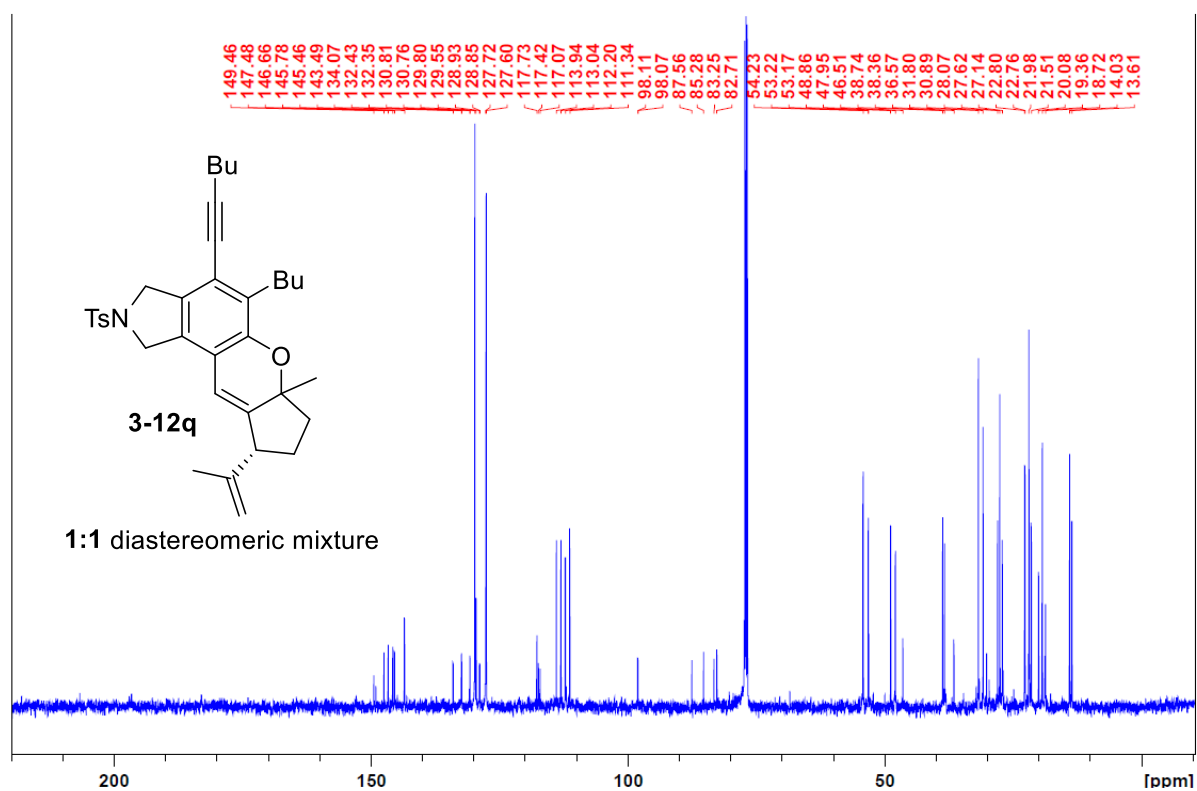
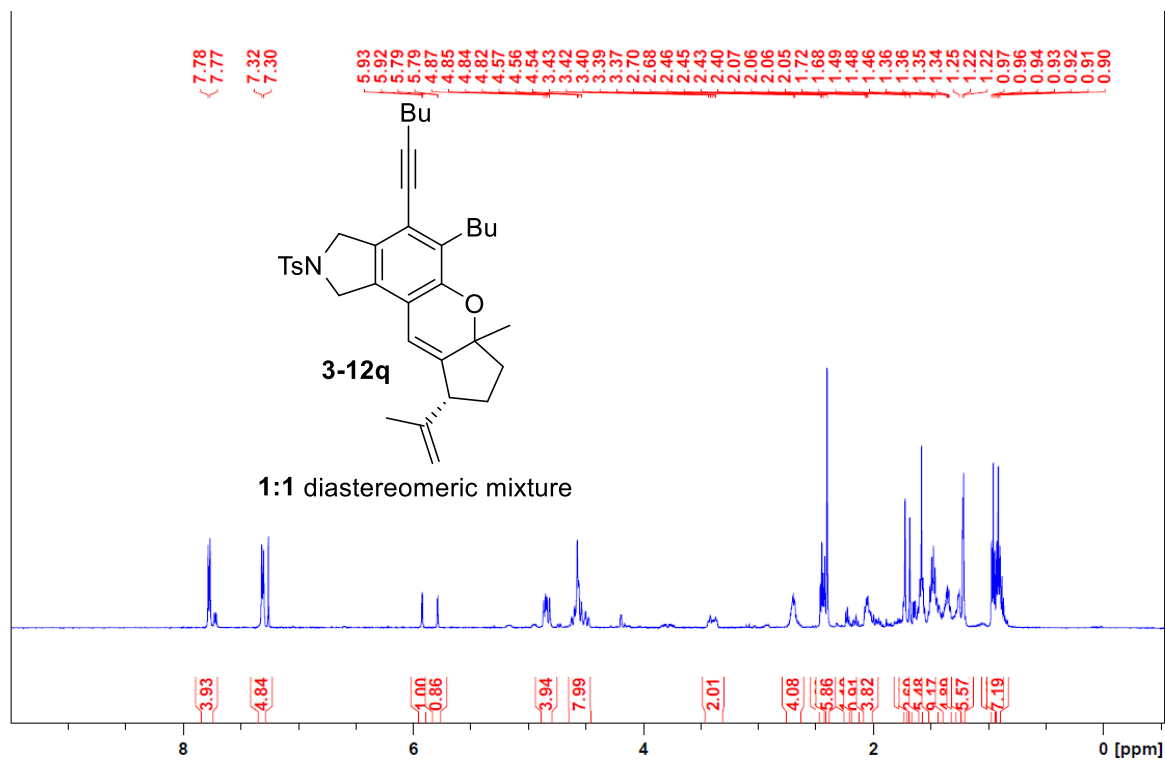


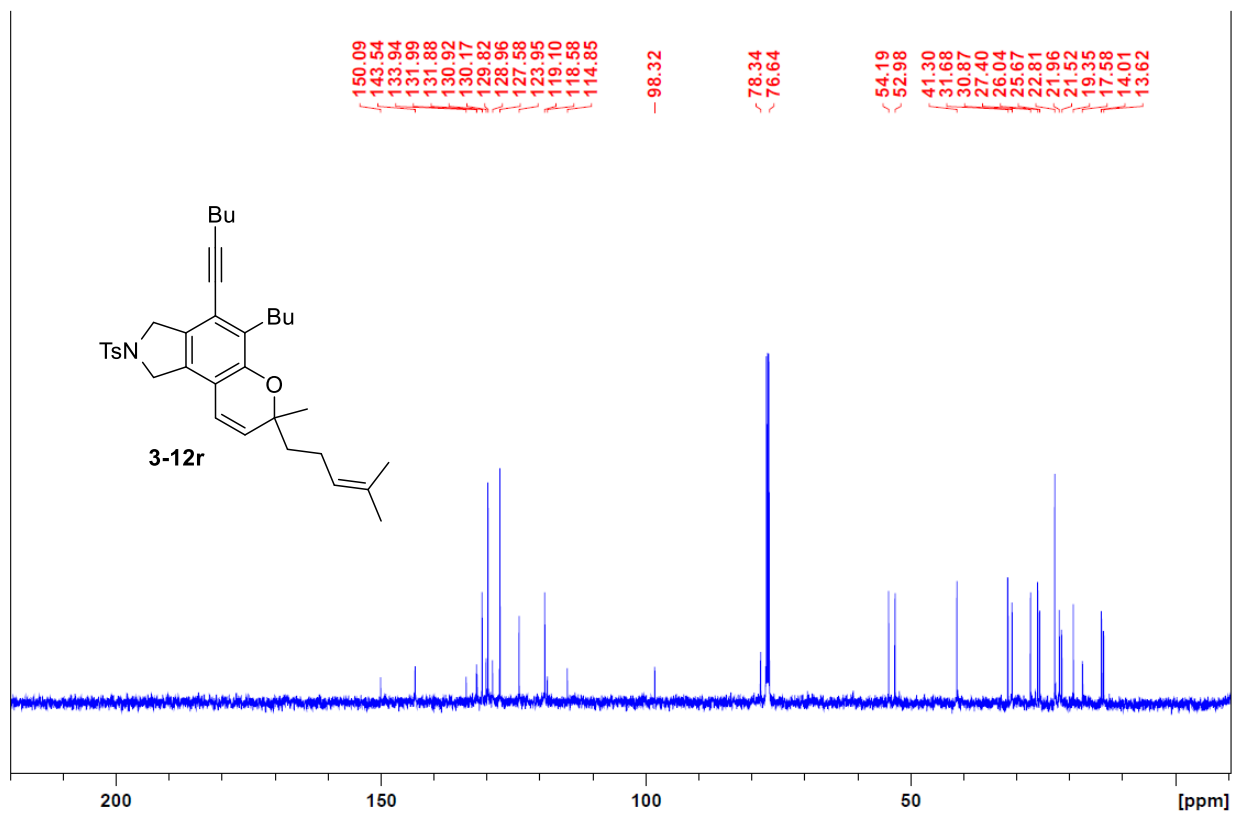
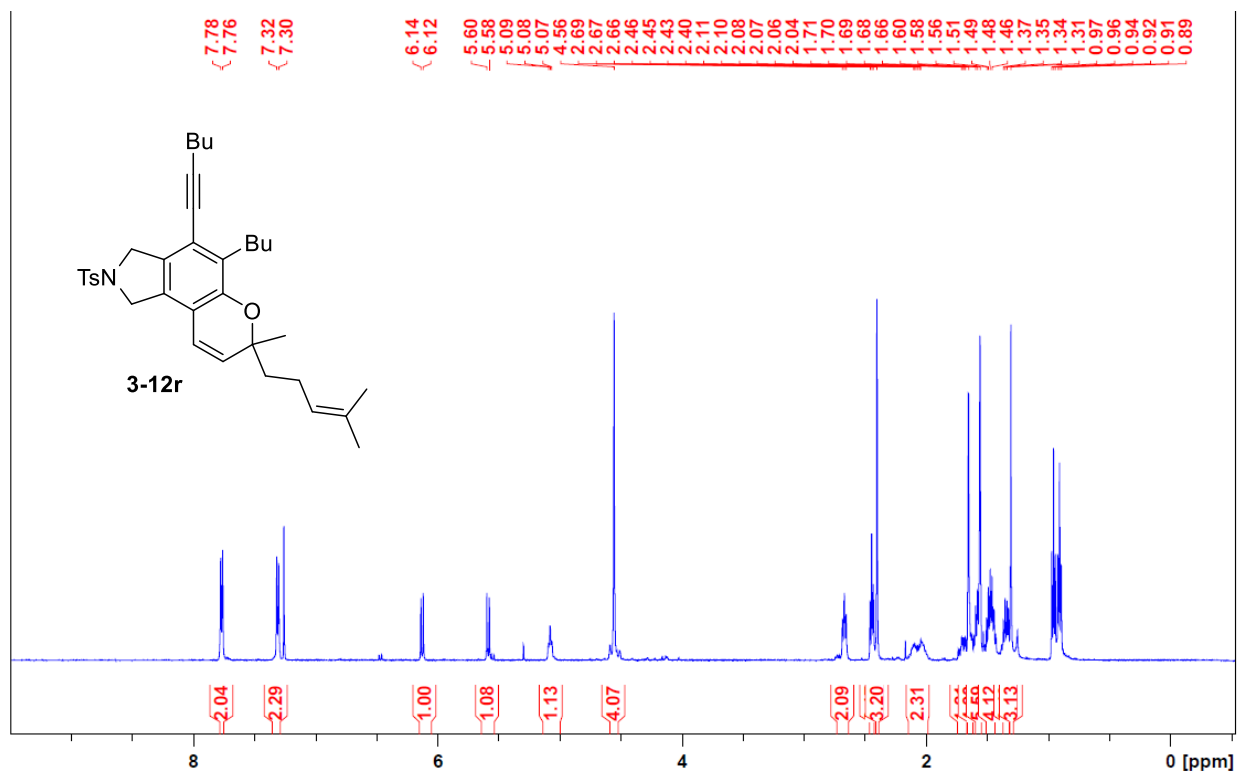


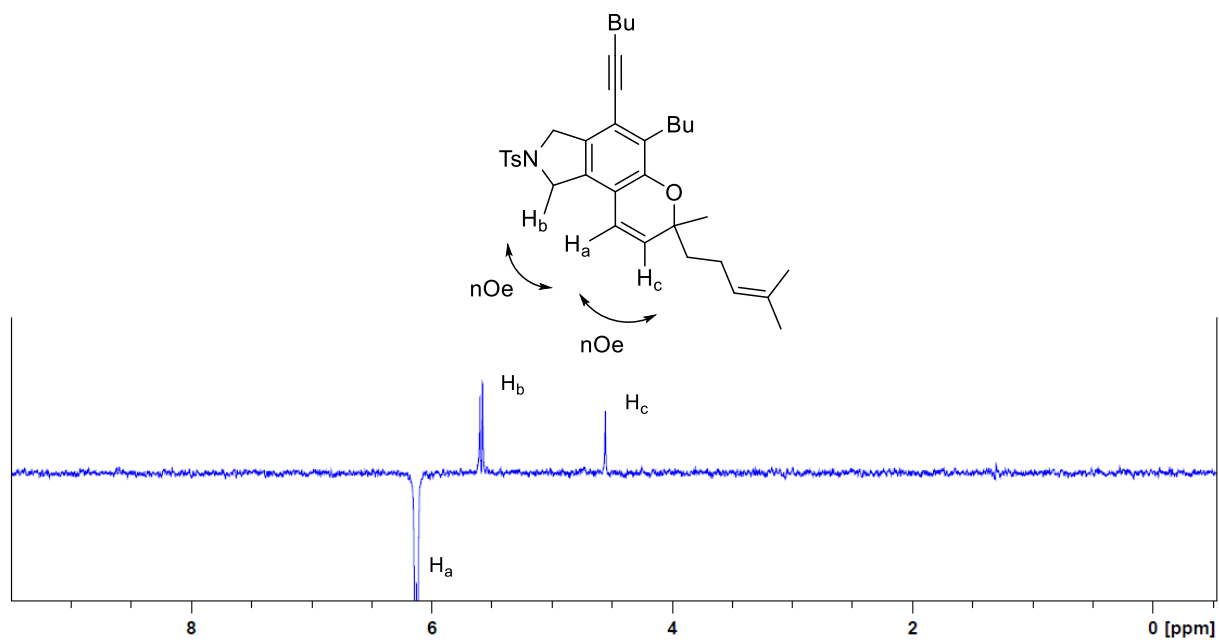


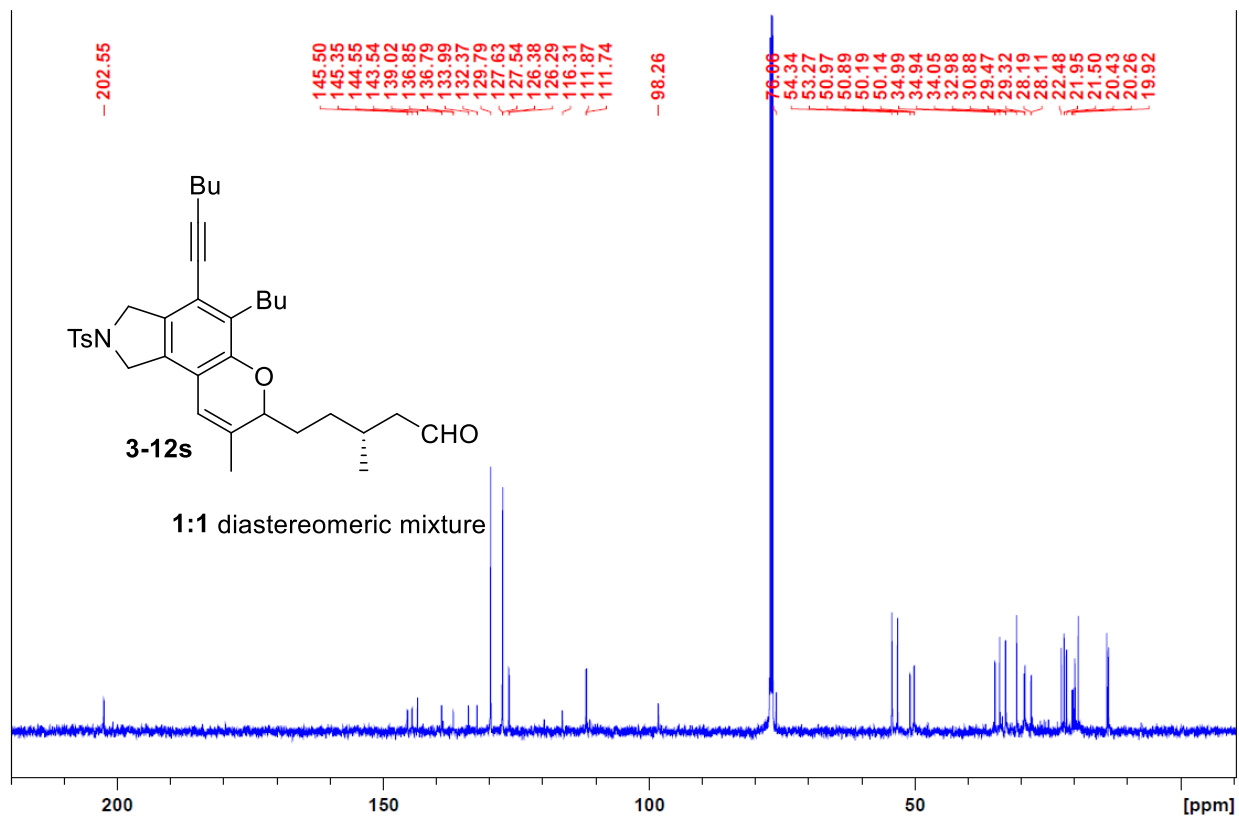
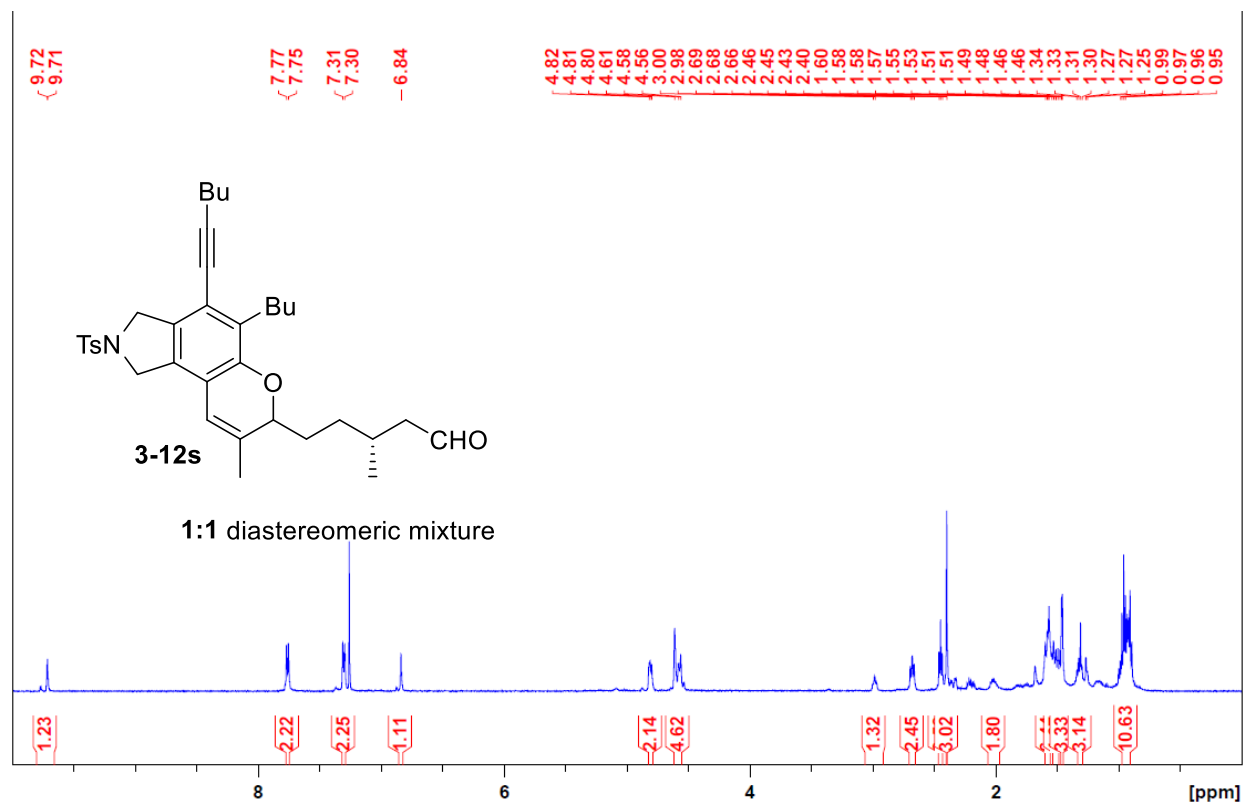


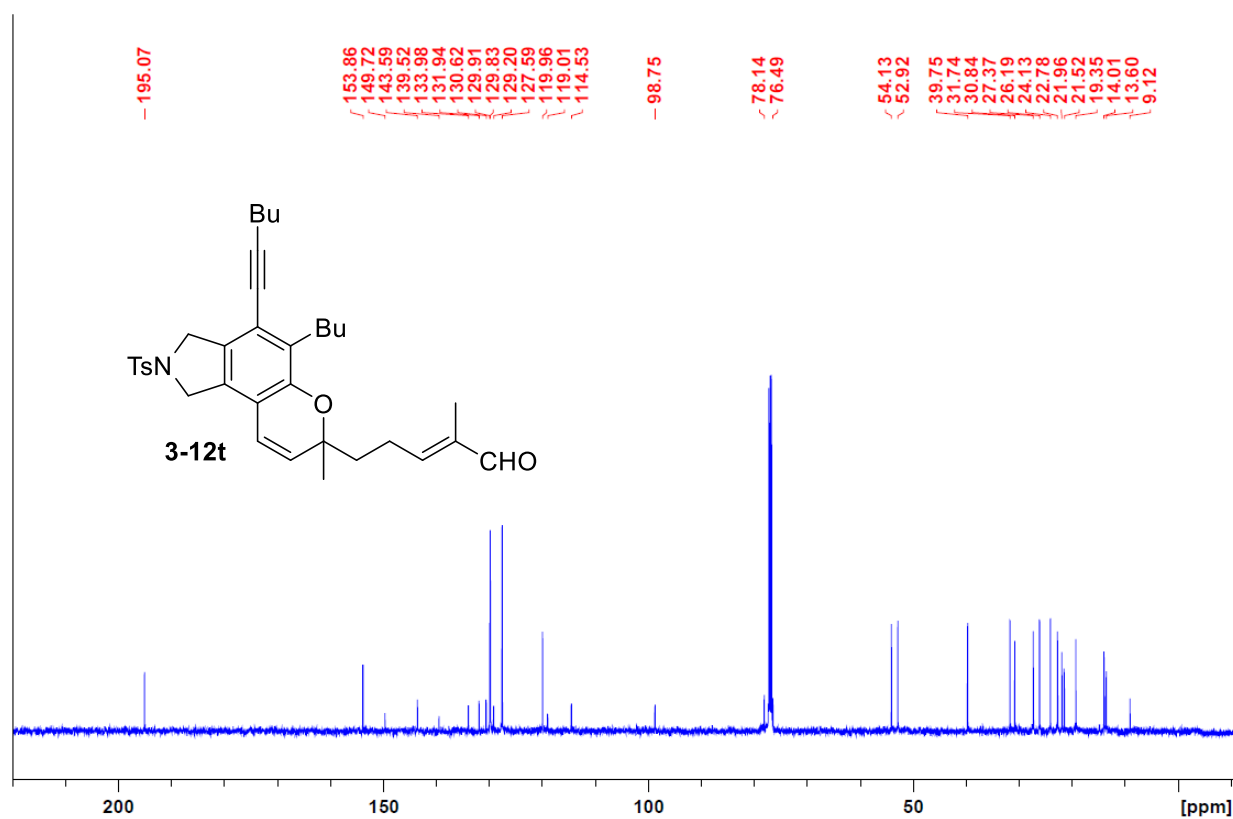
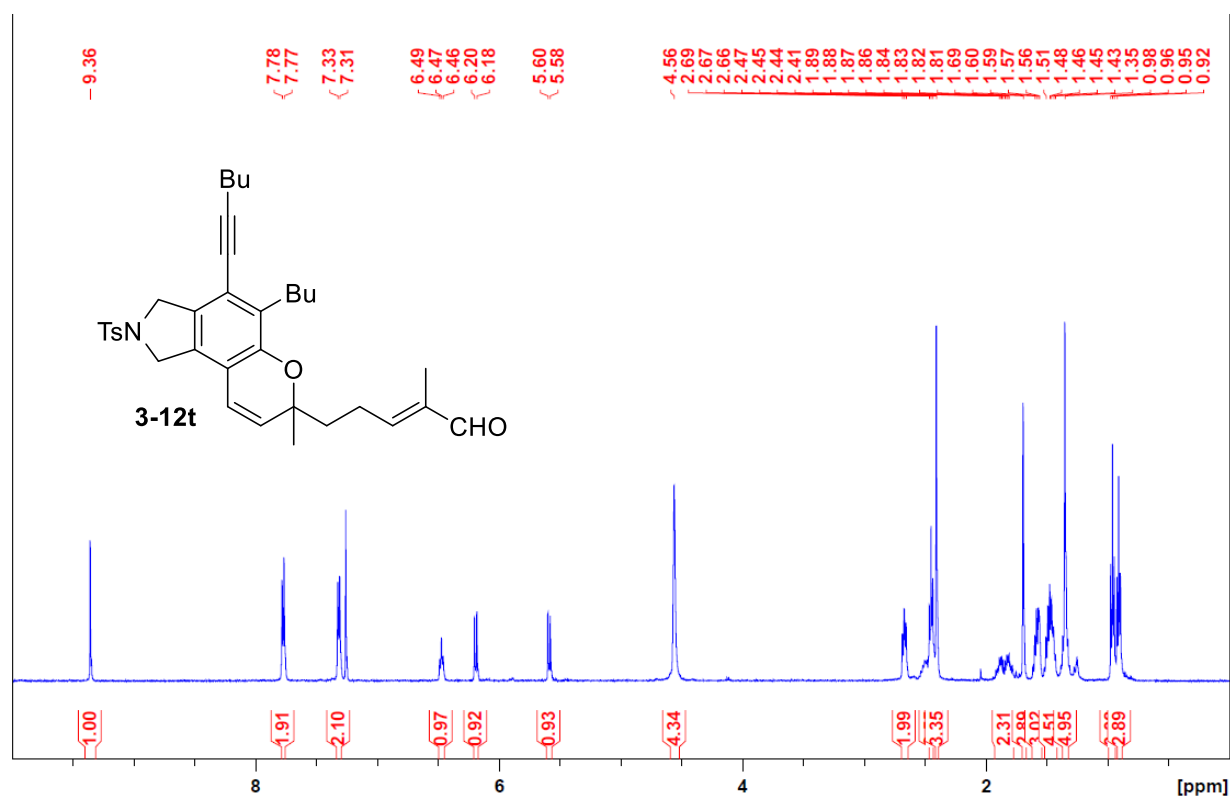


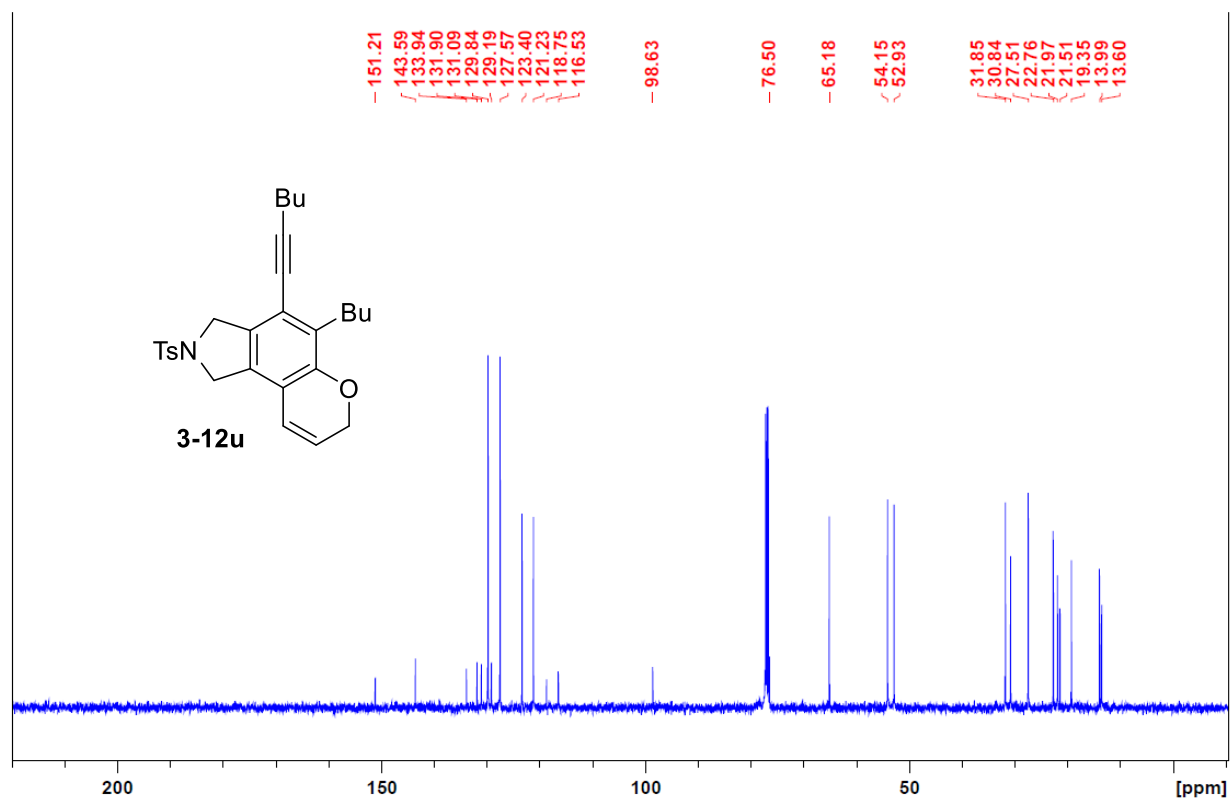
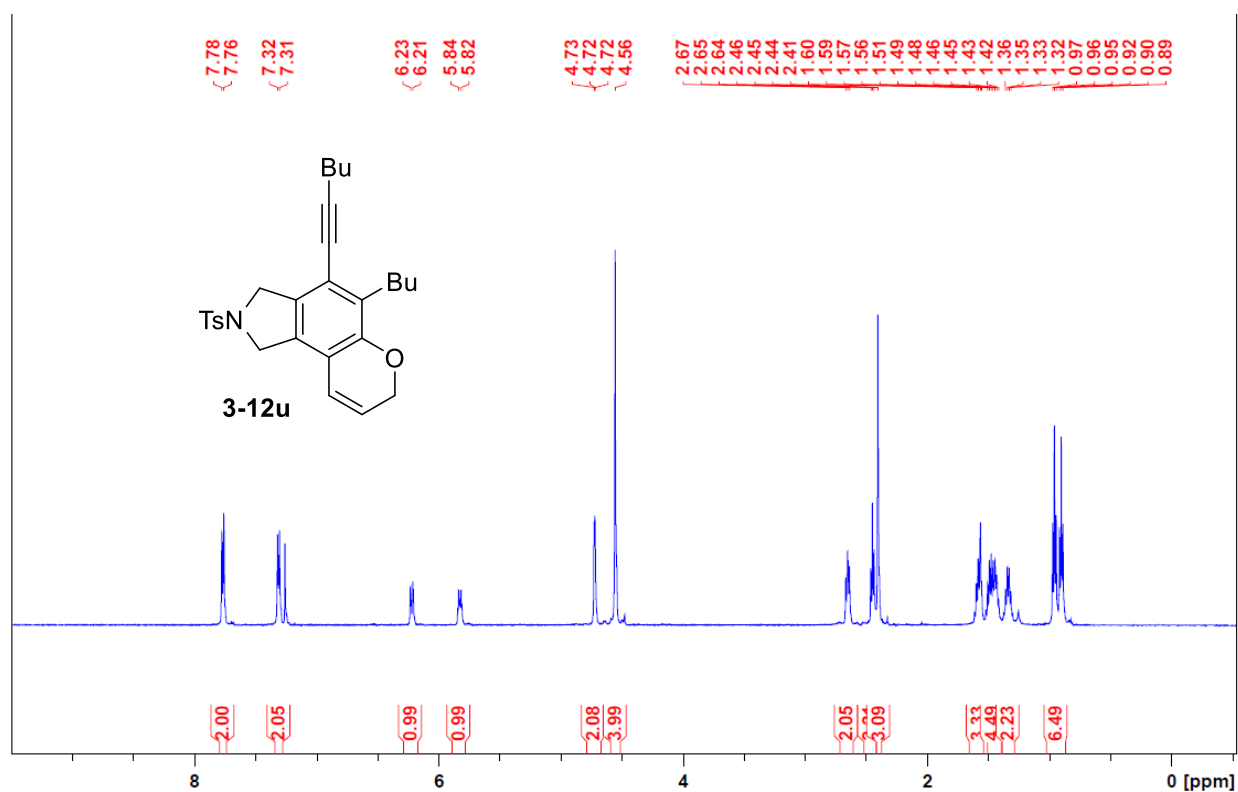


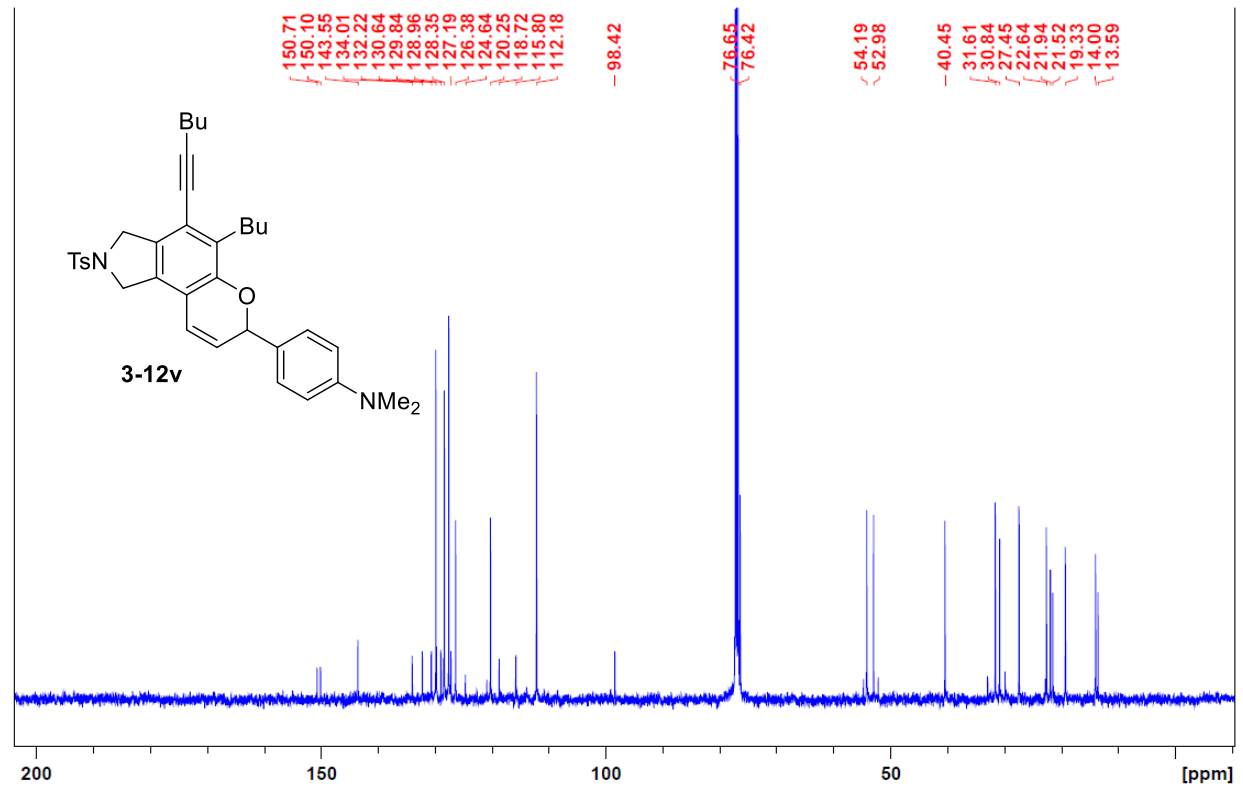
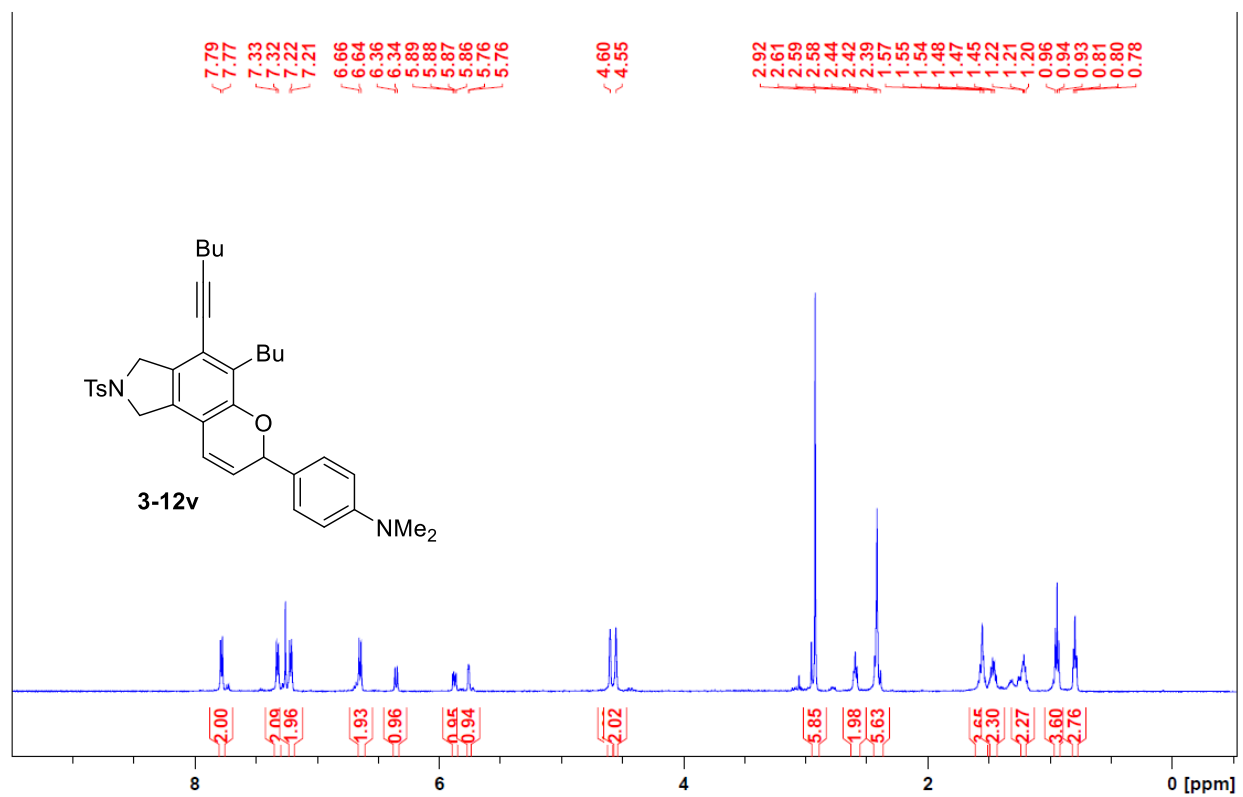


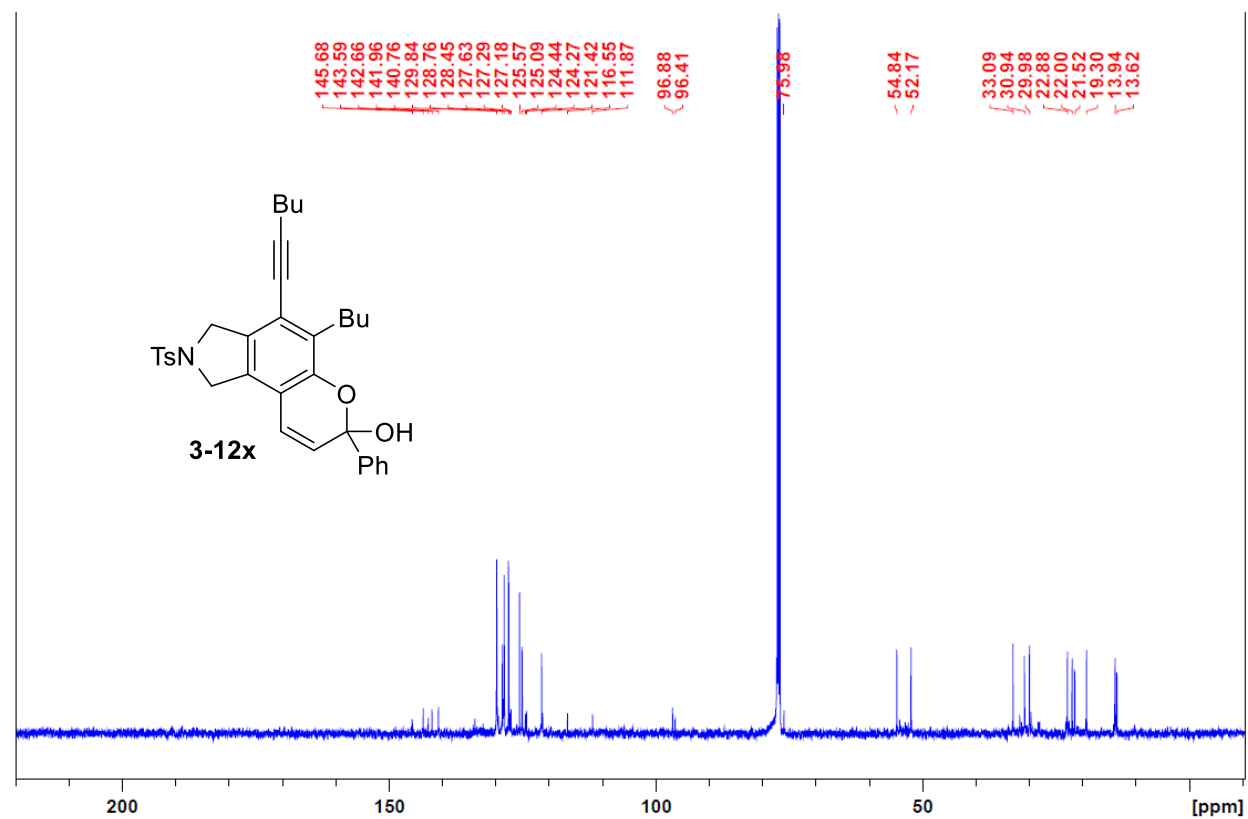
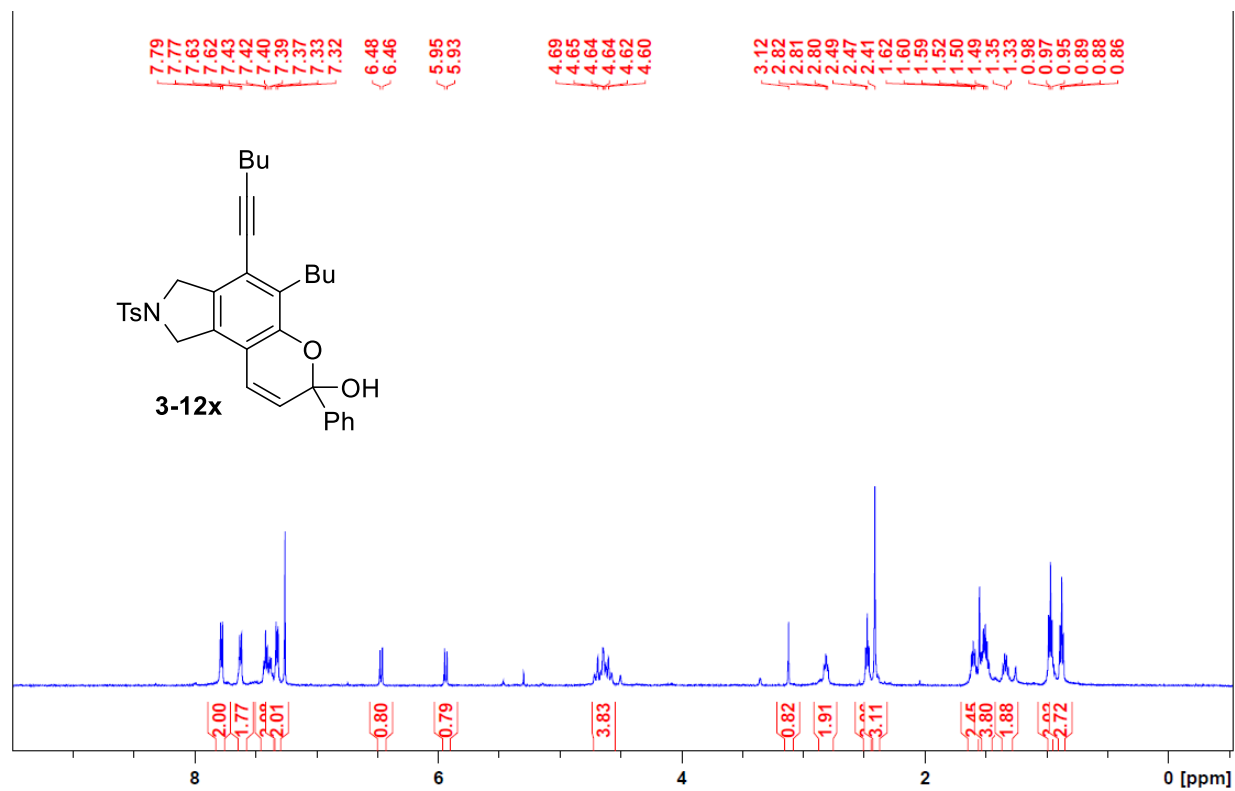


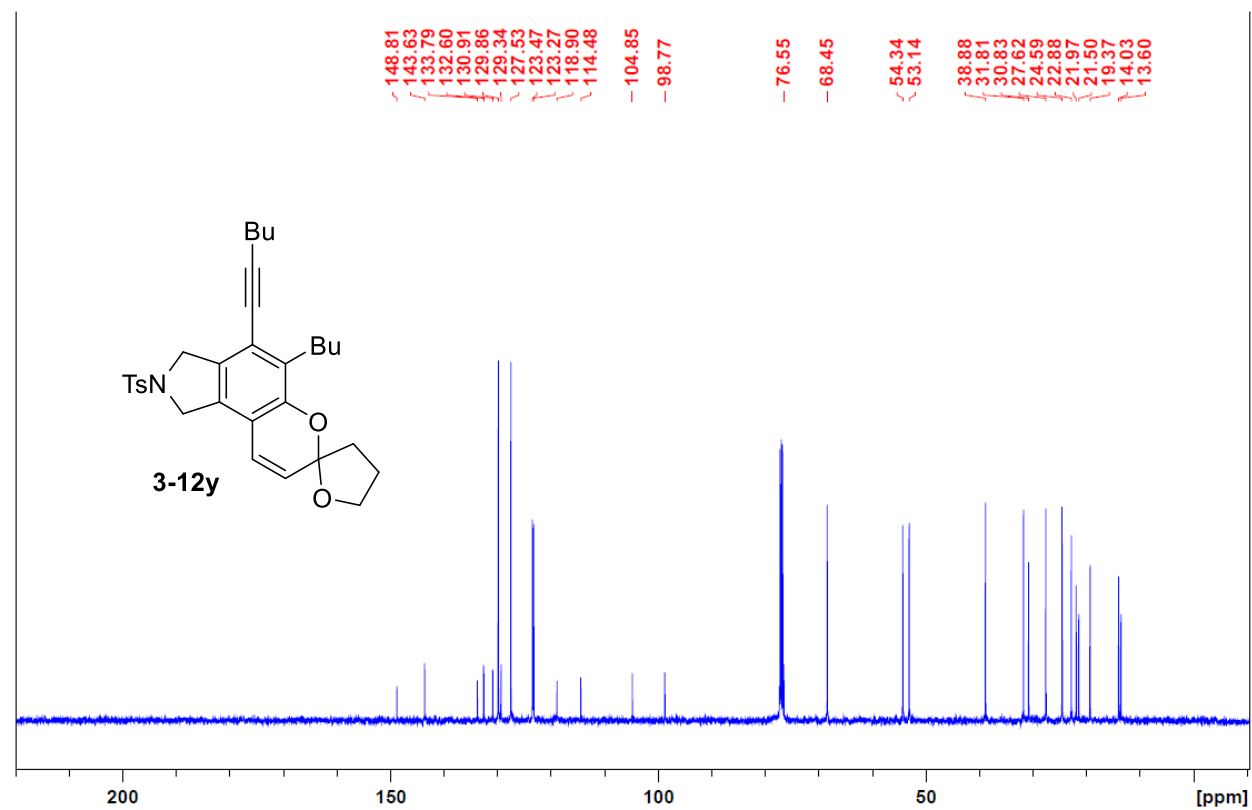
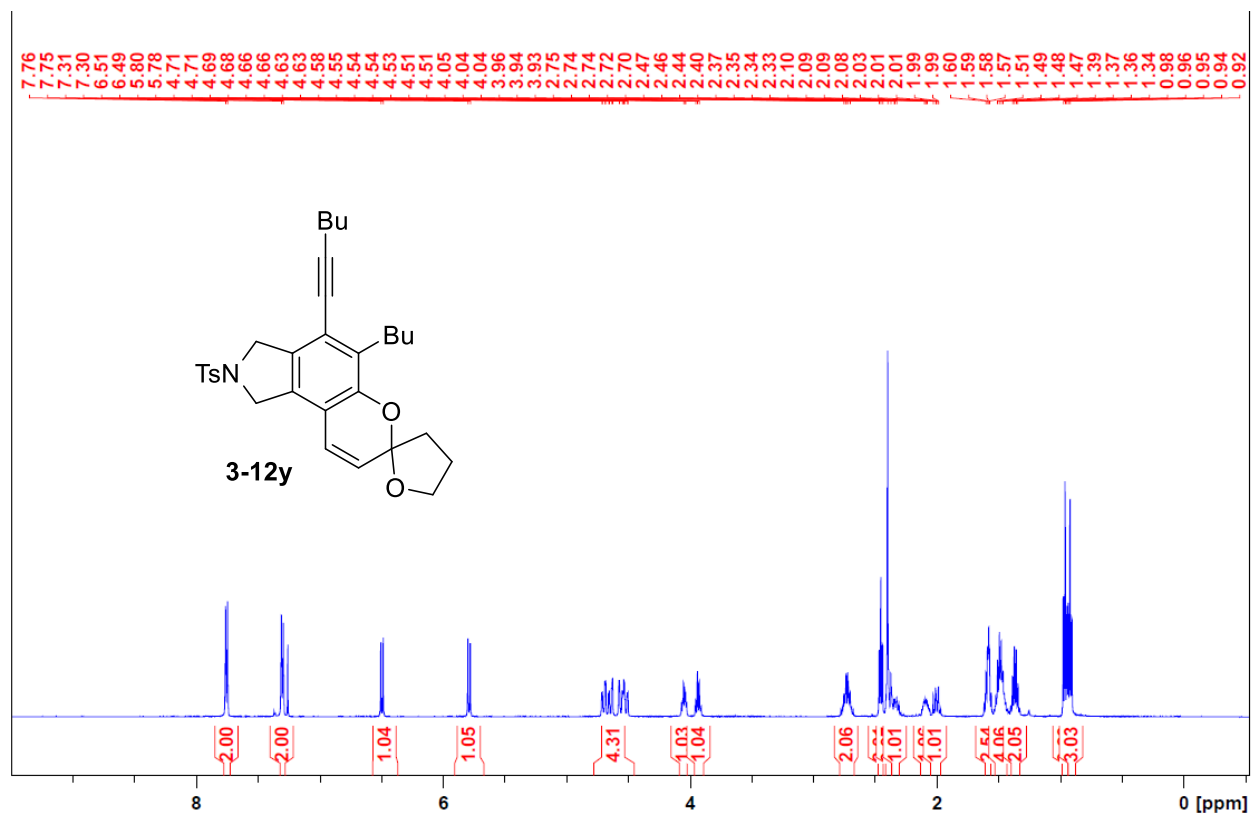


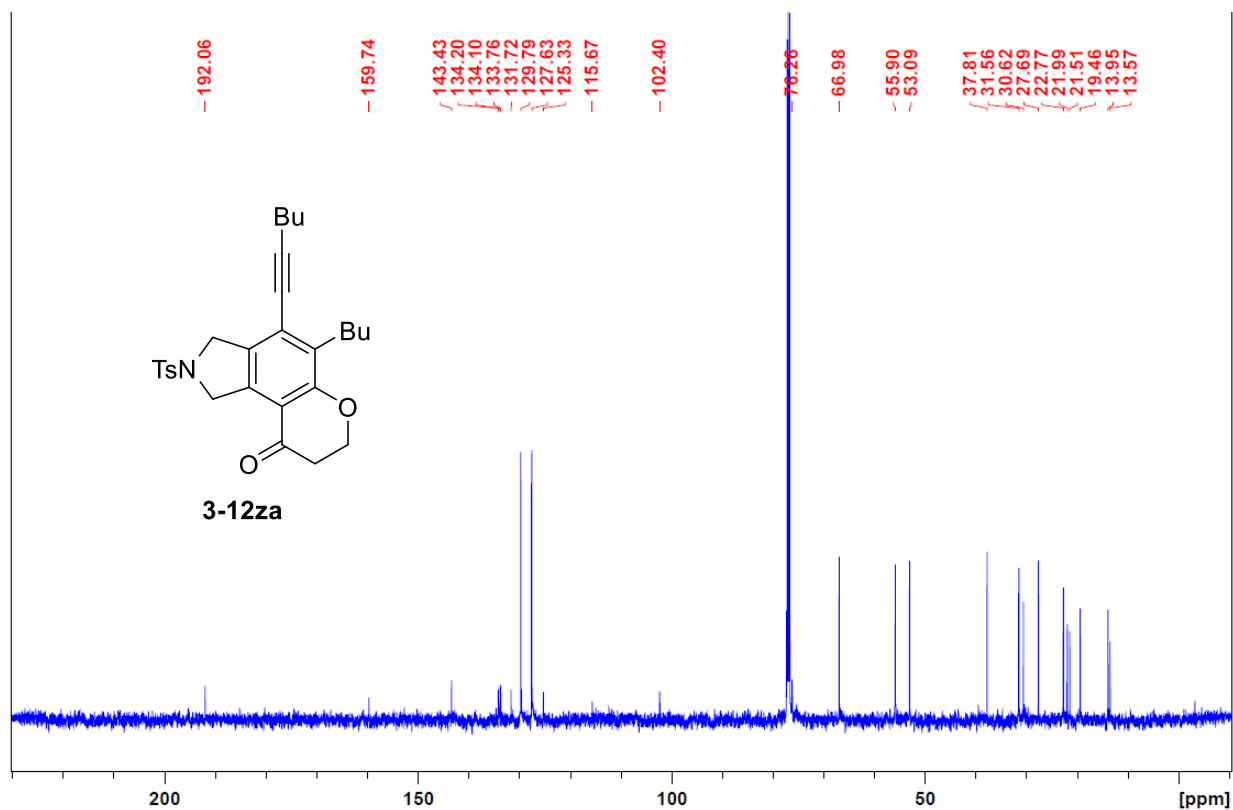
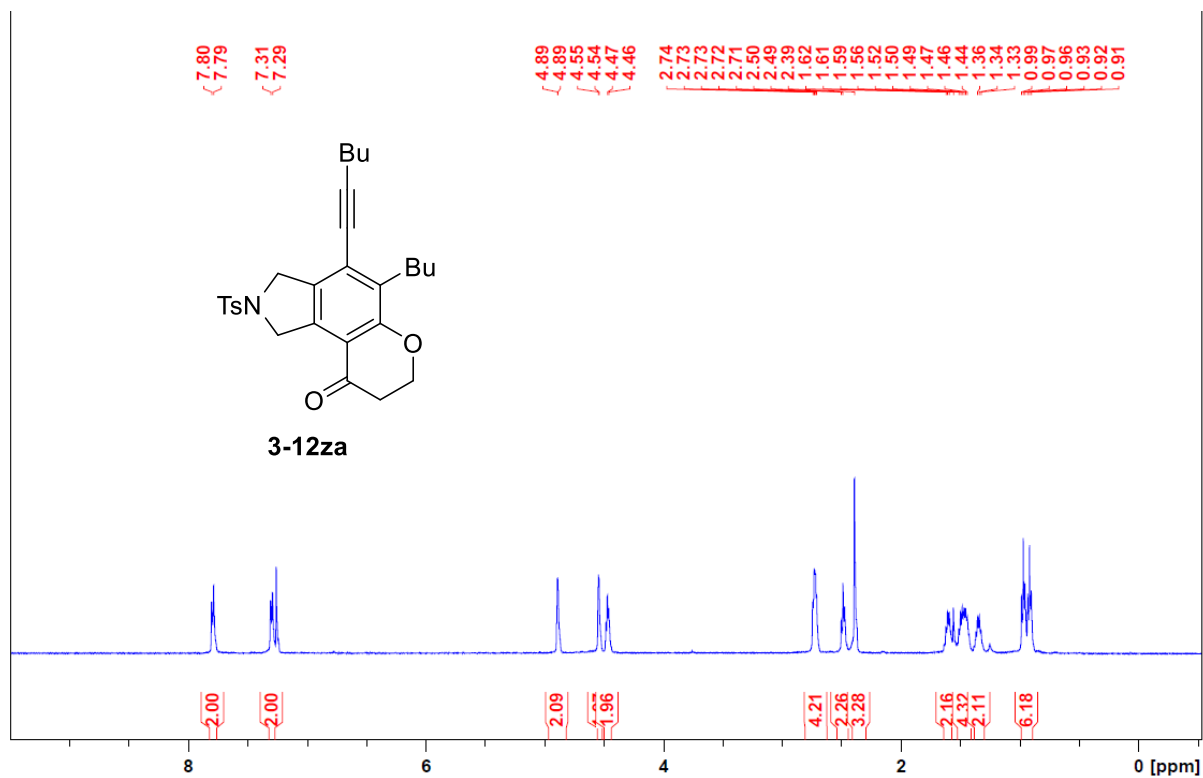


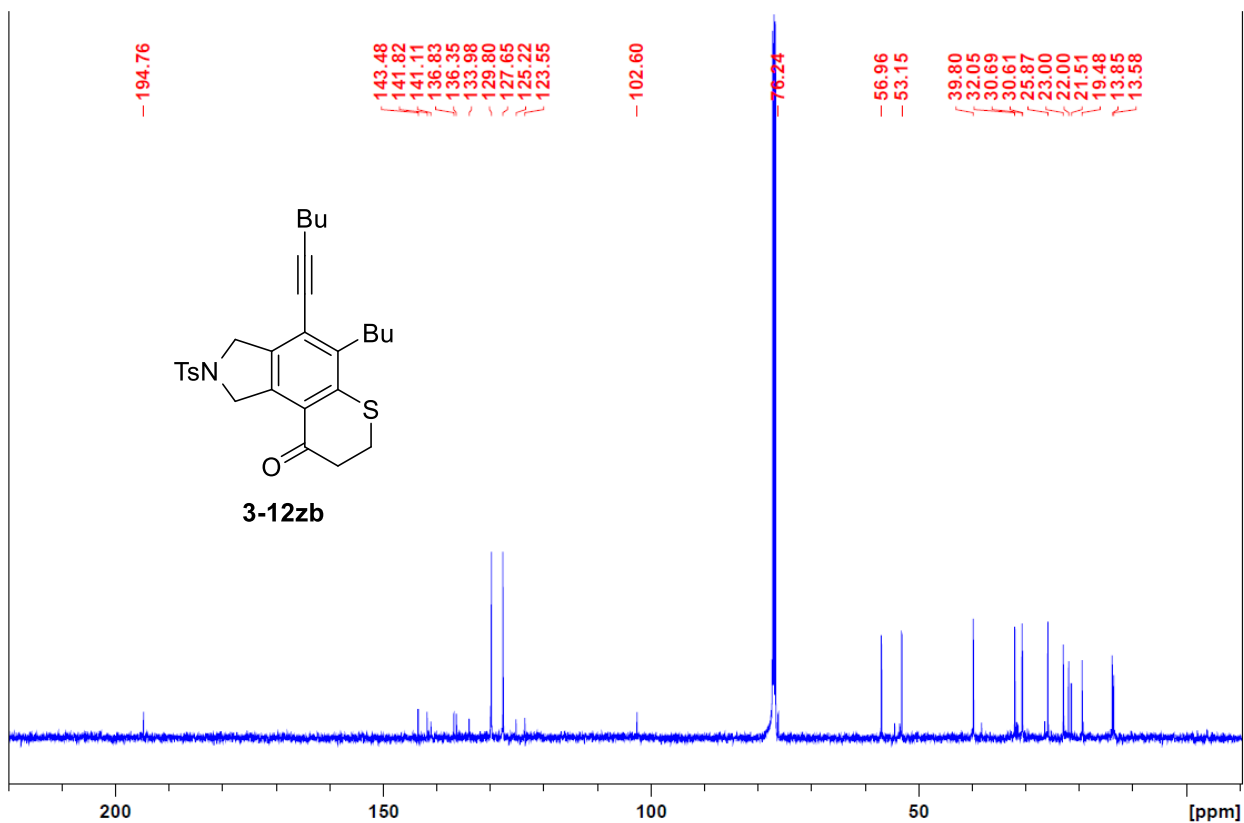
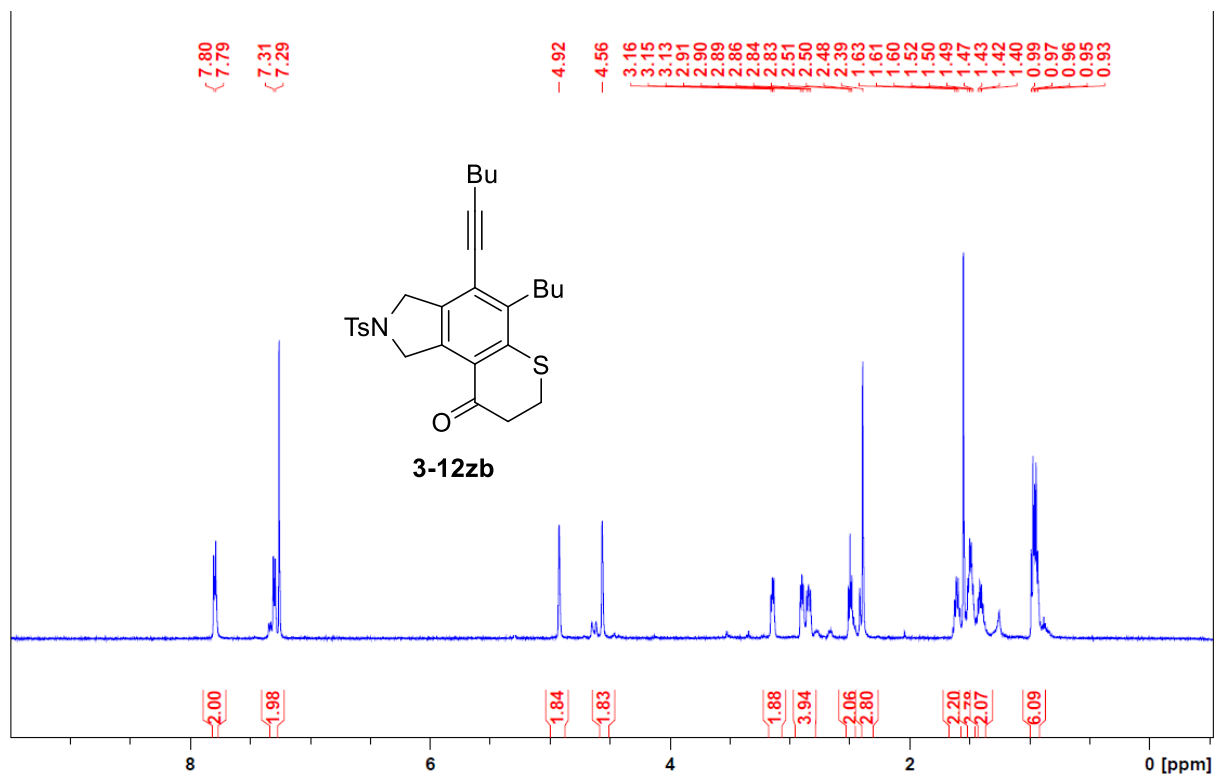


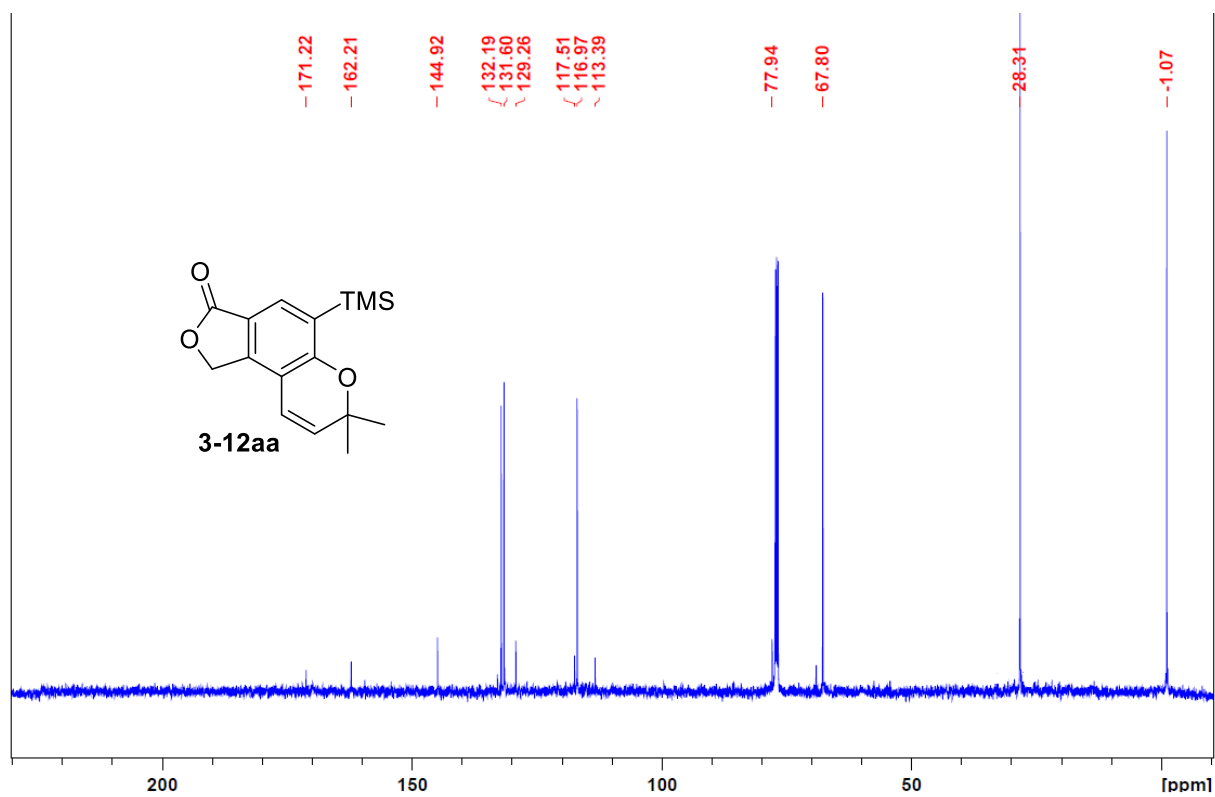
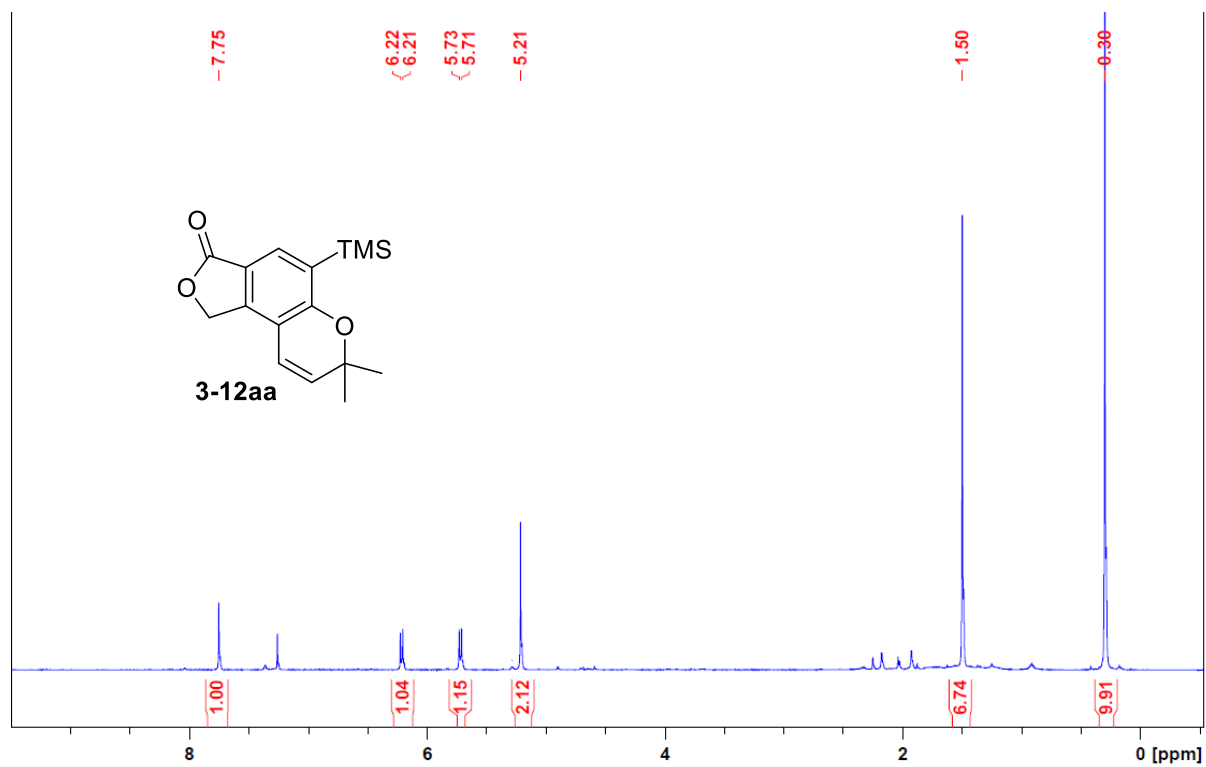


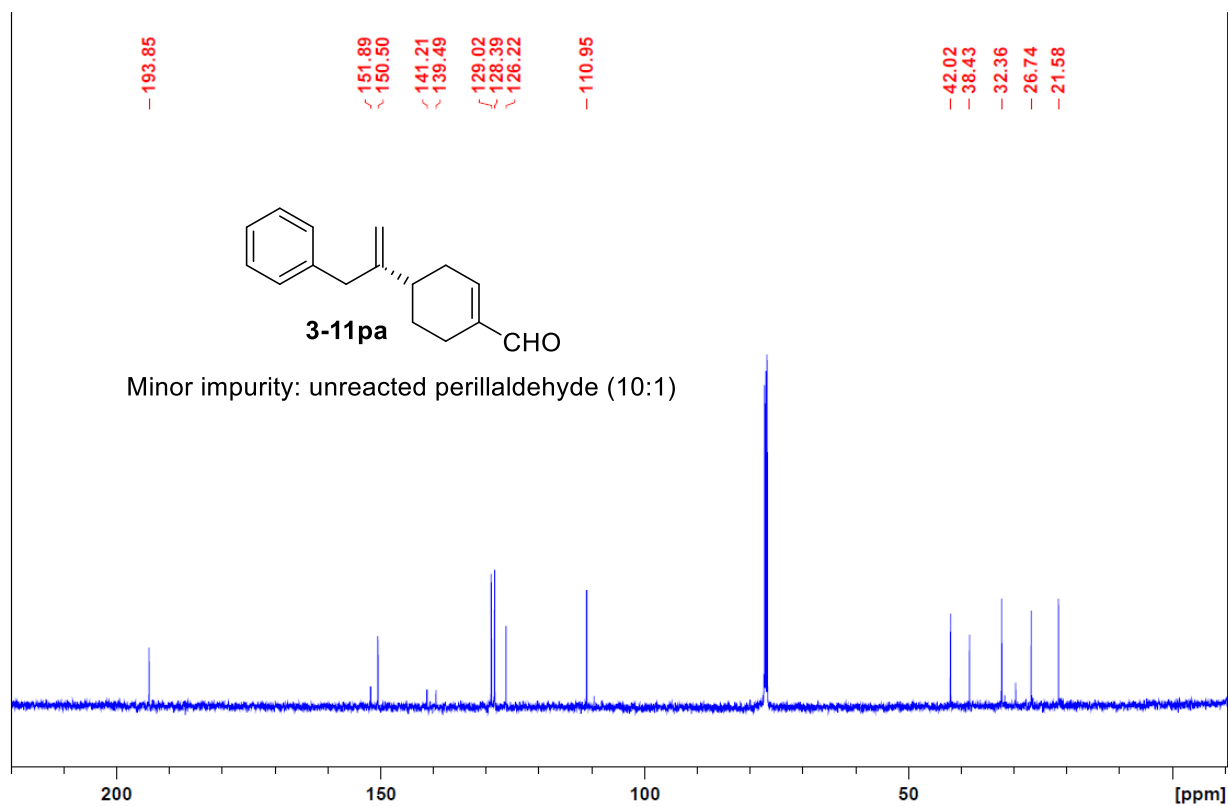
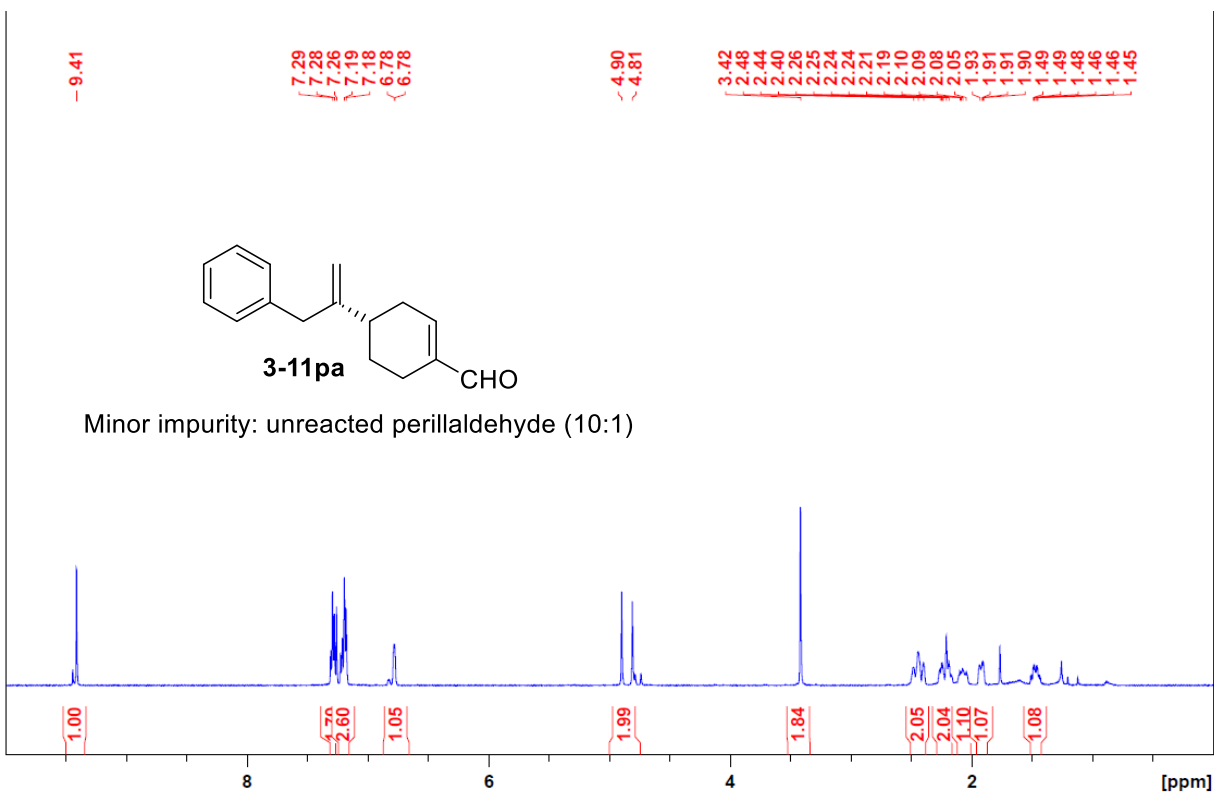




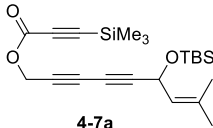
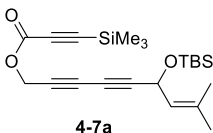


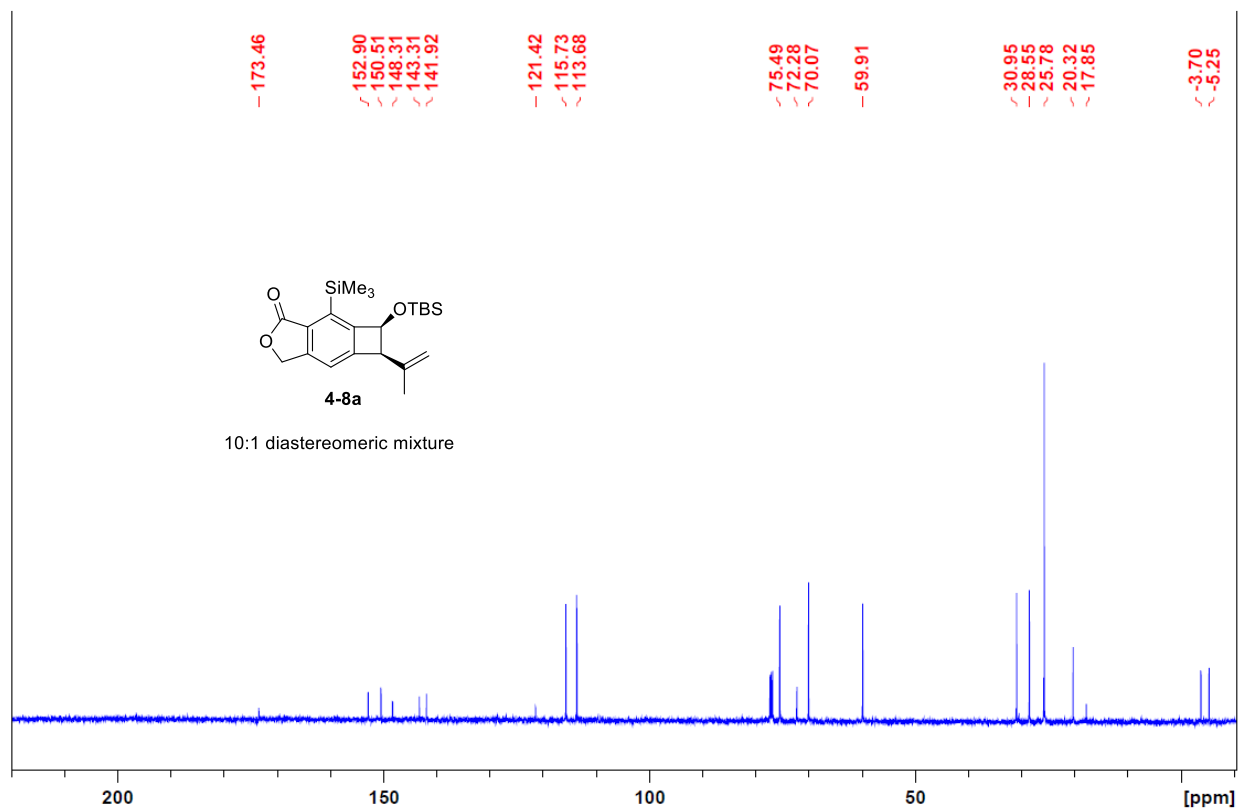
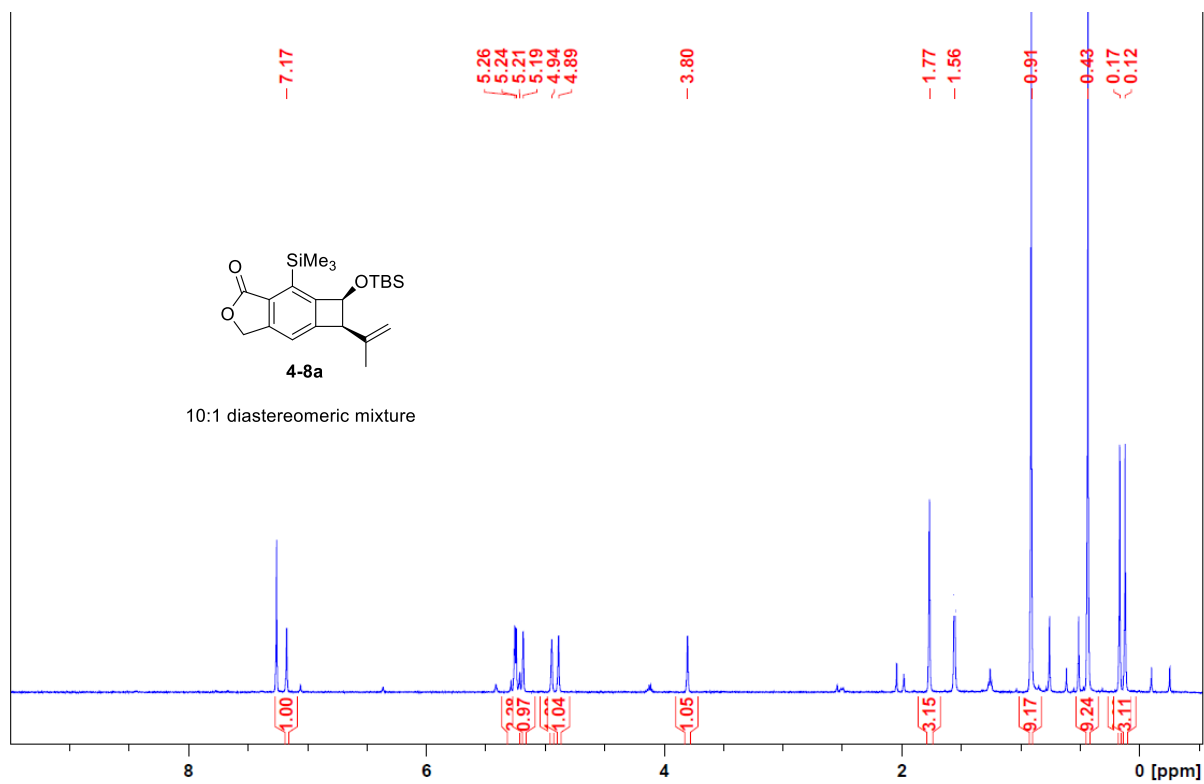


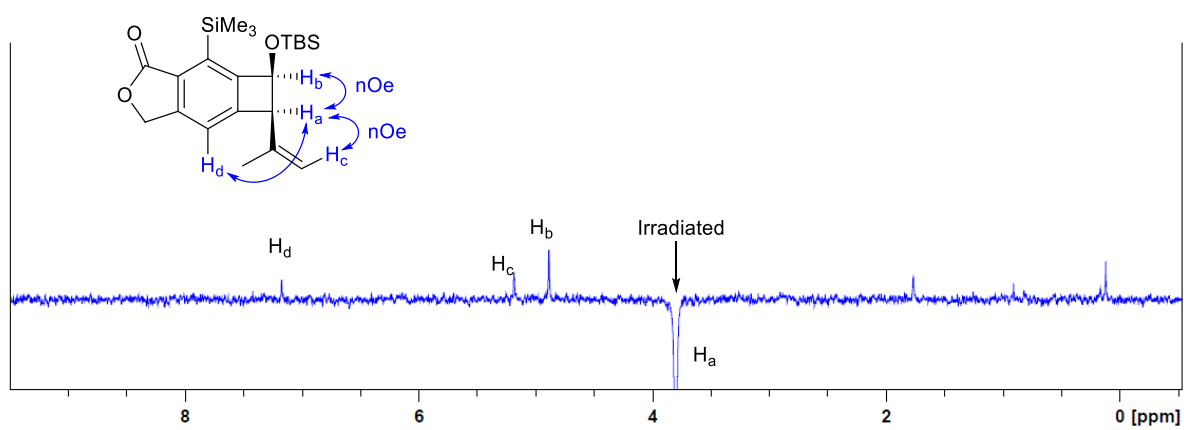


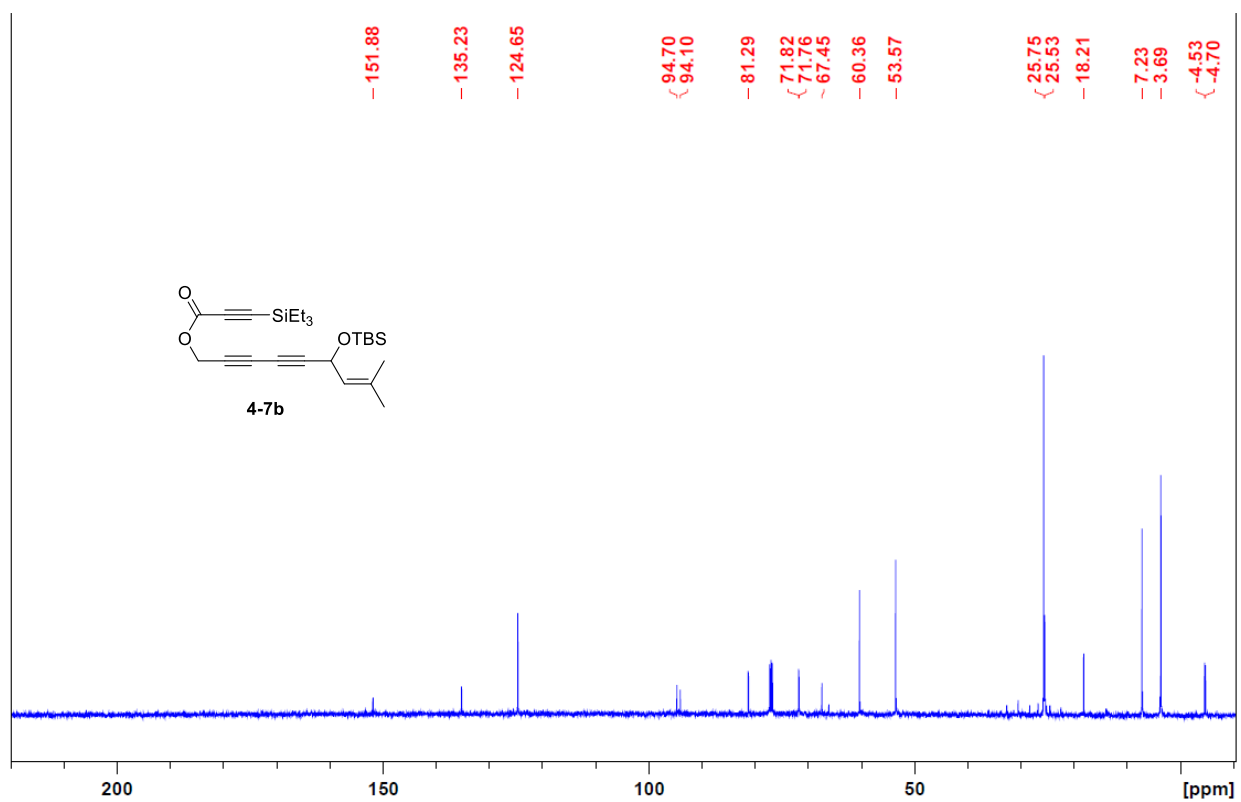
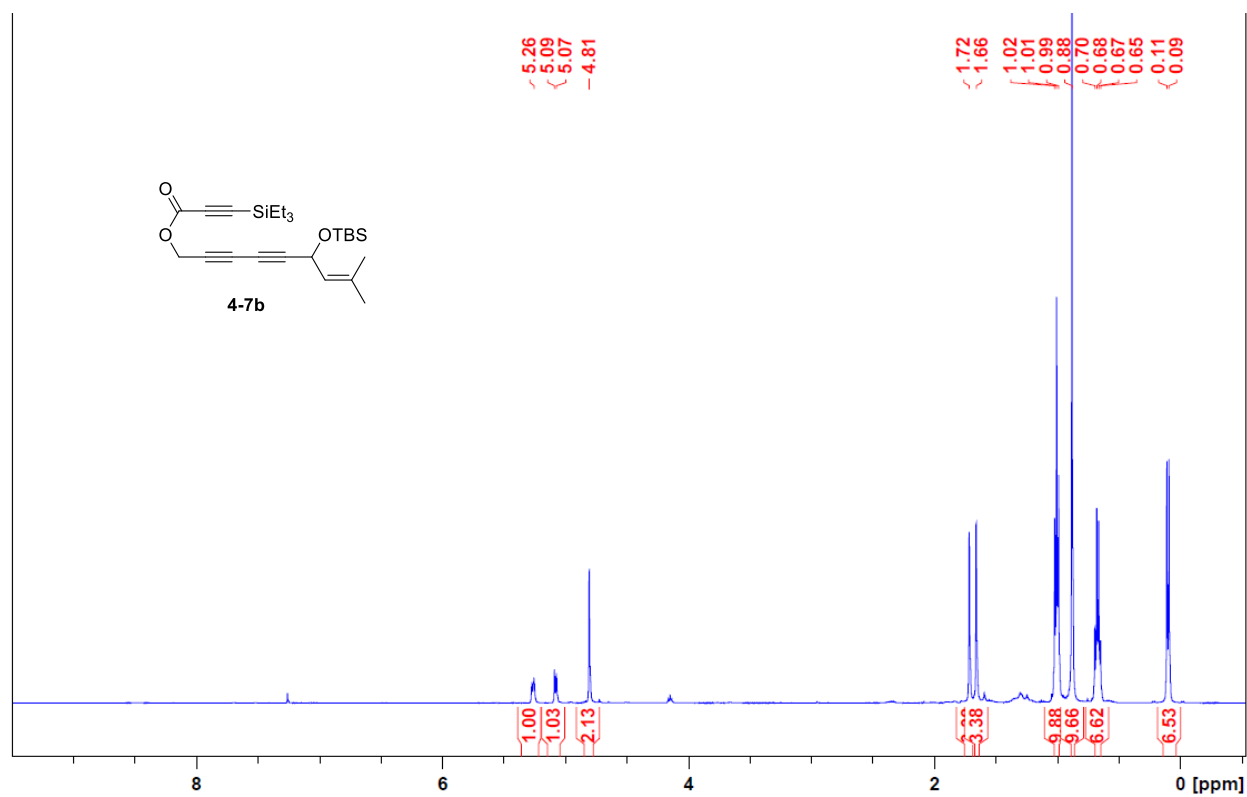


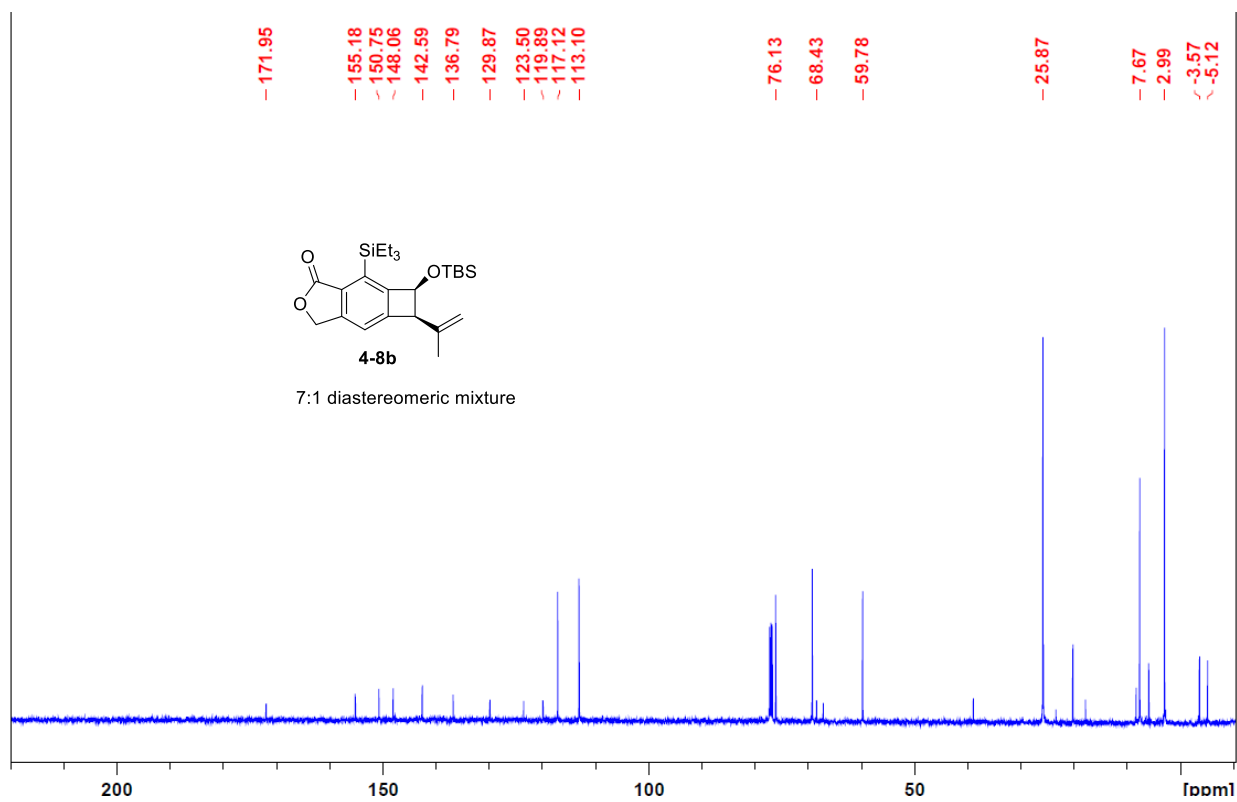
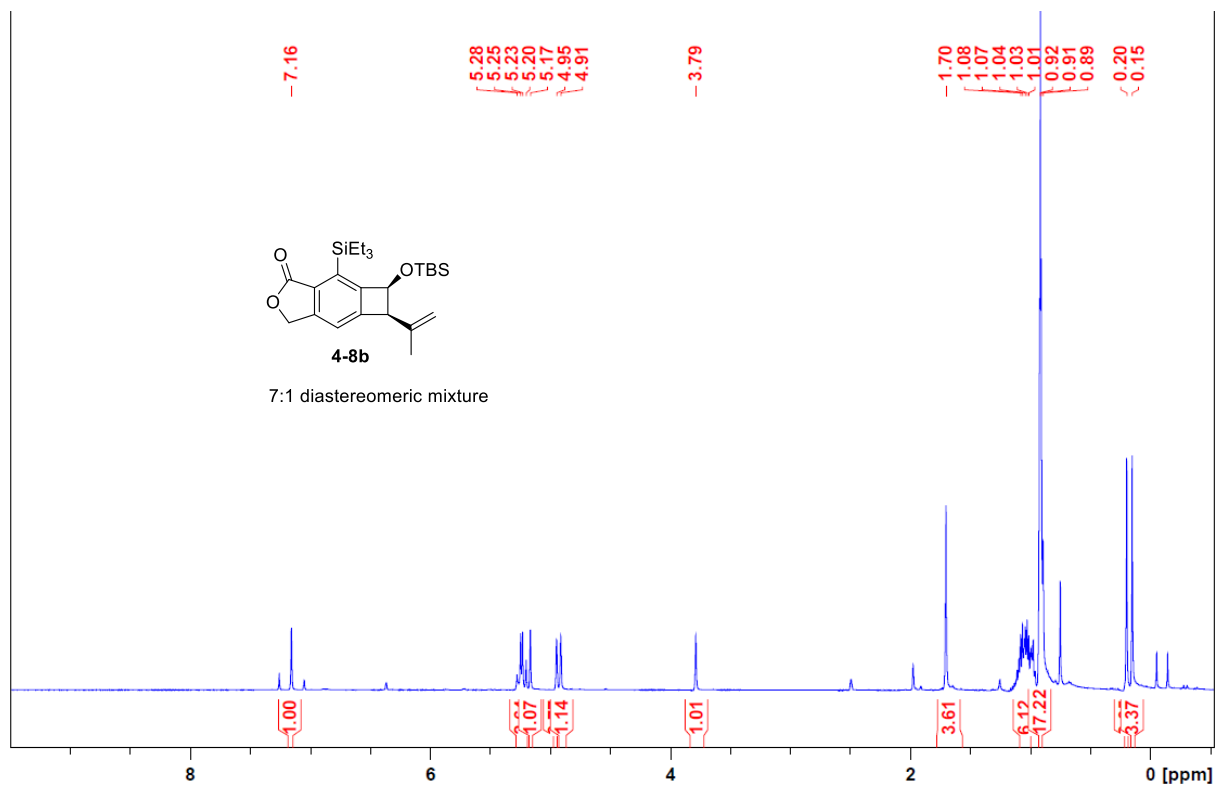
Appendix III
Selected NMR Spectra for Chapter 4

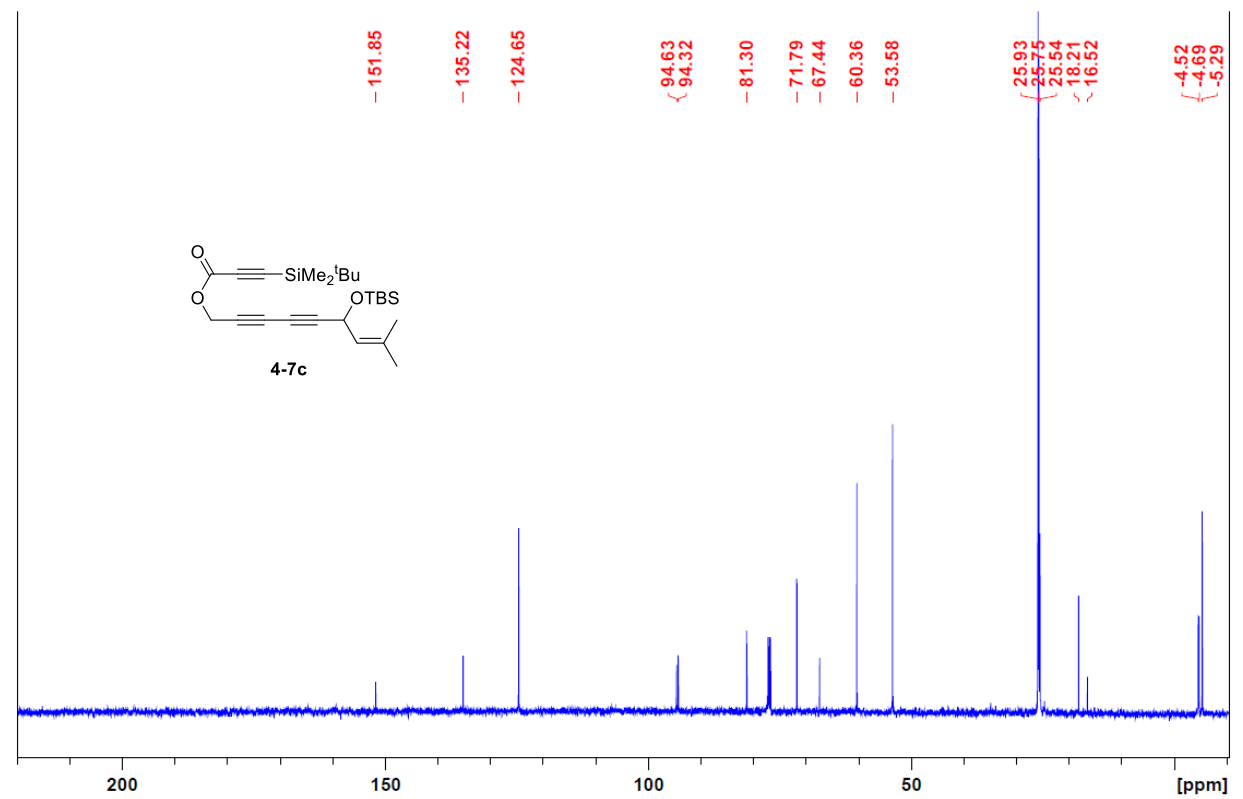
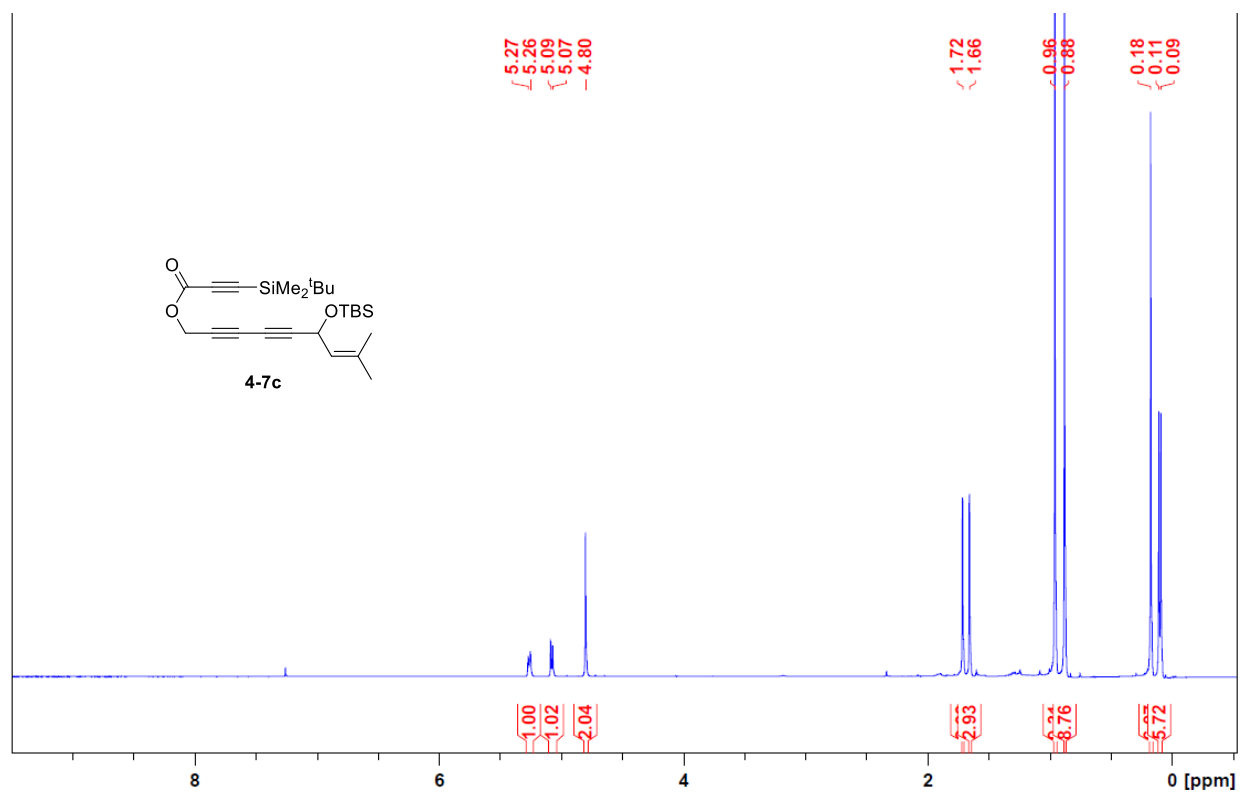


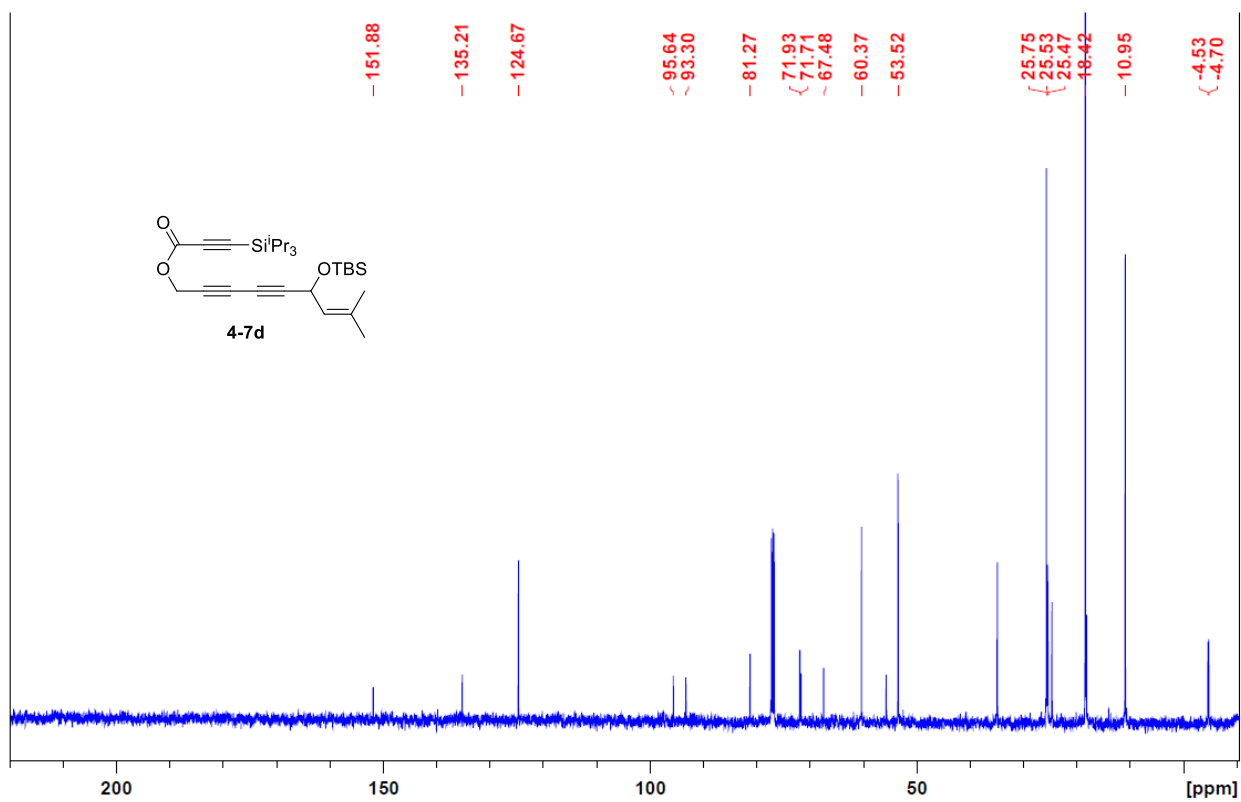
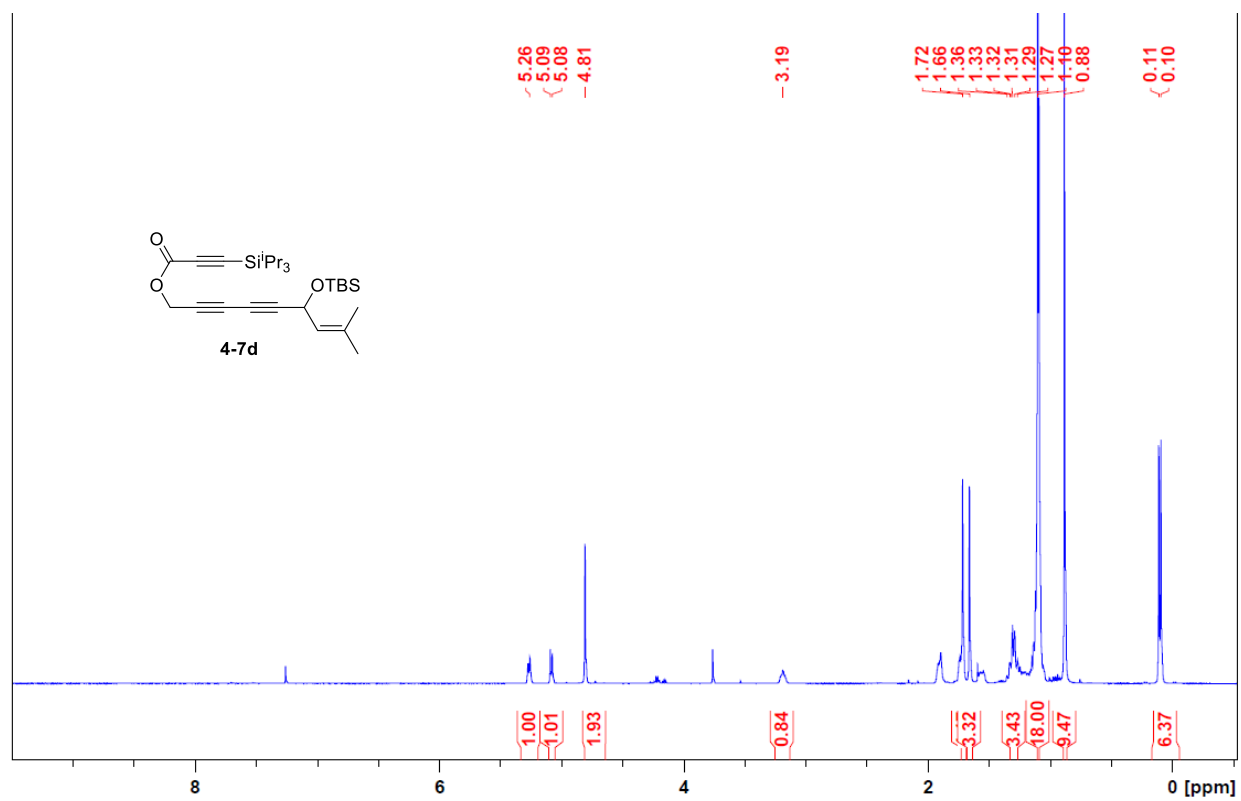


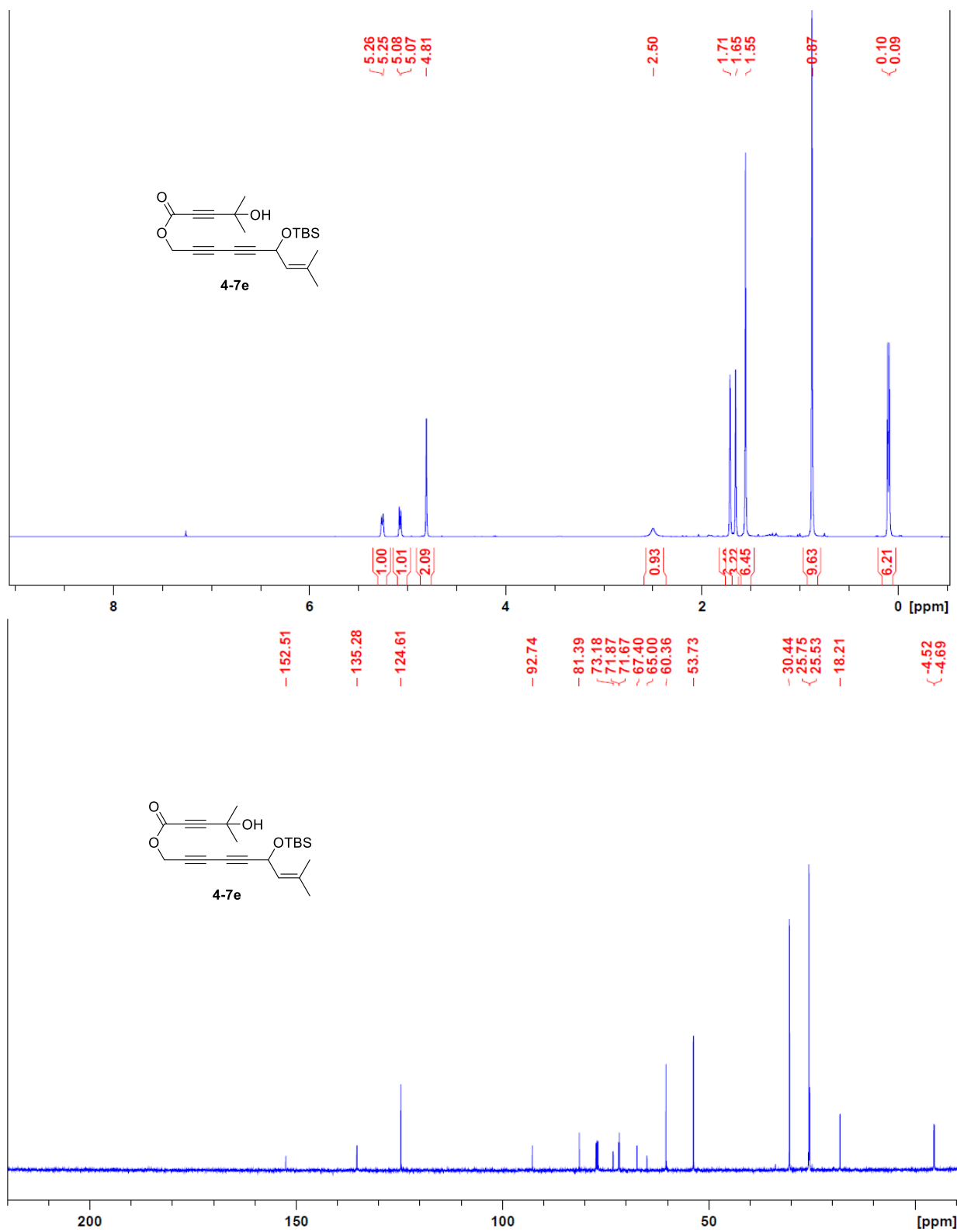


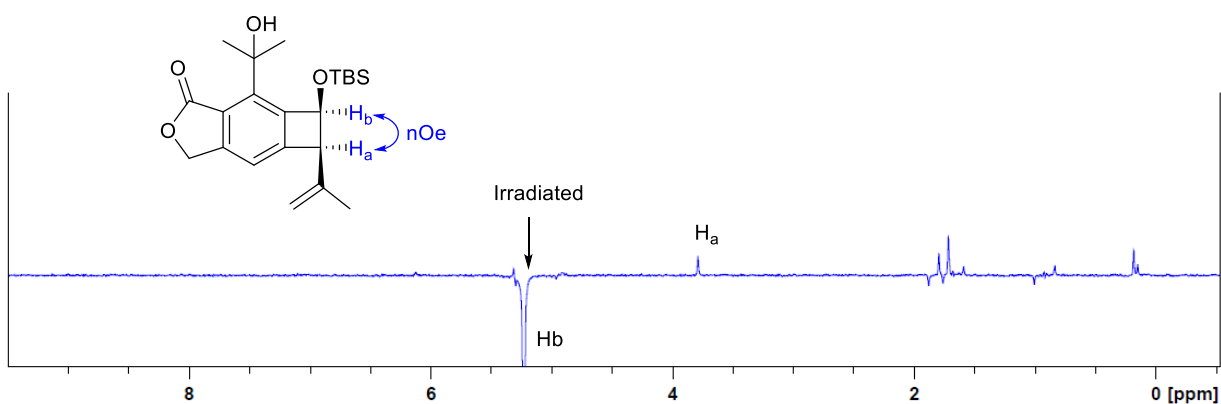
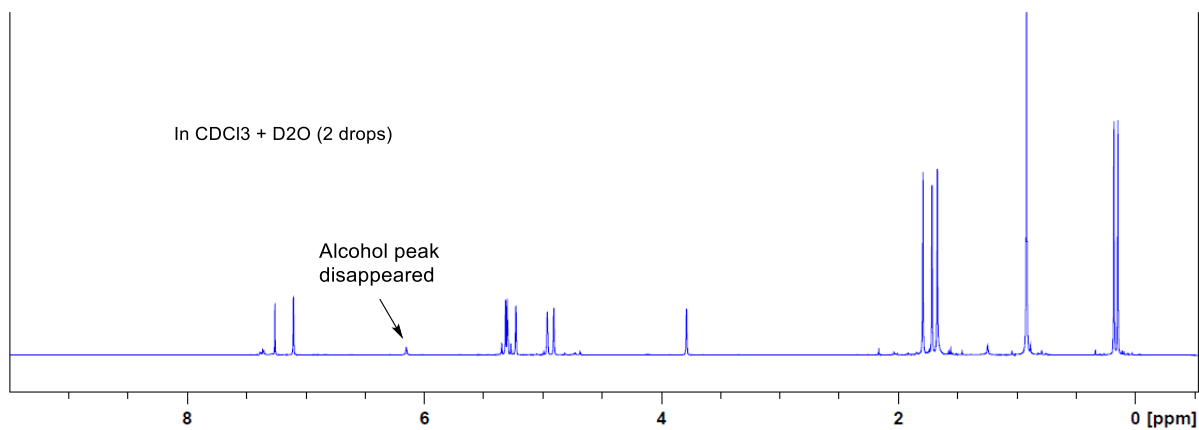


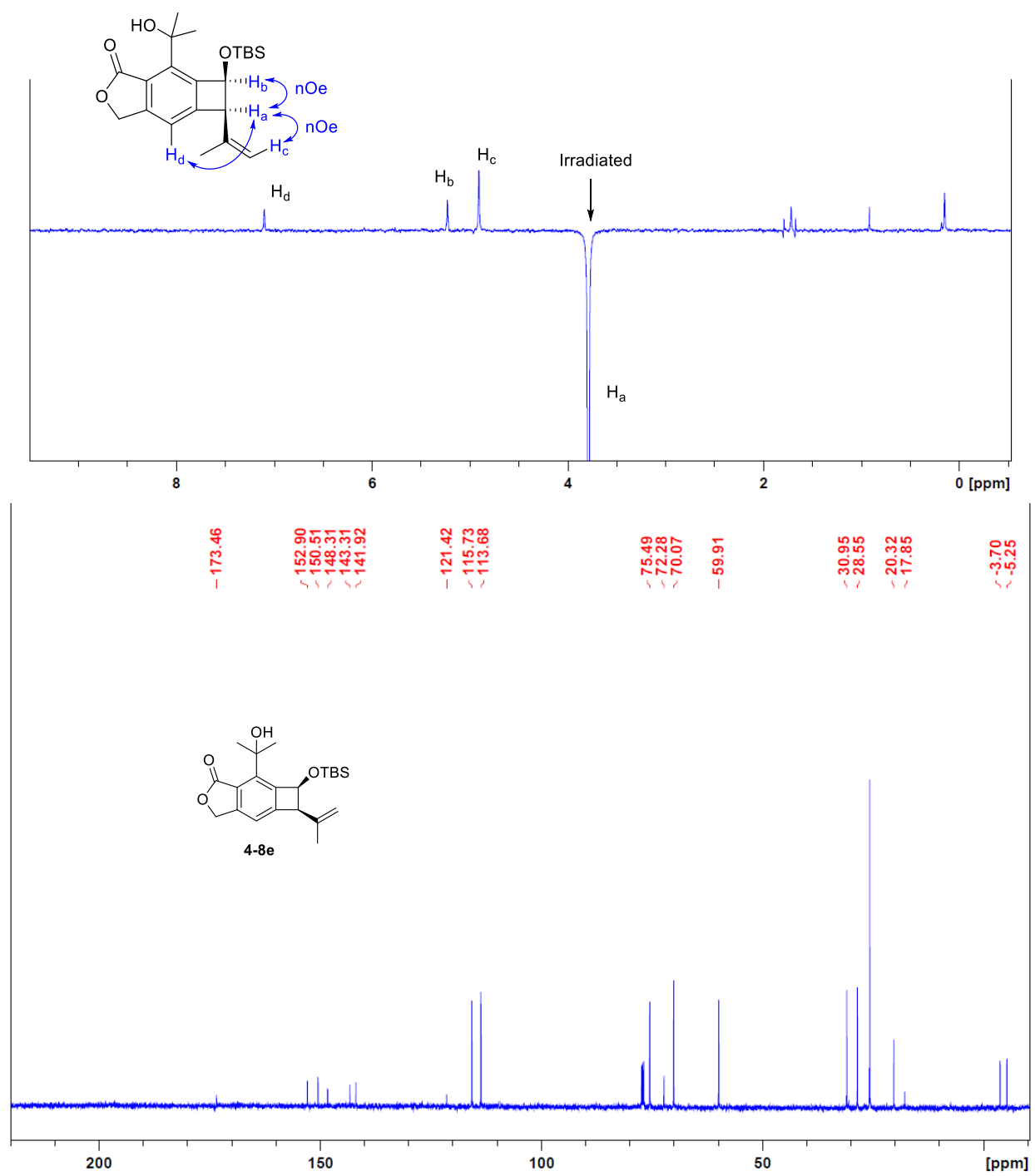


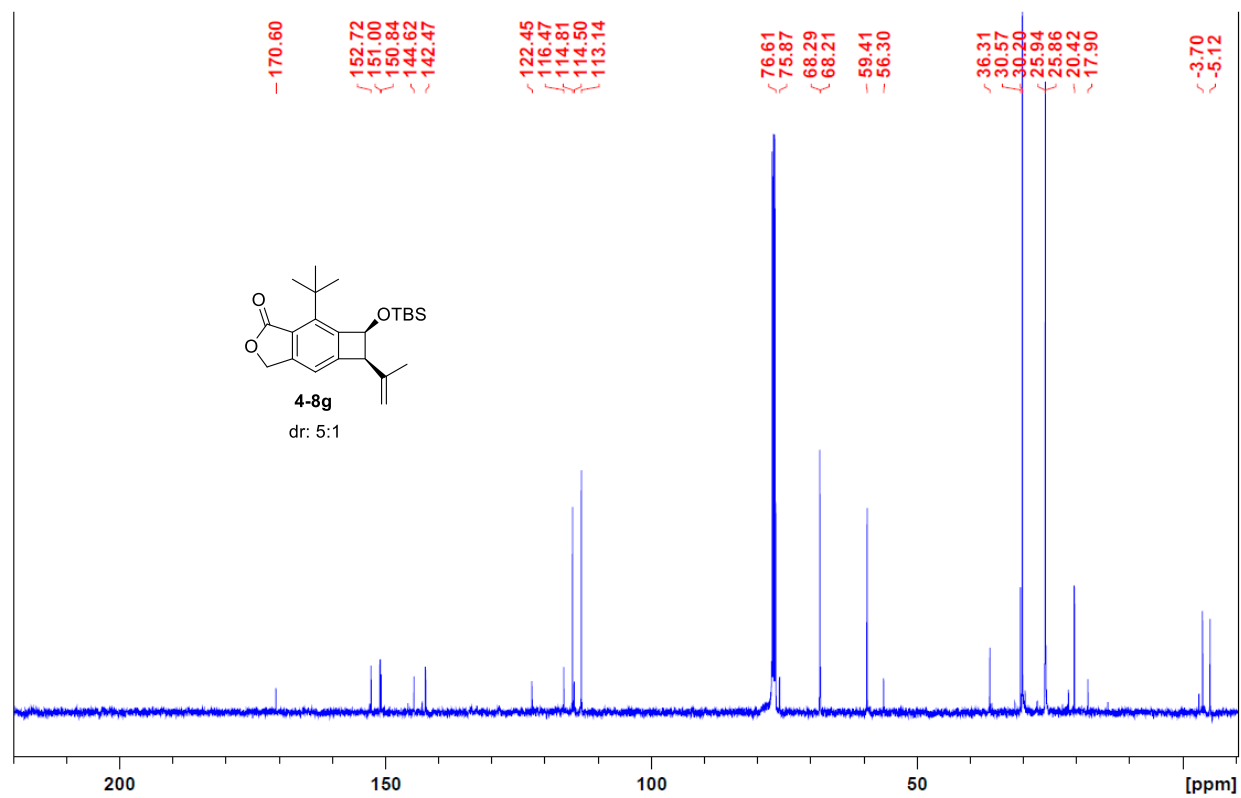
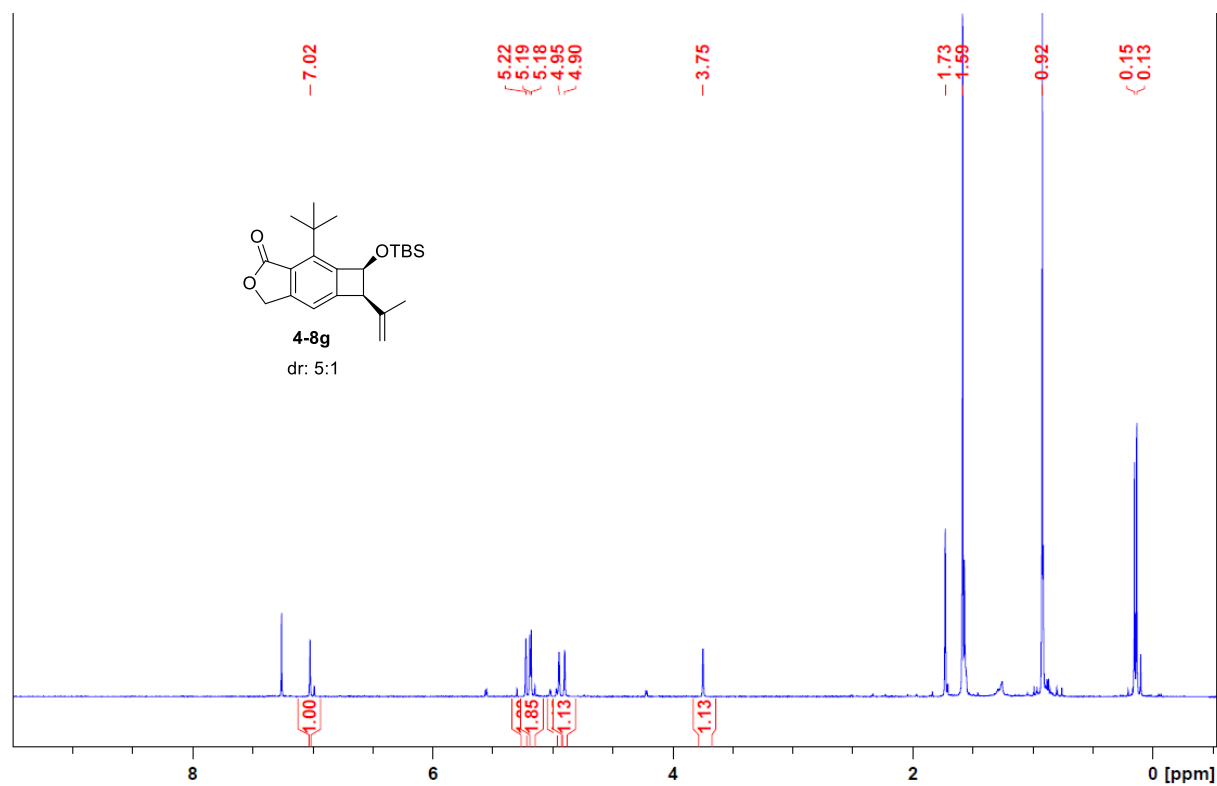


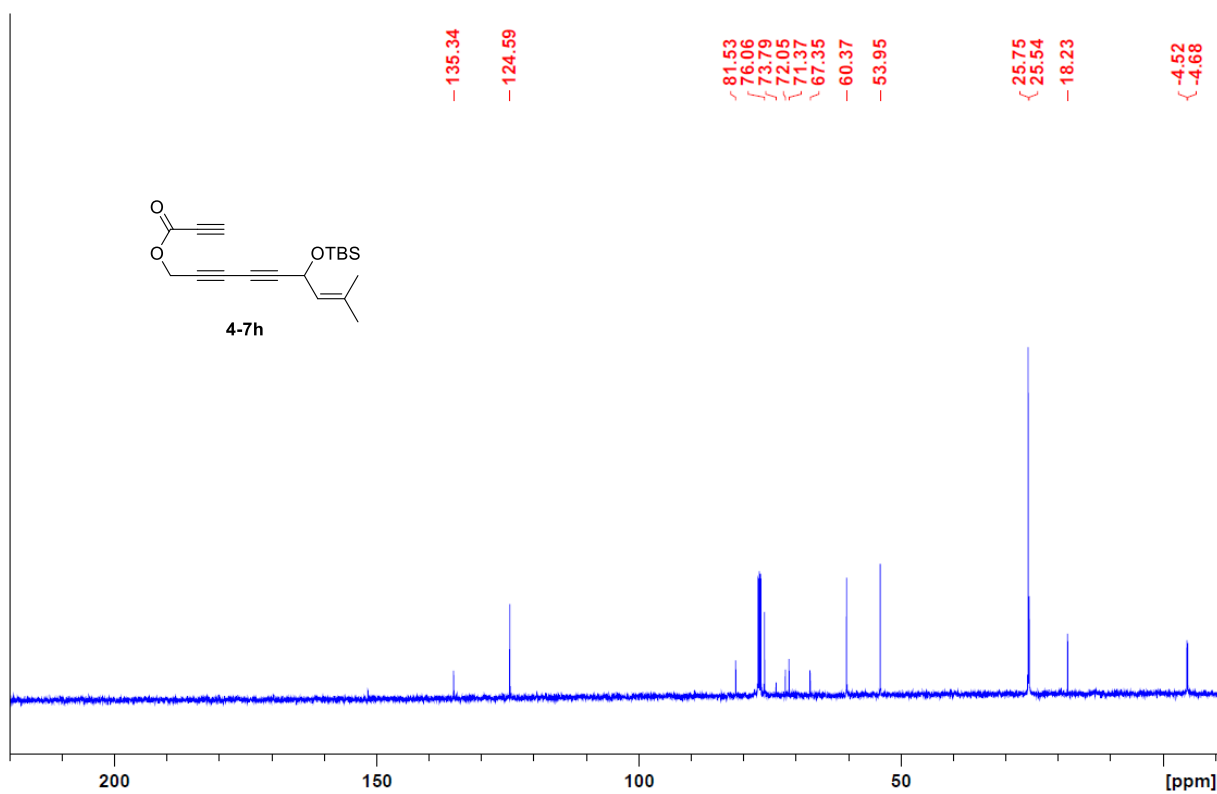
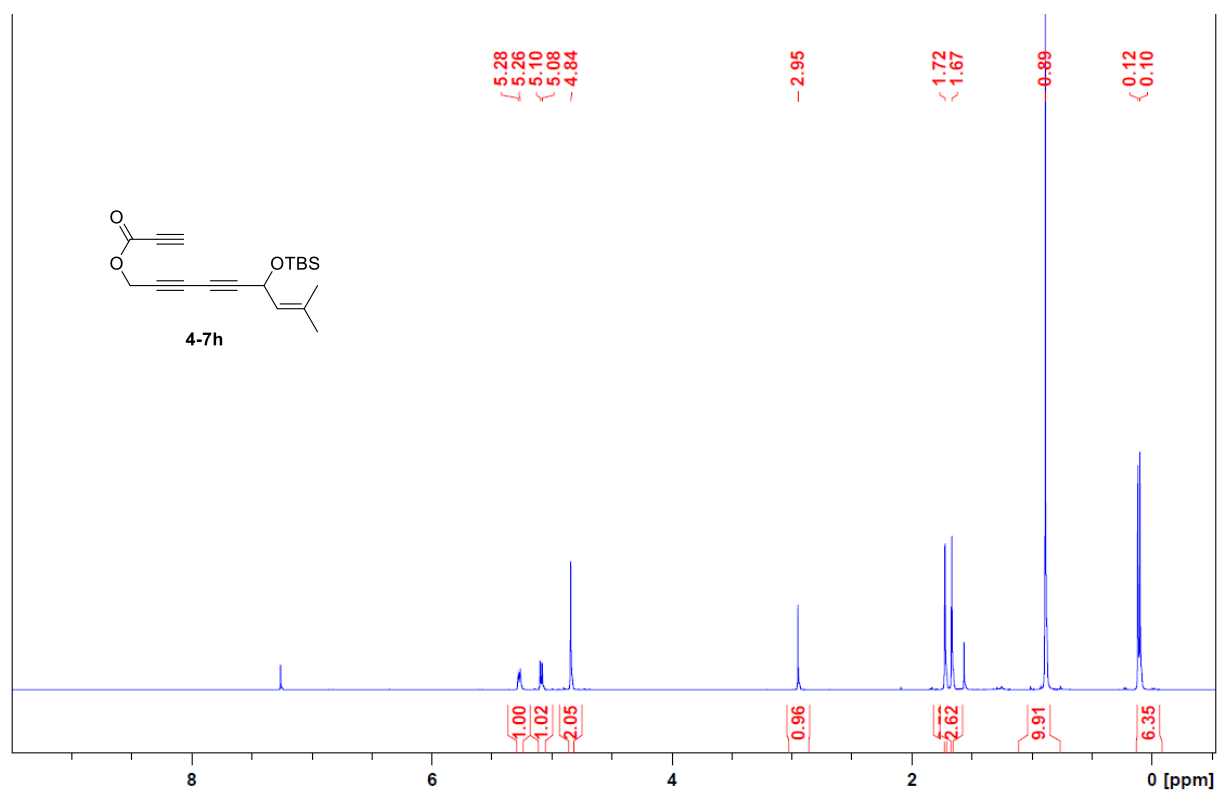


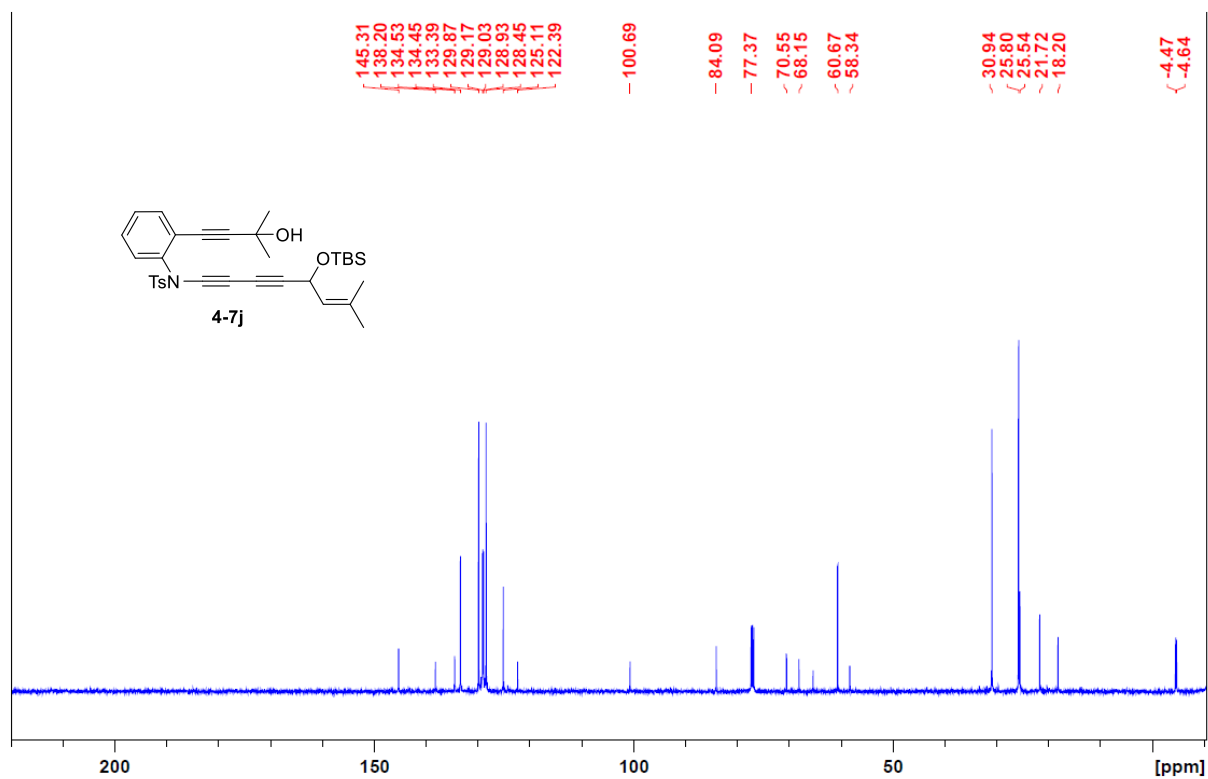
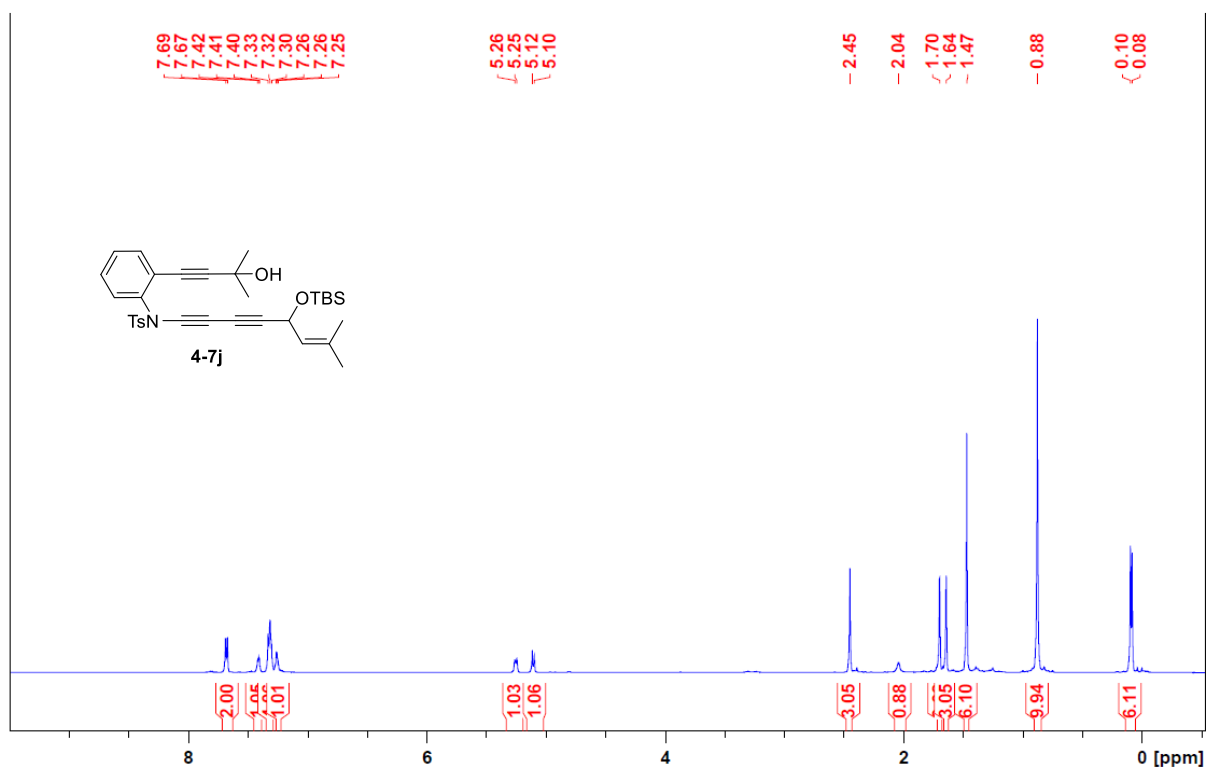


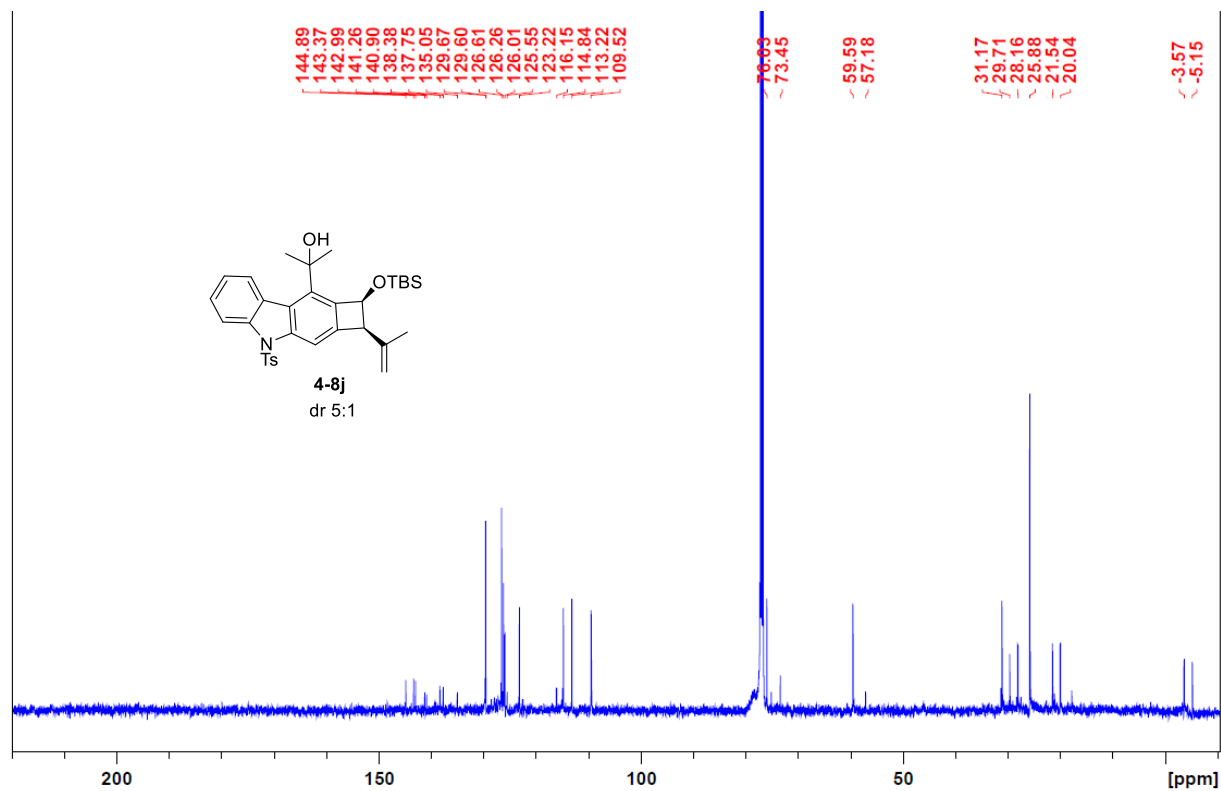
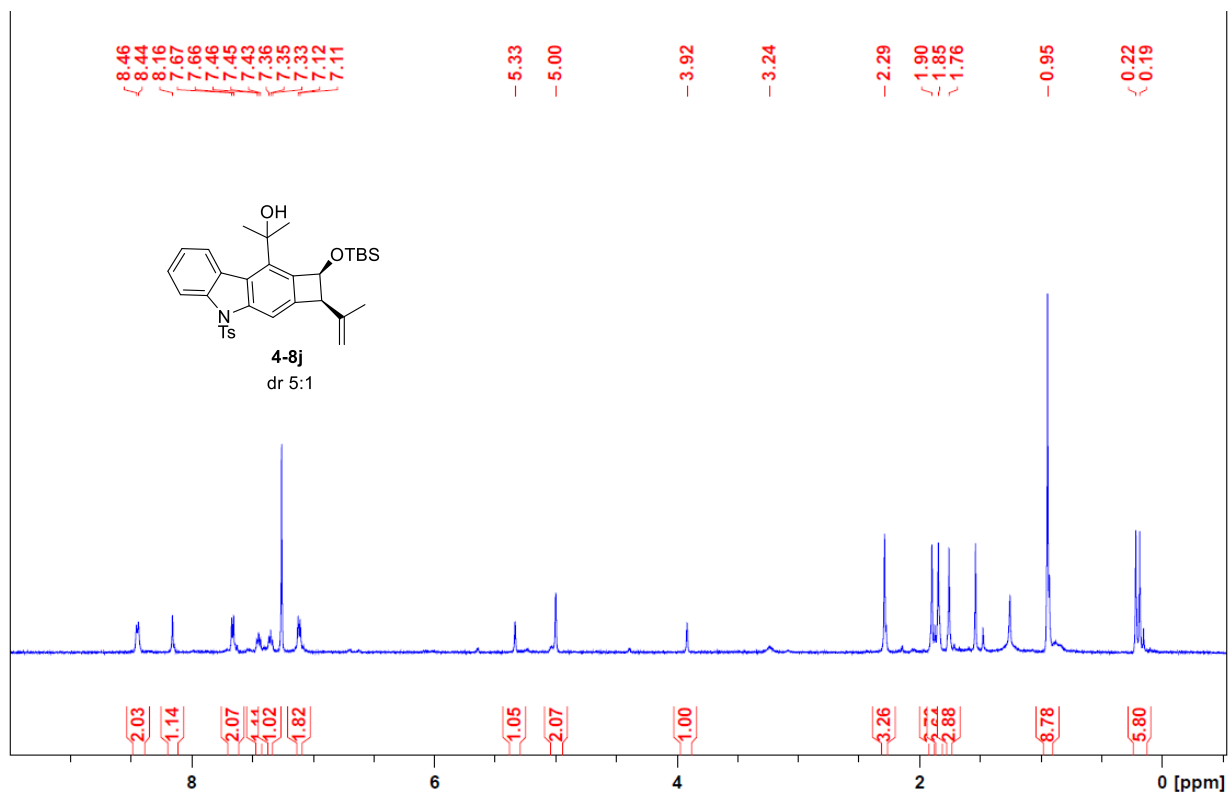


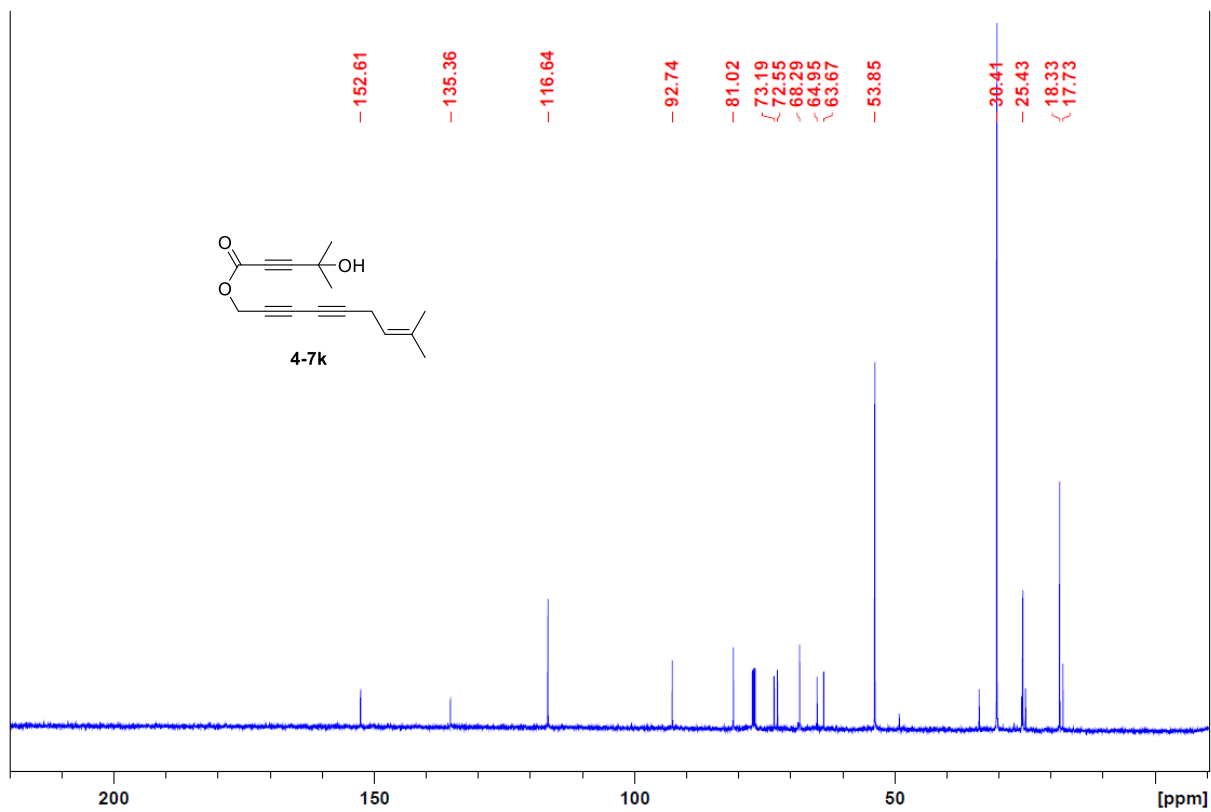
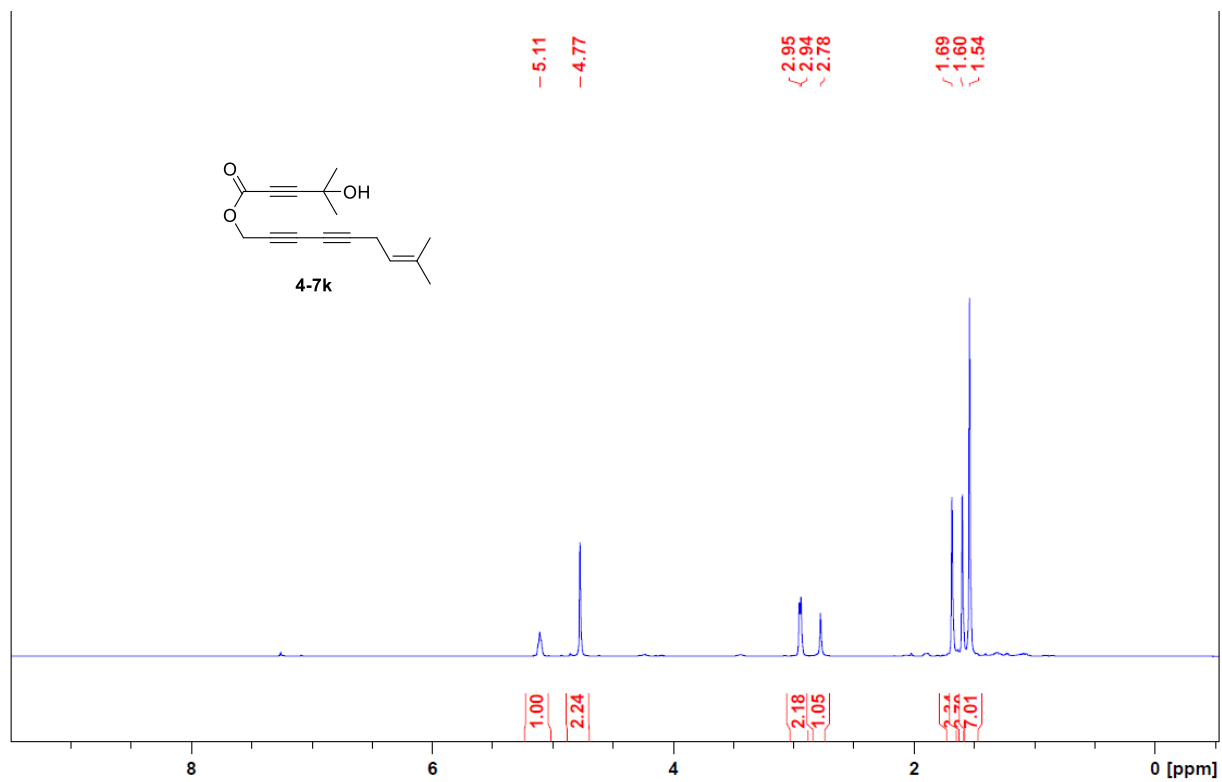


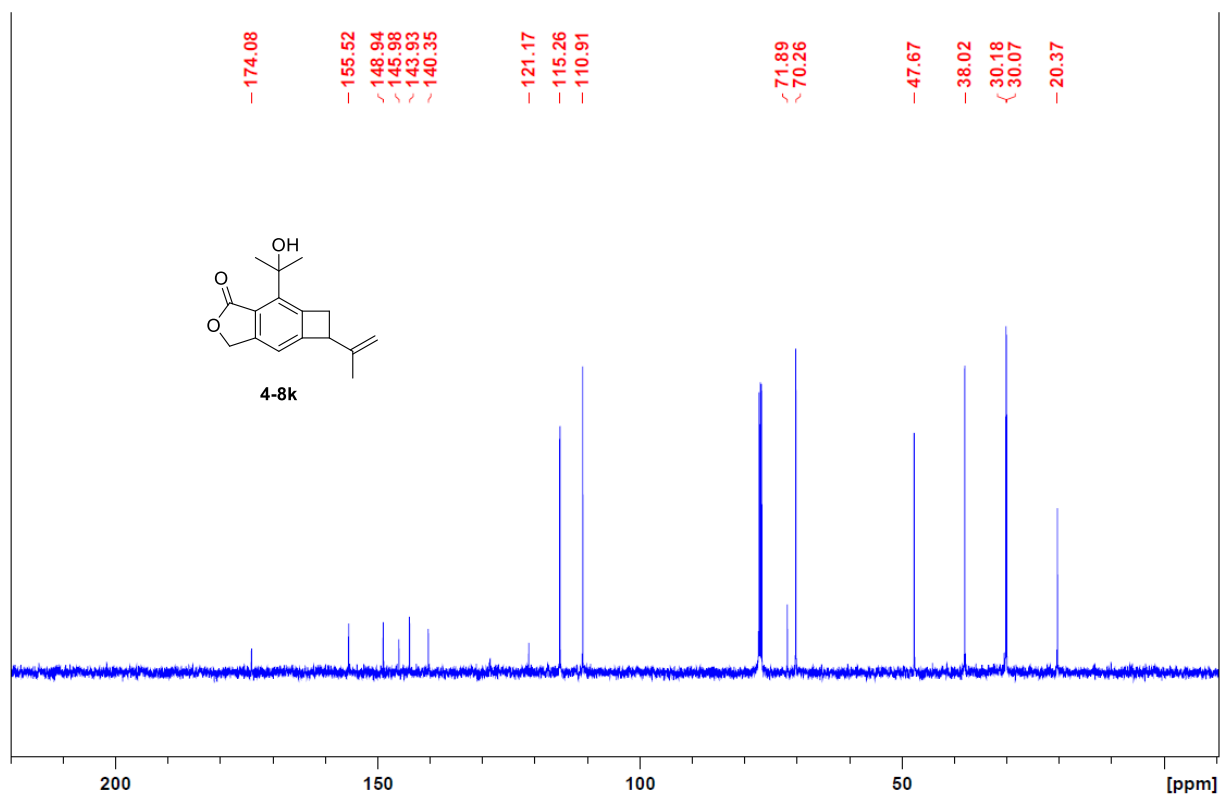
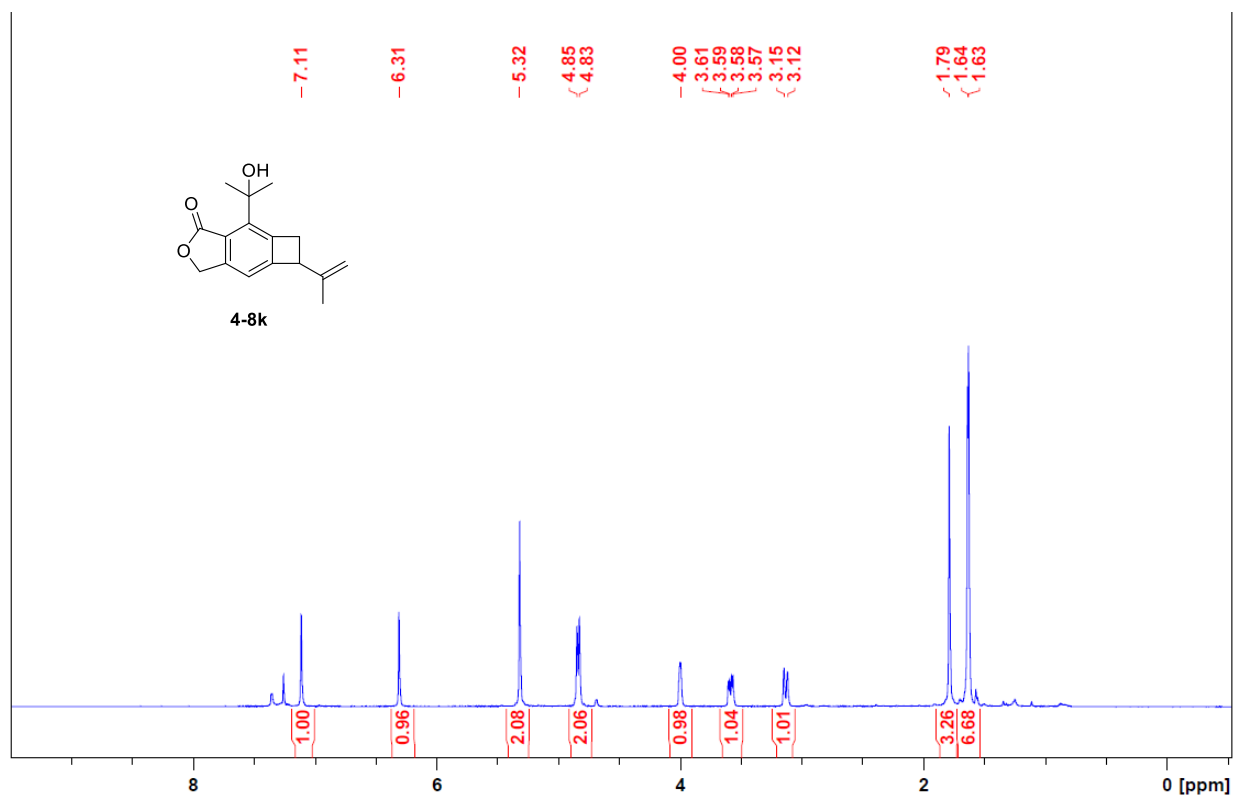


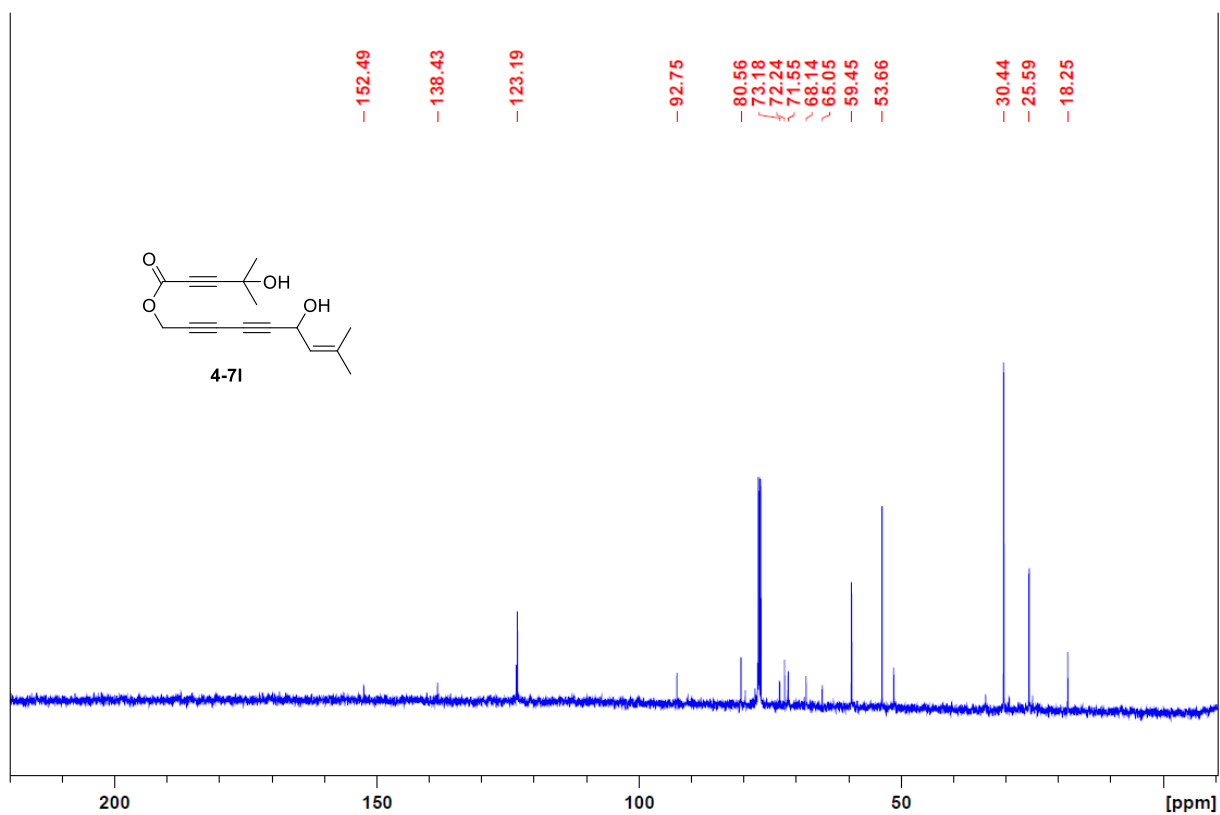
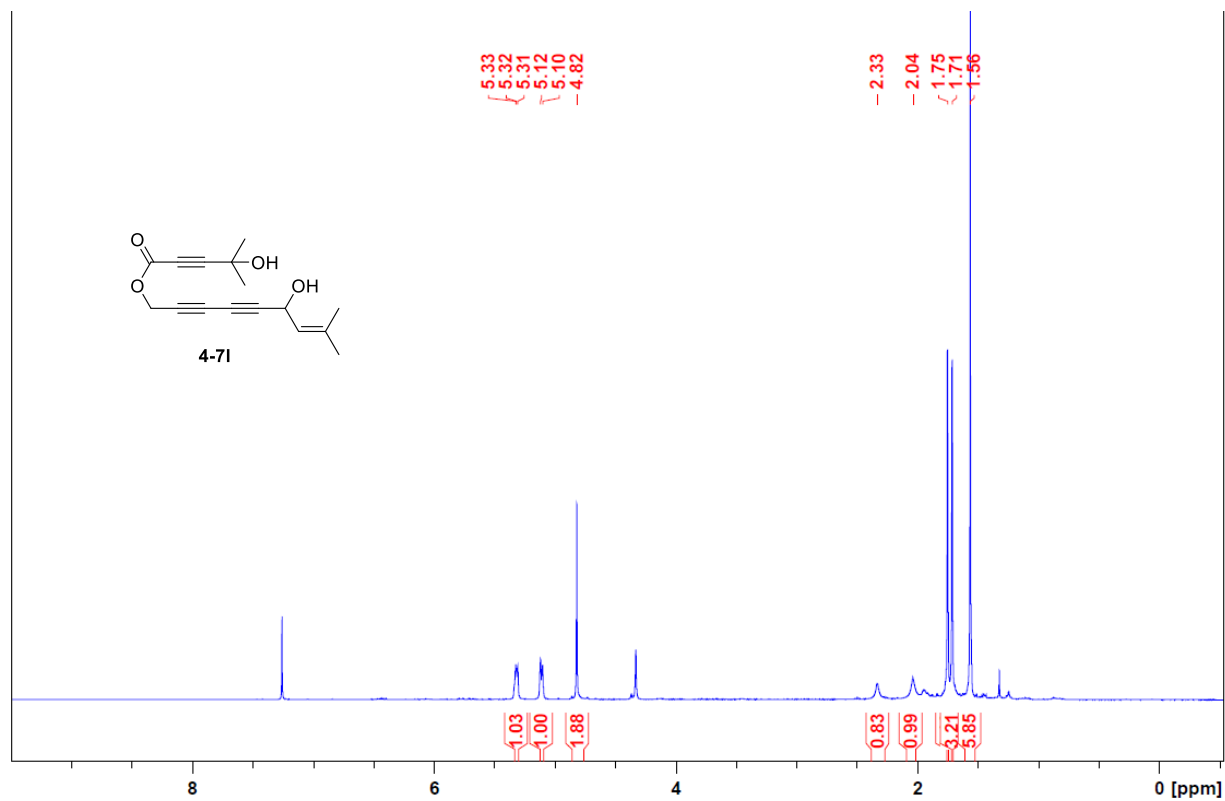


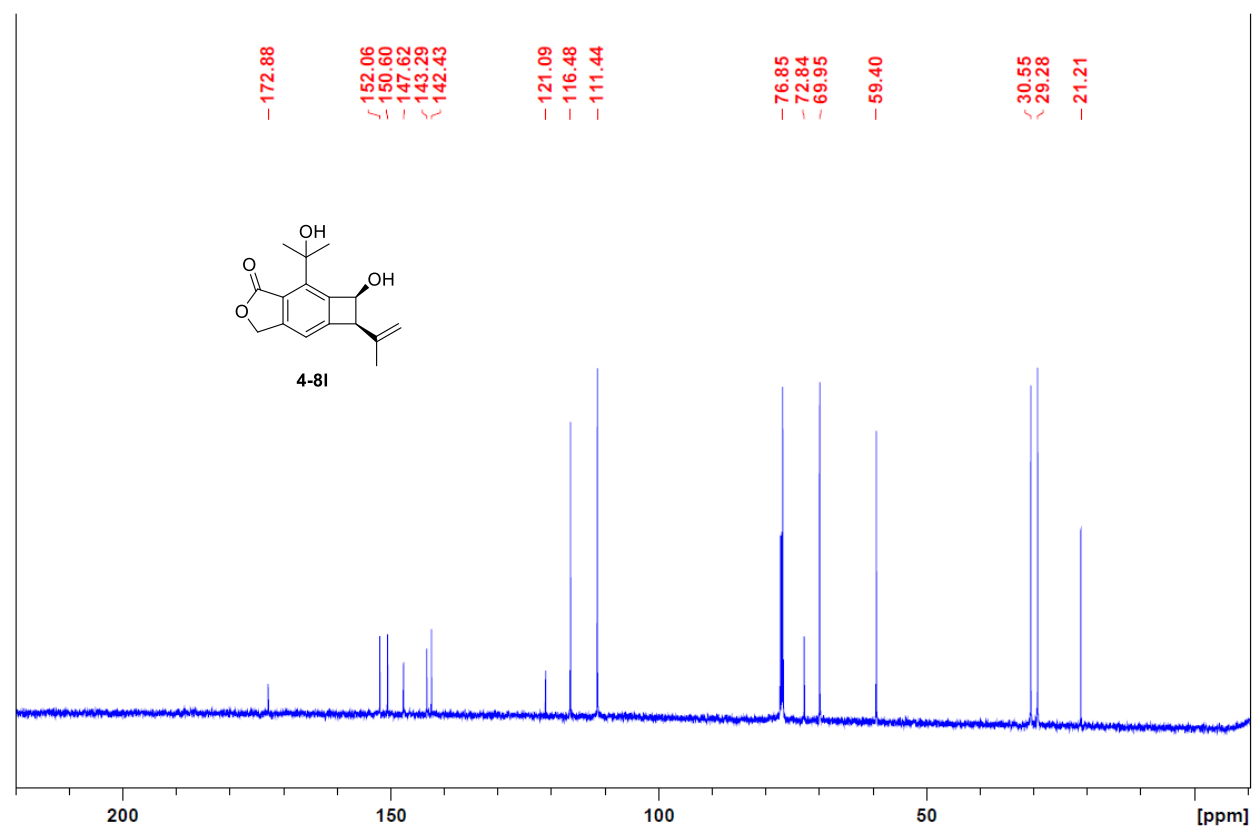
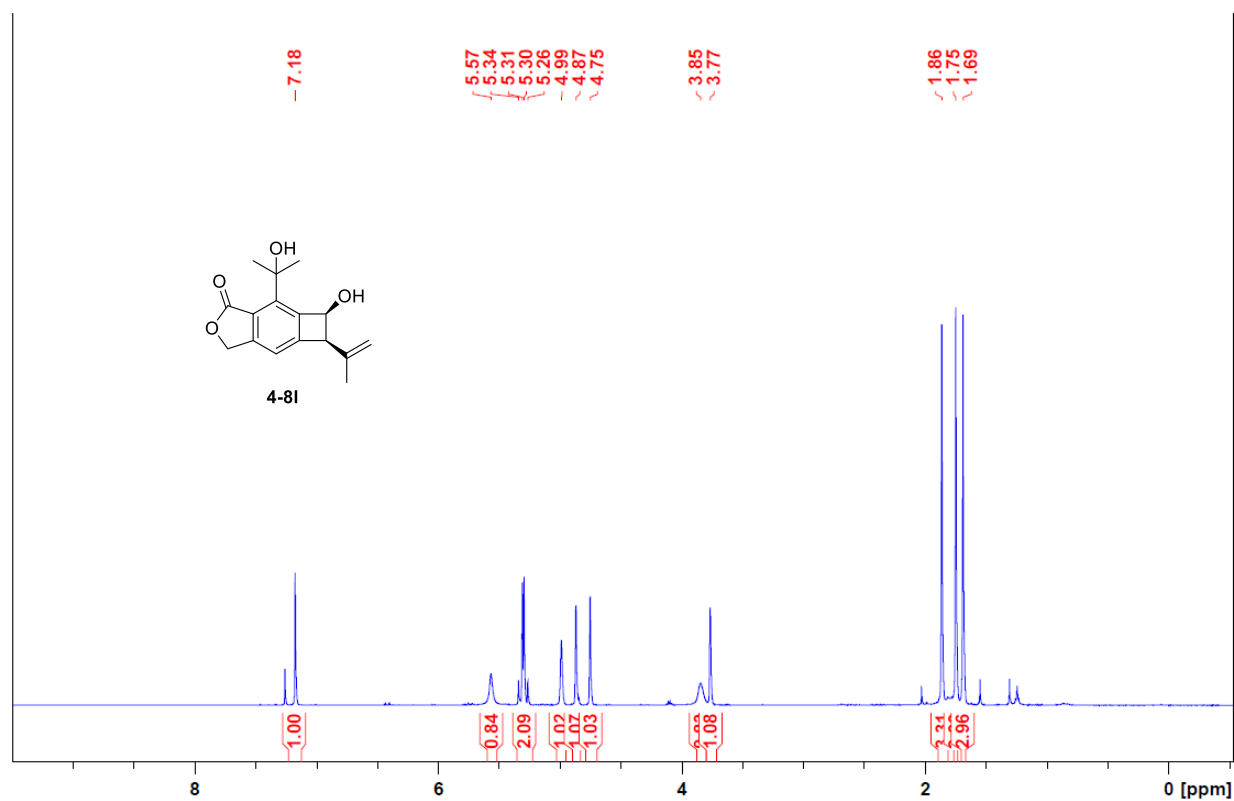


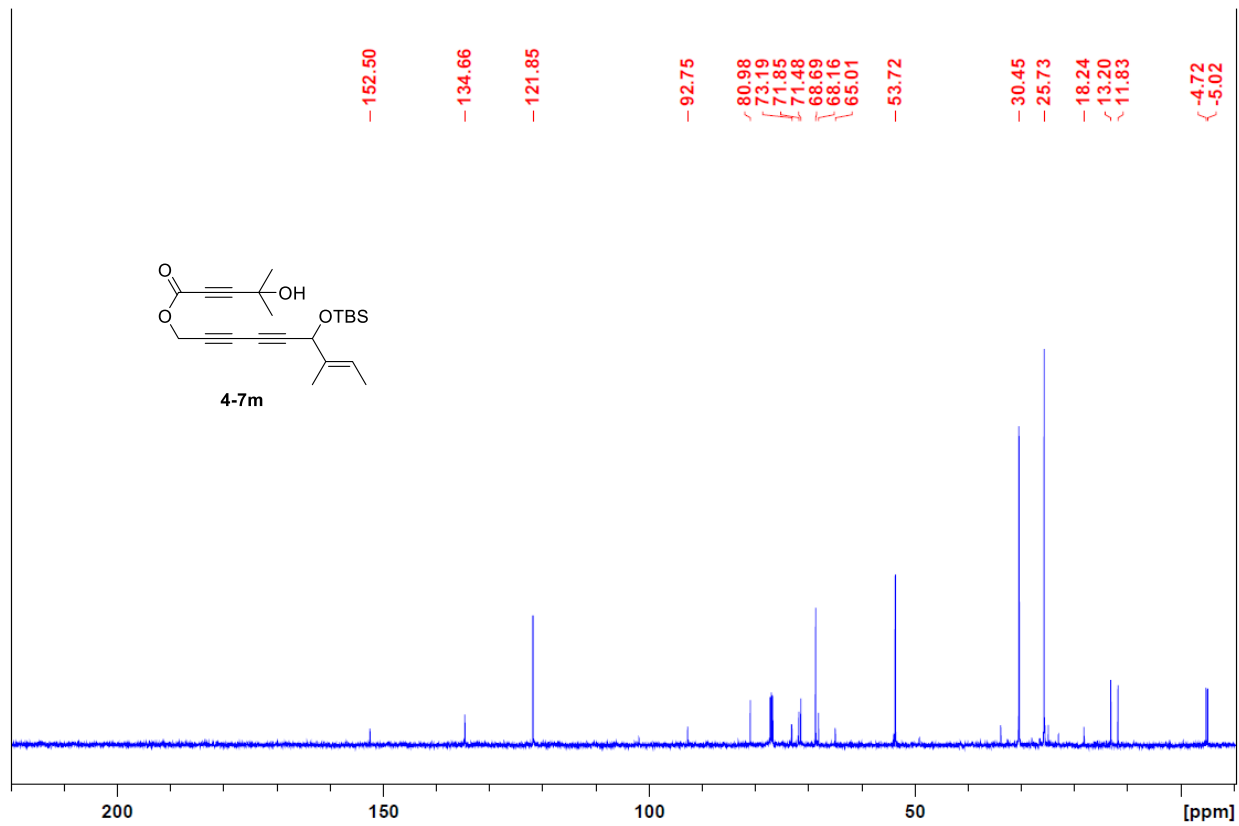
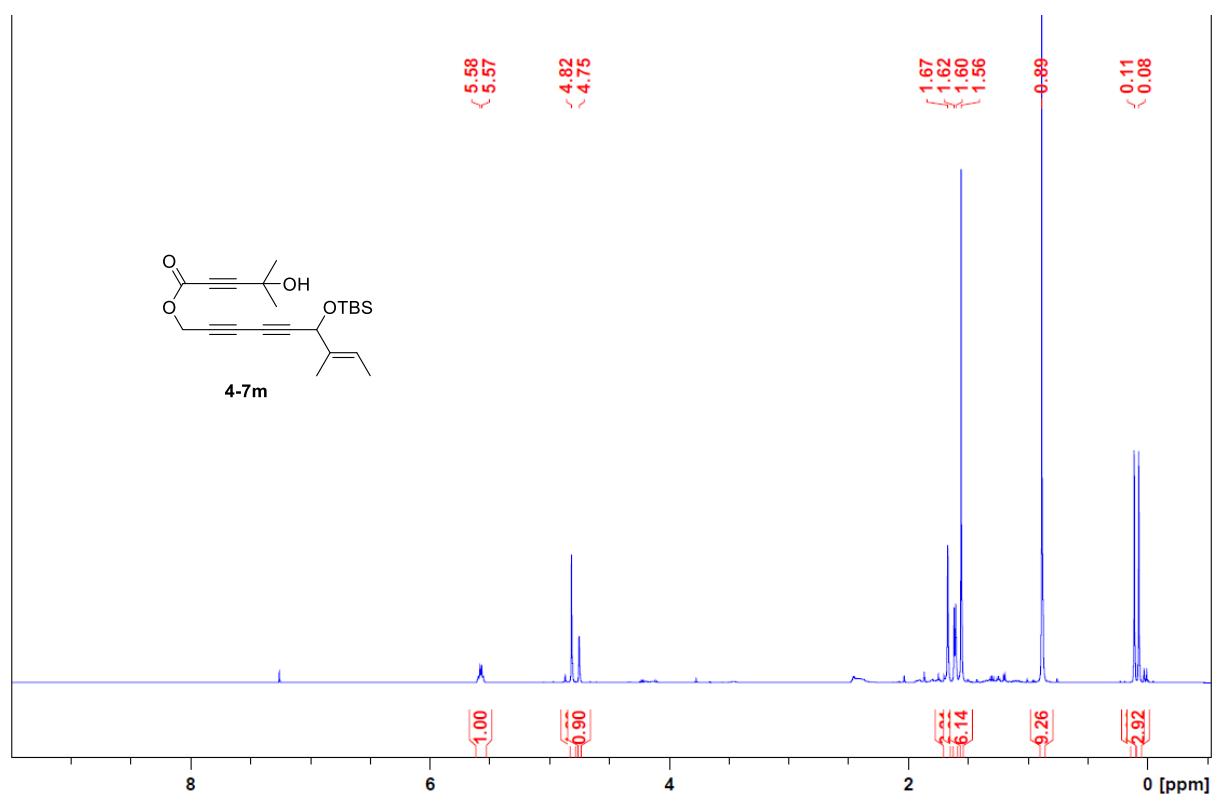


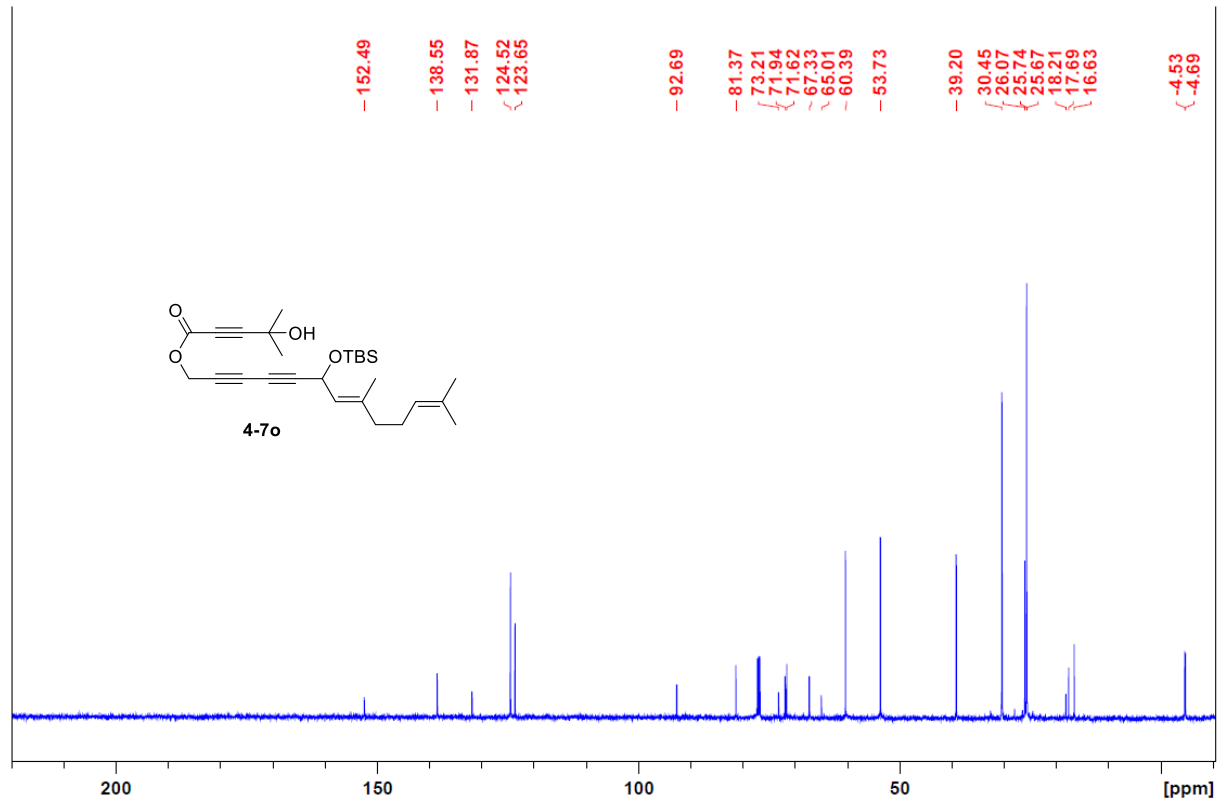
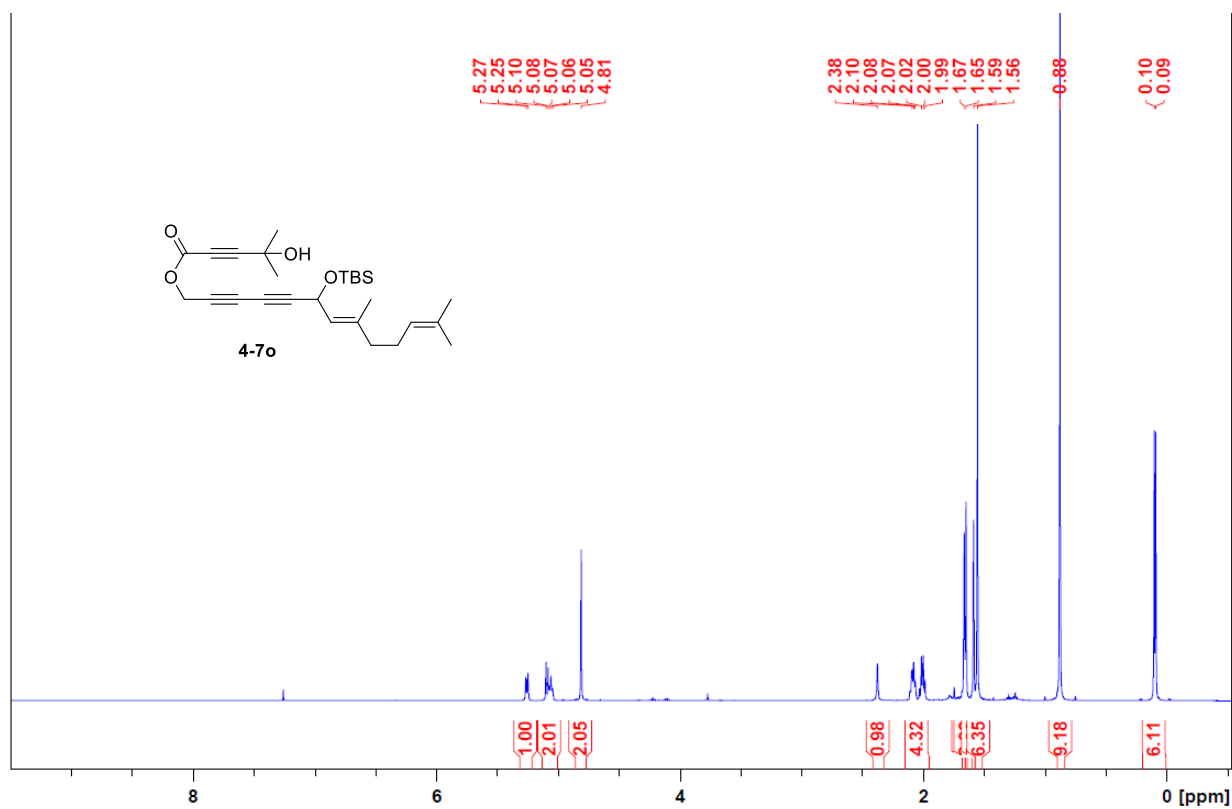


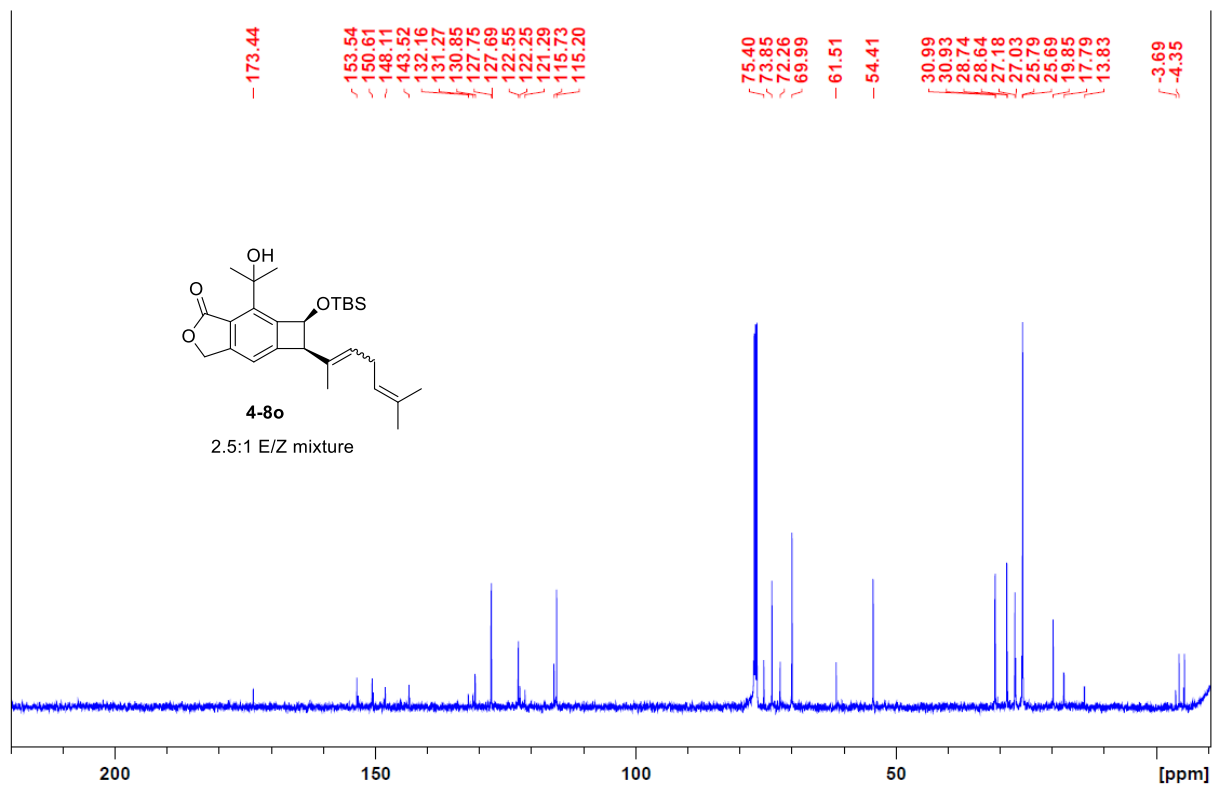
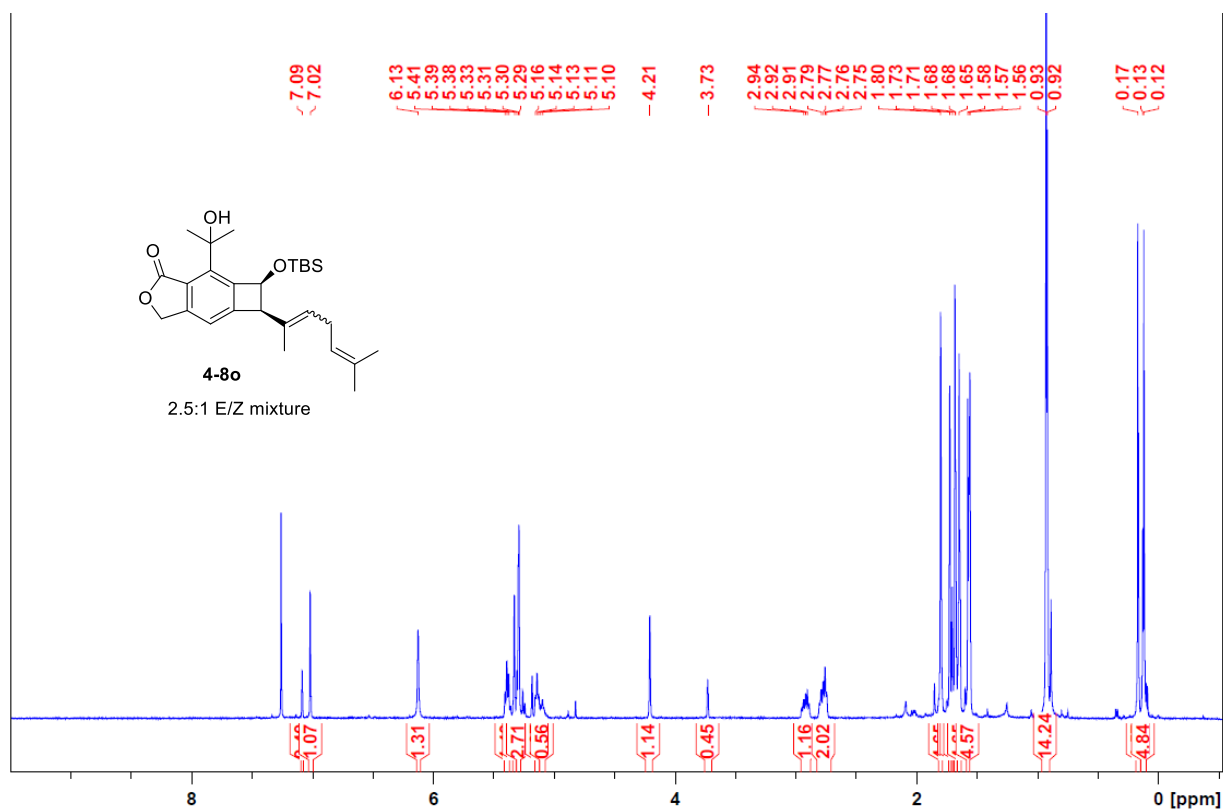


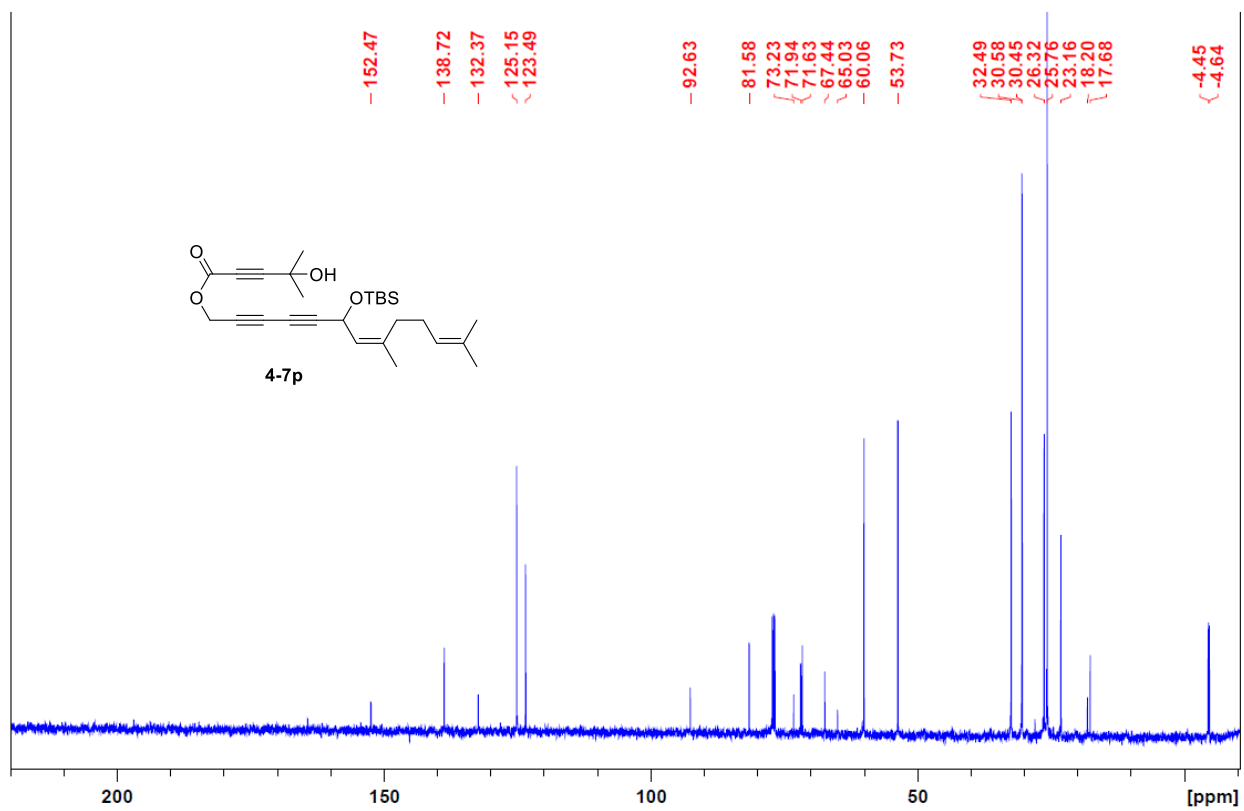
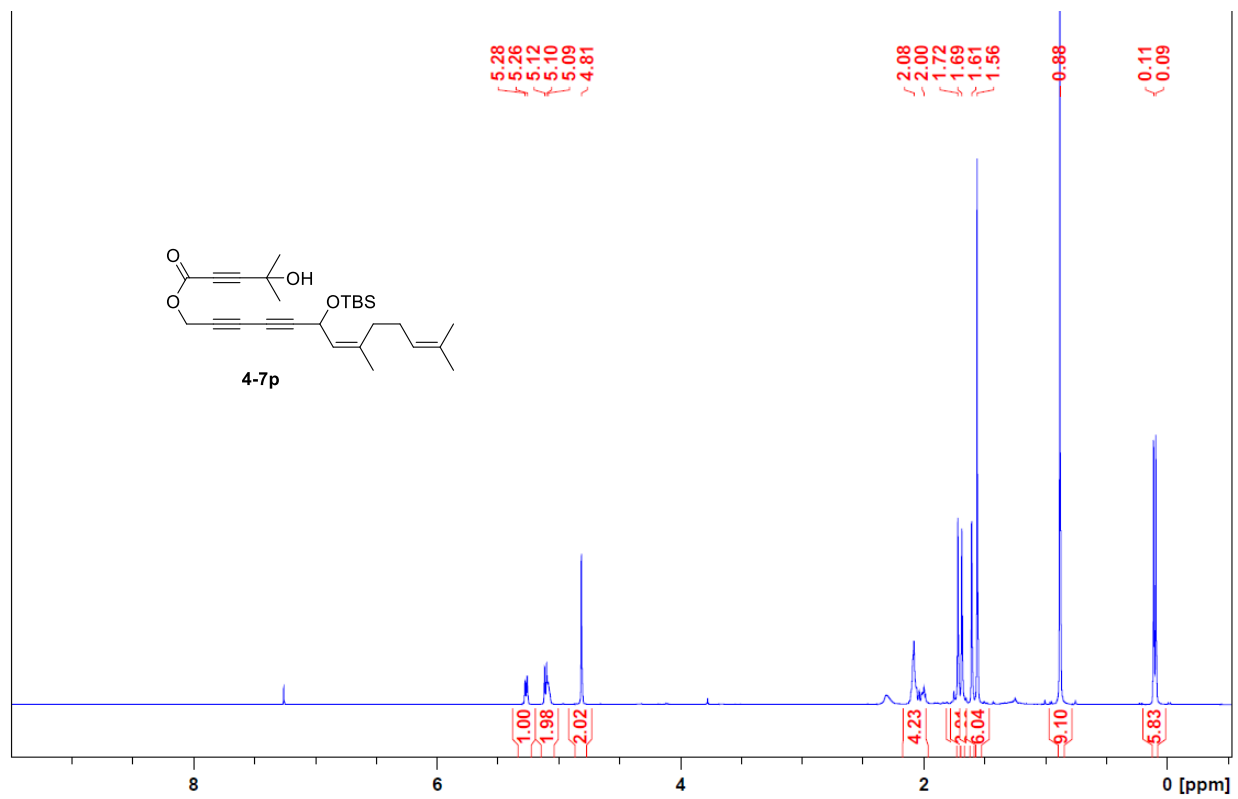


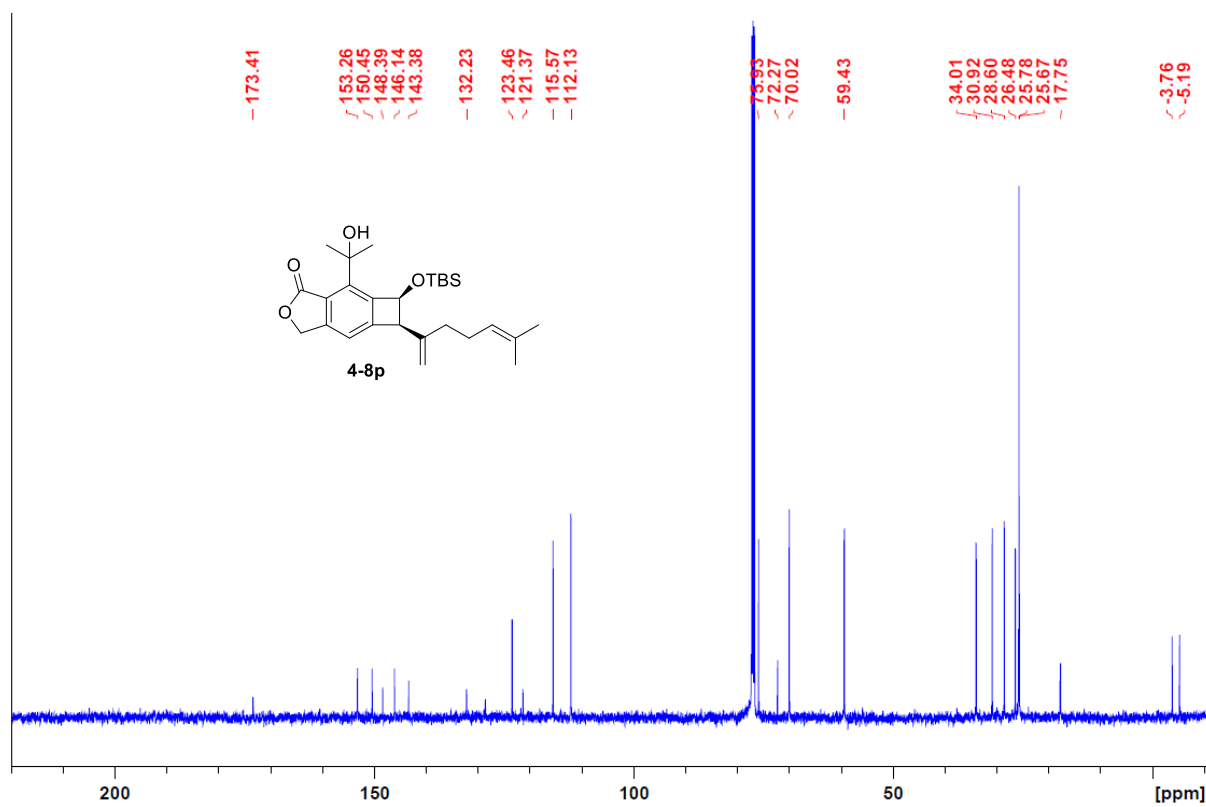
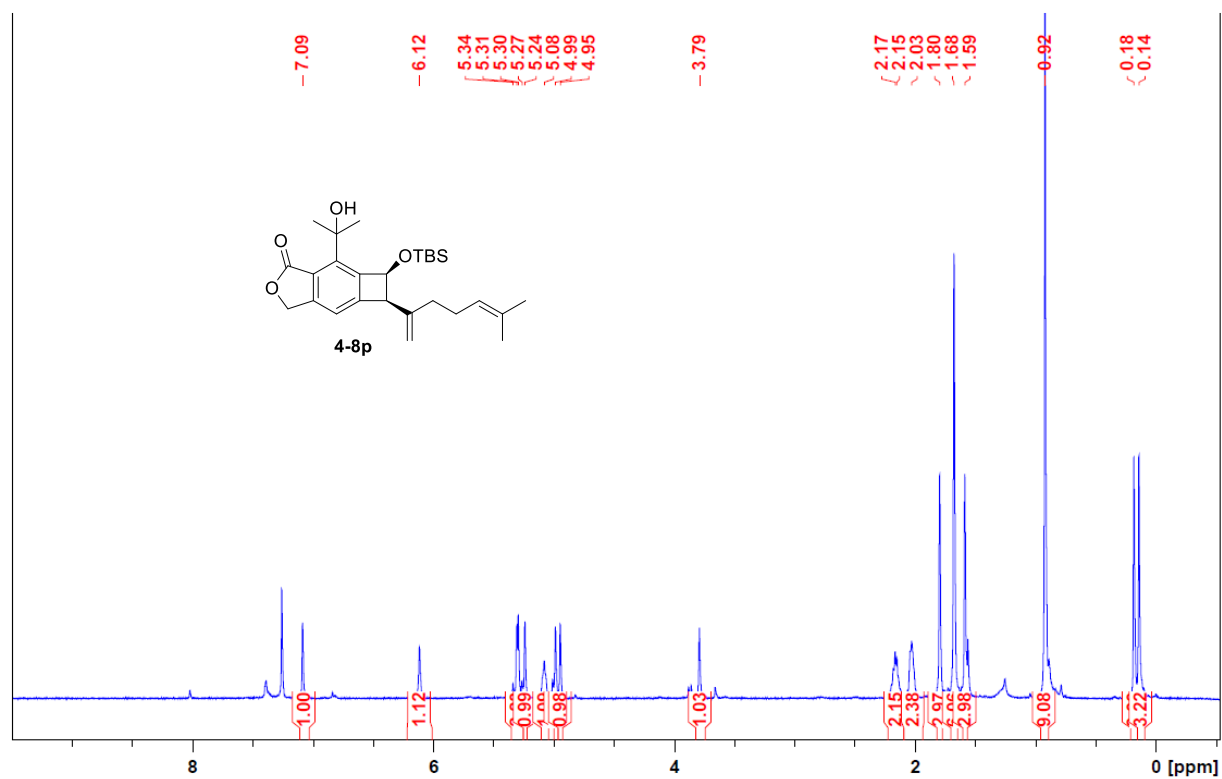


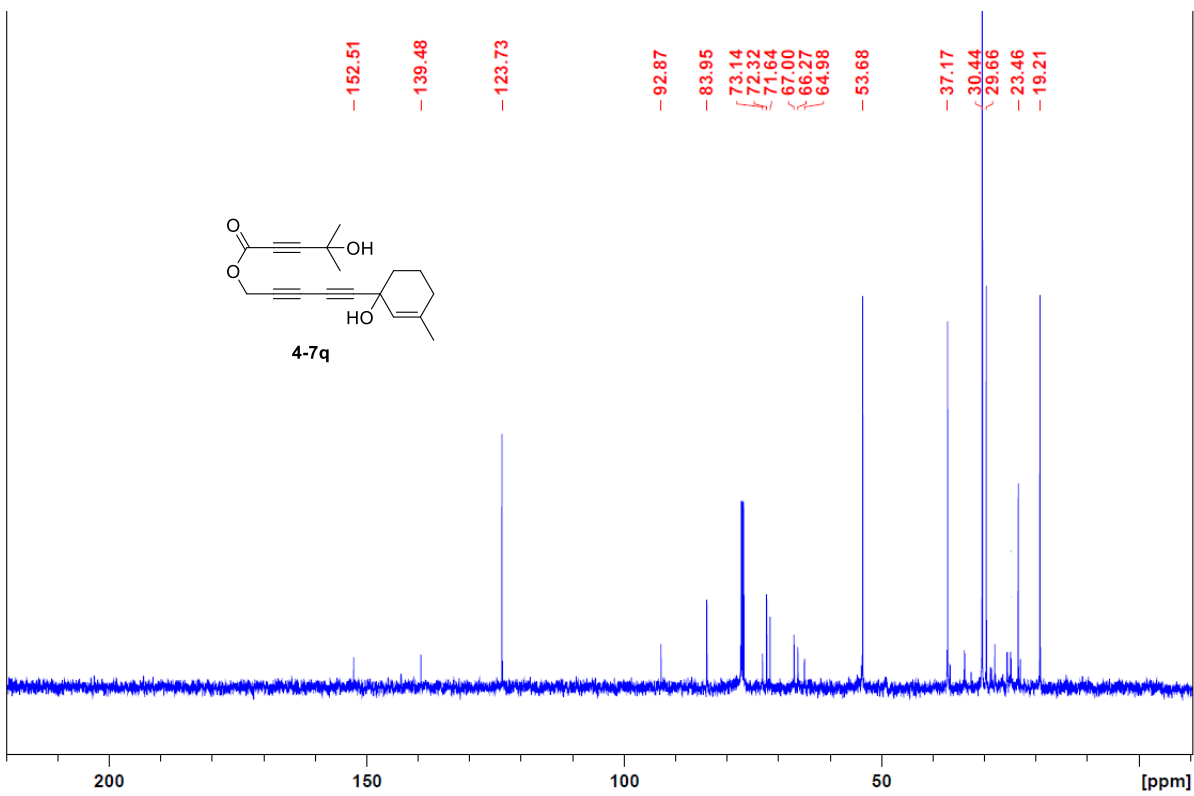
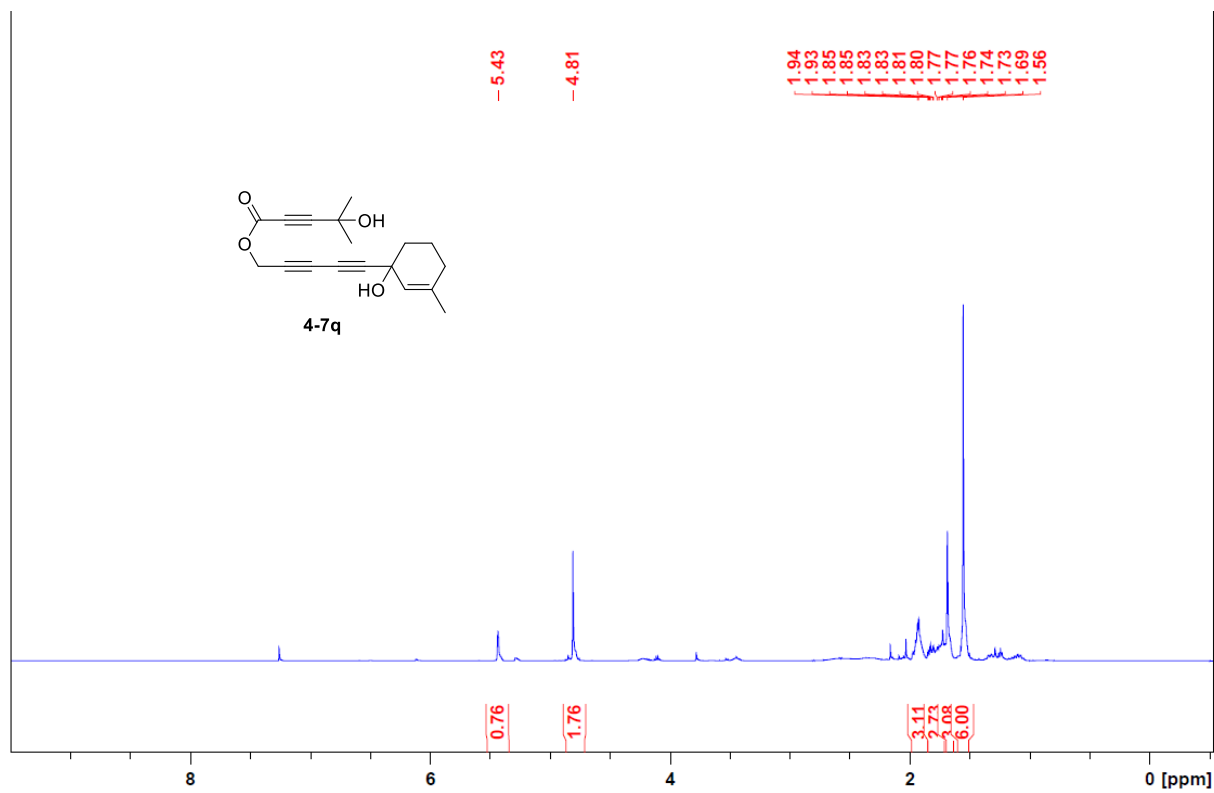


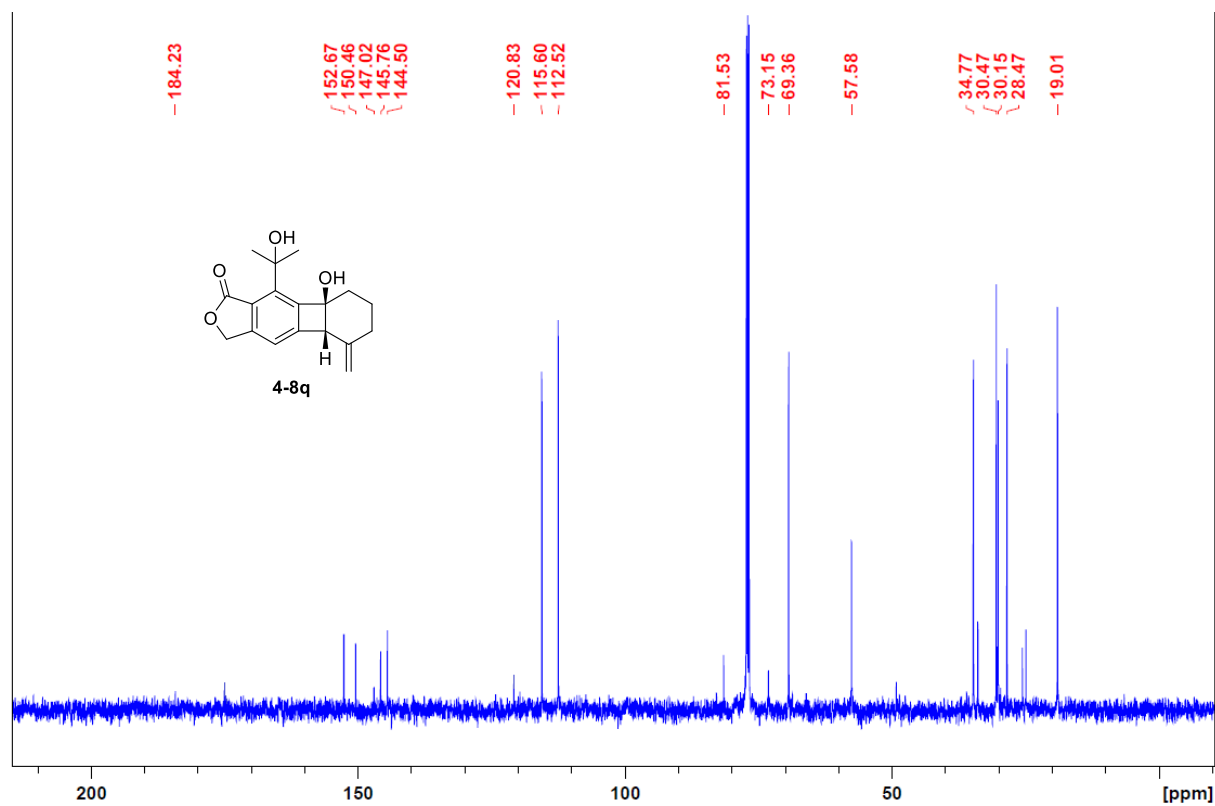
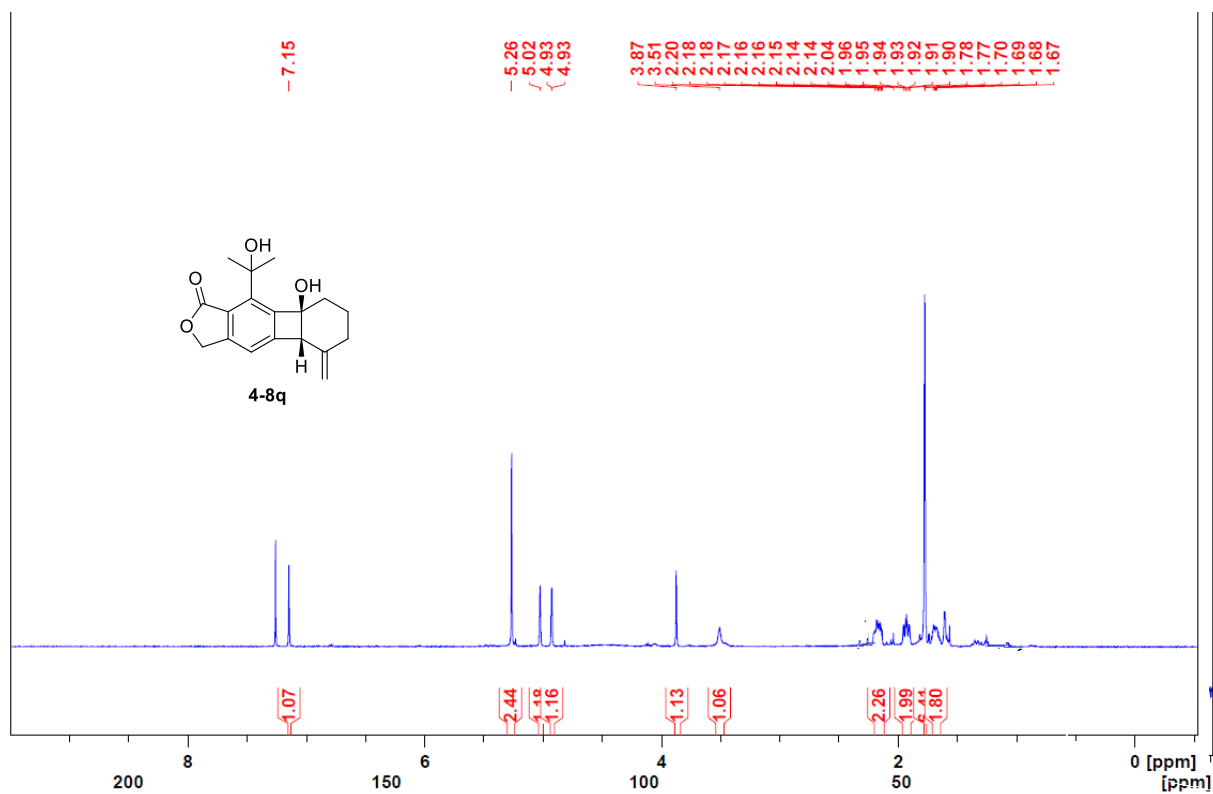


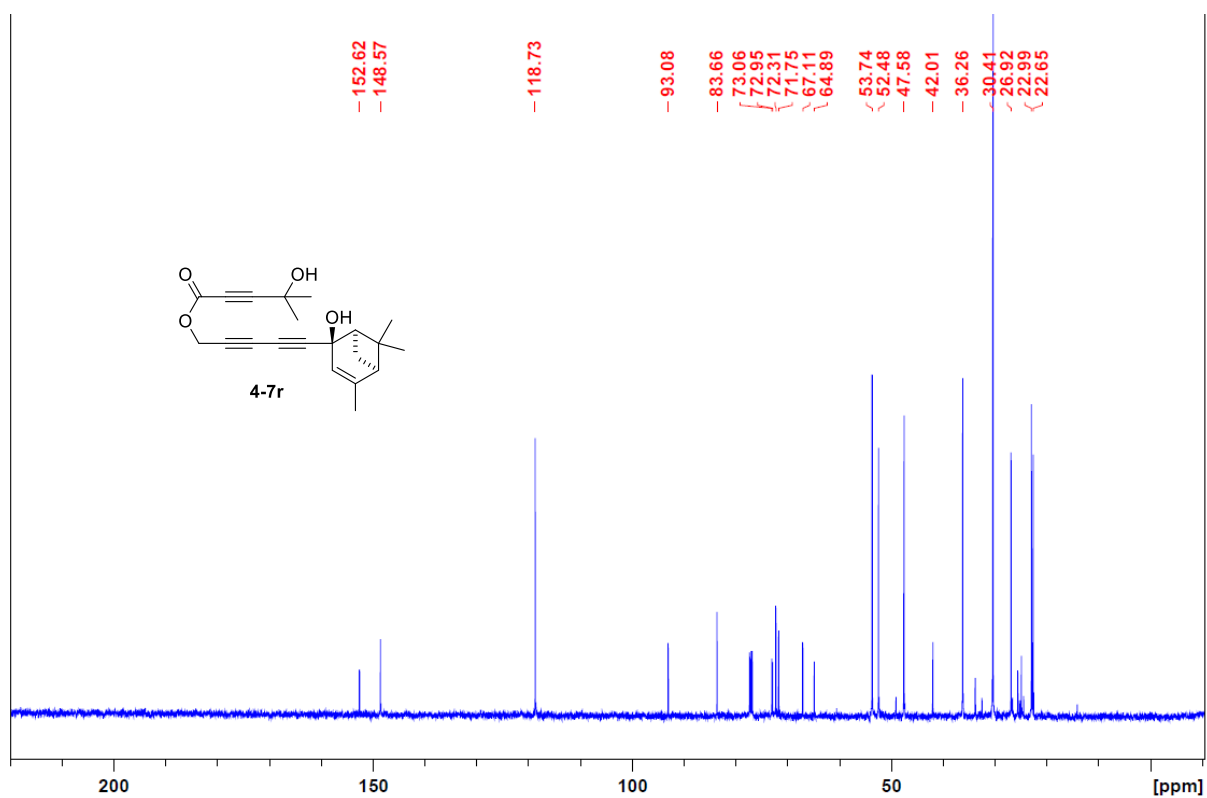
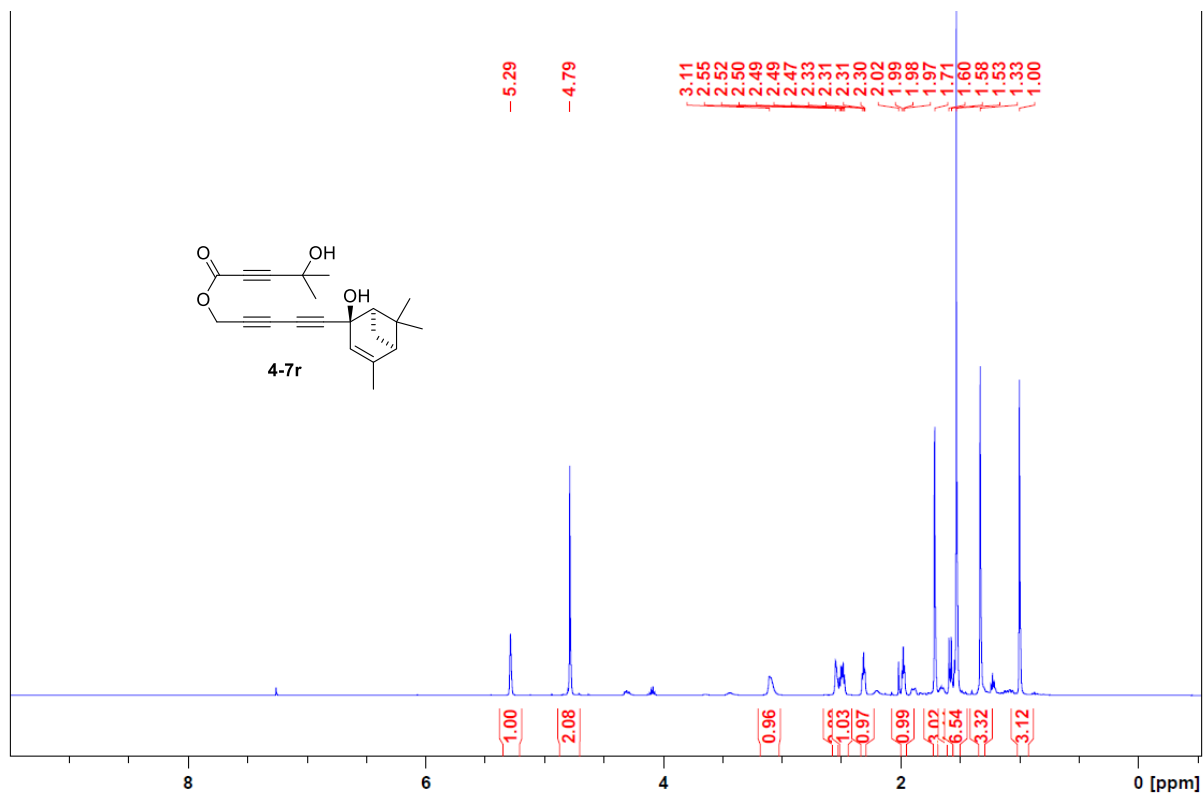


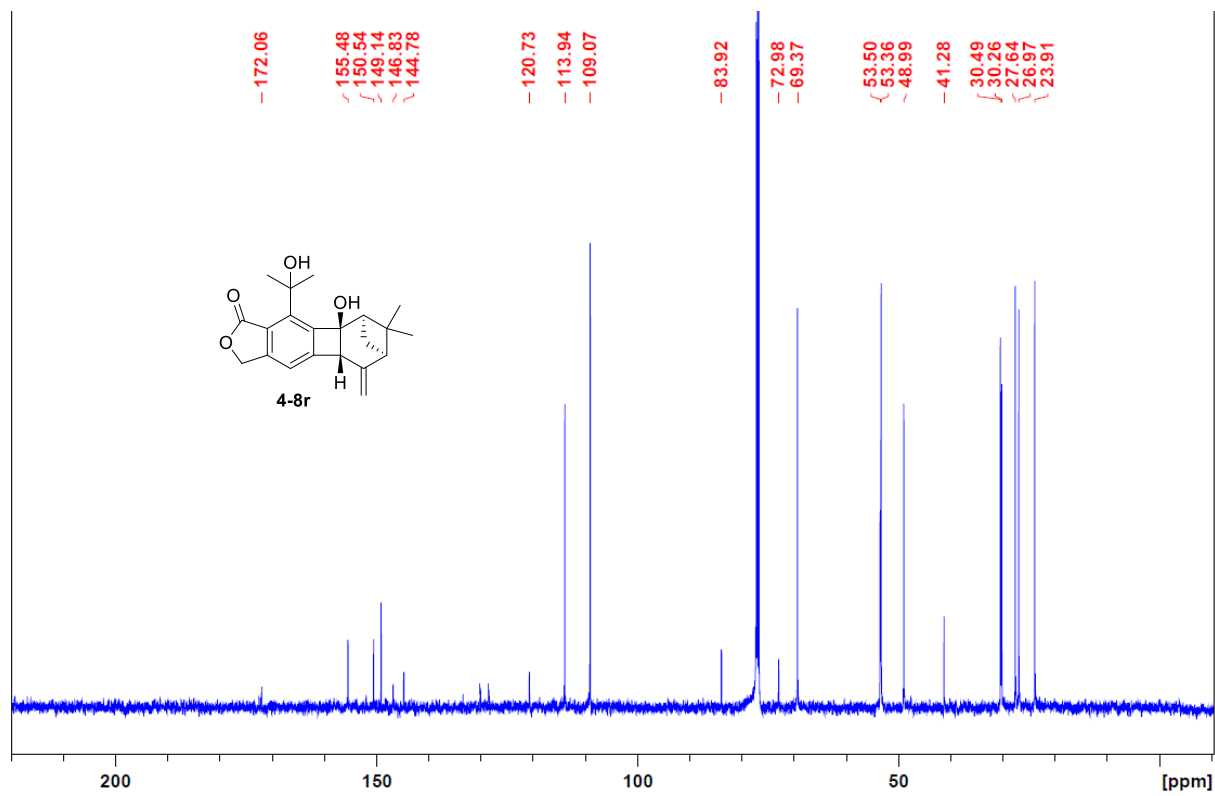
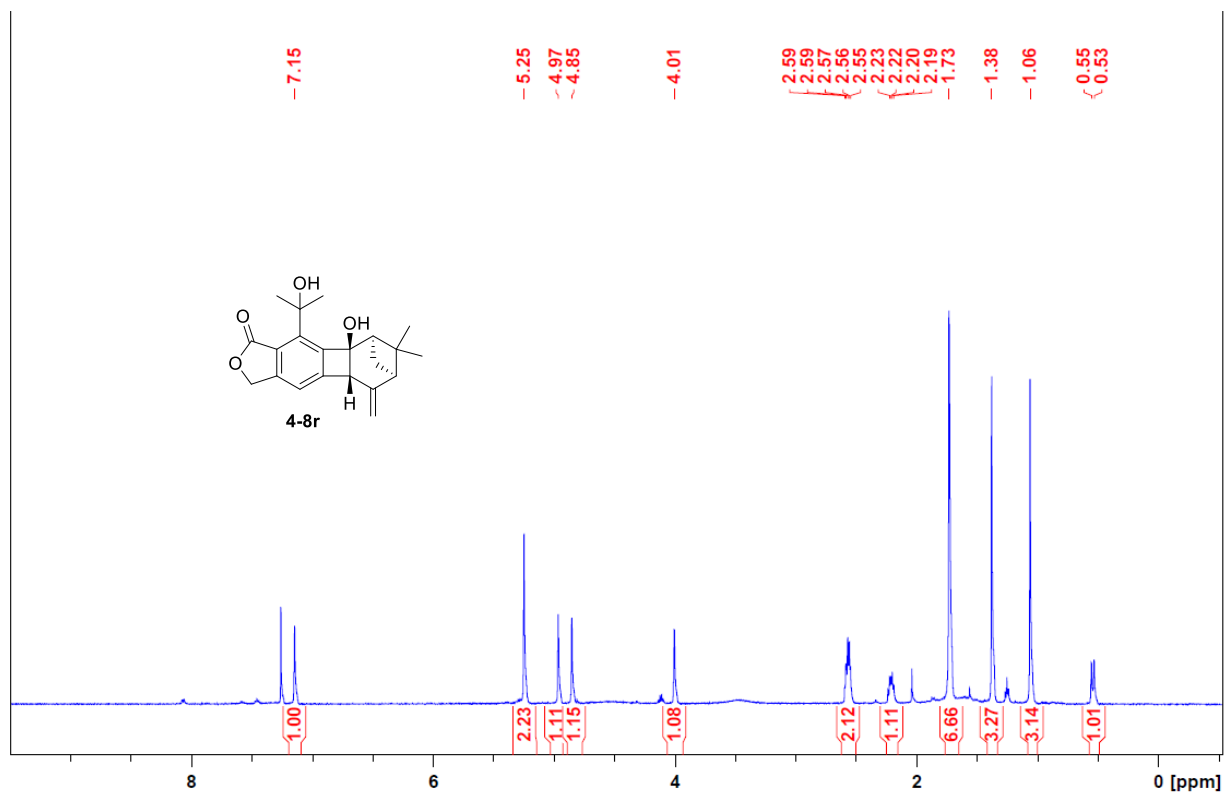


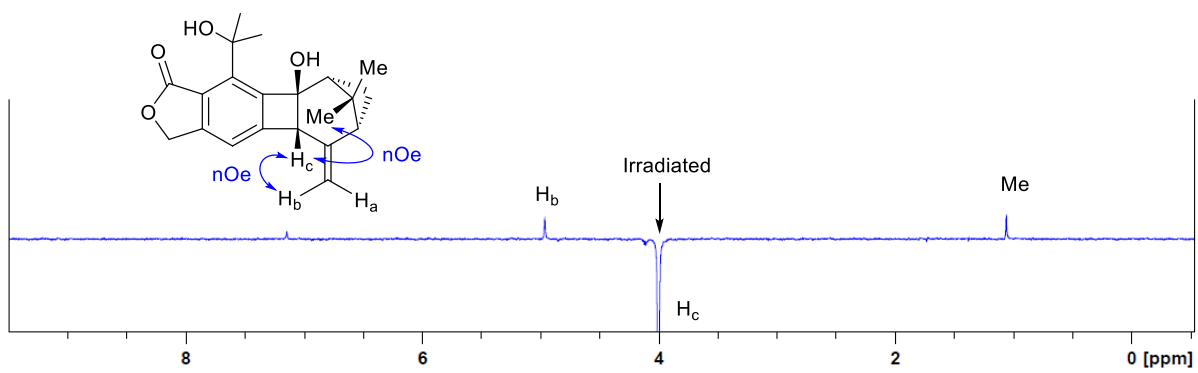


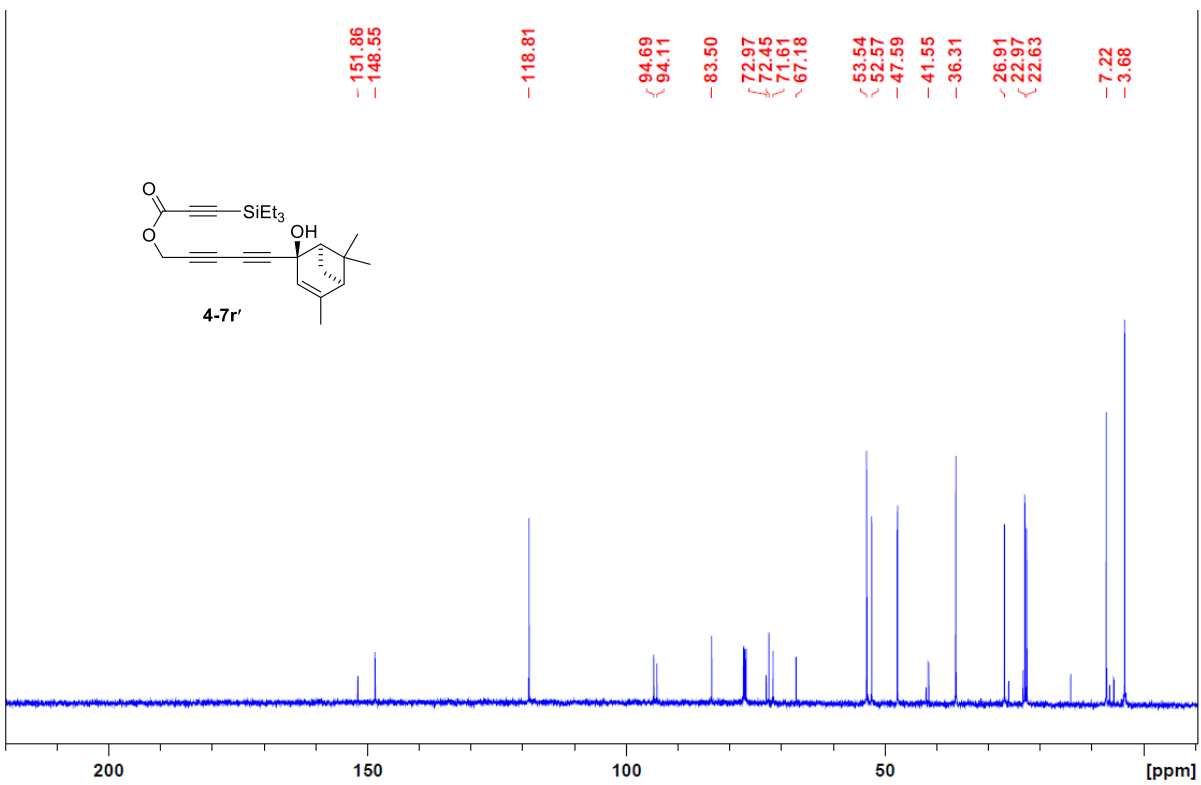
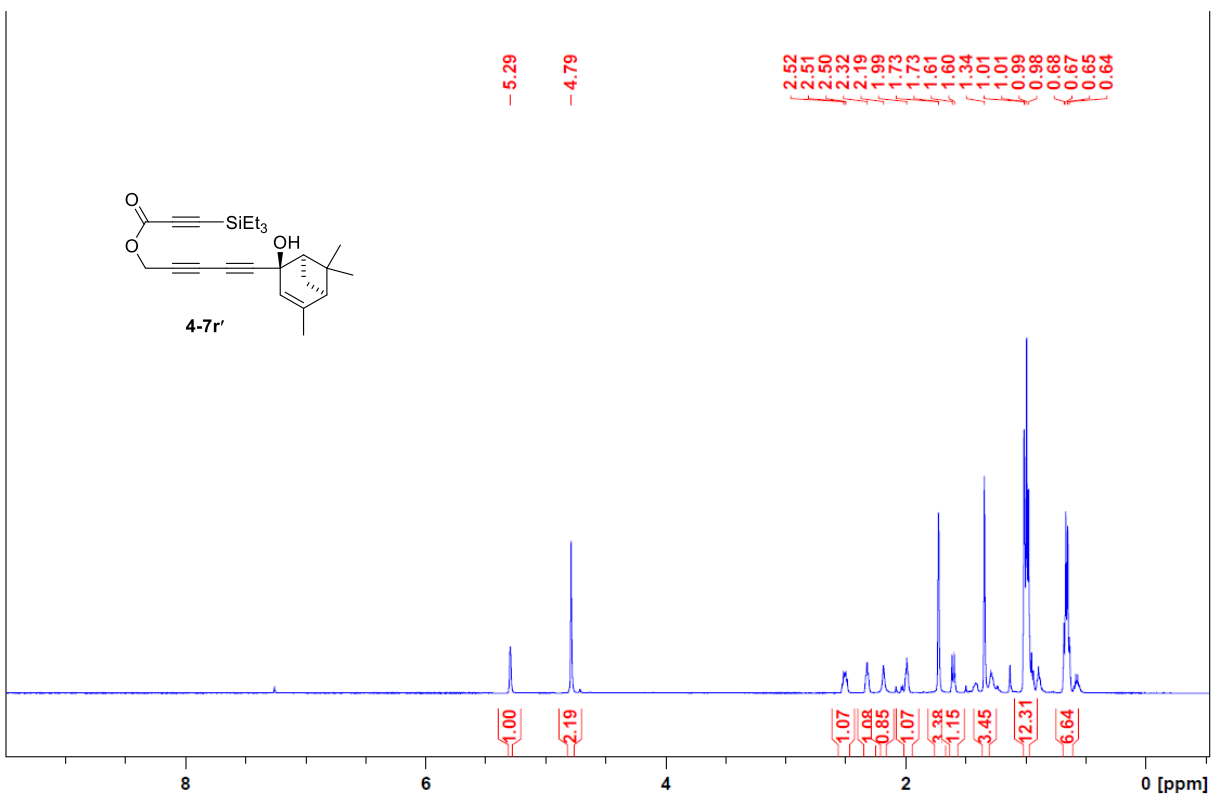


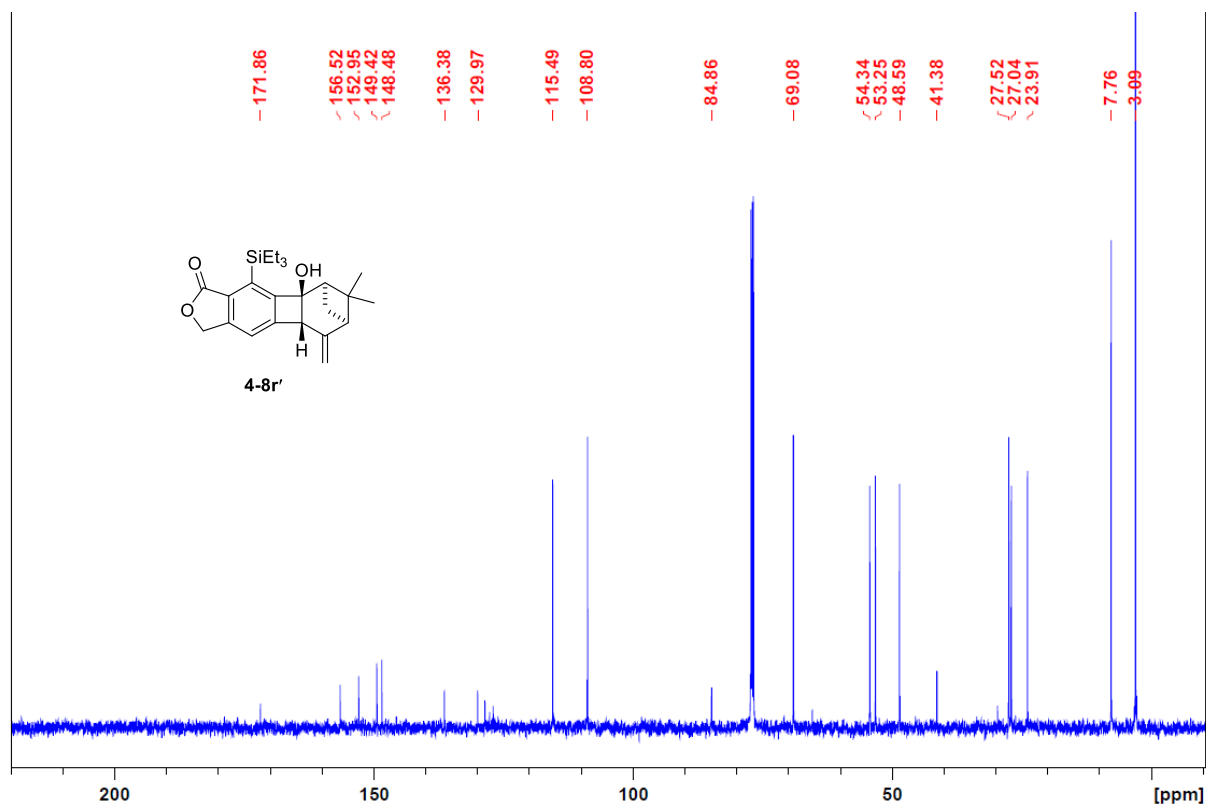
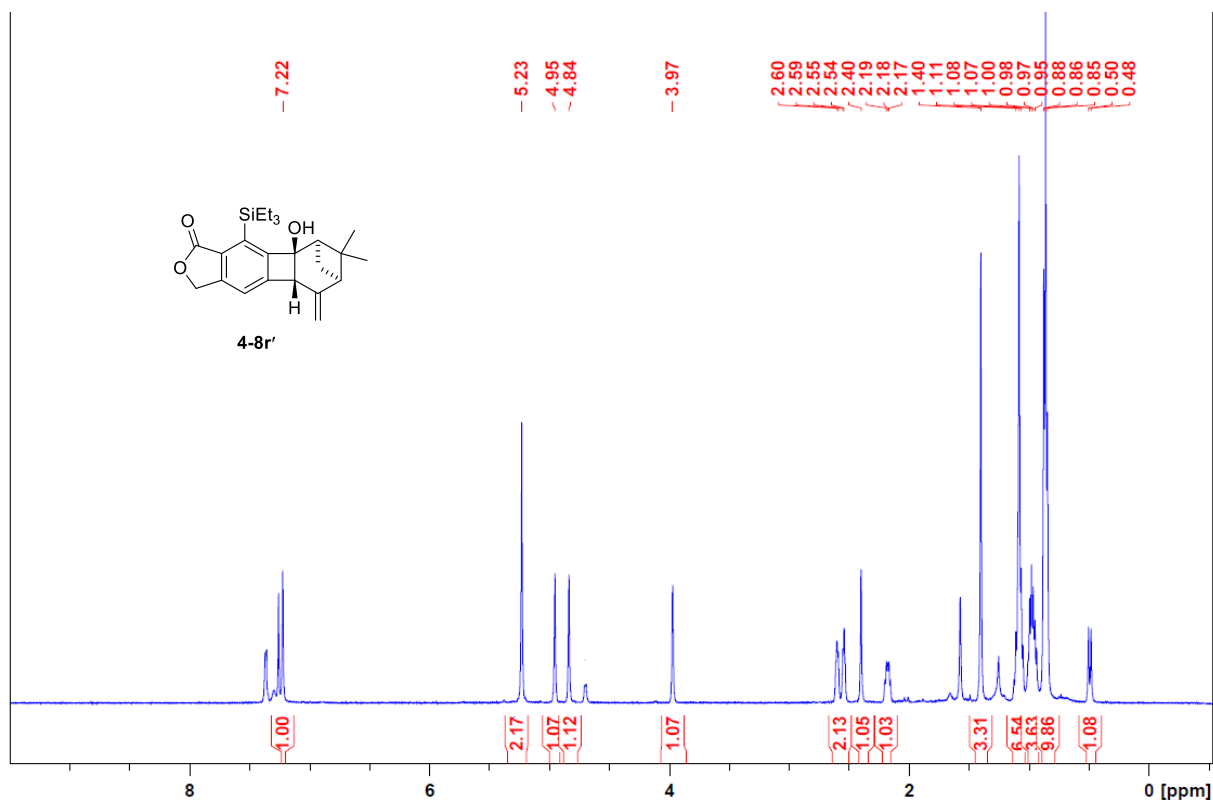


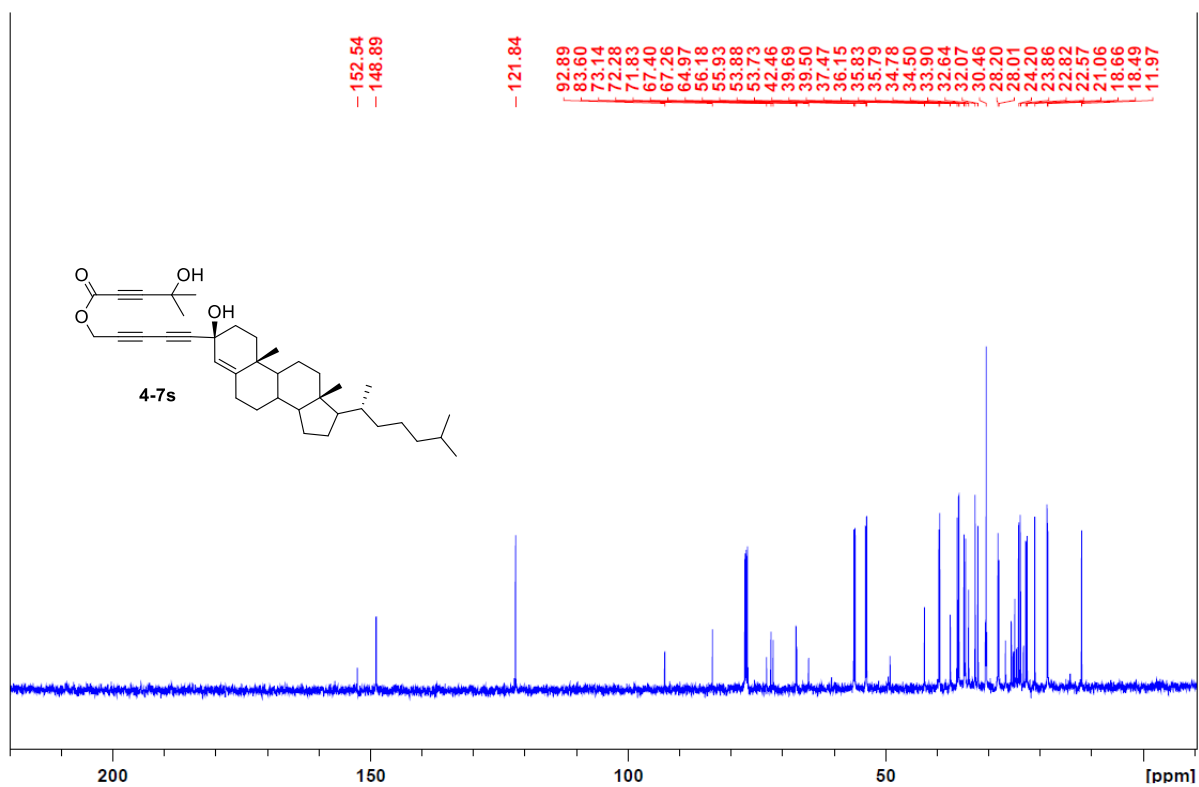
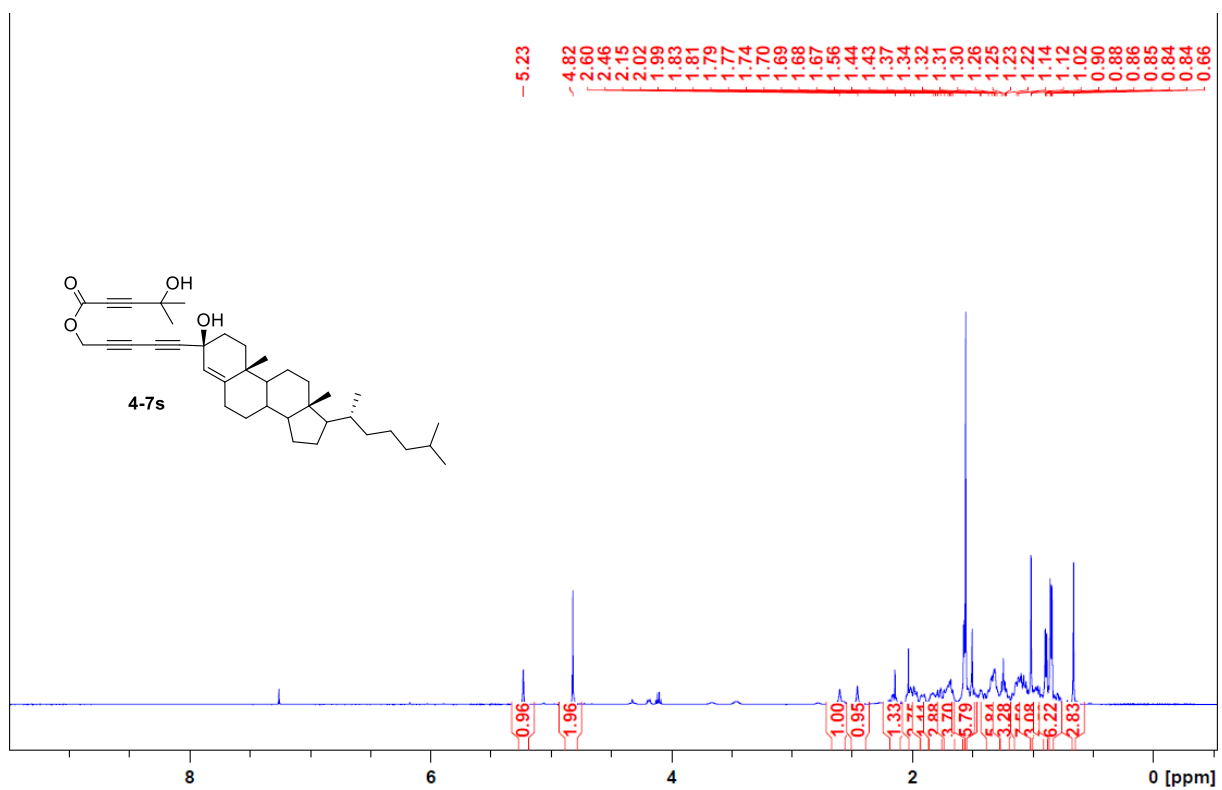


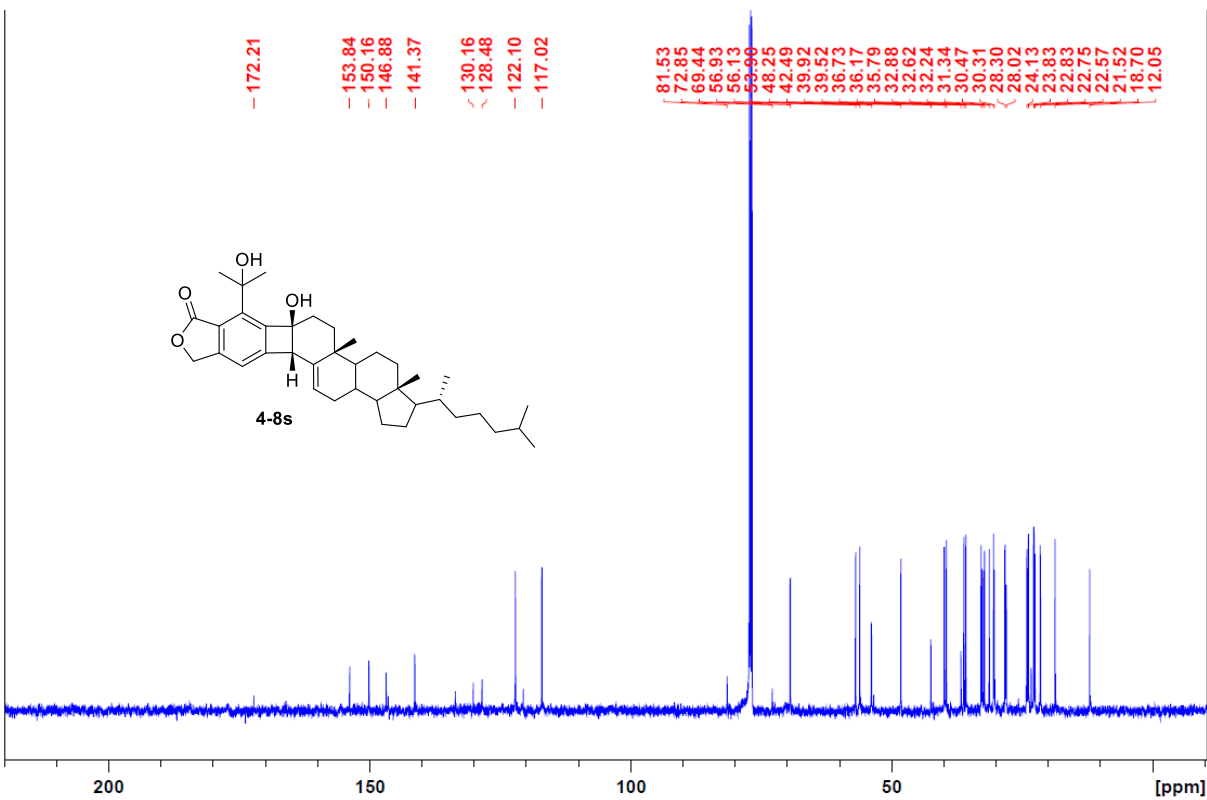
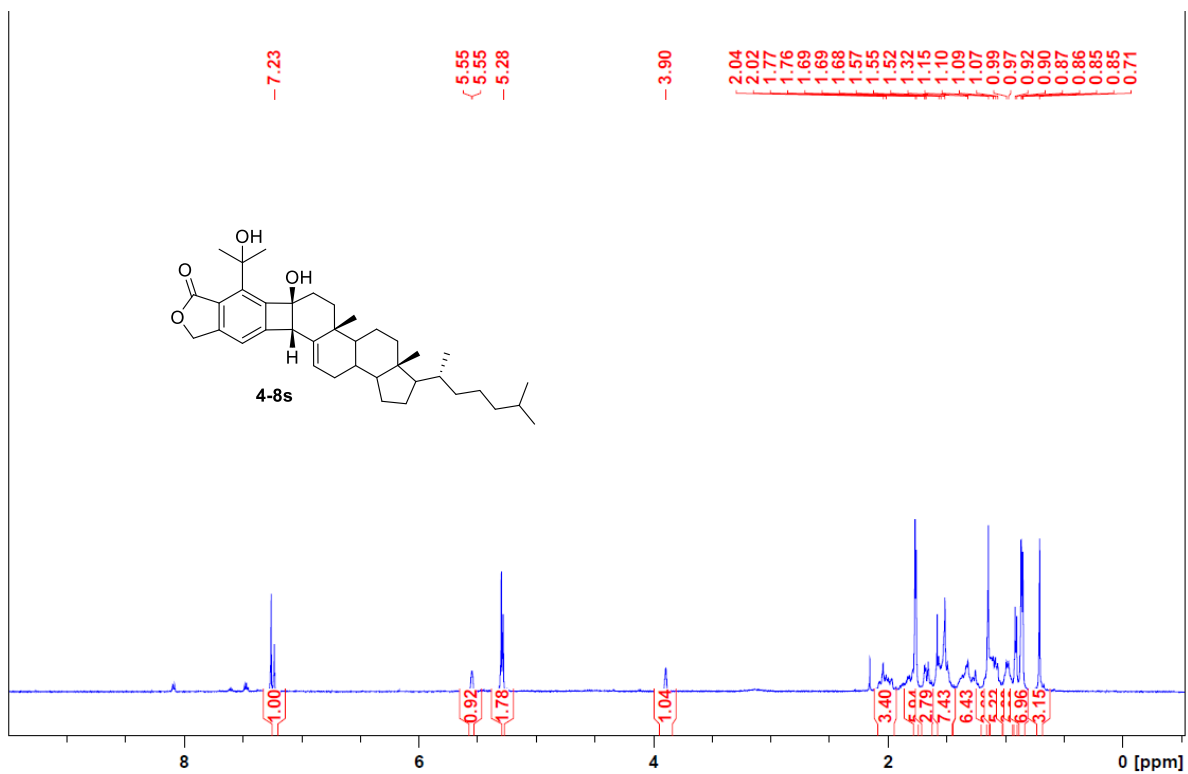


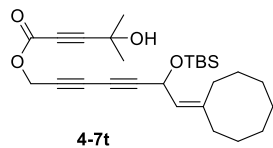
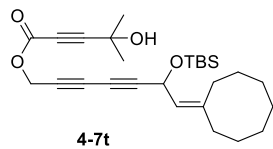


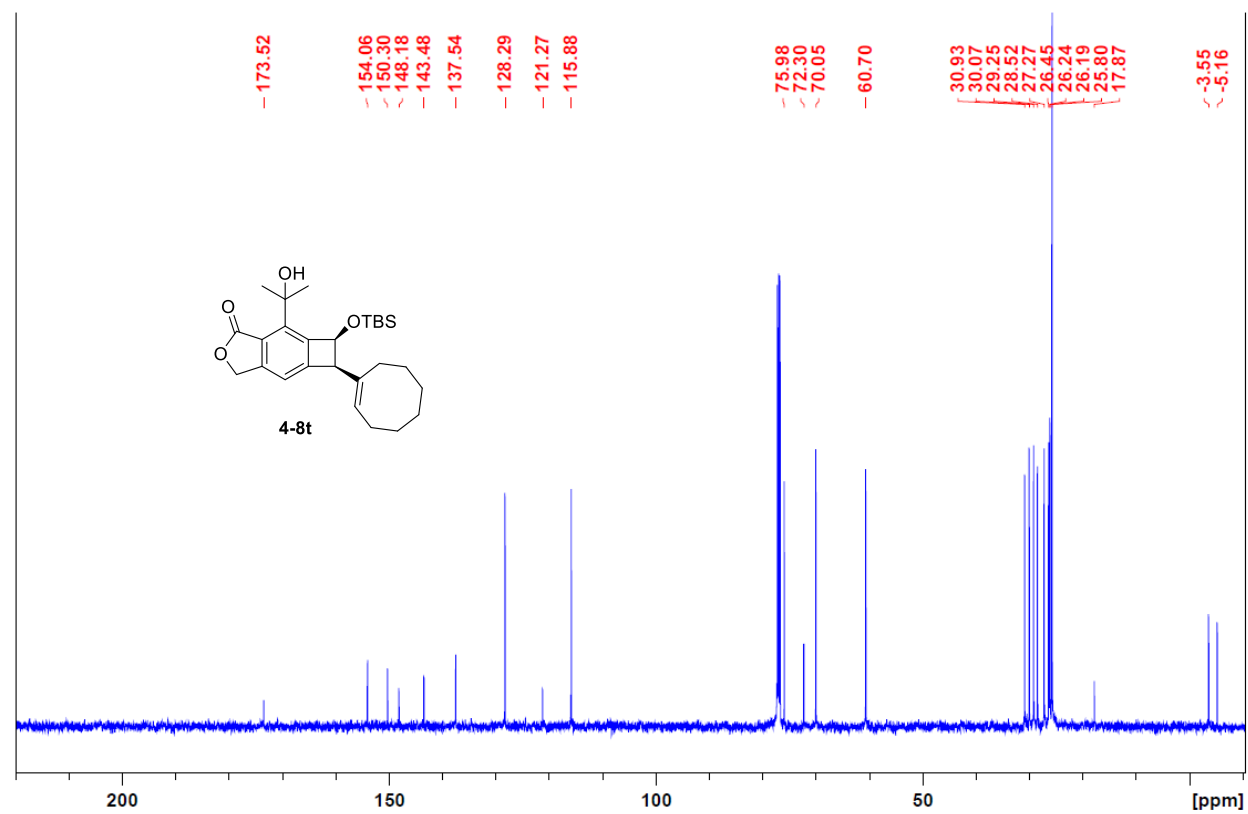
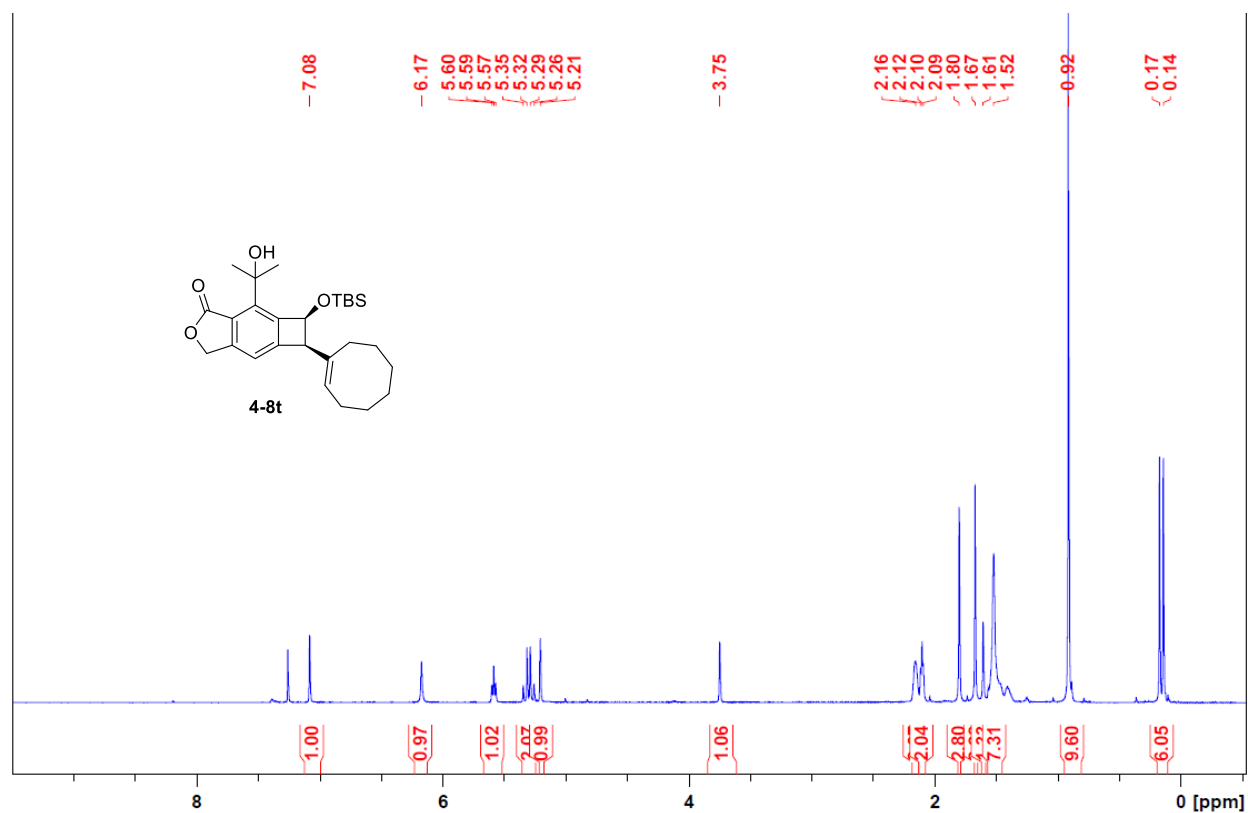


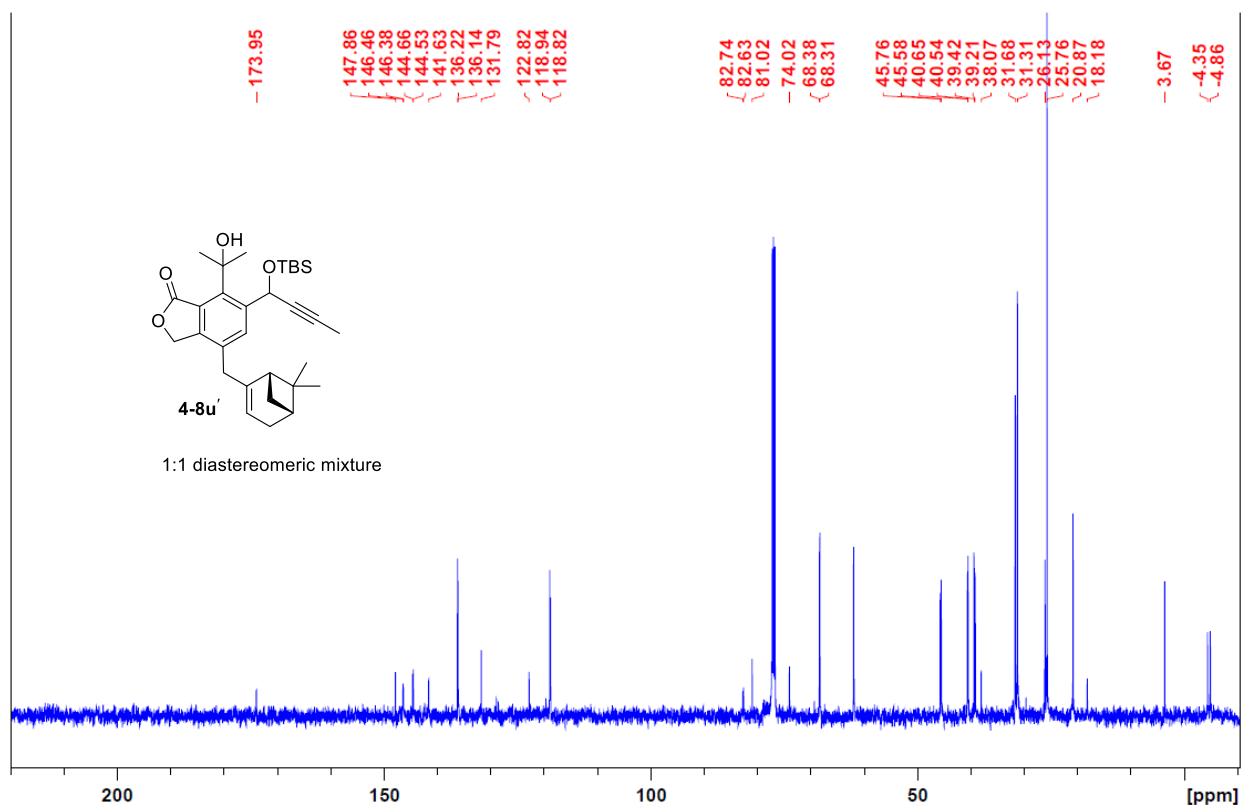
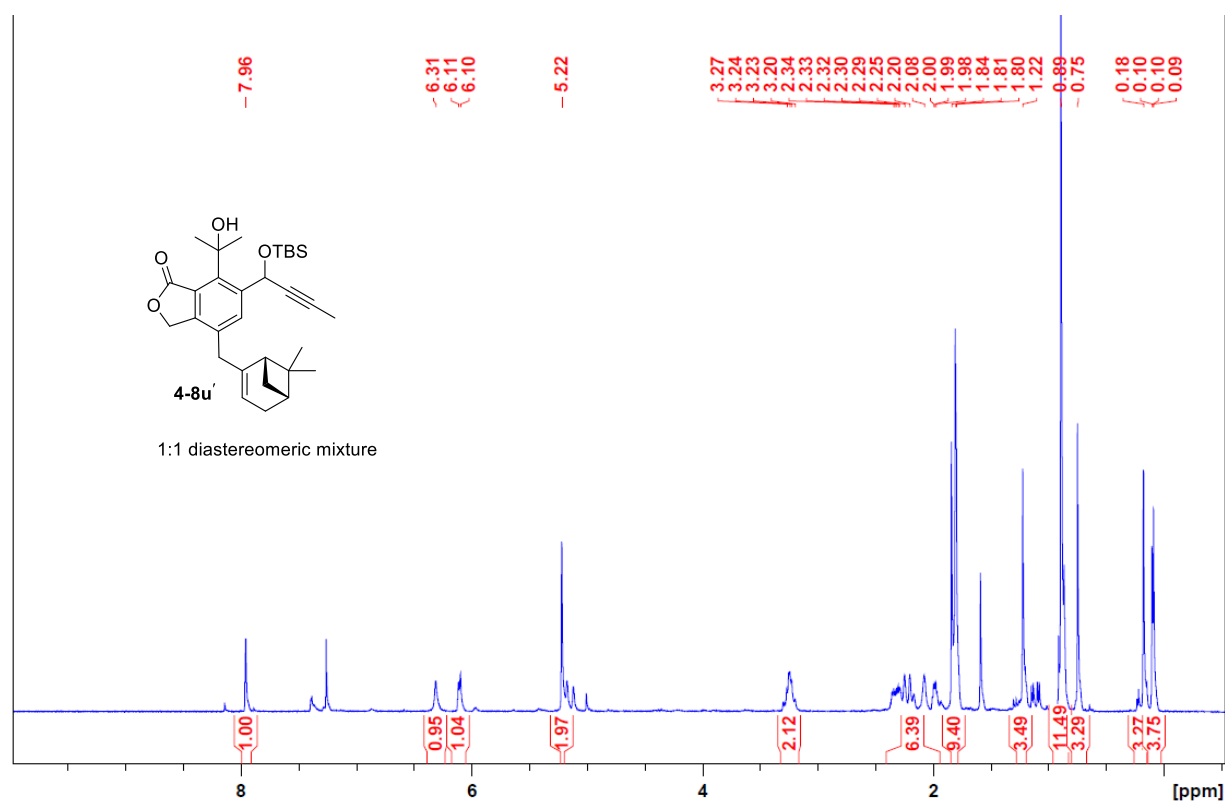


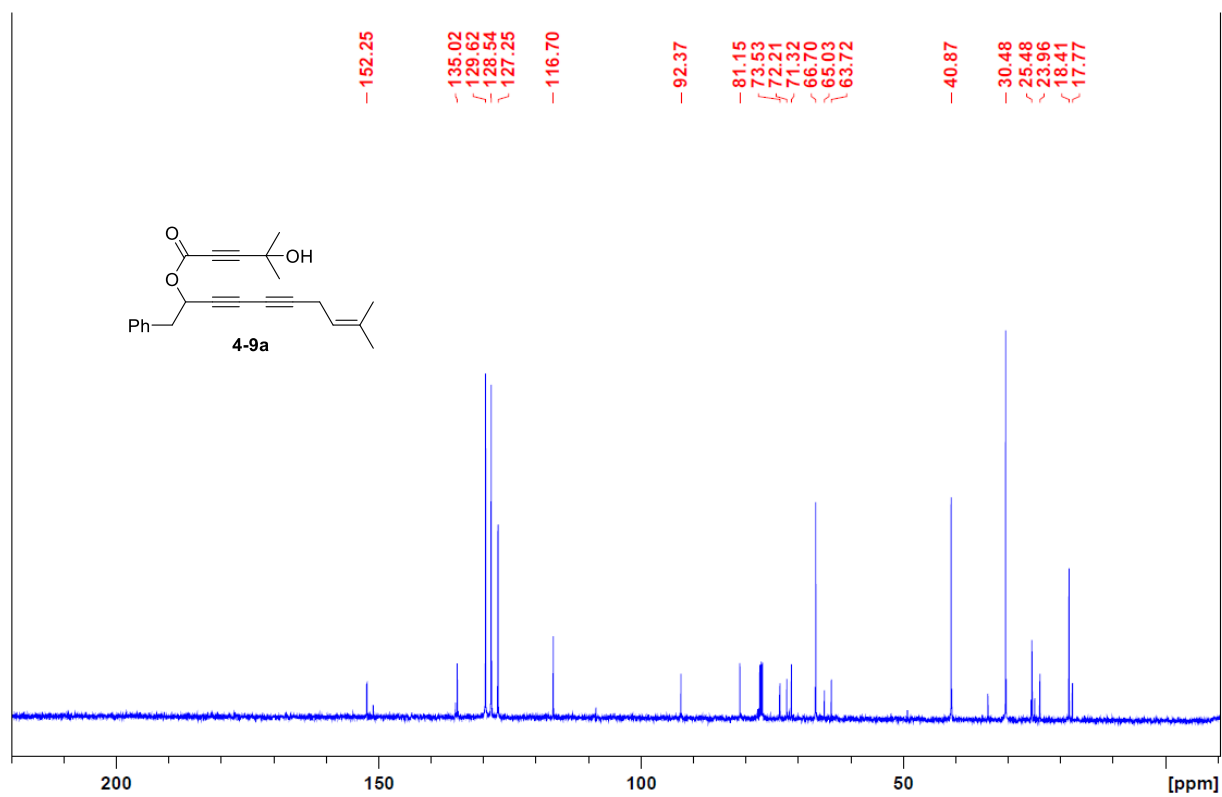
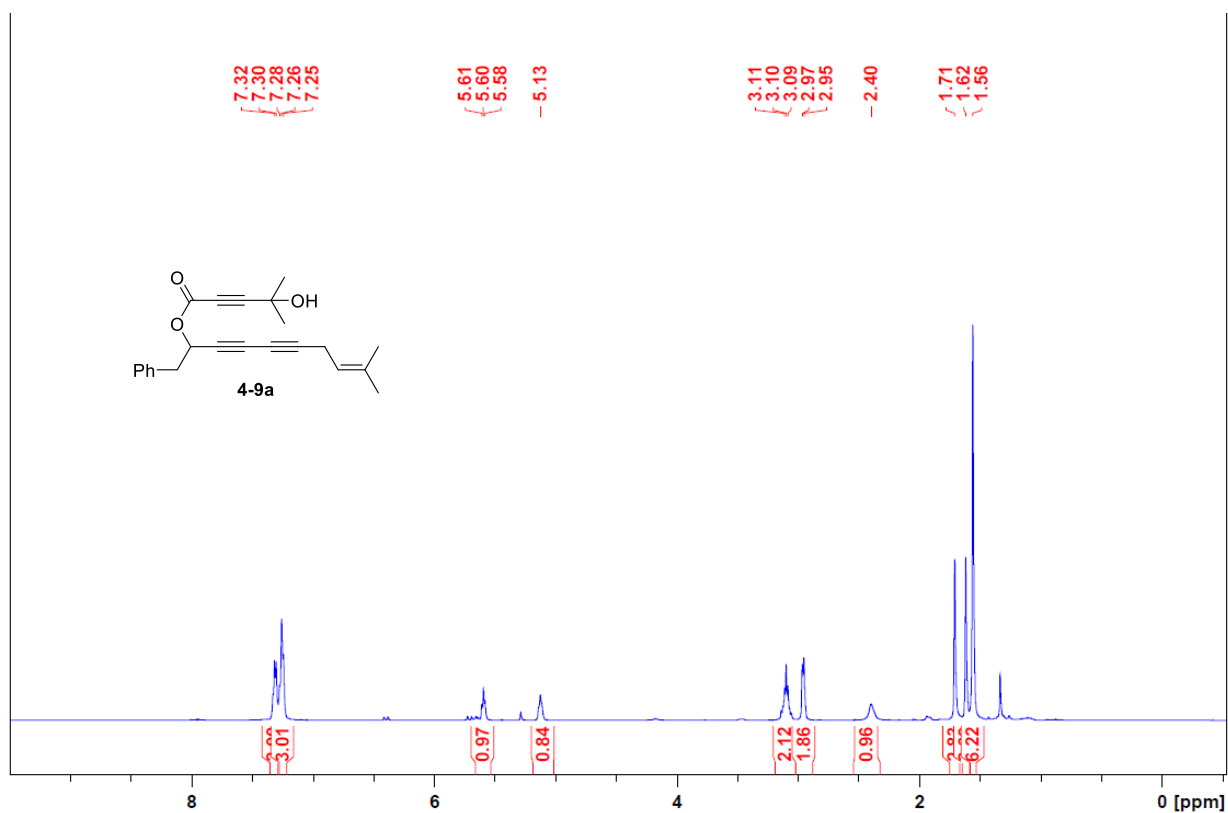


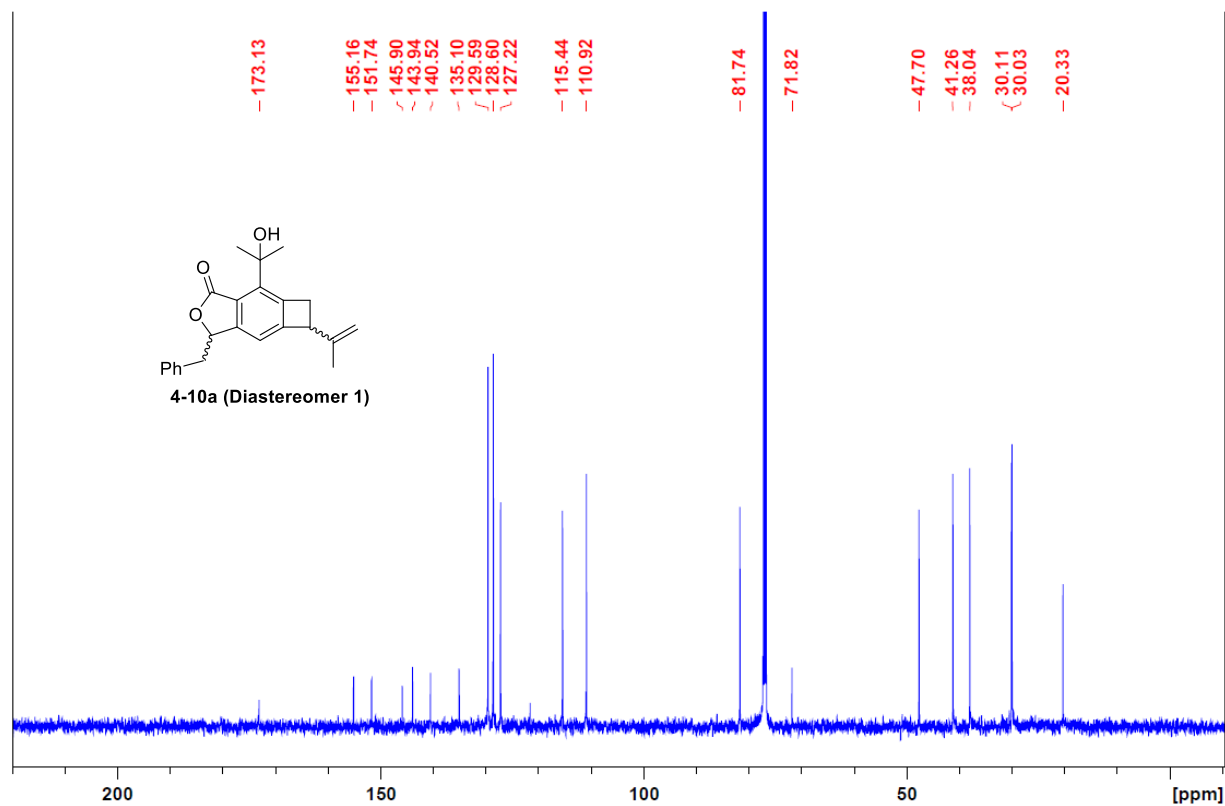
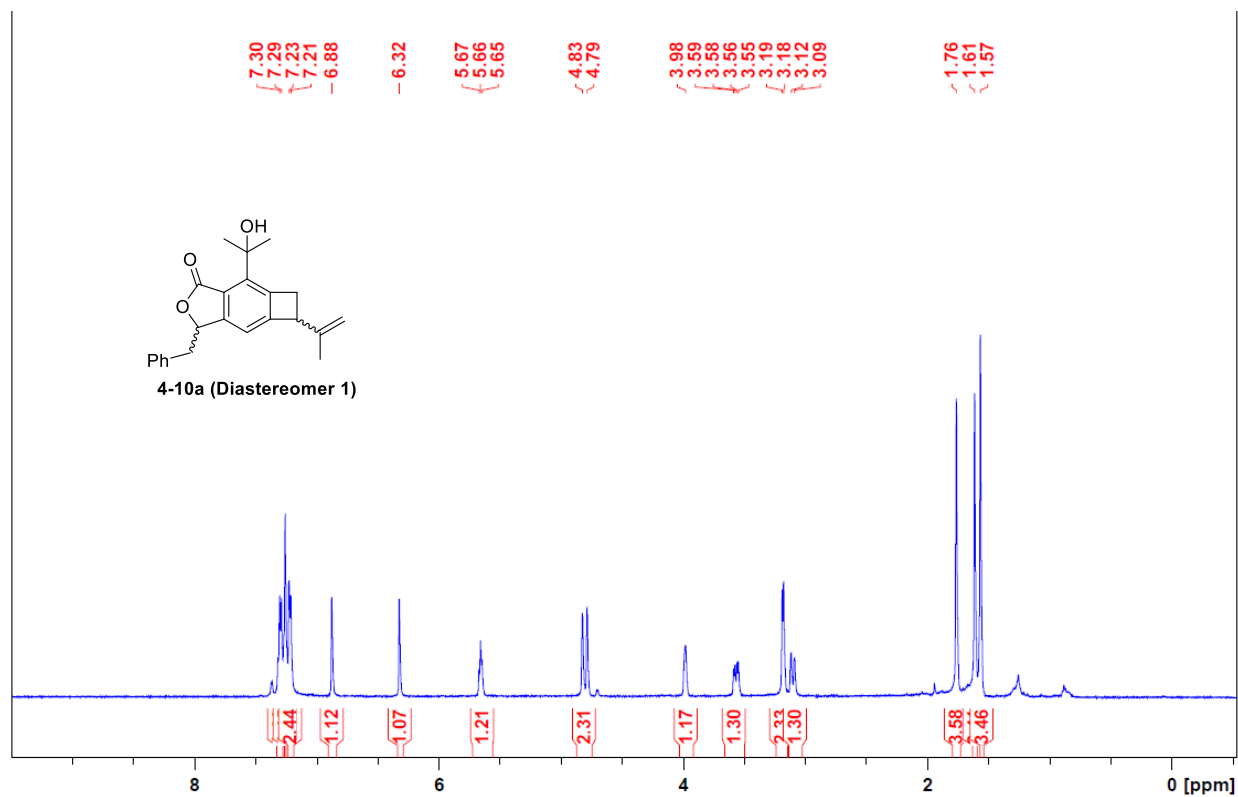


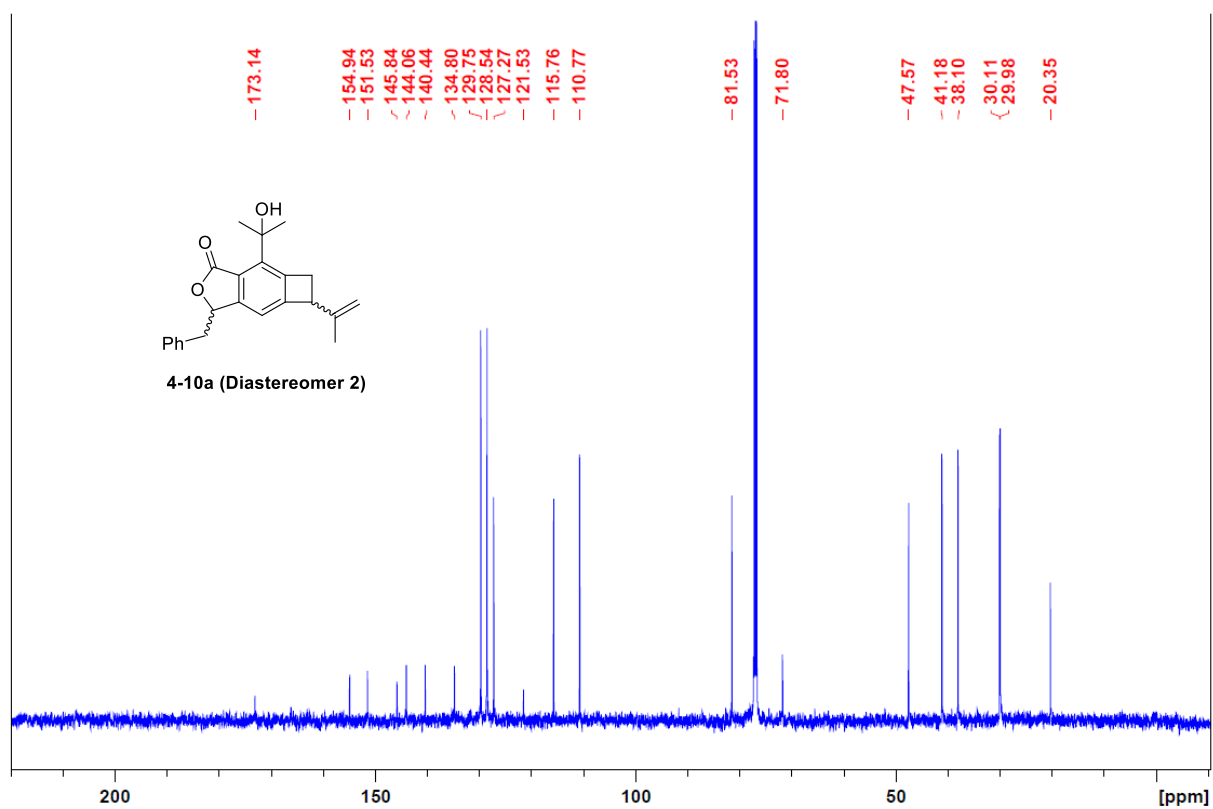
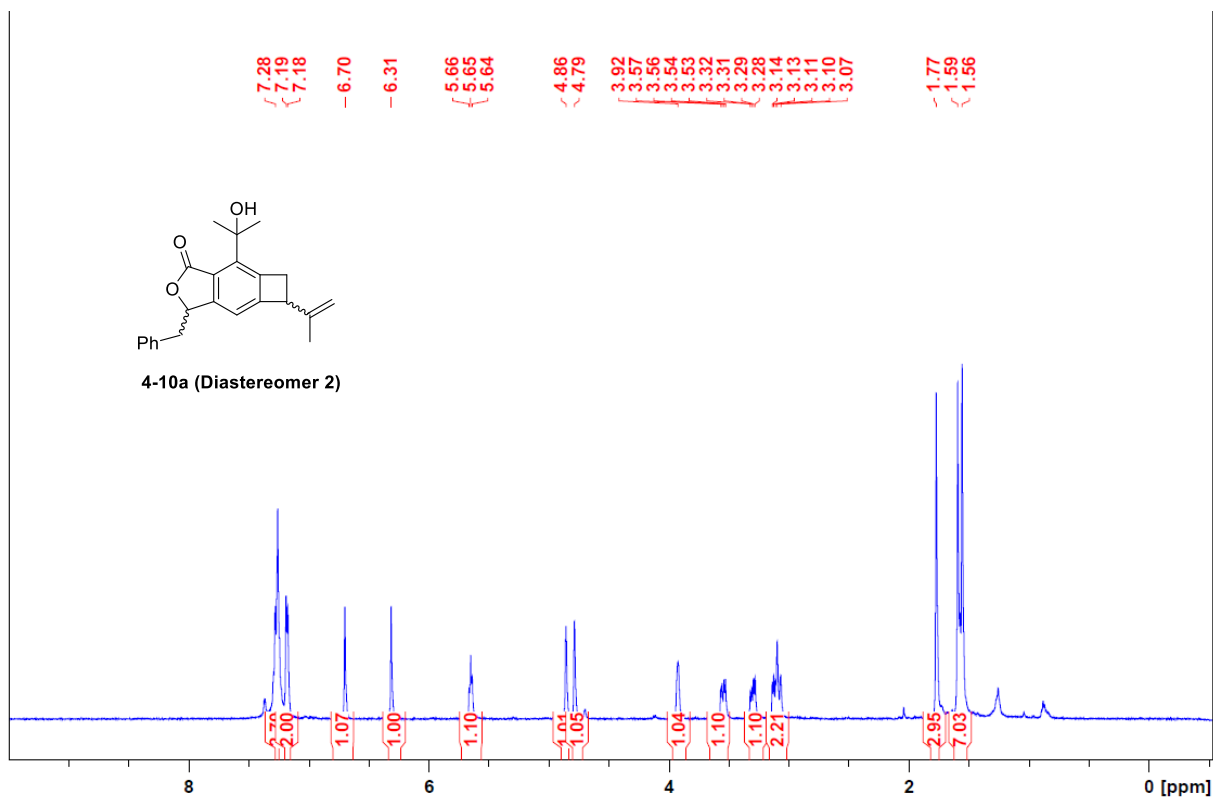


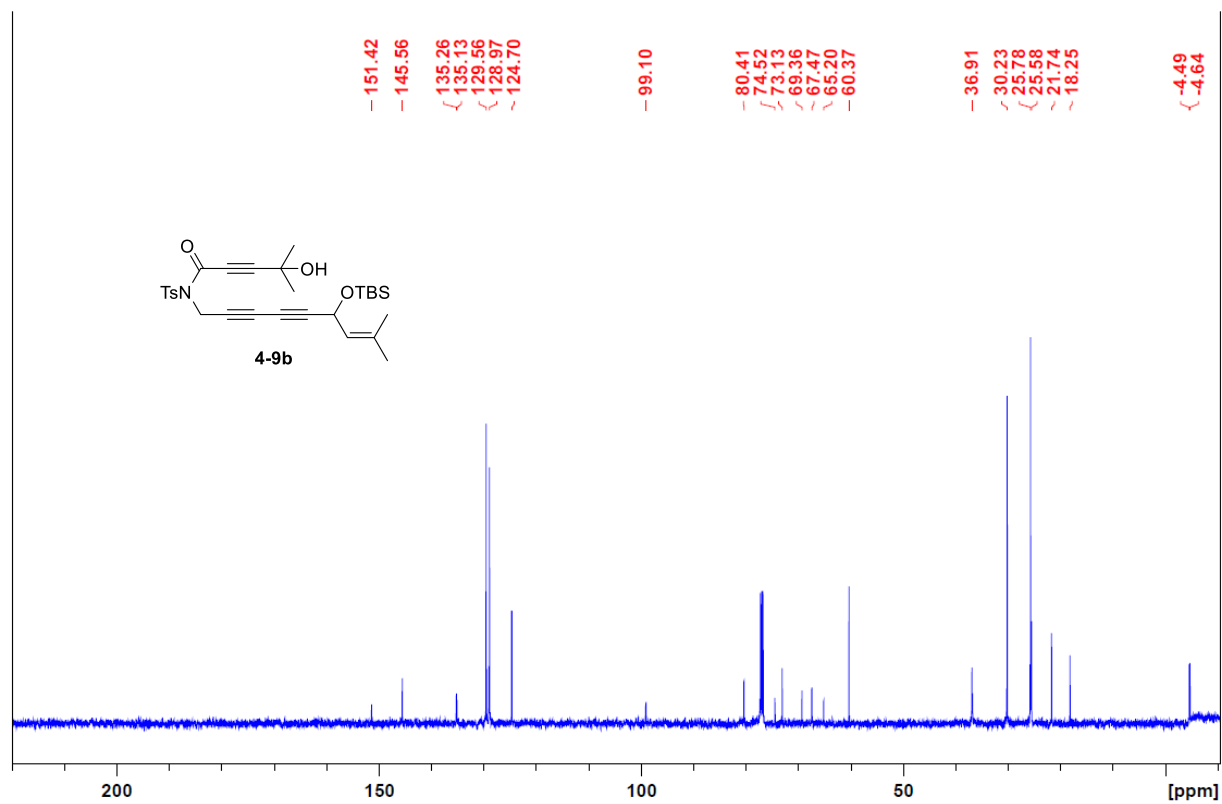
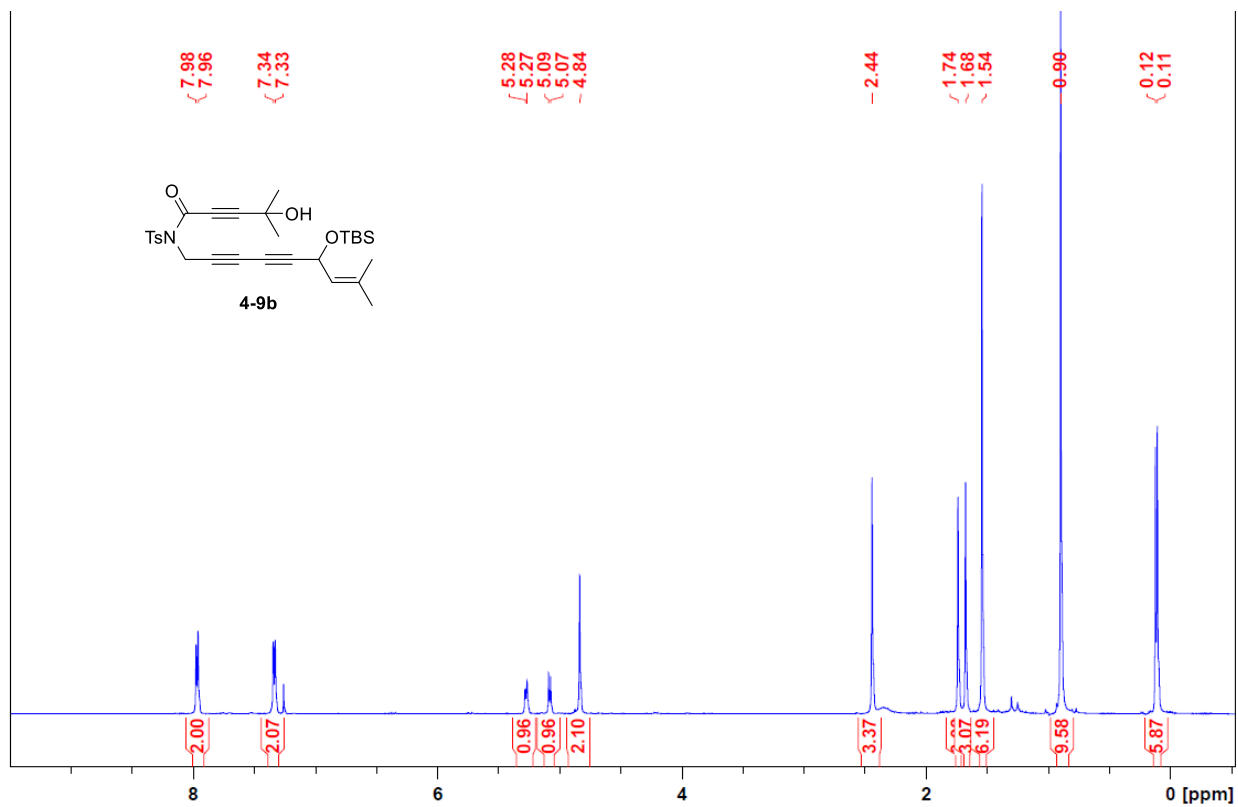


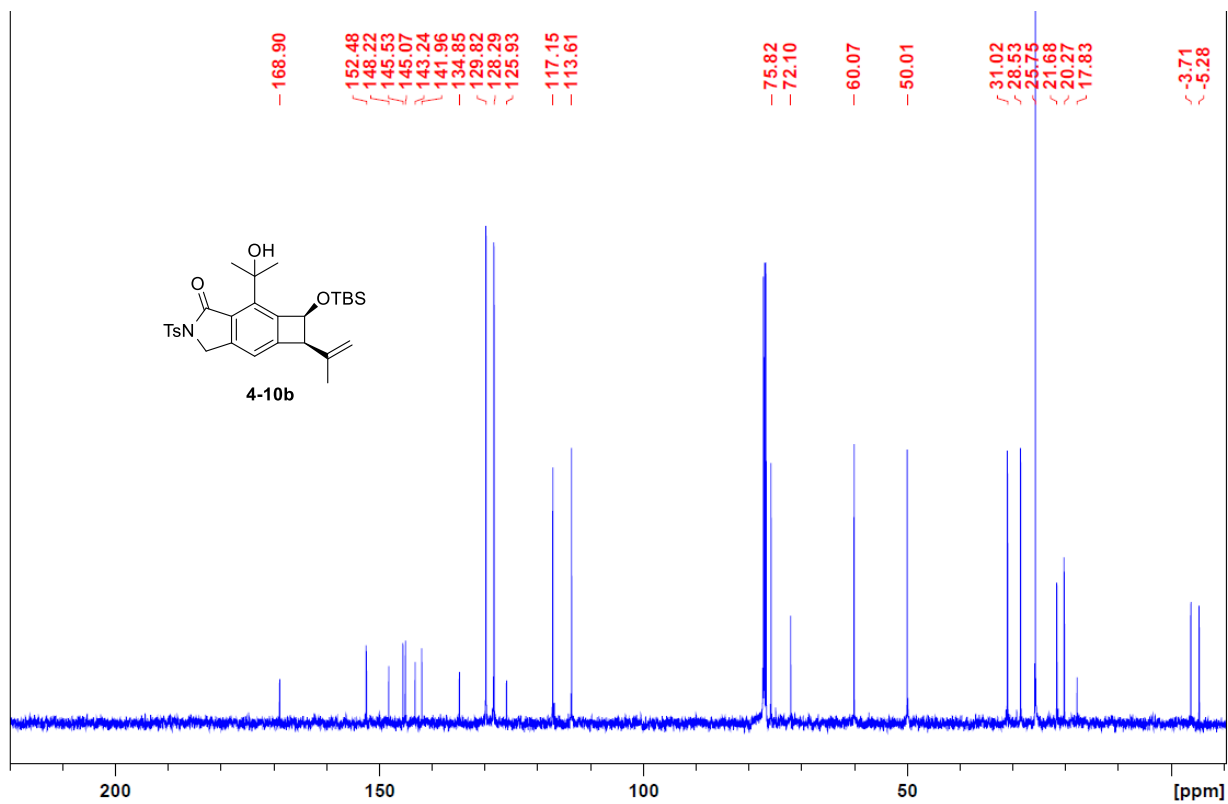
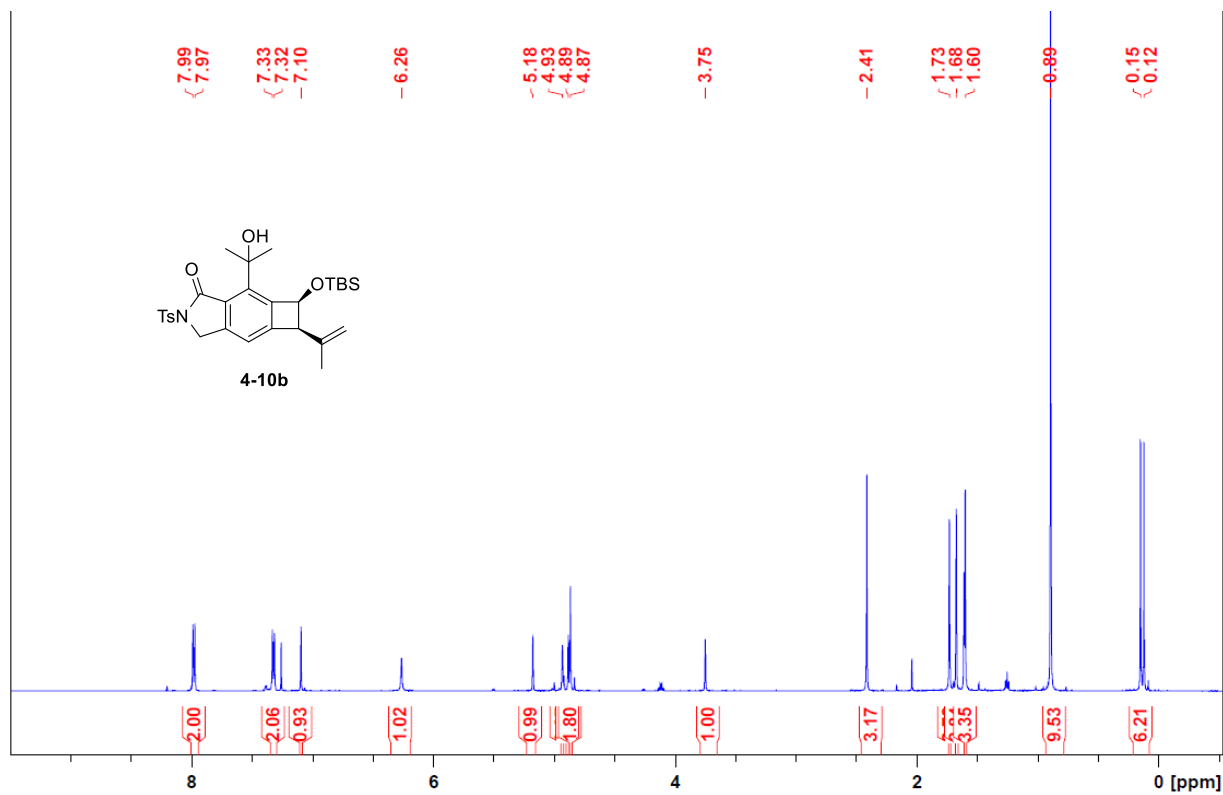


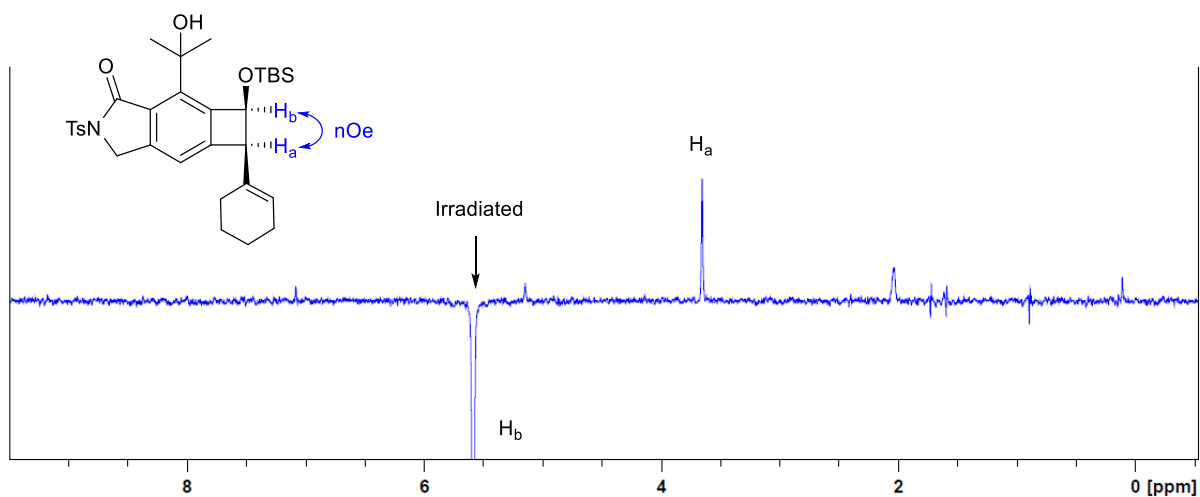
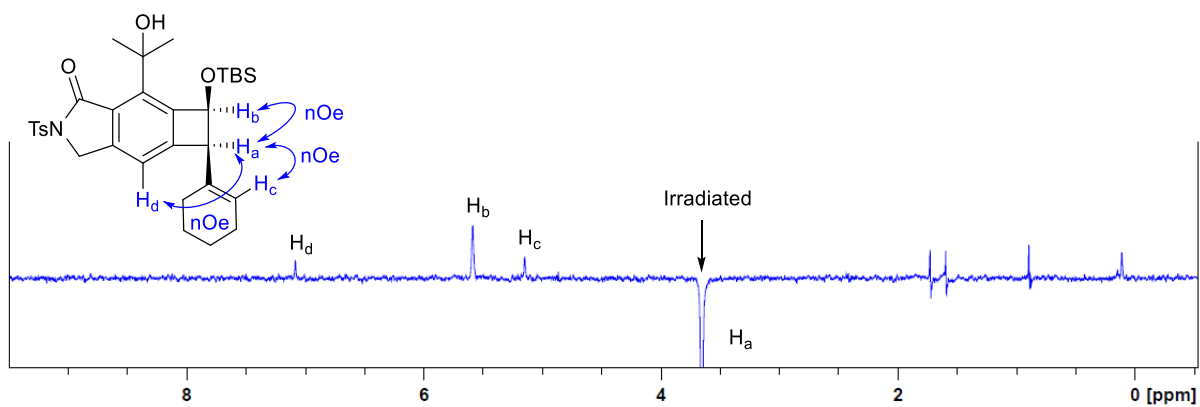


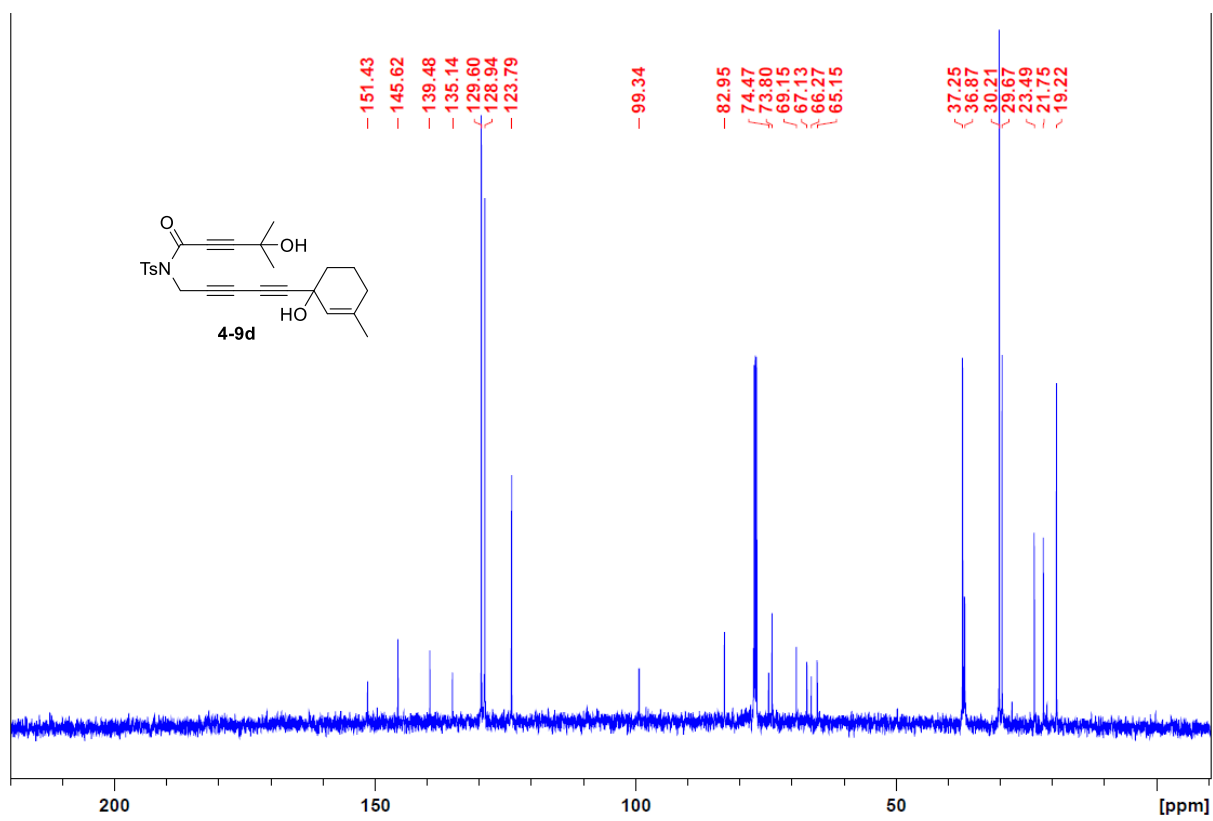
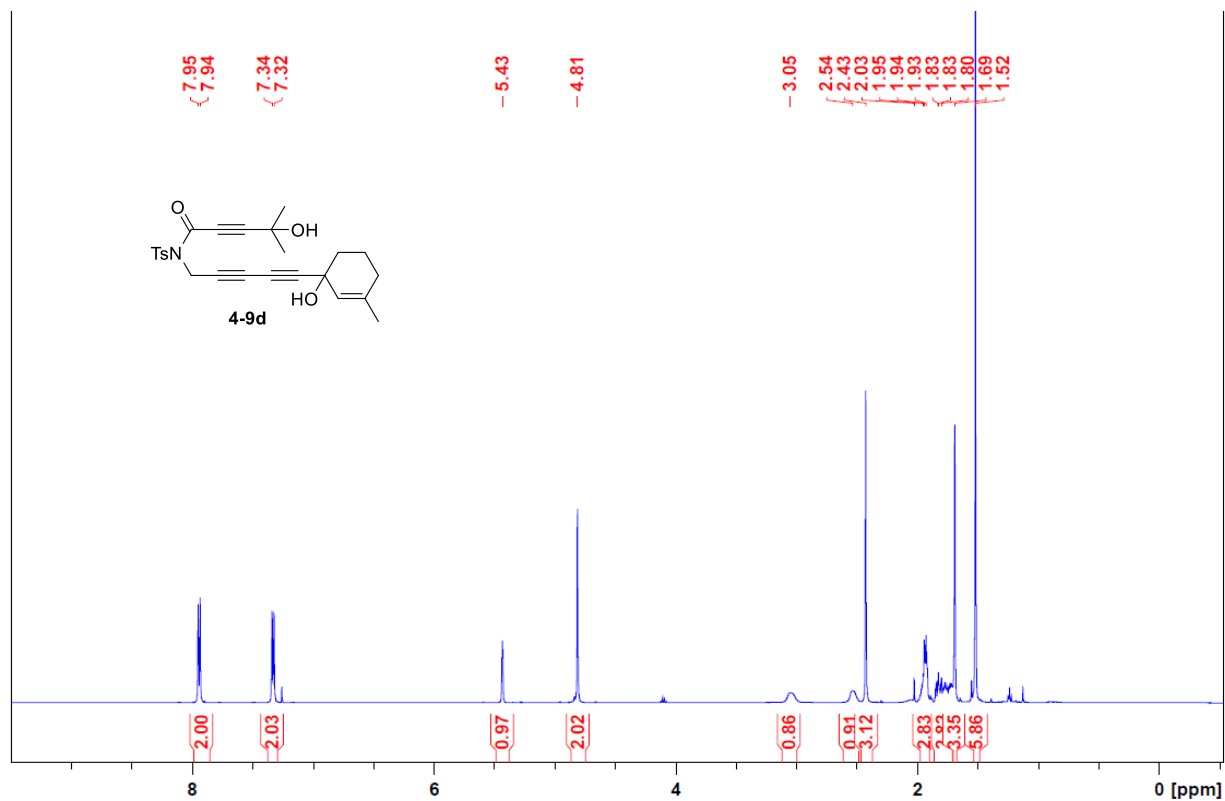


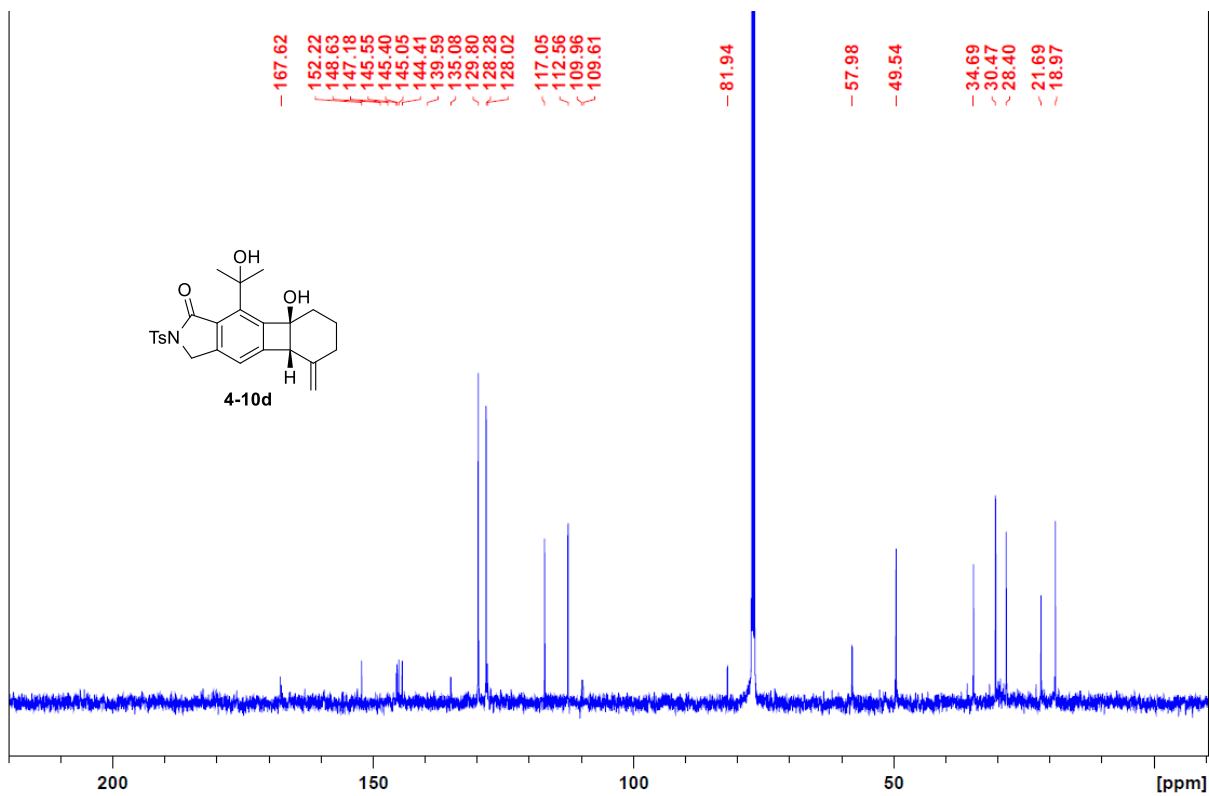
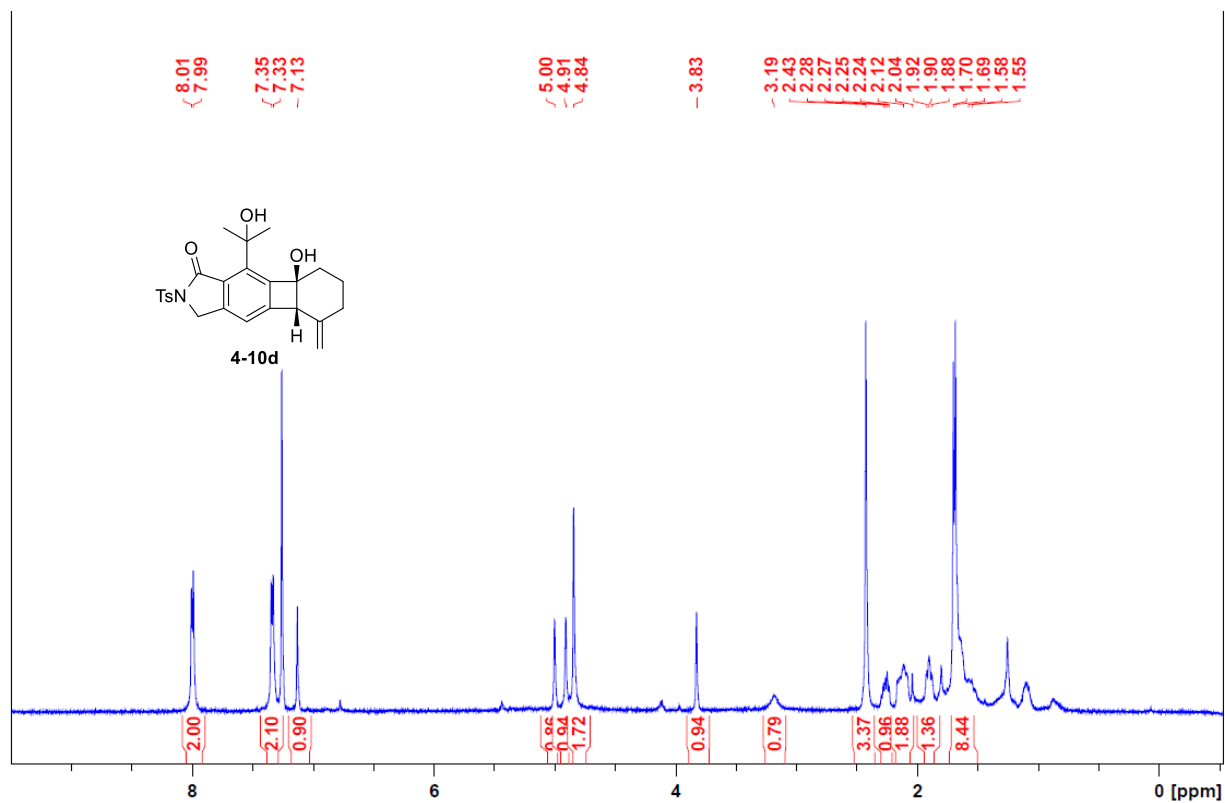


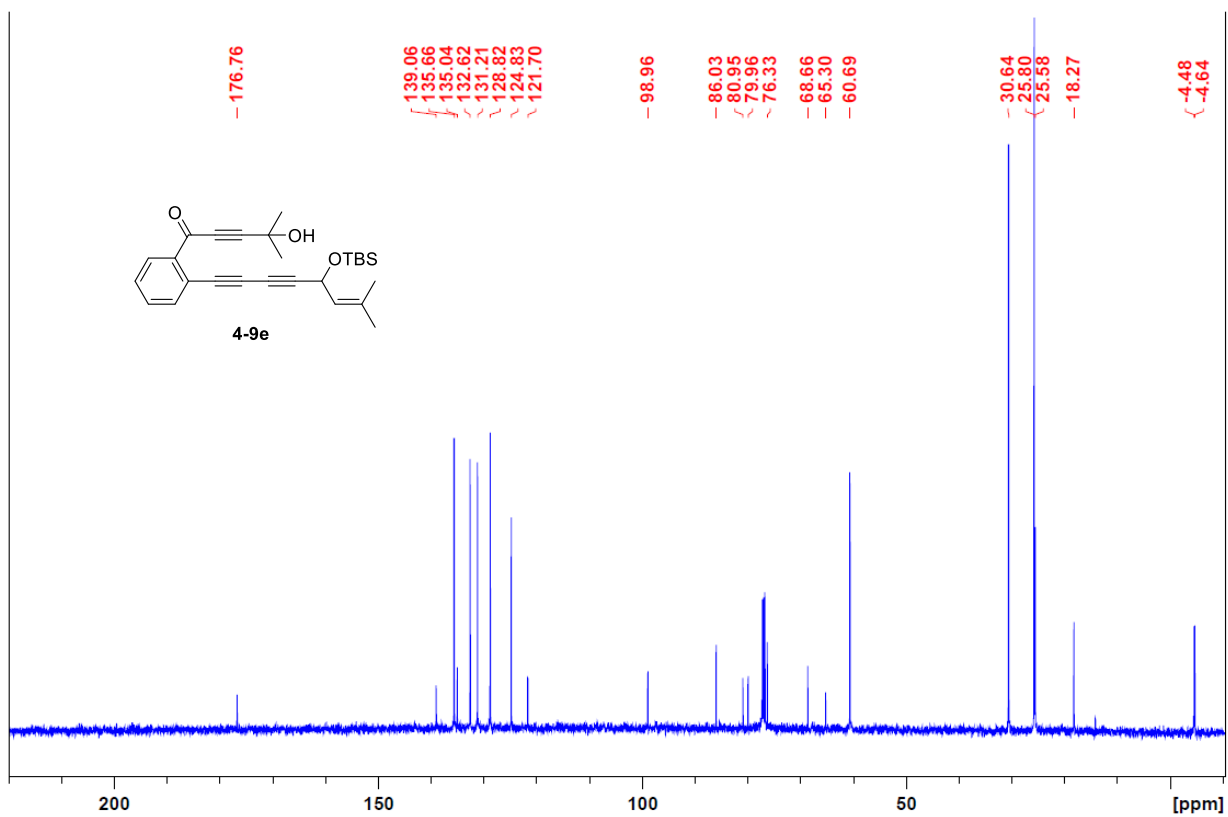
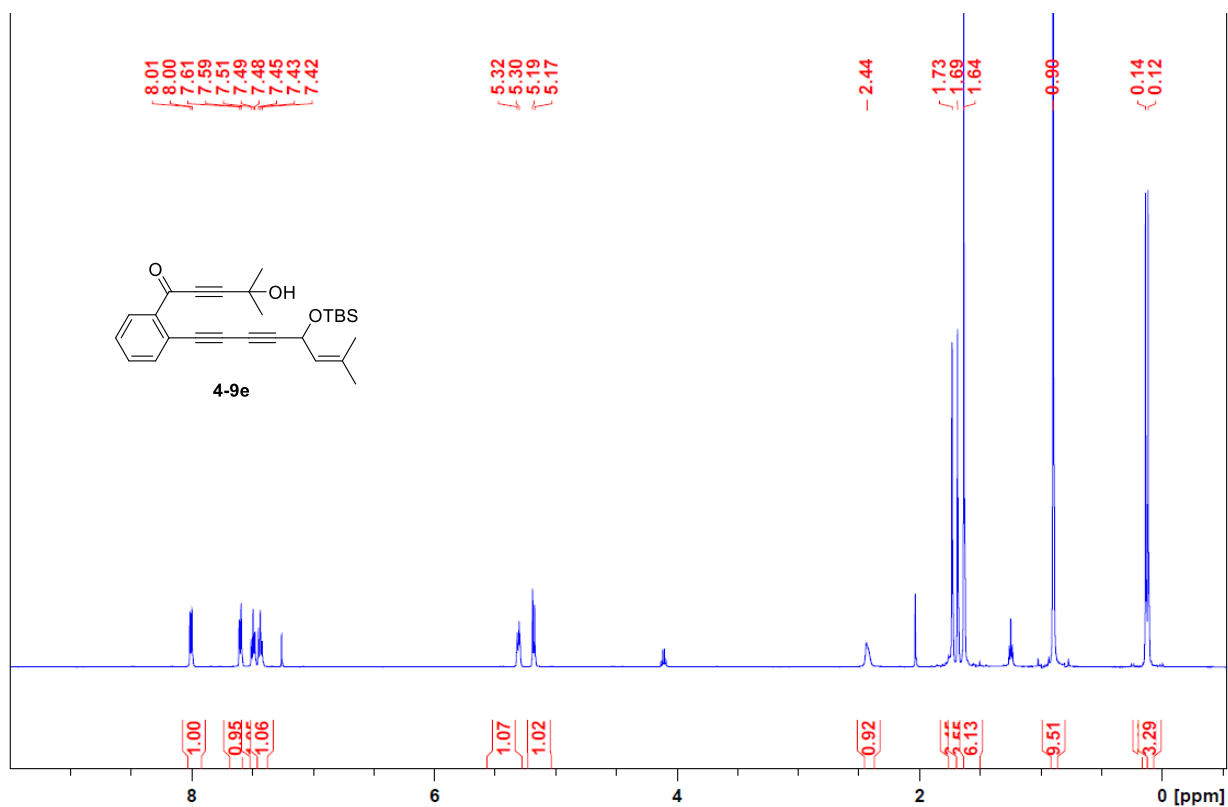


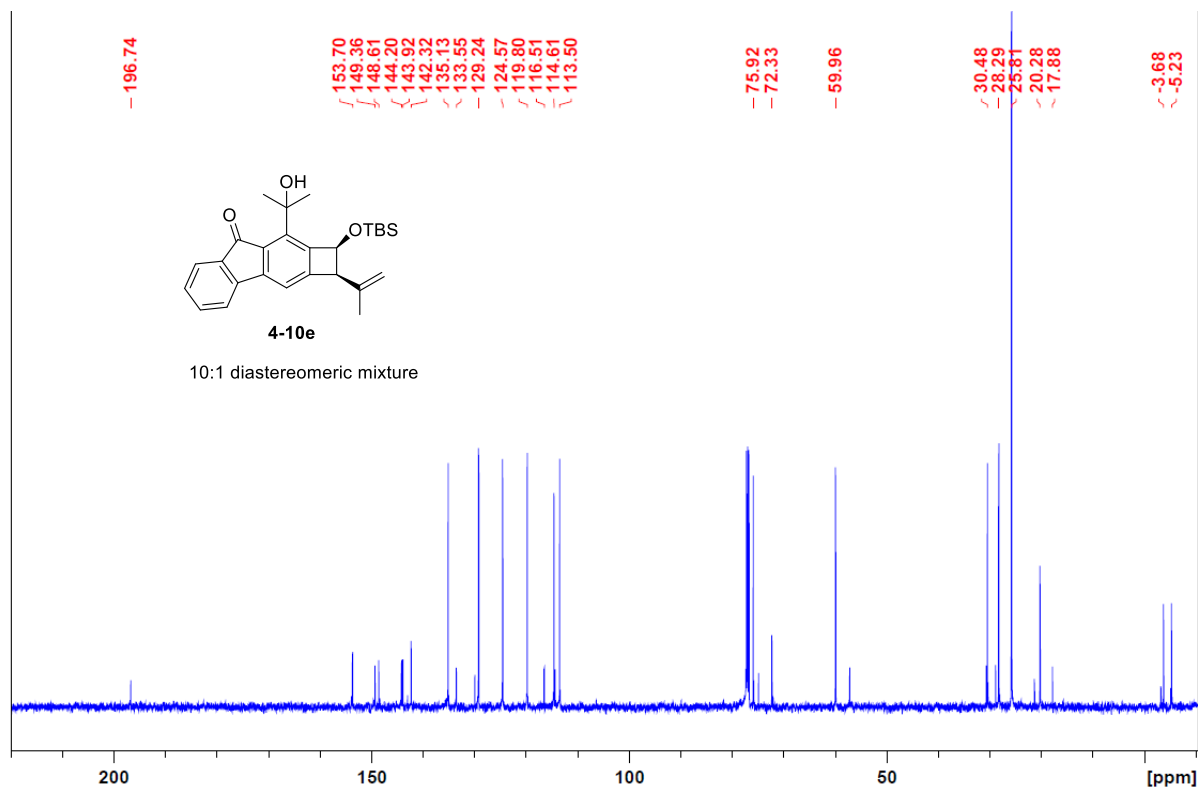
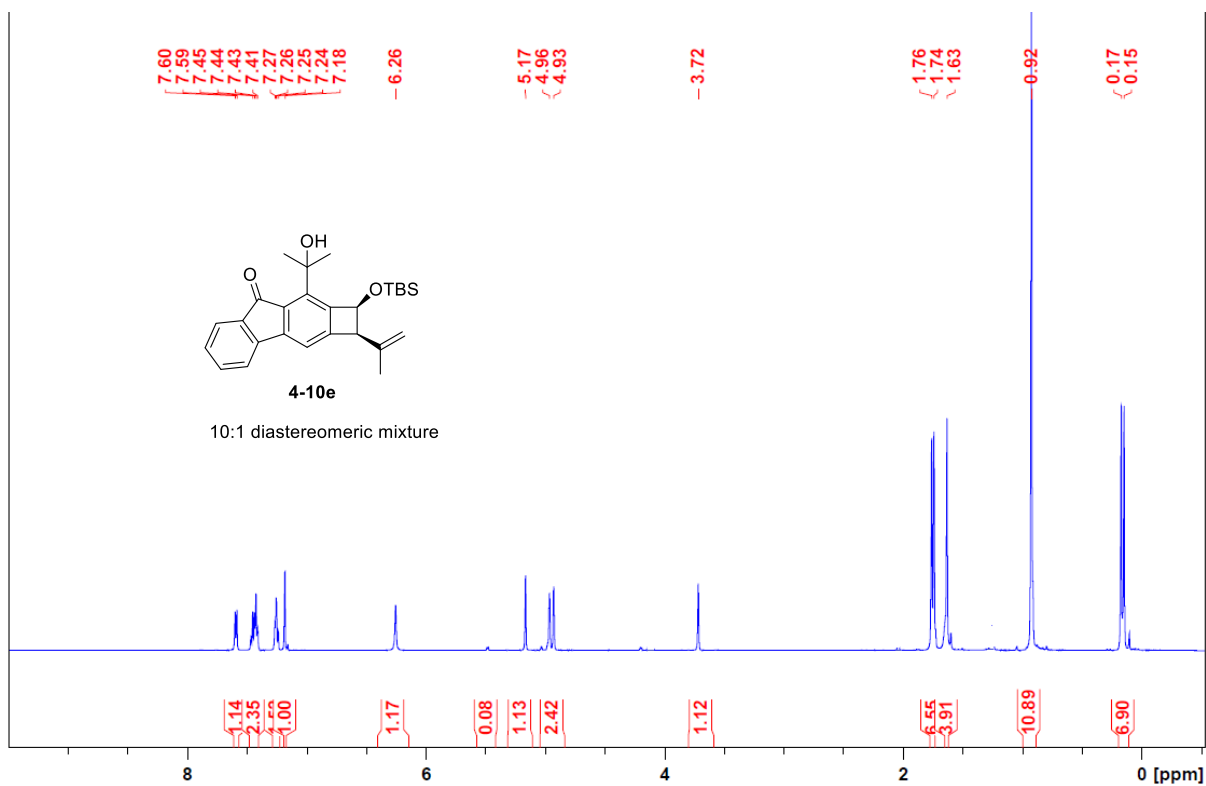


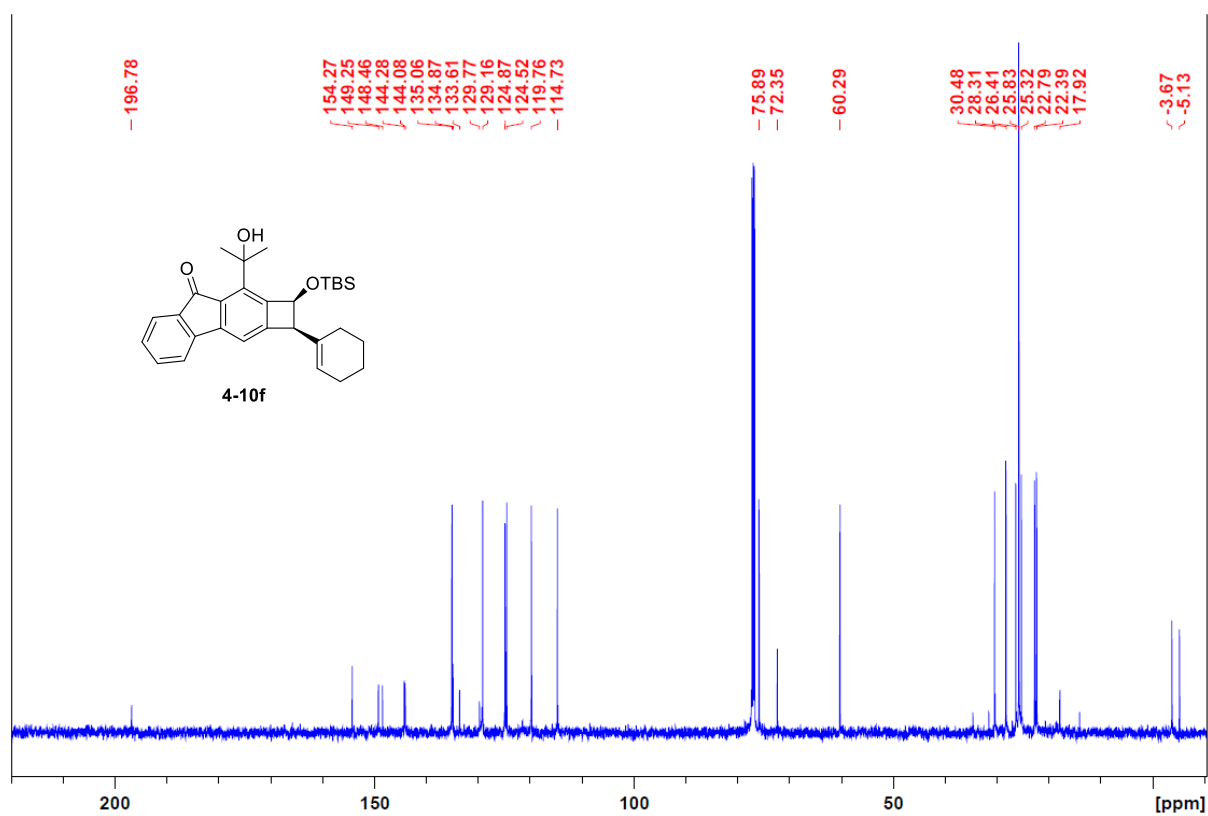
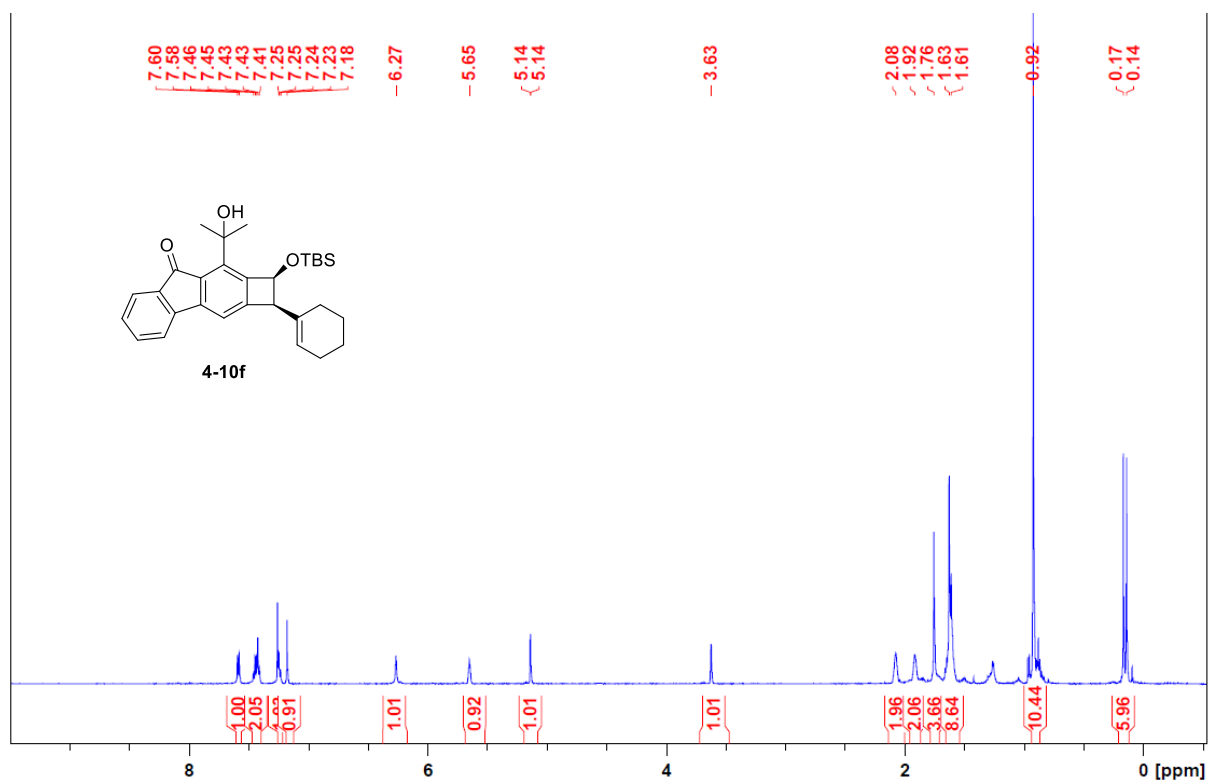


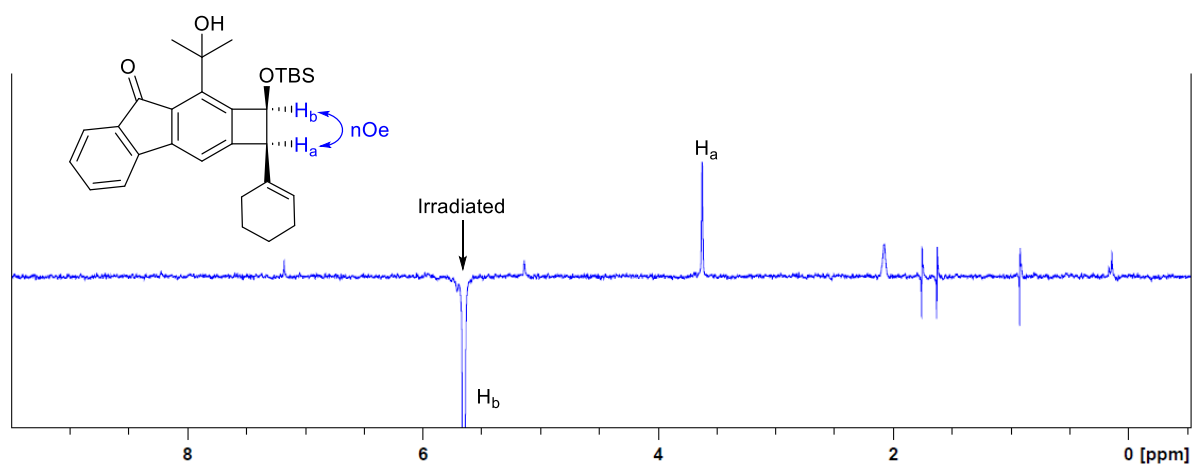


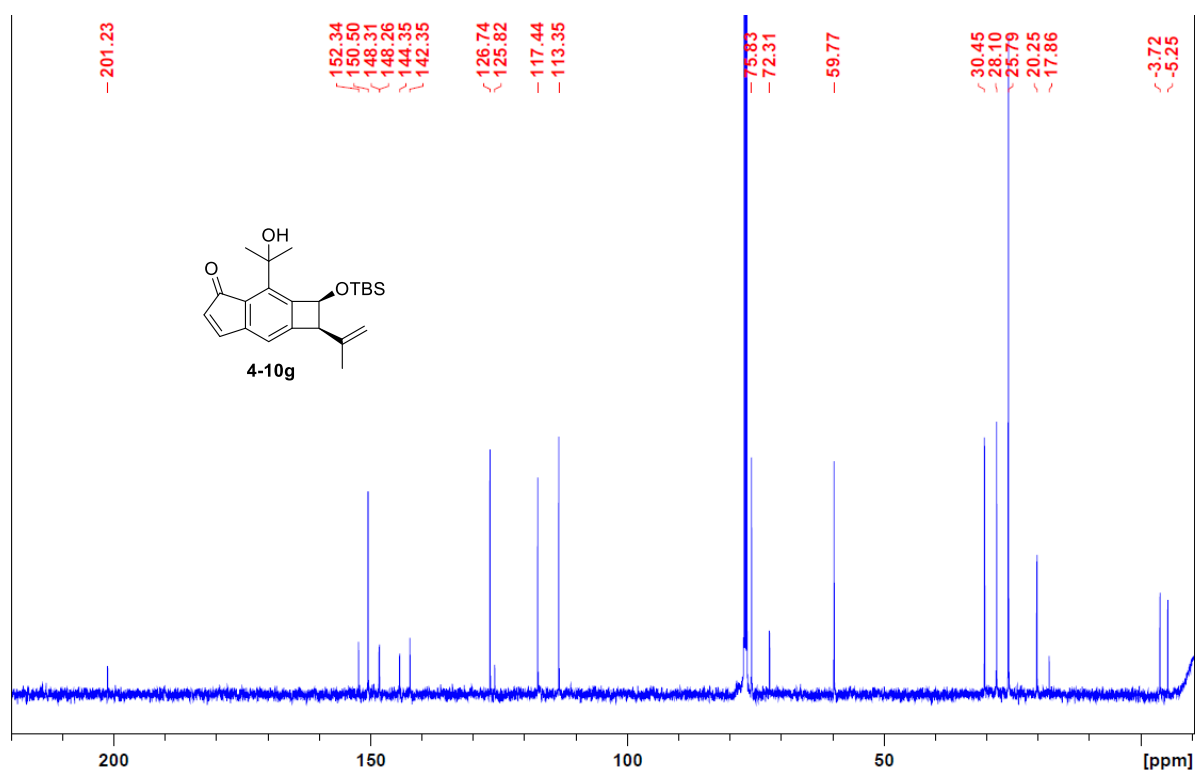
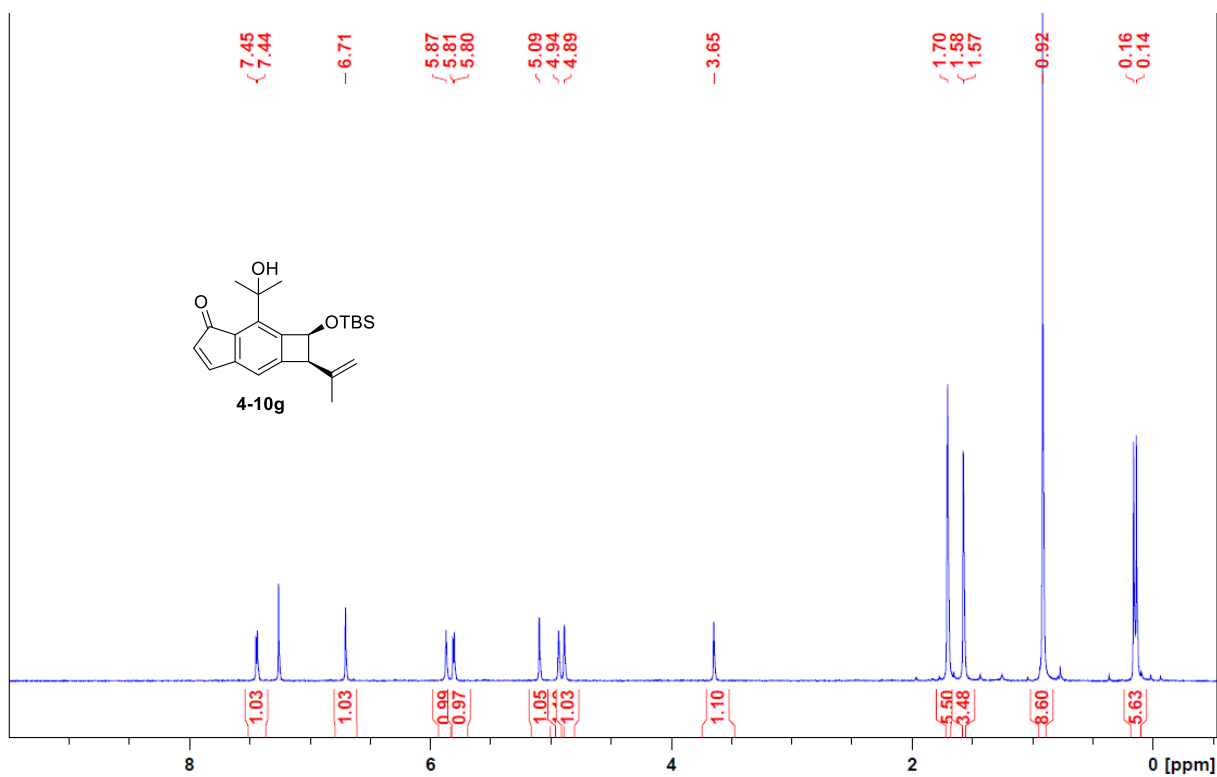


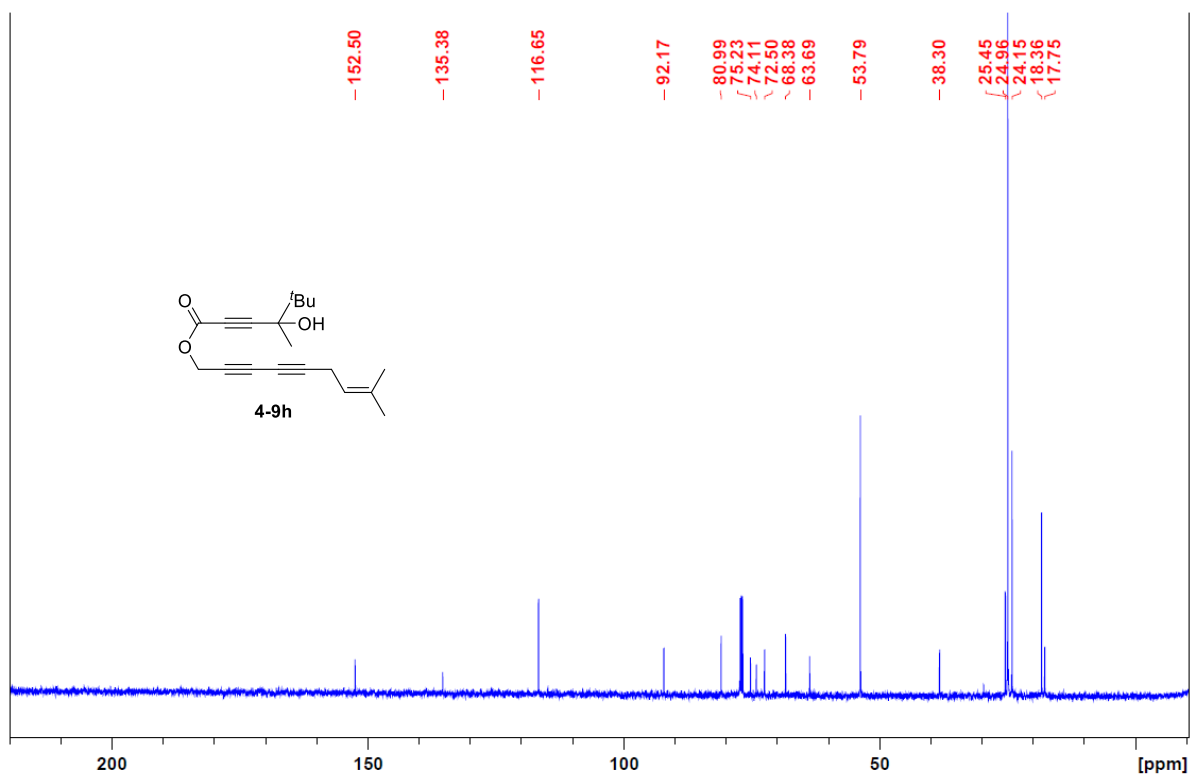
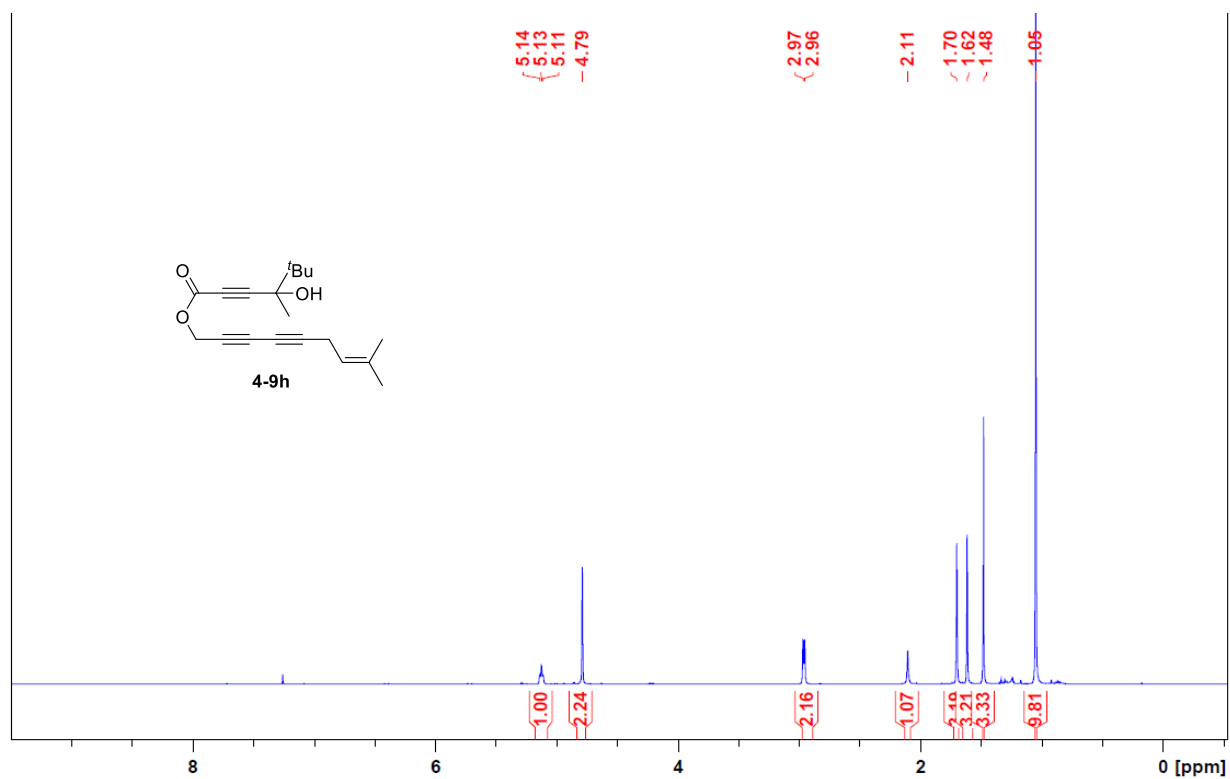


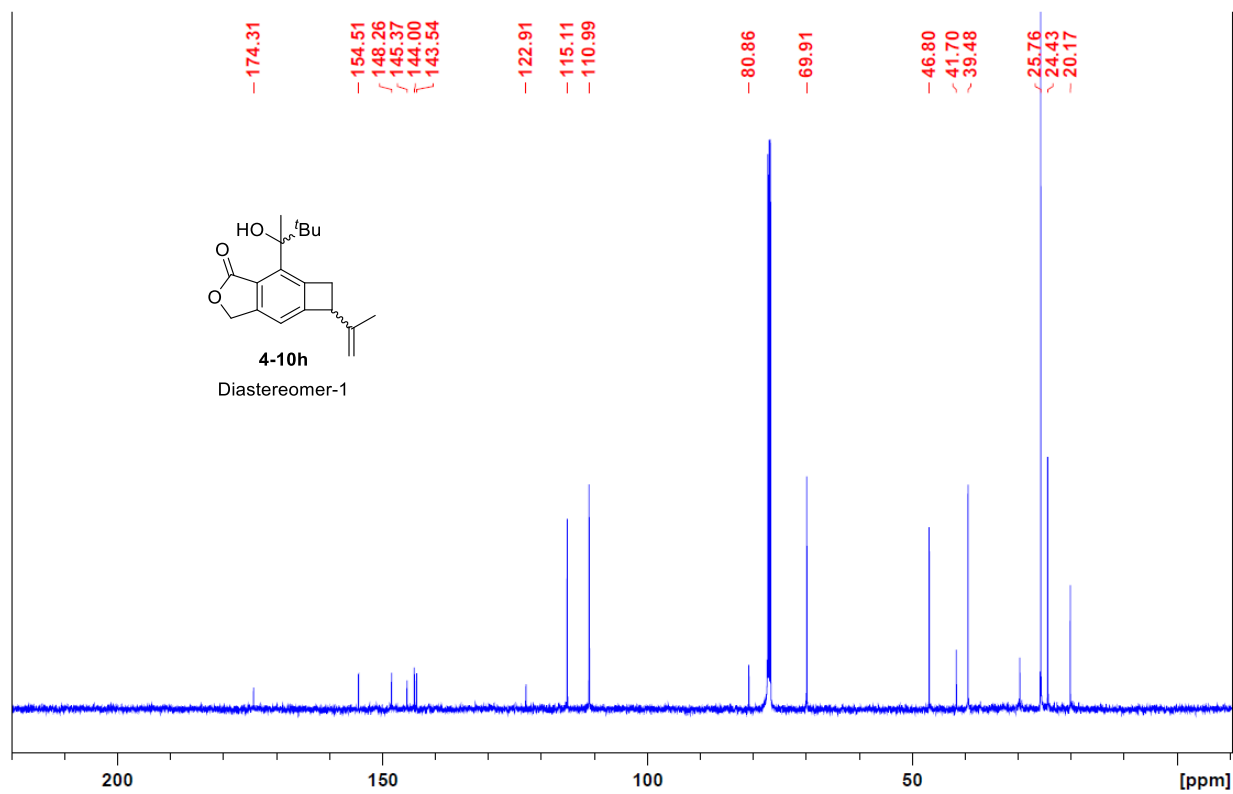
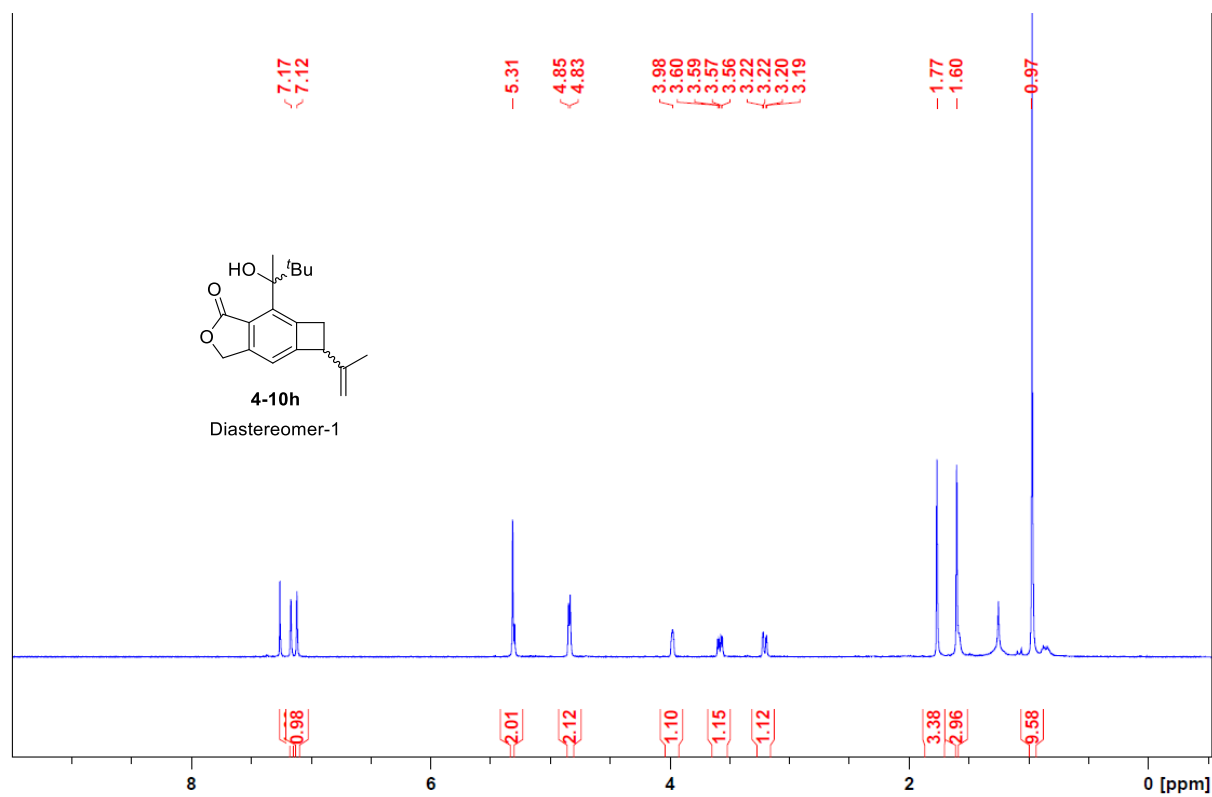


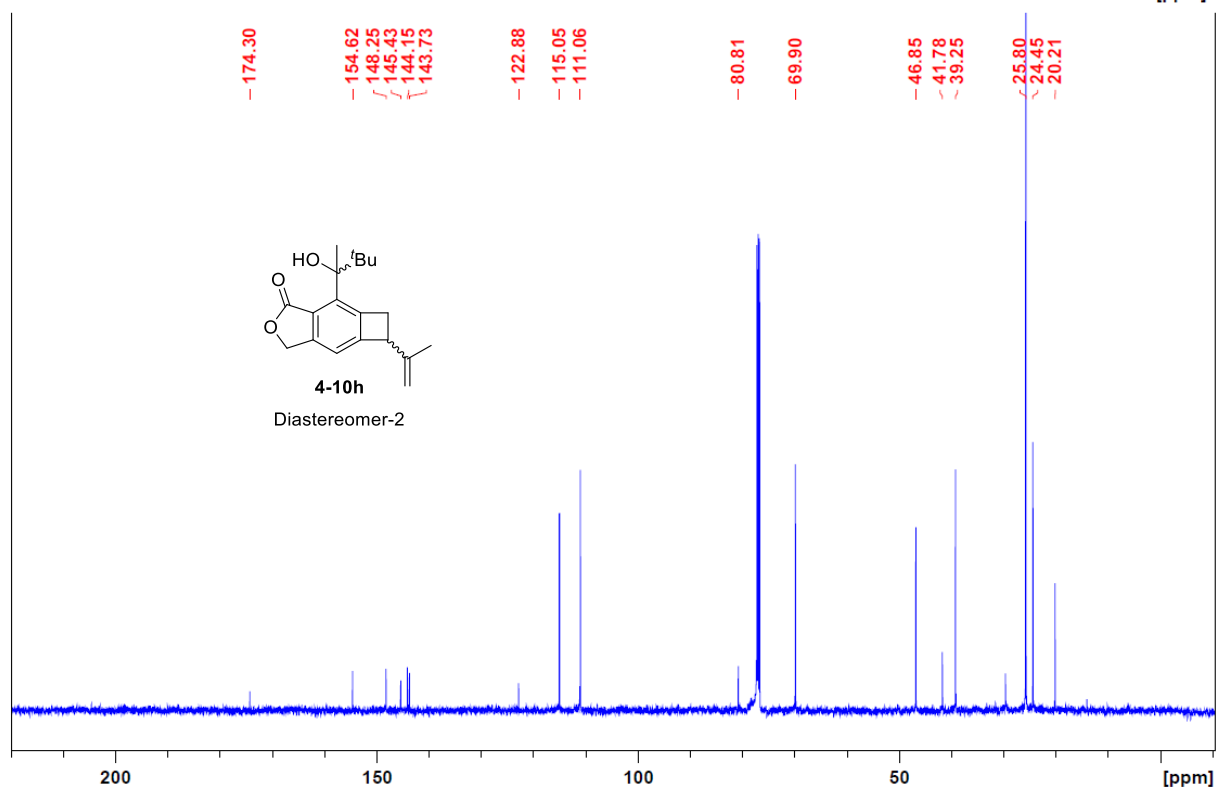
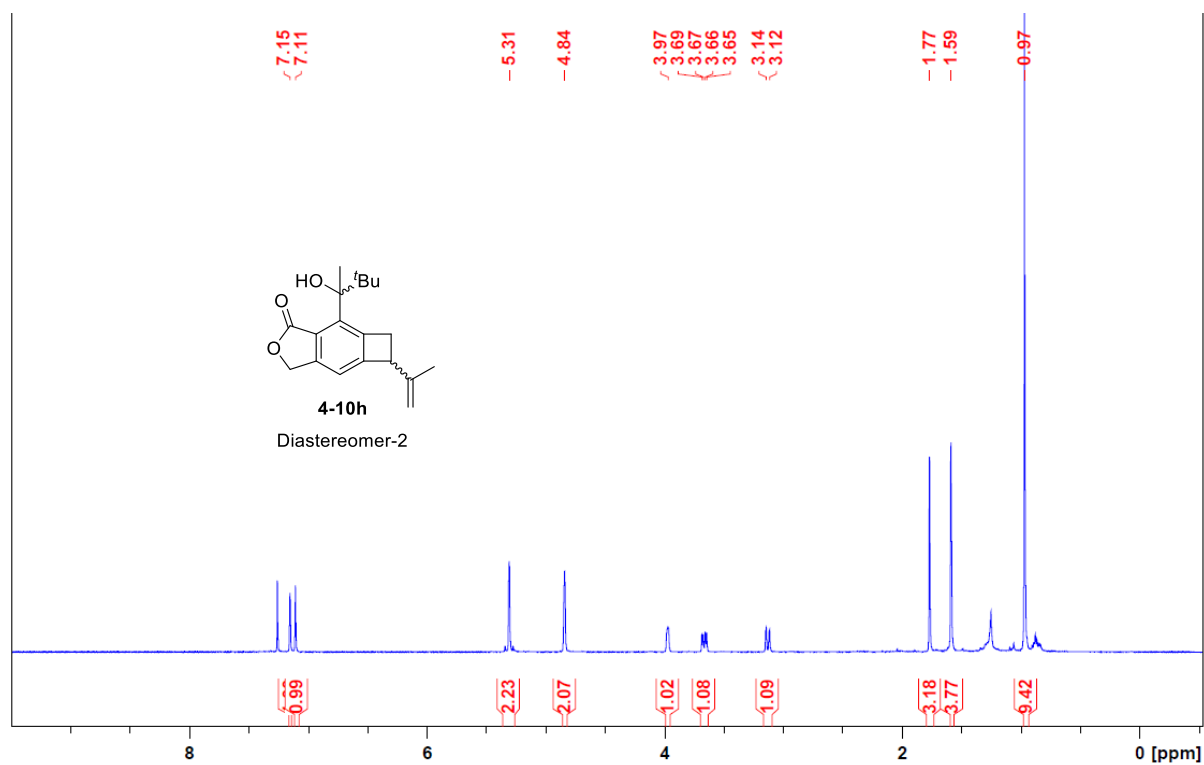


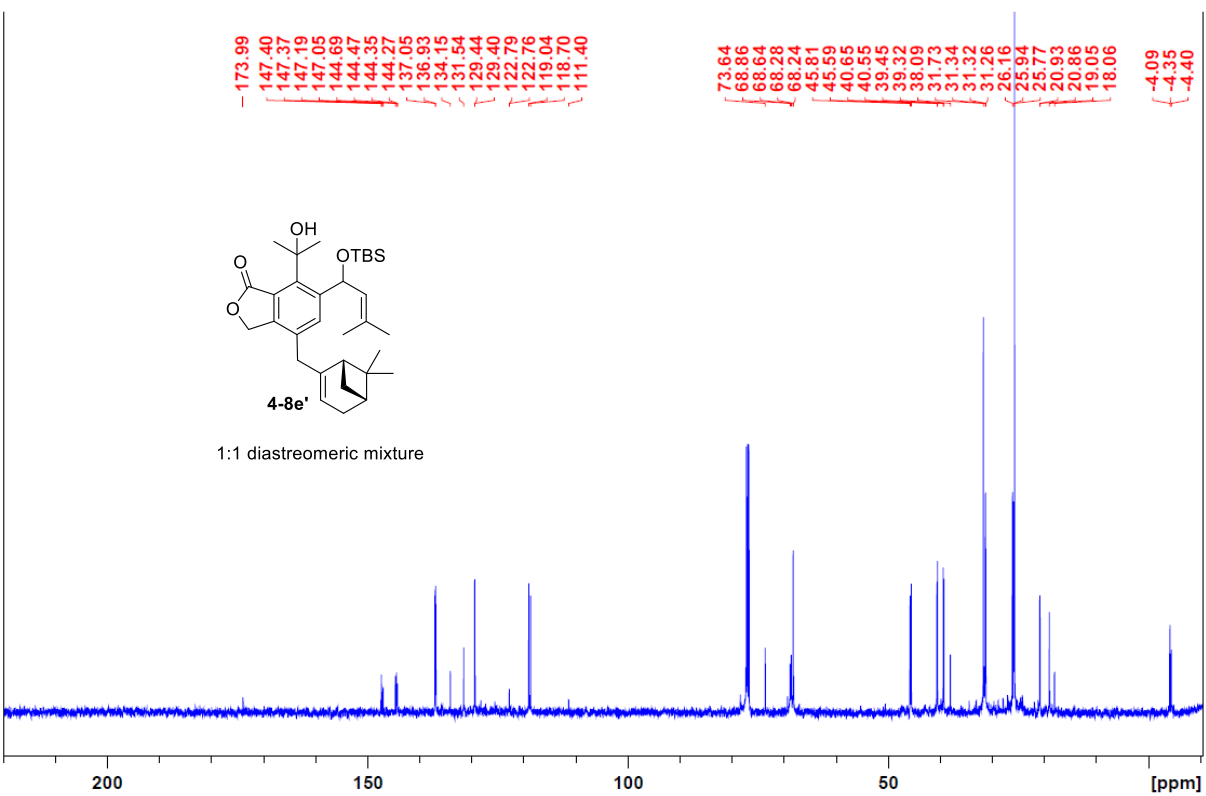
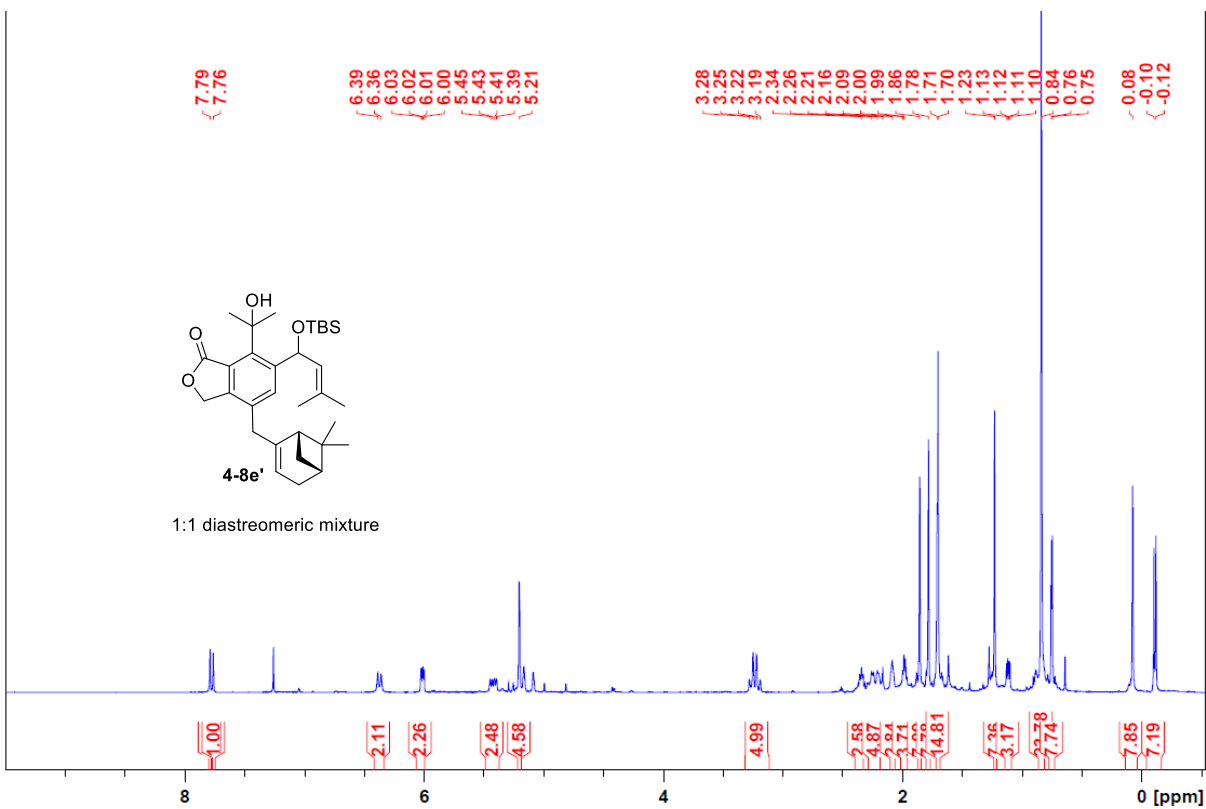


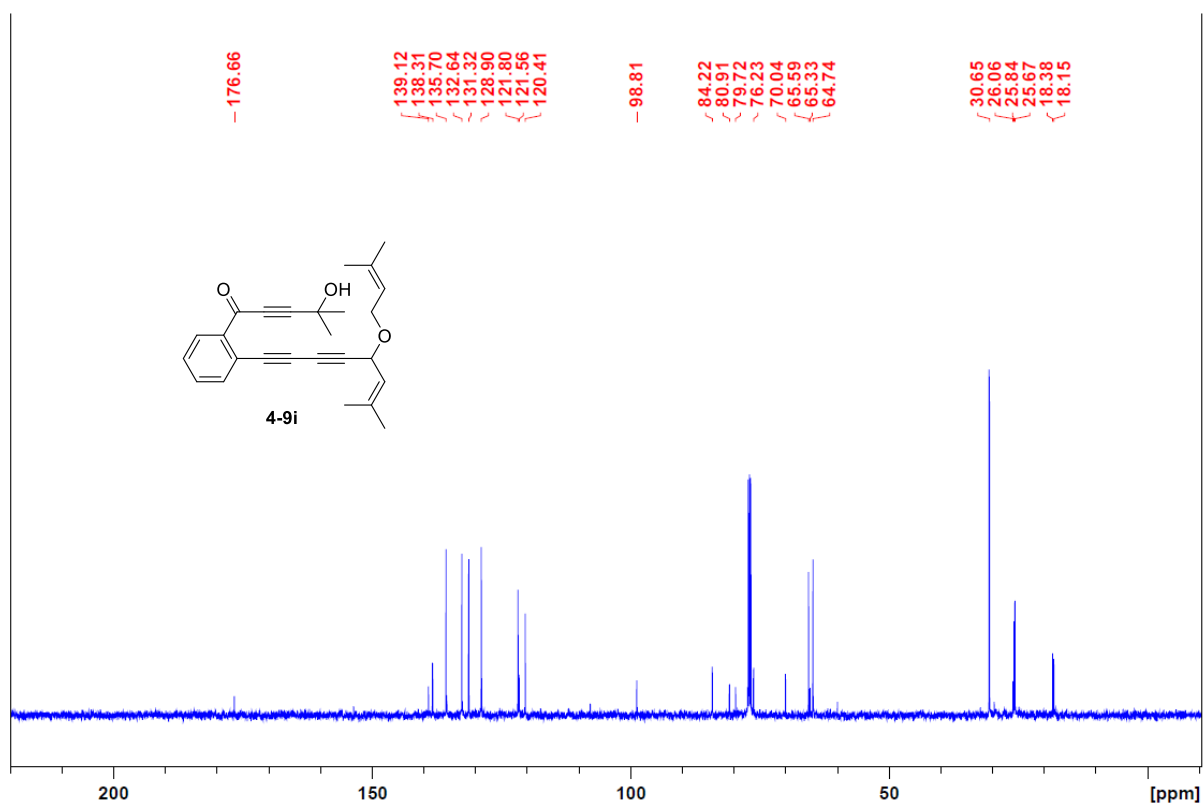
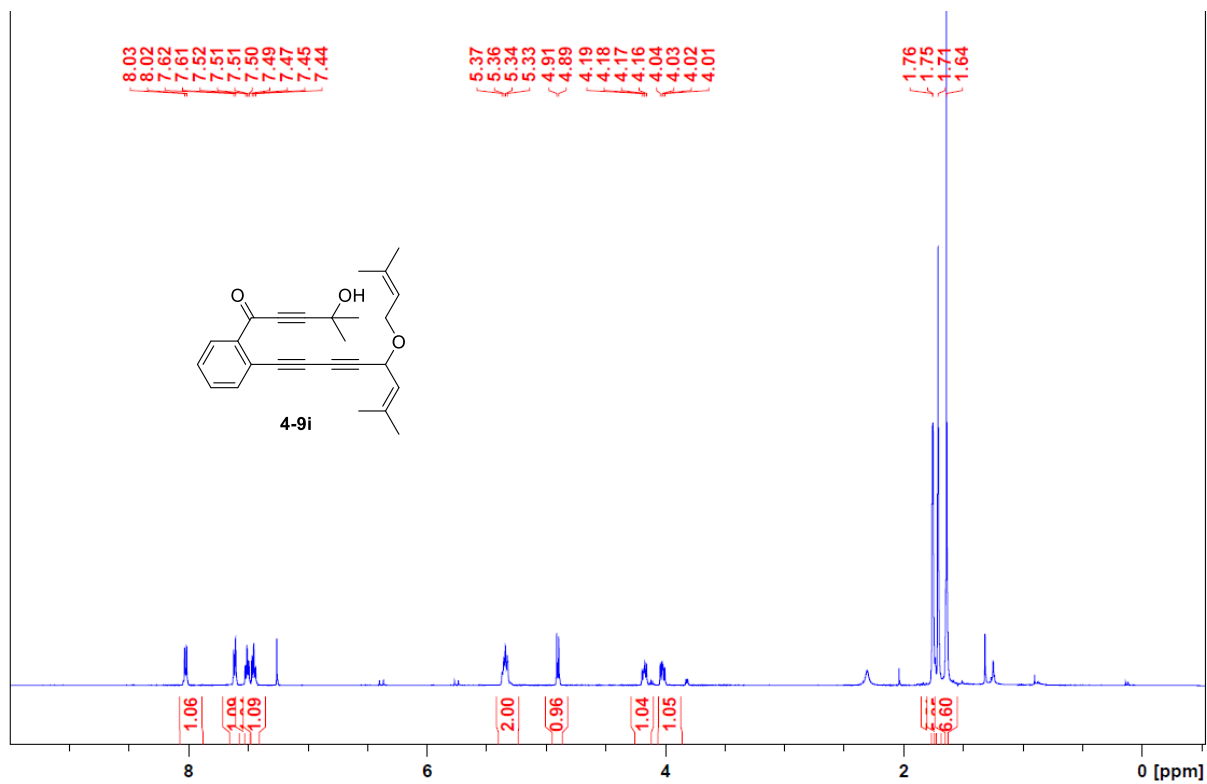


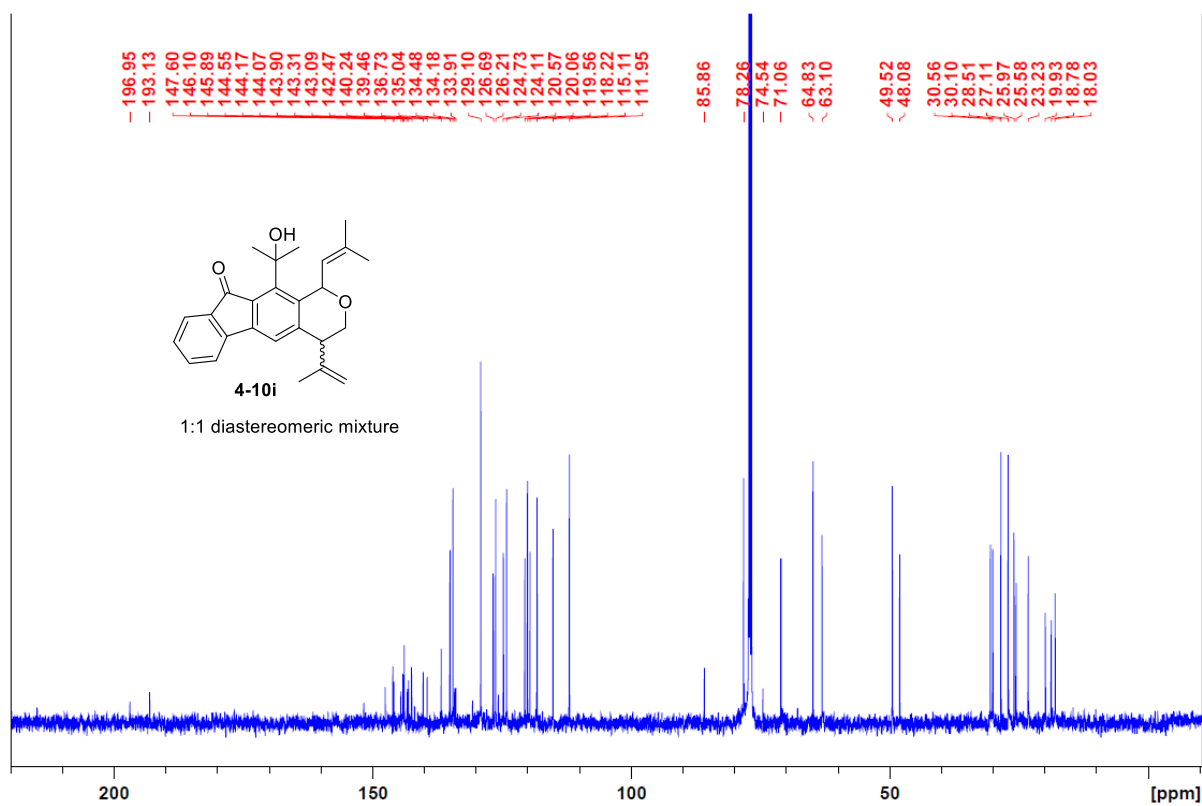
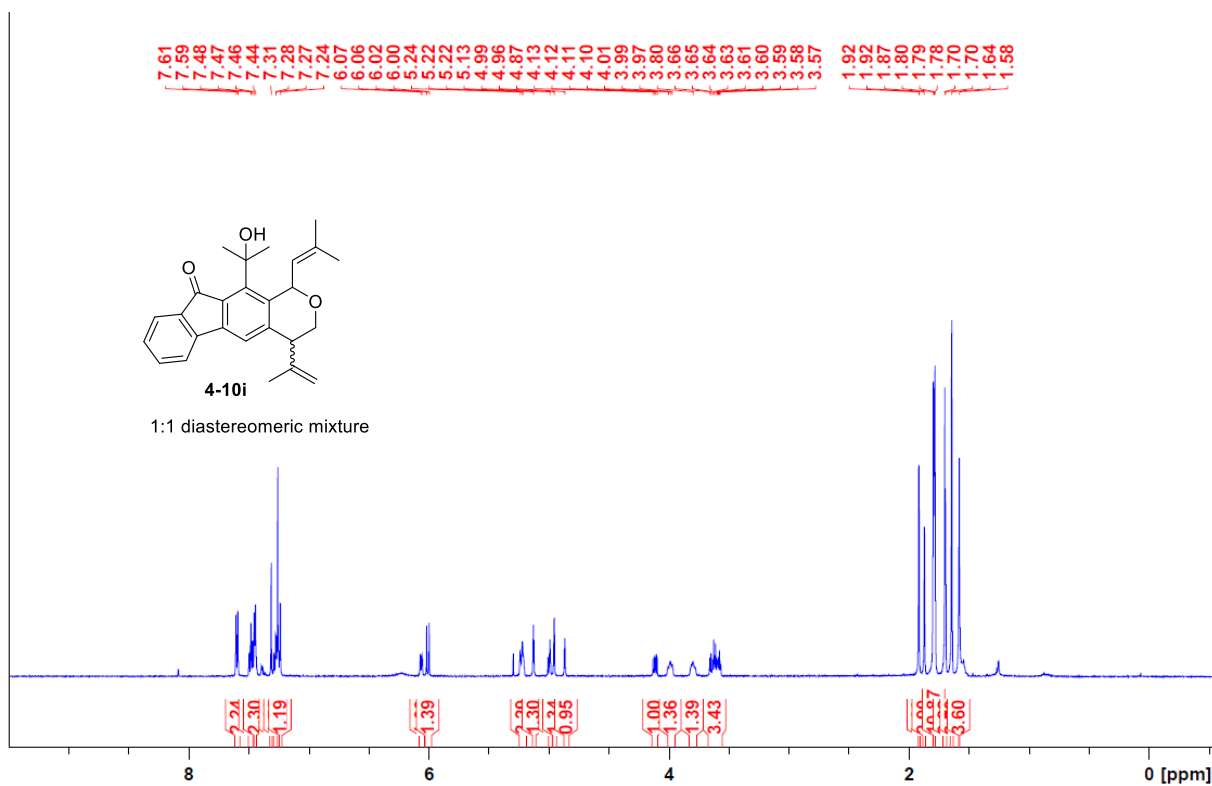


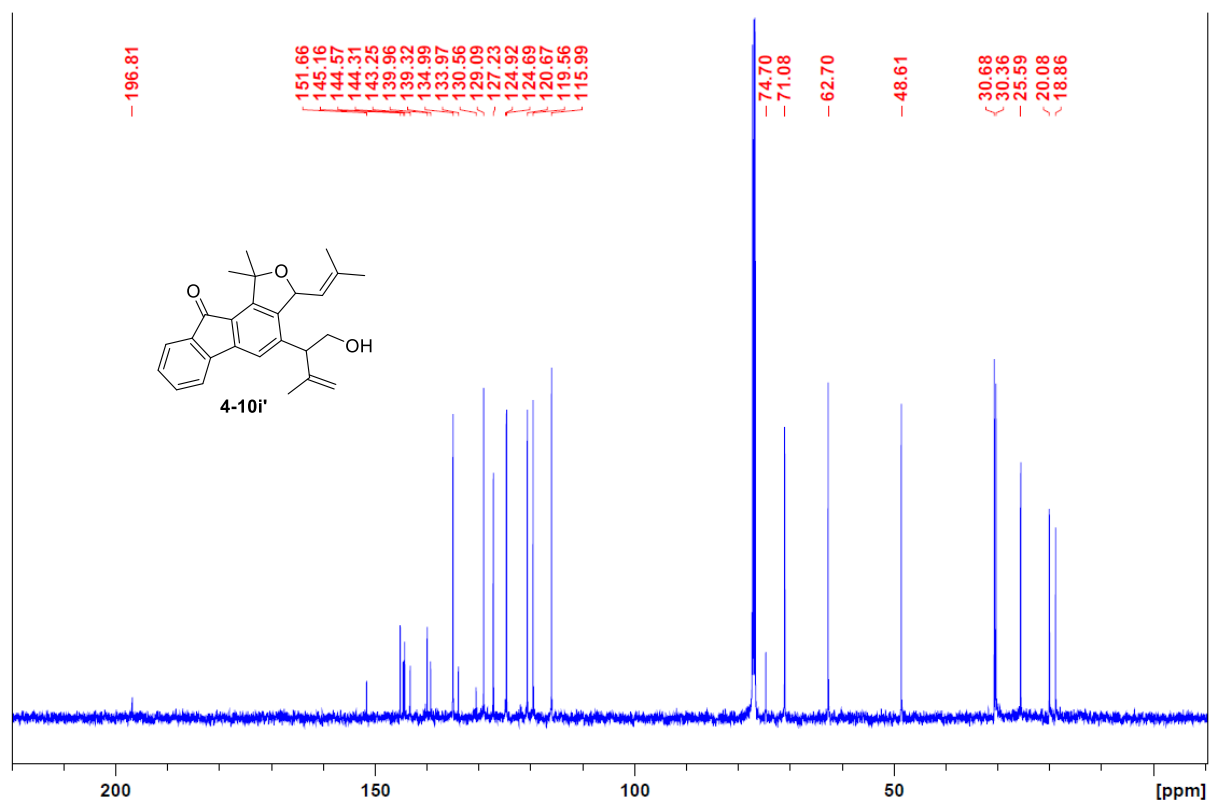
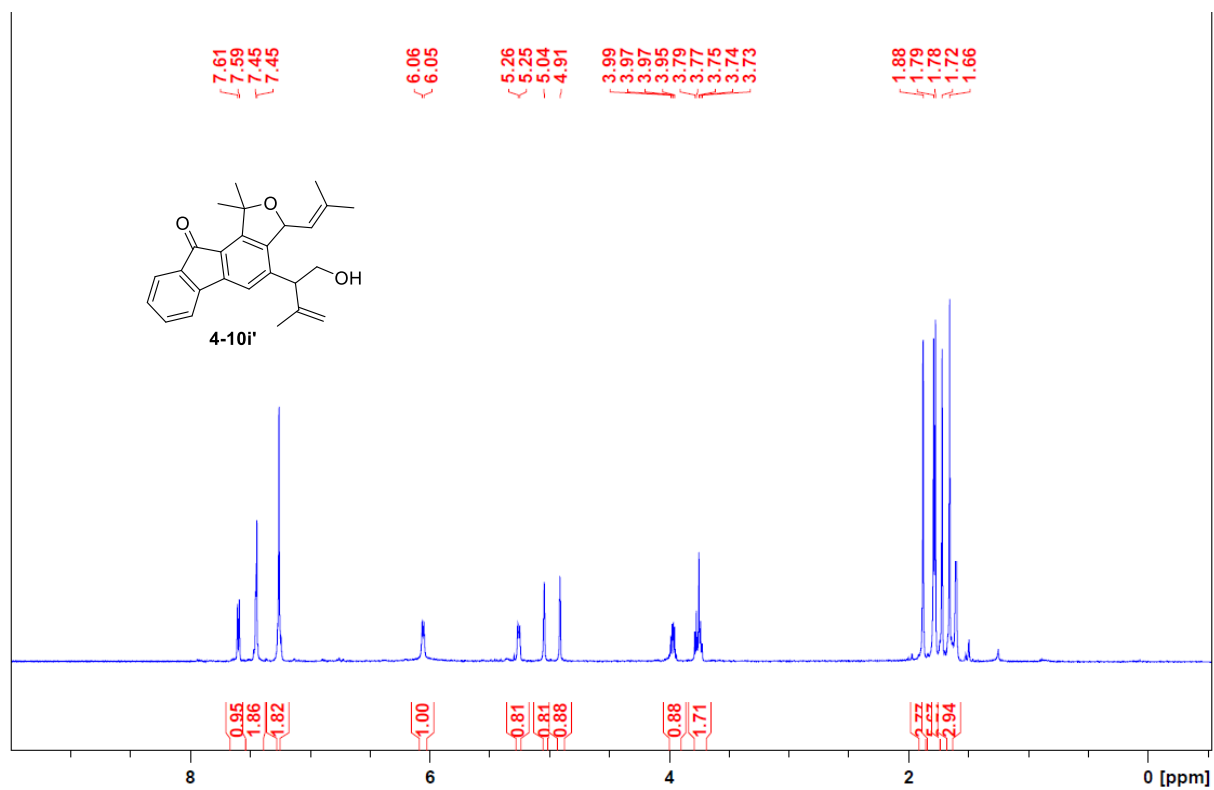


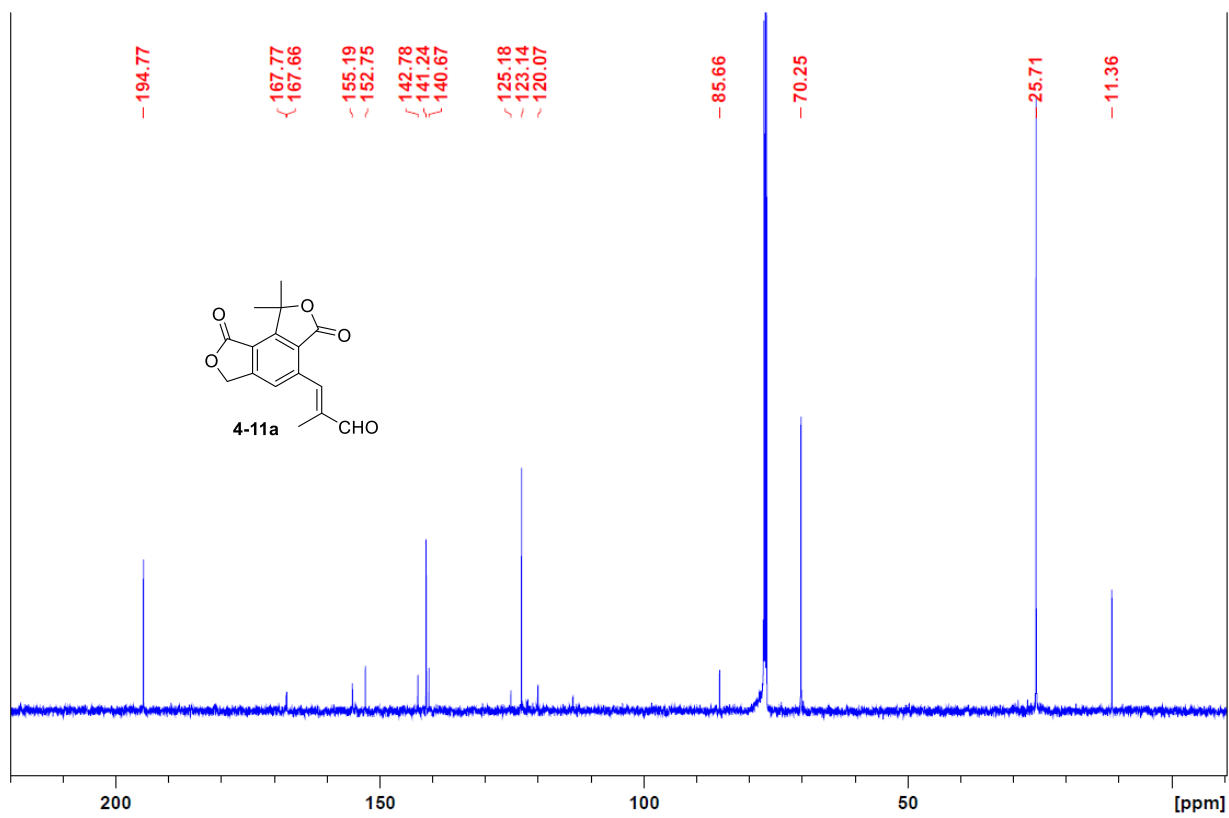
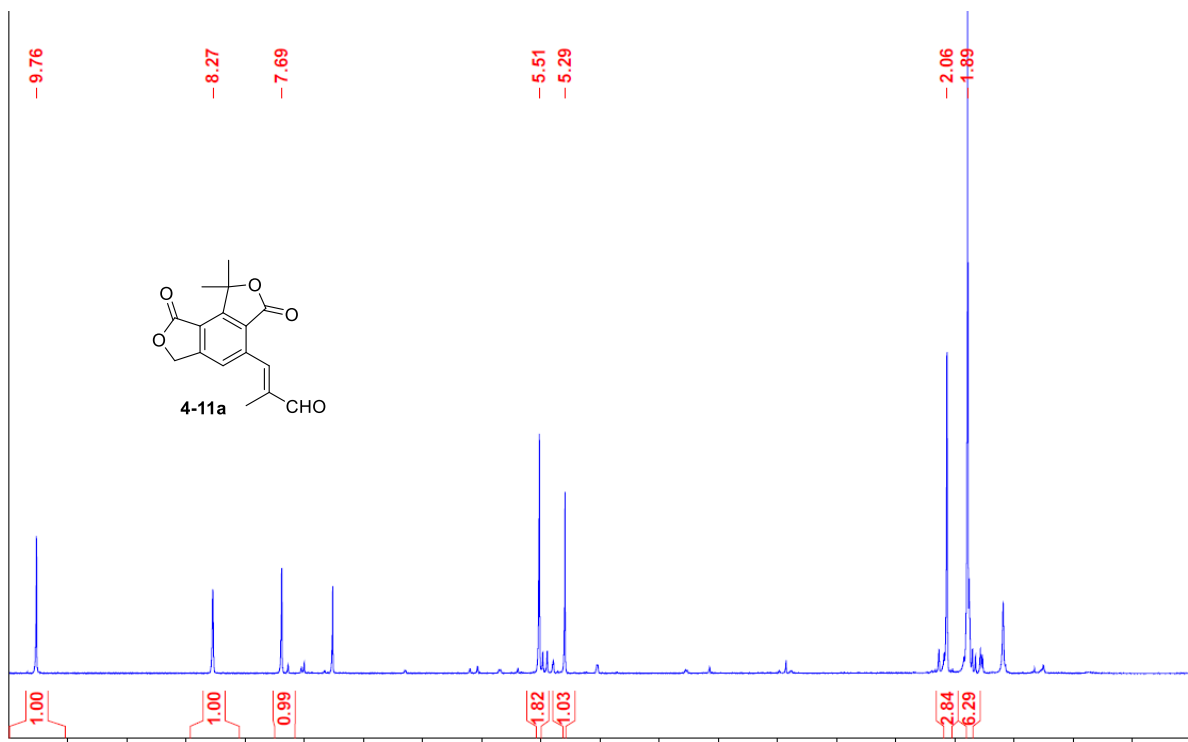


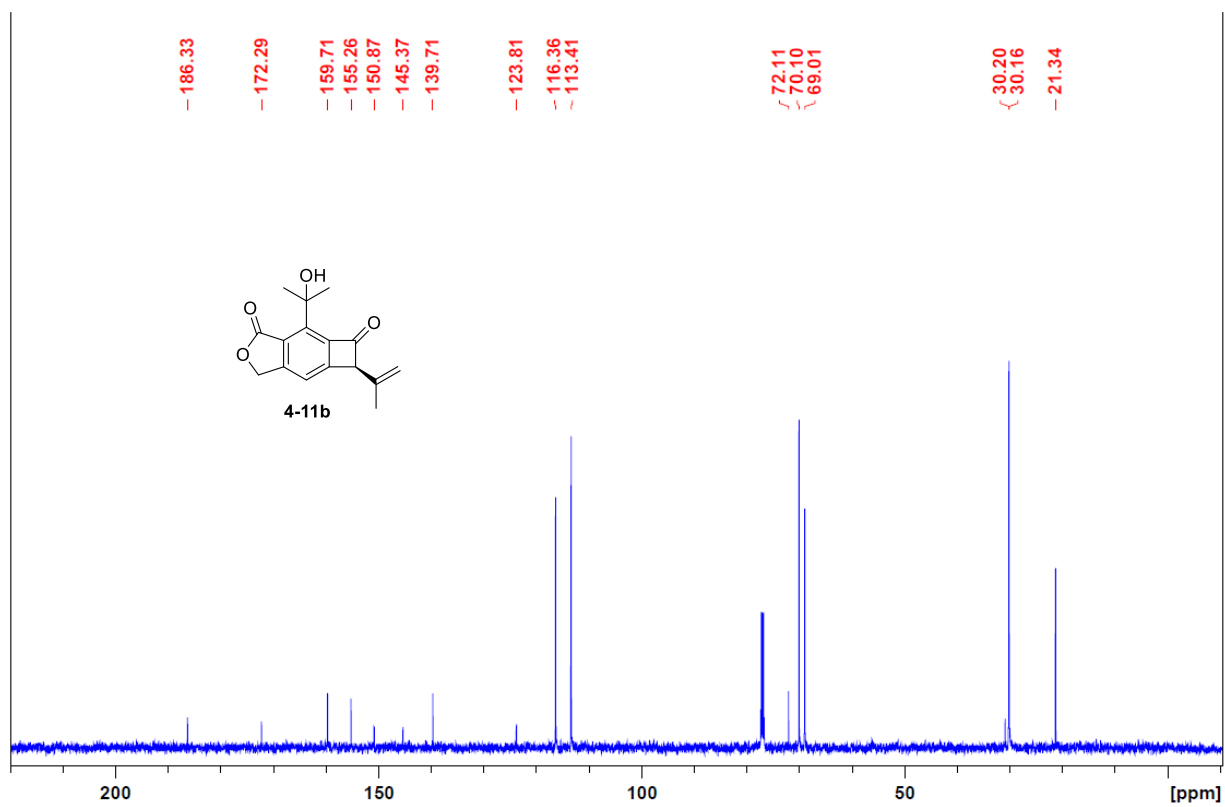
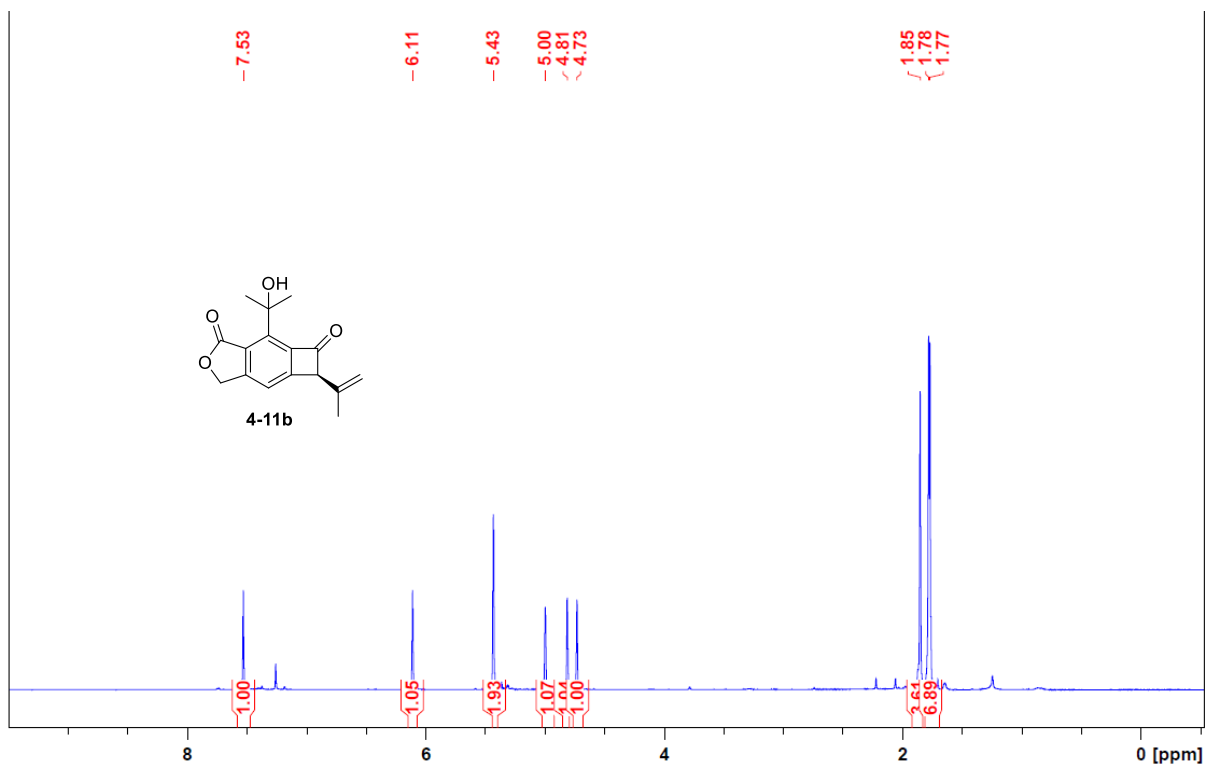


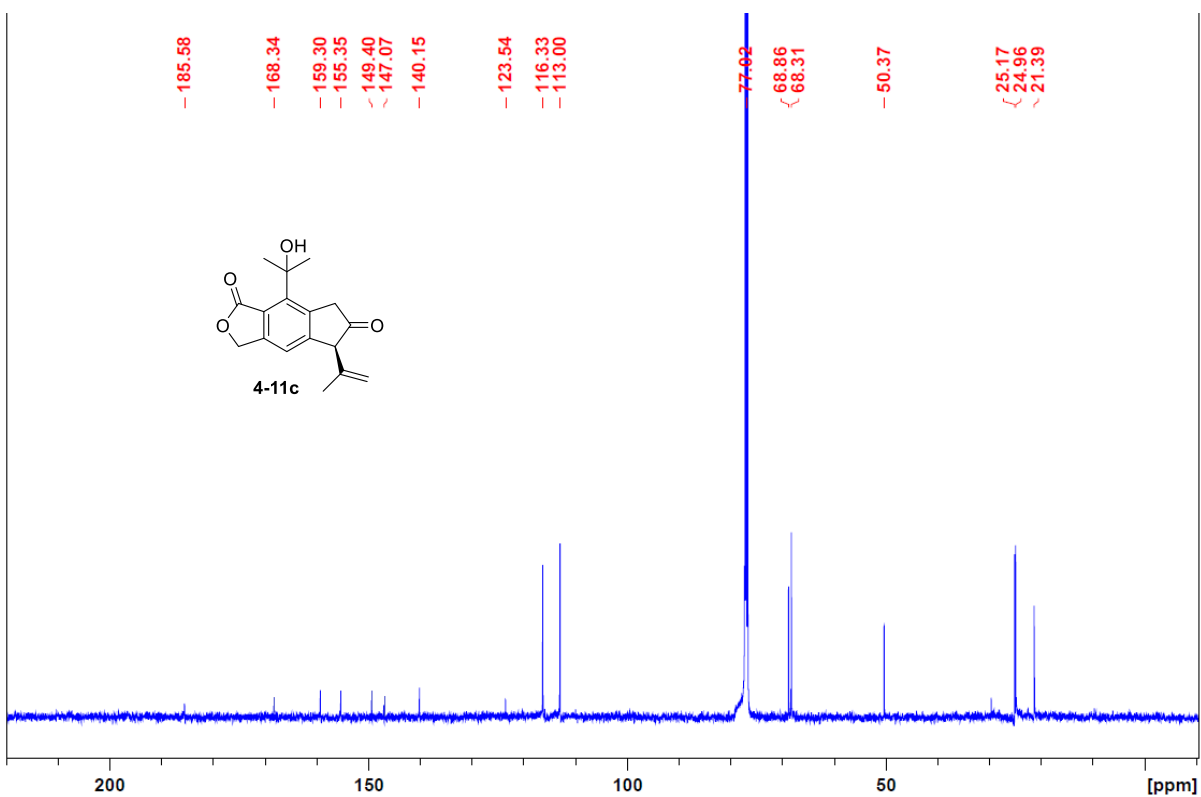
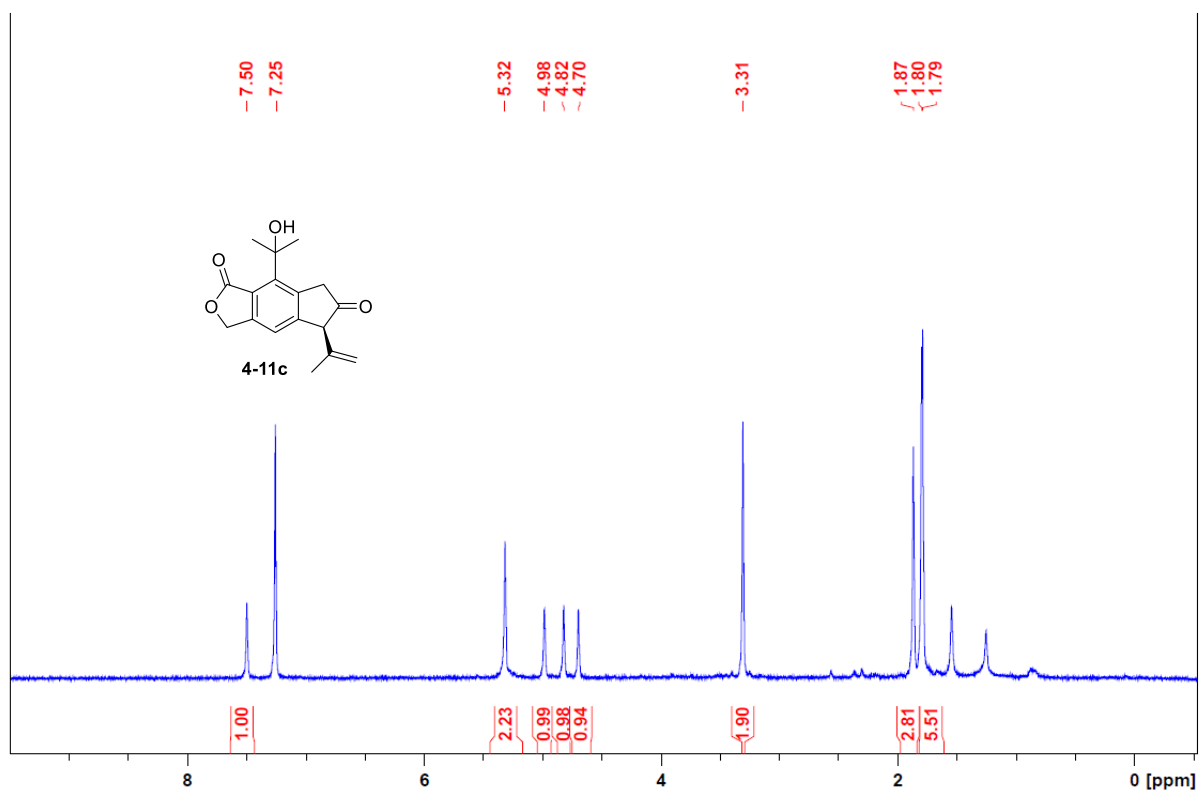


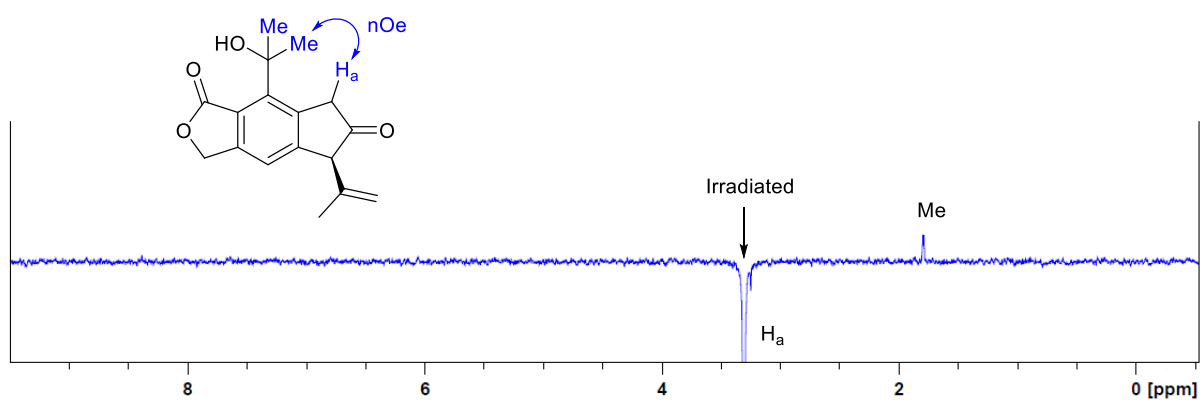


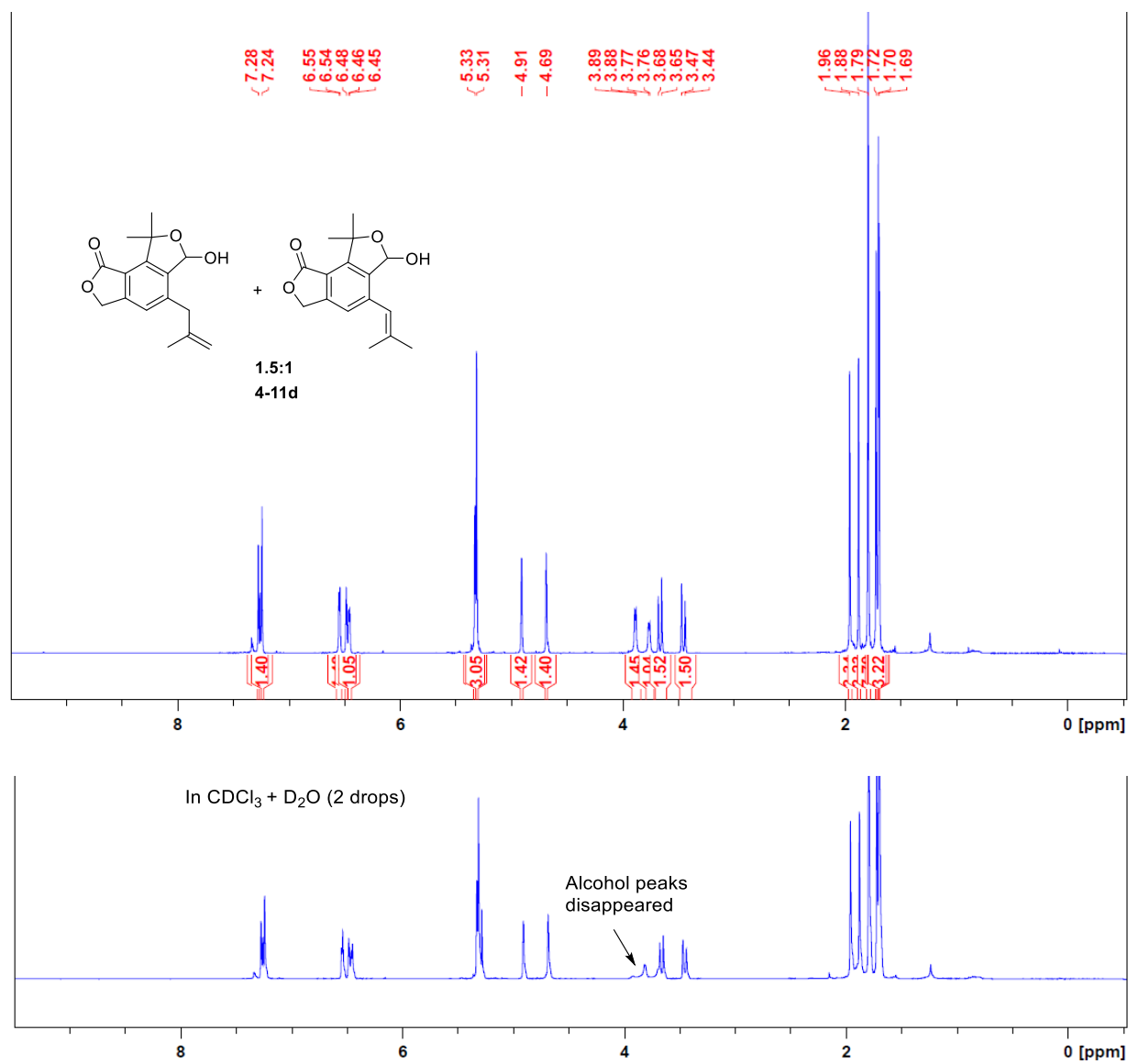


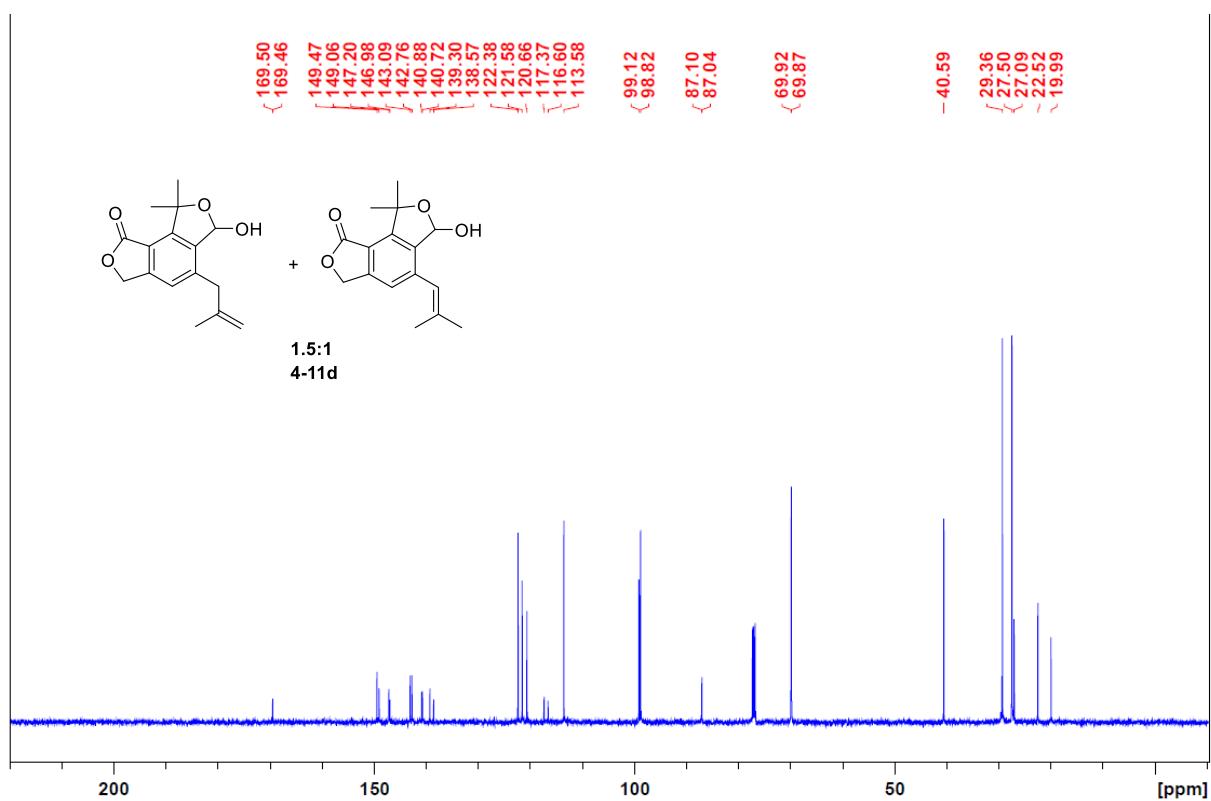


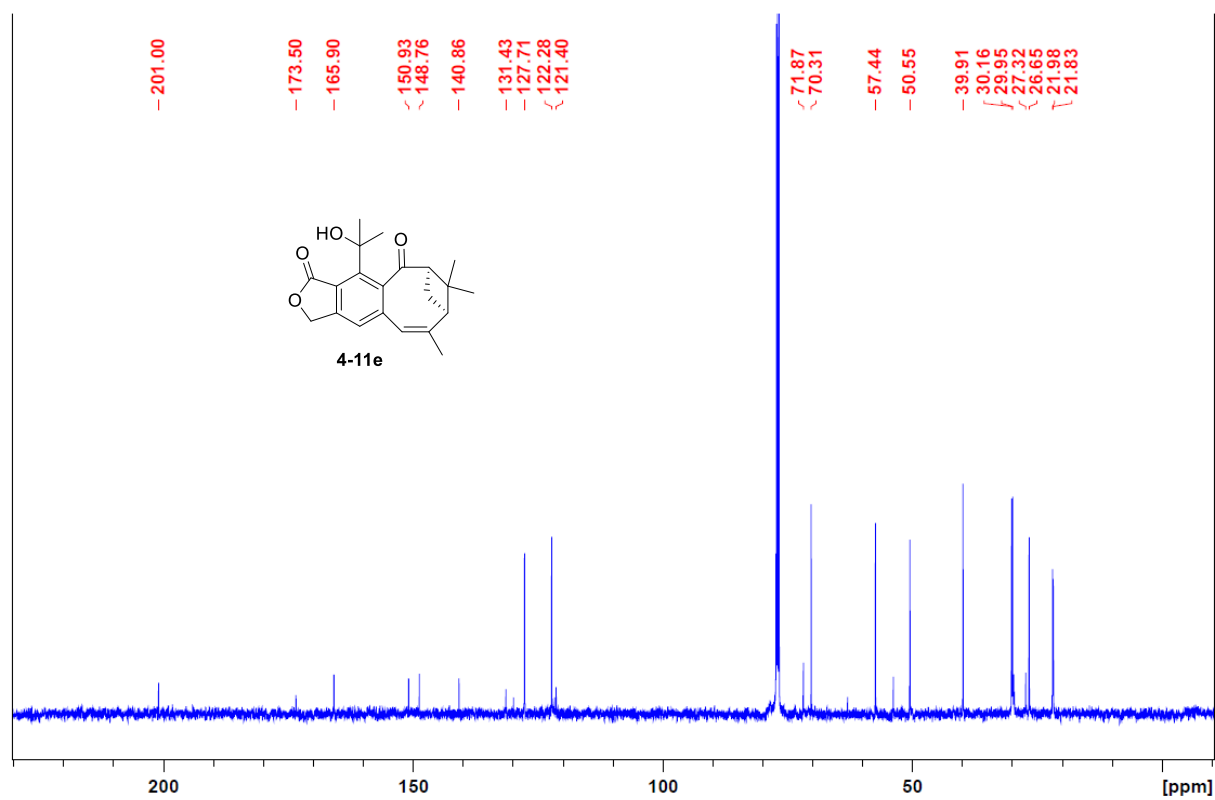
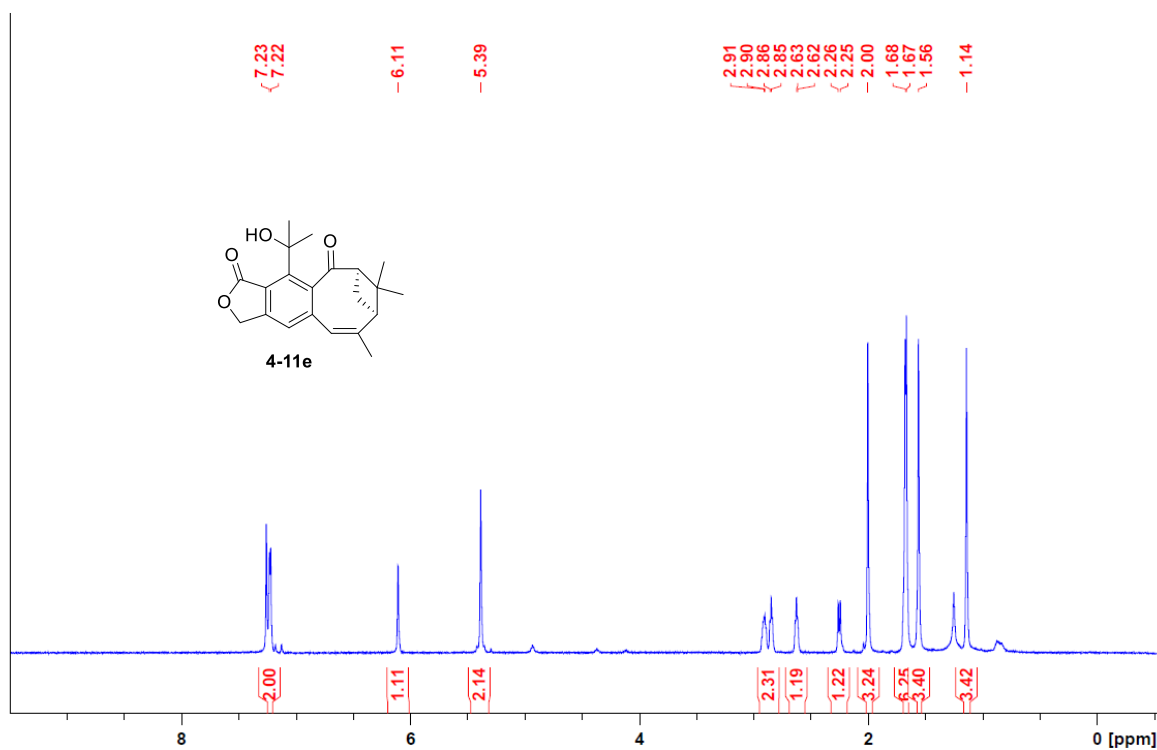




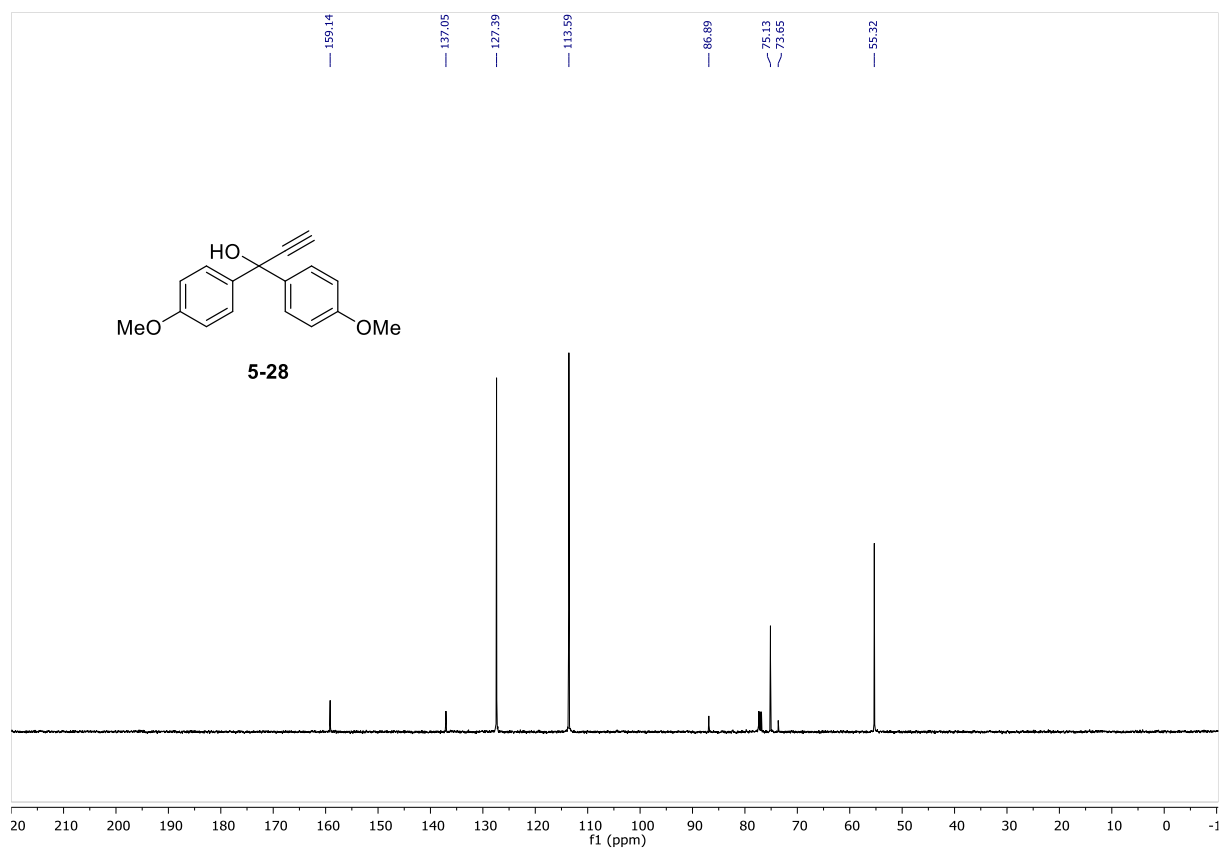
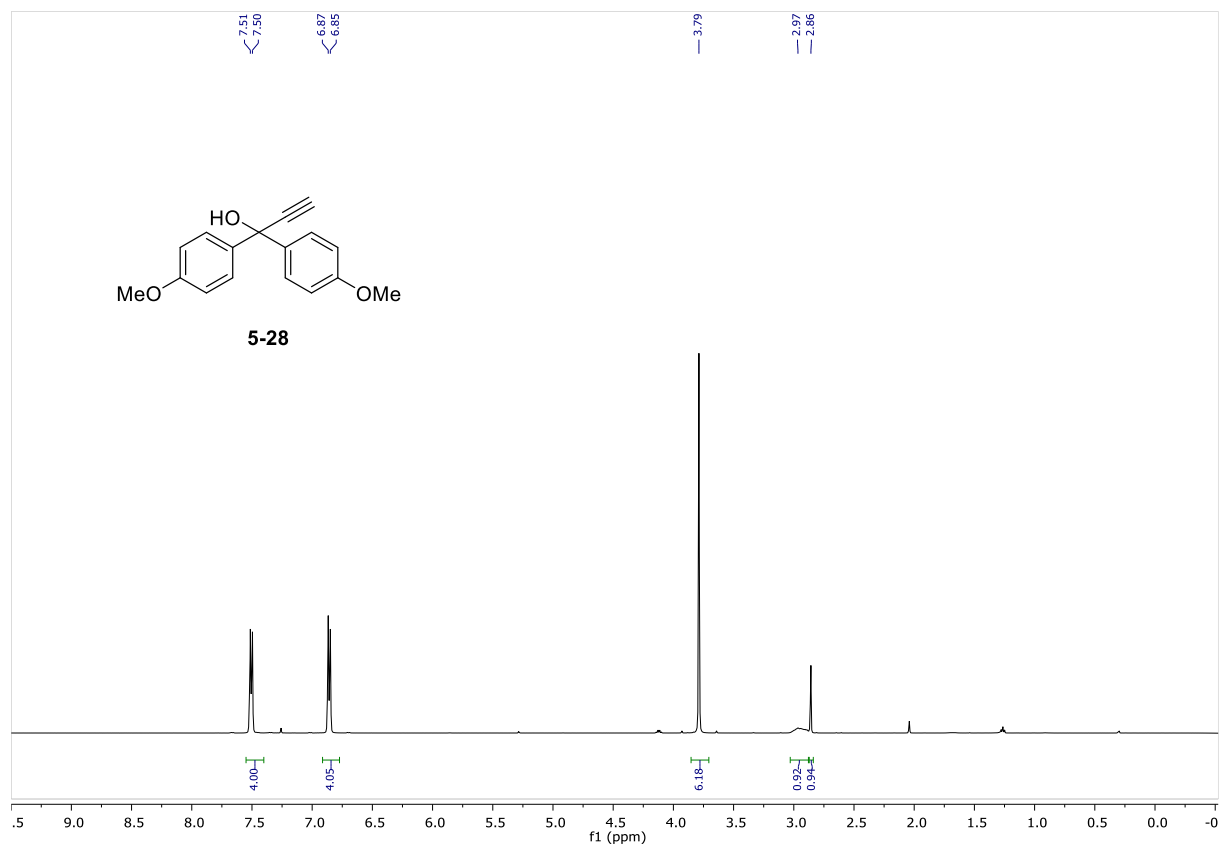


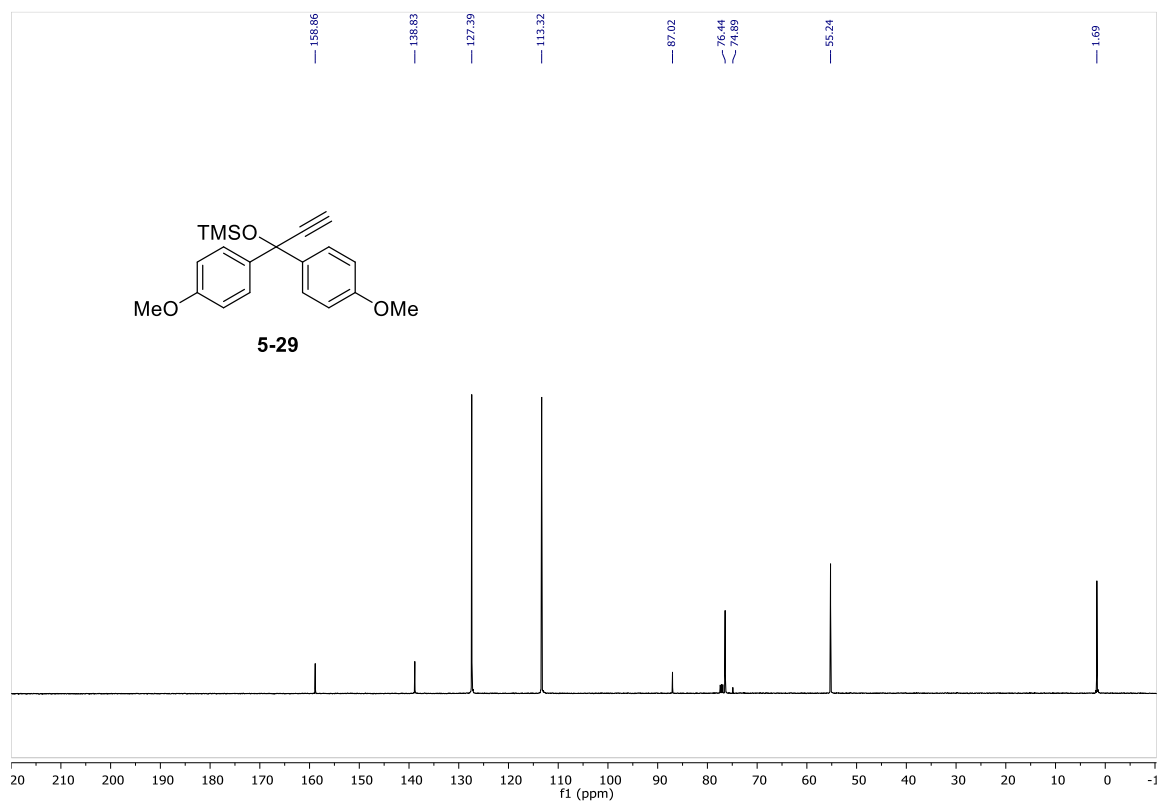
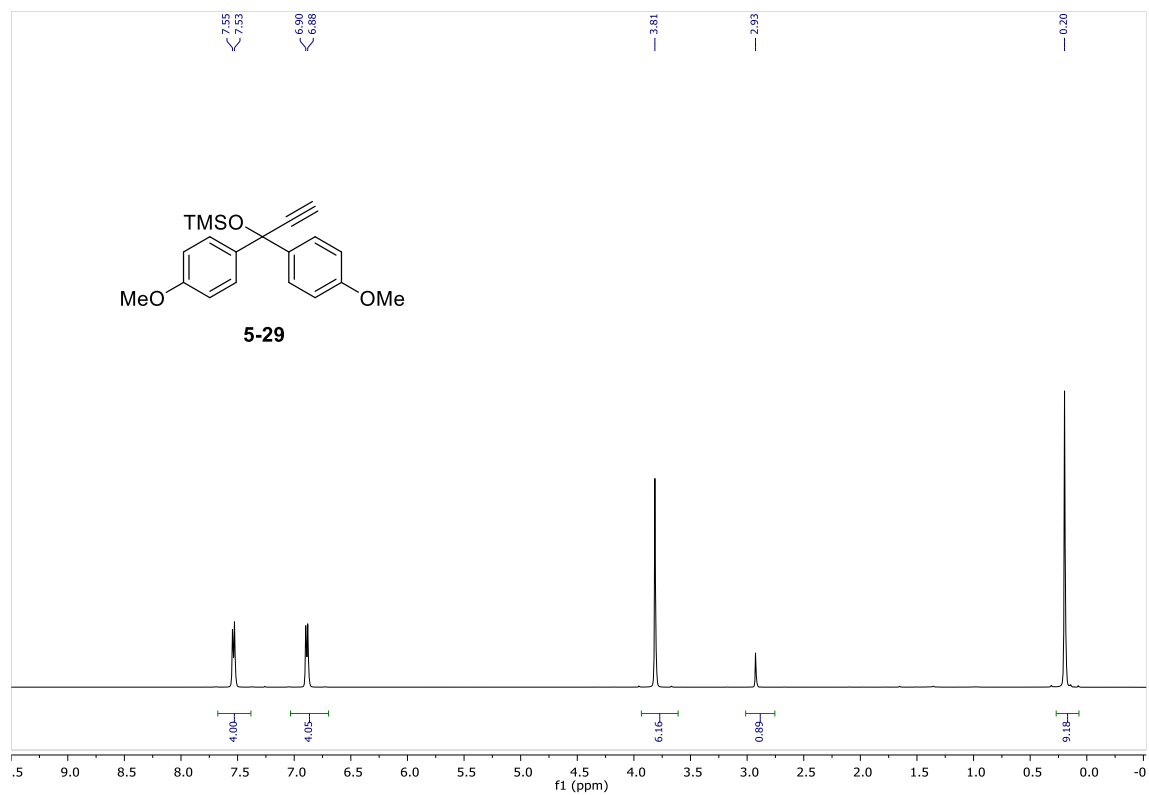


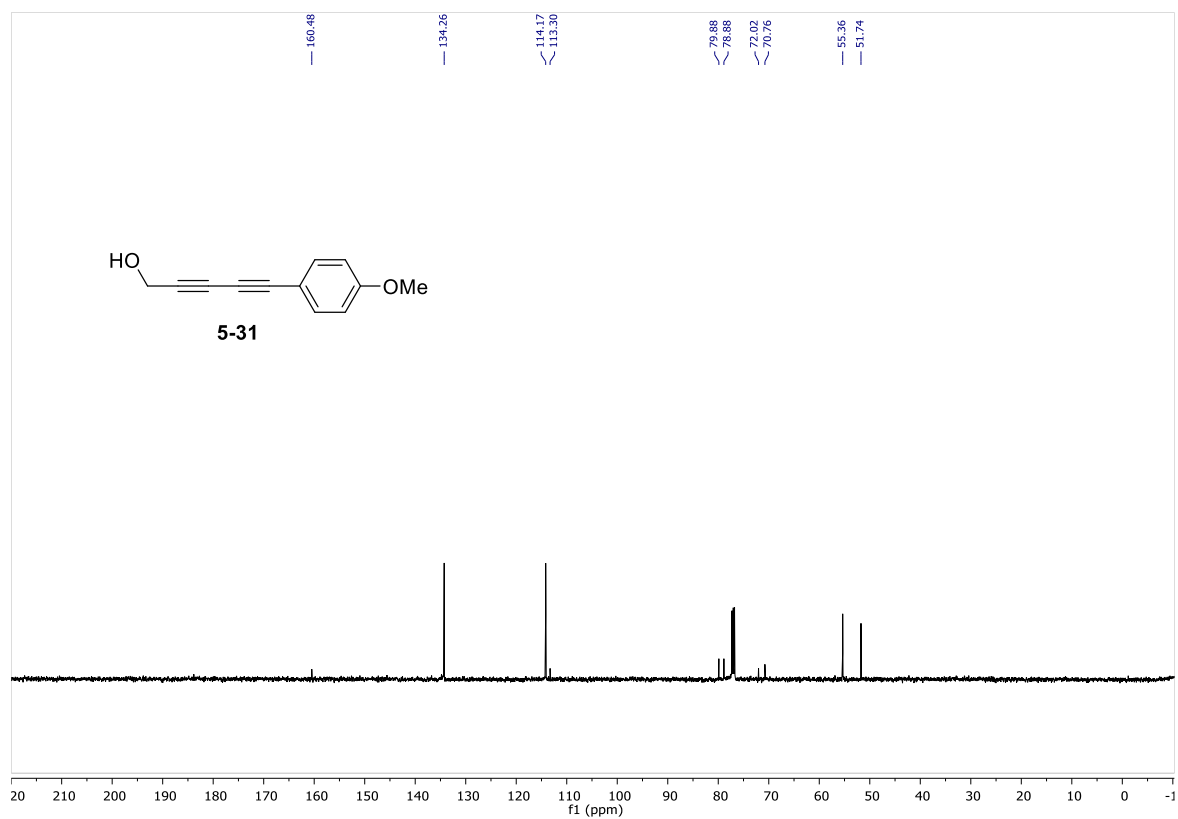
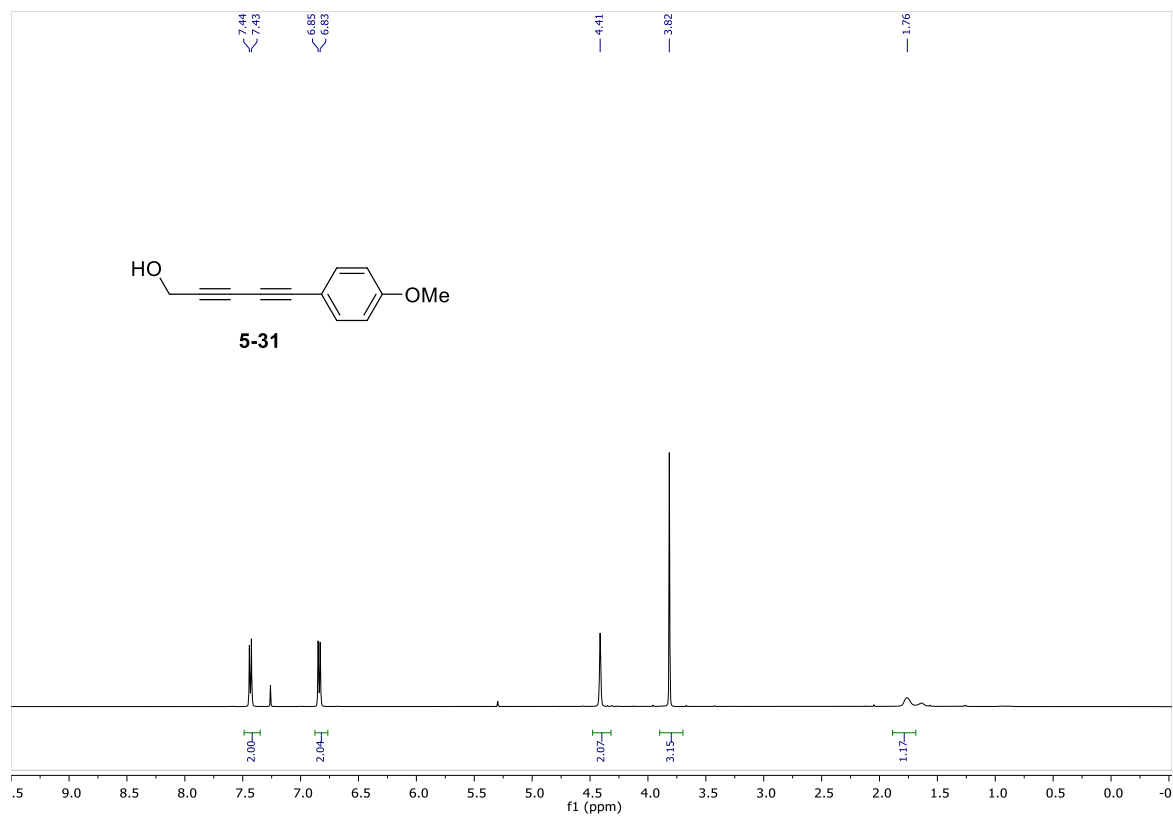


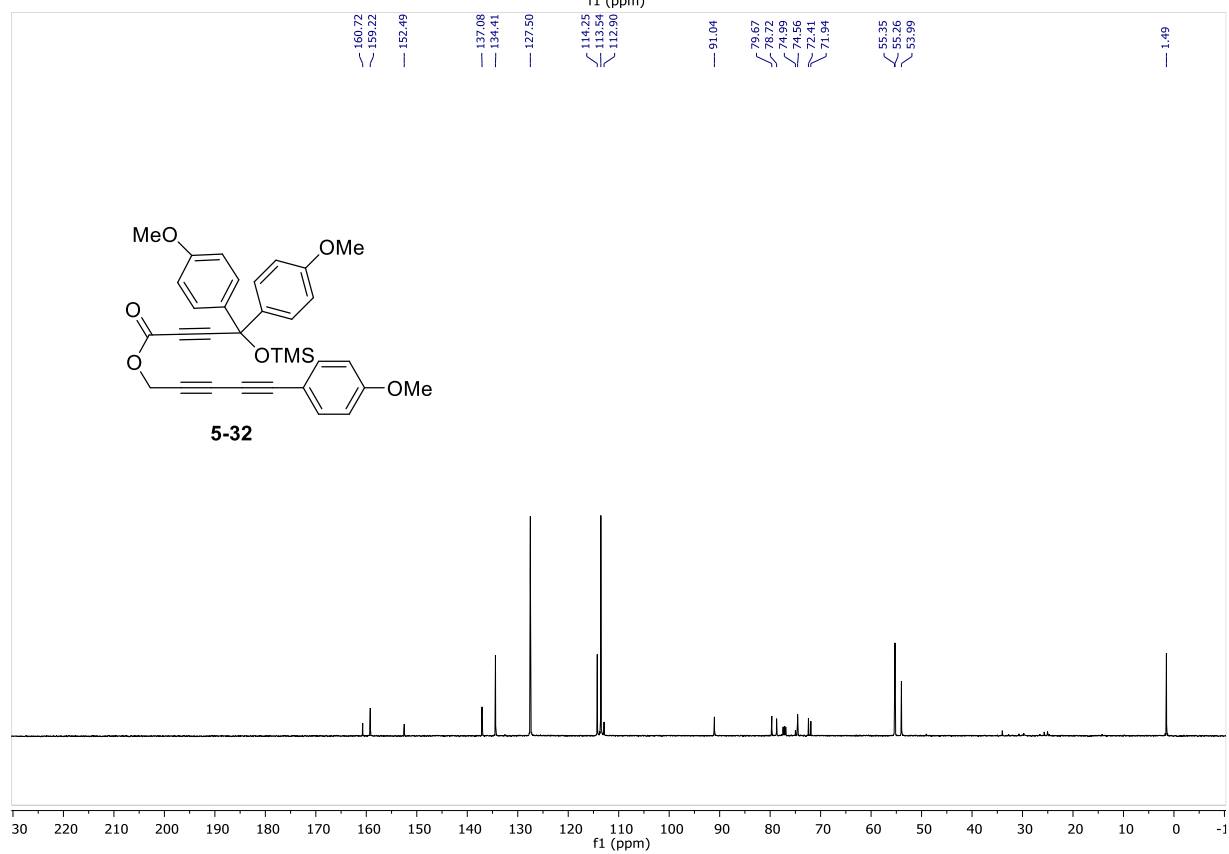
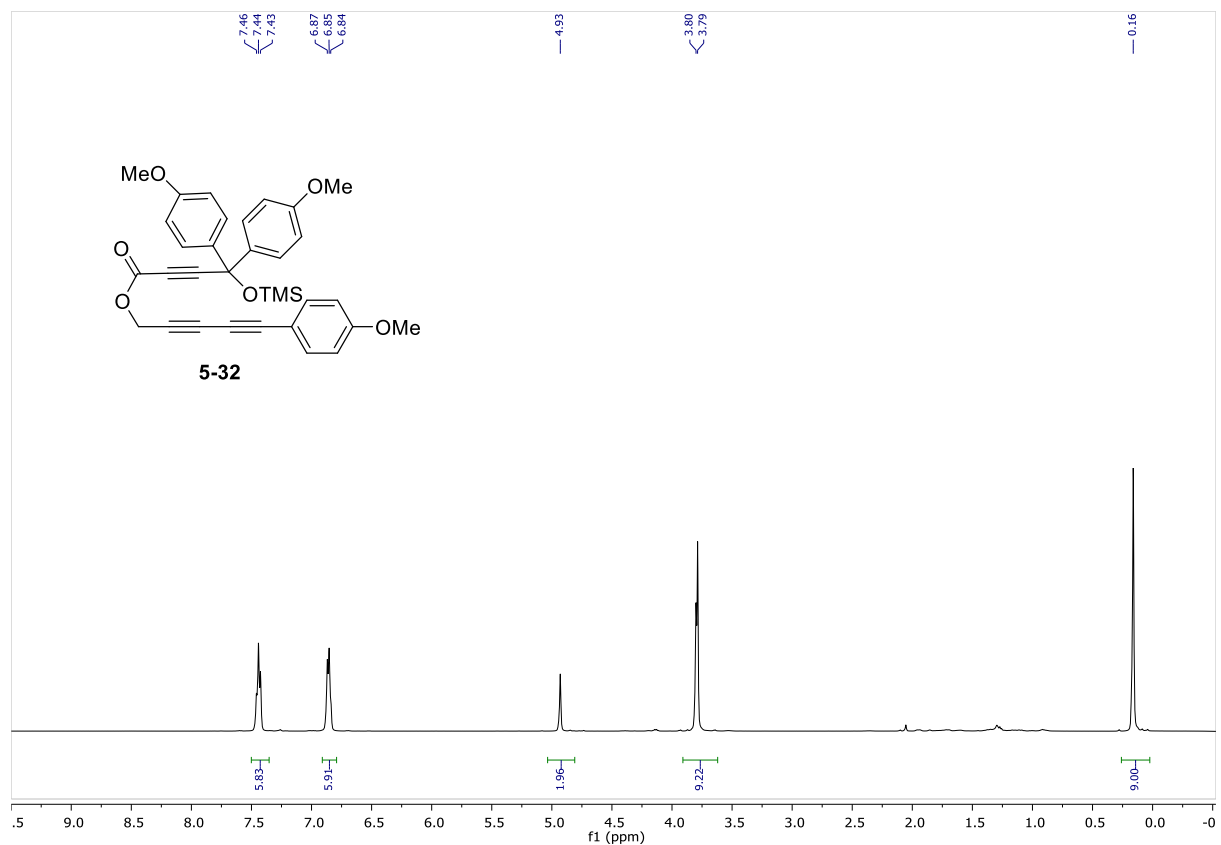


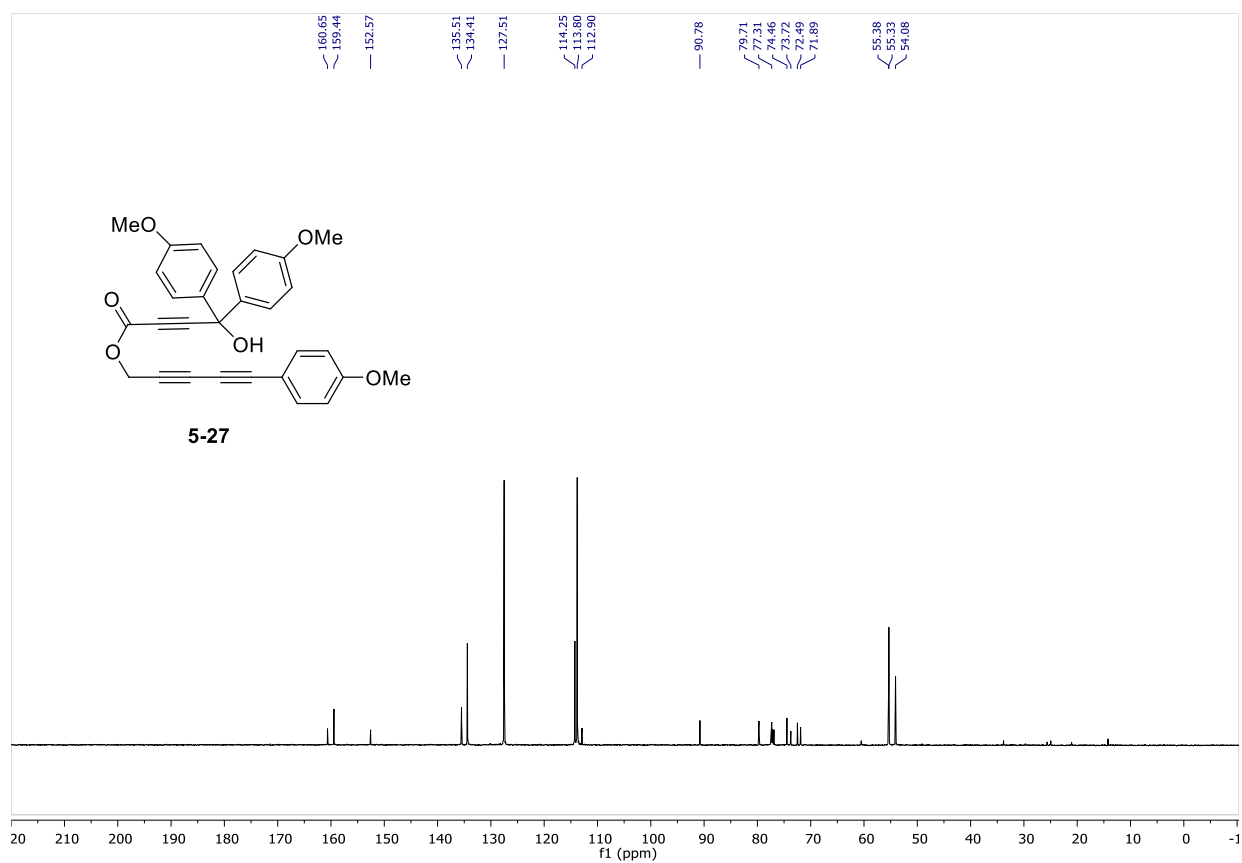
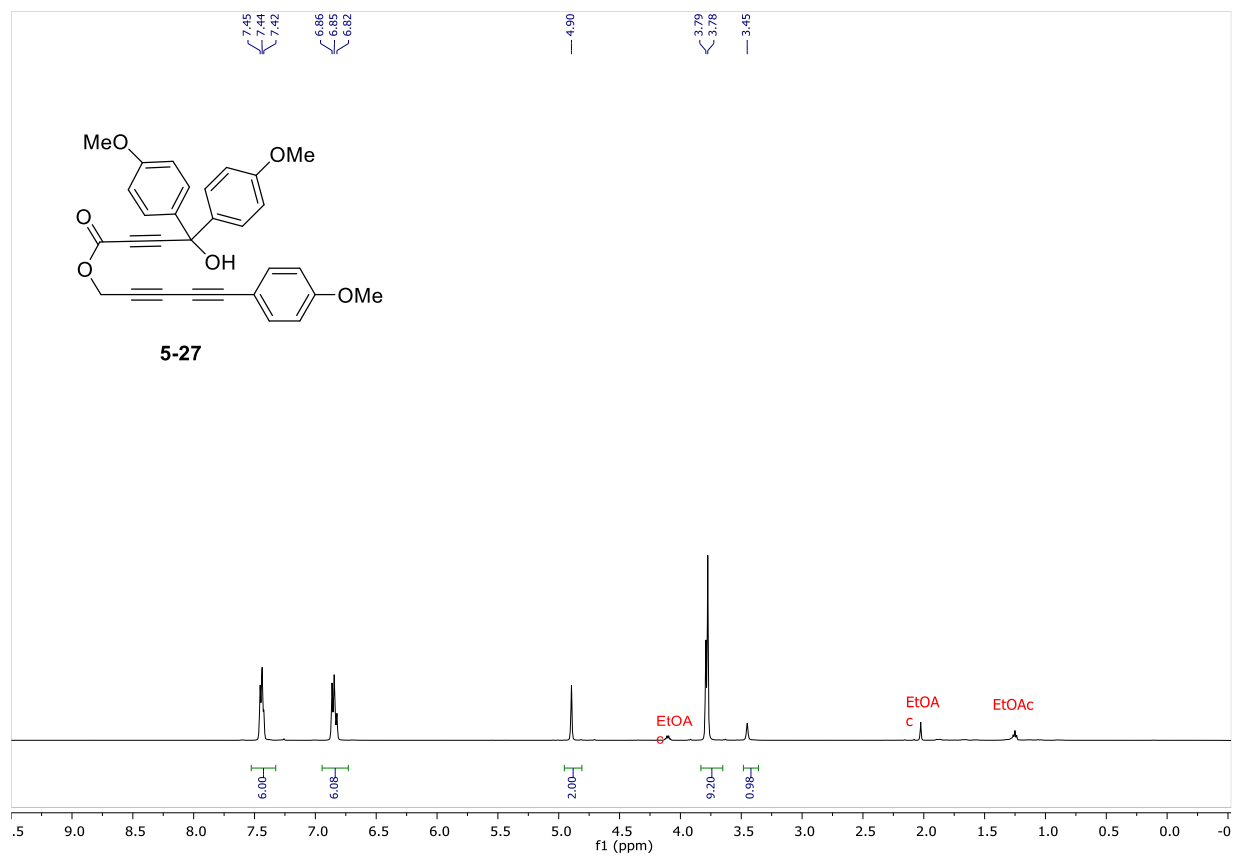
Appendix IV
Selected NMR Spectra for Chapter 5

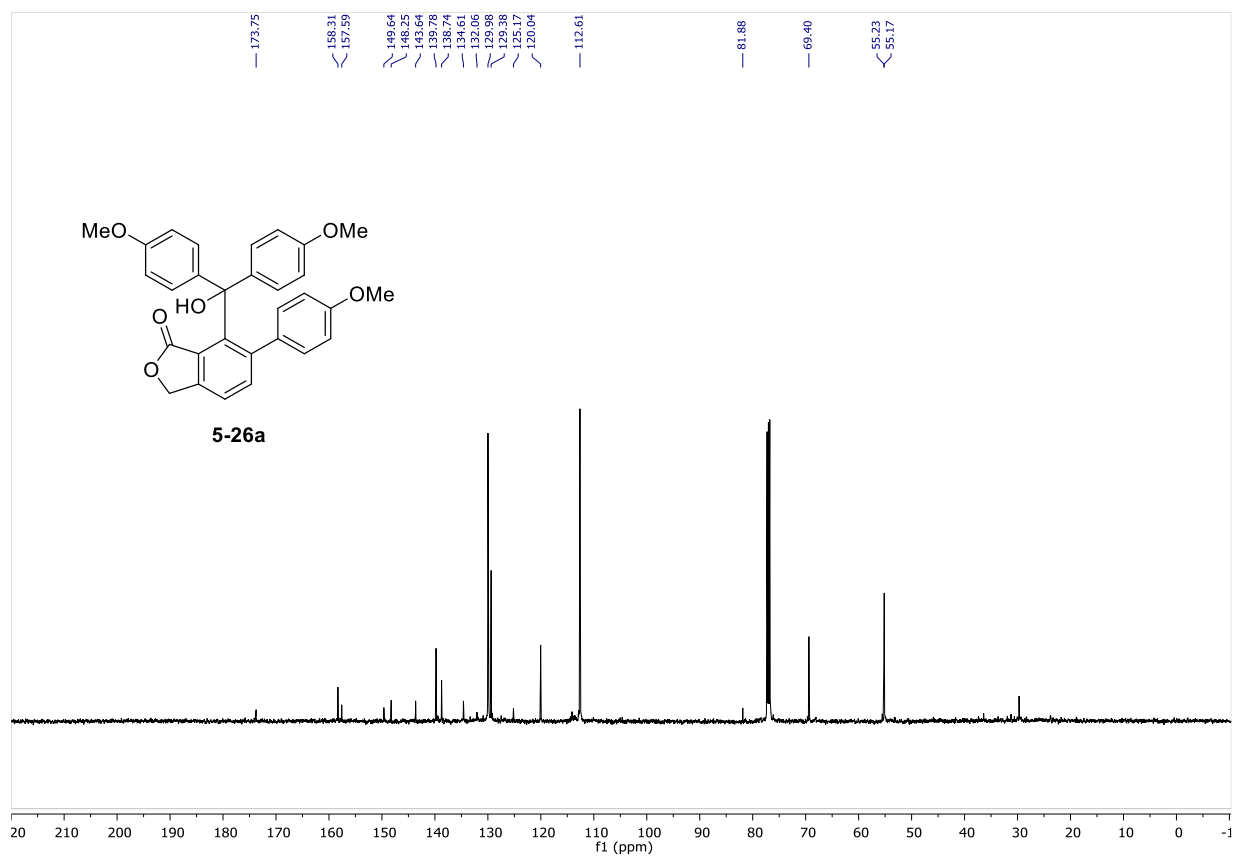
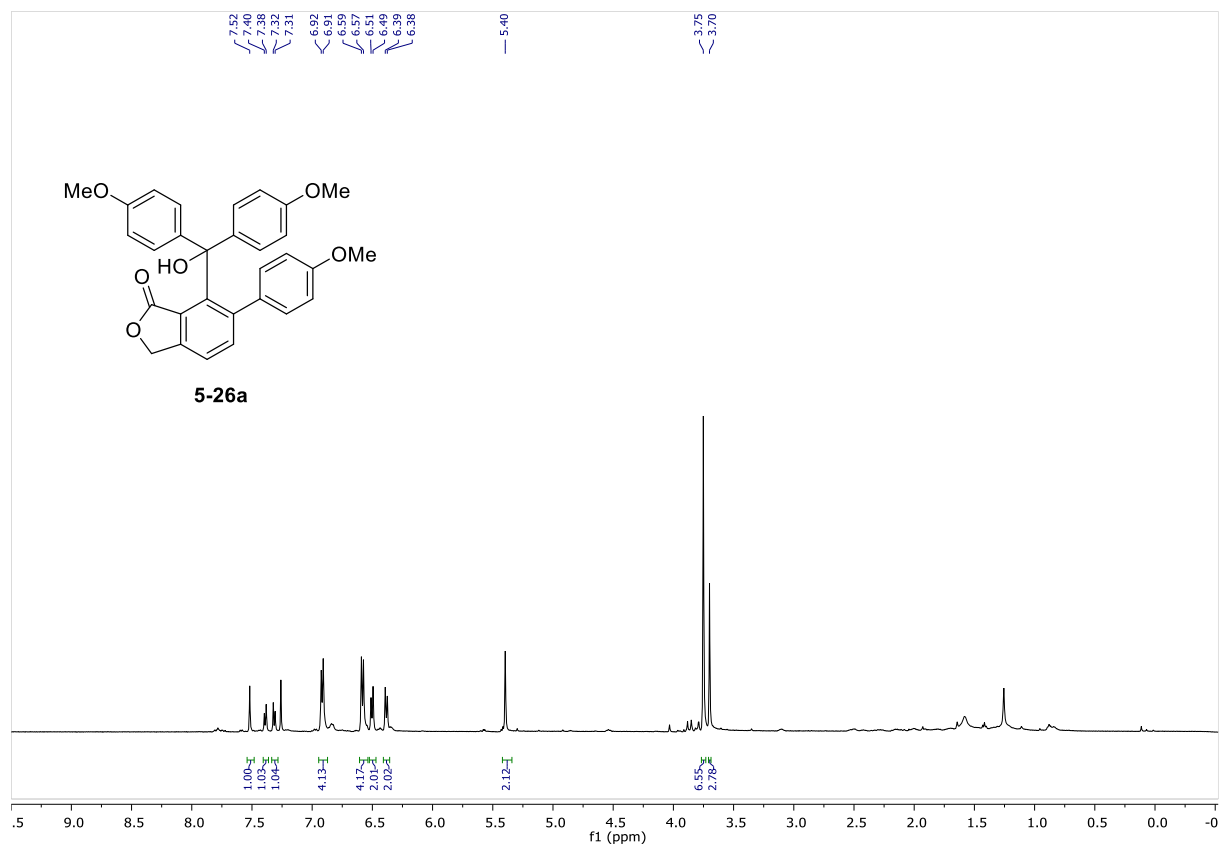


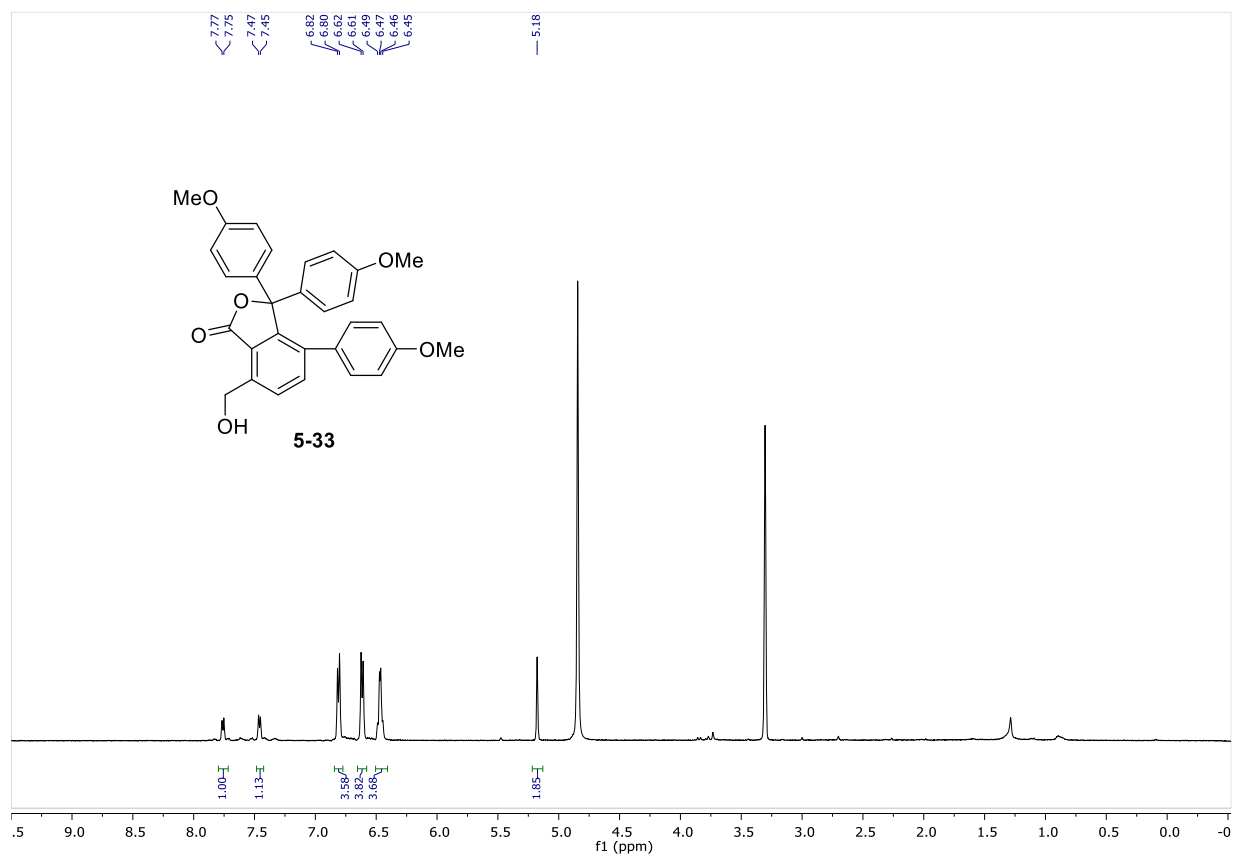
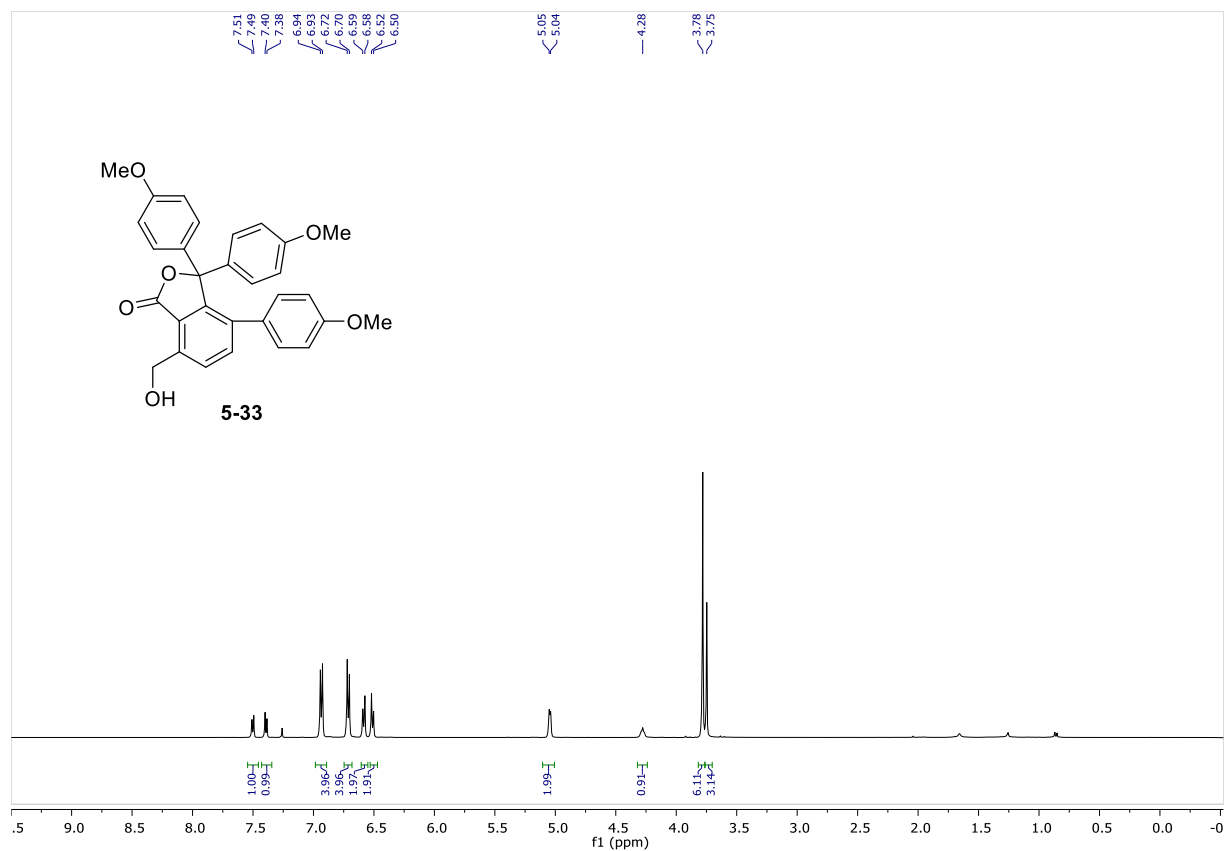


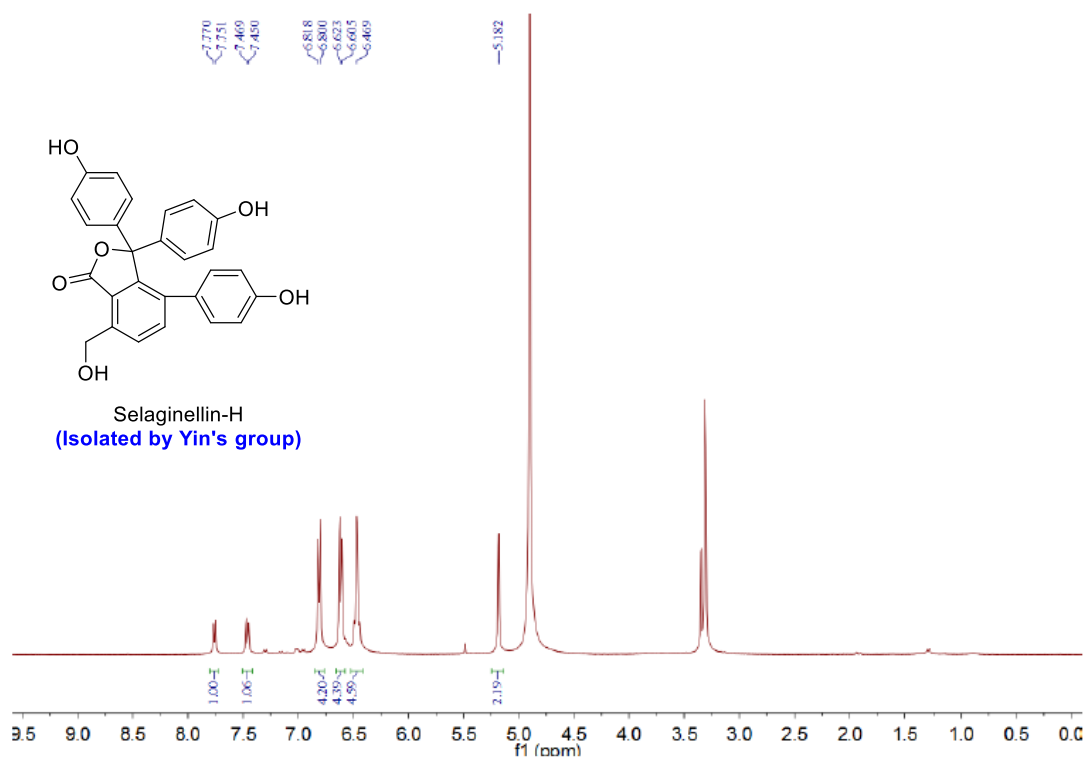
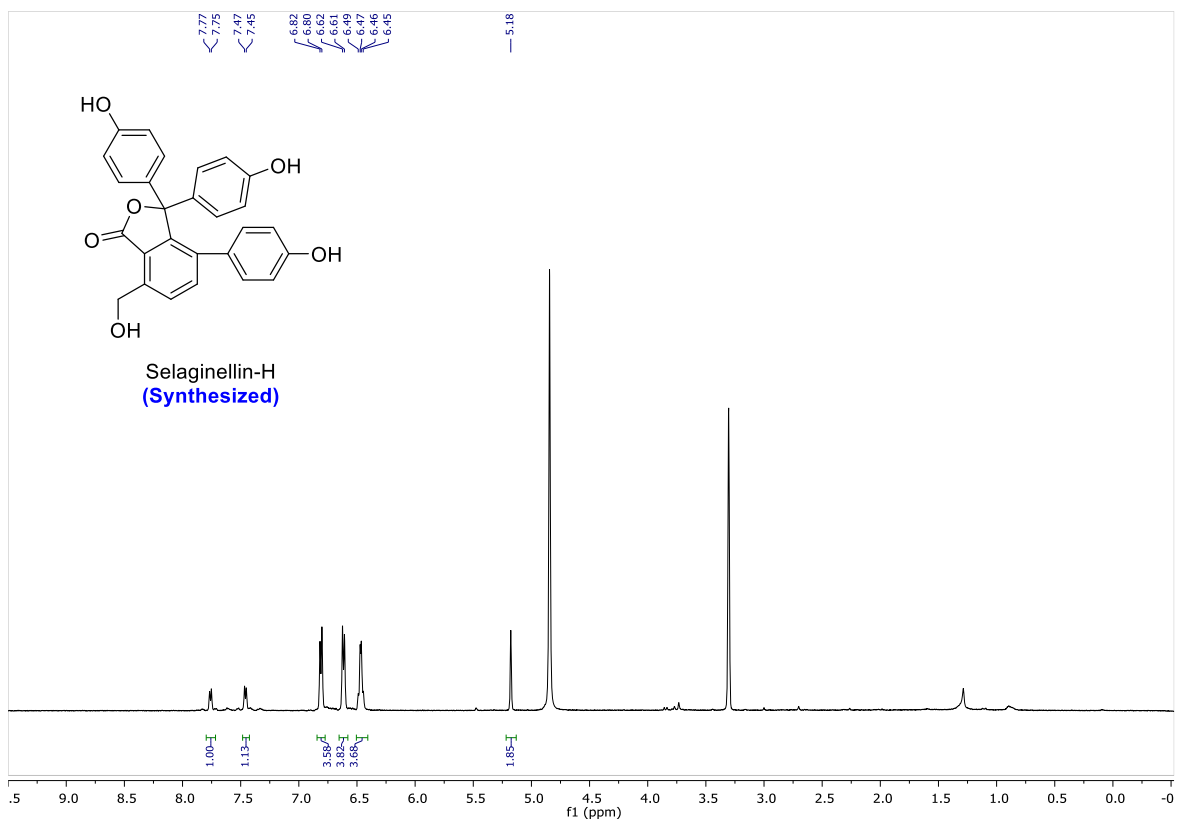


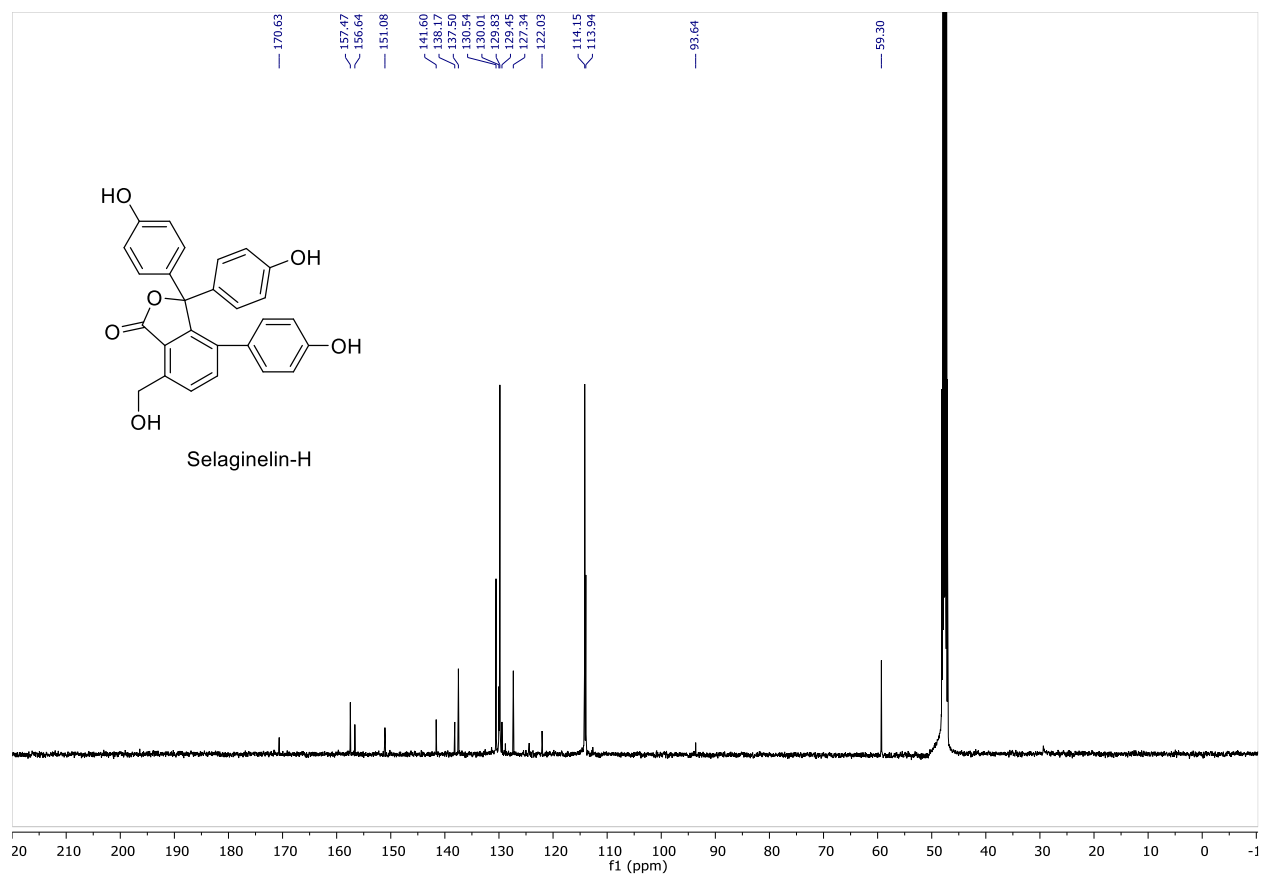


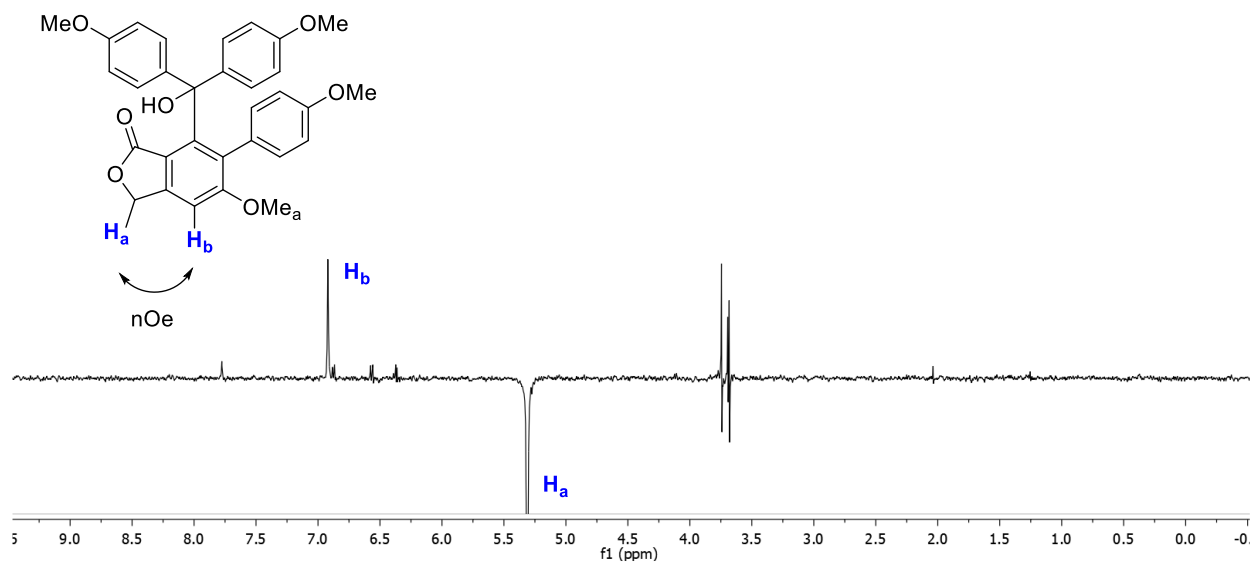
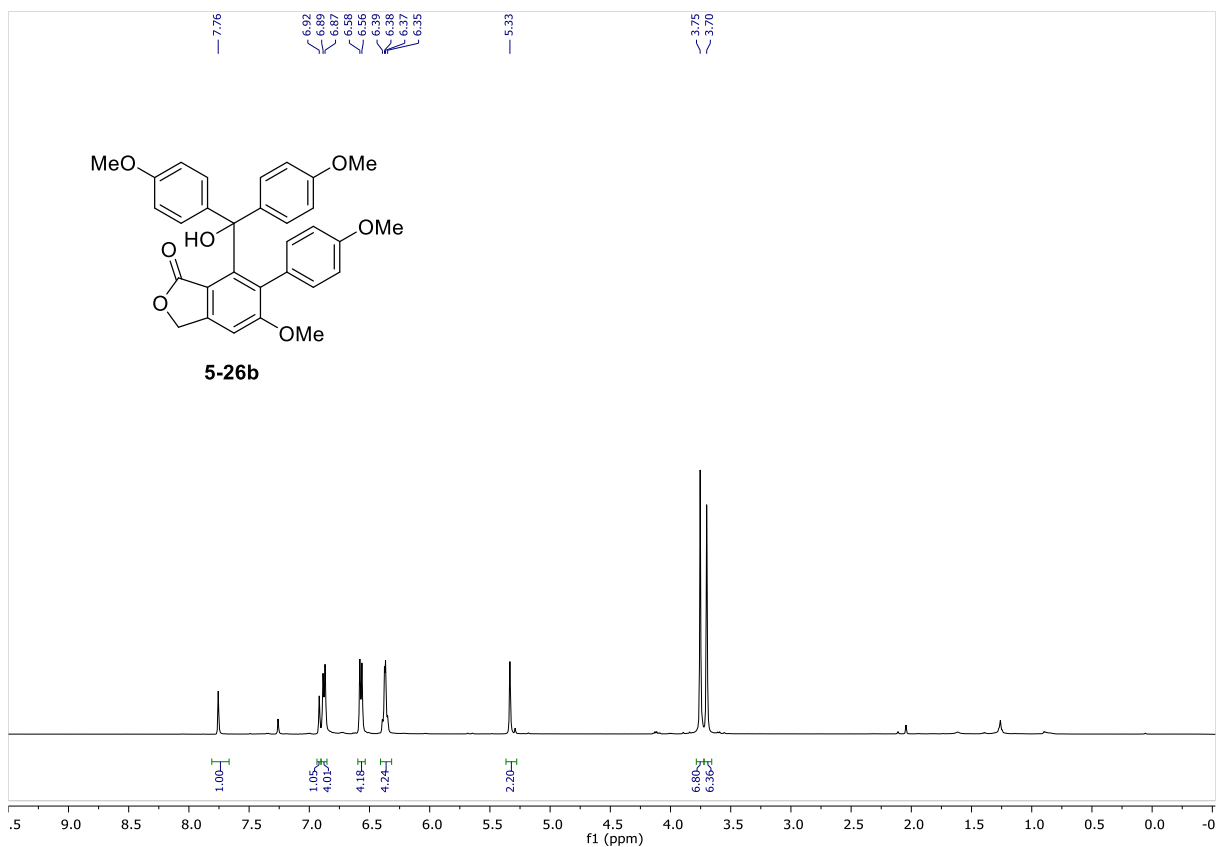


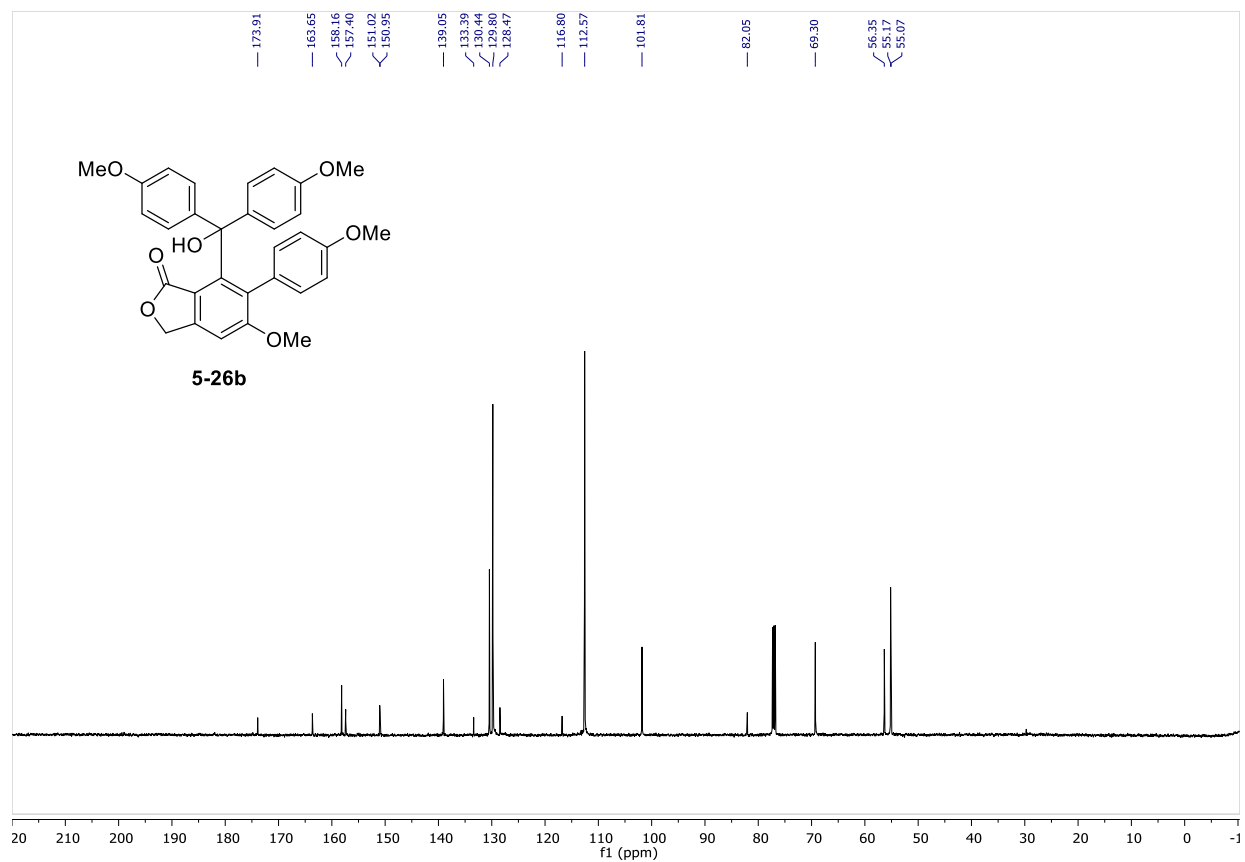


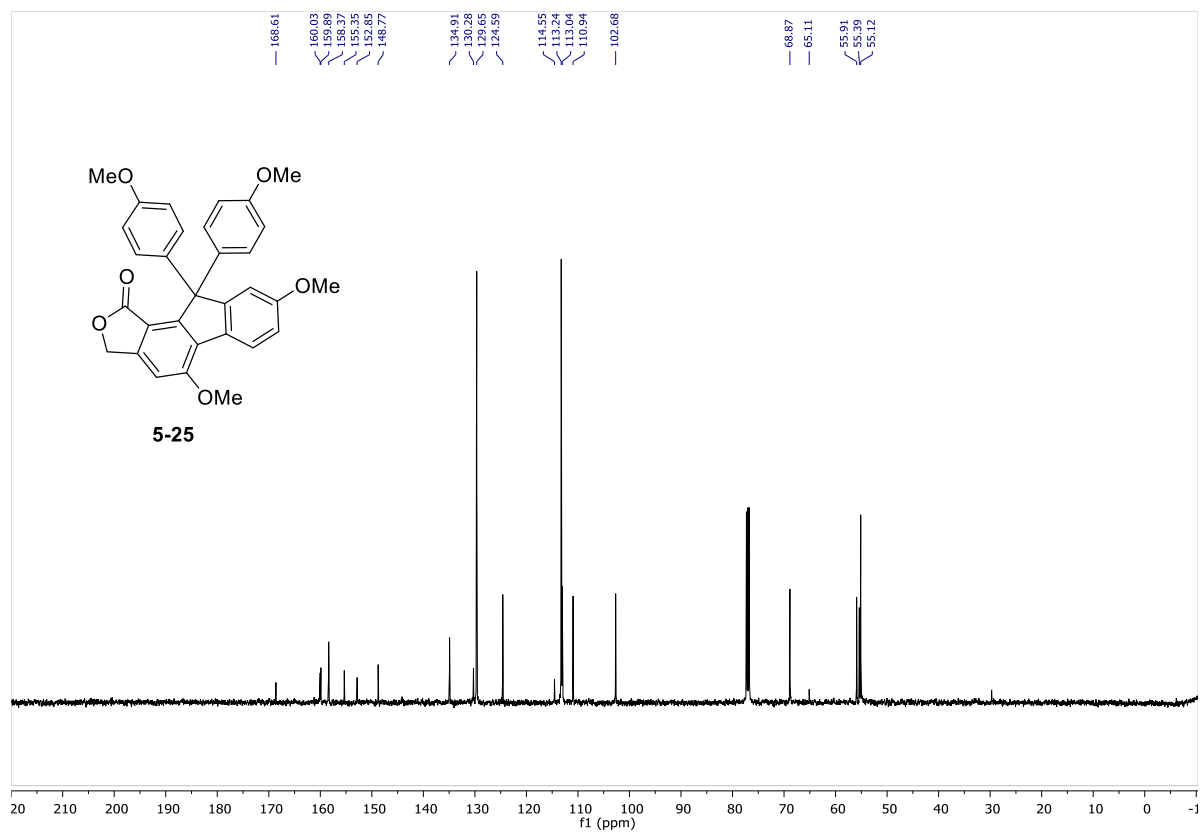
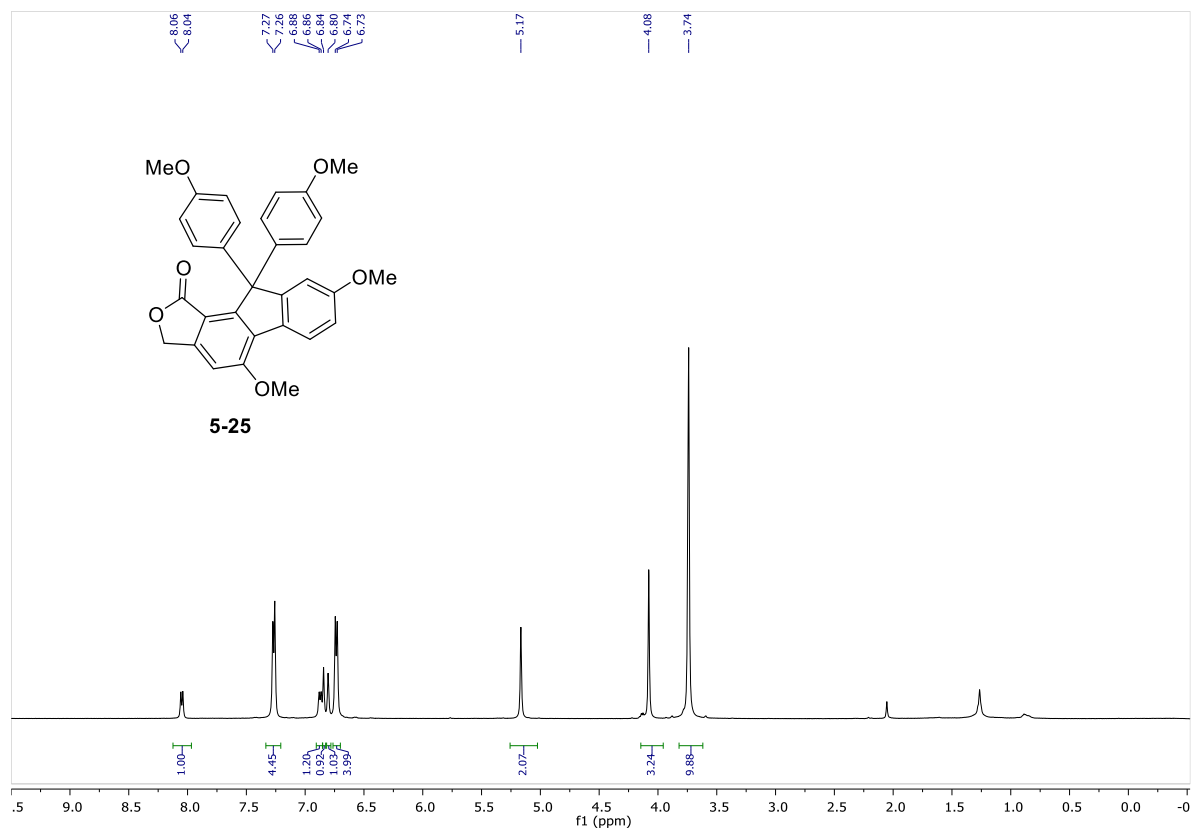


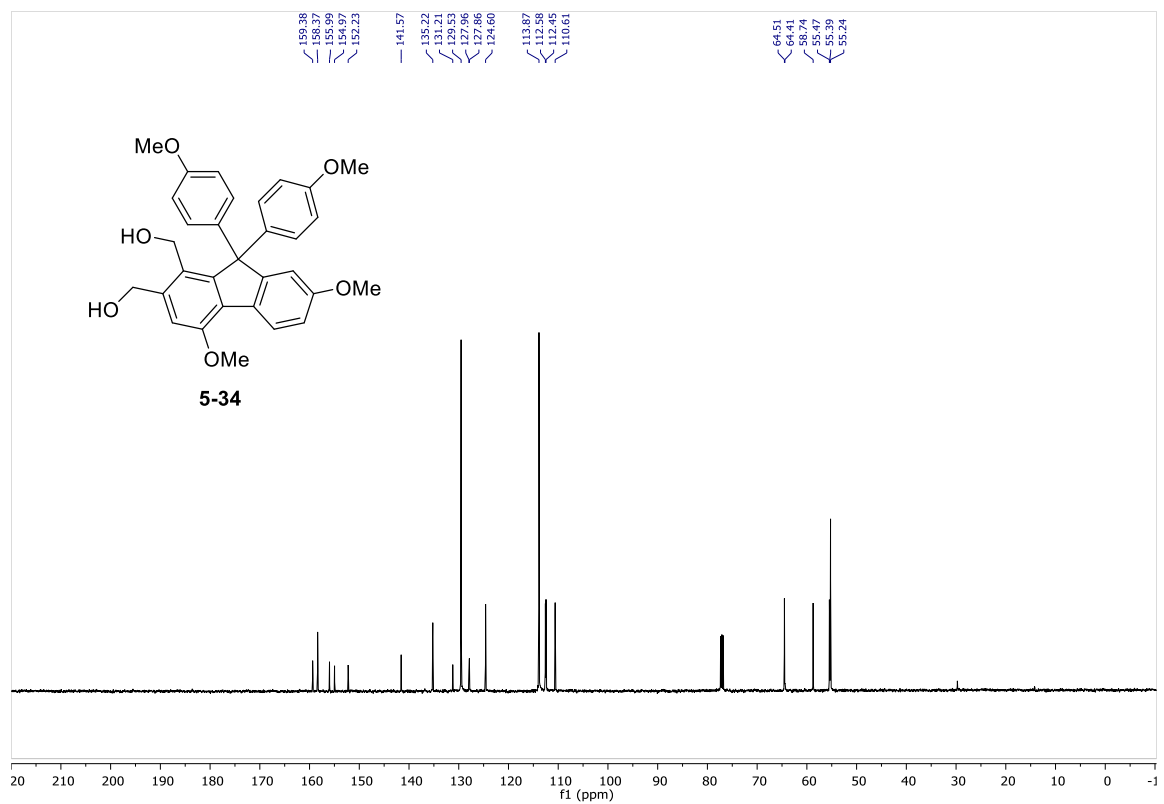
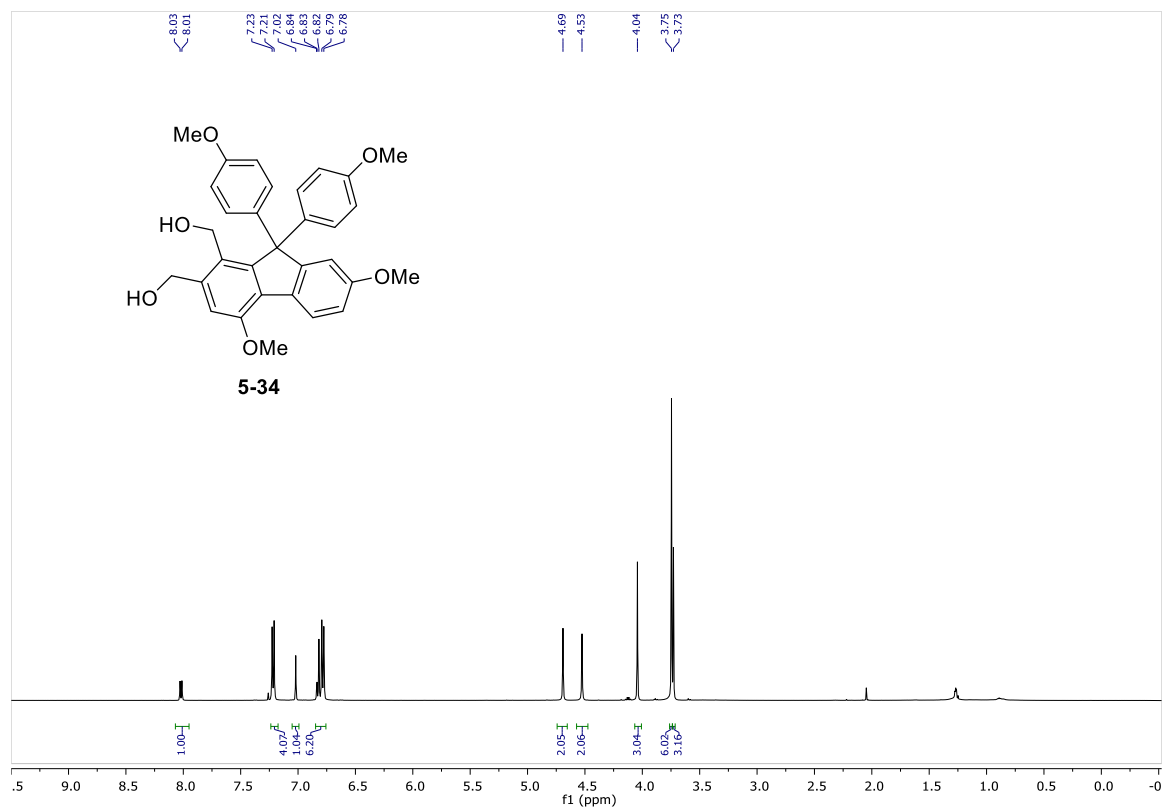


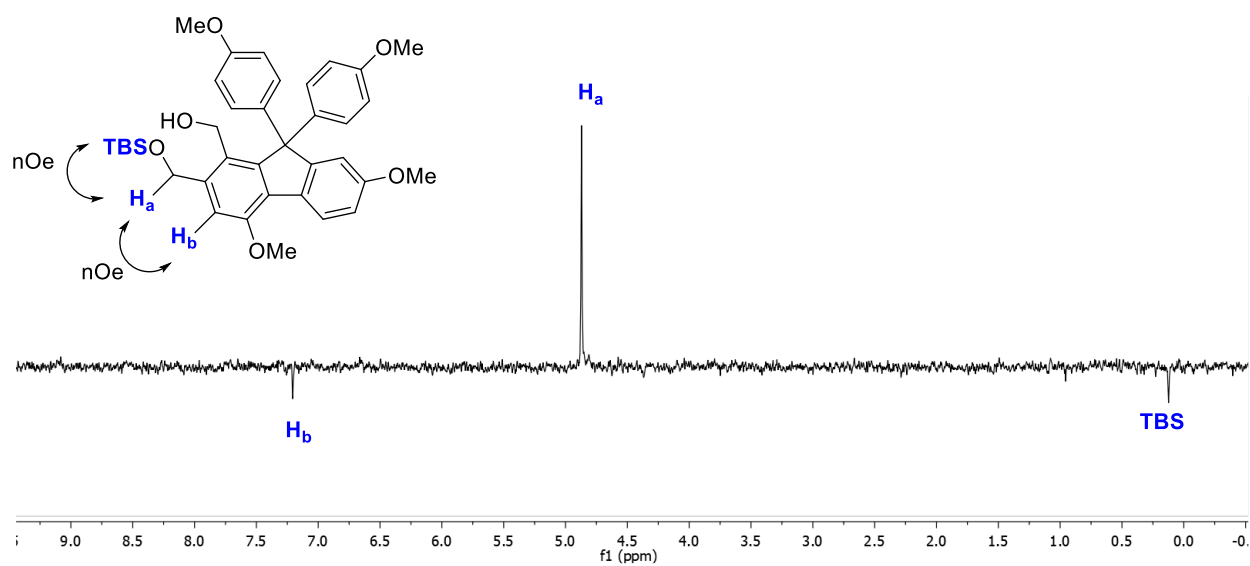
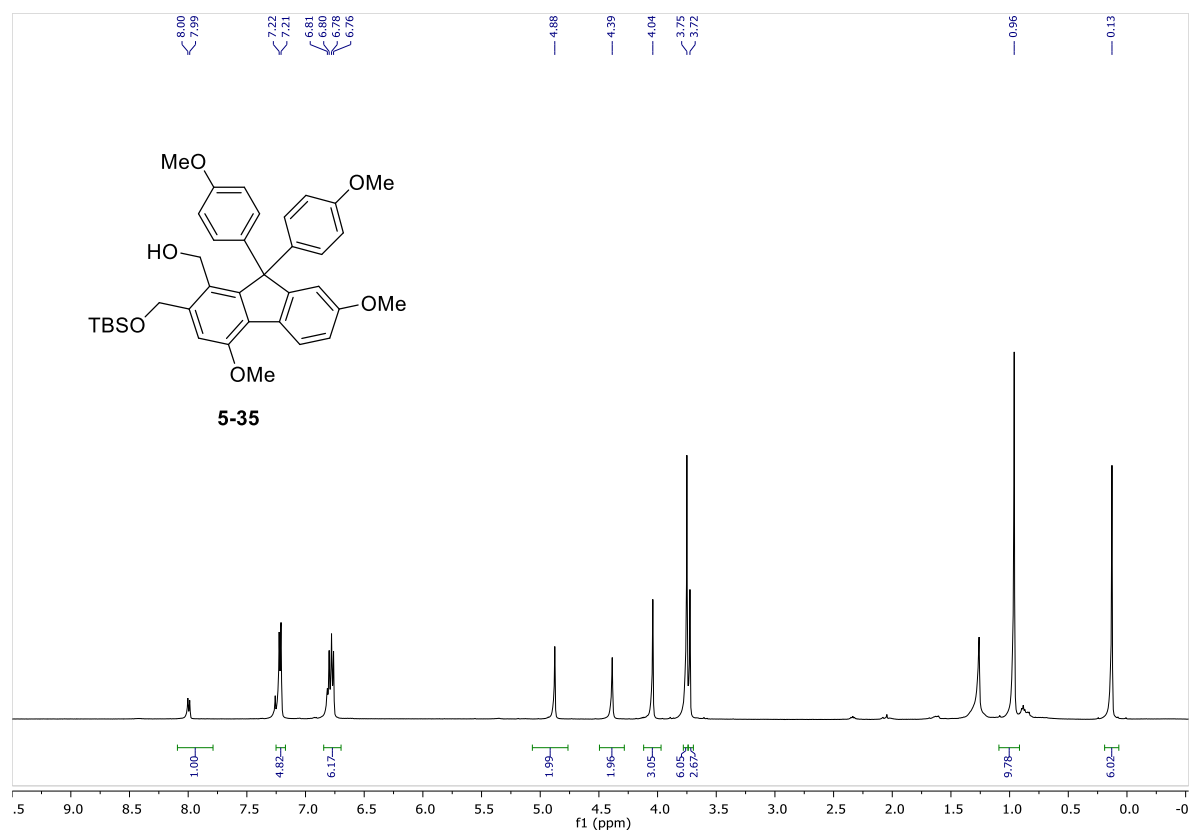


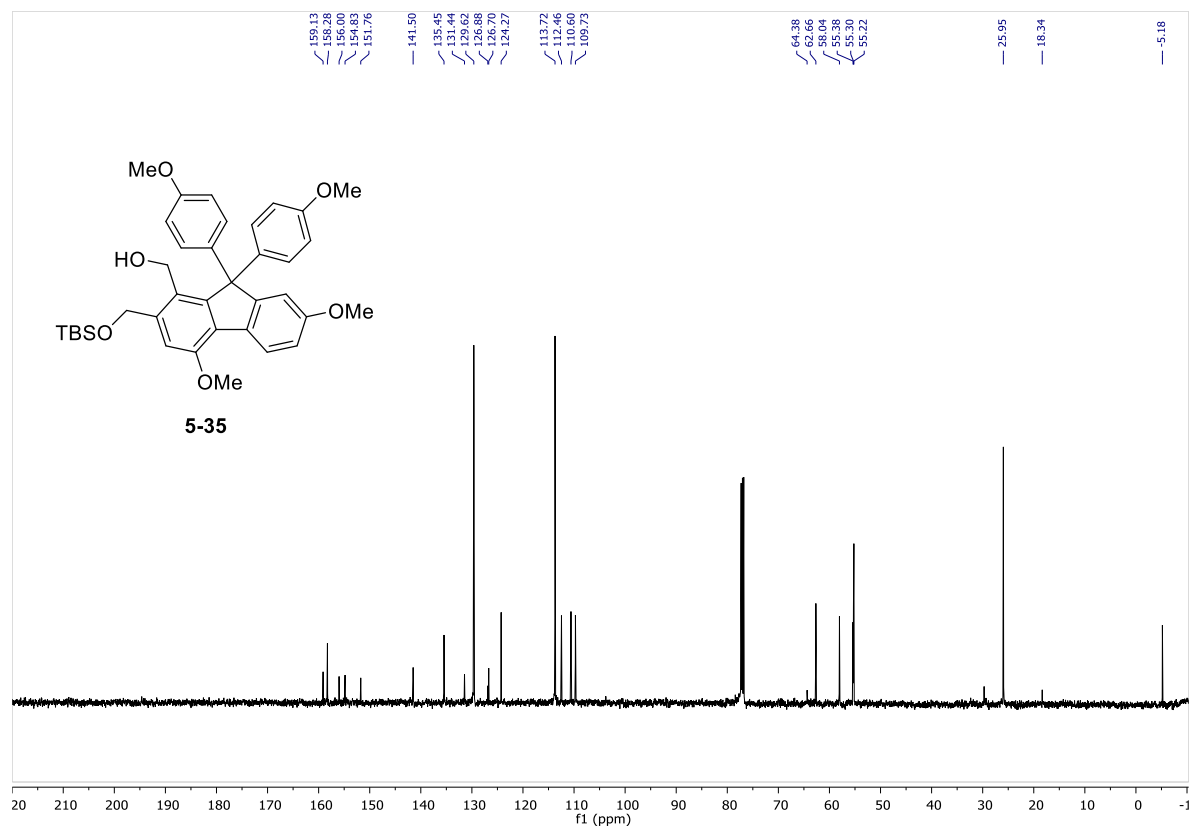


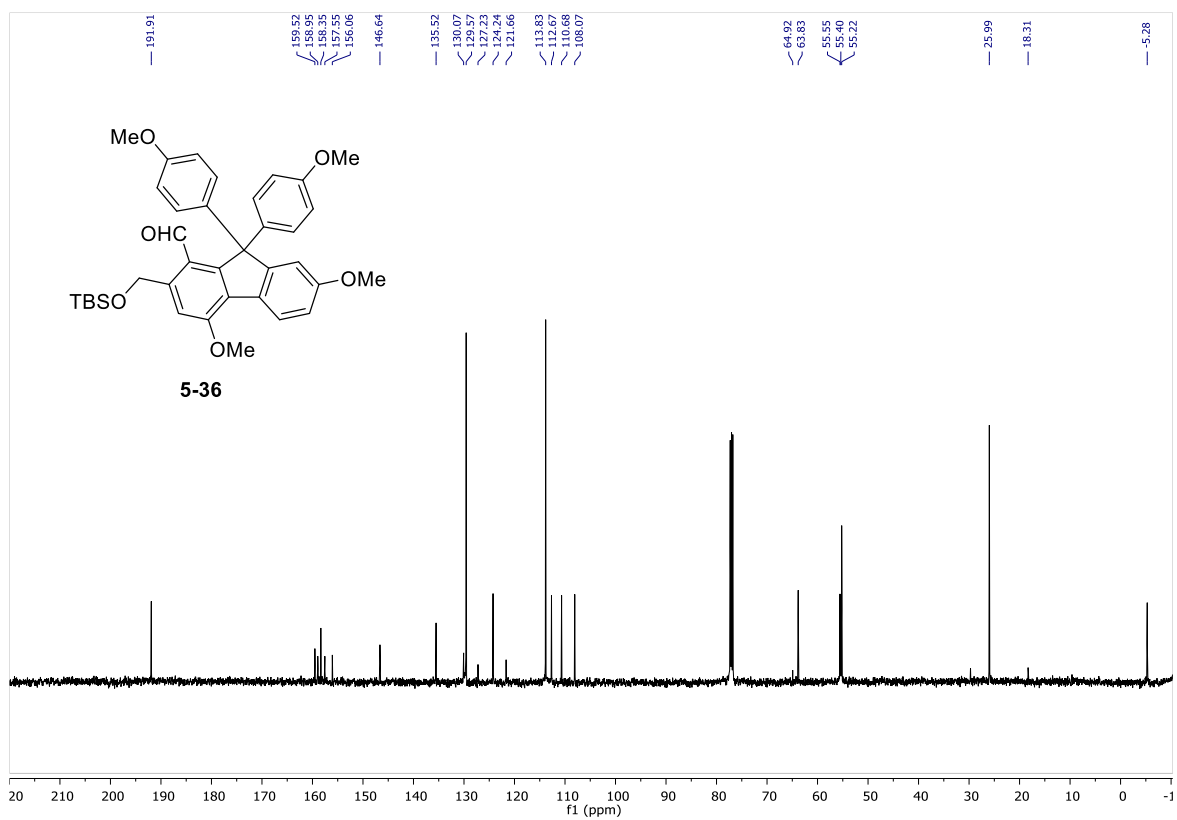
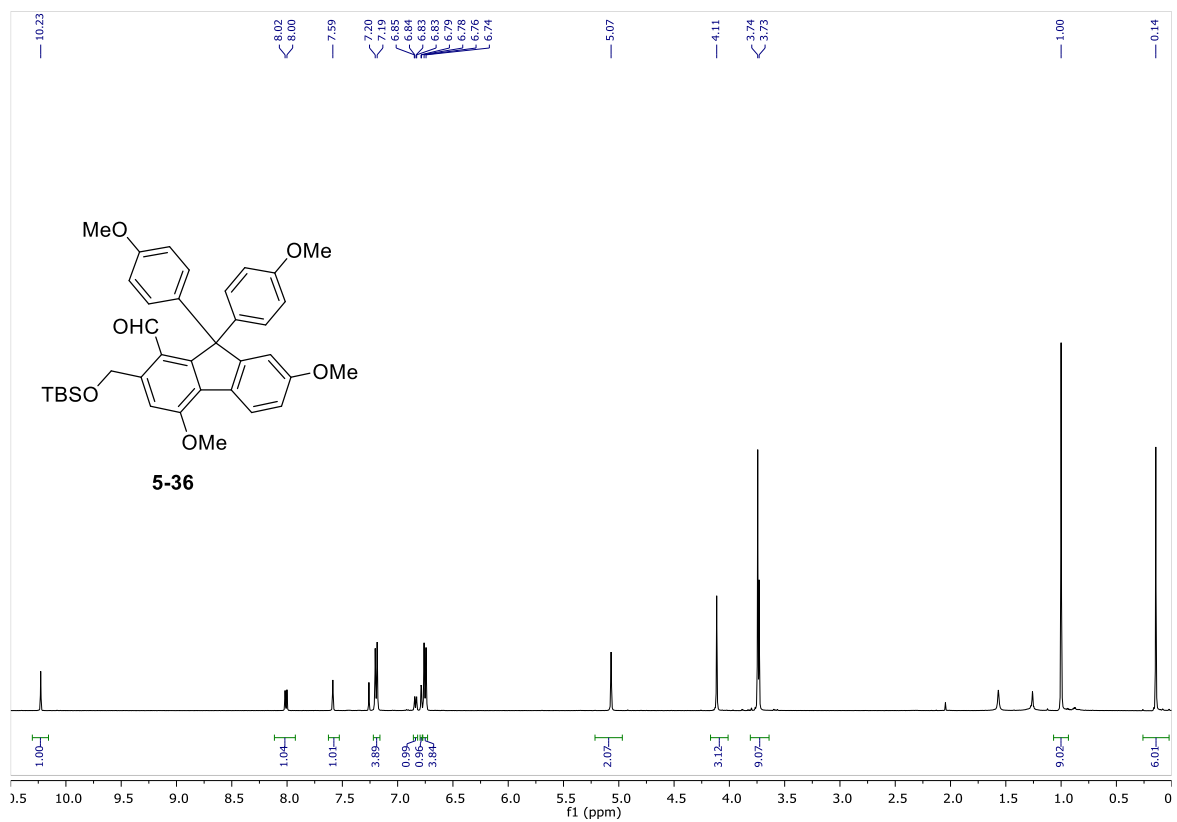


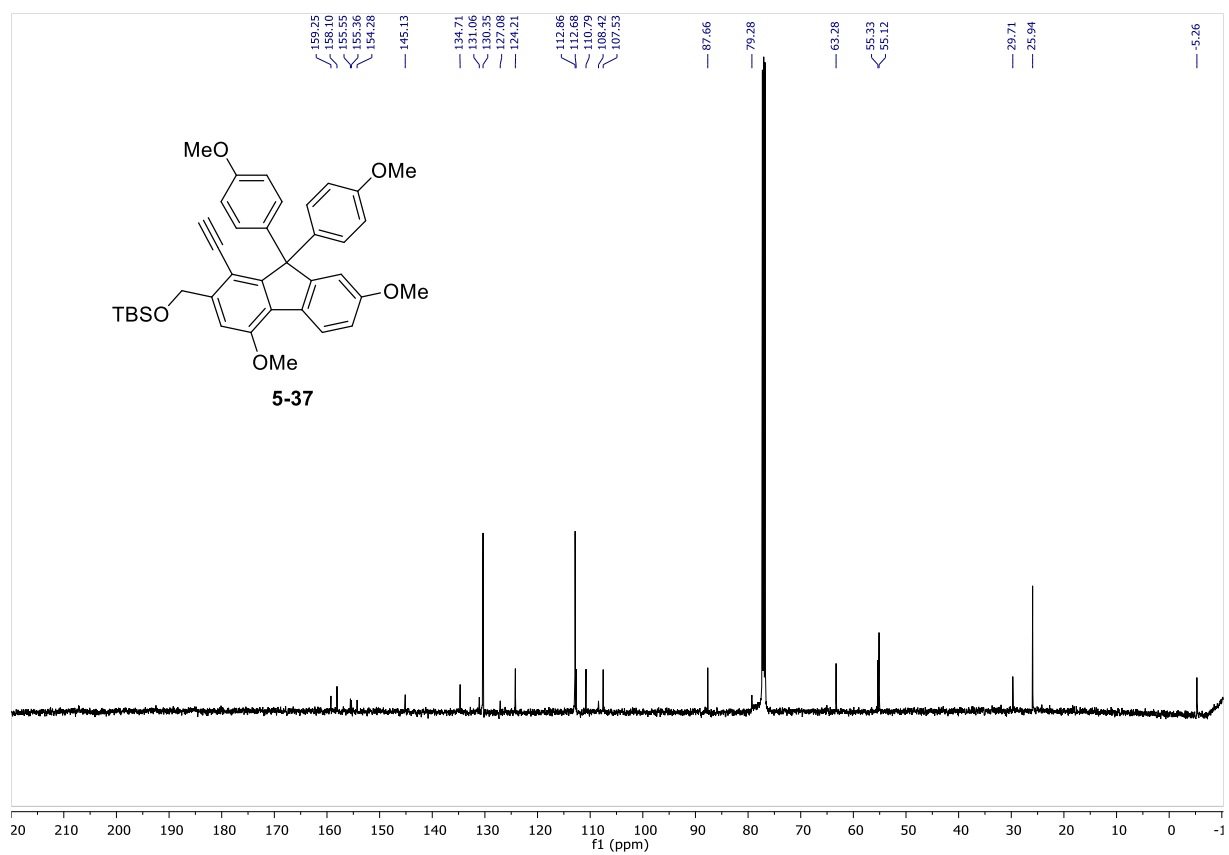
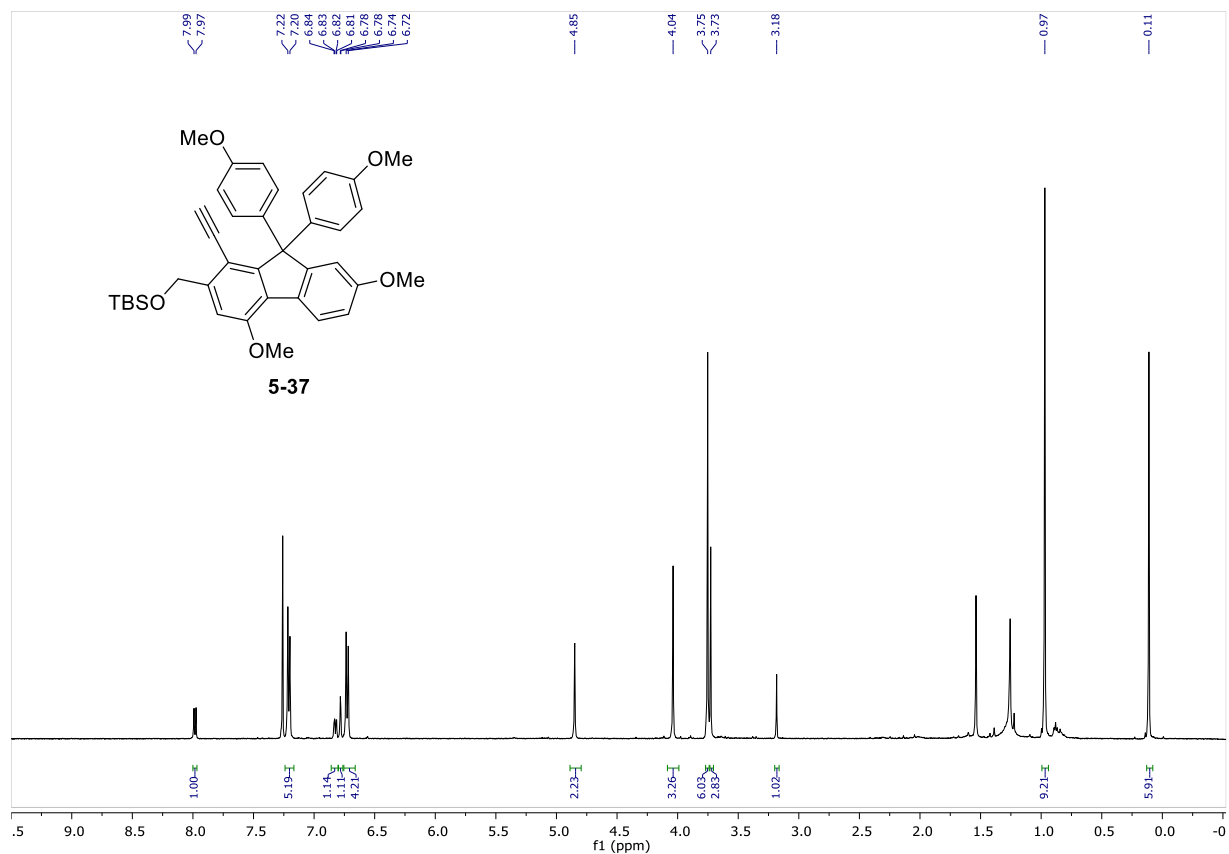


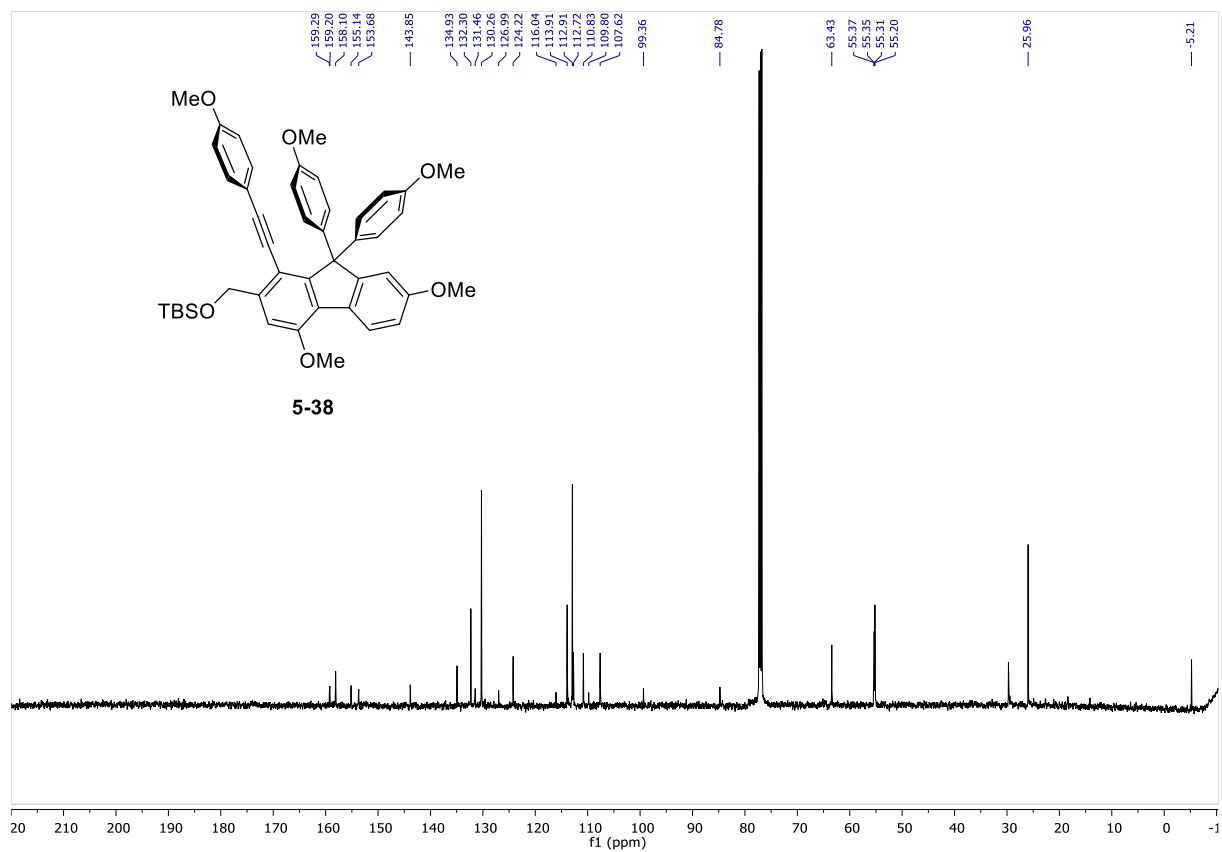
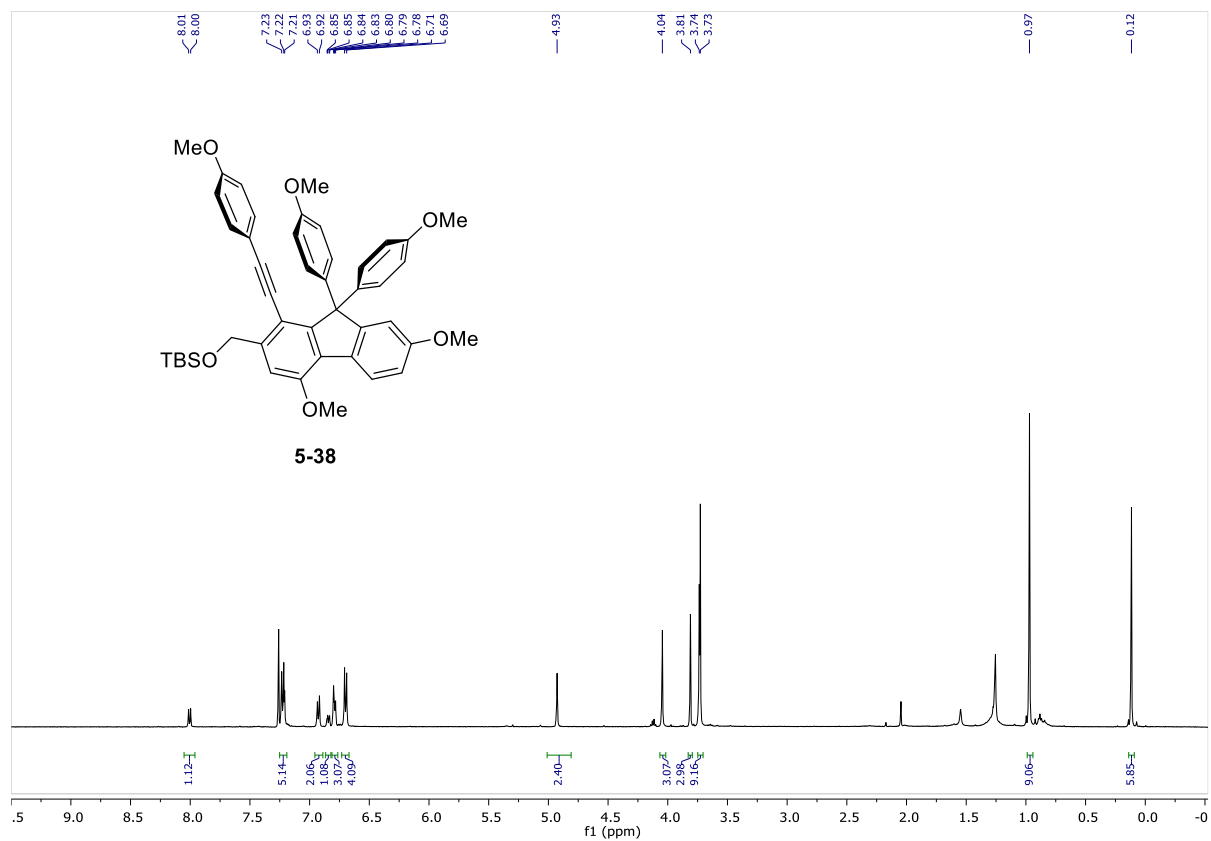




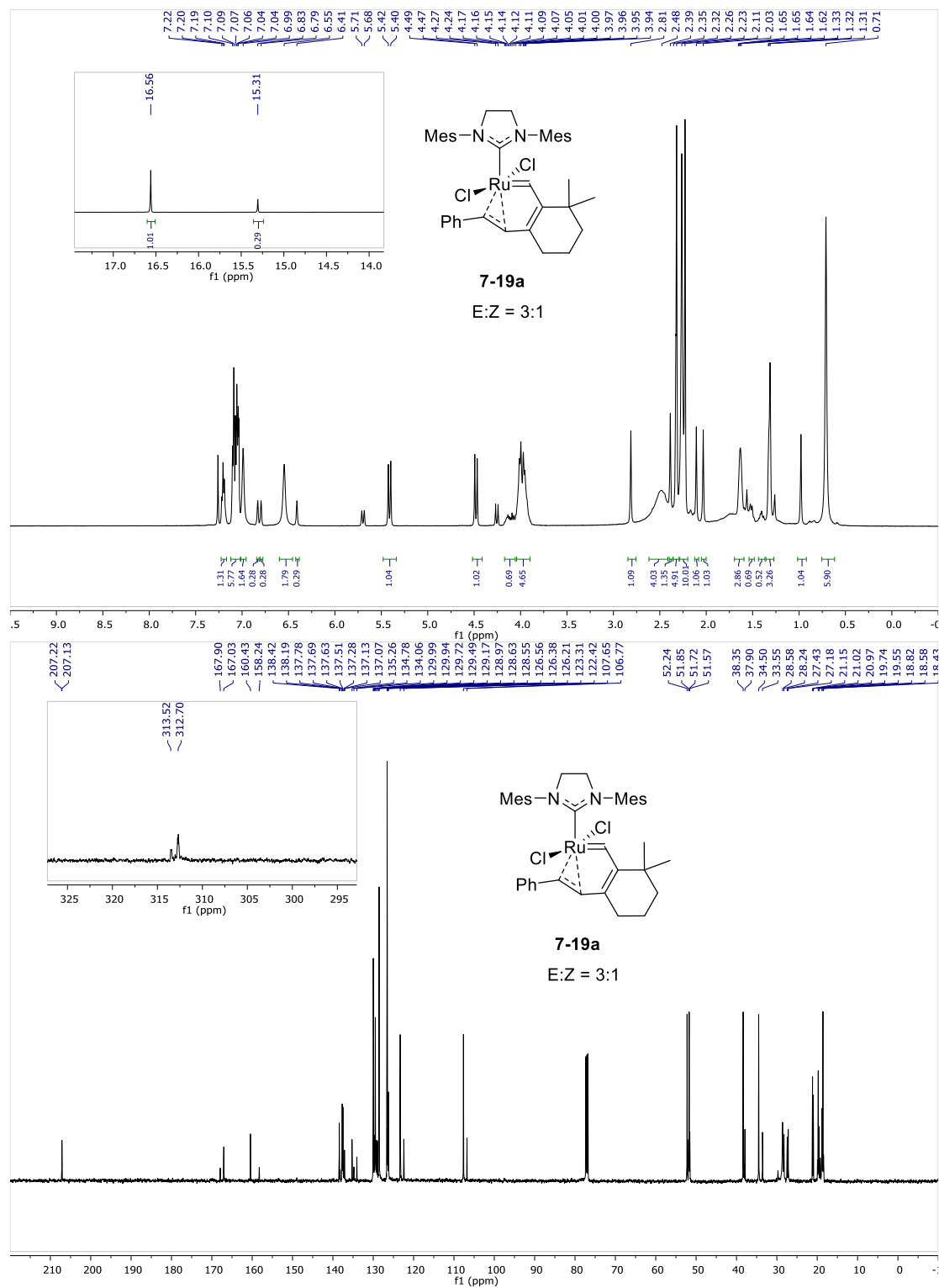


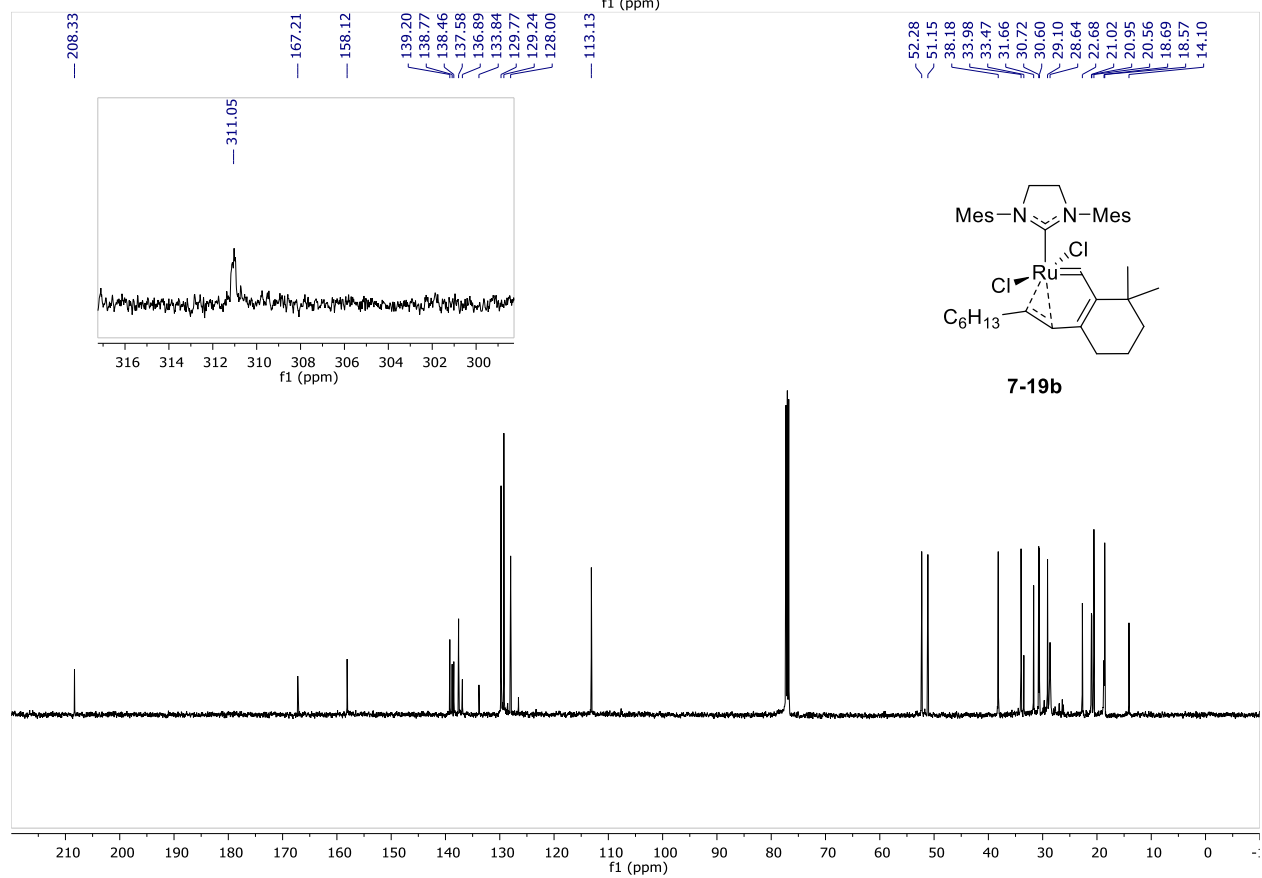
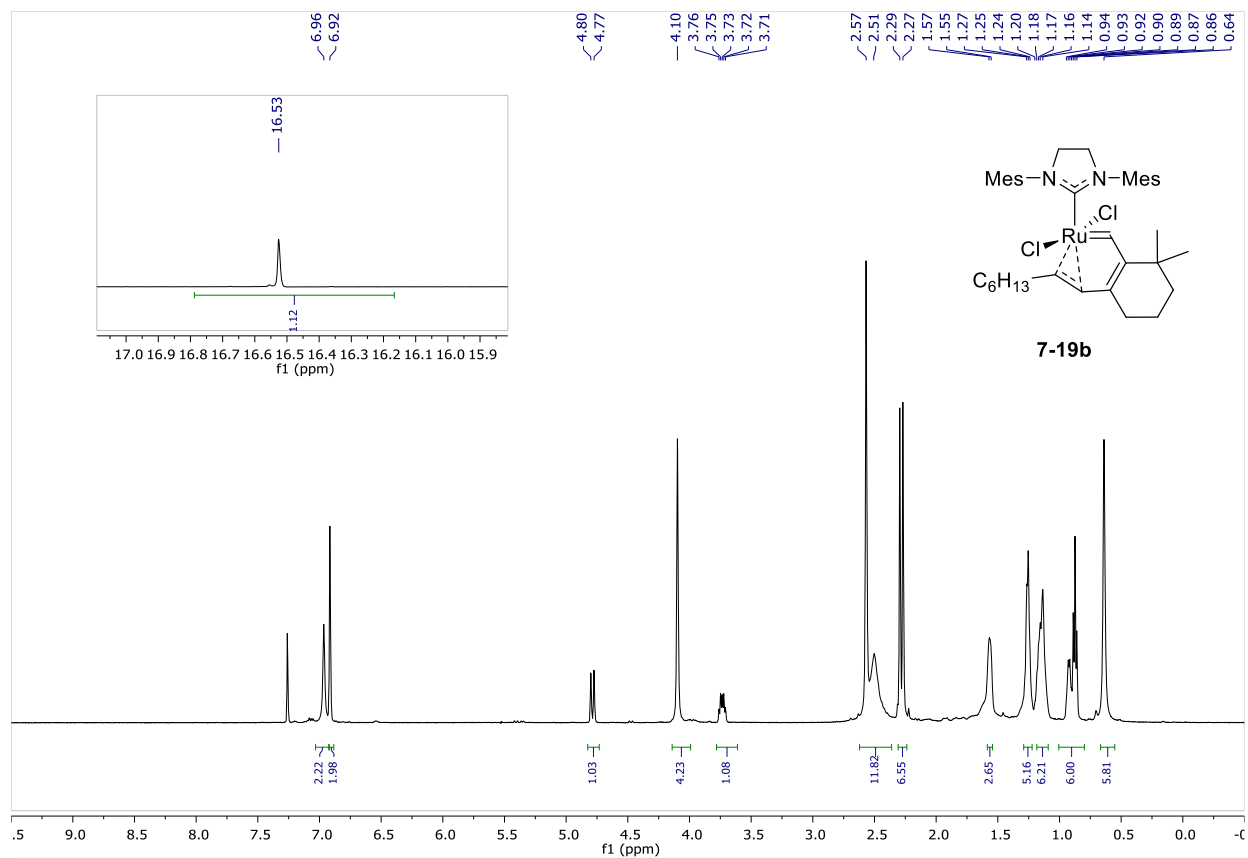


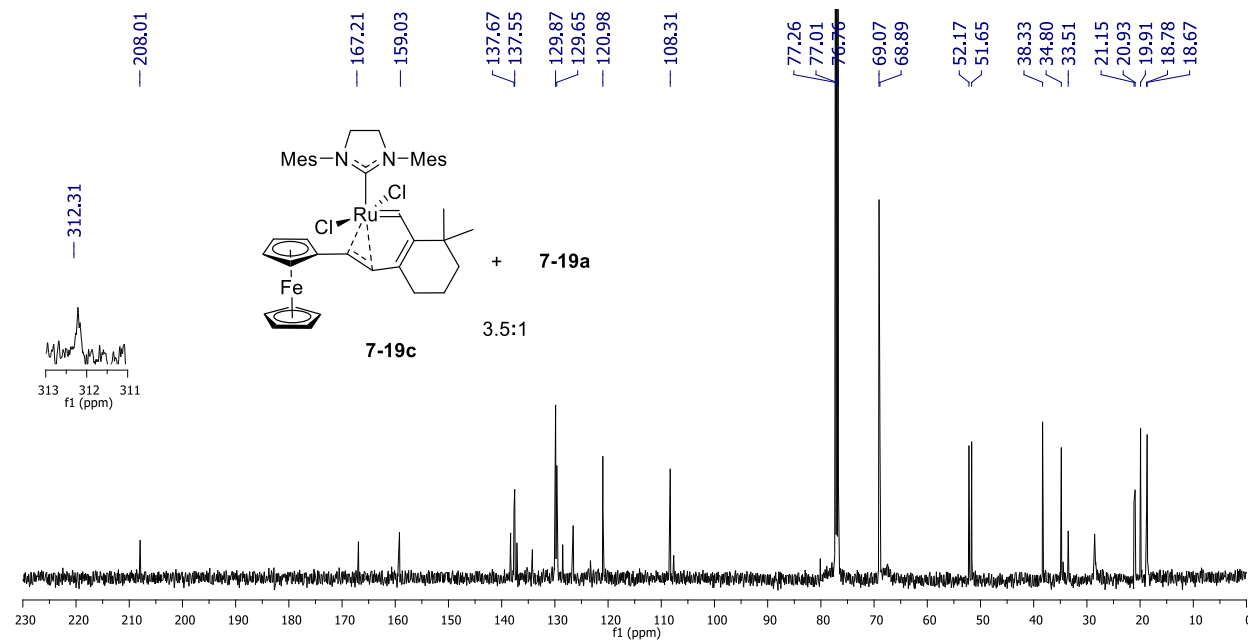
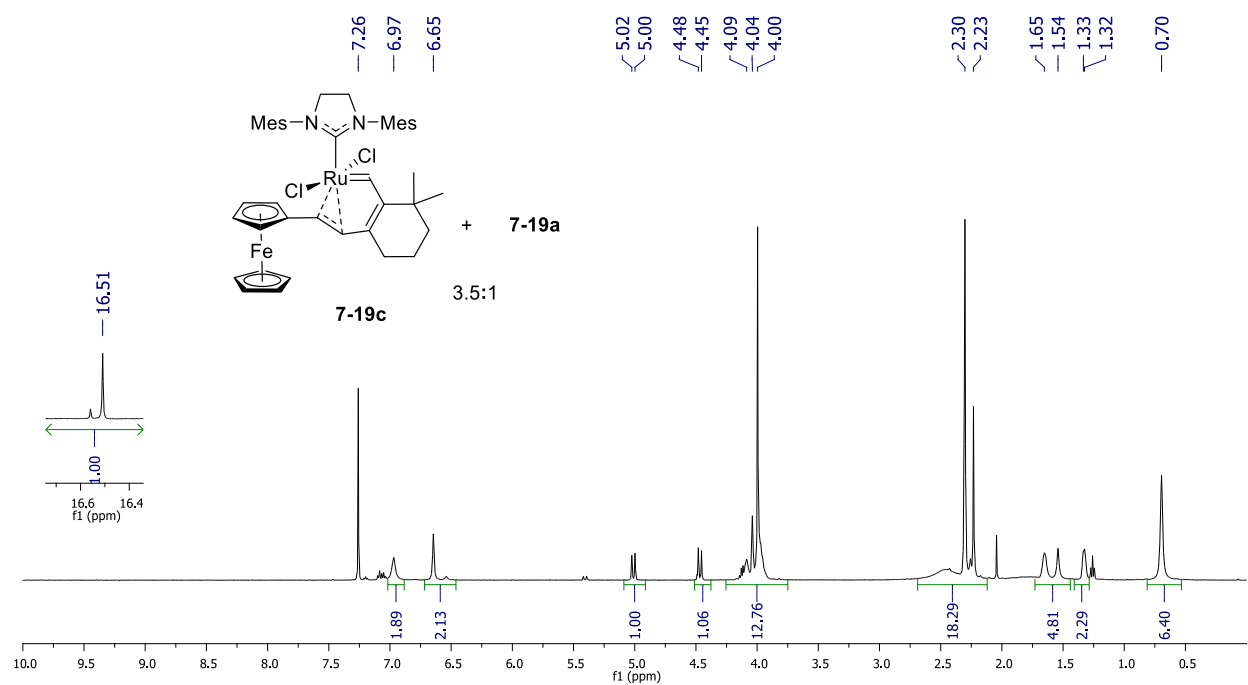


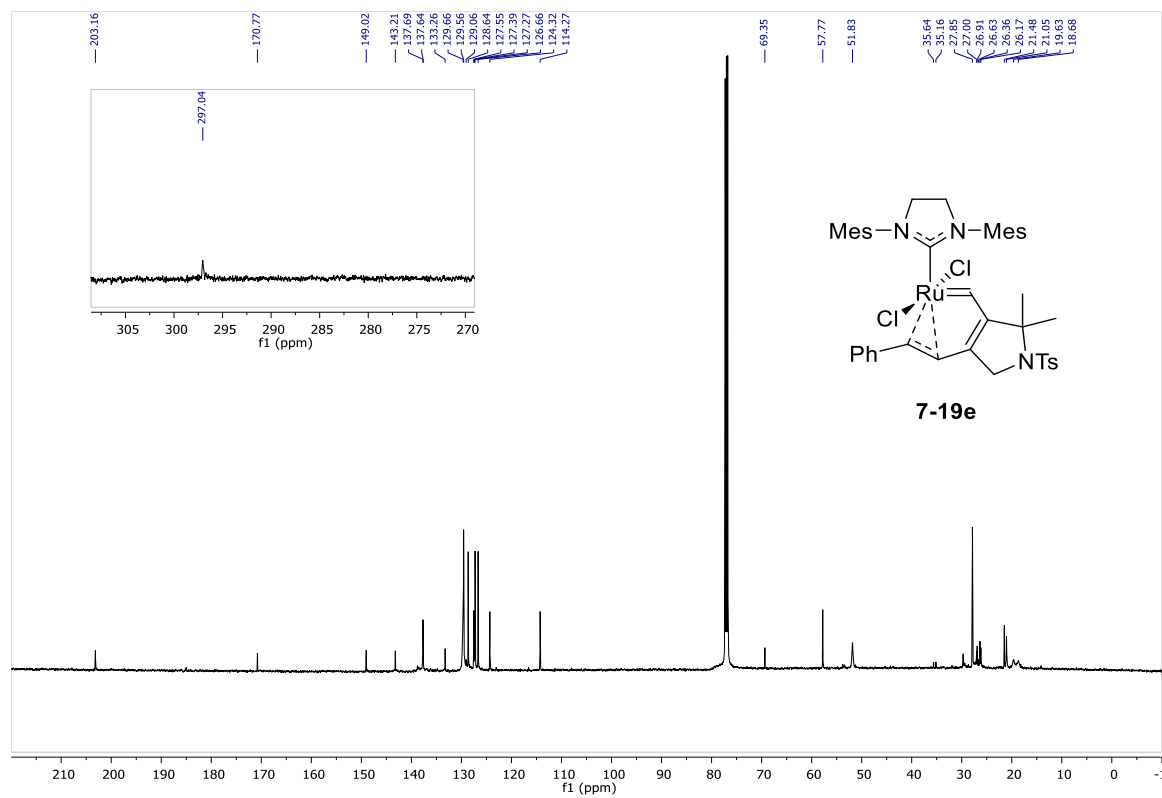
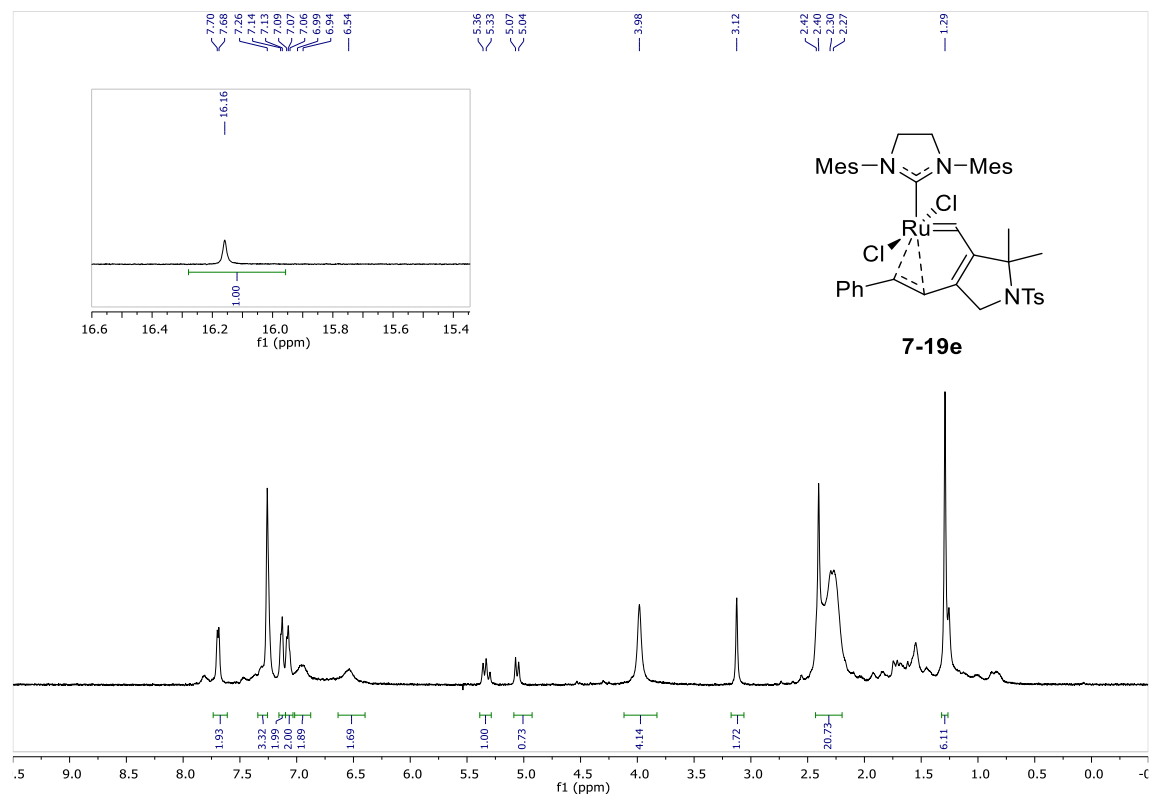


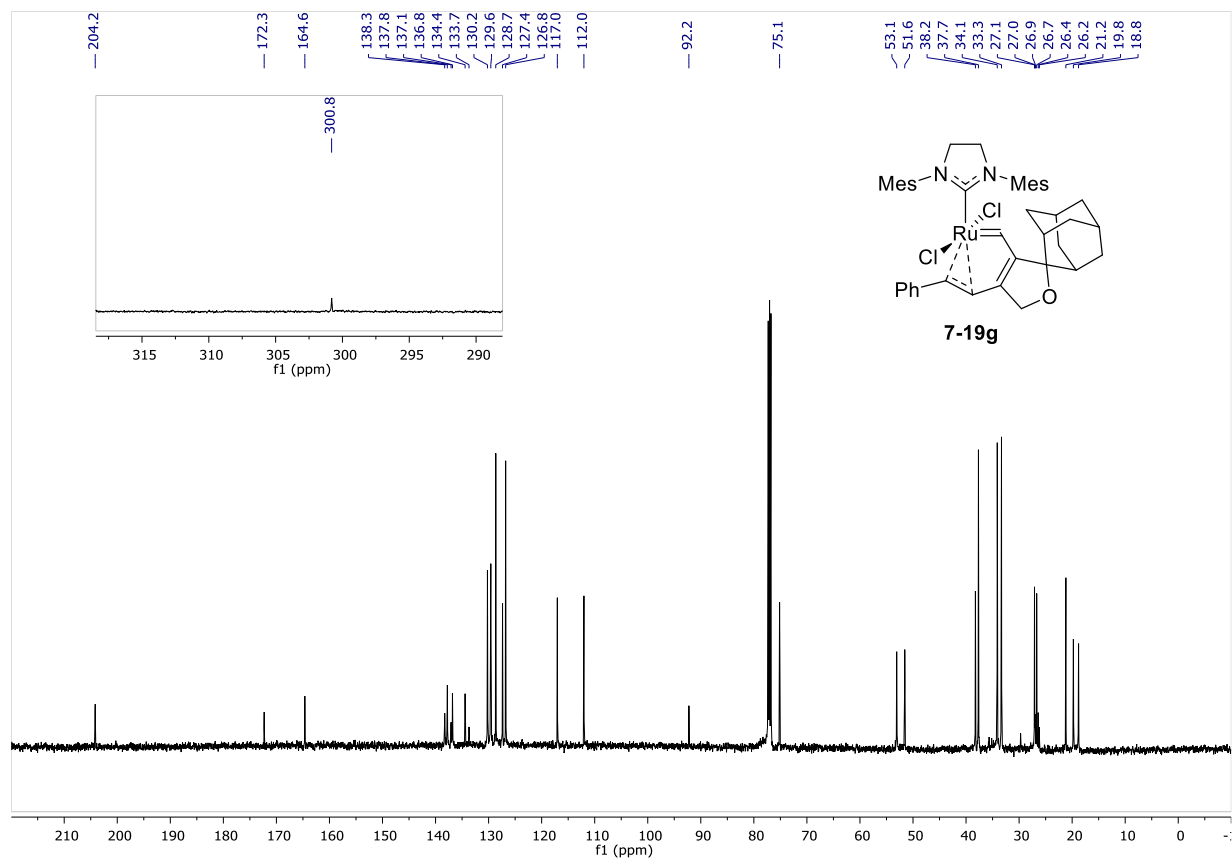
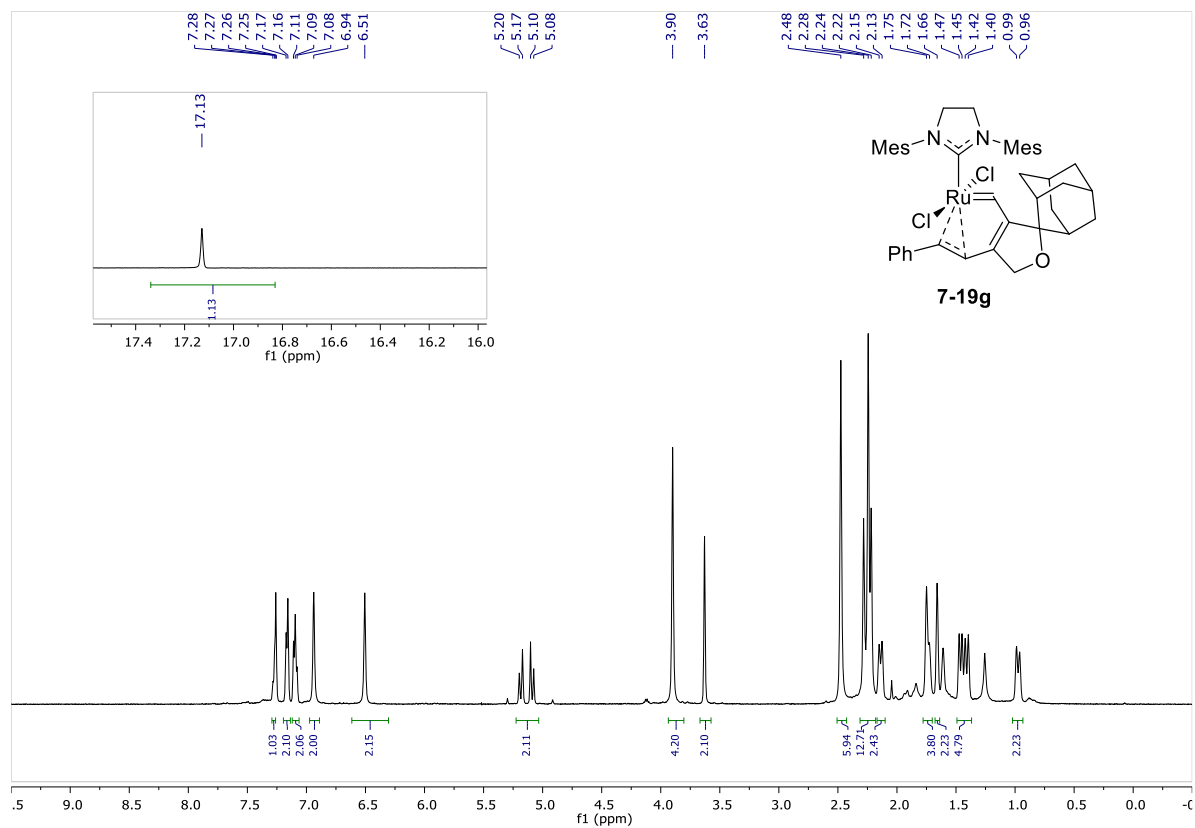
Appendix V
Selected NMR Spectra for Chapter 7

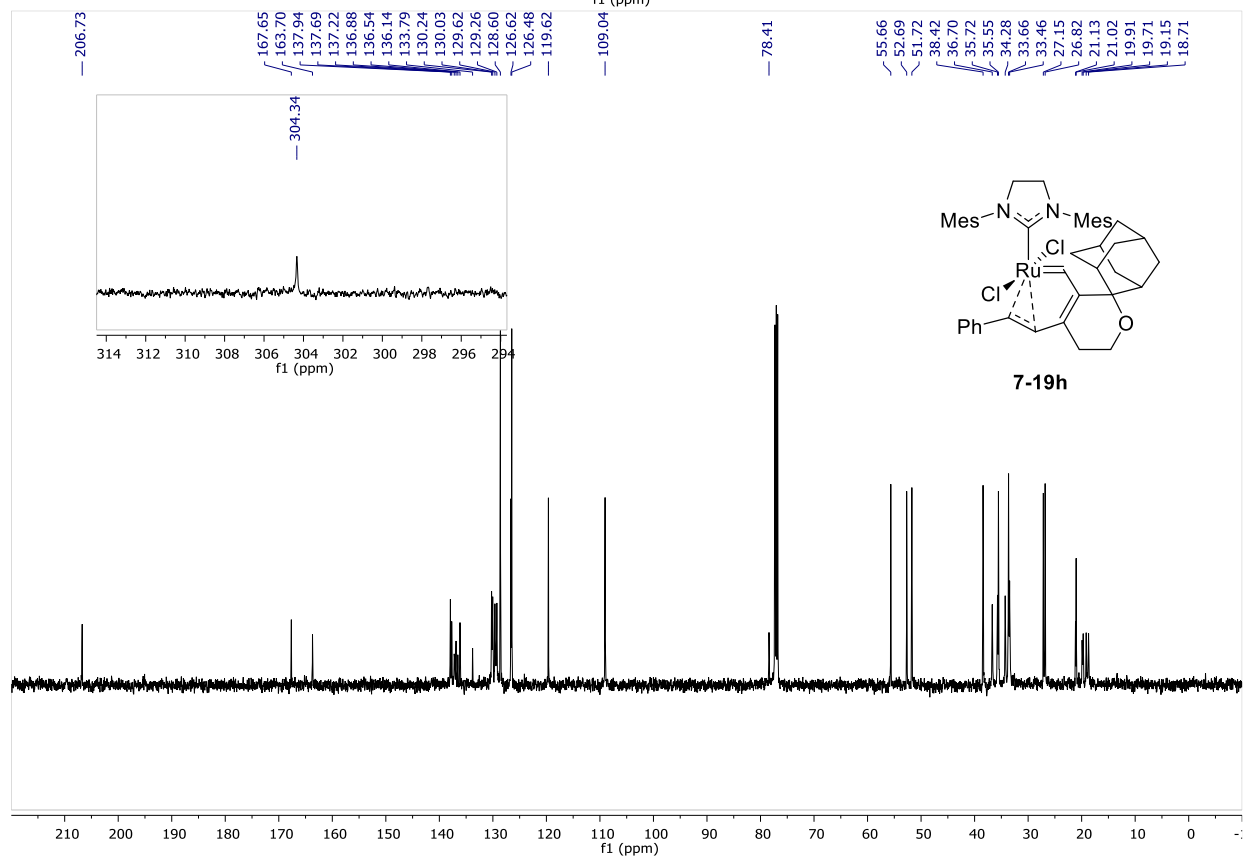
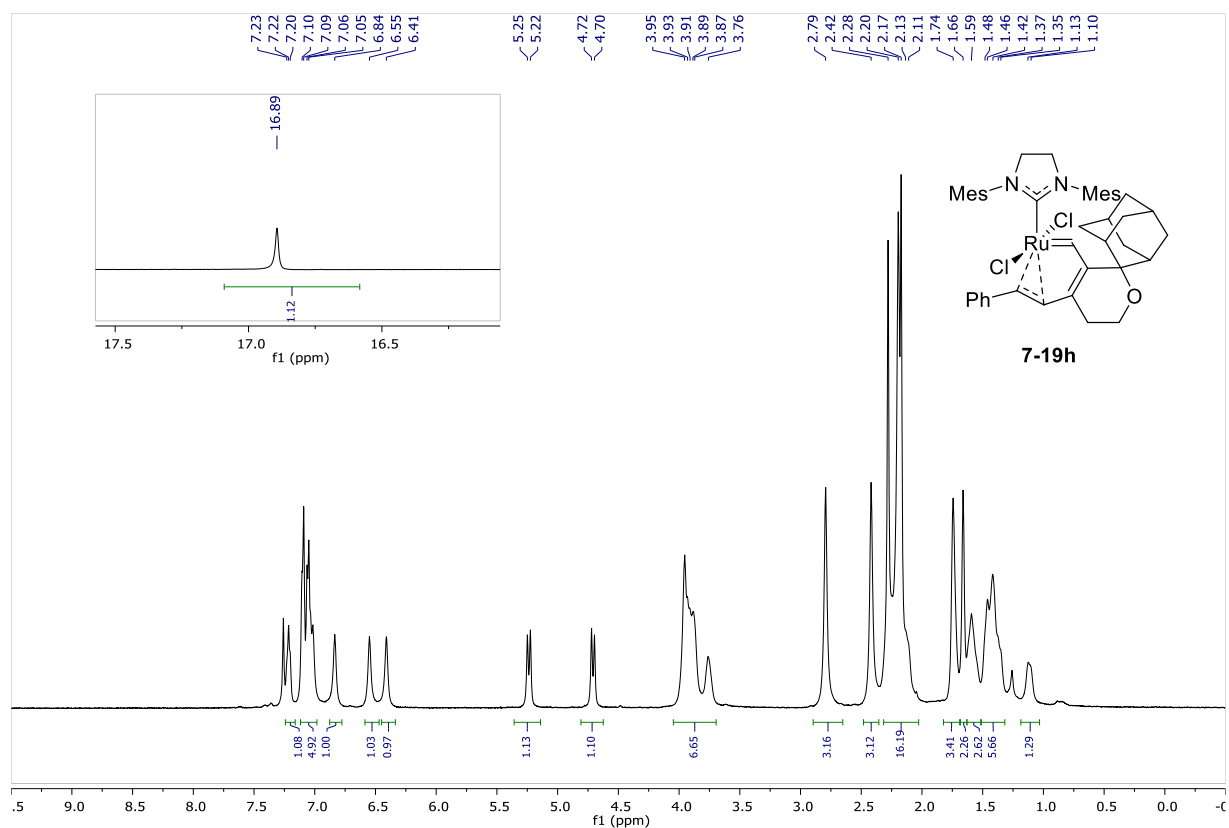


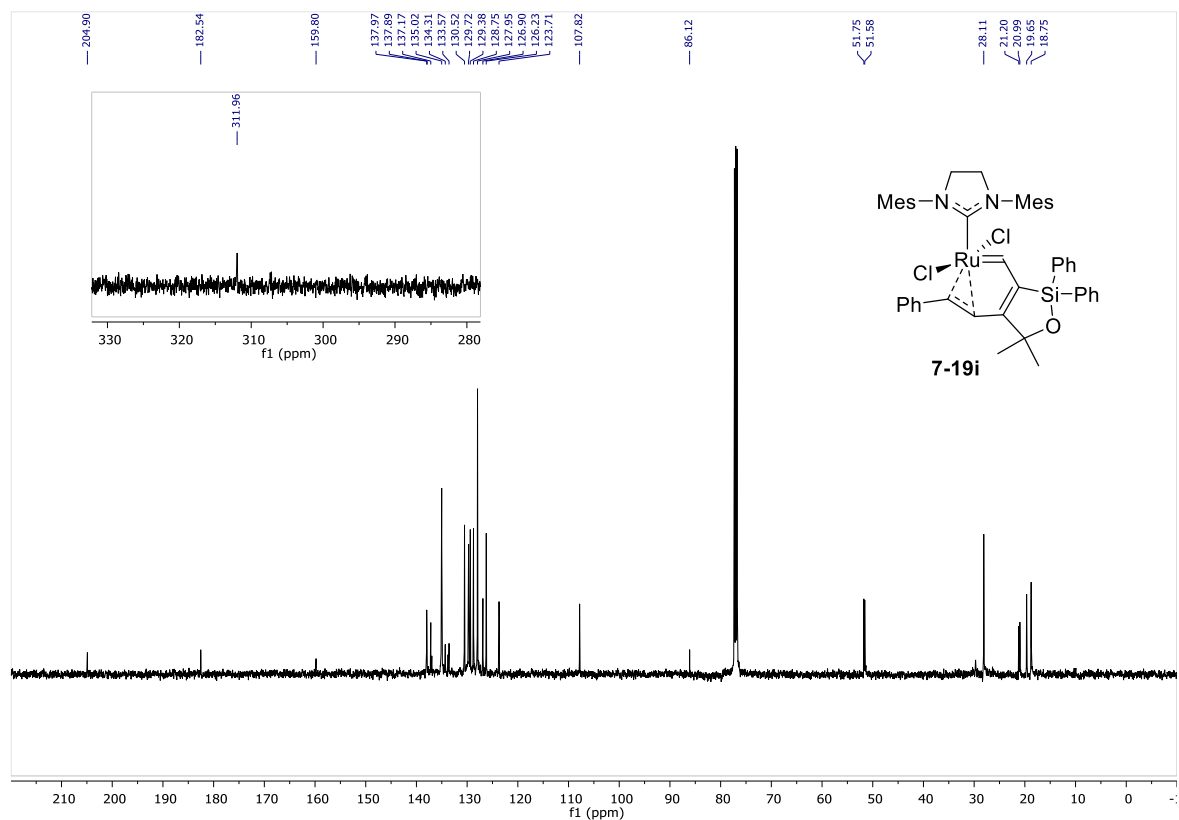
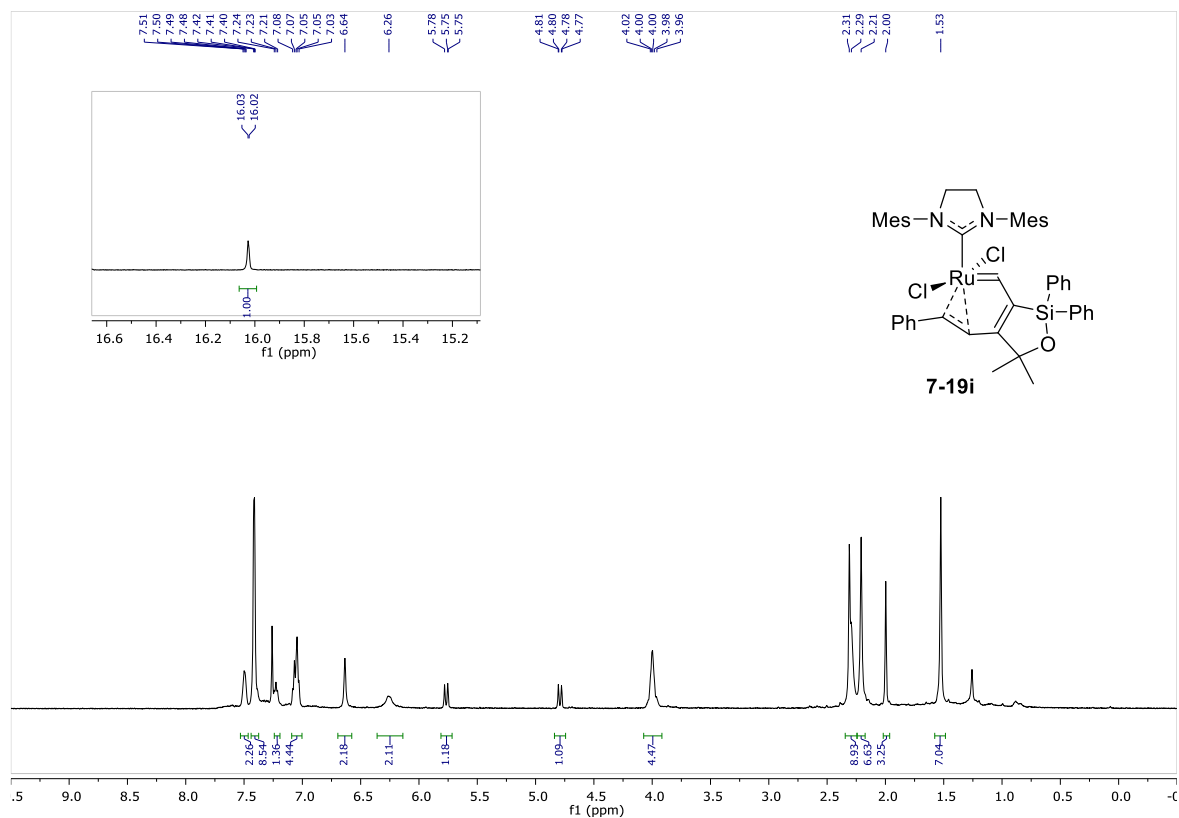


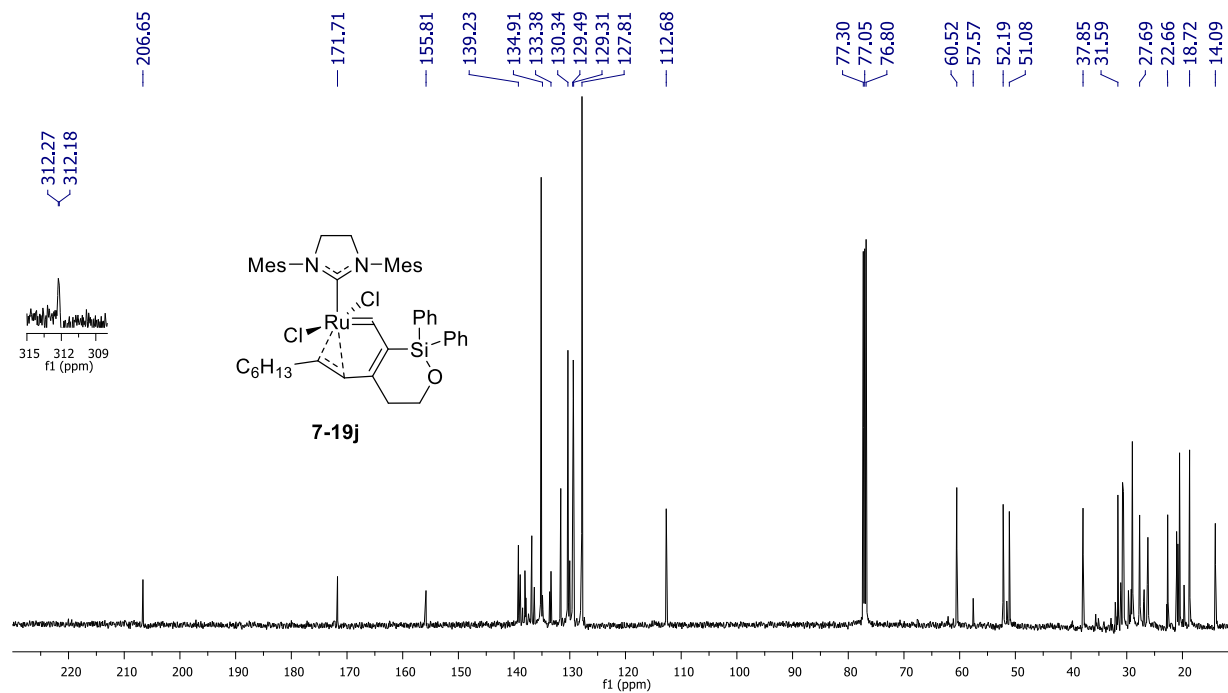
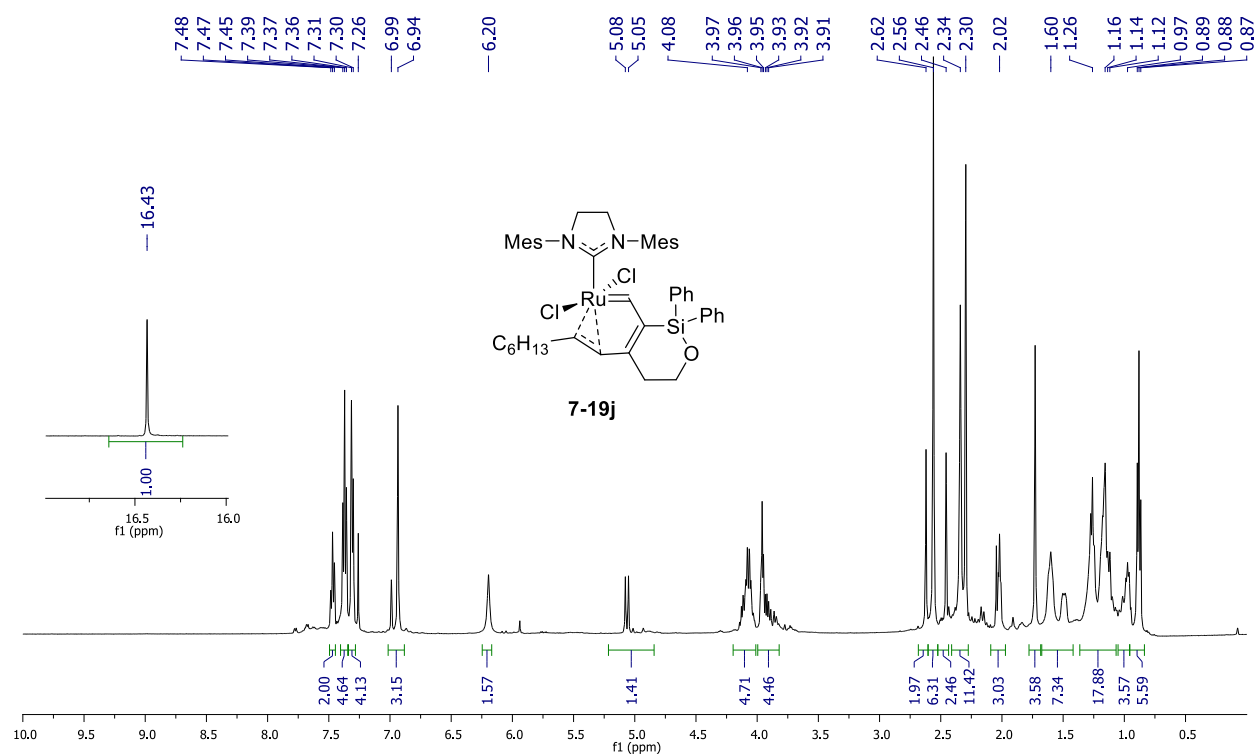


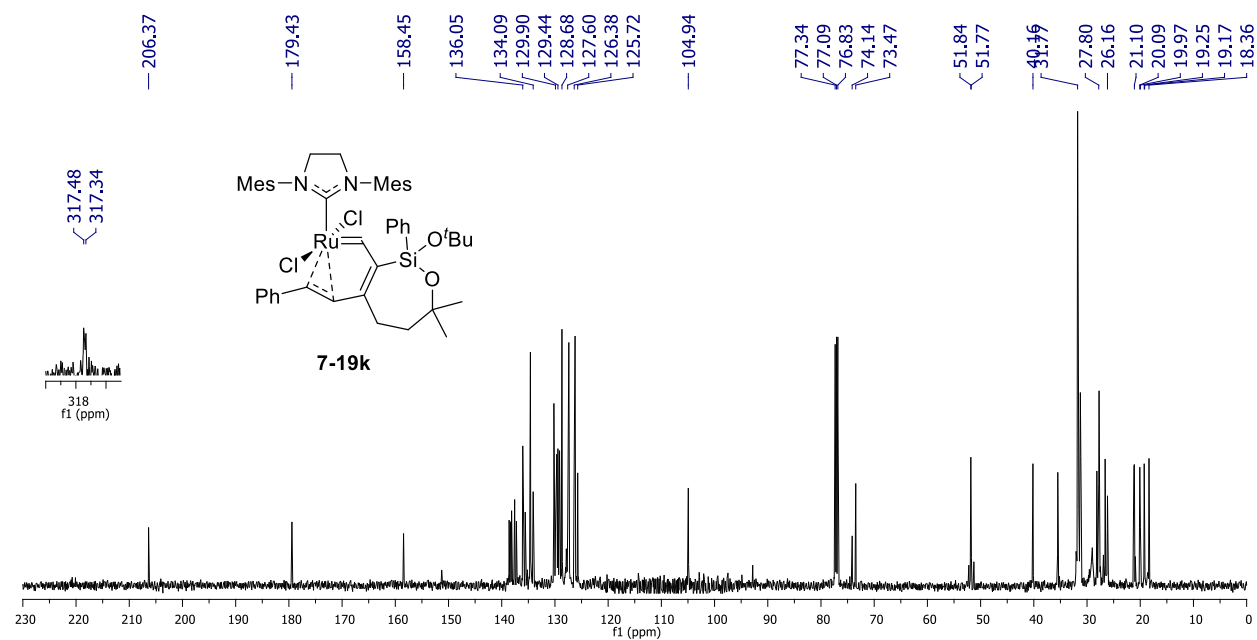
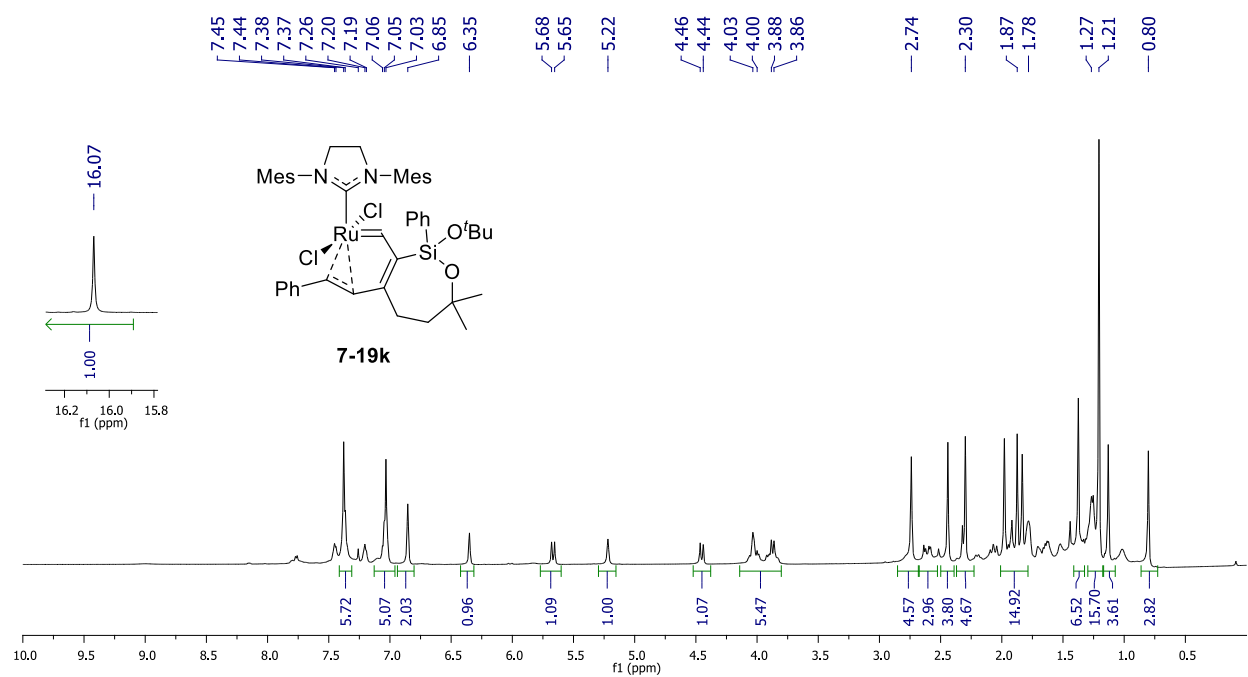


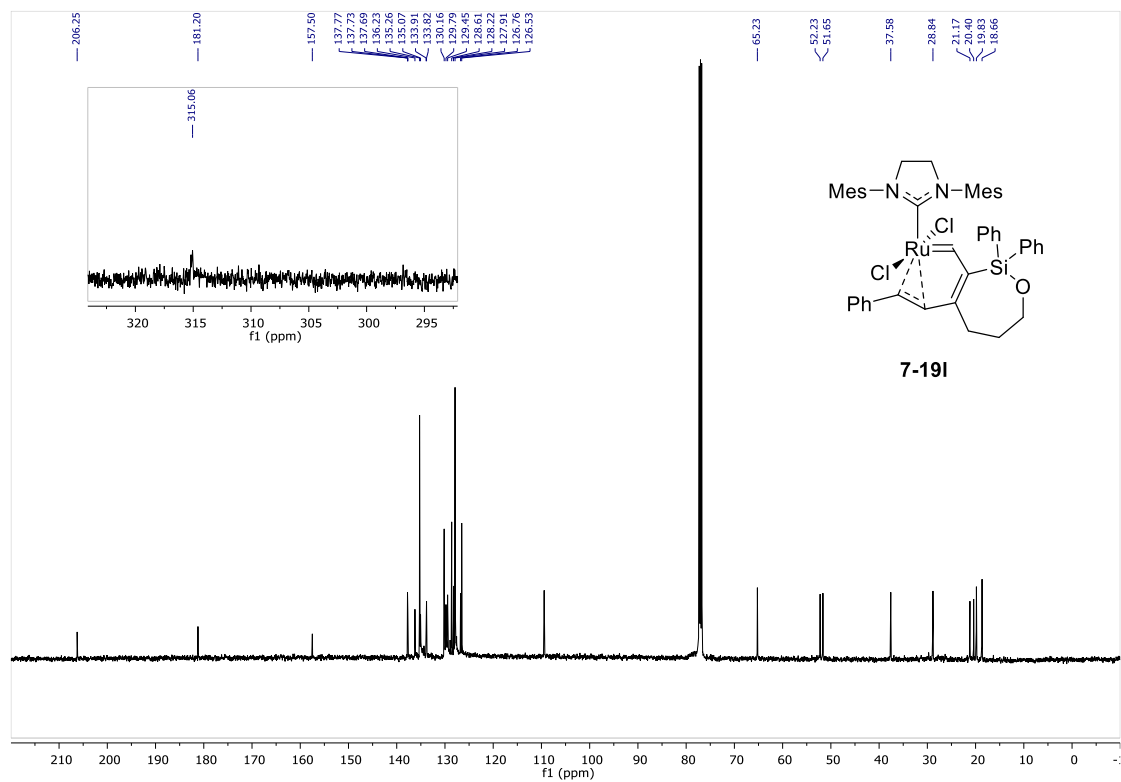
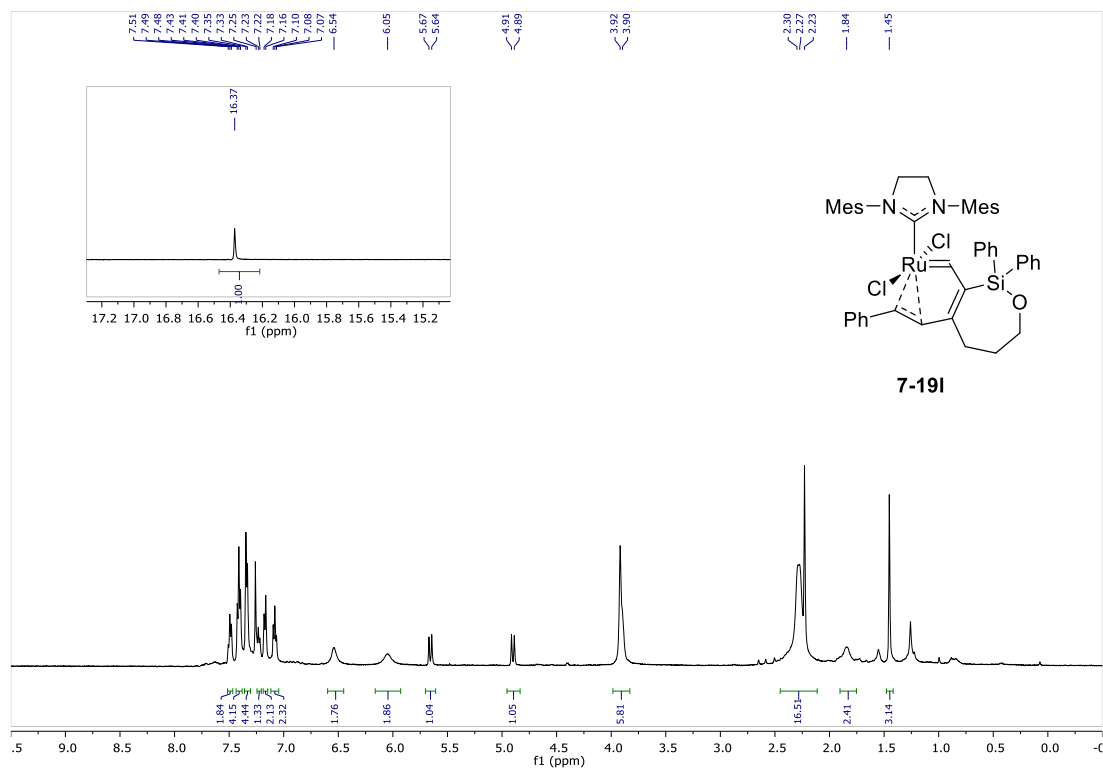


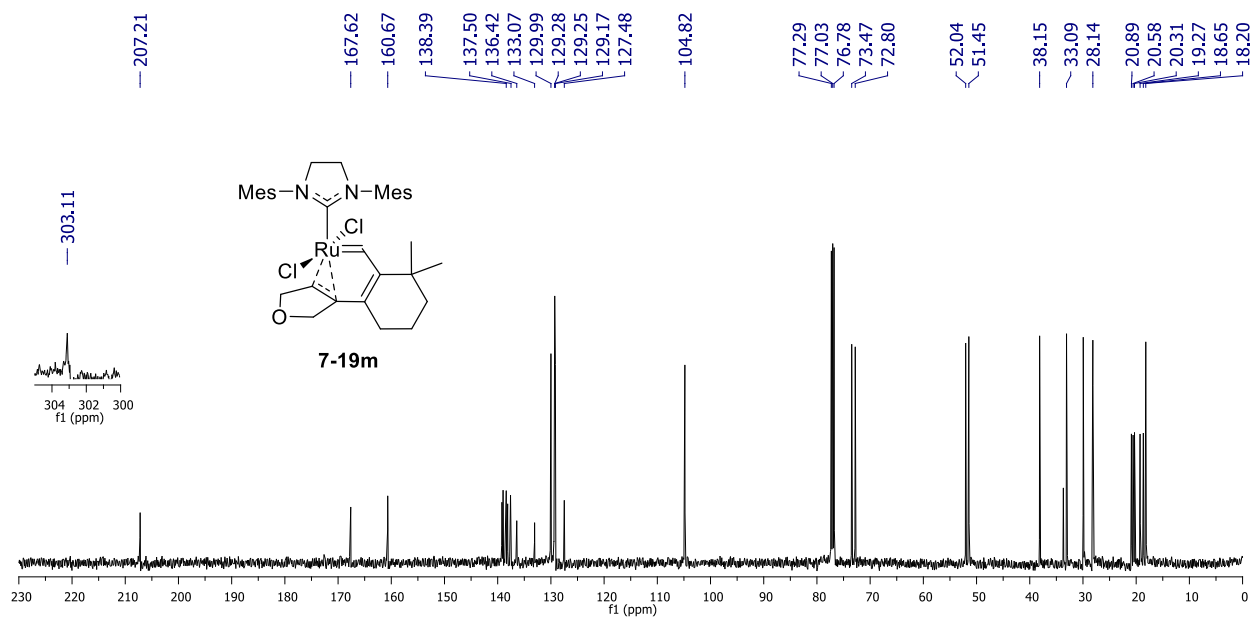
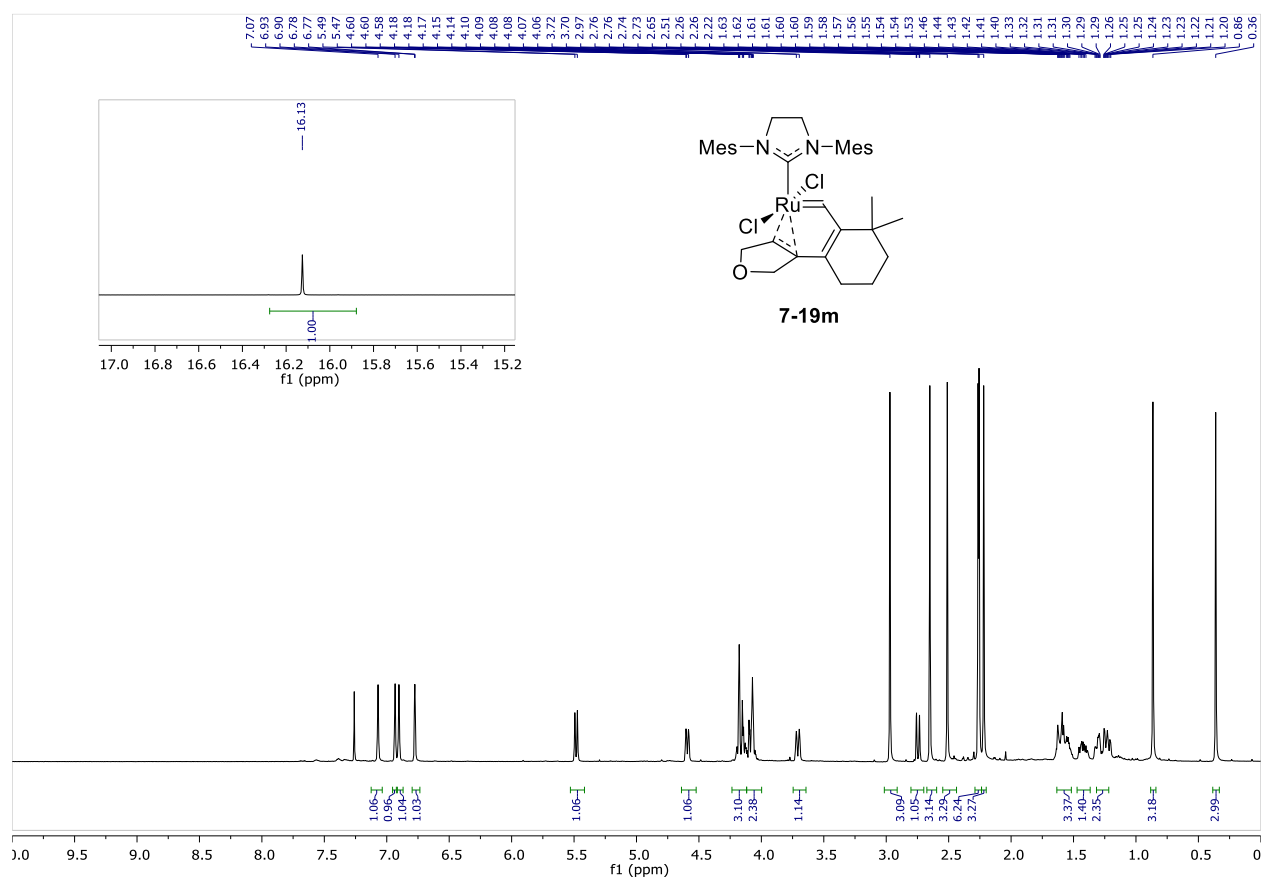


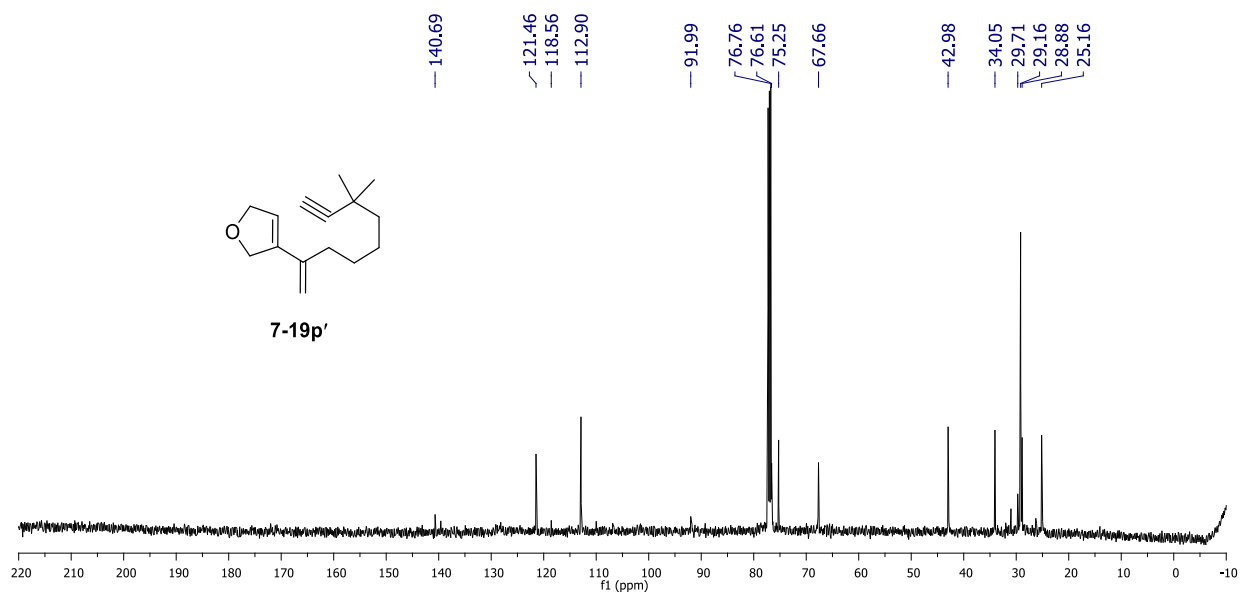
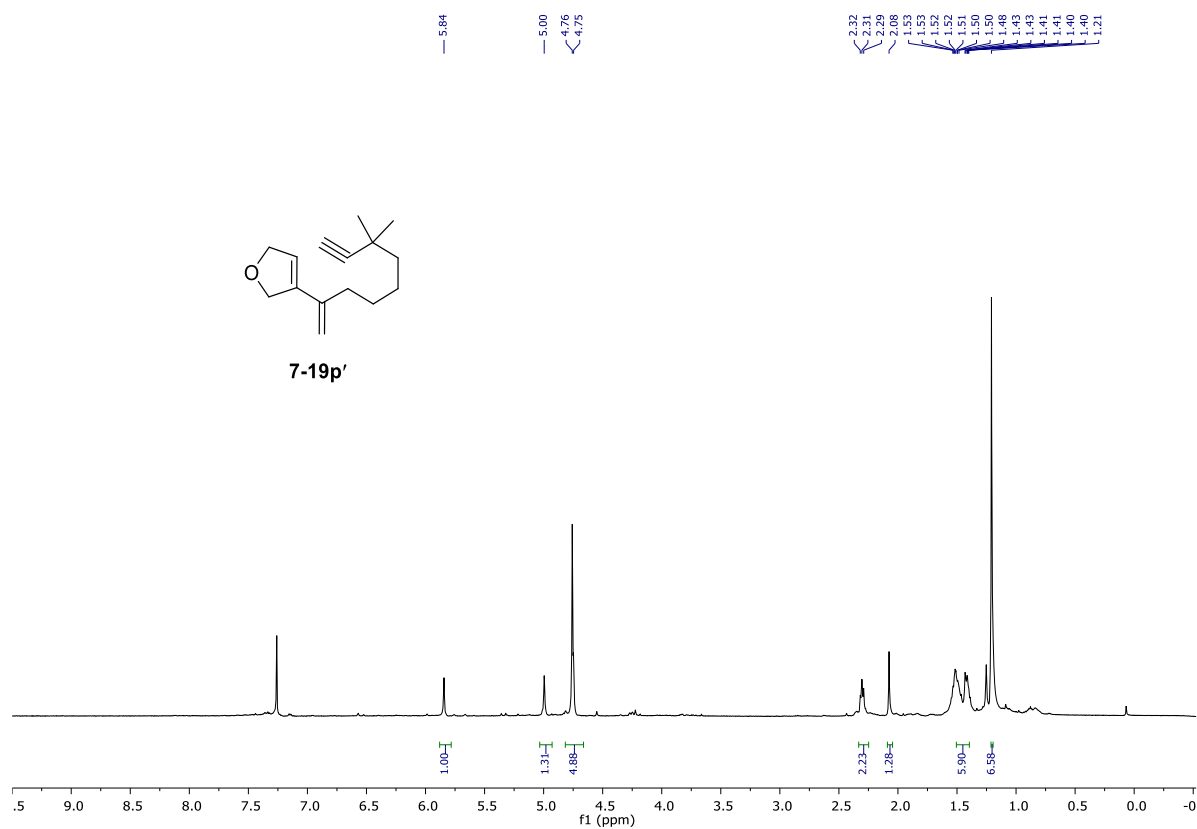


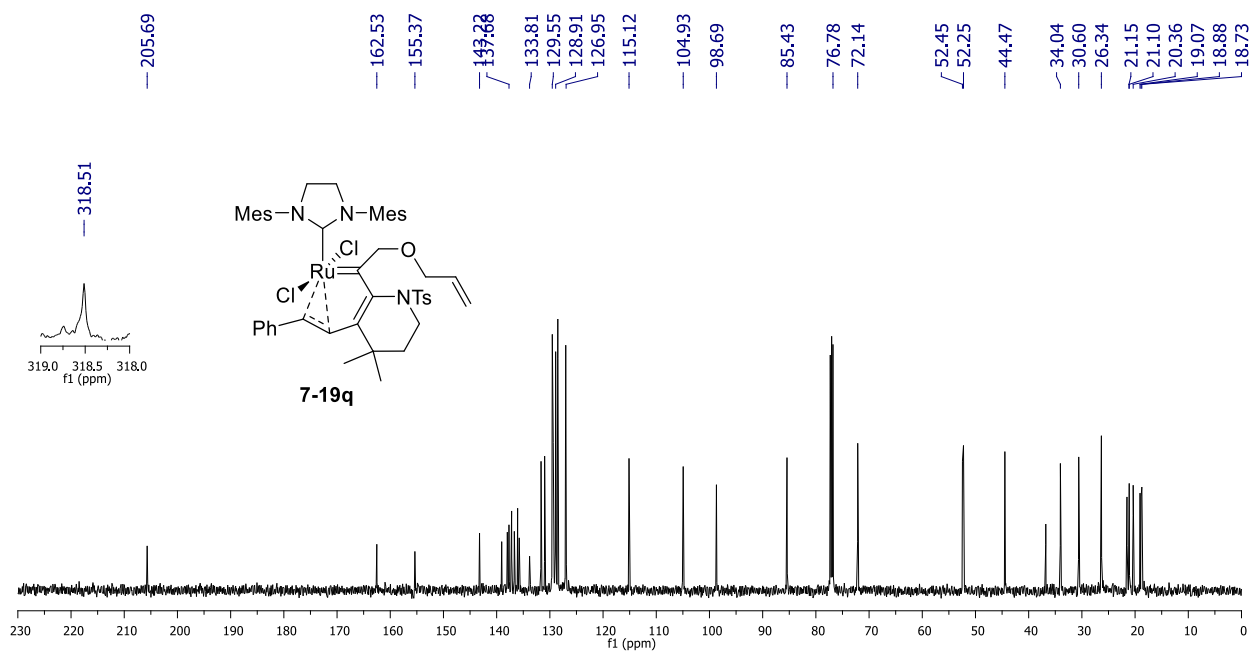
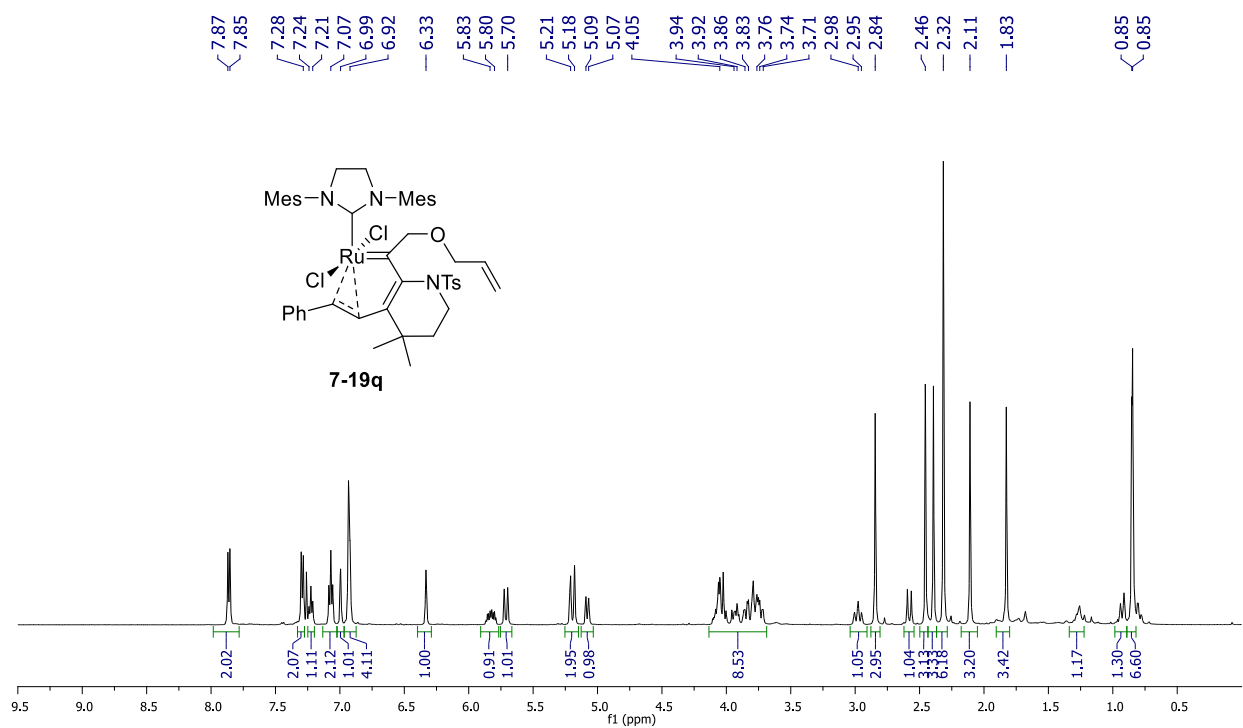


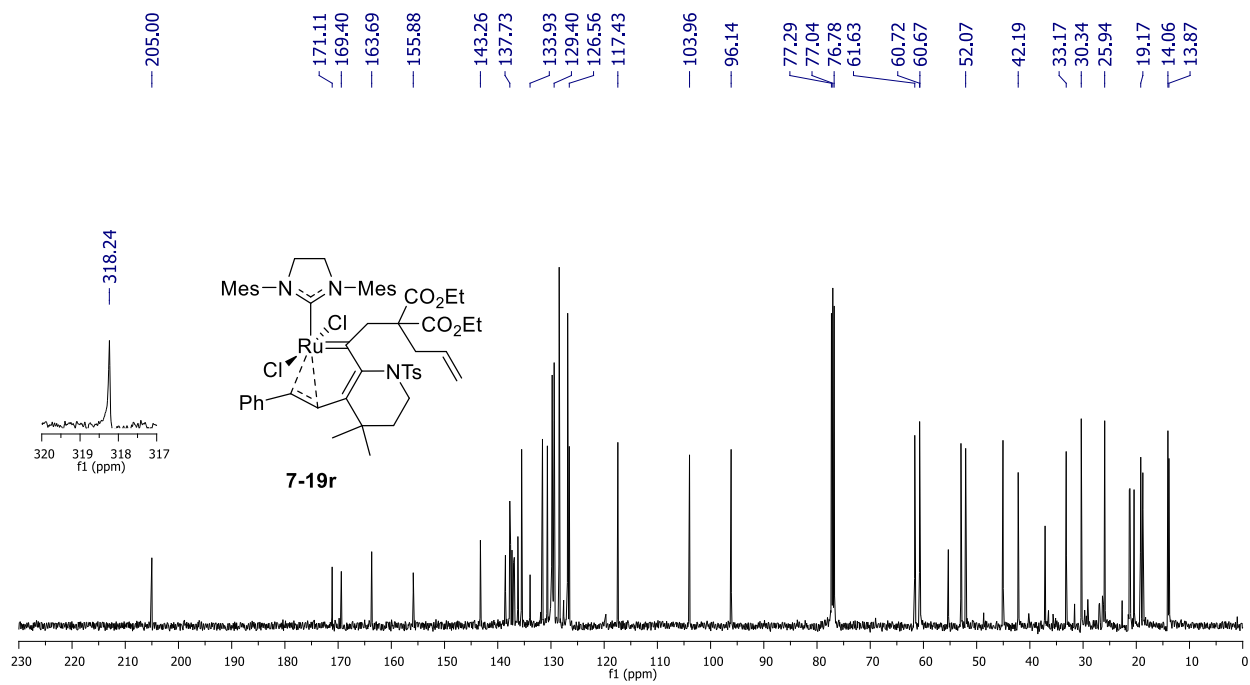
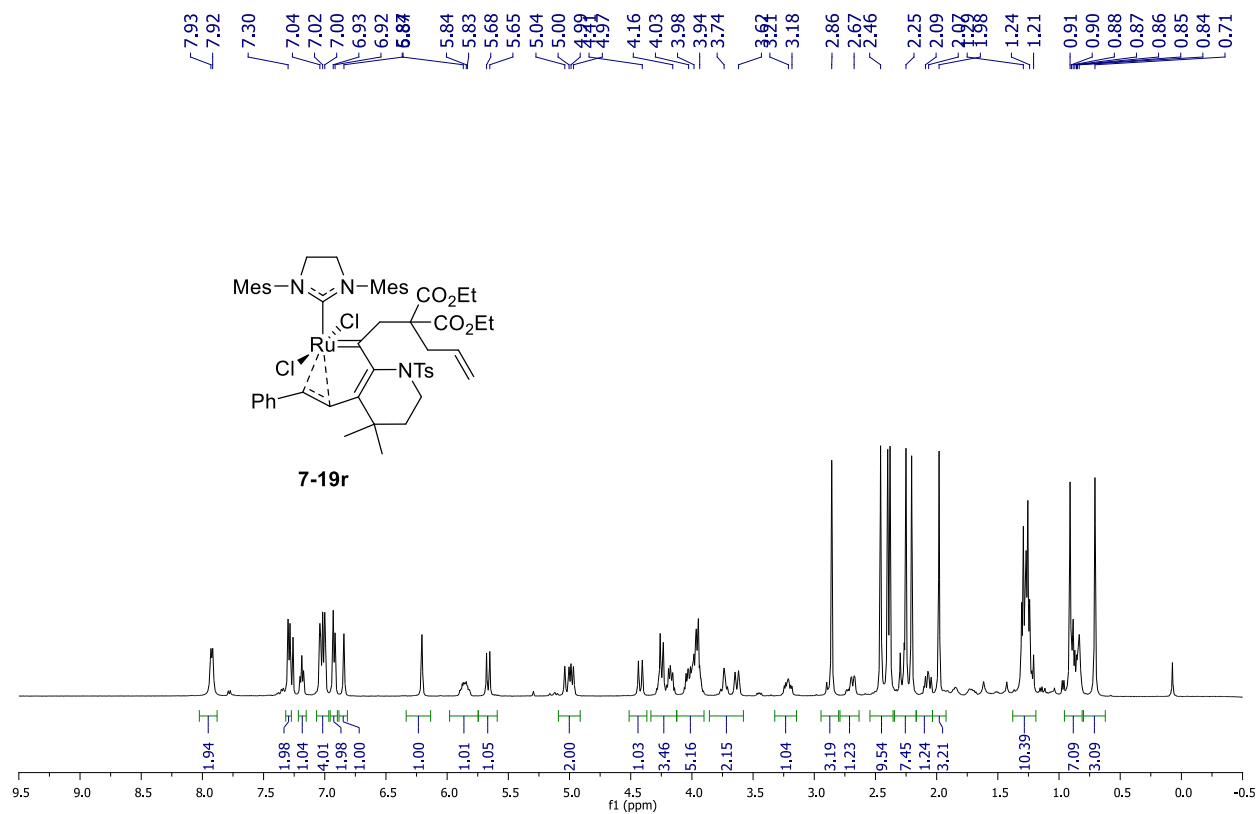


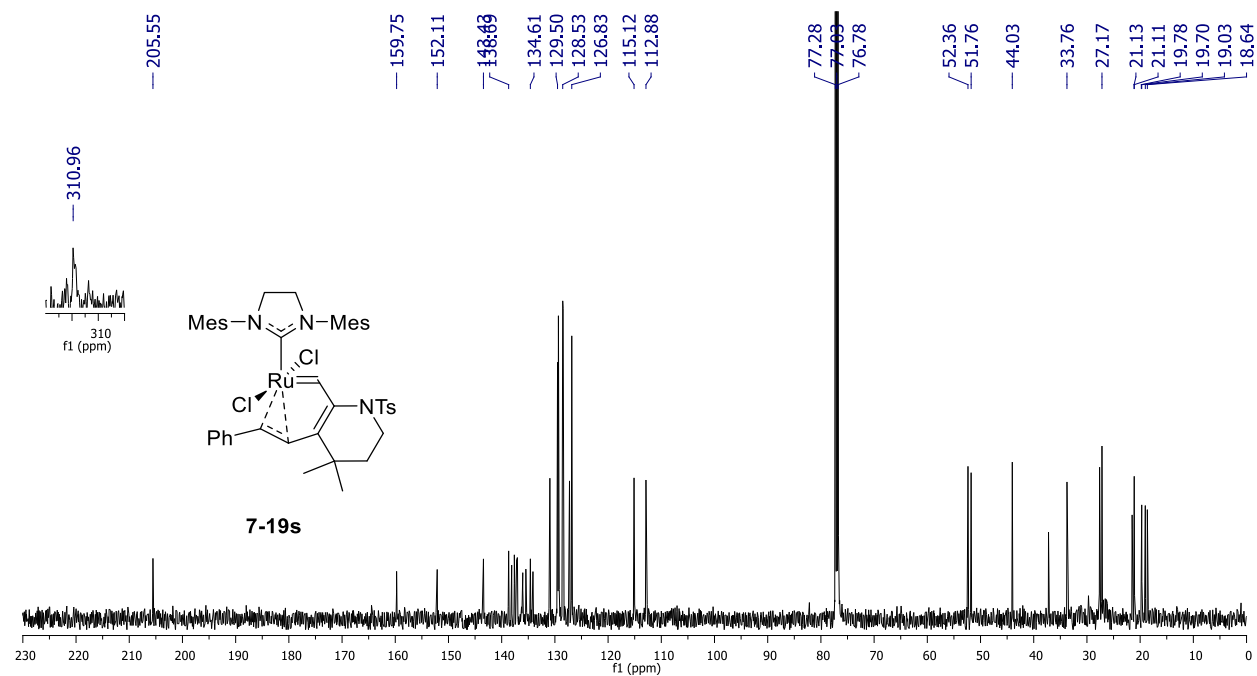
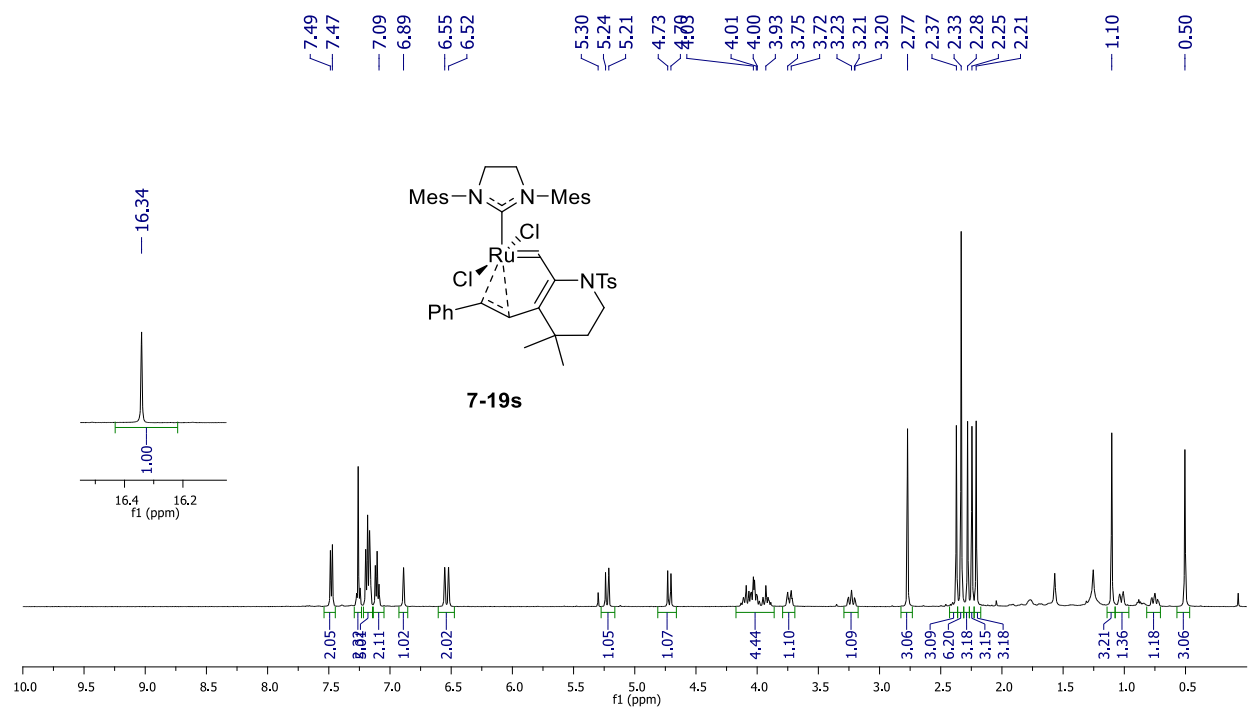


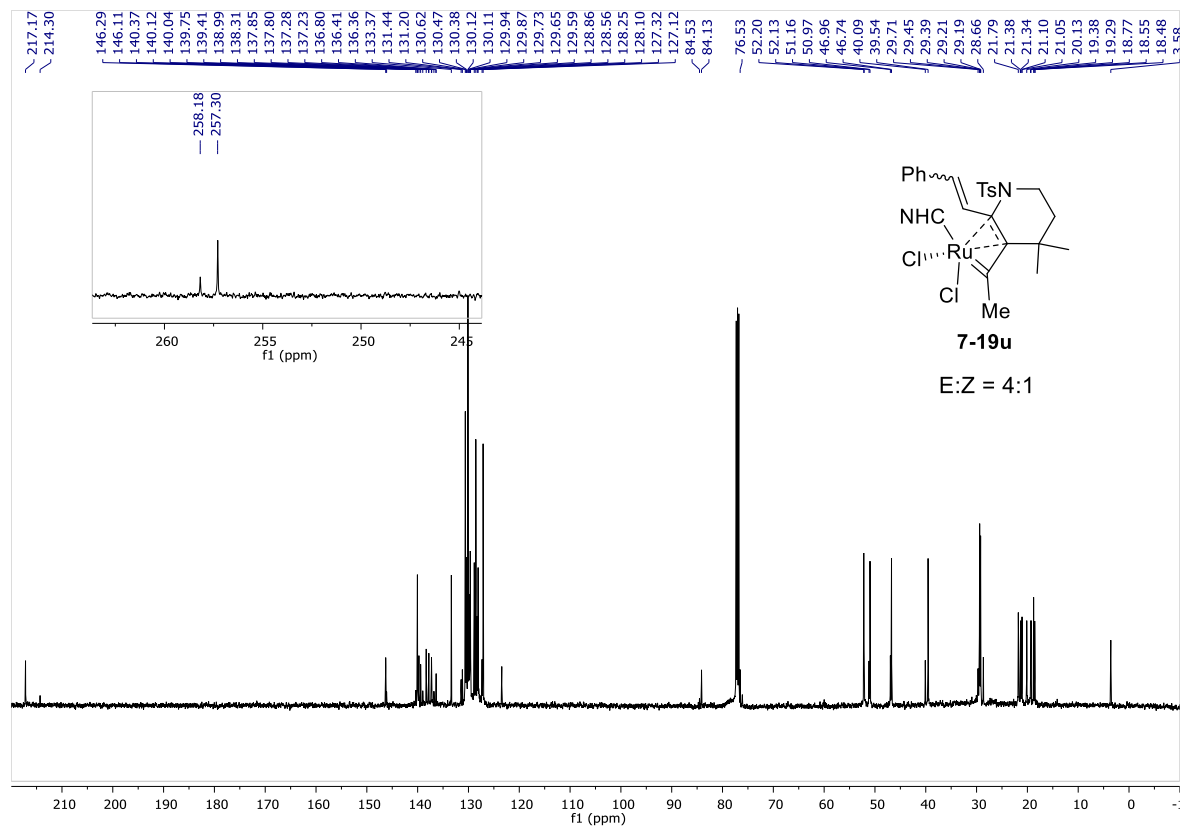
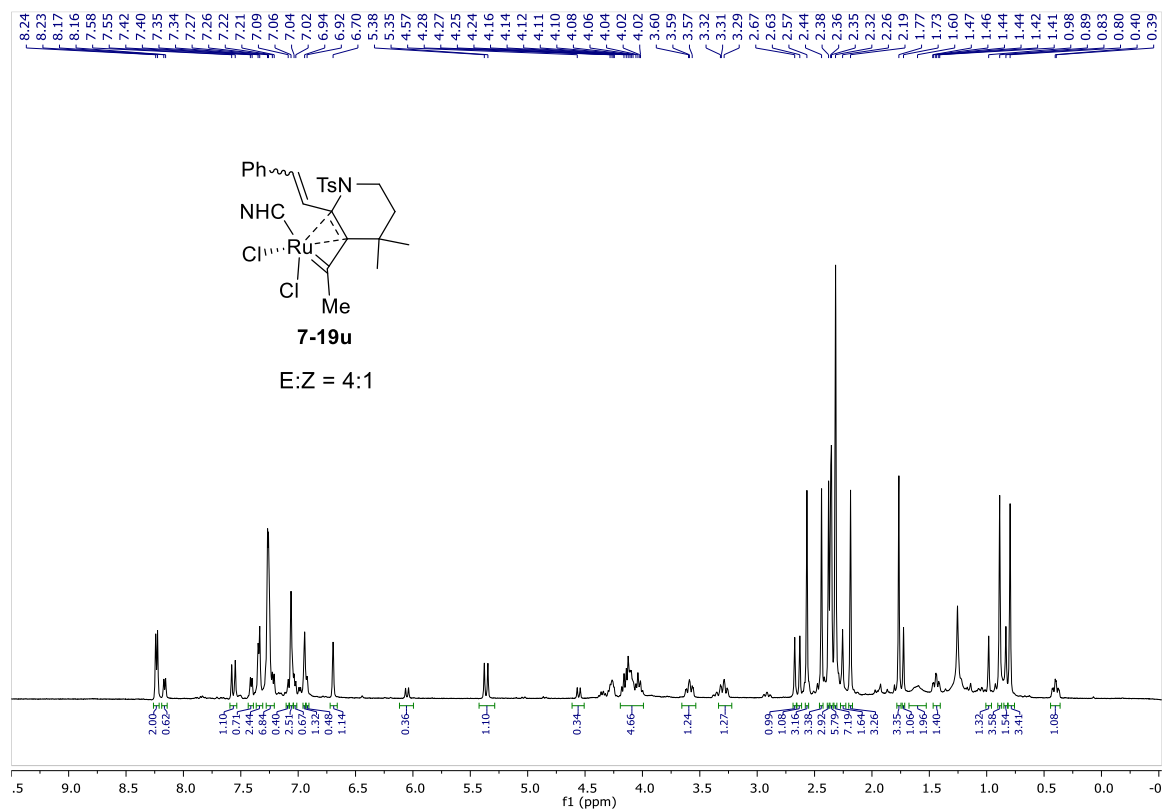


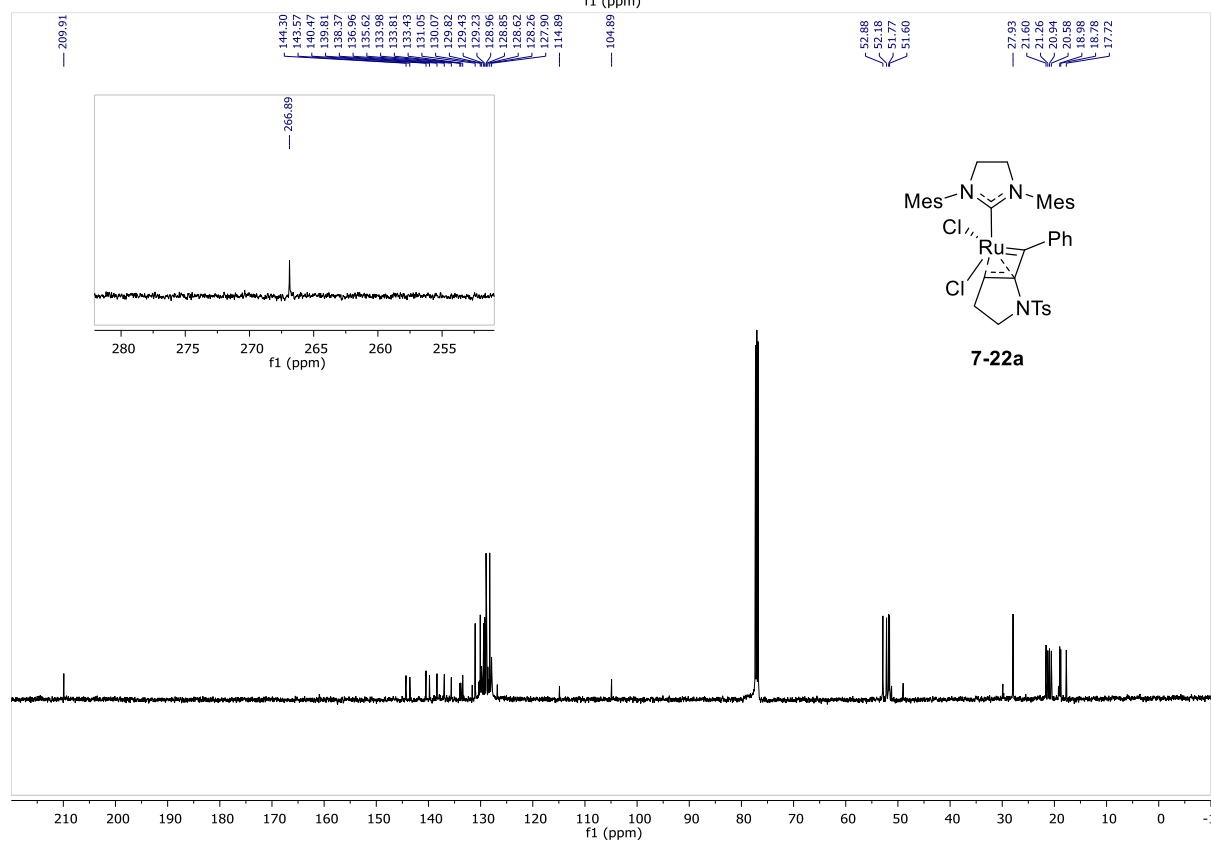
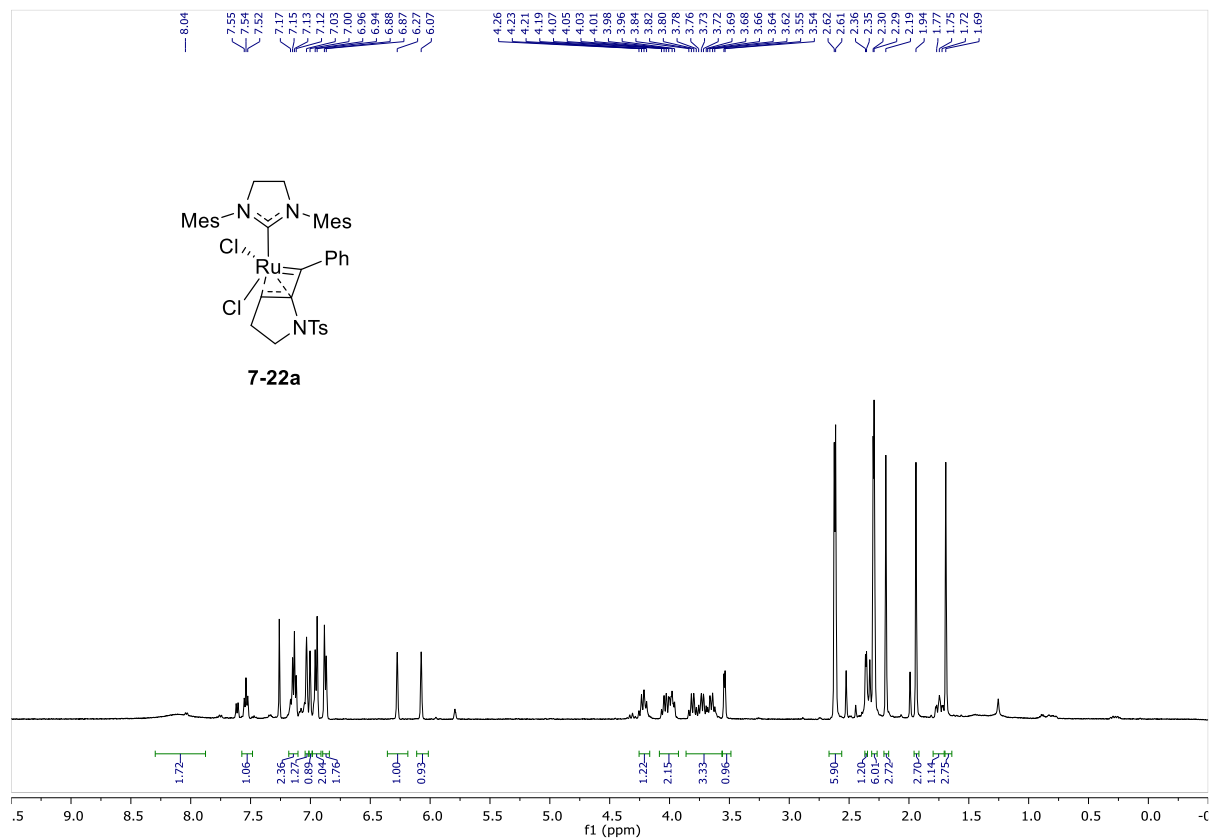


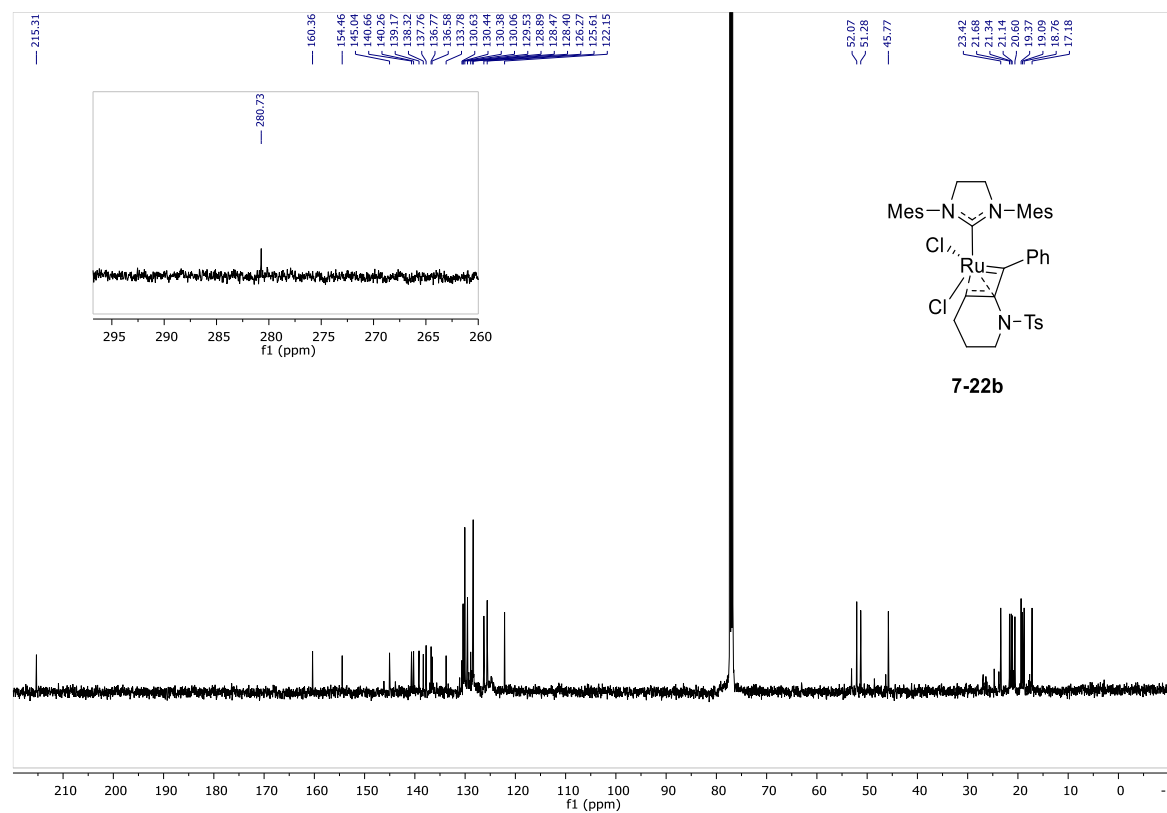
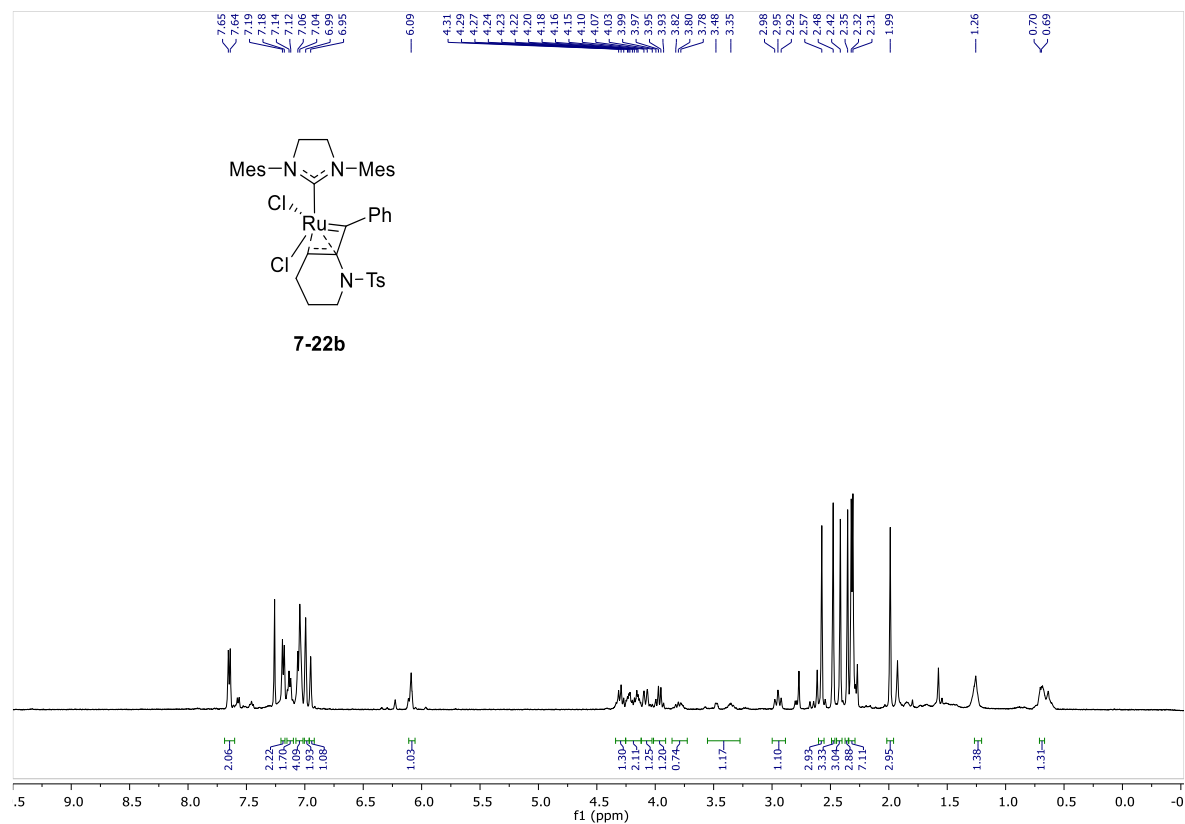


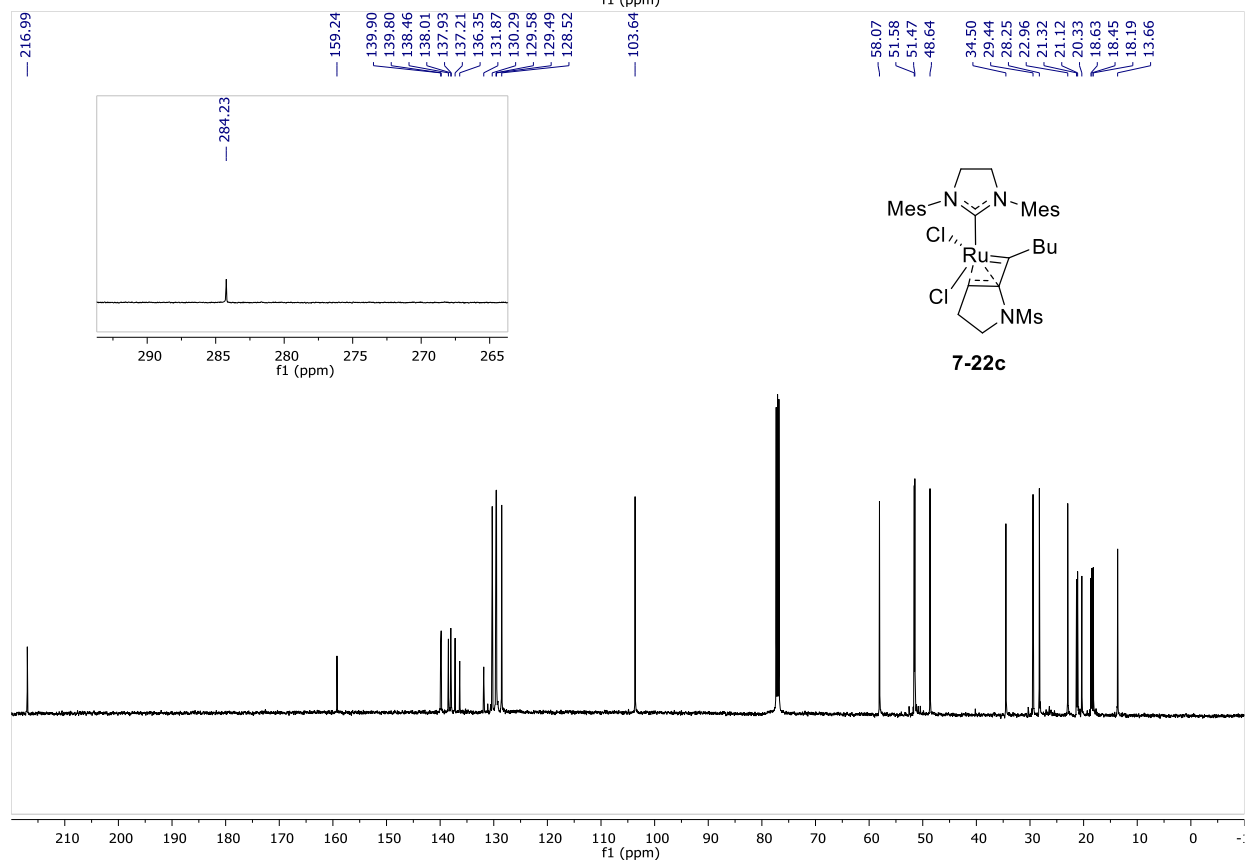
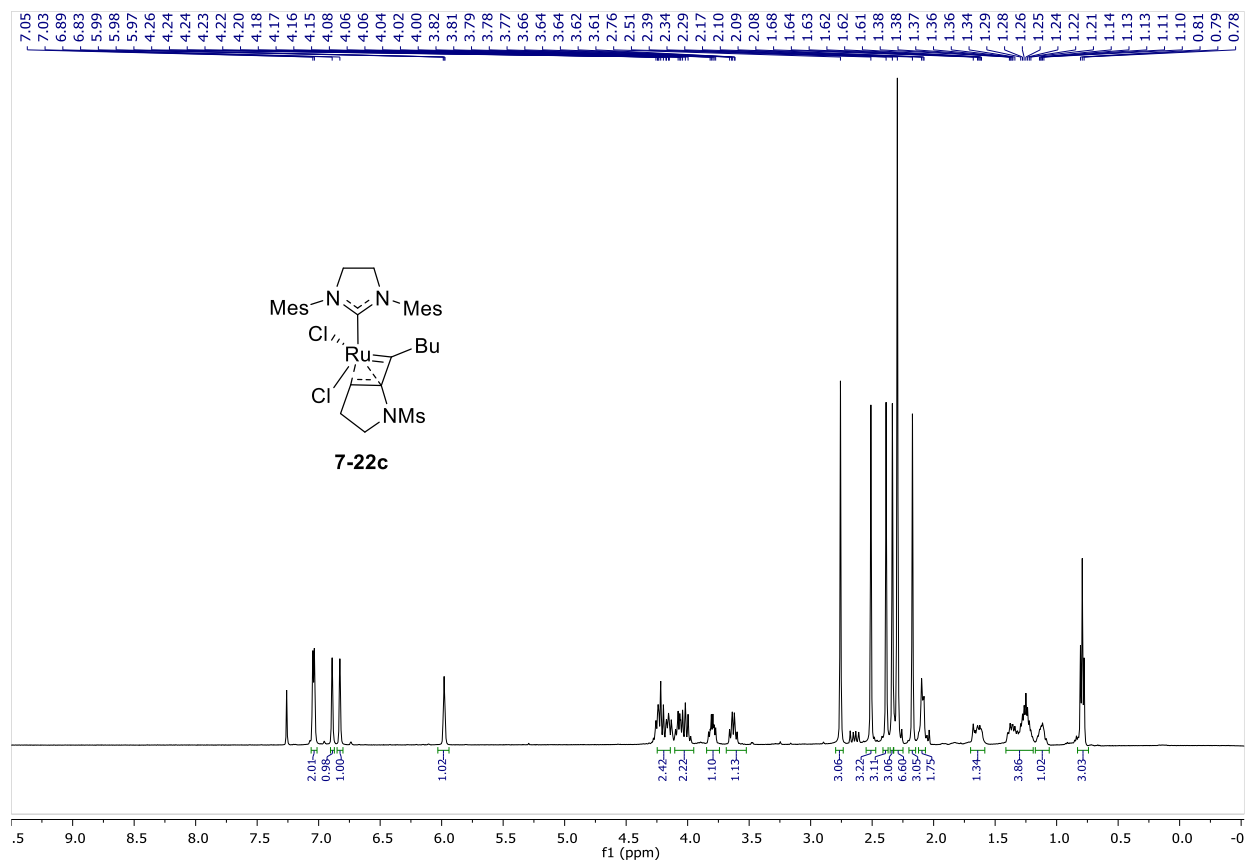


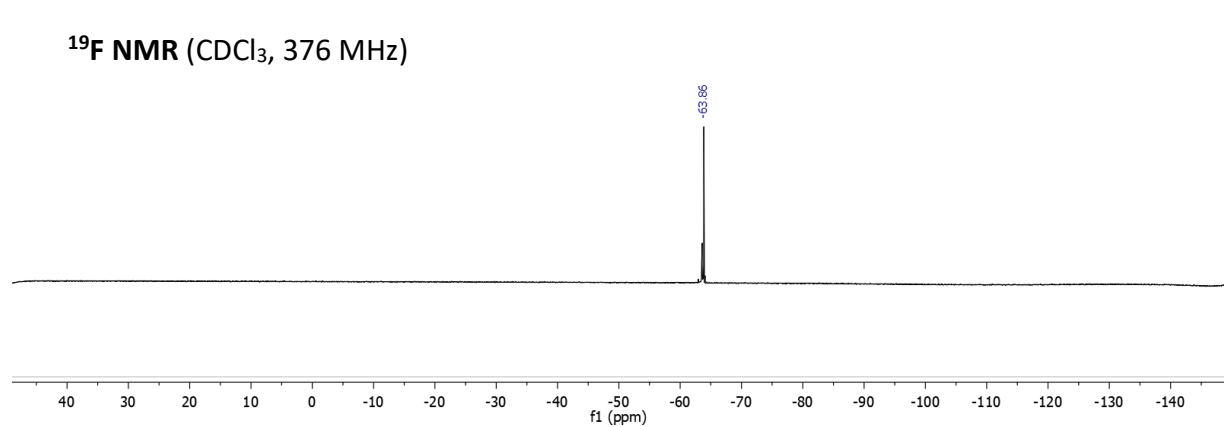
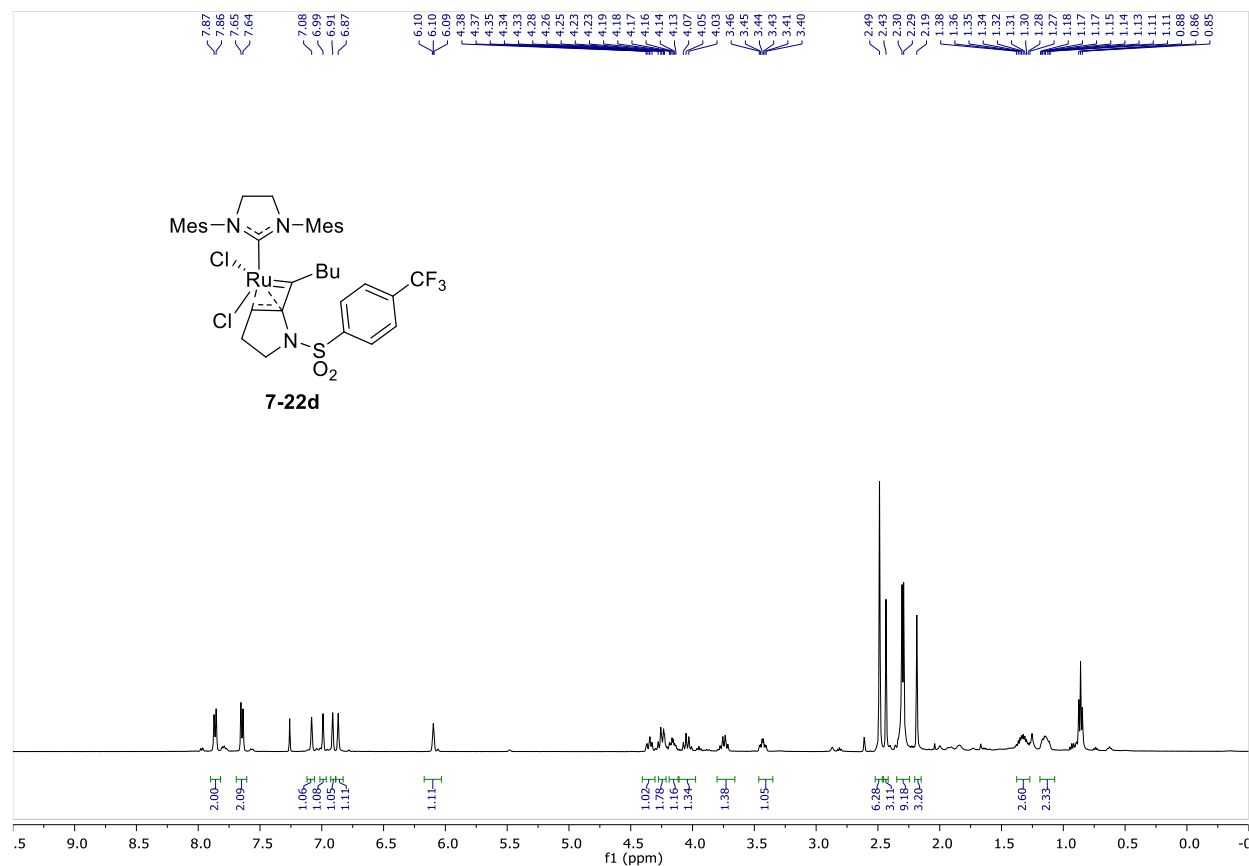


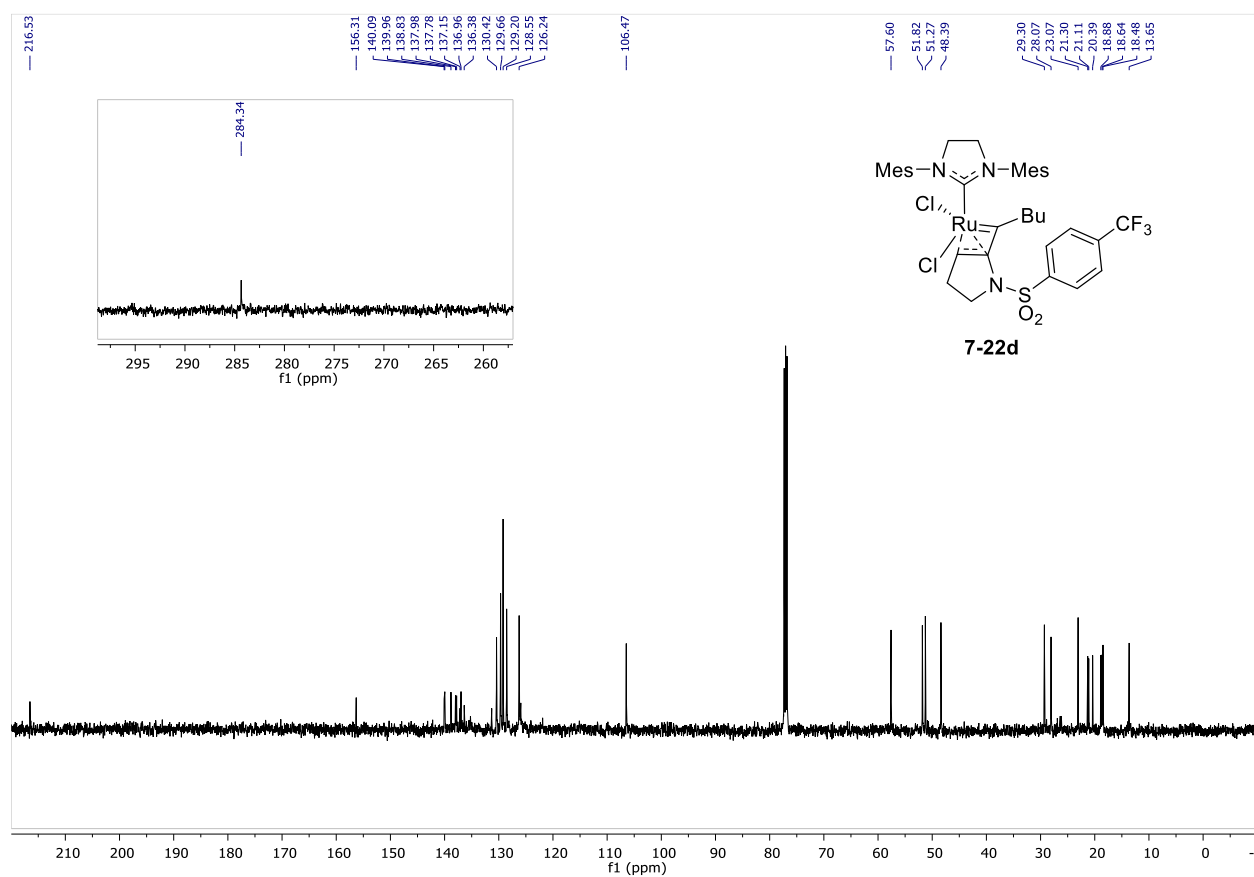


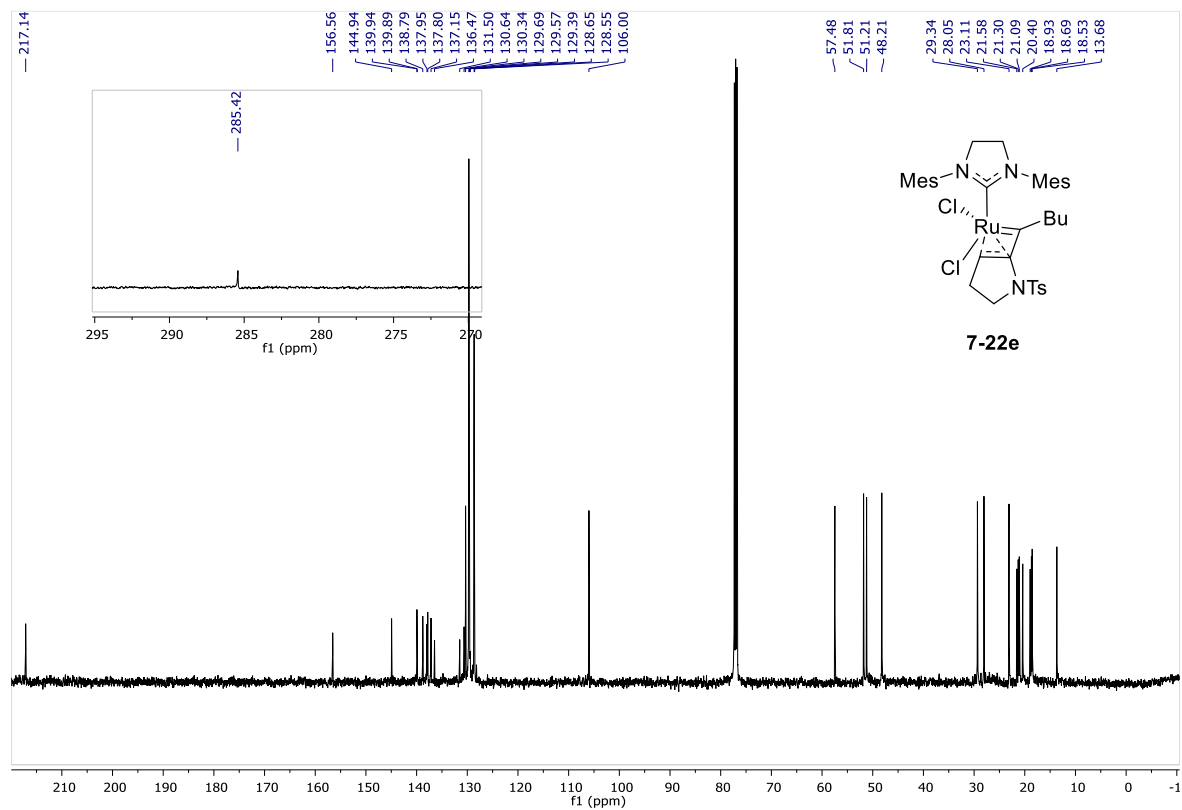
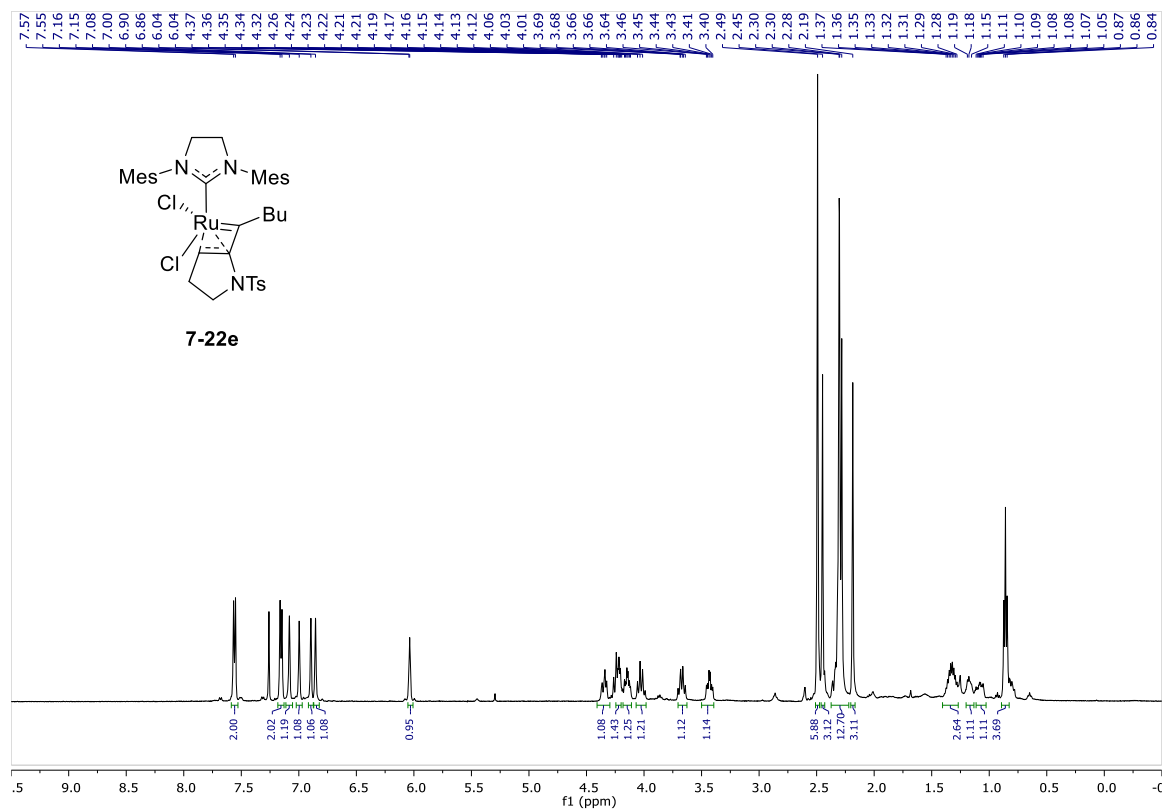


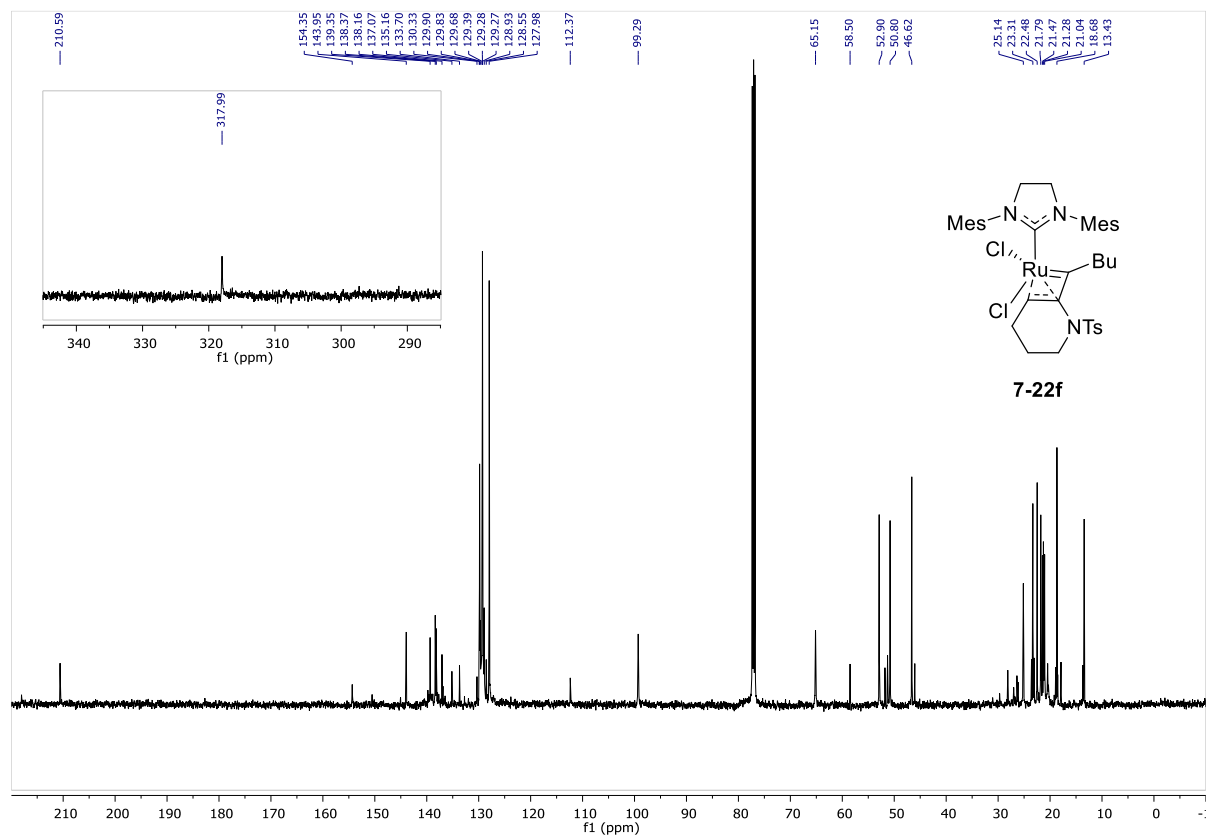
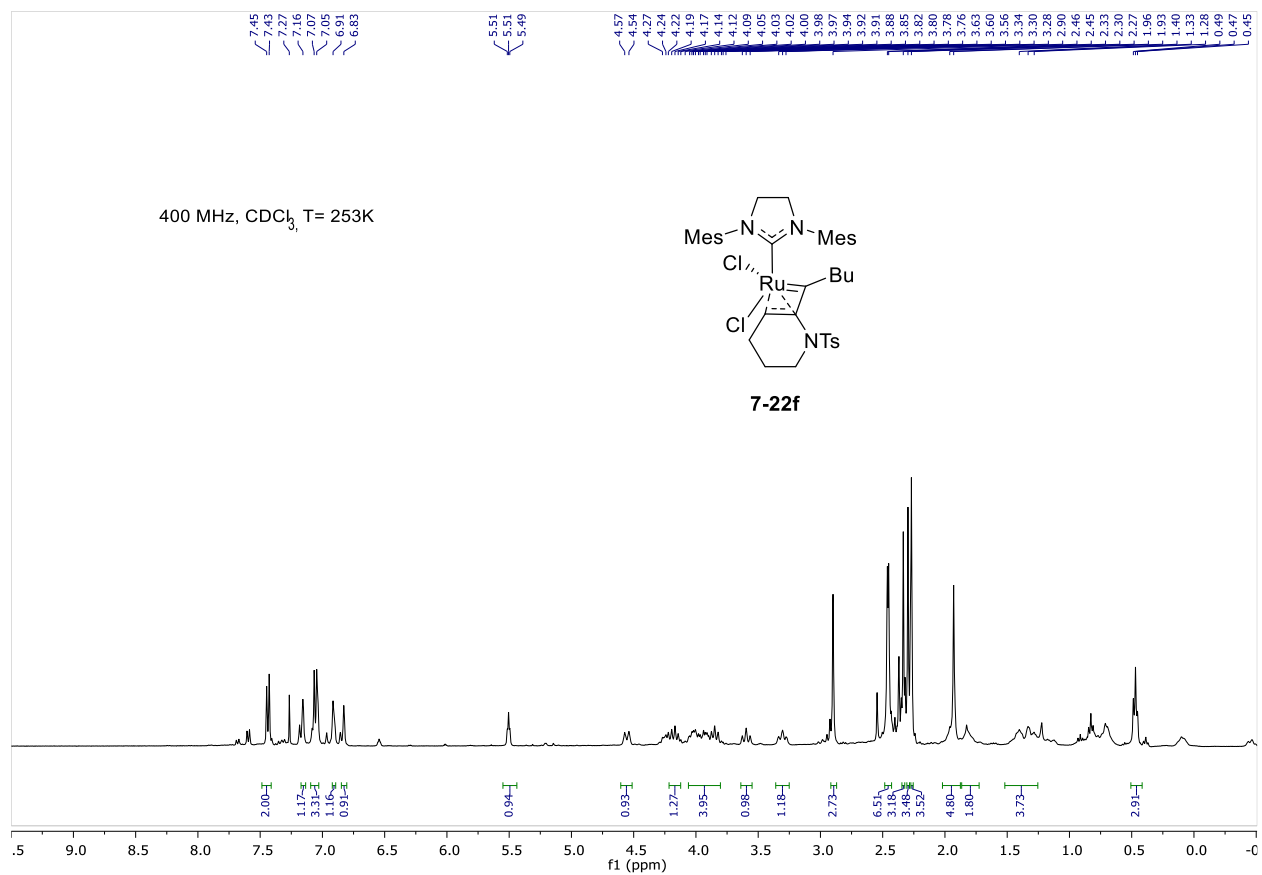


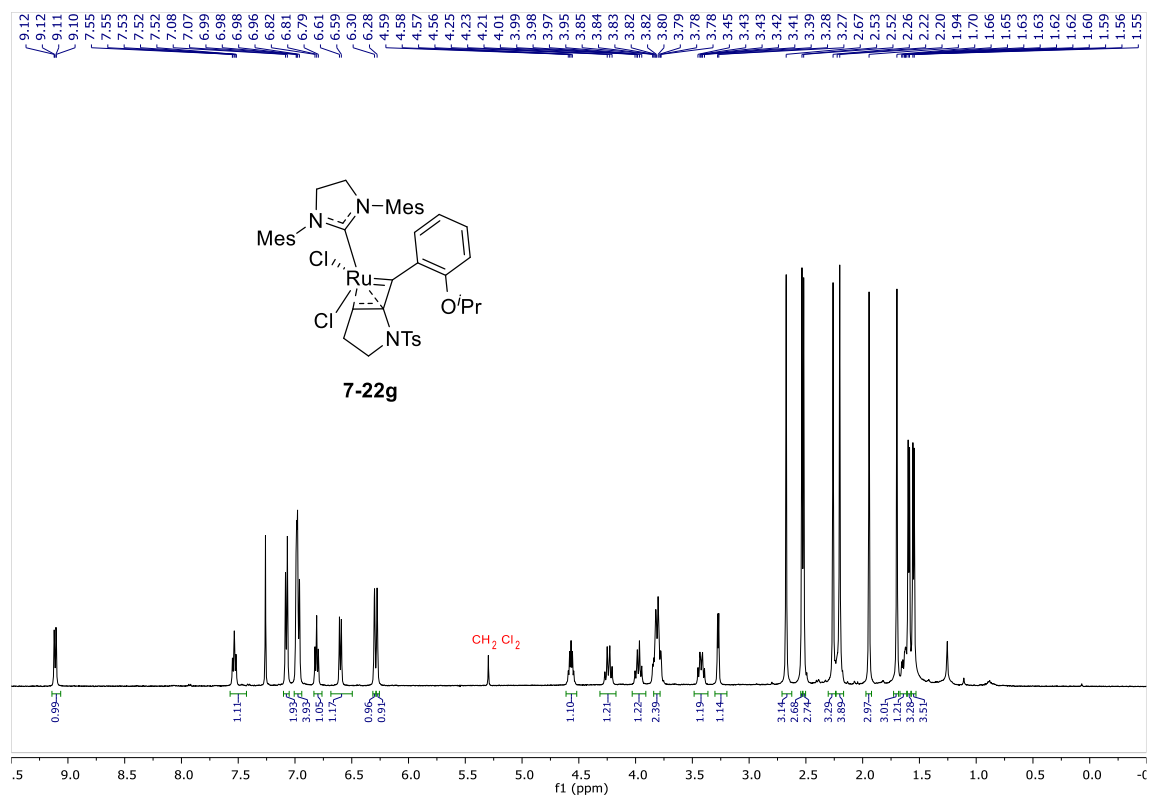


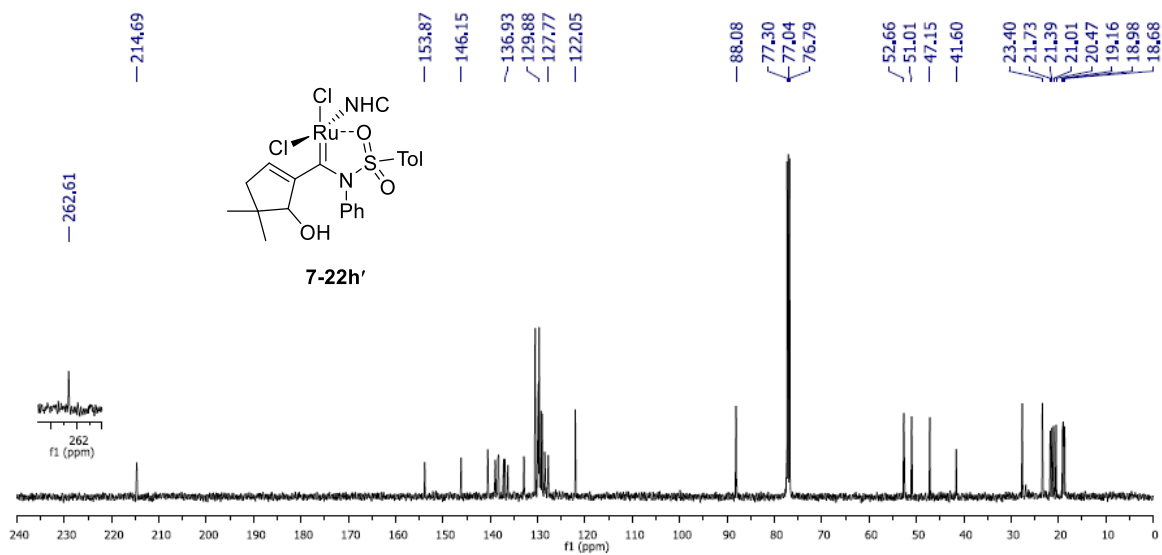
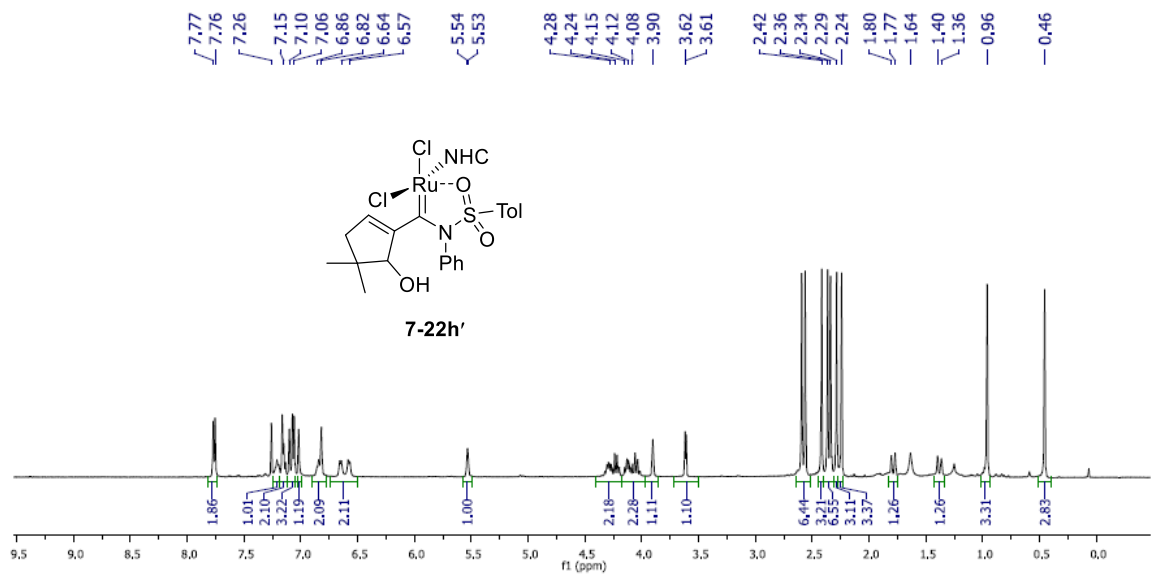


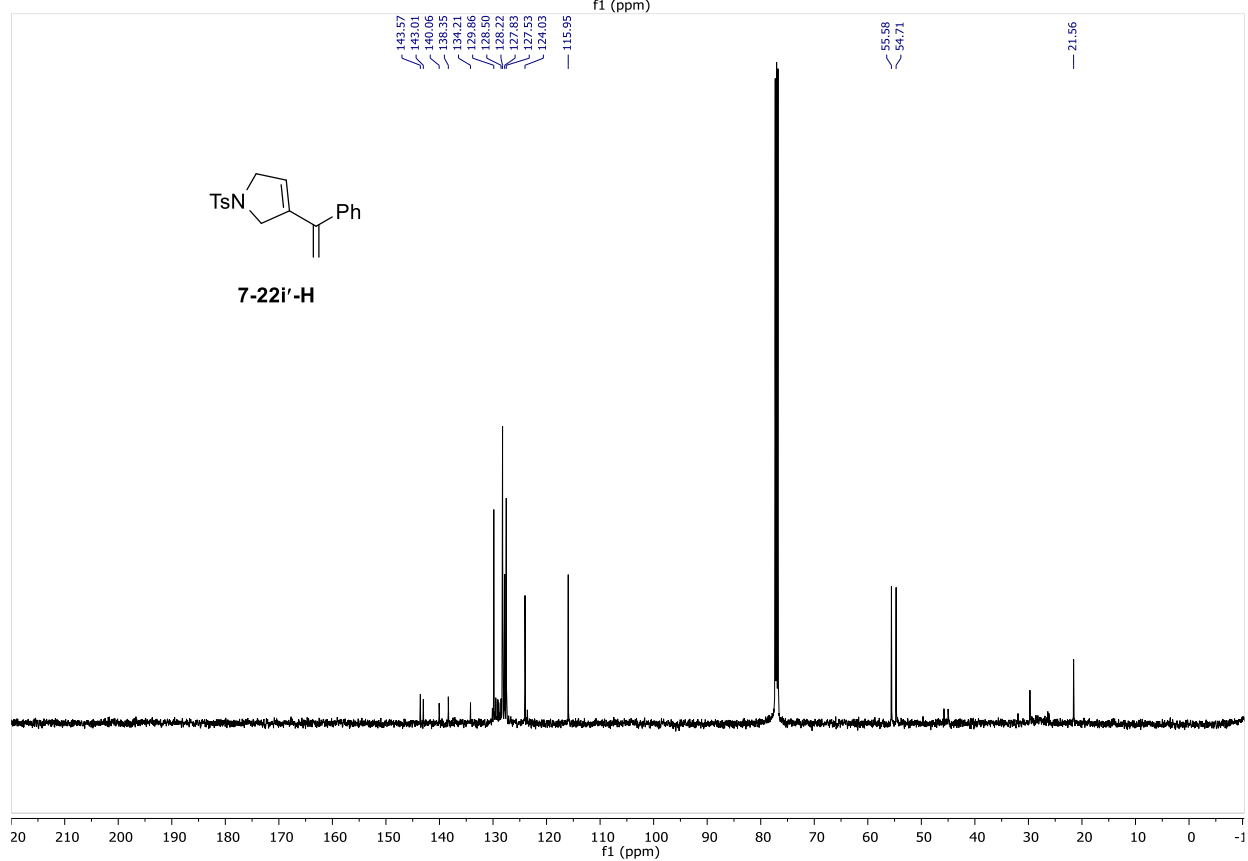
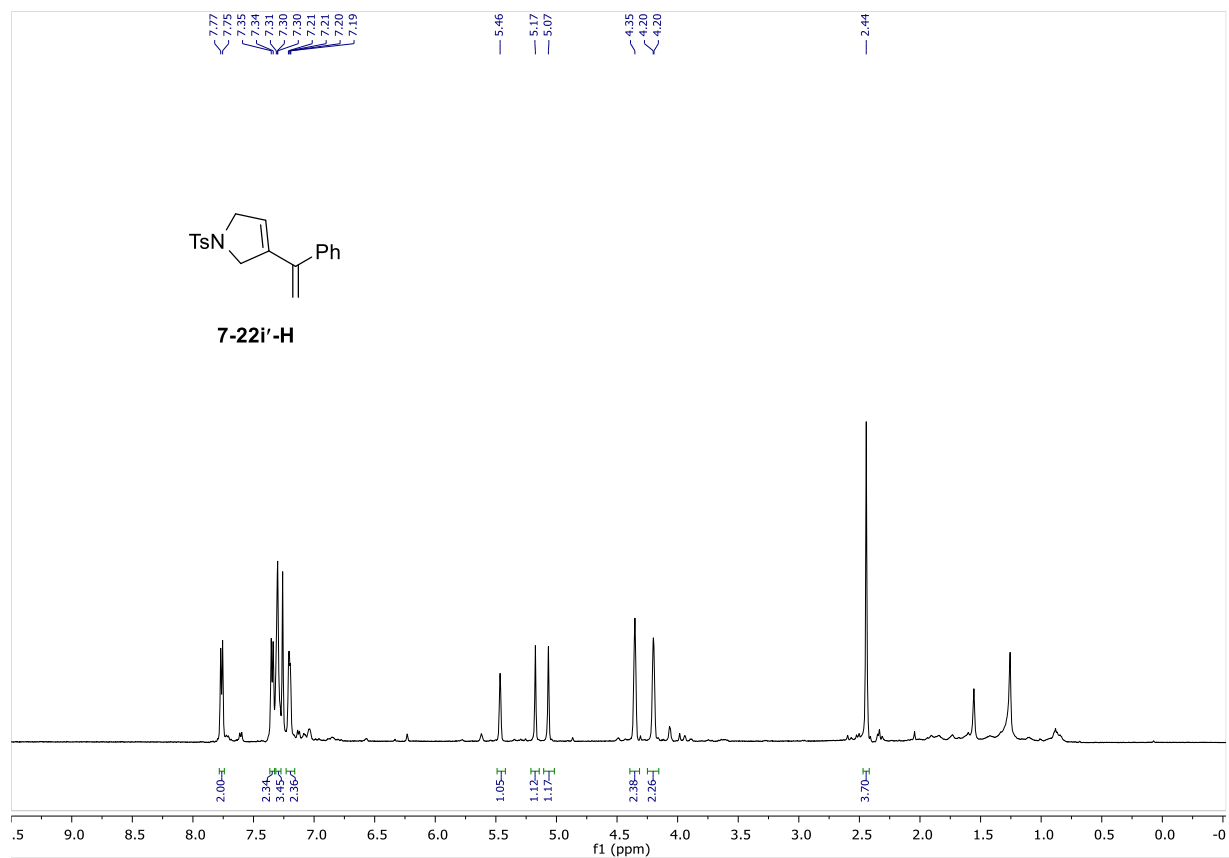


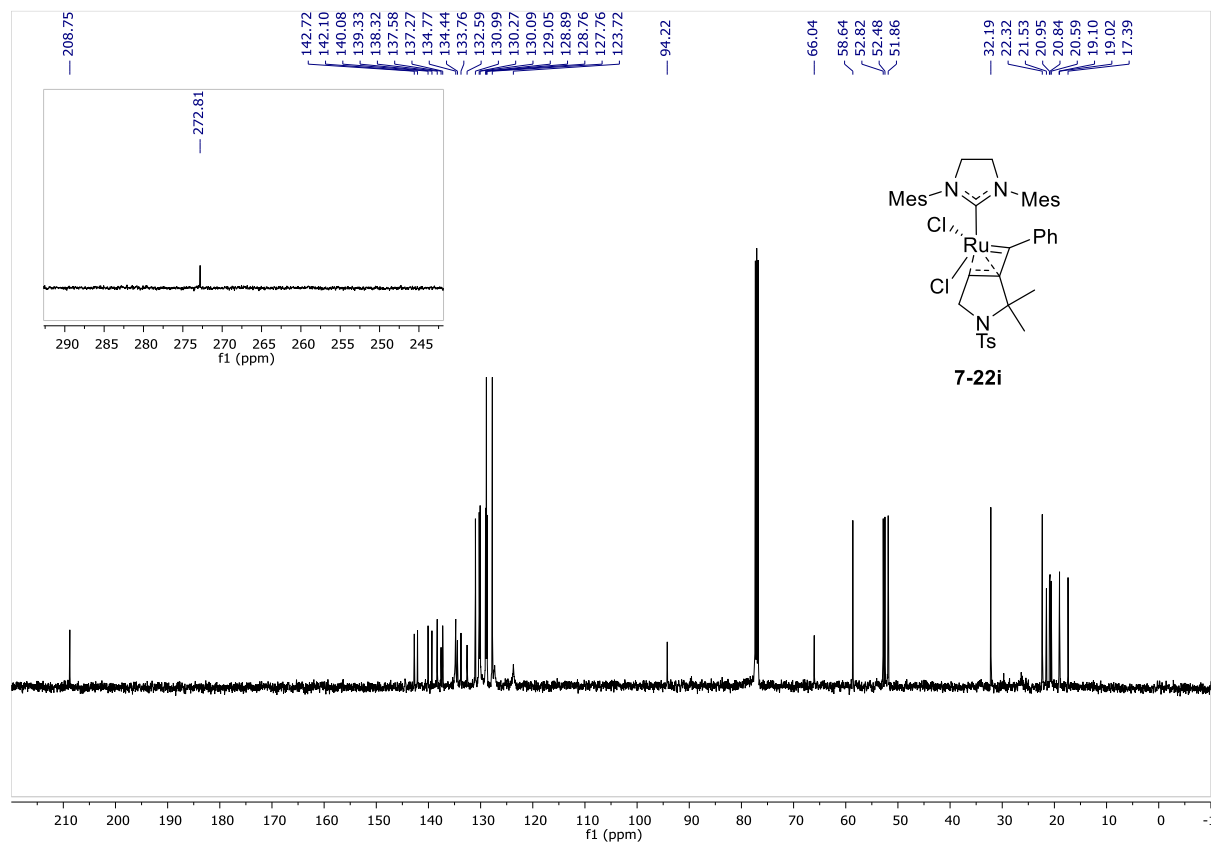
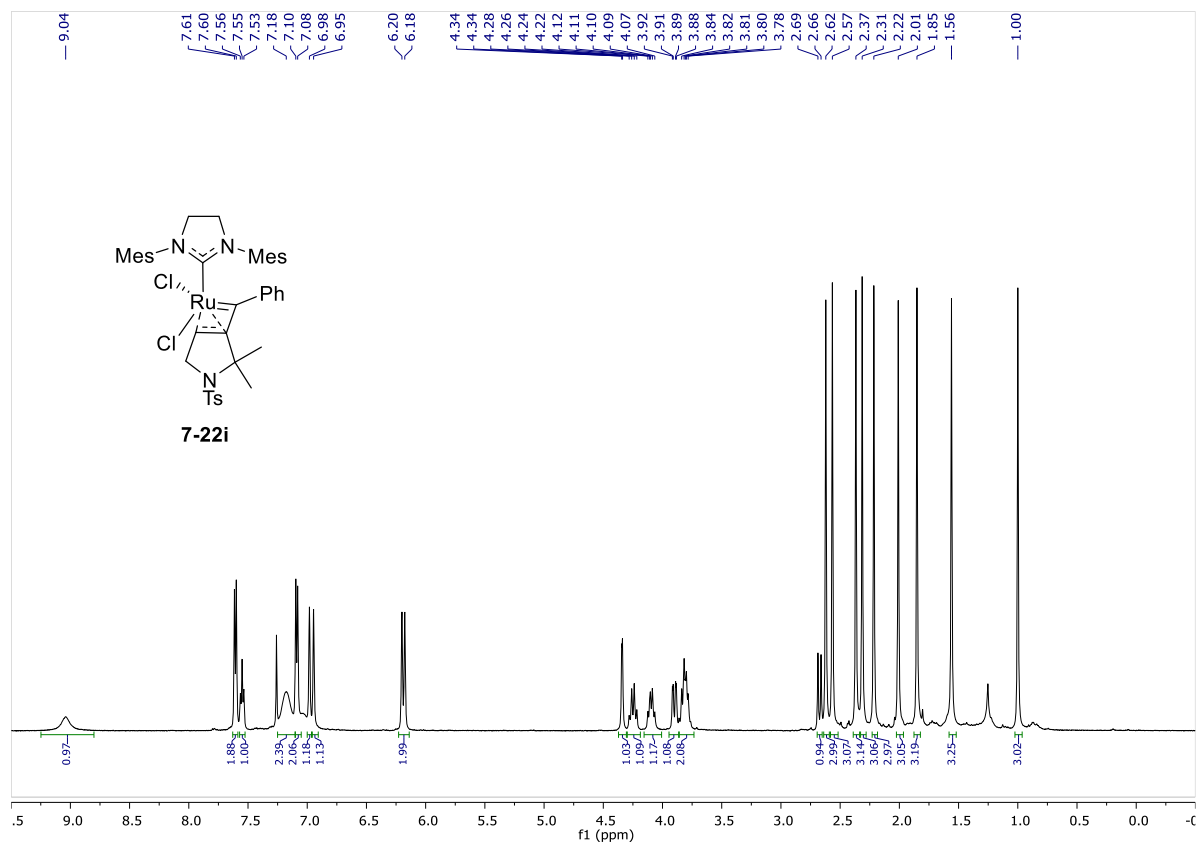


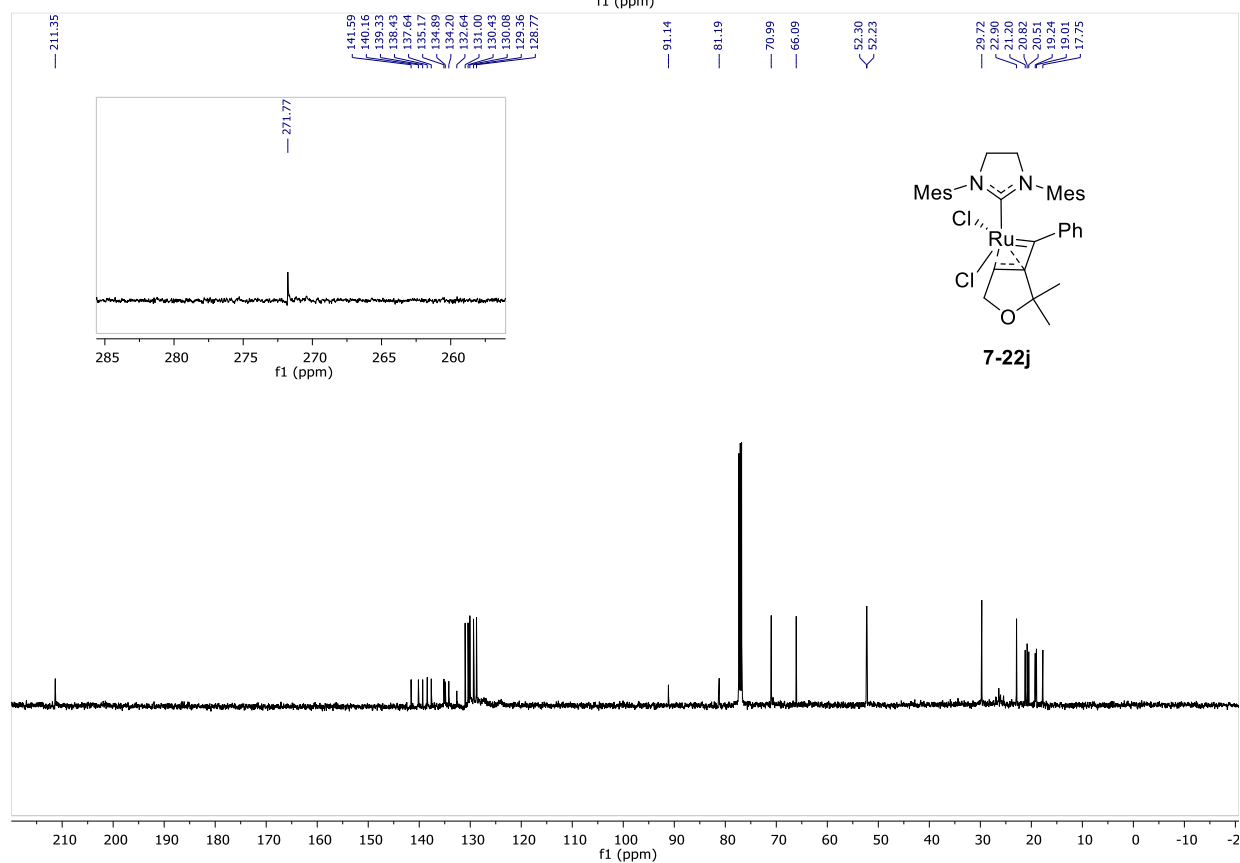
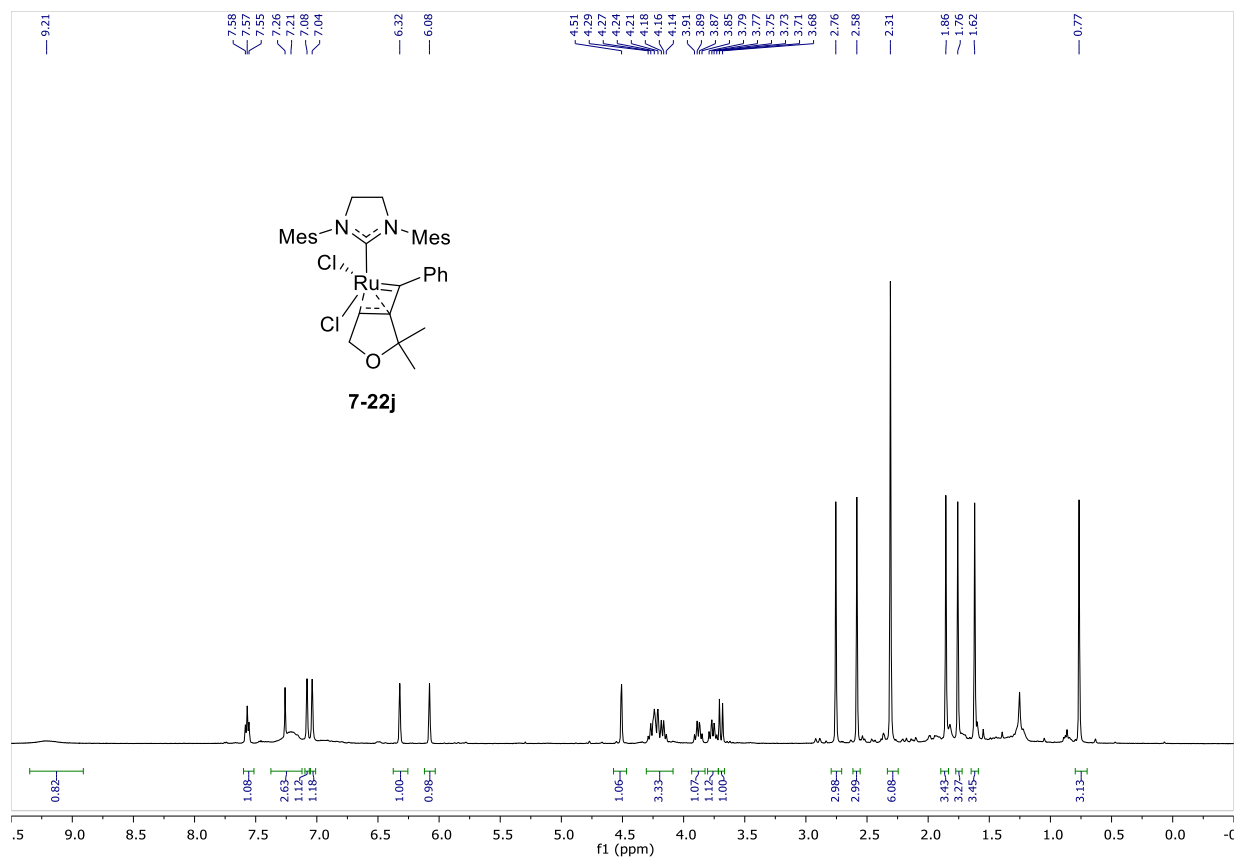


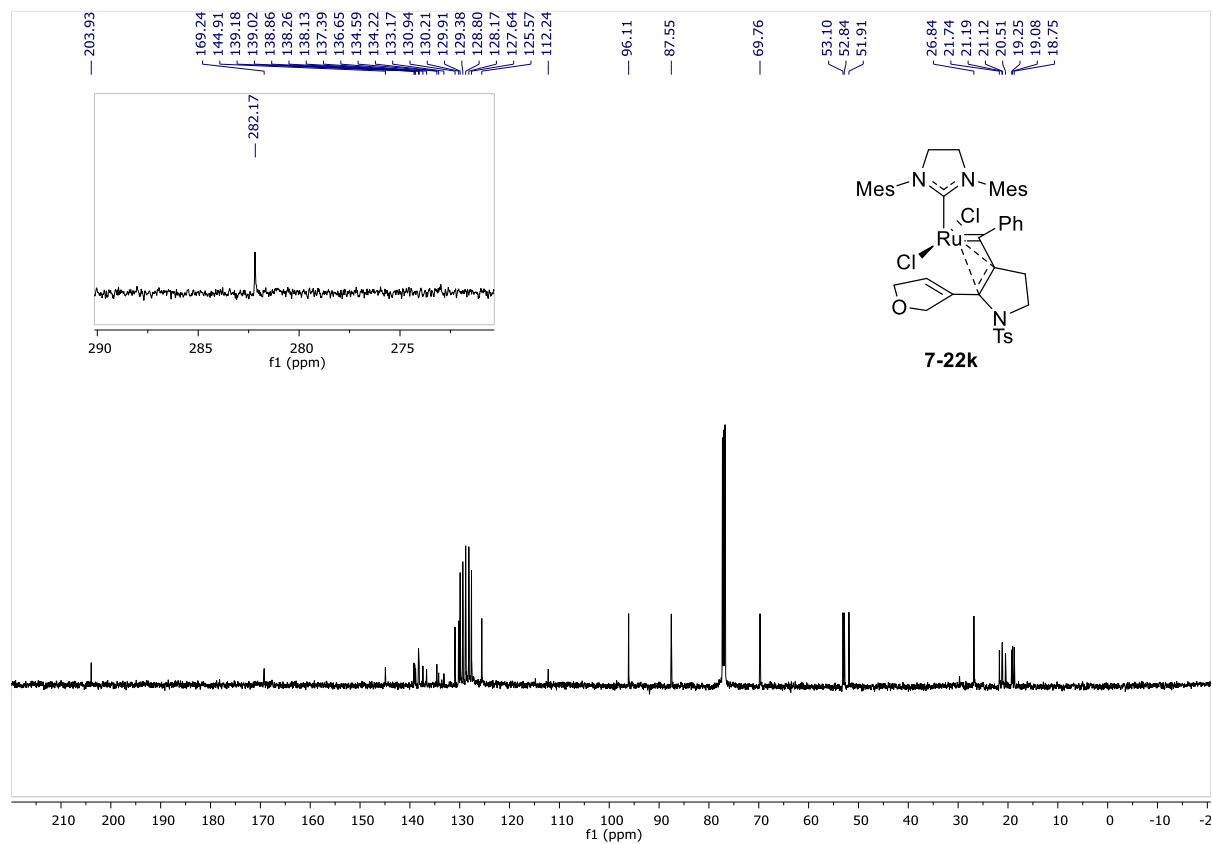
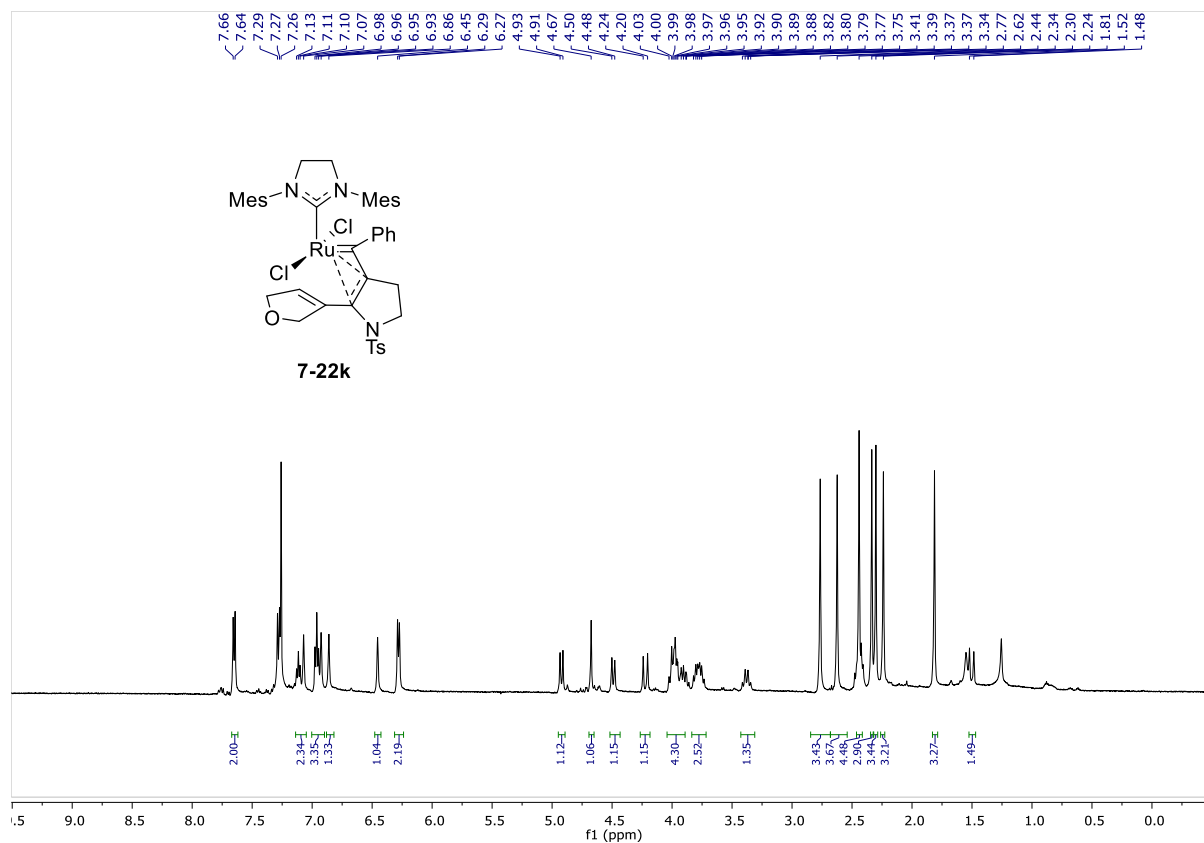


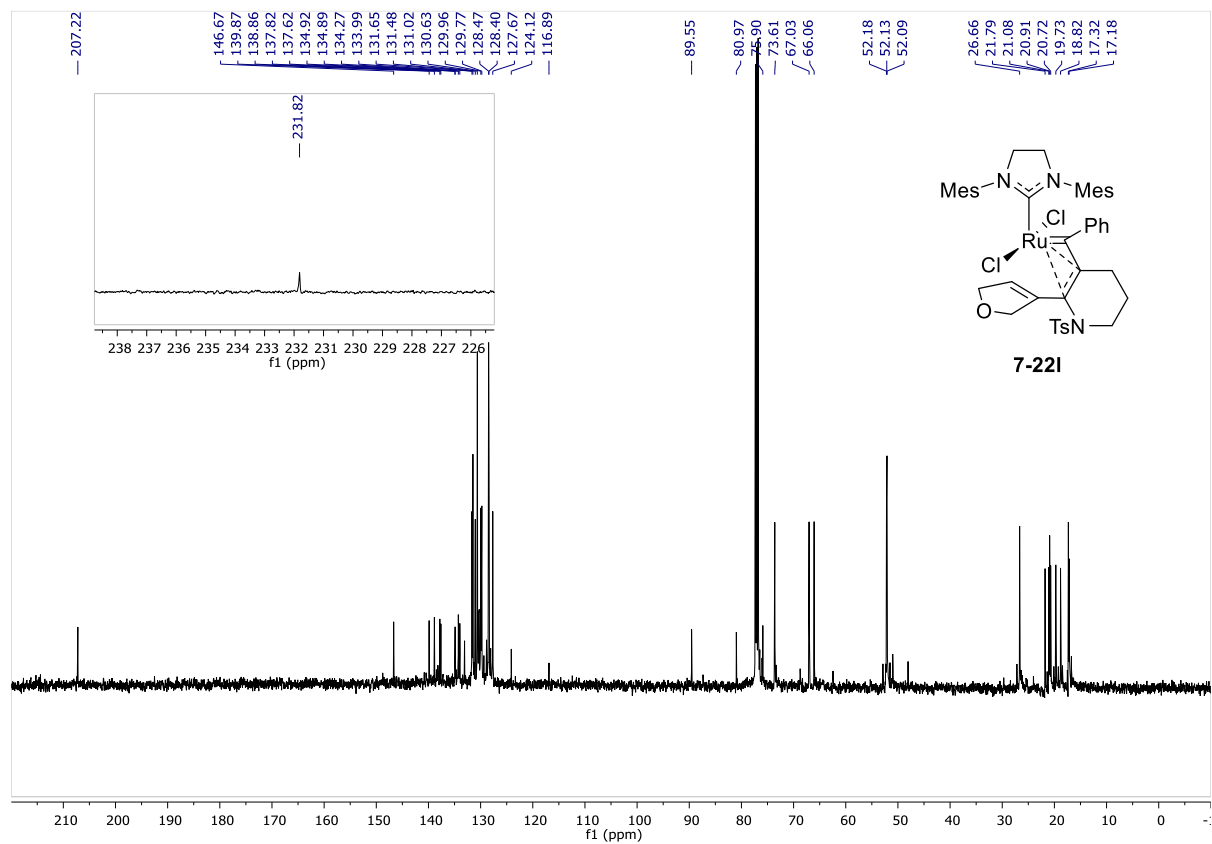
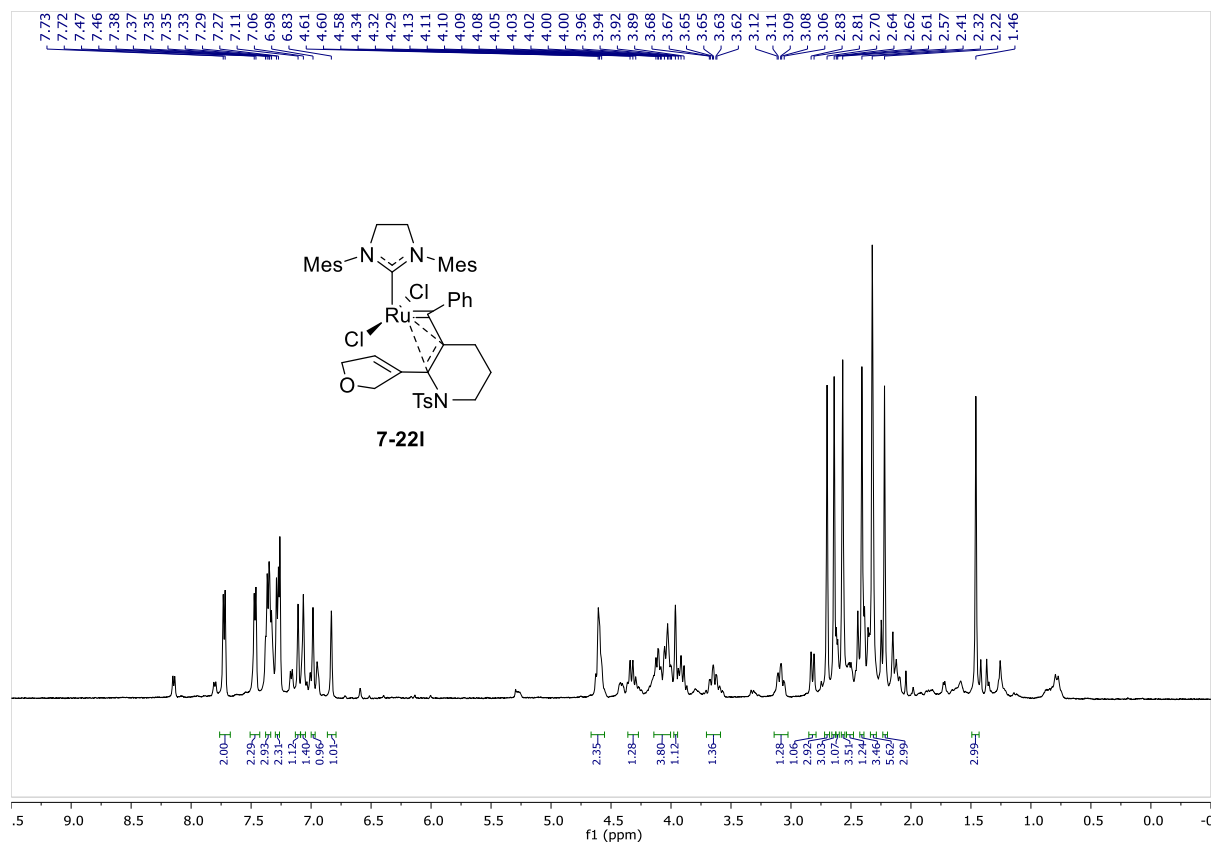


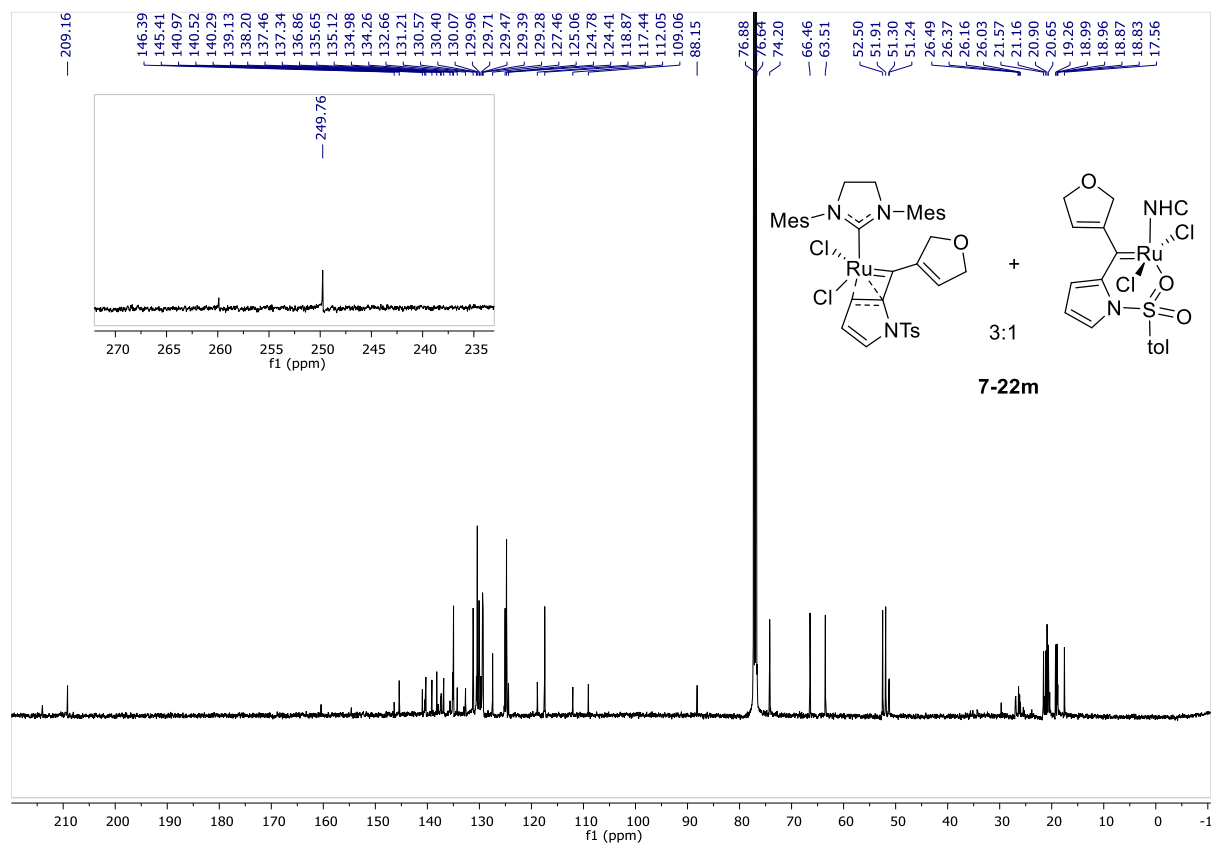
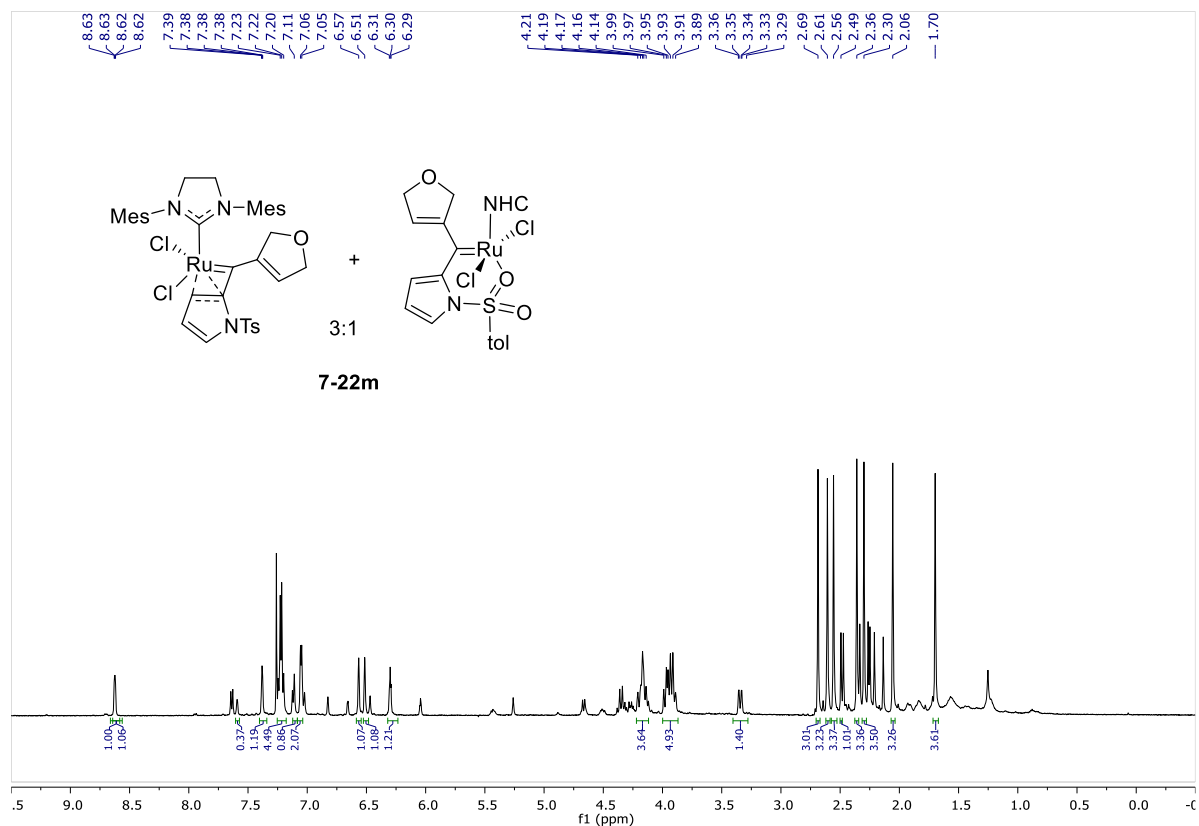


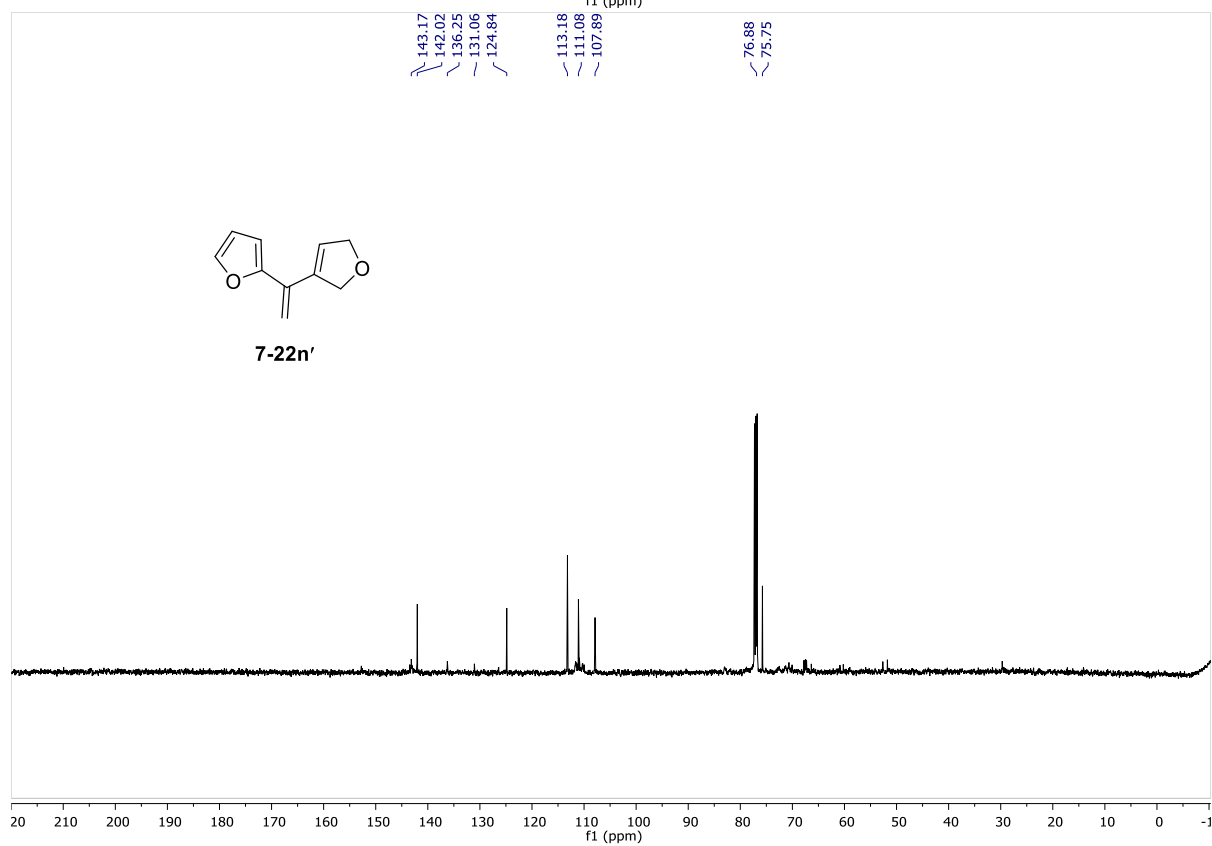
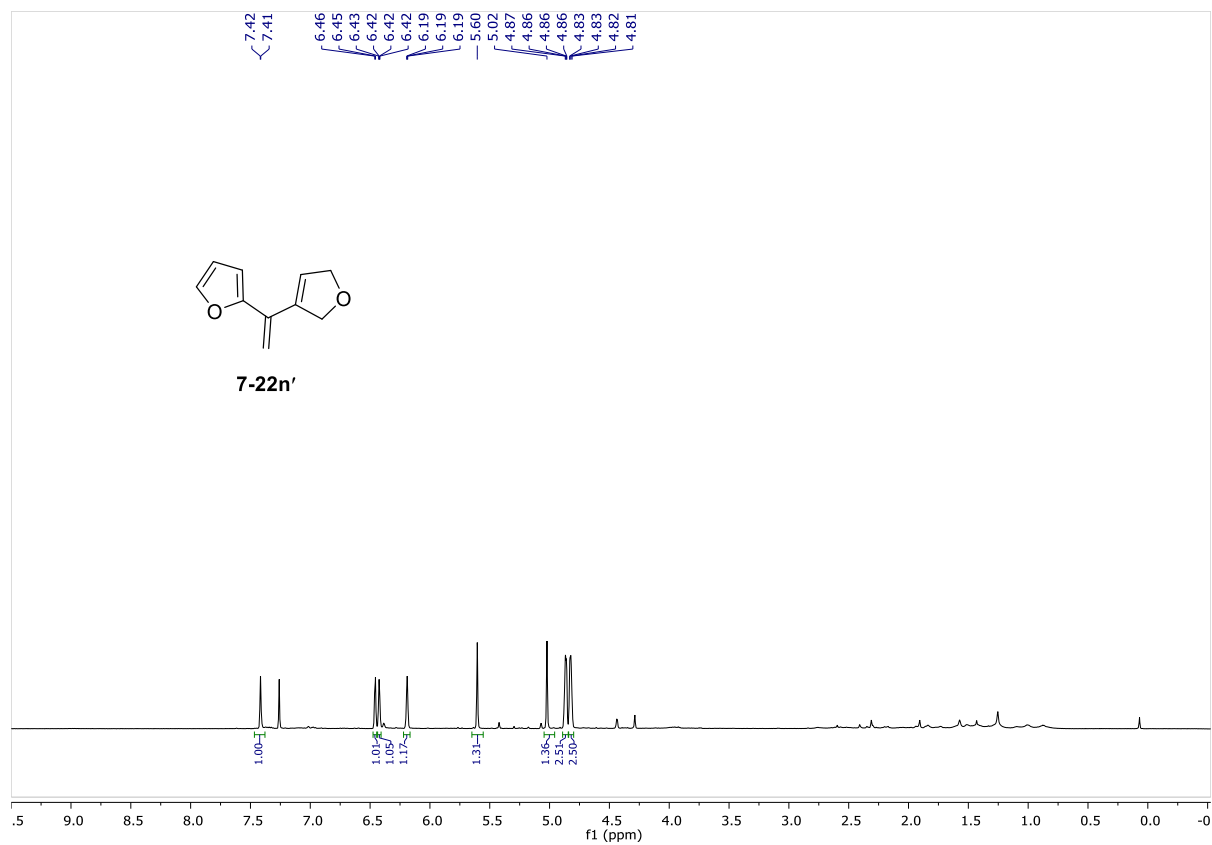


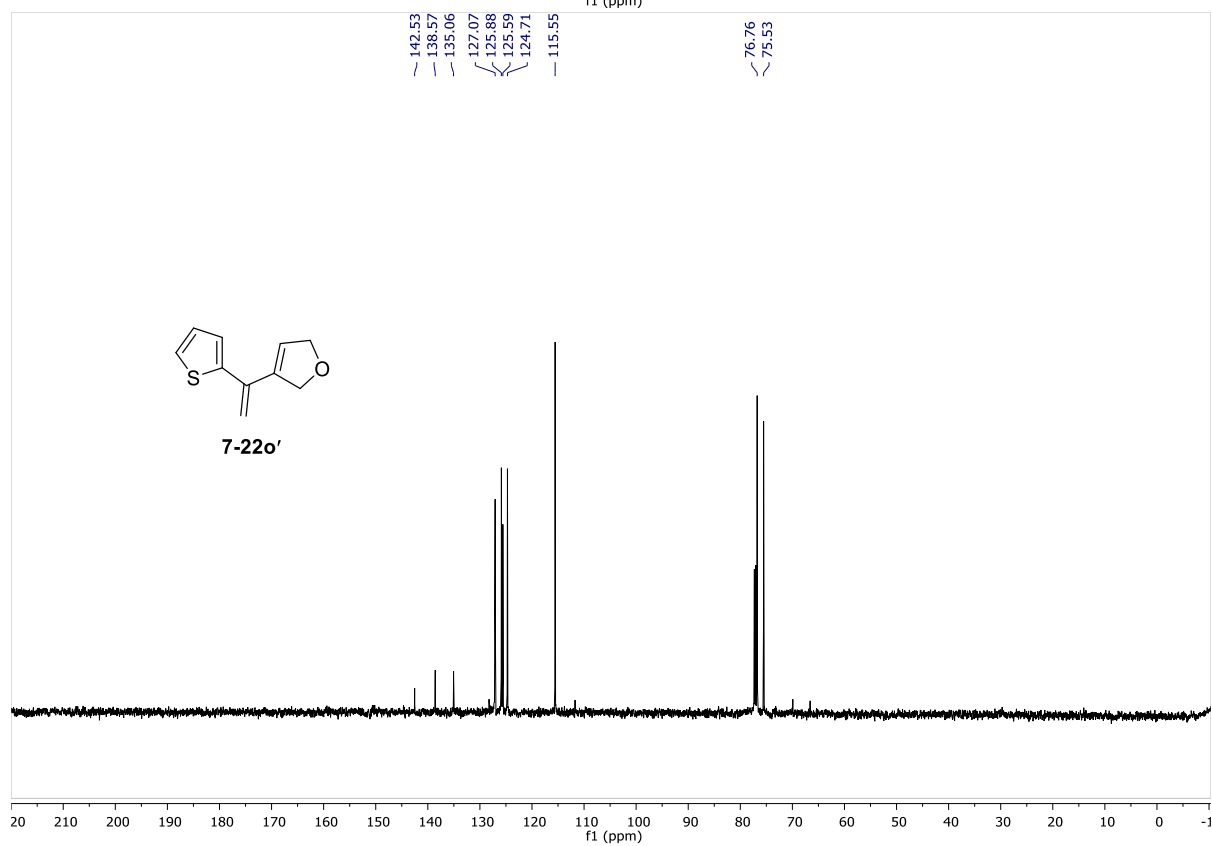
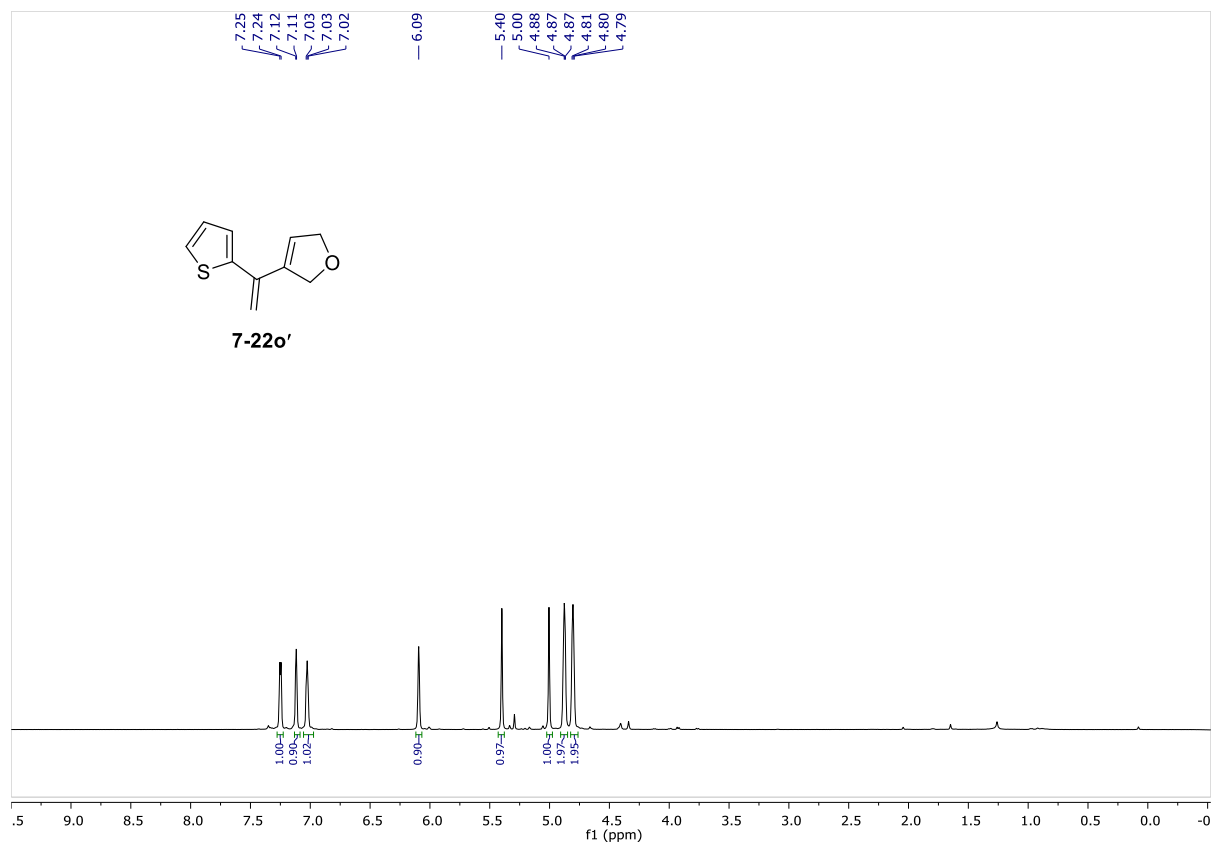


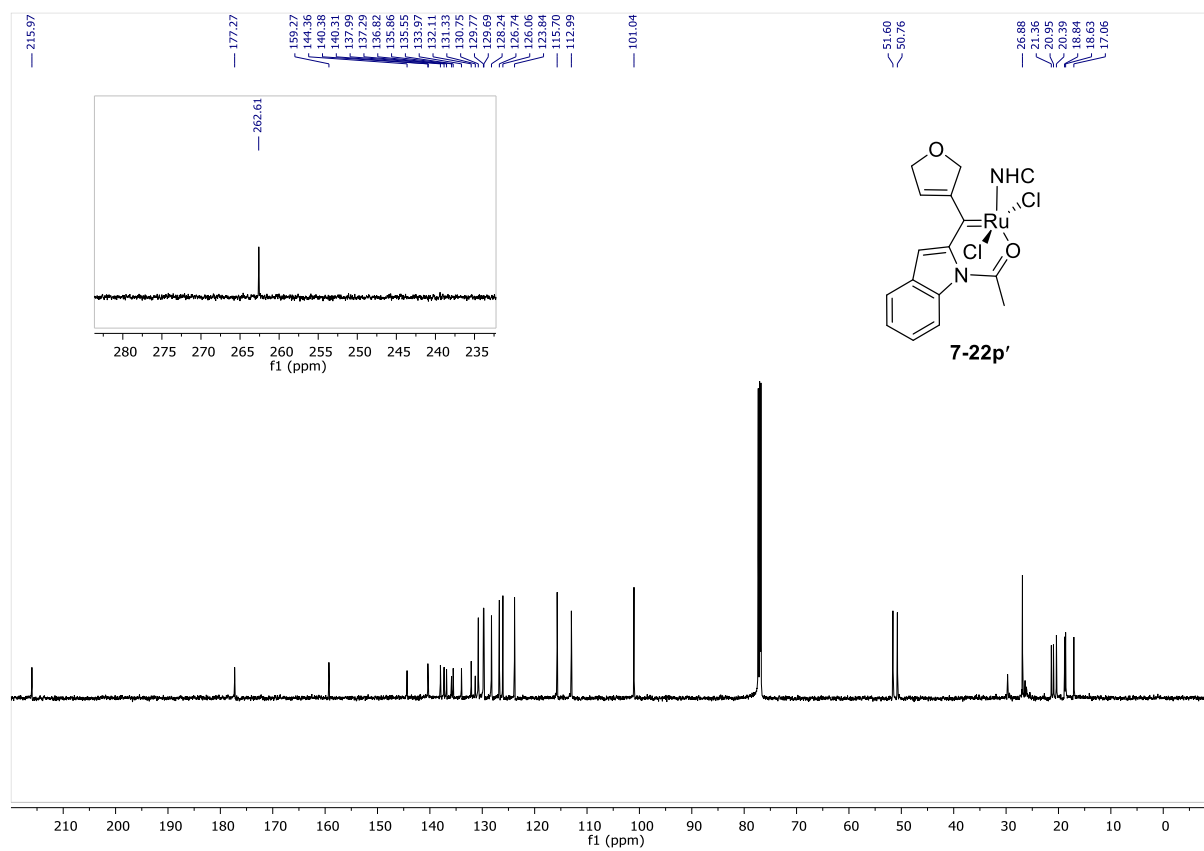
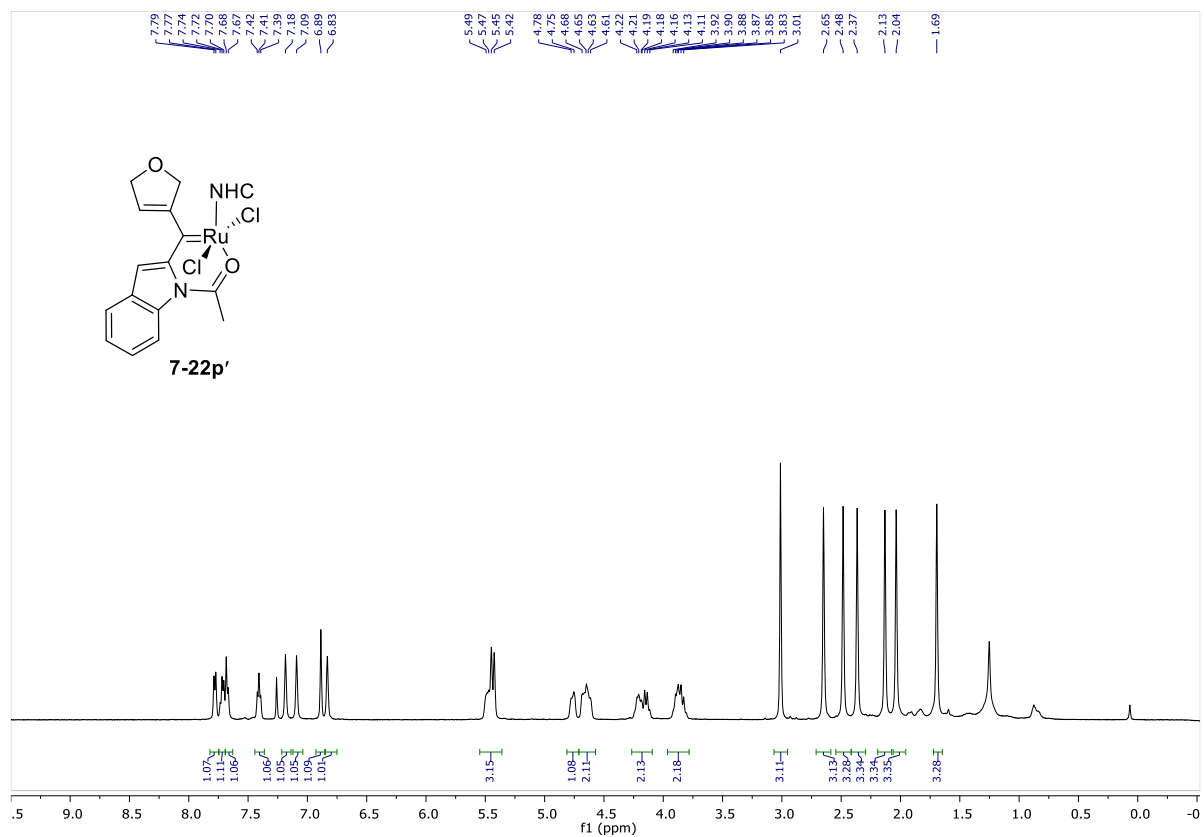


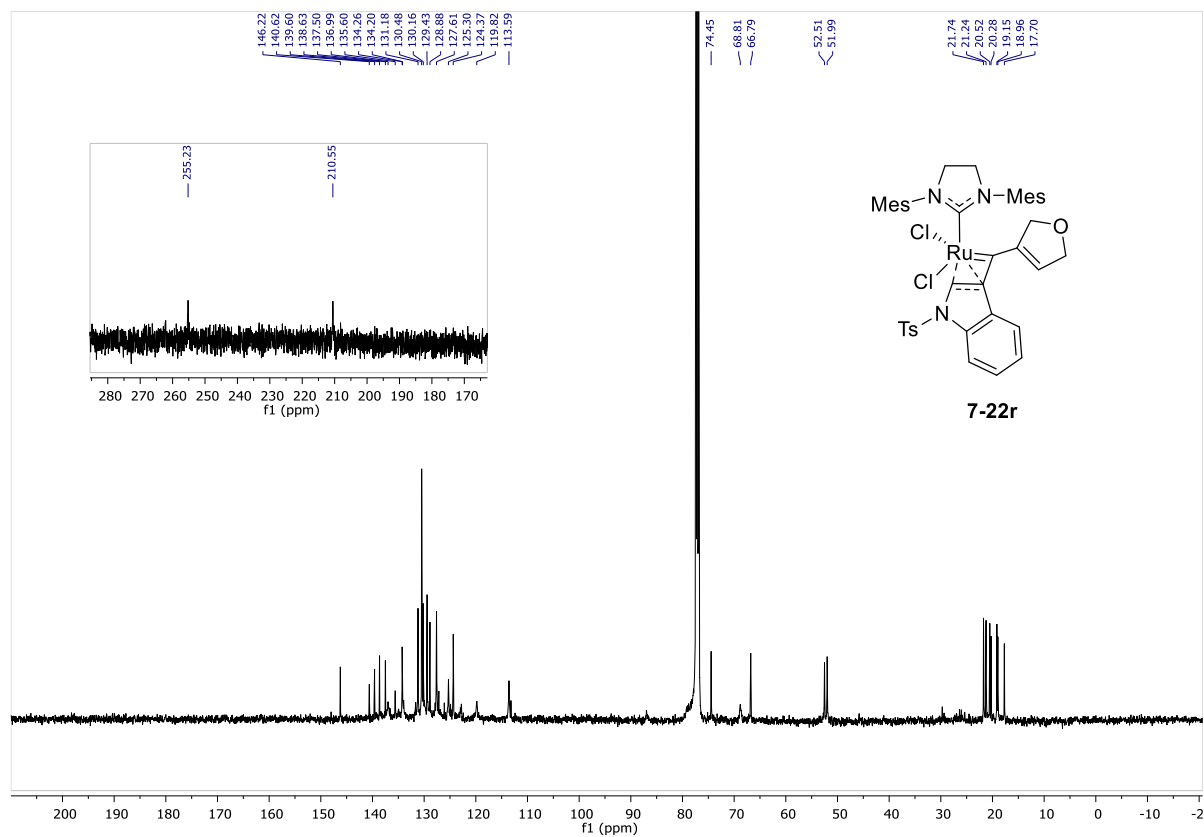
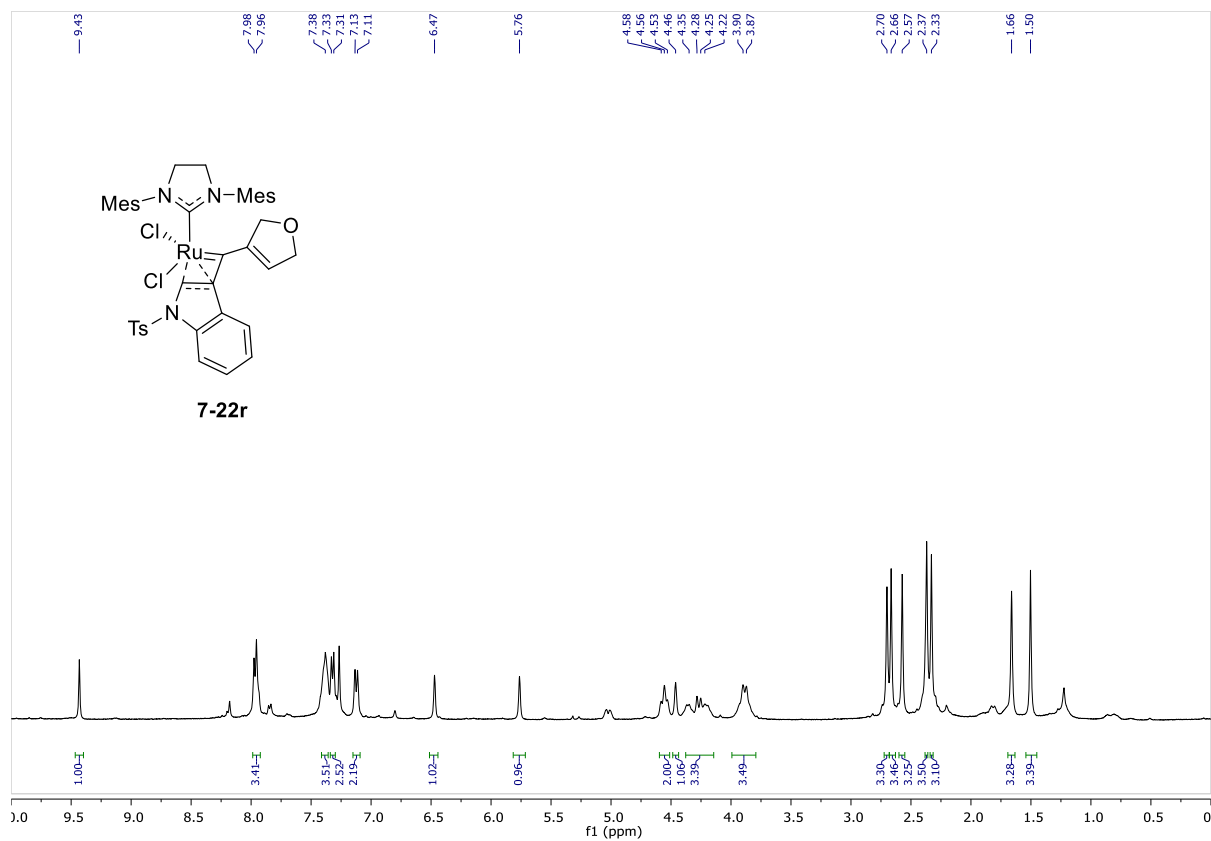


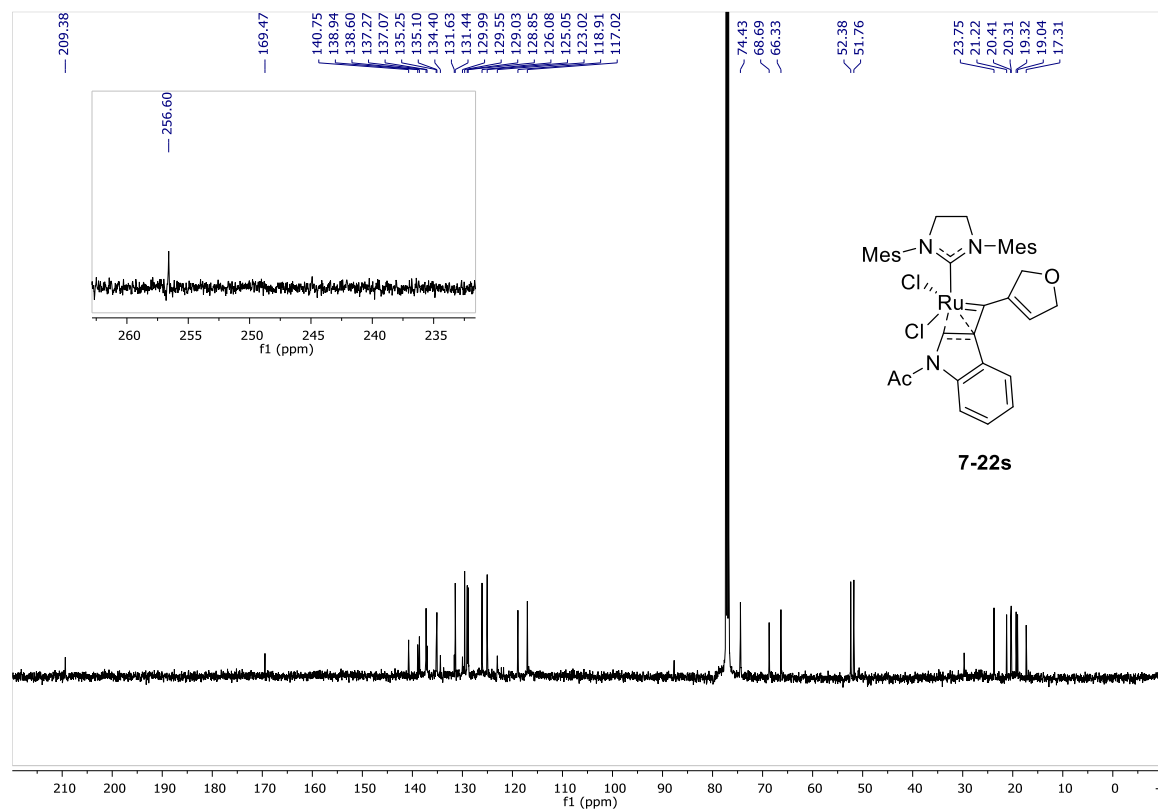
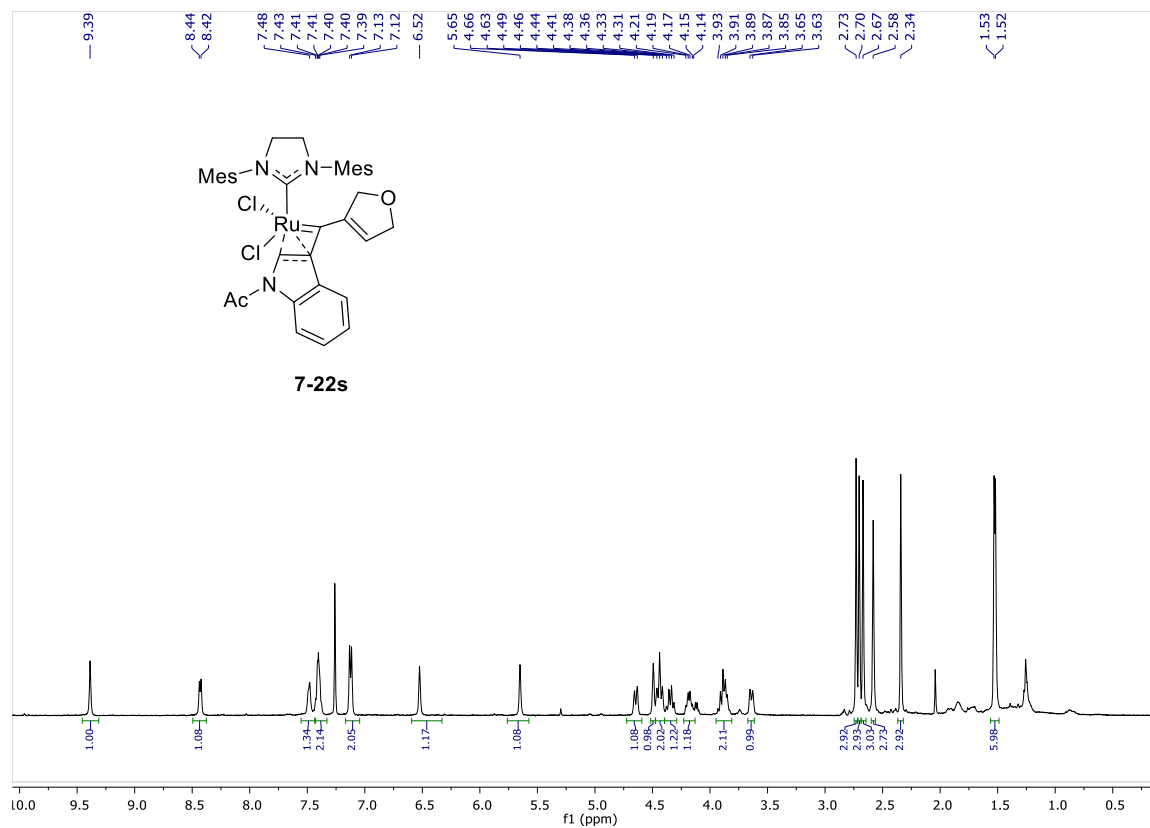


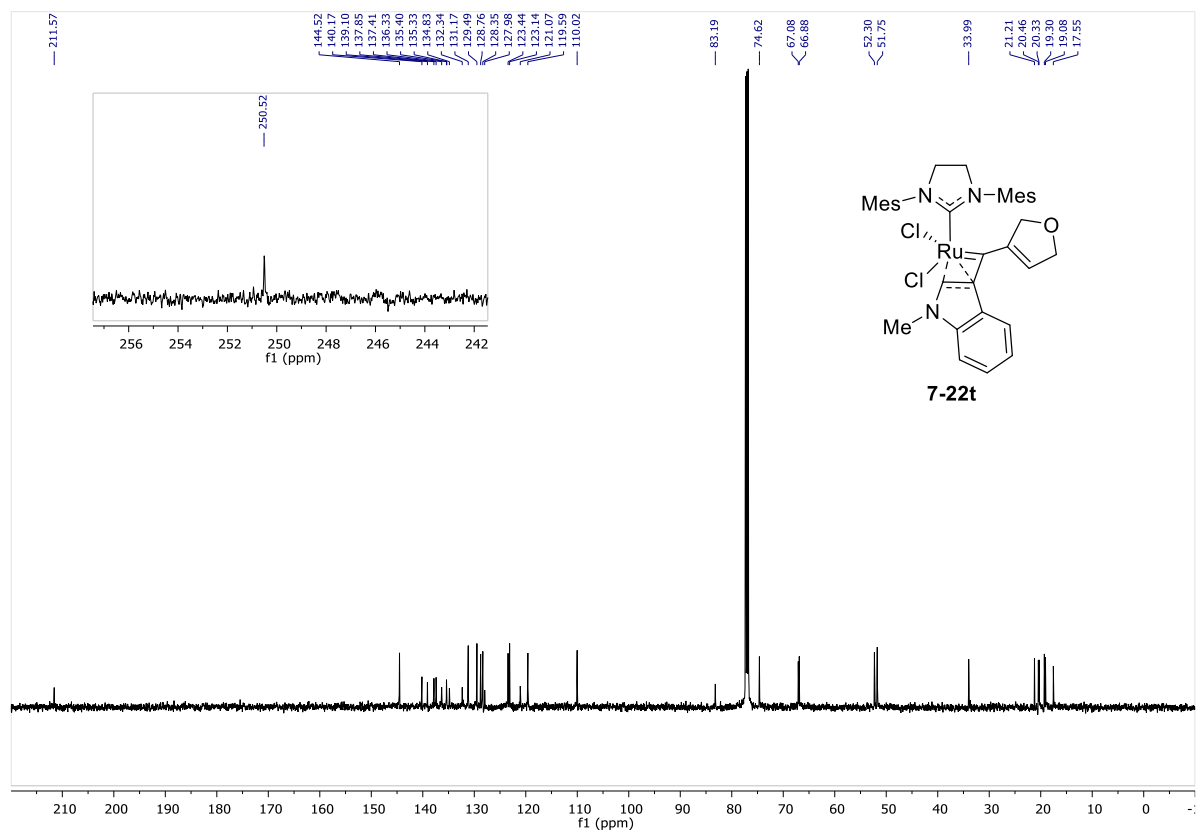
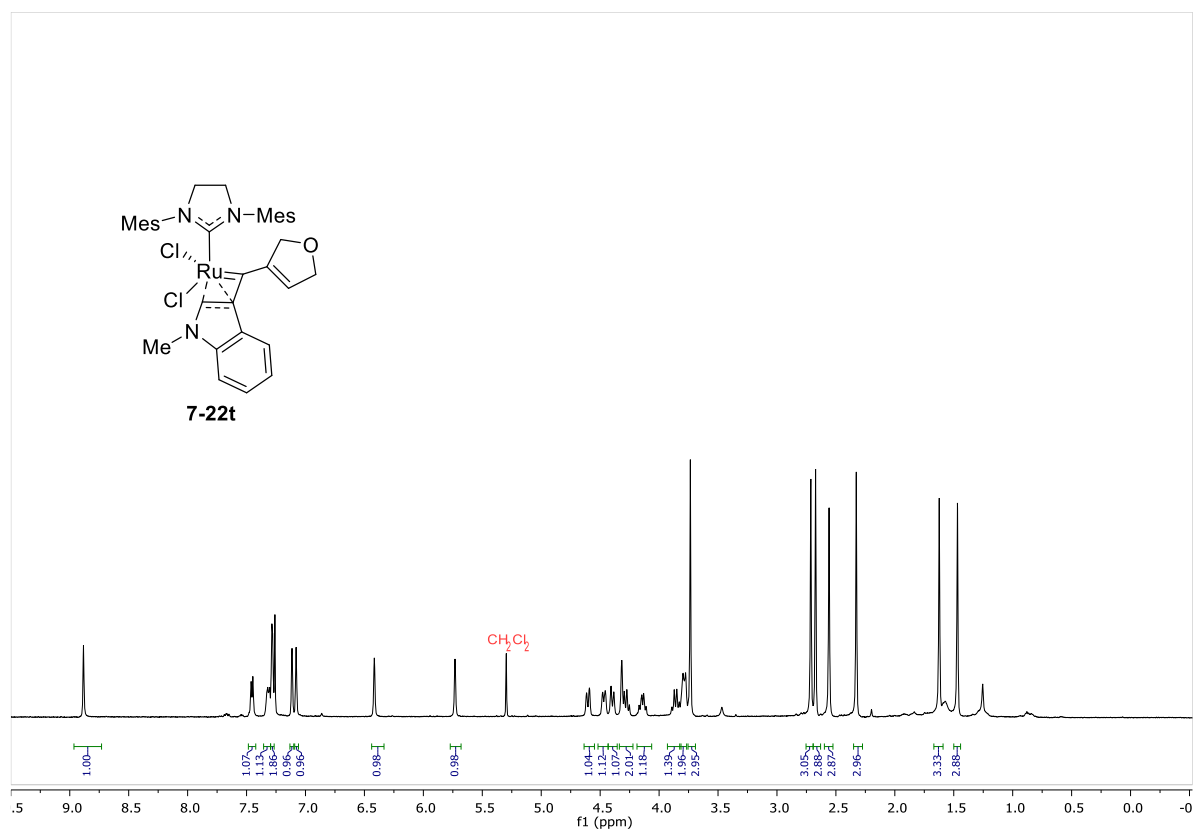


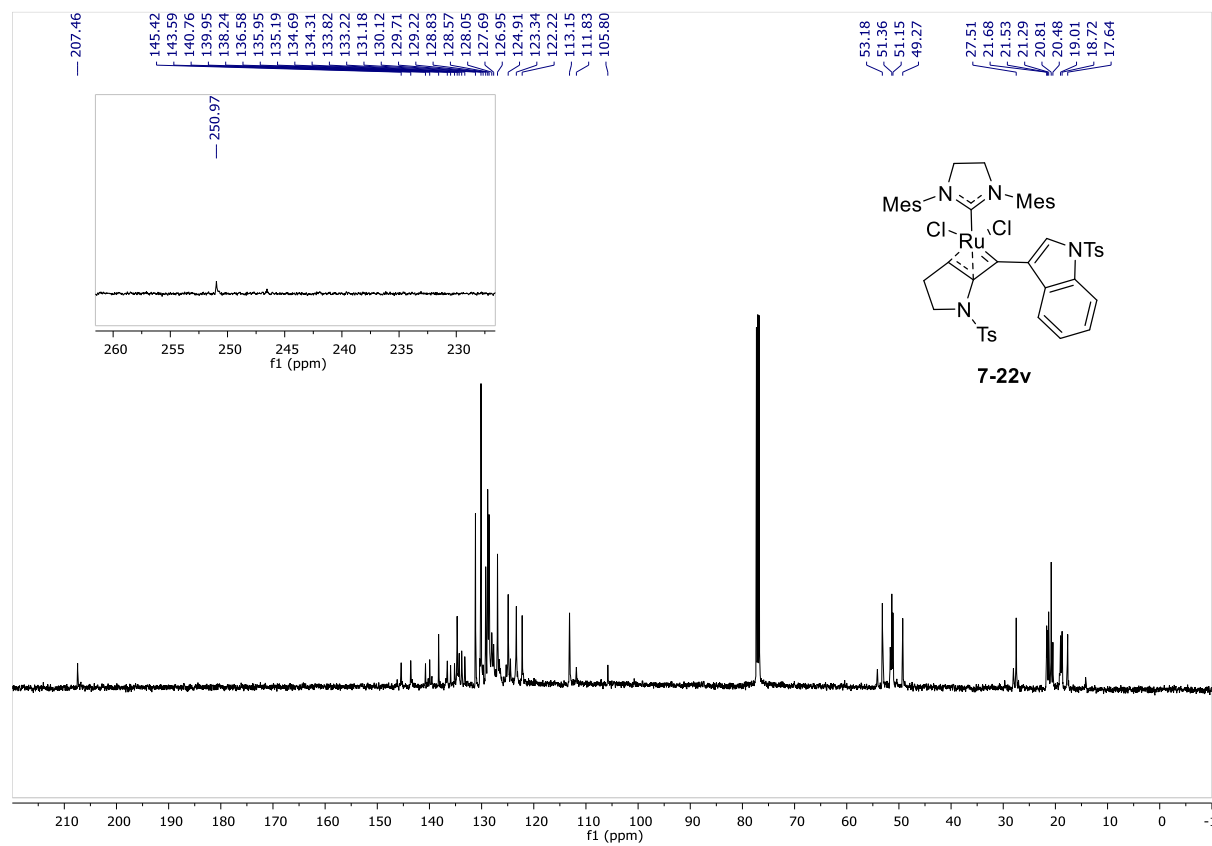
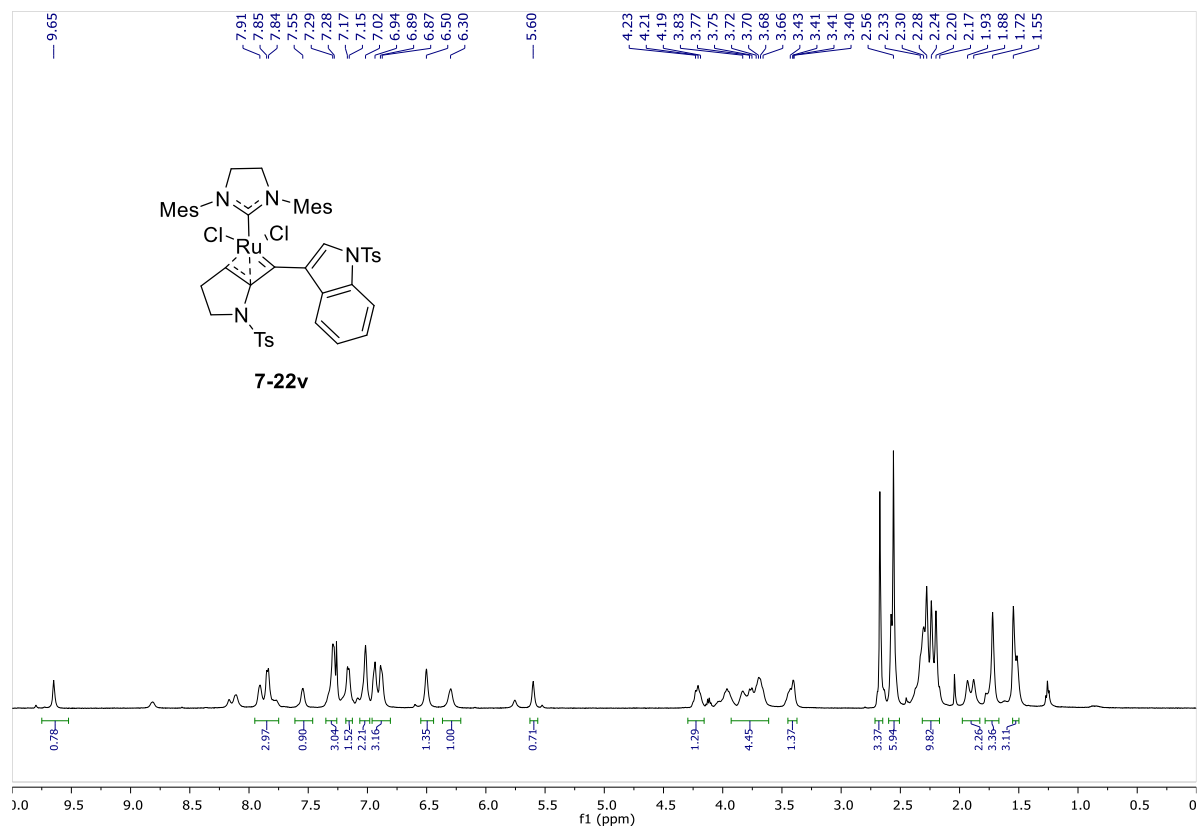




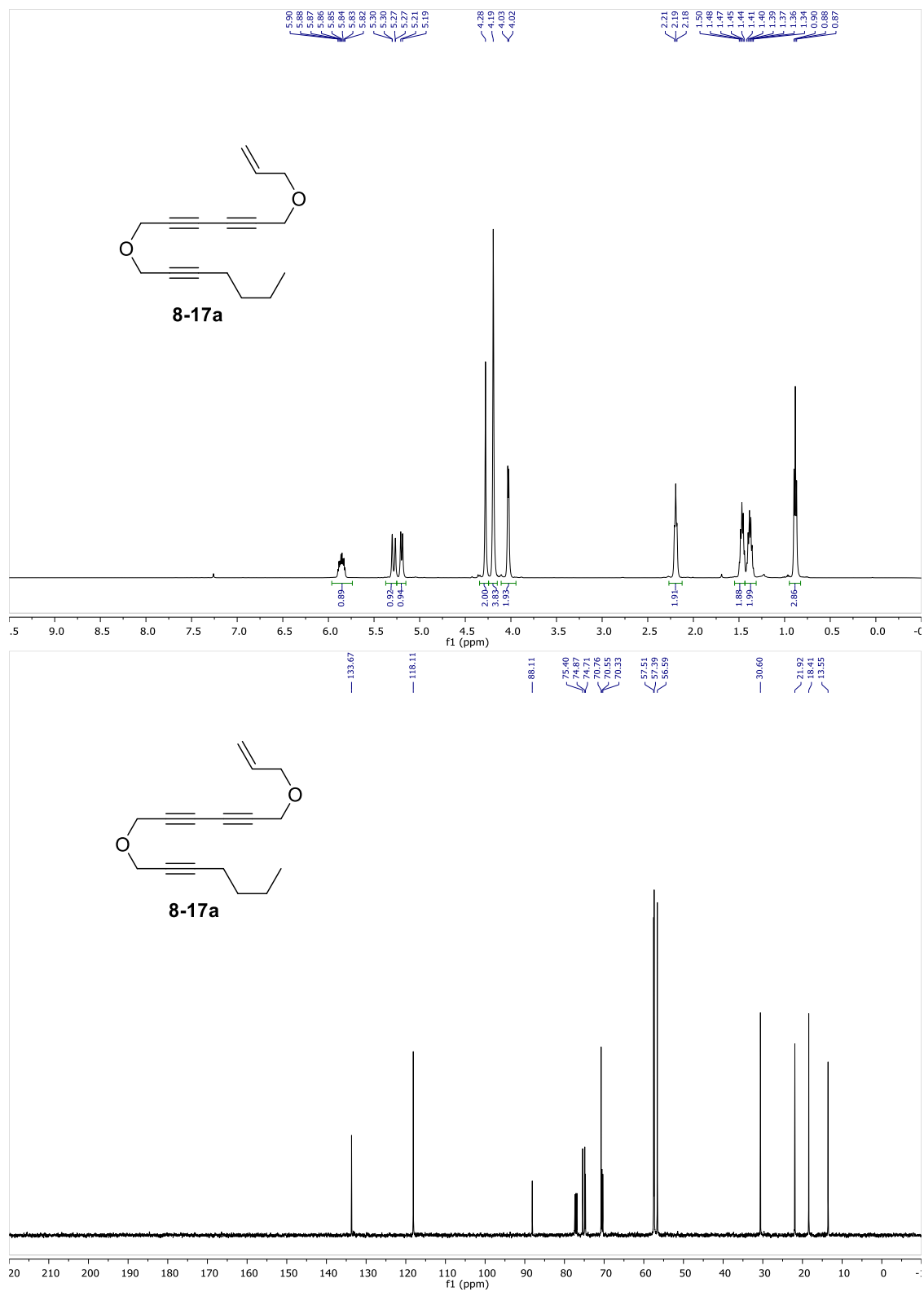


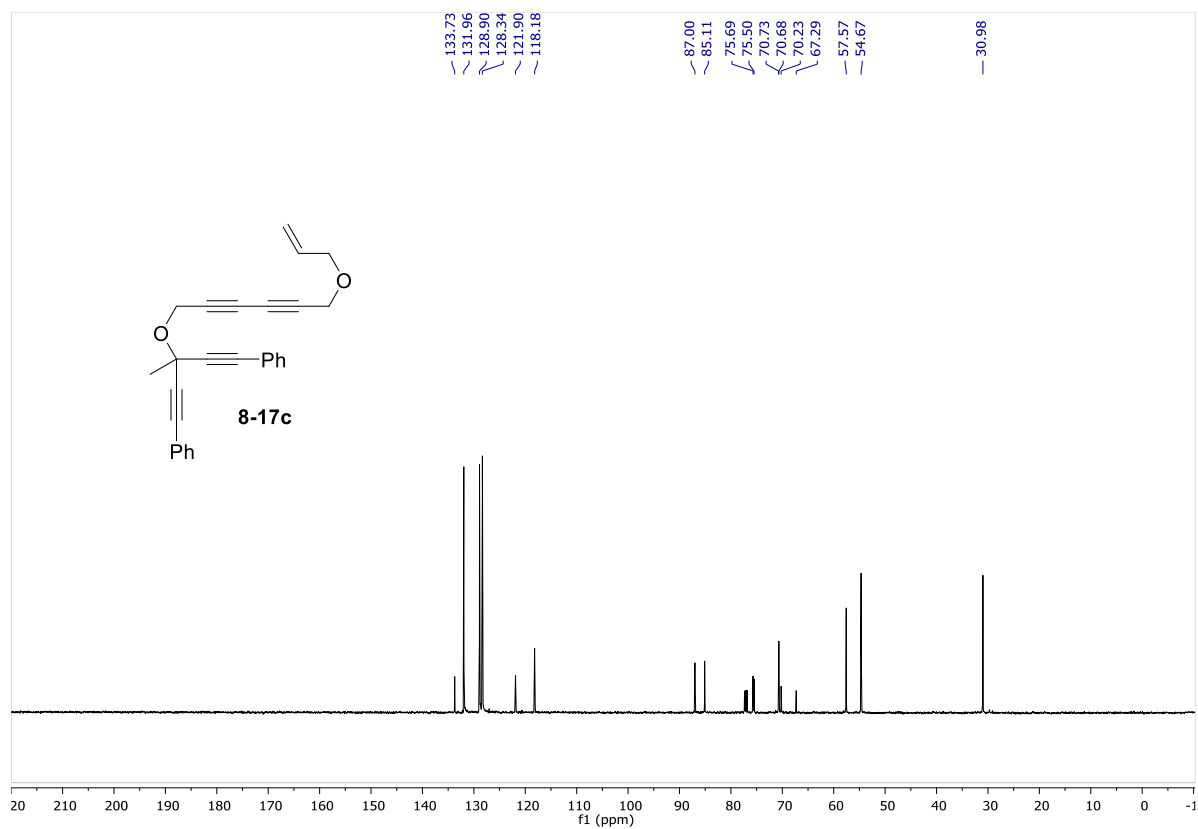
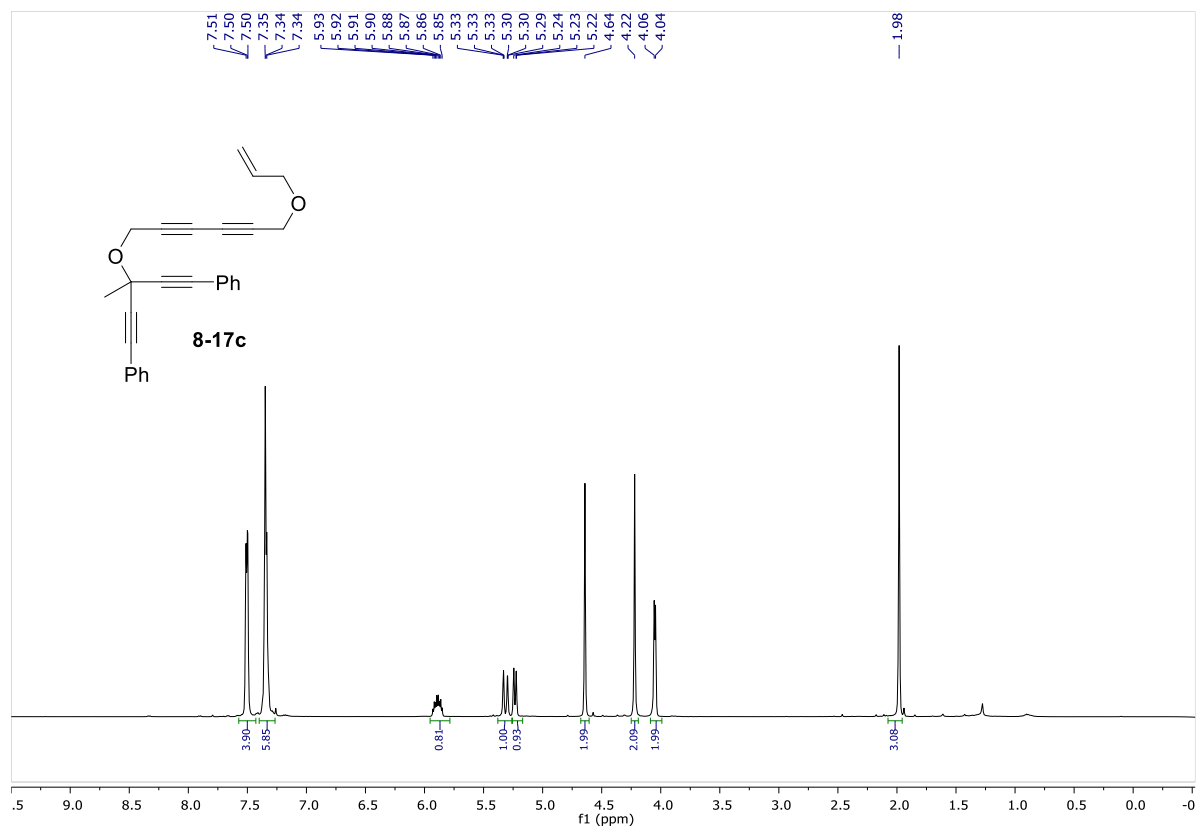


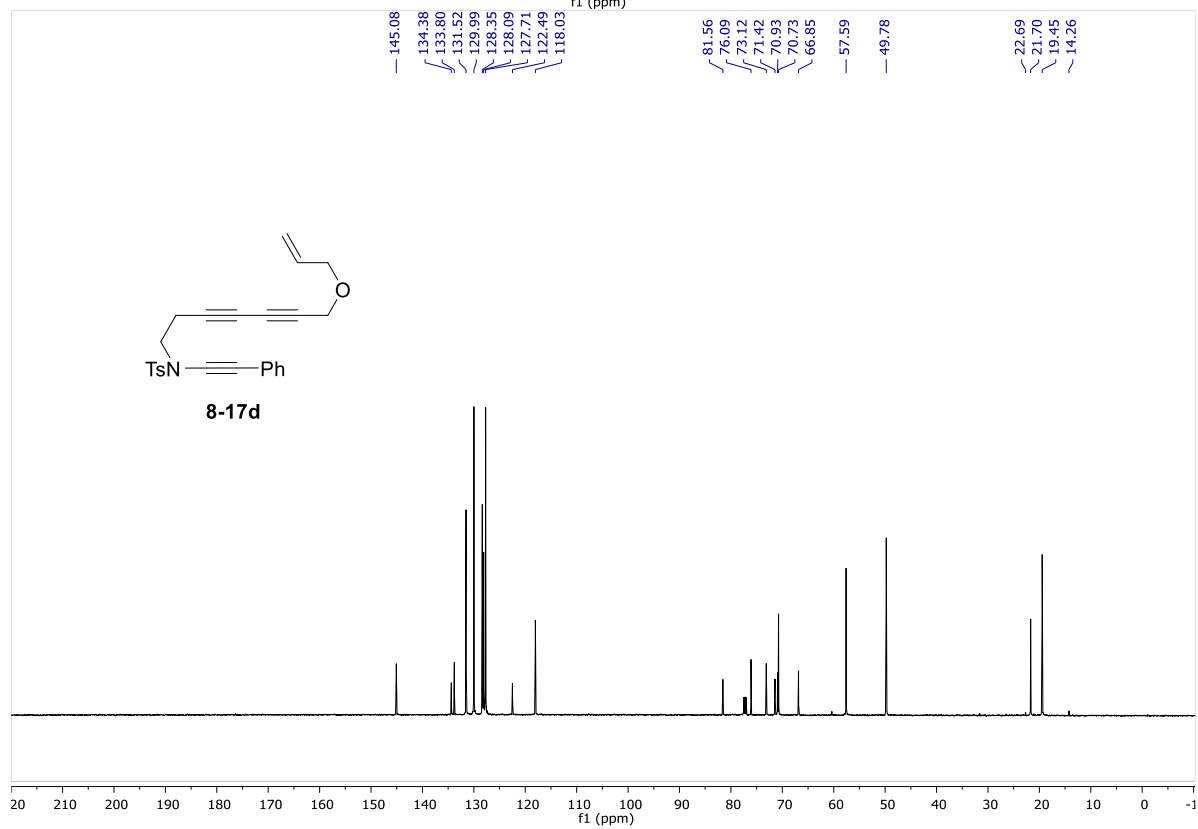
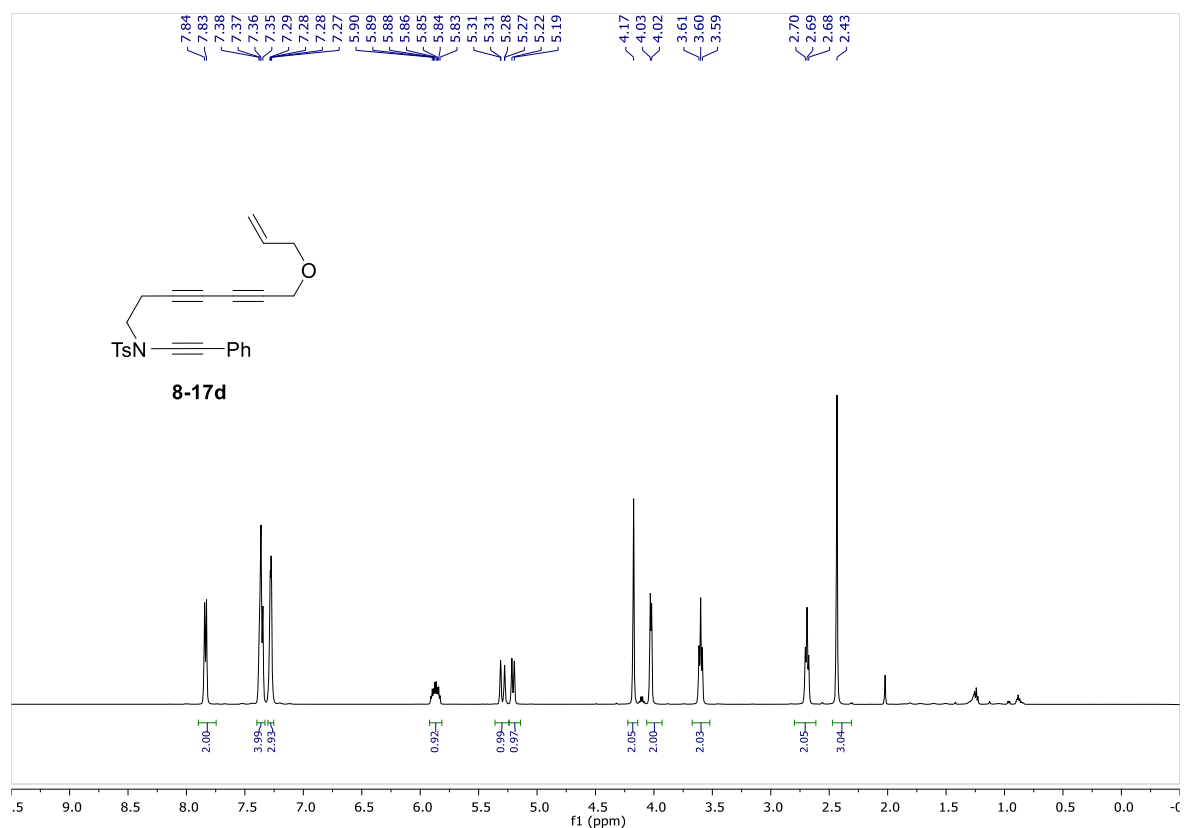


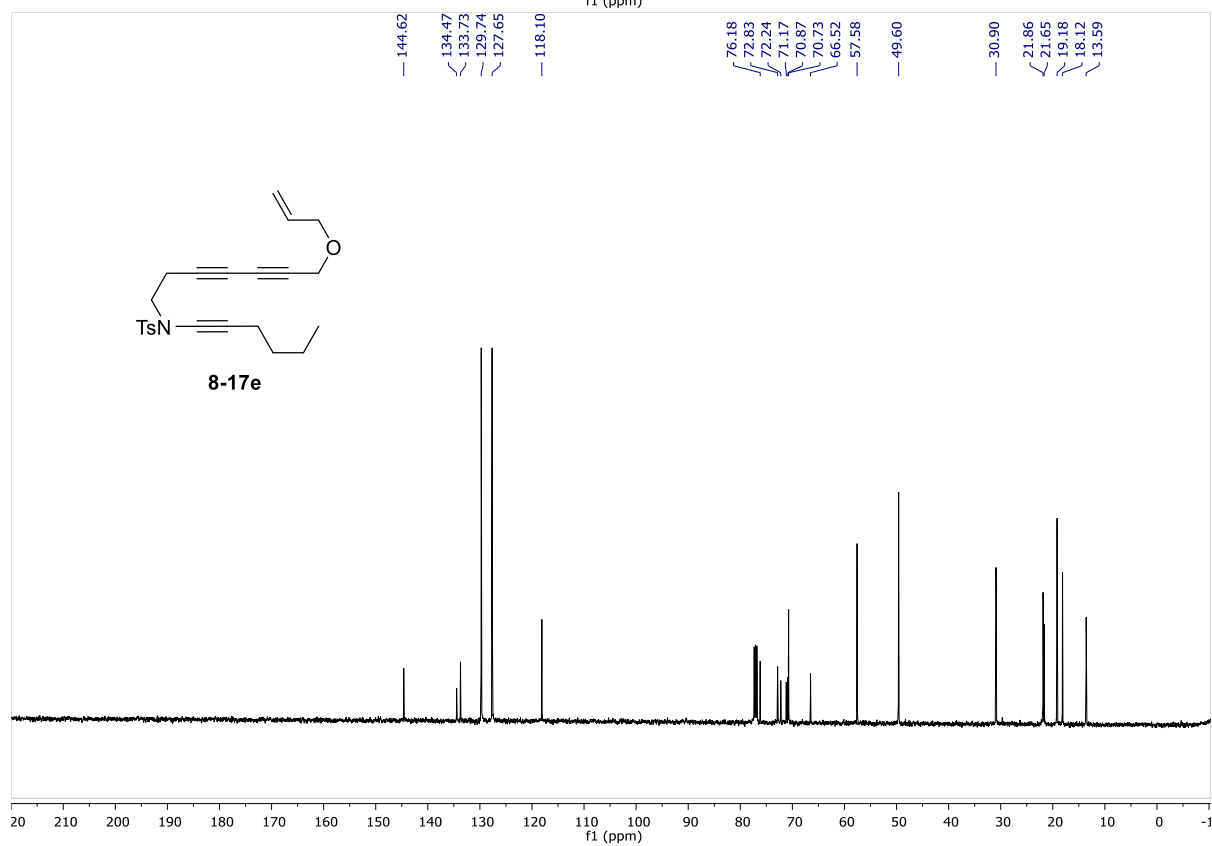
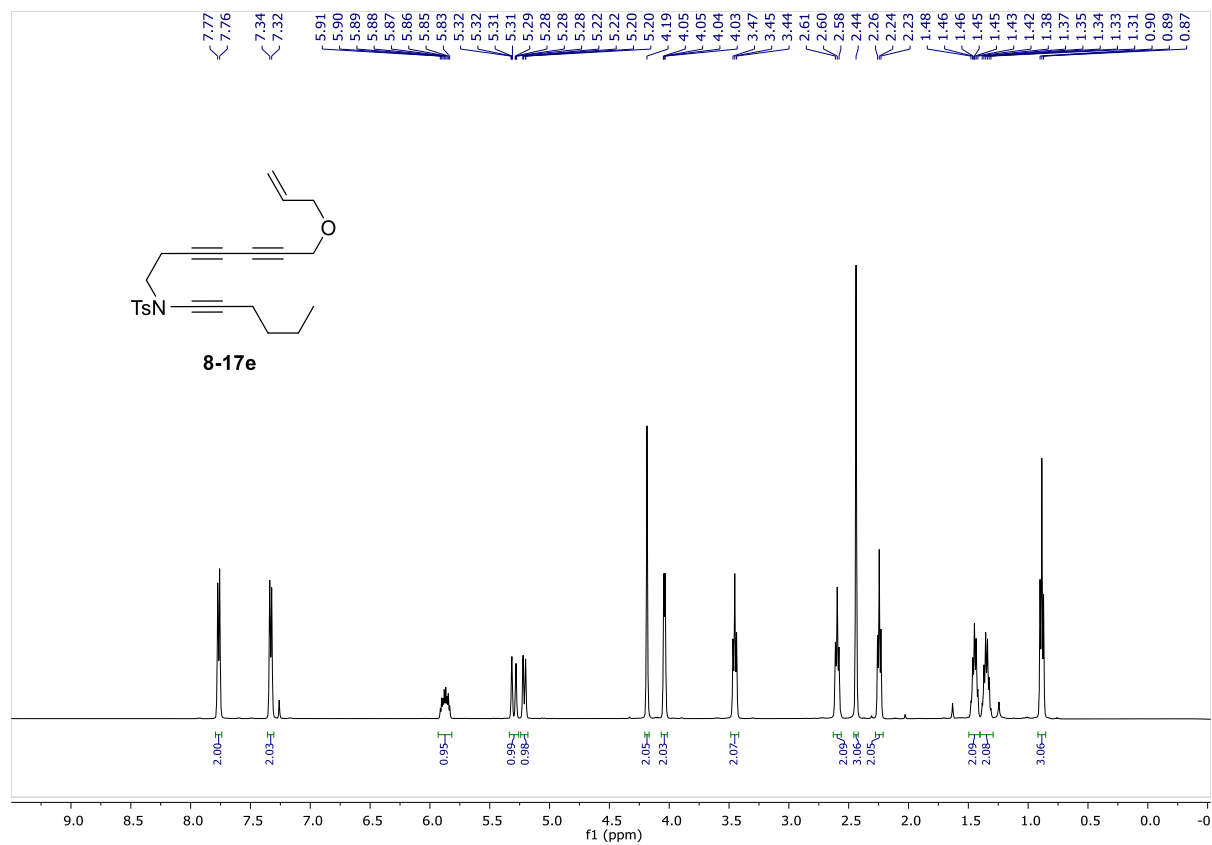


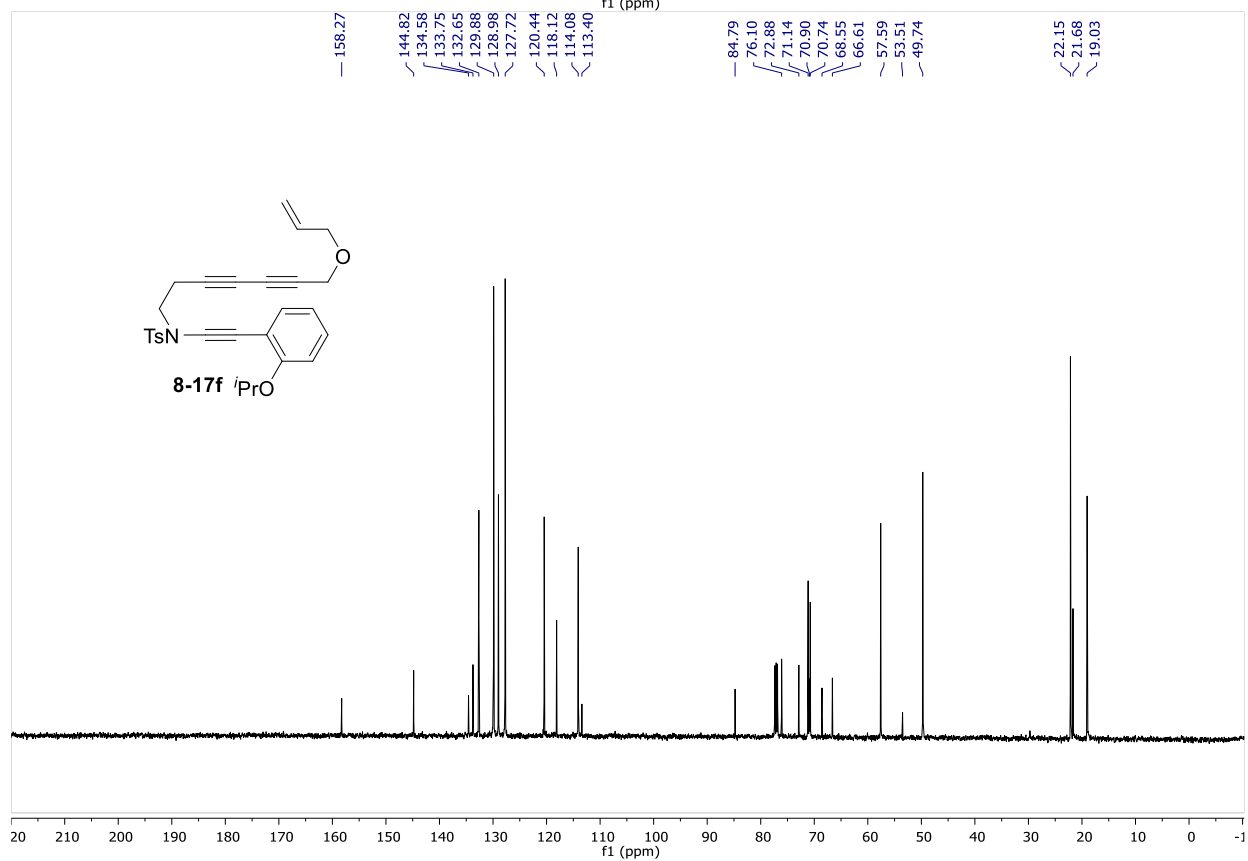
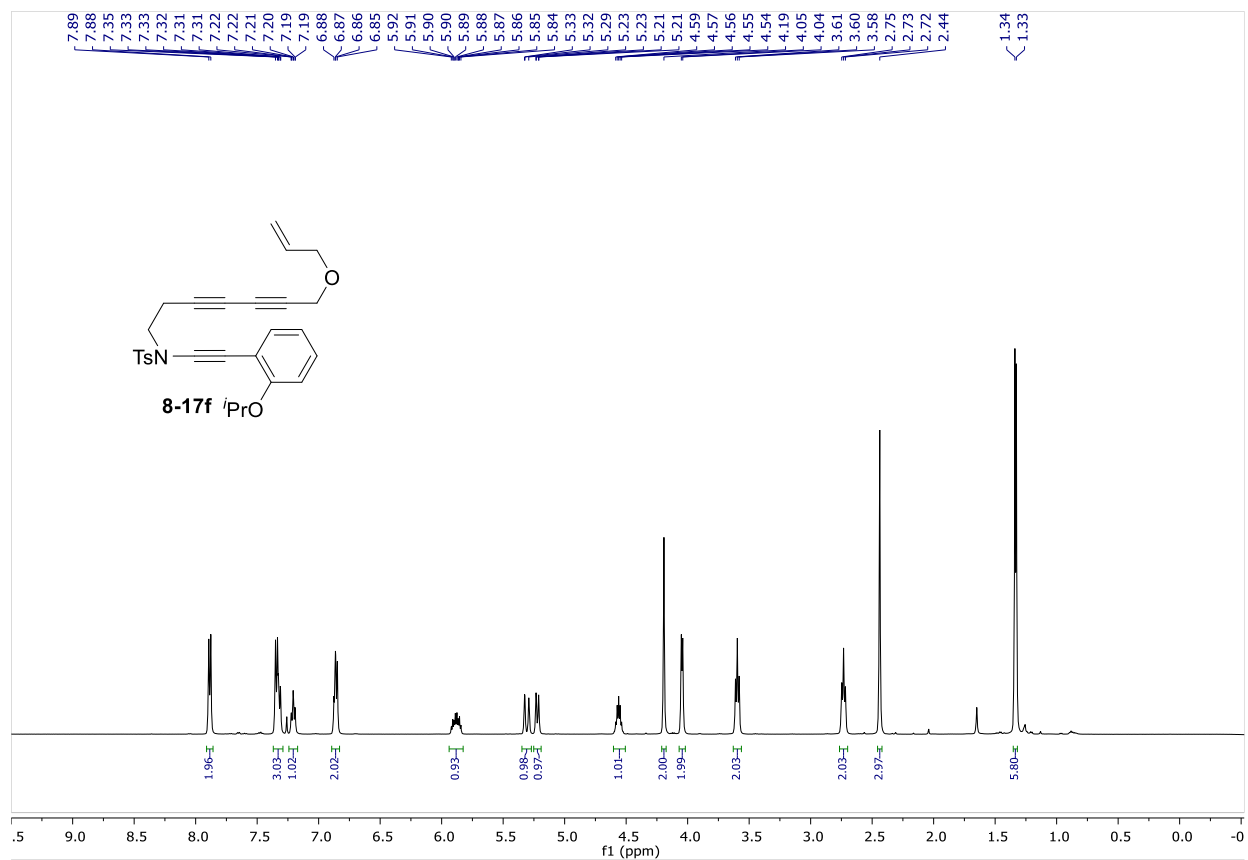
Appendix VI
Selected NMR Spectra for Chapter 8

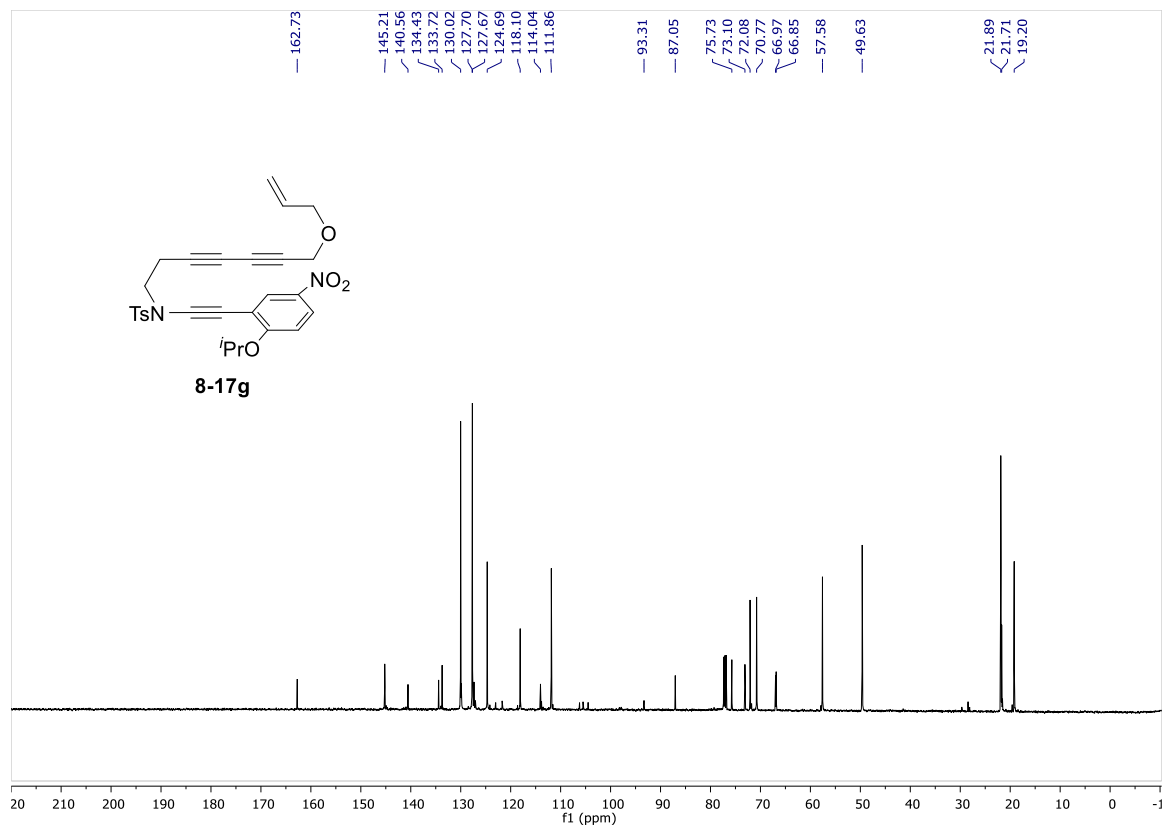
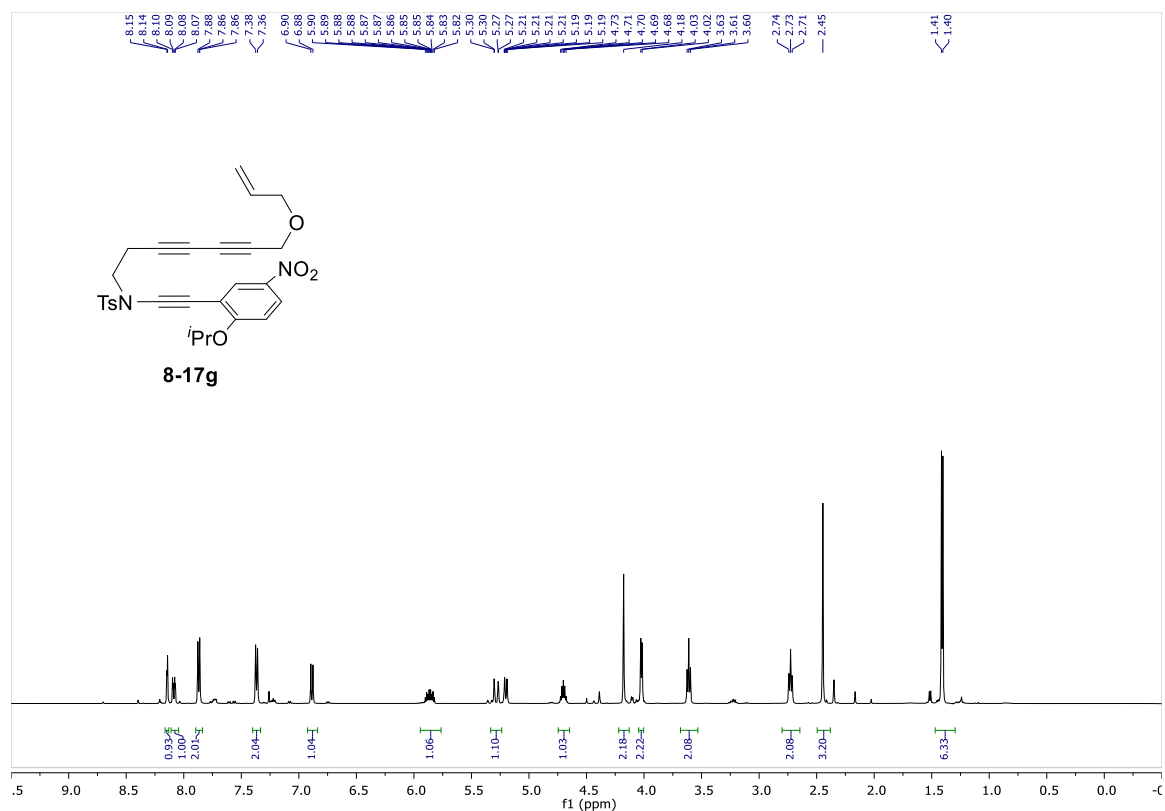


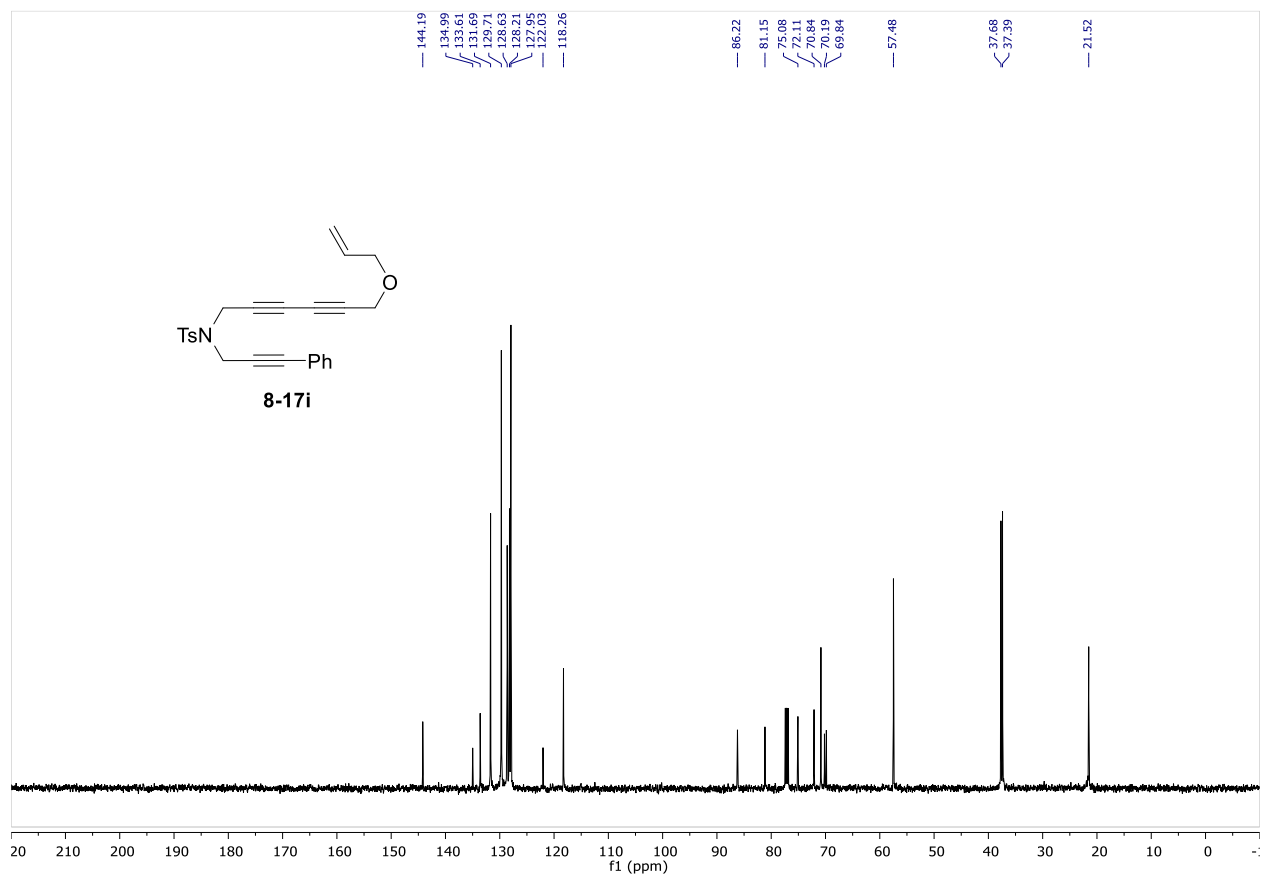
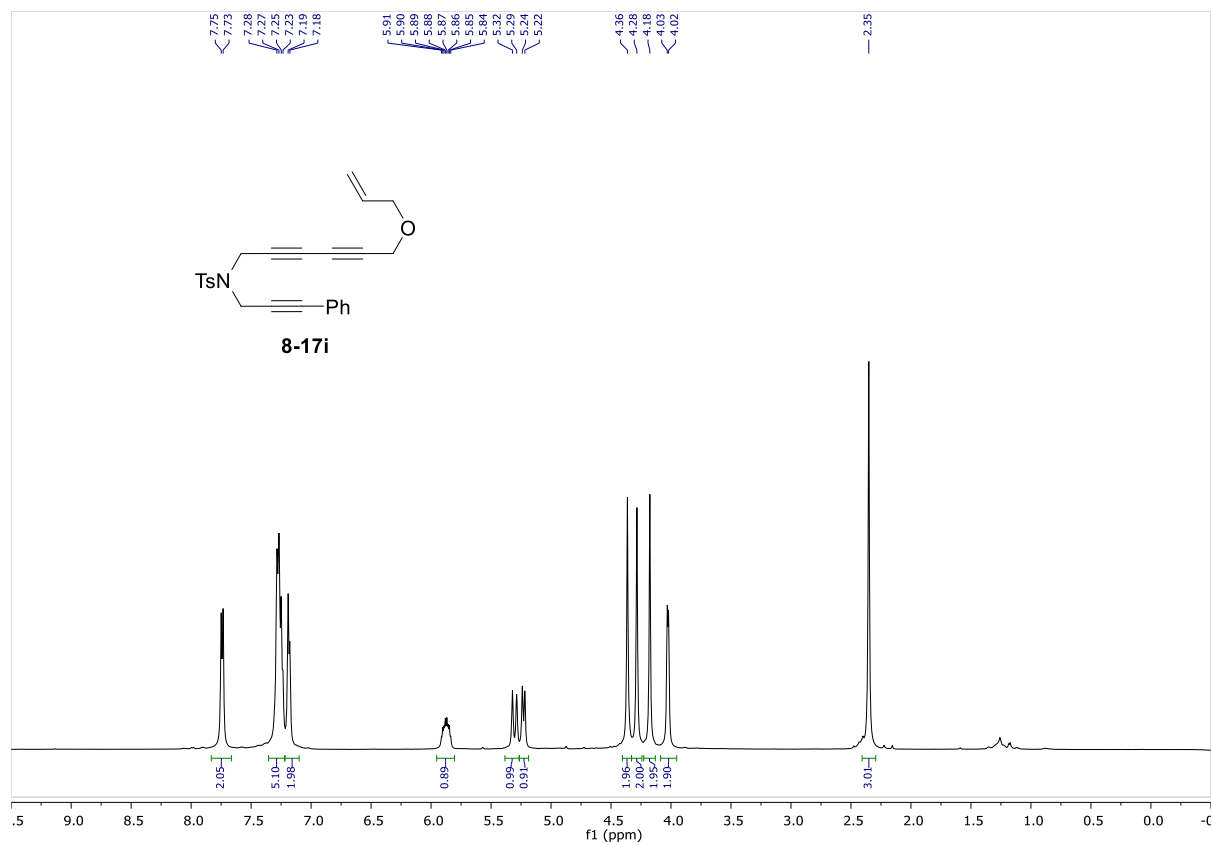


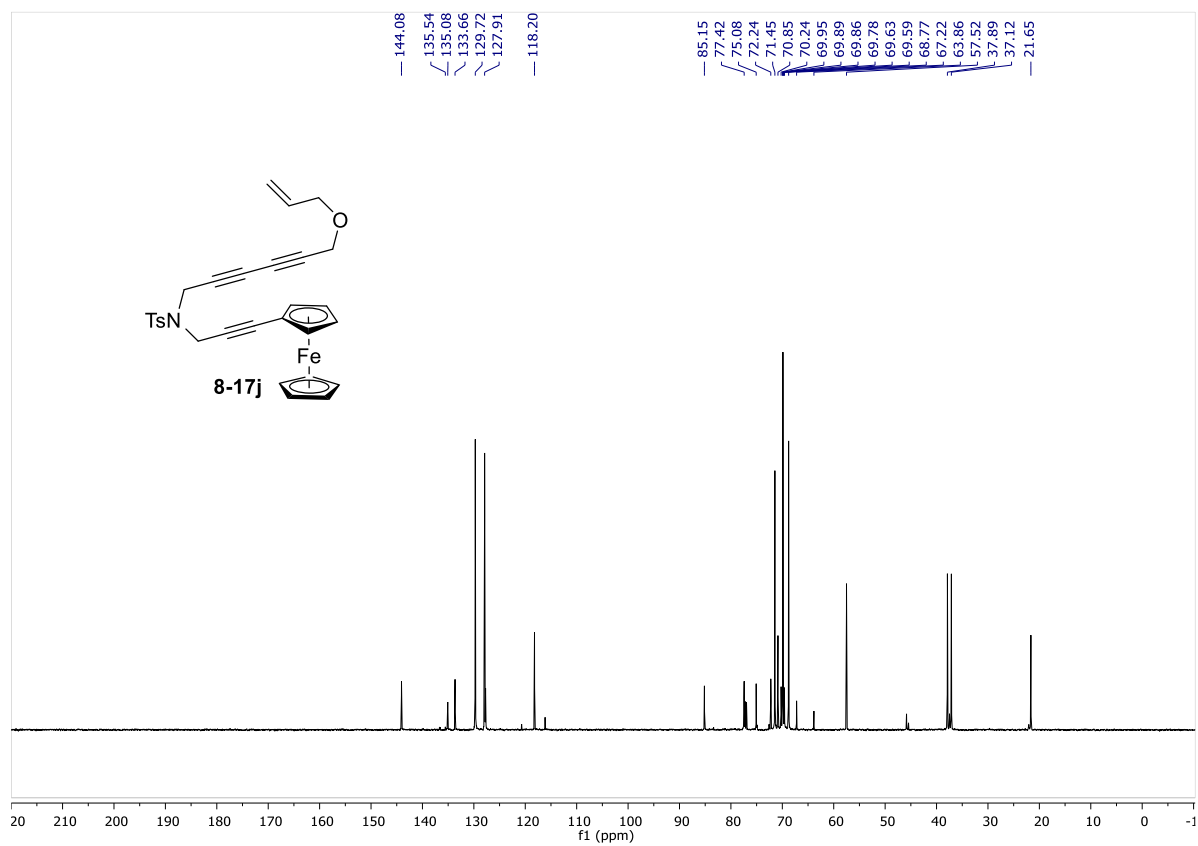


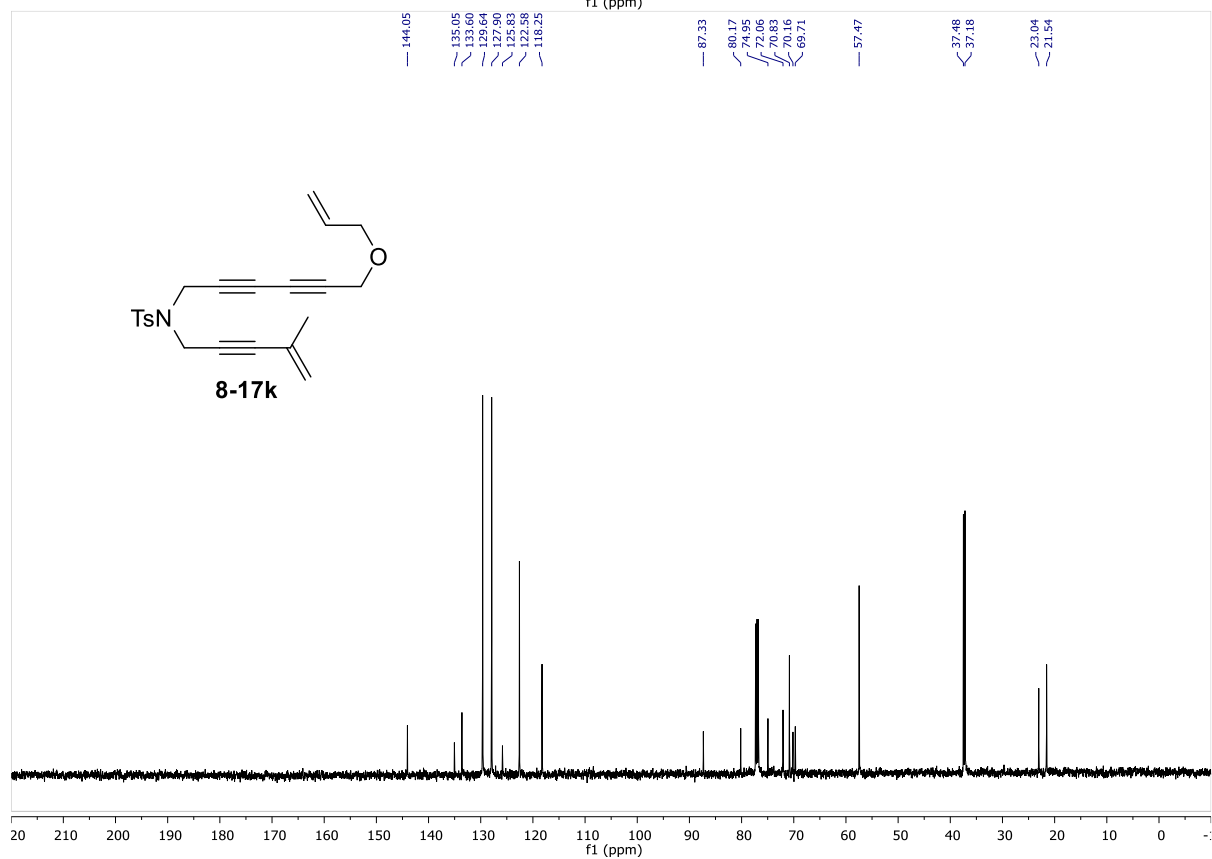
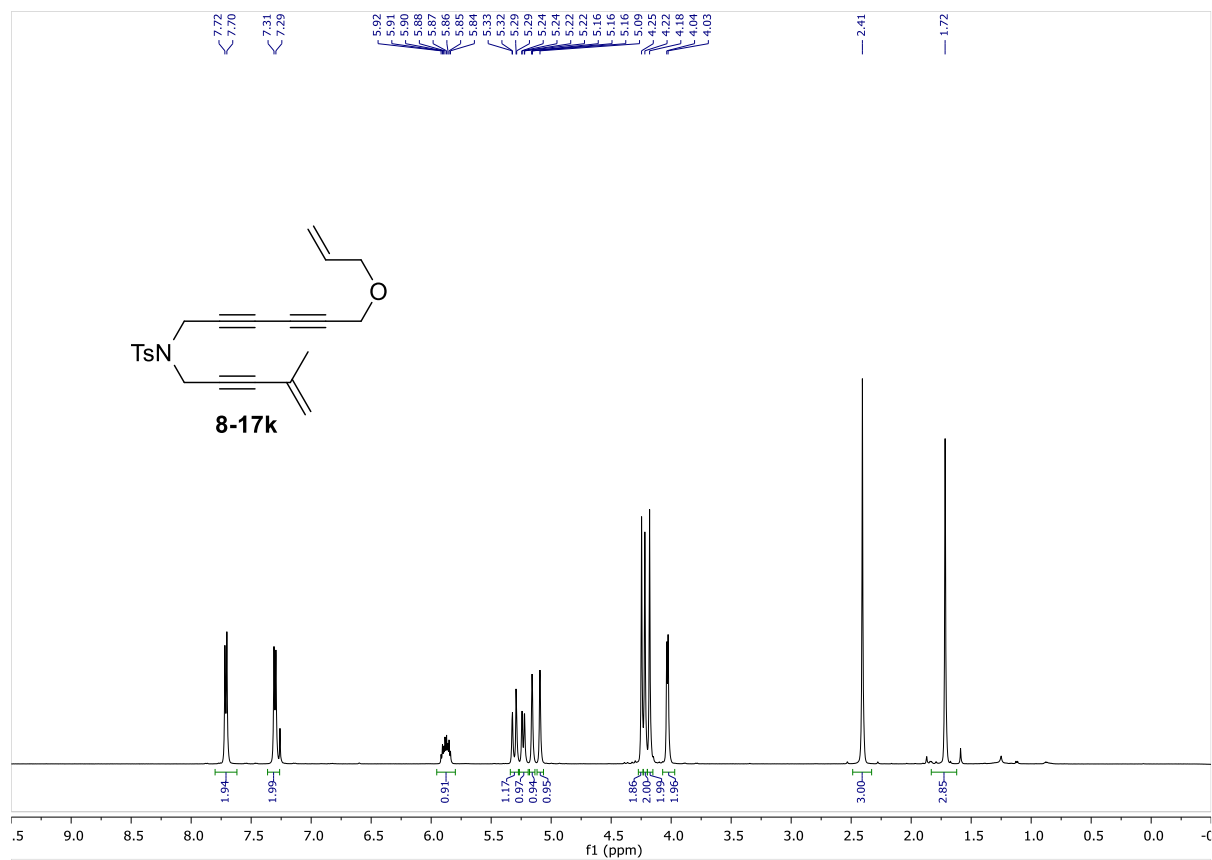


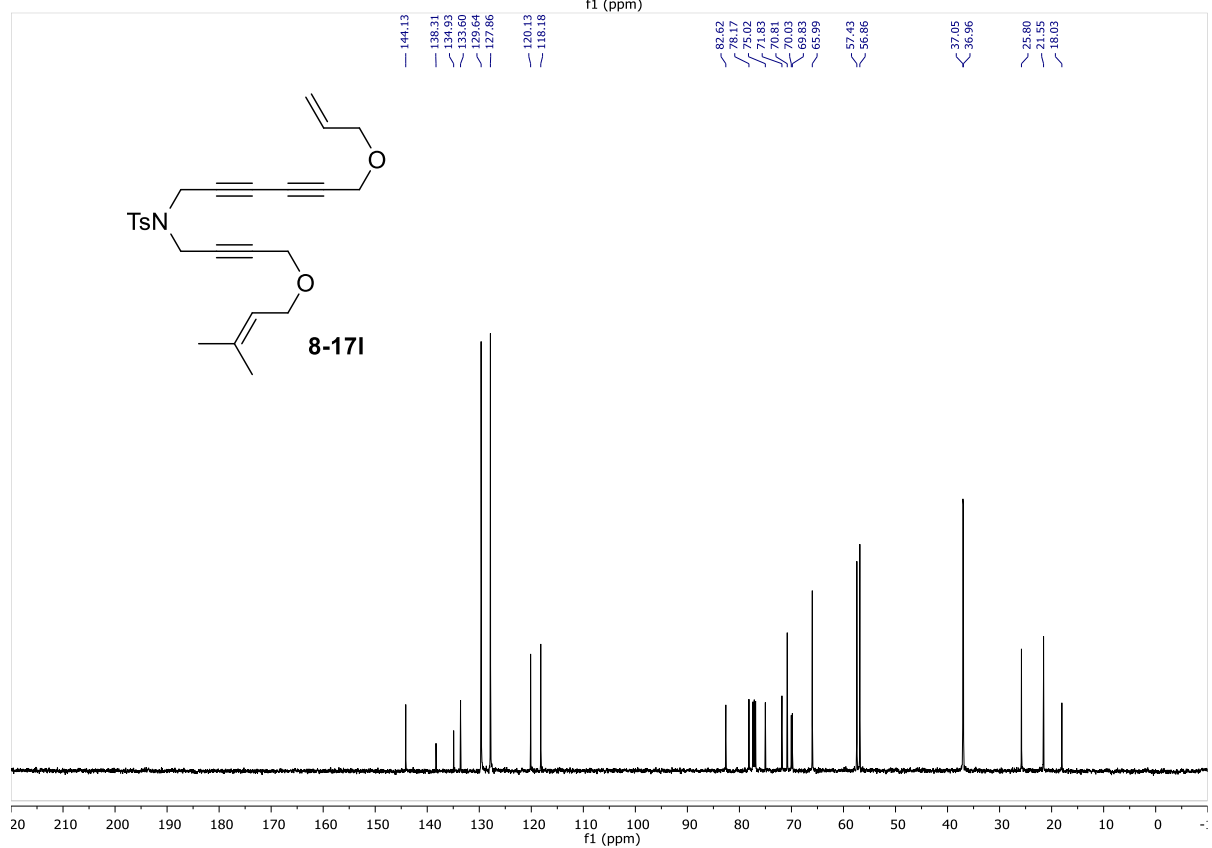
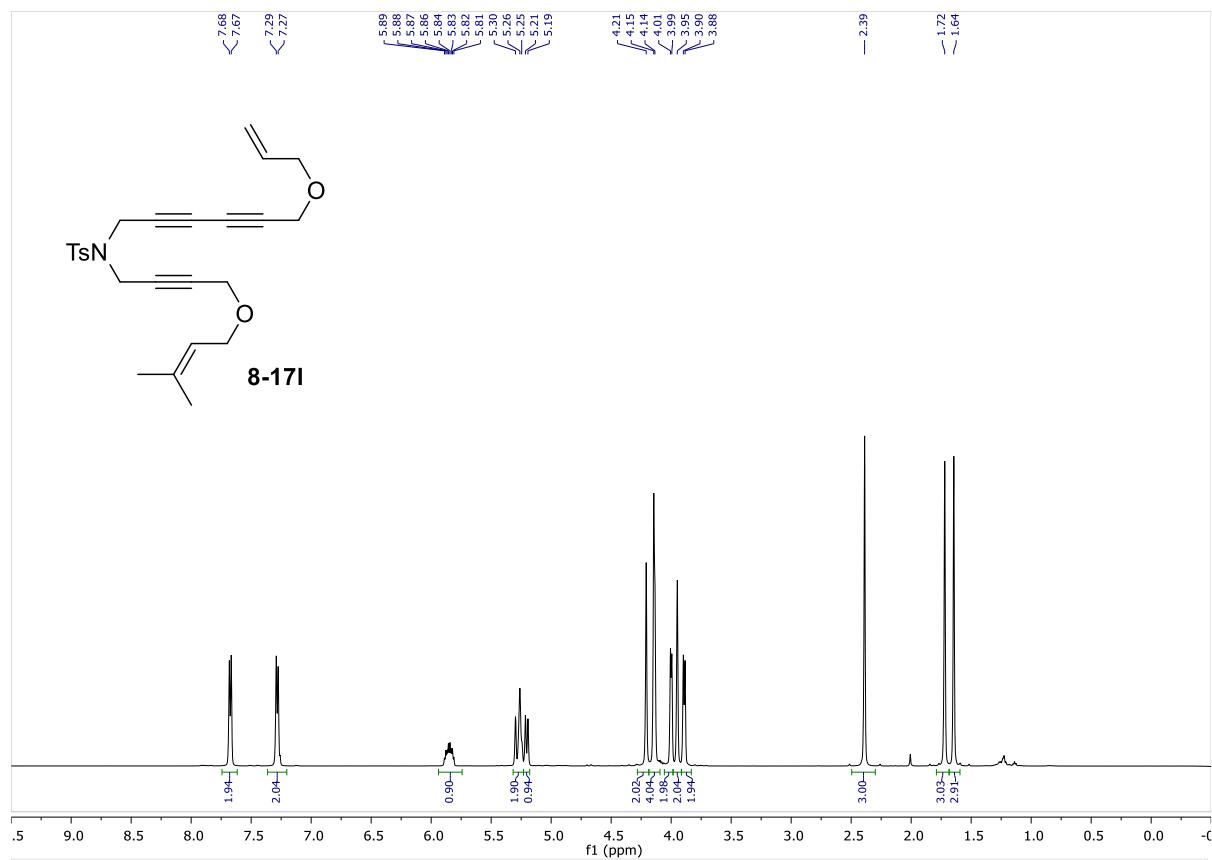


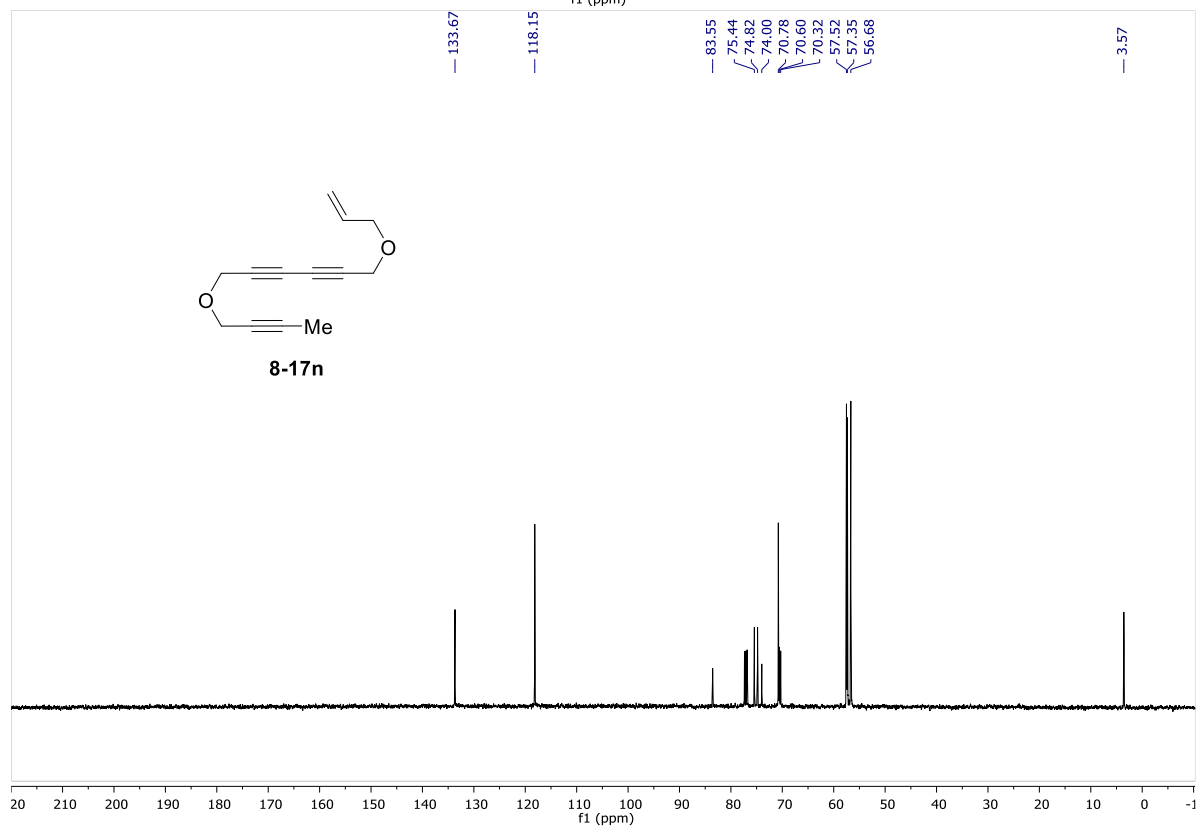
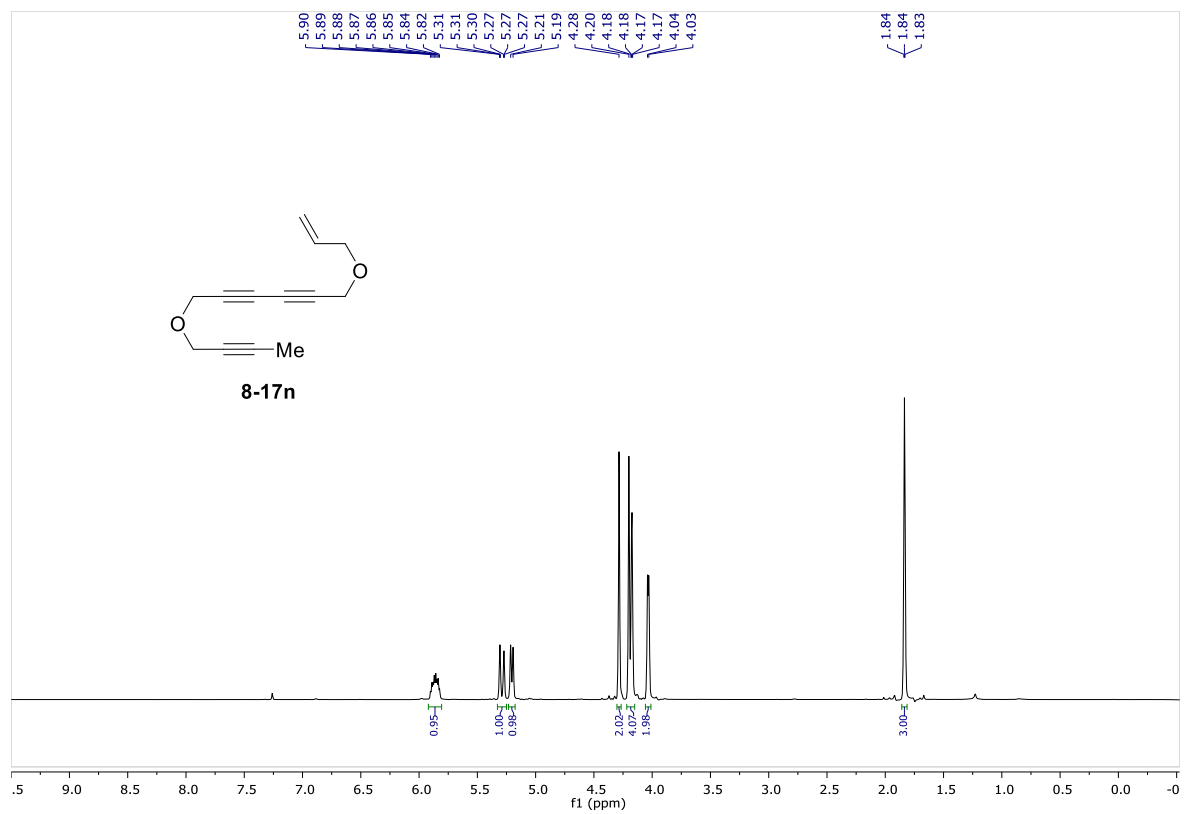


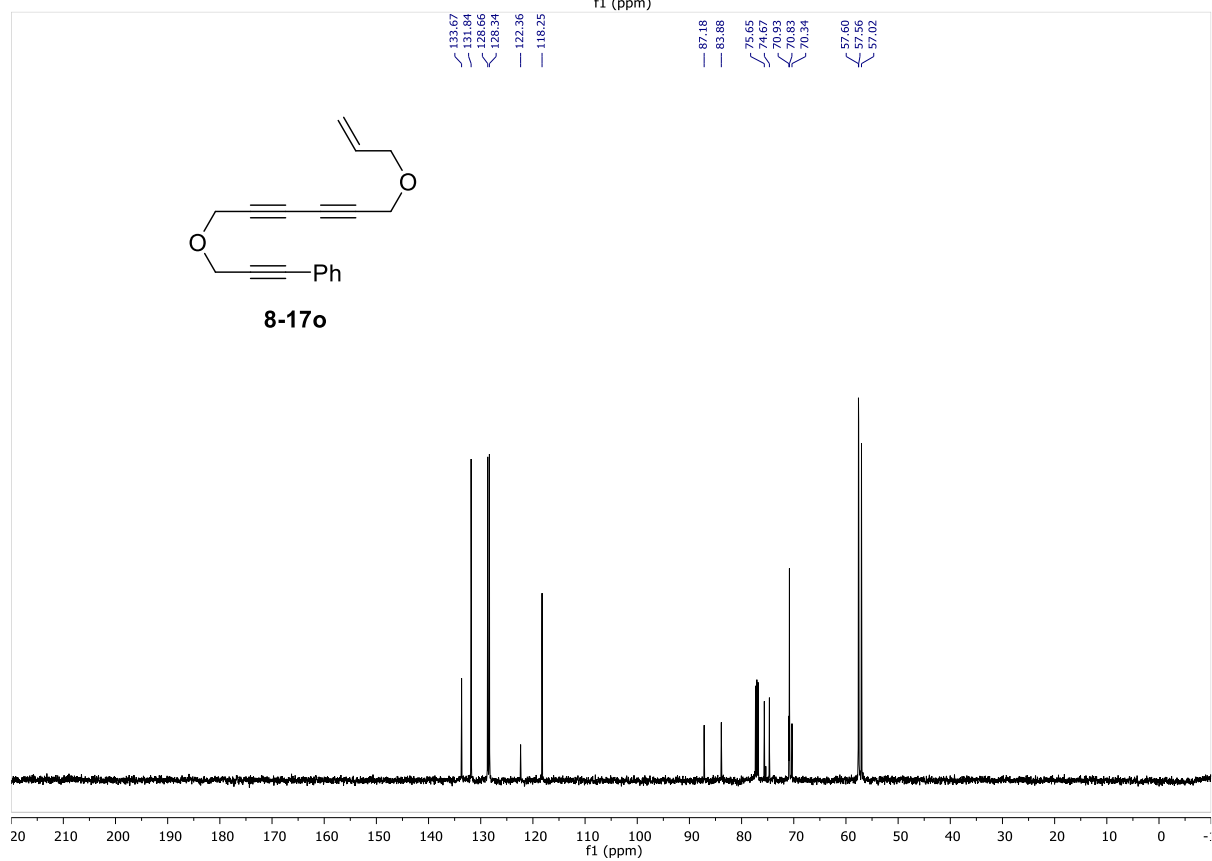
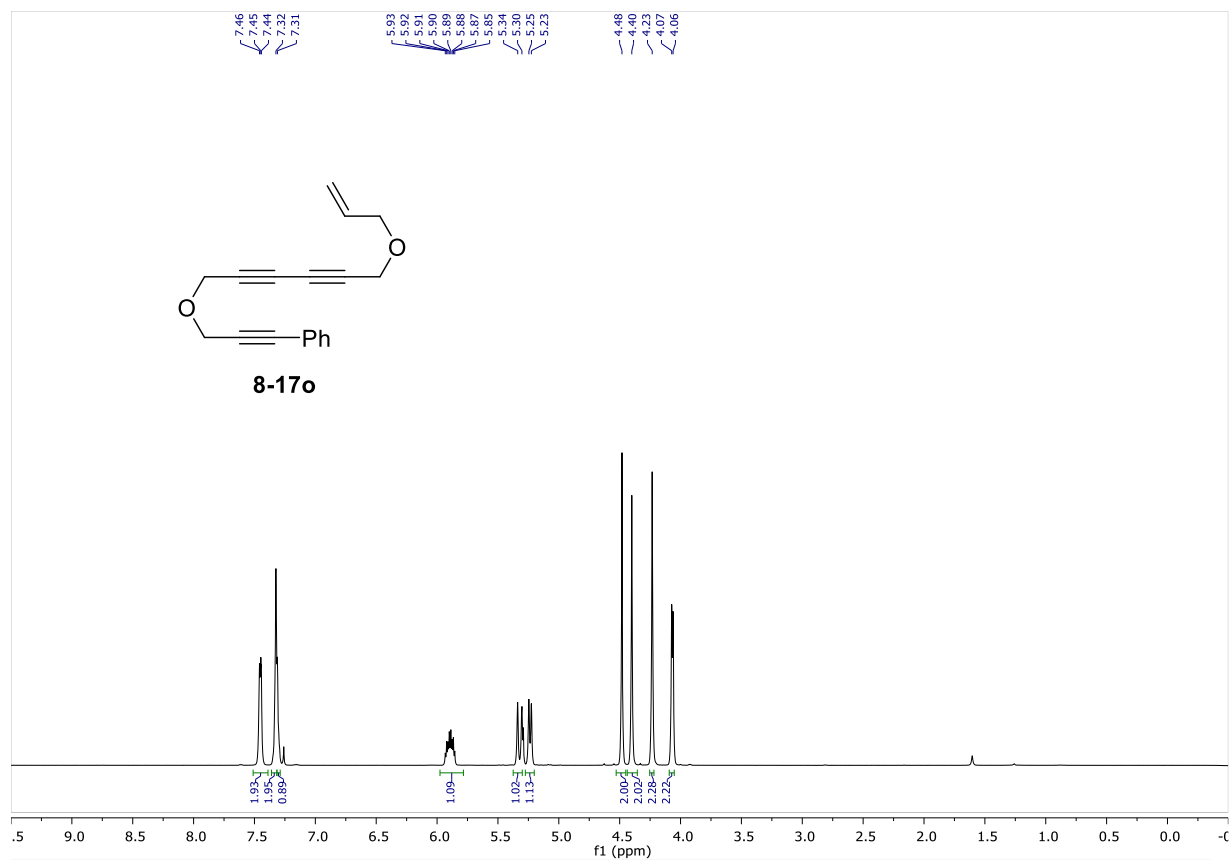


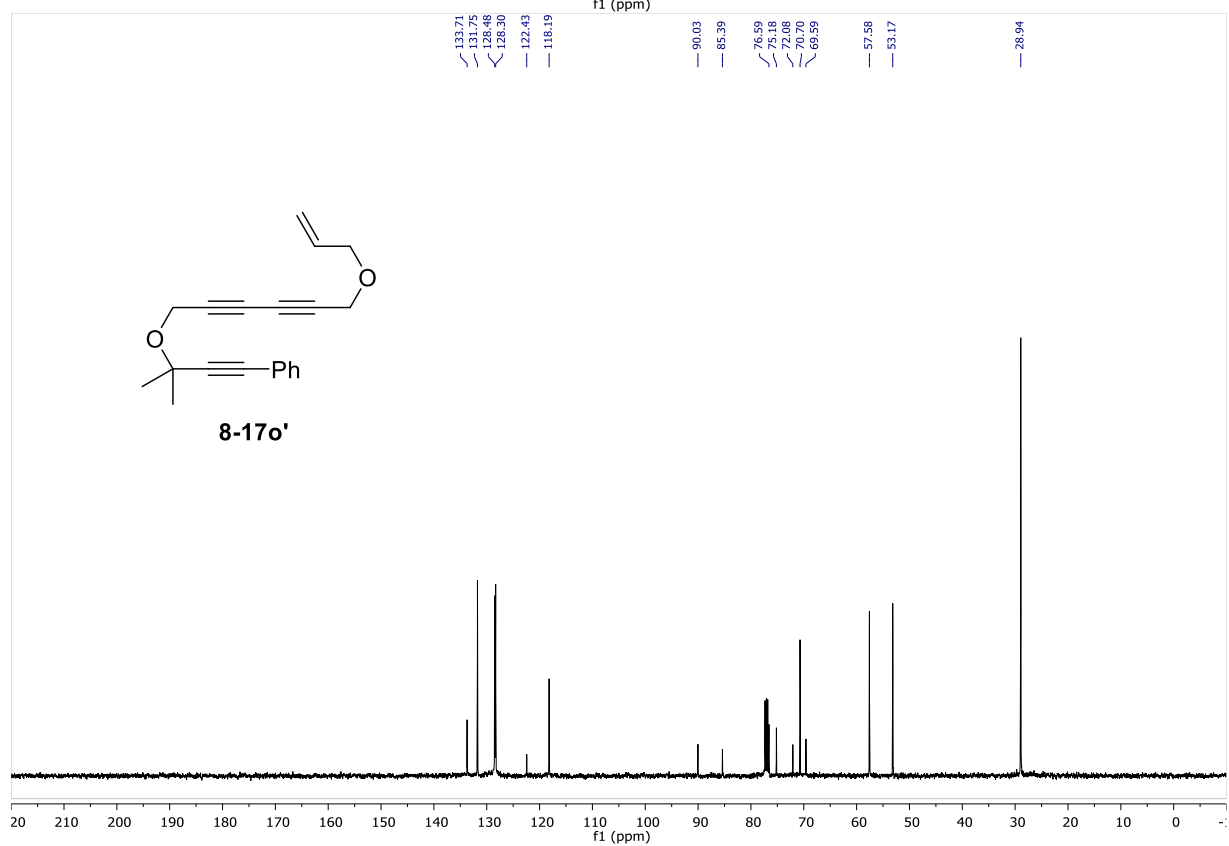


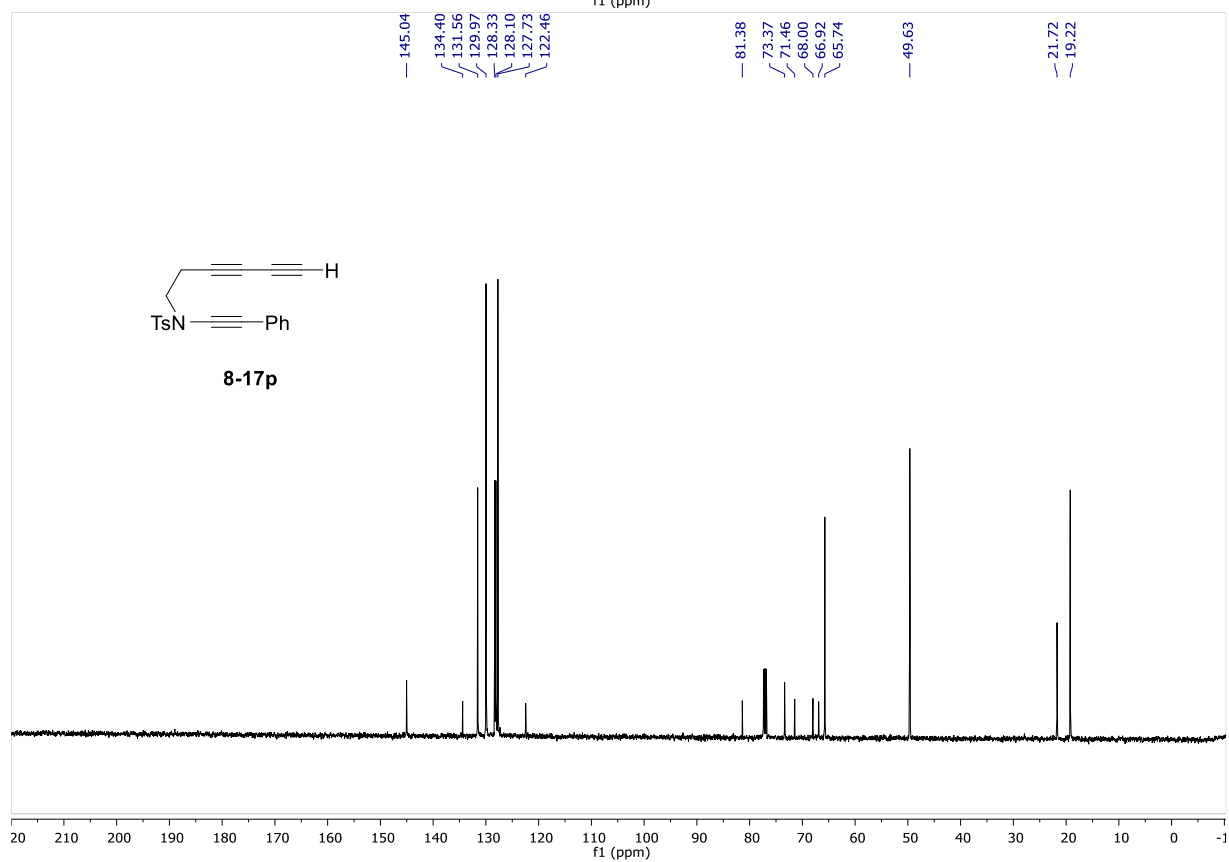
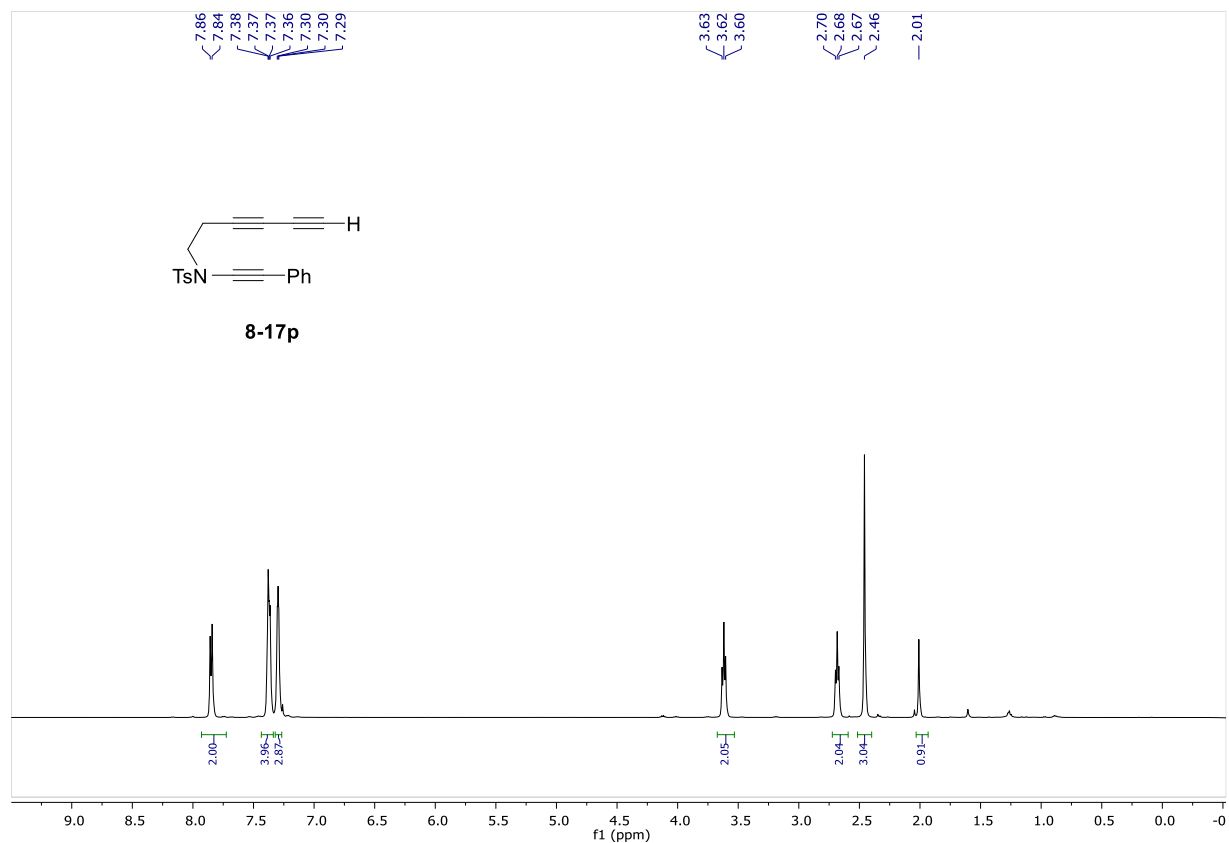


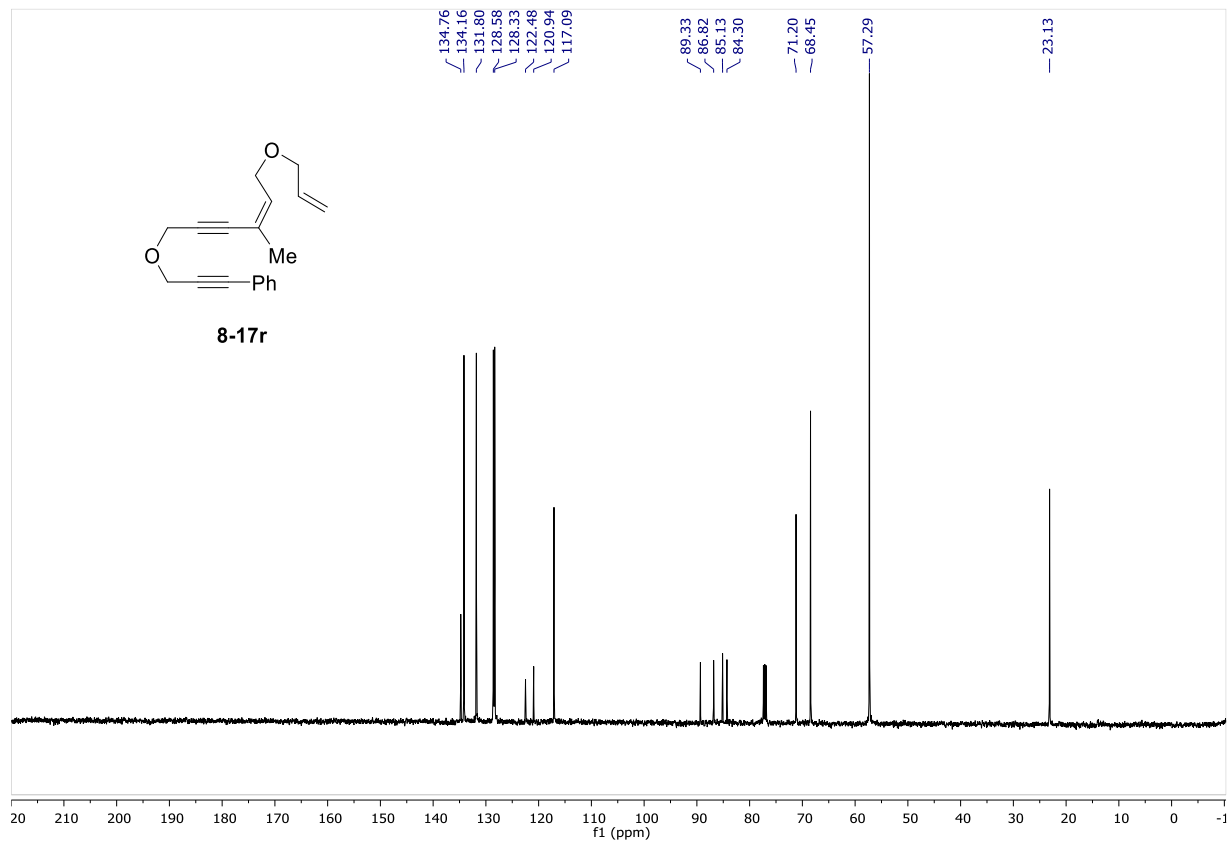
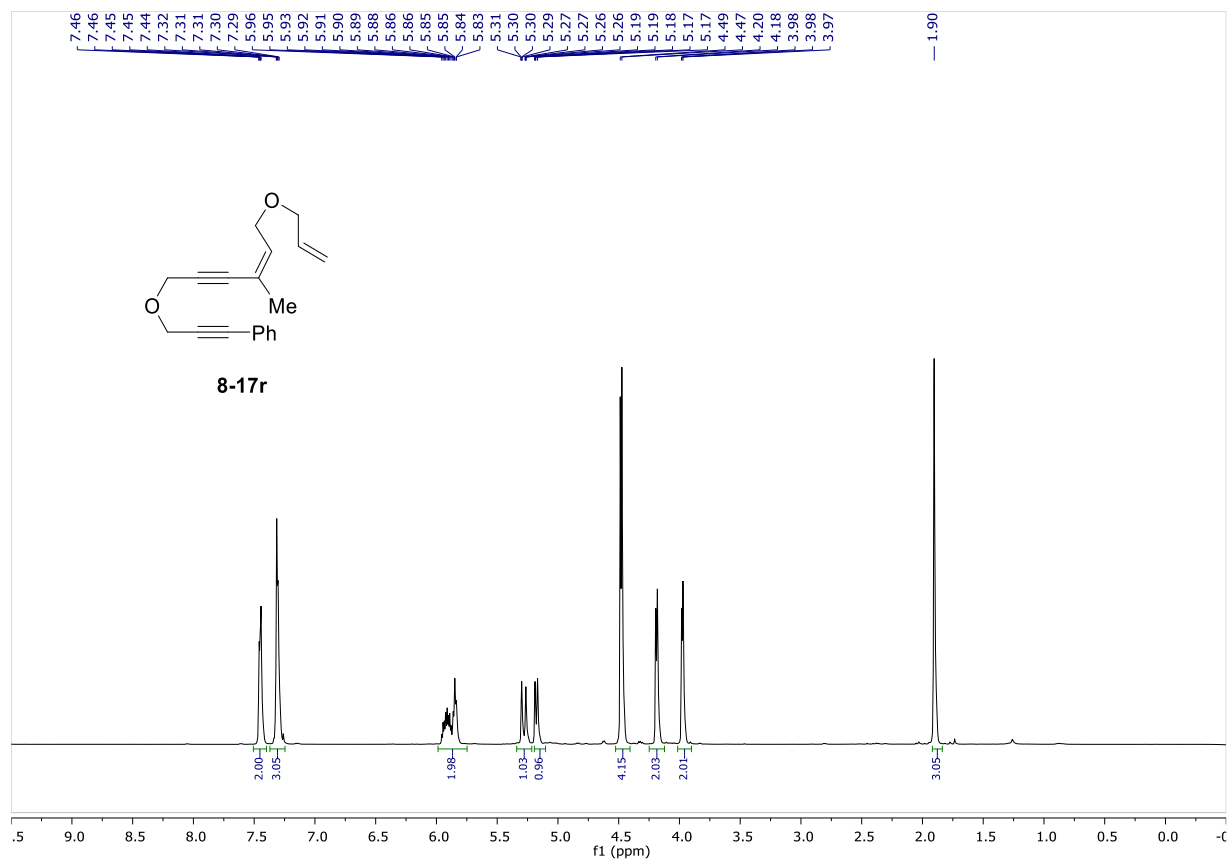


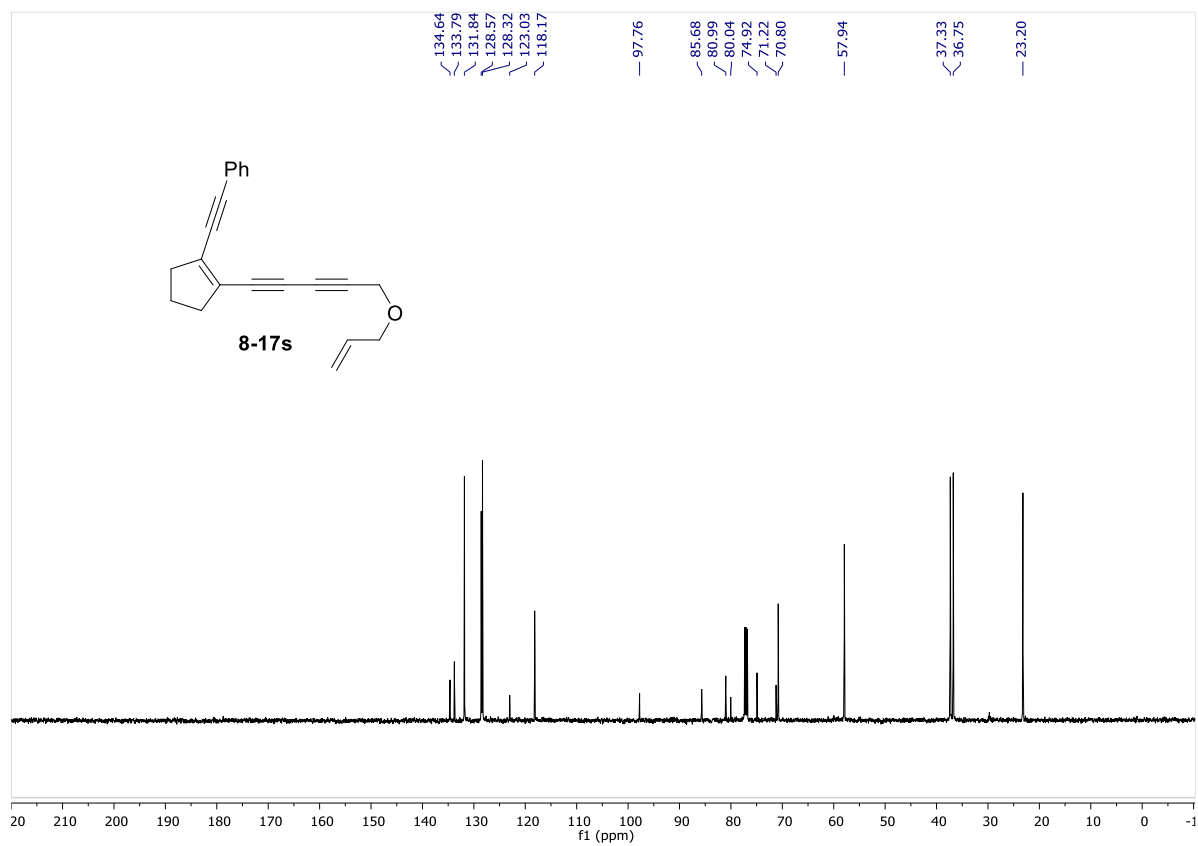
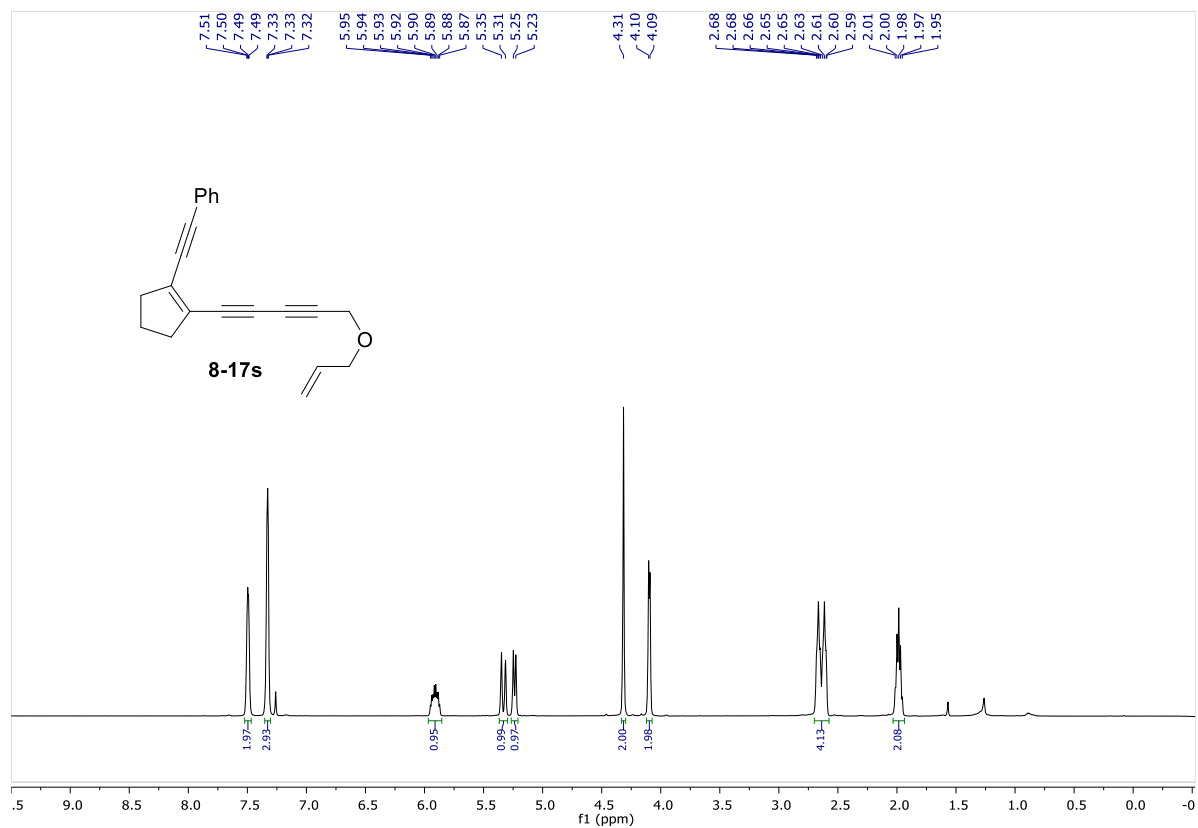


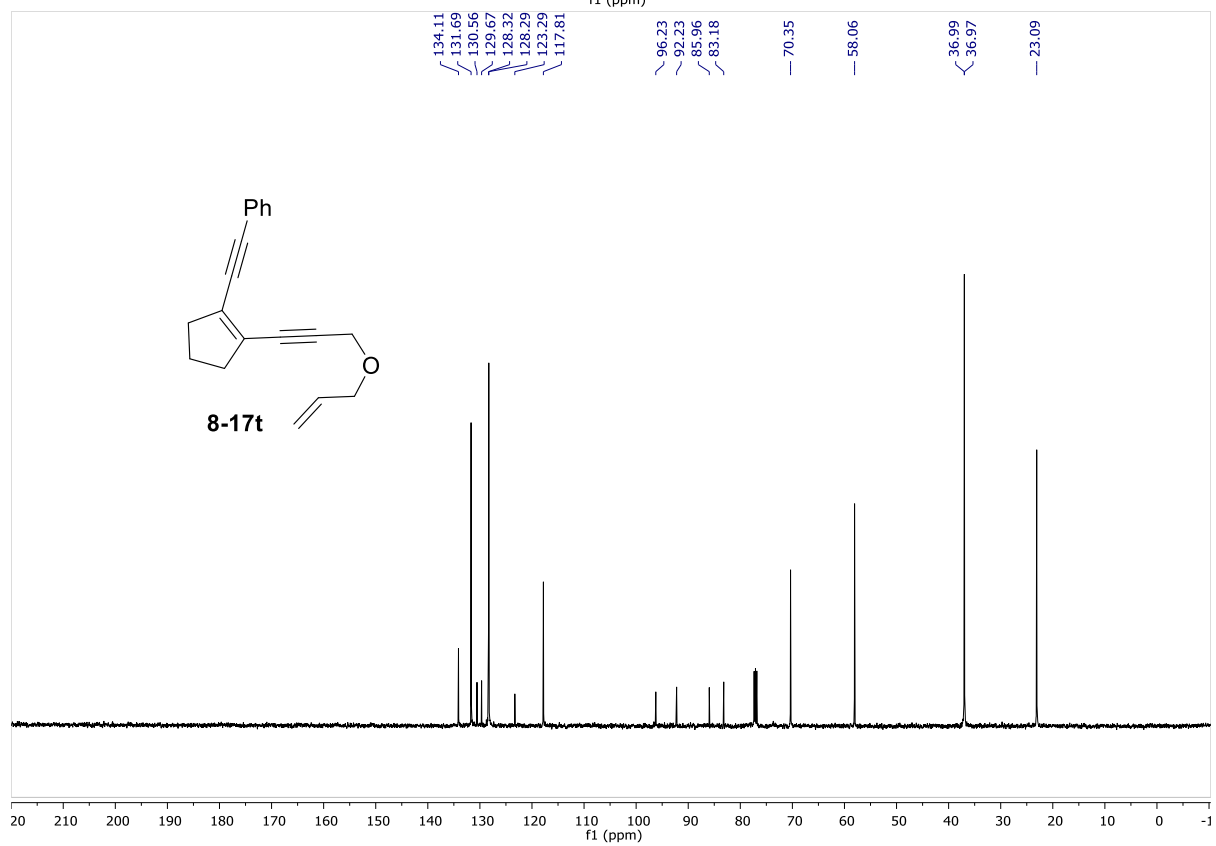
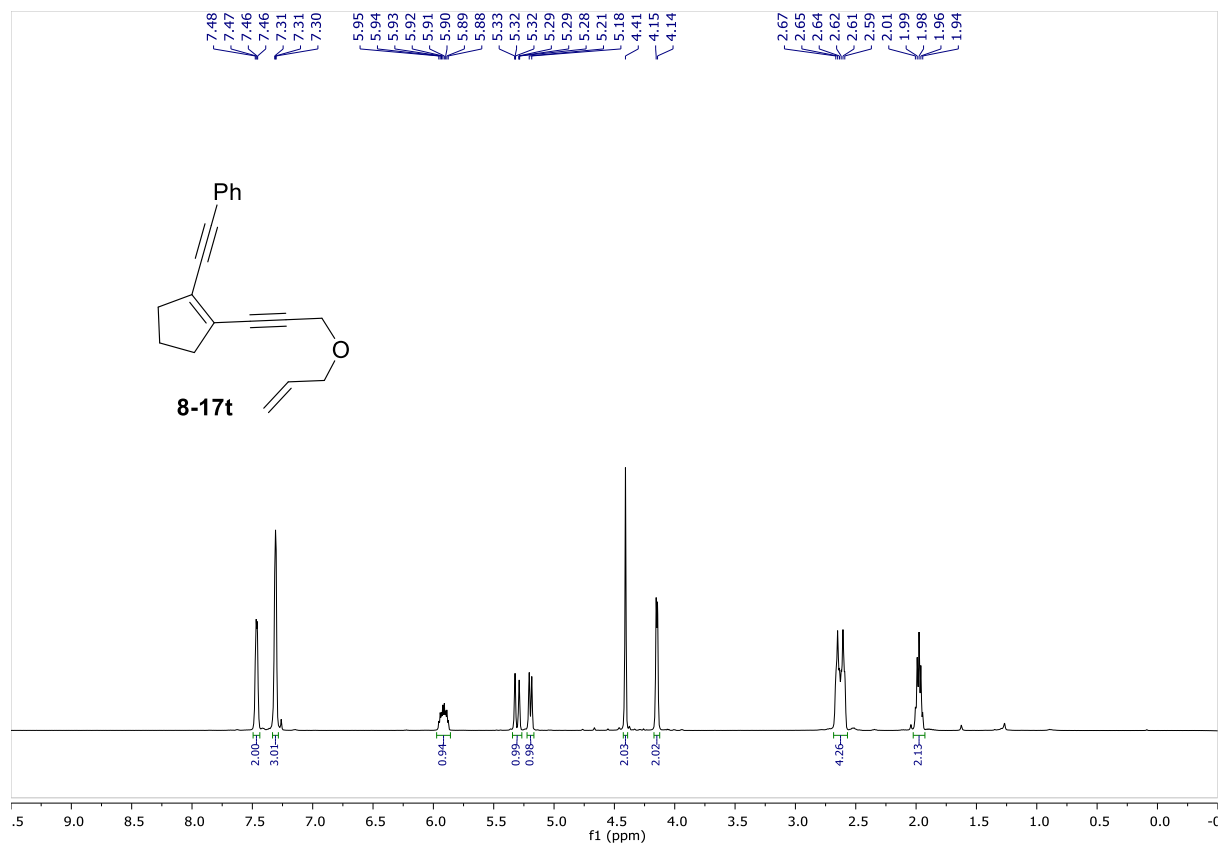


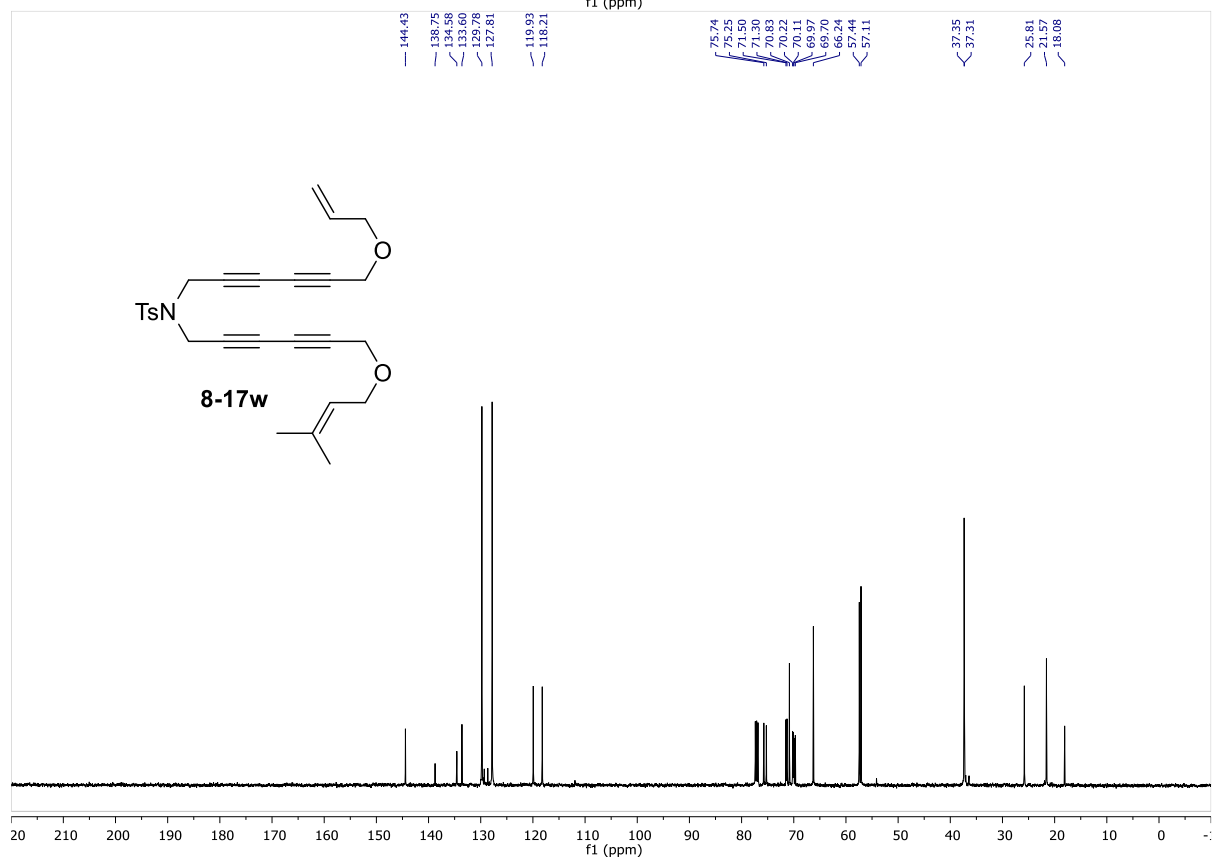
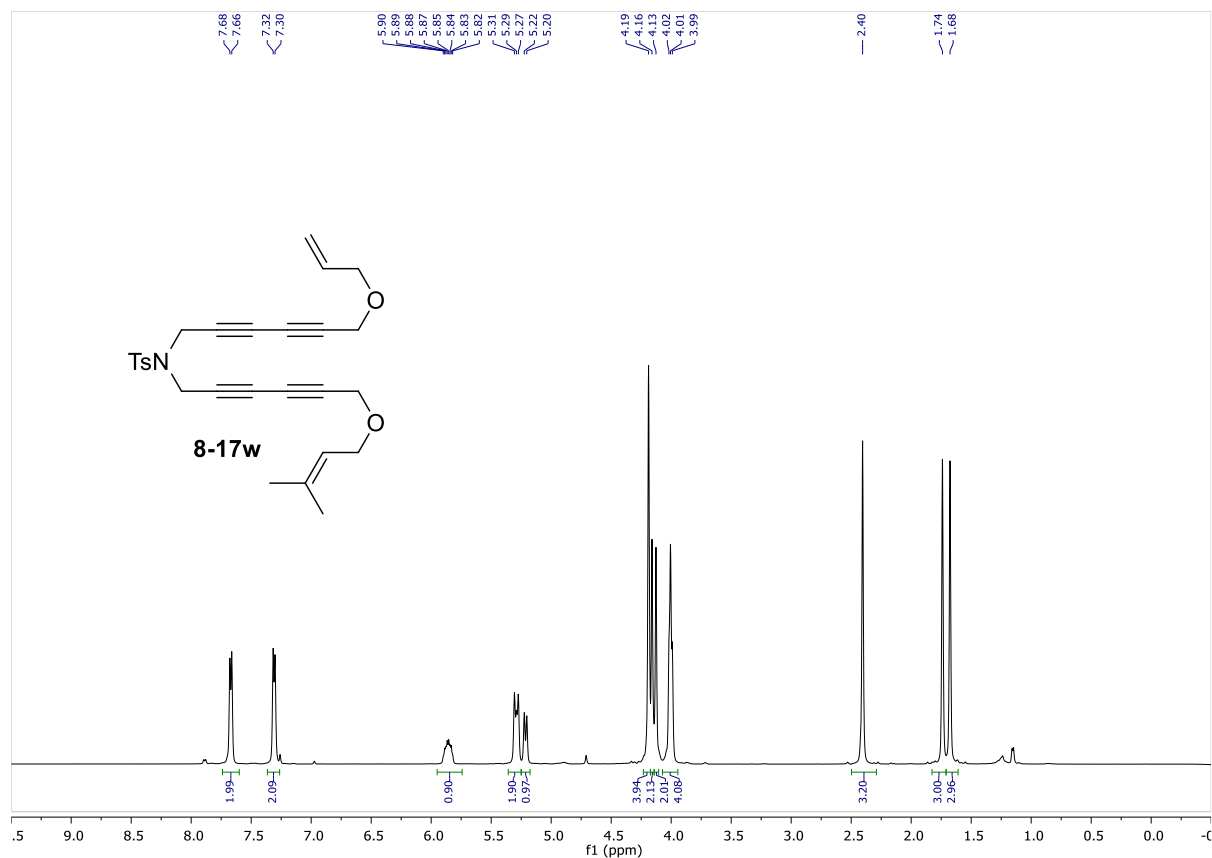




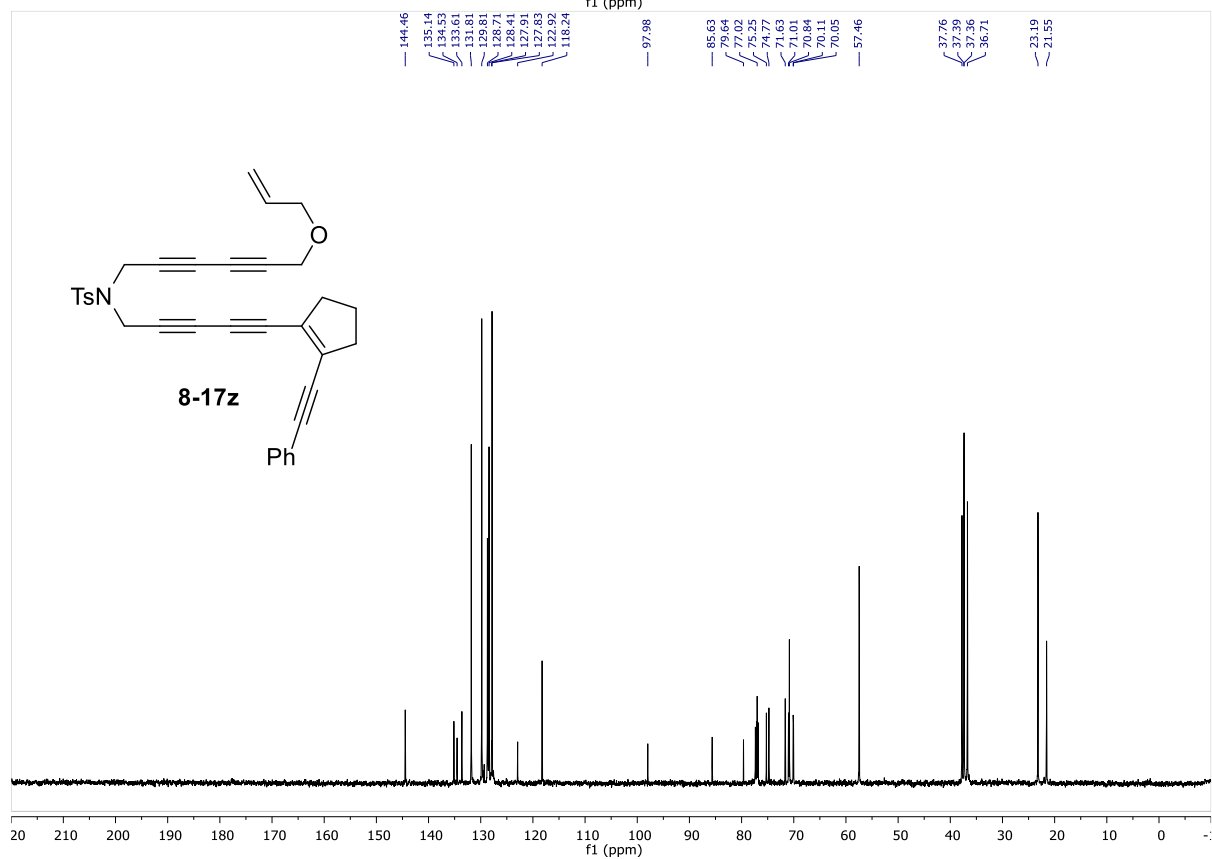
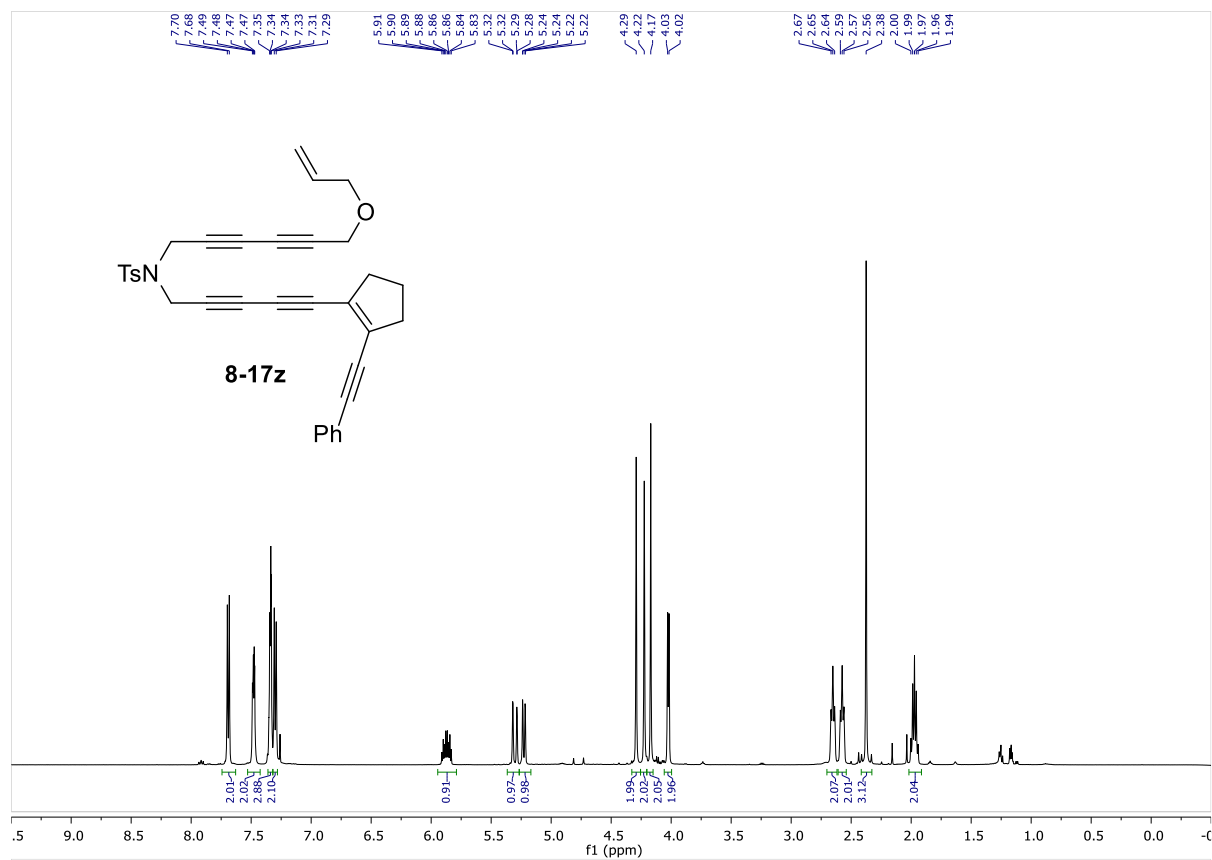


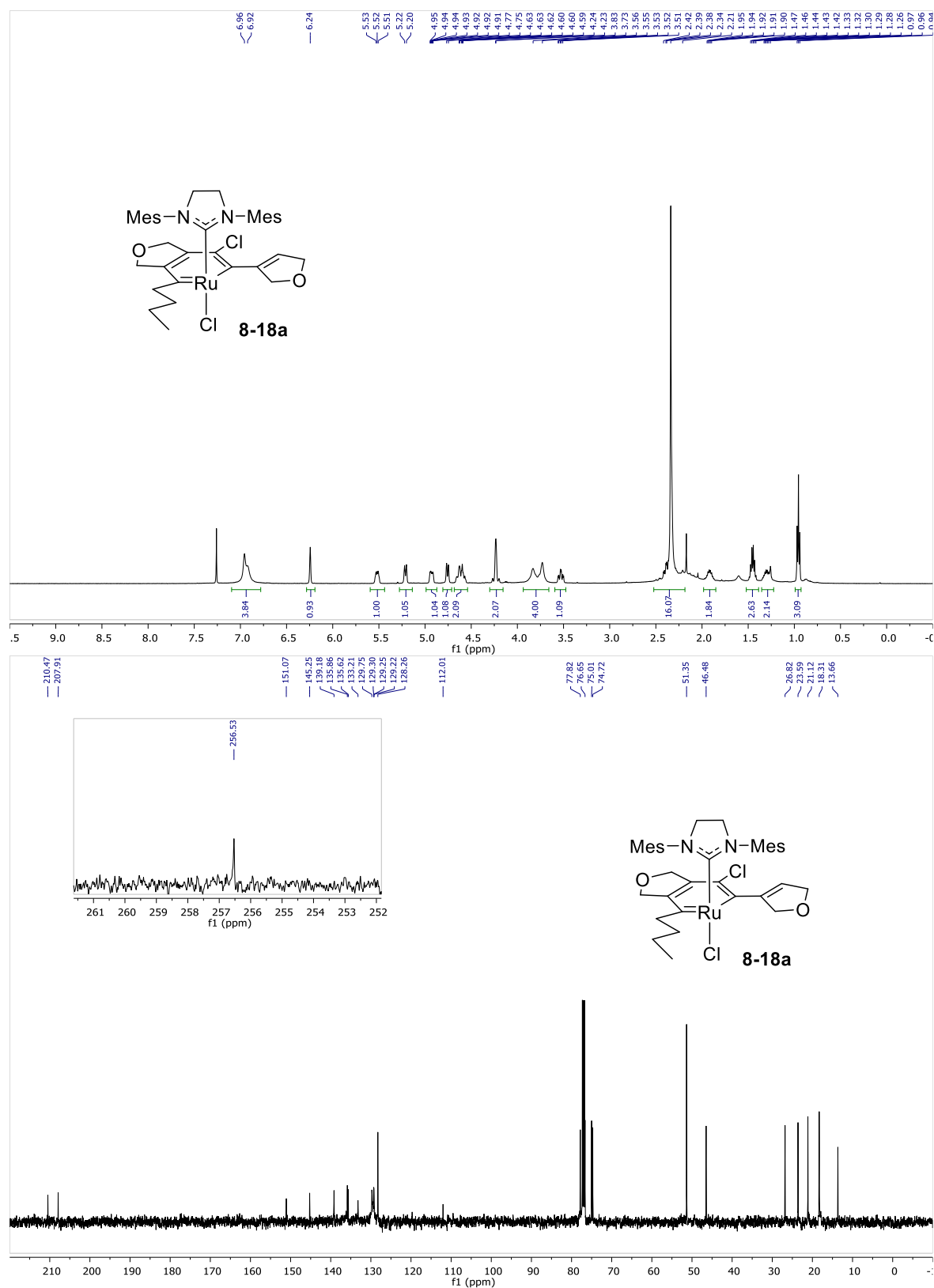


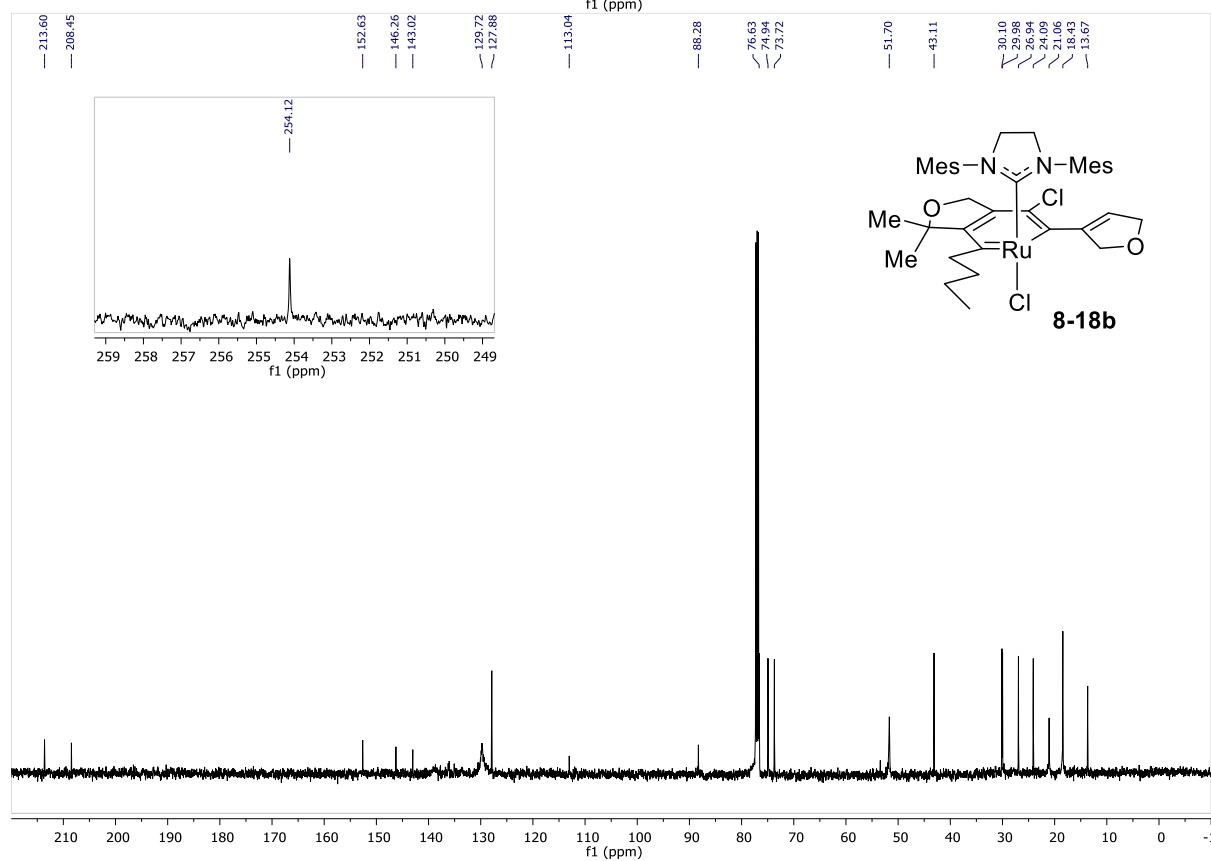
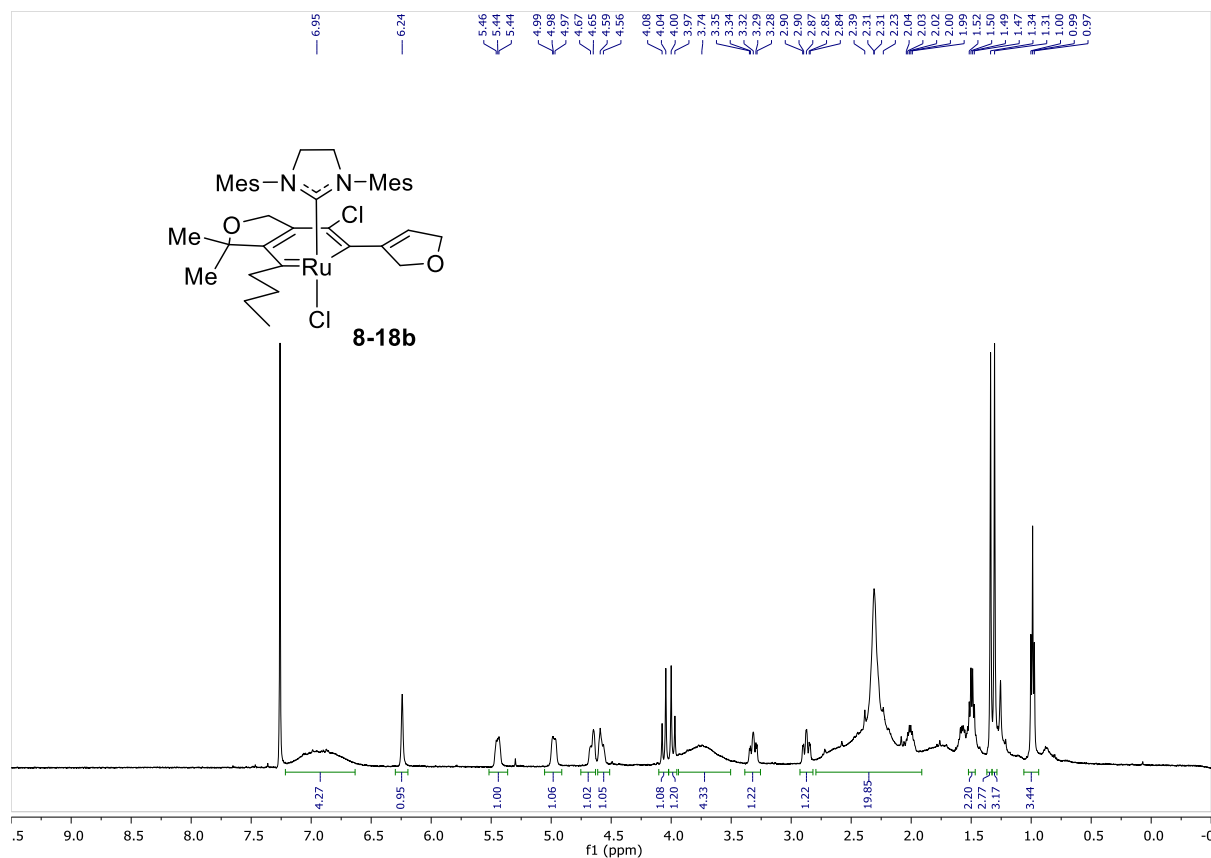


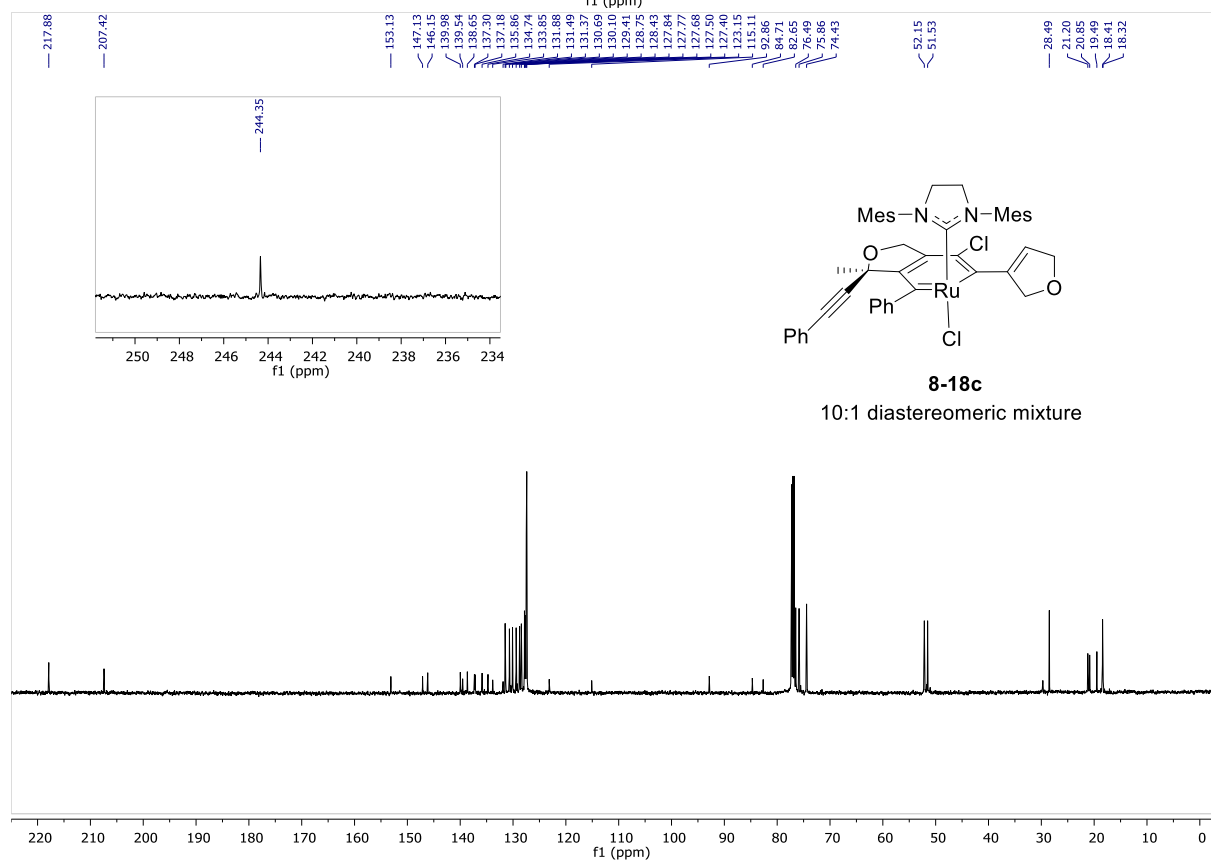
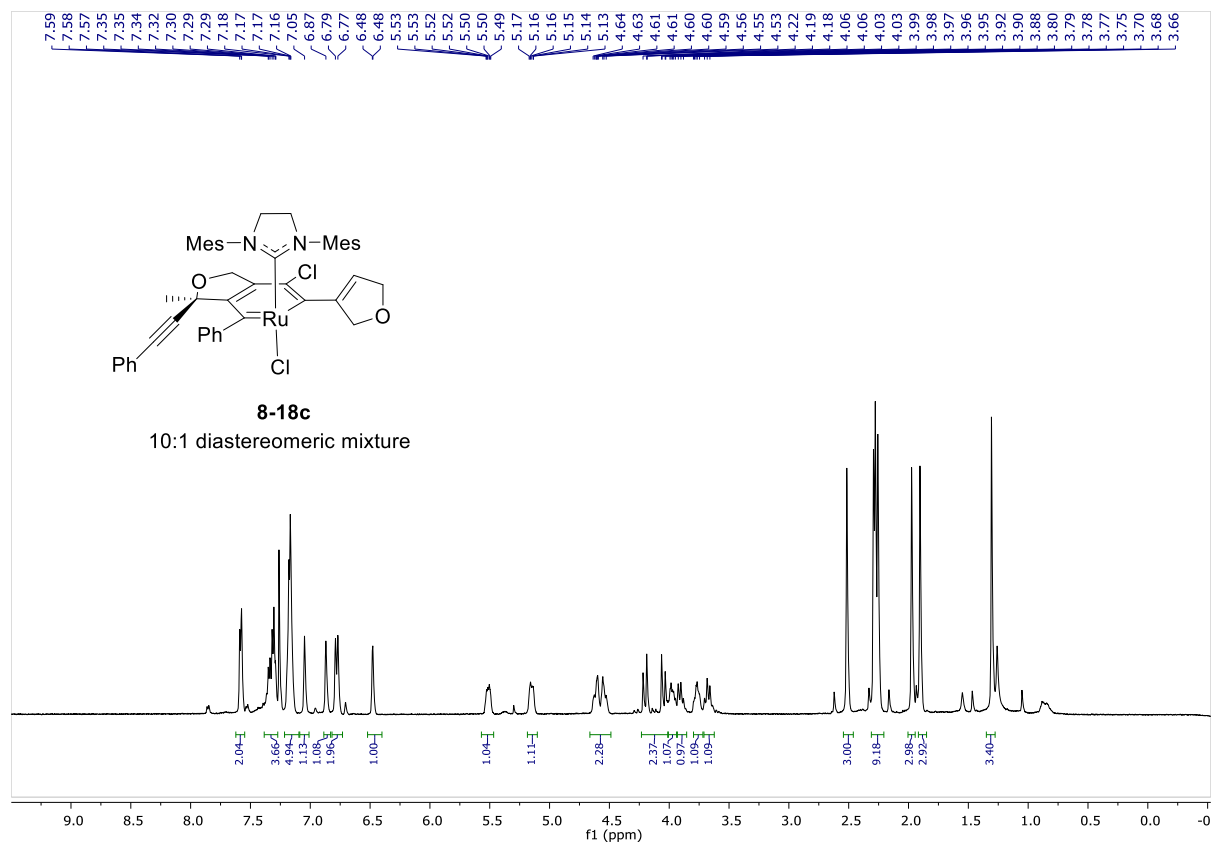


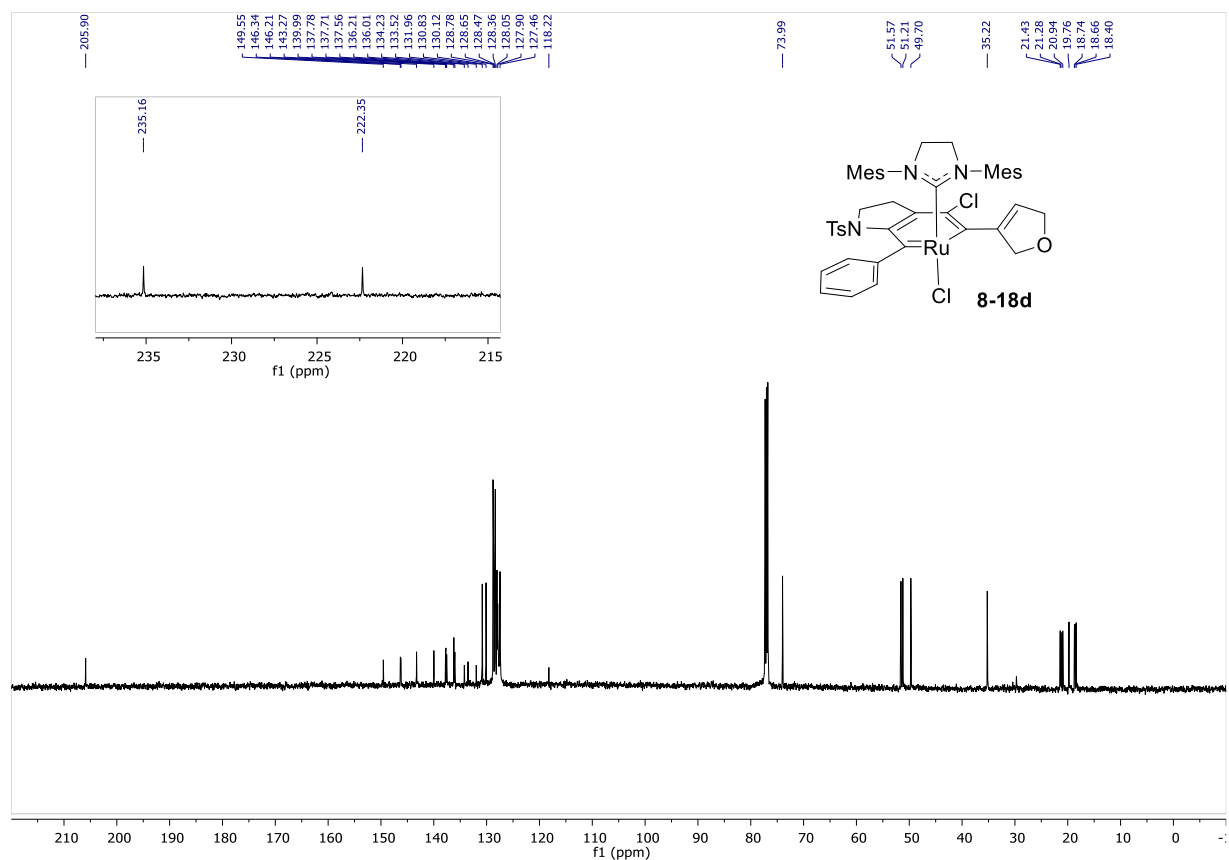
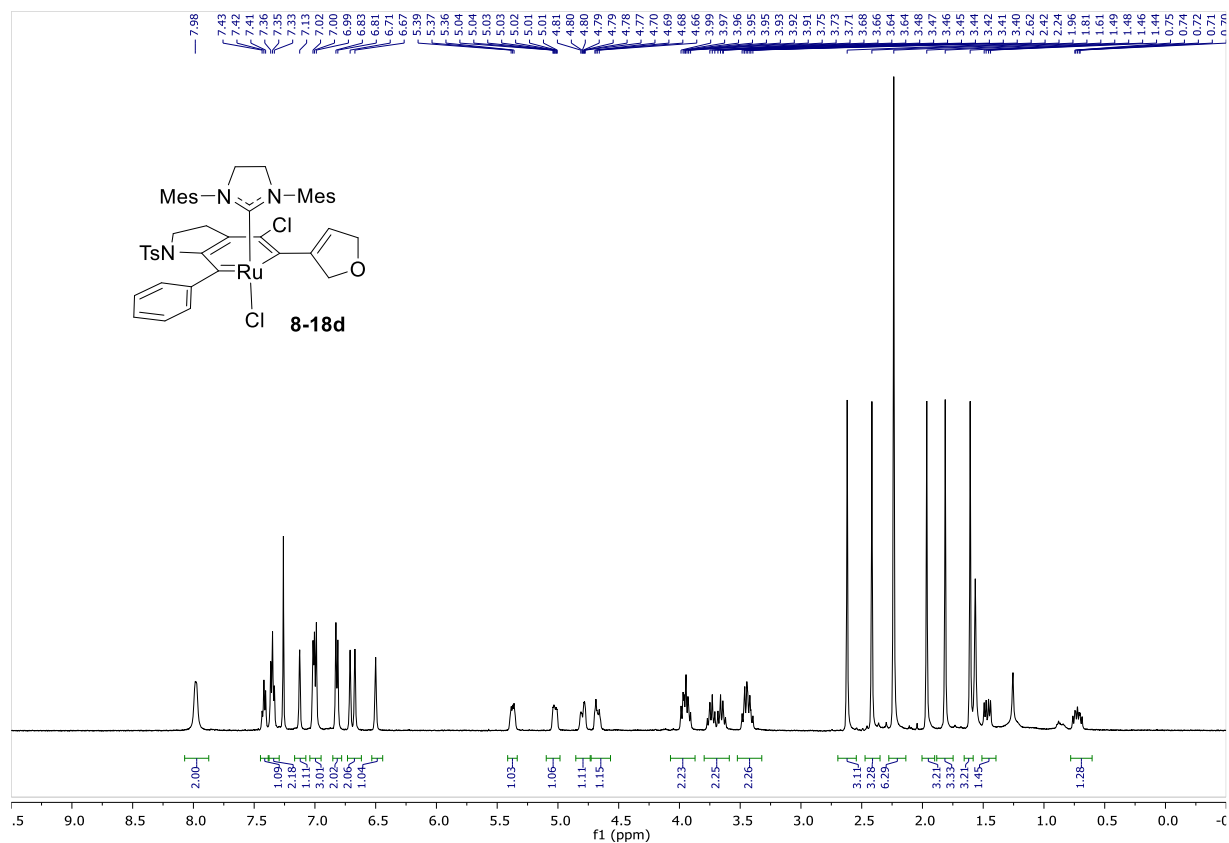


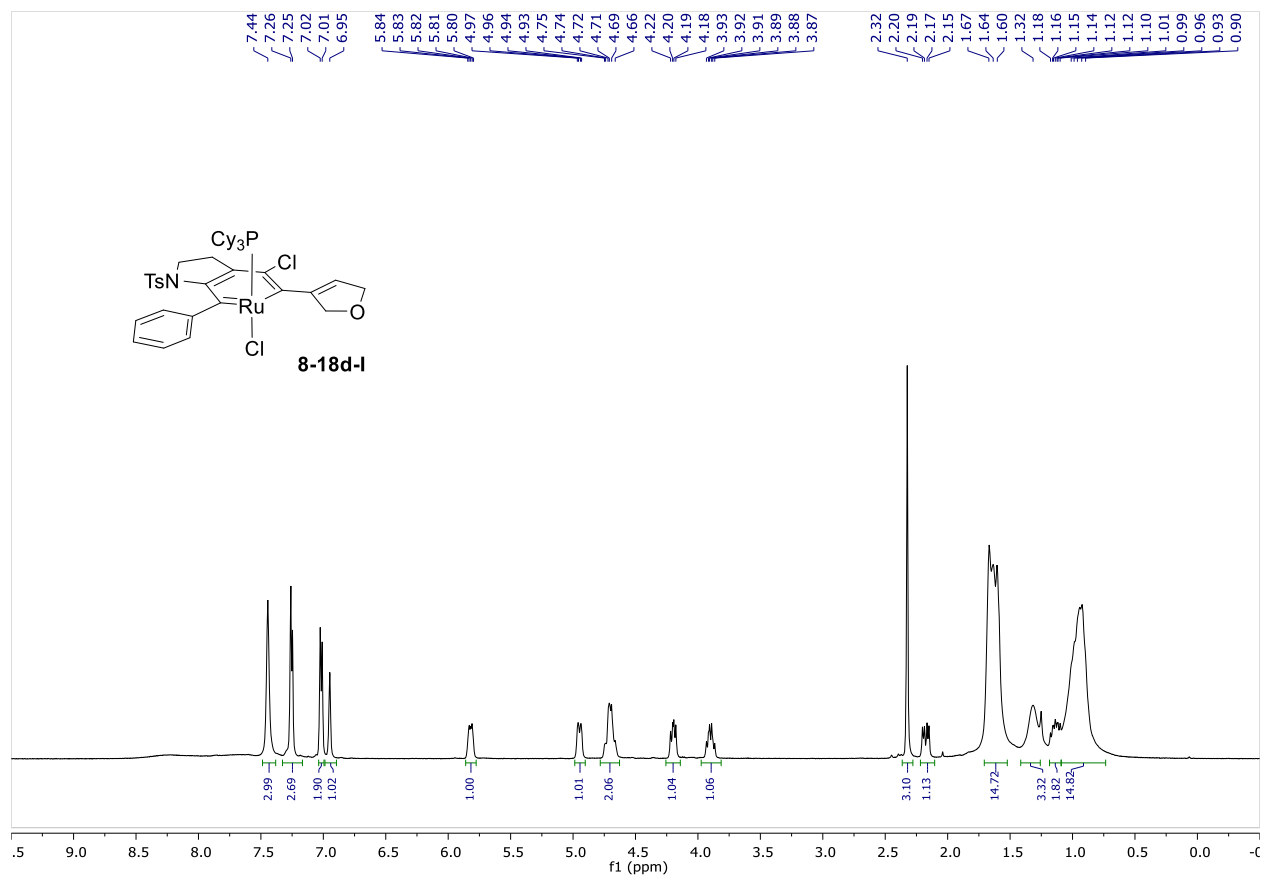




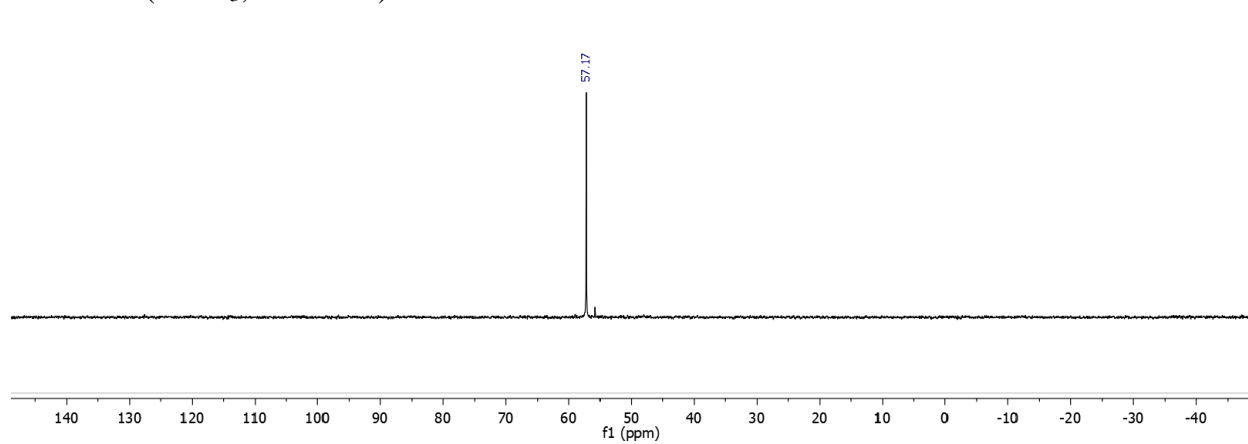


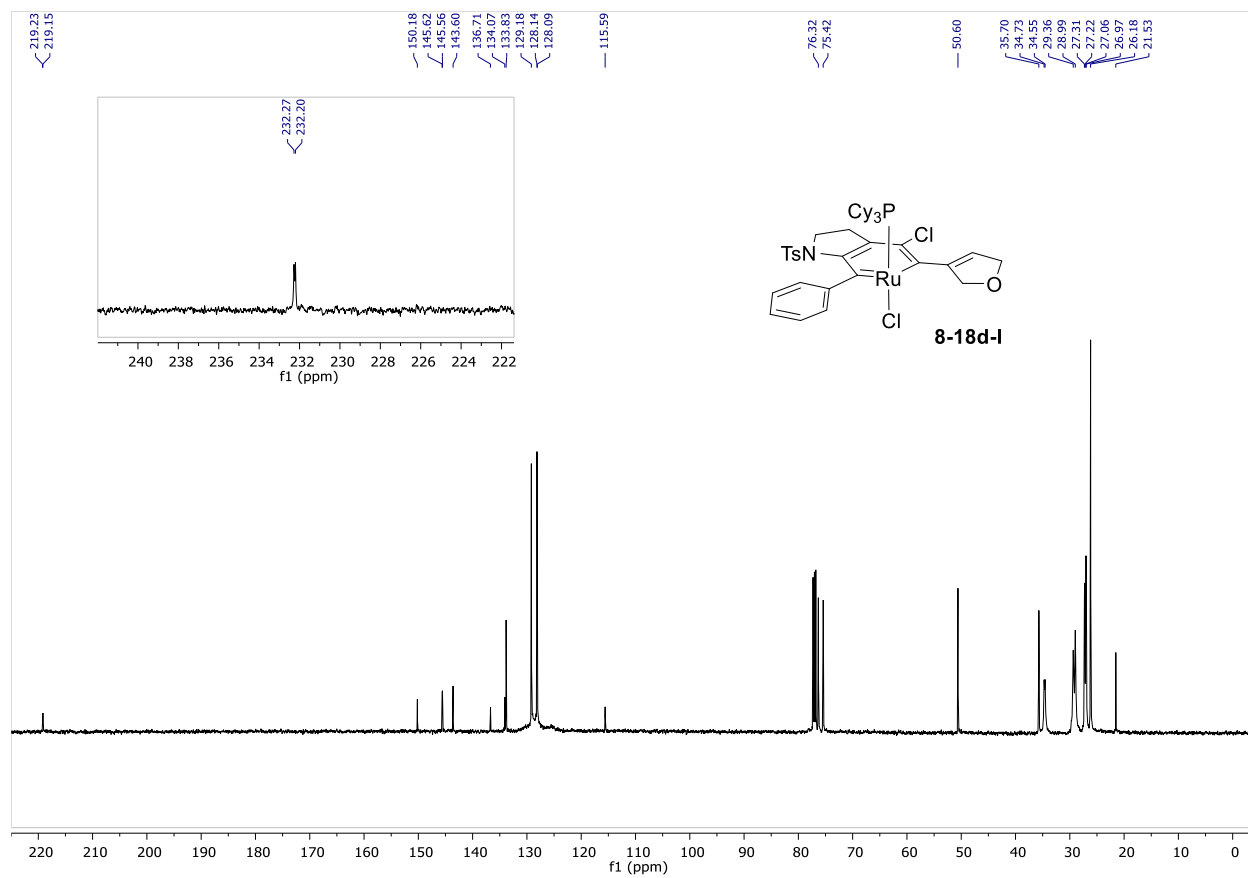


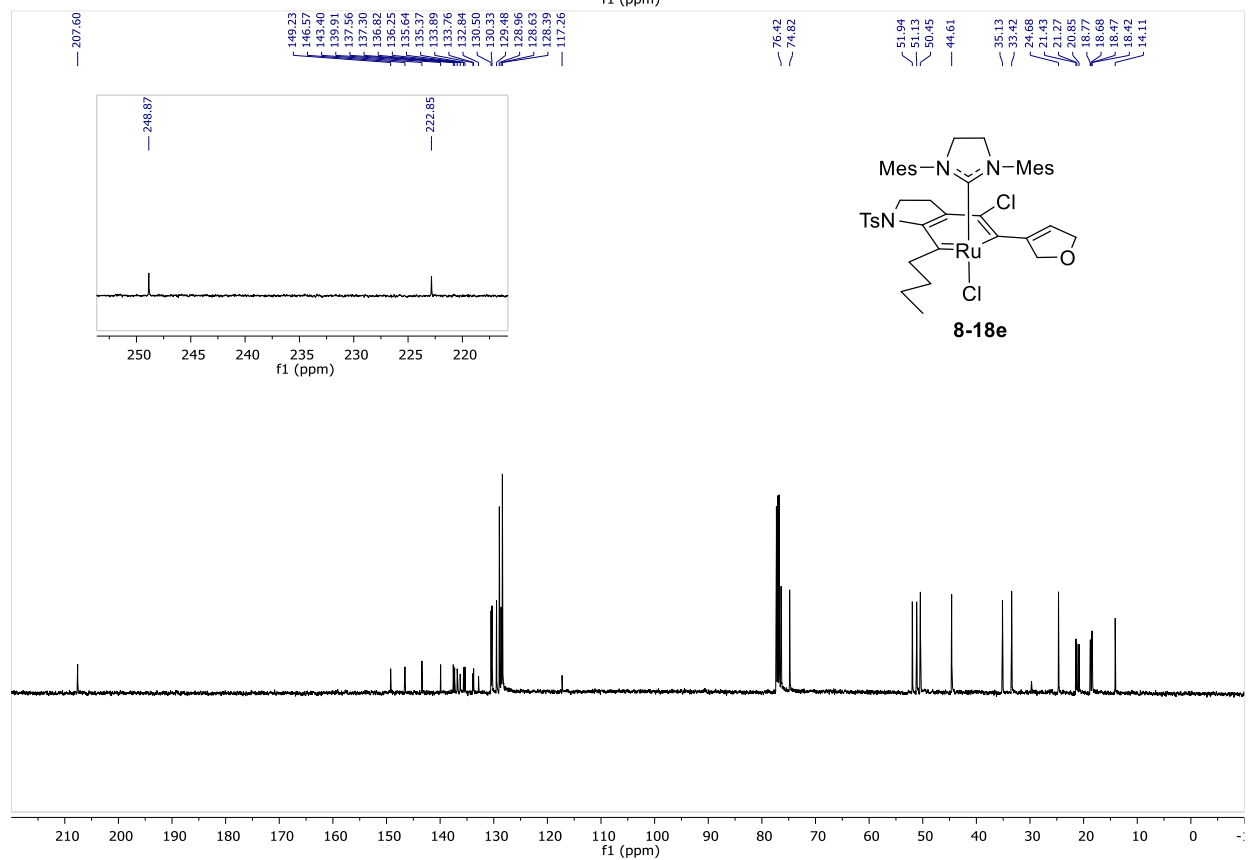
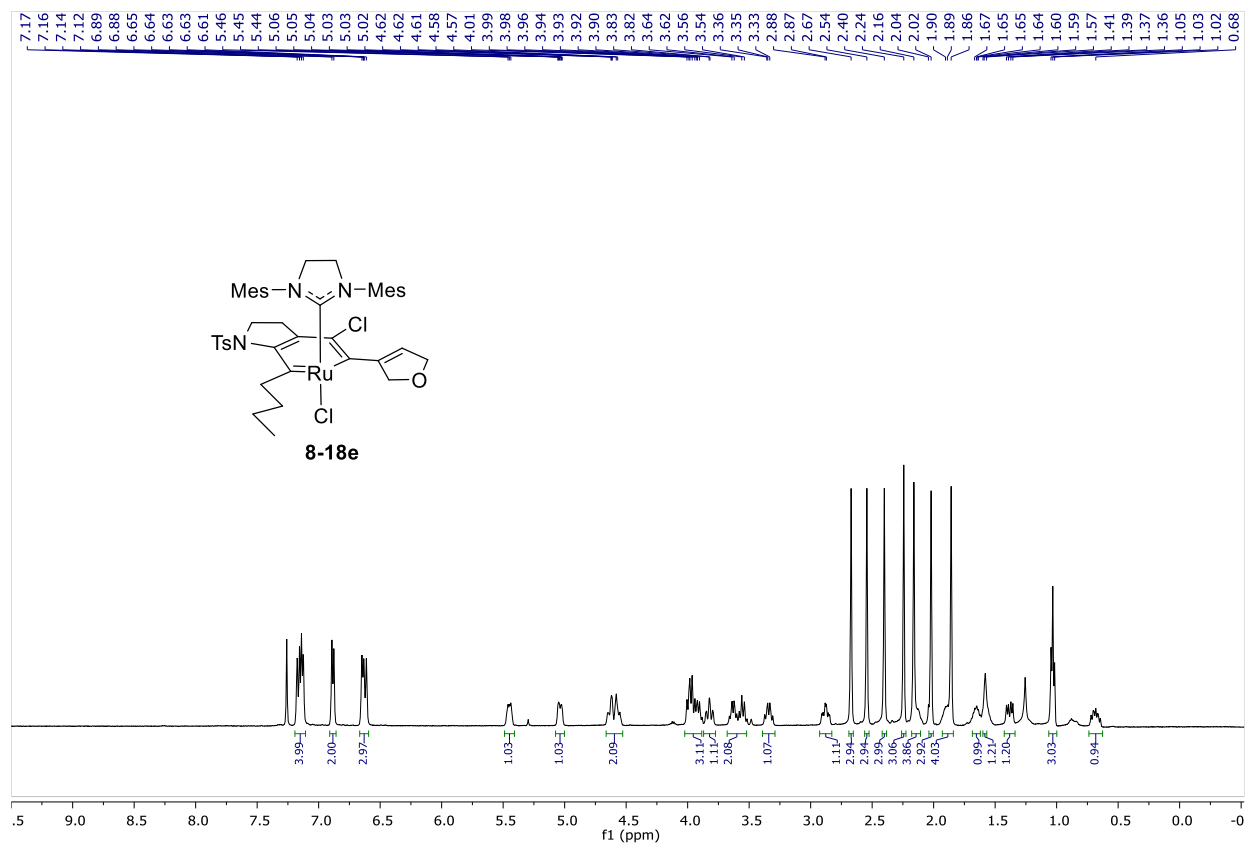


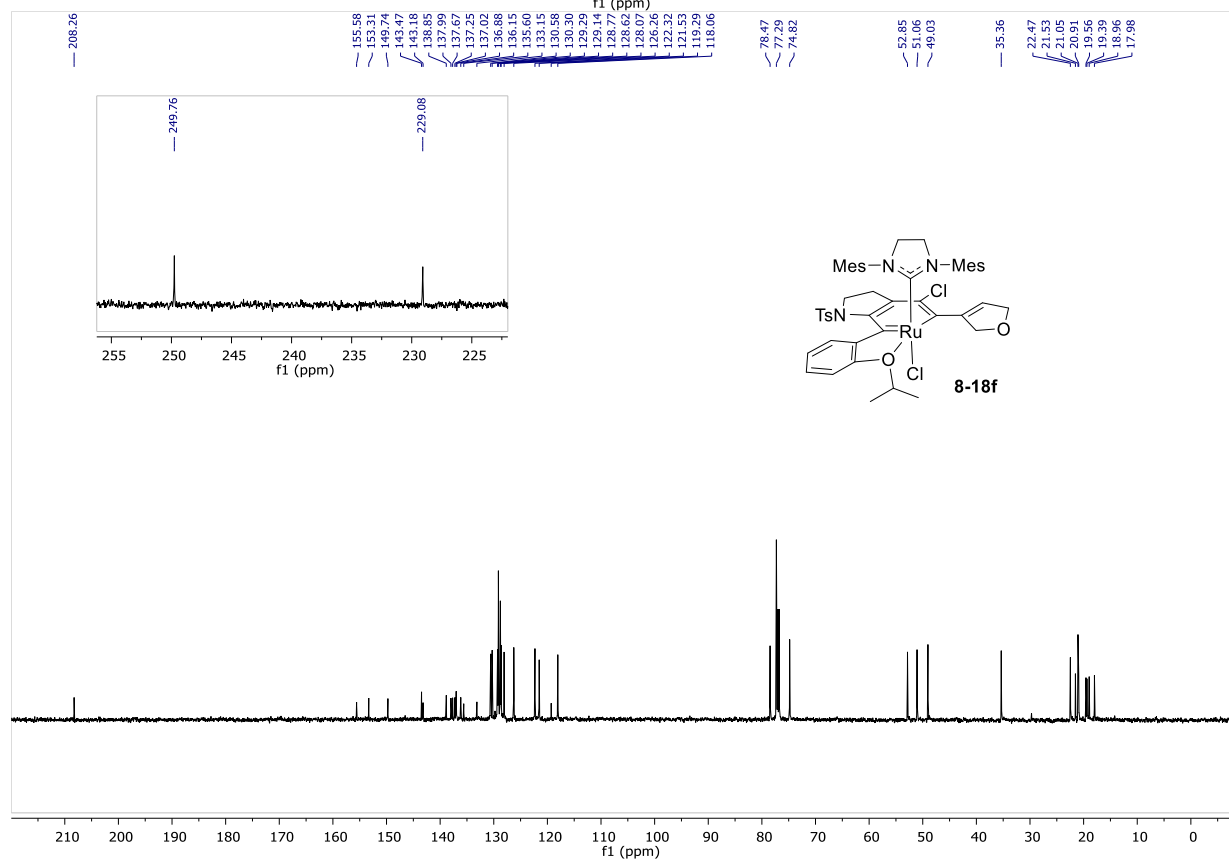
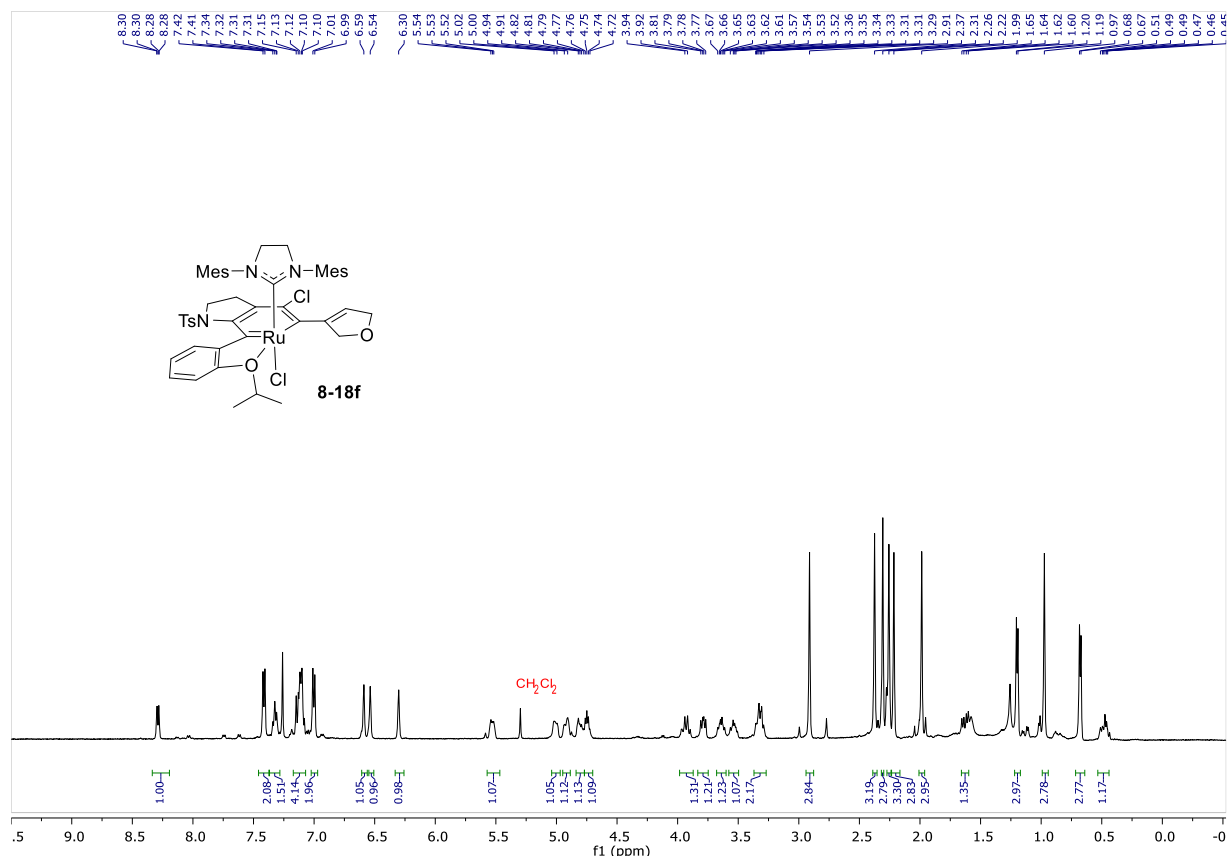


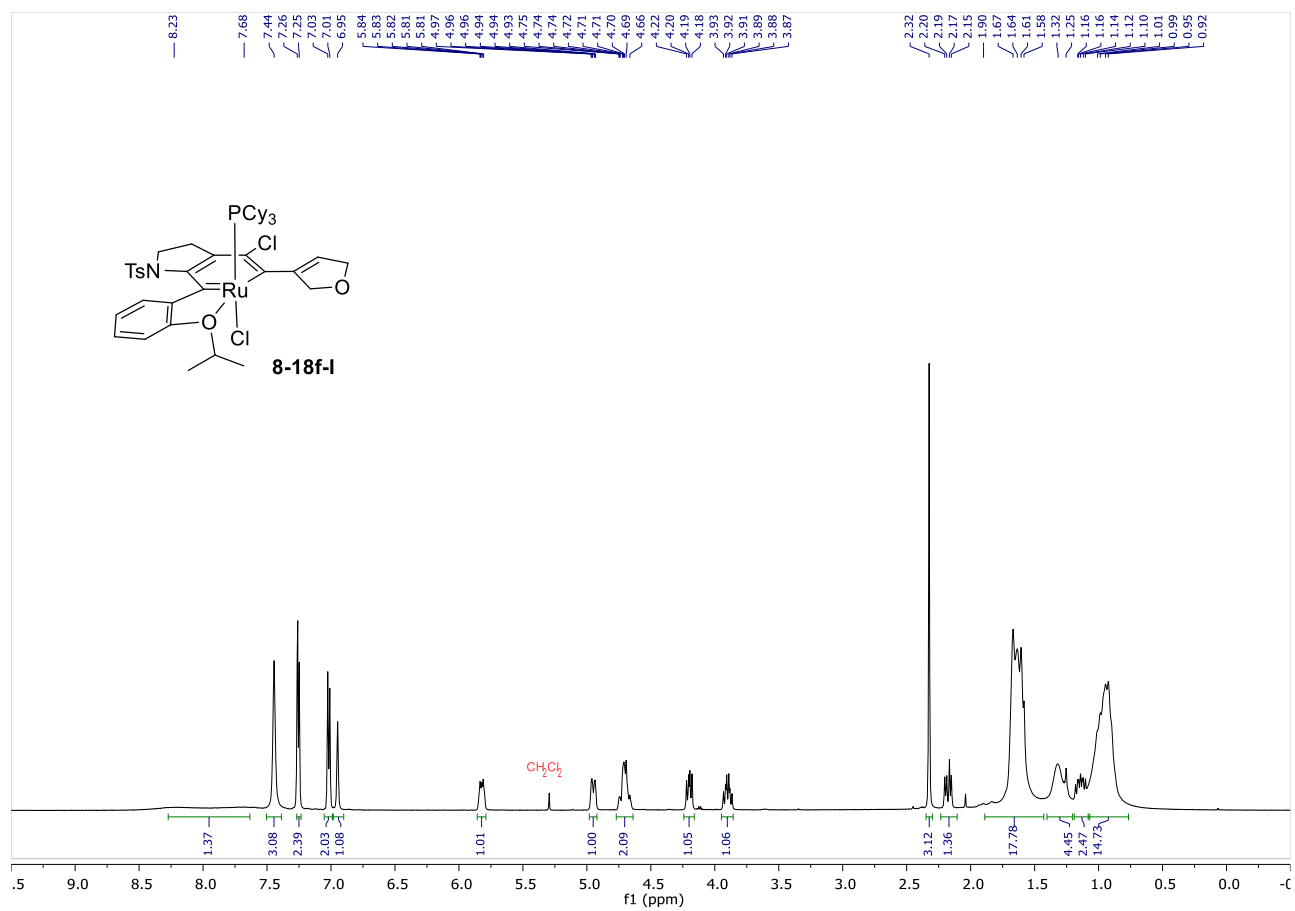
^1H NMR (CDCl₃, 203 MHz)



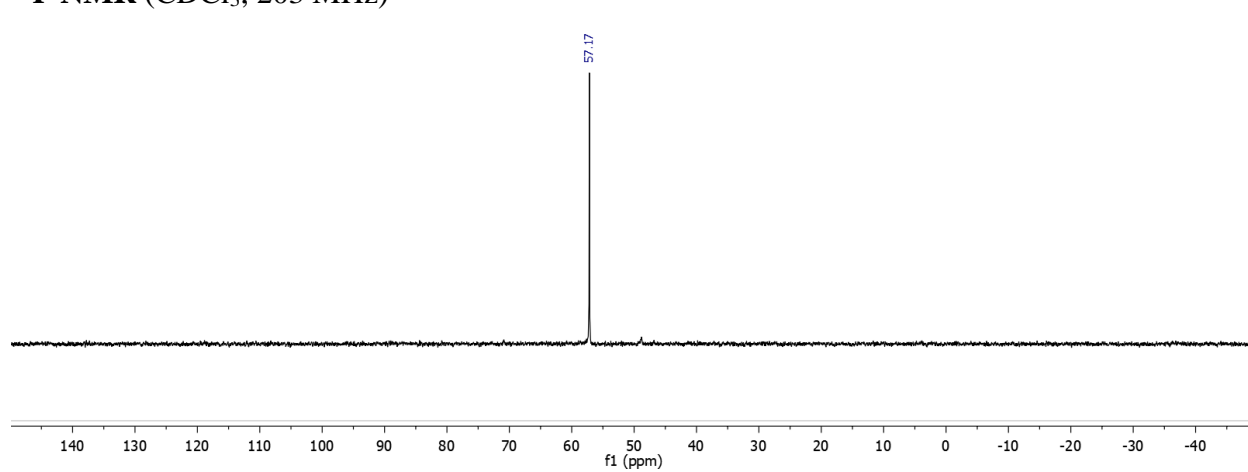


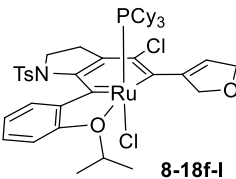




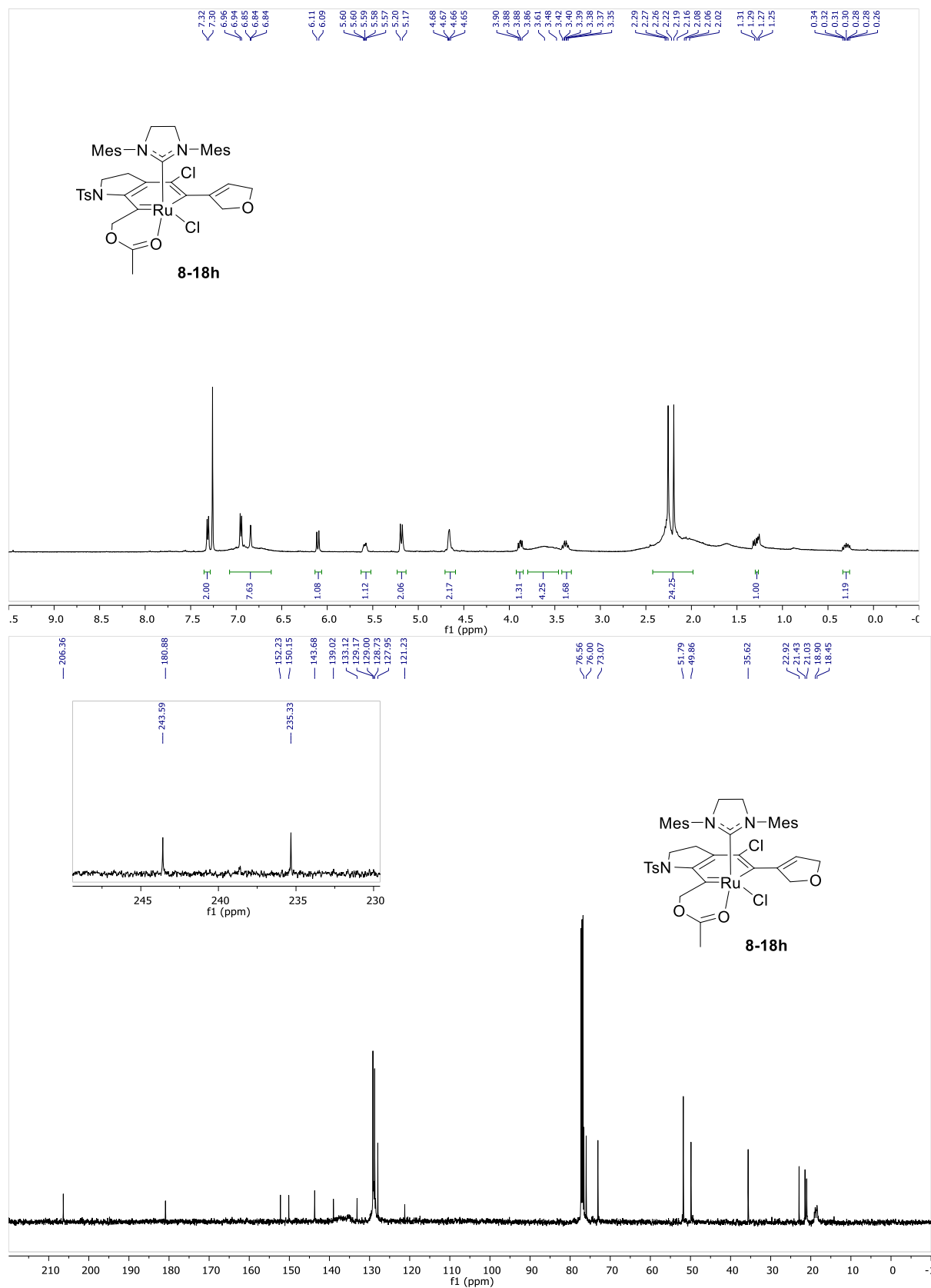


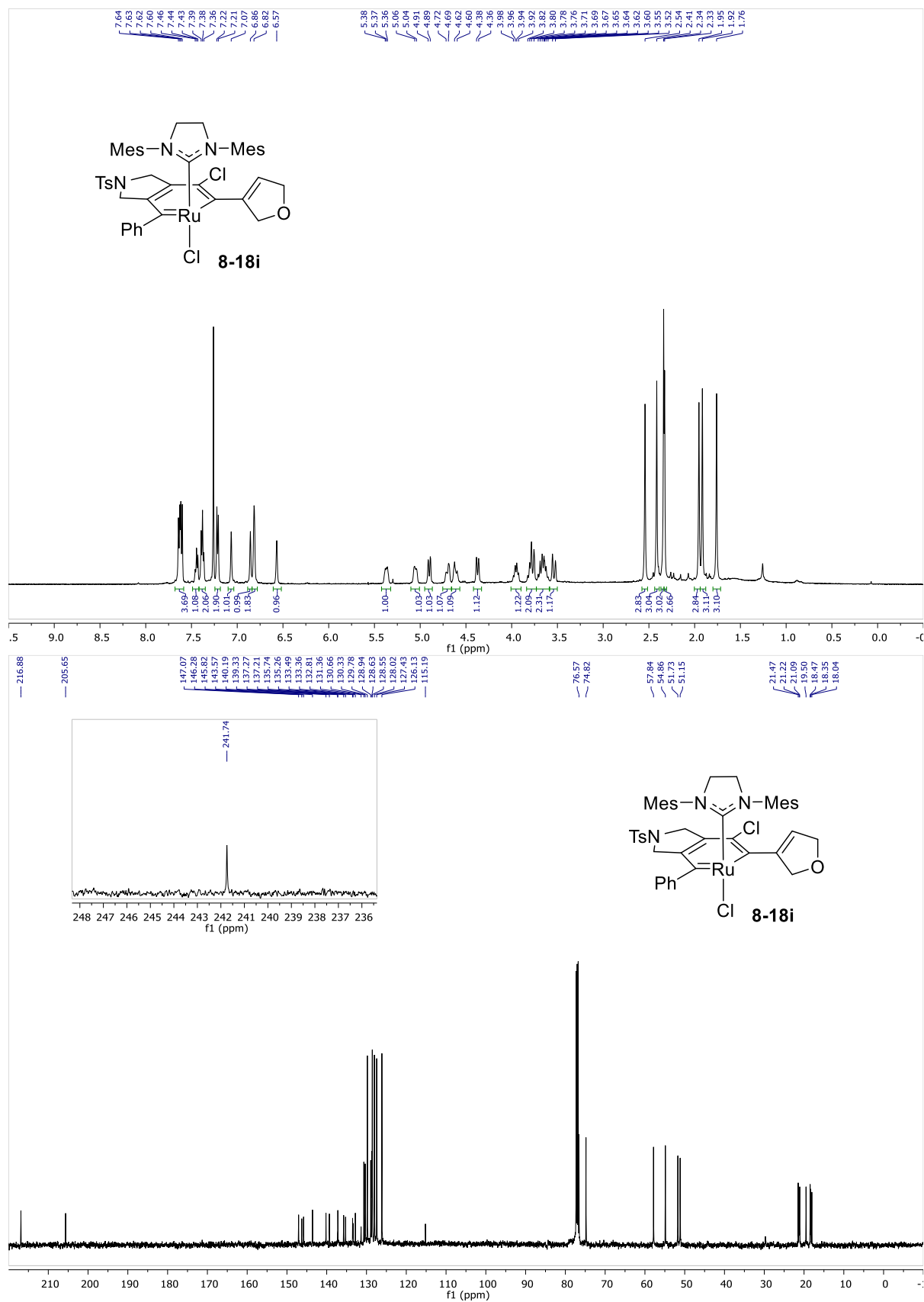
³¹P NMR (CDCl₃, 203 MHz)

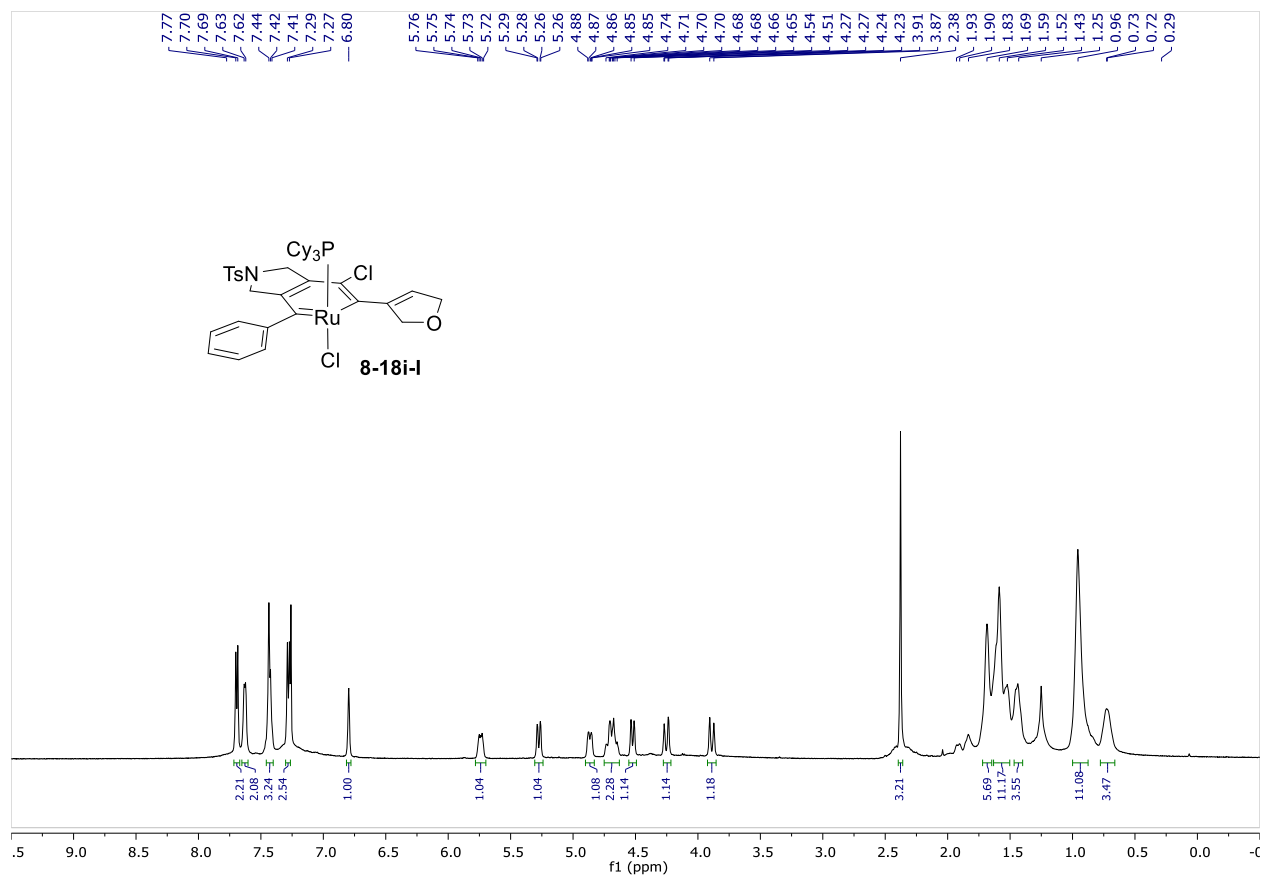




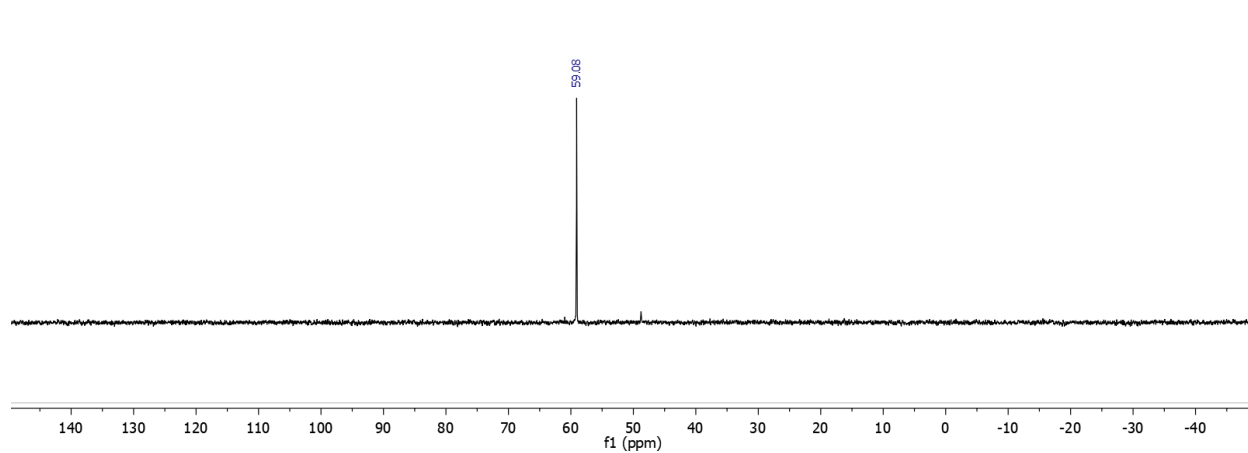


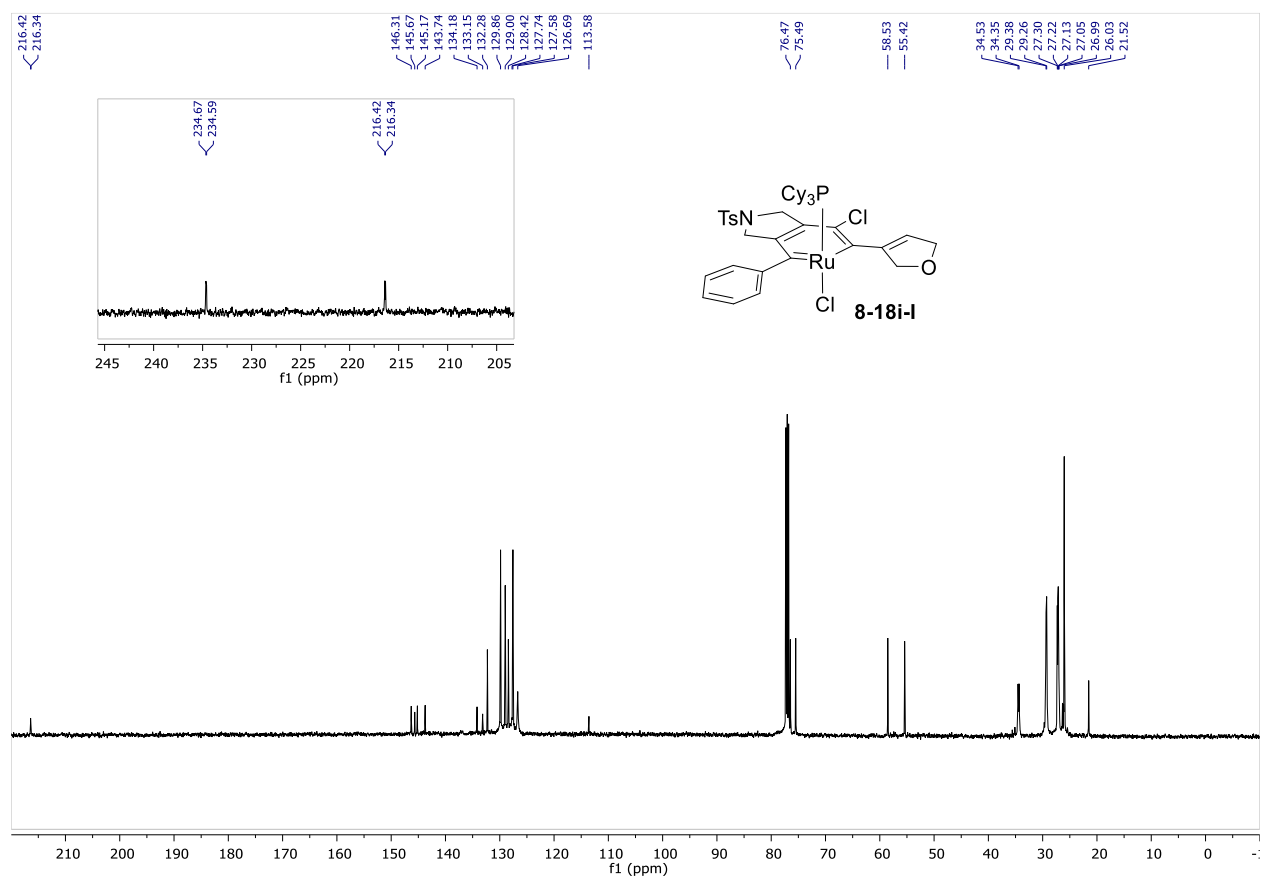


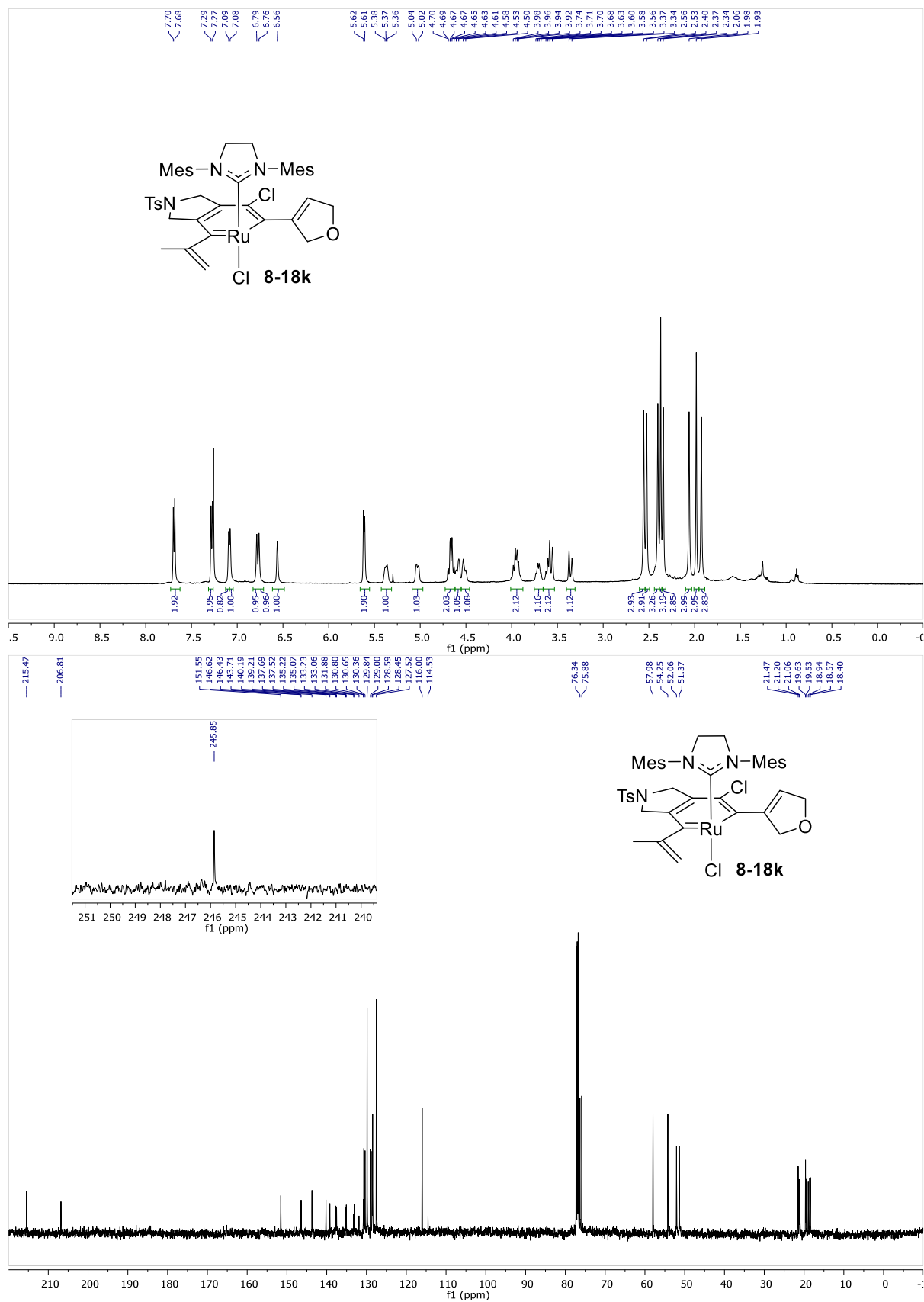


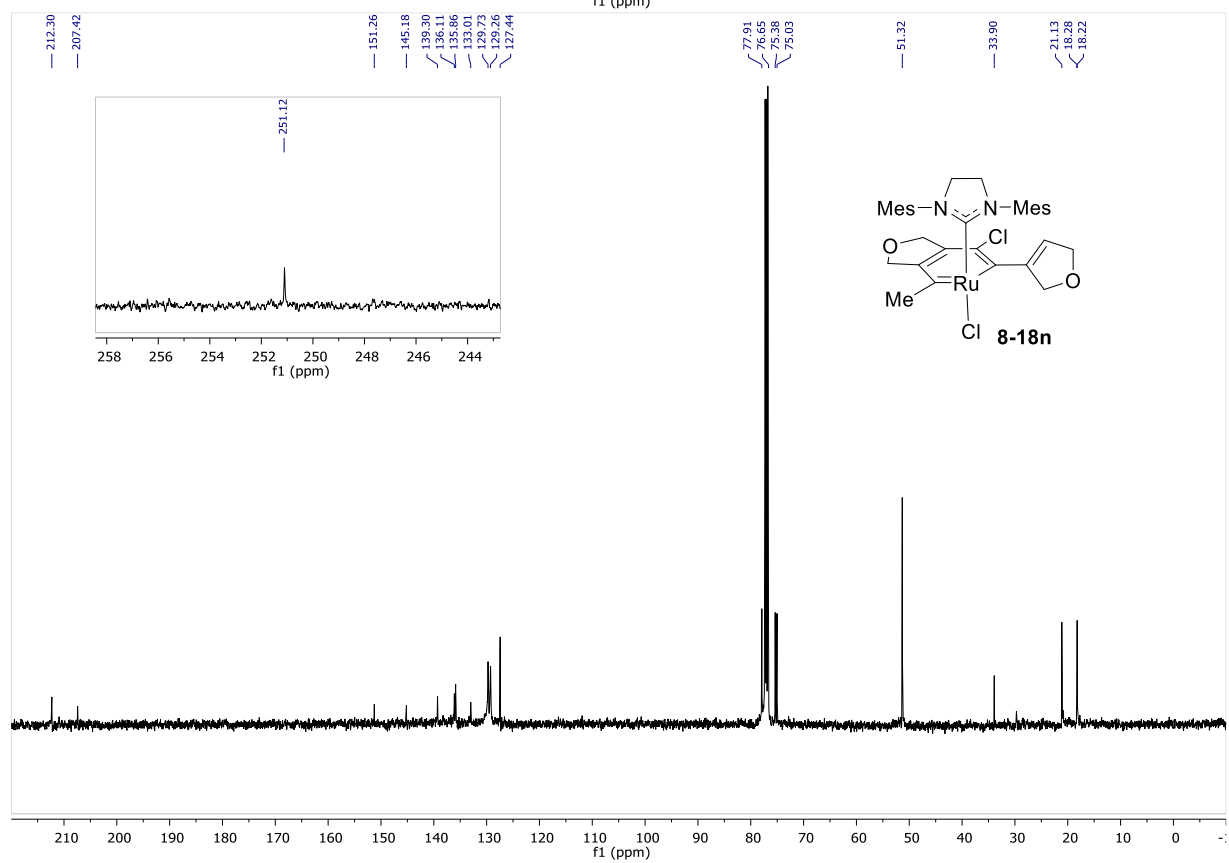
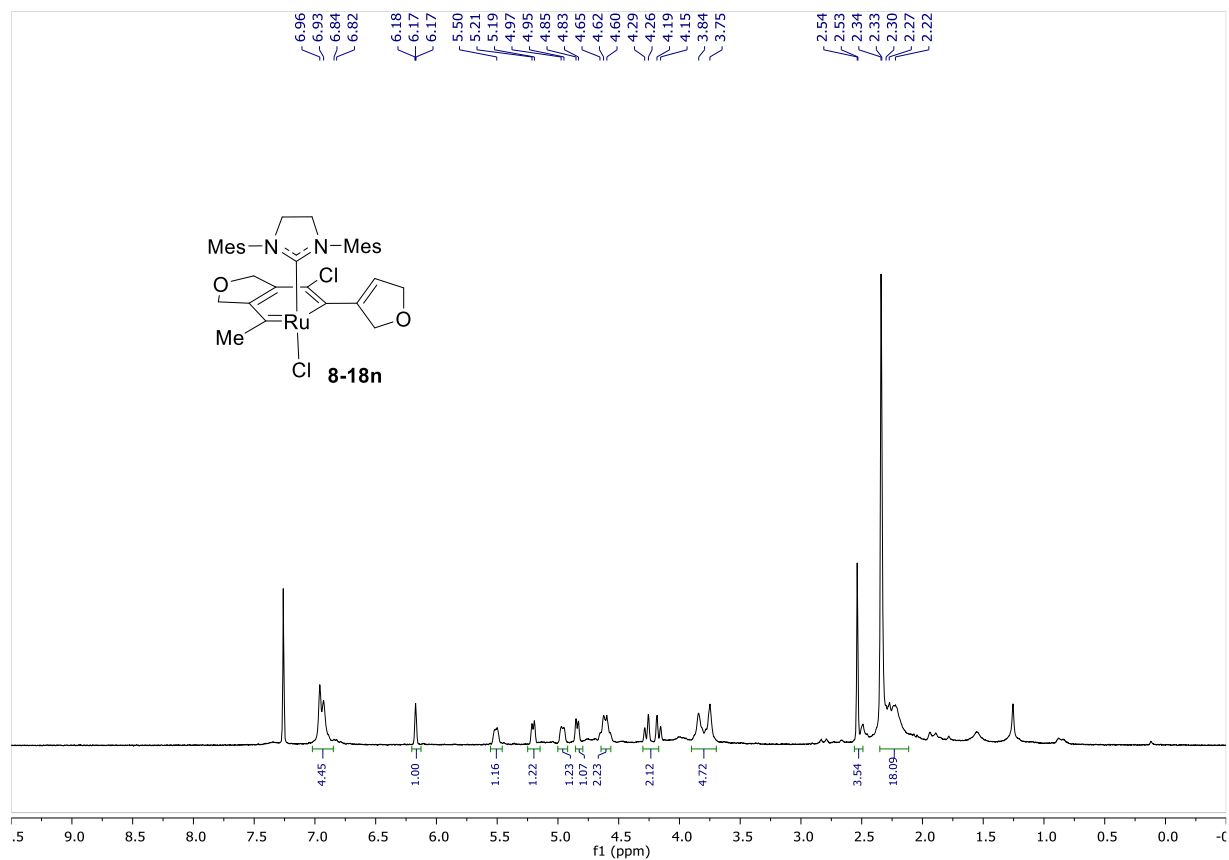


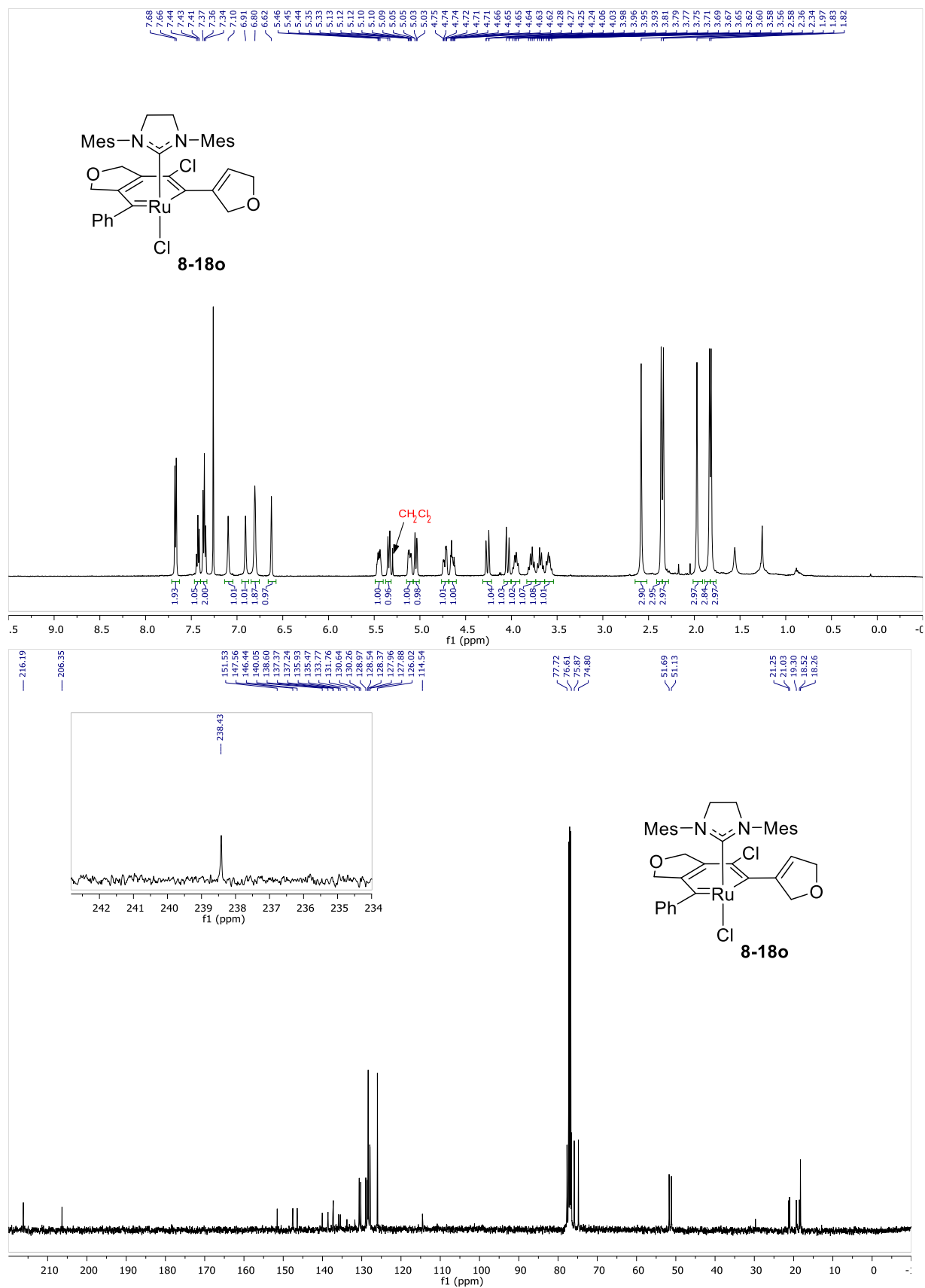
¹⁹P NMR (CDCl₃, 203 MHz)

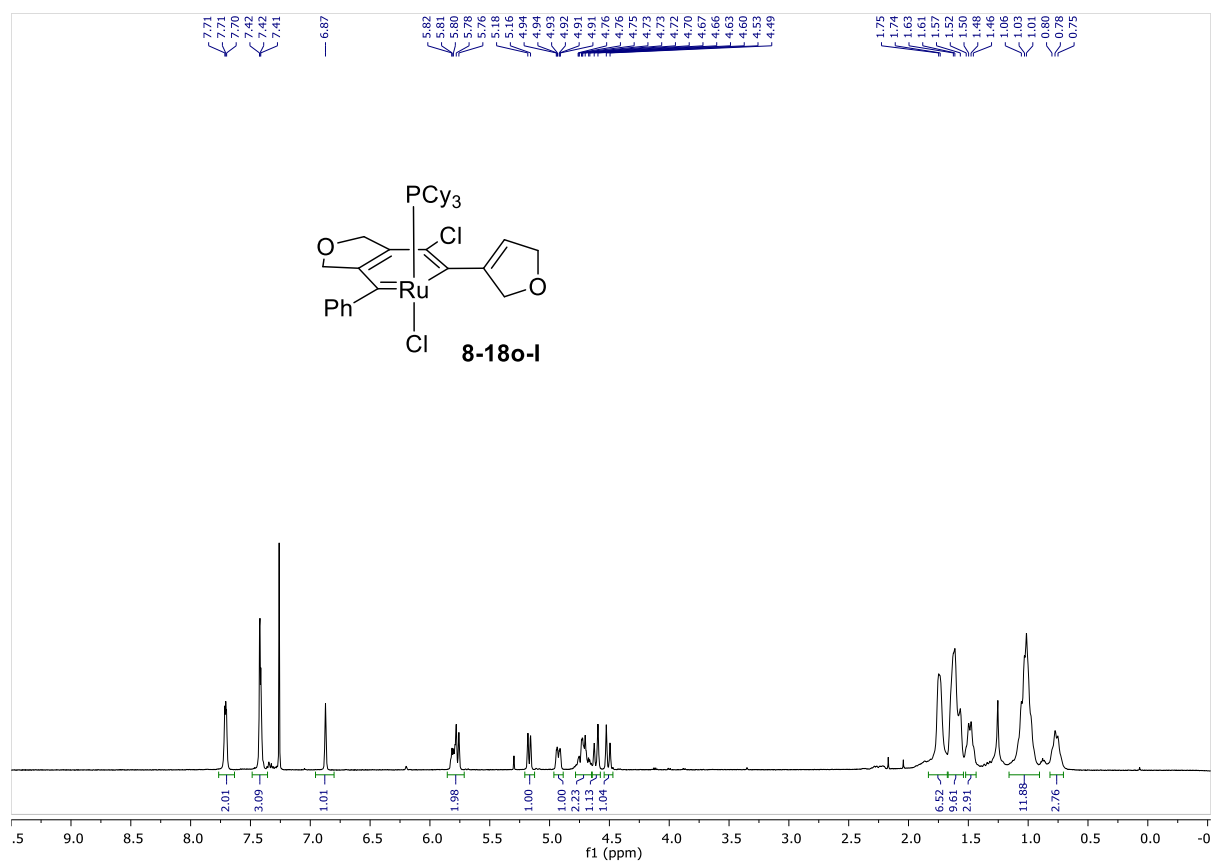




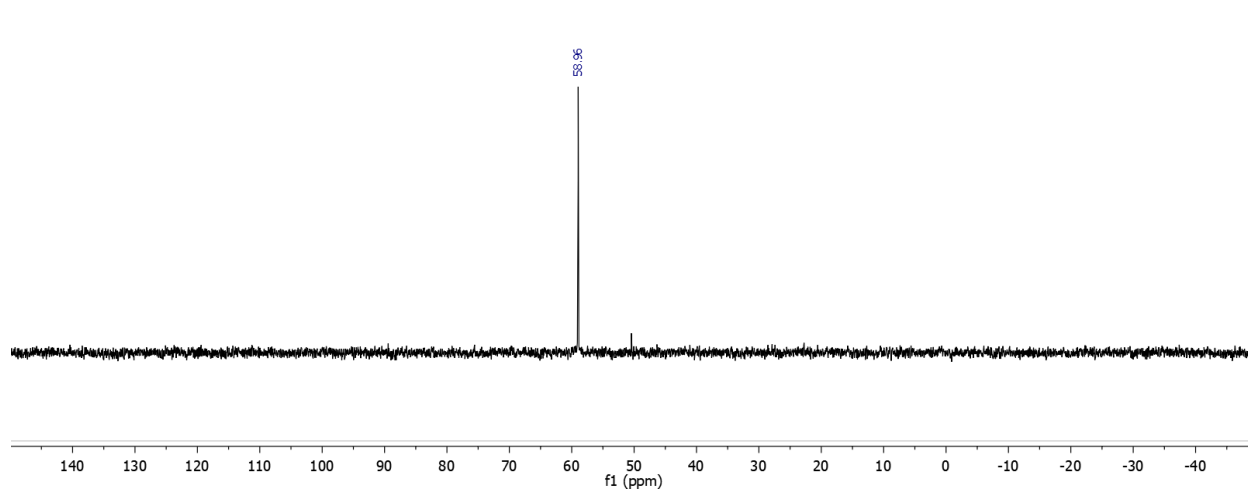


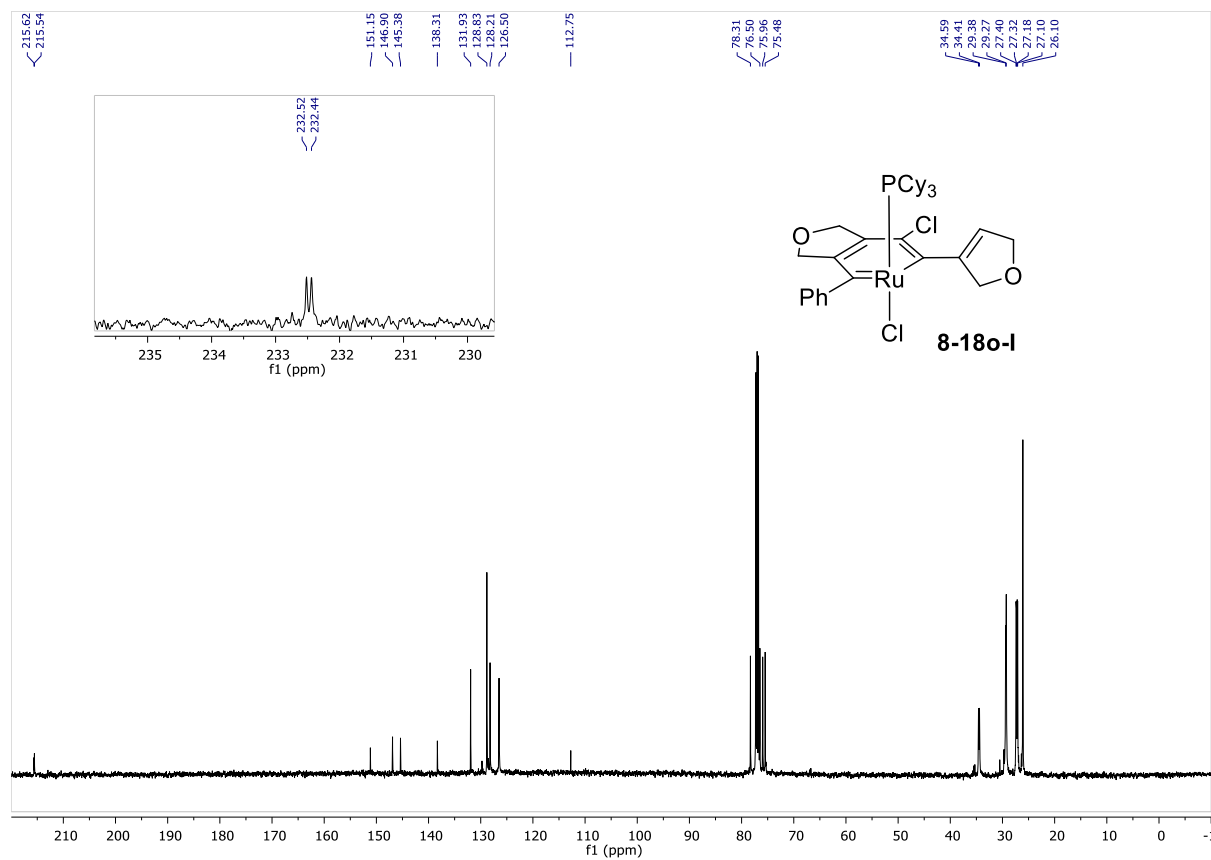


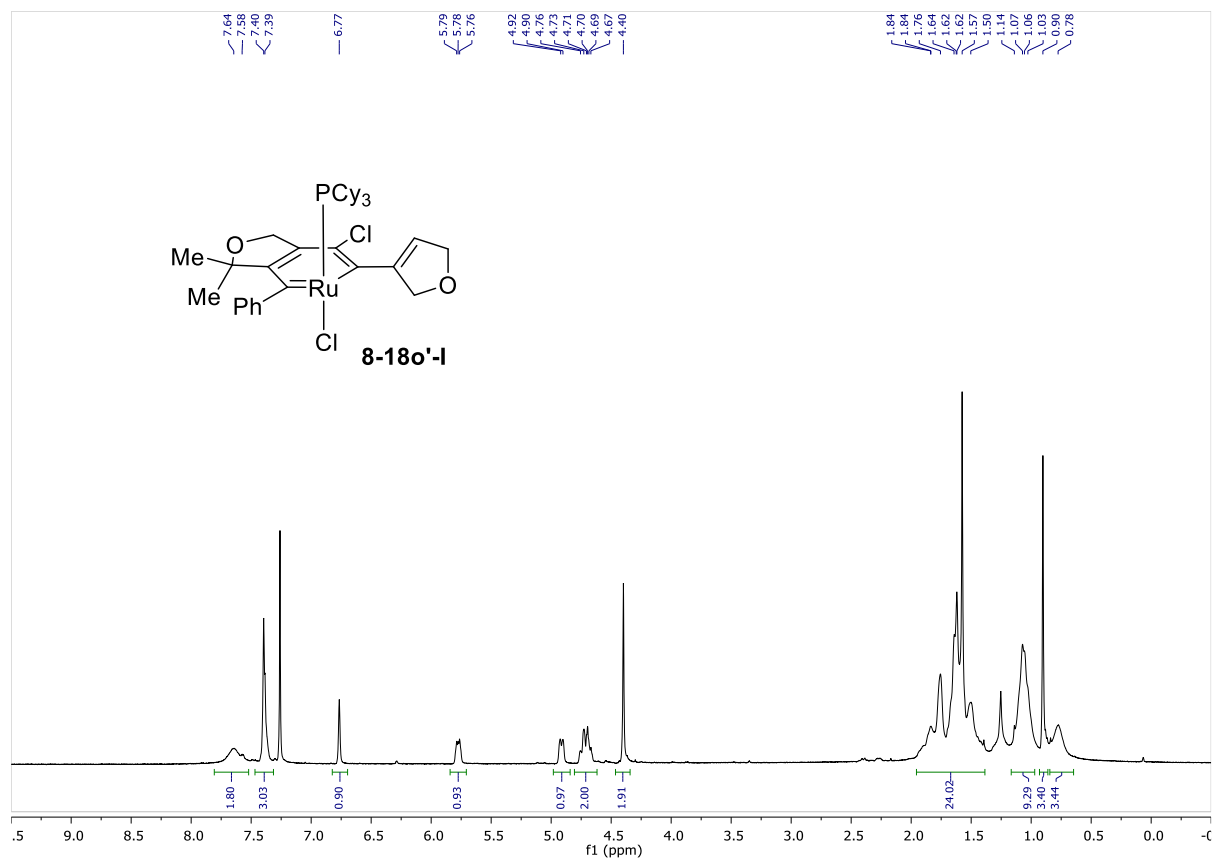




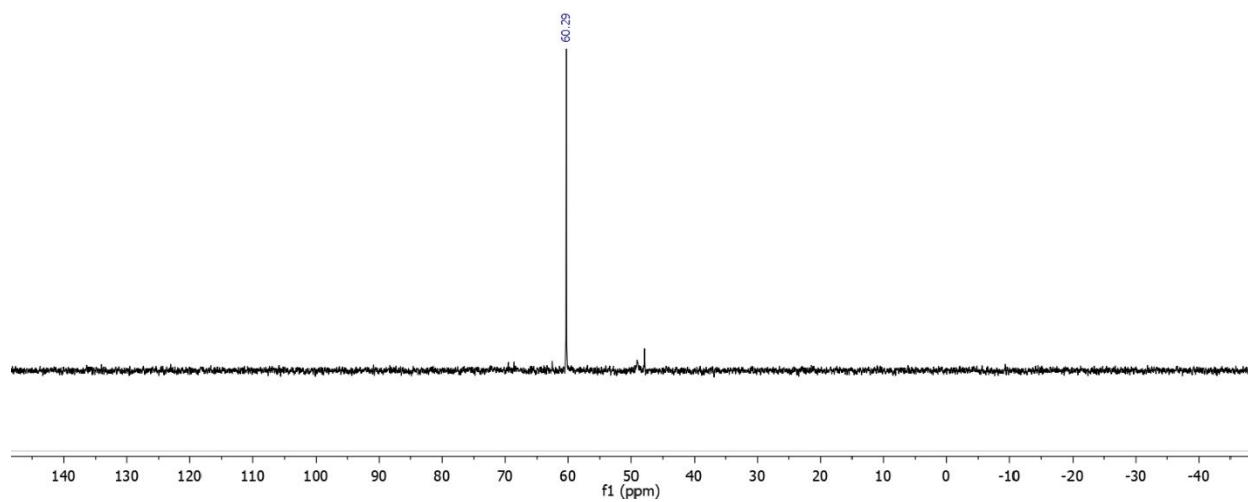
¹⁹P NMR (CDCl₃, 203 MHz)

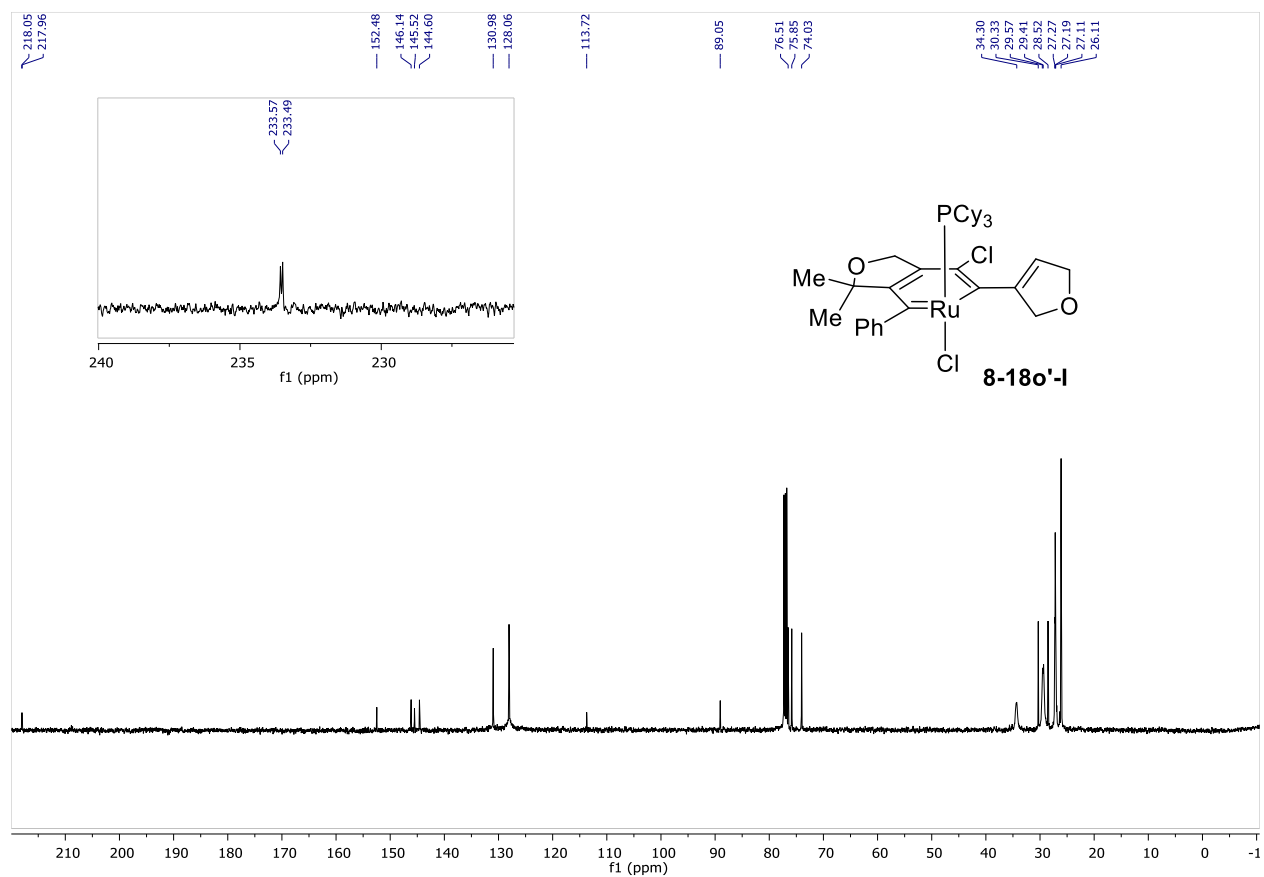


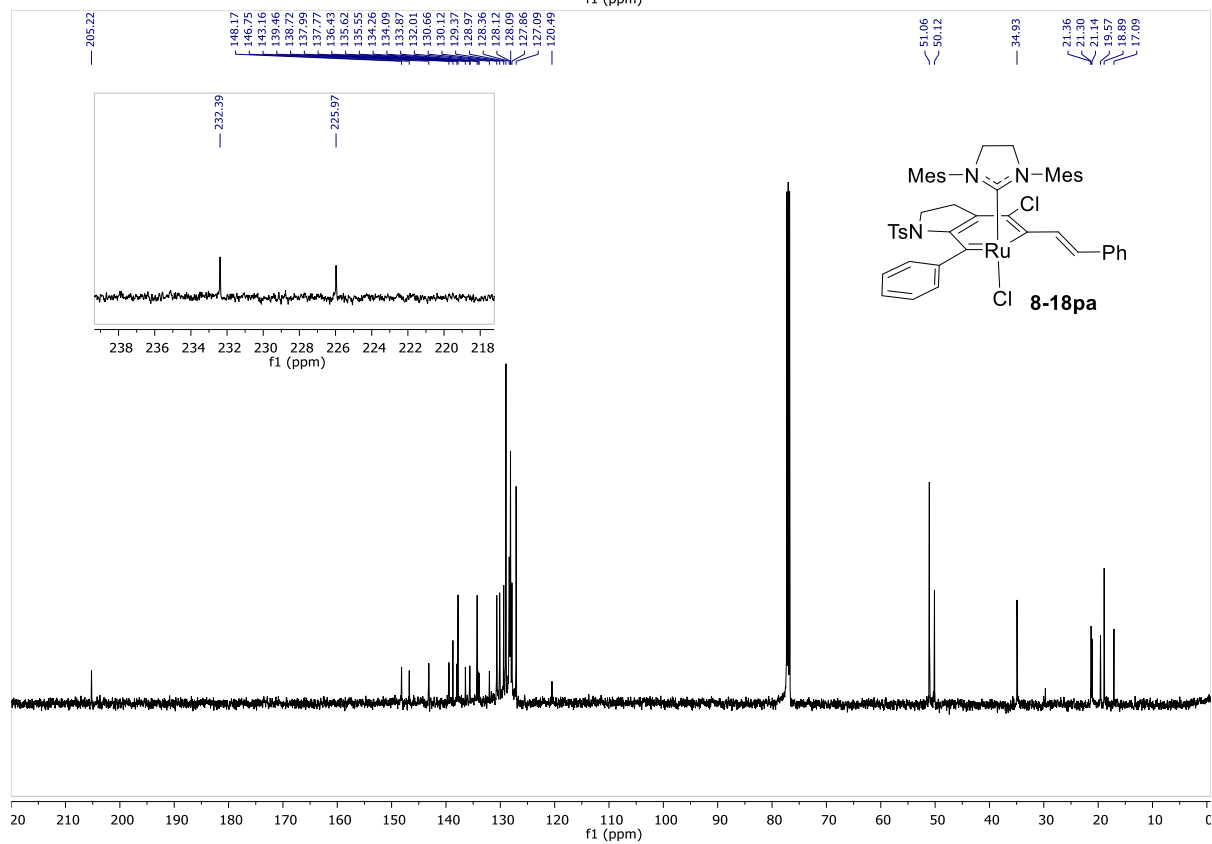
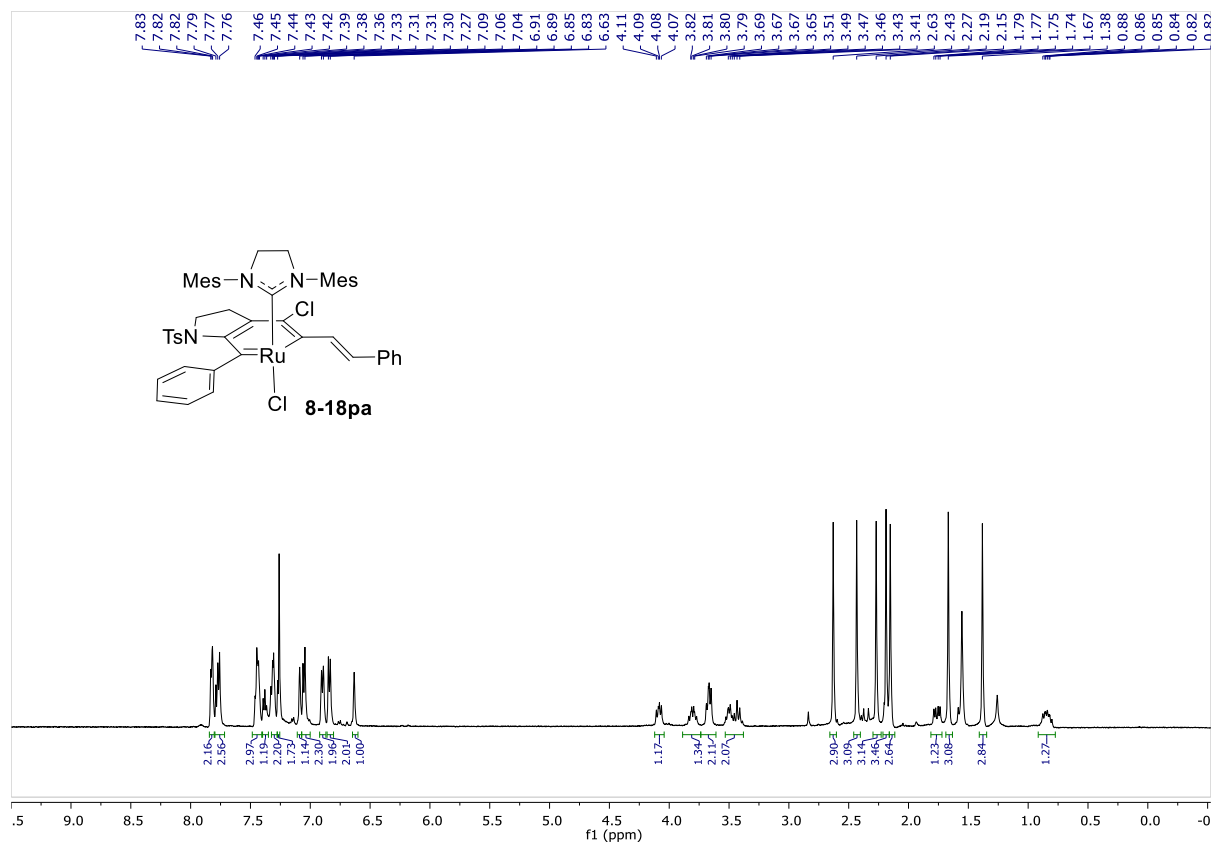


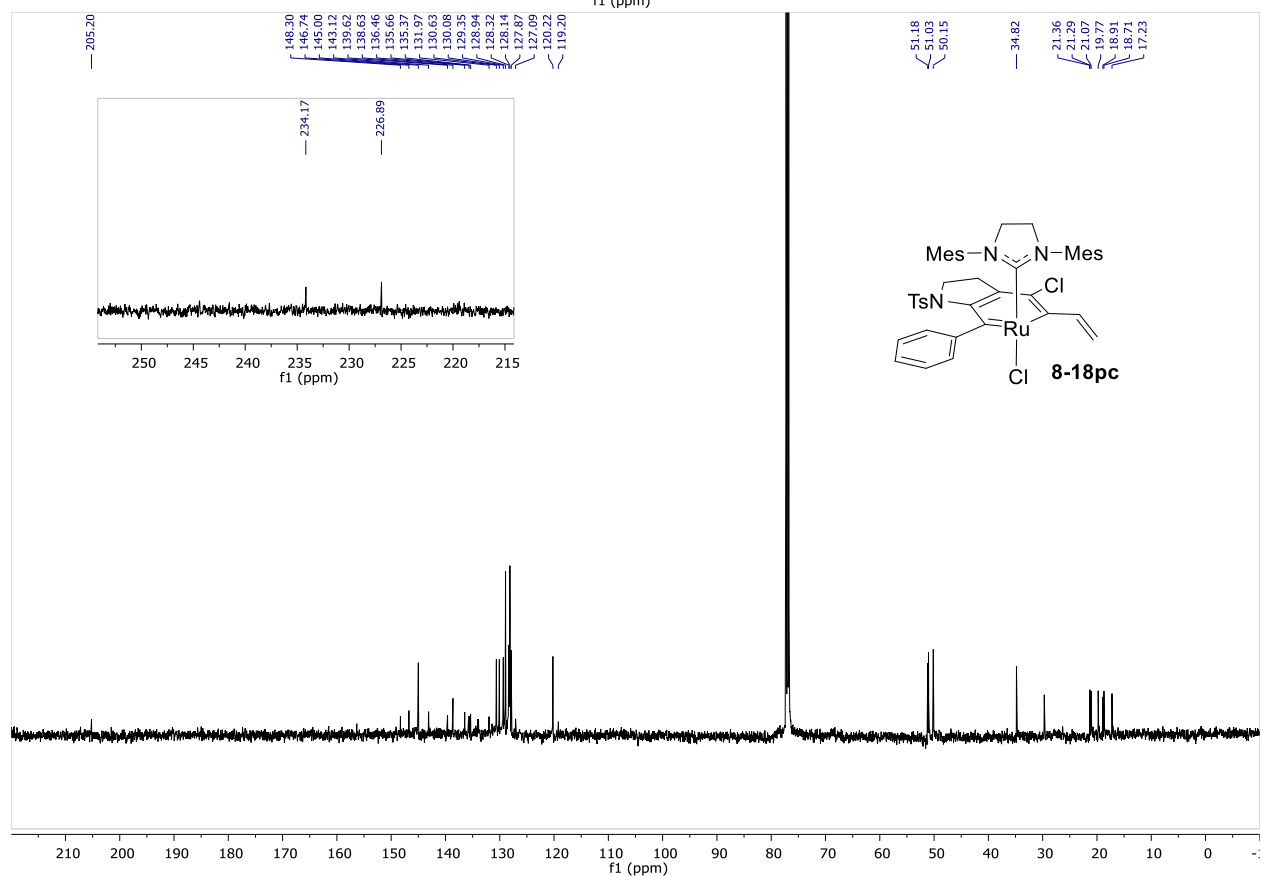
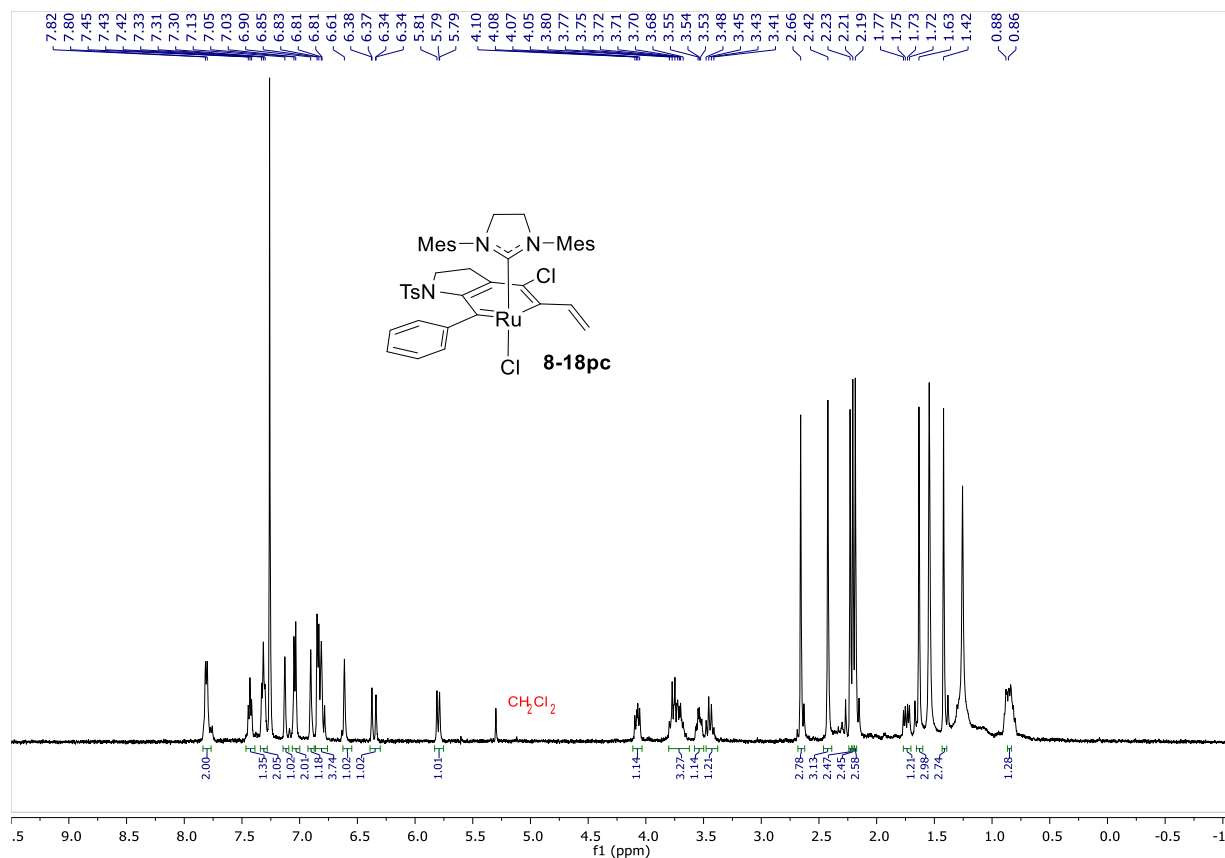


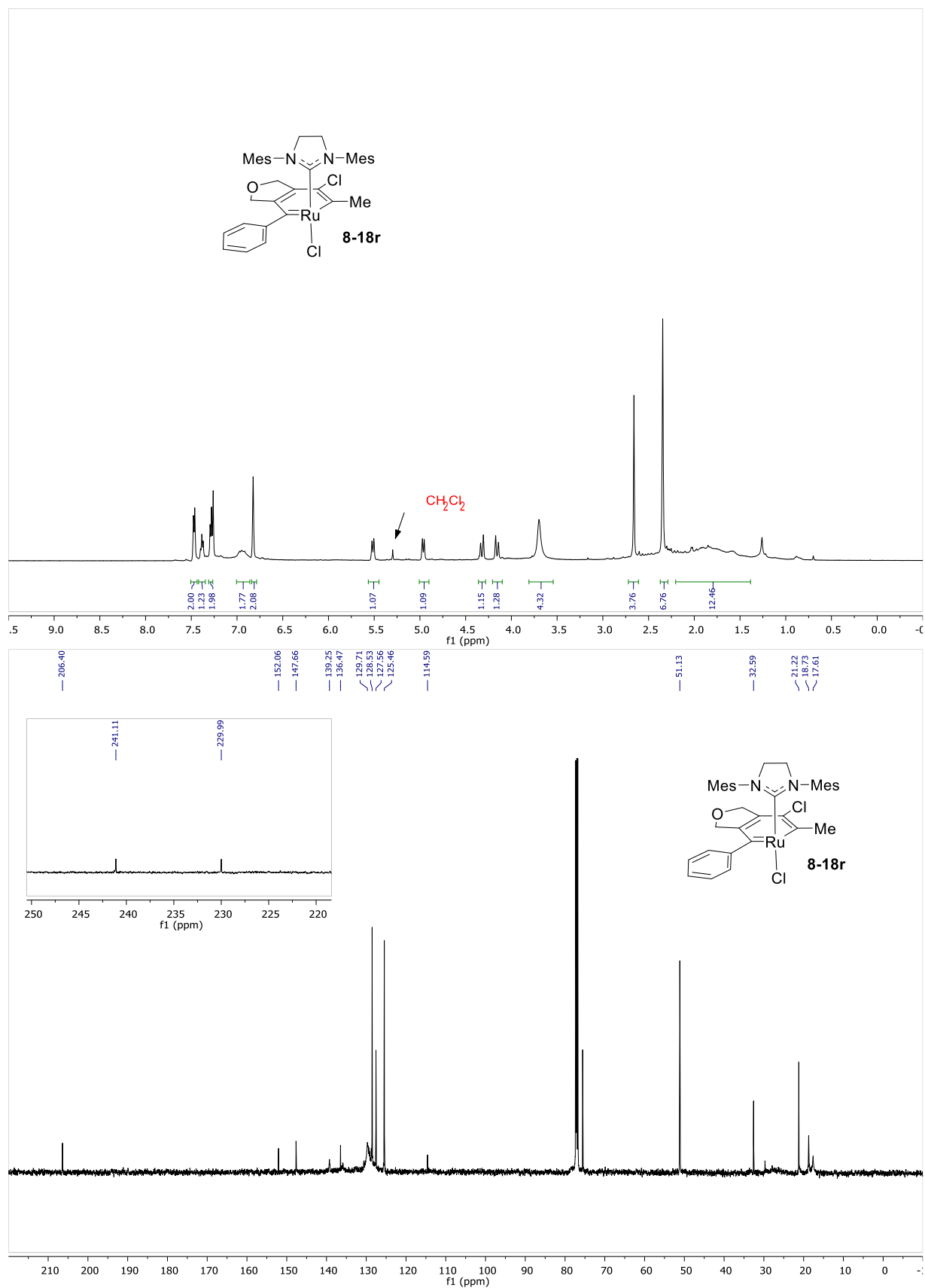
^{19}P NMR (CDCl₃, 203 MHz)

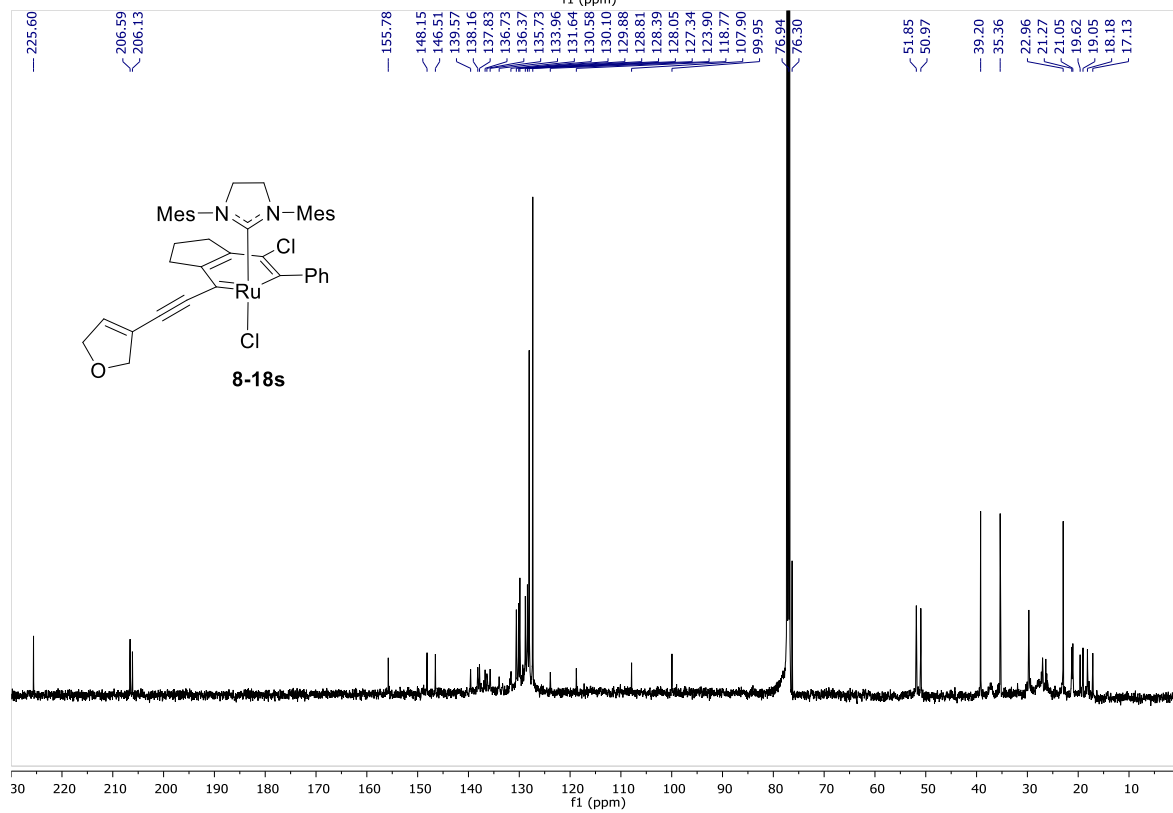


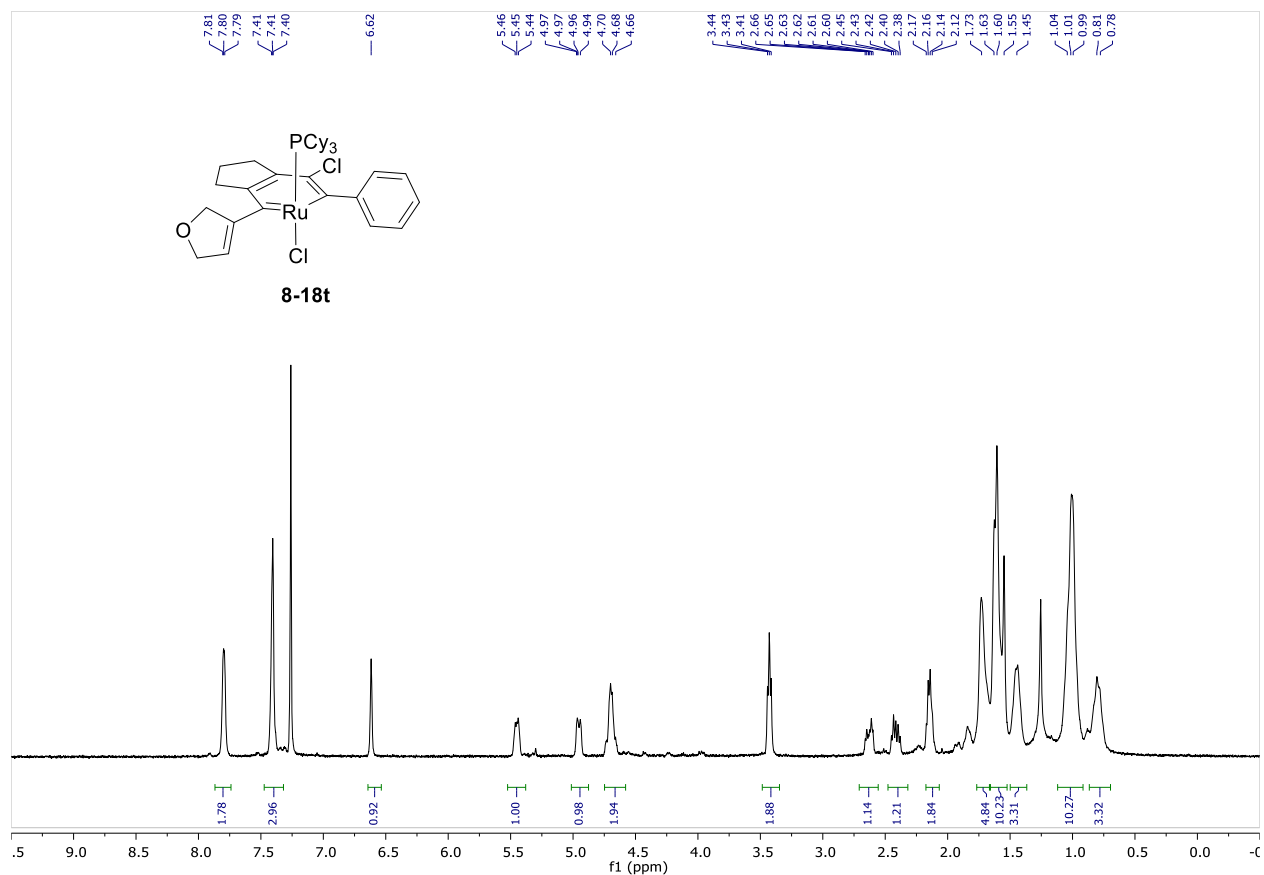




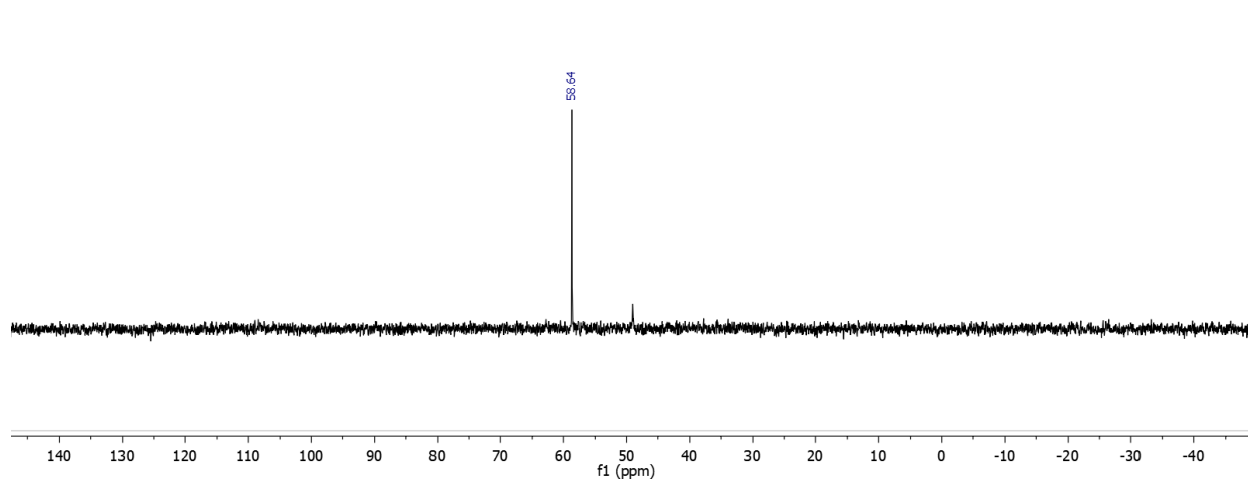


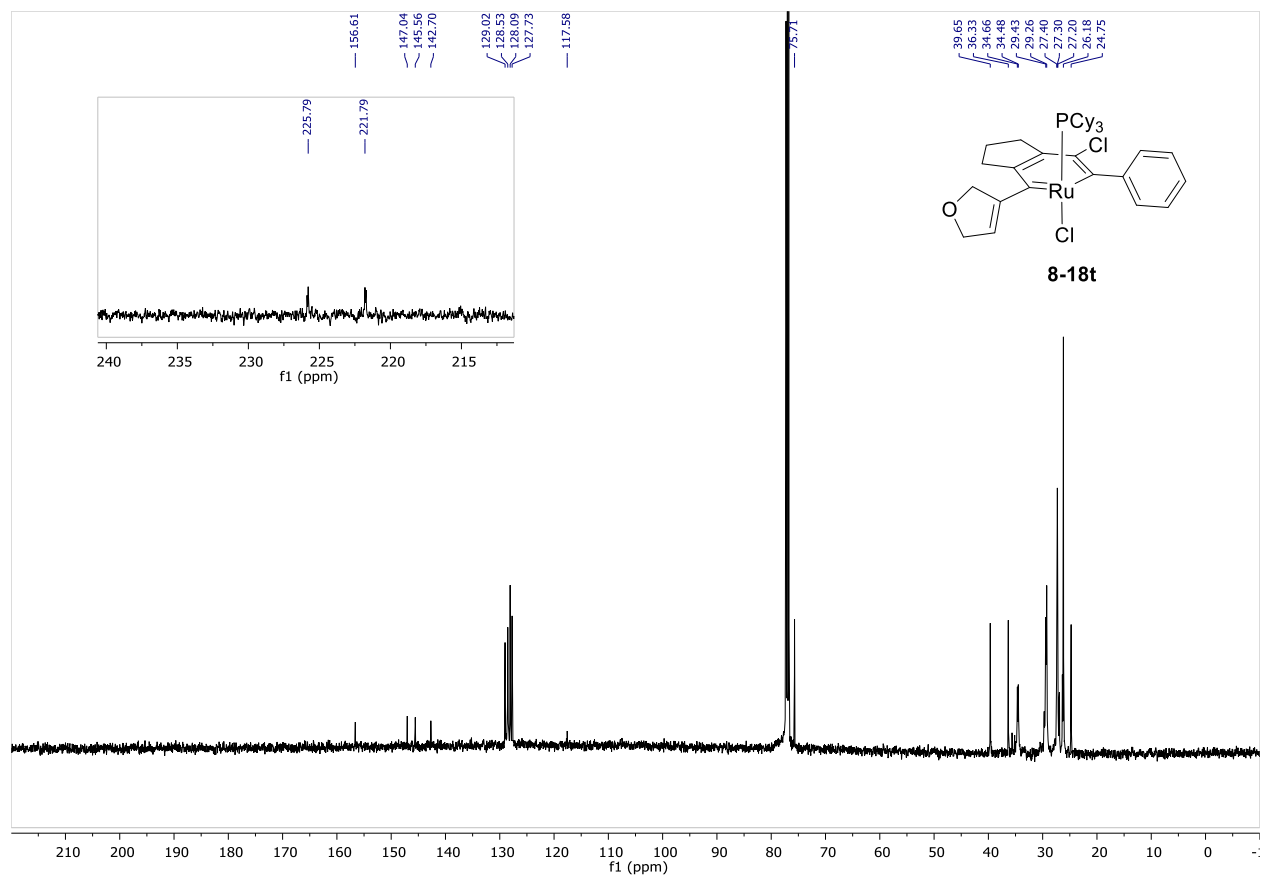


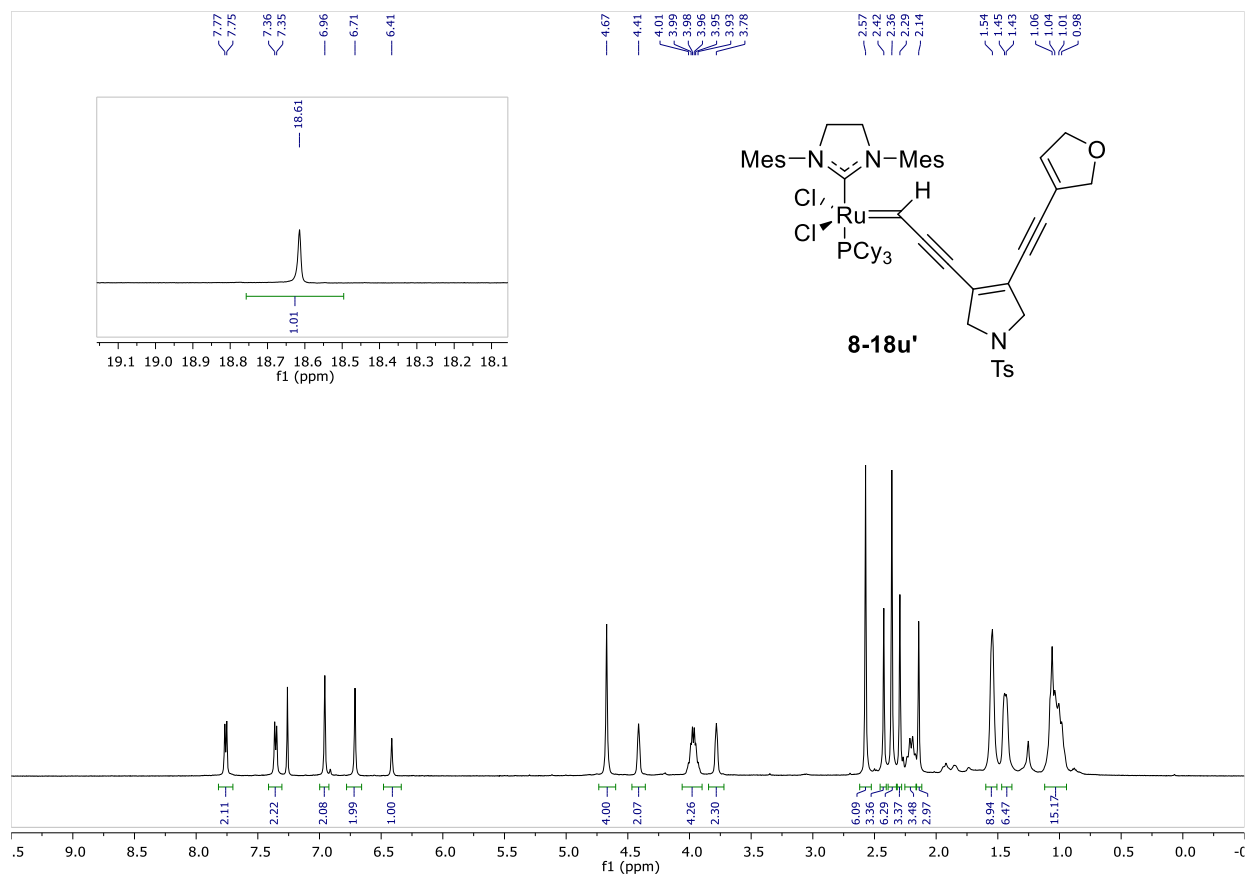




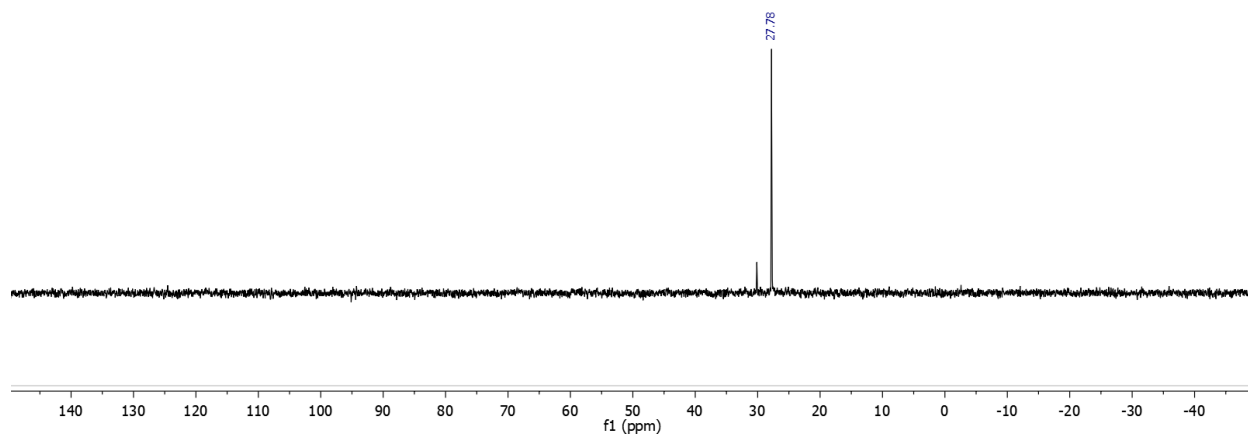
^{19}P NMR (CDCl₃, 203 MHz)

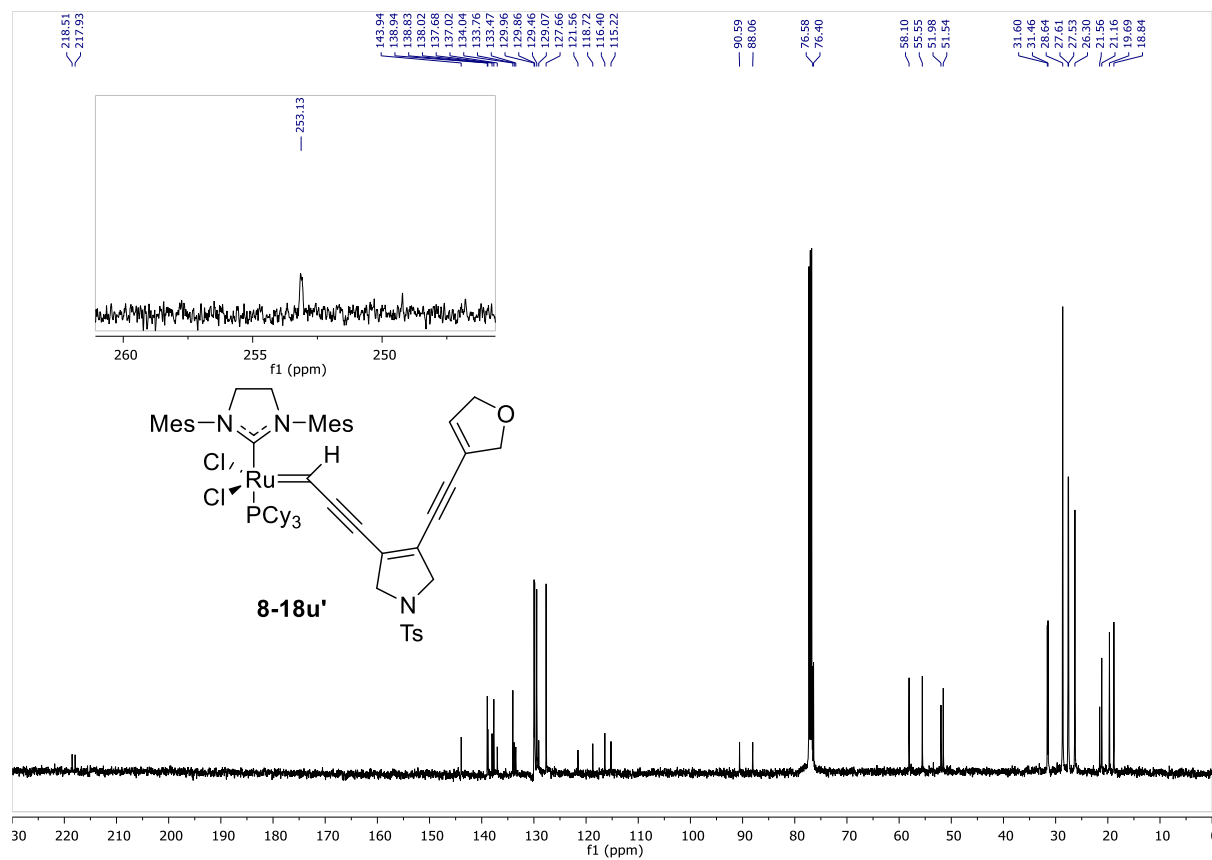


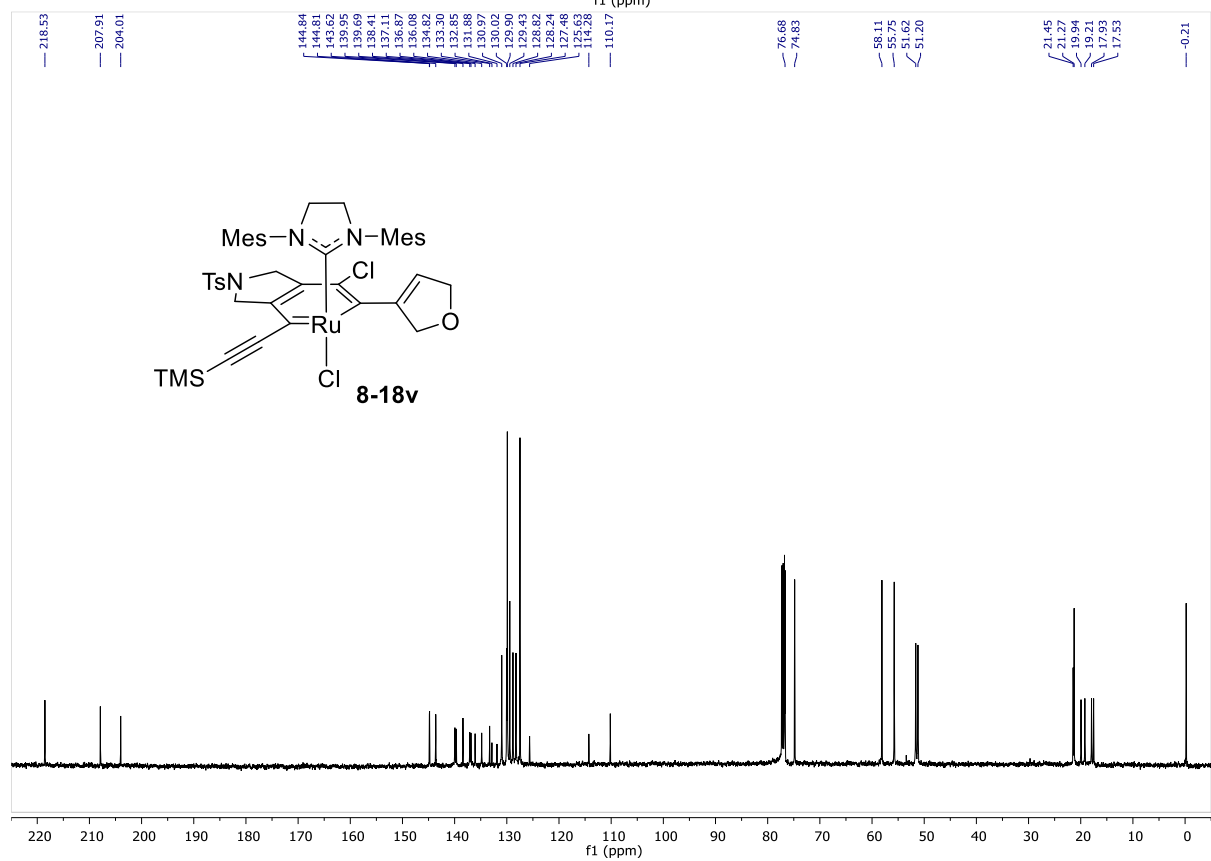
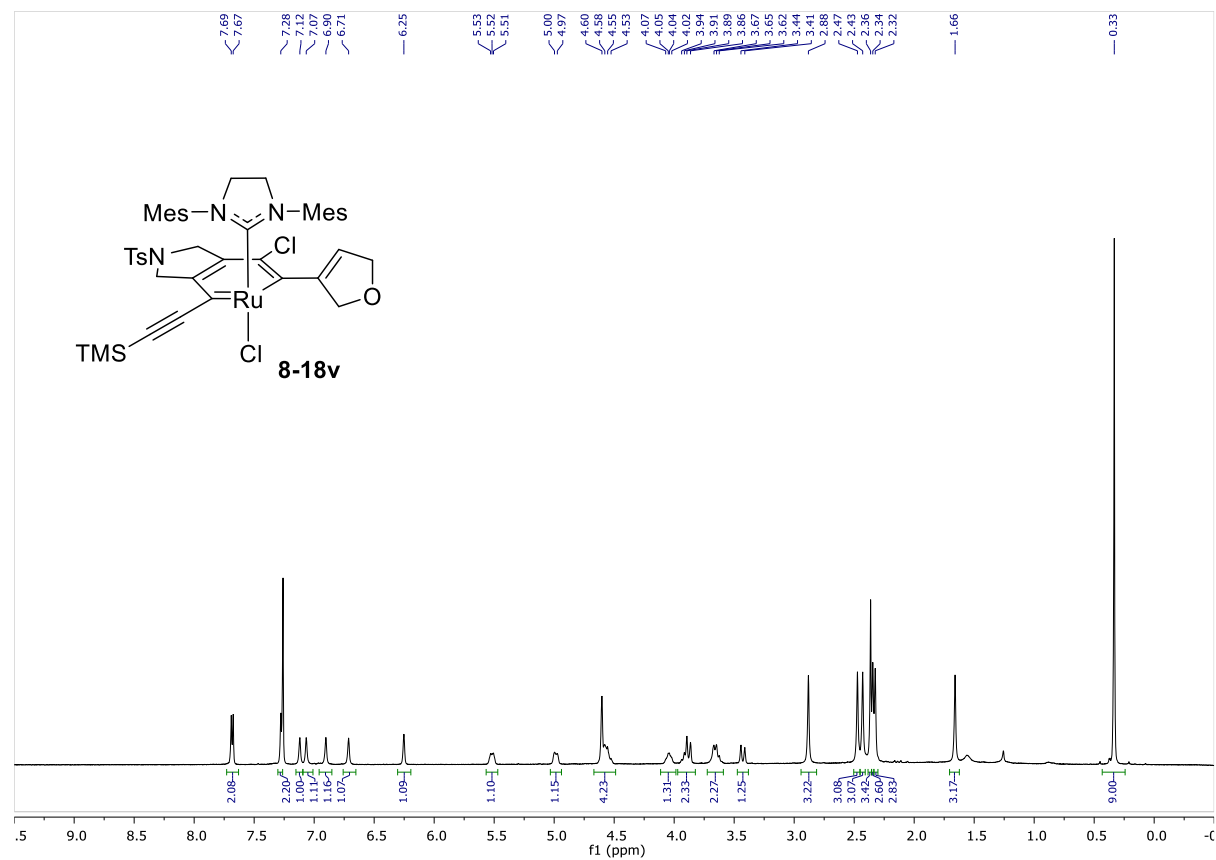


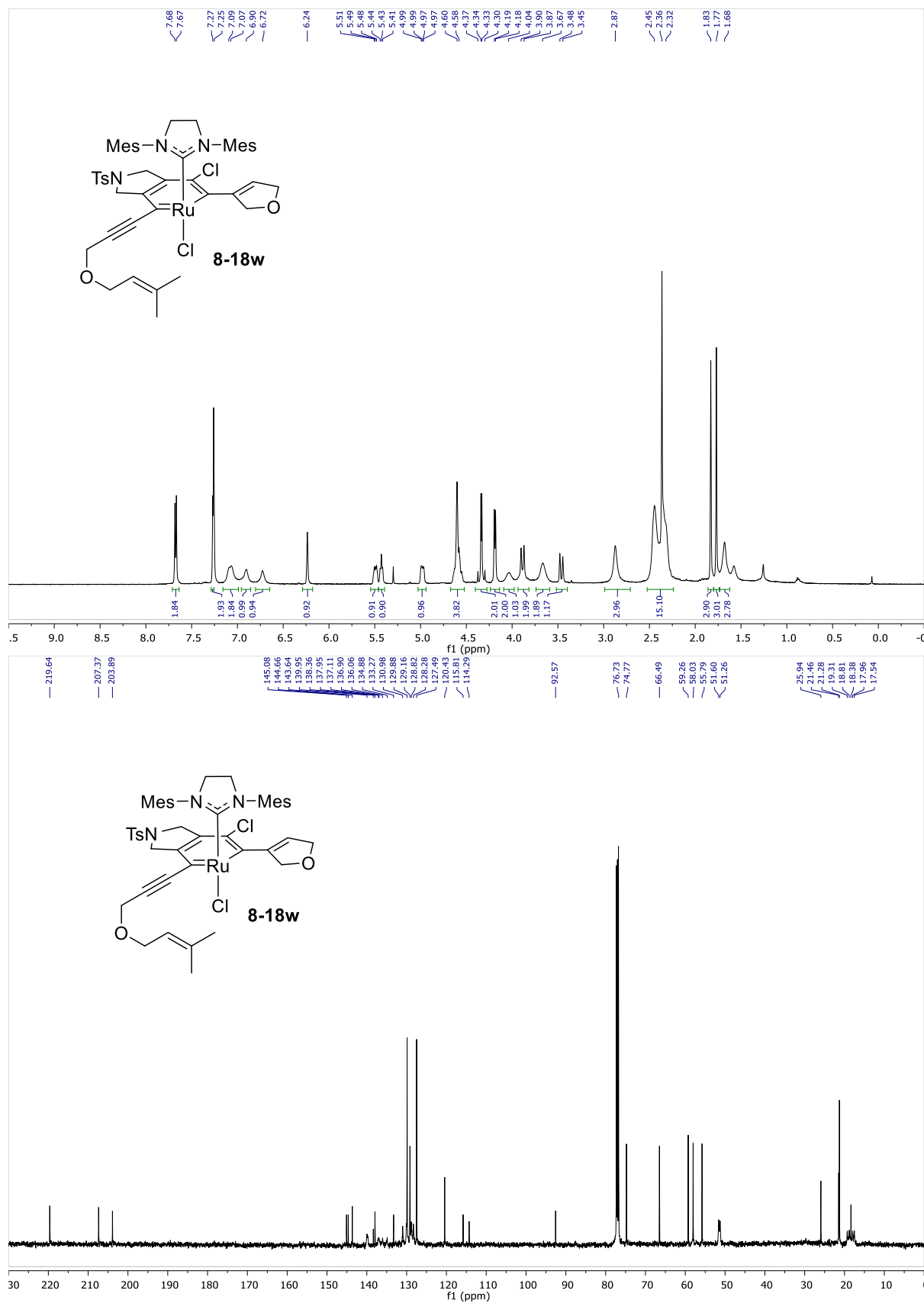


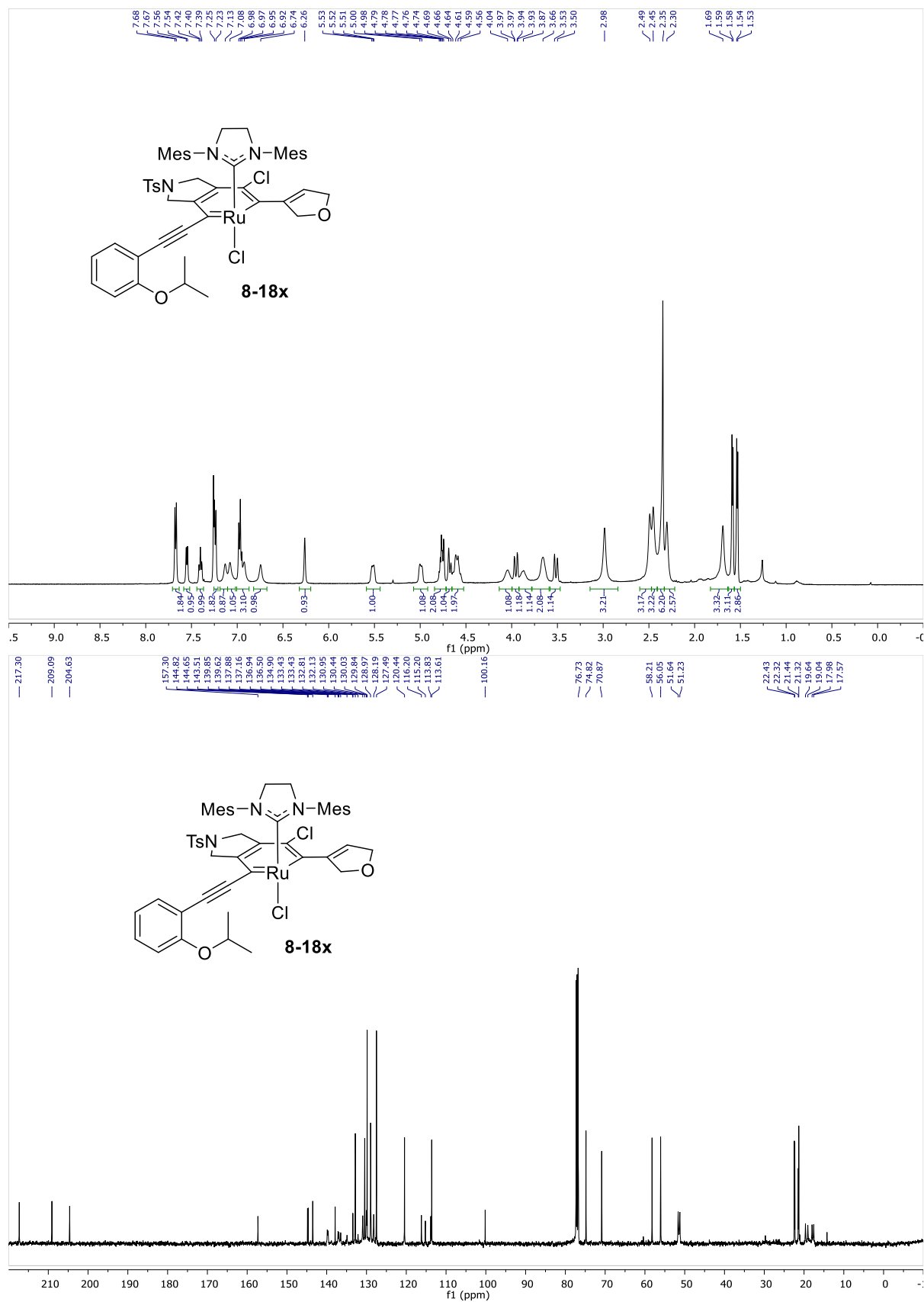
¹⁹P NMR (CDCl₃, 203 MHz)

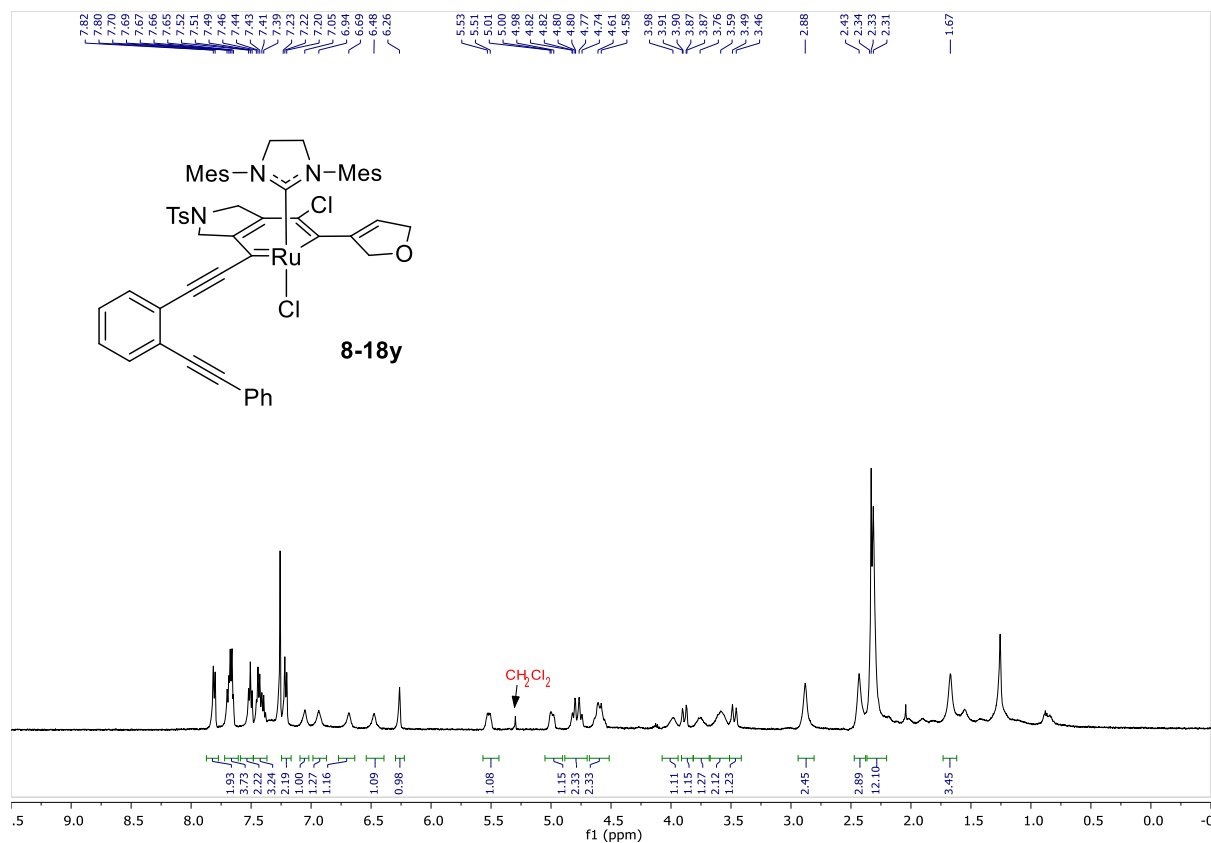


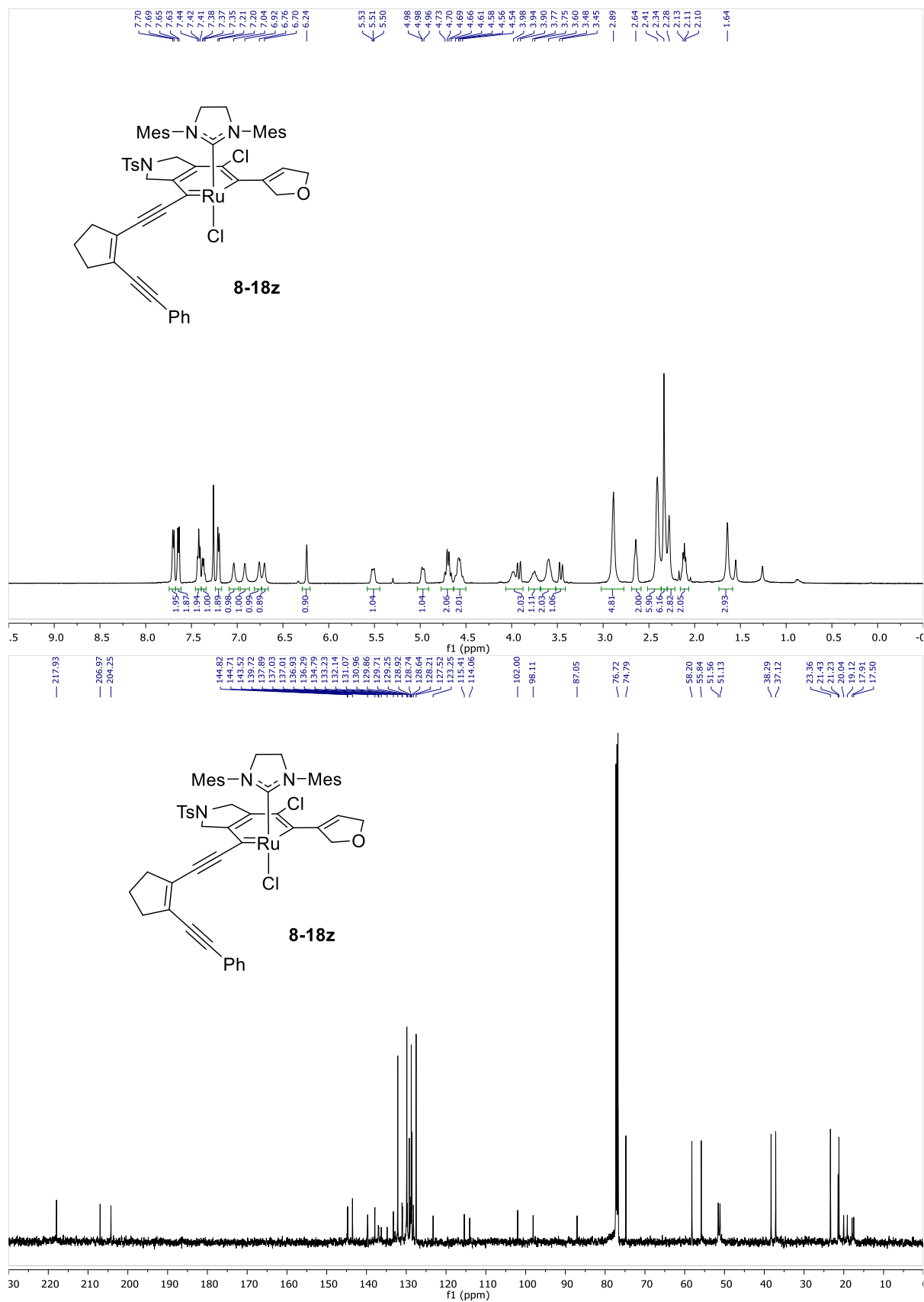


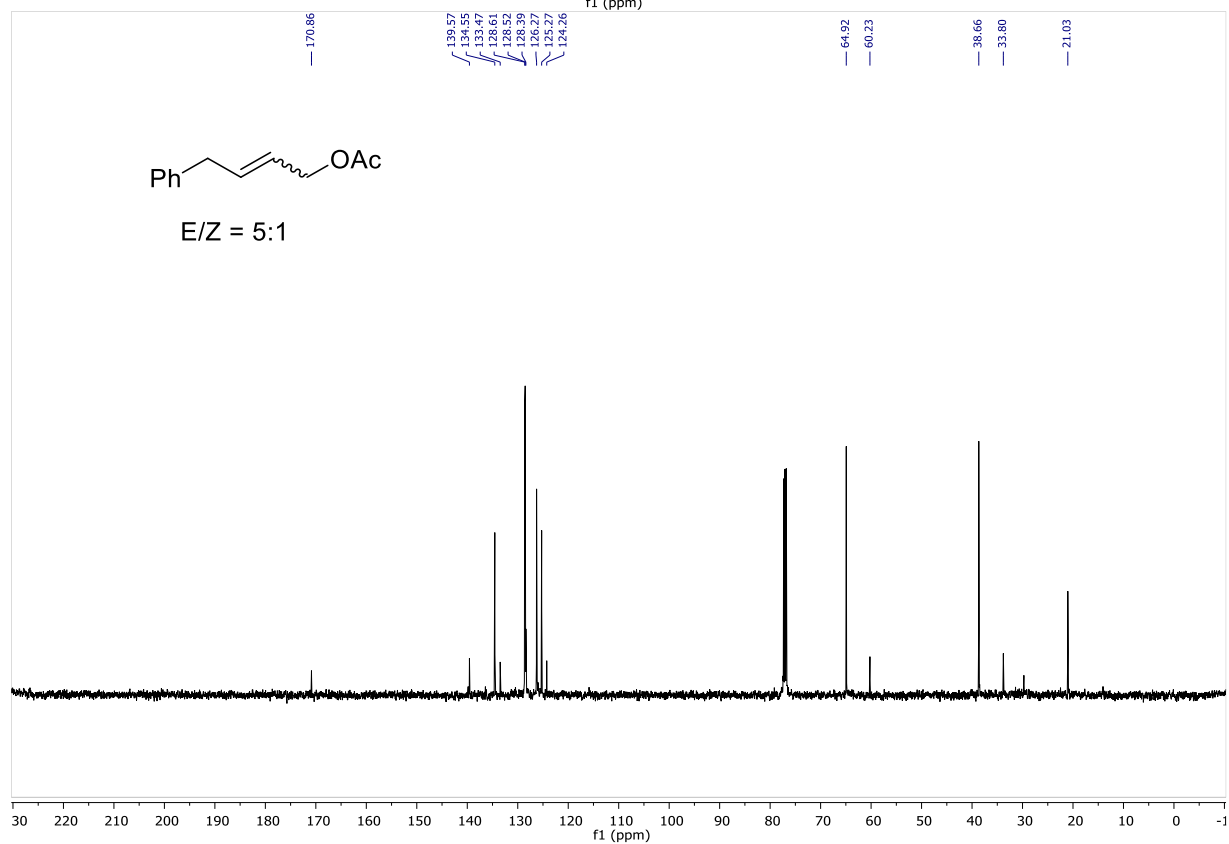
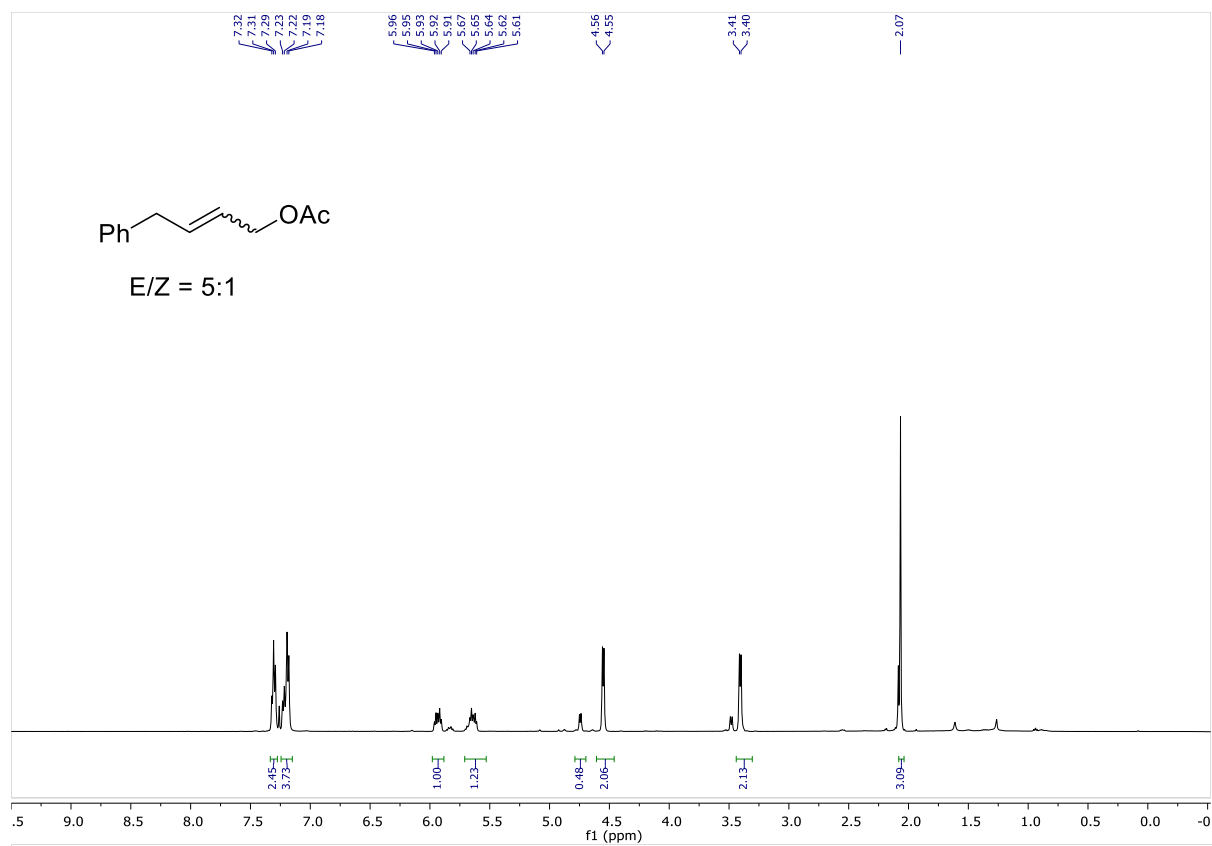


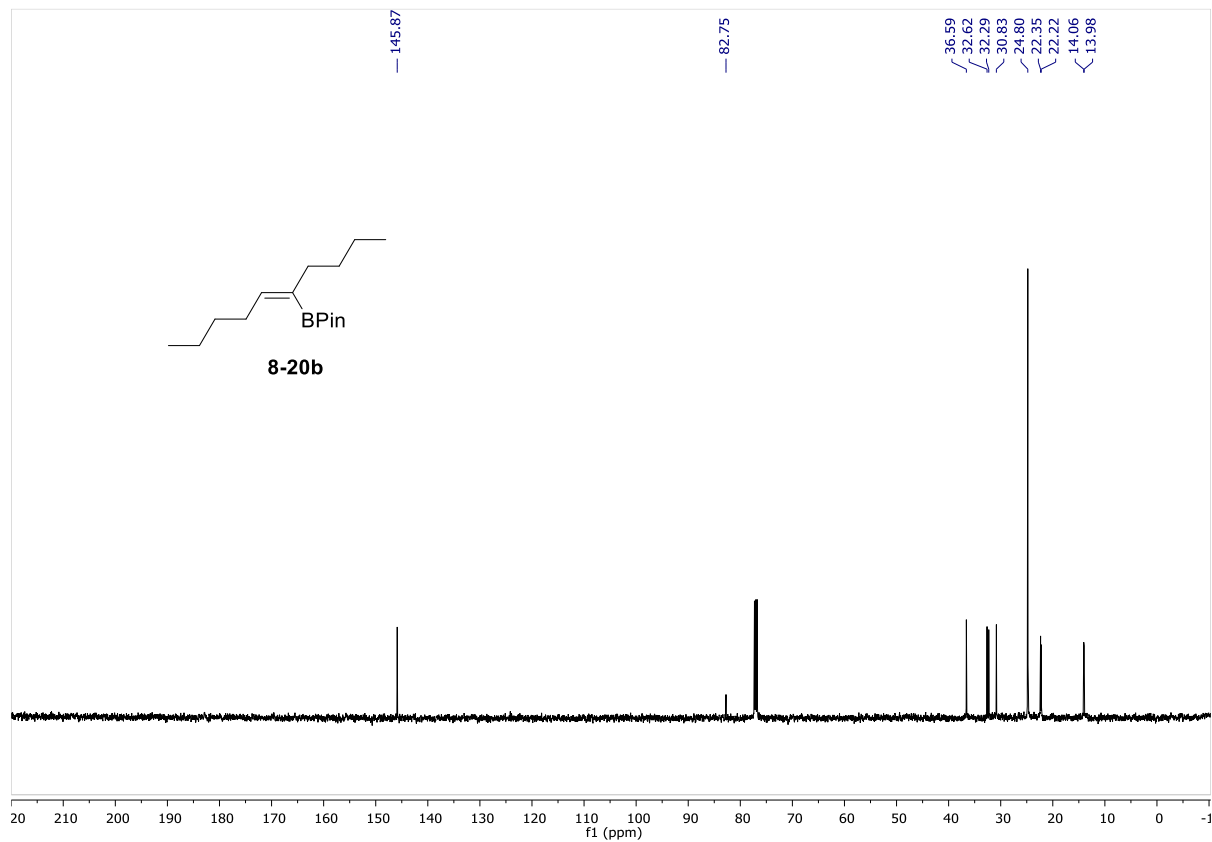
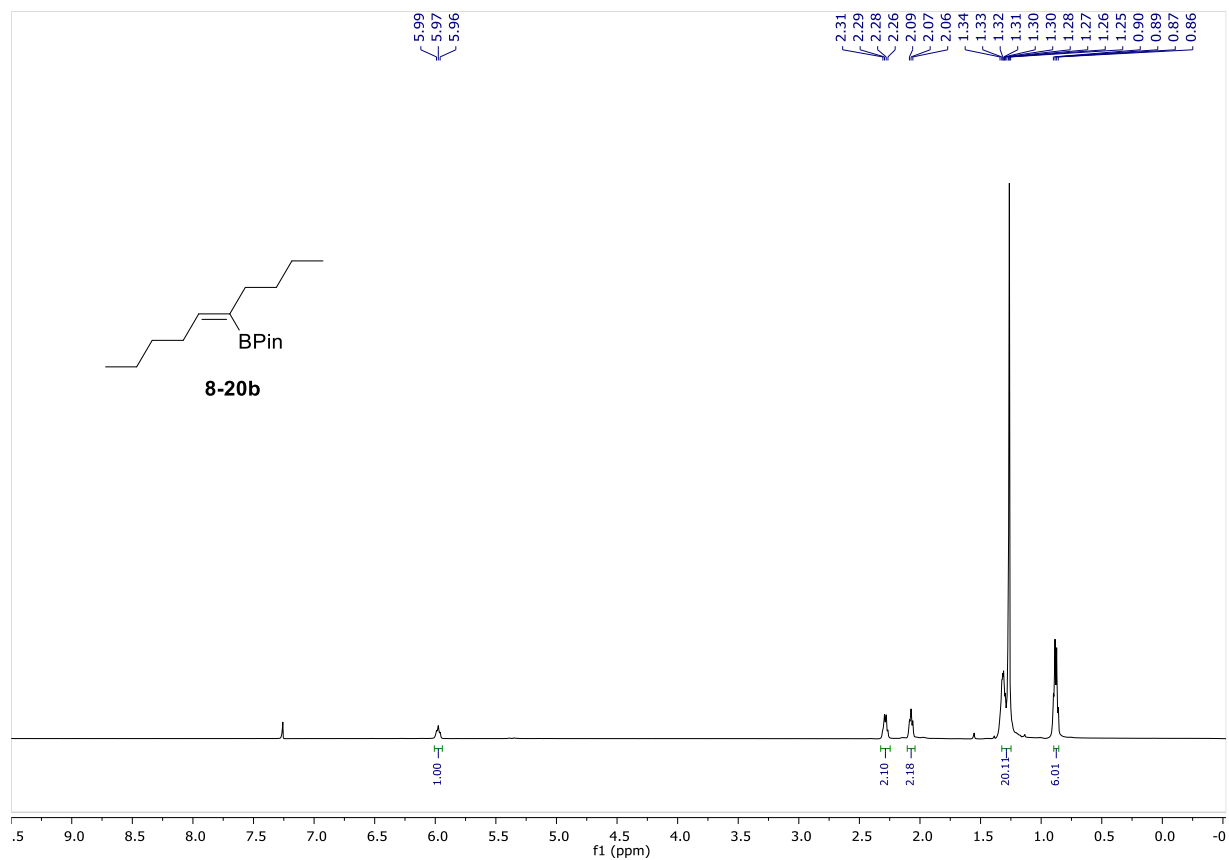


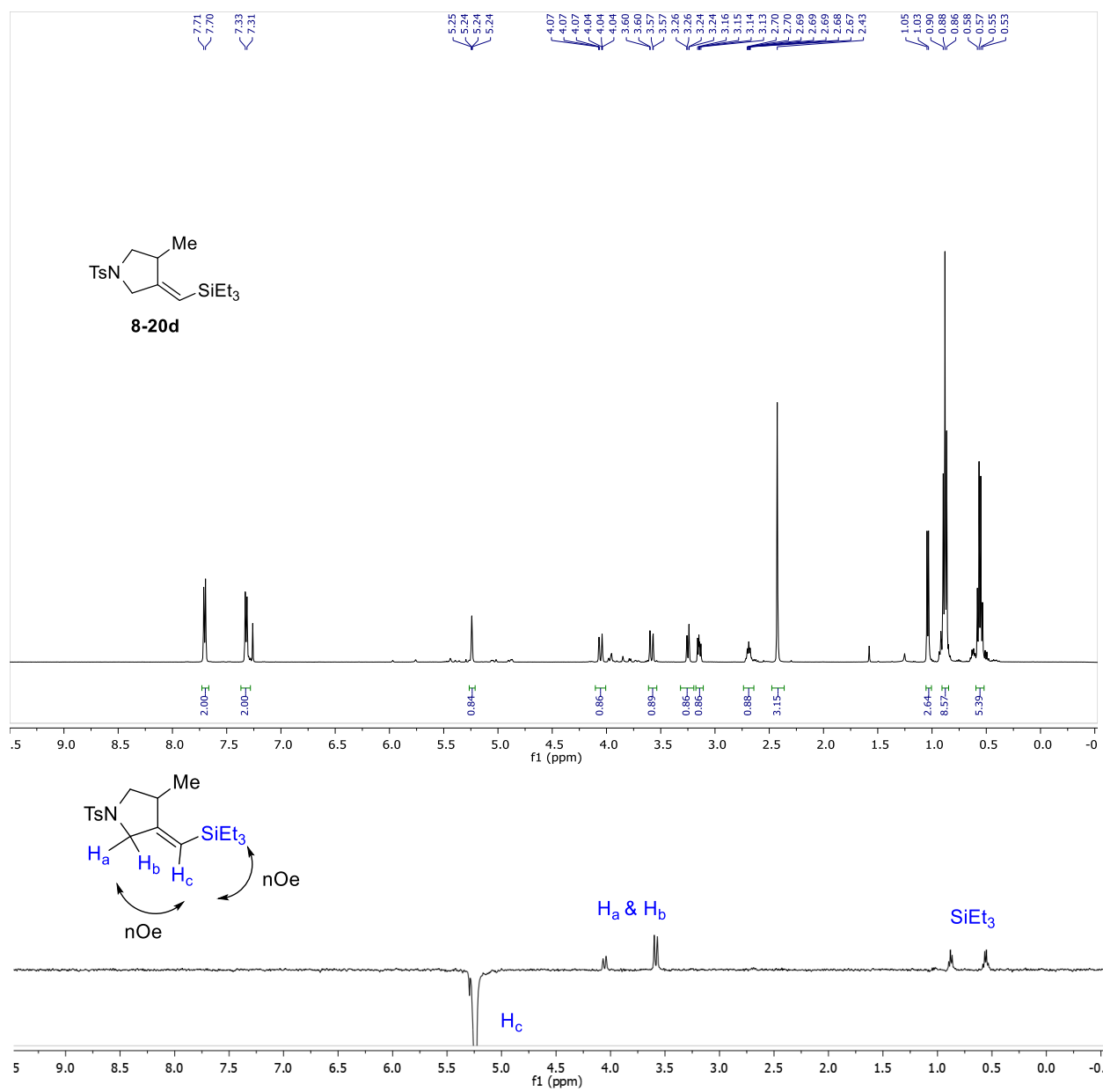


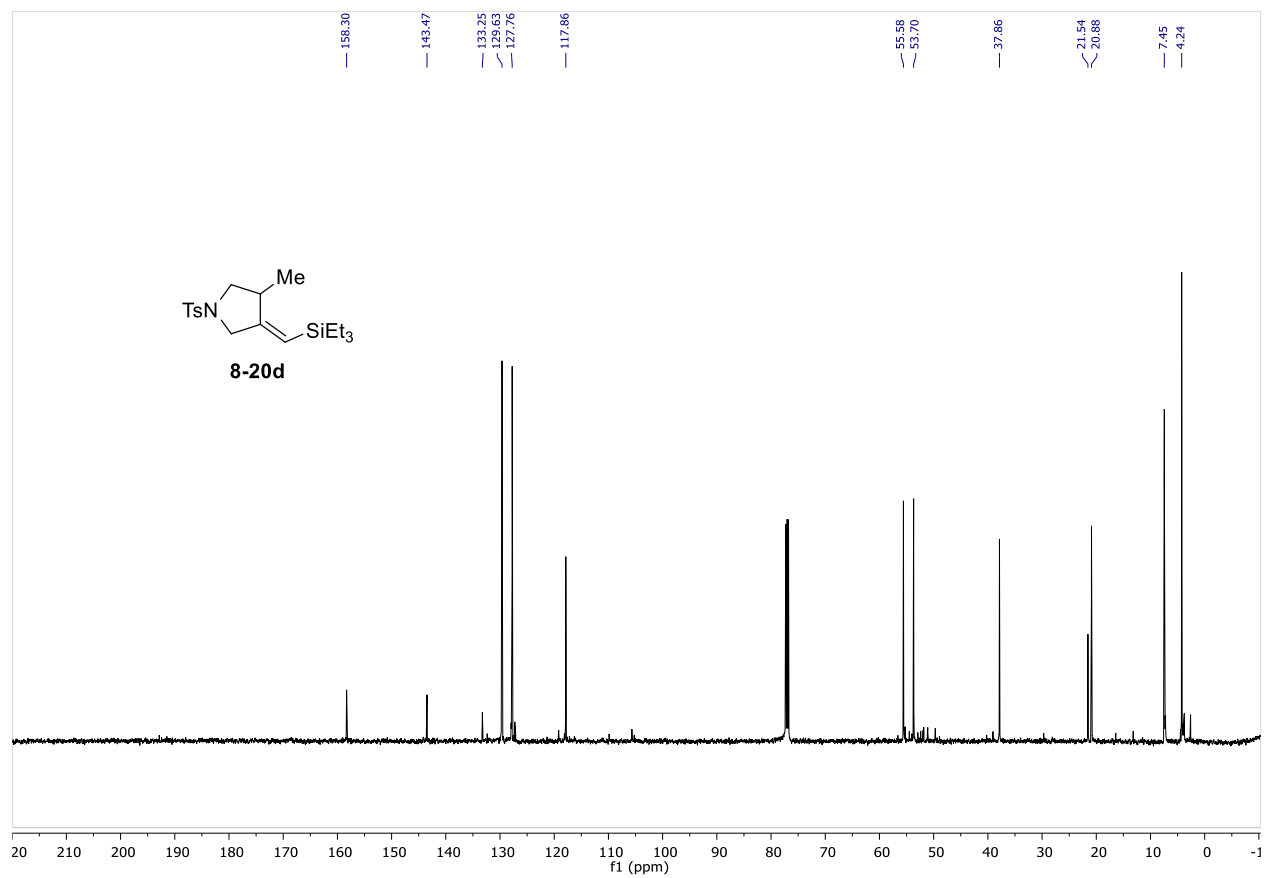












Appendix VII
Copyright Permission



Home



Help



Email Support



Sign in



Create Account

Reactivity and Selectivity in the Intermolecular Alder-Ene Reactions of Arynes with Functionalized Alkenes



Author: Saswata Gupta, Peipei Xie, Yuanzhi Xia, et al

Publication: Organic Letters

Publisher: American Chemical Society

Date: Oct 1, 2017

Copyright © 2017, American Chemical Society

PERMISSION/LICENSE IS GRANTED FOR YOUR ORDER AT NO CHARGE

This type of permission/license, instead of the standard Terms and Conditions, is sent to you because no fee is being charged for your order. Please note the following:

- Permission is granted for your request in both print and electronic formats, and translations.
- If figures and/or tables were requested, they may be adapted or used in part.
- Please print this page for your records and send a copy of it to your publisher/graduate school.
- Appropriate credit for the requested material should be given as follows: "Reprinted (adapted) with permission from {COMPLETE REFERENCE CITATION}. Copyright {YEAR} American Chemical Society." Insert appropriate information in place of the capitalized words.
- One-time permission is granted only for the use specified in your RightsLink request. No additional uses are granted (such as derivative works or other editions). For any uses, please submit a new request.

If credit is given to another source for the material you requested from RightsLink, permission must be obtained from that source.

[BACK](#)[CLOSE WINDOW](#)



Home



Help



Email Support



Sign in



Create Account

Alkene-Chelated Ruthenium Alkylidenes: A Missing Link to New Catalysts



Author: Saswata Gupta, Venkata R. Sabbasani, Siyuan Su, et al

Publication: ACS Catalysis

Publisher: American Chemical Society

Date: Feb 1, 2021

Copyright © 2021, American Chemical Society

PERMISSION/LICENSE IS GRANTED FOR YOUR ORDER AT NO CHARGE

This type of permission/license, instead of the standard Terms and Conditions, is sent to you because no fee is being charged for your order. Please note the following:

- Permission is granted for your request in both print and electronic formats, and translations.
- If figures and/or tables were requested, they may be adapted or used in part.
- Please print this page for your records and send a copy of it to your publisher/graduate school.
- Appropriate credit for the requested material should be given as follows: "Reprinted (adapted) with permission from {COMPLETE REFERENCE CITATION}. Copyright {YEAR} American Chemical Society." Insert appropriate information in place of the capitalized words.
- One-time permission is granted only for the use specified in your RightsLink request. No additional uses are granted (such as derivative works or other editions). For any uses, please submit a new request.

If credit is given to another source for the material you requested from RightsLink, permission must be obtained from that source.

[BACK](#)[CLOSE WINDOW](#)



Home



Help



Email Support



Sign in



Create Account

Ruthenabenzene: A Robust Precatalyst**Author:** Saswata Gupta, Siyuan Su, Yu Zhang, et al**Publication:** Journal of the American Chemical Society**Publisher:** American Chemical Society**Date:** May 1, 2021*Copyright © 2021, American Chemical Society***PERMISSION/LICENSE IS GRANTED FOR YOUR ORDER AT NO CHARGE**

This type of permission/license, instead of the standard Terms and Conditions, is sent to you because no fee is being charged for your order. Please note the following:

- Permission is granted for your request in both print and electronic formats, and translations.
- If figures and/or tables were requested, they may be adapted or used in part.
- Please print this page for your records and send a copy of it to your publisher/graduate school.
- Appropriate credit for the requested material should be given as follows: "Reprinted (adapted) with permission from {COMPLETE REFERENCE CITATION}. Copyright {YEAR} American Chemical Society." Insert appropriate information in place of the capitalized words.
- One-time permission is granted only for the use specified in your RightsLink request. No additional uses are granted (such as derivative works or other editions). For any uses, please submit a new request.

If credit is given to another source for the material you requested from RightsLink, permission must be obtained from that source.

[BACK](#)[CLOSE WINDOW](#)

VITA

Name: Saswata Gupta

Education: B.Sc., Chemistry, Presidency College, Kolkata, West Bengal, India, 2013

M.Sc., Chemistry, Indian Institute of Technology Kharagpur, West Bengal, India, 2015

Ph.D., Organic Chemistry, University of Illinois at Chicago, Chicago, Illinois, USA, 2020

TEACHING: Department of Chemistry, University of Illinois at Chicago, Chicago, Illinois: General Chemistry (CHEM 112), Organic Chemistry I (CHEM 232), Organic Chemistry II (CHEM 234) Organic Chemistry Laboratory (CHEM 233), Advanced Synthetic Laboratory (CHEM 333) for Undergraduates, 2015-2020

HONORS: INSPIRE Scholarship (Department of Science and Technology, India)
Junior Research Fellowship (JRF-CSIR), India
Student Presenter Award (University of Illinois at Chicago)
Moriarty Graduate Fellowship (University of Illinois at Chicago)

PUBLICATIONS: **Gupta, S.**; Su, S.; Zhang, Y.; Liu, P.; Wink, D. J.; Lee, D. "Ruthenabenzene: A Robust Precatalyst" *J. Am. Chem. Soc.* **2021**, *143*, 7490–7500; featured in [JACS Spotlights](#); highlighted in [Chemistry Views](#).

Gupta, S.*; Sabbasani, V. R.*; Su, S.; Wink, D. J.; Lee, D. "Alkene-Chelated Ruthenium Alkylidenes: A Missing Link to New Catalysts" *ACS Catal.* **2021**, *11*, 1977–1987.

Gupta, S.; Lee, D. "Aryne-mediated construction of fluorene skeleton and its application in total synthesis of Selaginplvillins" In *Strategies and Tactics in Organic Synthesis*. **2020** (Invited Book chapter), *in press*.

Gupta, S.; Lin, Y.; Xia, Y.; Wink, D. J.; Lee, D. "Alder-ene reactions driven by high steric strain and bond angle distortion to form benzocyclobutenes" *Chem. Sci.* **2019**, *10*, 2212–2217.

Gupta, S.; Lee, D. "Trimethylsilyldiazomethane (TMSCHN₂) in Carbon–Carbon and Carbon–Heteroatom Bond-Forming Reactions" *Aldrichimica Acta* **2018**, *51*, 77–87.

Xia, Y.; Lee, N.-K.; Sabbasani, V. R.; **Gupta, S.**; Lee, D. "Reaction of silylallenes with triplet molecular oxygen" *Org. Chem. Front.* **2018**, *5*, 2542–2546.

Lee, D.; **Gupta, S.** "Trimethylsilyldiazomethane" update in *Encyclopedia of Reagents for Organic Synthesis* **2018**.

Gupta, S.; Xie, P.; Xia, Y.; Lee, D. “Reactivity of arynes toward functionalized alkenes: intermolecular Alder-ene vs. addition reactions” *Org. Chem. Front.* **2018**, *5*, 2208–2213.

Sabbsani, V. R.; **Gupta, S.;** Yun, S. Y.; Lee, D. “A general approach for the formation of oxygen-chelated ruthenium alkylidene complexes relying on the Thorpe–Ingold effect” *Org. Chem. Front.* **2018**, *5*, 1532–1536.

Gupta, S.; Xie, P.; Xia, Y.; Lee, D.” Reactivity and Selectivity in the Intermolecular Alder–Ene Reactions of Arynes with Functionalized Alkenes” *Org. Lett.* **2017**, *19*, 5162–5165.

.

PRESENTATIONS: **Gupta, S.;** Su, S.; Zhang, Y.; Liu, P.; Wink, D. J.; Lee, D. “Ruthenabenzene: A Robust Catalyst”, ACS Spring 2021 National Virtual Meeting, April 5–30, **2021**. (oral)

Gupta, S.; Lin, Y.; Xia, Y.; Wink, D. J.; Lee, D. “Aryne-mediated intramolecular Alder-ene reaction to form benzocyclobutenes”, ACS National Meeting, Boston, Massachusetts, USA, August 19–23, **2018**. (poster)

Gupta, S.; Lee, D. “Aryne mediated intramolecular Alder-ene reactions to form benzocyclobutenes by overcoming a kinetic barrier with steric pressure”, 8th Chicago Organic Symposium, University of Illinois, Chicago, IL, USA, Sept 30, **2017**. (poster)

Gupta, S.; Xie, P.; Xia, Y.; Lee, D. “Intermolecular Alder-ene reaction of arynes with functionalized alkenes”, 7th Chicago Organic Symposium, Loyola University, Chicago, IL, USA, Oct 1, **2016**. (poster)